

NASA Contractor Report 189654

1N-39
125226
P. 631

LOW COST, SPF ALUMINUM CRYOGENIC TANK STRUCTURE FOR ALS

(NASA-CR-189654) LOW COST, SPF
ALUMINUM CRYOGENIC TANK STRUCTURE
FOR ALS Final Report, Apr. 1989 -
Jan. 1992 (Rockwell International
Corp.) 631 p

N93-18030

Unclas

G3/39 0125226

C. E. Anton, et. al

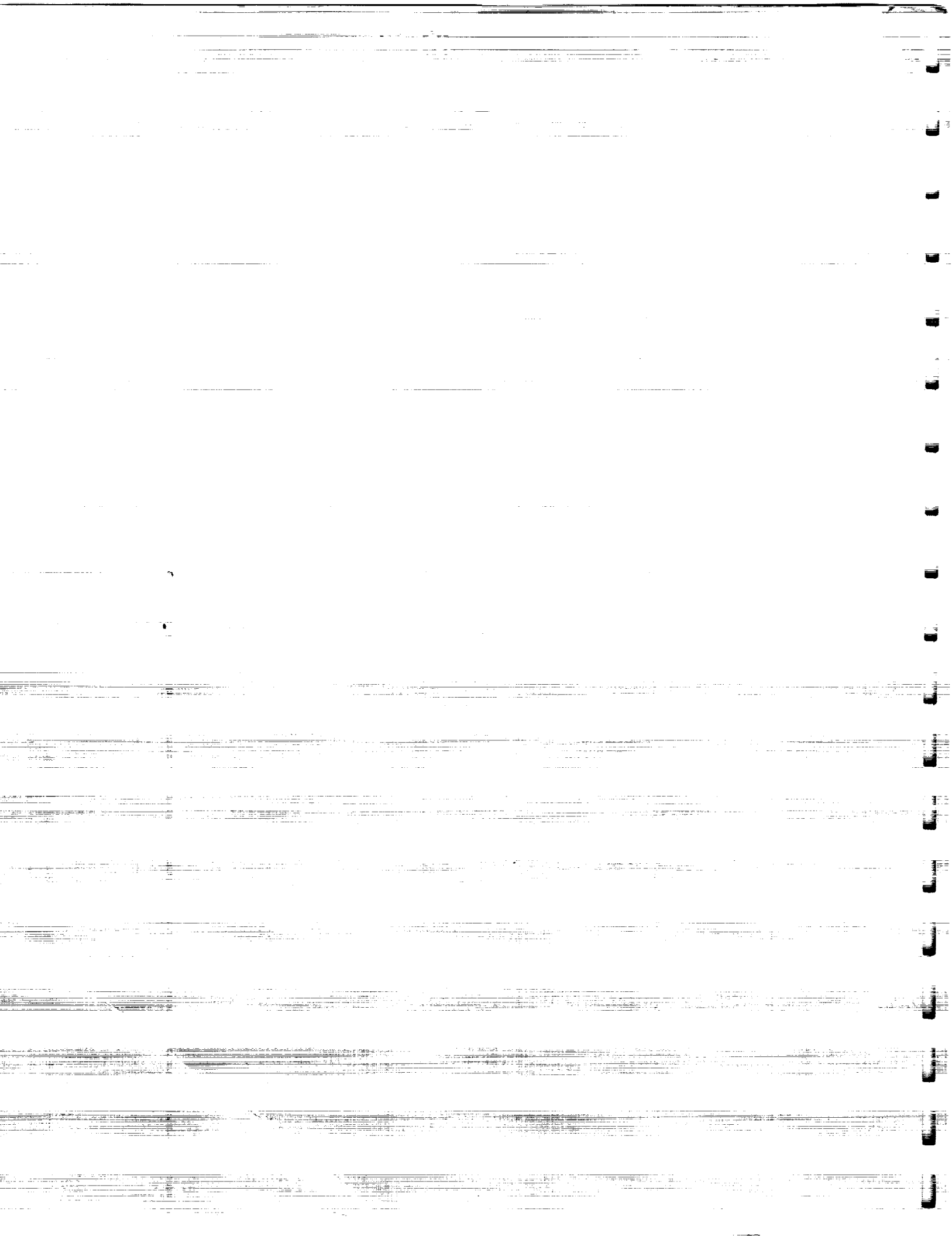
**Rockwell International North American Aircraft - Hypersonics
Downey, California**

**Contract NAS1-18590, Task 5: Technology for Hypersonic Vehicles
May 1992**



**National Aeronautics and
Space Administration**

**Langley Research Center
Hampton, Virginia 23665-5225**



FINAL TECHNICAL REPORT

September 22, 1992

CONTRACT: Technology For Hypersonic Vehicles, NAS 1-18590 TASK Order 5, "Low Cost, SPF Aluminum Cryogenic Tank Concepts for ALS."

Final REPORT

Activities For April 1989 Through January 1992

Prepared By:

C.E. Anton

C.E. Anton
Program Manager,
Low Cost, SPF Aluminum Cryogenic Tank
Concepts for ALS and Future Hypersonic Vehicles

Approved By:

K. Henn

K. Henn
Manager Structures, Design, Materials
Hypersonic Vehicles

DATE September 22, 1992
NO. OF PAGES Title + liii+ 425+ Appendices



Rockwell International

North American Aircraft Operations
Rockwell International Corporation
P.O. Box 92098
Los Angeles, California 90009

THIS PAGE INTENTIONALLY LEFT BLANK.

REPORT DOCUMENTATION PAGE

Form Approved
OMB No. 0704-0188

Public reporting burden for this collection of information is estimated to average 1 hour per response, including the time for reviewing instructions, searching existing data sources, gathering and maintaining the data needed, and completing and reviewing the collection of information. Send comments regarding this burden estimate or any other aspect of this collection of information, including suggestions for reducing this burden, to Washington Headquarters Services, Directorate for Information Operations and Reports, 1215 Jefferson Davis Highway, Suite 1204, Arlington, VA 22202-4302, and to the Office of Management and Budget, Paperwork Reduction Project (0704-0188), Washington, DC 20503.

1. AGENCY USE ONLY (Leave blank)		2. REPORT DATE September 1992		3. REPORT TYPE AND DATES COVERED Contractor Report	
4. TITLE AND SUBTITLE Low Cost, SPF Aluminum Cryogenic Tank Structures for ALS				5. FUNDING NUMBERS CNAS1-18590 WU 946-01-00-83	
6. AUTHOR(S) Claire E. Anton, Perry Rasmussen, Curt Thompson, Richard Latham, C. Howard Hamilton, Ben Ren, Chimata Gandhi, Dallis Hardwick					
7. PERFORMING ORGANIZATION NAME(S) AND ADDRESS(ES) Rockwell International North American Aircraft PO Box 92098 Los Angeles CA 90009-2098				8. PERFORMING ORGANIZATION REPORT NUMBER NA-92-1097	
9. SPONSORING / MONITORING AGENCY NAME(S) AND ADDRESS(ES) National Aeronautics and Space Administration Langley Research Center Hampton VA 23665-5225				10. SPONSORING / MONITORING AGENCY REPORT NUMBER NASA CR 189654	
11. SUPPLEMENTARY NOTES Langley Technical Monitor: John A. Wagner Task 5 Report					
12a. DISTRIBUTION / AVAILABILITY STATEMENT Unclassified - Unlimited Subject Category 26				12b. DISTRIBUTION CODE	
13. ABSTRACT (Maximum 200 words) Past production work has shown that cryogenic tank structure for the Shuttle booster rockets and the Titan system have very high life cycle costs for the fuel tank structure. The tanks are machined stiffener-skin combination that are subsequently formed into the required contour after machining. The material scrap rate for these configurations are usually high, and the loss of a tank panel due to forming or heat treatment problems is very costly. The idea of reducing the amount of scrap material and scrapped structural members has prompted the introduction of built-up structure for cryogenic tanks to be explored on the ALS program. A built-up structure approach that has shown improvements in life cycle cost over the conventional built-up approach is the use of SPF stiffened panels (reducing the overall part count and weight for the tank) resistance spot welded (RSW) to outer tank skin material. The stiffeners provide for general stability of the tank, while the skin material provides hoop direction continuity for the loads.					
14. SUBJECT TERMS Low Cost Cryogenic Tank Structure, SPF of Al and Al-Li, Resistance Spot Welding, Fusion Welding of Al-Li, Al-Li, Advanced Launch System				15. NUMBER OF PAGES 624	
				16. PRICE CODE	
17. SECURITY CLASSIFICATION OF REPORT Unclassified	18. SECURITY CLASSIFICATION OF THIS PAGE Unclassified	19. SECURITY CLASSIFICATION OF ABSTRACT Unclassified	20. LIMITATION OF ABSTRACT		

THIS PAGE INTENTIONALLY LEFT BLANK.

FOREWORD

The contract "Low Cost, SPF of Al Cryogenic Tank Structures for ALS" (Contract No. NAS1-18590, Task Assignment 5) was performed by Rockwell International North American Aircraft (NAA) Division - Hypersonics Group in conjunction with General Dynamics Space Systems Division. The program was funded out of the NASA Langley Research Center (LaRC), Hampton Virginia, during May 1989 under the Advanced Launch System (ALS) materials and structures technology Advanced Development Program (ADP) 3104. Mr. John Wagner of NASA Langley, was the NASA contract monitor, and the task manager for ADP 3104. Mr. Thomas Bales, located at NASA LaRC, was the Structures and Materials Area ADP Manager.

The Rockwell program manager was Mrs. Claire Anton co-located at the Rockwell International-SSD Downey Division and NAA-Hypersonics group. The General Dynamics Space Systems Division program manager was Mr. Perry Rasmussen. Principal investigators at Rockwell were Claire Anton - Materials and Process, Alfredo DelMundo - Advanced Design, and Curt Thompson and Richard Latham - Structural Analysis. Principal investigators at General Dynamics Space Systems Division were Perry Rasmussen - Advanced Design, Richard McCool - Structural Analysis, and Gerry Bjorkman - Manufacturing Technology. Additional contributions were provided by C. Howard Hamilton and Ben Ren of Washington State University, Ralph Bush and Peter Brouwer of the ALCOA Technical Center, and Chimata Gandhi, Clifford Bampton and Dallis Hardwick of the Rockwell Science Center, and Art Martinez of North American Aircraft.

THIS PAGE INTENTIONALLY LEFT BLANK.

TABLE OF CONTENTS

Section	Page
Foreword.....	i
List of Tables.....	v
List of Figures	x
Summary	xx
1.0 Introduction.....	1-1
2.0 Objectives	2-1
3.0 Program Plan.....	3-1
4.0 Technical discussion.....	4-1
4.0 Technical discussion.....	4-1
4.1 Design and Analysis	4-1
4.1.1 ALS Configuration.....	4-1
4.1.2 Material Design Allowables.....	4-1
4.1.3 Design Criteria.....	4-7
4.1.4 Built-Up Cryogenic Tank Design	4-7
4.1.5 Crippling Panel Design.....	4-15
4.1.5.1 PASCO Analysis.....	4-20
4.1.5.1.1 Stiffener Modeling -PASCO Approach.....	4-27
4.1.5.1.2 Typical PASCO Output.....	4-28
4.1.5.2 NASTRAN Analysis.....	4-32
4.1.6 Integrally Stiffened Structure	4-32
4.1.7 Column Buckling Panel.....	4-40
4.1.8 Doubler-Reinforced Fusion Weld.....	4-41
4.1.8.1 Modeling of Doubler-Reinforced Joint	4-43
4.1.8.2 Finite Element Model of Doubler-Reinforced Fusion Weld.....	4-44
4.1.8.3 Model Failure Load and Location Predictions	4-46
4.2 Superplastic Material Characteristics.....	4-51
4.2.1 Superplastic Forming (SPF) Material Characterization.....	4-51
4.2.1.1 7475 Aluminum	4-52
4.2.1.2 2090 Aluminum-Lithium	4-57
4.2.1.2.1 Metallurgical Analysis.....	4-58
4.2.1.2.2 Stress-Strain Rate Behavior.....	4-58
4.2.1.2.3 Superplastic Elongation Data	4-58
4.2.1.2.4 Flow Stress-Strain Data	4-59
4.2.1.2.5 Dynamic Grain Growth	4-59
4.2.1.2.6 Superplastic Cavitation	4-65
4.2.1.3 8090 Aluminum-Lithium	4-65
4.2.1.3.1 Metallurgical Analysis.....	4-68
4.2.1.3.2 Stress-Strain Rate Behavior.....	4-68
4.2.1.3.3 Flow Stress-Strain Data	4-68
4.2.1.3.4 Dynamic Grain Growth	4-71
4.2.1.3.5 Cavitation	4-71
4.2.1.4 Weldalite-049 Aluminum-Lithium.....	4-71
4.2.1.4.1 Metallurgical Analysis.....	4-80
4.2.1.4.2 Step-Strain Rate Testing.....	4-81
4.2.1.4.3 Flow Stress-Strain Data	4-82
4.2.1.4.4 Dynamic Grain Growth	4-83
4.2.1.4.5 Superplastic Cavitation	4-83

TABLE OF CONTENTS (CONTINUED)

<u>Section</u>	<u>Page</u>
4.2.2 Producibility Study	4-83
4.2.2.1 2090 and 8090 Aluminum-Lithium	4-98
4.2.2.2 Weldalite-049 (x2095) Aluminum-Lithium	4-99
4.2.3 Test Matrix and Coupon Configuration for 2090 and 8090 Aluminum-Lithium	4-100
4.2.3.1 Material Processing	4-100
4.2.3.3 Chemical Analysis	4-102
4.2.3.4 Ambient Tensile	4-105
4.2.3.4.1 Smooth Tensile Testing	4-106
4.2.3.4.2 Notched Tensile Testing	4-111
4.2.3.5 Cryogenic Tensile	4-117
4.2.3.6 Compression	4-120
4.2.3.7 Exfoliation Corrosion	4-120
4.2.3.8 Stress Corrosion Cracking	4-120
4.2.3.9 Residual Tensile Strength (Post-SCC)	4-125
4.2.3.10 Fracture Toughness	4-128
4.2.3.12 Smooth and Notched Axial Fatigue	4-129
4.2.3.13 Bearing Strength	4-143
4.2.3.14 Shear	4-144
4.2.4 Post-Superplastic Forming Heat Treatment Optimization for 2090 and 8090 Aluminum-Lithium	4-144
4.2.4.1 Heat Treatment Optimization Test Matrix and Experimental Procedures	4-146
4.2.4.1.1 Materials	4-149
4.2.4.1.2 Heat Treatment Evaluation	4-149
4.2.4.1.3 Mechanical Property Testing	4-151
4.2.4.1.4 Microstructure Evaluation	4-152
4.2.4.2 Results for Unrecrystallized Materials	4-153
4.2.4.2.1 Microstructure	4-153
4.2.4.2.2 Differential Scanning Calorimetry (DSC)	4-153
4.2.4.2.3 SHT + Natural Aging	4-153
4.2.4.2.4 SHT + Artificial Aging	4-159
4.2.4.2.5 Effect of Cooling Rate	4-159
4.2.4.2.6 Tensile Test Results	4-160
4.2.4.3 Superplastic Formed Materials	4-160
4.2.4.3.1 SHT + Natural Aging	4-175
4.2.4.3.2 SHT + Artificial Aging	4-175
4.2.4.3.3 Microstructure	4-175
4.2.4.3.4 Effect of Cooling Rate	4-183
4.2.4.3.5 Tensile Results	4-195
4.2.4.4 Discussion of Results	4-200
4.2.4.4.1 Microstructure	4-200
4.2.4.4.2 Heat Treatment Results	4-203
4.2.4.4.3 Cooling Rates	4-203
4.3 Joining	4-205
4.3.1 Adhesive Bonding	4-206
4.3.1.1 Material Selection	4-206

TABLE OF CONTENTS (CONTINUED)

<u>Section</u>	<u>Page</u>
4.3.2 Resistance Spot Weld Development	4-207
4.3.2.1 Resistance Spot Weld Characterization 7475-T62 to 2219-T81 Aluminum	4-209
4.3.2.1.1 Weld Cycle Development 7475-T62 Joined to 2219-T81 Aluminum	4-212
4.3.2.1.2 Ambient Test Data 7475-T62 Joined to 2219-T81 Aluminum	4-216
4.3.2.1.3 Cryogenic Test Data 7475-T62 Joined to 2219-T81 Aluminum	4-217
4.3.2.1.4 Exposure After Cleaning	4-219
4.3.2.1.5 Weld Cycle Tolerance	4-230
4.3.2.2 Resistance Spot Weld Characterization 2090-T62 to 2090-T83 Aluminum-Lithium	4-233
4.3.2.2.1 Weld Cycle Development	4-235
4.3.2.2.2 Ambient Test Data	4-240
4.3.2.2.3 Cryogenic Test Data	4-242
4.3.2.2.4 Exposure After Cleaning	4-243
4.3.2.2.5 Weld Cycle Tolerance	4-251
4.3.2.2.6 Weld Repair	4-251
4.3.3 Fusion Weld Development	4-256
4.3.3.1 2219-T81 Aluminum Fusion Weld Development	4-256
4.3.3.2 2090-T83 Aluminum-Lithium Fusion Weld Development	4-262
4.3.3.3 Doubler-Reinforced Fusion Weld Development	4-263
4.4 Panel Fabrication and Test	4-285
4.4.1 Fabrication and testing of crippling panels	4-285
4.4.1.1 Crippling Panel Fabrication	4-285
4.4.1.1.2 Crippling Panel Tool Design and Fabrication	4-285
4.4.1.2 Crippling Panel Test Plan	4-295
4.4.1.2.1 Introduction	4-295
4.4.1.2.2 Specimen Description	4-295
4.4.1.2.3 Test Temperature	4-303
4.4.1.2.4 Test Machine	4-303
4.4.1.2.5 Instrumentation	4-303
4.4.1.2.6 Test Fixtures	4-303
4.4.1.2.7 Test Procedure	4-309
4.4.1.2.8 Data Required	4-310
4.4.1.2.8 Test Report	4-311
4.4.1.3 Assembly of the Crippling Test Panels	4-311
4.4.1.4 Crippling Panel Test Evaluation	4-331
4.4.1.4.1 Initial Buckling	4-346
4.4.1.5 Crippling Panel Test Load Shortening Analysis	4-346
4.4.1.5.1 Results and Conclusion	4-353
4.4.1.6 Crippling Panel Test Conclusions	4-353
4.4.1.7 Crippling Panel Test Recommendations	4-354
4.4.2 Integrally Stiffened Panel Demonstration article	4-354
4.4.3 Column Buckling Panel Fabrication	4-357
4.4.4 Doubler-Reinforced Fusion Weld Panel	4-362
4.4.4.1 Bi-Axial Panel Fabrication	4-377
4.4.4.1.1 Test Procedure	4-377

TABLE OF CONTENTS (CONTINUED)

<u>Section</u>	<u>Page</u>
4.5 NDE & Quality Assurance.....	4-383
4.6 Life Cycle Cost Analysis.....	4-389
4.6.1 Ground Rules and Assumptions.....	4-390
4.6.2 Summary of Life Cycle Cost Analysis.....	4-406
4.7 Automation and Scale-Up.....	4-416
5.0 References.....	5-1
Appendix A: PASCO Input.....	A-1
Appendix B: PASCO Output.....	B-1
Appendix C: Column Buckling Panel Test Plan.....	C-1
Appendix D: R-Curves.....	D-1
Appendix E: Transmission Electron Microscopy and Diffraction Patterns of 2090 and 8090 Heat Treatment Analysis.....	E-1
Appendix F: Doubler Reinforced Fusion Weld Panel Test Plan.....	F-1

LIST OF TABLES

<u>Tables</u>	<u>Page</u>
1 Design Load Conditions	4-6
2 Room Temperature Material Properties	4-6
3 Average Material Allowables Utilized for PASCO Analysis.....	4-7
4a Qualitative Trade Study.	4-12
4b Qualitative Trade Study.	4-13
4c Qualitative Trade Study.	4-14
5 Summary of Baseline Design (Via Panda II).	4-16
6 Summary of PASCO Analysis Results for Stepped Hat and Beaded Web Hat Sections Formed from 7475 Al Joined to 2219-T81 Al Skins.	4-18
7 Summary of PASCO Analysis Results for Stepped Hat and Beaded Web Hat Sections Formed from 2090 Al-Li Joined to 2090-T83 Al-Li Skins.	4-18
8 Summary of PASCO Results for the 2090-T62 Al-Li 2-inch Stepped Hat Stiffener.....	4-22
9 Summary of PASCO Results for the 2090-T62 Al-Li 2.0-inch Beaded Hat Stiffener.....	4-22
10 Layered Modeling of 2090-T62 Al-Li 2.0-Inch Beaded Hat Stiffener Using the PASCO Analysis.....	4-23
11 Summary of the PASCO Results for the 2090-T62 Al-Li 2.5-Inch Stepped Hat.....	4-23
12 Typical PASCO Input for 7475 Al Stepped Hat Stiffener Concept.....	4-25
13 Typical PASCO Input for 7475 Al Beaded Hat Stiffener Concept.....	4-26
14 PASCO Output for the 15 Inch Long 7475-T62 Al Joined to	4-29
15 PASCO Output for the 15 Inch Long 7475-T62 Al Joined to	4-29
16 Summary of Parametric Study for 2.0 Inch Deep Hat Stiffener.....	4-36
17 Column Buckling Panel Predicted Failure Loading.....	4-41
18 Fusion Weld Test Case Data for 0.155" 2219-T81 VPPA Reinforced with 0.100" 7475-T62 Aluminum.	4-45
19 Superplastic Al and Al-Li Alloys Characterized During Program.....	4-52
20 Test Matrix for Uniaxial Duplex Strain Rate Testing.	4-55
21 Superplastic Tensile Elongations of 2090 Al-Li.....	4-63
22 Superplastic Tensile Elongations of 8090 Al-Li.....	4-72
23 Superplastic Two-Stage Strain Rate Longitudinal Tensile Elongations of 8090 Al-Li Alloy.....	4-72
24 Superplastic Two-Stage Strain Rate Transverse Tensile Elongations of 8090 Al- Li Alloy.	4-73
25 Summary of Optimum Superplastic Forming Parameters.....	4-92
26 Matrix for Post-SPF Material Testing.	4-101
27 Material Thermal Processing After SPF Prior to Testing.	4-102
28 Chemical Analysis of 2090 Al-Li in the Pre- and Post-SPF Conditions.	4-103
29 Chemical Analysis of 8090 Al-Li in the Pre- and Post-SPF Conditions.	4-104
30 Pre- and Post-SPF Longitudinal Ambient Tensile Results for 2090 Al-Li.....	4-106
31 Pre- and Post-SPF Transverse Ambient Tensile Results for 2090 Al-Li.....	4-107
32 Pre- and Post-SPF Mean Ambient Tensile Results for 2090 Al-Li.	4-108
33 Pre- and Post-SPF Longitudinal Ambient Tensile Results for 8090 Al-Li.....	4-111
34 Pre- and Post-SPF Transverse Ambient Tensile Results for 8090 Al-Li.....	4-112
35 Pre- and Post-SPF Mean Ambient Tensile Results for 8090 Al-Li.	4-113
36 2090 Notched Tensile Strength, Longitudinal Direction.	4-116
37 2090 Notched Tensile Strength, Transverse Direction.	4-116

LIST OF TABLES (CONTINUED)

Tables	Page
38 8090 Notched Tensile Strength, Longitudinal Direction.....	4-117
39 8090 Notched Tensile Strength, Transverse Direction.....	4-117
40 Cryogenic Temperature Smooth Tensile Test Results for 2090-T62 and 8090-T62 Pre- and Post-Superplastic Formed Sheet at -60°F.....	4-118
41 Cryogenic Temperature Smooth Tensile Test Results for 2090-T62 and 8090-T62 Pre- and Post-Superplastic Formed Sheet at -320°F.....	4-119
42 Compressive Strength of 2090 and 8090 Pre- and Post-Superplastic Formed Sheet Heat Treated to -T62.....	4-123
43 SCC Alternate Immersion Test Results for 2090 and 8090 Sheet.....	4-125
44 Smooth Room Temperature Tensile Testing After SCC Exposure of 2090 and 8090 Pre- and Post-SPF Sheet.....	4-126
45 Ambient Fracture Toughness for 2090-T62 and 8090-T62 Al-Li Materials in the L-T Direction, to = 0.090.....	4-129
46 Smooth Fatigue Testing of 2090-T62 Al-Li, L and T Orientations.....	4-135
47 Notched Fatigue Testing of 2090-T62 Al-Li, L and T Orientations.....	4-136
48 Smooth Fatigue Testing of 8090-T62 Al-Li, L and T Orientations.....	4-137
49 Notched Fatigue Testing of 8090-T62 Al-Li, L and T Orientations.....	4-138
50 Bearing Properties of 2090 Pre- and Post-Superplastic Formed Sheet Heat Treated to -T62.....	4-143
51 Bearing Properties of 8090 Pre- and Post-Superplastic Formed Sheet Heat Treated to -T62.....	4-144
52 Blanking Shear Properties of 2090 and 8090 Pre- and Post-Superplastic Formed Sheet Heat Treated to -T62.....	4-145
53 STAGE 1 Test Matrix for Unrecrystallized and Post-Formed 8090 and 2090 Aluminum-Lithium Alloys.....	4-147
54 STAGE 2 Test Matrix for Unrecrystallized and Post-Formed.....	4-148
55 Tensile Data for As-Received 2090 After Thermal Processing.....	4-173
56 Tensile Data for As-Received 8090 After Thermal Processing.....	4-174
57 Tensile Properties for SPF 8090 Alloy for Various Heat Treatment Parameters.....	4-198
58 Tensile Properties for SPF 2090 Alloy for Various Heat Treatment Parameters.....	4-199
59 Candidate Cryogenic Structural Adhesives.....	4-206
60 Adhesive Preliminary Test Results.....	4-207
61 L9 Taguchi Test Matrix for 0.100" 7475-T62 to 0.190" 2219-T81 Al Material Combination.....	4-209
62 Response Table for Weld Nugget Diameter (inches) of the 0.100" 7475-T62 to 0.190" 2219-T81 Material Combination.....	4-210
63 The Optimum Factor Levels were Selected Based Upon Response Table Results for Minimum Nugget Diameter.....	4-210
64 Confirmatory Test of Optimized Weld Schedule for Minimum Nugget Diameter.....	210
65 Response Table for Shear Test Values (pounds) of the 0.100" 7475-T62 to 0.190" 2219-T81 Material Combination.....	4-211
66 The Optimum Factor Levels were Selected Based Upon Response Table Maximum Lap Shear Test Results.....	4-211
67 Confirmatory Test of Optimized Weld Schedule for Maximum Lap Shear Result.....	211
68 L8 Taguchi Test Matrix for 0.100" 7475-T62 to 0.190" 2219-T81 Al Material Combination.....	4-212

LIST OF TABLES (CONTINUED)

Tables	Page
69 Test Results for Confirmatory Run on Schedule #1.....	4-213
70 Test Results for Confirmatory Run on Schedule #2.....	4-214
71 Test Results for Confirmatory Run on Schedule #3.....	4-214
72 Resistance Spot Spacing Test Results for 0.100 inch 7475-T62 to 0.190 inch 2219-T81 Aluminum.....	4-215
73 0.190" 2219-T81 Aluminum Skin Efficiency (or Reduction in Ultimate Tensile Strength) After Spot Welding of 0.100" 7475-T62 Stiffeners.....	4-217
74 Weld Schedule Certification 0.077" 7475-T62 Joined to 0.190" 2219-T81 Aluminum.....	4-218
75 0.190" 2219-T81 Aluminum Skin Efficiency (or Reduction in Ultimate Tensile Strength) After Spot Welding of 0.100" 7475-T62 Stiffeners.....	4-219
76 LN2 (-320°F) Cryogenic Resistance Spot Weld Test Results.0.100 inch 7475- T62 to 0.190 inch 2219-T81 Aluminum.....	4-220
77 LH2 (-423°F) Cryogenic Resistance Spot Weld Test Results.0.100 inch 7475- T62 to 0.190 inch 2219-T81 Aluminum.....	4-224
78 Results from Day One of Set One Pre-Weld Cleaning Test 0.100" 7475-T62 Joined to 0.190" 2219-T81 Aluminum.....	4-225
79 Results from Day Two of Set One Pre-Weld Cleaning Test 0.100" 7475-T62 Joined to 0.190" 2219-T81 Aluminum.....	4-226
80 Results from Day Three of Set One Pre-Weld Cleaning Test 0.100" 7475-T62 Joined to 0.190" 2219-T81 Aluminum.....	4-227
81 Results from Day One of Set Two Pre-Weld Cleaning Test 0.100" 7475-T62 Joined to 0.190" 2219-T81 Aluminum.....	4-228
82 Results from Day Two of Set Two Pre-Weld Cleaning Test 0.100" 7475-T62 Joined to 0.190" 2219-T81 Aluminum.....	4-228
83 Results from Day Three of Set Two Pre-Weld Cleaning Test 0.100" 7475-T62 Joined to 0.190" 2219-T81 Aluminum.....	4-229
84 Results from Day Four of Set Two Pre-Weld Cleaning Test 0.100" 7475-T62 Joined to 0.190" 2219-T81 Aluminum.....	4-229
85 Results from Day Five of the Pre-Weld Cleaning Test 0.100" 7475-T62 Joined to 0.190" 2219-T81 Aluminum.....	4-230
86 L9 Taguchi Test Matrix for 0.090" 2090-T62 Al-Li joined to 0.190" 2090-T83 Al-Li.....	4-233
87 Average Test Results for 0.090" 2090-T62 to 0.190" 2090-T83 Al-Li L9 Taguchi Array.....	4-234
88 Conformity Test Results for 0.090" 2090-T62 to 0.190" 2090-T83 Al-Li Optimized Resistance Spot Weld Schedule.....	4-234
89 Weld Certification Test Results for 0.090" 2090-T62 to 0.190" 2090-T83 Al-Li Optimized Resistance Spot Weld Schedule.....	4-235
90 Resistance Spot Spacing Test Results for 0.090 inch 2090-T62 to .190 inch 2090-T83 Aluminum-Lithium.....	4-238
91 0.190" 2090-T83 Aluminum-Lithium Skin Efficiency (or Reduction in Ultimate Tensile Strength) After Spot Welding of 0.090" 2090-T62 Stiffeners.....	4-240
92 Weld Schedule Certification Test for 2090 Crippling Test Panels.....	4-241
93 0.190" 2090-T83 Aluminum-Lithium Skin Efficiency (or Reduction in Ultimate Tensile Strength) After Spot Welding of 0.090" 2090-T62 Stiffeners.....	4-243
94 LN2 (-320°F) Cryogenic Resistance Spot Weld Test Results.0.090 inch 2090- T62 to 0.190 inch 2090-T83 Aluminum-Lithium.....	4-244

LIST OF TABLES (CONTINUED)

Tables	Page
95 LH2 (-423°F) Cryogenic Resistance Spot Weld Test Results.0.090 inch 2090-T62 to 0.190 inch 2090-T83 Aluminum-Lithium.....	4-245
96 Resistance Spot Welding Pre-Weld Cleaning Test Results for 0.090 inch 2090-T62 to 0.190 inch 2090-T83 Aluminum-Lithium.....	4-246
97 Defect Weld Schedules for 0.090" 2090-T62 Joined to 0.190" 2090-T83 Aluminum-Lithium.....	4-252
98 Repair Weld Schedules for 0.090" 2090-T62 Joined to 0.190" 2090-T83 Aluminum-Lithium.....	4-252
99 Tensile Strength of VPPA Fusion Welded 0.190" 2219-T81.....	4-257
100 Tensile Strength of VPPA Fusion Welded 0.155" 2219-T81.....	4-257
101 Tensile Response of Fusion Doubler Reinforce Testing for 2219-T81 Al with 7475-T62 Al Doubler.....	4-259
102 Fusion Weld Development of 0.155.....	4-262
103 Tensile Results of 0.155" 2090-T83 Two Pass VPPAW.....	4-263
104 Analysis Results for Longitudinal Joint for Various Spot Weld Stiffness Values.....	269
105 The Analysis Best Matched the Test Data When a Spot Weld Stiffness of 180,000 lb/in was Used.....	4-270
106 Summary of longitudinal joint dogbone tests comparing load distribution in joint with analysis.....	4-271
107 Spot Weld and VPPA Fusion Weld Strength Values for Various Joints.....	4-286
108 Predicted Ultimate Uniaxial Loads.....	4-310
109 Crippling Panel Weld Certification Testing.....	4-315
110 Crippling Panel Test Results for 7475-T62 Stiffener Joined to 2219-T81 Skin.....	4-326
111 2090 Al-Li Crippling Panel Weld Certification Testing.....	4-327
112 2090 Al-Li Crippling Panel Weld Certification Testing.....	4-328
113 Crippling Panel Test Results for 2090-T62 Stiffener Joined to 2090-T83 Skin.....	4-330
114 Summary of Predicted Loads and Failure Modes for the Crippling Test Panel.....	4-332
115 Strain Gage and Deflectometer Readings for Panel #14 (7475 Al) Obtained During Testing at General Dynamics Space Systems Division.....	4-347
116 Strain Gage and Deflectometer Readings for Panel #18 (2090 Al-Li) Obtained During Testing at General Dynamics Space Systems Division.....	4-348
117 Summary of the Crippling Crippling Panel Test Versus Predicted Loads.....	4-349
118 Comparison Summary of the Test Panel Versus Predicted Axial Stiffness (EA) of the Crippling Specimens.....	4-353
119 Test Results of the As-Welded 2219-T81 VPPA Fusion Weld Tensile Specimens.....	4-379
120 Test Results of the 2219-T81 VPPA Fusion Weld with the Bead Ground Down on One Side of Each Tensile Specimen.....	4-380
121 Test Results of the 2219-T81 VPPA Fusion Weld with the Bead Ground Down on Both Sides of Each Tensile Specimen.....	4-380
122 Results of 2090-T83 VPPA Fusion Weld Tensile Tests.....	4-381
123 Results of 2090-T83 VPPA Fusion Weld Tensile Tests, Weld Bead Ground Flush on One Side.....	4-381
124 Results of 2090-T83 VPPA Fusion Weld Tensile Test.....	4-382
125 Results of 2090-T83 VPPA Fusion Weld Tensile Tests, Weld Bead Ground Flush on One Side.....	4-382126
127 Cost Estimating Methodology for the LCC Analysis.....	4-405

LIST OF TABLES (CONTINUED)

Tables	Page
128 Ground Rules for LCC Analysis.....	4-406
129 LCC Weight Breakdowns for Each Configuration.	4-407
130 LCC Hours and Cost Information for Superplastic Formed Stiffened Panels for 2090 Aluminum LH2 Tank Structure at T1, T307 and T1000.	4-408
131 LCC Hours and Cost Information for Superplastic Formed Stiffened Panels for 7475 Aluminum LH2 Tank Structure at T1, T307 and T1000.	4-409
132 LCC Hours and Cost Information for Brake Formed Stiffened Panels for 2090 Aluminum LH2 Tank Structure at T1, T307 and T1000.	4-410
133 LCC Hours and Cost Information for Brake Formed Stiffened Panels for 2219 Aluminum LH2 Tank Structure at T1, T307 and T1000.	4-411
134 LCC Hours and Cost Information for "I" Extrusion Stiffened Panels for 2090 Aluminum LH2 Tank Structure at T1, T307 and T1000.	4-412
135 LCC Hours and Cost Information for "I" Extrusion Stiffened Panels for 2219 Aluminum LH2 Tank Structure at T1, T307 and T1000.	4-413
136 LCC Hours and Cost Information for Integrally Stiffened Machined Panels for 2219 Aluminum LH2 Tank Structure at T1, T307 and T1000.	4-414
137 Summary of Cost Trade Analysis.....	4-415
138 Summary of Weight Analysis.	4-415
139 Predicted LCC Behavior.	4-416
140 Cost Savings or Penalties for Cryogenic Tank Structures Versus the Integrally Machined Concept.	4-416

LIST OF FIGURES

Figures	Page
1 ALS-L Launch Vehicle Configuration.....	4-2
2 ALS-L Vehicle Load Level for the LH2 Tank, Ultimate NX at Max Alpha Q.....	4-3
3 ALS-L Vehicle Load Level for the LH2 Tank, Ultimate NX at Max Beta Q, Positive Mz.	4-4
4 ALS-L Vehicle Load Level for the LH2 Tank, Ultimate NX at Max Beta Q, Negative Mz.	4-5
5 Hat Stiffener-Ring Configuration.....	4-9
6 Effect of Spot Weld Pitch Versus Parent Metal Strength (Ref. MIL-HDBK-5).....	4-10
7 Baseline Conventional "T" and Hat Stiffener.....	4-10
8 Structural Efficiency Curves for Conventional Baseline Stiffener and SPF Designs.....	4-11
9 Initial SPF Stiffener Designs.....	4-11
10 Length Between Intermediate Rings Versus Hat tbar.....	4-17
11 Stiffener Height versus Hat tbar for the Stepped Hat. PASCO Analysis for Outward Thinning.	4-17
12 Selected Stepped Hat Concept Design for Type I Crippling Panels and the Theoretical Thinning at Selected Points on the Stiffener.....	4-20
13 Beaded Hat Concept Designs for Type I Crippling Panels and the Theoretical Thinning at Selected Points on the Stiffener.....	4-21
14 Final Type 1 Stepped Hat and Beaded Web Crippling Specimen Panel Designs.	4-24
15 2090 Al-Li PASCO Matrix for the Beaded Web Configuration.....	4-27
16 Typical Modal Shapes for Stepped Hat Stiffener Using PASCO Analysis.....	4-30
17 Typical Modal Shapes for Beaded Hat stiffener Using PASCO Analysis.	4-31
18 NASTRAN Finite Element Model.....	4-33
19 NASTRAN Buckling Analysis.....	4-34
20 NASTRAN Sixty Inch Modal Deformed Buckling Mode.....	4-36
21 NASTRAN Sixty Inch Multiple C-Bar Model with Center Support Frame, Eigen Value Factor = 1.09.....	4-37
22 NASTRAN Sixty Inch Multiple C-Bar Model with Center Support Frame, Eigen Value Factor = 1.89.....	4-37
23 NASTRAN Model of Column Buckling Panel Design.....	4-38
24 Column Buckling Panel Deflected (Solid) Under Mode 1 and Non-Deflected (Dashed) Uniaxial Load (Nx = 10,000 lb/in), Stiffener Spacing = 4.0", Integral Node I = 1.0 in4.....	4-39
25 Example of One Integral Node Configuration for SPF Stiffened Structure.....	4-39
26 Column Buckling Panel Configuration.....	4-40
27 Average Thickness At Flange and Cap for Column Buckling Panel.....	4-41
28 Vertical Doubler-Reinforced Joint on the ALS Vehicle.....	4-42
29 Schematic of Doubler-Reinforced Joint on the ALS Vehicle.	4-44
30 Stress-Stain Curve for Doubler-Reinforced Fusion Weld Joint.....	4-45
31 Top View of Stress Contour Plot for Hoop Loading = 7500 lb/in.....	4-47
32 Bottom View of Stress Contour Plot for Hoop Loading = 7500 lb/in.....	4-47
33 Top View of Stress Contour Plot for Hoop Loading = 5887 lb/in and Axial Load = -6307 lb/in.....	4-48
34 Bottom View of Stress Contour Plot for Hoop Loading = 5887 lb/in and Axial Load = -6307 lb/in.....	4-48
35 Stress Distribution Curves for Weld Joint Area Via FEM Model.....	4-49
36 Doubler-Reinforced Fusion Weld Joint.....	4-50

LIST OF FIGURES (CONTINUED)

Figures	Page
37 Superplastic Uniaxial Test Chamber with Hydrostatic Pressure Retort.	4-53
38 Superplastic Uniaxial Test Chamber with Data Acquisition System.	4-54
39 Microstructure of Superplastic 7475 Aluminum.	4-55
40 Flow Stress and Strain Rate Sensitivity Versus Strain Rate for 7475 Al.	4-56
41 Flow Stress Versus Strain for 7475 Al at Constant Strain Rate Values between 2E-4 and 8E-4/sec.	4-57
42 Microstructure of Superplastic 2090 Al-Li Material.	4-59
43 2090 Al-Li Longitudinal Flow Stress Versus Strain for Different Strain Rates.	4-60
44 2090 Al-Li Transverse Flow Stress Versus Strain for Different Strain Rates.	4-61
45 2090 Al-Li Uniaxial Superplastic Elongations with Back Pressure Tests Performed at 950°F with Duplex Strain Rate of 2E-3 and 2E-4 sec-1.	4-62
46 2090 Al-Li Flow Stress Versus Strain for Duplex Stage Strain Rates. (-T3 and - OE16 Temps)	4-64
47 2090 Al Transverse Flow Stress at 400 psi Back Pressure Versus Strain for Duplex Stage Strain Rates.	4-64
48 2090 Al Transverse Flow Stress at 600 psi Back Pressure Versus Strain for Duplex Stage Strain Rates.	4-65
49 2090 Al-Li Dynamic Grain Growth with Increase in Strain.	4-66
50 2090 Al-Li Dynamic Grain Growth Versus Superplastic Strain.	4-67
51 Microstructure of Superplastic 8090 Al-Li.	4-67
52 Flow Stress and Strain Rate Sensitivity Versus Strain Rate for 8090 Al-Li for Various Temperatures.	4-69
53 8090 Al-Li Uniaxial Superplastic Elongations with Back Pressure. Tests were Performed at 915°F with Duplex Strain Rate of 2E-3 and 2E-4 sec-1.	4-70
54 Superplastic Elongation Versus Forming Temperature for 8090 Al-Li at Various Levels of Back Pressure.	4-74
55 Average Grain Size Versus Superplastic Strain for 8090 Al-Li.	4-74
56 Dynamic Grain Growth and Superplastic Cavitation in 8090 Al-Li, Formed Without Back Pressure.	4-75
57 Dynamic Grain Growth in 8090 Al-Li Formed with 400 psi Back Pressure.	4-76
58 Flow Stress Versus Strain for 8090 Al-Li Formed with 200 psi Back Pressure.	4-77
59 Flow Stress Versus Strain for 8090 Al-Li Formed with 400 psi Back Pressure.	4-77
60 Flow Stress Versus Strain for 8090 Al-Li Formed with 600 psi Back Pressure.	4-78
61 Superplastic Elongation Versus Back Pressure for 8090 Al-Li at Various Forming Temperatures.	4-78
62 Severe Superplastic Cavitation for Strain of 1.7 in 8090 Al-Li Without Back Pressure versus Suppressed Cavitation for an Increase in Strain to 3.1 with 400 psi Back Pressure.	4-79
63 Microstructure of Weldalite-049 Al-Li Observed to be Non-Superplastic.	4-80
64 Microstructure of Weldalite-049 Al-Li Observed to be Superplastic.	4-81
65 Flow Stress and M-value Versus Strain Rate for Initial Batch of Weldalite-049 Al-Li Sheet, Longitudinal Direction Tested, at 915°F at 600 psi Back Pressure.	4-84
66 Flow Stress and M-value Versus Strain Rate for Initial Batch of Weldalite-049 Al-Li Sheet, Transverse Direction, Tested at 914°F at 600 psi Back Pressure.	4-85
67 Flow Stress and M-value Versus Strain Rate for Second Batch of Weldalite-049 Al-Li Sheet, Longitudinal Direction Tested, at 915°F at 600 psi Back Pressure.	4-86
68 Flow Stress and M-value Versus Strain Rate for Second Batch of Weldalite-049 Al-Li Sheet, Transverse Direction, Tested at 915°F (490°C) at 600 psi Back Pressure.	4-87

LIST OF FIGURES (CONTINUED)

Figures	Page
69 Strain Rate and Orientation Effects on Flow Stress and Elongation to Failure of SPF Weldalite-049 Sheet at 915°F with 600 psi Back Pressure.....	4-88
70 Temperature Effects on Elongation and Cavitation of SPF Weldalite-049 Sheet at $\epsilon = 3E-4/\text{sec}$ with 600 psi Back Pressure.....	4-89
71 Static Recrystallization and Grain Growth of SPF Weldalite-049 Sheet at Temperatures of 915°F and 930°F.	4-90
72 Back Pressure Effect on Cavitation in Weldalite-049 Al-Li Sheet Tested at 915°F at Strain Rate of $6E-4 \text{ sec}^{-1}$	4-91
73 Pressure Versus Time Profile for x2095 Al-Li Producibility Pan.....	4-93
74 Small Producibility Pans 6" x 6" x Depth were Fabricated for Each Material Examined During this Program. The Depth of the Tool was Altered with the Addition of Inserts into the Die Cavity.	4-93
75 Large Producibility Pan 18" x 18" x Depth was Fabricated for Materials Used During Weld Development and Post-SPF Property Testing The Depth of the Tool was Altered with the Addition of Inserts into the Die Cavity.....	4-94
76 Thickness Measurements for a 7475 Al Producibility Pan.....	4-95
77 Thickness Measurements for a 2090 Al-Li Producibility Pan.....	4-95
78 Thickness Measurements for a 8090 Al-Li Producibility Pan.....	4-96
79 Thickness Measurements for a x2095 Al-Li Producibility Pan.....	4-96
80 Photomicrograph of Cavitation for a 7475 Al Producibility Pan.....	4-97
81 Photomicrograph of Cavitation for a 2090 Al-Li Producibility Pan.	4-97
82 Photomicrograph of Cavitation for a 8090 Al-Li Producibility Pan.	4-98
83 Tensile Test Coupons - Smooth ($K_t = 1.0$) with no Center hole -Notched ($K_t = 2.5$) with Center Drill-hole.....	4-105
84 2090 Al-Li Ultimate Tensile Strength Versus Effective True Strain.....	4-108
85 2090 Al-Li Tensile Yield Strength Versus Effective True Strain.....	4-109
86 2090 Al-Li Ultimate Tensile and Yield Strengths Versus Effective True Strain.....	4-109
87 2090 Al-Li Tensile Elongation Versus Effective True Strain.....	4-110
88 2090 Al-Li Tensile Modulus Versus Effective True Strain.	4-110
89 8090 Al-Li Ultimate Tensile Strength Versus Effective True Strain.....	4-113
90 8090 Al-Li Tensile Yield Strength Versus Effective True Strain.....	4-114
91 8090 Al-Li Ultimate Tensile and Yield Strengths Versus Effective True Strain.....	4-114
92 8090 Al-Li Tensile Elongation Versus Effective True Strain.	4-115
93 8090 Al-Li Tensile Modulus Versus Effective True Strain.	4-115
94 Cryogenic Tensile Response of 2090-T62 Al-Li at -60°F.....	4-121
95 Cryogenic Tensile Response of 8090-T62 Al-Li at -60°F.....	4-121
96 Cryogenic Tensile Response of 2090-T62 Al-Li at -320°F.....	4-122
97 Cryogenic Tensile Response of 8090-T62 Al-Li at -320°F.....	4-122
98 Exfoliation Corrosion Results for 2090 and 8090 Al-Li Using the MASTMAASIS Test Methods.	4-124
99 Post-SCC Residual Tensile Strength of 2090-T62 Al-Li.	4-127
100 Post-SCC Residual Tensile Strength of 8090-T62 Al-Li.	4-127
101 Center Crack Tension Specimen Configuration.....	4-128
102 R-Curve for 2090 Al-Li, Non-Strained Material. $K_{IC} = 48.3$	4-130
103 R-Curve for 2090 Al-Li, Non-Strained Material. $K_{IC} = 52.0$	4-130
104 R-Curve for 2090 Al-Li, Formed Material. $K_{IC} = 39.4$	4-131
105 R-Curve for 2090 Al-Li, formed Material. $K_{IC} = 52.8$	4-131
106 R-Curve for 8090 Al-Li, Non-Strained Material. $K_{IC} = 52.9$	4-132

LIST OF FIGURES (CONTINUED)

Figures	Page
107 R-Curve for 8090 Al-Li, Non-Strained Material. $K_{IC} = 66.8$	4-132
108 R-Curve for 8090 Al-Li, Formed Material. $K_{IC} = 60.3$	4-133
109 R-Curve for 8090 Al-Li, formed Material. $K_{IC} = 48.8$	4-133
111 Smooth ($K_t = 1.02$) and Notched ($K_t = 2.5$) Fatigue Specimens With Continuous Radius.	4-134
111 Smooth Fatigue Life of 2090-T62 Al-Li.	4-139
112 Notched Fatigue Life of 2090-T62 Al-Li.	4-140
113 Smooth Fatigue Life of 8090-T62 Al-Li.	4-141
114 Notched Fatigue Life of 8090-T62 Al-Li.	4-142
115 Microstructure of the as-received 2090 alloy	4-154
116 Results of the differential scanning calorimetry conducted on the as-received 2090 alloy. Results indicate a solidus temperature of approximately 586°C (1087°F).....	4-155
117 Results of the differential scanning calorimetry conducted on the as-received 8090 alloy. Results indicate a solidus temperature of approximately 593°C (1099°F).....	4-156
118 Optical micrographs of the a. 8090 alloy and b. 2090 alloy after solution heat treatment at 510°C (950°F) for 1 hour followed by a water quench. Banding is present, however, some recrystallization appears to have taken place.....	4-157
119 Effect of natural aging on hardness of the as-received a. 8090, and b. 2090 alloys for various solution heat treatment temperatures.	4-158
120 Effect of the aging temperature (48 hours) on the hardness for several solution heat treatment temperatures	4-161
121 Effect of the aging temperature on the yield and ultimate strengths after solution treatment at 560°C (1040°F), water quenched, artificially aged for 48 hours.	4-162
122 Cooling rate characteristics measured for the sheet alloys for water quenching, slow air cooling, and fast air cooling.....	4-163
123 The effect of the cooling rate from 510°C (950°F) on the hardness of the 8090 and 2090 alloys after aging at 180°C (356°F) for 48 hours	4-164
124 Effect of cooling rate on the hardness developing with artificial aging time for as-received 8090 alloy, aged at 150°C (302°F) after solution heat treatment at a. 510°C (950°F), b. 545°C (1013°F), and c. 560°C (1040°F).....	4-165
125 Effect of cooling rate on the hardness developing with artificial aging time for as-received 8090 alloy, aged at 180°C (356°F) after solution heat treatment at a. 510°C (950°F), b. 545°C (1013°F), and c. 560°C (1040°F).....	4-167
126 Effect of cooling rate on the hardness developing with artificial aging time for as-received 2090 alloy, aged at 150°C (302°F) after solution heat treatment at a. 510°C (950°F), b. 545°C (1013°F), and c. 560°C (1040°F).....	4-169
127 Effect of cooling rate on the hardness developing with artificial aging time for as-received 2090 alloy, aged at 180°C (356°F) after solution heat treatment at a. 510°C (950°F), b. 545°C (1013°F), and c. 560°C (1040°F).	4-171
128 Effect of natural aging on hardness of the SPF-processed a. 8090, and b. 2090 alloys for various solution heat treatment temperatures and cooling rates as indicated on the graphs.....	4-176

LIST OF FIGURES (CONTINUED)

Figures	Page
129 Age hardening characteristics of the SPF-processed 8090 alloy after direct water quenching from the forming temperature, and after re-solution treatment at 545°C (1013°F) and 560°C (1040°F) aged at a. 150°C (302°F), and b. 180°C (356°F).....	4-177
130 Age hardening characteristics of the SPF-processed 8090 alloy re-solution treated at a. 545°C (1013°F), and b. 560°C (1040°F) and artificially aged at 150°C (302°F) or 180°C (356°F).....	4-178
131 Optical micrographs of the 8090 alloy, as-SPF processed (510°C, 950°F followed by a water quench), a. longitudinal, and b. transverse views.....	4-179
132 Optical micrographs of the 2090 alloy, as-SPF processed (510°C, 950°F followed by a water quench), a. longitudinal, and b. transverse views.....	4-180
133 TEM photograph of the 8090 alloy after forming and aging 510°C (950°F) followed by a water quench and artificially aged at 180°C (356°F) for 48 hours.....	4-181
134 Electron micrographs of the 2090 alloy in the condition formed at 510°C (950°F) followed by a water quench and artificially aged at 180°C (356°F) for 24 hours. The microstructure appears to have fully recrystallized grains of approximately 1 to 2 microns. A somewhat non-uniform distribution of precipitates was observed.....	4-182
135 Electron micrographs of the 2090 alloy in the condition formed at 510°C (950°F) followed by a water quench and artificial aging at 180°C (356°F) for 24 hours.....	4-184
136 Electron micrographs of the 2090 alloy in the condition formed at 510°C (950°F) followed by a water quench and artificial aging at 180°C (356°F) for 24 hours. The microstructure consists of the δ' as the background "mottled" structure, with the larger T1 platelets and larger spherical δ'.....	4-185
137 Effect of cooling rate on the strength of as-formed, water quenched, and artificially age hardened a. 8090 and b. 2090 alloys.....	4-186
138 Comparison of the quench-rate effect on the 8090 and 2090 alloys in the as-formed condition, water quenched and age hardened a. longitudinal orientation, and b. transverse orientation of the tensile test axis.....	4-187
139 Effect of cooling rate on the age hardening characteristics of the as-SPF processed 8090 alloy for aging at a. 150°C (302°F), and b. 180°C (356°F).....	4-188
140 Effect of cooling rate on the age hardening characteristics of the as-SPF processed 8090 alloy in the as-formed condition a. water quenched b. fast air cooled, and c. slow air cooled.....	4-189
141 Age hardening characteristics of the SPF-processed 2090 alloy after direct water quenching from the forming temperature, and after solution treatment at 545°C (1013°F) and 560°C (1040°F) aged at a. 150°C (302°F), and b. 180°C (356°F).....	4-191
142 Age hardening characteristics of the SPF-processed 2090 alloy a. as-formed and b. after solution treatment at 545°C (1013°F), and c. after solution treatment at 560°C (1040°F).....	4-192
143 Effect of cooling rate on the age hardening characteristics of the as-SPF processed 2090 alloy in the as-formed condition a. water quenched, and b. slow air cooled.....	4-194

LIST OF FIGURES (CONTINUED)

Figures	Page
144 Data showing the effect of the cooling rate on the longitudinal strength of 8090 alloy taken from Shakesheff et. al. and results of this work for comparison.....	4-196
145 Electron micrographs of the 8090 alloy in the as-formed condition followed by a quench and artificial aging at 180°C (356°F) for 24 hours. Cooling rates were a. water quenched, b. fast air cooling, and c. slow air cooling. An increase in grain boundary precipitation with decreasing cooling rate can be seen.....	4-197
146 Scanning electron fractographs taken from the failed tensile test specimens of the a. 2090 and b. 8090 alloys in the unformed but solution heat treated condition (510°C (950°F)) followed by a water quench and artificial age at 180°C (356°F) for 48 hours.....	4-201
147 Scanning electron fractographs taken from the failed tensile test specimens of the a. 2090 and b. 8090 alloys in the superplastic formed condition (510°C (950°F)) followed by a water quench and artificial age at 180°C (356°F) for 48 hours. The fracture mode is intergranular, but with ductile dimples on the grain facets.	4-202
148 Resistance Spot Welding Equipment at General Dynamics.....	4-208
149 Schematic for inter-spot spacing test.	4-215
150 Summary of Mechanical Lap Shear Test Results for 0.100" 7475-T62 joined to 0.190" 2219-T81 Al, and 0.090" 2090-T62 joined to 0.190" 2090-T83 Al-Li.....	4-221
151 Summary of Spot Weld Nugget Quality for 0.100" 7475-T62 joined to 0.190" 2219-T81 Al, and 0.090" 2090-T62 joined to 0.190" 2090-T83 Al-Li.....	4-222
152 Summary of Sheet Efficiency for 0.100" 7475-T62 joined to 0.190" 2219-T81 Al, and 0.090" 2090-T62 joined to 0.190" 2090-T83 Al-Li.	4-223
153 Weld Heat Sensitivity Versus Nugget Diameter for 0.100" 7475-T62 Al Joined to 0.190" and 0.090" 2090-T62 Joined to 0.190" 2090-T83 Al-Li.	4-231
154 Weld Heat Sensitivity Versus Nugget Penetration into Lower Sheet for 0.100" 7475-T62 Al Joined to 0.190" and 0.090" 2090-T62 Joined to 0.190" 2090-T83 Al-Li.	4-232
155 Weld Heat Sensitivity Versus Lap Shear for 0.100" 7475-T62 Al Joined to 0.190" and 0.090" 2090-T62 Joined to 0.190" 2090-T83 Al-Li.	4-232
156 Resistance Spot Weld Spacing Test. Nugget Diameter Versus Spot Spacing 0.090 inch 2090-T62 to 0.190 inch 2090-T8	4-237
157 Resistance Spot Weld Spacing Test. Lap Shear Versus Spot Spacing 0.090 inch 2090-T62 to 0.190 inch 2090-T8.....	4-237
158 Resistance Spot Weld Spacing Test. 0.090" Sheet Penetration Versus Spot Spacing for 0.090 inch 2090-T62 to 0.190 inch 2090-T8.....	4-239
159 Resistance Spot Weld Spacing Test. 0.190 inch Sheet Penetration Versus Spot Spacing for 0.090 inch 2090-T62 to 0.190 inch 2090-T8.....	4-240
160 Pre-weld Cleaning Test, Surface Resistance Versus Time.0.090 inch 2090-T62 to 0.190 inch 2090-T83.....	4-248
161 Pre-weld Cleaning Test, Lap Shear Versus Time.0.090 inch 2090-T62 to 0.190 inch 2090-T83.....	4-248
162 Pre-weld Cleaning Test, Nugget Diameter Versus Time.0.090 inch 2090-T62 to 0.190 inch 2090-T83.....	4-249
163 Pre-weld Cleaning Test, 0.090 inch Sheet Penetration Versus Time.....	4-250
164 Pre-weld Cleaning Test, 0.190 inch Sheet Penetration Versus Time.....	4-250
165 Diffusion Spot Weld in 0.090" 2090-T62 joined to 0.190" 2090-T83 Al-Li.....	4-253
166 Repaired Diffusion Spot Weld in 0.090" 2090-T62 joined to 0.190" 2090-T83 Al-Li.....	4-253

LIST OF FIGURES (CONTINUED)

Figures	Page
167 Undersized Spot Weld in 0.090" 2090-T62 joined to 0.190" 2090-T83 Al-Li.	4-254
168 Repaired Undersized Spot Weld in 0.090" 2090-T62 joined to 0.190" 2090-T83 Al-Li.	4-254
169 Spot Weld with Cracks and Voids in 0.090" 2090-T62 joined to 0.190" 2090-T83 Al-Li.	4-255
170 Spot Weld with Cracks and Voids Repaired in 0.090" 2090-T62 joined to 0.190" 2090-T83 Al-Li.	4-255
171 Variable Polarity Plasma Arc Fusion Weld Development for 0.155" 2219-T81.	4-258
172 Standard Tension Specimen for Fusion Weld Reinforcement.	4-260
173 Strain Gauge Locations for Fusion Weld Efficiency Testing.	4-261
174 Macro Cross-section of a Double Pass VPPA Weld of 2090-T83, (0.155 inch thickness sheet), some porosity was apparent.	4-264
175 Macro Cross-section of a Double Pass VPPA Weld of 2090-T83, (0.155 inch thickness sheet).	4-265
176 Longitudinal Joint Configuration and Nomenclature for the Even Row Spot Weld Pattern.	4-266
177 Longitudinal Joint Configuration and Nomenclature for the Staggered Row Spot Weld Pattern.	4-267
178 Model Representation of a Fusion Weld / Resistance Spotweld Doubler Reinforced Joint.	4-268
179 Standard Tension Specimen for the Longitudinal Spot Welded Splice Joint Tests.	4-272
180 Longitudinal Splice Joint Test Configuration for the Even Row Spot Weld Pattern.	4-273
181 Longitudinal Splice Joint Test Configuration for the Staggered Row Spot Weld Pattern.	4-274
182 Strain Gage Location for Test Specimen F4D1.	4-275
183 Strain Gage Location for Test Specimen F3D2.	4-276
184 Strain Gage Location for Test Specimen F2D4.	4-277
185 Strain Gage Location for Test Specimen F1D3.	4-278
186 Load Versus Microstrain for Front Strain Gages on Specimen F4D1.	4-279
187 Load Versus Microstrain for Back Strain Gages on Specimen F4D1.	4-280
188 Load Versus Microstrain for Specimen F3D2.	4-281
189 Load Versus Microstrain for Front Strain Gages on Specimen F2D4.	4-282
190 Load Versus Microstrain for Back Strain Gages on Specimen F2D4.	4-283
191 Load Versus Microstrain for Specimen F1D3.	4-284
192 Sensitivities of The Fusion Weld Stress and Spot Shear Load to a Variation in Doubler Thickness.	4-287
193 Sensitivities of The Fusion Weld Stress and Spot Shear Load to a Variation in Spot Weld Gage.	4-288
194 Sensitivities of The Fusion Weld Stress and Spot Shear Load to a Variation in Doubler Width.	4-289
195 Crippling Specimen Universal Die Box.	4-290
196 Crippling Stiffener Tool Inserts for Stepped Web Curved Cap Hat, Beaded Web Curved Cap Hat, and Beaded Web Flat Cap Hat.	4-291
197 Graphical Representation of the Crippling Tool Thermal Survey.	4-292
198 Schematic of Crippling Tool and Platen Thermocouple Layout and Temperature Print Out from Heat Survey.	4-292
199 Crippling Panel Pressure Versus Time Profile for 7475 Al.	4-293

LIST OF FIGURES (CONTINUED)

Figures	Page
200 Crippling Panel Pressure Versus Time Profile for 2090 Al-Li.	4-293
201 Crippling Panel Pressure Versus Time Profile for 8090 Al-Li.	4-294
202 Crippling Panel Pressure Versus Time Profile for 2095 Al-Li.	4-294
203 Application of Releasing Agent on Part Blank.	4-296
204 Hot Loading of Part Blank into Automated 300 Ton Press.	4-297
205 Hot Unload Formed Part.	4-298
206 Beaded Crippling Panel.	4-299
207 Part Blank and Identical Beaded Hat Sections.	4-300
208 Rough Trimmed Crippling Panels.	4-301
209 Crippling Specimen Drawing L9111392.	4-302
210 Strain Gauge Locations View 1.	4-304
211 Strain Gauge Locations View 2.	4-305
212 Crippling Specimen Strain Gage Location Drawing L9111398.	4-306
213 Test Support Fixture.	4-307
214 Crippling Specimen Support Fixture Drawing L9111397.	4-308
215 Critical Failure Areas for Stiffener Concepts as Determined by PASCO Modeling.	4-309
216 7475-T62 SPF Stepped Hat Stiffener and 2219-T81 Skin with Strain Gages.	4-312
217 SPF Stepped Hat Stiffener and Skin Clamped With Resistance Spot Spacing Tooling.	4-312
218 Resistance Spot Welding Crippling Test Panel Stiffener to Skin	4-313
219 SPF Stepped Hat and Stiffener Being Resistance Spot Welded.	4-314
220 End View of Welded Stepped Hat and Skin Combination.	4-314
221 Resistance Spot Welded SPF Crippling Test Panel.	4-317
222 Radiographic Image of Resistance Spot Welds for Test Panel 1.	4-318
223 Panel 5 Pre-test Spot Weld Nuggets 0.070" 7475-T62 joined to 0.190" 2219- T81 Al.	4-319
224 Panel 8 Pre-test Spot Weld Nuggets 0.070" 7475-T62 joined to 0.190" 2219- T81 Al.	4-320
225 Panel 11 Pre-test Spot Weld Nuggets 0.070" 7475-T62 joined to 0.190" 2219- T81 Al.	4-321
226 Panel 12 Pre-test Spot Weld Nuggets 0.070" 7475-T62 joined to 0.190" 2219- T81 Al.	4-322
227 Front View of Initial Test Panel at Completion of Testing at General Dynamics.	4-323
228 Side View of Initial Test Panel at Completion of Testing at General Dynamics with Deflectometers.	4-324
229 Back View of Initial Test Panel at Completion of Testing at General Dynamics.	4-325
230 Failure of Panel #4 - 7475 Al Stepped Hat (Front View).	4-333
231 Failure of Panel #4 - 7475 Al Stepped Hat (Rear View).	4-334
232 Typical Plots of Compression Strain Versus Load for the 7475-T62 Stepped Hat Stiffener - Panel 4 (Back-to-Back Strain Gages 1 and 6, 2 and 7, 3 and 8, 5 and 9, 5 and 10 are on the Skin).	4-335
233 Typical Plots of Compression Strain Versus Load for the 7475-T62 Stepped Hat Stiffener - Panel 4 (Strain Gages at Extreme Ends of Stepped Hat Stiffener).	4-336
234 Typical Plots of Compression Strain Versus Load for the 7475-T62 Stepped Hat Stiffener - Panel 4 (Strain Gages are on the Central portions of the Cap and Flange Area of the Hat).	4-337
235 Typical Strain Gage Locations for the Stepped Hat Panels.	4-338

LIST OF FIGURES (CONTINUED)

Figures	Page
236 Panel Deflection Versus Load for the 7475-T62 Stepped (Panel 4) and Beaded Hat (Panel 18) Configurations.	4-339
237 Compression Strain Versus Load for the 7475-T62 Beaded Web Curved Cap Hat Stiffener - Panel 8.....	4-340
238 Compression Strain Versus Load for the 7475-T62 Beaded Web Curved Cap Hat Stiffener - Panel 8 (Strain Gages on Upper portion of Web and Flange Areas).	4-341
239 Compression Strain Versus Load for the 7475-T62 Beaded Web Curved Cap Hat Stiffener - Panel 8 (Strain Gages on Lower portion of Web and Flange Areas).	4-342
240 Typical Strain Gage Locations for the Beaded Hat Panels.	4-343
241 Failure of Panel #8 - 7475 Beaded Web, Curved Cap (Front View).	4-344
242 Failure of Panel #8 - 7475 Beaded Web, Curved Cap (Rear View).	4-345
243 Load Shortening Analysis Panel #1 (65-3-7-28) Stepped Hat with Curved Cap (7475-T62 Al to 2219-T81 Al). Ultimate Load = 84,000 Lb.....	4-350
244 Load Shortening Analysis Panel #8 (7-1-7-20) Beaded Web with Curved Cap (7475-T62 Al to 2219-T81 Al). Ultimate Load = 66,300 Lb.....	4-350
245 Load Shortening Analysis Panel #12 (30-2-7-36) Beaded Web with Flat Cap (7475-T62 Al to 2219-T81 Al). Ultimate Load = 67,000 Lb.....	4-351
246 Load Shortening Analysis Panel #15 (126-3-2-91) Stepped Hat with Curved Cap (2090-T62 Al-Li to 2090-T83 Al-Li). Ultimate Load = 74,600 Lb.	4-351
247 Load Shortening Analysis Panel #19 (39-2-2-55) Beaded Web with Curved Cap (2090-T62 Al-Li to 2090-T83 Al-Li). Ultimate Load = 65,000 Lb.	4-352
248 Load Shortening Analysis Panel #23 (87-1-2-78) Beaded Web with Flat Cap (2090-T62 Al-Li to 2090-T83 Al-Li). Ultimate Load = 67,200 Lb.....	4-352
249 As-Formed and Cleaned Integrally Stiffened Panel.....	4-355
250 Welded and Trimmed Integrally Stiffened Panel.....	4-356
251 Column Buckling Panel Tooling Configuration.....	4-358
252 Column Buckling Panel Die Chamber.....	4-359
253 Loading of Column Buckling Panel Part Blank into Heated Die Chamber.	4-360
254 Hot Removal of Column Buckling Panel from 4500 Ton Press.	4-361
255 Trimmed and Cleaned Column Buckling Panels.....	4-363
256 Strain Gage Location for Inner Surface of Column Buckling Stiffener Panel #1, 7475-T62.	4-364
257 Close-up of Strain Gage Location for Inner Surface of Column Buckling Stiffener Panel #1, 7475-T62.	4-365
258 Strain Gage Location for Inner Surface of Column Buckling Skin Panel #1, 2219-T81.	4-366
259 Spot welding of Column Buckling Panel.	4-367
260 Spot welding of Column Buckling Panel with Tooling for Spot Weld Location.....	4-368
261 Close-up of Resistance Spot welding of Column Buckling Panel.	4-369
262 Welded Column Buckling Panel (Front View).....	4-370
263 Welded Column Buckling Panel (Back View).	4-371
264 Welded Column Buckling Panel Fixtured for Edge Clean-up.....	4-372
265 End View of Welded Column Buckling Panel Fixtured for Edge Machining.	4-373
266 Welded Column Buckling Panel Being Machined Flat and Parallel.	4-374
267 Welded Column Buckling Panel After Machining.	4-375
268 Close-up of Welded Column Buckling Panel After Machining.	4-376

LIST OF FIGURES (CONTINUED)

Figures	Page
269 Variable Polarity Plasma Arc Weld Macro of 0.155" 2219-T81 Al.....	4-378
270 Variable Polarity Plasma Arc Weld Macro of 0.155" 2090-T83 Al-Li.	4-378
271 Resistance Spot Welding of Doubler over the Fusion Weld.....	4-384
272 Resistance Spot Welding of Doubler Reinforced Fusion Weld with Stepped Hat Stiffeners.....	4-385
273 Front View of Doubler Reinforced Fusion weld.....	4-386
274 Back View of Doubler Reinforced Fusion weld.	4-387
275 End View of Doubler Reinforced Fusion Weld Panel With Stepped Hat Stiffeners.....	4-388
276 Life Cycle Cost Trade Flow.....	4-391
277 Cryogenic Tank Vehicle Concepts Utilized for Life Cycle Cost Analysis.	4-392
278 Cryogenic Tank Structural Options Investigated During the Life Cycle Cost Analysis.....	4-393
279 Built-Up SPF Stiffener Panel Configuration.....	4-394
280 Built-Up Brake Formed Stiffener Panel Configuration.	4-395
281 Built-Up Extrusion Stiffened Panel Configuration.	4-396
282 Machined Panel Configuration, Integrally Stiffened.....	4-397
283 Manufacturing Process Flow for 2090 Al-Li SPF Stiffener Panel Fabrication and Assembly Into Barrel Sections.....	4-398
284 Manufacturing Process Flow for 7475 Al SPF Stiffener Panel Fabrication and Assembly Into Barrel Sections.	4-399
285 Manufacturing Process Flow for 2090 Al-Li or 2219 Al Brake Formed Stiffener Components and Assembly Into Barrel Sections.	4-400
286 Manufacturing Process Flow for 2090 Al-Li or 2219 Al "T" Extrusion Stiffener Components and Assembly Into Barrel Sections.	4-401
287 Manufacturing Process Flow for Integrally Machined 2219 Al Panels and Assembly Into Barrel Sections.	4-402
288 Manufacturing Process Flow for Barrel Section Forming.	4-403
289 Manufacturing Process Flow for Major Cylinder Assembly.	4-404
290 Hot Loading Part Blank into Automated SPF Press.....	4-417
291 Hot Unloading Part.....	4-417
292 Hot Loading of Blank and Quench of Formed Part.....	4-418
293 Forming Blank and Loading Part for Thermal Processing.....	4-418
294 Heat Treatment, Trimming and Welding of Stiffened Panel to Outer Skin.	4-419
295 Assembly of Cryogenic Tank.	4-420

EXECUTIVE SUMMARY

Past production work has shown that cryogenic tank structure for the Shuttle booster rockets and the Titan system have very high life cycle costs for the fuel tank structure. The tanks are machined stiffener-skin combination that are subsequently formed into the required contour after machining. The material scrap rate for these configurations are usually high, and the loss of a tank panel due to forming or heat treatment problems is very costly. The idea of reducing the amount of scrap material and scrapped structural members has prompted the introduction of built-up structure for cryogenic tanks to be explored on the ALS program. A built-up structure approach that has shown improvements in life cycle cost over the conventional built-up approach is the use of SPF stiffened panels (reducing the overall part count and weight for the tank) resistance spot welded (RSW) to outer tank skin material. The stiffeners provide for general stability of the tank, while the skin material provides hoop direction continuity for the loads. The objective of this program was to design and fabricate integrally stiffened superplastic formed Al-Li panels that could be used for fabrication of low cost cryogenic tank structure for the ALS family of vehicles.

TASK 1: PANEL DESIGN AND ANALYSIS

The ALS vehicles have been designed for relatively high launch rates and high launch availability. The vehicle is intended to remain on the launch pad through quite severe weather conditions, and launch without a launch or umbilical tower. ALS loads (refer to Table S-1) were supplied to Rockwell International from the General Dynamics ALS-L vehicle configuration which was made up of a core and an external booster. The loading conditions took into account ground handling, ground winds, maximum flight winds (Max Alpha-Q / Max Beta-Q), and booster burn out.

Table S-1. Design Load Conditions

1. N_x = -4237 lb/in. N_y = 0 lb/in. N_{xy} = 1028 lb/in.	2. N_x = -8474 lb/in. N_y = 0 lb/in. N_{xy} = 416 lb/in.
3. N_x = +8474 lb/in. N_y = 0 lb/in. N_{xy} = 416 lb/in.	4. N_x = -7607 lb/in. N_y = +7002 lb/in. N_{xy} = -119 lb/in.
5. Ultimate Tank Pressure = 56 psi	
6. Temperature = Ambient	

The technology driven requirements when coupled with the high loading conditions typical of the ALS vehicles created some unique design challenges for optimizing the performance of light weight structure. The first step in the design of the panels was to establishment of the baseline design concept (refer to Figure S-1) and assess the structural efficiency of the conventional baseline concept versus the SPF stiffener designs.

Several SPF stiffener designs were developed that would carry the launch loads and provide for improvements in the structural efficiency of the stiffened panels. A qualitative trade study was conducted with Rockwell and General Dynamics personnel to down select three stiffener configurations that would be optimized, and tested as crippling stiffener panels: the selected

concepts were the stepped hat with curved cap, beaded web with flat cap, and the beaded web with the curved cap (refer to Figure S-2).

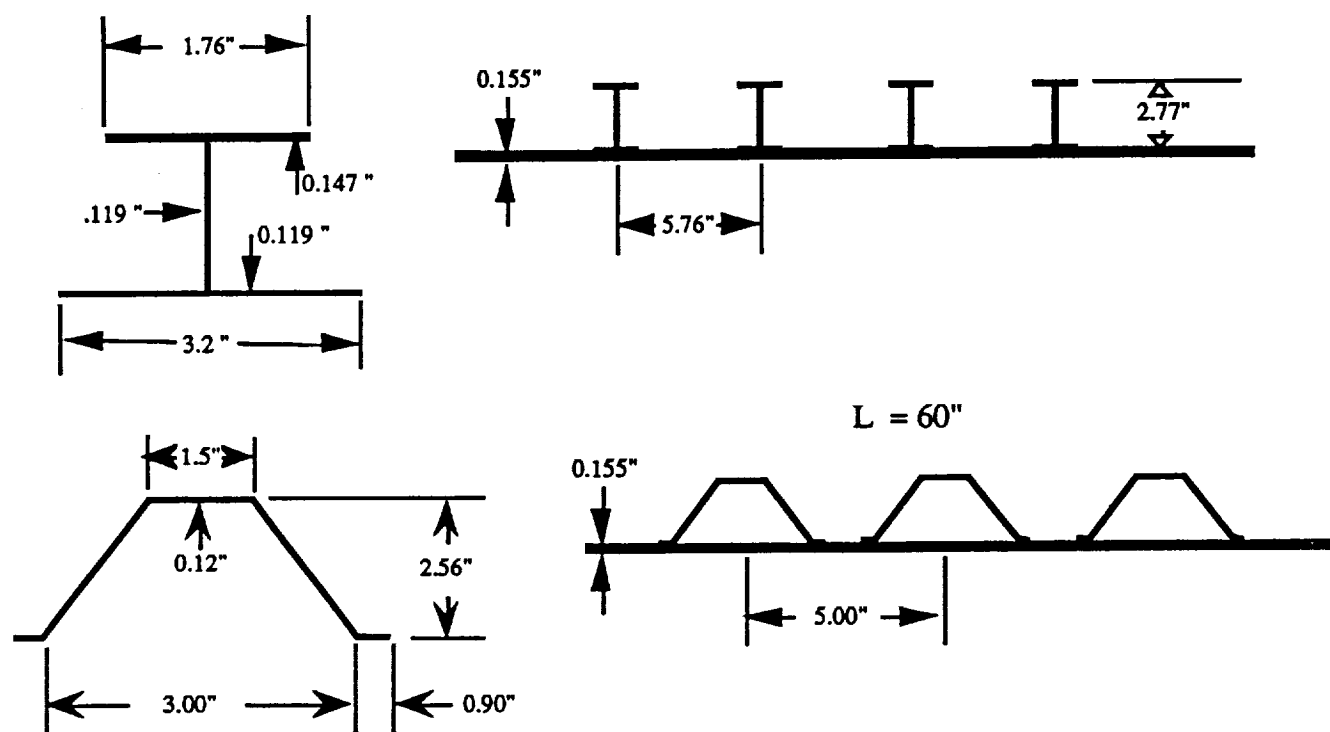


Figure S-1. Baseline Conventional "T" and Hat Stiffener.

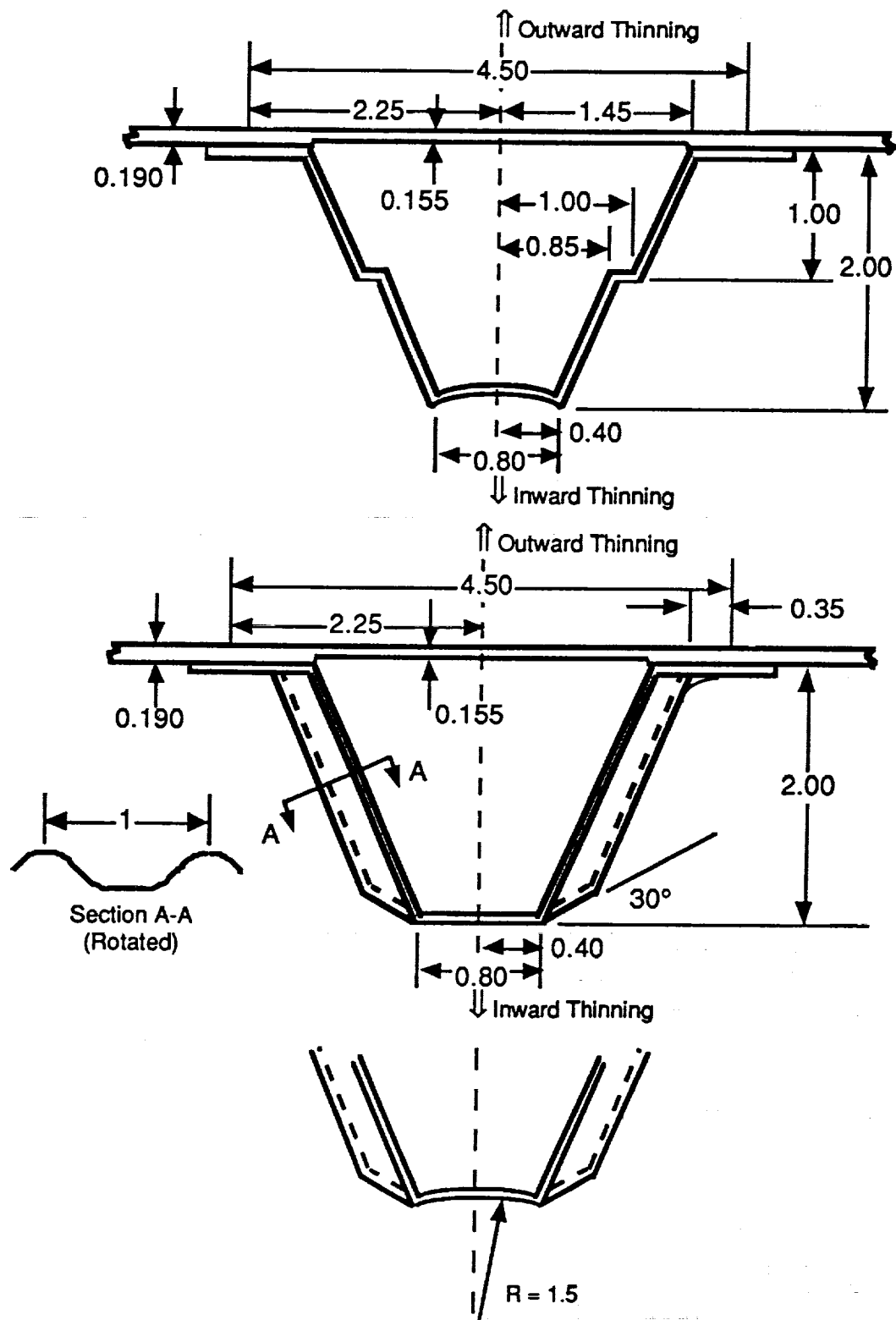
CRIPPLING PANEL DESIGN AND ANALYSIS:

A 15 inch length was selected to insure local buckling of the crippling specimen panels during testing. Single hat-stiffener NASTRAN finite element models were developed to study and visualize the buckling modes of the SPF stiffeners, and to compare results to the PASCO analysis. The NASTRAN buckling analysis solution resulted in an eigenfactor of 1.248 for the first buckling mode. This would be equivalent to a loading of $1.248 \times 10,000 \text{ lbs/in.} \times 6 \text{ in.} = 74,880 \text{ lbs}$ for the Type 1 specimen. The NASTRAN results were considered to be in close agreement with the PASCO program. The predicted failure modes and loads are tabulated in Table S-2.

TABLE S-2. Predicted Ultimate Uniaxial Loads.

Stiffener Type	Material Combinations		$\frac{t}{L}$	Predicted Ultimate Uniaxial Load	Critical Areas
	Skin	Stiffener			
Stepped Hat With Curved Cap	7475/2219 Al	7475 SPF Al	.256	76,800 Lb. 69,000 Lb.	Crippling Yield Skin
Stepped Hat With Curved Cap	2090 Al-Li	2090 SPF Al-Li	.252	68,000 Lb.	Comp Yield Hat
Beaded Web Flat or Curved Cap*	7475/2219 Al	7475 SPF Al	.264	60,000 Lb. 79,200 Lb.	Comp. Yield Skin Skin Wrinkle
Beaded Web Flat or Curved Cap*	2090 Al-Li	2090 SPF Al-Li	.252	60,000 Lb. 68,000 Lb.	Comp. Yield Hat

* Based upon PASCO analysis, the difference in the Ultimate loads for the flat or curved cap configurations was insignificant, thus both configurations are shown together in the table.



$t(\text{start}) = 0.100$ inch for 7475 Beaded and Stepped Hats
 $t(\text{start}) = 0.090$ inch for 2090 Beaded and Stepped Hats

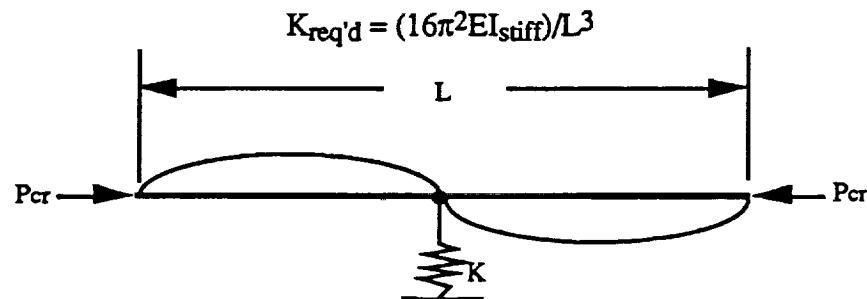
Figure S-2. Final Type 1 Stepped Hat and Beaded Web Crippling Specimen Panel Designs.

INTEGRALLY STIFFENED STRUCTURE:

The overall stability of the tank required intermediate frames to be placed along the vertical length of the tank at 30 inch intervals (as observed from singly stiffener models at 15, 30 and 60 inch intervals during the development of the optimum stiffener configuration). The objectives of the providing an integral ring design were as follows:

- Enforce a simple support node at the integral ring to prevent Euler column failure
- Fabricate the stiffeners and integral ring with one forming operation (one-step forming) to minimize fabrication cost
- Provide load path continuity for the N_x and N_y loads

The establishment of the integral ring stiffness utilized the "Theory of Elastic Stability" published by S. Timoshenko presented as follows: (8474 lb/in loading condition utilized for this analysis)



$$K_{req'd} = (16 \times 9.817 \times 11.5 \times 10^6 \times .48)/(60)^3 = 4035 \text{ lb/in (to enforce simple support node)}$$

The preliminary analysis indicated that for the particular loading scenario, an integral ring with an $I = 3 \text{ in}^4$ would enforce the node. As a result of the preliminary analysis, several node conditions were examined for the barrel section, along with the effects of the different loading conditions on the node geometry.

Optimization of the node intersection was continued with the development of a detailed NASTRAN finite element model on the a large scale panel with a 30" node to better simulate and optimize the panel behavior under different loading conditions. The sizing of the interim ring with the NASTRAN analysis resulted in a design that provides maximum efficiency for the node (refer to Figure S-3).

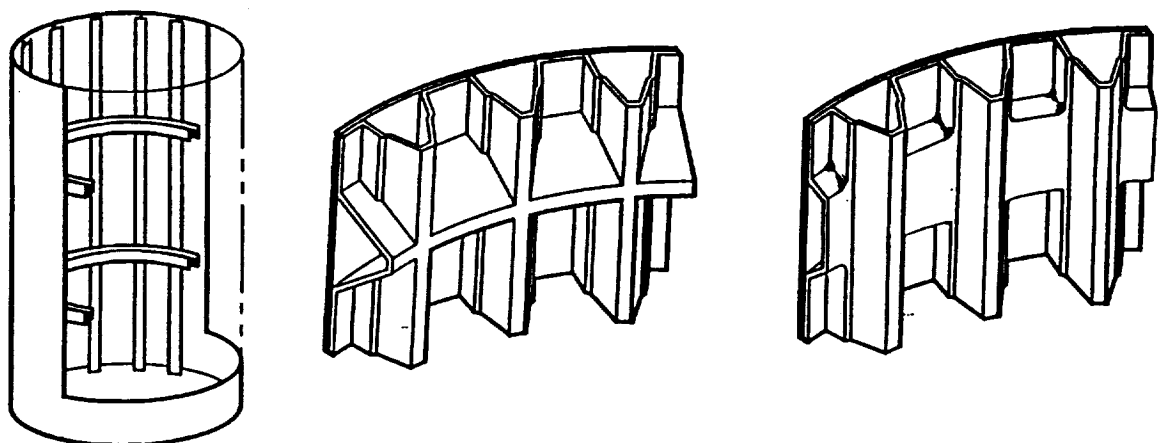


Figure S-3. Example of One Integral Node Configuration for SPF Stiffened Structure.

COLUMN BUCKLING PANEL:

At the completion of the crippling panel tests, the stepped hat stiffener configuration was chosen for continued development based on its load carrying capability. The stepped hat stiffener was modeled under NASTRAN and optimization of the stiffened structure was conducted. PASCO analysis of the stepped hat stiffener was conducted with a larger cap width to enhance the overall stability of the structure. The panel configuration was chosen based upon the desired length of the panel (column of at least 60 inches) and limited by the width of available material (48" minus sealing area). The resulting panel design (refer to Figure S-4 and S-5) maintained the inter-stiffener and inter-spot spacing developed during the development of the crippling stiffener panel. The column buckling panels projected load carrying capability is shown in Table S-3.

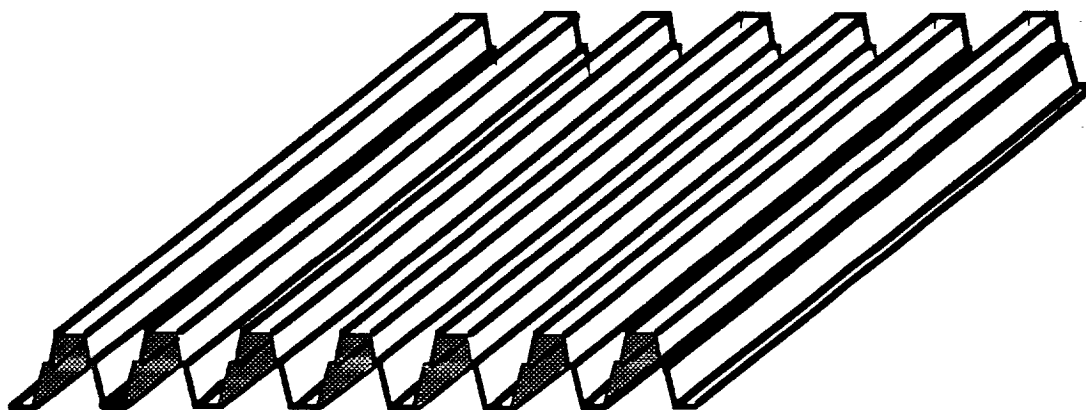


Figure S-4. Column Buckling Panel Configuration.

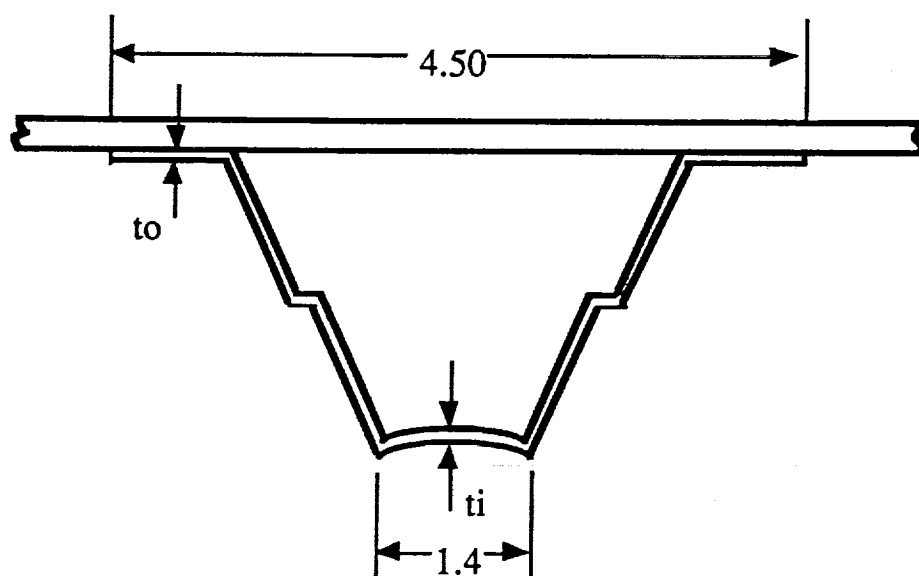


Figure S-5. Optimized Stepped Hat with Wider Cap Used for the Column Buckling Panel.

Table S-3. Column Buckling Panel Predicted Failure Loading.

SPF Material	t_{bar} (in.)	Predicted Column Failure Loading	Predicted Inter-spot Crippling	Thickness (in.)
7475 Al (0.100 Starting Gage)	0.255	6510 lb/in (25.5 Ksi)	41 Ksi	* t_o = 0.05 * t_i = 0.091
2090 Al-Li (0.090 Starting Gage)	0.245	6840 lb/in (27.9 Ksi)	37.4 Ksi	* t_o = 0.046 * t_i = 0.08

* Average measured thickness from Column Buckling Panel.

DOUBLER-REINFORCED FUSION WELD:

The final panel configuration examined during this program was the vertical fusion weld or panel-to-panel joint. This joint configuration was based upon past work at General Dynamics Space Systems Division on the ATLAS and Centaur upper stage. This doubler-reinforced concept (refer to Figure S-6) eliminates the need for machined weld lands (commonly used for launch vehicle pressure vessels at an increased fabrication cost, and weight penalty to the structure) to reinforce the joint by utilizing the doubler as a major load carrying member for the fusion weld. The development of the joint was based upon the fusion weld and resistance spot weld data generated during task 3 of this program. Specific doubler testing was conducted under task 3 that provided a greater understanding of the behavior of the doubler over the Variable Polarity Plasma Arc (VPPA) fusion weld for load transfer. The test data was then utilized with finite element modeling techniques to predict the behavior of the fusion weld joint during bi-axial (axial and hoop) loading conditions.

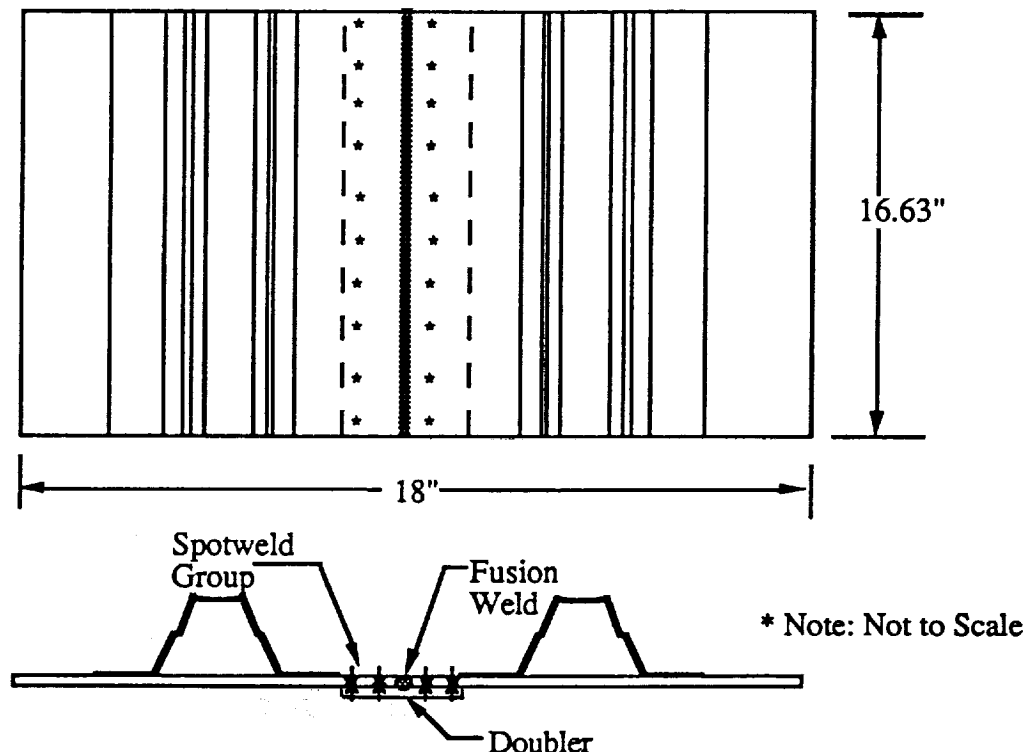


Figure S-6. Vertical Doubler-Reinforced Joint on the ALS Vehicle.

Two verification runs were made with the model. The first evaluation involved application of a compressive axial load of 1000 lb/in to the model and evaluate the uniformity of the load and the stress across the joint. The model produced a uniform stress in the plate elements of -3500 psi which correlated with the expected stress of -3921 psi (due to T_{bar} of the section = 0.255 inch and $\sigma = -1000$ lb per inch / 0.255 in, where the -1000 lb was taken from the elastic portion of the fusion weld stress strain curve). The second verification run utilized a failure load of 7500 lb/in, obtained from the dog-bone tests, for the hoop direction. The anticipated point of failure is in the first row of spot welds indicated by both the dog-bone test and the model, despite a 30,000 psi load across the fusion weld. It was concluded that the model produced a reasonable representation of the stress distribution across the joint for bi-axial testing, and that test results should be similar to the simulation.

TASK 2: SUPERPLASTIC MATERIAL CHARACTERISTICS

Superplastic characterization of the materials used during this program involved metallographic examination of the material prior to and after forming, static exposure to elevated temperature (for grain stability), uniaxial tensile testing at constant strain rate and variable strain rate with and without back pressure, and finally producibility forming trials. These characterization tests have been developed at Rockwell to provide information on the starting grain size of the material, stability of the grain size due to elevated temperature exposure, the presence or absence of recrystallization during forming or grain growth during forming, flow stress of the material at various strain rates, flow stress of the material with varying amounts of back pressure, flow stress whereby superplastic elongation is maximized, requirements for suppression of cavitation, and formability characteristics for each alloy.

The aluminum and aluminum-lithium materials examined during this program included 7475 Al, a material that has been used on several programs at Rockwell, two production Al-Li alloys, and one experimental Al-Li alloy. The characterization study for the 7475 Al material was limited to verification of uniaxial superplastic tensile properties and metallography in order to determine the quality of the material prior to fabrication. Additional tests were run on the 2090, 8090, and x2095 alloys to fully characterize each material. The optimum superplastic forming parameters are shown in Table S-4.

Table S-4. Summary of Optimum Superplastic Forming Parameters.

ALLOY	7475 AL	2090 AL-LI	8090 AL-LI	x2095 AL-LI WL-049
Forming Temp.(°F)	950	960	960	915
Strain Rate ($\times 10^{-3} s^{-1}$)	0.2	2.0/0.2	2.0/0.2	0.6
Flow Stress (ksi)	0.25	1.5/0.4	1.5/0.3	0.85
Back Pressure (psi)	400	400	400	600

The fabrication of producibility pans of 7475 Al, 2090 Al-Li, 8090 Al-Li, and the x2095 Al-Li (Weldalite-049) materials was conducted immediately following completion of the uniaxial characterization of each material. All of the materials used during the program were formed with existing tooling into simple pan shapes to ensure proper translation of the uniaxial data into the manufacturing environment. The initial pans formed from 2090 and 8090 Al-Li materials were immediately quenched (utilizing several different quench rates) upon removal from the tool, stored at 20°F to retard natural aging, sectioned, and shipped to Washington State University in dry ice

storage for inclusion in the heat treatment evaluation. Large producibility pans (18" x 18" x 6") were also fabricated from 7475 Al, 2090 and 8090 Al-Li during the program for use during the resistance spot weld parameter development at General Dynamics and for generation of engineering design data at Alcoa.

TEST MATRIX AND COUPON CONFIGURATION FOR 2090 AND 8090 ALUMINUM-LITHIUM:

A data base of mechanical property and corrosion resistance performance of the 2090 and 8090 Al-Li materials procured for this program was generated on formed and non-formed samples. The test material (both formed and unformed) was solution heat treated, quenched, and artificially aged to a peak -T62 condition.

Ambient Tensile

Ambient room temperature tensile tests were conducted in accordance with ASTM E8 specification. The ambient tensile data for 2090 Al-Li is represented in Table S-5 with the specimen orientation and forming strain.

Table S-5. Pre- and Post-SPF Mean Ambient Tensile Results for 2090 Al-Li.

Orientation	F _{tu} (ksi)	F _{ty} (ksi)	Elongation (%)	Effective True Strain	E (msi)
L	63.3	52.8	4.0	0.000	12.9
	64.2	50.3	5.0	0.189	14.3
	63.2	49.1	5.0	0.240	10.1
	60.5	48.3	4.0	0.279	11.2
	63.1	50.2	4.0	0.301	12.5
	63.3	50.6	3.0	0.319	11.0
	63.1	50.2	3.5	0.340	14.2
V	62.3	50.3	4.0	0.372	11.1
T	63.4	52.7	6.0	0.000	12.7
	62.6	50.7	9.0	0.217	14.4
	60.8	47.2	7.0	0.240	11.6
	62.0	47.9	9.0	0.254	10.9
	62.8	48.7	9.0	0.275	11.2
	62.1	48.0	9.0	0.304	14.5
	61.3	48.5	8.5	0.321	11.3
	60.1	47.8	7.0	0.366	11.3
V	59.1	47.8	7.0	0.439	11.7

The ambient tensile data for 8090 Al-Li is represented in Table S-6 with the specimen orientation and forming strain. As with the 2090 data, it was observed that the ambient tensile behavior of the 8090 Al-Li material does not change significantly with superplastic strain for either the longitudinal or transverse specimens.

Cryogenic Tensile

Smooth tensile tests were performed for 2090-T62 and 8090-T62 aluminum-lithium material at cryogenic temperatures. The cryogenic test results are shown on Table S-7 and S-8. The overall strengths and elongations increased with the decrease in temperature which is typical of aluminum materials. However, the ultimate and yield strengths of the coupons did decrease slightly with increasing forming strain.

Table S-6. Pre- and Post-SPF Mean Ambient Tensile Results for 8090 Al-Li.

Orientation	F _{tu} (ksi)	F _{ty} (ksi)	Elongation (%)	Effective True Strain	E (msi)
L	66.6	54.9	4.0	0.000	11.4
	67.8	57.8	3.0	0.111	13.0
	67.0	56.6	4.0	0.125	12.0
	64.0	57.1	2.0	0.139	13.0
	66.5	56.7	4.0	0.158	13.0
	66.2	57.8	4.0	0.168	12.0
	66.1	54.9	4.0	0.182	13.0
	66.8	56.2	5.0	0.198	12.4
V	62.7	54.4	4.0	0.236	11.0
T	60.1	47.7	7.0	0.000	11.0
	57.8	47.0	5.0	0.095	12.9
	65.4	52.3	5.0	0.108	12.0
	66.1	52.9	6.0	0.116	13.0
	66.2	52.8	6.0	0.136	13.0
	65.7	52.2	6.0	0.165	13.0
	64.7	50.3	8.0	0.198	10.6
	60.4	47.5	7.0	0.234	12.0
V	63.8	51.0	5.0	0.259	11.2

Table S-7. Cryogenic Temperature Smooth Tensile Test Results for 2090-T62 and 8090-T62 Pre- and Post-Superplastic Formed Sheet at -60°F.

Alloy Temper	Coupon I.D.	SPF Condition	Specimen Thickness (in)	Test Temp. (°F)	F _{tu} (ksi)	F _{ty} (ksi)	El (%)	Effective True Strain Thickness
2090-T62	316-1-L1	Pre-SPF	0.09045	- 60	68.1	54.0	4F	0
"	316-1-L2	Pre-SPF	0.09045	- 60	67.5	54.0	4F	0
"	316-1-T1	Pre-SPF	0.09010	- 60	65.3	52.9	10	0
"	316-1-T2	Pre-SPF	0.08995	- 60	65.1	52.9	10	0
"	322-L1	Post-SPF	0.06675	- 60	67.1	52.3	4F	0.2989
"	325-L2	Post-SPF	0.07000	- 60	67.9	51.5	5F	0.2513
"	324-L3	Post-SPF	0.07220	-60	66.6	51.3	4F	0.2204
"	323-L4	Post-SPF	0.06710	- 60	66.8	51.3	5F	0.2936
"	322-T1	Post-SPF	0.06395	- 60	62.9	50.4	6F	0.3417
"	325-T2	Post-SPF	0.07065	- 60	63.9	50.8	9	0.2421
"	324-T3	Post-SPF	0.07185	- 60	61.5	47.8	9	0.2252
"	323-T4	Post-SPF	0.07035	- 60	63.0	49.6	10	0.2463
8090-T62	315-3-L1	Pre-SPF	0.08730	- 60	70.4	55.5	7D	0
"	315-3-L2	Pre-SPF	0.08680	- 60	71.4	56.0	9	0
"	315-3-T1	Pre-SPF	0.08705	- 60	62.1	48.4	13D	0
"	315-3-T2	Pre-SPF	0.08715	- 60	62.0	48.3	13	0
"	361-L1	Post-SPF	0.08035	- 60	68.8	55.2	6F	0.0909
"	361-L2	Post-SPF	0.07870	- 60	68.7	56.1	6F	0.1117
"	359-L3	Post-SPF	0.07230	- 60	62.6	50.1	3F	0.1965
"	359-L4	Post-SPF	0.07315	- 60	65.5	50.9	6F	0.1848
"	359-T1	Post-SPF	0.07040	- 60	59.1	46.5	8D	0.2231
"	359-T2	Post-SPF	0.07195	- 60	60.5	43.3	7F	0.2014
"	359-T3	Post-SPF	0.07885	- 60	60.4	47.1	7F	0.1098
"	359-T4	Post-SPF	0.07600	- 60	60.8	47.5	8F	0.1466

D = Coupon Failed Outside of Middle of Gage Length.

F = Coupon Failed at Fillet.

Table S-8. Cryogenic Temperature Smooth Tensile Test Results for 2090-T62 and 8090-T62 Pre- and Post-Superplastic Formed Sheet at -320°F.

Alloy Temper	Coupon ID.	SPF Condition	Thickness (in)	Test Temp. (°F)	F _{tu} (ksi)	F _{ty} (ksi)	El (%)	Eff. True Strain Thickness
2090-T62	316-1-L1	Pre-SPF	0.09055	- 320	83.0	57.3	8F	0
"	316-1-L2	Pre-SPF	0.09050	- 320	85.1	56.6	12D	0
"	316-1-T1	Pre-SPF	0.09025	- 320	78.3	57.6	18	0
"	316-1-T2	Pre-SPF	0.09045	- 320	78.2	57.3	18	0
"	322-L1	Post-SPF	0.06765	- 320	82.8	55.0	9F	0.2989
"	325-L2	Post-SPF	0.06875	- 320	79.8	54.5	8D	0.2513
"	324-L3	Post-SPF	0.07290	- 320	83.6	54.3	10F	0.2204
"	323-L4	Post-SPF	0.06765	- 320	83.3	54.8	10F	0.2936
"	322-T1	Post-SPF	0.06060	- 320	75.7	53.7	15F	0.3417
"	325-T2	Post-SPF	0.07155	- 320	77.1	55.7	17	0.2421
"	324-T3	Post-SPF	0.06970	- 320	75.1	52.9	17	0.2252
"	323-T4	Post-SPF	0.06915	- 320	76.9	54.5	13F	0.2463
8090-T62	315-3-L1	Pre-SPF	0.08710	- 320	87.4	58.7	10D	0
"	315-3-L2	Pre-SPF	0.08680	- 320	88.0	58.8	17D	0
"	315-3-T1	Pre-SPF	0.08695	- 320	74.6	52.4	17D	0
"	315-3-T2	Pre-SPF	0.08710	- 320	74.8	59.1	83	0
"	361-L1	Post-SPF	0.07730	- 320	85.0	59.8	10F	0.0909
"	361-L2	Post-SPF	0.07900	- 320	87.2	54.7	9F	0.1117
"	359-L3	Post-SPF	0.06920	- 320	82.4	54.9	8F	0.1965
"	359-L4	Post-SPF	0.07570	- 320	81.7	51.3	12F	0.1848
"	359-T1	Post-SPF	0.07040	- 320	73.4	50.8	13F	0.2231
"	359-T2	Post-SPF	0.07305	- 320	73.4	52.1	12F	0.2014
"	359-T3	Post-SPF	0.07970	- 320	74.1	49.4	12F	0.1098
"	359-T4	Post-SPF	0.07690	- 320	72.6	47.5	8F	0.1466

D = Coupon Failed Outside of Middle of Gage Length. F = Coupon Failed at Fillet.

Compression

The compressive yield strength was determined in accordance with the ASTM E-9 specification for 2090-T62 and 8090-T62 Pre- and Post-Superplastic formed sheet. The compressive strength coupons were machined to a uniform thickness to prevent buckling or improper failure of the coupons during testing. The results from the compressive tests are shown in Table S-9.

Table S-9. Compressive Strength of 2090 and 8090 Pre- and Post-Superplastic Formed Sheet Heat Treated to -T62.

Alloy Temper	Coupon ID.	SPF Condition	Thickness (in)	Specimen Width (in)	F _{cy} (ksi)	Ave. F _{cy} (ksi)
2090-T62	316-2-L1	Pre-SPF	0.058	0.625	58.5	
"	316-2-L2	Pre-SPF	0.058	0.624	58.0	58.3
"	316-1-T1	Pre-SPF	0.091	0.623	56.6	
"	316-1-T2	Pre-SPF	0.091	0.622	56.4	56.5
"	360-L1	Post-SPF	0.066	0.625	59.6	
"	360-L2	Post-SPF	0.058	0.625	58.3	59.0
"	360-T1	Post-SPF	0.052	0.624	61.0	
"	360-T2	Post-SPF	0.060	0.625	59.1	60.0
8090-T62	315-2-L1	Pre-SPF	0.088	0.623	58.7	
"	315-2-L2	Pre-SPF	0.088	0.622	59.1	58.9
"	315-2-T1	Pre-SPF	0.088	0.622	51.6	
"	315-2-T2	Pre-SPF	0.088	0.621	51.9	51.8
"	357-L1	Post-SPF	0.063	0.625	57.0	
"	359-L2	Post-SPF	0.047	0.625	57.2	57.1
"	357-T1	Post-SPF	0.046	0.625	55.3	
"	359-T2	Post-SPF	0.059	0.625	55.1	55.2

* Specimens were machined to achieve uniform thickness.

Exfoliation Corrosion

Exfoliation corrosion test were carried out in accordance with ASTM G85 Annex 2 MASTMAASIS (Modified ASTM Acetic Acid Salt Intermittence Spray). All of the 2090 specimens received an exfoliation rating of A (mild exfoliation). Three of the four specimens exhibited only minor pitting and one specimen exhibited some pit blistering. All of the 8090 specimens received an exfoliation rating of C (severe pitting) and all experienced pit blistering. Protection of these materials for long periods of times in corrosive environments is recommended.

Fracture Toughness

Fracture toughness were tested using the center crack tension test for stable crack growth under static loading with a measurement of strain compliance with load increase. The fracture toughness (K_{Ic}) values at a maximum load are shown in Table S-10. There was substantial scatter in the results, however there was no direct evidence of an effect on the toughness of the material due to the SPF process. The 8090-T62 K_{Ic} values were slightly higher than those measured for 2090-T62, however, K_{Ic} is only one point on the R-curve and that general observation may not apply to the entire R-curve.

Table S-10. Ambient Fracture Toughness for 2090-T62 and 8090-T62 Al-Li Materials in the L-T Direction, $t_0 = 0.090$.

Alloy - Temper	SPF Condition	Fracture Toughness K_{Ic} (ksi $\sqrt{\text{in}}$)	Effective True Strain (ϵ)
2090-T62	Non-Formed	48.3	0
		52.0	0
	Formed	39.4	0.250
		52.8	0.207
8090-T62	Non-Formed	52.9	0
		66.8	0
	Formed	60.3	0.155
		48.8	0.208

POST-SUPERPLASTIC FORMING HEAT TREATMENT OPTIMIZATION FOR 2090 AND 8090 ALUMINUM-LITHIUM:

The Al-Li based alloys have been shown to offer highly desirable properties for the aerospace industry, particularly in the reduction of density and concurrent increase in the elastic modulus, leading to significant improvements in the specific modulus over the more conventional Al alloys. The development and application of these alloys, however, have been found to be significantly challenged by a number of technological difficulties which have included the achievement of high strength with sufficient ductility for structural applications.

Historically, thermomechanical processing of aluminum and aluminum-lithium alloys has been utilized to provide for a balance of strength and ductility for conventional product forms. However, superplastic forming (SPF) does not lend itself to stretching a completed part before aging for attainment of maximum strength. SPF processing, by its nature, involves forming of complex shapes at temperatures well in excess of those used for aging or annealing of the alloys (structural complexity can be increased far beyond conventional forming methods with the use of the SPF process). The formed configuration must then be solution heat treated, water quenched, and aged in order to attain peak strength or a -T62 condition in the material prior to use.

A study was initiated in order to assess the potential for elimination of the solution heat treatment (SHT) of the formed part from the manufacturing process. The aim of the study was to develop a thermal processing procedure for the alloys whereby the part could be quenched directly from the forming process and artificially aged prior to trimming without a sacrifice to material properties. The optimization of the heat treatment for 2090 and 8090 examined the strengthening response of the material with different solution heat treatment temperatures, quench rates, and aging practices. The issue of out of tool quench was examined as a replacement for solution heat treatment-quench processing of the formed parts to minimize distortion, solute depletion, and reduce overall cost during fabrication of the SPF parts.

Tensile Results

The tensile properties for both alloys aged after SPF processing without a solution heat treatment are as good as, or better than, those with a solution treatment at higher temperatures. The highest strengths were observed both of the materials when they were superplastically formed and directly quenched in water followed by artificial aging at 180°C (356°F). Both SPF processed alloys show some quench sensitivity, however, high strength values were obtained from all three quench rates used during the study. The test results indicated that the fastest cooling rate following SPF process provided the highest strength values after artificial aging.

Optimized heat treatment parameters were suitable for achieving the program goal of yield strength levels greater than 50 ksi for both alloys (2090 and 8090). Selected post-SPF heat treatments resulted in yield strengths of the order 50-54 ksi for the 8090 alloy and 57-70 ksi for the 2090 alloy. An unexpected, but interesting result observed was that the higher strengths were generally observed for the alloys when aged directly after forming, where the forming acted as the solution heat treatment. When the same material was solution heat treated and aged, the strength levels were no better, and in many cases lower than, those for the aforementioned condition. This result is highly desirable since it suggests that parts may be superplastically formed and heat treated without need to conduct an additional high temperature process, that of the solution heat treatment.

TASK 3: JOINING

The built-up cryogenic tank structure approach required attachment of the stiffeners to skin materials in such a way that the tank would remain sealed at both ambient and cryogenic temperatures. Historically, fuel tanks and lines used for cryogenic fuel systems have been fusion welded in order to assure a leak free structure. In the cryogenic fuel tank, the vertical welds (panel to panel) and the welds between the barrel sections and the major ring frames will be fusion welded in order to assure proper sealing of the pressure vessel. However, the attachment of the stiffeners to the outer skins required a permanent, leak free methodology that would be reliable both during storage of the tank and during flight. Since mechanical fastening of the stiffeners to the outer tank skins would not provide for a leak-free surface, alternative attachment methods were examined for the built-up configuration.

The primary method examined during this program was resistance spot welding of the stiffeners to the outer skin panels. The resistance spot welding approach provided a leak-free condition in the cryogenic tank for attachment of the stiffeners to the skins, whether the stiffeners were attached to the inner surface of the tank, or to the outer surface. The second method of attachment examined briefly during the program was adhesive bonding of the stiffeners to the skins on the external surface of the cryogenic tank. Several adhesive systems were examined and tested under laboratory conditions for evaluation of flat-wise tensile and shear behavior at ambient and cryogenic temperatures.

ADHESIVE BONDING:

An engineering survey of adhesive materials with cryogenic service capabilities was conducted. The list of adhesives that were selected as candidates for the cryogenic tank are shown as Table S-11.

Table S-11. Candidate Cryogenic Structural Adhesives.

Adhesive	Type	Curing Temperature (°F)
Hysol EA 9330	Epoxy Paste	Room Temp.
Crest 810 A&B	Polyurethane Paste	Room Temp.
Crest 7344 A&B	Epoxy Paste	Room Temp.
Crest 3710 A&B	Polyurethane Paste	Room Temp.
Crest 212 A&B	Polyurethane Paste	Room Temp.
PRC 1665	Polyurethane Paste	130
PRC 1649	Polyurethane Paste	130
BF Goodrich PL-777	Polyurethane Paste	250

Preliminary ambient and cryogenic adhesive testing were conducted with production-ready materials on an aluminum-lithium substrate. Lap shear (0.5 in² surface area) and flat-wise tensile (1 in² surface area) results are shown on Table S-12. Flat-wise tensile results that are reported as NC (not completed) failed the 2090-T83 parent metal in bearing rather than the adhesive. Overall the adhesives performed very well during the evaluation. However, the 7344 A&B was selected as the most promising material for cryogenic application.

Table S-12. Adhesive Preliminary Test Results.

ADHESIVE	TYPE	CURING TEMP. (°F)	LAP-SHEAR (psi)	FLATWISE TENSILE (psi)	TEST TEMP. (°F)
CREST'S 810 A&B	PASTE	RT	5970	NC	-320
			6030	NC	-165
			1576	650	RT
7344 A&B	PASTE	RT	2940	NC	-320
			4380	11941	-165
			4565	4542	RT
212 A&B	PASTE	RT	4690	NC	-320
			4680	NC	-165
			839	1927	RT
Products Rsch. Corp. PRC 1665	PASTE	130	7190	NC	-320
			5540	NC	-165
			676	1350	RT

RESISTANCE SPOT WELD DEVELOPMENT:

Characterization of the resistance spot weld (RSW) parameters for the materials used during this program utilized the Taguchi design of experiments. The Taguchi experiment process minimized the number of coupons that needed to be tested while evaluating the characteristics of the weld process as a function of the processing variables. Both the 7475-T62 to 2219-T81, and the 2090-T62 to 2090-T83 material combinations were examined with the Taguchi methodology. Once the optimum weld parameters had been isolated by this technique, standard test methodologies for development of the behavior of the weld were utilized.

Resistance Spot Weld Development for 7475-T62 Joined to 2219-T81

The test results for the optimum weld schedule developed for the 7475-T62/2219-T81 material combination using the Taguchi methodology is shown in Table S-13

Table S-13. Test Results for Optimized 7475-T62/2219-T81 RSW Schedule.

Coupon I.D.	Nugget Diameter inch	Nugget Penetration		Shear lbs
		% Upper Sheet	% Lower Sheet	
Average	0.351	68.8	32.9	3456

* Nugget penetration in 0.100" 7475-T62 sheet / penetration into 0.190" 2219-T81 sheet.

Weld schedules developed for the crippling test panels were verified through certification testing. The average lap shear test value for the schedule was 2909 pounds, the average nugget diameter was 0.303", nugget penetration into the 7475-T62 (the thinnest sheet) was recorded between 61 to 80% of the sheet thickness and nugget penetration into the 2219-T81 (the thicker) sheet was between 18 and 30%.

Sheet Efficiency

Sheet efficiency tests were performed on the 2219-T81 material in order to determine the "knockdown" to the ultimate tensile strength for a given skin section after spot welding. The sheet efficiency test results are shown in Table S-14 for 2219-T81 skin.

Table S-14. 0.190" 2219-T81 Aluminum Skin Efficiency (or Reduction in Ultimate Tensile Strength) After Spot Welding of 0.100" 7475-T62 Stiffeners.

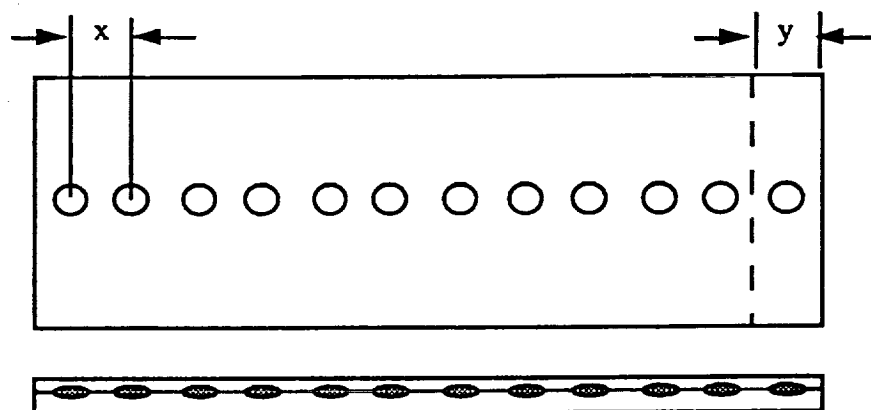
Material Type	Test Temperature (°F)	F _{tu} (ksi)	Sheet Efficiency (%)
2219-T81	20	62.1	62.1/65.6* = 94.75

* Note: Ratio taken from actual test data rather than allowable data.

Resistance Spot Weld Spacing

Resistance spot weld spacing tests were performed in order to determine the effects that inter-spot spacing has on weld strength and quality. Continuous sheet test specimens were welded from 0.100" 7475-T62 joined to 0.190" 2219-T81 using a certified weld schedule with inter-spot spacings of 0.75", 1.00", 1.25" and 1.5". Results from the tests are shown in Table S-14.

Schematic for inter-spot spacing test.



x = Inter-spot spacing
y = Width of Lap shear coupon

Table S-15. Resistance Spot Spacing Test Results for 0.100 inch 7475-T62 to 0.190 inch 2219-T81 Aluminum.

Schedule: Weld Heat (36 percent), Weld Time (6 cycles), Weld Force (15 psi), Forge Force (24 psi), Squeeze (55).

Spot Weld Spacing (inch)	Coupon I.D.	Nugget Diameter (inch)	Nugget Penetration Shear		Strength (Lbs)
			Upper Sheet (inch)	Lower Sheet (inch)	
0.75	1SS1-1	Diffusion	Diffusion	Diffusion	2292
	1SS1-2				
	1SS1-3	Diffusion	Diffusion	Diffusion	2413
	1SS1-4				
	1SS1-5	Diffusion	Diffusion	Diffusion	2431
	1SS1-6				
	1SS1-7	Diffusion	Diffusion	Diffusion	2379
	Average	Diffusion	Diffusion	Diffusion	
1.00	1SS2-1	Diffusion	Diffusion	Diffusion	2047
	1SS2-2				
	1SS2-3	0.300	.050	.020 - .040	2469
	1SS2-4				
	1SS2-5	0.260	.045	.015 - .040	2246
	1SS2-6				
	1SS2-7	0.290	.040	.010 - .030	2254
	Average	0.283	.045	.015 - .037	
1.25	1SS3-1	0.300	.045	.015 - .040	2569
	1SS3-2				
	1SS3-3	0.300	.045	.015 - .045	2908
	1SS3-4				
	1SS3-5	Diffusion	Diffusion	Diffusion	2685
	1SS3-6				
	1SS3-7	0.300	.050	.020 - .050	2721
	Average	0.300	.047	.017 - .045	
1.50	1SS4-1	0.300	.060	.020 - .045	2421
	1SS4-2				
	1SS4-3	0.300	.050	.020 - .040	2347
	1SS4-4				
	1SS4-5	0.290	.040	.010 - .025	2394
	1SS4-6				
	1SS4-7	0.325	.050	.025 - .050	2387
	Average	0.304	.050	.019 - .040	
Single Spot	1SS5-1	0.325	.050	.010 - .040	2267
	1SS5-2				
	1SS5-3	0.315	.045	.015 - .030	2769
	1SS5-4				
	1SS5-5	0.300	.045	.020 - .025	2432
	1SS5-6				
	1SS5-7	0.310	.050	.025 - .050	2489
	Average	0.313	.048	.018 - 0.036	

The spot spacing tests revealed that there was not a significant decrease in lap shear values as spot spacings decreased from 1.5" to 0.75", however, a decline in nugget diameters was noted. Furthermore, spot weld penetration into the 0.100" sheet showed a slight decrease with the decrease in spacing. The penetration into the 0.190" sheet resulted in a decrease in minimum penetration as spacing decreased but maximum penetration remained unchanged. The most important observation was that as the spot weld spacing decreased, the greater the shunting effect to the adjoining spot weld, which resulted in a greater probability for diffusion spot welds. A spot weld spacing of 1.25" was selected for panel design and fabrication.

Cryogenic Test Data 7475-T62 Joined to 2219-T81 Aluminum

Tests were performed on the 2219-T81 material in order to determine the effect that cryogenic temperature had on sheet efficiency (refer to Table S-16). A decrease was noted as temperature decreased.

Table S-16. 0.190" 2219-T81 Aluminum Skin Efficiency (or Reduction in Ultimate Tensile Strength) After Spot Welding of 0.100" 7475-T62 Stiffeners.

Material Type	Test Temperature (°F)	F _{tu} (ksi)	Sheet Efficiency (%)
2219-T81	-320	74.8	74.7/81.9* = 91.3
	-423	86.0	86.0/95.5* = 90.05

* Note: Ratio taken from actual test data rather than allowable data.

Tensile evaluation was performed at cryogenic temperature for the 7475-T62/2219-T81 material combination in order to assess the effect on lap shear to decrease in temperature. The results are shown in Tables S-17 and S-18. An increase in lap shear was recorded as the temperature decreased from ambient to cryogenic.

Table S-17. LN₂ (-320°F) Cryogenic Resistance Spot Weld Test Results 0.100 inch 7475-T62 to 0.190 inch 2219-T81 Aluminum.

Coupon ID	Nugget Diameter (inch)	Nugget Penetration		Shear (lbs)
		% Upper Sheet 7475-T62	% Lower Sheet 2219-T81	
Average	0.354	62.0	24.4	4346

Table S-18. LH₂ (-423°F) Cryogenic Resistance Spot Weld Test Results 0.100 inch 7475-T62 to 0.190 inch 2219-T81 Aluminum.

Coupon ID	Nugget Diameter (inch)	Nugget Penetration		Shear (lbs)
		% Upper Sheet 7475-T62	% Lower Sheet 2219-T81	
Average	0.349	62.0	23.6	4134

Exposure After Cleaning

Pre-weld "out-time" cleaning tests were performed in order to determine acceptable cleaning methods for aluminum alloys and determine the amount of time after cleaning that acceptable spot welds could be produced. The "out-time" test was planned for a period of ten days with three tests performed each day.

Prior to welding each day, the coupons were wire brushed and solvent wiped. The test was discontinued after day three due to weld expulsion however, the entire exposure test was repeated in order to verify the exposure requirements for the aluminum combination.

Batch two and three of set two were exposed to the environment and welded in order to assess the change in the weld quality with and without adjustments to the weld schedule. On the first day of the experiment, the materials from both of these groups were removed from the vacuum bags, wire brushed, and exposed to the atmosphere covered only with shop packing paper in order to simulate shop environment. Welds were made each day from each of the sets and evaluated for quality. The test was halted after five days due to the inability to produce acceptable welds in the exposed material.

Resistance Spot Weld Characterization 2090-T62 to 2090-T83 Aluminum-Lithium

The resistance spot weld schedule development was initiated for 0.090" 2090-T62 to 0.190" 2090-T83 aluminum-lithium material using a Taguchi L9 array. The optimum weld schedule derived from the response tables is as follows: Weld Time = 5 Cycles, Weld Force = 3000 pounds, Weld Heat = 32 percent, Forge Force = 7000 pounds. Confirmatory tests were conducted using the aforementioned schedule and are shown on Table S-19 and S-20.

Table S-19. Average Test Results for 0.090" 2090-T62 to 0.190" 2090-T83 Al-Li L9 Taguchi Array.

Test I.D.	Nugget Diameter (inch)	Nugget Penetration		Shear (pounds)	Sheet Efficiency (ratio, %)*
		% Upper Sheet	% Lower Sheet		
1	0.360	54.2	17.78	2661	91.3
2	0.406	61.15	30.28	3295	89.6
3	0.228	33.35	12.5	3480	88.2
4	0.376	44.43	23.03	2656	90.0
5	0.485	70.85	41.45	3447	87.3
6	0	0	0	0	0
7	0.404	51.4	34.20	2940	88.0
8	0.373	58.33	38.83	2700	0
9	0	0	0	0	0

*Note: Sheet efficiency is a ratio of the welded to non-welded FtU of the skin material.

Table S-20. Average Conformity Test Results for 0.090" 2090-T62 to 0.190" 2090-T83 Al-Li Optimized Resistance Spot Weld Schedule.

Nugget Diameter inch	Nugget Penetration		Shear Lbs.
	% Upper Sheet	% Lower Sheet	
0.4125	69.5	32.9	2759

Weld Cycle Development

Resistance spot weld certification tests were performed according to MIL-W-6858D class A requirements. The test was used to certify weld schedules developed by Taguchi design of experiments techniques for optimization of a process. The test results are reported in Table S-21.

Table S-21. Weld Certification Test Results for 0.090" 2090-T62 to 0.190" 2090-T83 Al-Li Optimized Resistance Spot Weld Schedule.

Coupon I.D.	Nugget Diameter inch	Nugget Penetration		Shear Lbs.
		% Upper Sheet	% Lower Sheet	
Average	0.406	62.2	33.0	3155

Resistance Spot Weld Spacing Tests were performed to determine the effects of the resistance spot weld spacing on weld strength and quality. The average single-spot lap shear was 3,417 lbs., and the 1.50", 1.25", 1.00", and 0.75" spot spacing average lap shear values were 3154, 2876, 3206, and 3024 lbs., respectively. There was a decrease of 263 lbs. from the single-spot value to the 1.50" spot spacing value. The lap shear values for spot spacing from 1.50" to 0.75" did not reveal any conclusive trends. The spot weld nugget penetration into the 0.090" sheet showed a slight increase in minimum penetration and a slight decrease in maximum penetration with the closer spot weld spacing. The penetration into the 0.190" sheet showed fairly uniform minimum

penetration, but the values for maximum penetration showed erratic behavior over the range tested. The overall change in nugget penetration in relationship to the spot spacing was insignificant.

In conclusion, the shunting effect of close spot spacing did not degrade the integrity of the spot weld for this material combination and spot weld schedule. This certified weld schedule could be used to spot weld 0.090" 2090-T62 to 0.190" 2090-T83 at spot spacings of 0.75" or greater.

Sheet Efficiency

Sheet efficiency tests were performed on the 2090-T83 material in order to determine the "knockdown" against the ultimate tensile strength after spot welding. The sheet efficiency test results are shown in Table S-22 for 2090-T83 skin.

Table S-22. 0.190" 2090-T83 Aluminum-Lithium Skin Efficiency (or Reduction in Ultimate Tensile Strength) After Spot Welding of 0.090" 2090-T62 Stiffeners.

Material Type	Test Temperature (°F)	F _{tu} (ksi)	Sheet Efficiency (%)
2090-T83	20	65.9	65.9/78.3* = 84.15

* Note: Ratio taken from actual test data rather than allowable data.

The weld schedules developed for the crippling test panels (modified weld schedule developed for thinner section based upon Taguchi response) were verified through certification testing. The results from the tests are shown in Tables S-23.

Table S-23. Weld Schedule Certification Test for 2090 Crippling Test Panels.

Coupon ID	Nugget Diameter (inch)	Nugget Penetration		Shear (lbs.)	2090-T62 Thickness (inch)
		% upper Sheet	% Lower Sheet		
Average	0.340	36 - 47	33.0	2175	0.072

Cryogenic Test Data

Sheet efficiency tests were performed under cryogenic temperature on the 2090-T83 material in order to determine the reduction in ultimate tensile strength after spot welding. The cryogenic sheet efficiency test results are shown in Table S-24 for 2090-T83 skin.

Table S-24. 0.190" 2090-T83 Aluminum-Lithium Skin Efficiency (or Reduction in Ultimate Tensile Strength) After Spot Welding of 0.090" 2090-T62 Stiffeners.

Material Type	Test Temperature (°F)	F _{tu} (ksi)	Sheet Efficiency (%)
2090-T83	-320	76.1	76.1/95.7 = 79.53
	-423	87.7	87.7/103.9 = 84.4

Cryogenic lap shear tests on the 0.090" 2090-T62 joined to 0.190" 2090-T83 material combination were performed in order to evaluate the response of the spot welds produced by the certified weld schedule operating under cryogenic temperatures. The lap shear and weld nugget measurements are shown in Table S-25 and Table S-26.

Table S-25. LN₂ (-320°F) Cryogenic Resistance Spot Weld Test Results.0.090 inch 2090-T62 to 0.190 inch 2090-T83 Aluminum-Lithium

Coupon ID	Nugget Diameter (inch)	Nugget Penetration		Shear (lbs)
		% Upper Sheet	% Lower Sheet	
Average	0.412	52.2	50.0	4206
Min / Max		38.9 / 66.6	33.3 / 77.8	

Table S-26. LH₂ (-423°F) Cryogenic Resistance Spot Weld Test Results.0.090 inch 2090-T62 to 0.190 inch 2090-T83 Aluminum-Lithium

Coupon ID	Nugget Diameter (inch)	Nugget Penetration		Shear (lbs)
		% Upper Sheet	% Lower Sheet	
Average	0.423	52.2	47.2	4299
Min / Max		33.3 / 66.6	33.3 / 72.2	

Exposure After Cleaning

Pre-Weld Cleaning Tests were performed to determine acceptable cleaning methods for the aluminum-lithium alloy and determine the out-time after cleaning duration in which acceptable spot welds could be produced with the 0.090" 2090-T62 to 0.190" 2090-T83 material. Lap shear values did not vary significantly from Day 1 to 15. The average shear value was 3,330 lbs., compared to the spot weld certification value of 3,154 lbs. The high and low values were 3,490 lbs. and 3,128 lbs., respectively, giving a range of 362 lbs. These high and low values varied from -6% to +5% of the 3,330 lbs. average value. Nugget diameters did not vary significantly from Day 1 to 15. The average nugget diameter was 0.423", compared to the spot weld certification value of 0.406". The high and low values were 0.431 and 0.407", respectively, giving a range of 0.024". These high and low values varied from -4% to +2% of the 0.406" average value. In conclusion, the 0.090" 2090-T62 to 0.190" 2090-T83 weld material combination can be successfully resistance spot welded per MIL-W-6858D requirements up to fifteen days after chemical cleaning with only paper (blue-line) packaging.

Weld Repair

The objective of this task was to determine the feasibility of repairing defective resistance spot welds in the 0.090" 2090-T62 to 0.190" 2090-T83 aluminum-lithium alloy combination. Defective spot welds were intentionally produced with the aluminum-lithium material combination from variations to the original certified spot weld schedule. Three groups of defective welds were made: diffusion welds (a reduction in 11 percentage points of heat from the original certified schedule), undersized nuggets (a reduction in 8 percentage points of heat from the original certified schedule), and nuggets with cracks or voids (a reduction in 2 percentage points of heat and the elimination of the forge force from the original certified schedule).

Fifteen specimens were spot welded per defect group, and sent to radiographic inspection for verification of the defect. The coupons were re-welded, using resistance spot weld repair schedules, and re-examined by radiographic inspection to verify correction of the defect.

The examination of the "diffusion weld" specimens resulted in the removal of the defect by the repair process. The average shear strength of the diffusion weld was 2203 pounds and the average shear strength of the repair weld was 3344 pounds. Examination of the "undersized spot weld" specimens resulted in the removal of the defect by the repair process. The average shear strength of the undersized weld was 2721 pounds and the average shear strength of the repair weld was 3441 pounds. Examination of specimens with "cracks and voids in the weld" resulted in the

removal of the defect by the repair process. The average shear strength of the cracks and voids in the weld was 3108 pounds and the average shear strength of the repair weld was 3639 pounds.

It was determined that the repair weld process can be successfully used for all of the defect types examined during this program with the aluminum-lithium materials. However, the repairs were accomplished with additional heat placed into the system, which is anticipated to further decrease the skin efficiency. Any quantifiable reduction in skin efficiency is unknown and would depend upon the total heat input.

FUSION WELD DEVELOPMENT:

Fusion welding is utilized for both the vertical panel to panel joints, and the barrel to major frame joints. In order to fabricate the doubler reinforced weld joint, fusion weld parameters had to be developed for both the 0.155" 2219-T81 aluminum and 0.155" 2090-T83 aluminum-lithium materials, and the theory of the joint explored through mechanical testing of coupons. Variable Polarity Plasma Arc (VPPA) fusion weld studies were initiated with the aforementioned material systems using a 300 Amp Hobart VPPA welder. A helium purge box was adapted to the VPPA welder so that all of the welding would be controlled under a shielded environment.

2219-T81 Aluminum Fusion Weld Development

The variable polarity plasma arc (VPPA) fusion weld development process was initiated and weld certification panels were welded, radiographic inspected and sectioned into tensile test and macro cross-section specimens. The preliminary results of tensile testing on 0.190" and 0.155" thick 2219-T81 aluminum sheet are shown in Table S-27 and S-28.

Table S-27. Tensile Strength of VPPA Fusion Welded 0.190" 2219-T81

Coupon I.D.	Width (in)	Thickness (in)	Area (sq. in)	Load (lbs)	F _{tu} (psi)
1	0.962	0.192	0.185	7565	40,957
2	0.960	0.191	0.183	7680	41,907
3	0.966	0.190	0.184	7522	40,983
4	0.936	0.191	0.179	7010	39,232
5	0.921	0.191	0.176	6909	39,276
6	0.949	0.189	0.179	7093	39,567
7	0.930	0.188	0.174	6867	39,402
8	0.946	0.187	0.164	6818	38,644
9	0.986	0.187	0.184	7082	38,429
				Average	39,822

The fusion weld specimens were machined into a tensile coupon (dogbone) configuration and chemically cleaned (doubler and outer skin material) prior to resistance spot welding of a 7475-T62 Al doubler onto the 2219-T81 Al fusion weld specimen. The completed uniaxial specimens were strain gauged and tested at ambient temperature (refer to Table S-29).

All of the test specimens failed in the 2219-T81 skin along the first row of spot welds near the edge of the doubler. There were not any indications of spot weld failure during testing, or permanent deformation in the fusion weld. Weld efficiencies for the test specimens were lower than predicted due to the close doubler inter-spot spacing (0.075 inch) used during welding.

The results of the doubler reinforced fusion weld testing showed that the in-line configuration provided the best reinforcement of the fusion weld. However, neither reinforcement joint configuration (in-line or staggered) were optimized. As a result of the tests and evaluations of

the joint at General Dynamics and Rockwell the inter-spot weld spacing was increased and the center-line offset of the reinforce joint was readjusted.

Table S-28. Tensile Strength of VPPA Fusion Welded 0.155" 2219-T81

Coupon I.D.	Width (in)	Thickness (in)	Area (sq. in)	Load (lbs)	F _{tu} (psi)
A1	0.962	0.145	0.139	5850	41,938
B1	1.027	0.146	0.150	6113	40,769
C1	0.992	0.147	0.146	5953	40,823
				Average	41,177
A2	0.997	0.132	0.129	5031	39,011
B2	0.989	0.130	0.129	4794	37,287
C2	1.020	0.135	0.138	5163	37,494
				Average	37,930
A3	0.996	0.142	0.141	5310	37,544
B3	1.010	0.141	0.142	5521	38,768
C3	0.9665	0.142	0.137	5244	38,210
				Average	38,174

Table S-29. Tensile Response of Fusion Doubler Reinforce Testing for 2219-T81 Al with 7475-T62 Al Doubler.

Specimen ID	Spot Weld Pattern	Width (inch)	Thickness (inch)	Area (sq. in.)	Ultimate Load (pounds)	F _{tu} (Ksi)	Weld Efficiency (percent)
1-F4D1	In-Line	4.84	0.155	0.750	36712	48.9	77.7
1-F3D2	In-Line	4.84	0.155	0.750	41151	54.9	87.0
2-F1D3	Staggered	4.02	0.155	0.620	34720	55.7	88.5
2-F2D4	Staggered	4.02	0.155	0.623	34727	55.7	88.5

2090-T83 Aluminum-Lithium Fusion Weld Development

Parameter development on VPPA welding of the 0.155" 2090-T83 material was performed. Radiographic inspection of the single pass welds revealed high quality fusion joints with full penetration, however, the visual appearance of the welds showed small amounts of undercut along the weld length. The initial goal of developing a single pass VPPA weld with full penetration (Keyhole) without a 'cosmetic' cover pass to fill undercut was desirable since panel distortion appeared to be most noticeable after the cover pass. However, the single pass weld schedule could not be enhanced in order to remove the under-cut, and the program goal was modified to include the cover-pass.

The preliminary test panel, 0.155" 2090-T83 Al-Li, was welded and radiographically inspected. The panel passed the acceptance criteria for fusion welding of aluminum and was processed for tensile and metallographic analysis. Data provided for the development work is shown in Table S-30 and S-31.

Table S-30. Single Pass Fusion Weld Development of 0.155: 2090-T83 Al-Li.

Coupon I.D.	Test Area (sq. in.)	Load (pounds)	F _{tu} (psi)	Elongation (%)
1	0.141	5871	41,562	5
2	0.144	5269	36,626	5
3	0.141	5766	41,010	4
4	0.146	5313	36,463	5
5	0.145	5276	36,426	5
Average	0.143	5499	38,417	5

Table S-31. Tensile Results of 0.155" 2090-T83 Two Pass VPPAW

Coupon LD.#	Width inch	Thickness inch	Test Area sq. inch	F _{tu} psi	Elongation %
1	0.954	0.156	0.149	41169	5
2	1.009	0.157	0.158	41752	5
3	1.005	0.156	0.157	41759	4
4	1.015	0.156	0.158	39832	5
Average			0.156	41128	5

TASK 4: PANEL FABRICATION AND TEST

CRIPPLING PANEL FABRICATION:

The crippling panel designs were based upon the analysis of the three selected stiffener configurations. The designs were analyzed and optimized for fabrication and structural testing. The crippling specimens were superplastic formed, heat treated, trimmed, inspected, spot welded to outer skin material and assembled into the test fixtures. Testing was performed on the three configurations and compared with predicted behavior of the stiffened structures.

The part blanks of each material were coated with releasing agent, hot loaded into the SPF press, formed, hot unloaded and allowed to slow air cool. The panels were formed, heat treated, trimmed to a net shape configuration and inspected. The stiffener and skin combination was cleaned, internal strain gauges were applied, and the panel was welded to the skin. The panels were examined for weld integrity by radiographic analysis and prepared for structural testing. The welded panels were trimmed, assembled into the test fixture, and tested. Each specimen was mounted and aligned in the test machine for compression loading as shown in Figure S-7.

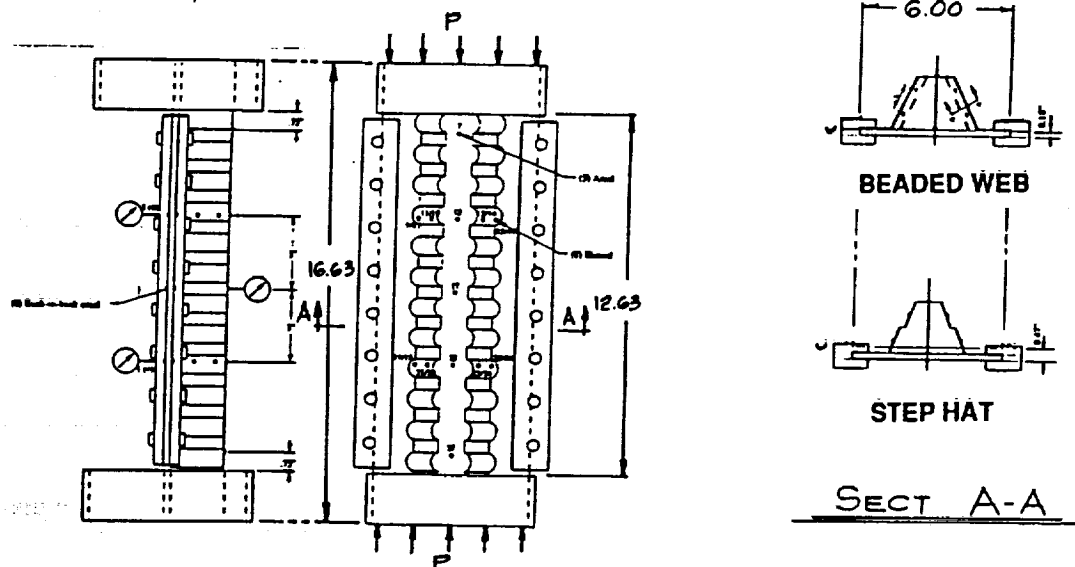


Figure S-7. Crippling Stiffener Structural Test Set-up.

The initial fully strain gauged crippling panel test was performed on a 7475-T62/2219-T81 stepped hat configuration. Buckling initiated at 77,000 lbs for the stepped hat stiffener but continued to carry load up to 84,000 Lb. The spot welds did not fail during the testing for either the test set-up panel or the initial stepped hat panel.

The predicted ultimate uniaxial test loads for crippling in the hats are re-iterated for comparison purposes in the following table:

Predicted Ultimate Uniaxial Test Panel Loads
Aluminum

Stepped Hat	7475-T62 to 2219-T81 Al	76,800 Lb.
Beaded Flat or Curved Cap	7475-T62 to 2219-T81 Al	60,000 Lb.

Aluminum-Lithium

Stepped Hat	2090-T62 to 2090-T83 Al-Li	68,000 Lb.
Beaded Flat or Curved Cap	2090-T62 to 2090-T83 Al-Li	68,000 Lb.

The test results of the 7475-T62/2219-T81 and 2090-T62/2090-T83 aluminum and aluminum-lithium panels are summarized in Table S-32 and S-33.

Table S-32. Crippling Panel Test Results for 7475-T62/2219-T81.

Panel and I.D.	Panel Type	Ultimate Compressive Load (Lbs)	Comments
Test Panel 1 (47-3-7-23)	Stepped Hat	84,000	
Test Panel 2 (50-3-7-26)	Stepped Hat	79,400	Cracked Spot Welds 1, 2, 14
Test Panel 3 (43-3-7-3)	Stepped Hat	83,400	Cracked Spot Weld 2
Test Panel 4 (1-1-7-7)	Beaded Web (CC)	66,500	
Test Panel 5 (3-1-7-16)	Beaded Web (CC)	67,900	
Test Panel 6 (7-1-7-20)	Beaded Web (CC)	66,300	Cracked Spot Weld 19
Test Panel 7 (26-2-7-62)	Beaded Web (FC)	63,000	Popped Spot Welds 8, 9, 10, 14, 15, 16
Test Panel 8 (27-2-7-63)	Beaded Web (FC)	67,500	Popped Spot Welds 19, 20, 21
Test Panel 9 (30-2-7-36)	Beaded Web (FC)	67,000	Cracked Spot Welds 2, 3, 13
			Cracked Spot Welds 1, 2

Table S-33. Crippling Panel Test Results for 2090-T62/2090-T83.

Test Panel	I.D.	Panel Type	Ultimate Compressive Load (Lbs)
14	(17-3-2-15)	Stepped Hat	70,300
15	(126-3-2-91)	Stepped Hat	74,600
16	(60-3-2-42)	Stepped Hat	73,800
18	(35-2-2-51)	Beaded Web (FC)	65,000
19	(39-2-2-55)	Beaded Web (FC)	65,000
20	(70-2-2-58)	Beaded Web (FC)	65,200
21	(12-1-2-10)	Beaded Web (CC)	65,800
23	(87-1-2-78)	Beaded Web (CC)	67,200
24	(91-1-2-82)	Beaded Web (CC)	63,770

The test load values were for the 7475-T62 to 2219-T81 aluminum and the 2090-T62 to 2090-T83 aluminum-lithium stiffener and skin combination were slightly higher than the predicted load values. The higher results have been attributed to conservative estimates for spot weld strength which translated into reductions in outer skin and stiffener allowables.

The basic failure mode for each stiffener was face wrinkling of the skin, as would be expected with a heavy skin-light stiffener combination. It was noted that very soon after the skin wrinkling

for the stepped hat, the web buckled because of the change in skin support condition. The failure of a typical stepped hat is shown in Figures S-8 and S-9.

Results and Conclusion

The comparisons of the PASCO model axial stiffness and that obtained through the crippling test specimen values are summarized in Table S-34. The column of the $E(t_{\text{bar}})x$ specimen width was included as an additional check of the values obtained. The PASCO models presented a satisfactory axial stiffness simulation of the crippling test specimens.

Table S-34. Comparison Summary of the Test Panel Versus Predicted Axial Stiffness (EA) of the Crippling Specimens.

Panel No.	Stiffener Type	Material (Stiff/Skin)	A ₁₁ Model (xE6)	PASCO EA (xE6)	Test EA (xE6)	Stiffener t_{bar} (in)	Approximate $E t_{\text{bar}} \times \text{width}$ (Lb x E6 = EA)	Ratio Test to Model
#1	SH	7475/2219	2.618	15.7	15.2	0.256	15.4*	0.97
#8	BCC	7475/2219	2.269	13.62	12.8	N/A	N/A	0.94
#12	BFC	7475/2219	2.269	13.62	13.4	N/A	N/A	0.98
#15	SH	2090/2090	2.90	17.4	16.7	0.252	17.1**	0.96
#23	BCC	2090/2090	2.28	13.68	12.9	N/A	N/A	0.94
#19	BFC	2090/2090	2.28	13.68	13.7	N/A	N/A	1.0

* Effective Modulus, Assumed = 10 Msi, ** Effective Modulus, Assumed = 11.3 Msi

t_{bar} = Effective Stiffener to skin thickness

SH = Stepped Hat, BCC = Beaded Curved Cap, BFC = Beaded Flat Cap

Test EA = $P/\delta/L = P/\epsilon \text{ ave. strain}$ δ = shortening of specimen (in.), L = Length of Specimen (in.)

PASCO EA = (A₁₁ x Width) A₁₁ = Stiffness per inch of width, W = Specimen Width (6 in.)

N/A = Not applicable for beaded web panel the PASCO t_{bar} for the beaded web includes the webs, however, the beaded web contribution to the axial load capability of the stiffener is minimal.

Crippling Panel Test Conclusions

The following summary conclusions are based on the crippling panel test results:

1. The correlation between test and predicted loads was satisfactory.
2. The mode of initial buckling failure, face wrinkling (similar to column buckling of a beam on an elastic foundation), was expected, since this is typical of a heavy skin-light stiffener combination.
3. Spotweld strength was sufficient for this application; e.g., no unzipping was observed after the face wrinkling failures of the specimens.
4. Since the t_{bar} for the beaded hat and stepped hat are quite close, the stepped hat offers about 10-14% more efficiency on the basis of initial buckling for the same material.
5. Comparing the ratio of the initial buckling to material density (F_{bu}/ρ) for 2090 and 7475 stepped hats indicates that the 2090 material is slightly more efficient for this application.
6. Since the initial buckling and yield strength were quite close, all the designs appeared to produce a very good optimum structure.
7. All designs met the required design criterion of 51,000 lbs (8474 lbs/in.) uniaxial compression loading for local buckling.
8. The SPF beaded hat could be made a more structurally efficient configuration if the webs were chem-milled to a lower thickness; however, this would increase the cost of fabrication.
9. An improved theoretical thinning profile would be useful in considering any other possible variations of the SPF hat-stiffener configuration.
10. The stepped-hat configuration will be utilized as the column buckling test panel design to maximize stiffener load carrying ability.

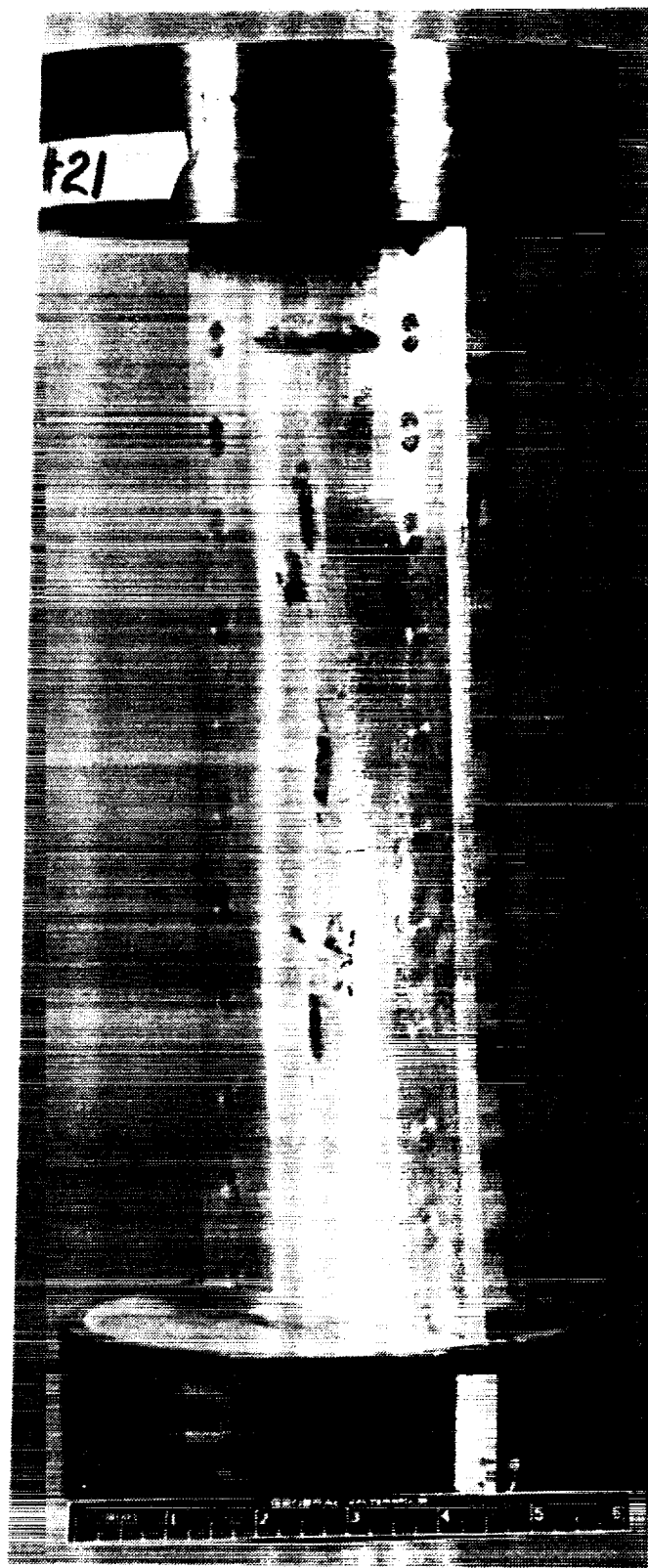
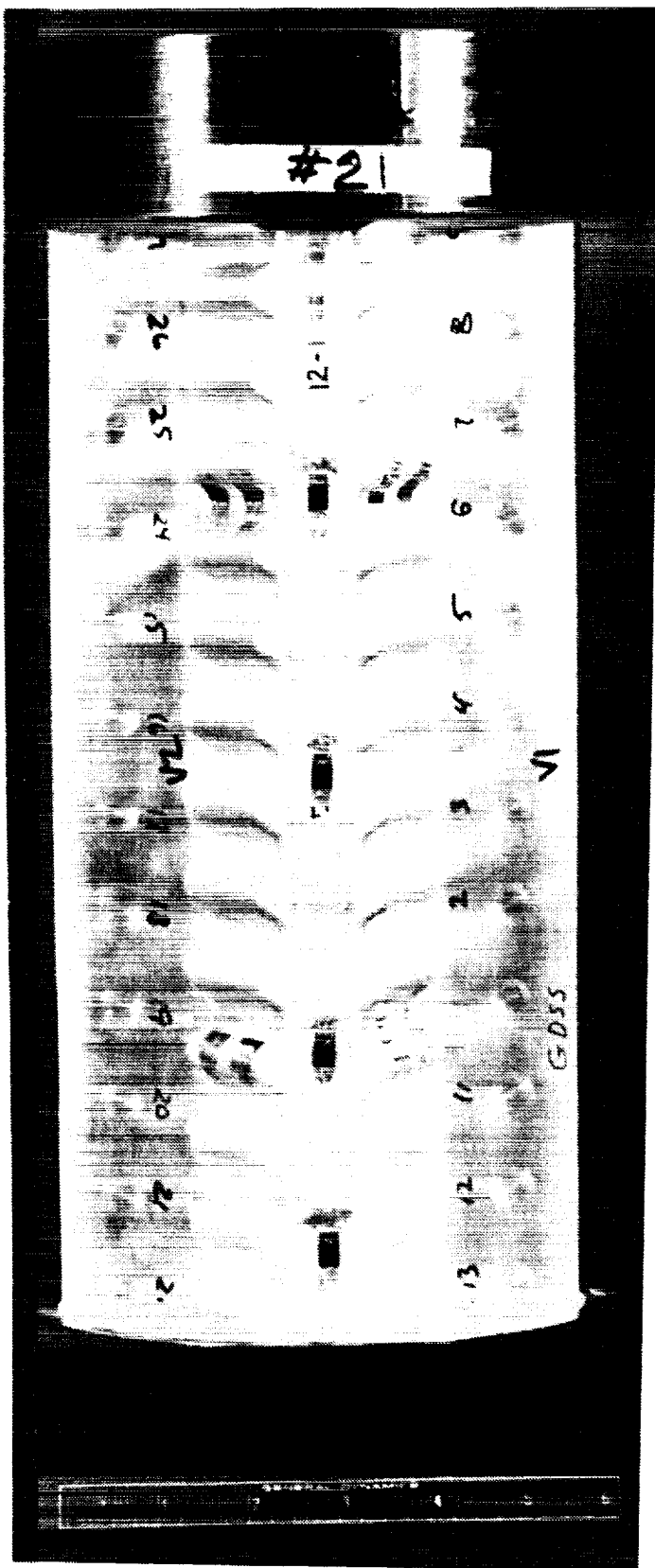


Figure S-8. Typical Failure of Beaded Web Stiffener.

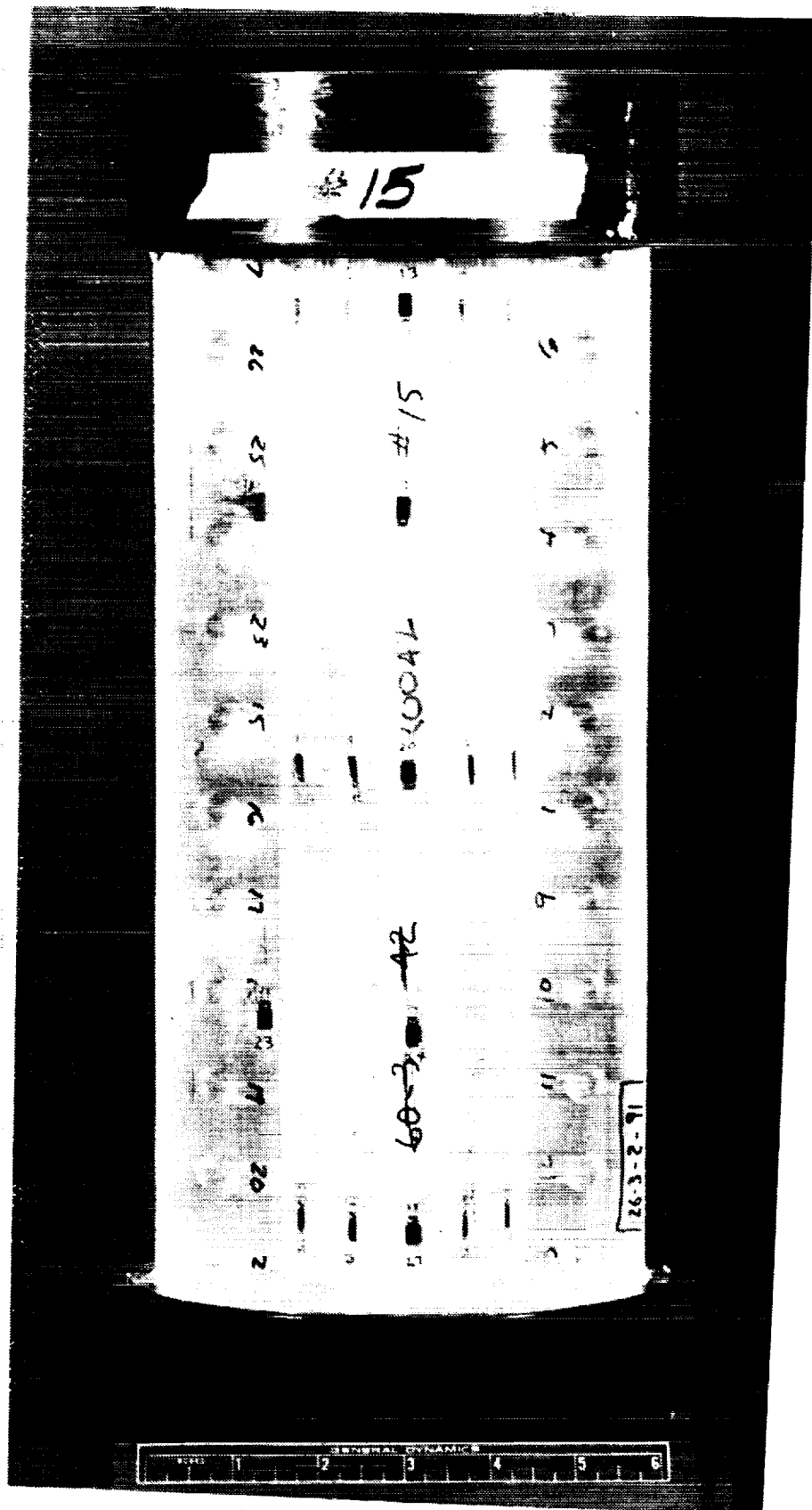


Figure S-9. Typical Failure of Stepped Hat Stiffener.

INTEGRALLY STIFFENED PANEL DEMONSTRATION ARTICLE:

The integrally stiffened panel (shown in Figure S-10) was fabricated as a demonstration article. The panel was fabricated as a representation of the type of configuration that could be fabricated for an integral SPF stiffener configuration without optimization of the stiffener or node configuration. Integrally stiffened structure (vertical stiffeners and hoop-wise supports integrally formed into the panel) would utilize the beaded web stiffener concept to minimize load transfer through the side walls of the stiffener which could lead to large moments at the point of intersection in the panel. The integrally stiffened panel was not addressed during the panel test and evaluation portion of this program, however, the concept appears to be viable (due to the performance of the structural test specimens and through evaluation of the stress analysis efforts under this program) for vertical and hoop-wise strengthening of built-up cryogenic tank structure.

COLUMN BUCKLING PANEL FABRICATION:

At the completion of the crippling panel tests, the stepped hat stiffener configuration was chosen for continued development based on its load carrying capability. The panel configuration was chosen based upon the desired length of the panel (column of at least 60 inches) and limited by the width of available material (48" minus sealing area). The resulting panel design maintained the inter-stiffener and inter-spot spacing optimized for the crippling stiffener panels.

The tooling concept for the universal die chamber and insert combination used a base-plate for assured release of the gas pressure during forming with separate stiffener configurations indexed onto the gas plate with locator pins. The stiffeners were machined separately out of bar stock in order to minimize material scrap and keep handling of the tooling configuration simple. The gas pressure plate was chamfered along the bottom periphery and grooved to allow for gas flow away from the final part to the gas outlets.

The column buckling test panels were formed (refer to Figure S-11), solution heat treated, water quenched, straightened, artificially aged, trimmed, chemically cleaned, and strain gauged prior to shipment of the panels to General Dynamics for final assembly. After completion of the welding process, the panels were inspected and final machined to net dimensions. The panels were shipped directly to NASA LaRC for final assembly and testing.

DOUBLER-REINFORCED FUSION WELD PANEL:

The final panel configuration examined during this program was the vertical fusion weld or panel-to-panel joint. The joints are fusion butt-welded together and reinforced with a spot-welded doubler over the weld. This doubler-reinforced concept eliminates the need for machined weld lands (commonly used for launch vehicle pressure vessels at an increased fabrication cost, and weight penalty to the structure) to reinforce the joint by utilizing the doubler as a major load carrying member for the fusion weld. The development of the joint was based upon the fusion weld and resistance spot weld data generated during task 3 of this program. Specific doubler testing was conducted under task 3 that provided a greater understanding of the behavior of the doubler over the Variable Polarity Plasma Arc (VPPA) fusion weld for load transfer. The test data was then utilized with finite element modeling techniques to predict the behavior of the fusion weld joint during bi-axial (axial and hoop) loading conditions.

The fusion weld test panels were fabricated from two skins (machined from 0.190" to 0.155" thickness) fusion welded together with a doubler attached to the outer skin over the fusion weld and two crippling stiffeners attached to the skin material. Prior to assembly of the panels, weld

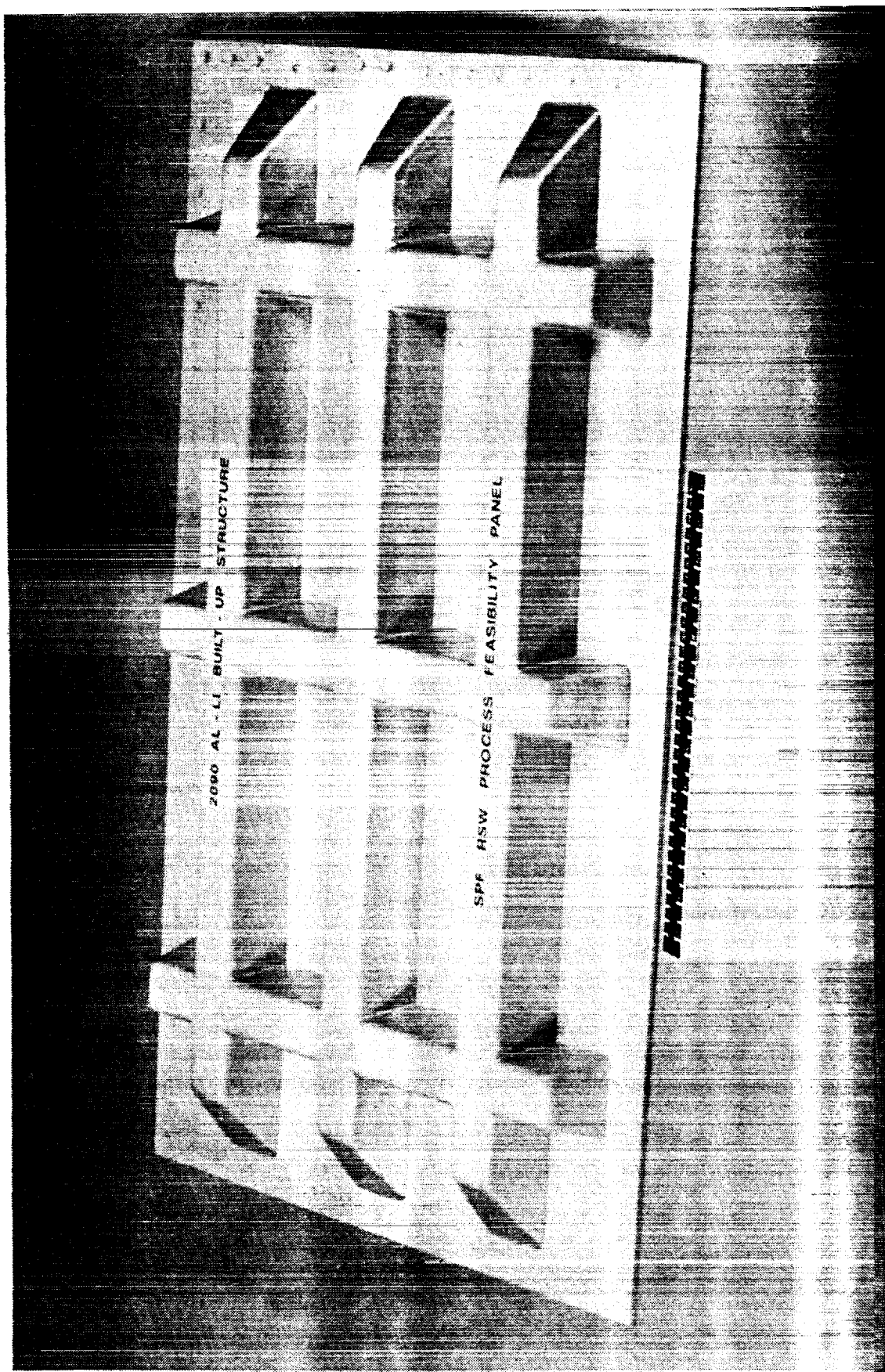


Figure S-10. Integrally Stiffened Demonstration Panel.



Figure S-11. Hot Removal of Column Buckling Panel from 4500 Ton Press.

verification testing was performed on the fusion weld. Welding of the 2219-T81 and 2090-T83 fusion weld panels were completed and inspected (visually and radiographically).

The fusion welded panels were accepted after weld verification testing, and machined to a net shape condition. The reinforcement doubler was resistance spot welded onto panel over the shaved weld bead (refer to Figure S-12). The SPF stepped hat stiffeners were subsequently located and welded onto the test panel and the entire panels was inspected. The finished test panels were machined to final contour (flat and parallel) and inspected for dimensional integrity. Final assembly of the fusion weld panels into the test fixture was initiated at General Dynamics. The doubler reinforced fusion weld panels were shipped to NASA Langley for completion of assembly and final testing.

TASK 5: NDE & QUALITY ASSURANCE

The NDE and quality assurance of SPF structure and resistance spot weld joints was evaluated and enhanced wherever possible during the program. Existing process specifications for aluminum at Rockwell were modified to include 2090 and 8090 Al-Li. The modifications to the specification were based upon uniaxial test data and producibility analysis (based upon the predictive modeling of the material prior to forming) carried out under this program. The main areas that were critical for understanding the materials were the strain rate and forming temperature that result in the lowest flow stress (with the highest uniform elongation) and the cavitation behavior of each material. The evaluation of the superplastic material variables resulted in selection of a duplex strain rate for both the 2090 and 8090 materials ($2E-3$ for strains up to 0.5 after which the strain rate is decreased to $2E-4$ for the remainder of the forming process), thermal control of $950 \pm 10^\circ\text{F}$ with a maximum back pressure of 600 psi (minimum of 200 psi).

The welding NDE and quality control issues were addressed during resistance spot welding development. The evaluation of weld quality was based upon monitoring of the process parameters for resistance spot welding (forge force, heat, current, etc.) that were recorded during each welding operation and evaluating the parameters for an acceptable versus unacceptable weld. The out-of-tolerance control areas for the welding process were determined through evaluations of information generated during the Taguchi design of experiment tests and the heat sensitivity testing. The acceptable limits for each variable in the welding process were identified and used as boundaries (upper and lower limits) for the fabrication of acceptable resistance spot welds (however, radiographic inspection, lap shear testing, and metallographic examination of welds was performed during this program in order to fully characterize the process). The next step for complete NDE of the resistance spot weld process would be to include automatic feed-back control (or in-process control) for the welding equipment that would control the settings of the weld equipment so that out-of-tolerance welds could not be made. However, investigation of automatic feedback control for resistance spot welding was out of the scope of this program.

TASK 6: LIFE CYCLE COST ANALYSIS

The "Low Cost, SPF Aluminum Cryogenic Tank Structures for ALS and Future Hypersonic Vehicles" examined the application of superplastic formed (SPF) structure as a cost effective means to fabricate a cryogenic tank. The goal of the life cycle cost (LCC) study was to evaluate the cost savings or penalty associated with utilizing a built-up structures approach versus integrally machined structure for the Hydrogen tank. The built-up concept uses stiffeners, specifically, superplastically formed stiffener panels, brake formed hat sections, or "I" extrusions, joined to a skin panel. The flow of the LCC study included evaluation of three built-up concepts represented by two different material systems, and a baseline concept, integral machining.

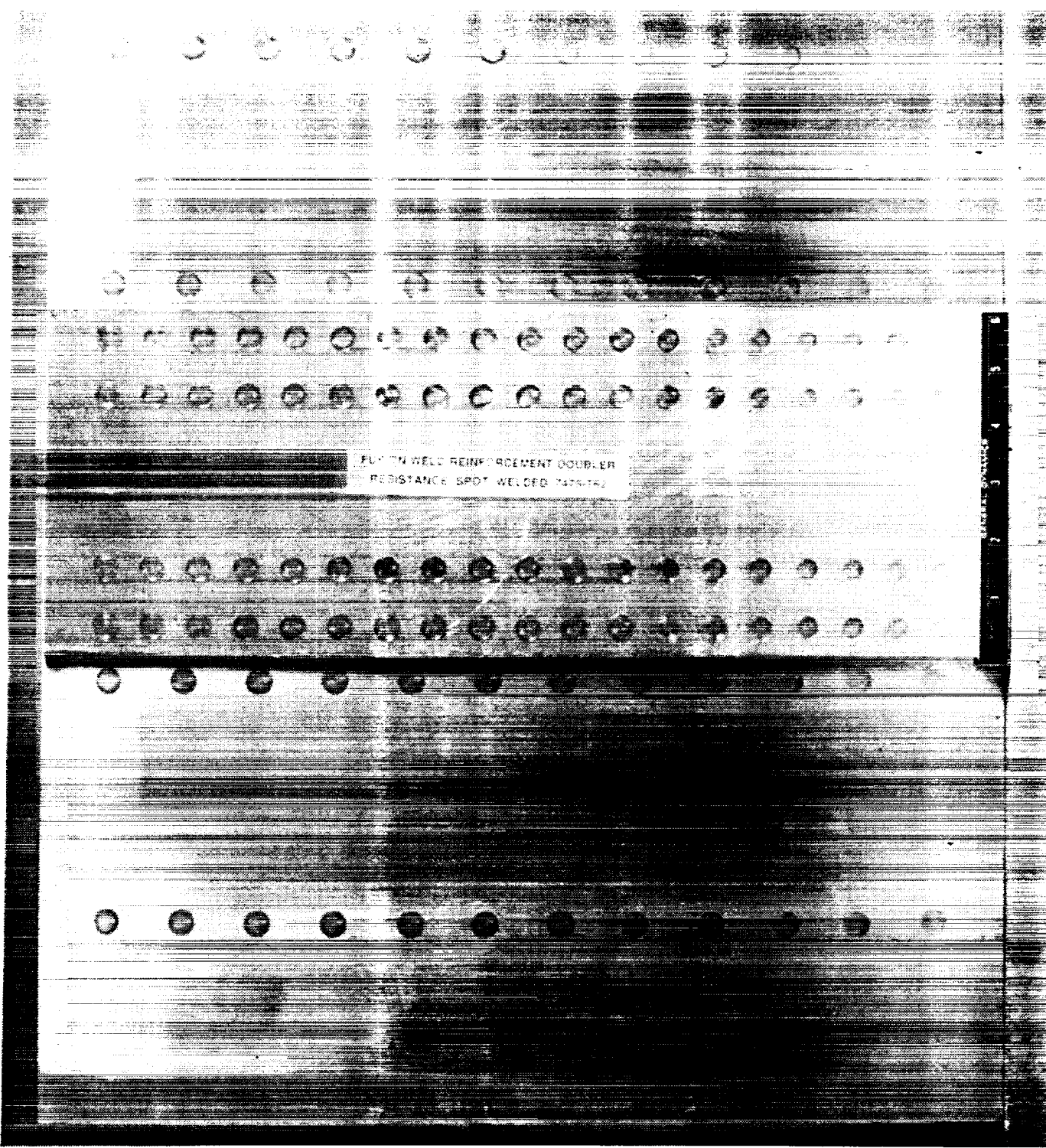


Figure S-12. Doubler Reinforced Fusion Weld Panel.

The results of the analysis showed the cost to fabricate one vehicles cryogenic tanks (T1 dollars, two tanks per vehicle), 307 vehicles (T307 dollars, two tanks per vehicle), and a projected build of 1000 vehicles (T1000, two tanks per vehicle). A summary of the costs for the tanks are shown as Table S-35. The integrally machined configuration (integrally machined 2219 Al) is the most costly system at T1, and at T307 (or the 307th vehicle built) however at T1000, the disparity in purchase price between built-up configurations and the integrally machined concept begins to become less apparent.

Table S-35. Summary of Cost Trade Analysis.

Fabrication Method - Material	T1 Dollars	T307 Dollars	T1000 Dollars
Built-Up Structures			
Superplastic Forming Al-Li	3,563,000	2,922,100	2,603,200
Superplastic Forming Al	3,039,000	2,610,300	2,321,600
Brake Forming Al-Li	3,831,000	3,019,200	2,716,300
Brake Forming Al	3,535,000	2,670,200	2,420,400
Extrusion Al-Li	4,163,000	3,231,500	2,895,000
Extrusion Al	3,782,000	2,763,100	2,498,900
Integrally Machined Al	4,225,000	3,610,000	2,649,600

In the course of the program, it was difficult to ascertain the value of weight to the vehicle versus amount of payload that would have to be sacrificed for each pound of structural weight. However, if the value were similar to a Shuttle type vehicle in that each pound saved for the vehicle allowed for increase to the payload manifest, each pound could be worth up to \$300. In that case the modified purchase price, due to weight savings or penalty, (refer to Table S-36) is shown in Table S-37 for each configuration (based off of the integrally machined concept). Using the \$300/lb ratio, the SPF Al-Li concepts provide for approximately 40 to 48% cost savings over the integrally machined concept, while the SPF Al concept provided a 17 to 26% cost savings. The cost savings or penalties are shown as Table S-38. Since this is an expendable vehicle, the goal of minimization of fabrication and material cost is of the utmost importance. However, weight savings should be kept in the picture as it relates to potential payload into space.

In summary, the built-up approach can provide significant cost savings over conventionally machined cryogenic tank structure. This analysis was performed with standard manufacturing methods and realistic data inputs. It is believed that the aluminum-lithium family of materials can provide additional benefits to an NLS type vehicle by reducing overall structural weight. Additional cost savings can be realized with utilization of alternative fabrication methods for cryogenic tank structure.

Table S-36. Summary of Weight Analysis.

FABRICATION METHOD - MATERIAL	STRUCTURAL WEIGHT (LBS)
Built-Up Structures	
Superplastic Forming Al-Li	28,836
Superplastic Forming Al	32,505
Brake Forming Al-Li	31,306
Brake Forming Al	35,576
Extrusion Al-Li	31,627
Extrusion Al	35,970
Integrally Machined Al	32,356

Table S-37. Cost Savings or Penalties for Cryogenic Tank Structures Versus the Integrally Machined Concept.

Fabrication Method - Material	T1 Savings	T307 Savings	T1000 Savings
Built-Up Structures			
Superplastic Forming Al-Li	40.7 %	48.3 %	41.6 %
Superplastic Forming Al	17.5 %	26.5 %	10.7 %
Brake Forming Al-Li	16.8 %	25.1 %	9.4 %
Brake Forming Al	(6.5 %)	(0.7 %)	(27.8 %)
Extrusion Al-Li	6.6 %	16.5 %	1 %
Extrusion Al	(15.2 %)	(6.6 %)	(35.7 %)
Integrally Machined Al	0	0	0

Table S-38. Predicted LCC Behavior.

Fabrication Method - Material	T1 Dollars	T307 Dollars	T1000 Dollars
Built-Up Structures			
Superplastic Forming Al-Li	2,507,000	1,866,100	1,547,200
Superplastic Forming Al	3,486,000	2,655,000	2,366,300
Brake Forming Al-Li	3,516,000	2,704,200	2,401,300
Brake Forming Al	4,501,000	3,636,200	3,386,400
Extrusion Al-Li	3,944,300	3,012,800	2,676,300
Extrusion Al	4,866,200	3,847,300	3,583,100
Integrally Machined Al	4,225,000	3,610,000	2,649,600

TASK 7: AUTOMATION AND SCALE-UP

Investigations into automation of the fabrication process for NLS cryogenic tanks were limited to planning the type of facilities that could be most cost-effective for the nation. An automated fabrication cell for superplastic forming. The automated fabrication well would provide for automatic loading of a part blank, forming, part removal and quenching (air quench if aluminum-lithium materials are to be utilized). The parts would be loaded immediately after forming into a cleaning and heat treatment carousel after which time it would be trimmed and welded onto the outer skins. The welded panels would then be joined into barrel sections and finally into cryogenic tank structure. The preliminary plan would utilize existing facilities where available (or modify existing facilities if possible) in order to minimize any re-facilitization costs.

1.0 INTRODUCTION

The work reported herein covers the design, analysis, and structural testing of the Type I hat-stiffened crippling panels for the NASA contract NAS 1-18590 Task Order 5, "Low Cost SPF Aluminum Cryogenic Tank Concepts for ALS", C. E. Anton, Program Manager.

The crippling specimens (Type 1 panels) utilized during this program were designed and structurally tested to determine a differentiation between the three efficient Superplastically Formed (SPF) designs. The basis for this examination into the use of aluminum (Al) or aluminum-lithium (Al-Li) stiffener concepts welded onto outer skin material was to reduce the life cycle cost of cryogenic tank structure for the Advance Launch System (ALS) family of vehicles.

Past production work has shown that cryogenic tank structure for the Shuttle booster rockets and the Titan system have very high life cycle costs for the fuel tank structure. The tanks are machined stiffener-skin combination that are subsequently formed into the required contour after machining. The material scrap rate for these configurations are usually high, and the loss of a tank panel due to forming or heat treatment problems is very costly. The idea of reducing the amount of scrap material and scrapped structural members has prompted the introduction of built-up structure for cryogenic tanks to be explored on the ALS program. A built-up structure approach that has shown improvements in life cycle cost over the conventional built-up approach is the use of SPF stiffened panels (reducing the overall part count and weight for the tank) resistance spot welded (RSW) to outer tank skin material. The stiffeners provide for general stability of the tank, while the skin material provides hoop direction continuity for the loads.

The three Type 1 crippling SPF stiffener concepts were designed by Rockwell International based upon past work performed by NASA-Langley on titanium stiffener concepts. The General Dynamics ALS loading requirements and RSW allowables were used in conjunction with past experience at Rockwell International with SPF of Al and Al-Li materials during the design of the stiffener components. The stiffener concepts were designed, structurally analyzed, fabricated, and tested during the initial part of this program (NAS1-18590 Task 5). The pre- and post-test analysis covered in this technical file document (TFD) along with the methodology utilized for the design analysis, and fabrication methodology of the Type 1 panels.

The objective of this program was to design and fabricate SPF stiffened panels that could be used for fabrication of low cost cryogenic tank structure for the ALS family of vehicles. The two-fold objectives of the crippling panel design and testing was to validate the structural efficiency of SPF stiffeners versus conventional stiffened configurations, and to differentiate between the structural performance of the three optimized SPF stiffener designs and between the two material systems (7475-T62 Al stiffeners joined to 2219-T81 Al skins, and 2090-T62 Al-Li stiffeners joined to 2090-T83 outer skins) used for the study.

THIS PAGE INTENTIONALLY LEFT BLANK.

2.0 OBJECTIVES

Three superplastic formed (SPF) hat stiffener concepts were designed by Rockwell to utilize the SPF process in combination with resistance spotwelding (RSW) for use as non-pressure stabilized cryogenic tank structure. The purpose of the optimized stiffener-to-skin concepts was to reduce the manufacturing and life cycle cost of large cryogenic LH₂ tank designs associated with ALS.

THIS PAGE INTENTIONALLY LEFT BLANK.

3.0 PROGRAM PLAN

The intent of the program is to investigate the application of Al and Al-Li superplastically formed structure (SPF) as a low cost manufacturing method for expendable launch vehicle structure. The tasks involved in this investigation include:

Task 1 - Structural Concept Selection

This task includes the development and optimization of structurally efficient and cost effective SPF stiffener design concepts, utilizing ALS prime contractor loading.

Task 2 - Superplastic Forming Study

This task develops the SPF parameters for fabrication of the compression panels, develops post-SPF thermal processing parameters, and generates material design data.

Task 3 - Joining Studies

This task develops resistance welding parameters for the material combinations selected during task 1 and 2, and examines the application of adhesive bonding in conjunction with the SPF stiffener panels.

Task 4 - Compression Panel Fabrication, Test, and Evaluation

This task includes the fabrication of four compression panel configurations (single stiffener, multiple stiffener, large-scale stiffened panel, and large-scale stiffened panel to panel joining and structural test and evaluation of the first three panel types.

Task 5 - NDE & Quality Assurance

This task will be conducted during the entire program and will result in a plan to fabricate quality SPF structure and resistance weldments.

Task 6 - Life Cycle Cost Estimating

This task will assess the cost benefits that SPF will provide to fabrication of cryogenic tank stiffened panels.

Task 7 - Automation and Scale-up

This task will develop a manufacturing plan to fabricate full-scale tank structure.

Task 8 - Reporting

This task assured documentation and transmission of data developed during this program.

THIS PAGE INTENTIONALLY LEFT BLANK.

4.0 TECHNICAL DISCUSSION

4.1 DESIGN AND ANALYSIS

4.1.1 ALS CONFIGURATION

The ALS vehicle loads supplied to Rockwell International were derived from the ALS-L vehicle configuration (refer to Figure 1) for a variety of loading conditions. These loading conditions consisted of ground handling, ground winds, maximum flight winds (Max Alpha-Q / Max Beta-Q), and booster burn out. The loads imposed by these conditions are critical for different areas of the vehicle depending upon the location along the vehicle length. The forward end of the vehicle was sized by flight winds and the aft end of the vehicle was sized by booster burn out and ground wind loads.

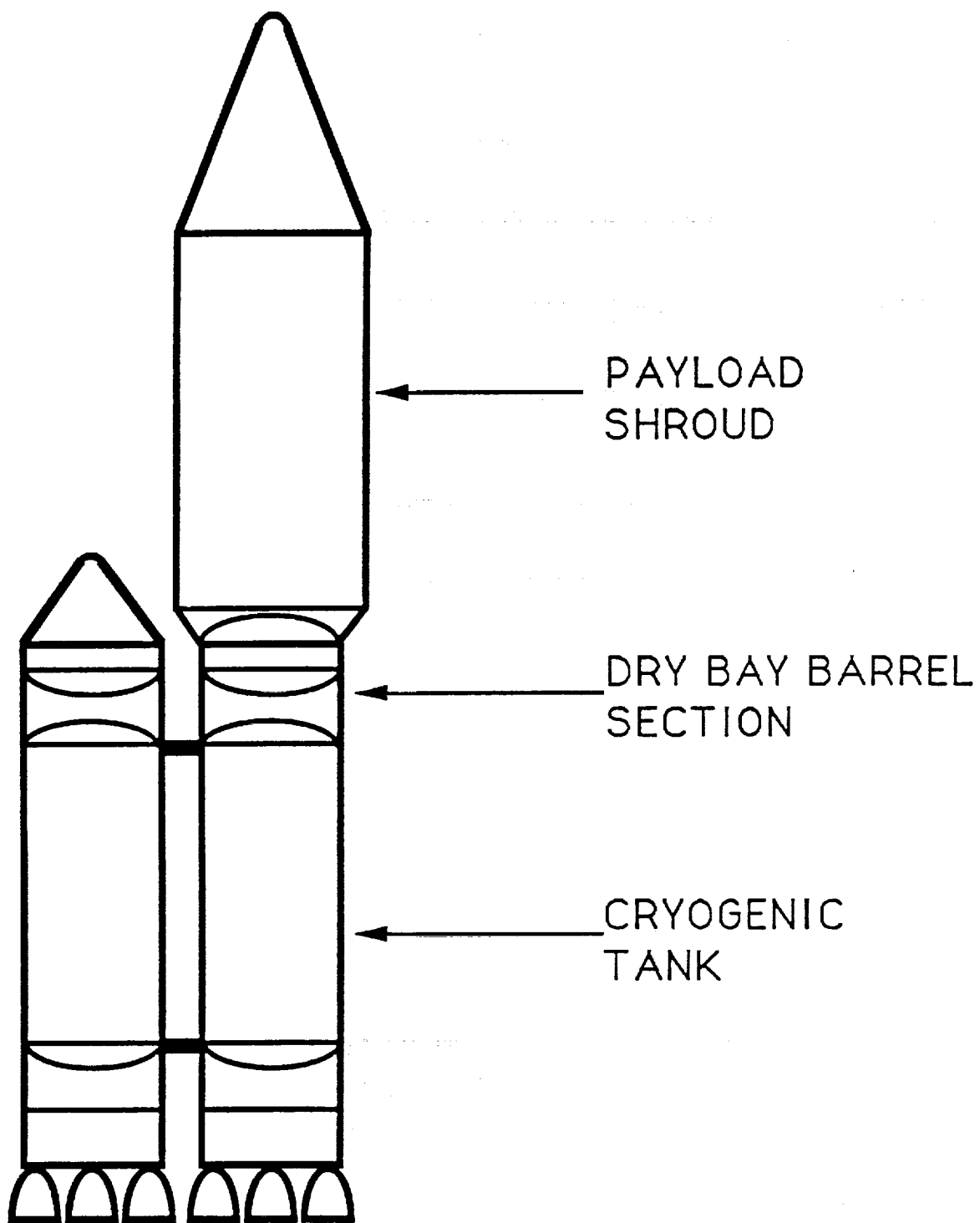
The ALS vehicles have been designed for relatively high launch rates and high launch availability as compared to previous launch vehicles. The vehicle is intended to remain on the launch pad through quite severe weather conditions, and launch without a launch or umbilical tower. The latter constraints require the vehicle to react the high ground wind loads while cantilevered from the aft end producing a very high bending moment near the aft end of the vehicle.

The increased launch availability of the ALS, requires the vehicle to fly through severe weather conditions, and high winds while aloft. This produces the maximum bending moments in the forward and central regions of the vehicle during Max Alpha-Q and Max Beta-Q flight periods. Representative load levels in the LH2 tank cylindrical section are depicted geometrically in Figures 2, 3, and 4. Figures 3 and 4 show where the loads, due to side winds at maximum Beta-Q can be interpolated with a plus or minus Mz component in the axial load (Nx) calculations.

The highest bending in the far aft end of the vehicle occurs just prior to booster burn out. This large moment is caused by the booster engine thrust pushing eccentrically on the core vehicle. At this time, most of the booster thrust is transferred to the core since the booster is nearly empty and provides very little inertia reaction against the thrust load. A summary of the design loads and additional design parameters for this program are summarized in Table 1.

4.1.2 MATERIAL DESIGN ALLOWABLES

The material properties used during design of the crippling panel SPF stiffener concepts, and the sizing of the outer tank skins are summarized in Tables 2 and 3.

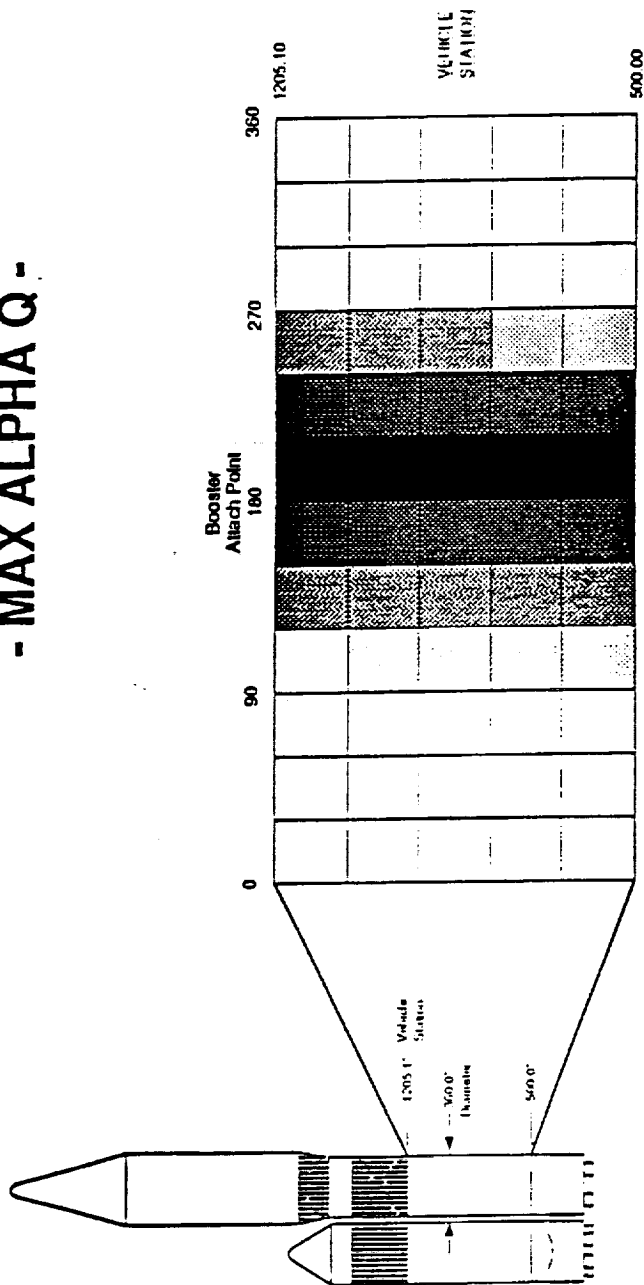


ALS CONCEPT

Figure 1. ALS-L Launch Vehicle Configuration.

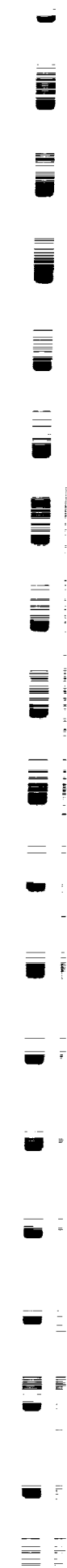
ALS-L Vehicle
"Baseline"

- MAX ALPHA Q -



FLAT PATTERN REPRESENTATION OF THE LOAD
LEVELS ON THE CORE TANK SECTION

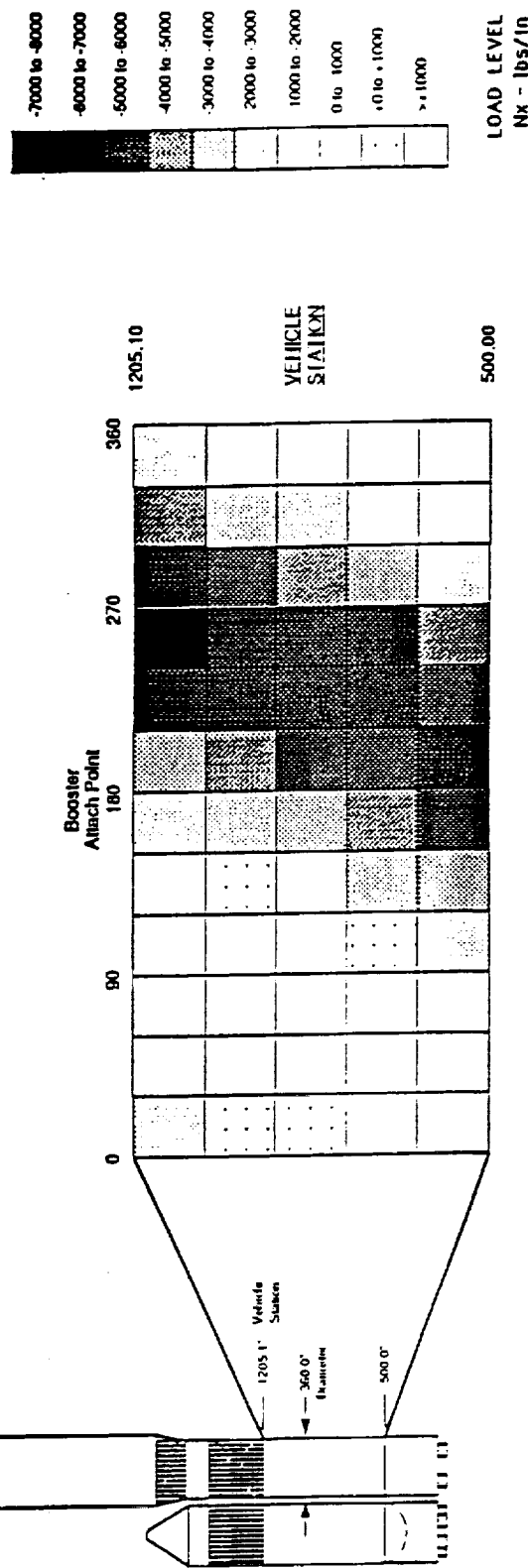
Figure 2. ALS-L Vehicle Load Level for the LH₂ Tank, Ultimate NX at Max Alpha Q.



The figure displays 18 individual gel electrophoresis results, numbered 1 through 18 from top to bottom. Each gel shows multiple horizontal bands of varying intensity and position, representing different DNA fragment sizes. The labels below each gel include sample identifiers such as 'S-1', 'S-2', 'S-3', 'S-4', 'S-5', 'S-6', 'S-7', 'S-8', 'S-9', 'S-10', 'S-11', 'S-12', 'S-13', 'S-14', 'S-15', 'S-16', 'S-17', and 'S-18'. Some gels also have additional labels like 'L' or 'H'.

ALS-L Vehicle "Baseline"

- MAX BETA Q - Negative Mz



FLAT PATTERN REPRESENTATION OF THE LOAD
LEVELS ON THE CONE TANK SECTION

Figure 4. ALS-L Vehicle Load Level for the LH₂ Tank, Ultimate NX at Max Beta Q, Negative Mz.

Table 1. Design Load Conditions ¹

1. N_x	=	-4237 lb/in.	2. N_x	=	-8474 lb/in.
N_y	=	0 lb/in.	N_y	=	0 lb/in.
N_{xy}	=	1028 lb/in.	N_{xy}	=	416 lb/in.
3. N_x	=	+8474 lb/in.	4. N_x	=	-7607 lb/in.
N_y	=	0 lb/in.	N_y	=	+7002 lb/in.
N_{xy}	=	416 lb/in.	N_{xy}	=	-119 lb/in.
5. Ultimate Tank Pressure	=	56 psi			
6. Temperature	=	Ambient			

On the basis of initial PASCO runs, Conditions 2, 4, & 5 sized the parts.

Table 2. Room Temperature Material Properties²

Material ⇒	2090-T83 Al-Li	2219-T81 Al-Li	7475-T62 Al. Post-SPF	2090-T62 Al-Li. Post-SPF	8090-T6 Al-Li	
Basis ⇒	S	B	S	Average	S	
Property ↓↓						
Ftu, Ksi	L	75	63	74	58	64
	45°	65				
	LT	73	63	75	60	57
Fty, Ksi	L	70	48	65	48	45
	45°	57				
	LT	66	47	64	50	48
Fcy, Ksi	L	63	49	64	47	50
	45°	60				
	LT	71	50	68	45	47
Fsu, Ksi		37	36	45	29	27
Fbru, Ksi						
	e/D = 1.5	100	78	97	75	68
	e/D = 2.0	126	95	110	95	77
E, Msi	L	11.5	10.5	10	11.3	11.5
	45°	11			10.9	
	LT	11.5			11.3	
Ec, Msi	L	11.8	10.8	10.5	11.7	11.7
	45°	11.4				
	LT	11.8				
μ		0.33	0.33	0.33	0.34	0.33
G, Msi		4.4	4.0	3.8	4.4	4.4
ρ, lb/cu in.		0.093	0.102	0.101	0.093	0.092

Table 3. Average Material Allowables Utilized for PASCO Analysis.³

Property ↓	7475-T62 SPF Stiffener	2219-T81 Outer Skin	2090-T62 SPF Stiffener	2090-T83 Outer Skin
F _{tu} , Ksi	74	63	58	65
F _{cy} , Ksi	64	50	45	60
F _{su} , Ksi	45	36	29	37
E, Msi	10	10.5	11.3	11.5
G, Msi	3.8	4	4.4	4.4
μ	0.33	0.33	0.34	0.33
ρ, lb/cu in	0.101	0.102	0.093	0.093

4.1.3 DESIGN CRITERIA

The design loads were generated from the ALS "L" configuration on the General Dynamics vehicle, and were represented (refer to Table 1) of a down-scale of the launch requirements for the vehicle. Specifically the reductions were in the ground wind requirements for the vehicle. The sizing of the outer skin thickness was based upon:

$$t_{\text{skin min.}} = P_{\text{ult}} \times R / F_{\text{tu}}$$

$$P_{\text{ult}} = (40 \text{ psi} \times 1.25) + (4.3 \text{ psi} \times 1.4) = 50 + 6 = 56 \text{ psi}$$

$$R = \text{Outer radius of the tank}$$

The preliminary spot weld spacing for the stiffened panels was determined as follows:

$$P_{\text{cr}} = \text{Critical Column Buckling Load} = (\pi^2 EI) / L^2$$

$$L^2 = (\pi^2 EI) / P_{\text{cr}} \quad L = \text{Length between spot weld}$$

$$\sigma_{\text{cr}} = (N_x) / t$$

$$N_x = 8474 \text{ Lb/in}, \quad t = 0.039 \text{ inch (required per the optimization analysis)}$$

$$\text{Assume that } P_{\text{cr}} = \sigma_{\text{cr}} \times A = (8474 / 0.25) \times .7 \times 0.039$$

$$L^2 = (9.87 \times 11.5 \times 10^6 \times (1/12) \times .7 \times (0.039)^3) / 925 = 393 / 925 = 0.4249$$

$$L = 0.65 \text{ inch}$$

4.1.4 BUILT-UP CRYOGENIC TANK DESIGN

The design and analysis of the built-up cryogenic tank structure was developed with the merger of SPF technology, resistance spotwelding parameters, and the LH₂ cryogenic tank structural loads for the ALS-L vehicle configuration. The design was also developed in keeping

with the overall ALS program objective of maintaining low life cycle costs. During the design and analysis phase, it became apparent that in a number of cases, that specific requirements of one technology diametrically opposed those required for the second technology or even within its own technology. An example of particularly severe opposing constraints observed with the use of resistance spot welding are illustrated with the example below and in Figure 5.

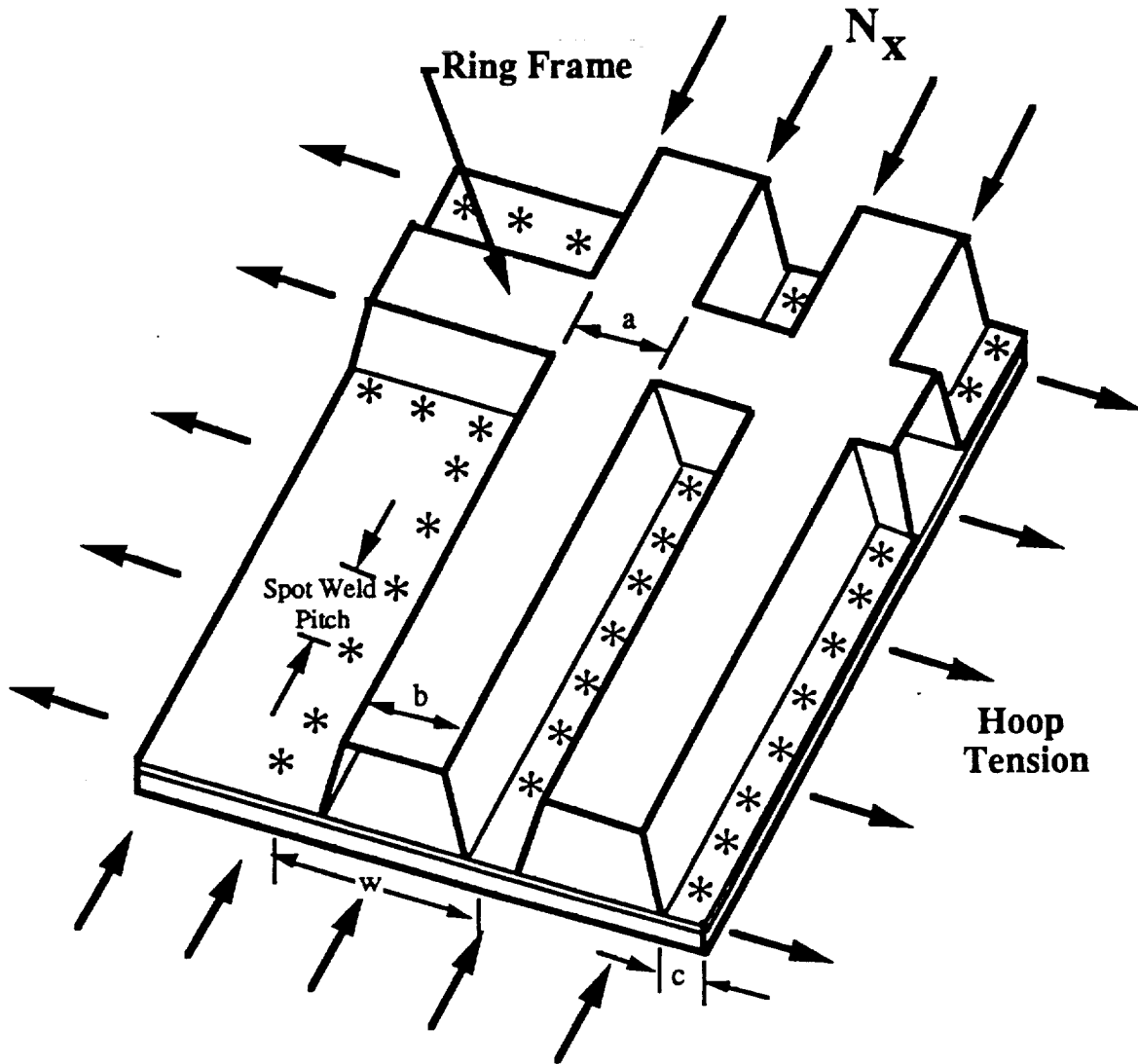
- The LH₂ tank is under internal pressure which drives the resistance inter-spotweld spacing (spotweld pitch) towards a maximum in order to minimize the degradation of the skin's parent metal strength (refer to Figure 6).
- Conversely, the axial loading (Nx) on the tank drives the inter-spotweld spacing towards a minimum to prevent inter-spot crippling.
- In addition, the spotweld process requires maximum inter-spot spacing to prevent electrode shunting during the weld operation.

The technology driven requirements when coupled with the high loading conditions typical of the ALS vehicles created some unique design challenges for optimizing the performance of light weight structure. In addition, general missile tank structural requirements dictate that stiffener failures (buckling) in the tank be local in nature rather than catastrophic, and that reduction in parent metal strength in the skin due to spotwelding should not result in rupture of the outer skin. Thus, the Rockwell International built-up tank structure integrated all the aforementioned design challenges into the development of the stiffened panels. The first step in the design of the panels was to establish the baseline design concept (refer to Figure 7) and assess the structural efficiency of the conventional baseline concept versus the SPF stiffener designs. The assessment of the structural efficiency is shown as Figure 8.

Several SPF stiffener designs were developed that would carry the launch loads and provide for improvements in the structural efficiency of the stiffened panels. The preliminary designs developed are shown in Figure 9. A qualitative trade study was conducted with Rockwell and General Dynamics personnel to down select three stiffener configurations that would be optimized, and tested as crippling stiffener panels. The results from the qualitative analysis (refer to Table 4) were very close due to the structural efficiency and producibility of each design, however, three stiffener configurations were selected that appeared to have high payoff for continued evaluation as crippling stiffener panels; stepped hat with curved cap, beaded web with flat cap, and the beaded web with the curved cap.

Three built-up stiffener concepts were analyzed with the established load conditions: a "Tee" section, a superplastic formed hat which optimizes the web thickness, overall weight, and

height, and a brake-formed constant-web-thickness hat section (refer to Table 5). An equivalent plate thickness per inch (t-bar) of the built-up stiffened panel geometry, was calculated from the combination of the skin and stiffener configuration and utilized during design optimization as the weight of the panel.



- | | | |
|---|---|---|
| a | = | Integral unsupported cap width at ring-to-stiffener intersection |
| b | = | Cap width |
| c | = | Stiffener-to-skin flange (Critical point for stiffener support of skin against wrinkling) |
| w | = | Spotweld hoop-wise pitch |

Figure 5. Hat Stiffener-Ring Configuration.

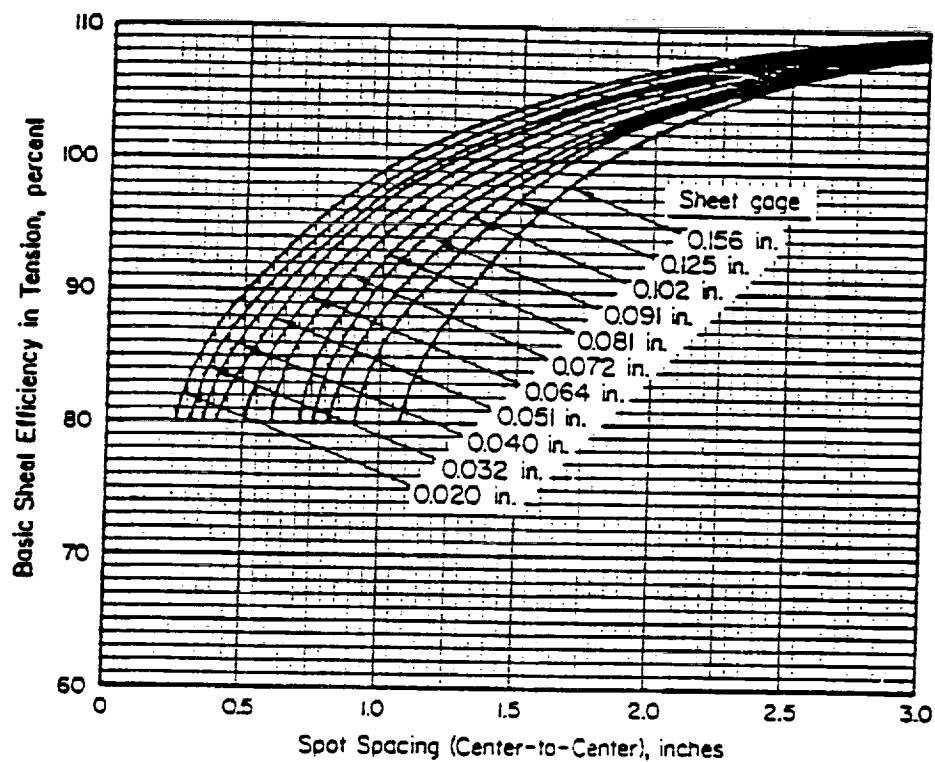


Figure 6. Effect of Spot Weld Pitch Versus Parent Metal Strength (Ref. MIL-HDBK-5).⁴

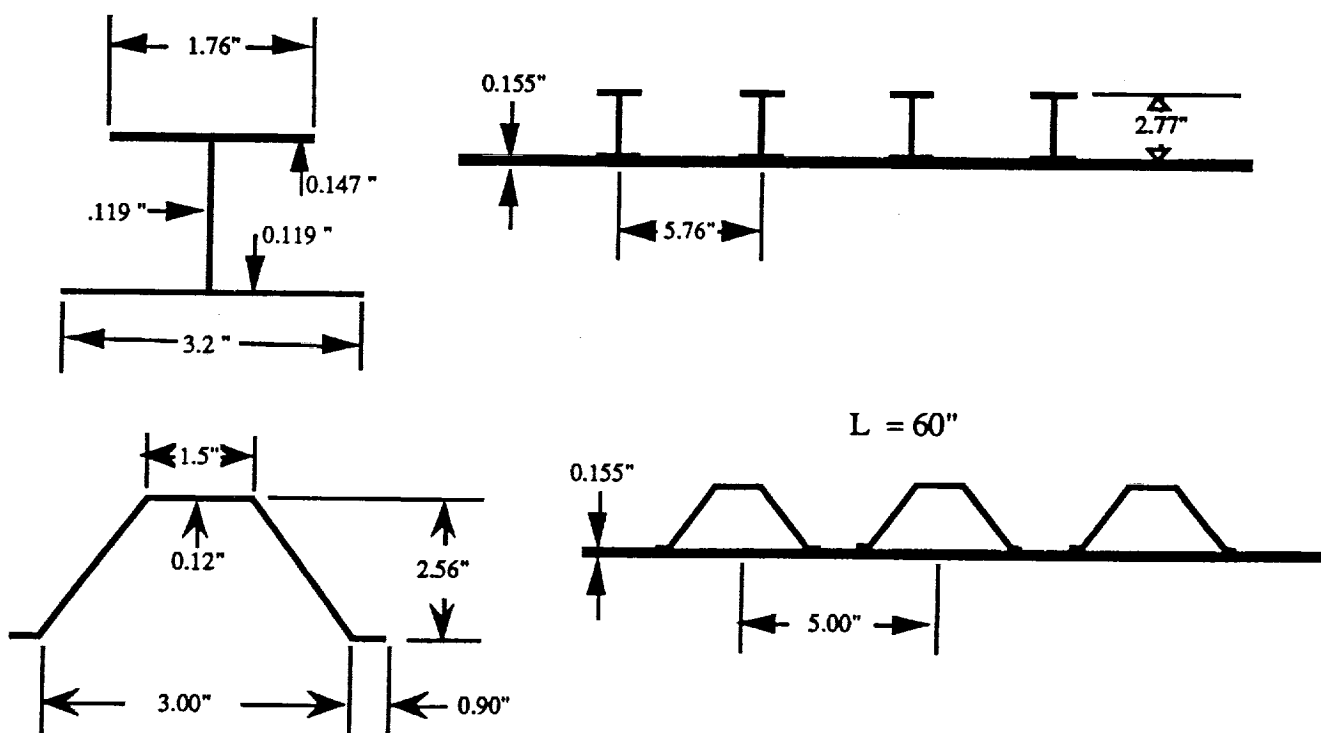


Figure 7. Baseline Conventional "T" and Hat Stiffener.

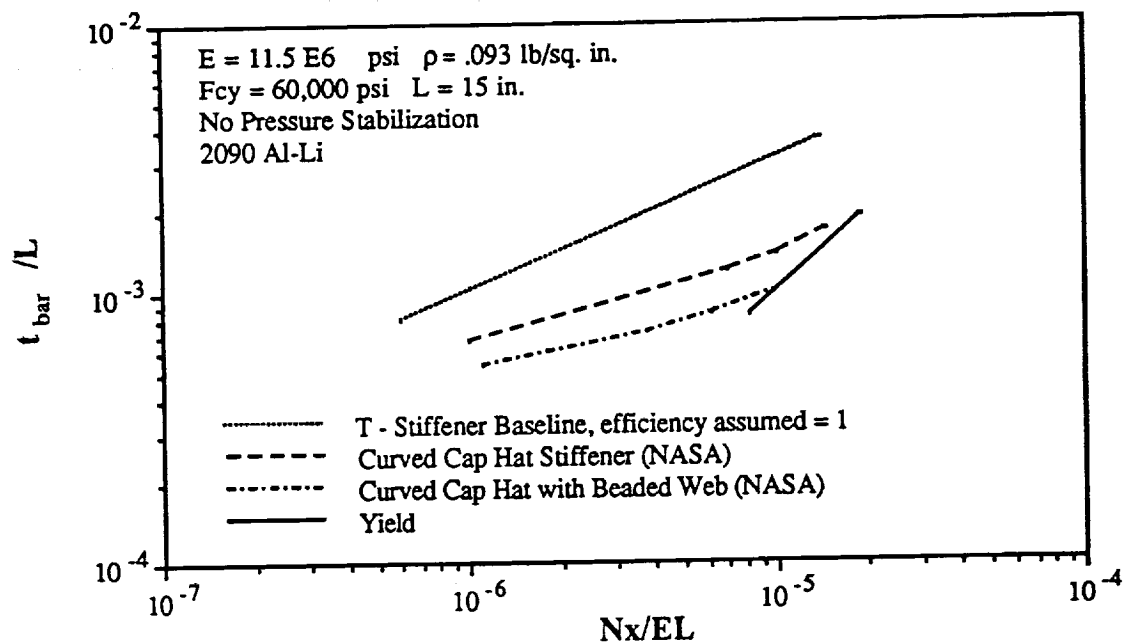
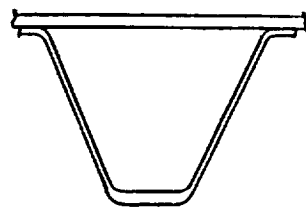
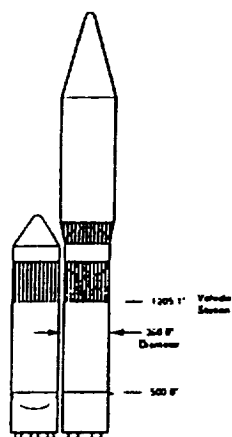
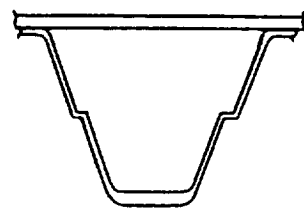


Figure 8. Structural Efficiency Curves for Conventional Baseline Stiffener and SPF Designs.

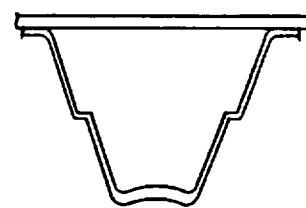
ALS-L Vehicle
"Baseline"



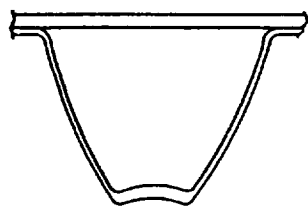
**BASIC HAT
STIFFENER**



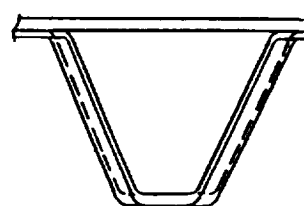
**STEP HAT
STIFFENER**



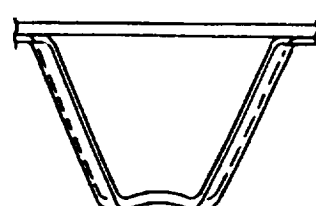
**STEP HAT W/
CURVED CAP**



CURVED HAT



BEADED WEB



**BEADED WEB W/
CURVED CAP**

Figure 9. Initial SPF Stiffener Designs.

Table 4a. Qualitative Trade Study.⁵

The qualitative trade study examines the relative ranking of the superplastic stiffener panels in relation to each other. The areas that were explored for the trade are listed below with explanations of their area of analysis.

Structural Efficiency = Subjective measurement based upon load bearing qualifications.

- | | | |
|---|---|---|
| 1 | = | Highly efficient design (comparable to "T" stiffener) |
| 2 | = | Efficiency close to the "T" stiffener. |
| 3 | = | Average structural efficiency. |
| 4 | = | Nominal structural efficiency. |
| 5 | = | Minimal structural efficiency. |

The structural efficiency of each stiffener panel is based upon the preliminary analysis performed on each design. The different designs (only SPF configurations were included in this analysis) were examined for their anticipated structural performance relative to an ideal "T" stiffener panel.

Labor Intensity = Number of manufacturing steps involved in fabrication of the panel.

- | | | |
|---|---|---------------------------------|
| 1 | = | 3 to 15 manufacturing steps. |
| 2 | = | 16 to 30 manufacturing steps. |
| 3 | = | 31 to 50 manufacturing steps. |
| 4 | = | 51 to 70 manufacturing steps. |
| 5 | = | 71 or more manufacturing steps. |

Manufacturing steps are defined as the number of different stations the part must go through to be completed (i.e., blank sheet, route edges, form, inspect, clean, heat treatment, check and straighten, chemically process, prime and paint, bond, cure, and final inspection). This example of a manufacturing process consists of 12 steps which break down into a labor intensity of 1.

Inspection Method = The values depend on the labor intensity and overall cost of the inspection method being examined.

- | | | |
|---|---|--|
| 1 | = | Production proven methods can be used, i.e., visual, configuration and identification. |
| 2 | = | Production proven methods (high skill radiographic or ultrasonic tests). |
| 3 | = | Limited experience methods (in production elsewhere). |
| 4 | = | Limited experience methods II (experimental). |
| 5 | = | No experience. |

The inspection methods include visual, penetrant, x-ray or experimental for the SPF panels only.

Table 4b. Qualitative Trade Study.

Confidence or Risk = This value is strictly subjective. It was determined by the past experience of the contractor in fabricating parts similar to designs for the material being used.

- 1 = The part being examined is similar to parts that have been production-fabricated with scrap rates less than 10 percent.
- 2 = The part being examined is similar to parts that have been production-fabricated with scrap rates of 30 to 50 percent.
- 3 = The part being examined is similar to laboratory demonstration parts of similar size and complexity.
- 4 = The part being examined is similar to laboratory parts, but smaller and simpler in design.
- 5 = The part being evaluated is feasible, but the contractor has no experience in making this part.

Tooling = The weighting values depend upon the complexity of the required tooling and its normality.

- 1 = No special tooling is required.
- 2 = No special tooling except weld jigs, assembly jig, etc.
- 3 = Special tooling similar to that used with other production parts.
- 4 = Special tooling similar to that used with smaller and simpler parts.
- 5 = Special tooling feasible but no history.

Definition: Weighting Factor = These weighting factors apply to the overall weighting for each phase in the analysis.

- 1 = Little effect on cost.
- 2 = Moderately low cost driver.
- 3 = Moderate cost driver.
- 4 = Moderately high cost driver.
- 5 = Major cost driver.

Table 4c. Qualitative Trade Study.

Weighting Factor =>	5		4		3		5		3		
Component Configuration	Structural Efficiency		Labor Intensity		Inspection Method		Confidence or Risk		Tooling		Total
Beaded Hat Stiffener (Superplastic Formed)	2	10	1	4	1	3	2	10	4	12	39
Curved Cap Hat Stiffener (Superplastic Formed)	3	15	1	4	1	3	2	10	3	9	41
Stepped Hat Stiffener (Superplastic Formed)	3	15	1	4	1	3	2	10	3	9	41
Stepped Curved Cap (A) (Superplastic Formed)	3	15	1	4	1	3	2	10	3	9	41
Beaded Curved Cap (Superplastic Formed)	2	10	1	4	1	3	2	10	4	12	39
Stepped Curved Cap (B) (Superplastic Formed)	3	15	1	4	1	3	5	25	5	15	62

The PANDA II computer modeling program⁶ and the design criteria loads were used to determine the optimum frame spacing that would provide general stability for the tank using the baseline T-stiffened design. Various runs with the PANDA II program indicated that major frames should be placed every 60 inches and that an intermediate frame should be placed every 30-inches (i.e., one intermediate frame between major frames, as shown in Figure 10) could produce a t_{bar} that would be competitive with the baseline concept. Parametric PASCO runs were made using the theoretical thinning profile generated for the SPF designs with 2.0- and 2.5-inch hat height and a 3.6-inch spotweld pitch. The same procedure was performed for the extruded hat-stiffened panels with optimized web thickness and height, and with the brake-formed hat-stiffened panels with constant-web-thickness. The minimum skin thickness required on all of the design concepts to contain the internal tank pressure of 56.0 psi ultimate ($t_{skin} = Pr/F_w$) resulted in a minimum outer-skin thickness requirement of 0.155 inch for the 2090-T83 Al-Li concept.

Thinning of the stiffener during the SPF process is dependent upon direction of forming. Forming that resulted with minimum thickness in the flange (outward thinning) required a male tool, and forming that resulted with the minimum thickness in the cap (inward thinning) required a female tool. The PASCO runs showed a lower t_{bar} for inward thinning with the 2.5-inch stiffener

(yielding a thick flange for prevention of inter-spotweld crippling), however, outward thinning was selected on the basis of increasing the cap thickness to alleviate local buckling in the unsupported length of the hat-frame cap and also for its ability to increase the Euler column allowable of the stiffened panels. The outward thinning 2-inch depth hat was selected over the outward thinning 2.5-inch depth hat on the basis of having a slightly lower t_{bar} (refer to Figure 11) thus reducing the overall Life Cycle Cost of the vehicle. The beaded web radius (0.25 inch) was used in the design based on successful designs that used the standard sinusoid bead configuration in several Rockwell aircraft configurations.

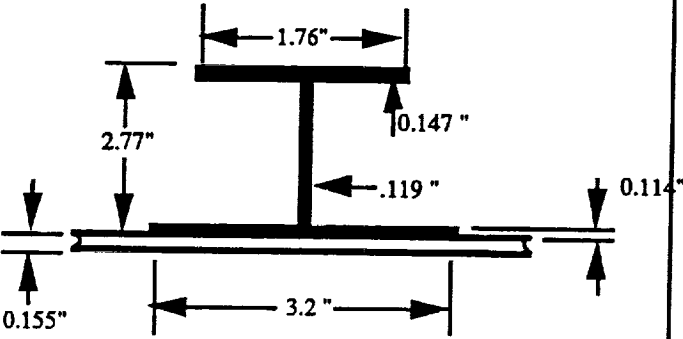
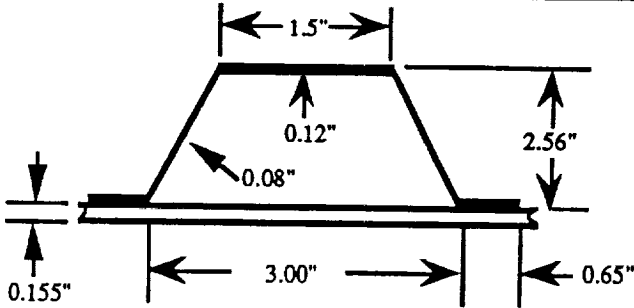
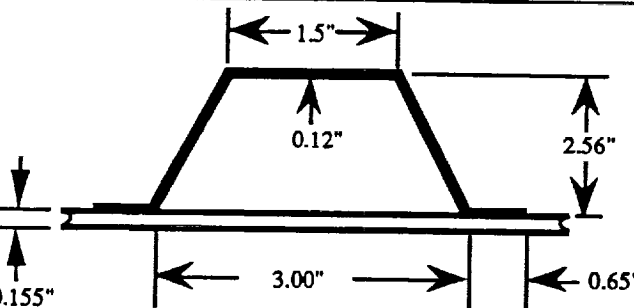
The hoop-wise spotweld pitch (refer to Figure 5) for the crippling panels was selected in order to provide clearance for the spotwelding equipment during fabrication and to minimize the fabrication costs by maintaining one row of spotweld between each stiffener. The one remaining requirement to be addressed during the panel design was the minimum spot weld pitch (refer to Figure 5). The pitch was selected based upon the requirement to minimize inter-spot crippling during axial loading on the specimen, while preventing severe reductions in outer skin parent metal strengths or shunting during welding. An inter-spot pitch of one inch was initially selected to maximize the performance of the spot welds during testing, but was increased to 1.125 inches based upon further analysis of reductions in parent skin strength and structural performance of the skin-stringer structure.

In summary, the initial ALS LH₂ vehicle superplastic formed stiffener designs were based on a 2 inch depth hat configuration, that utilized a 4.5-inch hoop-wise spotweld spacing, a 1.125 inch inter-spotweld pitch, and with 30-inch intermediate frames required between the 60 inch major ring frames.

4.1.5 CRIPPLING PANEL DESIGN

A length of 15 inches was selected to insure local buckling in the (refer to PASCO results shown in Table 6 and 7) crippling specimen panels during testing. Material was procured at two thicknesses at the onset of the program based upon predicted loads on the ALS-L vehicle in order to alleviate supply problems during fabrication. The fluctuations in the loading requirements for the program resulted in thicker stiffener configurations and outer skin materials for the crippling panels than the final loading requirements necessitated. Thus the improvements in panel weight (driving the life cycle cost savings up) and performance due to the change in thickness would further benefit the overall built-up concept approach.

Table 5. Summary of Baseline Design (Via Panda II).

Configuration	Frame Pitch (in.)	Stiffener to Skin (Area Ratio)	Moment of Inertia (INA)	Stiffener Centroid \bar{y} (in.)	Stiffener Pitch (in.)	t_{bar} (in.)
 <p>I Stiffened Baseline</p>	60	1.6	1.9	0.81	5.76	0.277 0.318 with spotweld requirement
 <p>Regular Hat (Opt. Web)</p>	60	1.48	1.3	0.92	5.0	0.295
 <p>Regular Brake Formed Hat</p>	60	2.08	>1.3		5.0	0.347

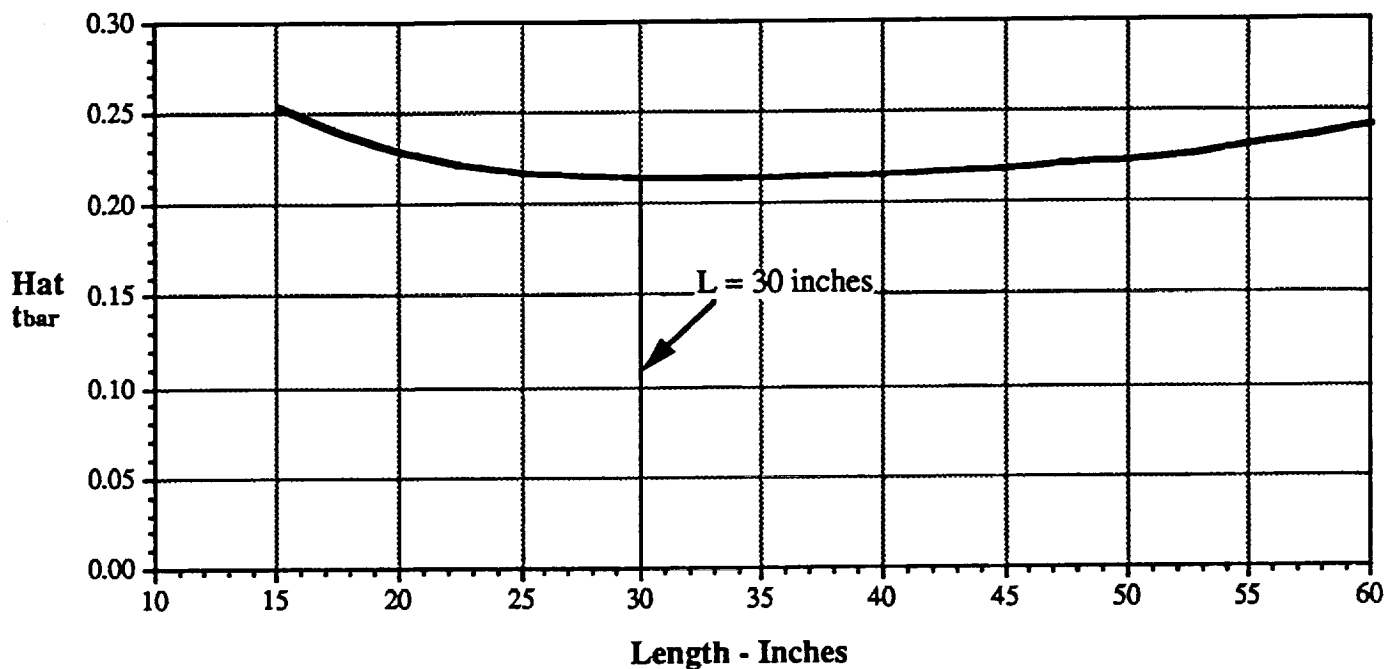


Figure 10. Length Between Intermediate Rings Versus Hat t_{bar}



Figure 11. Stiffener Height versus Hat t_{bar} for the Stepped Hat. PASCO Analysis for Outward Thinning.

Table 6. Summary of PASCO Analysis Results for Stepped Hat and Beaded Web Hat Sections Formed from 7475 Al Joined to 2219-T81 Al Skins.

Stiffener Length (in.)	Cap Width (in.)	Vehicle Loading (Lbs.)	Stiffener/Skin Factor (in./in.)	Failure Mode
15 (S.H.) 15 (S.H.)	0.8 0.8	Nx = 10,000 Nx = +7607 Ny = -7002	1.16 1.10	Buckling L = 3.75" Local Skin Tension
30 (S.H.) 30 (S.H.)	0.8 0.8	Nx = 10,000 Nx = +7607 Ny = -7002	1.05 1.28	Buckling L = 30" Local Skin Tension
15 (B.H.) 30 (B.H.) 30 (B.H.)	0.8 0.8 0.8	Nx = 10,000 Nx = 10,000 Nx = +7607 Ny = -7002	1.00 0.72 0.95	Buckling L = 3.75" Buckling L = 30" Buckling L = 30"
15 (S.H.) 15 (S.H.) 15 (S.H.)	1.1 1.4 1.4	Nx = 10,000 Nx = 10,000 Nx = +7607 Ny = -7002	1.22 1.20 1.10	Local Skin Compression Buckling L = 3.75 Local Skin Tension
30 (S.H.) 30 (S.H.)	1.4 1.4	Nx = 10,000 Nx = +7607 Ny = -7002	1.20 1.10	Buckling L = 3.3" Local Skin Tension

Table 7. Summary of PASCO Analysis Results for Stepped Hat and Beaded Web Hat Sections Formed from 2090 Al-Li Joined to 2090-T83 Al-Li Skins.

Stiffener Length (in.)	Cap Width (in.)	Vehicle Loading (Lbs.)	Stiffener/Skin Factor (in./in.)	Failure Mode
15 (S.H.) 15 (S.H.)	0.8 0.8	Nx = 10,000 Nx = +7607 Ny = -7002	1.13 1.14	Local Hat Compression Local Hat Compression
30 (S.H.) 30 (S.H.)	0.8 0.8	Nx = 10,000 Nx = +7607 Ny = -7002	1.13 1.14	Local Hat Compression Local Hat Compression
15 (B.H.) 30 (B.H.) 30 (B.H.)	0.8 0.8 0.8	Nx = 10,000 Nx = 10,000 Nx = +7607 Ny = -7002	1.00 0.78 1.00	Buckling L = 3.75" Buckling L = 30" Buckling L = 30"

An advantage of the SPF process over conventional sheet metal forming practices is that thinning in the part can be tailored per design requirements. Thinning for the stiffener during the SPF process is dependent upon direction of forming and forming strain rate. Figures 12 and 13 depict the theoretical thinning profile for the crippling stiffener test specimens (the stepped hat and beaded hat stiffeners respectively), from the Rockwell International-SPF thinning and flow stress/strain code. The Rockwell pressure versus time modeling tool was developed under internal research and development funding during the 1970's and 1980's. The model utilizes superplastic uniaxial flow stress and strain hardening behavior of a desired material system in conjunction with the required part or tool geometry. The model generates a forming pressure profile, based upon the aforementioned parameters, and a stage-by-stage (simple cup forming to complex side wall and corner forming) prediction of the thinning behavior of the material during the forming operation. The model has been successfully used for aluminum, aluminum-lithium materials, titanium (SPF and SPF/DB), and other high temperature materials.

Parametric runs using PASCO were made using the theoretical thinning profile of both stepped hat and the beaded hat stiffened panels at various lengths and are shown in the matrix below. The results from the analysis are summarized in Tables 8 through 11.

Parametric Runs

- a. Frame spacings; 15.0 inches; 30.0 inches; and 60.0 inches
- b. Depth of the stiffeners: 2.0 inches and 2.5 inches
- c. Inward and Outward Forming

The crippling stiffeners were fabricated from the 7475-SPF Aluminum (starting gage = 0.100 inch) and 2090-SPF Al-Li the (starting gage = 0.090 inch). The measured thinning profile from the formed parts resulted in range of flange thickness from 0.060 to 0.070 inch. The resulting allowable inter-spot pitch was equal to 1.125 inches. The resulting nugget diameter obtained during welding was 0.040 inch with an inter-spot crippling strength of 50,000 psi. The inter-spot crippling strength was slightly above the yield for the skin material which yielded a 95% hoop tension efficiency; hence, a satisfactory compromise was accomplished for the design of the Type 1 crippling specimens.

The cross-sections of the selected crippling stiffeners are shown in Figure 14 and Reference Drawing L9111392 shown in section 4.4.1.2, Figure 214. A 0.190 inch skin thickness was utilized to preclude the generation of an additional resistance spot weld schedule so as not to

impact the program schedule. The skin was machined as shown in the drawings to provide for local failure of the stiffener component.

4.1.5.1 PASCO Analysis

The PASCO (Panel Optimization/Analysis) program developed by NASA-Langley Research Center⁷ was used to develop and analyze the SPF stiffener configurations. The PASCO program has the ability to handle curved parts along with thinning differences that are indicative of the SPF process⁸. The input to the PASCO program for the stepped hat and the beaded hat configurations are shown in Tables 12 and 13 and Appendix A. These inputs utilized the average thicknesses that were measured on the formed stiffener configurations for the inputs into the program.

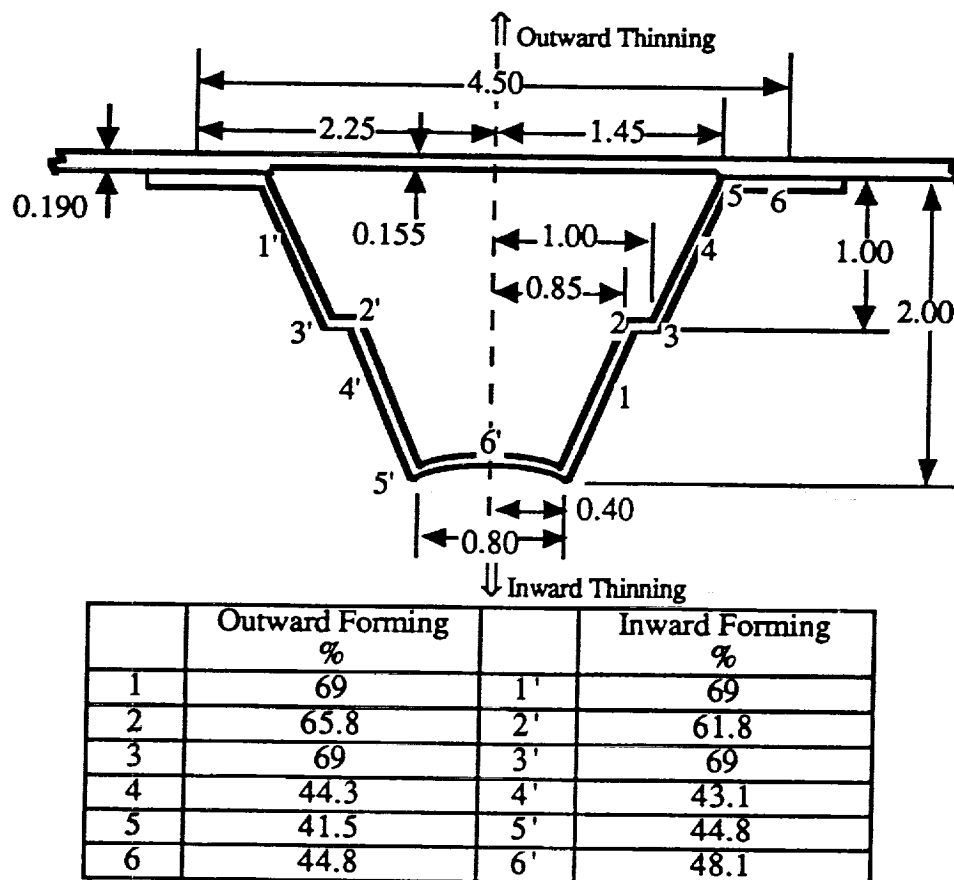
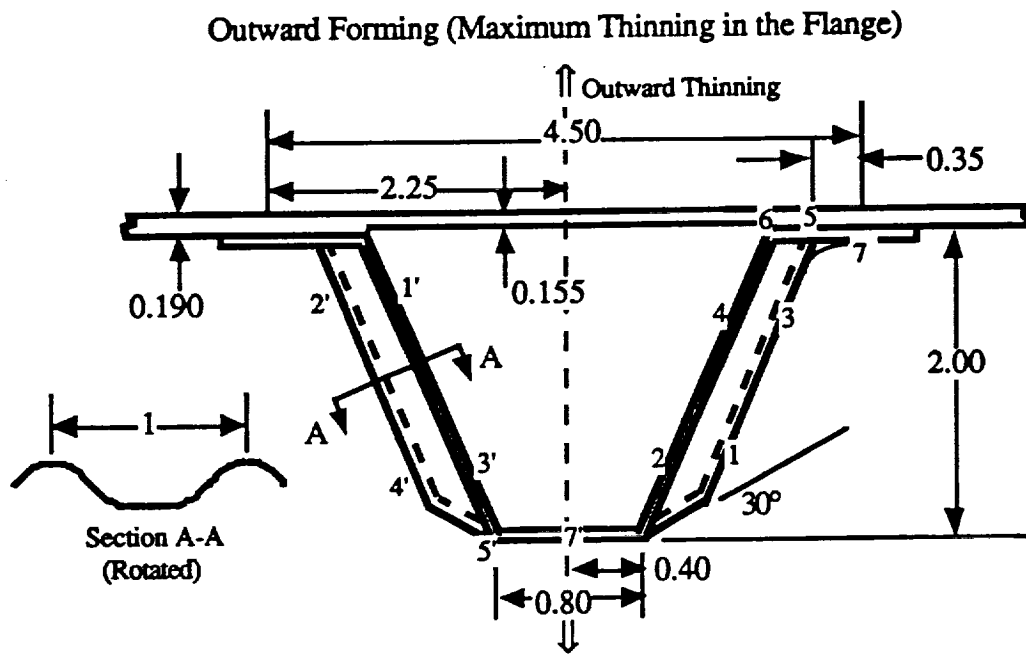
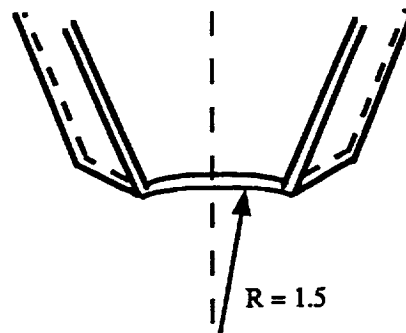


Figure 12. Selected Stepped Hat Concept Design for Type I Crippling Panels and the Theoretical Thinning at Selected Points on the Stiffener.



a) Beaded Web with Flat Cap



b) Beaded Web with Curved Cap

	Inward Forming %		Outward Forming %
1'	67.2	1	75.1
2'	45.2	2	50.2
3'	47.7	3	66.0
4'	31.9	4	44.1
5'	44.8	5	41.8
6'		6	29.0
7'	47.7	7	44.1

Figure 13. Beaded Hat Concept Designs for Type I Crippling Panels and the Theoretical Thinning at Selected Points on the Stiffener.

Table 8. Summary of PASCO Results for the 2090-T62 Al-Li 2-inch Stepped Hat Stiffener.

Ring Pitch (in.)	t_{bar}	Mode	λ (Wavelength)	Eigenvalue Factor	t_f (in.)	t_c (in.)
OUTWARD THINNING						
15	0.248 + 3 Integral Frames	1	15.0	4.064	0.039	0.090
		2	3.75	1.514	0.039	0.090
		3	3.0	1.548	0.039	0.090
30	0.248 + 1 Integral Frames	1	30.0	1.925	0.039	0.090
		2	6.0	1.698	0.039	0.090
		3	4.286	1.542	0.039	0.090
		4	3.75	1.515	0.039	0.090
60	0.382	1	60	0.9918	0.093	0.217
		2	12	16.04	0.093	0.217
INWARD THINNING						
15	0.241 + 3 Integral Frames	1	15.0	4.332	0.086	0.040
		2	3.75	1.432	0.086	0.040
		3	3.0	1.461	0.086	0.040
30	0.241 + 1 Integral Frames	1	30.0	1.333	0.086	0.040
		2	6.0	1.801	0.086	0.040
		3	4.286	1.482	0.086	0.040
60	0.413	1	60	0.8223	0.118	0.254
		2	12	15.36	0.118	0.254

Skin Thickness = 0.156, Sized from the pressure loads on the LH2 tank.

t_f = Flange Thickness, t_c = Cap Thickness

Based Upon: N_x = -7606 lb/in, N_y = +7002 lb/in, N_{xy} = -119 lb/in, Pressure = 56 psi

Table 9. Summary of PASCO Results for the 2090-T62 Al-Li 2.0-inch Beaded Hat Stiffener.

Ring Pitch (in.)	t_{bar}	Mode	λ (Wavelength)	Eigenvalue Factor	t_f (in.)	t_c (in.)
OUTWARD THINNING						
15	0.306 + 3 Integral Frames	1	15.0	6.065	0.052	0.139
		2	3.0	2.5	0.052	0.139
		3	2.5	2.88	0.052	0.139
30	0.306 + 1 Integral Frames	1	30.0	2.045	0.052	0.139
		4	3.33	2.66	0.052	0.139
		6	2.72	2.65	0.052	0.139

Skin Thickness = 0.156, Sized from the pressure loads on the LH2 tank.

t_f = Flange Thickness, t_c = Cap Thickness

Based Upon: N_x = -7606 lb/in, N_y = +7002 lb/in, N_{xy} = -119 lb/in, Pressure = 56 psi

Table 10. Layered Modeling of 2090-T62 Al-Li 2.0-Inch Beaded Hat Stiffener Using the PASCO Analysis.

Ring Pitch (in.)	t_{bar}	Mode	λ (Wavelength)	Eigenvalue Factor	t_f (in.)	t_c (in.)
30	0.264	1	30.0	1.99	0.039	0.90
	+	4	4.287	1.44	0.039	0.90
	1 Integral Frames	6	2.308	1.47	0.039	0.90

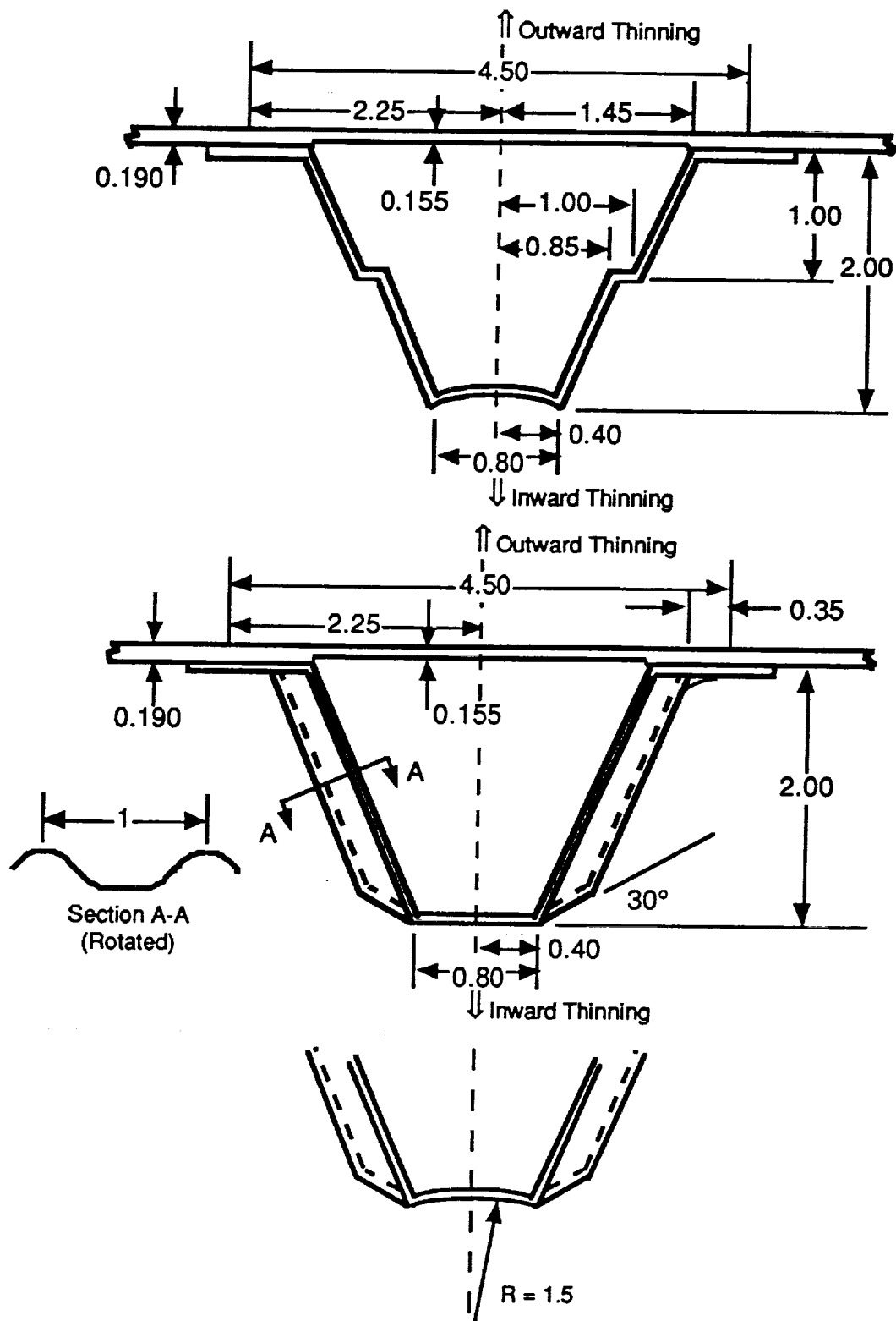
Table 11. Summary of the PASCO Results for the 2090-T62 Al-Li 2.5-Inch Stepped Hat.

Ring Pitch (in.)	t_{bar}	Mode	λ (Wavelength)	Eigenvalue Factor	t_f (in.)	t_c (in.)
OUTWARD THINNING						
30	0.25 +	1	30.0	2.976	0.039	0.090
	1 Integral Frames	3	4.286	1.238	0.039	0.090
60	0.272	1	60	0.9958	0.148	0.110
		2	12	2.851	0.148	0.110
INWARD THINNING						
30	0.240 +	1	30.0	2.086	0.086	0.040
	1 Integral Frames	3	4.286	1.125	0.086	0.040
60	0.413	1	60	0.9731	>0.17	>0.074

Skin Thickness = 0.156, Sized from the pressure loads on the LH2 tank.

t_f = Flange Thickness, t_c = Cap Thickness

Based Upon: N_x = -7606 lb/in, N_y = +7002 lb/in, N_{xy} = -119 lb/in, Pressure = 56 psi



$t(\text{start}) = 0.100$ inch for 7475 Beaded and Stepped Hats
 $t(\text{start}) = 0.090$ inch for 2090 Beaded and Stepped Hats

Figure 14. Final Type 1 Stepped Hat and Beaded Web Crippling Specimen Panel Designs.

Table 12. Typical PASCO Input for 7475 Al Stepped Hat Stiffener Concept.

```

Stepped Hat 4.5 " wide with 0.8" Cap - WA15 - 7475 Hat, 2219 Skin
$CONDATS
$SPANEL
MAXJJJ = 0
B = 0.3, 3.9, 0.5, 1.096586, 0.15, 1.096586, 0.8, 1.0, 0.4103647,
T = 0.0775, 0.031, 0.031, 0.031, 0.031, 0.035,
THET = 0.0, 0.0, 0.0,
LINK = 0,
MAT(1,1) = 1,
MAT(2,1) = 2,
MAT(3,1) = 2,
MAT(4,1) = 2,
MAT(5,1) = 2,
MAT(6,1) = 2,
KWALL(1,1) = 1, 2,
KWALL(1,2) = 1,
KWALL(1,3) = 2,
KWALL(1,4) = 3,
KWALL(1,5) = 4,
KWALL(1,6) = 5,
KWALL(1,7) = 6,
IWALL = 1, 2, 3, 4, 5, 6, 7, 1, 1,
HCARD = 4, -11, 4, -9, 8,
        4, -12, 6, -9, 8,
        4, -13, 4, 9, 8,
        4, -14, 6, 9, 8,
        10, 20, 3, 11, 5, 12, 7, 14, 5, 13, 3,
        5, 30, 1, 2, -20, 1,
ICARD = 5, 1, 2, 1, -990, 9000,
        5, 2, 11, 2, 3, 3,
        3, 3, 4, 11,
        3, 4, 5, 5,
        3, 5, 6, 12,
        3, 6, 7, 7,
        3, 7, 8, 14,
        3, 8, 9, 5,
        3, 9, 10, 13,
        3, 10, 11, 3,
        3, 11, 12, 1,
        3, 12, -990, 9000,
        EL = 15.0, IP = -2, JPRINT = 1,
MINLAM = 15, NOBAY = 1, FSTIFF = 1.0, NLAM(1) = 5, 7, 9, 11, 13, 15,
NX(1) = 10000,
NY(1) = 0,
NXY(1) = 0,
$
$MATER
E1(1) = 10.5 E6, E2(1) = 10.5 E6, E12(1) = 4.0 E6, ANU1(1) = 0.33, RHO(1) = 0.102,
E1 = 10.5 E6, E2(2) = 10.5 E6, E12(2) = 3.8 E6, ANU1(2) = 0.33, RHO(2) = 0.102,
ALLOW(1,1) = 1, 50.0 E3, -63.0 E3, 50.0 E3, -50.0 E3, 36.0 E3,
ALLOW(1,2) = 1, 64.0 E3, -74.0 E3, 64.0 E3, -64.0 E3, 45.0 E3,
$

```

Table 13. Typical PASCO Input for 7475 Al Beaded Hat Stiffener Concept.

```

Regular Hat with Beaded Web - HA15 - 7475 Hat, 2219 Skin - Measured
$CONDAT$
$PANEL
B = 0.3, 3.9, 0.65, 3*.718022, 1.0, 1.0, 0.3713907,
T = -0.0775, 0.030, 0.090, 0.045, 0.040,
THET = 5*0.0,
MAT(1,1) = 1,
MAT(2,1) = 1,
MAT(3,1) = 2,
MAT(4,1) = 3,
MAT(5,1) = 1,
KWALL(1,1) = 1, 2,
KWALL(1,2) = 1,
KWALL(1,3) = 2,
KWALL(1,4) = 3, 4,
KWALL(1,5) = 3, 4,
KWALL(1,6) = 3, 4,
KWALL(1,7) = 5,
IWALL = 1, 2, 3, 4, 5, 6, 7, 1, 1,
HCARD = 4, -11, 4, -9, 8,
        4, -12, 5, -9, 8,
        4, -13, 6, -9, 8,
        4, -14, 6, 9, 8,
        4, -15, 5, 9, 8,
        4, -16, 4, 9, 8,
        10, 20, 3, 11, 12, 13, 7, 14, 15, 16, 3,
        5, 30, 1, 2, -20, 1,
ICARD = 5, 1, 2, 1, -990, 9000,
        5, 2, 11, 2, 3, 3,
        3, 3, 4, 11,
        3, 4, 5, 12,
        3, 5, 6, 13,
        3, 6, 7, 7,
        3, 7, 8, 14,
        3, 8, 9, 15,
        3, 9, 10, 16,
        3, 10, 11, 3,
        3, 11, 12, 1,
        3, 12, -990, 9000,
        EL = 15.0, IP = -2, JPRINT = 1, MAXJJJ = 0
MINLAM = 15, NOBAY = 1, FSTIFF = 1.0, NLAM(1) = 5, 7, 9, 11, 13, 15,
NX(1) = 10000,
NY(1) = 0,
NXY(1) = 0,
$
$MATER
E1(1) = 10.5 E6, E2(1) = 10.5 E6, E12(1) = 4.0 E6, ANU1(1) = 0.33, RHO(1) = 0.101,
E1(2) = 2.51 E4, E2(2) = 3.36 E6, E12(2) = 4.14 E5, ANU1(2) = 0.0, RHO(2) = 0.021,
E1(3) = 2.21 E4, E2(3) = 1.13 E6, E12(3) = 5.87 E5, ANU1(3) = 0.0, RHO(3) = 0.021,
ALLOW(1,1) = 1, 50.0 E3, -63.0 E3, 50.0 E3, -63.0 E3, 36.0 E3,
ALLOW(1,2) = 1, 64.0 E3, -74.0 E3, 64.0 E3, -74.0 E3, 45.0 E3,
ALLOW(1,3) = 1, 64.0 E3, -74.0 E3, 64.0 E3, -74.0 E3, 45.0 E3,
$

```

4.1.5.1.1 Stiffener Modeling -PASCO Approach

The stepped hat had a relatively straightforward input for the PASCO analysis; however, the beaded web stiffener input utilized the approach suggested by Dr. Davis of NASA-LaRC⁹. The Davis approach utilized three equivalent layers for modeling the sine wave web. The sine wave A and D matrices were determined by using an individual model of the sine wave web with PASCO. After the matrices were determined, a program was used that had been developed and furnished by Dr. Randall Davis, to determine the positive moduli and the pseudo-orthotropic layer thicknesses required by the PASCO program simulation. An example of the matrix for the 2090 beaded stiffener is shown as Figure 15. The average actual measured web thickness was 0.05 inch. (This translated for the 0.25 inch radius sine wave bead to the following stiffness matrices¹⁰.)

$$\begin{bmatrix} A & B \\ B & D \end{bmatrix} = \begin{bmatrix} 0.623E4 & 0 & 0 & 0 & 0 & 0 & 0 \\ 0 & 0.678E6 & 0 & 0 & 0 & 0 & 0 \\ 0 & 0 & 0.131E6 & 0 & 0 & 0 & 0 \\ 0 & 0 & 0 & 0.390E2 & 0 & 0 & 0 \\ 0 & 0 & 0 & 0 & 0.517E4 & 0 & 0 \\ 0 & 0 & 0 & 0 & 0 & 0 & 0.563E3 \end{bmatrix}$$

where

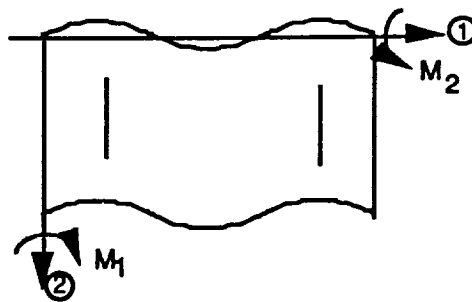


Figure 15. 2090 Al-Li PASCO Matrix for the Beaded Web Configuration
Sine wave web radius = 0.25 inch.

Using the PASCO program¹¹, the required PASCO input (3 orthotropic layer (symmetric)) was as follows:

$$h_{\text{layer 1}} = h_{\text{layer 3}} = 0.09$$

$$\begin{aligned} \epsilon_{11} &= 2.4069\text{E}4 & \epsilon_{12} &= 3.25\text{E}5 \\ \epsilon_{22} &= 3.2334\text{E}6 & \nu_{12} &= \nu_{21} = 0 \end{aligned}$$

R. Davis 3-Layer
Equivalent Program

$$h_{\text{layer 2}} = 0.09$$

$$\begin{aligned} \epsilon_{11} &= 2.117\text{E}4 & \epsilon_{12} &= 8.119\text{E}5 \\ \epsilon_{22} &= 1.067\text{E}6 & \nu_{12} &= \nu_{21} = 0 \end{aligned}$$

where ϵ_{11} = Modulus in 1 direction
 ϵ_{22} = Modulus in 2 direction
 ϵ_{12} = Shear Modulus
 $\nu_{12} = \nu_{21}$ = Poisson's Ratio

The actual web was not a perfect sine wave; however, an evaluation of the bending stiffness about the 1 axis of the actual web versus a sine wave indicated close agreement, which prompted the use of the sine wave simulation.

In order to have the weight of the sine wave web (or beaded stiffener) determined by the PASCO program, the weight factor was multiplied by the density of each pseudo layer. The result equal to 0.017 was obtained from $[(0.05 \text{ in} \times 0.093 \text{ lb/cu in}) / (3 \times .090 \text{ in})] = \{[\text{thickness} \times \text{density of the alloy (in this case it was 2090 Al-Li)}] / [3 \text{ (for three layers)} \times \text{original material thickness}]\}$. The moduli and layer thickness values developed with the Davis Methodology (described above), were used in the prediction of beaded web crippling panel failure loads. Similar matrices were used for the 7475 Al beaded webs as for the 2090 Al-Li beaded panels.

4.1.5.1.2 Typical PASCO Output

Each configuration was analyzed both for uniaxial loading (to compare with the panel test data) and for bi-axial loading of the actual tank structure. The output for the PASCO program produced the buckling wavelength (λ), the eigenvalue factor for λ , and the projected t_{bar} for the skin (0.155 inch) and stiffener combination. Thus, from PASCO, for the 15 inch long stepped-hat crippling panel fabricated from 7475-T62 stiffener joined to 2219-T81 skin the eigen value, wavelength, and failure mode are shown in Table 14.

Table 14. PASCO Output for the 15 Inch Long 7475-T62 Al Joined to 2219-T81 Al Stepped Hat Crippling Specimen.

t_{bar} (inches)	Mode	λ (inches)	Eigen Value	Length (inches)
0.256	1 (Yield)	15	2.79	15
	2 (Compression)	3.75	1.16	15

$$N_x \text{ applied to model} = 10,000 \text{ lbs./in.}$$

The lowest eigenvalue was obtained with the mode 2 failure and was recorded as 1.16. The failure load was calculated using the N_x loading, the lowest eigen value and the specimen width (10,000 lbs./in. x 1.16 x 6 in.) = 69,600 lbs.

The ultimate load of the part was calculated with the lowest material yield strength of the stiffener to skin combination, multiplied by the stiffener area (i.e., t_{bar}) and the specimen width

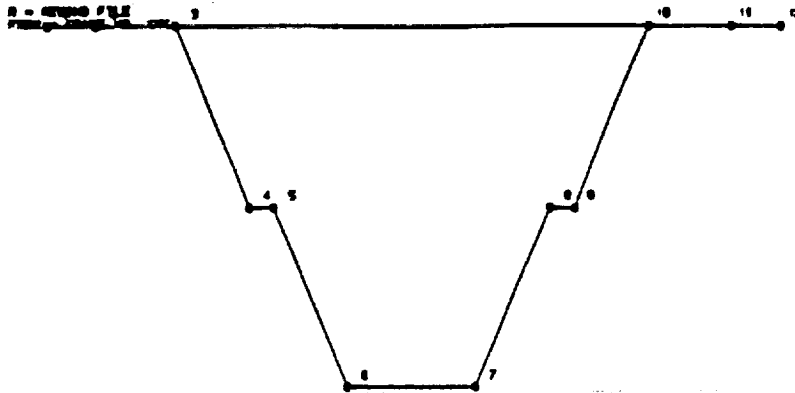
$$P_{ult} = 50,000 \text{ psi} \times 0.256 \text{ in.} \times 6 \text{ in.} = 76,800 \text{ lbs.} \quad (\text{yield of 2219-T81 skin})$$

The PASCO analysis, for the 15 inch long beaded web crippling panel fabricated from 7475-T62 stiffener joined to 2219-T81 skin resulted in the eigen value, wavelength, and failure mode shown in Table 15.

Table 15. PASCO Output for the 15 Inch Long 7475-T62 Al Joined to 2219-T81 Al Beaded Web Crippling Specimen.

t_{bar} (inches)	Mode	λ (inches)	Eigen Value	Length (inches)
0.264	1 (Yield)	15	1.83	15
	2 (Crippling)	3.75	1.00	15

Thus, initial buckling = 10,000 lbs./in. x 1.00 x 6 in. = 60,000 lbs. and Pult. panel = 50,000 psi x 0.264 in. x 6 in. = 79,200 lbs. The detailed output of the PASCO program may be seen in Appendix B. The choice of length, 15 inch length of the crippling panels, was selected to insure that the Euler column buckling responsible for failure was much larger than the yield strength of the skin. Included in the output format are the modal shapes at the various eigenvalues. The shapes for the stiffeners are shown in Figures 16 and 17.



Stepped Hat 4.5" Wide 0.8" Cap - WA15, 7475-T62 Hat with 2219-T81 Skin

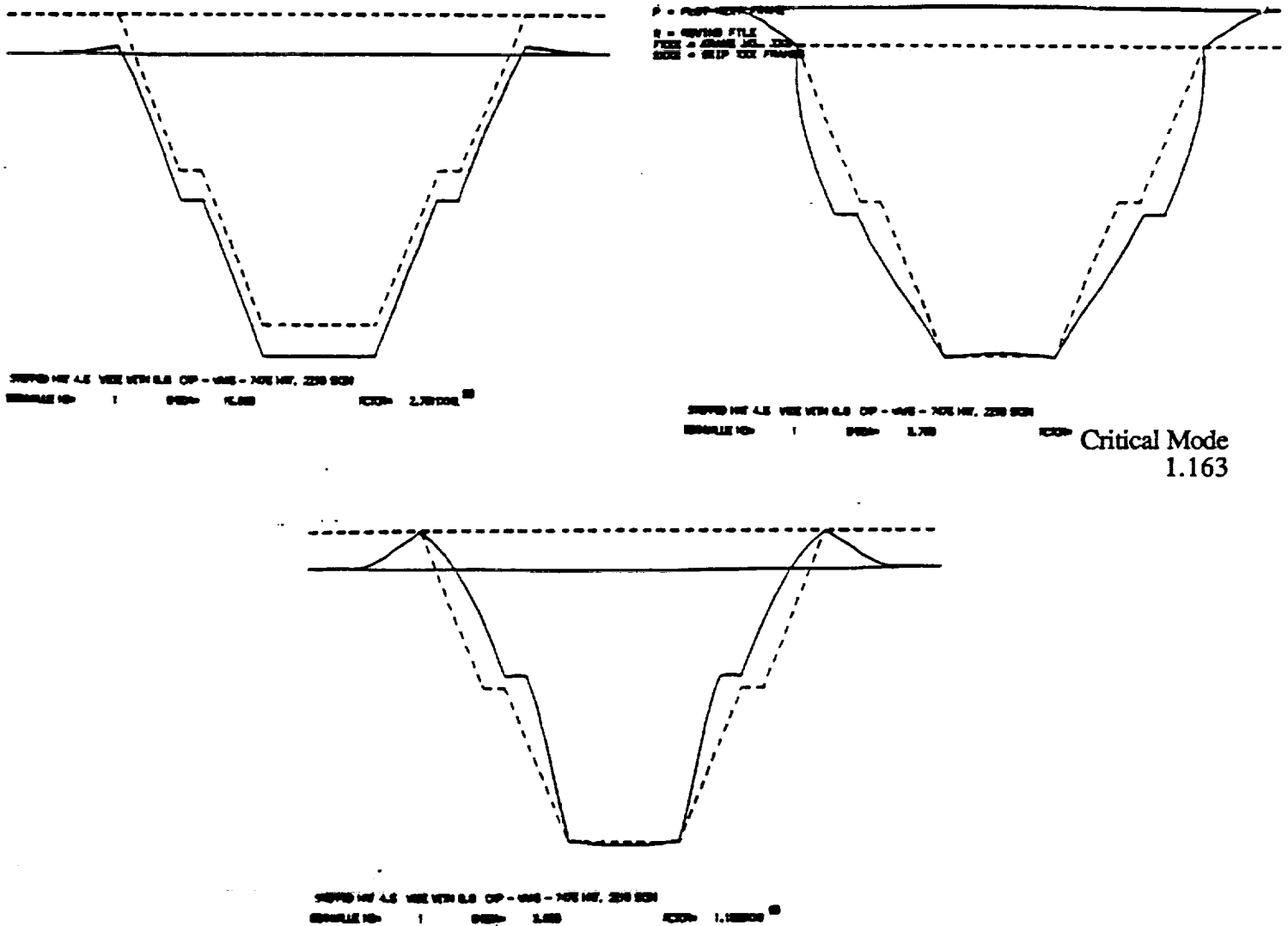
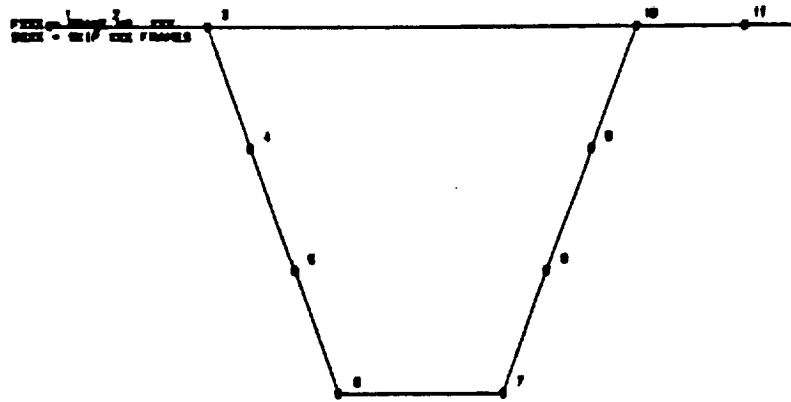
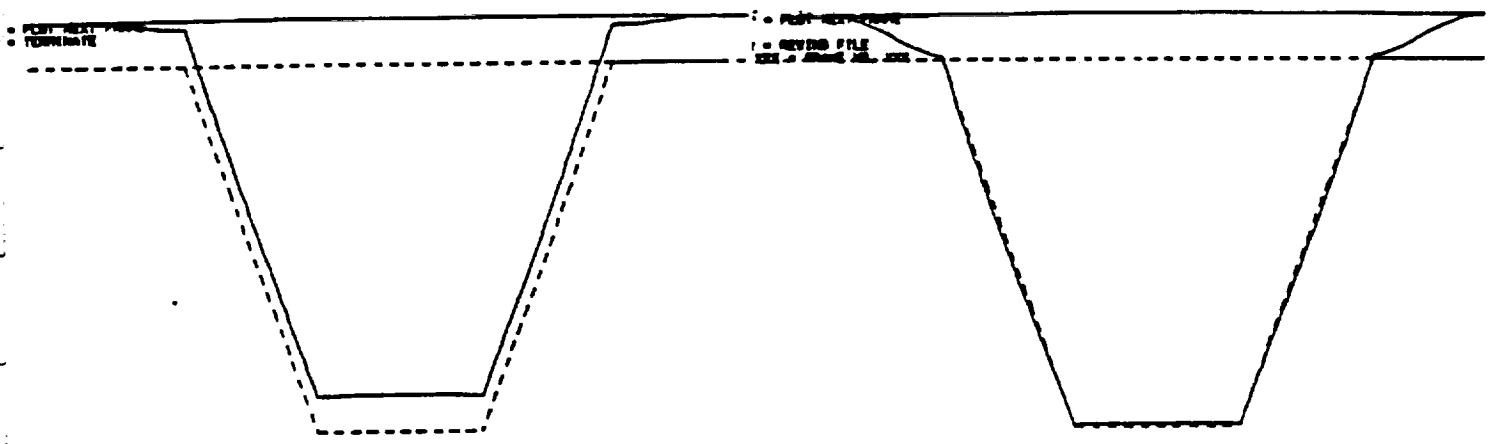


Figure 16. Typical Modal Shapes for Stepped Hat Stiffener Using PASCO Analysis.



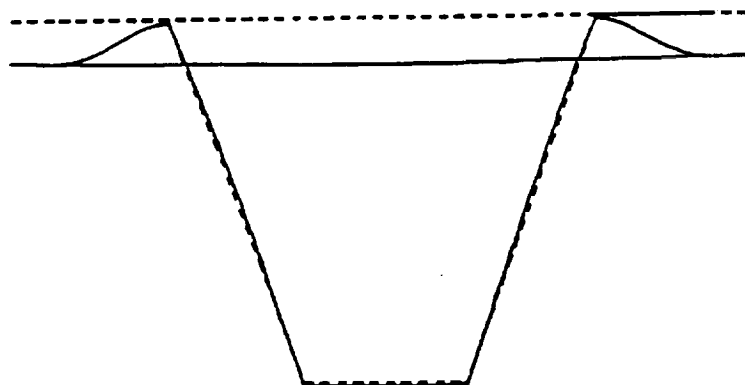
Regular Hat with Beaded Web 4.5" Wide 0.8" Cap - HA15, 7475-T62 Hat with 2219-T81 Skin



REGULAR HAT STIFFER WEB - HAT - 7475 T62 SKIN - PAPERED
 ELEMENT NO. 1 SPAN 15.000 SECTION 1.00000

REGULAR HAT STIFFER WEB - HAT - 7475 T62 SKIN - PAPERED
 ELEMENT NO. 1 SPAN 15.000 SECTION 1.00000

Critical Mode
 1.000



REGULAR HAT STIFFER WEB - HAT - 7475 T62 SKIN - PAPERED
 ELEMENT NO. 1 SPAN 15.000 SECTION 1.00000

Figure 17. Typical Modal Shapes for Beaded Hat stiffener Using PASCO Analysis.

4.1.5.2 NASTRAN Analysis

Single hat-stiffener NASTRAN finite element models were developed to study and visualize the buckling modes of the SPF stiffeners, and to compare results to the PASCO analysis. Initially, a 3 inch long finite element NASTRAN model was generated to study the local buckling modes for the stiffener configurations. Figure 18 presents the deformed shape for the first analysis mode. The eigenfactor of 1.085 would be equivalent to an allowable buckling load of 65,100 pounds for a 6-inch-wide Type 1 crippling specimen. Figure 19 presents the 15-inch-long finite element model of the stepped-hat specimen. The model is half of the SPF stiffener test specimen with symmetric boundary constraints at the center of the hat section. The model is uniaxially loaded with 10,000 lbs/in. distributed proportionally to the cross section area at each node. The NASTRAN buckling analysis solution resulted in an eigenfactor of 1.248 for the first buckling mode. This would be equivalent to a loading of $1.248 \times 10,000 \text{ lbs/in.} \times 6 \text{ in.} = 74,880 \text{ lbs}$ for the Type 1 specimen. The NASTRAN results were considered to be in close agreement with the PASCO program, as would be expected.

4.1.6 INTEGRALLY STIFFENED STRUCTURE

The overall stability of the tank required intermediate frames to be placed along the vertical length of the tank at 30 inch intervals (as observed from singly stiffener models at 15, 30 and 60 inch intervals during the development of the optimum stiffener configuration). The objectives of the providing an integral ring design were as follows:

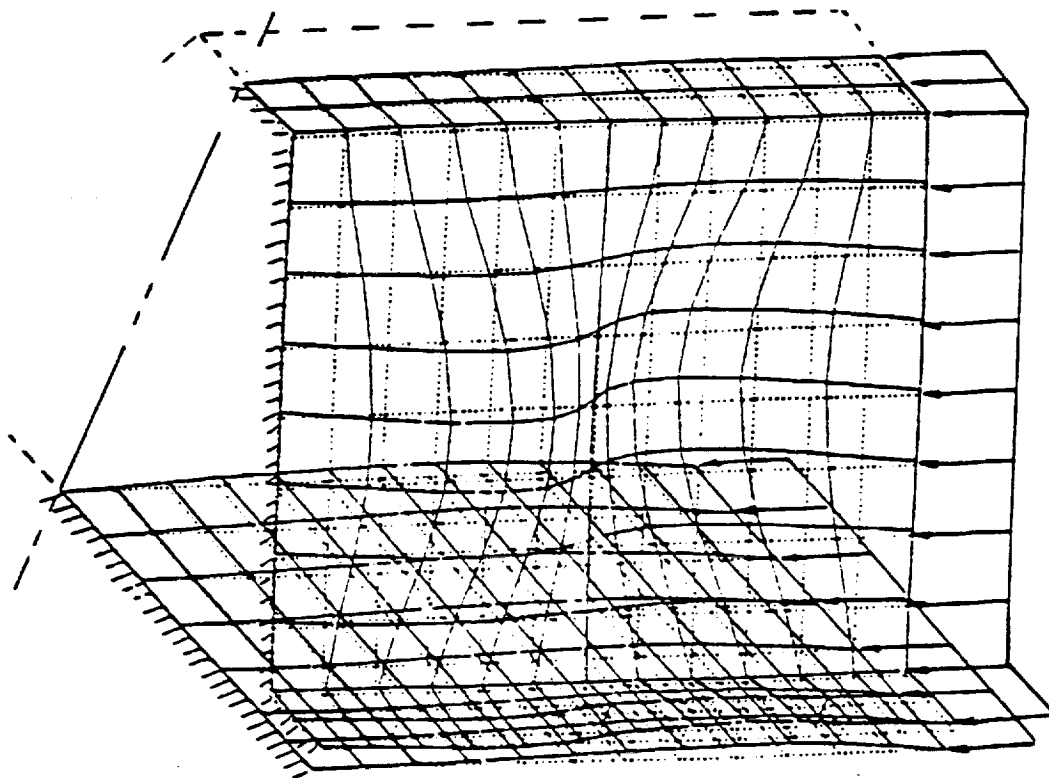
- Enforce a simple support node at the integral ring to prevent Euler column failure
- Fabricate the stiffeners and integral ring with one forming operation (one-step forming) to minimize fabrication cost
- Provide load path continuity for the N_x and N_y loads

The initial node concepts included several different configurations shown in Figure 20. These different approaches included an integral node ("pinch down" configuration), scab-on "T" frame, and a integral frame with a scab-on overlap ("J" frame).

The "pinch down integral frame" configuration allowed for one-step fabrication of the stiffened panels, however, due to past experience with a similar frame configuration (a door fabricated for an IR&D program at Rockwell on the B-1), beam column and "Kick" load effects can present eccentricity problems to the design. The other two concepts shown in Figure 20 (A2, and A3) required additional fabrication steps from the basic integral SPF version, which would result in an undesirable increase in manufacturing cost from the one step SPF process.

3 Inch Hat Stiffener

$N_x = 10,000 \text{ lb./in.}$



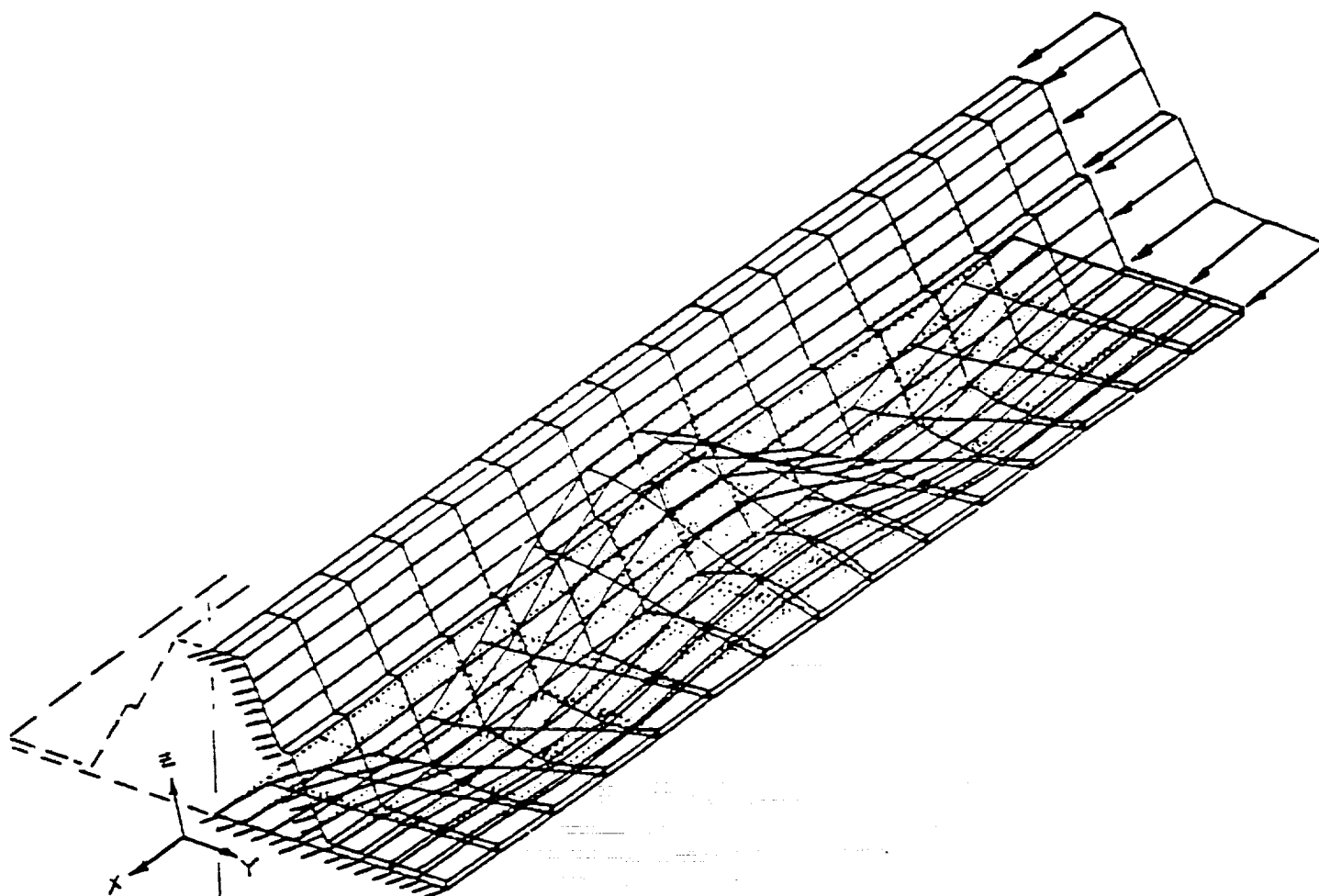
Eigen Factor = 1.085

Buckling Allowable Load: $1.085 \times 10,000 \text{ lb./in.} \times 6 \text{ inch} = 65,000 \text{ lbs.}$

Figure 18. NASTRAN Finite Element Model.

15 Inch Stepped Hat Stiffener (ALS 15S3.Bulk.Data)

$N_x = 10,000 \text{ lb./in.}$



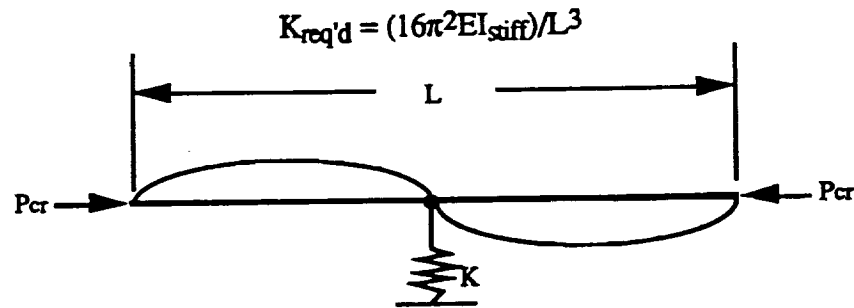
Eigen Factor = 1.248

Buckling Allowable Load: $1.248 \times 10,000 \text{ lb./in.} \times 6 \text{ inch} = 74,880 \text{ lbs.}$

Figure 19. NASTRAN Buckling Analysis.

Thus further evaluation of the joint configuration and the overall behavior of the tank was necessary prior to completion of the joint design.

The establishment of the integral ring stiffness utilized the "Theory of Elastic Stability" published by S. Timoshenko presented as follows: (8474 lb/in loading condition utilized for this analysis)



$$K_{req'd} = (16 \times 9.817 \times 11.5 \times 10^6 \times .48)/(60)^3 = 4035 \text{ lb/in (to enforce simple support node)}$$

The preliminary analysis indicated that for the particular loading scenario, an integral ring with an $I = 3 \text{ in}^4$ would enforce the node. As a result of the preliminary analysis, several node conditions were examined for the barrel section, along with the effects of the different loading conditions on the node geometry.

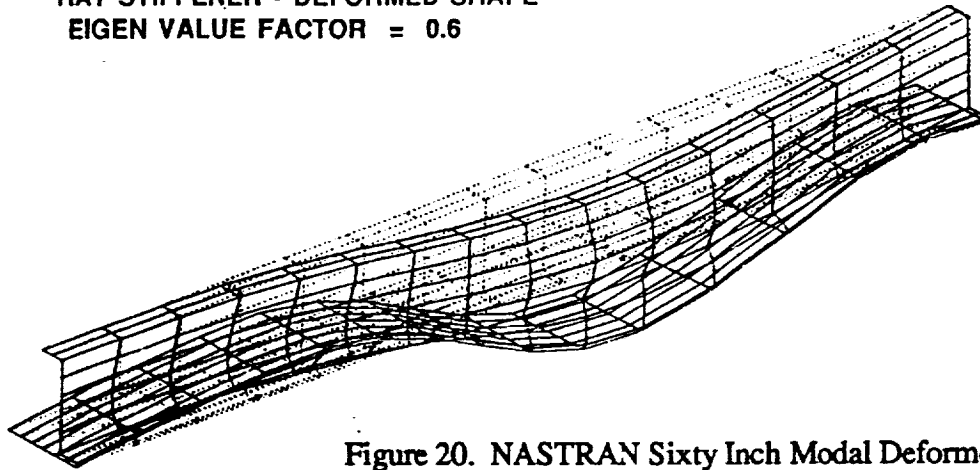
A parametric analysis was performed to correlate the results of the PANDA II, PASCO, NASTRAN and hand calculations. The PASCO analysis provided margin of safety and critical element failure modes for the stiffeners. For buckling modes, the wavelengths and load factor to failure was obtained. The allowable stiffener loading, which becomes critical as the stiffener length increases, was compared to the Euler column allowable.

$$P_{cr} = (\pi^2 EI)/L^2$$

Single hat stiffener NASTRAN models with lengths of fifteen, thirty and sixty inches were created to study the buckling modes. Figure 20 presents the sixty inch model deformed buckling mode. Table 16 presents a summary of the analysis studies for a two inch deep brake formed hat stiffener. An additional sixty inch long NASTRAN model was created with multiple stiffeners and a center C-Bar frame support. The NASTRAN model was used to determine the moment of inertia requirements for the intermediate ring (node) to enforce a nodal point. Previous hand calculations indicated that 3 in^4 was required to enforce the nodal point, however, the PANDA II results indicated approximately 0.5 in^4 while the NASTRAN results indicate approximately 1.0 in^4 . The latter result appears the most acceptable based upon Rockwell previous experience with structural

analysis using the NASTRAN program. Figures 21 and 22 present the first two modes and eigen factors from the multiple stiffener model.

60 INCH NASTRAN FINITE ELEMENT MODEL
HAT STIFFENER - DEFORMED SHAPE
EIGEN VALUE FACTOR = 0.6



CASE	4
DEFORMED SHAPE	
SF =	1.0E+01
TYPE =	ALL
DIST H =	1.00
Y =	1.00
ROT. X =	0.0
Y =	15.0
Z =	-15.0
SD =	1.0E+05
MODEL	
DATE :	02/06/98
TIME :	11:33:33

Figure 20. NASTRAN Sixty Inch Modal Deformed Buckling Mode.

Table 16. Summary of Parametric Study for 2.0 Inch Deep Hat Stiffener.

Ring Pitch	t _{bar}	Analysis Type	Mode	Lamda (Wavelength)	Eigen Value Factor	t _f	t _c
15 Inch	.295	PASCO	1	15 Inch	6.98	.080	.080
			4	1.67 Inch	2.4		
		NASTRAN (C-Bar Model)	1	15 Inch	7.56		
		NASTRAN (Plate Model)		2.0 Inch	2.7		
		Euler Column		15 Inch	6.7		
V	V	Compression Allowable		Local	1.95	V	V
30 Inch	.295	PASCO	1	30 Inch	2.18	.080	.080
			4	2.0 Inch	2.43		
		NASTRAN (C-Bar Model)	1	30 Inch	1.88		
		NASTRAN (Plate Model)		2.5 Inch	1.4		
		Euler Column		30 Inch	1.67		
V	V	Compression Allowable		Local	1.95	V	V
60 Inch	.295	PASCO	1	60 Inch	0.58	.080	.080
		NASTRAN (C-Bar Model)	1	60 Inch	0.47		
		NASTRAN (Plate Model)	1	60 Inch	0.6		
		Euler Column		60 Inch	0.42		
V	V	NASTRAN (Multiple C-Bars with center frame support-TYPE 3)		60 Inch	1.09	V	V

t_f = thickness of flange, t_c = thickness of cap

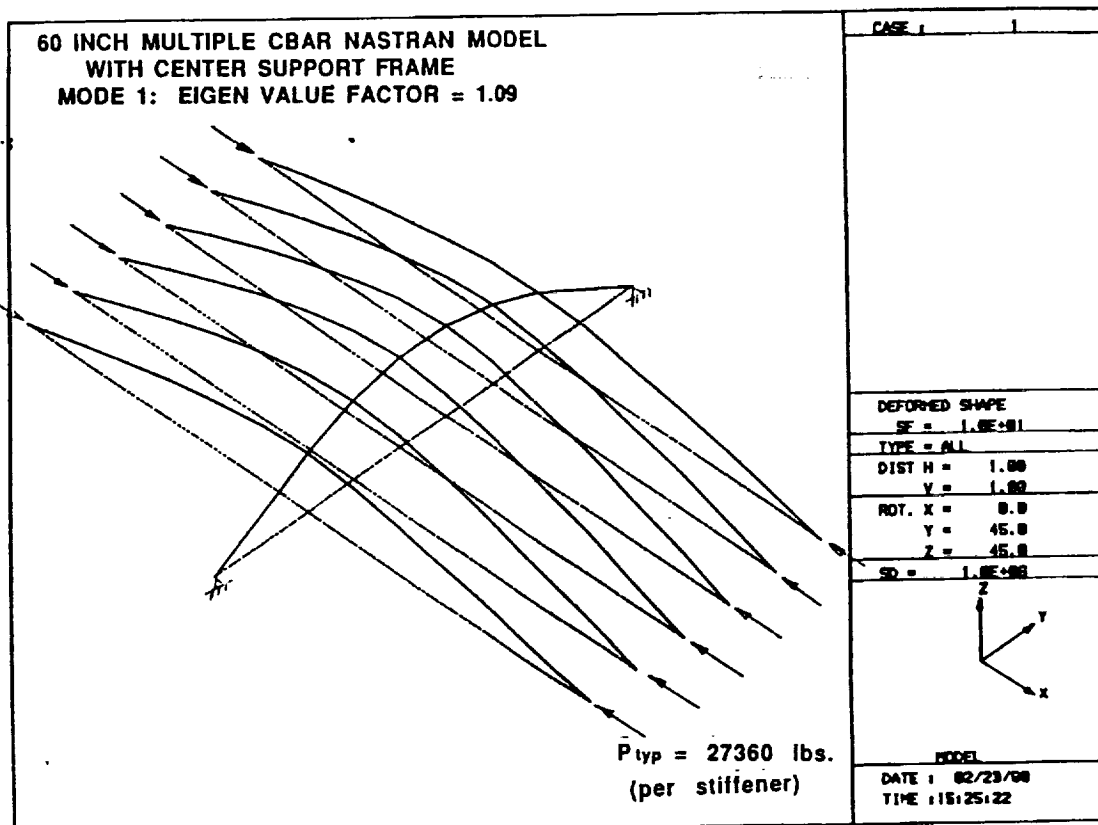


Figure 21. NASTRAN Sixty Inch Multiple C-Bar Model with Center Support Frame, Eigen Value Factor = 1.09

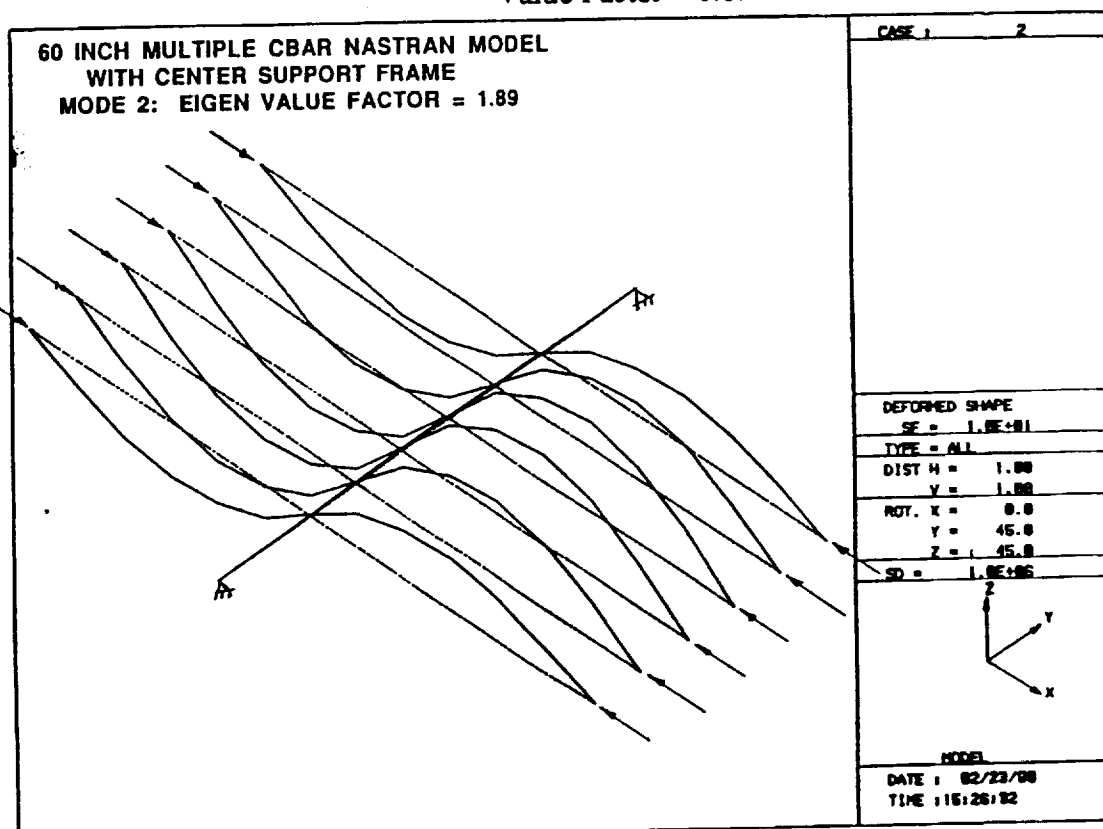


Figure 22. NASTRAN Sixty Inch Multiple C-Bar Model with Center Support Frame, Eigen Value Factor = 1.89

Optimization of the node intersection was continued with the development of a detailed NASTRAN finite element model (as shown in Figure 23) on the a large scale panel with a 30" node to better simulate and optimize the panel behavior under different loading conditions. The NASTRAN model utilized C-Bar elements as a cost effective means to evaluate the ring sizing necessary to enforce the node with both axial and bi-axial loading scenarios. A typical result of the node analysis is shown in Figure 24. The sizing of the interim ring with the NASTRAN analysis resulted in a design that provides maximum efficiency for the node (refer to Figure 25) with some sacrifice to overall manufacturability of the design. Additional designs were developed that would also satisfy the objective of node reinforcement and minimal manufacturing cost.

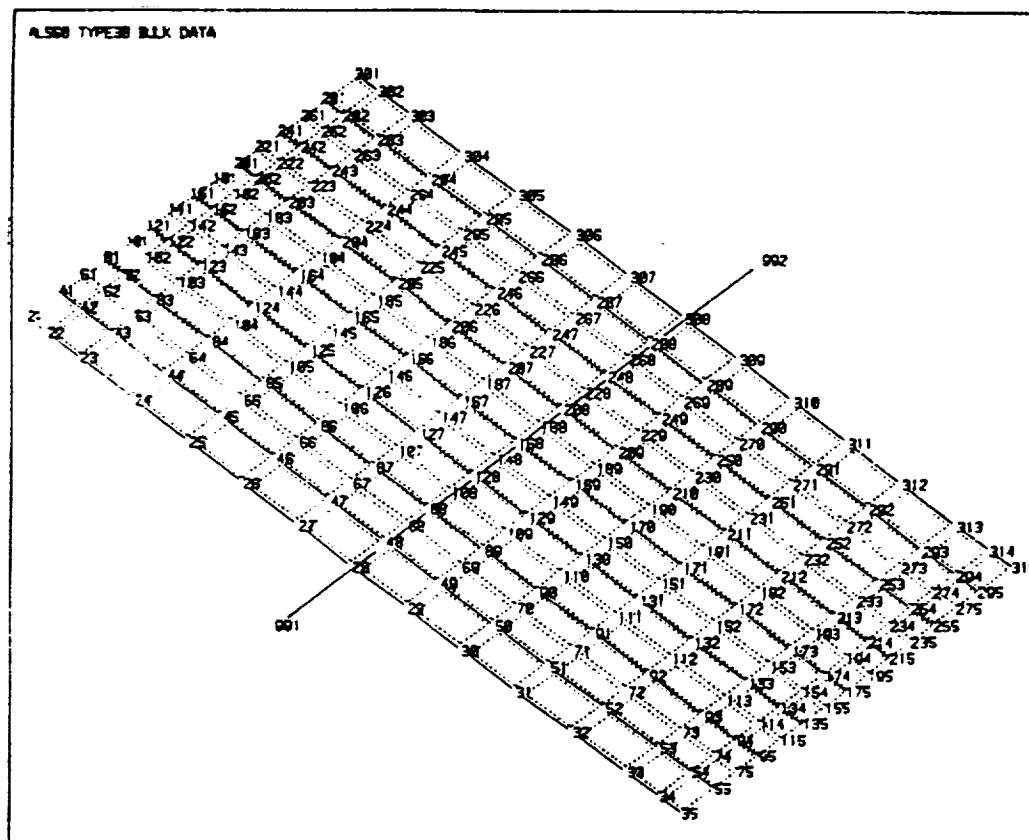


Figure 23. NASTRAN Model of Column Buckling Panel Design.

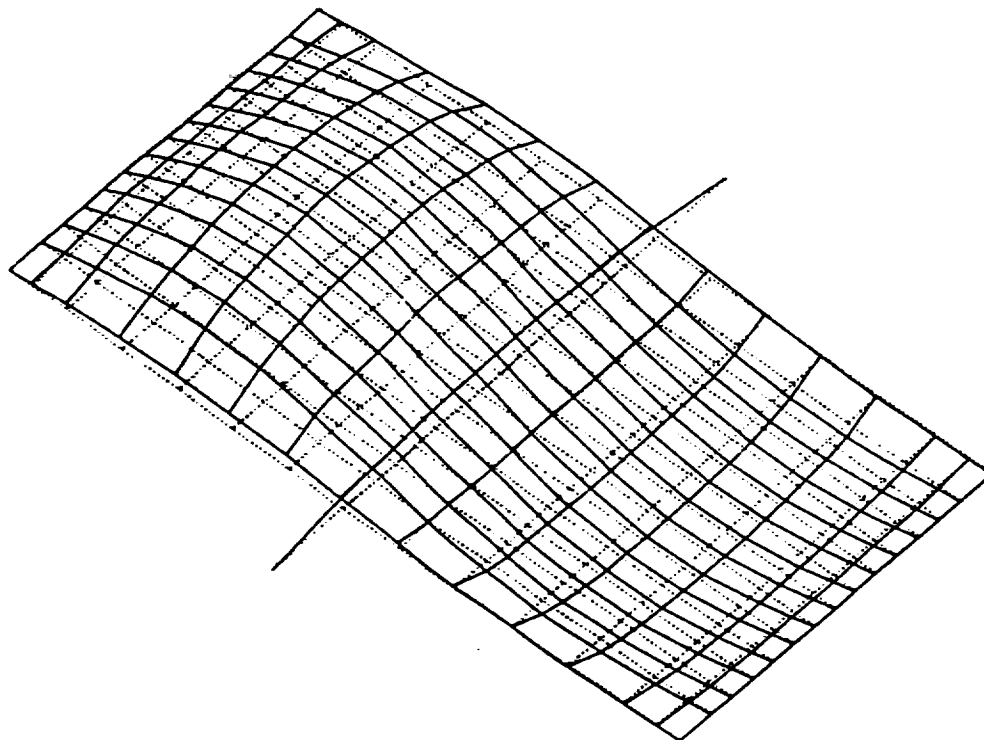


Figure 24. Column Buckling Panel Deflected (Solid) Under Mode 1 and Non-Deflected (Dashed) Uniaxial Load ($N_x = 10,000$ lb/in), Stiffener Spacing = 4.0", Integral Node I = 1.0 in⁴.

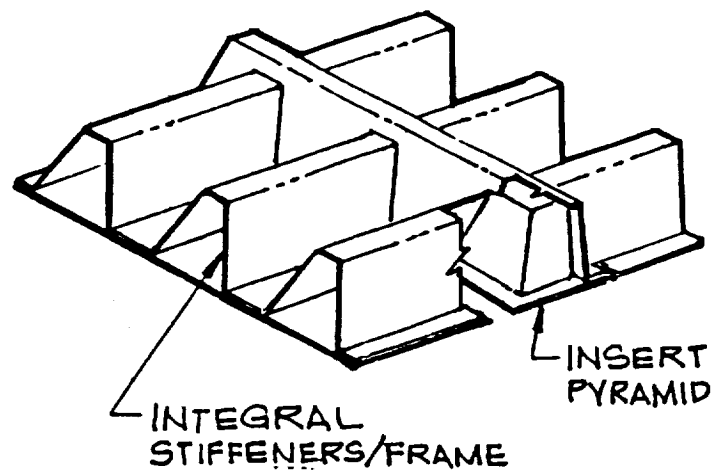


Figure 25. Example of One Integral Node Configuration for SPF Stiffened Structure.

4.1.7 COLUMN BUCKLING PANEL

At the completion of the crippling panel tests, the stepped hat stiffener configuration was chosen for continued development based on its load carrying capability. The stepped hat stiffener was modeled (refer to section 4.1 6) under NASTRAN and optimization of the stiffened structure was conducted. PASCO analysis of the stepped hat stiffener was conducted with a larger cap width to enhance the overall stability of the structure. The panel configuration was chosen based upon the desired length of the panel (column of at least 60 inches) and limited by the width of available material (48" minus sealing area). The resulting panel design (refer to Figure 26) maintained the inter-stiffener and inter-spot spacing developed during the development of the crippling stiffener panel.

The PASCO program was used in conjunction with a revised thinning profile (obtained from average measurements on the formed column buckling panels (7475 and 2090 aluminum materials)) shown in Figure 27. The failure loads were developed on the panels and are shown in Table 17 with the failure modes that resulted in beam column failure and inter-spot crippling. The primary failure mode was column failure, with inter-spot crippling occurring as a secondary failure mode. The test plan for the column buckling panel is included as Appendix C.

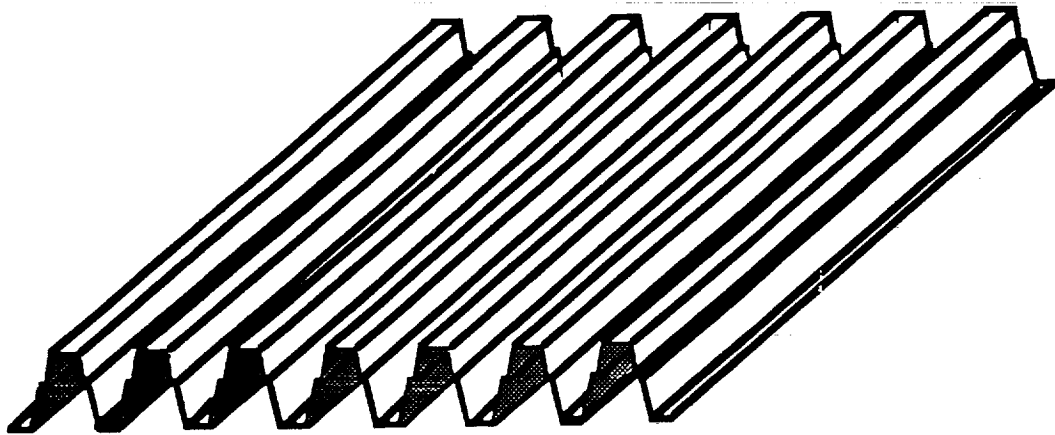


Figure 26. Column Buckling Panel Configuration.

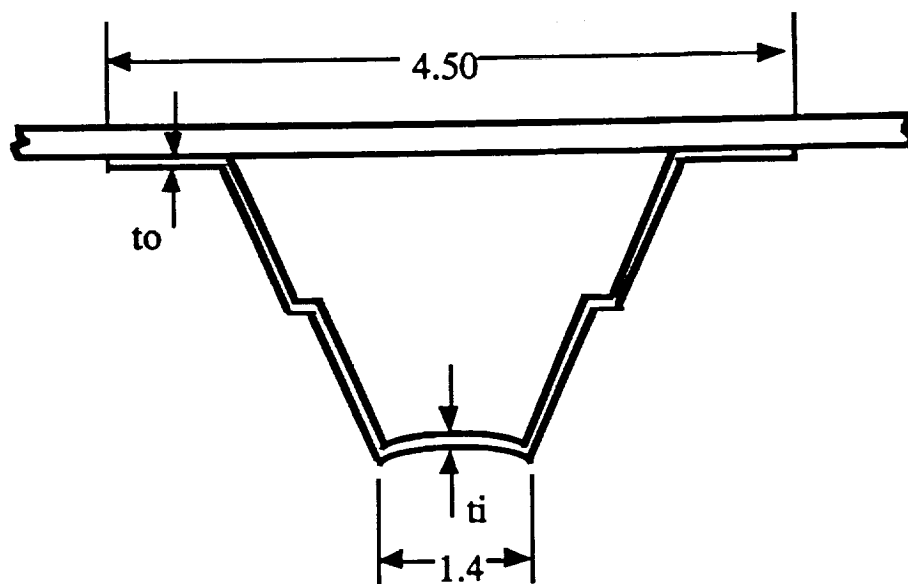


Figure 27. Average Thickness At Flange and Cap for Column Buckling Panel.

Table 17. Column Buckling Panel Predicted Failure Loading.

Material	t_{bar} (in.)	Predicted Column Failure Loading	Predicted Inter-spot Crippling	Thickness (in.)
7475 Al (0.100 Starting Gage)	0.255	6510 lb/in (25.5 Ksi)	41 Ksi	* t_o = 0.05 * t_i = 0.091
2090 Al-Li (0.090 Starting Gage)	0.245	6840 lb/in (27.9 Ksi)	37.4 Ksi	* t_o = 0.046 * t_i = 0.08

* Average measured thickness from Column Buckling Panel.

** Gage unavailable at this time, however, would have been preferable.

4.1.8 DOUBLER-REINFORCED FUSION WELD

The final panel configuration that was examined during this program was the vertical fusion weld or panel-to-panel joint. This joint configuration was based upon past work at General Dynamics Space Systems Division on the ATLAS and Centaur upper stage. The current ATLAS and Centaur pressure stabilized tanks are entirely fabricated from stainless steel foil. The joints are fusion butt-welded together and reinforced with a spot-welded doubler over the weld. This doubler-reinforced concept eliminates the need for machined weld lands (commonly used for launch vehicle pressure vessels at an increased fabrication cost, and weight penalty to the structure) to reinforce the joint by utilizing the doubler as a major load carrying member for the fusion weld.

The success of the General Dynamics use of the doubler-reinforced joint prompted the translation of the joint into an integral part of the ALS program for the vertical joint (refer to Figure 28). The development of the joint was based upon the fusion weld and resistance spot weld data generated during task 3 (section 4.3) of this program. Specific doubler testing was conducted under task 3 that provided a greater understanding of the behavior of the doubler over the Variable Polarity Plasma Arc (VPPA) fusion weld for load transfer. The test data was then utilized with finite element modeling techniques to predict the behavior of the fusion weld joint during bi-axial (axial and hoop) loading conditions.

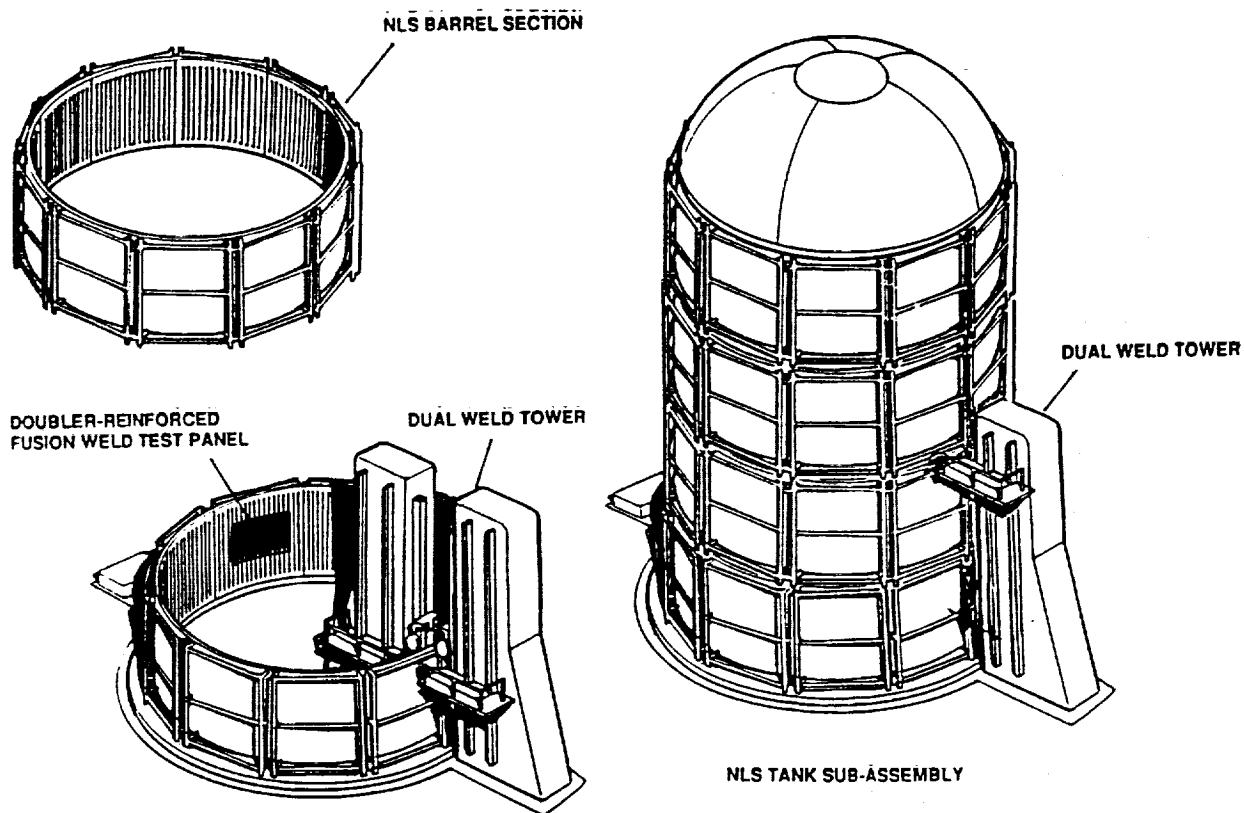


Figure 28. Vertical Doubler-Reinforced Joint on the ALS Vehicle.

4.1.8.1 Modeling of Doubler-Reinforced Joint

The IDEAS (a post-processing model developed by "Structural Dynamics Research Corporation" to maximize information gathered under current finite element models) and the NASTRAN finite element model (FEM) programs were used to predict the failure modes of the fusion weld panel. The weld joint was analyzed as a non-linear structure, hence it is a complex joint to model. The goal of the analysis was to provide a theoretical approximation of the stresses in the joint that can be compared to the test results to assess the reinforced joint efficiency. The joint configuration was comprised of several parameters listed below:

- Spot-weld pitch was averaged at 1 inch for both the doubler reinforced joint and the application of the stiffeners.
- C-Bar elements were used to simulate the attachment of the doubler or stiffener to the skin by resistance spotwelding.
- C-Quad 4 elements were used to simulate bending and membrane stresses for skin, doubler, stiffener configurations and fusion weld.
- Material properties for the materials as summarized in Table 2 and 3.
- The fusion weld is considered to be a major non-linear element of the overall joint.
- The approach to simulation of the non-linear effect is to use the secant modulus of the test article stress strain curve (doubler reinforced tensile tests were conducted earlier this year and are discussed under Task 3, section 4.3 of this report).

The bi-axial test panel has been designed to simulate the weld joint configuration of the built-up cryogenic tank sections (refer to Figure 29). The panels consists of two skin sections fusion welded together by the variable polarity plasma arc (VPPA) process, two stiffener sections, and a doubler for reinforcement of the fusion weld joint. The doubler reinforcement joint is welded over the shaved fusion weld using an in-line spot-weld pattern. The configuration was designed to minimize the cost to fabricate the weld joint (eliminating machining of a heavy weld land) while providing maximum joint efficiency at the lowest weight. The test panel was designed to be loaded bi-axially to simulate bending in the vehicle and thrust, and internal fuel pressure.

The joint configuration was based upon the General Dynamics dog-bone joint efficiency tests, and past experience with the Atlas configuration. The dog-bone tests showed a non-linear joint response to the imposed load. A true non-linear finite element analysis would include a NASTRAN iterating approach with non-linear material effects. However, due to program funding constraints, this effort was beyond the scope of the remaining program. Thus the goal of the finite element modeling effort was to construct a model that would provide for reasonable predictions of

the stress distribution across the joint for comparison with test data. The prediction should also show the anticipated load at failure, and the location of the failure.

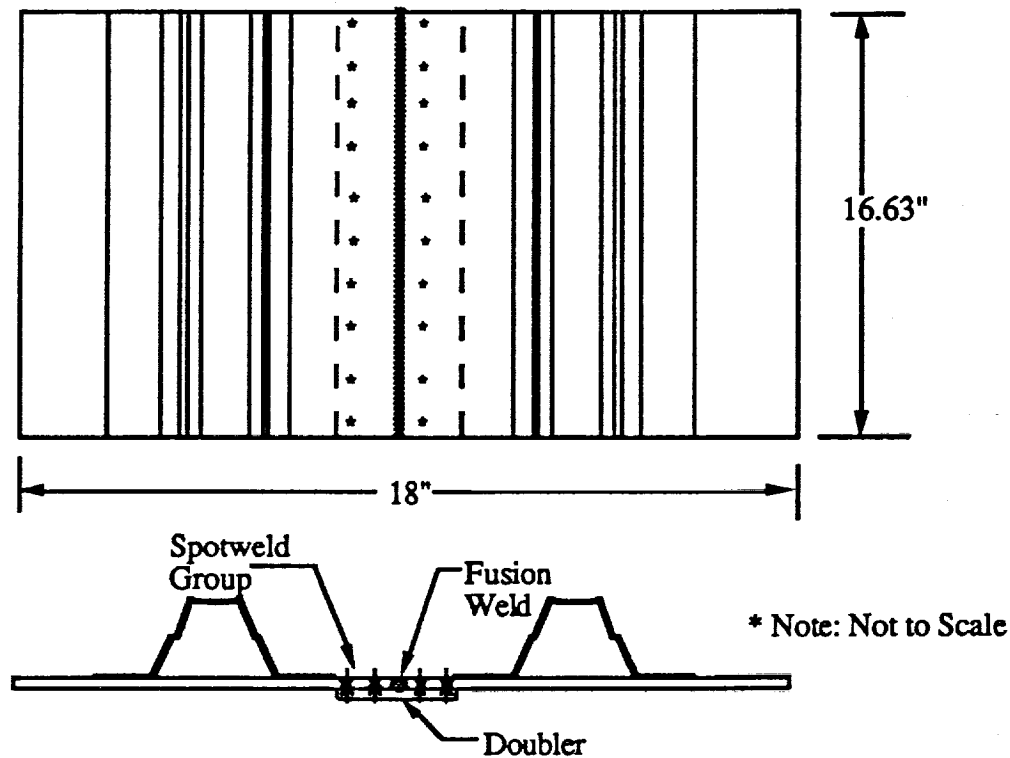


Figure 29. Schematic of Doubler-Reinforced Joint on the ALS Vehicle.

4.1.8.2 Finite Element Model of Doubler-Reinforced Fusion Weld

The results and constraints of the model are summarized as follows:

- Spot weld pitch measurements are set at 1 inch to facilitate the model.
- The IDEAS model was utilized to develop a NASTRAN model of the joint. A static NASTRAN run was performed with post-processing and stress contour plots in the IDEAS program.
- C-Quad 4 elements were used to simulate the plates. Stiff C-BAR elements were used to simulate the spot-welds. A C-Quad 4 element was used for the fusion weld area.
- The non-linear effect was simulated by using a reduced modulus of the fusion weld area at discrete load points as shown by the General Dynamics dog-bone test stress strain curves of the fusion weld joint (shown in Table 18 and Figure 30).

Table 18. Fusion Weld Test Case Data for 0.155" 2219-T81 VPPA Reinforced with 0.100" 7475-T62 Aluminum.

Load (lbs)	Area (in ²)	$\sigma = P/A$ (psi)	δ (in)	$\Sigma = \delta/L$	E_s (Msi)
766 (1532 lb/in)	0.0784	9750	0.0005	0.001 (1000 in/in)	9.75
1347 (2694 lb/in)	0.0784	17148	0.002	0.004 (4000 in/in)	4.29
1400 (2800 lb/in)	0.0784	17755	0.0022	0.0044 (4400 in/in)	4.0
1600 (3200 lb/in)	0.0784	20369	0.0035	0.007 (7000 in/in)	2.91
1800 (4000 lb/in)	0.0784	22915	0.00545	0.0109 (10900 in/in)	2.1
2000 (4000 lb/in)	0.0784	25461	0.0082	0.0164 (16400 in/in)	1.55
3050 (*6100 lb/in)	0.0784	38828	0.14	N.A.	0.139 (plastic)

* Failure

Note: Half of Gage Section Width = 0.5025" (Ave), $t_{ave} = 0.156"$, Area = 0.0784 in²

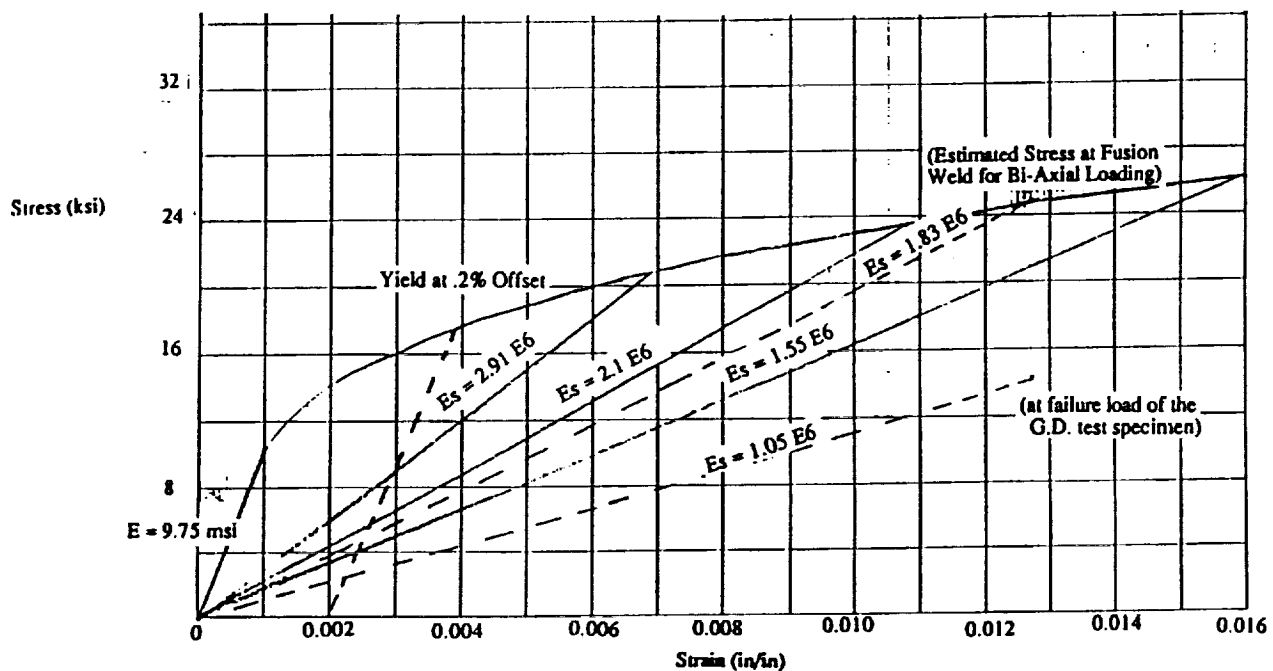


Figure 30. Stress-Strain Curve for Doubler-Reinforced Fusion Weld Joint.

Two verification runs were made with the model. The first evaluation involved application of a compressive axial load of 1000 lb/in to the model and evaluate the uniformity of the load and the stress across the joint. The model produced a uniform stress in the plate elements of -3500 psi which correlated with the expected stress of -3921 psi (due to T_{bar} of the section = 0.255 inch and $\sigma = -1000 \text{ lb per inch} / 0.255 \text{ in}$, where the -1000 lb was taken from the elastic portion of the fusion weld stress strain curve). The second verification run utilized a failure load of 7500 lb/in, obtained from the dog-bone tests, for the hoop direction. A reduced fusion weld secant modulus of $E_s = 1.05E6$ (estimated from stress strain curves) was utilized. The stress contour plots from the IDEAS program is shown as Figures 31 and 32. The model indicated that the bending stress is centralized in the joint area plates with the highest stress carried by the first row of spot welds. The anticipated point of failure is in the first row of spot welds indicated by both the dog-bone test and the model, despite a 30,000 psi load across the fusion weld. It was concluded that the model produced a reasonable representation of the stress distribution across the joint for bi-axial testing, and that test results should be similar to the simulation.

4.1.8.3 Model Failure Load and Location Predictions

The bi-axial failure loading predicted by simple hand calculation was as follows:

- Hoop = +5807 lb/in and Axial = -6307 lb/in

The joint loading in the model utilized a secant modulus of $1.83E6$ for the fusion weld pre-determined by the stress strain curves generated from the dog-bone testing. The resulting stress contours observed in the joint with the model are shown in Figures 33 and 34. It was concluded that the finite element model shows a failure in the first row of spot welds at a loading of 29,000 psi (which correlates with the G.D. uniaxial dog-bone tests). A comparison of the average plate stress for the hoop loading and for the bi-axial loading conditions are shown in Figure 35. The resulting stress distribution across the joint appeared similar to that observed for a bonded lap joint, which would be expected based upon the type of spotwelding attachment used during this program. The final joint configuration that was developed as a result of the test data and analysis is shown as Figure 36.

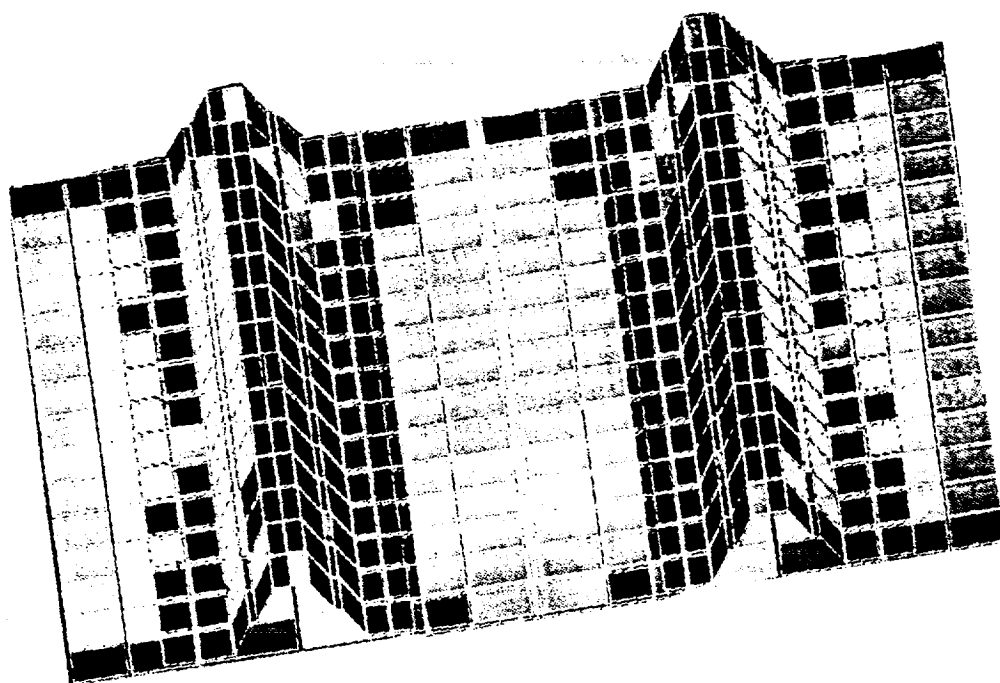


Figure 31. Top View of Stress Contour Plot for Hoop Loading = 7500 lb/in.

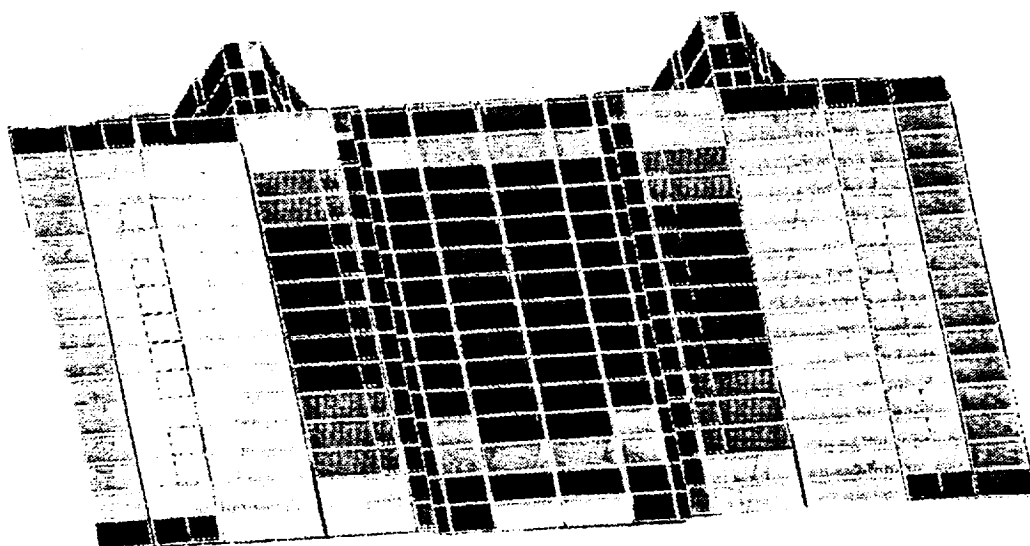


Figure 32. Bottom View of Stress Contour Plot for Hoop Loading = 7500 lb/in.

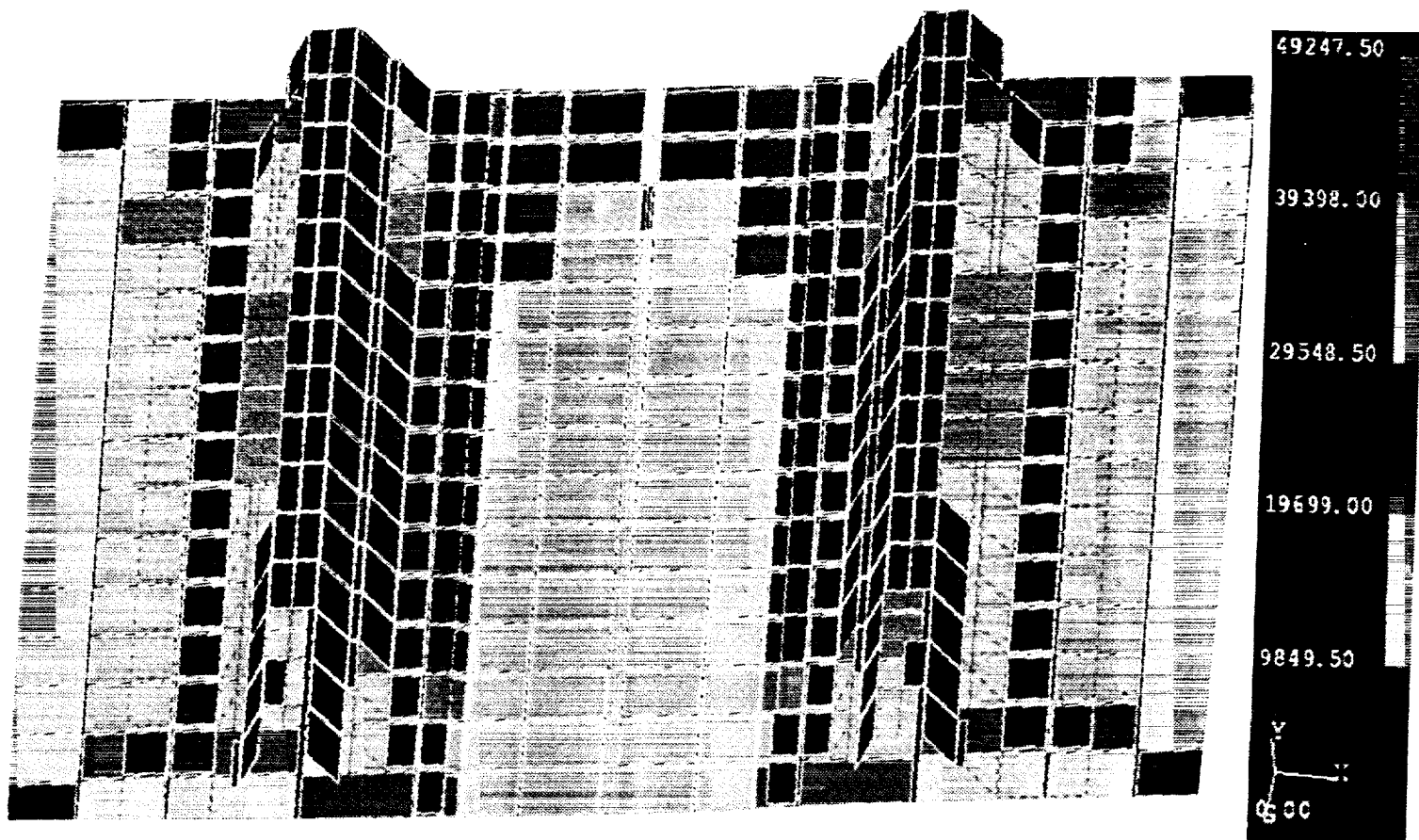


Figure 33. Top View of Stress Contour Plot for Hoop Loading = 5887 lb/in and Axial Load = -6307 lb/in.

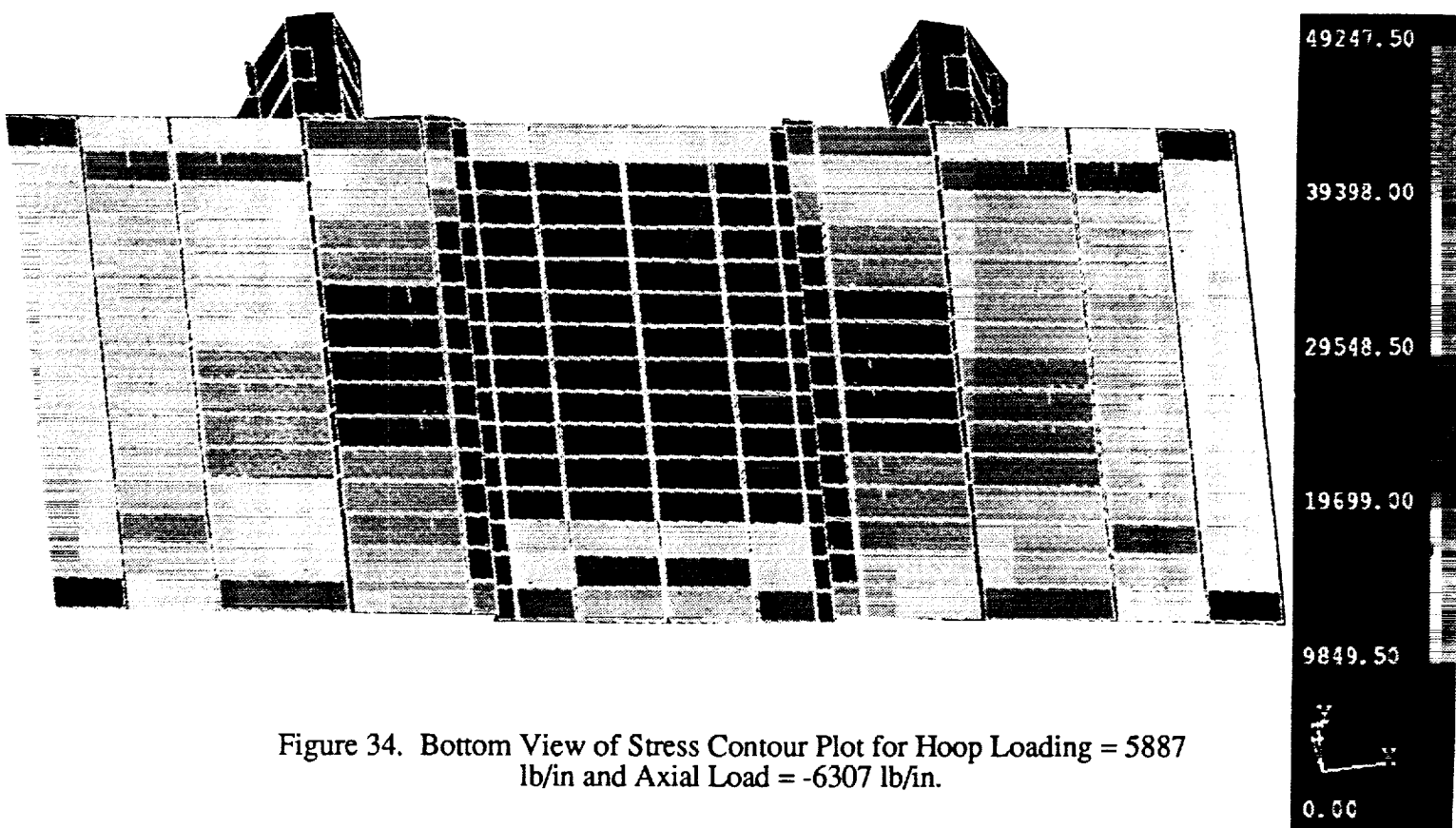


Figure 34. Bottom View of Stress Contour Plot for Hoop Loading = 5887 lb/in and Axial Load = -6307 lb/in.

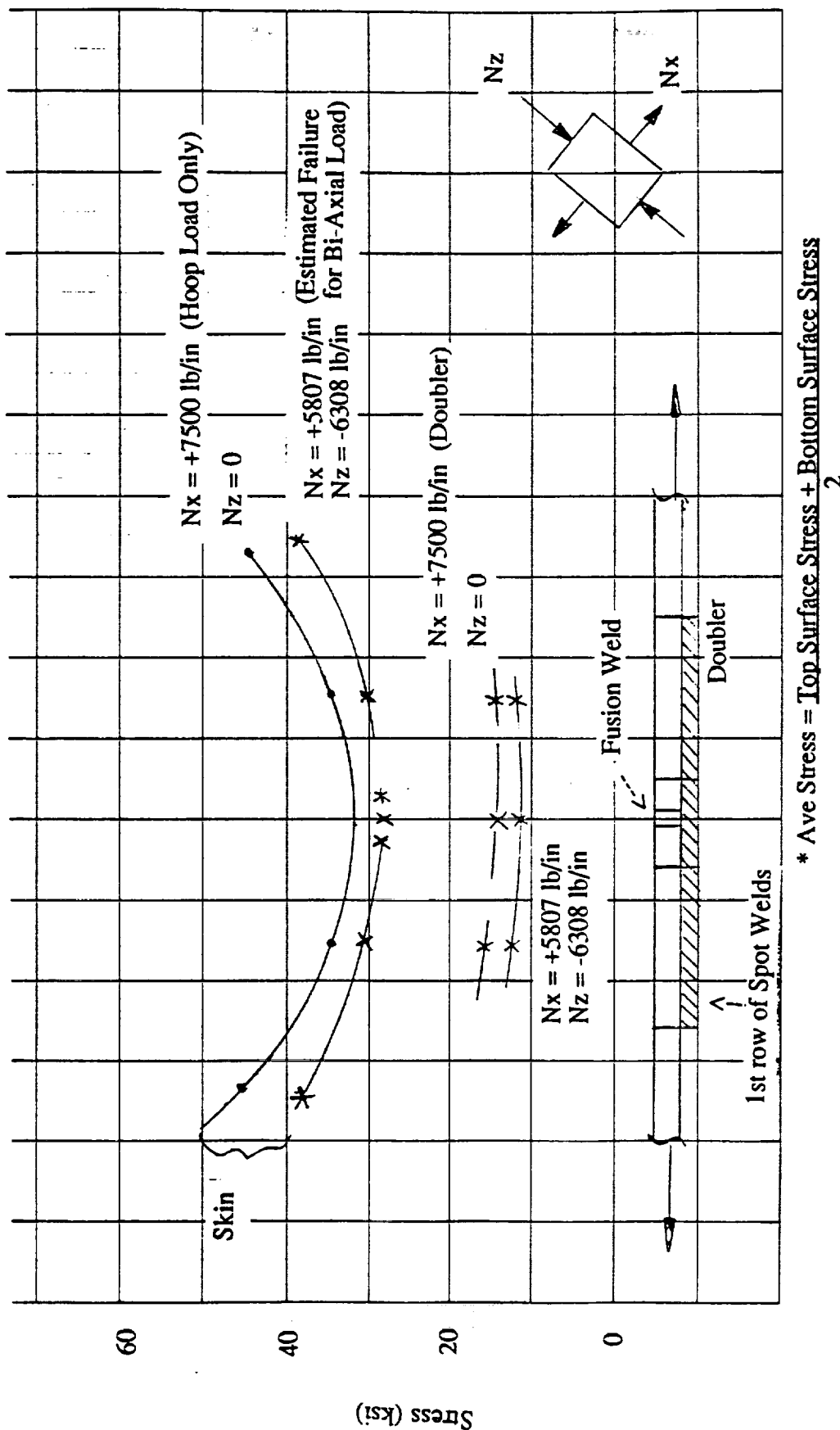


Figure 35. Stress Distribution Curves for Weld Joint Area Via FEM Model.

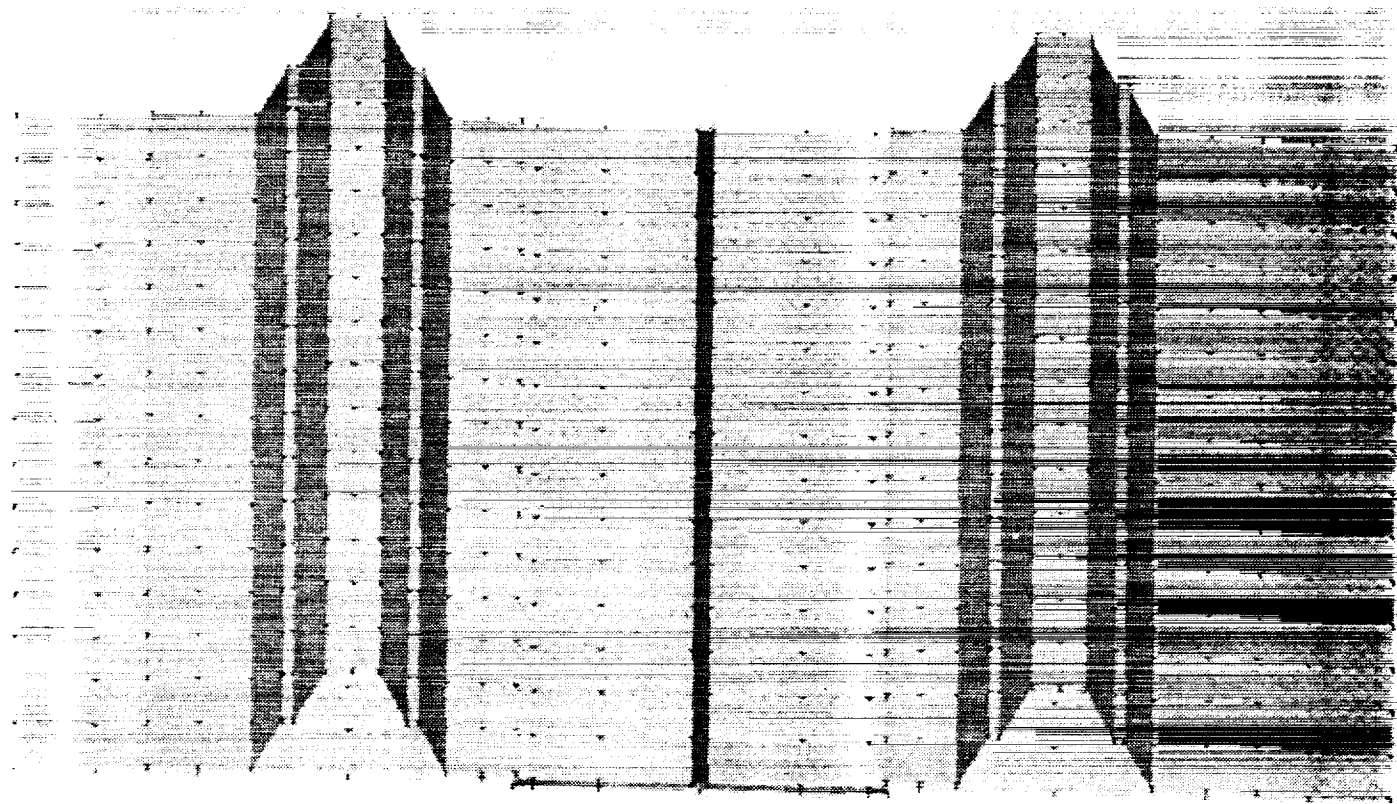


Figure 36. Doubler-Reinforced Fusion Weld Joint.

4.2 SUPERPLASTIC MATERIAL CHARACTERISTICS

4.2.1 SUPERPLASTIC FORMING (SPF) MATERIAL CHARACTERIZATION

Superplastic characterization of the materials used during this program involved metallographic examination of the material prior to and after forming, static exposure to elevated temperature (for grain stability), uniaxial tensile testing at constant strain rate and variable strain rate with and without back pressure, and finally producibility forming trials. These characterization tests have been developed at Rockwell to provide information on the starting grain size of the material, stability of the grain size due to elevated temperature exposure, the presence or absence of recrystallization during forming or grain growth during forming, flow stress of the material at various strain rates, flow stress of the material with varying amounts of back pressure, flow stress whereby superplastic elongation is maximized, requirements for suppression of cavitation, and formability characteristics for each alloy.

There are various other points of information that can be obtained during testing that include strain hardening, or softening as was the case with the second batch of Weldalite-049 (x2095 Al-Li) obtained during the program, the strain at which cavitation initiates for each material at various levels of back pressure, etc. All of these various data points are used during the development of a forming process for structural components. The information gathered during the characterization phase of the program is placed into the Rockwell superplastic forming computer model and when combined with the configuration of the article to be fabricated, a thinning profile and forming pressure versus time profile is generated for the component to be formed.

The aluminum and aluminum-lithium materials examined during this program included 7475 Al, a material that has been used on several programs at Rockwell, two production Al-Li alloys, and one experimental Al-Li alloy (refer to Table 19). The characterization study for the 7475 Al material was limited to verification of uniaxial superplastic tensile properties and metallography in order to determine the quality of the material prior to fabrication. Additional tests were run on the 2090, 8090, and x2095 alloys to fully characterize each material.

Superplastic tensile tests were carried out on an Instron machine equipped with a computer-aided controller that maintained constant strain rate with a superimposed hydrostatic pressure for suppressing cavitation during testing (refer to Figure 37 and 38). The uniaxial testing machine is equipped with a five zone furnace with a 12-inch-long uniform temperature zone that maintains temperatures up to $\pm 2^{\circ}\text{C}$, and equipped with a retort that is capable of maintaining vacuum or gas pressures up to 600 psi. The specimen and pullrod assembly are placed within the retort with an

on-line load cell (water cooled) which allows for load measurement during testing with superimposed hydrostatic pressure.

Table 19. Superplastic Al and Al-Li Alloys Characterized During Program.

Material =>	7475 Al	2090 Al-Li	8090 Al-Li	x2095 Al-Li (Weldalite-049)
Full Characterization		X	X	X
Verification Characterization	X			

Stepped strain rate tests were carried out for each material type at specified test temperatures. This test was computer-controlled in order to sequentially determine the initial plastic flow stress at each constant strain rate. The load and extension data collected by the control computer were processed to provide: true stress versus true strain rate data, a least-squares-fit, third or fourth order polynomial equation for Log(true stress) versus Log(true strain rate) and strain rate sensitivity index (m-value) versus log(true strain rate).

Constant true strain rate tests were carried out for each material type at each specified test temperature with strain rates selected from the analysis of the stepped strain rate test data. The load and extension data were collected by the control computer and processed to give a graphical plot of true stress versus true strain. Multi-stage constant true strain rate tests were conducted for 2090 and 8090 Al-Li materials in order to take advantage of the effects that dynamic recrystallization can provide for enhancement of superplastic elongations during forming. A standard test matrix that was utilized for the duplex or multi-stage strain rate testing is shown in Table 20.

4.2.1.1 7475 Aluminum

Uniaxial and microstructural evaluations were performed on 7475 Al (Reynolds MD254) for verification of SPF forming parameters prior to use on the program. Figures 39 through 41 show the results from the verification testing on the 7475 Al material procured for this program. Uniaxial testing and microstructural evaluations revealed some differences from past evaluations of the 7475 Al material at Rockwell. However, the material did fall within acceptable ranges of formability for 7475 Al.

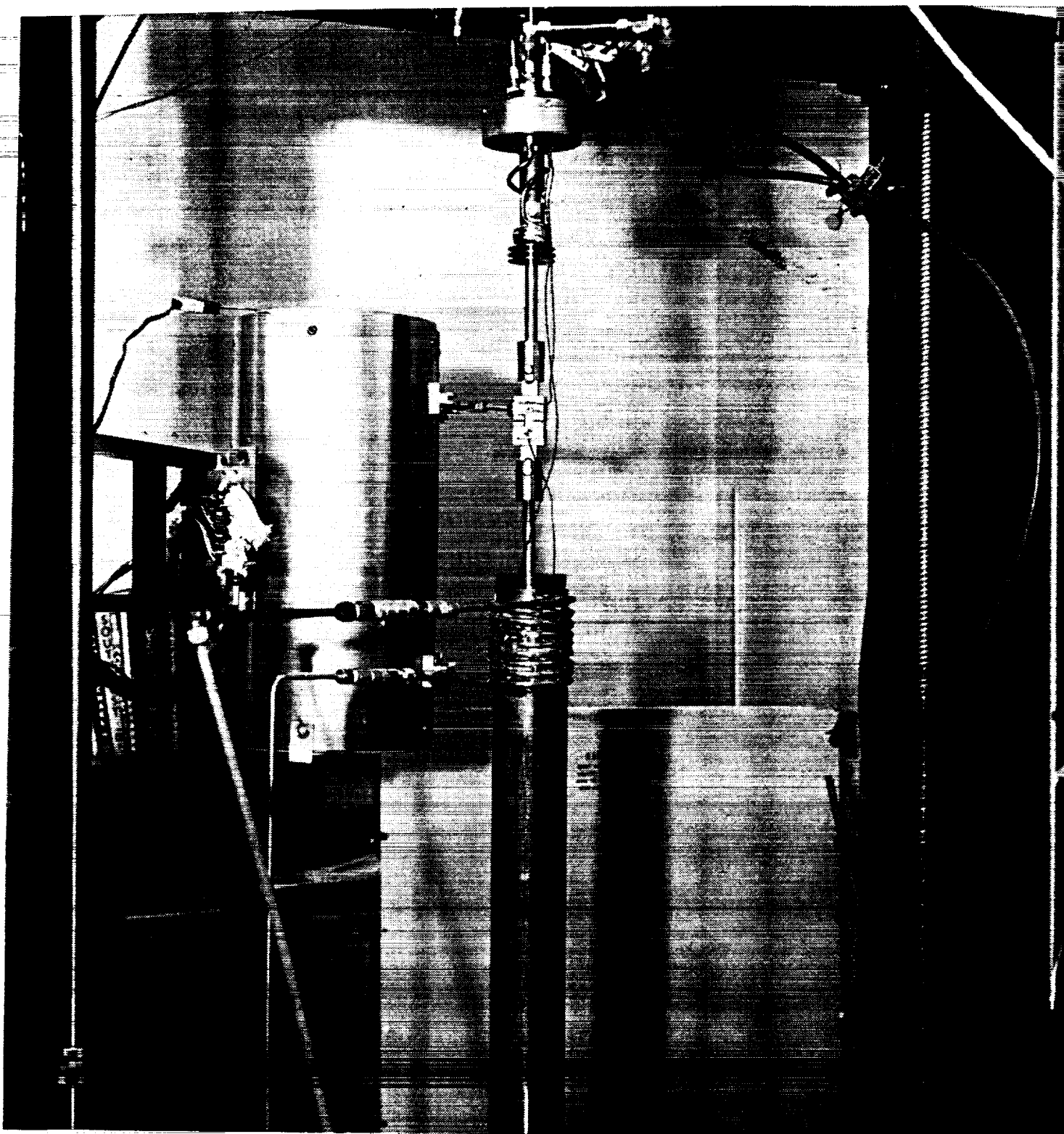


Figure 37. Superplastic Uniaxial Test Chamber with Hydrostatic Pressure Retort.

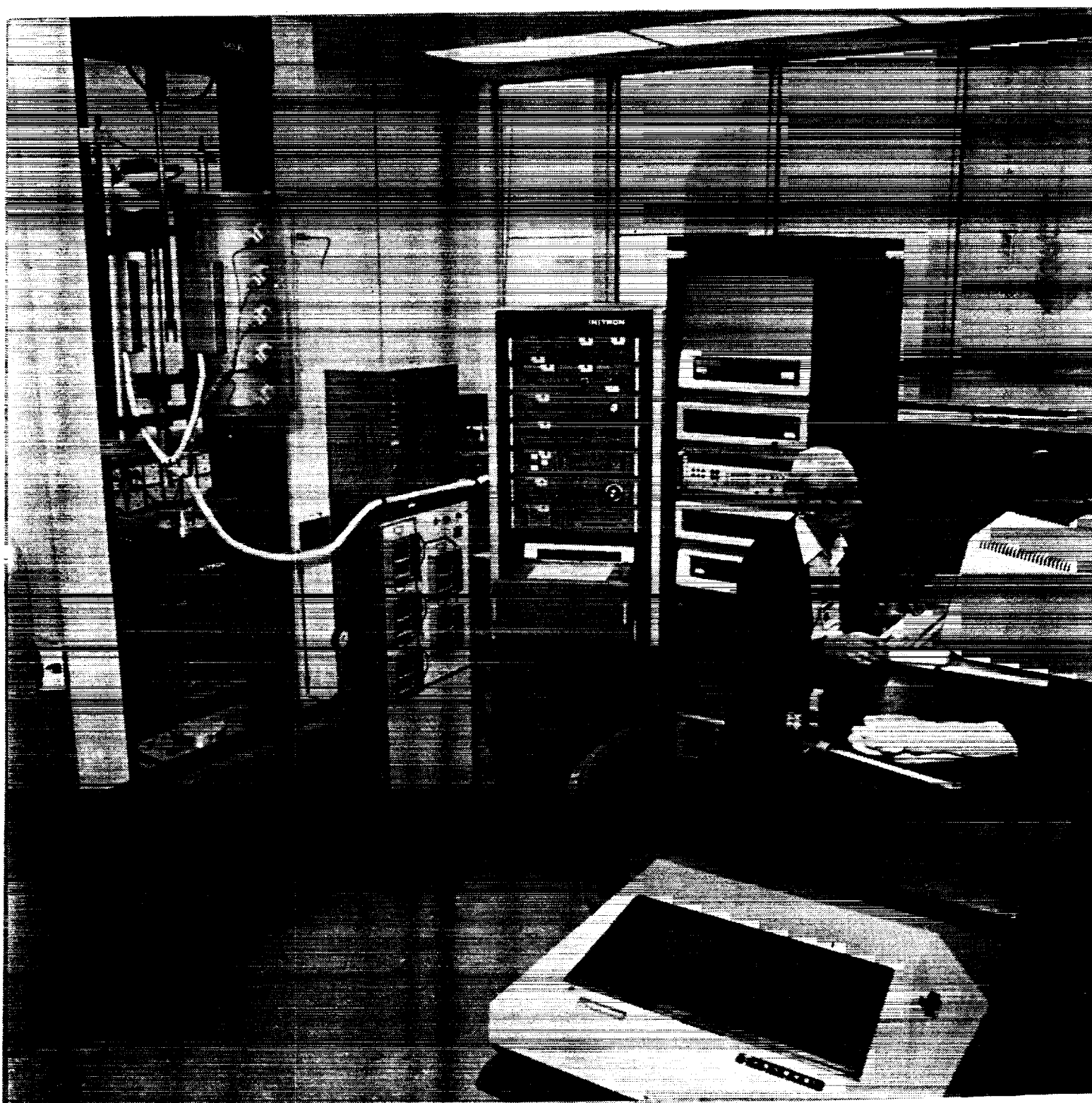


Figure 38. Superplastic Uniaxial Test Chamber with Data Acquisition System.

Table 20. Test Matrix for Uniaxial Duplex Strain Rate Testing.

Temperature (°F)	Back Pressure (psi)	Strain Rate #1 (per second)	Strain 0 to X	Strain Rate #2 (per second)	Strain X to End
914	Ambient	2E-3	0.72	2E-4	End of Test
914	200	2E-3	0.72	2E-4	End of Test
914	600	2E-3	0.72	2E-4	End of Test
950	Ambient	2E-3	0.72	2E-4	End of Test
950	200	2E-3	0.72	2E-4	End of Test
950	600	2E-3	0.72	2E-4	End of Test
986	Ambient	2E-3	0.72	2E-4	End of Test
986	200	2E-3	0.72	2E-4	End of Test
986	600	2E-3	0.72	2E-4	End of Test

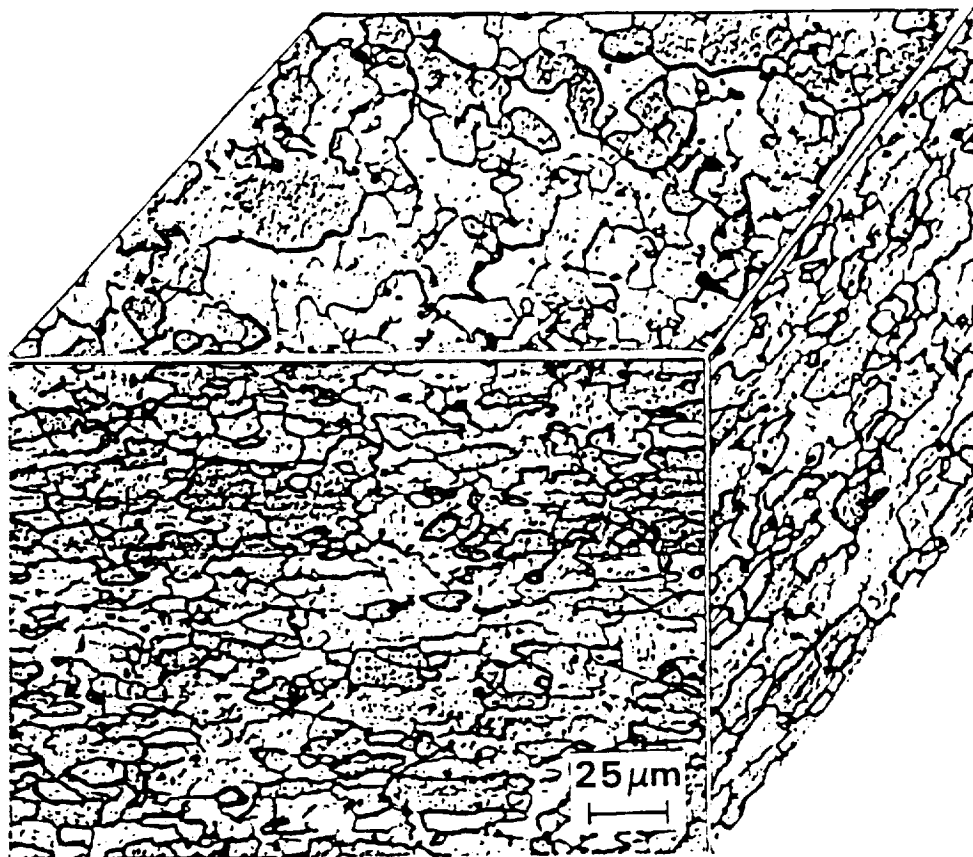


Figure 39. Microstructure of Superplastic 7475 Aluminum.

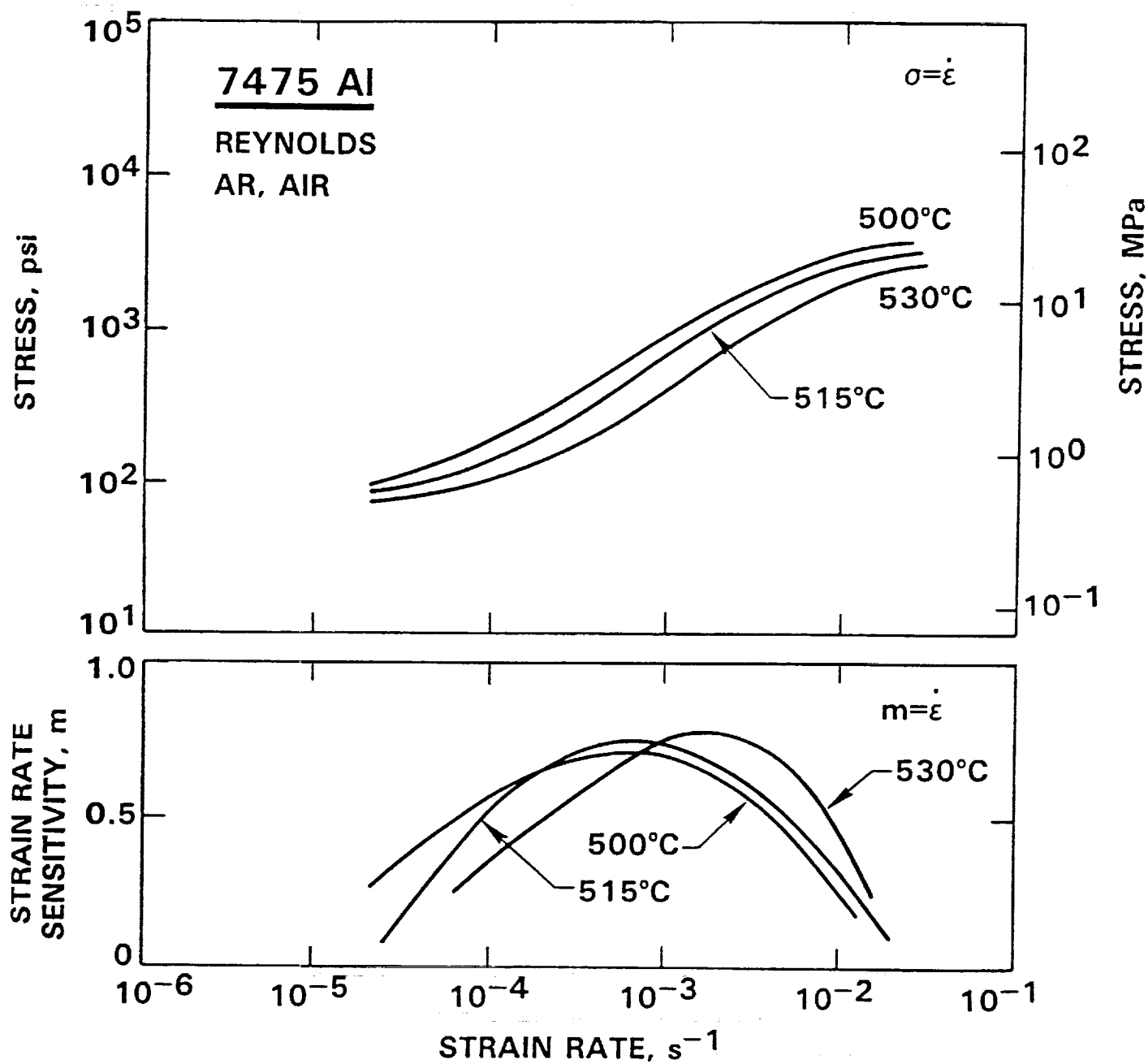


Figure 40. Flow Stress and Strain Rate Sensitivity Versus Strain Rate for 7475 Al.

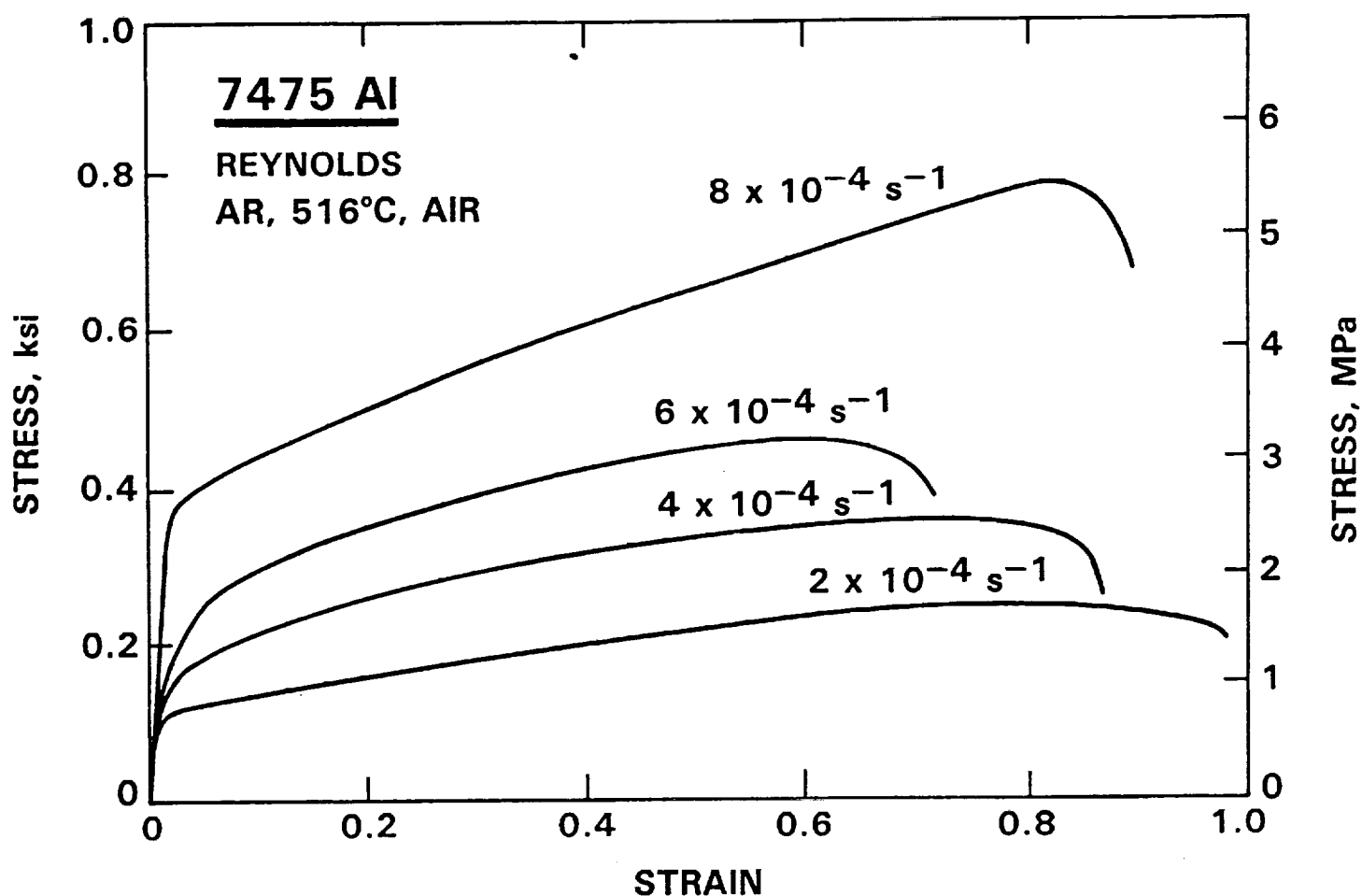


Figure 41. Flow Stress Versus Strain for 7475 Al at Constant Strain Rate Values between 2E-4 and 8E-4/sec.

4.2.1.2 2090 Aluminum-Lithium

A metallurgical and superplastic characterization of 2090 Al-Li sheets was conducted for both the -OE16 and -T3 condition. The preliminary metallographic and tensile tests showed that the material obtained in the -T3 condition was not inherently superplastic. However, the evaluation of the -OE16 material showed a fine grained material with excellent superplastic behavior. The chemical composition of the materials evaluated on this program are shown in the table below.

Cu	Mg	Si	Fe	Mn	Zn	Zr	Li	Cr	Ti	Ag	Other	Al
2.4	0.25	.010	0.12	0.05	0.10	0.15	2.6	0.05	0.15		0.20	Rem
3.0						0.08	1.9					

4.2.1.2.1 Metallurgical Analysis

The as-received 2090-OE16 Al-Li alloy contained fine subgrains ($2.93 \times 2.35 \times 3.65 \mu\text{m}$) were slightly elongated in the final rolling direction as shown in Figure 42. However, the fine subgrain structure coarsened rapidly at temperatures in the range of 950 to 986°F (510 to 530°C). The average grain size of 2090-OE16 increased to $7.8 \mu\text{m}$ in two hours during exposure at the aforementioned temperatures. Thus hot loading of a part for SPF is recommended during forming of parts in order to prevent excessive static grain growth.

4.2.1.2.2 Stress-Strain Rate Behavior

Stepped strain rate tests were performed on the as-received 2090-OE16 material at 914, 950, and 986°F (490, 510, and 530°C) in air to determine the flow stress levels and strain rate sensitivity values of the material as a function of strain rate. The flow stress-strain rate data in the longitudinal and transverse directions are shown in Figures 43 and 44. The results from the tests showed a decrease in flow stress with an increase in test temperature, and an increase in flow stress with an increase in strain rate. The maximum strain rate sensitivity for the material was obtained at an intermediate strain rate ($1\text{E-}3/\text{sec}$) which is consistent with other superplastic aluminum materials. Differences in the flow properties of this material in the longitudinal and long-transverse directions were observed. The flow stress levels were slightly higher in the long-transverse samples than in the longitudinal, and the optimum strain rates which correspond to the maximum strain rate sensitivity (m values) obtained from the jump tests differed by a factor of two. The longitudinal samples showed more symmetric m -curves (with the implication of higher superplastic elongations) than the transverse samples.

4.2.1.2.3 Superplastic Elongation Data

Several elongation tensile tests were performed under two strain rates ($2\text{E-}3/\text{sec}$ until a strain of 0.72 and $2\text{E-}4/\text{sec}$ until coupon failure) at 914, 950, and 986 °F in air and under back pressure (200 to 600 psi). The elongation data on the 2090-OE16 material is shown on Table 21. The results indicate that 2090-OE16 exhibits very high superplastic elongations using the two stage strain rate uniaxial test conditions at 950 °F. The elongations can be improved from 400 % in air (or without back pressure) to over 1425 % with back pressures up to 600 psi (refer to Figure 45). The increase in uniaxial elongations with back pressure is attributed to the suppression of superplastic cavitation which formed in the material during testing in air.

4.2.1.2.4 Flow Stress-Strain Data

Flow stress-strain curves for the two stage strain rate testing are shown in Figures 46 through 48. The material exhibits strain hardening during the first stage of testing ($2\text{E-}3/\text{sec}$) for strains between 0 and 0.4 which is followed by a softening effect. The flow stress levels during the second stage of deformation (where the strain rate has been reduced to $2\text{E-}4/\text{sec}$) are dramatically reduced, when compared with the first stage flow stress values, to approximately 400 psi. Strain hardening in the 2090-OE16 material in the second stage of deformation is negligible and the small increase in flow stress during the second stage is attributed to dynamic grain growth in the material.

4.2.1.2.5 Dynamic Grain Growth

Metallographic examination of the tensile tested samples showed extensive grain growth with superplastic deformation (refer to Figures 49 and 50). The grain size increased from $7.8\text{ }\mu\text{m}$ in the grip area (strain = 0) to $13.5\text{ }\mu\text{m}$ at a strain of 3.0. The grain structure in the deformed area is more equiaxed than in the grip section. The excessive grain growth in this alloy causes higher flow stress levels and promotes cavitation when tested in air.

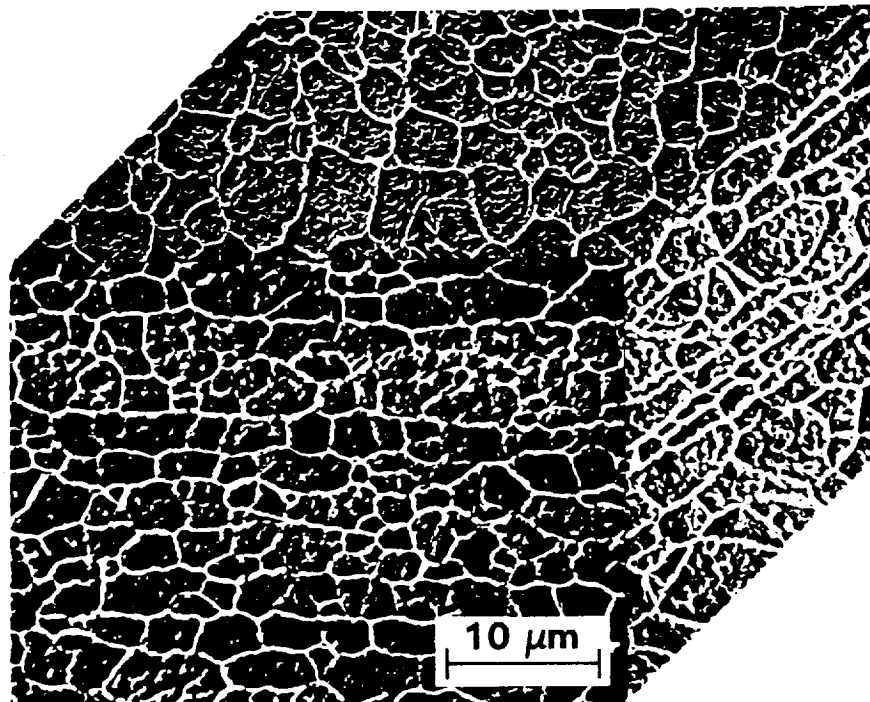


Figure 42. Microstructure of Superplastic 2090 Al-Li Material.

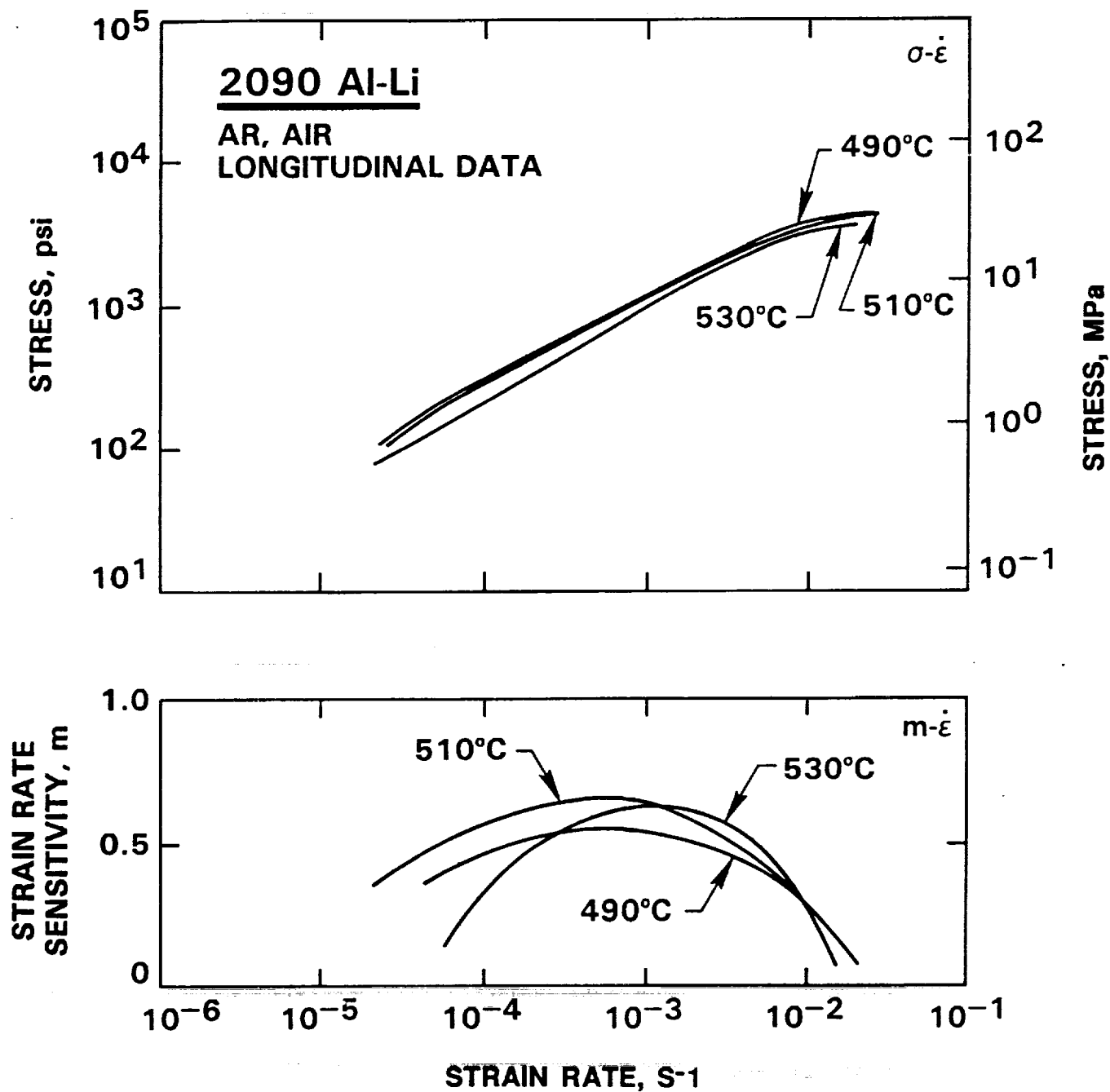


Figure 43. 2090 Al-Li Longitudinal Flow Stress Versus Strain for Different Strain Rates.

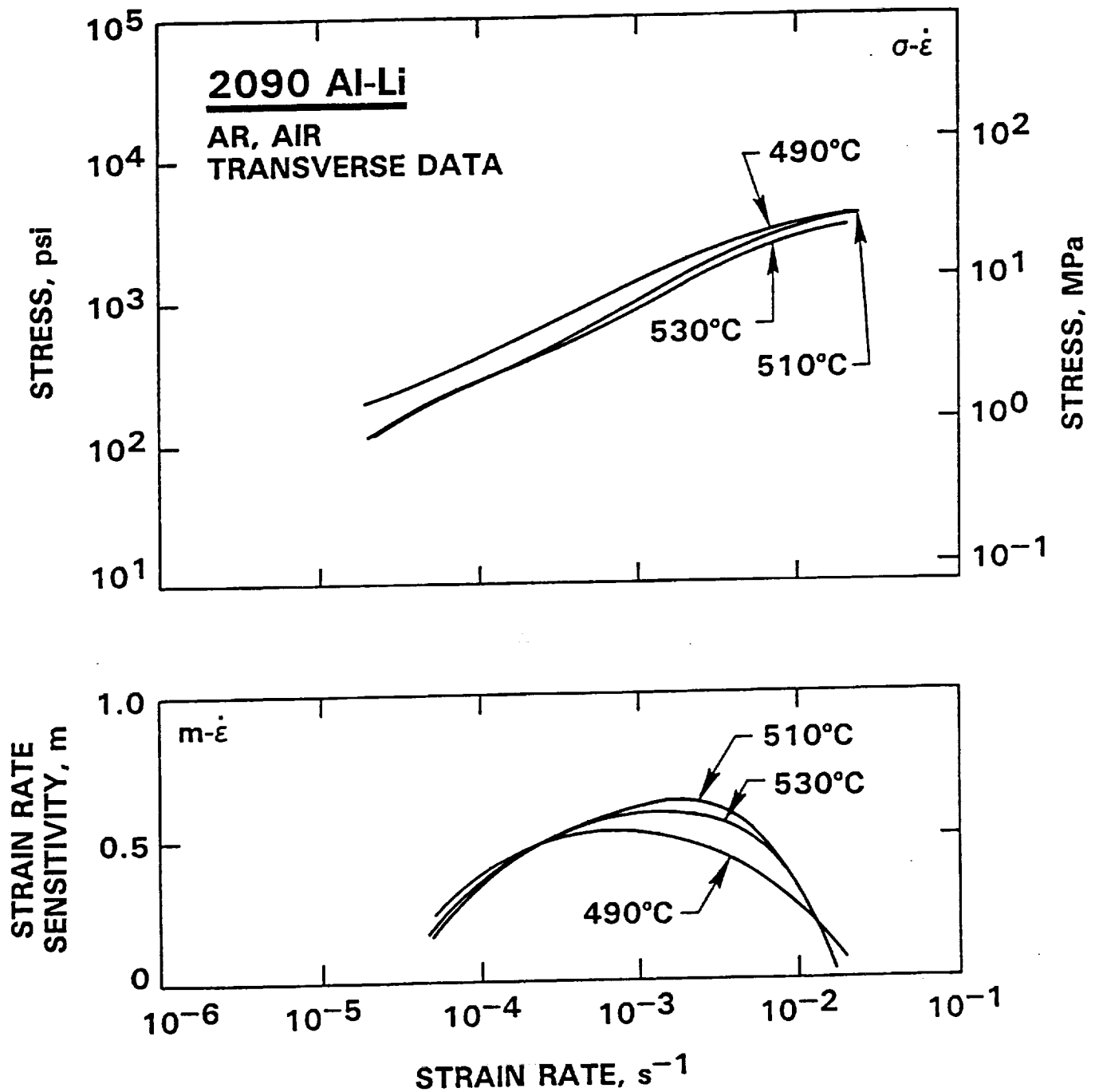


Figure 44. 2090 Al-Li Transverse Flow Stress Versus Strain for Different Strain Rates.

600 psi 1425%



400 psi 1050%



UNTESTED



Figure 45. 2090 Al-Li Uniaxial Superplastic Elongations with Back Pressure. Tests Performed at 950°F with Duplex Strain Rate of 2E-3 and 2E-4 sec⁻¹.

Table 21. Superplastic Tensile Elongations of 2090 Al-Li.

ALLOY	TMT	TEMP (°F)	PRESSURE (PSI)	STRAIN RATE (Per Second)	ELONGATION (%)
2090	OE16	914	Air	$2 \times 10^{-3} / 2 \times 10^{-4}$	246L
2090	OE16	950	Air	$2 \times 10^{-3} / 2 \times 10^{-4}$	392L
2090	OE16	986	Air	$2 \times 10^{-3} / 2 \times 10^{-4}$	444L
2090	OE16	1022	Air	$2 \times 10^{-3} / 2 \times 10^{-4}$	341L
2090	OE16	914	Air	$2 \times 10^{-3} / 2 \times 10^{-4}$	441T
2090	OE16	950	Air	$2 \times 10^{-3} / 2 \times 10^{-4}$	484T
2090	OE16	986	Air	$2 \times 10^{-3} / 2 \times 10^{-4}$	339T
2090	OE16	1022	Air	$2 \times 10^{-3} / 2 \times 10^{-4}$	431T
2090	OE16	914	200	$2 \times 10^{-3} / 2 \times 10^{-4}$	644L
2090	OE16	950	200	$2 \times 10^{-3} / 2 \times 10^{-4}$	758L
2090	OE16	986	200	$2 \times 10^{-3} / 2 \times 10^{-4}$	820L
2090	OE16	1022	200	$2 \times 10^{-3} / 2 \times 10^{-4}$	631L
2090	OE16	914	200	$2 \times 10^{-3} / 2 \times 10^{-4}$	427T
2090	OE16	950	200	$2 \times 10^{-3} / 2 \times 10^{-4}$	630T
2090	OE16	986	200	$2 \times 10^{-3} / 2 \times 10^{-4}$	658T
2090	OE16	1022	200	$2 \times 10^{-3} / 2 \times 10^{-4}$	546T
2090	OE16	914	400	$2 \times 10^{-3} / 2 \times 10^{-4}$	613L
2090	OE16	950	400	$2 \times 10^{-3} / 2 \times 10^{-4}$	854L *
2090	OE16	986	400	$2 \times 10^{-3} / 2 \times 10^{-4}$	702L
2090	OE16	1022	400	$2 \times 10^{-3} / 2 \times 10^{-4}$	905L
2090	OE16	914	400	$2 \times 10^{-3} / 2 \times 10^{-4}$	662T
2090	OE16	950	400	$2 \times 10^{-3} / 2 \times 10^{-4}$	743T
2090	OE16	986	400	$2 \times 10^{-3} / 2 \times 10^{-4}$	1049T
2090	OE16	1022	400	$2 \times 10^{-3} / 2 \times 10^{-4}$	709T
2090	OE16	914	600	$2 \times 10^{-3} / 2 \times 10^{-4}$	1016L
2090	OE16	950	600	$2 \times 10^{-3} / 2 \times 10^{-4}$	1425L *
2090	OE16	986	600	$2 \times 10^{-3} / 2 \times 10^{-4}$	1100L
2090	OE16	1022	600	$2 \times 10^{-3} / 2 \times 10^{-4}$	820L
2090	OE16	914	600	$2 \times 10^{-3} / 2 \times 10^{-4}$	812T
2090	OE16	950	600	$2 \times 10^{-3} / 2 \times 10^{-4}$	1063T
2090	OE16	986	600	$2 \times 10^{-3} / 2 \times 10^{-4}$	1275T
2090	OE16	1022	600	$2 \times 10^{-3} / 2 \times 10^{-4}$	720T

L: longitudinal, and T: transverse direction to final rolling., * Not Fractured

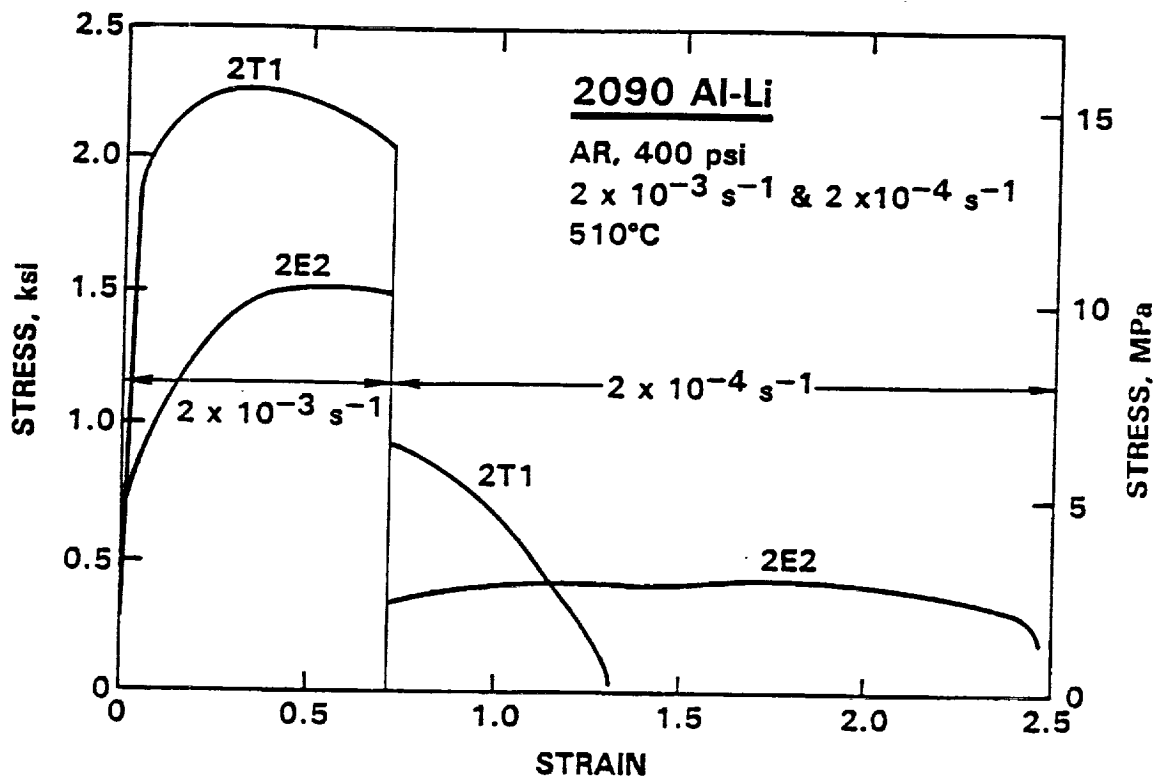


Figure 46. 2090 Al-Li Flow Stress Versus Strain for Duplex Stage Strain Rates. (-T3 and -OE16 Temps)

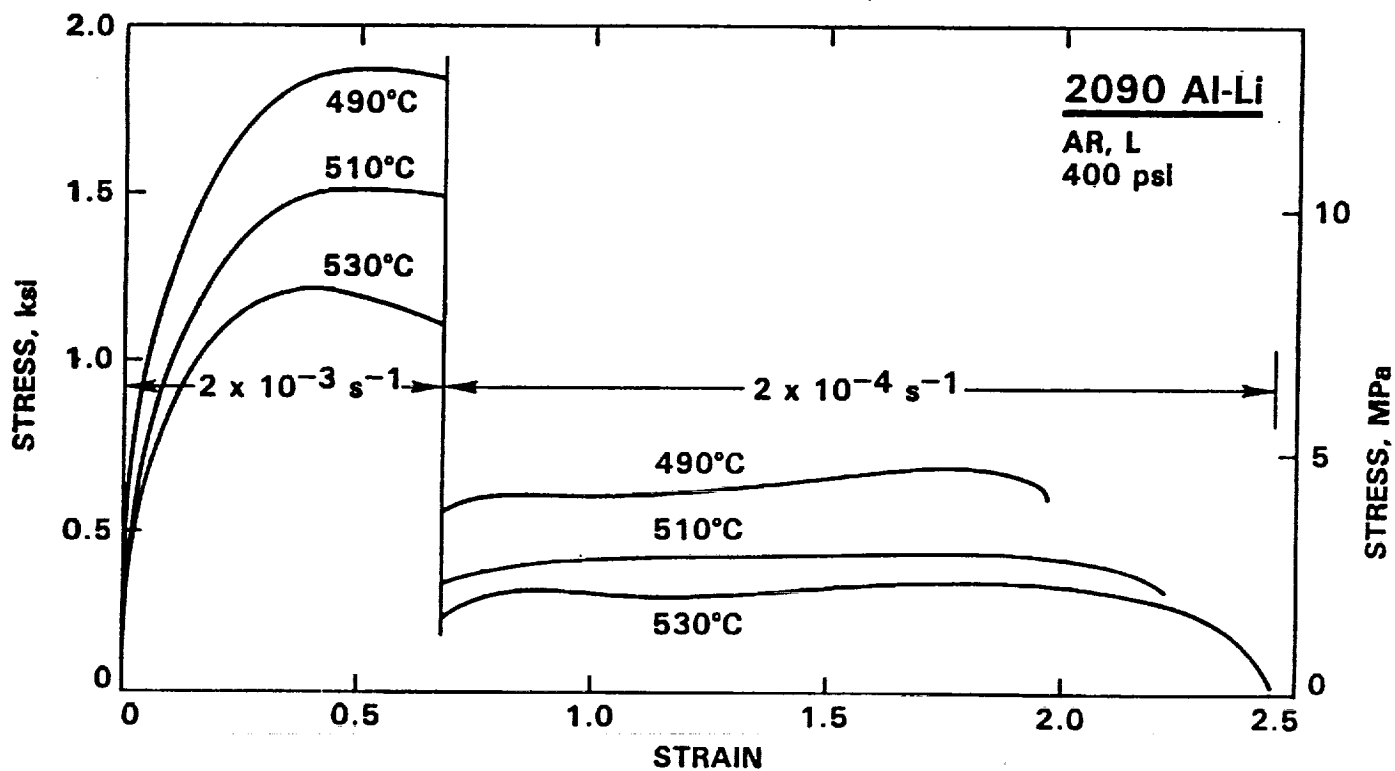


Figure 47. 2090 Al Transverse Flow Stress at 400 psi Back Pressure Versus Strain for Duplex Stage Strain Rates.

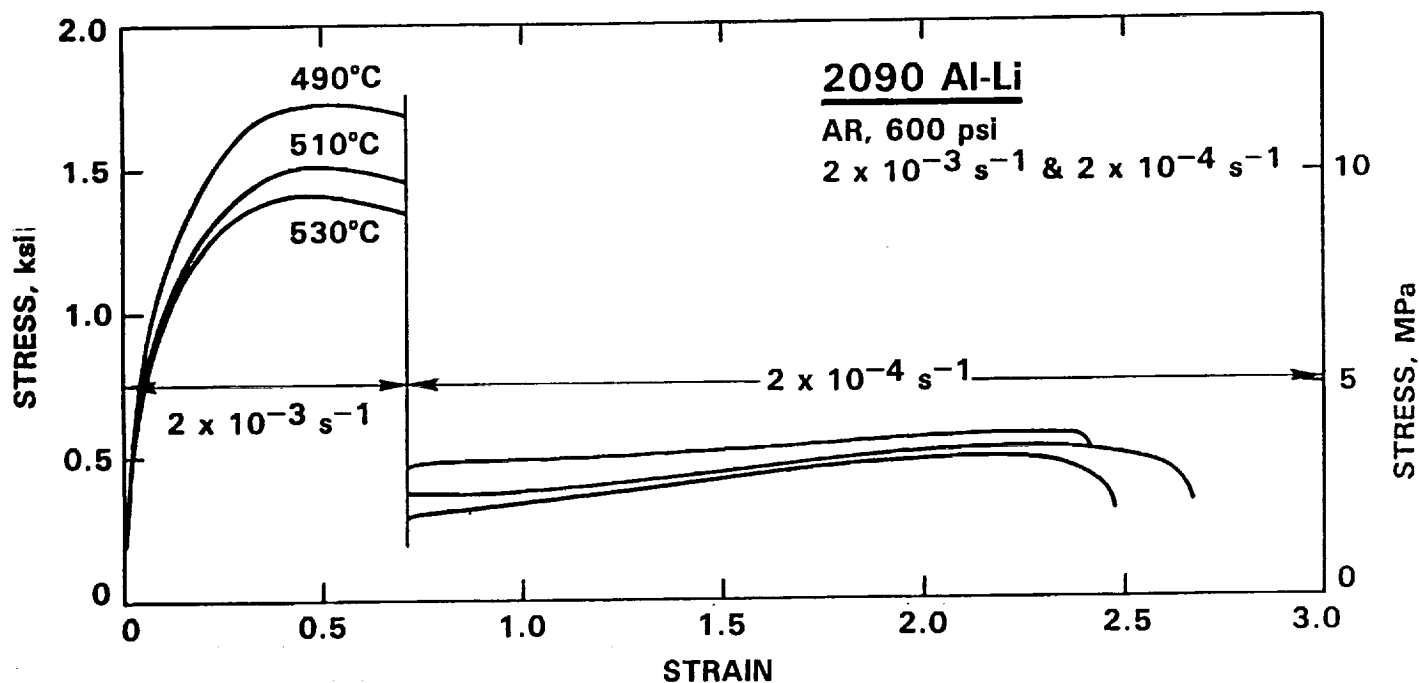


Figure 48. 2090 Al Transverse Flow Stress at 600 psi Back Pressure Versus Strain for Duplex Stage Strain Rates.

4.2.1.2.6 Superplastic Cavitation

Tensile samples tested up to strains of 2.0 with and without back pressure were examined metallographically for evidence of cavitation. The coupons tested in air showed extensive cavitation at strains of 1.0 while those tested with back pressure (400 psi) up to strains of 2.0 did not show any indication of superplastic cavitation.

4.2.1.3 8090 Aluminum-Lithium

The 8090 Al-Li material utilized during the study was supplied in the SPF condition from Alcan Aerospace. Chemical test certification supplied by Alcan on the material is as follows:

Cu	Mg	Si	Fe	Mn	Zn	Zr	Li	Cr	Ti	Ag	Al
1.18	0.61	.011	0.04	.001	0.03	0.12	2.35	.001	0.03		Rem

(510°C, 400 psi, $2 \times 10^{-3} \text{ s}^{-1}$ AND $2 \times 10^{-4} \text{ s}^{-1}$)

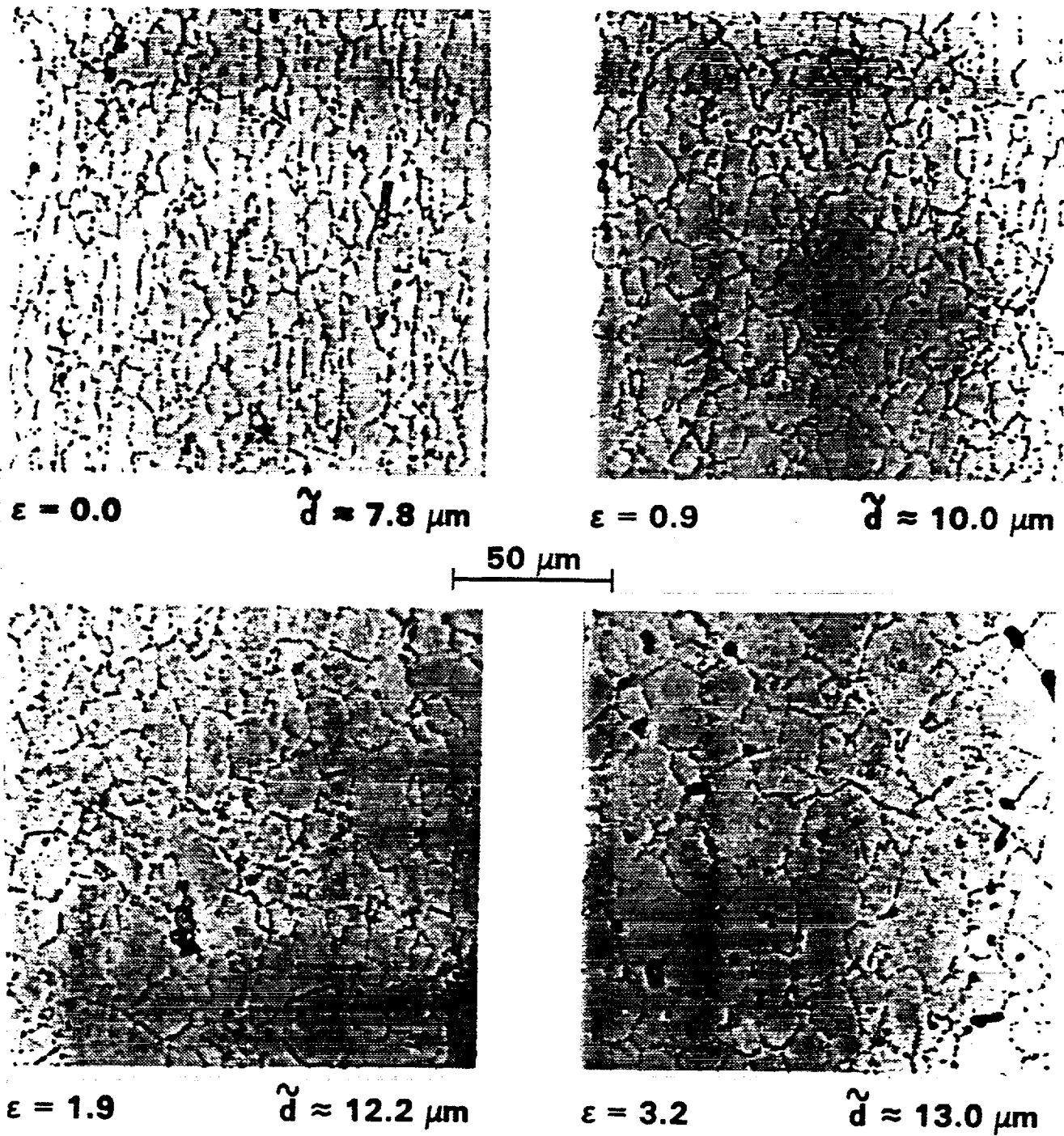


Figure 49. 2090 Al-Li Dynamic Grain Growth with Increase in Strain.

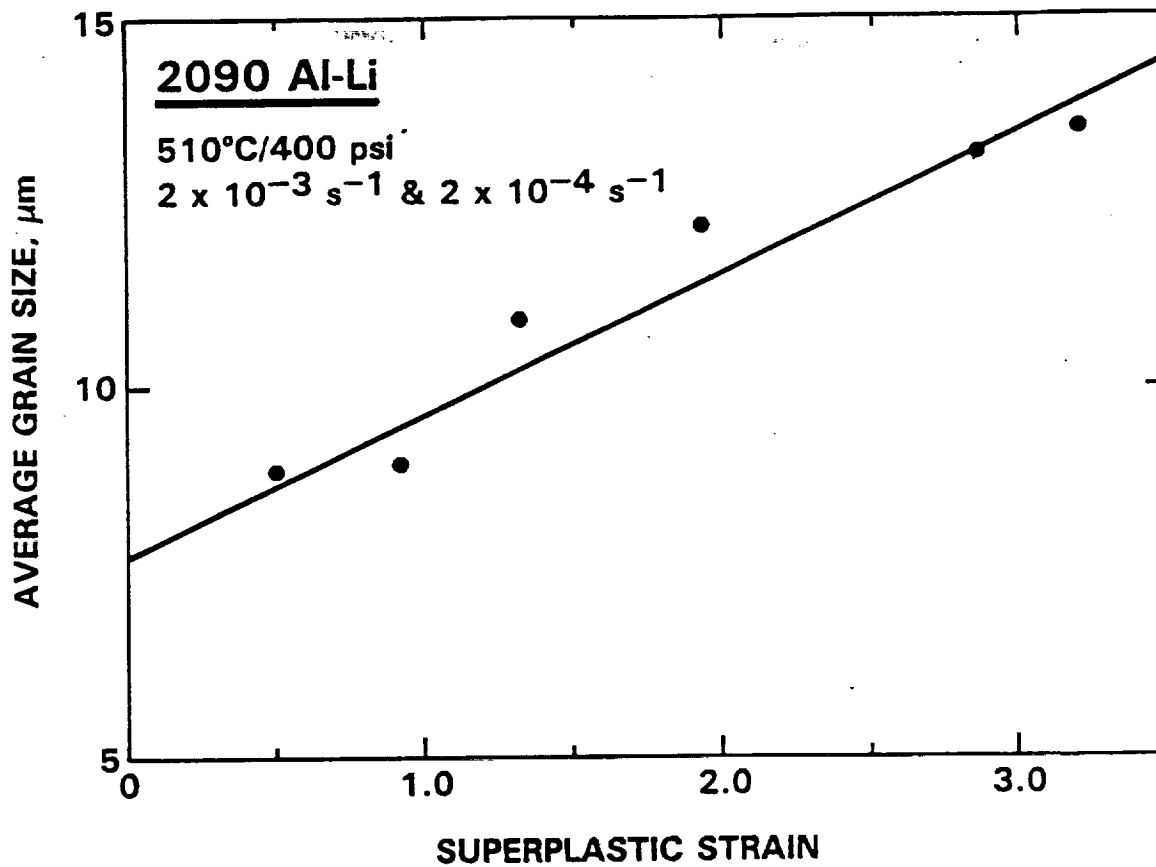


Figure 50. 2090 Al-Li Dynamic Grain Growth Versus Superplastic Strain.

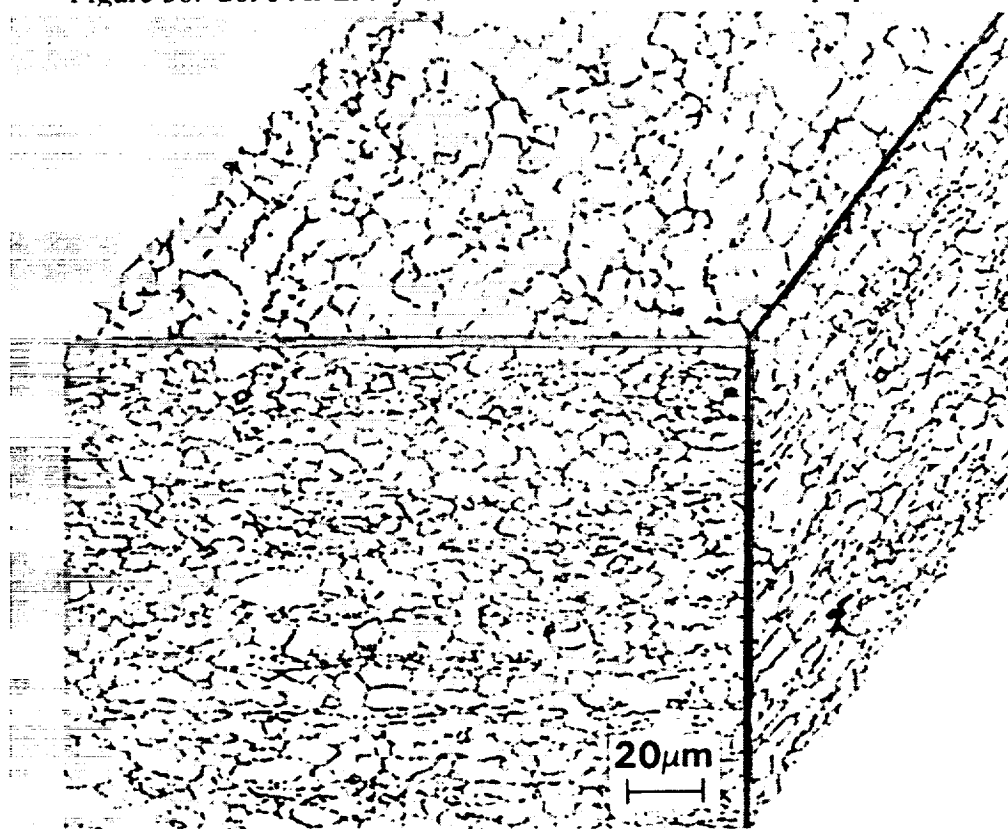


Figure 51. Microstructure of Superplastic 8090 Al-Li.

4.2.1.3.1 Metallurgical Analysis

Microstructural evaluation was performed on heat treated samples of the material (refer to Figure 51: solution heat treated at 968°F for 1 hour, water quenched and artificially aged at 374°F for 4 hours) in order to reveal the substructures of the material. The as-received material was fine grained with slightly elongated grains in the final rolling direction. The average grain sizes were approximately $3.3 \times 5.4 \times 5.2 \mu\text{m}$ in three directions. Static grain growth was observed to be moderate for the 8090 Al-Li alloy in the temperatures range of 914 to 986°F.

4.2.1.3.2 Stress-Strain Rate Behavior

Flow stress and strain rate sensitivity (m) measurements are shown versus strain rate in Figure 52 for 8090-SPF Al-Li material (uniaxial stepped strain rate tests were conducted without back pressure) for temperatures ranging from 914°F (490°C) to 986°F (530°C). The sigmoidal shape of the flow stress versus strain rate curves indicated that the material was superplastic at the intermediate strain rate. This conclusion is further corroborated by the measurement of strain rate sensitivity (m) with strain rate. The optimum SPF strain rate is shown to lie within 10^{-3} /second with a maximum strain rate sensitivity value of 0.6.

4.2.1.3.3 Flow Stress-Strain Data

Uniaxial testing of the 8090 Al-Li material was conducted to determine the optimum forming parameters for the material (refer to Figure 53). Initial testing briefly compared single strain rate deformation with two stage deformation (refer to Table 22). The results from the brief comparison yielded increased total SPF elongations with the two stage strain rate deformation versus the single stage strain rate.

Additional uniaxial tests were performed on the 8090 Al-Li material with the two stage strain rate deformation condition in order to optimize material forming parameters. The two stage strain rate tensile samples were initially pulled at a constant strain rate of 2×10^{-3} /second up to a strain of 0.72, after which the strain rate was reduced to 2×10^{-4} /second until failure of the samples occurred (due to test fixture limitations, samples that did not fail in the range of 1400 to 1600 percent superplastic elongation were removed from the test fixture). The aforementioned two stage uniaxial tests were performed at temperatures of 878°F to 1022 °F with back pressures of 200, 400, and 600 psi. The results (refer to Tables 23 and 24) showed that the 8090 Al-Li material exhibited excellent superplastic elongations which exceeded 1275% (in the longitudinal direction) with back pressures of 600 psi. The transverse samples showed slightly higher elongations with

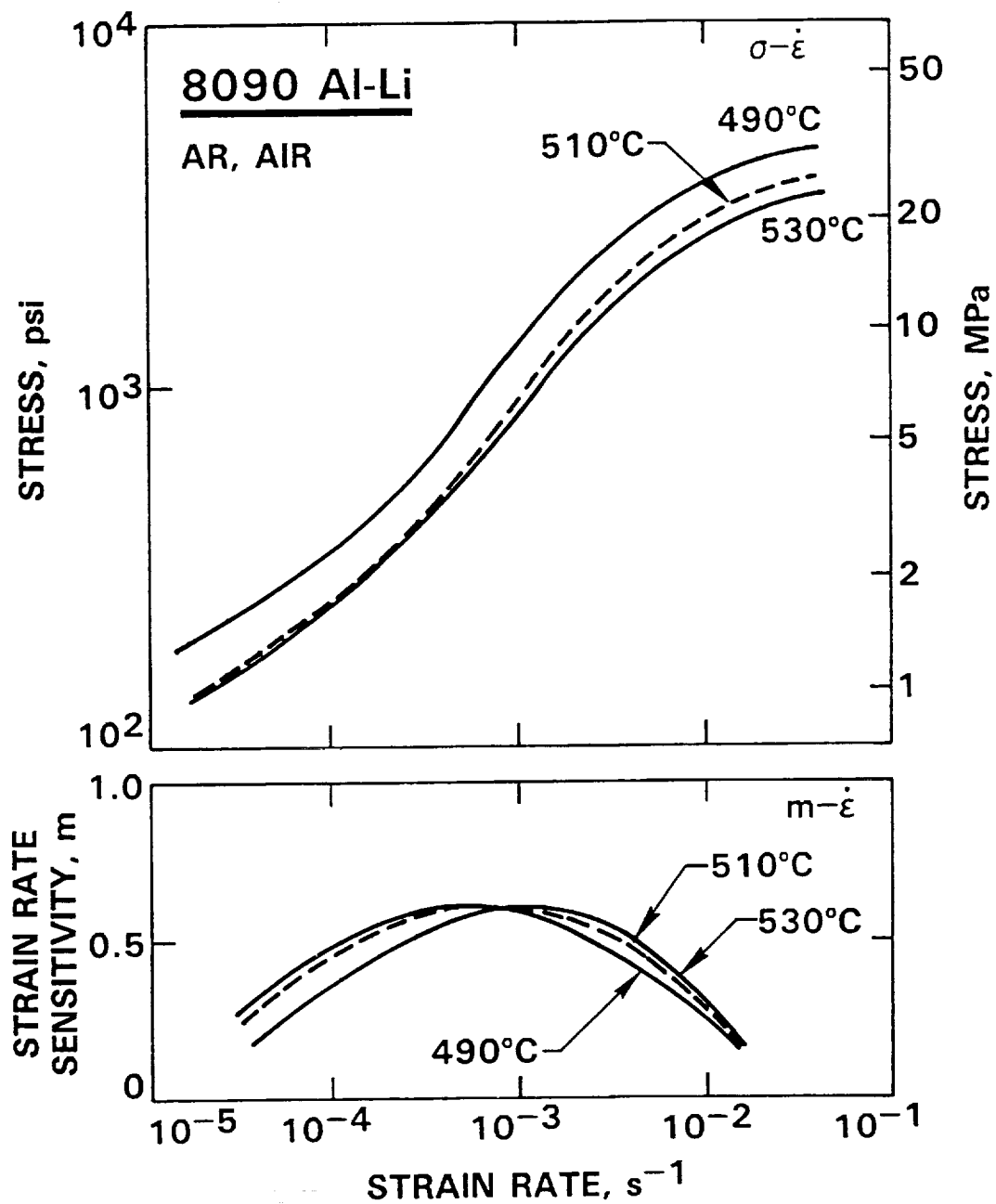


Figure 52. Flow Stress and Strain Rate Sensitivity Versus Strain Rate for 8090 Al-Li for Various Temperatures.

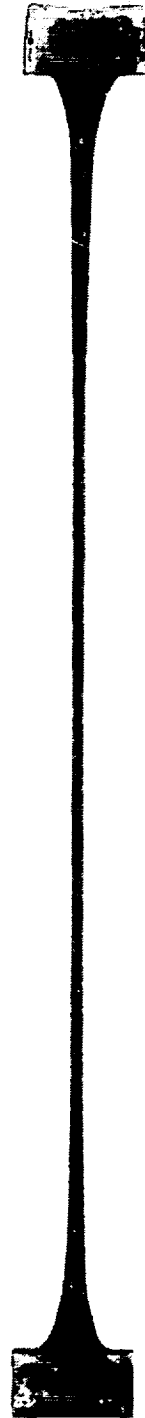
SC51875



UNTESTED



AIR, 450%



600 psi, 1225%

Figure 53. 8090 Al-Li Uniaxial Superplastic Elongations with Back Pressure. Tests were Performed at 915°F with Duplex Strain Rate of $2E-3$ and $2E-4 \text{ sec}^{-1}$.

the 600 psi back pressure and lower SPF temperatures than the longitudinal samples (refer to Table 24). The variation in elongation with test temperature and back pressure are shown graphically on Figure 54.

4.2.1.3.4 Dynamic Grain Growth

Dynamic grain growth was examined in conjunction with the two stage (duplex) strain rate forming condition. Grain growth was detected in the 8090 Al-Li material at all forming temperatures with increases in superplastic strain. The results from the evaluations at 914°F (490°C) without back pressure and with 400 psi back pressure are shown on Figures 55, 56, and 57. The increase in grain size of the material caused an increase in flow stress as shown in Figures 58, 59, and 60 of flow stress versus SPF strain.

4.2.1.3.5 Cavitation

Superplastic elongations of 8090 Al-Li were dramatically improved (refer to Figure 61) with the application of back pressure. The 8090 Al-Li alloy exhibited the same type of increase in superplastic elongations with increase in back pressure as the 7475 Al alloy throughout the test temperature range for the material. SPF elongations at low to moderate back pressure levels (levels at or below 400 psi are considered moderate by Rockwell) were optimum for forming temperatures between 914°F (490°C) and 1022°F (550°C). Intergranular cavitation of greater than 1 percent was observed in air tested samples (without back pressure) at strain levels as low as 0.6 (refer to Figure 56) while samples tested under back pressures at or greater than 400 psi did not show cavitation at strains up to 2.1 (refer to Figures 57 and 62). 8090 Al-Li (similarly to 7475 Al) requires higher back pressure levels to suppress cavitation at lower test temperatures (refer to Figure 61) and requires less back pressure to suppress cavitation as the forming temperature increases.

4.2.1.4 Weldalite-049 Aluminum-Lithium

Weldalite-049 aluminum-lithium material was developed by Martin Marietta Corp. and licensed to Reynolds Metals for fabrication. Its early development consisted of various iterations of the composition in order to obtain a balance of weldability, high strength, and acceptable toughness. The composition that was examined during this program is shown in the table below. The evaluation of the material was performed on two shipments of the material.

Cu	Mg	Si	Fe	Mn	Zn	Zr	Li	Cr	Ti	Ag	Al
4.47	0.4	0.02	0.06	.001		0.16	1.32			0.39	Rem

Table 22. Superplastic Tensile Elongations of 8090 Al-Li.

ALLOY	TMT	TEMP (°F)	PRESSURE (PSI)	STRAIN RATE (Per Second)	ELONGATION (%)
8090	AR	914	400	5×10^{-4}	695L
8090	AR	950	400	5×10^{-4}	547L
8090	AR	986	400	5×10^{-4}	424L
8090	AR	878	400	$2 \times 10^{-3} / 2 \times 10^{-4}$	754L
8090	AR	914	400	$2 \times 10^{-3} / 2 \times 10^{-4}$	863L
8090	AR	914	400	$2 \times 10^{-3} / 2 \times 10^{-4}$	913T
8090	AR	950	400	$2 \times 10^{-3} / 2 \times 10^{-4}$	797T
8090	AR	986	400	$2 \times 10^{-3} / 2 \times 10^{-4}$	796T
8090	AR	878	600	$2 \times 10^{-3} / 2 \times 10^{-4}$	829L
8090	AR	914	600	$2 \times 10^{-3} / 2 \times 10^{-4}$	877L

L: longitudinal, and T: transverse direction to final rolling., AR: as-received

Table 23. Superplastic Two-Stage Strain Rate Longitudinal Tensile Elongations of 8090 Al-Li Alloy.

ALLOY	TMT	TEMP (°F)	PRESSURE (PSI)	STRAIN RATE (Per Second)	ELONGATION (%)
8090	AR	878	AIR	$2 \times 10^{-3} / 2 \times 10^{-4}$	450L
8090	AR	878	200	$2 \times 10^{-3} / 2 \times 10^{-4}$	366L
8090	AR	878	400	$2 \times 10^{-3} / 2 \times 10^{-4}$	754L
8090	AR	878	600	$2 \times 10^{-3} / 2 \times 10^{-4}$	829L
8090	AR	914	AIR	$2 \times 10^{-3} / 2 \times 10^{-4}$	496L
8090	AR	914	200	$2 \times 10^{-3} / 2 \times 10^{-4}$	766L
8090	AR	914	400	$2 \times 10^{-3} / 2 \times 10^{-4}$	863L
8090	AR	914	600	$2 \times 10^{-3} / 2 \times 10^{-4}$	877L
8090	AR	950	AIR	$2 \times 10^{-3} / 2 \times 10^{-4}$	555L
8090	AR	950	200	$2 \times 10^{-3} / 2 \times 10^{-4}$	760L
8090	AR	950	400	$2 \times 10^{-3} / 2 \times 10^{-4}$	914L
8090	AR	950	600	$2 \times 10^{-3} / 2 \times 10^{-4}$	948L
8090	AR	986	AIR	$2 \times 10^{-3} / 2 \times 10^{-4}$	548L
8090	AR	986	200	$2 \times 10^{-3} / 2 \times 10^{-4}$	917L
8090	AR	986	400	$2 \times 10^{-3} / 2 \times 10^{-4}$	836L
8090	AR	986	600	$2 \times 10^{-3} / 2 \times 10^{-4}$	939L
8090	AR	1022	AIR	$2 \times 10^{-3} / 2 \times 10^{-4}$	550L
8090	AR	1022	200	$2 \times 10^{-3} / 2 \times 10^{-4}$	278L
8090	AR	1022	400	$2 \times 10^{-3} / 2 \times 10^{-4}$	979L
8090	AR	1022	600	$2 \times 10^{-3} / 2 \times 10^{-4}$	620L

L: longitudinal direction to final rolling. AR: as-received

Bold Highlight: Selected Forming Parameters

Table 24. Superplastic Two-Stage Strain Rate Transverse Tensile Elongations of 8090 Al-Li Alloy.

ALLOY	TMT	TEMP (°F)	PRESSURE (PSI)	STRAIN RATE (Per Second)	ELONGATION (%)
8090	AR	878	AIR	$2 \times 10^{-3} / 2 \times 10^{-4}$	445T
8090	AR	878	200	$2 \times 10^{-3} / 2 \times 10^{-4}$	365T
8090	AR	878	400	$2 \times 10^{-3} / 2 \times 10^{-4}$	355T
8090	AR	878	600	$2 \times 10^{-3} / 2 \times 10^{-4}$	1275T
8090	AR	914	AIR	$2 \times 10^{-3} / 2 \times 10^{-4}$	448T
8090	AR	914	200	$2 \times 10^{-3} / 2 \times 10^{-4}$	345T
8090	AR	914	400	$2 \times 10^{-3} / 2 \times 10^{-4}$	913T
8090	AR	914	600	$2 \times 10^{-3} / 2 \times 10^{-4}$	1225T
8090	AR	950	AIR	$2 \times 10^{-3} / 2 \times 10^{-4}$	621T
8090	AR	950	200	$2 \times 10^{-3} / 2 \times 10^{-4}$	666T
8090	AR	950	400	$2 \times 10^{-3} / 2 \times 10^{-4}$	797T
8090	AR	950	600	$2 \times 10^{-3} / 2 \times 10^{-4}$	952T
8090	AR	986	AIR	$2 \times 10^{-3} / 2 \times 10^{-4}$	652T
8090	AR	986	200	$2 \times 10^{-3} / 2 \times 10^{-4}$	926T
8090	AR	986	400	$2 \times 10^{-3} / 2 \times 10^{-4}$	796T
8090	AR	986	600	$2 \times 10^{-3} / 2 \times 10^{-4}$	1125T
8090	AR	1022	AIR	$2 \times 10^{-3} / 2 \times 10^{-4}$	485T
8090	AR	1022	200	$2 \times 10^{-3} / 2 \times 10^{-4}$	264T
8090	AR	1022	400	$2 \times 10^{-3} / 2 \times 10^{-4}$	942T
8090	AR	1022	600	$2 \times 10^{-3} / 2 \times 10^{-4}$	743T

T: Transverse direction to final rolling. AR: as-received
Bold Highlight: Selected Forming Parameters

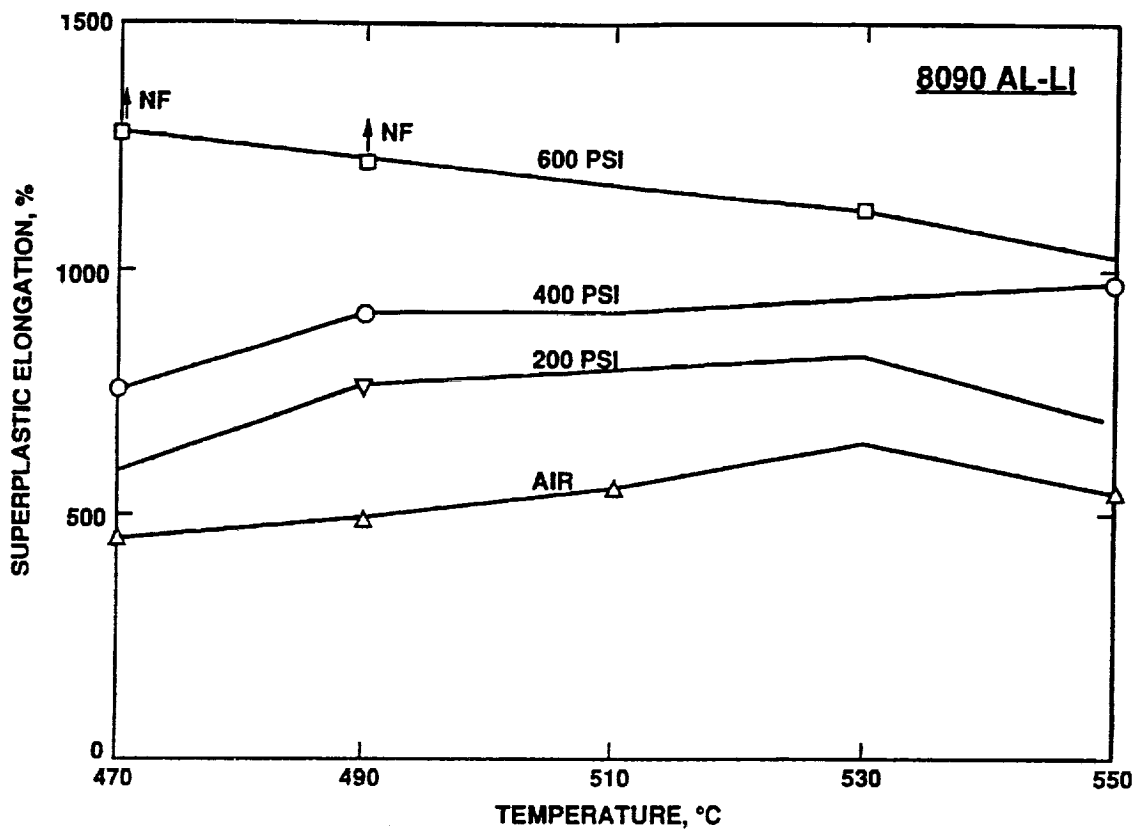


Figure 54. Superplastic Elongation Versus Forming Temperature for 8090 Al-Li at Various Levels of Back Pressure.

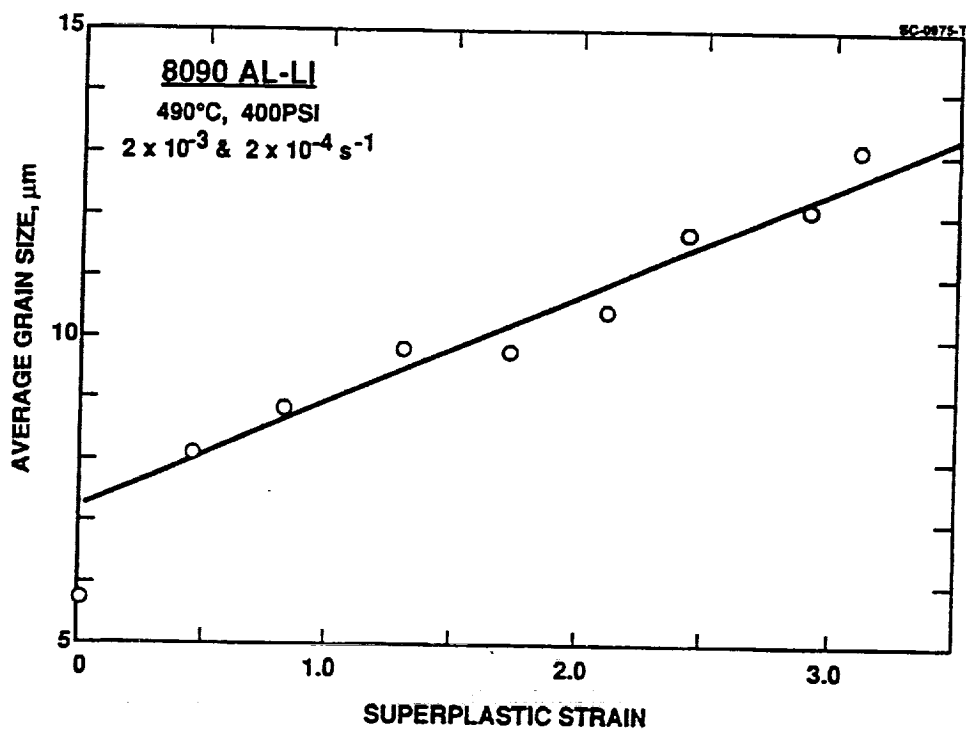
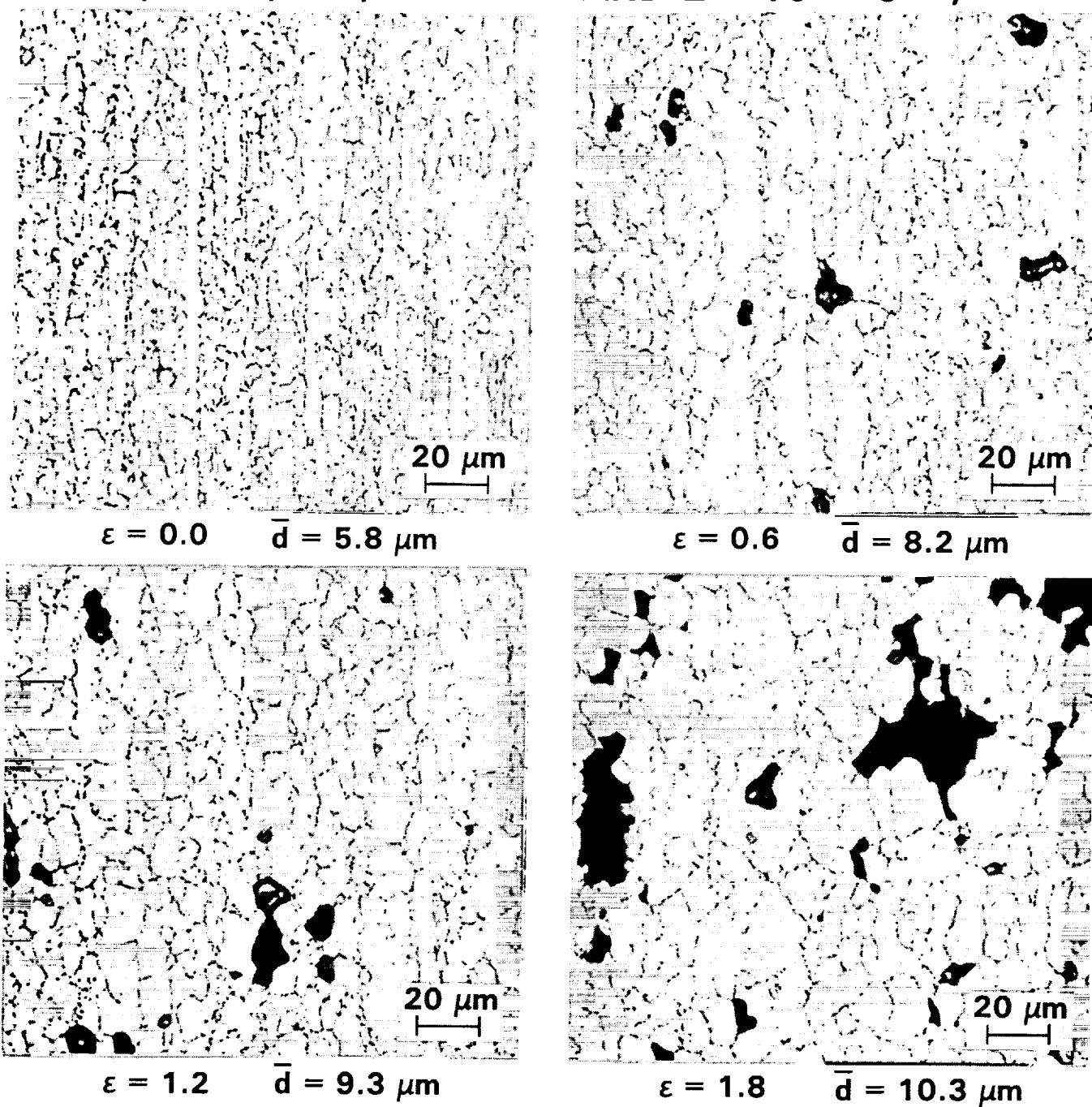


Figure 55. Average Grain Size Versus Superplastic Strain for 8090 Al-Li.

(490°C, AIR, 2×10^{-3} AND $2 \times 10^{-4} \text{ s}^{-1}$)

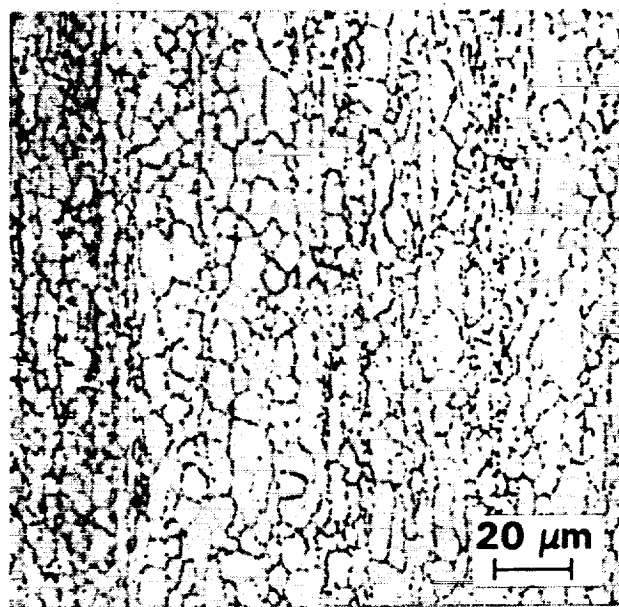


Rockwell International

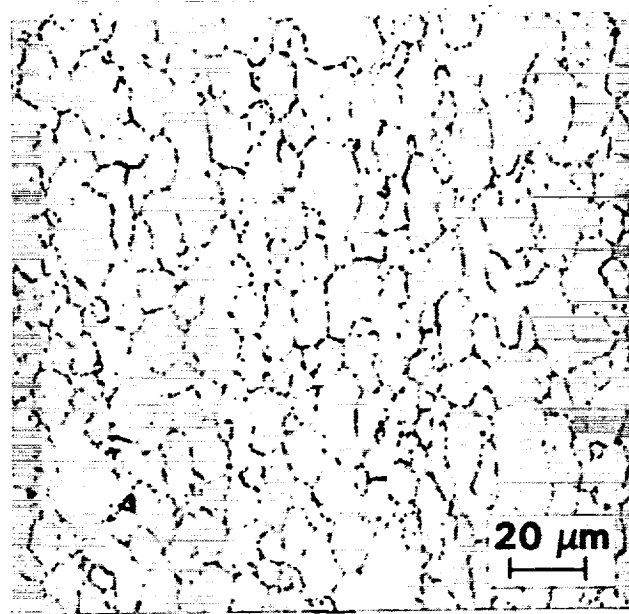
Figure 56. Dynamic Grain Growth and Superplastic Cavitation in 8090 Al-Li, Formed Without Back Pressure.

(490°C, 400 psi, 2×10^{-3} AND $2 \times 10^{-4} \text{ s}^{-1}$)

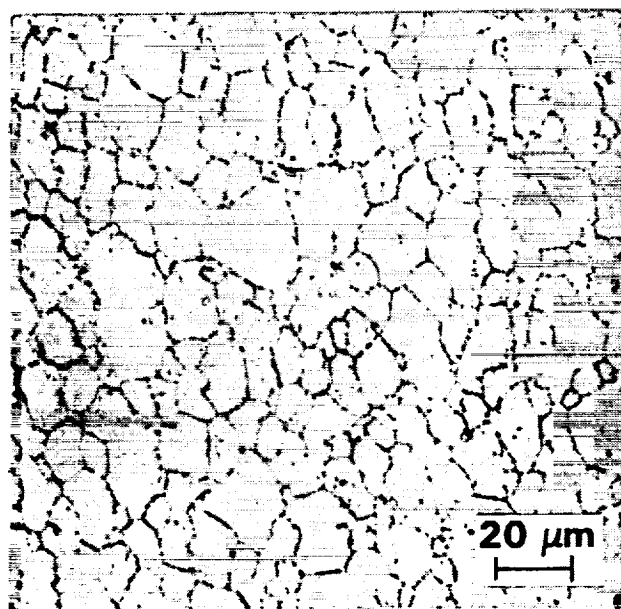
SC51840



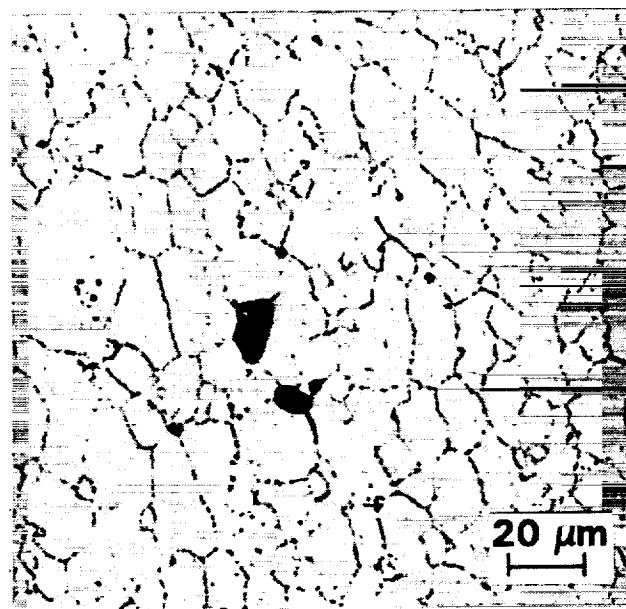
$\varepsilon = 0.0$ $\bar{d} = 5.8 \mu\text{m}$



$\varepsilon = 0.8$ $\bar{d} = 8.8 \mu\text{m}$



$\varepsilon = 2.1$ $\bar{d} = 10.4 \mu\text{m}$



$\varepsilon = 3.1$ $\bar{d} = 13.1 \mu\text{m}$



Rockwell International

Figure 57. Dynamic Grain Growth in 8090 Al-Li Formed with 400 psi Back Pressure.

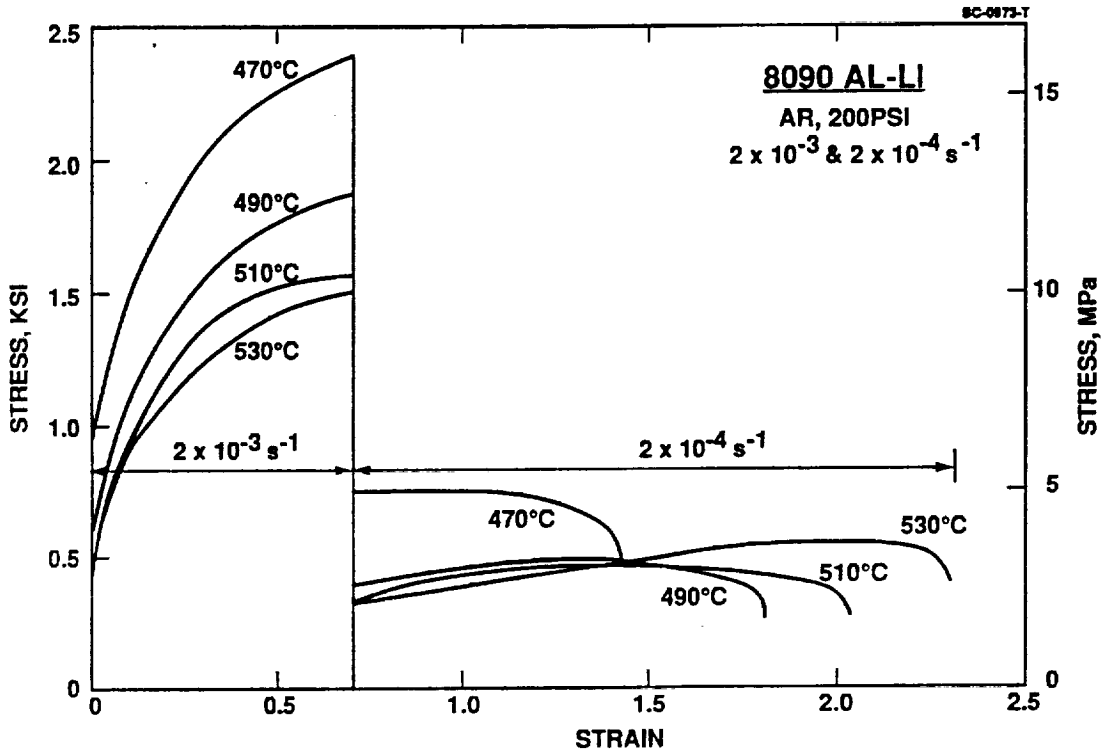


Figure 58. Flow Stress Versus Strain for 8090 Al-Li Formed with 200 psi Back Pressure.

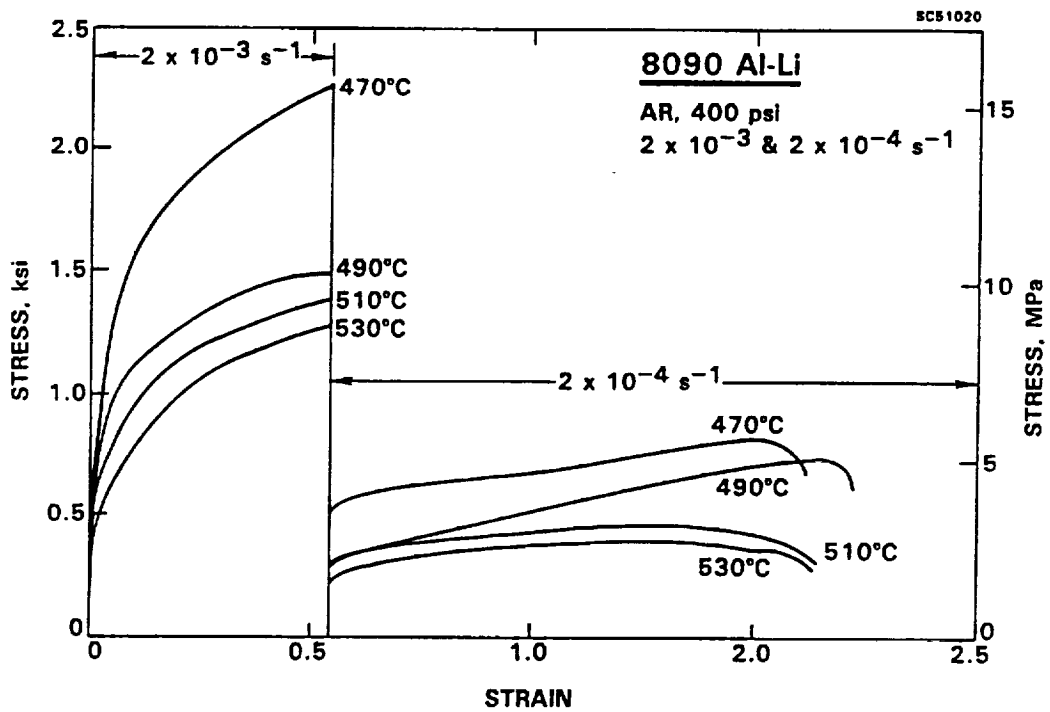


Figure 59. Flow Stress Versus Strain for 8090 Al-Li Formed with 400 psi Back Pressure

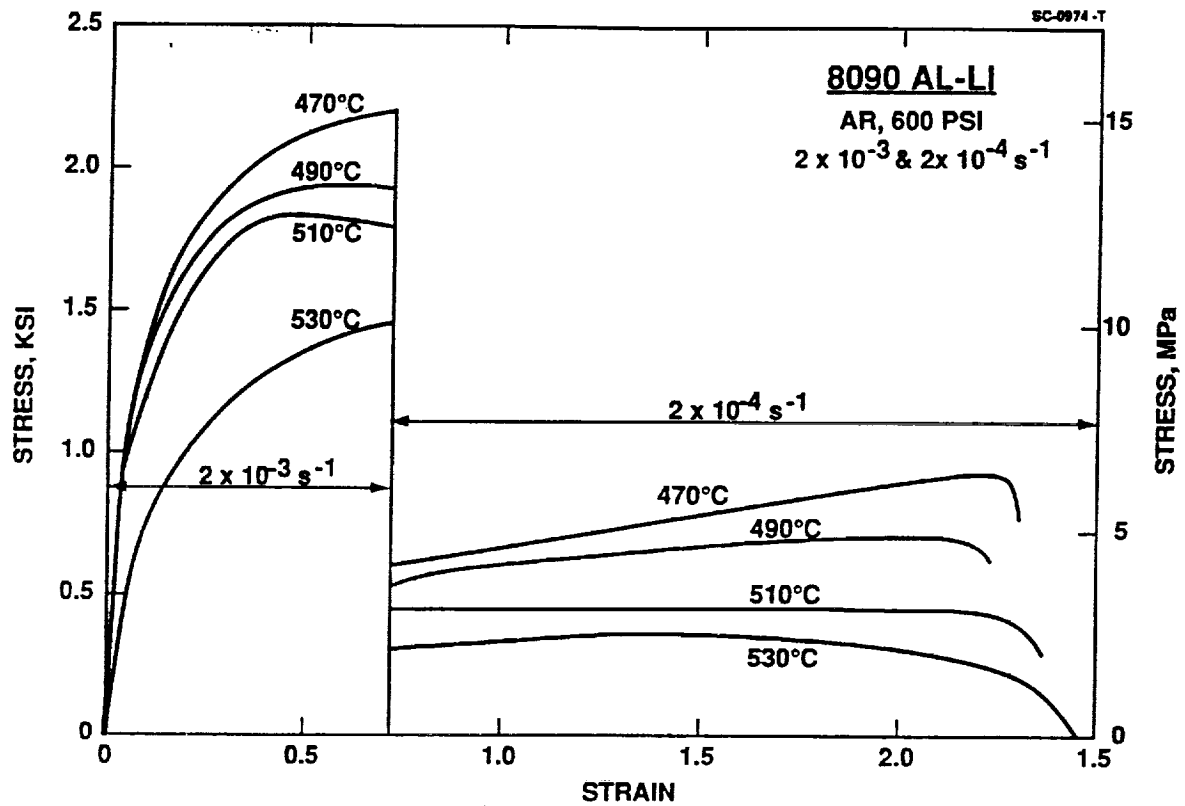


Figure 60. Flow Stress Versus Strain for 8090 Al-Li Formed with 600 psi Back Pressure.

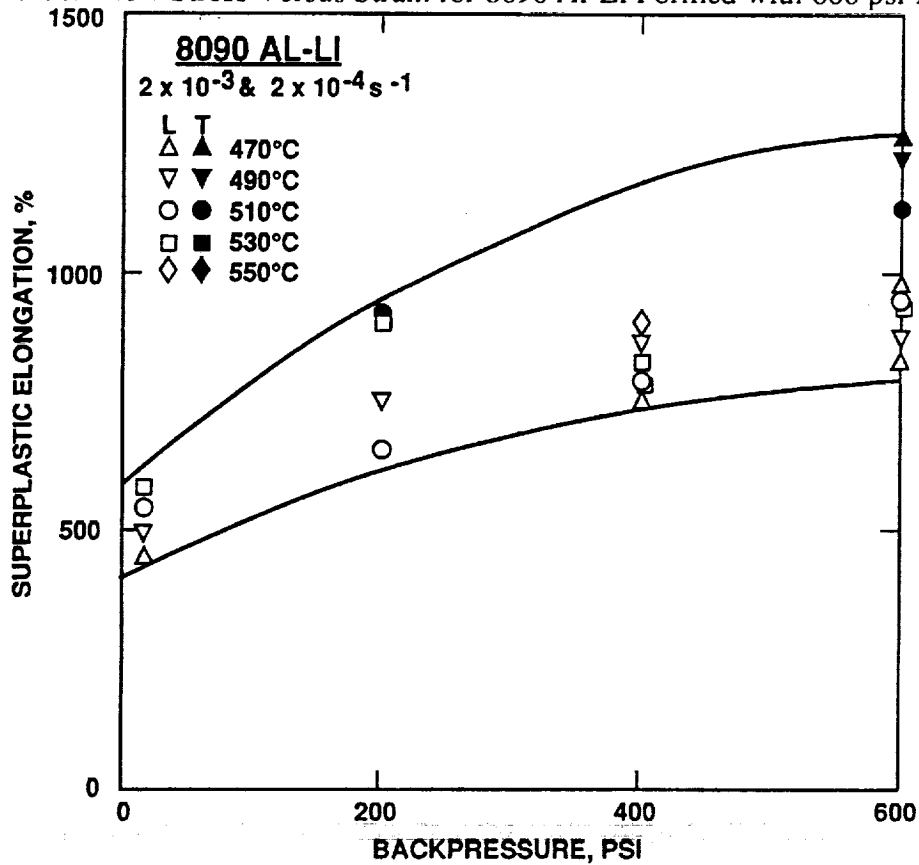
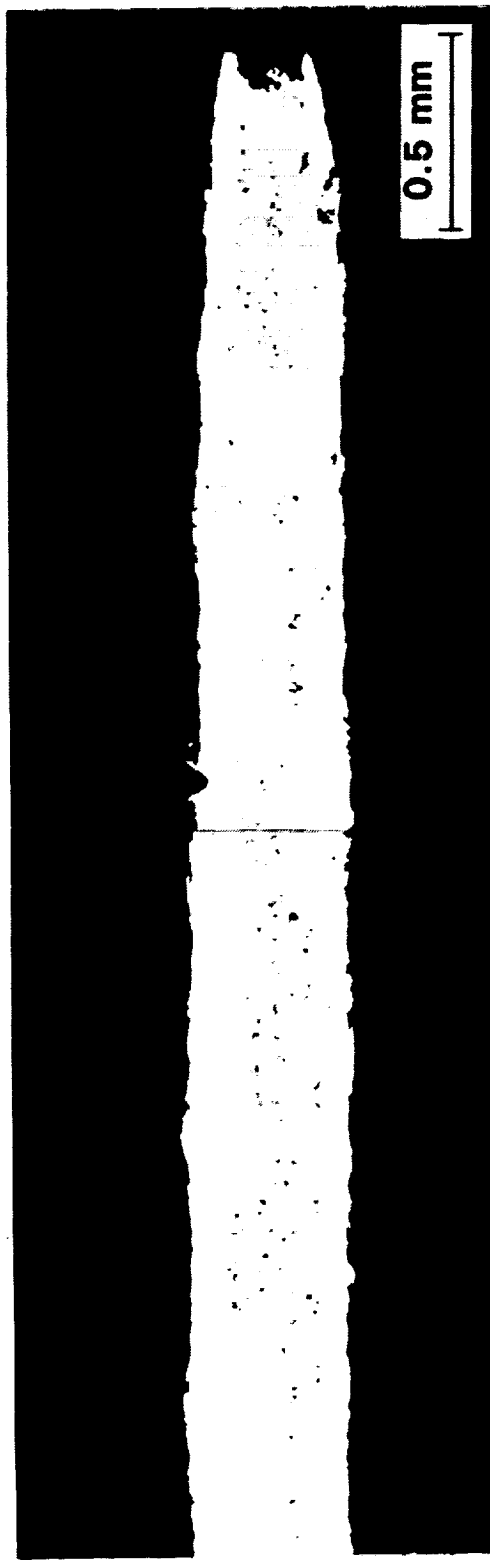


Figure 61. Superplastic Elongation Versus Back Pressure for 8090 Al-Li at Various Forming Temperatures.



AIR (NO BACKPRESSURE), $\epsilon = 1.7$



BACK PRESSURE 400 psi, $\epsilon = 3.1$



Rockwell International
Science Center

Figure 62. Severe Superplastic Cavitation for Strain of 1.7 in 8090 Al-Li Without Back Pressure versus Suppressed Cavitation for an Increase in Strain to 3.1 with 400 psi Back Pressure.

4.2.1.4.1 Metallurgical Analysis

The initial lot of Weldalite-049 material procured for the program did not appear to be superplastic during microstructural evaluation (refer to Figure 63). However, uniaxial testing was performed on two samples in order to corroborate the microstructural evaluation and verify the conclusion that the material was not superplastic. Further testing was delayed with the alloy until SPF quality material could be obtained. Microstructural examination of the second lot obtained for the program was performed and compared to the material that was observed to be non-superplastic. The microstructure of the second lot (Weldalite 049-RT72 sheet) was fine grained with a noticeable banded appearance (refer to Figure 64) which projected a more favorable uniaxial tensile response than the previous lot. It was unclear as to the reason for the initial lot's non-superplastic characteristics, but was assumed that a mistake had been made and conventional sheet material had been shipped for evaluation.

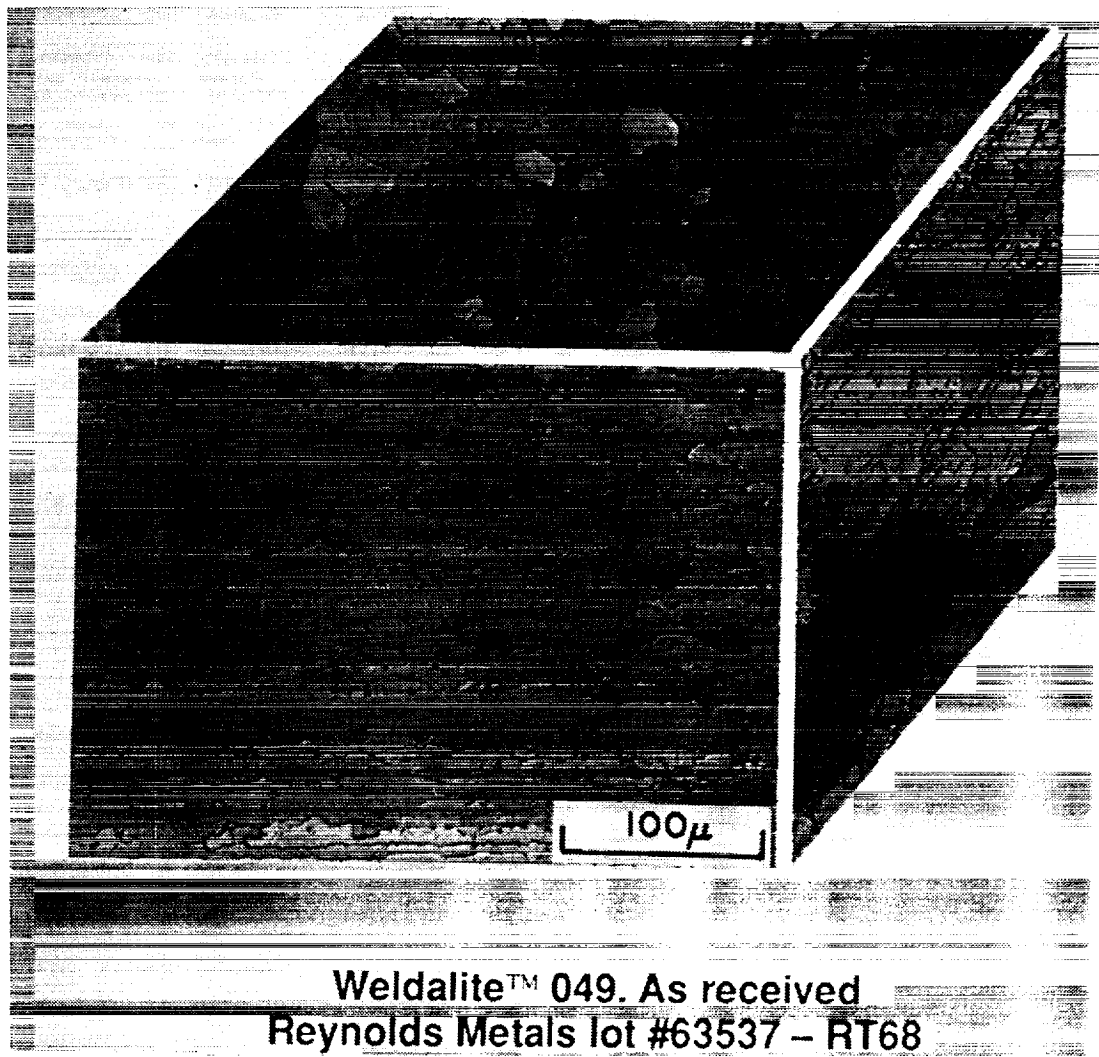


Figure 63. Microstructure of Weldalite-049 Al-Li Observed to be Non-Superplastic.

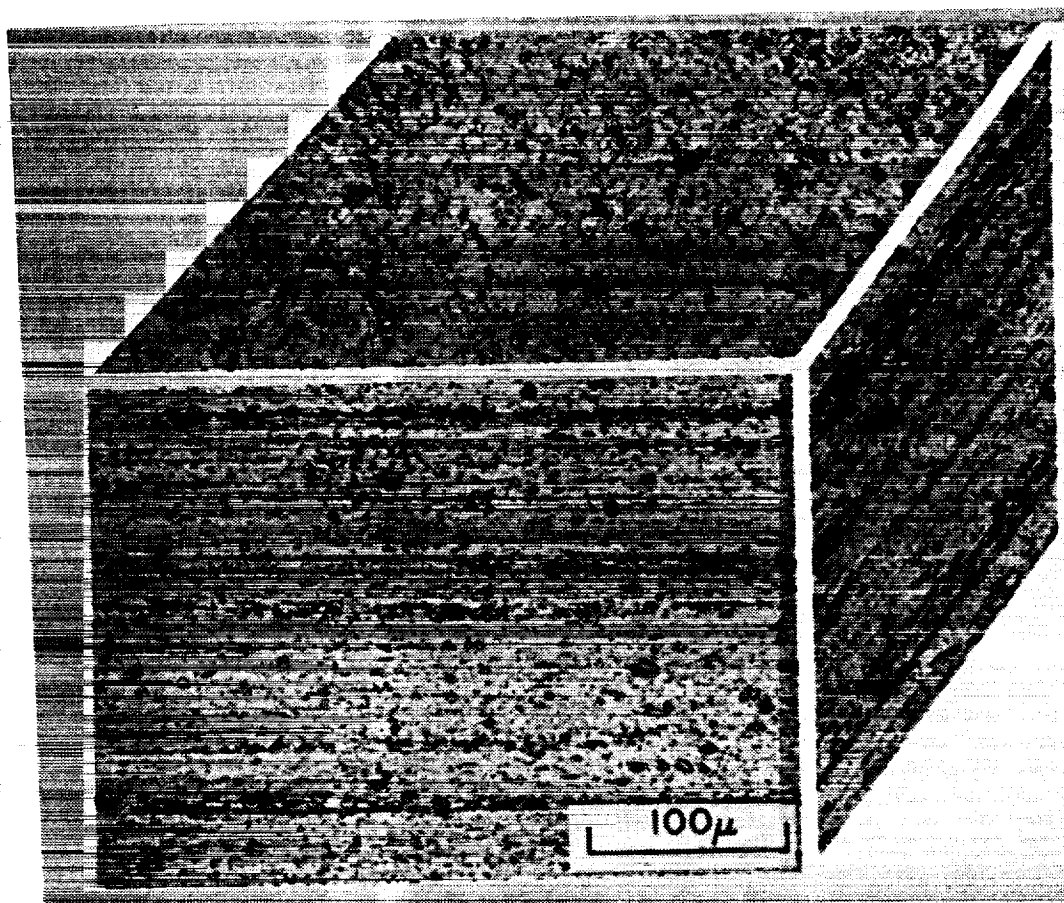


Figure 64. Microstructure of Weldalite-049 Al-Li Observed to be Superplastic.

4.2.1.4.2 Step-Strain Rate Testing

Stepped strain rate tests were performed on the two lots of material obtained for the program. The initial tests (refer to Figure 65 and 66) show the flow stress of the material and the m -value versus strain rate. The test results from the initial lot of material resulted in the non-superplastic rating for the material. The flow stress versus strain rate graphs resulting from the tests with the initial batch of material were linear and did not follow the sigmoidal trend normally associated with superplastic materials, and the m -value versus strain rate curves were nearly flat. The non-superplastic rating was based upon the combination of the stepped strain rate test results, the presence of extreme necking in the samples during uniaxial testing, and the microstructure of the as-received material.

The stepped strain rate tests performed on the second batch of Weldalite-049 (x2095 Al-Li) material received during the program was also evaluated for uniaxial behavior at elevated

temperature. The flow stress and m-value versus strain rate curves are shown as Figures 67 and 68. The behavior of the second lot of material during uniaxial superplastic deformation showed that the material was indeed superplastic although the optimum forming temperature for the material was significantly lower than other aluminum based materials previously examined.

4.2.1.4.3 Flow Stress-Strain Data

The uniaxial testing of the Weldalite 049-RT72 sheet revealed that the optimum parameters for longitudinal direction testing have generated true strains of up to 2.5. The parameters used for the longitudinal tests were temperature of 914°F (490°C) with 600 psi back pressure for strain rates of 3×10^{-4} /sec. The Long-transverse direction test results at the identical parameters yielded true strains of 1.6. The anisotropy observed in the SPF constant strain rate tests between L and L-T directions and the apparent "strain softening" behavior of the material during the uniaxial testing will require further investigation in order to pinpoint the cause of this behavior and verify its existence from lot to lot.

The effect of strain rate and coupon orientation on the elongation and flow stress were examined for the superplastic Weldalite material. It was observed that the maximum elongations occurred in the longitudinal direction, and in the range of $\epsilon = 3E^{-4}$ and $6E^{-4}$ per second (refer to Figure 69). Flow stress levels were lowest for the coupons tested at slower strain rates and elongation appeared to be very uniform without significant necking in the test coupons. The higher strain rates produced good to excellent elongations in the test coupons, but as the strain rate was increased, the propensity for necking in the coupon increased (refer to the flow stress curve at $\epsilon = 1E^{-3}$ per second). Some anisotropy was encountered during uniaxial testing of the weldalite material at Rockwell. Prior to fabrication of producibility hardware with the weldalite material, technical contact was made with Lockheed Aeronautical Systems Company on their recent experience with the testing and formability of the material. Lockheed did not observe the degree of anisotropy that was present during the Rockwell evaluation of the material. The disparity in results from this program and other studies, indicates that the processing of the weldalite material is still in its infancy, and that variations in behavior from lot-to-lot will continue to be observed during the development of the material.

The temperature effects of the Weldalite-049 SPF sheet on the elongation during superplastic forming are shown in Figure 70. All of the tests were performed at constant strain rate of $3E^{-4}$ per second under 600 psi back pressure. The elongation was maximized at the forming temperature of 915°F. Since the material appears to have a very narrow range of optimal

superplastic behavior, it is recommended that very rigorous thermal control is maintained during the forming of all structural components as loose control will result in non-uniform formability and the propensity for cavitation in the out-of-tolerance regions (refer to Figure 70).

4.2.1.4.4 Dynamic Grain Growth

The effects on the superplastic Weldalite-049 material after static thermal exposures of 915 or 930°F for three hours were evaluated in order to determine the reasons for reductions in elongation to failure for material tested at 930°F. The observation from the test (refer to Figure 71) was that exposure for the Weldalite-049 material to 930°F resulted in an increase in recrystallized grain structure and static grain growth over those exposed to 915°F. The amount of static grain growth observed in the three hour exposure test verified that the material is quite sensitive to changes in temperature during forming and that thermal control of the samples should be tightly controlled during part fabrication.

4.2.1.4.5 Superplastic Cavitation

Cavitation in behavior of the superplastic Weldalite-049 material was evaluated for material formed with 10 psi, 200 psi, and 600 psi back pressure (refer to Figure 72) during uniaxial testing. A back pressure of 600 psi provided the maximum suppression of cavity formation during elongation. The lower levels of back pressure (200 psi) reduced the formation of cavitation, but did not eliminate it from areas of high elongation in the samples. The indications observed in the uniaxial specimens suggest that at low levels of strain required for most parts, that back pressures between 200 and 600 psi should readily suppress cavitation in formed parts. The hypothesis was tested during the forming trials for the Weldalite-049 material and is reported in the producibility section of this report.

4.2.2 PRODUCIBILITY STUDY

The fabrication of producibility pans of 7475 Al, 2090 Al-Li, 8090 Al-Li, and the x2095 Al-Li (Weldalite-049) materials was conducted immediately following completion of the uniaxial characterization of each material. All of the materials used during the program were formed with existing tooling into simple pan shapes to ensure proper translation of the uniaxial data into

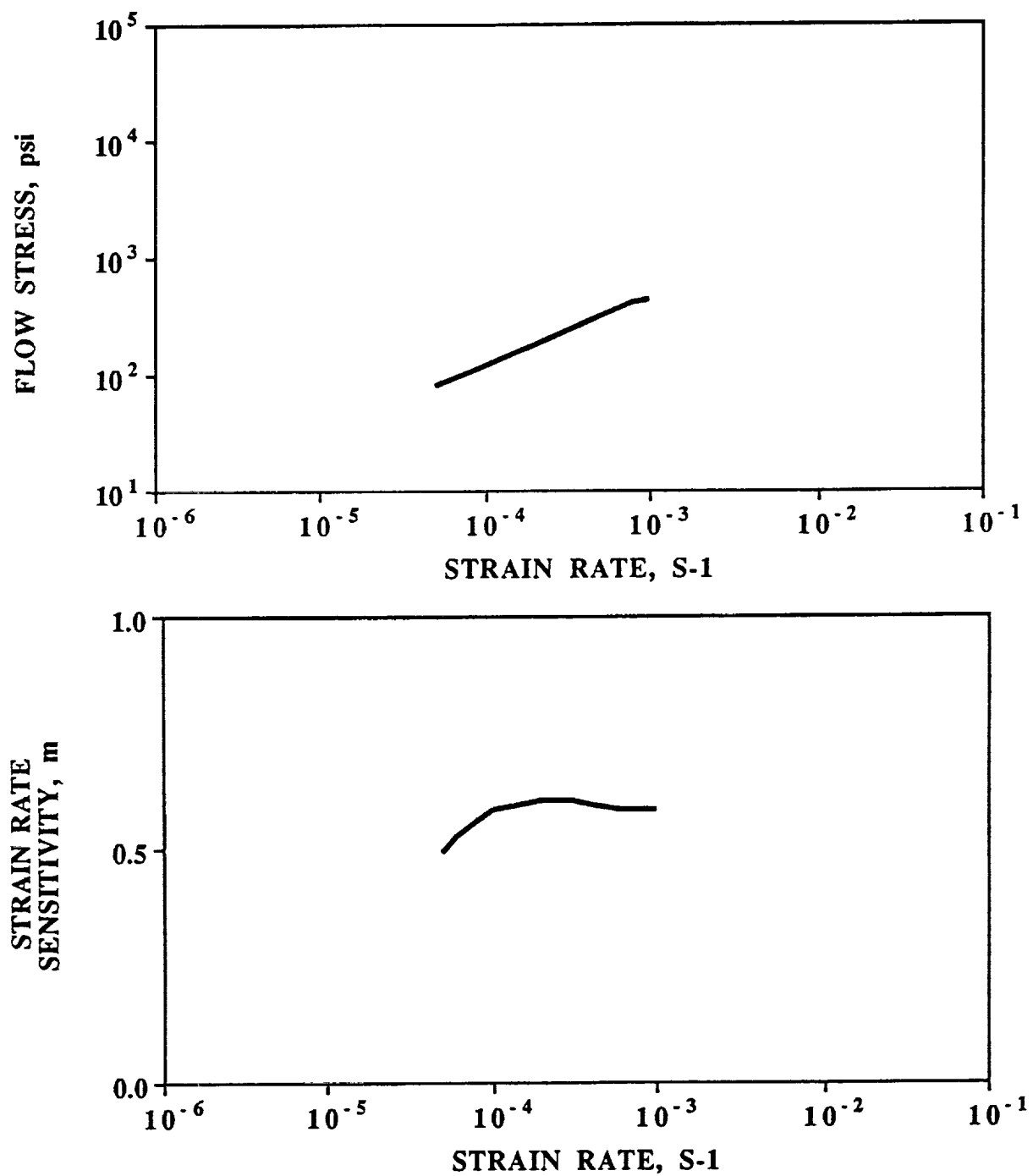


Figure 65. Flow Stress and M-value Versus Strain Rate for Initial Batch of Weldalite-049 Al-Li Sheet, Longitudinal Direction Tested, at 915°F at 600 psi Back Pressure.

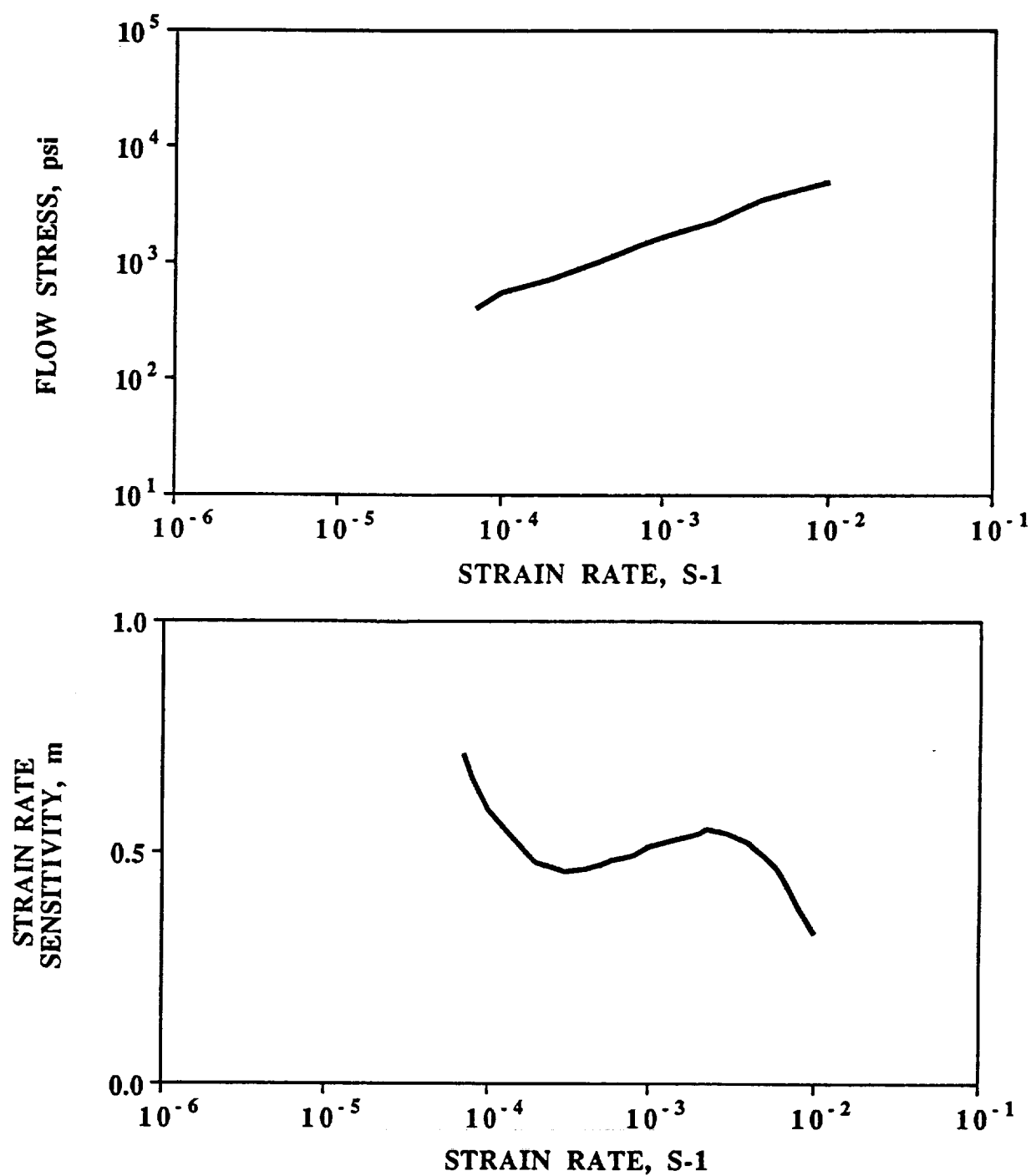


Figure 66. Flow Stress and M-value Versus Strain Rate for Initial Batch of Weldalite-049 Al-Li Sheet, Transverse Direction, Tested at 914°F at 600 psi Back Pressure.

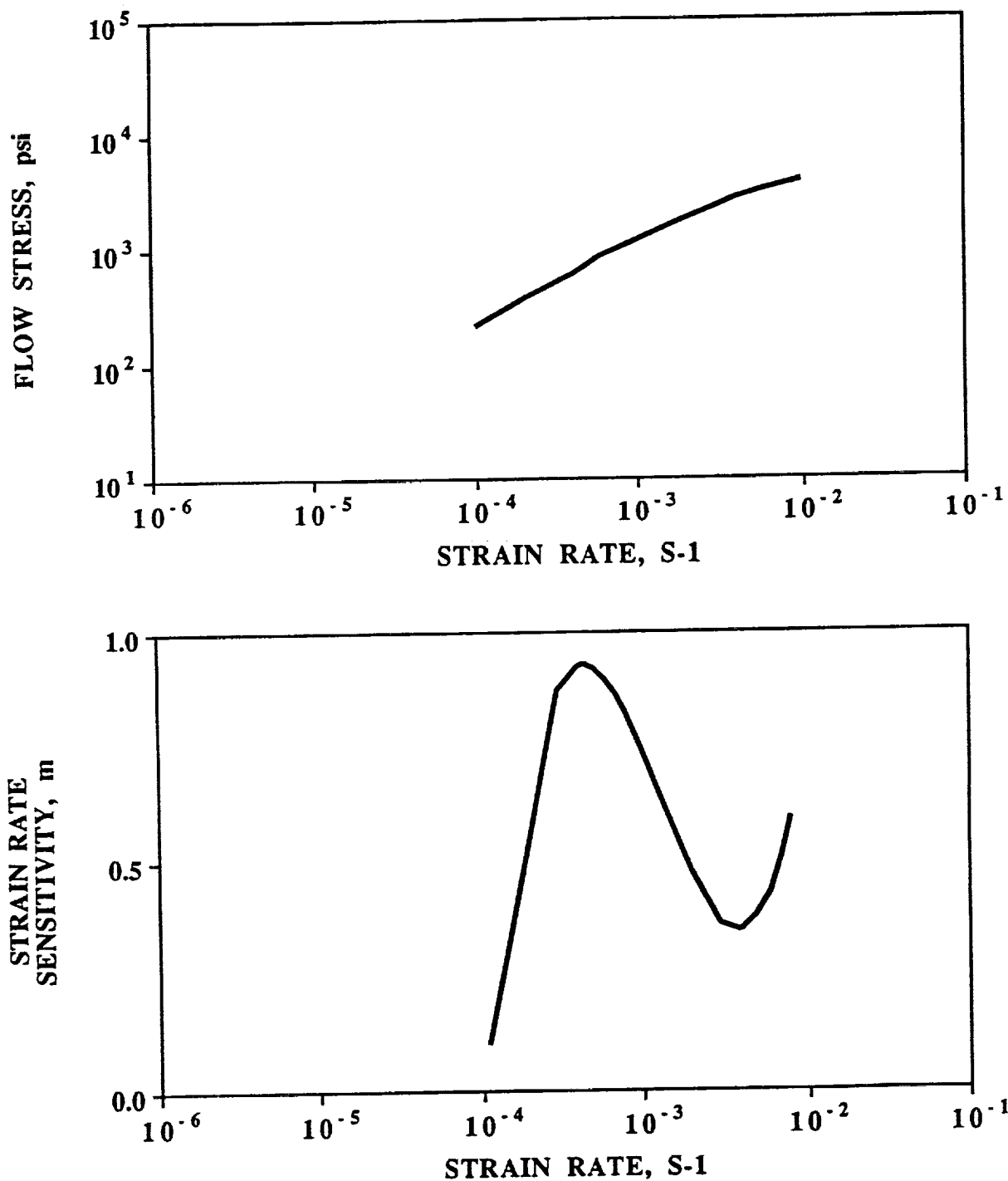


Figure 67. Flow Stress and M-value Versus Strain Rate for Second Batch of Weldalite-049 Al-Li Sheet, Longitudinal Direction Tested, at 915°F at 600 psi Back Pressure.

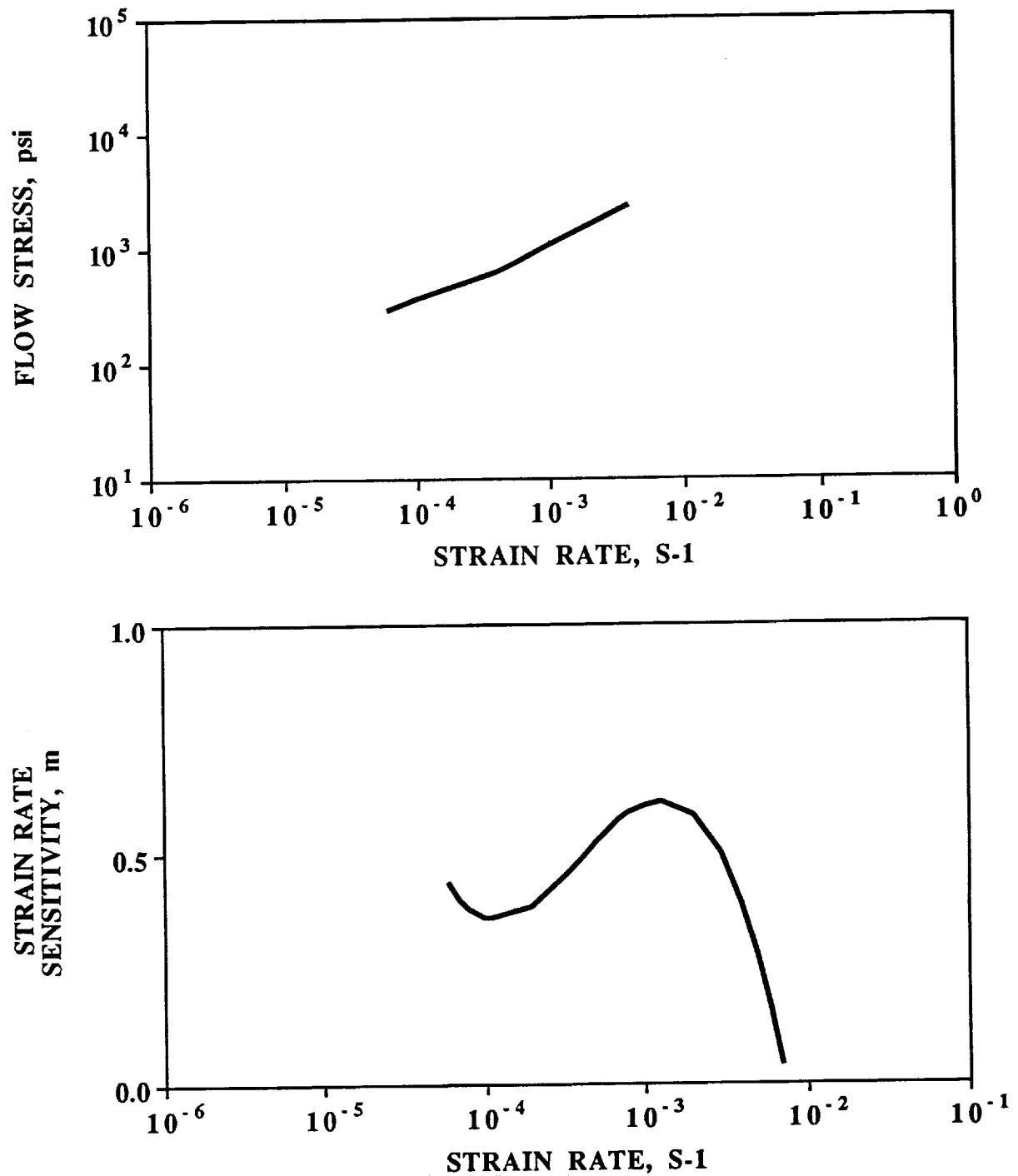


Figure 68. Flow Stress and M-value Versus Strain Rate for Second Batch of Weldalite-049 Al-Li Sheet, Transverse Direction, Tested at 915°F (490°C) at 600 psi Back Pressure.

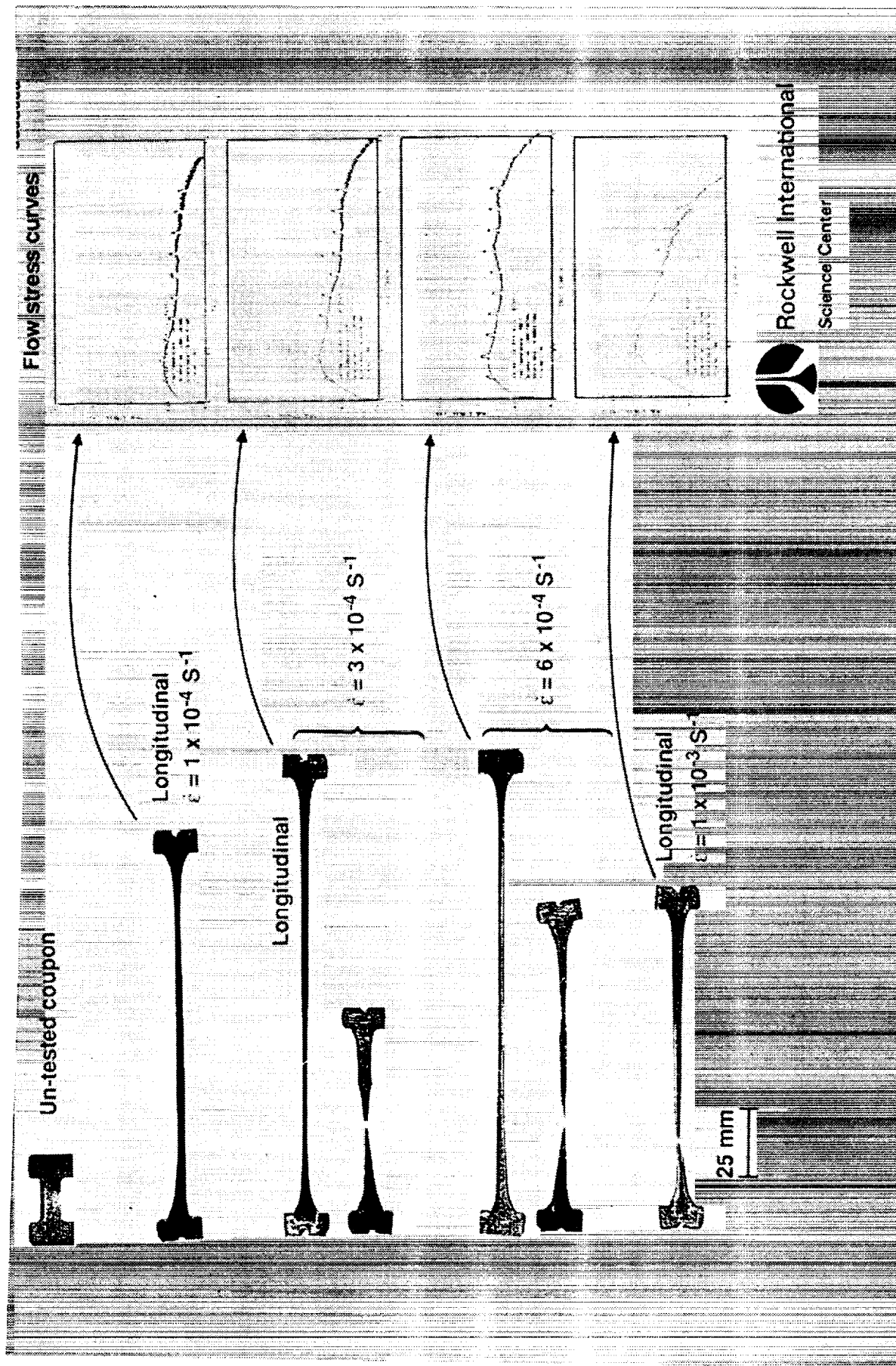


Figure 69. Strain Rate and Orientation Effects on Flow Stress and Elongation to Failure of SPF Weldalite-049
Sheet at 915°F with 600 psi Back Pressure.

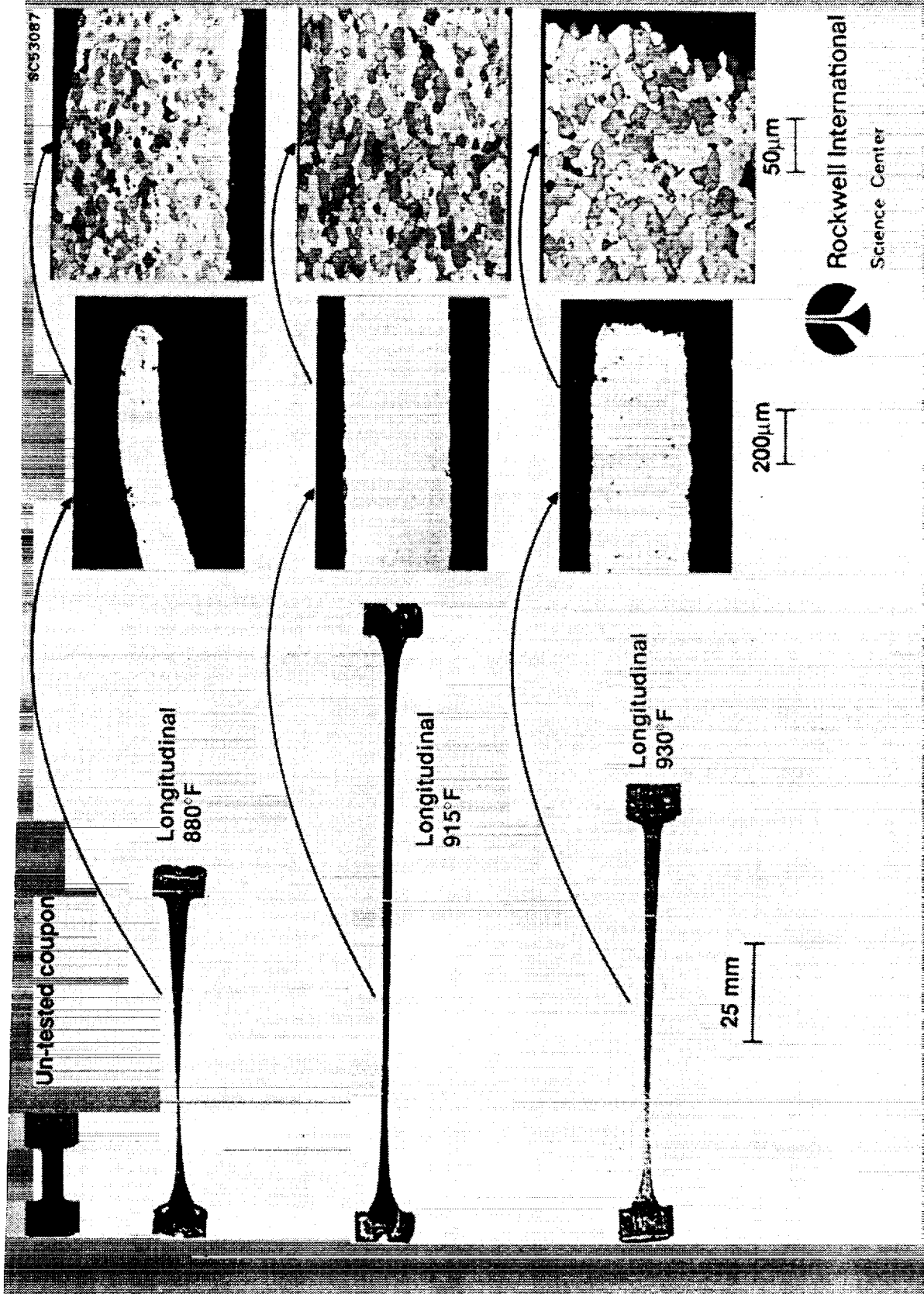


Figure 70. Temperature Effects on Elongation and Cavitation of SPF Weldalite-049 Sheet at $\epsilon = 3E-4/\text{sec}$ with 600 psi Back Pressure.

SC53089

- Micrographs from grips of superplastics tensile coupons
- Thermal exposures without strain



(a) 915°F



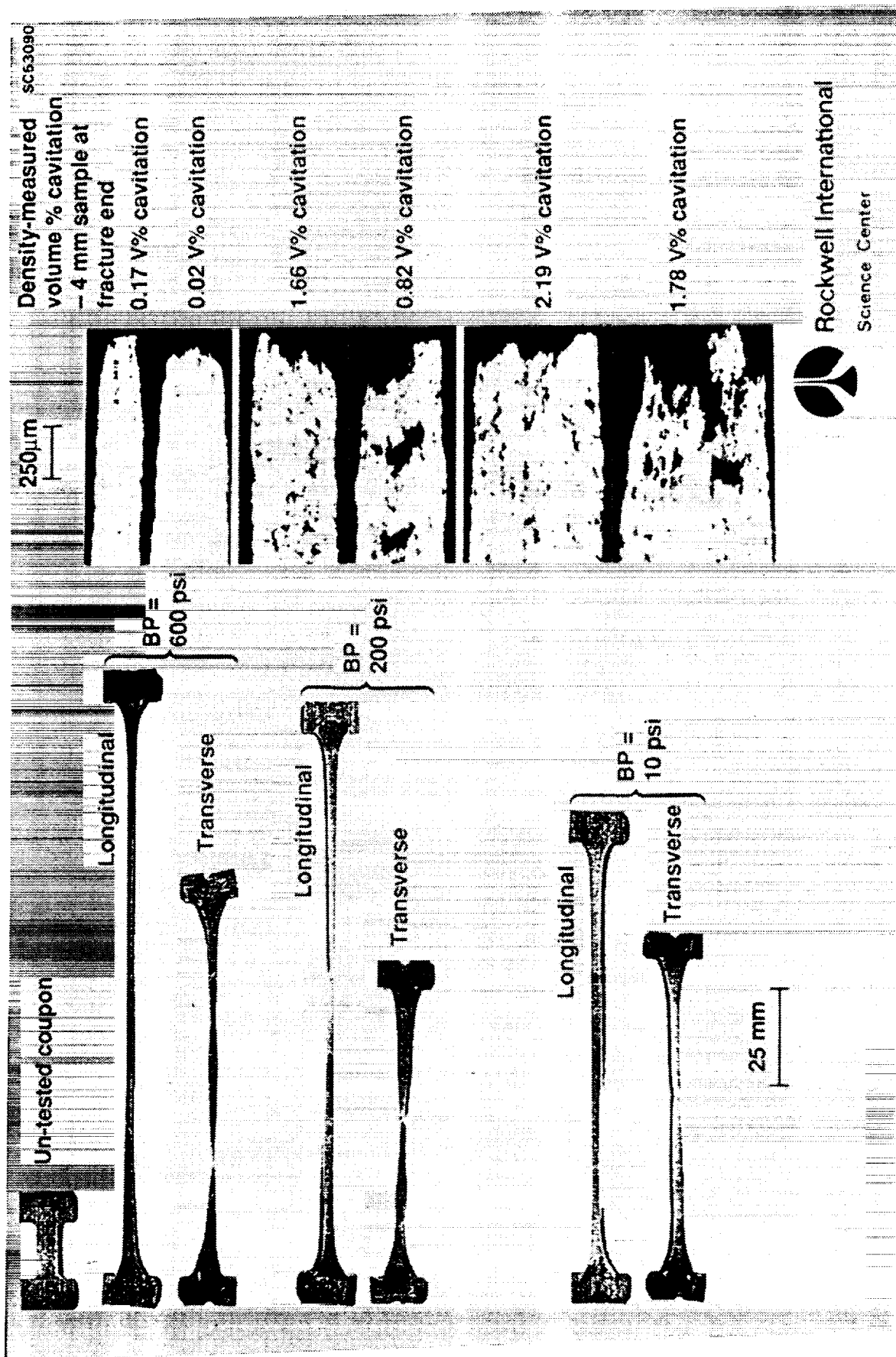
(b) 930°F

- Slightly more recrystallized grains
- Significant grain growth in recrystallized grains



Rockwell International
Science Center

Figure 71. Static Recrystallization and Grain Growth of SPF Weldalite-049 Sheet at Temperatures of 915°F and 930°F.



Rockwell International
Science Center

Figure 72. Back Pressure Effect on Cavitation in Weldalite-049 Al-Li Sheet Tested at 915°F at Strain Rate of 6E-4 sec⁻¹.

formability data. Optimal forming temperatures and strain rates obtained during the characterization study (refer to Table 25) were utilized for development of pressure-versus-time profiles and for establishing thermal stability requirement for the manufacturing environment. Pressure versus time profiles were generated for the small pans (an example of a cycle is shown as Figure 73) for each of the alloys utilizing the Rockwell SPF model in conjunction with the superplastic material parameters developed under this program. The preliminary parts (6" x 6" x 2.5", refer to Figure 74) were formed from each material utilized during the program. The initial pans formed from 2090 and 8090 Al-Li materials were immediately quenched (utilizing several different quench rates) upon removal from the tool, stored at 20°F to retard natural aging, sectioned, and shipped to Washington State University in dry ice storage for inclusion in the heat treatment evaluation. Large producibility pans (18" x 18" x 6", refer to Figure 75) were also fabricated from 7475 Al, 2090 and 8090 Al-Li during the program for use during the resistance spot weld parameter development at General Dynamics and for generation of engineering design data at Alcoa.

Table 25. Summary of Optimum Superplastic Forming Parameters.

ALLOY	7475 AL	2090 AL-LI	8090 AL-LI	x2095 AL-LI WL-049
Forming Temp. (°F)	950	960	960	915
Strain Rate ($\times 10^{-3} \text{ s}^{-1}$)	0.2	2.0/0.2	2.0/0.2	0.6
Flow Stress (ksi)	0.25	1.5/0.4	1.5/0.3	0.85
Back Pressure (psi)	400	400	400	600

The work, conducted on the small producibility pans included identification of forming constraints with the aforementioned materials, actual versus predicted thinning behavior for the pans, and cavitation within the formed part. Thickness measurements for the small producibility pans were obtained using a caliper model ultrasonic gauge (Krautkramer-Branson model CL204). The schematic thickness measurements (recorded in inches) are shown in Figures 76 through 79. Cavitation measurements were conducted on the formed 7475 Al, 2090, 8090 and x2095 Al-Li materials. The cavitation evaluation show the percentage of relative void volume for as-received versus formed material, along with the effect of percent SPF thickness strain on the relative volume of cavities (refer to Figures 80 through 82 and 72).

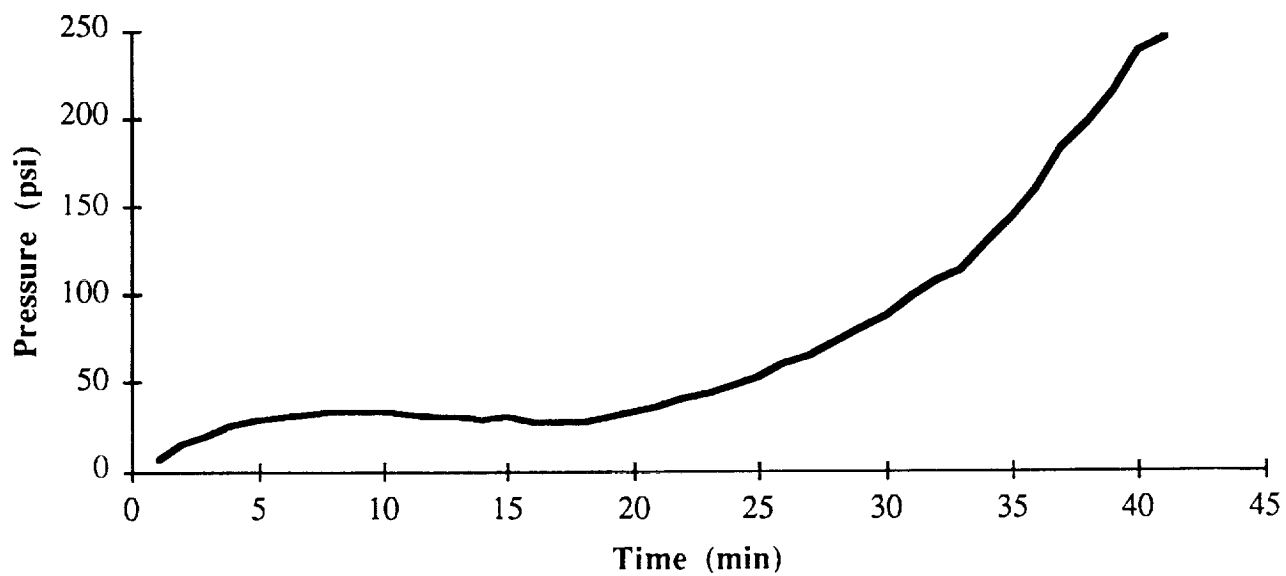


Figure 73. Pressure Versus Time Profile for x2095 Al-Li Producibility Pan.

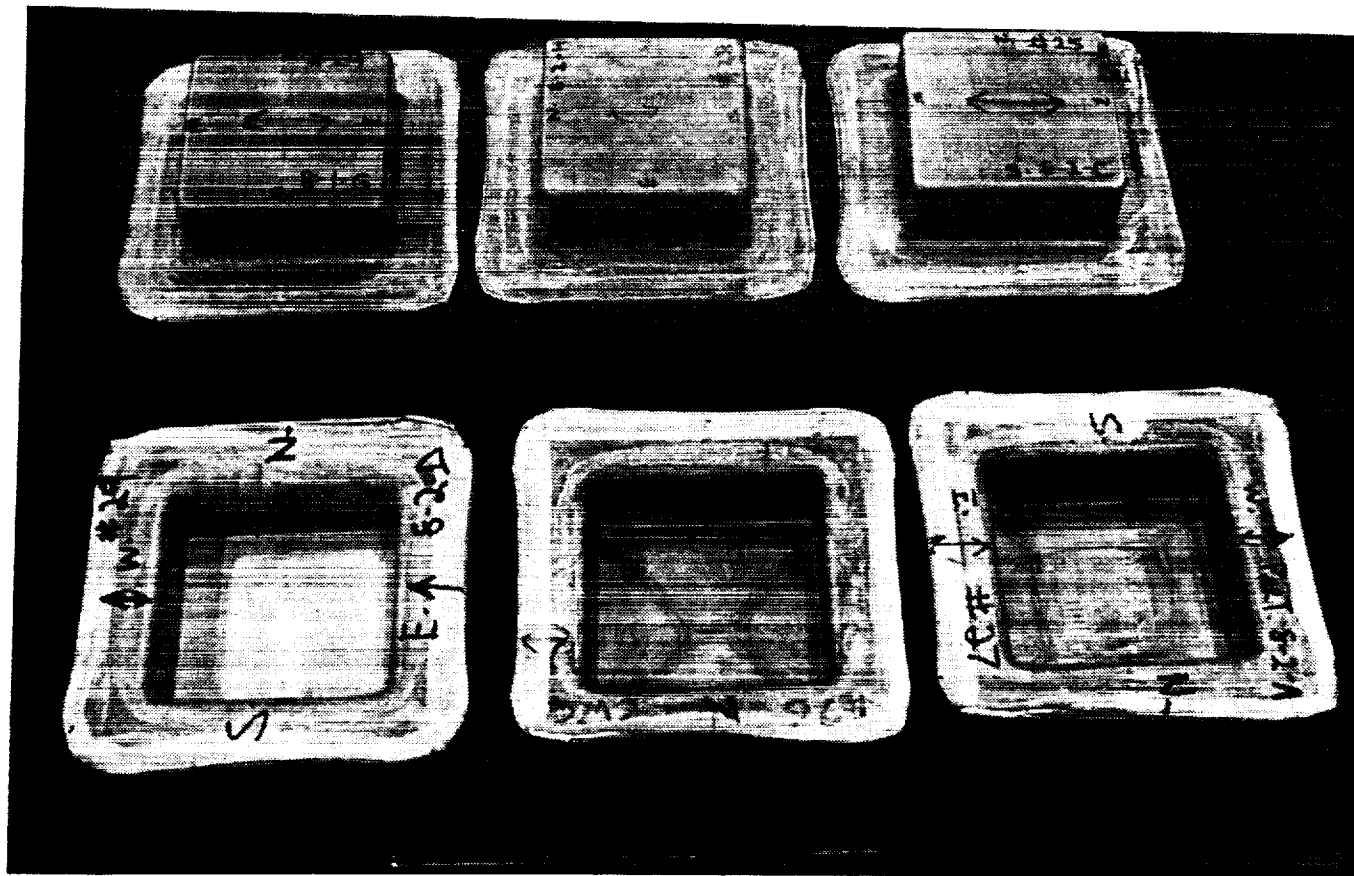
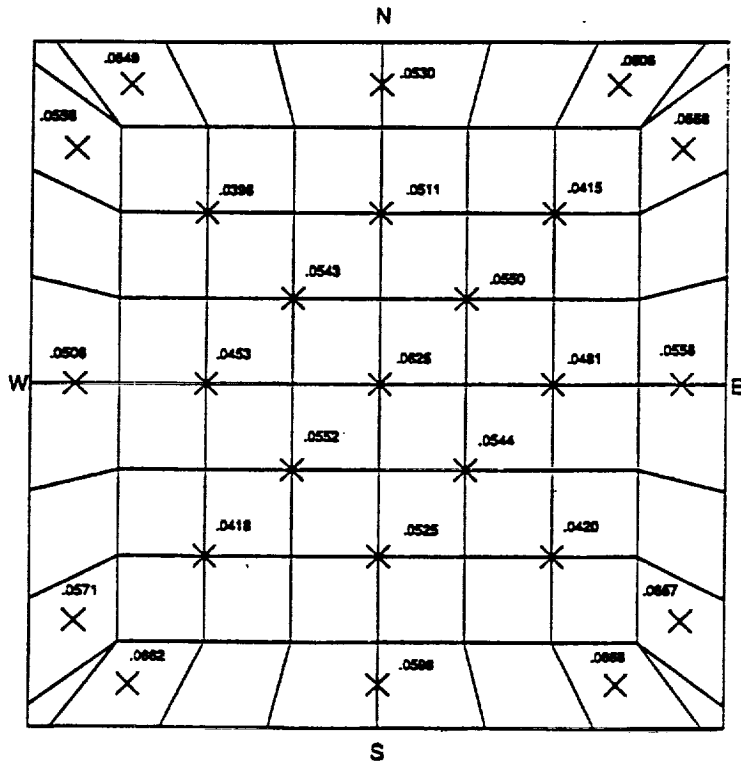


Figure 74. Small Producibility Pans 6" x 6" x Depth were Fabricated for Each Material Examined During this Program. The Depth of the Tool was Altered with the Addition of Inserts into the Die Cavity.

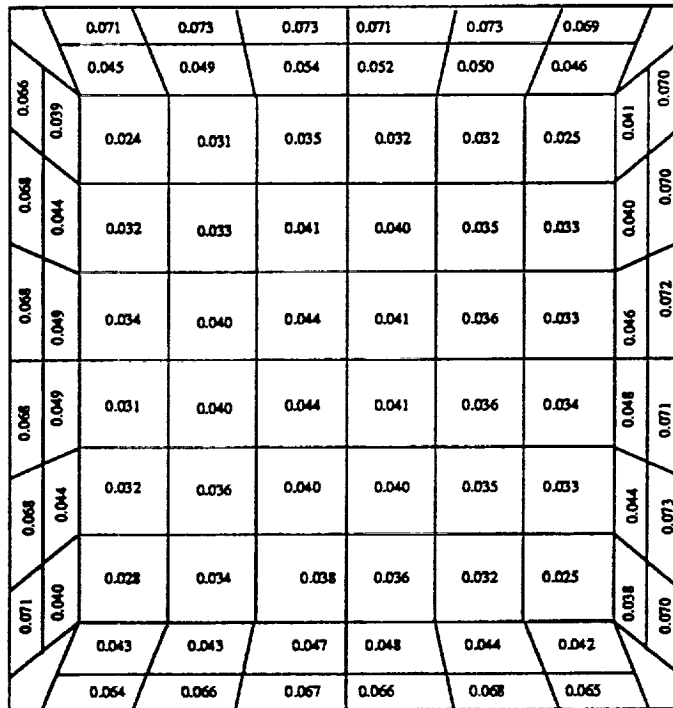


Figure 75. Large Productivity Pan 18" x 18" x Depth was Fabricated for Materials Used During Weld Development and Post-SPF Property Testing The Depth of the Tool was Altered with the Addition of Inserts into the Die Cavity.



8090 Al-Li Pan 25
 $t_0 = 0.090"$
 6" x 6" x 3" Plain Pan

Figure 78. Thickness Measurements for a 8090 Al-Li Producibility Pan.



Weldalite-049 (x2095) Al-Li Pan 4
 $t_0 = 0.124"$
 6" x 6" x 3" Plain Pan

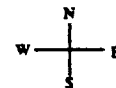
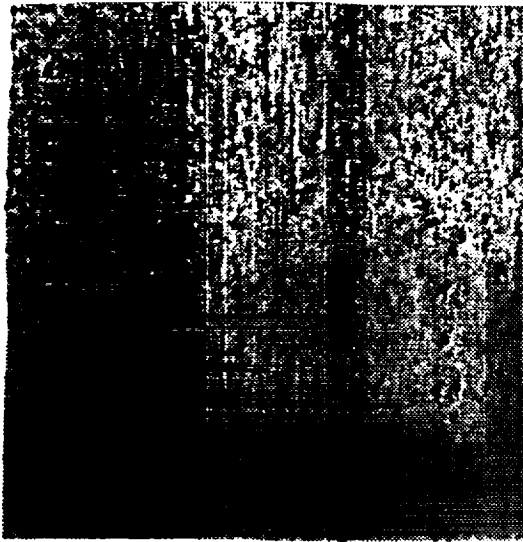
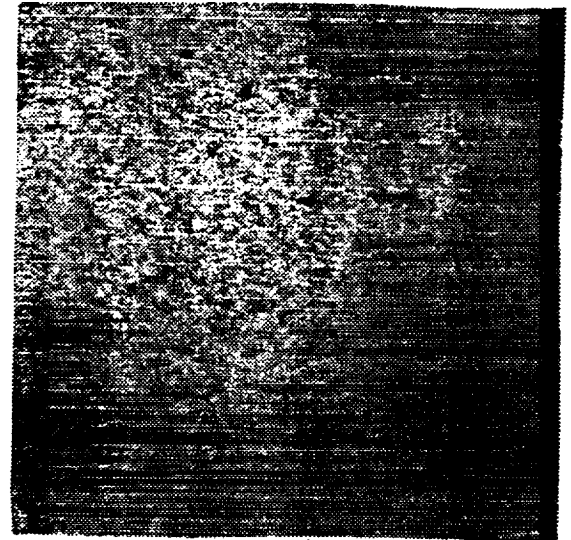


Figure 79. Thickness Measurements for a x2095 Al-Li Producibility Pan.



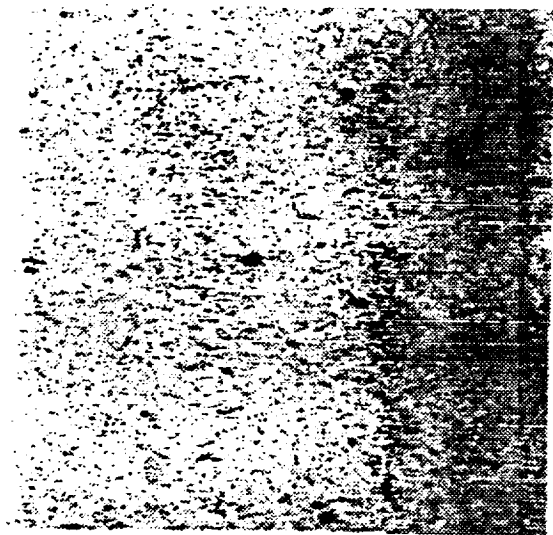
Longitudinal, As-Received
% Voids = 0.23
Magnification 100X



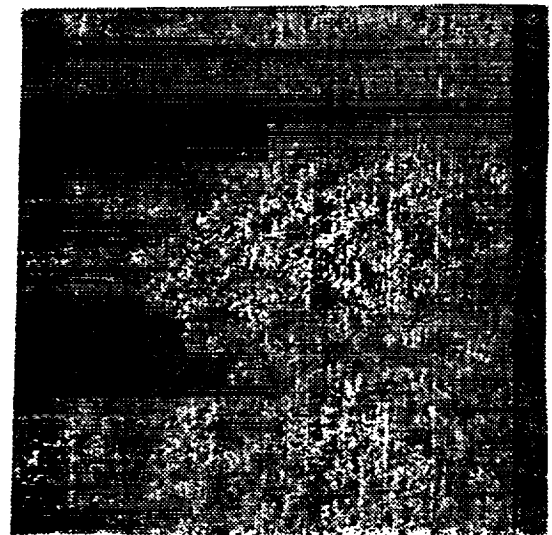
Longitudinal, 54% Strain
% Voids = 0.05
Magnification 100X

7475 Al Pan 101, $t_0 = 0.100''$
18" x 18" x 3" Plain Pan, Back Pressure = 350 psi

Figure 80. Photomicrograph of Cavitation for a 7475 Al Producibility Pan.



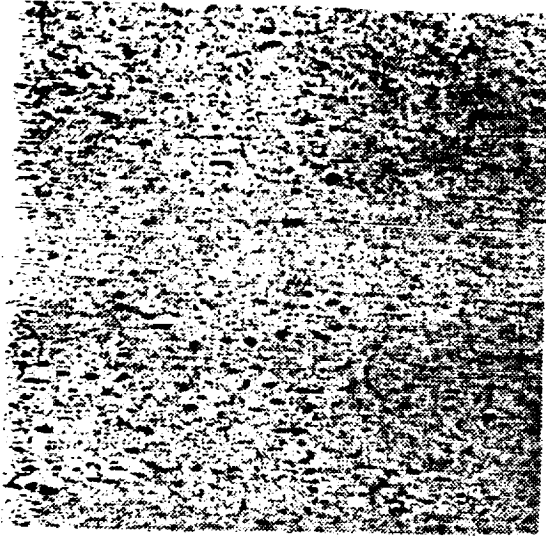
Longitudinal, As-Received
% Voids = 0.48
Magnification 100X



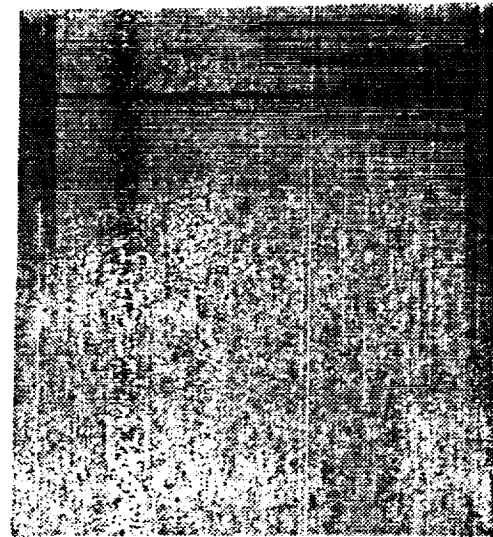
Longitudinal, 67% Strain
% Voids = 0.13
Magnification 100X

2090 Al-Li Pan 18, $t_0 = 0.090''$
6" x 6" x 3" Plain Pan, Back Pressure = 350 psi

Figure 81. Photomicrograph of Cavitation for a 2090 Al-Li Producibility Pan.



Longitudinal, As-Received
% Voids = 0.64
Magnification 100X



Longitudinal, 34% Strain
% Voids = None
Magnification 100X

8090 Al-Li Pan 107, $t_0 = 0.090''$
6" x 6" x 3" Plain Pan, Back Pressure 350 psi

Figure 82. Photomicrograph of Cavitation for a 8090 Al-Li Producibility Pan.

4.2.2.1 2090 and 8090 Aluminum-Lithium

Uniaxial SPF test information was used in conjunction with past experience with SPF of aluminum based materials resulting in selection of the following forming parameters for 2090 and 8090 Al-Li:

Forming Temperature

The forming temperature range of 950 to 960°F was selected in order to maintain low flow stress levels and to minimize and/or prevent static grain growth, incipient melting, and minimize the formation of lithium oxide and hydroxides on the surface of the material.

Strain Rate

A two stage strain rate (2×10^{-3} /second for bi-axial strains of 0.2 minimum to 0.5 maximum followed by 2×10^{-4} /second for the remainder of the cycle) was selected in order to provide for maximum elongation in the material, due to dynamic recrystallization at the onset of SPF strain, and for minimizing manufacturing time without sacrificing structural integrity.

Formability

The materials were hot loaded, and a thermal equilibration time was allowed for prior to the onset of the forming profile. The thermal control of the platens and tool were controlled during the entire cycle and recorded through the automated thermal control system during forming. At the completion of the pressure-time profile, the part was removed from the tool, quenched, and stored under refrigeration for further evaluation. The formability of both the 2090 and 8090 materials was excellent. Scale-up for fabrication of structural element was not considered as a problem for either material.

4.2.2.2 Weldalite-049 (x2095) Aluminum-Lithium

Uniaxial SPF test information was used in conjunction with past experience with SPF of aluminum based materials resulting in selection of the following forming parameters for x2095 Al-Li:

Forming Temperature

A forming temperature of 915°F was selected in order to maintain low flow stress levels and to minimize and/or prevent static grain growth, incipient melting and minimize the formation of lithium oxide and hydroxides on the surface of the material.

Strain Rate

A single stage strain rate of 6×10^{-4} /second was selected in order to maximize elongation in the material during forming without sacrificing structural integrity.

Formability

The material was hot loaded, and a thermal equilibration time was allowed for prior to the onset of the forming profile. The thermal control of the platens and tool were controlled during the entire cycle and recorded through the automated thermal control system during forming. At the completion of the pressure-time profile, the part was removed from the tool, allowed to slow air cool and evaluated for thinning behavior and cavitation. The formability of the x2095 Al-Li material was excellent, although it was less sensitive to gas pressure fluctuations than standard aluminum materials. The x2095 Al-Li material formability is similar to Ti-6Al-4V but requires very high level of back pressure to consolidate during forming. Scale-up for fabrication of structural elements is not considered as a problem for the material.

4.2.3 TEST MATRIX AND COUPON CONFIGURATION FOR 2090 AND 8090 ALUMINUM-LITHIUM

A data base of mechanical property and corrosion resistance performance of the 2090 and 8090 Al-Li materials procured for this program was generated on formed and non-formed samples. The test matrix utilized during the program is shown in Table 26. This matrix and testing details described in this section provide for direct comparison with existing material test data for SPF of aluminum and other SPF Al-Li materials. A group of the Pre- and Post-SPF material was heat treated to the condition designated as -T62 prior to testing.

4.2.3.1 Material Processing

Test coupons from post-SPF material were obtained by superplastically forming rectangular sectioned deep pans; the basic female cavity used to provide the deep pans was 18- by 18- by 6- inches deep. The large flat walls and base of the deep pans provided the material for the formed test coupons. The superplastic forming conditions used to fabricate the deep pans were taken from the characterization tests which were later utilized for fabrication of the structural test parts during the program. The differential pressurization cycles were calculated using an experimentally derived relationship between the materials' tensile flow stress and the effective true strain at the given temperature and strain rate.

The test material (both formed and unformed) was solution heat treated, quenched, flattened where noted, and artificially aged to a peak -T62 condition. The heat treatment parameters utilized during the program are outlined Table 27.

The effective true strains incurred during SPF were determined for the critical areas of each test coupon from thickness measurements. The effective true strains can be calculated by placing an etched grid onto the surface of the material prior to forming, and measuring the major and minor diameters of the etched grid pattern after SPF. The post-SPF grid measurements are then compared with the etched grid circle diameter before SPF according to the equation.

$$\epsilon = 1.155 (\epsilon_1^2 + \epsilon_2^2 + \epsilon_1 \epsilon_2)^{1/2}$$

where ϵ is the effective true strain, ϵ_1 is the true strain in the major tensile direction and ϵ_2 is the true strain in the minor tensile direction; i.e., $\epsilon = \ln (d_1/d_0)$ where d_1 = etched grid diameter after SPF and d_0 = original etched grid circle diameter. In cases where it is not possible to utilize a local

Table 26. Matrix for Post-SPF Material Testing.

TEST	NUMBER OF COUPONS		TEST	NUMBER OF COUPONS	
	PRE-SPF -T62	Post-SPF -T62		PRE-SPF -T62	Post-SPF -T62
Tensile Strength (Smooth) Longitudinal Transverse	3	12	Fatigue Crack Propagation R = +0.1 R = +0.3 R = +0.5	1	1
	3	12		1	1
Tensile Strength (Notched) Longitudinal Transverse	2	4		1	1
	2	4	Compression Strength Longitudinal Transverse	2	2
Cryogenic Temp. Tensile (Smooth) -60°F Longitudinal Transverse	2	4		2	2
	2	4	Shear Strength	4	4
-320 °F Longitudinal Transverse	2	4			
	2	4	Bearing Strength e/d = 1.5 e/d = 2.0	2	2
Fracture Toughness (R Curve)	2	2		2	2
	2	2	Exfoliation Corrosion	1	3
Smooth Fatigue Life (3 at each load) Longitudinal Transverse	6	9			
	6	9	Stress Corrosion Stresses at 1/2 yield strength Unstressed	3	3
Notch Fatigue Life (3 at each load) Longitudinal Transverse	6	9		0	3
	6	9	Residual Tensile Strength (Post-SCC)		
Chemical Analysis	1	3		3	6

etched grid pattern, the true thickness strain is determined from thickness measurement using the equation $\epsilon_3 = \ln (t_1/t_0)$ where ϵ_3 is the thickness true strain, t_1 = the sheet thickness after SPF, and t_0 is the original sheet thickness. The thickness true strain is a close approximation to the effective true strain ($\epsilon = -\epsilon_3$ for equi-biaxial strain and $\epsilon = 1.155 \epsilon_3$ for plane strain). The Effective uniaxial tensile elongations were derived from the effective true strains using the equation:

$$\epsilon = (\text{anti loge } \epsilon)^{-1}.$$

Table 27. Material Thermal Processing After SPF Prior to Testing.

Material V	Solution Heat Treatment Temperature (°F)	Solution Heat Treatment Time (minutes)	Quench Media	Artificial Age Temperature (°F)	Artificial Age Time (hours)
2090 Al-Li	1000	30	Water	350	20
8090 Al-Li	1013	30	Water	300	38 to 40

4.2.3.3 Chemical Analysis

Chemical analysis was performed at the surface of the material, and at the center (T/2) plane via Quantometer analysis. The classifications of the test data are broken down into material condition: Pre-SPF (unformed but solution heat treated-quenched-artificially aged) and Post-SPF (formed-solution heat treated-quenched-artificially aged). The goal of the evaluation of the composition of the material was to determine whether any changes had occurred in the composition due to the forming process that could alter the mechanical behavior of the material, or anomalies in the composition of the material when compared to the maximum and minimums associated with the registered composition. The results of the evaluation are shown in Table 28 and 29.

The composition of the 2090 aluminum-lithium material (refer to Table 28) was within the range of the registered composition except for the amount of lithium depletion at the surface of the material. The amount of lithium in the Pre-SPF (1.6 ± 0.21) condition versus the Post-SPF (1.7 ± 0.09) condition at the surface of the samples was virtually identical. The lithium measured at the center of the specimen (T/2) for the Pre-SPF was 2.26 ± 0.05 and for the Post-SPF material was 2.3 ± 0.15 ; thus it was concluded that Li depletion (approximately 0.42 weight percent lithium for

Table 28. Chemical Analysis of 2090 Al-Li in the Pre- and Post-SPF Conditions.

Alloy Temper	Material Cond.	Location	Si	Fe	Cu	Mn	Mg	Cr	Ni	Zn	Ti	V	Zr	Li	Al
2090-T62	Pre-SPF	Surface	0.04	0.06	2.5	0	0.01	0	0.01	0.02	0.02	0.01	0.13	1.5	Rem
—	Pre-SPF	Surface	0.05	0.06	2.6	0	0.01	0	0.01	0.02	0.02	0.01	0.13	1.8	Rem
—	Pre-SPF	Surface	0.04	0.06	2.6	0	0.01	0	0.01	0.02	0.02	0.01	0.13	1.6	Rem
—	Post-SPF	Surface	0.05	0.06	2.5	0	0.01	0	0.01	0.02	0.02	0.01	0.13	1.6	Rem
—	Post-SPF	Surface	0.05	0.05	2.5	0	0.01	0	0.01	0.02	0.02	0.01	0.13	1.7	Rem
—	Post-SPF	Surface	0.05	0.06	2.6	0	0.01	0	0.01	0.02	0.02	0.01	0.13	1.9	Rem
—	Post-SPF	Surface	0.05	0.06	2.5	0	0.01	0	0.01	0.02	0.02	0.01	0.13	1.7	Rem
—	Post-SPF	Surface	0.04	0.05	2.5	0	0.01	0	0.01	0.02	0.02	0.01	0.13	1.7	Rem
—	Post-SPF	Surface	0.05	0.05	2.6	0	0.01	0	0.01	0.01	0.02	0.01	0.13	1.7	Rem
—	Pre-SPF	T/2	0.04	0.05	2.5	0	0.01	0	0.01	0.02	0.02	0.01	0.13	2.2	Rem
—	Pre-SPF	T/2	0.05	0.06	2.6	0	0.01	0	0.01	0.02	0.02	0.01	0.13	2.3	Rem
—	Pre-SPF	T/2	0.04	0.06	2.6	0	0.01	0	0.01	0.02	0.02	0.01	0.13	2.3	Rem
—	Post-SPF	T/2	0.05	0.06	2.6	0	0.01	0	0.01	0.02	0.02	0.01	0.13	2.4	Rem
—	Post-SPF	T/2	0.04	0.06	2.6	0	0.02	0	0.01	0.02	0.02	0.01	0.12	2.4	Rem
—	Post-SPF	T/2	0.04	0.06	2.6	0	0.01	0	0.01	0.02	0.02	0.01	0.13	2.4	Rem
—	Post-SPF	T/2	0.05	0.06	2.6	0	0.01	0	0.01	0.02	0.02	0.01	0.13	2.3	Rem
—	Post-SPF	T/2	0.05	0.06	2.6	0	0.01	0	0.01	0.02	0.02	0.01	0.13	2.3	Rem
—	Post-SPF	T/2	0.04	0.05	2.4	0	0.01	0	0.01	0.02	0.02	0.01	0.13	2.0	Rem
2090-T62	Max		0.1	0.12	3.0	0.05	0.25	0.05		0.1	0.15		0.15	2.6	Rem
	Min				2.4								0.08	1.9	Rem

Table 29. Chemical Analysis of 8090 Al-Li in the Pre- and Post-SPF Conditions.

Alloy Temper	Material Cond.	Location	Si	Fe	Cu	Mn	Mg	Cr	Ni	Zn	Ti	V	Zr	Li	Al
8090-T62	Pre-SPF	Surface	0.02	0.05	1.1	0	0.60	0	0.01	0.02	0.02	0	0.13	2.3	Rem
	Pre-SPF	Surface	0.02	0.05	1.0	0	0.60	0	0.01	0.02	0.02	0	0.11	2.2	Rem
	Pre-SPF	Surface	0.02	0.05	1.1	0	0.50	0	0.01	0.02	0.02	0	0.11	2.0	Rem
	Post-SPF	Surface	0.03	0.05	1.5	0	0.60	0	0.01	0.02	0.02	0	0.12	2.0	Rem
	Post-SPF	Surface	0.03	0.05	1.5	0	0.60	0	0.01	0.02	0.02	0	0.12	2.0	Rem
	Post-SPF	Surface	0.03	0.04	1.1	0	0.7	0	0.01	0.02	0.02	0	0.12	2.6	Rem
	Post-SPF	Surface	0.02	0.04	1.0	0	0.6	0	0.01	0.02	0.02	0	0.11	2.4	Rem
	Post-SPF	Surface	0.03	0.04	1.5	0	0.6	0	0.01	0.02	0.02	0	0.12	2.2	Rem
	Post-SPF	Surface	0.03	0.04	1.4	0	0.6	0	0.01	0.02	0.02	0	0.12	2.2	Rem
	Pre-SPF	T/2	0.02	0.04	1.0	0	0.60	0	0.01	0.02	0.03	0	0.11	2.4	Rem
	Pre-SPF	T/2	0.02	0.05	1.0	0	0.60	0	0.01	0.02	0.02	0	0.12	2.4	Rem
	Pre-SPF	T/2	0.02	0.05	1.6	0	0.70	0	0.01	0.02	0.02	0	0.12	2.4	Rem
	Post-SPF	T/2	0.03	0.04	1.4	0	0.60	0	0.01	0.02	0.03	0	0.12	2.4	Rem
	Post-SPF	T/2	0.03	0.05	1.5	0	0.70	0	0.01	0.02	0.03	0	0.12	2.5	Rem
	Post-SPF	T/2	0.02	0.04	0.9	0	0.6	0	0	0.02	0.02	0	0.12	2.2	Rem
	Post-SPF	T/2	0.02	0.04	1.0	0	0.6	0	0.01	0.02	0.02	0	0.12	2.4	Rem
	Post-SPF	T/2	0.02	0.04	1.3	0	0.6	0	0	0.02	0.02	0	0.12	2.0	Rem
V	Post-SPF	T/2	0.03	0.04	1.4	0	0.6	0	0.01	0.02	0.03	0	0.12	2.4	Rem
8090-T62	Max		0.2	0.3	1.6	0.1	1.3	0.1		0.25	0.1		0.16	2.7	Rem
	Min				1.0		0.6						0.04	2.2	Rem

the material) did not occur during the forming process, but rather, occurred during the solution heat treatment of the material prior to artificial aging.

The composition of the 8090 aluminum-lithium material (refer to Table 29) was within the range of the registered composition. The amount of lithium at the surface of the Pre-SPF (2.16 ± 0.15) condition versus the Post-SPF (2.2 ± 0.23) condition was virtually identical. The lithium measured at the center of the specimen (T/2) for the Pre-SPF was 2.4 ± 0.0 and for the Post-SPF material was 2.3 ± 0.18 ; thus it was concluded that Li depletion (approximately 0.07 weight percent lithium for the material) was within experimental error for the equipment. Thus it was concluded that forming and/or solution heat treatment of the material did not seriously alter the composition of the alloy.

4.2.3.4 Ambient Tensile

Ambient room temperature tensile tests were conducted in accordance with ASTM E8 specification. Test specimens were prepared in two directions: one parallel with the sheet rolling direction (L) and perpendicular to the sheet rolling direction (L-T). Subscale test specimens were used as shown in Figure 83. The shortened (1.0- inch) gauge length was selected in order to minimize the effects of thickness variations in the post-SPF material.

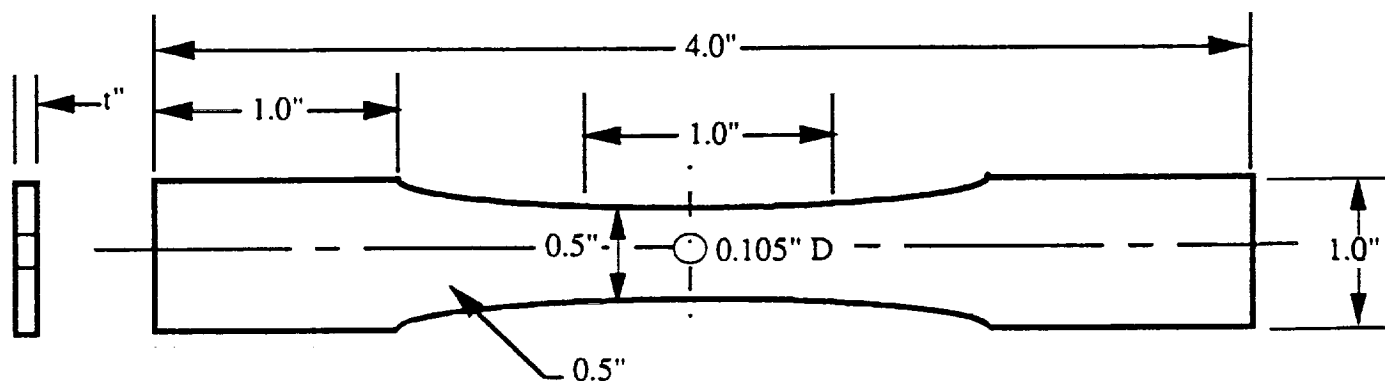


Figure 83. Tensile Test Coupons - Smooth ($K_T = 1.0$) with no Center hole - Notched ($K_T = 2.5$) with Center Drill-hole.

4.2.3.4.1 Smooth Tensile Testing

The smooth ambient temperature tensile tests were performed on the 2090 and 8090 Al-Li materials in the -T62 condition. The processing history of the materials are shown in Table 27. The ambient tensile data for 2090 Al-Li is represented in Table 30 and 31 with the specimen orientation and forming strain. Median tensile values are shown at the bottom of the table along with the standard deviation. The data was evaluated for possible reductions in tensile properties with increase in superplastic elongation. It was observed (refer to Table 32) that the ambient tensile behavior does not change significantly with superplastic strain for either the longitudinal or transverse specimens. Graphical representation of the ambient tensile properties of 2090 Al-Li is shown in Figures 84 through 88 versus superplastic effective true strain.

Table 30. Pre- and Post-SPF Longitudinal Ambient Tensile Results for 2090 Al-Li.

Orientation	F _{tu} (ksi)	F _{ty} (ksi)	Elong. (%)	Effective True Strain	E (msi)
L	66.9	55.8	4.0	0.000	12.9
	63.3	54.1	3.0	0.000	13.2
	64.8	52.8	3.0	0.000	13.3
	64.7	52.4	5.0	0.000	11.4
	63.2	52.5	4.0	0.000	11.3
	62.7	53.6	4.0	0.000	13.5
	61.2	51.5	4.0	0.000	10.0
	65.0	52.2	5.0	0.176	14.3
	64.2	50.3	5.0	0.189	12.6
	61.7	48.5	5.0	0.193	16.1
	63.2	49.1	5.0	0.240	10.1
	65.7	54.9	3.0	0.273	11.2
	60.2	48.3	5.0	0.279	9.8
	60.5	46.4	4.0	0.285	12.6
	62.8	50.0	3.0	0.297	11.2
	63.1	50.2	4.0	0.301	14.6
	64.0	53.6	5.0	0.303	12.5
	63.3	50.6	3.0	0.319	11.0
	63.3	50.3	4.0	0.330	17.6
	62.8	50.1	3.0	0.349	10.8
	61.2	48.3	4.0	0.365	12.0
V	63.3	52.3	4.0	0.378	10.2
Mean	63.2	51.3	4.0	0.194	12.373
STD Dev.	1.6	2.4	0.8	0.145	2.007

**Table 31. Pre- and Post-SPF Transverse Ambient Tensile Results
for 2090 Al-Li**

Orientation	F _{tu} (ksi)	F _{ty} (ksi)	Elong. (%)	Effective True Strain	E (msi)
T	65.10	52.70	6.00	0.000	13.0
T	61.90	52.80	5.00	0.000	12.7
T	65.00	54.60	8.00	0.000	13.6
T	62.40	50.90	4.00	0.000	10.9
T	63.40	51.40	7.00	0.000	11.2
T	62.30	50.10	8.00	0.215	14.0
T	62.80	51.20	10.00	0.219	14.7
T	60.80	47.20	7.00	0.227	11.6
T	61.20	46.70	7.00	0.230	13.9
T	60.20	45.80	7.00	0.240	9.5
T	60.80	48.60	8.00	0.241	13.0
T	63.00	49.70	10.00	0.246	9.7
T	61.80	48.20	9.00	0.253	10.6
T	62.10	47.50	9.00	0.254	11.1
T	62.80	48.90	9.00	0.272	11.3
T	61.60	48.00	9.00	0.273	11.0
T	63.10	48.50	9.00	0.276	10.7
T	62.70	50.50	7.00	0.277	12.6
T	62.60	48.50	9.00	0.301	11.8
T	61.50	47.50	9.00	0.306	17.2
T	61.50	48.80	8.00	0.318	11.1
T	61.10	48.20	9.00	0.324	11.5
T	60.10	47.80	7.00	0.366	11.3
T	59.10	47.80	7.00	0.439	11.7
Mean	62.04	49.25	7.83	0.220	12.07
STD Dev.	1.41	2.14	1.49	0.125	1.72

Table 32. Pre- and Post-SPF Mean Ambient Tensile Results for 2090 Al-Li.

Orientation	F _{tu} (ksi)	F _{ty} (ksi)	Elongation (%)	Effective True Strain	E (msi)
L	63.3	52.8	4.0	0.000	12.9
	64.2	50.3	5.0	0.189	14.3
	63.2	49.1	5.0	0.240	10.1
	60.5	48.3	4.0	0.279	11.2
	63.1	50.2	4.0	0.301	12.5
	63.3	50.6	3.0	0.319	11.0
	63.1	50.2	3.5	0.340	14.2
V	62.3	50.3	4.0	0.372	11.1
T	63.4	52.7	6.0	0.000	12.7
	62.6	50.7	9.0	0.217	14.4
	60.8	47.2	7.0	0.240	11.6
	62.0	47.9	9.0	0.254	10.9
	62.8	48.7	9.0	0.275	11.2
	62.1	48.0	9.0	0.304	14.5
	61.3	48.5	8.5	0.321	11.3
	60.1	47.8	7.0	0.366	11.3
V	59.1	47.8	7.0	0.439	11.7

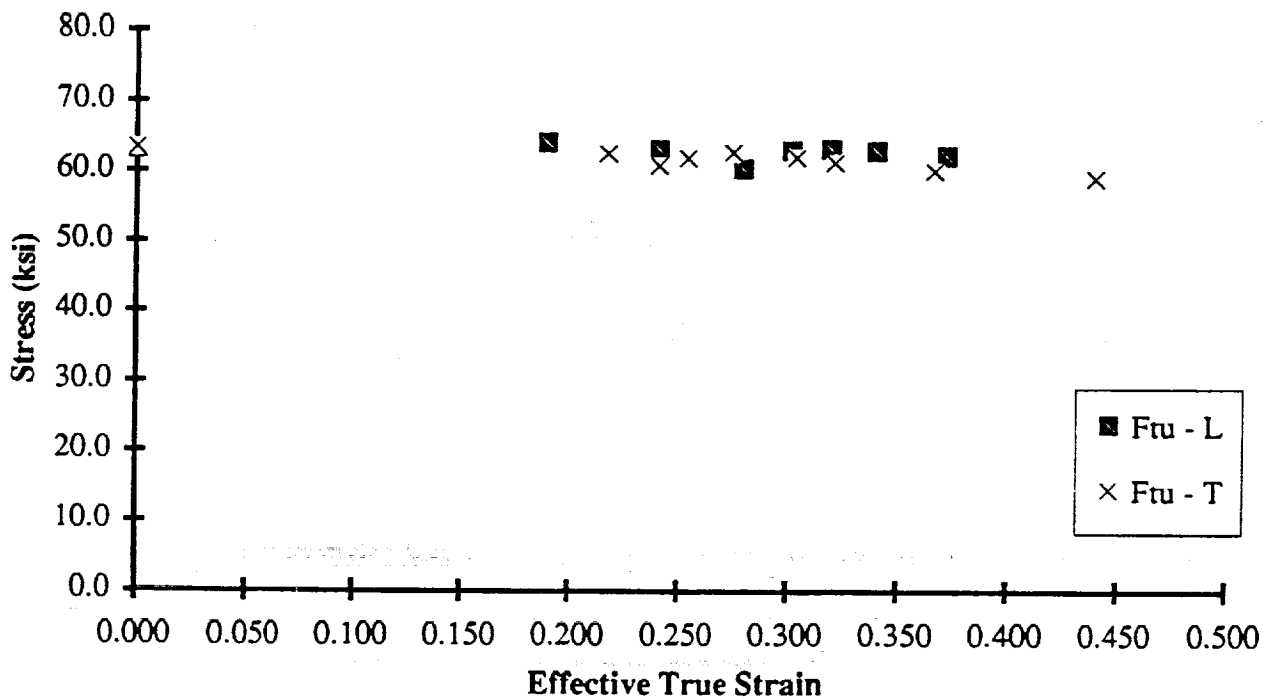


Figure 84. 2090 Al-Li Ultimate Tensile Strength Versus Effective True Strain.

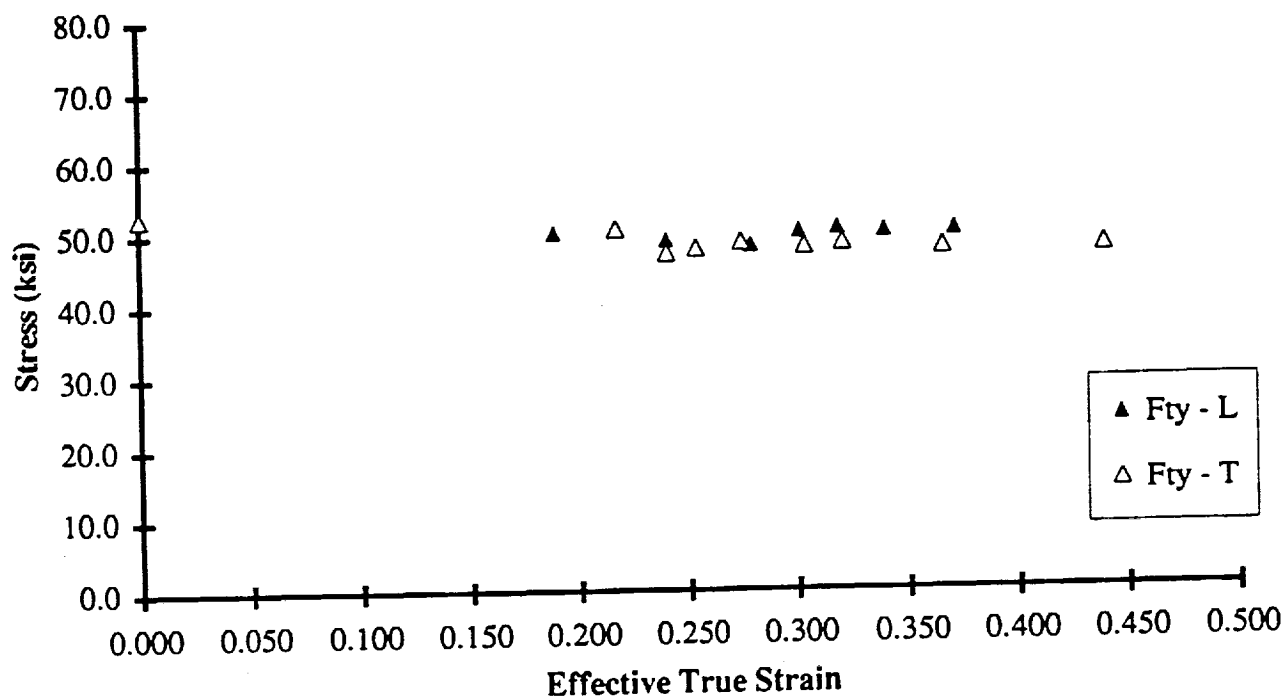


Figure 85. 2090 Al-Li Tensile Yield Strength Versus Effective True Strain.

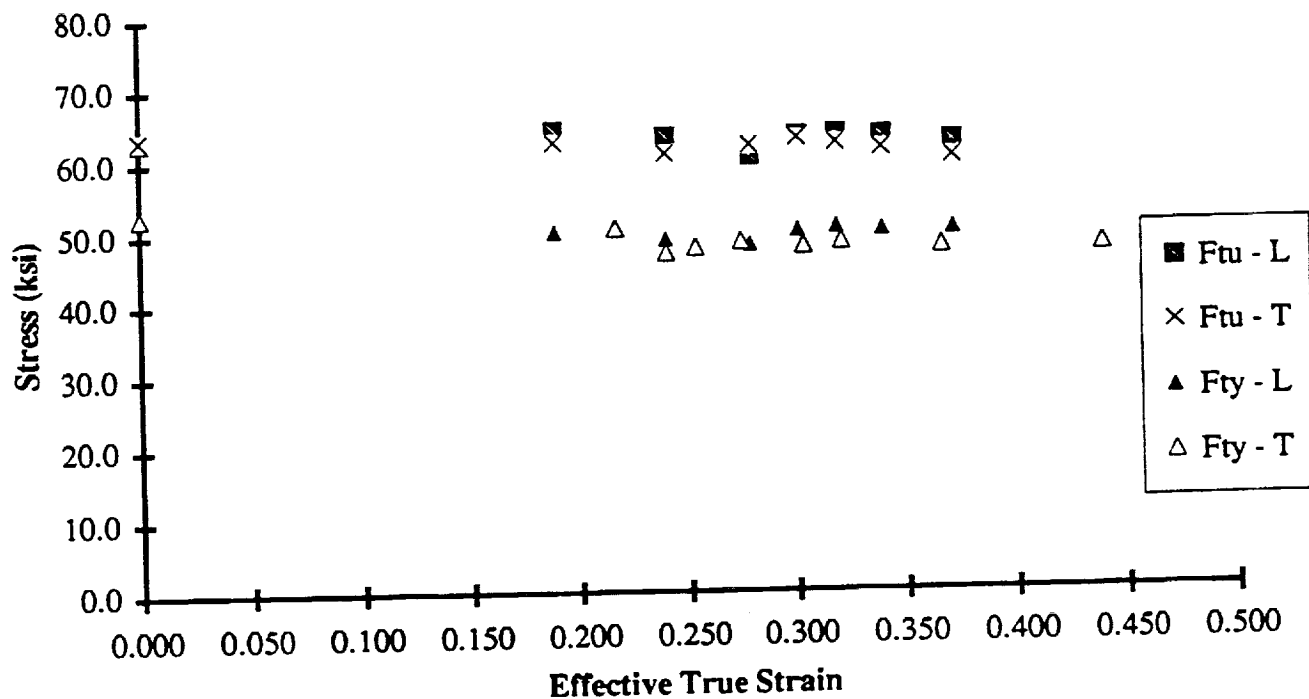


Figure 86. 2090 Al-Li Ultimate Tensile and Yield Strengths Versus Effective True Strain.

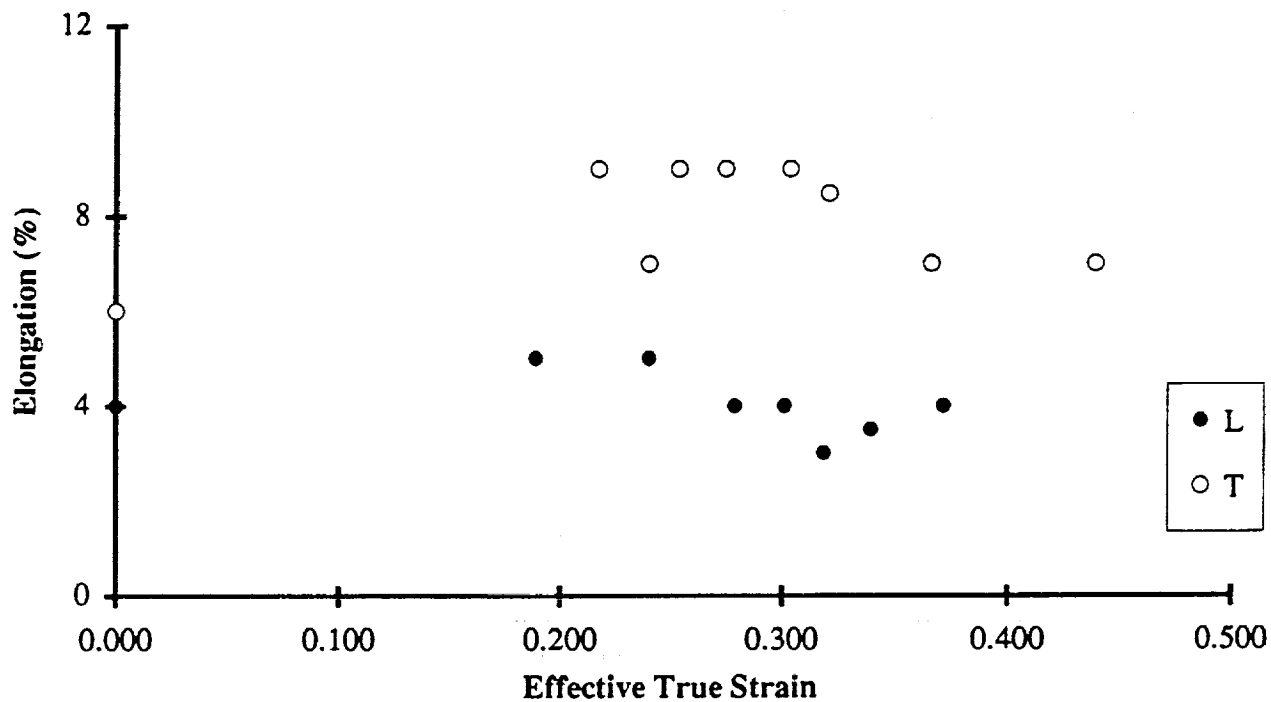


Figure 87. 2090 Al-Li Tensile Elongation Versus Effective True Strain.

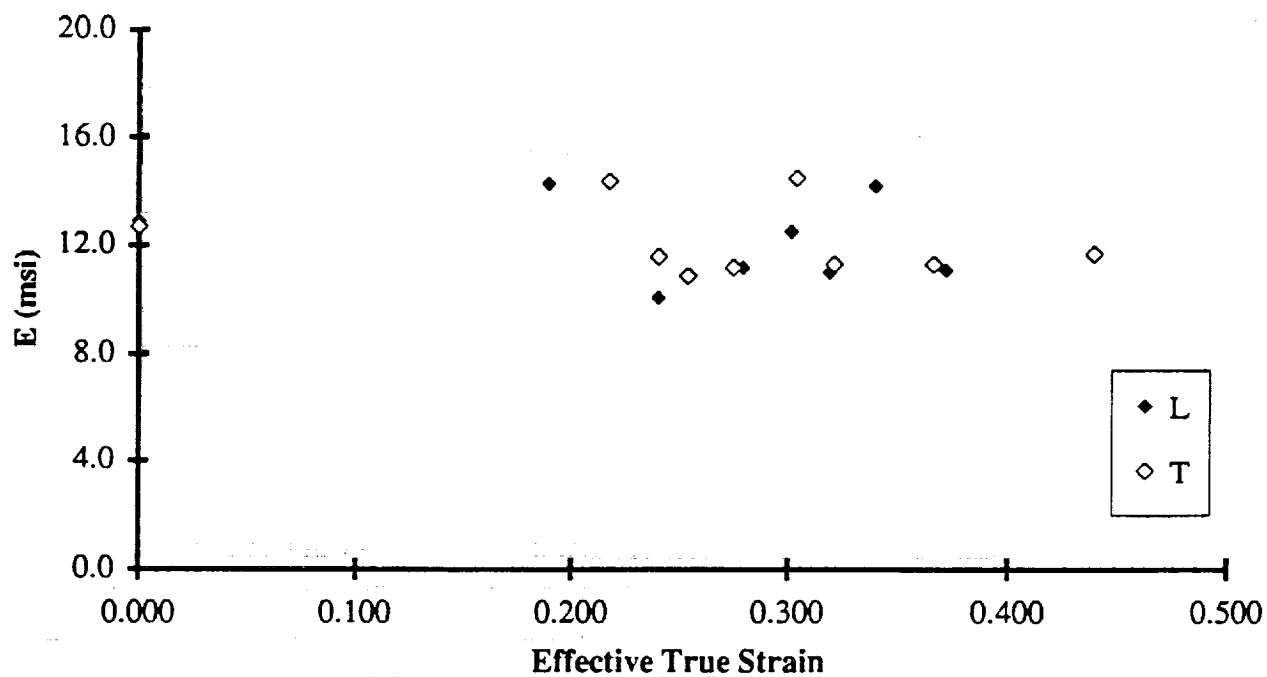


Figure 88. 2090 Al-Li Tensile Modulus Versus Effective True Strain.

The ambient tensile data for 8090 Al-Li is represented in Table 33 and 34 with the specimen orientation and forming strain. Median tensile values are shown at the bottom of the table along with the standard deviation. The data was evaluated for possible reductions in tensile properties with increase in superplastic elongation. As with the 2090 data, it was observed (refer to Table 35) that the ambient tensile behavior of the 8090 Al-Li material does not change significantly with superplastic strain for either the longitudinal or transverse specimens. Graphical representation of the ambient tensile behavior of 8090 Al-Li is shown in Figures 89 through 93 versus superplastic effective true strain.

Table 33. Pre- and Post-SPF Longitudinal Ambient Tensile Results for 8090 Al-Li.

Orientation	F _{tu} (ksi)	F _{ty} (ksi)	Elong. (%)	Effective True Strain	E (msi)
L	63.9	55.0	3.0	0.000	11.6
	65.6	54.8	5.0	0.000	11.1
	66.7	54.9	5.0	0.000	11.4
	67.2	54.8	4.0	0.000	12.1
	66.6	55.0	4.0	0.000	11.7
	66.7	54.9	4.0	0.000	10.8
	65.9	54.7	4.0	0.000	10.9
	68.0	58.0	3.0	0.105	12.4
	67.6	57.6	3.0	0.116	13.0
	66.4	57.7	3.0	0.123	12.0
	67.6	55.5	4.0	0.127	12.5
	62.3	50.8	3.0	0.134	13.8
	66.5	57.1	2.0	0.139	11.1
	64.0	58.4	1.0	0.141	12.7
	67.9	55.6	4.0	0.155	14.8
	65.1	57.8	3.0	0.161	11.7
	67.6	58.2	5.0	0.165	11.2
	64.8	57.3	2.0	0.171	12.5
	66.5	58.3	3.0	0.181	13.4
	65.7	51.5	5.0	0.183	12.4
	66.8	56.2	5.0	0.198	12.4
V	62.7	54.4	4.0	0.236	11.0
Mean	66.0	55.8	4.0	0.11	12.11
STD Dev.	1.6	2.1	1.0	0.08	1.02

4.2.3.4.2 Notched Tensile Testing

Notched tensile tests were carried out as described for the smooth tensile tests, however, the sub-scale test coupons contained a 0.105-inch diameter drill-hole in the center of the gauge length (as shown in Figure 83). The ratio of hole diameter to coupon width was determined for a $K_T = 2.5$ from "Stress Concentration Factors," R. E. Peterson, John Wiley and sons, 1974. Center-hole specimens were used rather than sharp edge notch specimens for improved

reproducibility in the thin sheet material, lower specimen costs, and to closely represent a typical stress concentration in airframe structures (i.e., fastener holes) which are clearly understood for prediction of structural behavior.

The 2090, and 8090 -T62 open hole tensile specimens were solution heat treated, quenched, and artificially aged according to the parameters laid out in Table 27. The results from the testing of the notched tensile specimens are shown in Tables 36 through 39. The 2090 specimens did not show a trend towards decrease in notched tensile strength with superplastic strain for either the longitudinal or transverse specimens. A constant notch yield ratio was obtained for the 2090 specimens with forming strain (approximately 1.18) which implies that there is no effect on the notch tensile data by the SPF process.

**Table 34. Pre- and Post-SPF Transverse Ambient Tensile Results
for 8090 Al-Li**

Orientation	F _{tu} (ksi)	F _{ty} (ksi)	Elong. (%)	Effective True Strain	E (msi)
T	60.1	47.7	8.0	0.000	10.9
	61.0	48.1	8.0	0.000	11.1
	60.2	47.7	8.0	0.000	11.2
	58.6	46.8	4.0	0.000	10.6
	59.9	47.4	6.0	0.000	11.3
	60.8	48.0	7.0	0.000	11.2
	60.0	48.0	7.0	0.000	11.4
	57.8	47.0	5.0	0.095	12.9
	65.2	52.3	5.0	0.107	12.3
	66.5	52.2	5.0	0.108	12.1
	65.4	52.9	5.0	0.108	11.3
	65.6	53.4	5.0	0.113	13.0
	66.5	52.4	7.0	0.118	12.3
	65.7	53.2	5.0	0.127	13.7
	66.7	52.3	7.0	0.144	12.7
	65.7	52.2	6.0	0.161	15.5
	61.4	47.4	5.0	0.165	10.8
	66.6	52.3	7.0	0.167	13.2
	64.7	50.3	8.0	0.198	10.6
	59.4	45.8	6.0	0.232	12.4
V	61.4	49.1	8.0	0.235	11.1
	63.8	51.0	5.0	0.259	11.2
Mean	62.9	49.9	6.0	0.11	11.95
STD Dev.	3.0	2.5	1.0	0.09	1.21

Table 35. Pre- and Post-SPF Mean Ambient Tensile Results for 8090 Al-Li.

Orientation	F _{tu} (ksi)	F _{ty} (ksi)	Elongation (%)	Effective True Strain	E (msi)
L	66.6	54.9	4.0	0.000	11.4
	67.8	57.8	3.0	0.111	13.0
	67.0	56.6	4.0	0.125	12.0
	64.0	57.1	2.0	0.139	13.0
	66.5	56.7	4.0	0.158	13.0
	66.2	57.8	4.0	0.168	12.0
	66.1	54.9	4.0	0.182	13.0
	66.8	56.2	5.0	0.198	12.4
V	62.7	54.4	4.0	0.236	11.0
T	60.1	47.7	7.0	0.000	11.0
	57.8	47.0	5.0	0.095	12.9
	65.4	52.3	5.0	0.108	12.0
	66.1	52.9	6.0	0.116	13.0
	66.2	52.8	6.0	0.136	13.0
	65.7	52.2	6.0	0.165	13.0
	64.7	50.3	8.0	0.198	10.6
	60.4	47.5	7.0	0.234	12.0
V	63.8	51.0	5.0	0.259	11.2

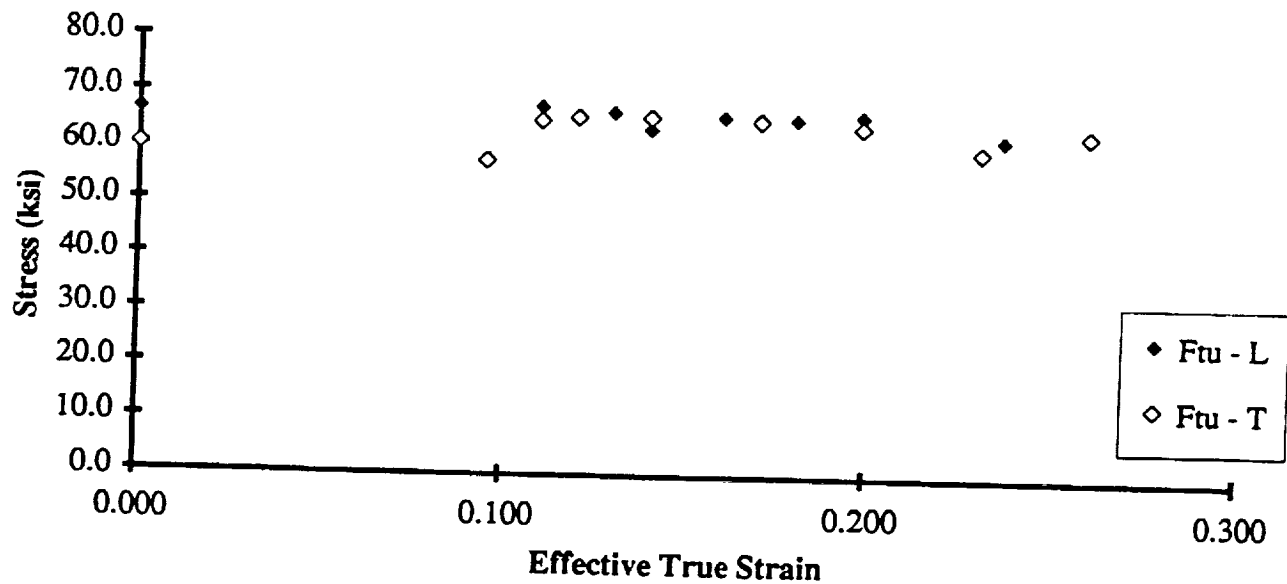


Figure 89. 8090 Al-Li Ultimate Tensile Strength Versus Effective True Strain.

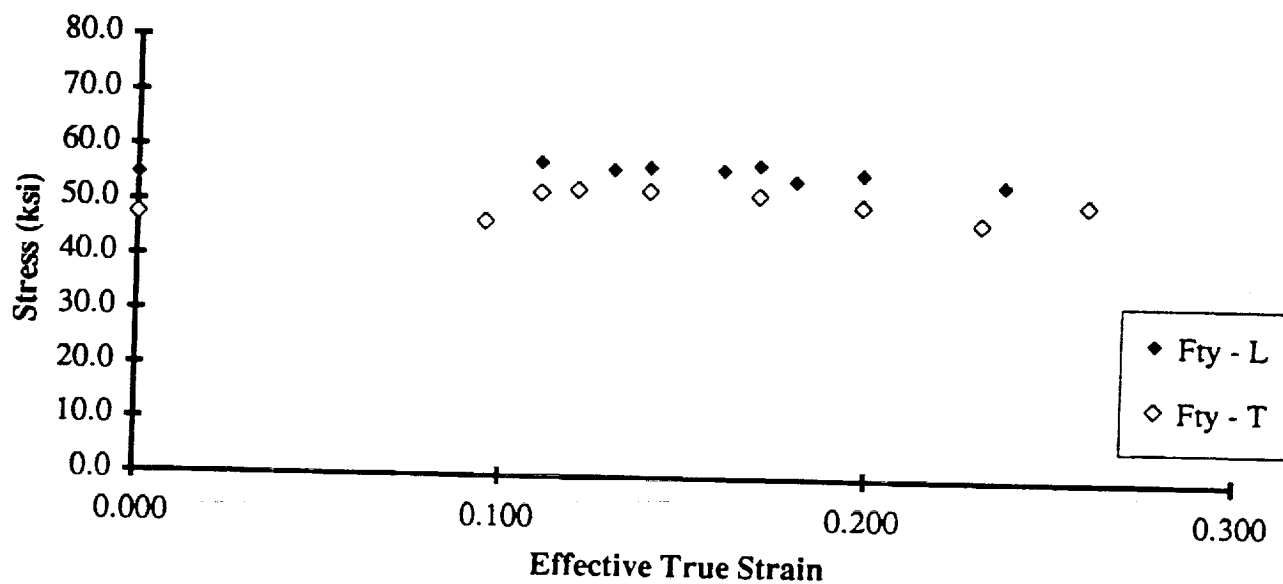


Figure 90. 8090 Al-Li Tensile Yield Strength Versus Effective True Strain.

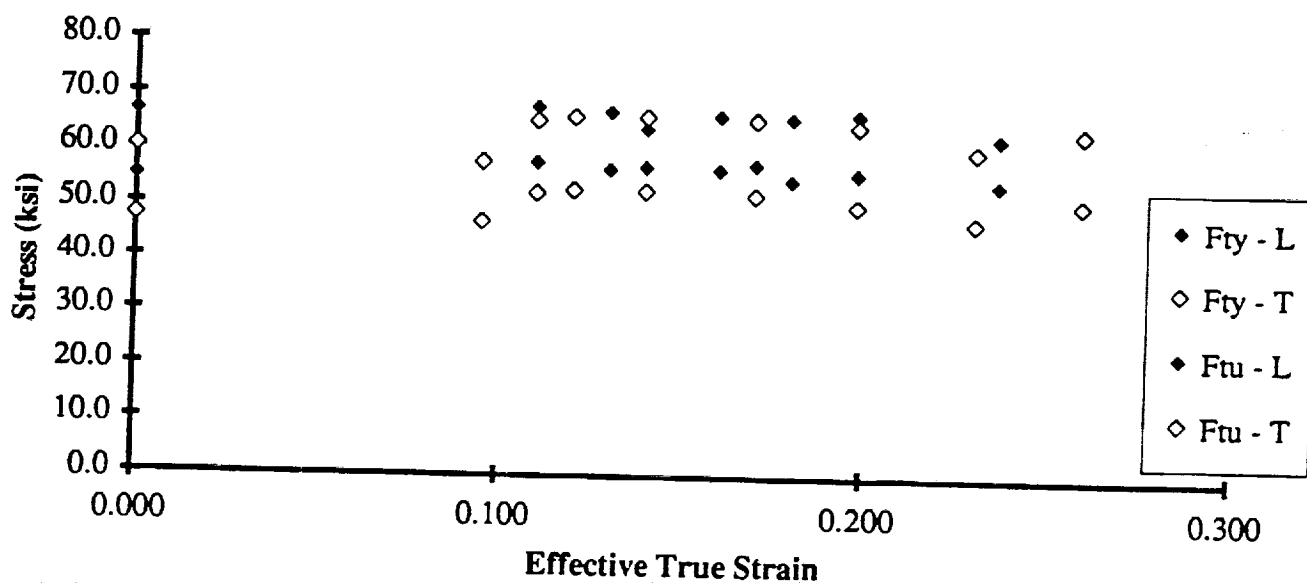


Figure 91. 8090 Al-Li Ultimate Tensile and Yield Strengths Versus Effective True Strain.

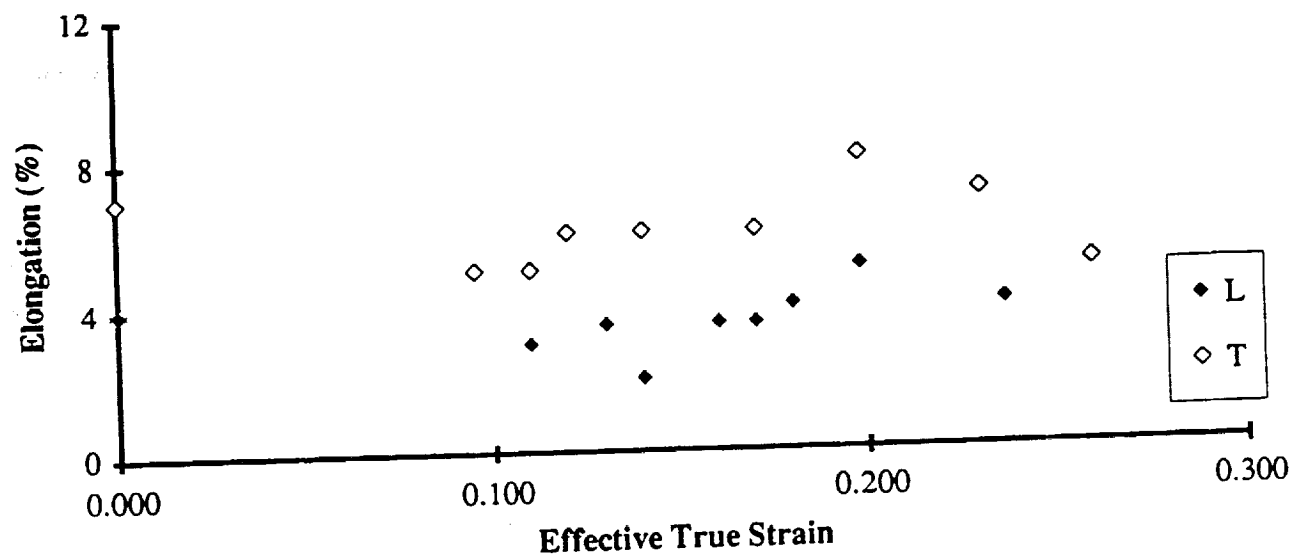


Figure 92. 8090 Al-Li Tensile Elongation Versus Effective True Strain.

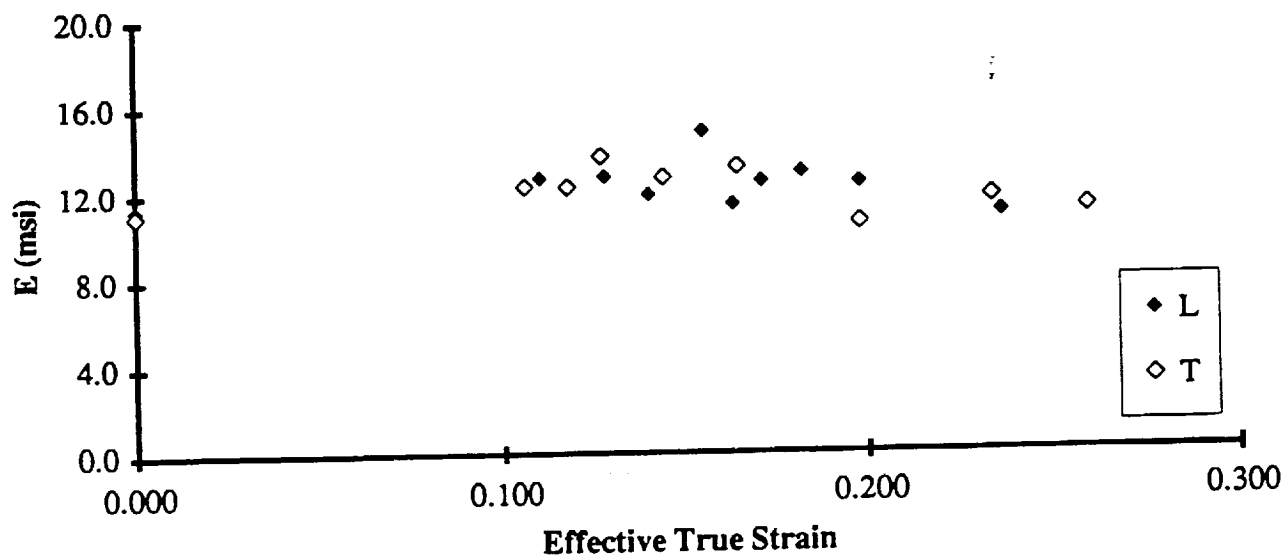


Figure 93. 8090 Al-Li Tensile Modulus Versus Effective True Strain.

The 8090 specimens did show a slight trend towards a decrease in notched tensile strength with increased superplastic strain for the longitudinal specimens. The median notch yield ratio obtained for the longitudinal 8090 specimens was 1.14 while the median obtained for the transverse specimens was 1.18. One explanation for the disparity in the values between the longitudinal specimens (low to high forming strain) could be the low copper content of some of the material. One low Cu post-SPF specimen exhibited a 6 ksi decrease in the notched tensile strength as compared with the non-formed material (material with strain of 0). This low copper effect may also be attributed to the lower response that some of the ambient smooth tensile specimens showed during testing, however, since this program was aimed at acceptability of the properties and not in an in-depth analysis of each characteristic, it is sufficient to say that the notch yield behavior of the material was acceptable, and that no serious deficiencies were found during the testing.

Table 36. 2090 Notched Tensile Strength, Longitudinal Direction.

Orientation	F _{tu} (ksi)	F _{tu} Nominal (ksi)	Notch Yield Ratio	Effective True Strain
L	48.00	61.00	1.19	0.000
L	48.00	61.00	1.19	0.000
L	46.20	58.80	1.15	0.270
L	47.20	59.80	1.17	0.319
L	49.30	61.40	1.20	0.213
L	48.00	60.90	1.19	0.213
Mean	47.78	60.48	1.18	0.17
STD Dev.	1.03	0.98	0.02	0.14

Table 37. 2090 Notched Tensile Strength, Transverse Direction.

Orientation	F _{tu} (ksi)	F _{tu} Nominal (ksi)	Notch Yield Ratio	Effective True Strain
T	45.70	57.90	1.18	0.000
T	46.50	59.10	1.20	0.000
T	46.10	58.60	1.19	0.361
T	46.30	58.90	1.20	0.185
T	44.20	56.20	1.14	0.232
T	47.00	59.80	1.21	0.229
Mean	45.97	58.42	1.19	0.17
STD Dev.	0.97	1.25	0.03	0.14

Table 38. 8090 Notched Tensile Strength, Longitudinal Direction.

Orientation	F _{tu} (ksi)	F _{tu} Nominal (ksi)	Notch Yield Ratio	Effective True Strain
L	49.50	62.80	1.12	0.000
L	51.10	64.90	1.16	0.000
L	51.20	65.20	1.17	0.190
L	51.60	65.50	1.17	0.177
L	50.90	64.70	1.16	0.130
L	46.40	58.80	1.05	0.205
Mean	50.12	63.65	1.14	0.12
STD Dev.	1.96	2.56	0.05	0.09

Table 39. 8090 Notched Tensile Strength, Transverse Direction.

Orientation	F _{tu} (ksi)	F _{tu} Nominal (ksi)	Notch Yield Ratio	Effective True Strain
T	45.20	57.40	1.15	0.000
T	45.70	58.00	1.16	0.000
T	46.70	59.40	1.19	0.229
T	47.30	60.10	1.20	0.171
T	48.40	61.50	1.23	0.147
T	45.70	58.20	1.17	0.179
Mean	46.50	59.10	1.18	0.12
STD Dev.	1.20	1.53	0.03	0.10

4.2.3.5 Cryogenic Tensile

Smooth tensile tests were conducted in accordance with the ASTM E8 specification at temperatures of approximately -60 °F to -320 °F (using industry conditions for cryogenic temperature testing two temperatures, both -60 and -320 should be used). Test coupons were as shown in Figure 83 for $K_T = 1.0$.

Smooth tensile tests were performed for 2090-T62 and 8090-T62 aluminum-lithium material at cryogenic temperatures. The cryogenic test results are shown on Table 40 and 41. Several of the coupons failed outside the middle of the gage length (denoted by F or D) which has been attributed to improper alignment of the grips and possible incomplete deburring of the tensile specimens prior to testing. The remaining test specimen and set-ups were re-examined prior to

testing in order to eliminate the problem. The elongations of the specimens that did fail in the gage length were in the range of 9 to 13 percent, which is an improvement of the ambient tensile test results of 4 to 5 percent shown in the ambient tensile section of this report.

Table 40. Cryogenic Temperature Smooth Tensile Test Results for 2090-T62 and 8090-T62 Pre- and Post-Superplastic Formed Sheet at -60°F.

Alloy Temper	Coupon I.D.	SPF Condition	Specimen Thickness (in)	Test Temp. (°F)	F _{tu} (ksi)	F _{ty} (ksi)	El (%)	Effective True Strain Thickness
2090-T62	316-1-L1	Pre-SPF	0.09045	- 60	68.1	54.0	4F	0
"	316-1-L2	Pre-SPF	0.09045	- 60	67.5	54.0	4F	0
"	316-1-T1	Pre-SPF	0.09010	- 60	65.3	52.9	10	0
"	316-1-T2	Pre-SPF	0.08995	- 60	65.1	52.9	10	0
"	322-L1	Post-SPF	0.06675	- 60	67.1	52.3	4F	0.2989
"	325-L2	Post-SPF	0.07000	- 60	67.9	51.5	5F	0.2513
"	324-L3	Post-SPF	0.07220	-60	66.6	51.3	4F	0.2204
"	323-L4	Post-SPF	0.06710	- 60	66.8	51.3	5F	0.2936
"	322-T1	Post-SPF	0.06395	- 60	62.9	50.4	6F	0.3417
"	325-T2	Post-SPF	0.07065	- 60	63.9	50.8	9	0.2421
"	324-T3	Post-SPF	0.07185	- 60	61.5	47.8	9	0.2252
"	323-T4	Post-SPF	0.07035	- 60	63.0	49.6	10	0.2463
8090-T62	315-3-L1	Pre-SPF	0.08730	- 60	70.4	55.5	7D	0
"	315-3-L2	Pre-SPF	0.08680	- 60	71.4	56.0	9	0
"	315-3-T1	Pre-SPF	0.08705	- 60	62.1	48.4	13D	0
"	315-3-T2	Pre-SPF	0.08715	- 60	62.0	48.3	13	0
"	361-L1	Post-SPF	0.08035	- 60	68.8	55.2	6F	0.0909
"	361-L2	Post-SPF	0.07870	- 60	68.7	56.1	6F	0.1117
"	359-L3	Post-SPF	0.07230	- 60	62.6	50.1	3F	0.1965
"	359-L4	Post-SPF	0.07315	- 60	65.5	50.9	6F	0.1848
"	359-T1	Post-SPF	0.07040	- 60	59.1	46.5	8D	0.2231
"	359-T2	Post-SPF	0.07195	- 60	60.5	43.3	7F	0.2014
"	359-T3	Post-SPF	0.07885	- 60	60.4	47.1	7F	0.1098
"	359-T4	Post-SPF	0.07600	- 60	60.8	47.5	8F	0.1466

D = Coupon Failed Outside of Middle of Gage Length.

F = Coupon Failed at Fillet.

Table 41. Cryogenic Temperature Smooth Tensile Test Results for 2090-T62 and 8090-T62 Pre- and Post-Superplastic Formed Sheet at -320°F.

Alloy Temper	Coupon I.D.	SPF Condition	Specimen Thickness (in)	Test Temp. (°F)	F _{tu} (ksi)	F _{ty} (ksi)	El (%)	Effective True Strain Thickness
2090-T62	316-1-L1	Pre-SPF	0.09055	- 320	83.0	57.3	8F	0
"	316-1-L2	Pre-SPF	0.09050	- 320	85.1	56.6	12D	0
"	316-1-T1	Pre-SPF	0.09025	- 320	78.3	57.6	18	0
"	316-1-T2	Pre-SPF	0.09045	- 320	78.2	57.3	18	0
"	322-L1	Post-SPF	0.06765	- 320	82.8	55.0	9F	0.2989
"	325-L2	Post-SPF	0.06875	- 320	79.8	54.5	8D	0.2513
"	324-L3	Post-SPF	0.07290	- 320	83.6	54.3	10F	0.2204
"	323-L4	Post-SPF	0.06765	- 320	83.3	54.8	10F	0.2936
"	322-T1	Post-SPF	0.06060	- 320	75.7	53.7	15F	0.3417
"	325-T2	Post-SPF	0.07155	- 320	77.1	55.7	17	0.2421
"	324-T3	Post-SPF	0.06970	- 320	75.1	52.9	17	0.2252
"	323-T4	Post-SPF	0.06915	- 320	76.9	54.5	13F	0.2463
8090-T62	315-3-L1	Pre-SPF	0.08710	- 320	87.4	58.7	10D	0
"	315-3-L2	Pre-SPF	0.08680	- 320	88.0	58.8	17D	0
"	315-3-T1	Pre-SPF	0.08695	- 320	74.6	52.4	17D	0
"	315-3-T2	Pre-SPF	0.08710	- 320	74.8	59.1	83	0
"	361-L1	Post-SPF	0.07730	- 320	85.0	59.8	10F	0.0909
"	361-L2	Post-SPF	0.07900	- 320	87.2	54.7	9F	0.1117
"	359-L3	Post-SPF	0.06920	- 320	82.4	54.9	8F	0.1965
"	359-L4	Post-SPF	0.07570	- 320	81.7	51.3	12F	0.1848
"	359-T1	Post-SPF	0.07040	- 320	73.4	50.8	13F	0.2231
"	359-T2	Post-SPF	0.07305	- 320	73.4	52.1	12F	0.2014
"	359-T3	Post-SPF	0.07970	- 320	74.1	49.4	12F	0.1098
"	359-T4	Post-SPF	0.07690	- 320	72.6	47.5	8F	0.1466

D = Coupon Failed Outside of Middle of Gage Length.

F = Coupon Failed at Fillet.

The overall strengths and elongations increased with the decrease in temperature which is typical of aluminum materials. However, the ultimate and yield strengths of the coupons did

decrease slightly with increasing forming strain. The graphical results of yield strength versus SPF thickness strain are shown as Figures 94 through 97.

4.2.3.6 Compression

The compressive yield strength was determined in accordance with the ASTM E-9 specification for 2090-T62 and 8090-T62 Pre- and Post-Superplastic formed sheet. The compressive strength coupons were machined to a uniform thickness to prevent buckling or improper failure of the coupons during testing. Past experience with the testing of formed SPF material has resulted in the practice of machining prior to testing to prevent premature failure in the coupons due to load discontinuities. The results from the compressive tests are shown in Table 42.

4.2.3.7 Exfoliation Corrosion

Exfoliation corrosion test were carried out in accordance with ASTM G85 Annex 2 MASTMAASIS (Modified ASTM Acetic Acid Salt Intermittence Spray) which is the most representative accelerated corrosion test for aluminum-lithium alloys.¹² The exfoliation test results are shown in Figure 98 with appropriate test ratings. All of the 2090 specimens received an exfoliation rating of A (mild exfoliation). Three of the four specimens exhibited only minor pitting and one specimen exhibited some pit blistering. All of the 8090 specimens received an exfoliation rating of C (severe pitting) and all experienced pit blistering. Protection of these materials for long periods of times in corrosive environments is recommended.

4.2.3.8 Stress Corrosion Cracking

The stress corrosion cracking testing performed under ASTM G44 is designed to expose the specimen to alternate immersion in 3.5 percent NaCl solution while under stress¹³. It is used to test the environmental effects of moderate to highly loaded structure that is allowed to dry between exposures (which could simulate the effects of long term storage of a cryogenic tank in a seacoast environment). The alternate immersion test utilizes a 1 hour exposure cycle which includes 10 minutes in the aqueous solution, followed by a 50 minute drying period. The cyclic exposure is continued 24 hours per day for typically 20 to 90 days, depending upon the resistance of the alloy to corrosion by saltwater.

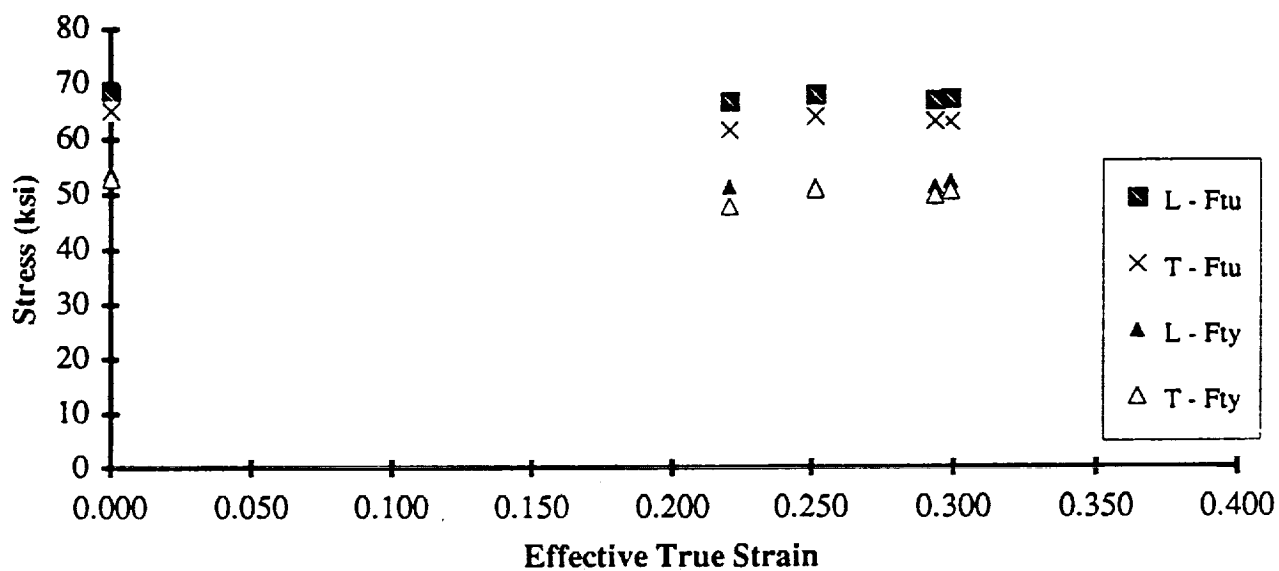


Figure 94. Cryogenic Tensile Response of 2090-T62 Al-Li at -60°F.

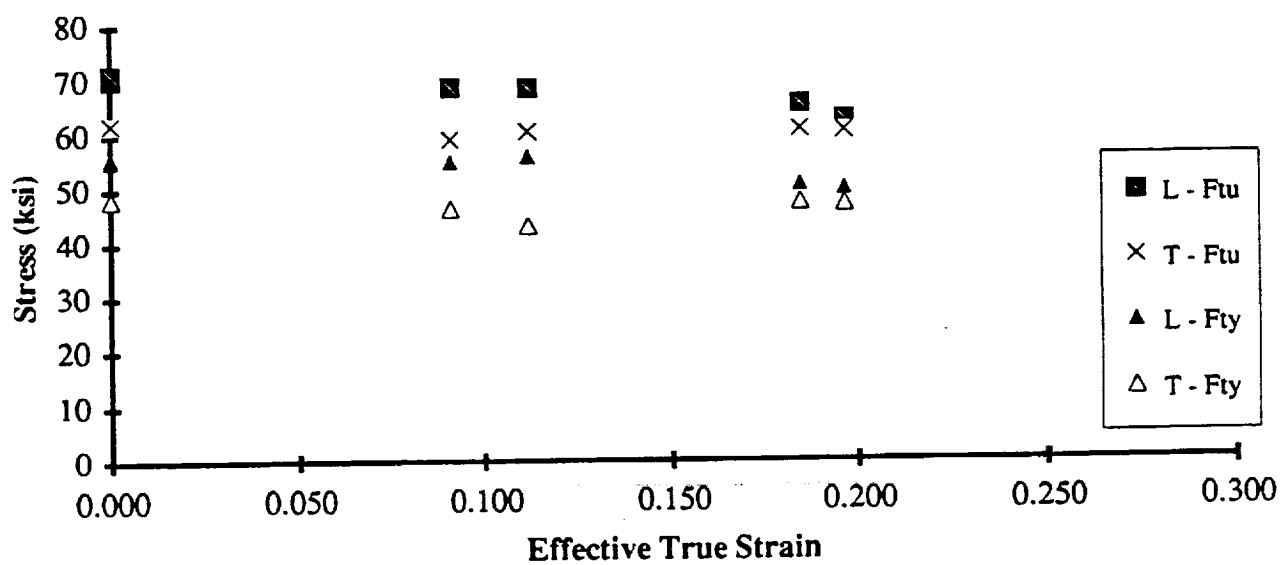


Figure 95. Cryogenic Tensile Response of 8090-T62 Al-Li at -60°F.

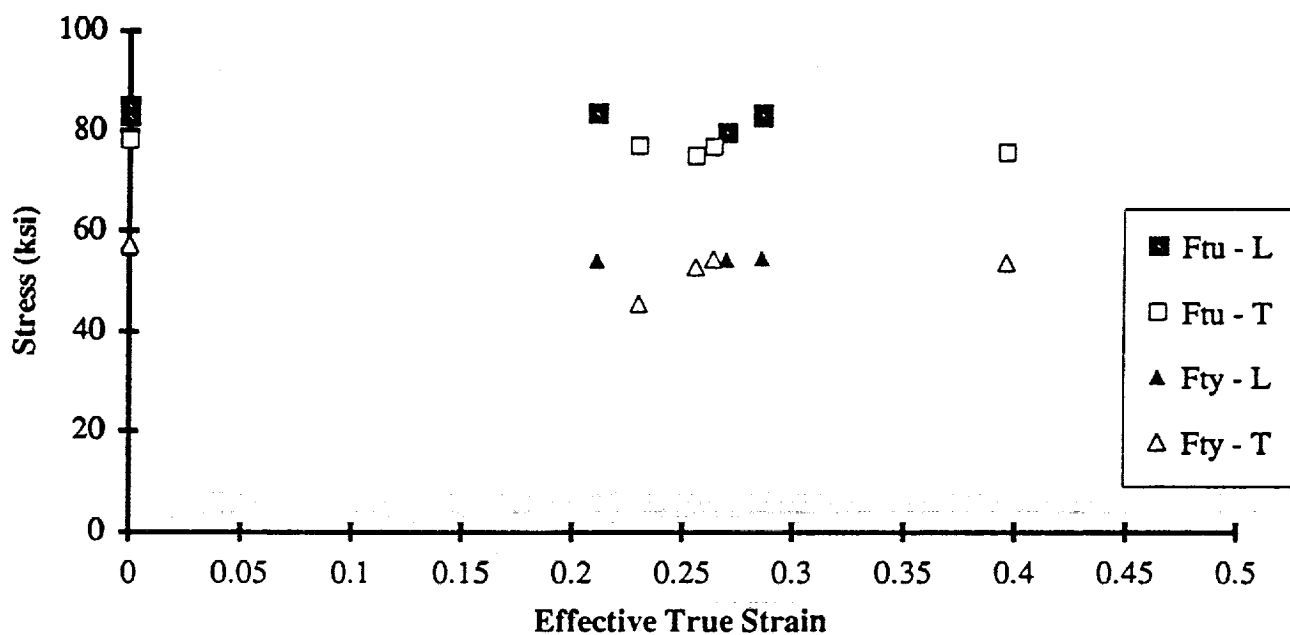


Figure 96. Cryogenic Tensile Response of 2090-T62 Al-Li at -320°F.

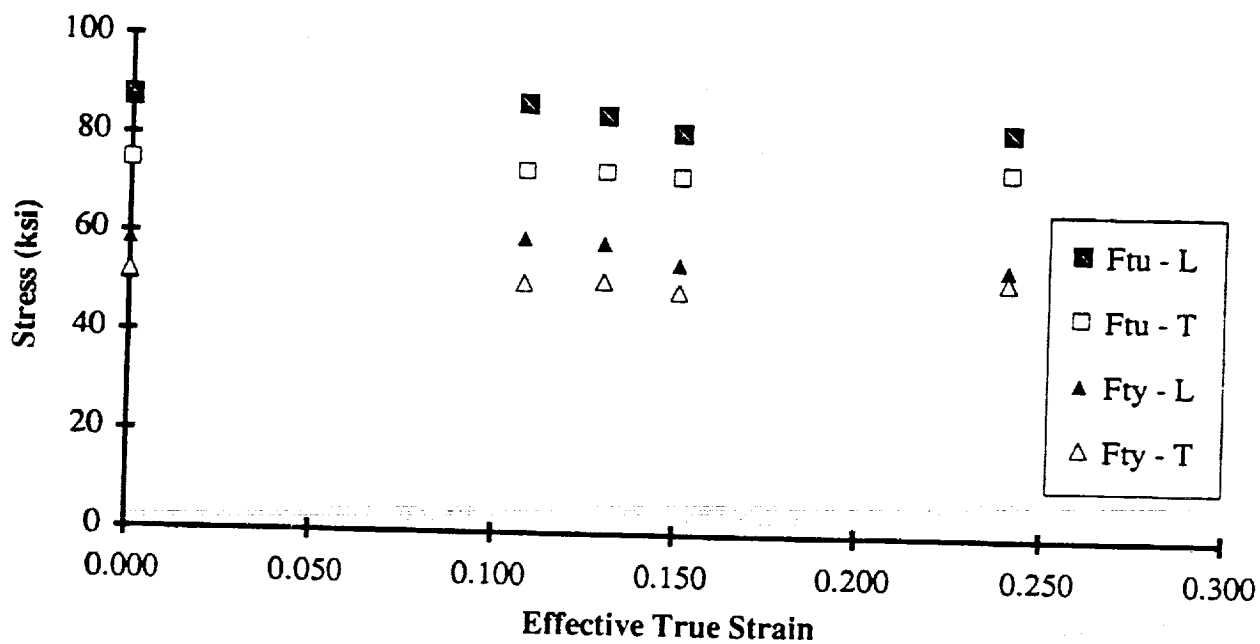


Figure 97. Cryogenic Tensile Response of 8090-T62 Al-Li at -320°F.

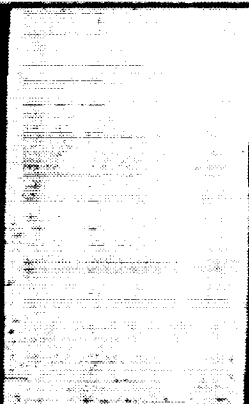
Table 42. Compressive Strength of 2090 and 8090 Pre- and Post-Superplastic Formed Sheet Heat Treated to -T62.

Alloy Temper	Coupon I.D.	SPF Condition	Specimen Thickness (in)	Specimen Width (in)	Compressive Yield Strength (ksi)	Compressive Ave. Yield (ksi)
2090-T62	316-2-L1	Pre-SPF	0.058	0.625	58.5	58.3
"	316-2-L2	Pre-SPF	0.058	0.624	58.0	
"	316-1-T1	Pre-SPF	0.091	0.623	56.6	56.5
"	316-1-T2	Pre-SPF	0.091	0.622	56.4	
"	360-L1	Post-SPF	0.066	0.625	59.6	59.0
"	360-L2	Post-SPF	0.058	0.625	58.3	
"	360-T1	Post-SPF	0.052	0.624	61.0	60.0
"	360-T2	Post-SPF	0.060	0.625	59.1	
8090-T62	315-2-L1	Pre-SPF	0.088	0.623	58.7	58.9
"	315-2-L2	Pre-SPF	0.088	0.622	59.1	
"	315-2-T1	Pre-SPF	0.088	0.622	51.6	51.8
"	315-2-T2	Pre-SPF	0.088	0.621	51.9	
"	357-L1	Post-SPF	0.063	0.625	57.0	57.1
"	359-L2	Post-SPF	0.047	0.625	57.2	
"	357-T1	Post-SPF	0.046	0.625	55.3	55.2
"	359-T2	Post-SPF	0.059	0.625	55.1	

* Specimens were machined to achieve uniform thickness.

The significance of the testing for this application is to provide valid comparisons for the superplastic formed 2090 and 8090 aluminum-lithium materials with other aluminum materials used in current launch systems. Although the alternate immersion test is an accelerated test, it is considered to be representative of certain natural exposure conditions. However, it is not intended to predict the performance of the material under specialized chemical environments where other failure modes may dominate. In several high strength aluminum alloys (specifically the copper bearing alloys with minimum cross sectional areas), severe pitting can interfere with the initiation of stress-corrosion cracks and can complicate failure mode identification.¹⁴ Since the panels used for the program were to be loaded in both the N_X and N_{XY} directions and exposed to severe environmental conditions both in storage and prior to launch, it seemed advisable to investigate the SCC resistance of the materials into the test matrix.

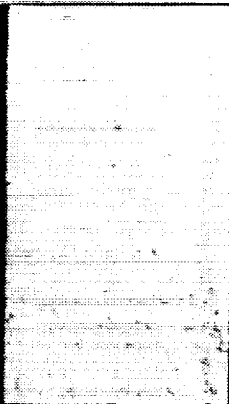
2090 PRE-SPF



S-NO. 590316-3

RATING - P A

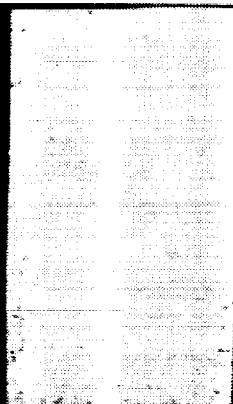
2090 POST-SPF



S-NO. 590323-3

RATING - PB A

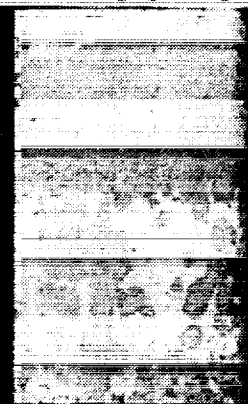
2090 POST-SPF



S-NO. 590322-1

RATING - P A

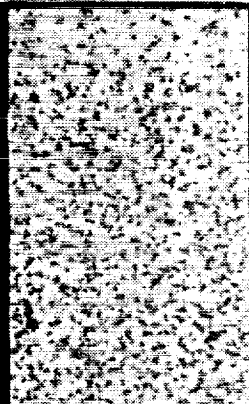
2090 POST-SPF



S-NO. 590324-1

RATING - P A

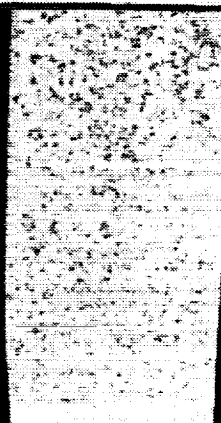
8090 PRE-SPF



S-NO. 590315-1

RATING - PB C

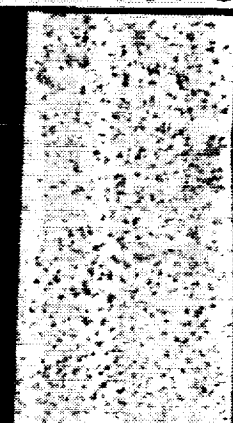
8090 POST-SPF



S-NO. 590319-3

RATING - PB C

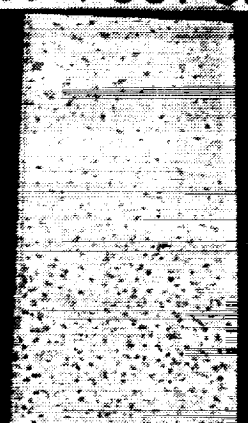
8090 POST-SPF



S-NO. 590319-3

RATING - PB C

8090 POST-SPF



S-NO. 590320-3

RATING - PB C

RATINGS:

A = MILD

C = SEVERE

P = PITTING

PB = PIT BLISTERING

EXFOLIATION
(MASTMAASIS)
(2 WEEKS)

Figure 98. Exfoliation Corrosion Results for 2090 and 8090 Al-Li Using the MASTMAASIS Test Methods.

For this group of test specimens, the coupons were fabricated from two sources; superplastic formed material and non-formed or as-received but thermally processed material. All of the test coupons were heat treated to a -T62 condition prior to testing, thus effectively eliminating all residual stress that may have been in the materials due to forming or mill processing. The 2090 and 8090 Al-Li materials were tested oriented in the long-transverse direction for both the stressed (loaded in a spring fixture) and unstressed condition. The coupons that were placed under stress (six of each alloy) were loaded to 50 percent of their yield strength (26 ksi for 2090 Al-Li, 25.5 ksi for 8090 Al-Li) in the test fixture. No failures occurred during the thirty day exposure for either alloy under stressed or unstressed conditions as shown in Table 43.

A portion of the SCC test results were performed with material that had been straightened after solution treatment and quenching to eliminate coupon distortion. The superplastic formed 8090 Al-Li coupons (identified by effective true strain values greater than zero) were the only SCC coupons not straightened. The use of check and straightening for elimination of distortion caused by solution heat treatment and quenching is a standard practice with sheet metal parts in production. Thus, the use of straightened coupons would be representative of areas in a final structural component. Theoretically, material that had been straightened would create areas of moderate localized stress in the coupon (depending upon the amount of warpage in the specimen) decreasing its SCC resistance. However, there was essentially no difference in the SCC results for any of the coupons or in the post-SCC tensile response of the straightened versus non-straightened 8090 Al-Li material. The results led to the conclusion that the amount of strain placed into the system due to a minimal check and straighten operation was not sufficient to aggravate the SCC response in sheet metal.

Table 43. SCC Alternate Immersion Test Results for 2090 and 8090 Sheet.

SCC of 2090				SCC of 8090			
Unstressed F/N	Days	Stressed F/N	Days	Unstressed F/N	Days	Stressed F/N	Days
0/3	----	0/6	----	0/3	----	0/6	----

4.2.3.9 Residual Tensile Strength (Post-SCC)

The post-SCC smooth room temperature tensile coupons for the 2090 and 8090 sheet materials were tested and the results are tabulated in Table 44. The variables tracked are the amount of strain introduced into the part due to superplastic forming (including the non-formed

condition), and the level of stress used on the coupons during SCC testing. The percent of property loss was computed by comparing the material properties of the post SCC tensile tests with the smooth tensile properties of the materials taken from the identical pan or sheet that had not been exposed to the NaCl solution.

Table 44. Smooth Room Temperature Tensile Testing After SCC Exposure of 2090 and 8090 Pre- and Post-SPF Sheet.

Alloy/ Temper	Stressed/ Unstressed	Specimen Thickness (in.)	Specimen Width (in.)	Tensile Properties @ Room Temperature				Effective True Strain
				F _{tu} (ksi)	Change (%)	F _{ty} (ksi)	Change (%)	
2090	Stressed	0.0902	0.503	58.5	-8.6	51	-4.5	0
2090	Stressed	0.0908	0.503	59.3	-7.3	50	-6.4	0
2090	Stressed	0.0901	0.503	59.9	-6.4	52.9	-0.9	0
2090	Stressed	0.0674	0.503	62.2	-0.2	56.1	12	0.289
2090	Stressed	0.0703	0.502	56.5	-9.3	48.6	-3	0.247
2090	Stressed	0.0704	0.503	57.5	-7.4	48.6	0.6	0.246
2090	Unstressed	0.0665	0.503	57.2	-4	48.2	0.8	0.303
2090	Unstressed	0.0656	0.503	57.4	-5.6	48.4	-0.4	0.316
2090	Unstressed	0.0692	0.502	59	-5	49.3	2.1	0.263
8090	Stressed	0.0883	0.502	57.4	-5	44.6	-7.1	0
8090	Stressed	0.0885	0.502	57.5	-4.8	44.4	-7.5	0
8090	Stressed	0.0885	0.502	57	-5.6	44.3	-7.7	0
8090	Stressed	0.0799	0.502	57.3	-3.5	46.6	1.7	0.097
8090	Stressed	0.0788	0.501	57.9	-2.5	46.1	0.7	0.11
8090	Stressed	0.0755	0.502	59.1	-0.5	45.9	0.2	0.153
8090	Unstressed	0.0782	0.501	55.9	-5.9	46.2	0.9	0.118
8090	Unstressed	0.0796	0.501	58.8	-1	47.1	2.8	0.1
8090	Unstressed	0.0817	0.502	57.4	-3.4	46.4	1.3	0.074

Notes: 8090 material Stressed at 25.5 ksi, 2090 material Stressed at 26.0 ksi. All material exposed to 3.5% NaCl Solution Alternate Immersion for 30 Days Both Stressed and Unstressed Specimen thickness was measured at the minimum thickness of the gauge section.

The tensile yield and ultimate strengths of 2090 and 8090 are shown after exposure to an alternate immersion 3.5 percent NaCl environment for 30 days in Figures 99 and 100. The results are plotted versus thickness strain (0 strain values are for material that was in the as-received condition and heat treated).

The primary reason for conducting residual strength tests is to discriminate between alloys and conditions with small differences in the ultimate tensile strength (F_{tu}) caused by increased rates of stress corrosion crack growth rates and hence longer cracks in one set of specimens. Since there is not any significant difference in F_{tu} between either the pre- and post-SPF or stressed and

unstressed specimens in either alloy, it is concluded that the superplastic forming process does not affect the SCC behavior of the material.

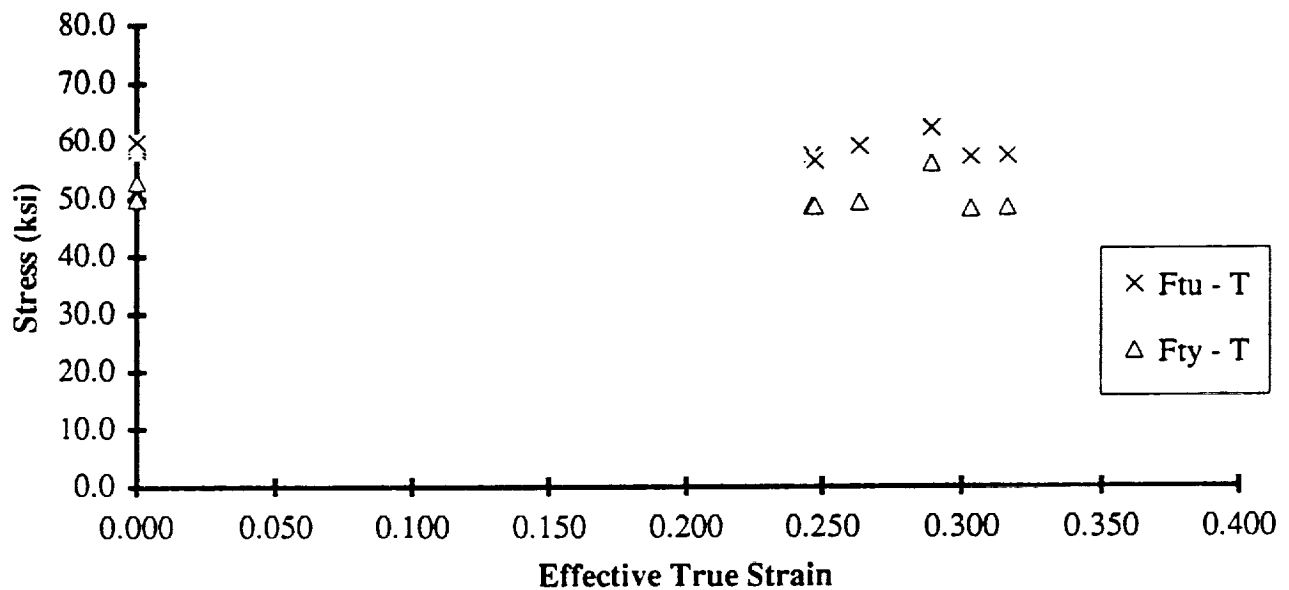


Figure 99. Post-SCC Residual Tensile Strength of 2090-T62 Al-Li.

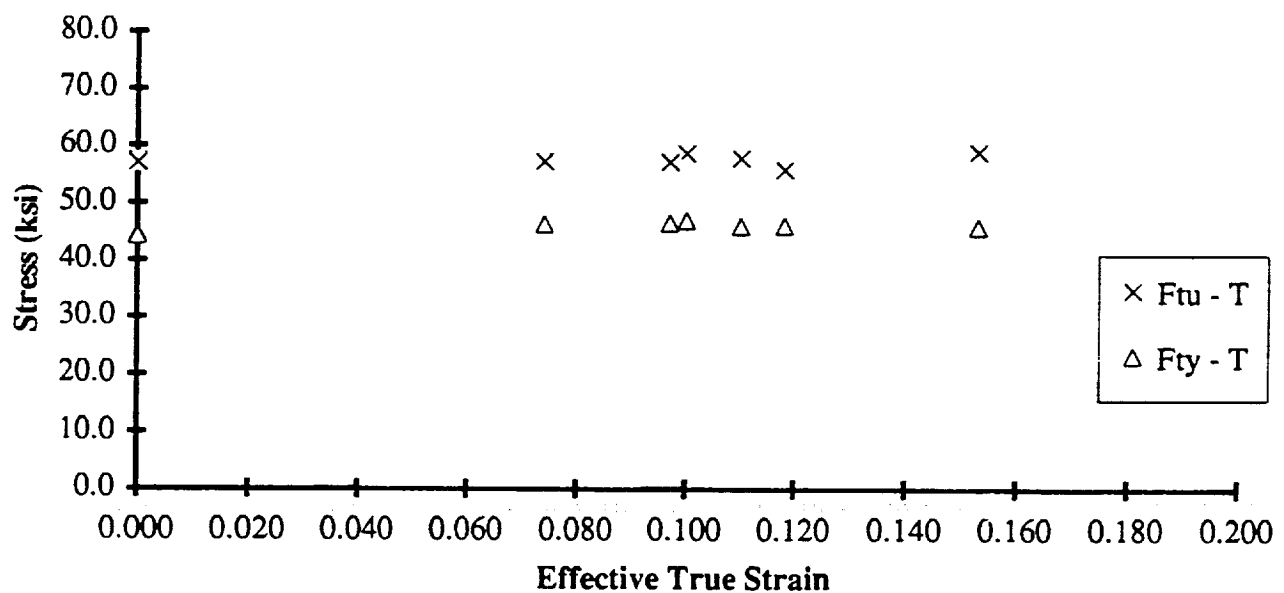


Figure 100. Post-SCC Residual Tensile Strength of 8090-T62 Al-Li.

4.2.3.10 Fracture Toughness

Fracture toughness were tested using the center crack tension (m (T)) coupon test for stable crack growth under static loading with a measurement of strain compliance with load increase. The R-curve test is described in ASTM STD E561-78T and B-646. Figure 101 shows the test specimen configuration that was utilized during this program. The specimens were oriented in the L-T direction with a non-formed thermally processed specimen as a control, and the remaining specimens removed from formed pans which were heat treated prior to testing.

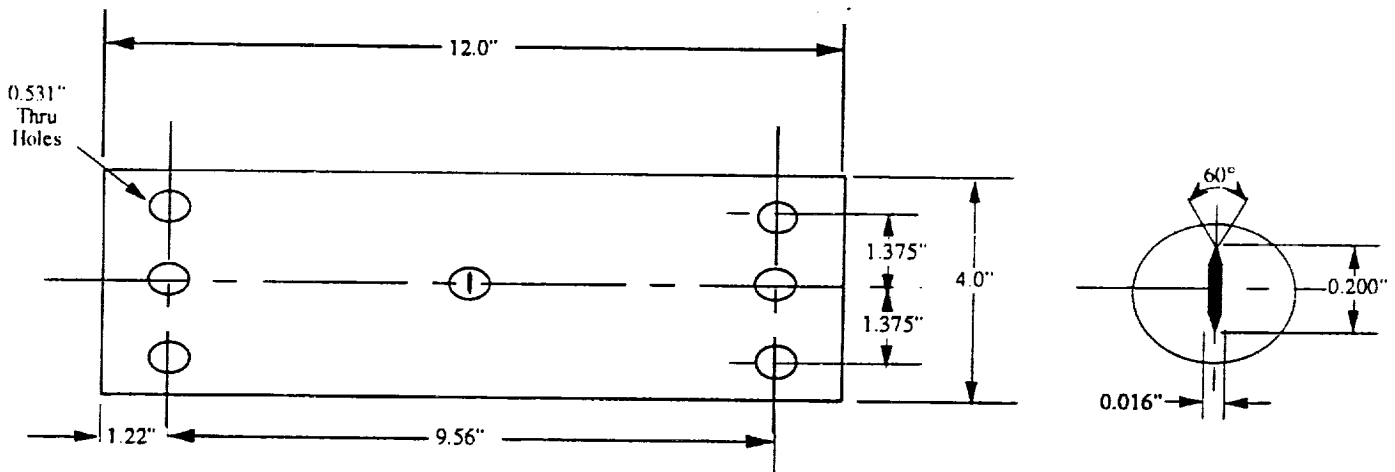


Figure 101. Center Crack Tension Specimen Configuration.

Fracture toughness has been used as a key property for utilization of a number of aluminum alloys in the Aerospace industry. In spite of all of the interest in this rating of materials several different test techniques and configurations exist and no single method exists to cover a number of the product lines or dimensional ranges involved. Plane-strain fracture toughness, K_{Ic} , is widely used in the Aerospace industry principally for the high strength alloys. Valid measurements for K_{Ic} can be made only for relatively thick sections, however test methods have been developed for measuring the "toughness" of sheet sections (previously mentioned as ASTM STD E561-78T and B-646).

Generally, for either quality assurance or material release purposes, the critical (or maximum) stress intensity factor for monotonically loaded center-slotted panels is recommended as the index of fracture toughness. This value is designated K_C for purposes of this practice. Specimen widths less than 15 or 16 in. can be used for quality assurance or lot release testing, but since the maximum, or critical stress intensity factor is dependent upon the interaction of the crack-driving force which is a function of specimen width and the crack-resistance curve, the resulting

value is both specimen width and thickness dependent. The value for K_{Ic} decreases with decreasing specimen width, all other factors being identical.

The fracture toughness (K_{Ic}) values at a maximum load are shown in Table 45. There was substantial scatter in the results, however there was no direct evidence of an effect on the toughness of the material due to the SPF process. The 8090-T62 K_{Ic} values were slightly higher than those measured for 2090-T62, however, K_{Ic} is only one point on the R-curve and that general observation may not apply to the entire R-curve. The test data are enclosed as Appendix D.

Table 45. Ambient Fracture Toughness for 2090-T62 and 8090-T62 Al-Li Materials in the L-T Direction, $t_0 = 0.090$.

Alloy - Temper	SPF Condition	Fracture Toughness K_{Ic} (ksi√in)	Effective True Strain (ϵ)
2090-T62	Non-Formed	48.3	0
		52.0	0
	Formed	39.4	0.250
		52.8	0.207
8090-T62	Non-Formed	52.9	0
		66.8	0
	Formed	60.3	0.155
		48.8	0.208

4.2.3.11 Fatigue Crack Propagation

Fatigue crack propagation rate tests (da/dn) were carried out according to ASTM E647-78T. Center-cracked tension specimens (four-inches wide) were used, as shown in Figure 101. Single specimens were tested with crack growth rates in the range 10^{-7} - 10^{-4} da/dn with three different stress ratios: $R = +0.1$, $+0.3$, and $+0.5$. The specimens were all oriented in the L-T direction with as-received and formed materials heat treated to the -T62 condition. Testing was conducted in ambient laboratory air at 10 Hz. The resulting R-curves are shown as Figures 102 through 109.

4.2.3.12 Smooth and Notched Axial Fatigue

Smooth and notched fatigue tests were carried out at constant amplitude in axial tension-tension. A minimum/maximum stress ratio (R) of $+0.1$ was used for all cases according to ASTM E-466 specification. Tests were performed in laboratory air at ambient temperature using

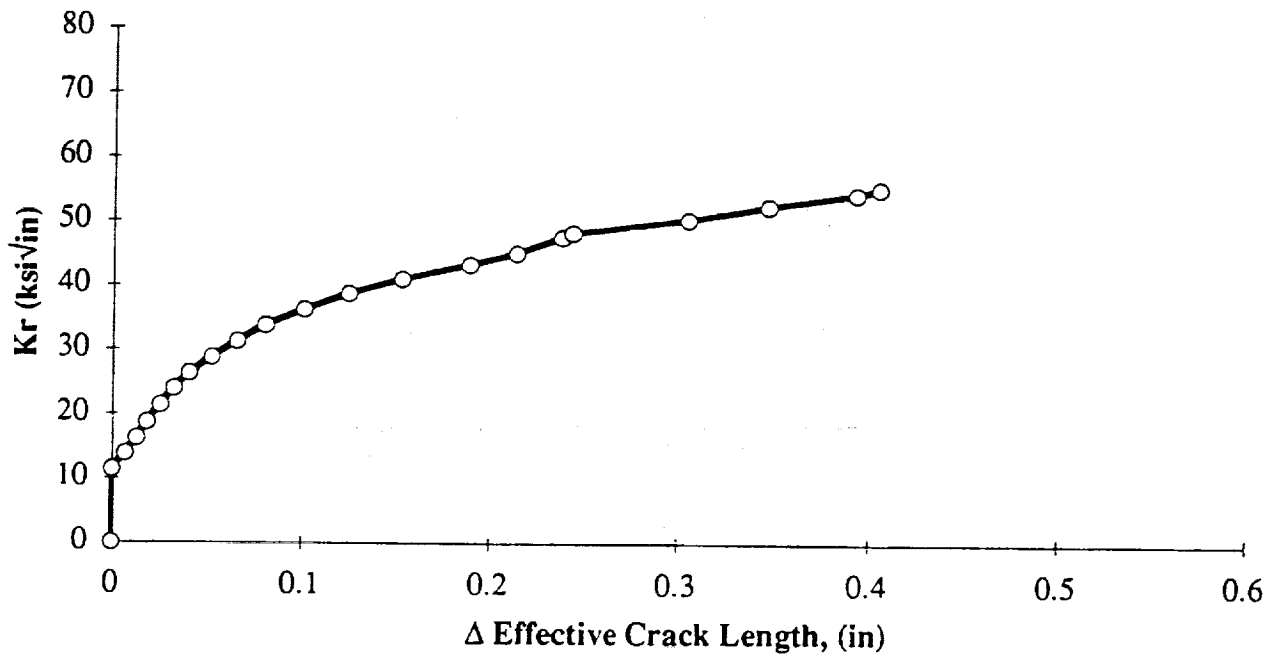


Figure 102. R-Curve for 2090 Al-Li, Non-Strained Material. $K_c = 48.3$.

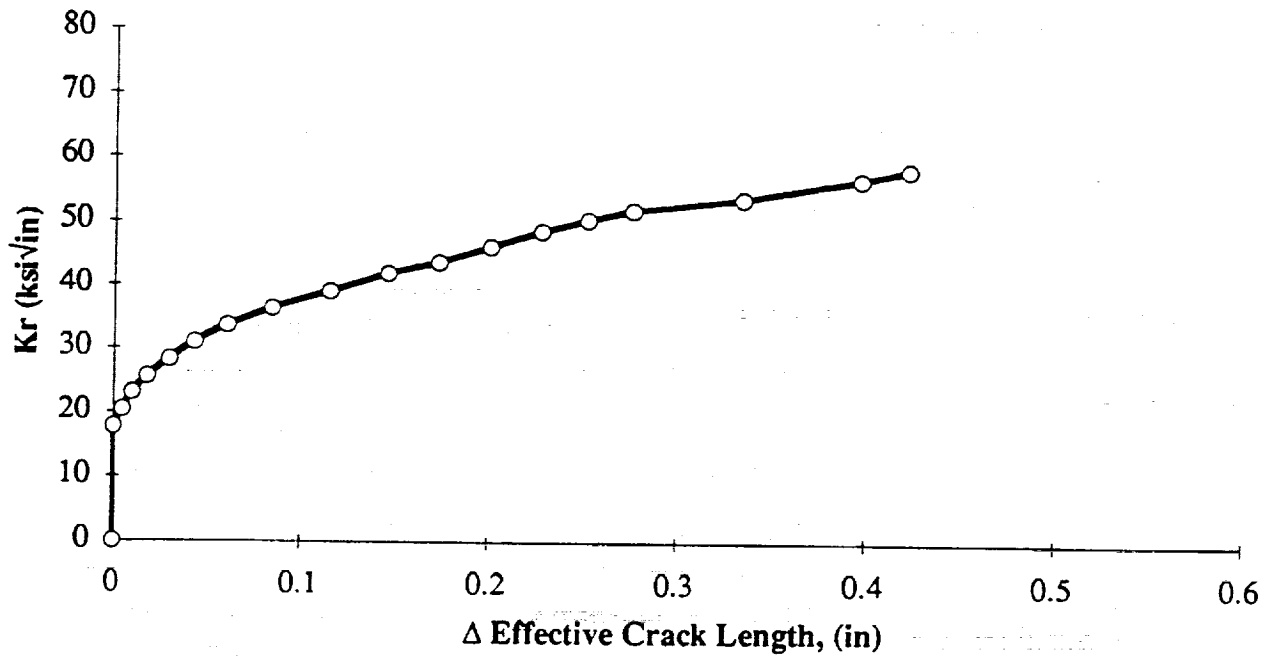


Figure 103. R-Curve for 2090 Al-Li, Non-Strained Material. $K_c = 52.0$.

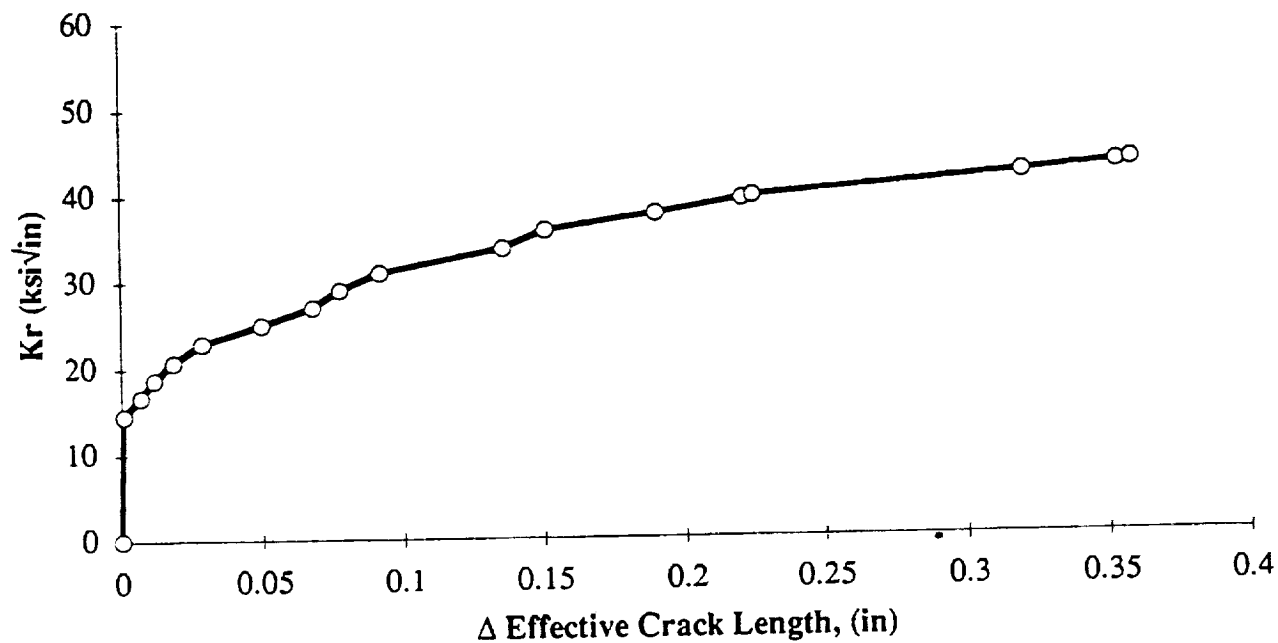


Figure 104. R-Curve for 2090 Al-Li, Formed Material. $K_c = 39.4$.

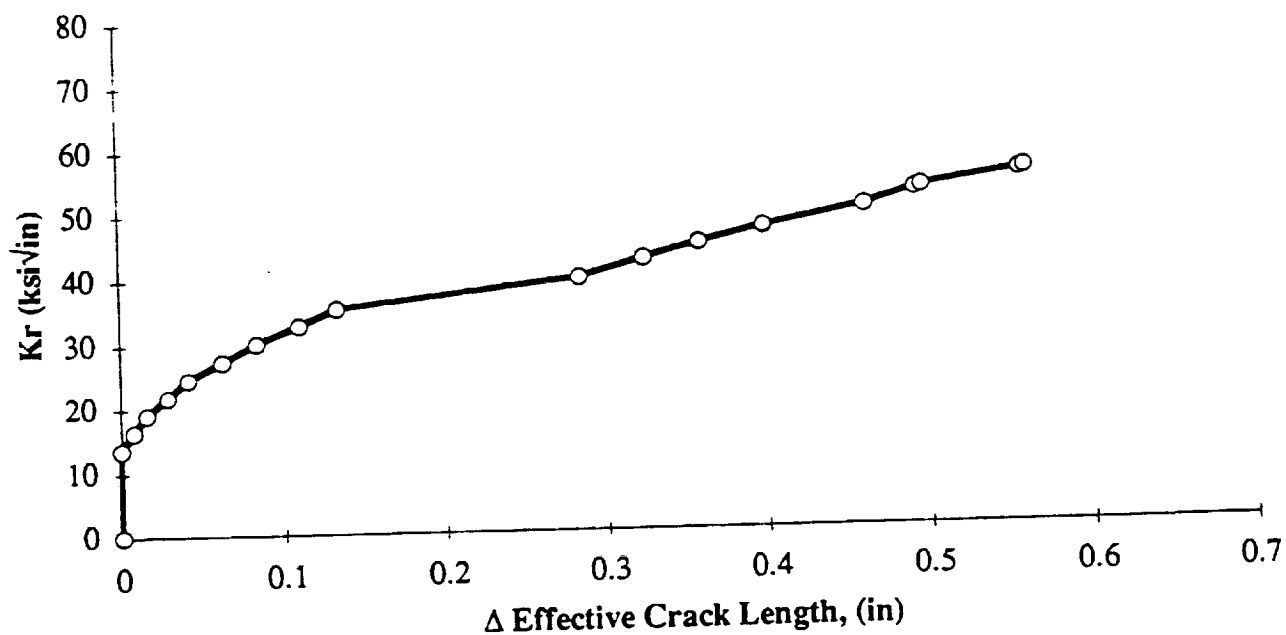


Figure 105. R-Curve for 2090 Al-Li, formed Material. $K_c = 52.8$.

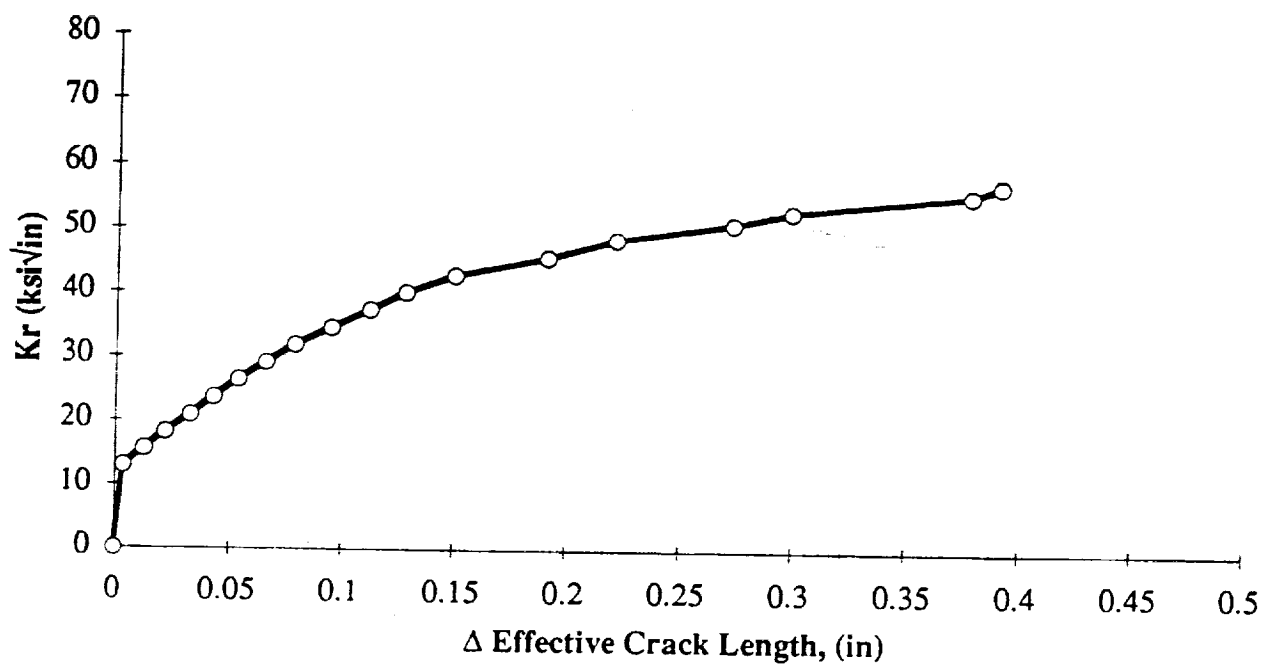


Figure 106. R-Curve for 8090 Al-Li, Non-Strained Material. $K_c = 52.9$.

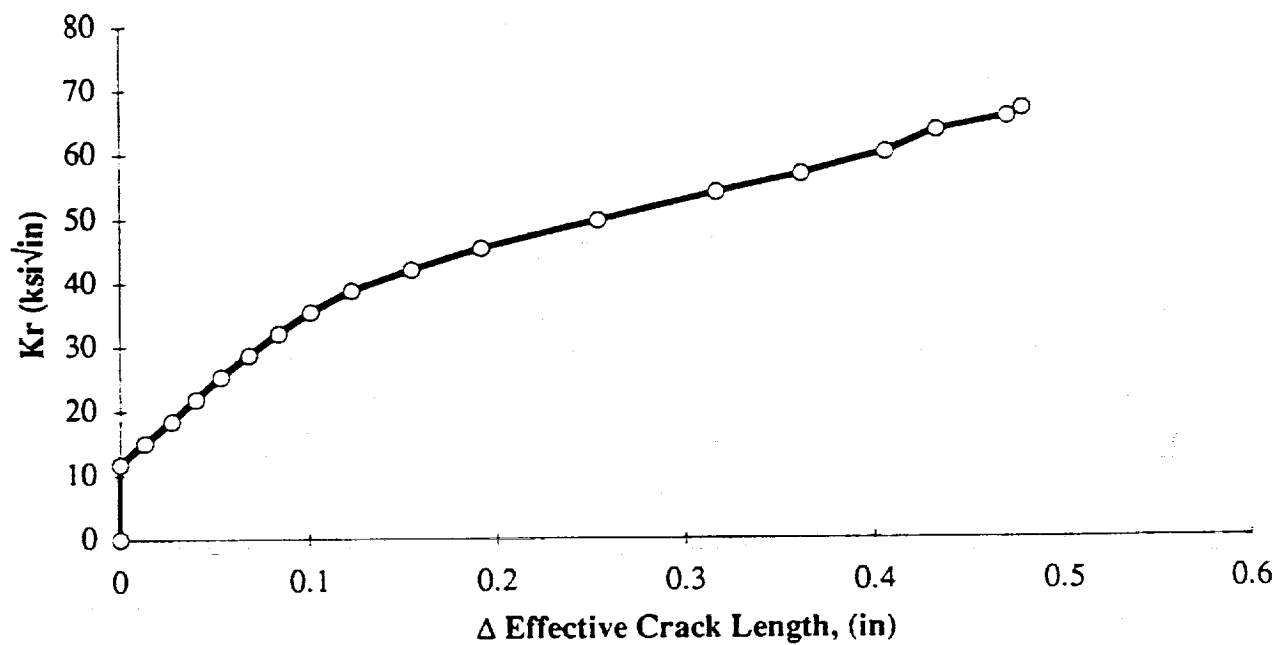


Figure 107. R-Curve for 8090 Al-Li, Non-Strained Material. $K_c = 66.8$.

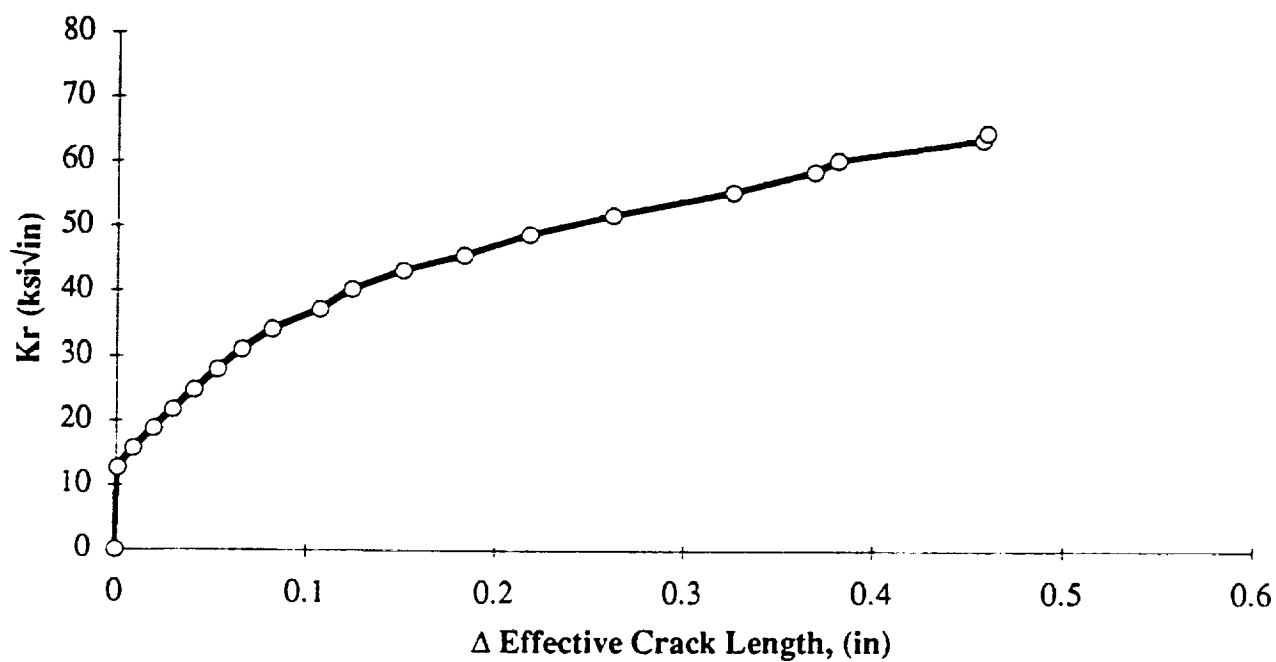


Figure 108. R-Curve for 8090 Al-Li, Formed Material. $K_c = 60.3$.

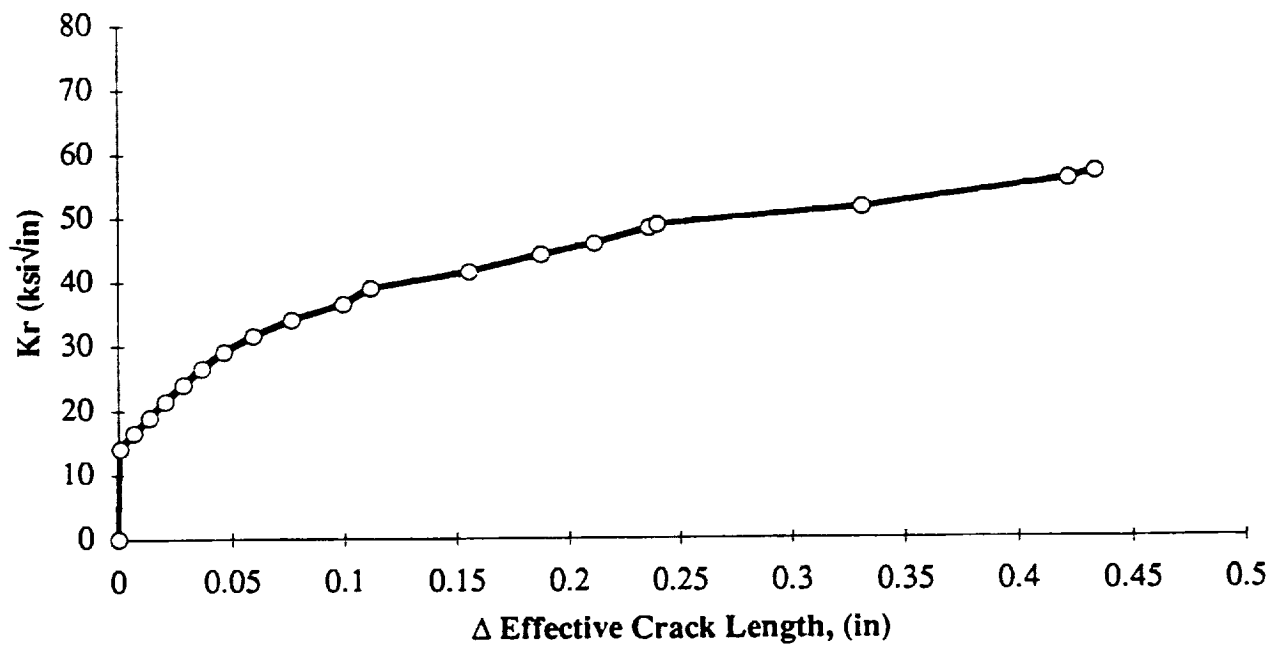


Figure 109. R-Curve for 8090 Al-Li, formed Material. $K_c = 48.8$.

specimens fabricated with a continuous radius as shown in Figure 110. This specimen form was chosen so that the position of fatigue crack initiation and growth was predictable even in the presence of thickness variations and internal cavitation. Specimens were sectioned in both the L and T directions.

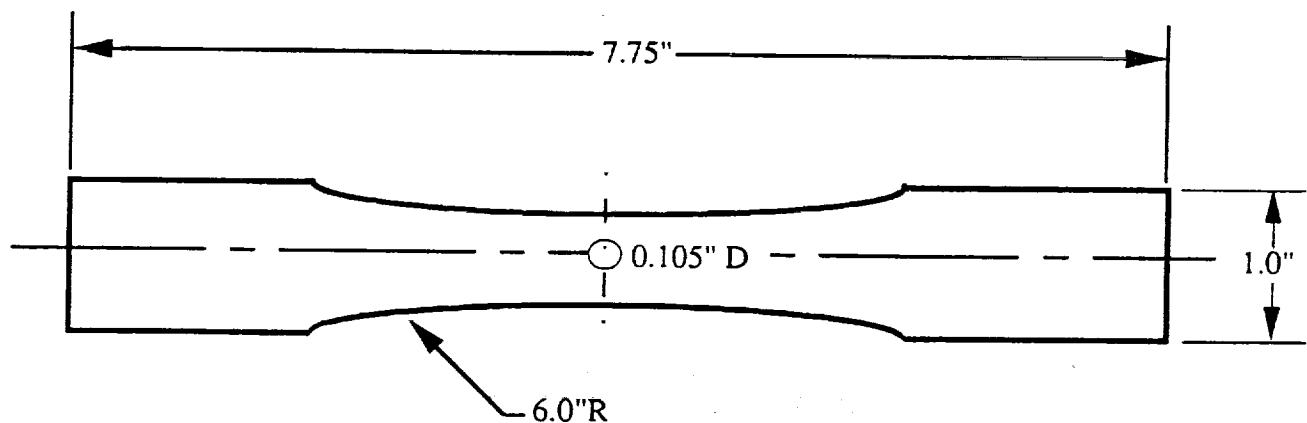


Figure 111. Smooth ($K_t = 1.02$) and Notched ($K_t = 2.5$) Fatigue Specimens With Continuous Radius.

The results from the smooth and notched axial fatigue testing of 2090-T62 and 8090-T62 SPF material are shown in Tables 46 through 49. The tables include information describing specimen processing sequence, SPF condition, and effective true forming strain in addition to the test stress and cycles to failure.

Smooth and notched axial fatigue results for the 2090-T62 material are shown in Figures 111 and 112. There was no observable effect on the fatigue life due to forming strains of approximately 50%. The pre-SPF smooth L specimen at the 28 ksi stress level failed prematurely at 200,000 cycles due to a surface defect crack (approximately 0.015" wide by .010 to 0.015" deep) that had not been detected prior to testing.

Smooth and notched axial fatigue results for the 8090-T62 material are shown in Figures 113 and 114. Again, there was no observable degradation in fatigue life due to the superplastic forming process. There was little or no difference in the smooth fatigue lives of 2090-T62 and 8090-T62. The notched fatigue performance (net stress) showed that there was little difference between the notched fatigue performance of 8090 and 2090 SPF material. All but three of the 8090 and eight of the 2090 fatigue specimens were flattened after solution heat treatment. The flattening would be expected to alter the fatigue response primarily through changes in tensile properties caused by strain enhanced precipitation strengthening. However, there was no evidence

Table 46. Smooth Fatigue Testing of 2090-T62 Al-Li, L and T Orientations.
Longitudinal

Condition	Fatigue Cycles	Stress Level (ksi)	Eff. True Strain (ϵ)	Comments
Pre-SPF	1.5E+05	40	0.000	Re-SHT, Flattened
Post-SPF	9.3E+04	40	0.234	Re-SHT, Flattened
Pre-SPF	8.9E+04	40	0.000	SHT
Post-SPF	5.8E+04	40	0.220	Re-SHT, Flattened
Pre-SPF	4.6E+05	30	0.000	Re-SHT, Flattened
Post-SPF	5.9E+04	45	0.152	Re-SHT, Flattened
Pre-SPF	1.1E+05	45	0.000	Re-SHT, Flattened
Pre-SPF	6.2E+04	45	0.000	Re-SHT, Flattened
Pre-SPF	2.0E+05	28	0.000	Re-SHT, Flattened
Post-SPF	1.1E+06	28	0.219	Re-SHT, Flattened, Radius Edge F
Post-SPF	1.4E+05	40	0.236	Re-SHT, Flattened
Post-SPF	6.7E+04	45	0.310	Re-SHT, Flattened
Post-SPF	1.3E+07	28	0.307	Re-SHT, Flattened, Did Not Fail
Post-SPF	1.1E+07	28	0.220	Re-SHT, Flattened, Did Not Fail
Post-SPF	6.2E+04	45	0.237	Re-SHT, Flattened

Transverse

Condition	Fatigue Cycles	Stress Level (ksi)	Eff. True Strain (ϵ)	Comments
Post-SPF	1.3E+07	28	0.207	Re-SHT, Flattened, Did Not Fail
Post-SPF	1.1E+05	40	0.194	Re-SHT, Flattened
Post-SPF	4.9E+04	45	0.330	SHT, Flattened
Post-SPF	4.4E+05	28	0.301	SHT, Flattened
Pre-SPF	1.7E+07	28	0.000	Re-SHT, Flattened, Did Not Fail
Post-SPF	1.3E+07	28	0.176	Re-SHT, Flattened Did Not Fail
Pre-SPF	2.5E+05	28	0.000	Re-SHT, Flattened
Post-SPF	5.1E+04	45	0.304	Re-SHT, Flattened
Pre-SPF	1.5E+05	45	0.000	SHT
Post-SPF	4.2E+04	45	0.261	SHT, Flattened
Pre-SPF	2.6E+05	45	0.000	Pre-SPF
Post-SPF	6.1E+04	40	0.264	Re-SHT, Flattened
Pre-SPF	1.4E+05	40	0.000	Re-SHT, Flattened
Post-SPF	8.8E+04	40	0.230	Re-SHT, Flattened
Pre-SPF	1.6E+05	40	0.000	SHT

Table 47. Notched Fatigue Testing of 2090-T62 Al-Li, L and T Orientations.
Longitudinal

Condition	Fatigue Cycles	Stress Level (ksi)	Eff. True Strain (ϵ)	Comments
Pre-SPF	2.7E+05	19	0.000	SHT
Pre-SPF	1.5E+05	19	0.000	Re-SHT, Flattened
Pre-SPF	8.2E+04	25	0.000	Re-SHT, Flattened
Pre-SPF	7.0E+04	25	0.000	Re-SHT, Flattened
Pre-SPF	2.9E+04	38	0.000	SHT
Pre-SPF	4.9E+04	38	0.000	SHT
Post-SPF	1.6E+05	19	0.189	Re-SHT, Flattened
Post-SPF	7.1E+04	25	0.203	Re-SHT, Flattened
Post-SPF	1.5E+04	38	0.207	Re-SHT, Flattened
Post-SPF	3.5E+05	19	0.209	Re-SHT, Flattened
Post-SPF	7.6E+04	25	0.220	Re-SHT, Flattened
Post-SPF	2.7E+05	19	0.229	Re-SHT, Flattened
Post-SPF	2.0E+04	38	0.251	Re-SHT, Flattened
Post-SPF	2.3E+04	38	0.332	Re-SHT, Flattened
Post-SPF	9.4E+04	25	0.355	Re-SHT, Flattened

Transverse

Condition	Fatigue Cycles	Stress Level (ksi)	Eff. True Strain (ϵ)	Comments
Pre-SPF	2.1E+05	15	0.000	Re-SHT, Flattened
Pre-SPF	2.7E+05	15	0.000	Re-SHT, Flattened
Pre-SPF	1.6E+05	20	0.000	Re-SHT, Flattened
Pre-SPF	1.8E+05	20	0.000	Re-SHT, Flattened
Pre-SPF	7.1E+04	25	0.000	Re-SHT, Flattened
Pre-SPF	3.6E+04	30	0.000	Re-SHT, Flattened
Post-SPF	2.3E+05	19	0.309	Re-SHT, Flattened
Post-SPF	2.4E+05	19	0.204	Re-SHT, Flattened
Post-SPF	4.4E+05	19	0.256	Re-SHT, Flattened
Post-SPF	5.0E+04	25	0.219	Re-SHT, Flattened
Post-SPF	7.0E+04	25	0.279	Re-SHT, Flattened
Post-SPF	7.1E+04	25	0.222	Re-SHT, Flattened
Post-SPF	1.1E+04	38	0.201	SHT, Flattened
Post-SPF	1.3E+04	38	0.241	Re-SHT, Flattened
Post-SPF	1.8E+04	38	0.220	Re-SHT, Flattened

Table 48. Smooth Fatigue Testing of 8090-T62 Al-Li, L and T Orientations.
Longitudinal

Condition	Fatigue Cycles	Stress Level (ksi)	Eff. True Strain (ϵ)	Comments
Pre-SPF	6.6E+4	40	0.000	Re-SHT, Flattened
Post-SPF	1.1E+5	40	0.236	Re-SHT, Flattened
Pre-SPF	7.8E+4	40	0.000	
Post-SPF	2.5E+5	40	0.189	Re-SHT, Flattened
Pre-SPF	3.3E+4	45	0.000	
Post-SPF	7.8E+4	45	0.174	Re-SHT, Flattened
Pre-SPF	5.7E+4	45	0.000	Re-SHT, Flattened
Post-SPF	1.1E+5	45	0.280	Re-SHT, Flattened
Pre-SPF	1.1E+7	28	0.000	Re-SHT, Flattened, Did Not Fail
Post-SPF	1.2E+6	28	0.227	Re-SHT, Flattened
Pre-SPF	1.5E+7	28	0.000	Re-SHT, Flattened, Did Not Fail
Post-SPF	1.1E+7	28	0.190	Re-SHT, Flattened, Did Not Fail
Post-SPF	1.3E+5	40	0.103	
Post-SPF	5.6E+4	45	0.129	
Post-SPF	7.4E+5	28	0.309	

Transverse

Condition	Fatigue Cycles	Stress Level (ksi)	Eff. True Strain (ϵ)	Comments
Pre-SPF	2.8E+5	40	0.000	Re-SHT, Flattened
Post-SPF	1.3E+5	40	0.115	
Pre-SPF	2.7E+5	40	0.000	Re-SHT, Flattened
Post-SPF	1.5E+5	40	0.257	
Pre-SPF	7.1E+4	45	0.000	
Post-SPF	9.4E+4	45	0.237	Re-SHT, Flattened
Pre-SPF	7.9E+4	45	0.000	Re-SHT, Flattened
Post-SPF	1.0E+5	45	0.292	Re-SHT, Flattened
Pre-SPF	1.1E+6	28	0.000	Re-SHT, Flattened
Post-SPF	1.2E+6	28	0.099	
Pre-SPF	7.4E+5	28	0.000	Re-SHT, Flattened
Post-SPF	8.3E+5	28	0.077	
Post-SPF	1.8E+5	40	0.067	
Post-SPF	5.9E+4	45	0.219	
Post-SPF	4.9E+5	28	0.193	

Table 49. Notched Fatigue Testing of 8090-T62 Al-Li, L and T Orientations.
Longitudinal

Condition	Fatigue Cycles	Stress Level (ksi)	Eff. True Strain (ϵ)	Comments
Pre-SPF	2.7E+4	30	0.000	Re-SHT, Flattened
Post-SPF	3.0E+4	30	0.285	Re-SHT, Flattened
Pre-SPF	2.8E+5	20	0.000	
Post-SPF	3.1E+5	20	0.219	Re-SHT, Flattened
Pre-SPF	7.8E+5	15	0.000	Re-SHT, Flattened
Post-SPF	6.6E+5	15	0.205	
Pre-SPF	3.0E+4	30	0.000	Re-SHT, Flattened
Post-SPF	3.1E+4	30	0.250	Re-SHT, Flattened
Pre-SPF	3.3E+5	20	0.000	Re-SHT, Flattened
Post-SPF	5.1E+5	20	0.208	Re-SHT, Flattened
Pre-SPF	1.1E+7	15	0.000	Re-SHT, Flattened, Did Not Fail
Post-SPF	1.1E+7	15	0.180	Re-SHT, Flattened, Did Not Fail
Post-SPF	4.3E+4	30	0.237	Re-SHT, Flattened
Post-SPF	5.4E+5	20	0.173	
Post-SPF	1.3E+6	15	0.273	

Transverse

Condition	Fatigue Cycles	Stress Level (ksi)	Eff. True Strain (ϵ)	Comments
Pre-SPF	4.0E+4	30	0.000	Re-SHT, Flattened
Post-SPF	4.0E+4	30	0.232	Re-SHT, Flattened, Did Not Fail
Pre-SPF	4.2E+5	20	0.000	Re-SHT, Flattened
Post-SPF	5.4E+5	20	0.261	Re-SHT, Flattened
Pre-SPF	1.1E+7	15	0.000	Re-SHT, Flattened, Did Not Fail
Post-SPF	1.0E+7	15	0.156	Did Not Fail
Pre-SPF	3.7E+4	30	0.000	Re-SHT, Flattened
Post-SPF	5.3E+4	30	0.117	
Pre-SPF	2.3E+5	20	0.000	Re-SHT, Flattened, Did Not Fail
Post-SPF	4.9E+5	20	0.089	
Pre-SPF	2.6E+6	15	0.000	Re-SHT, Flattened, Did Not Fail
Post-SPF	1.1E+7	15	0.076	Did Not Fail
Post-SPF	4.8E+4	30	0.080	
Post-SPF	3.7E+5	20	0.236	
Post-SPF	2.3E+6	15	0.166	

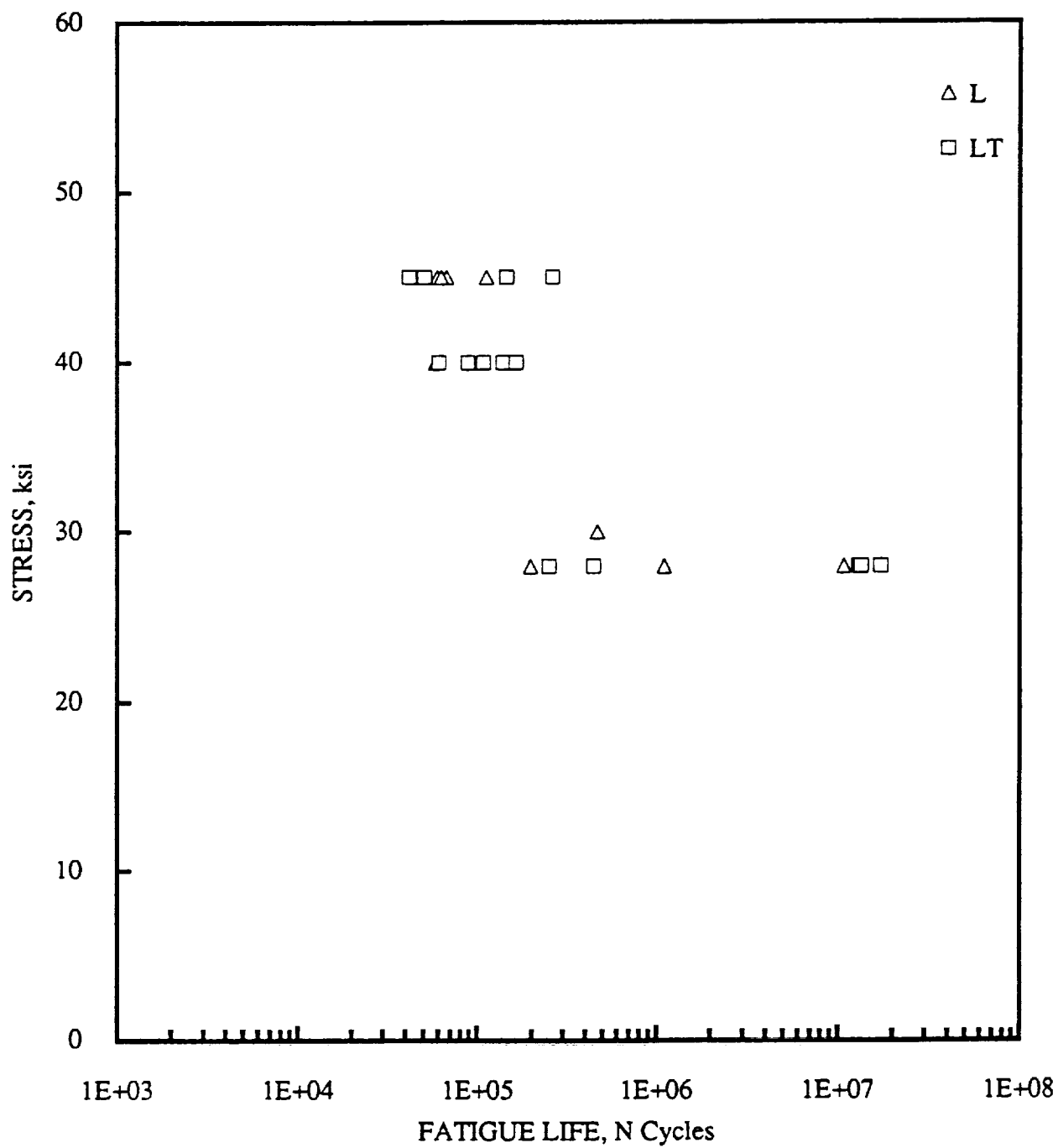
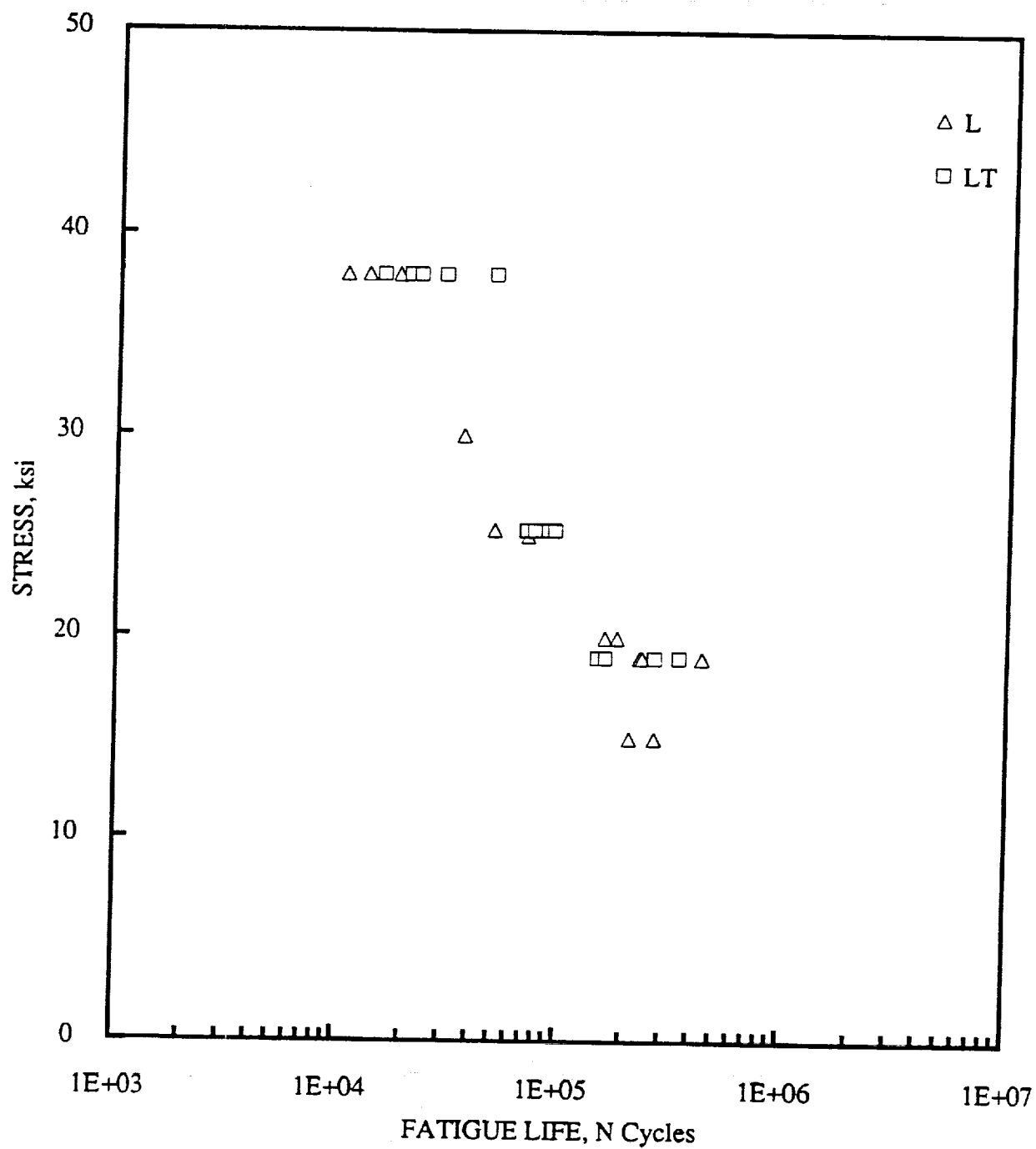


Figure 111. Smooth Fatigue Life of 2090-T62 Al-Li.



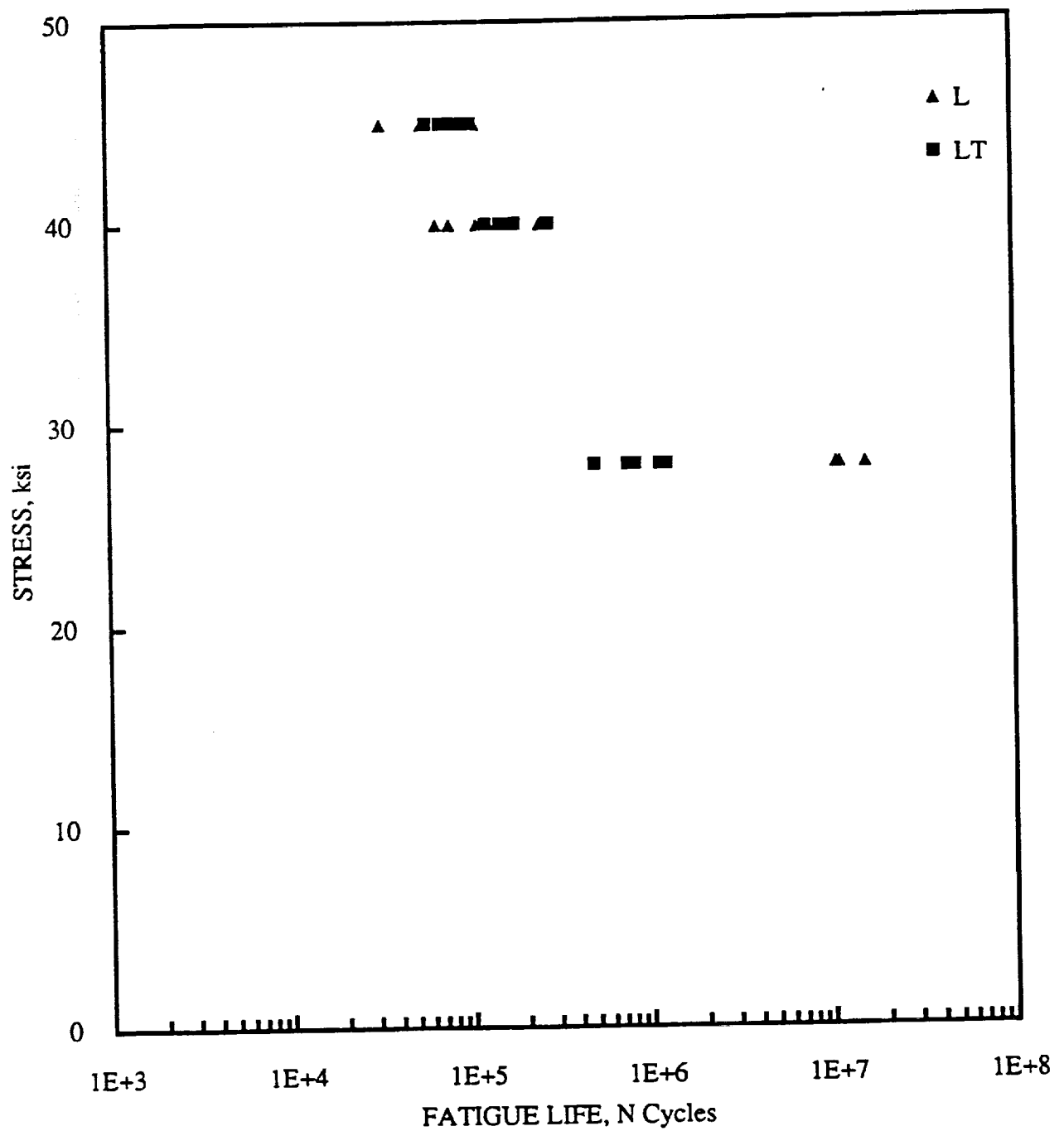


Figure 113. Smooth Fatigue Life of 8090-T62 Al-Li.

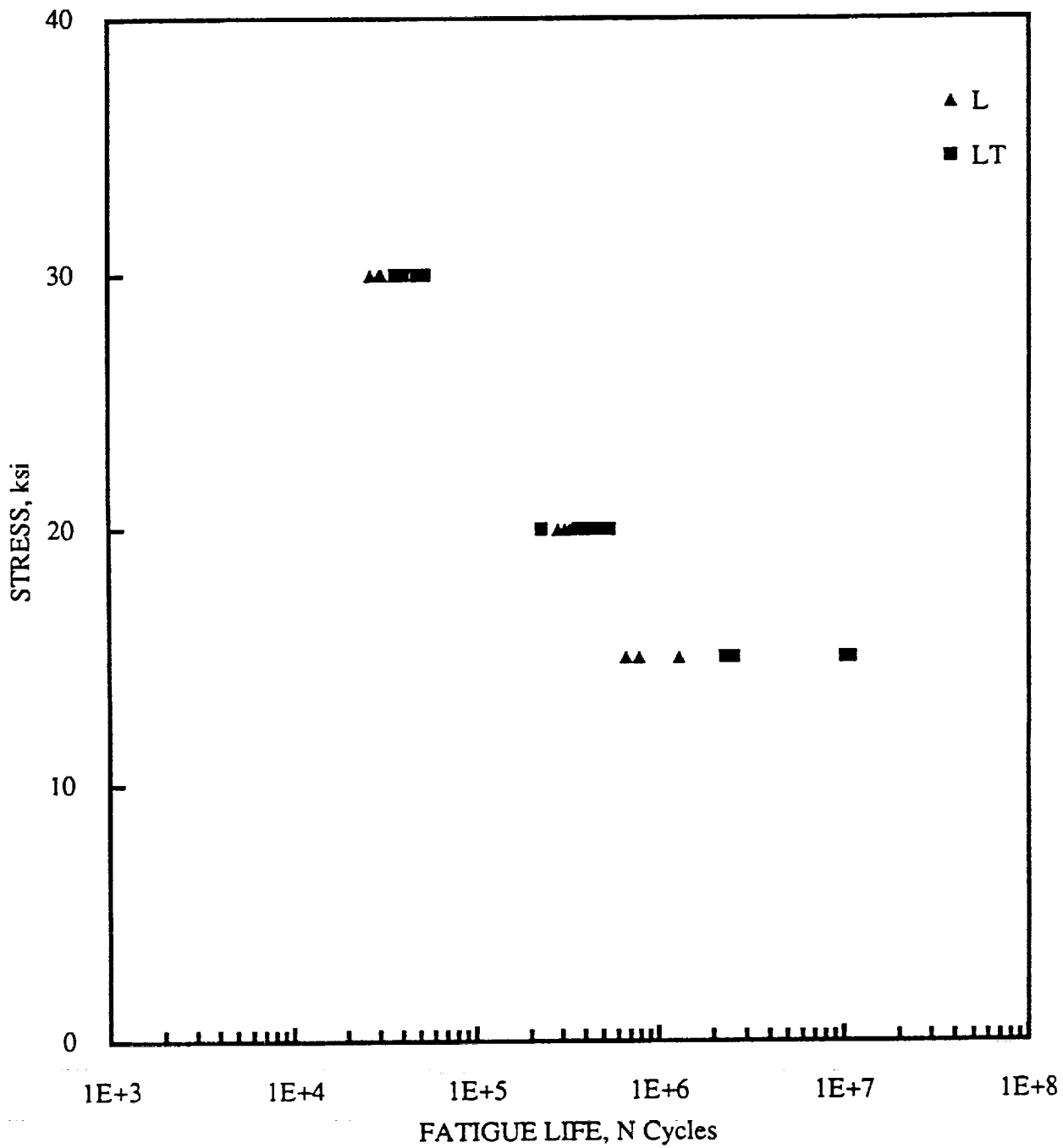


Figure 114. Notched Fatigue Life of 8090-T62 Al-Li.

of to suggest that any difference in fatigue lives exists between specimens which had undergone flattening and those that had not been flattened. Also, there was no observable difference between specimens that had been solution heat treated once, and those that were re-solution heat treated.

4.2.3.13 Bearing Strength

Pin-type bearing tests were conducted according to ASTM E238-68 for both the 2090 and 8090-T62 material systems. Although it seemed unlikely that fasteners would be used in the cryogenic tank, mechanical fastening was evaluated as a back-up for resistance spot-welding for attachment of a non-integral intermediate hoop frame to the caps of the stiffener members. The results from the tests are shown as Tables 50 and 51.

Table 50. Bearing Properties of 2090 Pre- and Post-Superplastic Formed Sheet Heat Treated to -T62.

Orientation	e/D	B _{ru} (ksi)	B _{ry} (ksi)	Effective True Strain	Failure Type
L	1.5	84.00	71.60	0.000	1
L	1.5	81.20	68.70	0.000	1
L	1.5	80.00	62.90	0.251	2
L	1.5	79.80	62.70	0.248	2
L	2	104.40	87.10	0.000	2
L	2	109.30	93.80	0.000	2
L	2	106.40	83.10	0.213	1
L	2	100.30	79.60	0.213	1
T	1.5	80.20	72.70	0.000	1
T	1.5	83.90	73.80	0.000	1
T	1.5	82.80	69.90	0.237	1
T	1.5	80.70	72.00	0.260	1
T	2	101.40	85.60	0.000	1
T	2	102.90	88.30	0.000	1
T	2	96.30	83.40	0.237	2
T	2	97.50	79.60	0.232	1

Failure Type: 1 = Shear, 2 = Shear-Tension, 5 = Crushing

Table 51. Bearing Properties of 8090 Pre- and Post-Superplastic Formed Sheet Heat Treated to -T62.

Orientation	E/D	Bru (ksi)	Bry (ksi)	Effective True Strain	Failure Type
L	1.5	81.50	70.70	0.000	1
L	1.5	84.00	70.80	0.000	1
L	1.5	79.20	64.60	0.104	5
L	1.5	79.90	68.70	0.159	5
L	2	104.20	87.90	0.000	1
L	2	102.20	87.60	0.000	1
L	2	101.90	82.00	0.165	5
L	2	100.00	83.50	0.190	5
T	1.5	79.30	68.90	0.000	5
T	1.5	79.50	69.50	0.000	1
T	1.5	78.60	66.40	0.248	5
T	1.5	78.80	67.60	0.206	1
T	2	98.10	88.00	0.000	1
T	2	100.50	86.80	0.000	1
T	2	96.20	82.20	0.173	1
T	2	97.60	83.00	0.265	1

4.2.3.14 Shear Failure Type: 1 = Shear, 2 = Shear-Tension, 5 = Crushing

Blanking shear was performed using 4 in. x 4 in. panels and tested according to the Alcoa punch shear test. The blanking shear tests provide for shear values through the thickness of the sheet material (in the case of puncture). The blanking shear specimens were machined on one side to accommodate the test equipment (thickness ≤ 0.064 inches) and the test was performed on the non-machined surface. The tests were conducted for 2090-T62 and 8090-T62 aluminum-lithium materials and the results are shown in Table 52. The results did not reveal any significant differences between the shear strength of the Pre- and Post-SPF sheet for either 2090-T62 or 8090-T62 aluminum-lithium materials.

4.2.4 POST-SUPERPLASTIC FORMING HEAT TREATMENT OPTIMIZATION FOR 2090 AND 8090 ALUMINUM-LITHIUM

The Al-Li based alloys have been shown to offer highly desirable properties for the aerospace industry, particularly in the reduction of density and concurrent increase in the elastic modulus, leading to significant improvements in the specific modulus over the more conventional Al alloys. The development and application of these alloys, however, have been found to be

significantly challenged by a number of technological difficulties which have included the achievement of high strength with sufficient ductility for structural applications.

Table 52. Blanking Shear Properties of 2090 and 8090 Pre- and Post-Superplastic Formed Sheet Heat Treated to -T62.

Alloy Temper	Coupon I.D.	SPF Condition	Specimen Thickness	Shear Strength (ksi)	Shear Strength Ave. (ksi)
2090-T62	316-3-BS1	Pre-SPF	0.0615	31.3	31.10
"	316-2-BS2	Pre-SPF	0.0613	31.8	
"	316-2-BS3	Pre-SPF	0.0598	32.0	
"	316-2-BS4	Pre-SPF	0.0588	29.3	
"	324-BS1	Post-SPF	0.0584	31.4	
"	323-BS2	Post-SPF	0.0606	28.3	
"	323-BS3	Post-SPF	0.0571	32.1	31.22
"	323-BS4	Post-SPF	0.0578	33.1	
8090-T62	315-1-BS1	Pre-SPF	0.0599	31.3	33.40
"	315-2-BS2	Pre-SPF	0.0619	31.8	
"	315-2-BS3	Pre-SPF	0.0606	32.0	
"	315-2-BS4	Pre-SPF	0.0620	29.3	
"	357-BS1	Post-SPF	0.0618	31.4	
"	357-BS2	Post-SPF	0.0585	28.3	
"	357-BS3	Post-SPF	0.0581	32.1	32.50
"	357-BS4	Post-SPF	0.0613	33.1	

* Specimens were machined on one side only and tested with the machined surface face down.

Historically, thermomechanical processing of aluminum and aluminum-lithium alloys has been utilized to provide for a balance of strength and ductility for conventional product forms. However, with the advent of superplastic forming of aluminum and aluminum-lithium materials as a fabrication methodology for producing low cost net-shape structures, alternate thermal conditions had to be utilized to achieve peak strength for the material in its final form. Superplastic forming (SPF) does not lend itself to stretching a completed part before aging for attainment of maximum strength. SPF processing, by its nature, involves forming of complex shapes at temperatures well in excess of those used for aging or annealing of the alloys (structural complexity can be increased far beyond conventional forming methods with the use of the SPF process). The formed configuration must then be solution heat treated, water quenched, and aged in order to attain peak strength or a -T62 condition in the material prior to use.

A past effort was conducted on superplastically formed 8091 Al-Li structures in order to establish optimized thermal treatments after forming^{15,16}. Solution heat treatment (SHT) and artificial aging (AA) treatment parameters were established which met program goals, and were considered suitable for the processing of structures for aerospace applications. While the strength

levels produced were not as high as those obtained with pre-straining (a -T8 condition), they were nonetheless considered suitable for use in the application of the high specific stiffness alloy. The heat treatment resulting from this study involved solution treatment after forming, water quenching, and isothermally aging to peak strength.

Subsequent interest emerged in the potential for SPF processing 2090 and 8090 Al-Li alloys. The interest was based on material availability, production of superplastic sheet, and the desire to eliminate the solution heat treatment (SHT) of the formed part from the manufacturing process. The elimination of the SHT from the manufacturing process was anticipated to minimize part distortion, solute depletion, and processing steps after forming. The aim of the study was to develop a thermal processing procedure for the alloys whereby the part could be quenched directly from the forming process and artificially aged prior to trimming without a sacrifice to material properties. The parts would be formed, quenched, artificially aged and trimmed prior to use as a structural element on the Advanced Launch System (ALS).

4.2.4.1 Heat Treatment Optimization Test Matrix and Experimental Procedures

The optimization of the heat treatment for 2090 and 8090 examined the strengthening response of the material with different solution heat treatment temperatures, quench rates, and aging practices. The issue of out of tool quench was examined as a replacement for solution heat treatment-quench processing of the formed parts to minimize distortion, solute depletion, and reduce overall cost during fabrication of the SPF parts. The evaluation of the heat treatment parameters for the SPF-processed materials was conducted in two chronological stages: Stage 1 and Stage 2. An outline of the approach used in these stages is presented below and in Tables 53 and 54 for Stage 1 and Stage 2 respectively. The initial screening of solution treatment and aging temperature was conducted using hardness testing, and confirmation of eight selected heat treatment cycles was then conducted using tensile tests. The objective of Stage 2 was to further isolate and verify the best solution treatment and age (STA) process, and then study the effects of quench on the resulting properties of the most promising STA heat treatment.

Stage 1 (SPF Material, 8090 Alloy and for 2090 Alloy)

- 1) Characterization of the microstructure: Optical microscopy and Transmission Electron Microscopy (TEM). This work was done to predict the Post-SPF heat treatment response of the material and to determine the precipitation reactions that are facilitated during the heat treatment process.
- 2) Differential Thermal Analysis (DTA) of both alloys in order to establish the solvus and solidus temperatures.

- 3) Establish baseline hardness values : Solution heat treatment (established by DTA analysis) followed by a water quench (to maximize strengthening potential), and either a natural age (NA) for 4 to 6 weeks or an artificial age (AA) for up to 100 hours.
- 4) Evaluation of effects on hardness of different quench rates: Solution heat treatment (established by DTA analysis) followed by either a water quench (WQ), still or slow air cool (SAC), or a forced air cool (FAC), and finally artificially aged to peak hardness.
- 5) Evaluation of effects on hardness of different SHT Temperature: Three solution heat treatment temperatures (including the SPF temperature) will be evaluated at the optimum artificial age (established during item 3) for 3 to 100 hours of age.

Table 53. STAGE 1 Test Matrix for Unrecrystallized and Post-Formed 8090 and 2090 Aluminum-Lithium Alloys.

Differential Thermal Analysis (DTA): Establish solvus and solidus temperatures. Determine suitable SHT temperature range. Selection of T1, T2, and T3 below based upon DTA results.									
<u>Solution Heat Treatment Evaluation:</u>									
SHT:	T1			T2			T3		
QUENCH:	WQ SAC FAC			WQ SAC FAC			WQ SAC FAC		
Natural Age:	to 4 weeks			to 4 weeks			to 4 weeks		
Hardness Tests:	36			36			36		
Art. Age:	T1a	T2a	T3a	T1a	T2a	T3a	T1a	T2a	T3a
	2hr	2hr	2hr	2hr	2hr	2hr	2hr	2hr	2hr
	4hr	4hr	4hr	4hr	4hr	4hr	4hr	4hr	4hr
	8hr	8hr	8hr	8hr	8hr	8hr	8hr	8hr	8hr
	24hr	24hr	24hr	24hr	24hr	24hr	24hr	24hr	24hr
	48hr	48hr	48hr	48hr	48hr	48hr	48hr	48hr	48hr
	76hr	76hr	76hr	76hr	76hr	76hr	76hr	76hr	76hr
	100hr	100hr	100hr	100hr	100hr	100hr	100hr	100hr	100hr
Hardness Tests: After each thermal exposure and screen the hardness response for down-selection of the eight best cycles for tensile evaluation.									

A range of the optimized heat treatment parameters was evaluated for the 2090 and 8090 Al-Li alloys in both the as-received and superplastically formed (SPF) conditions. The heat treat response of the as-rolled material (unformed, fine-grain material) was first established in order to baseline the thermal processing response of the SPF alloy to elevated temperature straining. Identical solution treatment and aging parameters were imposed on the unformed and deformed

samples in order to ascertain their effectiveness on an unrecrystallized and on a dynamically recrystallized microstructure.

Hardness tests were initially utilized to determine those solution heat treatment (SHT) and aging parameters which would yield the highest values for the as-rolled materials. Selection of the thermal processing parameters for continuation of the study were based upon the initial results on the unrecrystallized material. Verification of the heat treatment hardness response was conducted with formed and thermally processed material. The final evaluation of the thermal processing response was performed through measurement of the resulting strength and ductility properties which were conducted with smooth sub-scale tensile testing.

Stage 2 (SPF Material, 8090 Alloy and for 2090 Alloy)

Optimization of the best post-formed heat treatment processes for each material and generation of tensile data for prediction of behavior after thermal processing of formed materials.

Table 54. STAGE 2 Test Matrix for Unrecrystallized and Post-Formed 8090 and 2090 Aluminum-Lithium Alloys.

<u>Solution Heat Treatment Evaluation:</u>			
SHT:	T1 (SPF)	T2 (545°C)	T3 (560°C)
QUENCH:	WQ	WQ	WQ
Artificial Age:	4 T, t combinations established in Stage 1		
Tensile Tests:	8	8	8
<u>Quench Rate Evaluation:</u>			
SHT:	T1	T1	T1
Quench:	Water	Forced Air Cool	Slow Air Cool
Artificial Age:	4 T, t combinations established in Stage 1		
Fundamentals: Optical, SEM, and TEM analysis to elucidate mechanisms. Specimens and parameters to be selected based on results of hardness and tensile tests.			
Recommend Heat Treatment Parameters: Heat treatment processing parameters will be identified as a result of all test data.			

4.2.4.1.1 Materials

The 2090 and 8090 Al-Li alloys utilized in this study were produced by Alcoa and British Alcan respectively. The alloys were specifically processed for superplastic forming at the mill. The approximate chemistry (in weight percent) of the alloys are as follows:

Alloy	Li	Cu	Mg	Zr	Fe	Si	Al
8090	2.8	1.3	0.7	0.12	0.05	0.02	Bal.
2090	2.2	2.7	---	0.1	0.06	0.04	Bal

The unrecrystallized materials were utilized in 1ft² sheets and the superplastically formed materials were obtained from rectangular, box-shaped, flat-bottomed test pans that had been exposed to different cooling rates after superplastic forming (SPF). The SPF test pans were formed at 510°C (950°F) using a back pressure of 350 psi to prevent cavitation and were cooled by water quenching, static air cooling, and forced air cooling to provide for an evaluation of the quench rate effects on the age hardened properties. The formed and quenched materials were packed in dry ice and stored under refrigeration to prevent natural aging of the material prior to evaluation.

4.2.4.1.2 Heat Treatment Evaluation Solution Heat Treatment

Initially, differential scanning calorimetry analysis was conducted using a Perkin-Elmer Delta Series differential scanning calorimeter (DSC) on both as-received materials to obtain information of suitable temperature range for solution treatment without encountering incipient melting. All DSC analysis was conducted using a scanning rate of 5°C (9°F) per minute. The DSC measurements were made to assist in identifying the potential range of temperatures suitable for solution treatment, especially the temperature at which incipient melting would be expected. Subsequently, solution heat treatment of both alloy samples were performed at four selected temperatures (510°C (950°F), 530°C (986°F), 545°C (1013°F), and 560°C (1040°F)) in order to determine the optimum hardening response at a specific SHT temperature. All solution treating was conducted in air using a Marshall cylindrical tube furnace with temperature control maintained to within $\pm 2^\circ\text{C}$ (3.6°F).

Since the SPF forming temperature for 2090 and 8090 (510°C (950°F)) was selected as a solution heat treatment during the study, SPF parts were quenched directly from the forming

operation and evaluated without any subsequent solution heat treatment process. The form and quench procedure was considered to be of particular interest to the program since it would potentially eliminate a post-formed solution heat treatment and quench from the manufacturing process, which would translate itself into cost savings from both re-work due to distortion and through savings from number of processing steps after forming. The reported low quench sensitivity of the 8090 alloy in particular was instrumental in stimulating this approach and it seemed worthwhile to assess the response of the 2090 alloy to the same process.

Natural and Artificial Aging

After the solution heat treatment, natural and artificial aging studies were conducted on both alloys under unformed and deformed conditions. The strengthening kinetics of the alloys during different artificial aging were monitored using Rockwell Superficial Hardness tests (30T scale). Hardness testing was also conducted on the naturally aged samples. Initially the artificial aging temperatures used for the study were 120°C (248°F), 150°C (302°F), 180°C (356°F), and 210°C (410°F) in order to maximize the data obtained through the analysis, however, subsequent evaluations included 165°C (329°F), and 195°C (383°F) in order to better determine the optimum aging temperature. The samples were exposed to the aging temperatures for various times with hardness measurements taken periodically. The artificial aging time was limited to 100 hours for practical manufacturing reasons, with the intent to identify a suitable aging process for times under 48 hours. All isothermal artificial aging treatments were conducted in air using the same Marshall cylindrical tube furnace as was utilized for the solution heat treatment evaluation.

Effect of the Cooling Rate After SHT and SPF

For the as-received materials, the effect of the cooling rate on mechanical properties after various SHT temperatures was examined. Hardness tests were conducted following artificial aging at 150°C (302°F) and 180°C (356°F). A computer controlled Nicolet 4094A digital oscilloscope was utilized to measure the cooling rate. For both air cooling and slow air cooling tests, a hole was drilled in the specimens for inserting a thermocouple. For the slow cooling rate, two pieces of Al sheet of 1mm thickness were wrapped around the test specimens and the specimens were then air cooled.

For the SPF materials, the effect of the cooling rate on mechanical properties after superplastic forming was also addressed. After the pans were superplastically formed, they were

cooled in air using a fan for fast air cooling, room air cooled for the slow air cooling study, and water quenched. As soon as the pans were cooled to ambient temperature, they were stored in a freezer to prevent natural aging prior to any direct artificial aging. Initial evaluation was conducted by hardness testing, and final assessment of selected heat treatment parameters was conducted by tensile testing.

4.2.4.1.3 Mechanical Property Testing Hardness Testing

Initially, the strengthening kinetics of both alloys in the as-received and SPF conditions during different thermal cycles were monitored entirely through Rockwell superficial hardness tests (30T scale) conducted according to ASTM standard E18. Each data point was determined as an average of at least 5 measurements of hardness. For the as-formed materials, in order to minimize the hardness scatter caused by uneven thickness or specimen warpage, a small base or anvil was utilized on the hardness tester. The surface of each specimens was ground to remove the oxidation and alloy depleted layer which could reflect different properties than the bulk. After the screening tests (combination of solution heat treatment and artificial aging) were completed, the optimum thermal cycles based on the hardness results were selected for ambient temperature tensile tests for both alloys in the as-received and SPF processed conditions.

Tensile Testing

All tensile specimens were machined to the ASTM standard B557 (sub-sized specimens, 1.25 inch gage length) and tensile testing was conducted on an Instron series 2150 servomechanical testing. Tensile specimens for the SPF-processed materials were oriented in both longitudinal (rolling) and transverse (90° to rolling) directions for determining the anisotropy of strength. A strain gage extensometer was employed to facilitate determination of the elastic modulus (E) and yield strength ($\sigma_{0.2}$). Additional quantities determined from these tests include the ultimate tensile strength (σ_{ult}) and percent elongation at failure. A Model 2 FAM X-Y recorder was utilized for recording the tests data. Due to the thickness variation of the tensile specimens for the as-SPF materials, three measurements of cross-sectional area on each specimen were made in order to accurately determine the yield and ultimate strength.

Tensile test specimens were tested in the as-formed surface condition (without any removal of the oxide layer), since it would be representative of SPF parts. It is recognized that there could be surface oxidation and some related alloy depletion. However, removal of such a surface

condition would require additional operations and costs, and the data developed without redressing the surface would represent results of the lower cost processing with maximum applicability to the program requirements.

4.2.4.1.4 Microstructure Evaluation

Optical, transmission and scanning electron microscopy were utilized to evaluate the microstructure corresponding to various thermal treatments.

Optical Metallography

Optical metallographic specimens were prepared using a cold mounting technique followed by electrochemical etching for 40 seconds in Barker's etch (7 ml HBF_4 and 200 ml H_2O) at 20mV to create an optical active anodized surface. The microstructures were examined under polarized light on an Olympus MG optical metallurgical microscope.

Transmission Electron Microscopy

Foils for transmission electron microscopy (TEM) were made using a Metal Thin Jet Thinner with 10% nitric acid in methanol solution cooled to -20°C (-4°F) by dry ice. A thinning duration of approximately 1 minute was utilized with a current of 60mA and a voltage of 16 V. TEM observations were conducted using a Hitachi H-600 microscope with an accelerating voltage of 100 KeV adjusted for bright field imaging. Additional TEM work was performed on a Phillips CM-30 operated at 300 KeV for weak field imaging (for structures at precipitate interfaces including dislocations), bright field and dark field imaging to aid in precipitate imaging.

Scanning Electron Microscopy

Samples for scanning electron microscopy were cut directly from the tensile test specimens. The fracture surfaces for different thermal conditions were examined to determine the fracture mode using a computerized JSM 6400 scanning electron microscope operating under 20KeV with a working distance of 39 mm. Back scatter electron scanning technique was utilized to examine the thickness of the depleted layer due to SPF processing.

4.2.4.2 Results for Unrecrystallized Materials

4.2.4.2.1 Microstructure

The unrecrystallized alloys (as-received or unformed SPF materials) were evaluated in order to obtain basic information on the alloy as it had been received and thermally processed. The post-formed microstructure would then be compared to the unrecrystallized material in order to determine what effect, if any, the difference in elevated temperature strain had on the microstructure after thermal processing. The microstructure of the as-received materials are shown in Figure 115a (optical) and Figure 115b (TEM). As can be seen from these figures, the material contains a relatively high defect density in the form of dislocation tangles and some cell structure. This condition is similar to that observed for most superplastic Al-Li alloys containing Zr.

4.2.4.2.2 Differential Scanning Calorimetry (DSC)

The results of DSC scans conducted on the unrecrystallized materials are shown in Figure 116 and 117 (for 2090 and 8090 alloys respectively). The heat flow (heat capacity) versus temperature curves in Figure 116 and 117 are interpreted in terms of endothermic peak (due to dissolution reaction) and exothermic dips (due to precipitation reactions) superimposed on the heat capacity of the aluminum rich solid solution, including previously formed precipitates. The DSC results are particularly useful in indicating suitable temperature range for solution heat treatment without encountering incipient melting. The critical temperatures found for the incipient melting were 575°C (1067°F) for 2090 alloy and 592°C (1097°F) for 8090 alloy.

The alloys appear to undergo some static recrystallization on solution treating at 510°C (950°F) and above, as can be seen in Figure 118. However, there is some evidence of residual banding, indicating that the static recrystallization did not develop a uniform distribution of equiaxed grains of high misorientation angle.

4.2.4.2.3 SHT + Natural Aging

Figure 119 shows hardness curves that illustrate the natural aging behavior of the as-received 8090 and 2090 Al-Li alloys following four different SHT temperatures. The SHT time was one hour followed by a cold water quench. It appears that initially, the as-quenched hardness of the 2090 alloy is higher than that of the 8090, presumably the result of greater solid solution hardening resulting from the greater alloy content. Subsequent natural aging resulted in hardness levels for the 8090 as high as, or higher than, those for the 2090 alloy. It also appears that there is about a 30 hour incubation period before the hardness begins to rise for the 8090 whereas

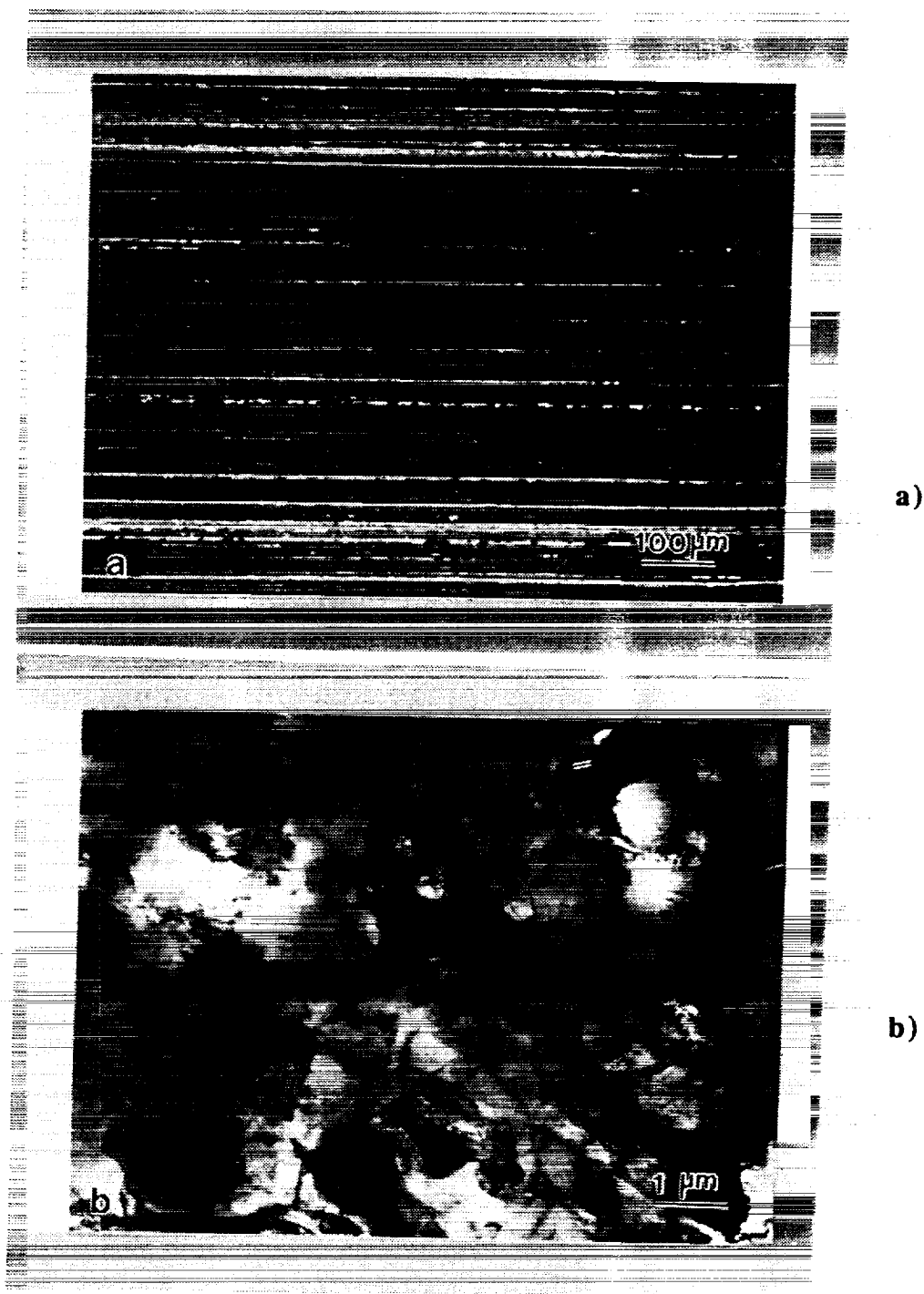


Figure 115. Microstructure of the as-received 2090 alloy: a. optical micrograph showing the unrecrystallized, heavily worked structure and b. TEM photograph showing the heavily dislocated structure. The microstructure of the 8090 alloy was similar to that shown above.

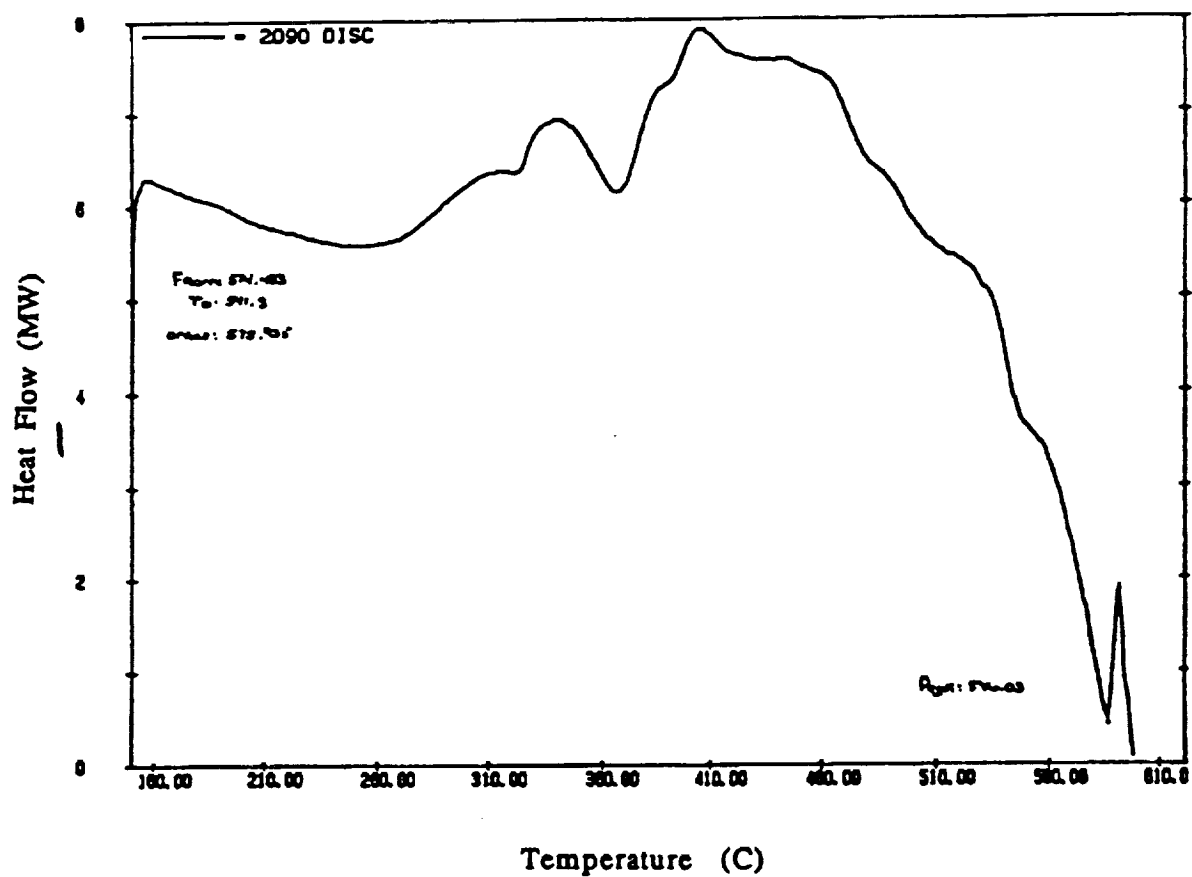


Figure 116. Results of the differential scanning calorimetry conducted on the as-received 2090 alloy. Results indicate a solidus temperature of approximately 586°C (1087°F).

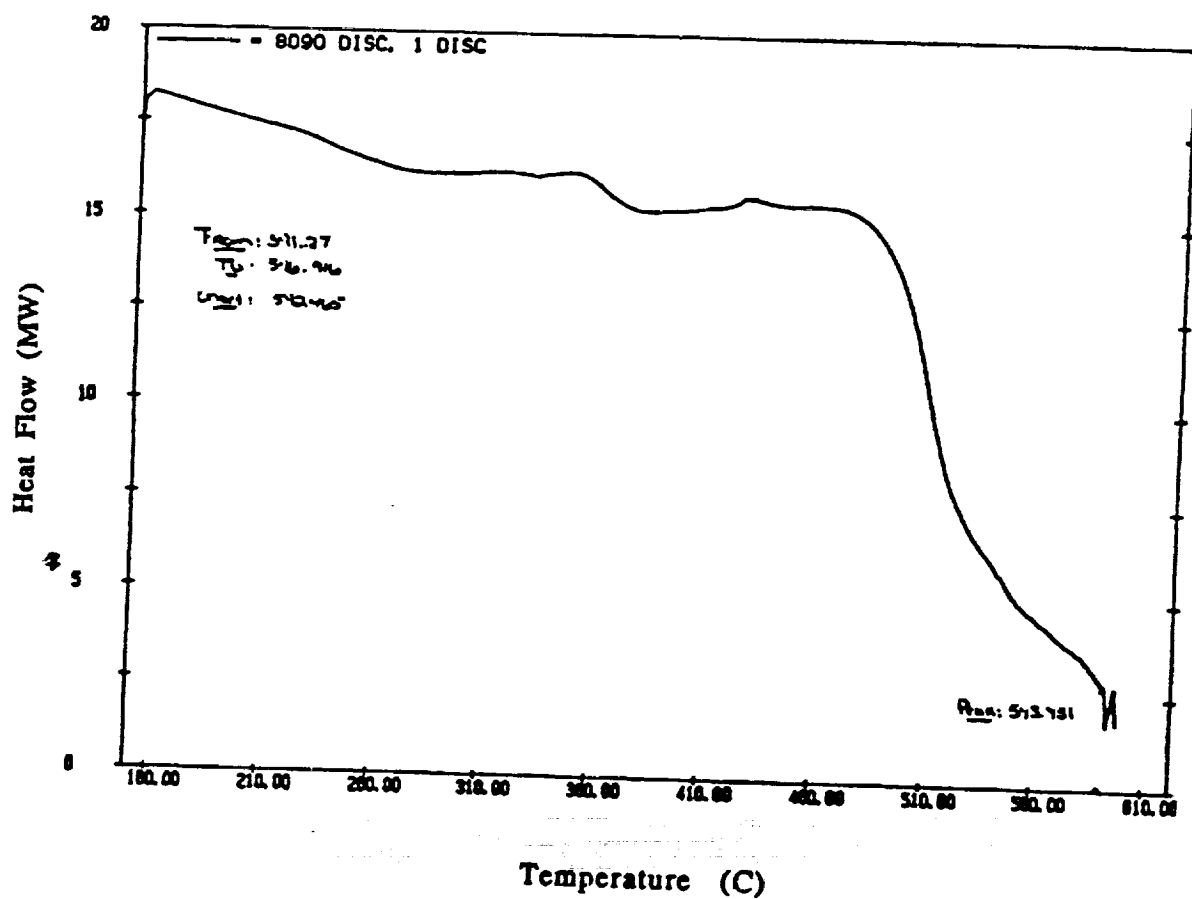
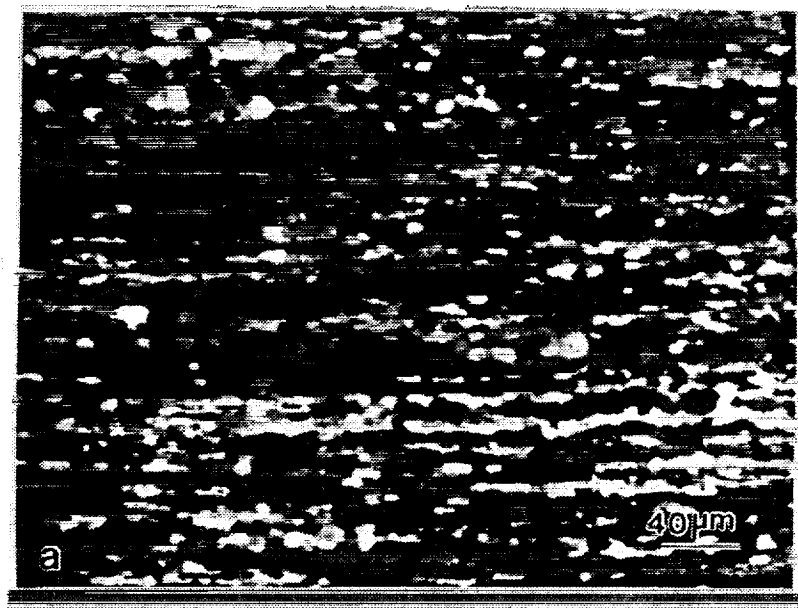
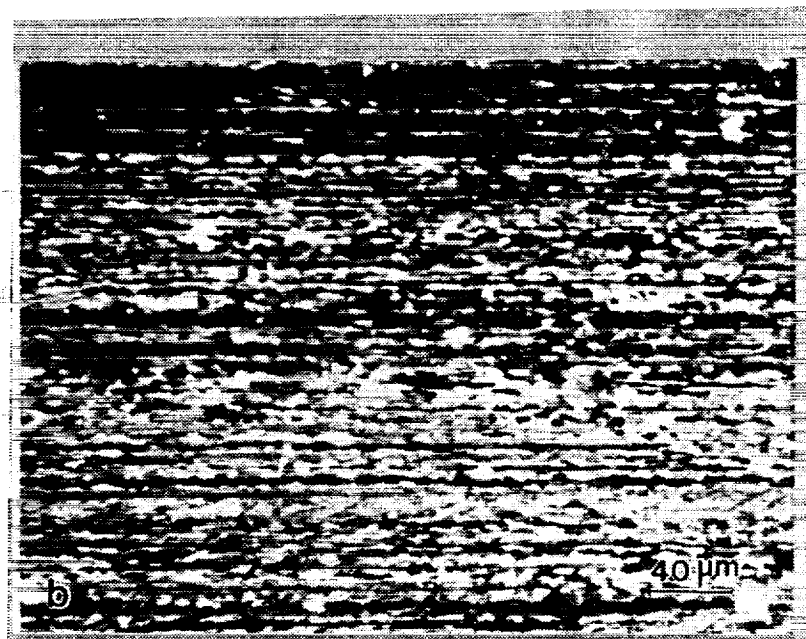


Figure 117. Results of the differential scanning calorimetry conducted on the as-received 8090 alloy. Results indicate a solidus temperature of approximately 593°C (1099°F).



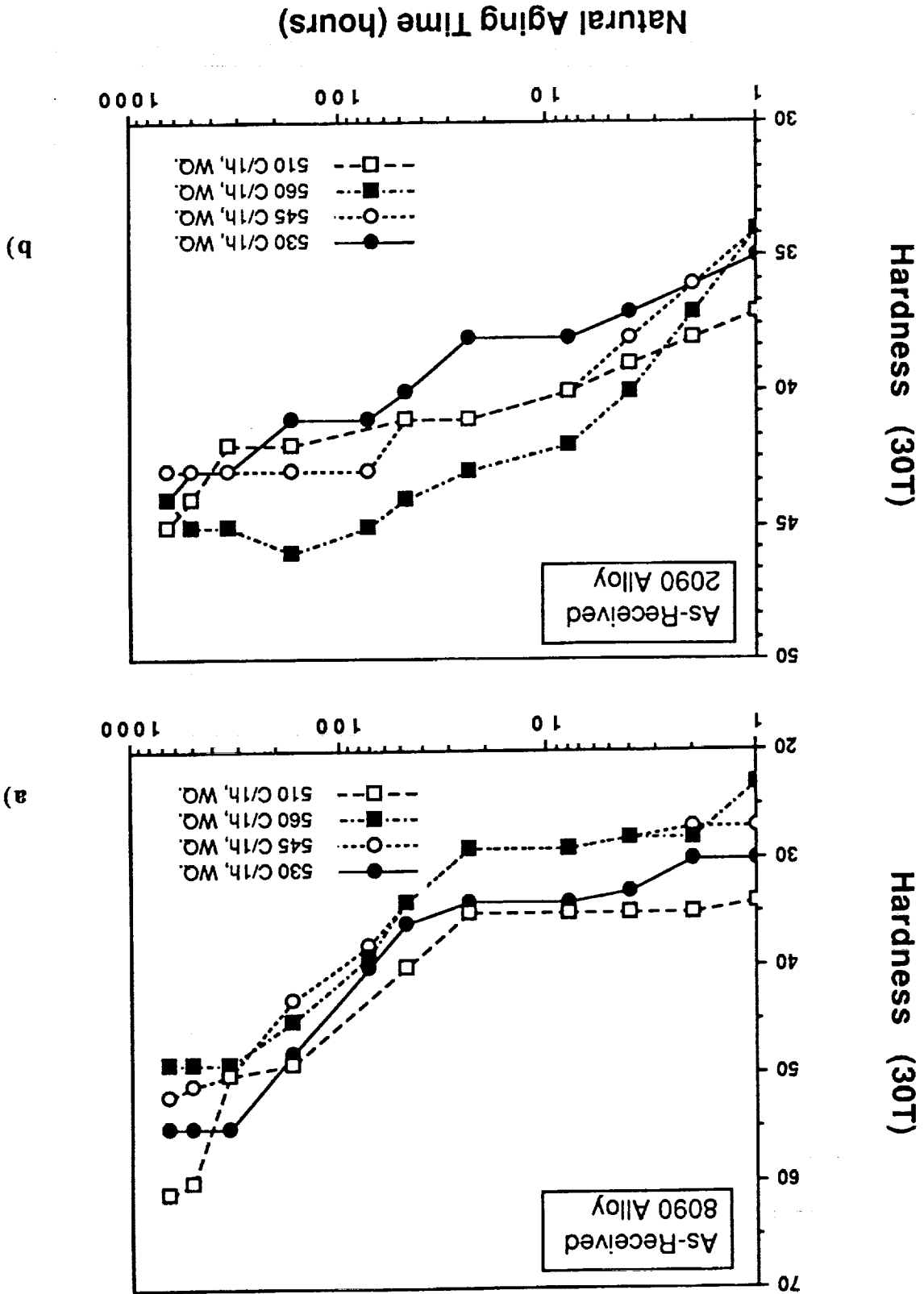
a)



b)

Figure 118. Optical micrographs of the a. 8090 alloy and b. 2090 alloy after solution heat treatment at 510°C (950°F) for 1 hour followed by a water quench. Banding is present, however, some recrystallization appears to have taken place.

Figure 119. Effect of natural aging on hardness of the as-received a. 8090, and b. 2090 alloys for various solution heat treatment temperatures.



hardness begins increasing quickly for the 2090 alloy. An interesting characteristic can be observed in these curves whereby the lowest SHT temperature, 510°C (950°F), resulted in hardness values at long times which were as high as, or higher than, those for other SHT temperatures. It would normally be expected that higher SHT temperature would tend to increase the amount of solute in solution and subsequently increase the hardness after precipitation had taken place.

4.2.4.2.4 SHT + Artificial Aging

The results of screening heat treatments for both alloys processed in the as-received condition are summarized in Figure 120. These heat treatments include four different solution heat treatment temperatures each with four different artificial aging temperatures. It appears that, for both alloys, the trend in hardness measurements during aging is for higher values at higher SHT temperatures, with the exception of SHT temperature at 510°C (950°F as-formed) and artificially aged at 150°C (302°F) and 180°C (356°F). It appears that there is a peak hardness at the 180°C (356°F) age for both alloys at all SHT temperatures used. Aging temperatures at or above 210°C (410°F) result in an over-aged condition for both alloys as shown by decreasing hardness.

The interesting characteristic which appeared in the SHT + natural aging study also appeared in the SHT + artificial aging study. This characteristic is the high age-hardened strength developed after solution treating at 510°C (950°F), which appear to be better than 530°C (986°F) or 545°C (1013°F) and competitive with the 560°C (1040°F) SHT temperature. The data developed suggests a peak in the age hardened strength of the alloys for a solution temperature around 510°C (950°F). A study was conducted to further explore the optimum solution heat treatment temperature in this range. A series of solution heat treatments followed by aging at 180°C (356°F) for 24 hours was conducted. Hardness results show that there is a peak around 510°C (950°F) for both alloys. Such a peak is unexpected since it would normally be thought that the higher temperature would place more solute in solution leading to a greater age hardening response. The peak hardening for aging at 180°C (356°F) was supported by subsequent tensile tests on the as-received alloys as shown in Figure 121.

4.2.4.2.5 Effect of Cooling Rate

The cooling rate measured for the various quenching techniques are shown in Figure 122. The average cooling rates from 510°C (950°F) to 100°C for the slow cooling, air cooling, and water quenching are approximately 0.4, 1.2, and 500°C per second respectively.

Figures 123, and 124-127 show the effect of the cooling rate on hardness after SHT at various temperatures and then aging at two peak aging temperatures. It appears that the 8090 alloy is less cooling rate sensitive than the 2090 alloy. However, the 8090 alloy does exhibit some quench rate sensitivity as the cooling rates are reduced, such as may be experienced with air cooling of thicker sheet alloy. It appears that the 8090 alloy may permit air cooling and aging directly to achieve good strength properties if the thickness of the parts is not too great. The 2090 alloy does appear to be more sensitive to the cooling rate, and it seems that this alloy will need to be solution treated after superplastic forming if maximum strength is to be achieved.

4.2.4.2.6 Tensile Test Results

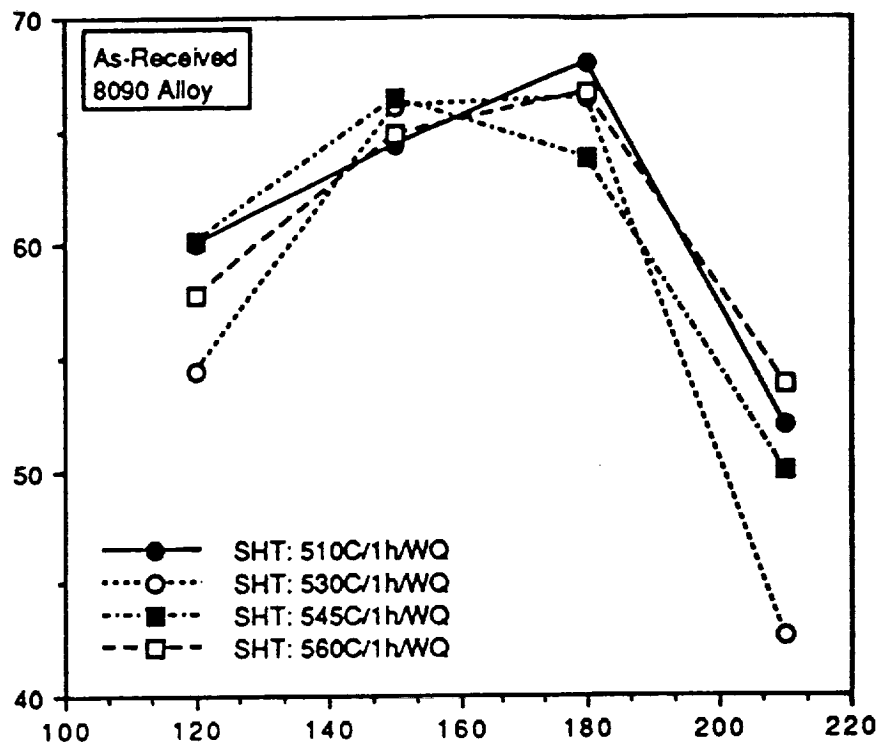
Tensile tests were conducted after the initial heat treatment screening process. The tensile specimens were processed using the best heat treatment cycles developed during screening of hardness data. The results of the tensile tests for a variety of heat treatment parameters are presented in Tables 55 and 56. The trend of the tensile data appears to be consistent with the hardness results reported previously. Particularly noteworthy are the 8090 alloy results for the solution treatment temperature of 510°C (950°F) which surprisingly results in strengths as good as or better than the higher temperatures. A similar response is seen for the 2090 alloy, but not quite so striking as for the 8090 alloy.

The effect of quench rate was also evaluated using the tensile tests. As can be seen from Tables 55 and 56, both alloys exhibit slight quench-rate sensitivity as indicated by the tensile properties. The loss in strength from air cooling is generally only 1 to 3 ksi as compared to the water quenched specimens.

4.2.4.3 Superplastic Formed Materials

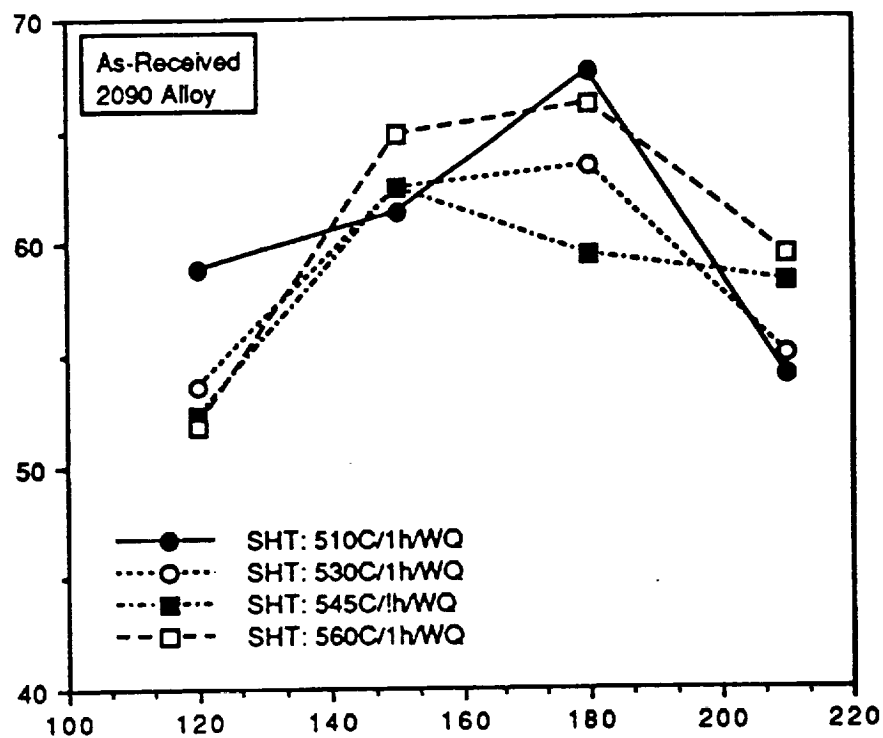
Based on results of the tests on the as-received alloys, the solution heat treatment temperatures selected for the SPF-processed materials were: 510°C (950°F the SPF temperature), 545°C (1013°F), and 560°C (1040°F). Correspondingly, the aging temperature selected were 150°C (302°F) and 180°C (356°F). For those materials to be solution heat treated at 510°C (950°F), it was assumed that the forming process provided the solution treatment, and the material was aged in the as-formed condition. For the other two solution treatments, the materials were re-solution heat treated after the forming process and then aged.

Hardness (30T)



a)

Hardness (30T)



b)

Artificial Aging Temperature (48 hours)

Figure 120. Effect of the aging temperature (48 hours) on the hardness for several solution heat treatment temperatures: a. 8090 alloy, and b. 2090 alloy.

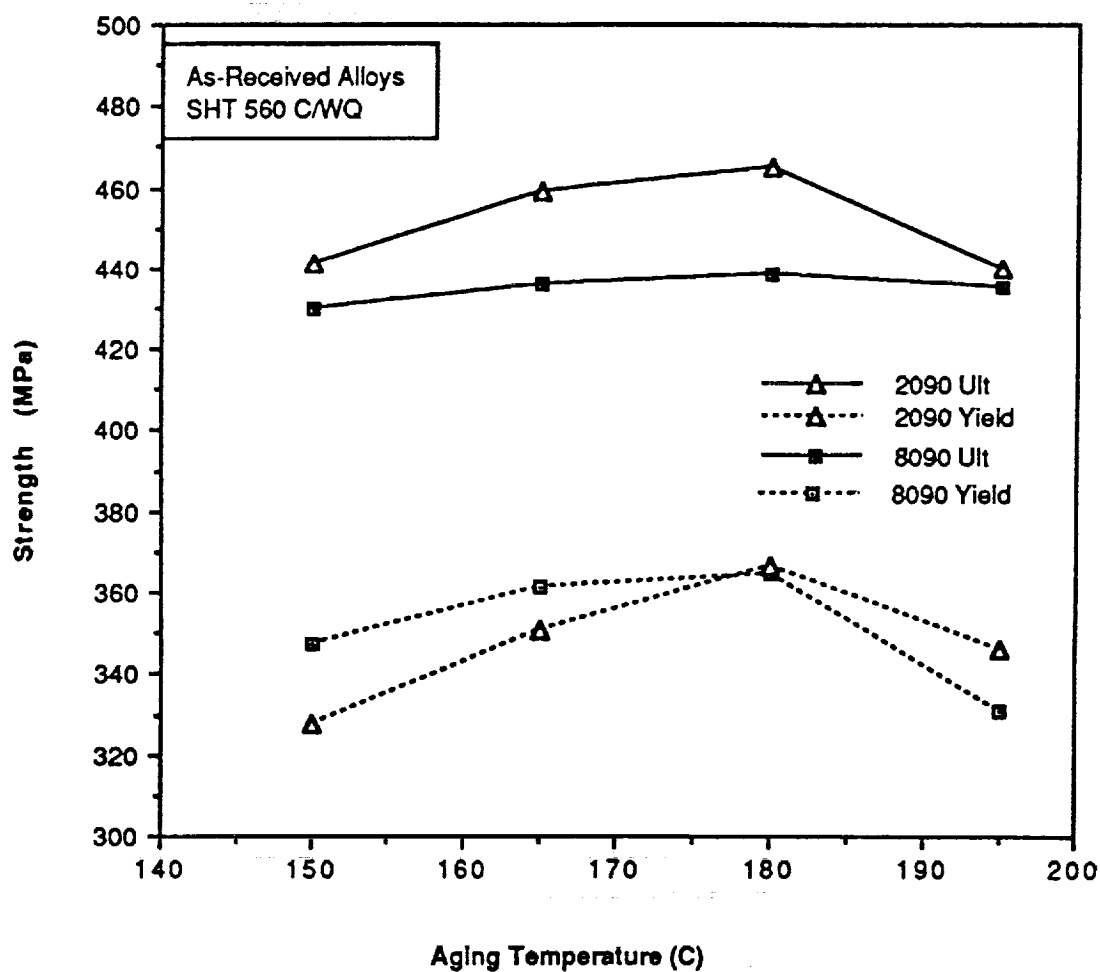


Figure 121. Effect of the aging temperature on the yield and ultimate strengths after solution treatment at 560°C (1040°F), water quenched, artificially aged for 48 hours.

As-Received 8090, 2090 Al. SHT: 510 C/1h.

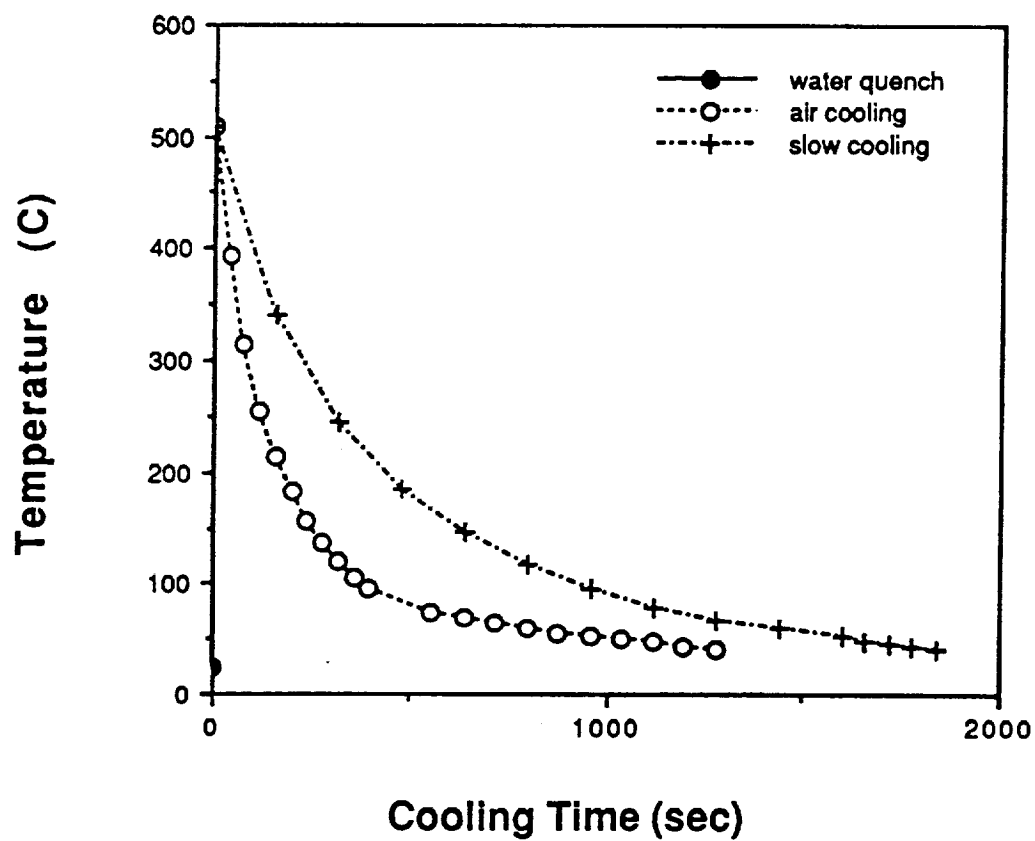


Figure 122. Cooling rate characteristics measured for the sheet alloys for water quenching, slow air cooling, and fast air cooling.

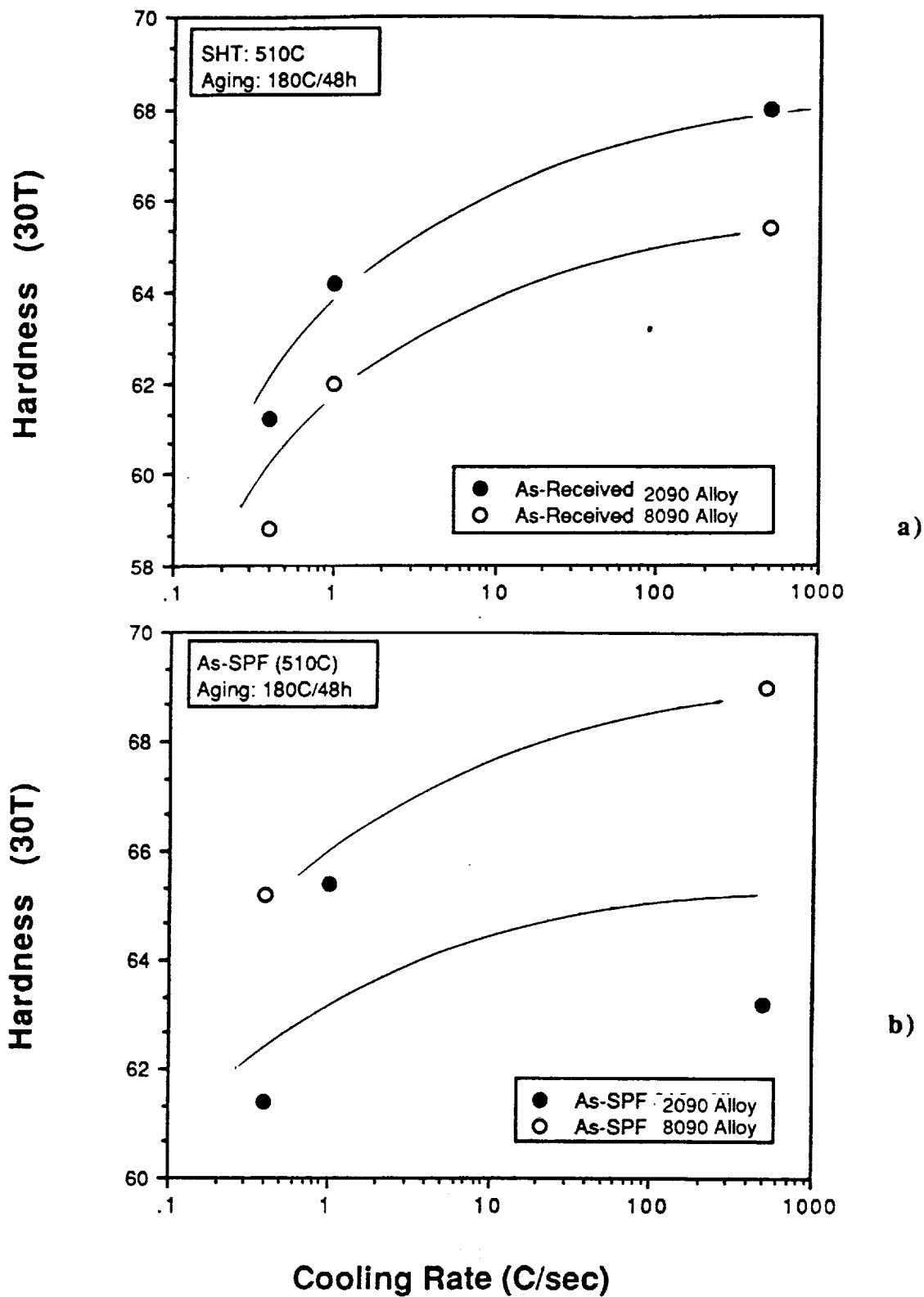
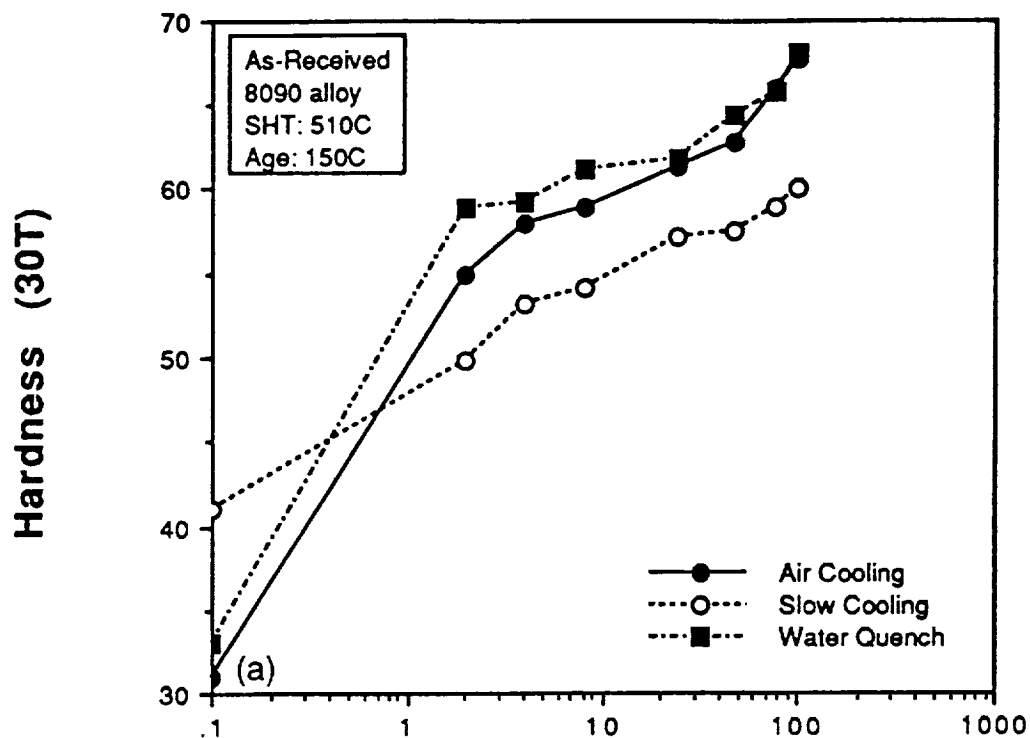
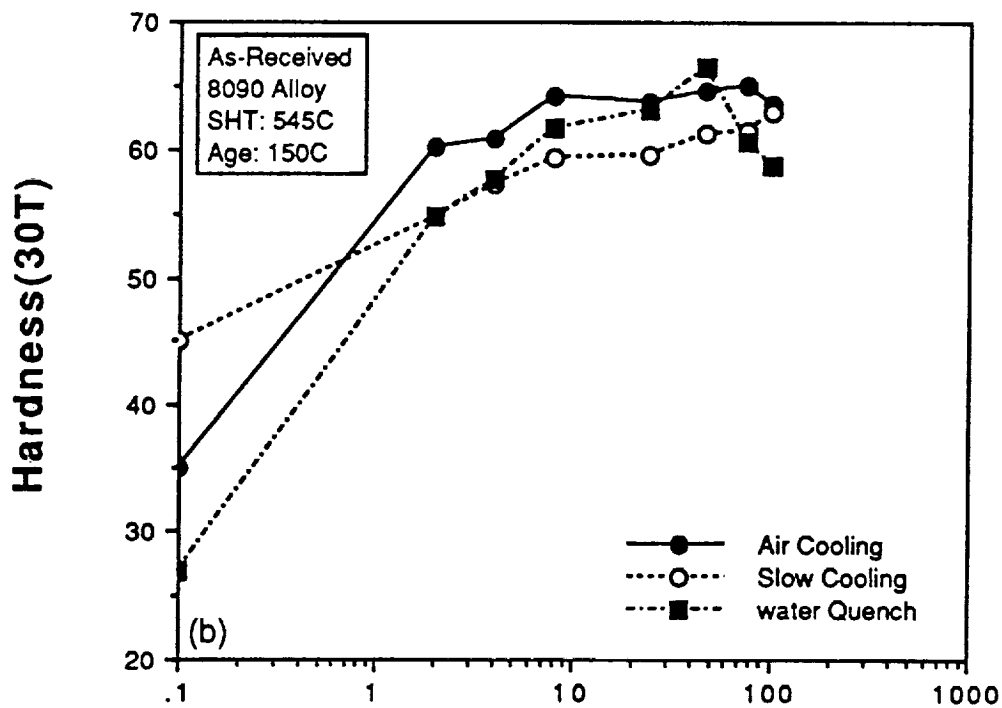


Figure 123. The effect of the cooling rate from 510°C (950°F) on the hardness of the 8090 and 2090 alloys after aging at 180°C (356°F) for 48 hours: a. as-received alloys, and b. as-SPF processed alloys.



a)



b)

Artificial Aging Time(hours)

Figure 124. Effect of cooling rate on the hardness developing with artificial aging time for as-received 8090 alloy, aged at: 150°C (302°F) after solution heat treatment at a. 510°C (950°F), b. 545°C (1013°F), and c. 560°C (1040°F).

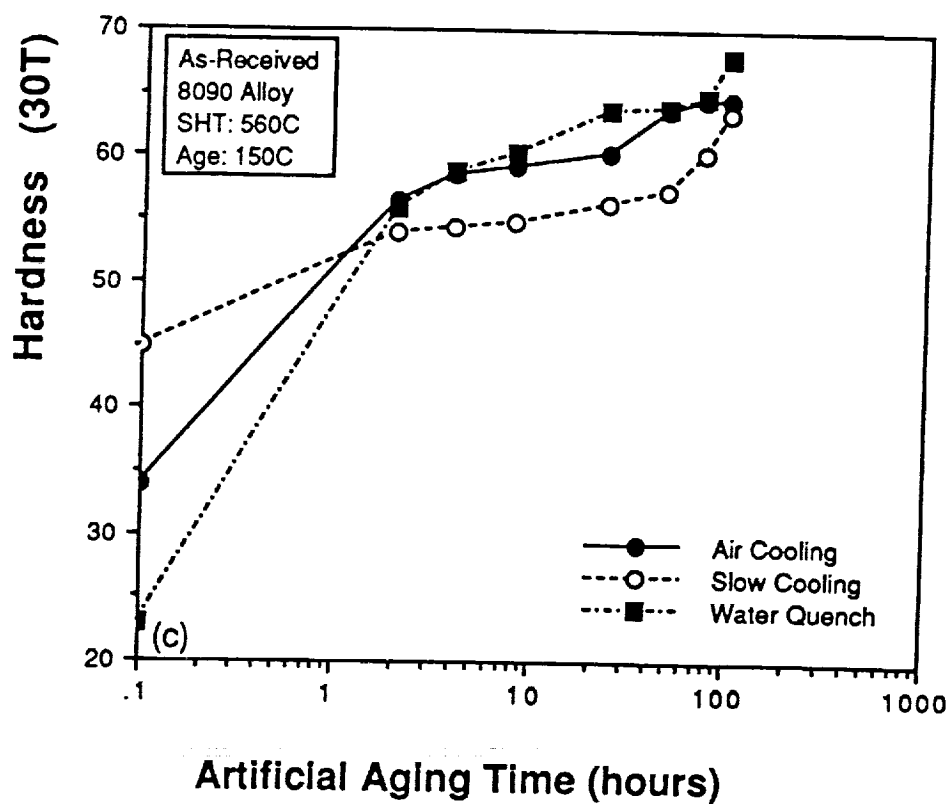


Figure 124 (continued). Effect of cooling rate on the hardness developing with artificial aging time for as-received 8090 alloy, aged at: 150°C (302°F) after solution heat treatment at a. 510°C (950°F), b. 545°C (1013°F), and c. 560°C (1040°F).

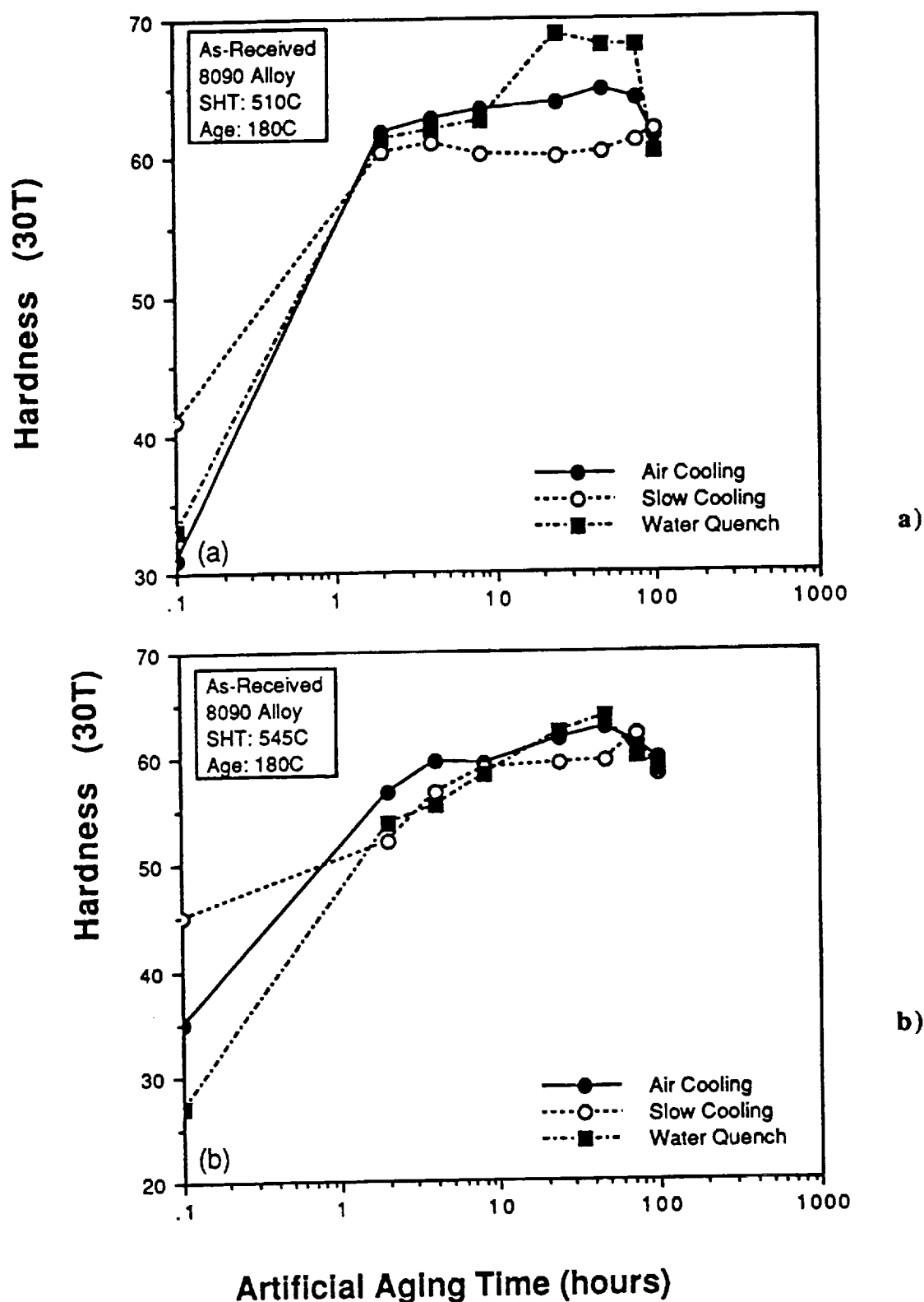


Figure 125. Effect of cooling rate on the hardness developing with artificial aging time for as-received 8090 alloy, aged at: 180°C (356°F) after solution heat treatment at a. 510°C (950°F), b. 545°C (1013°F), and c. 560°C (1040°F).

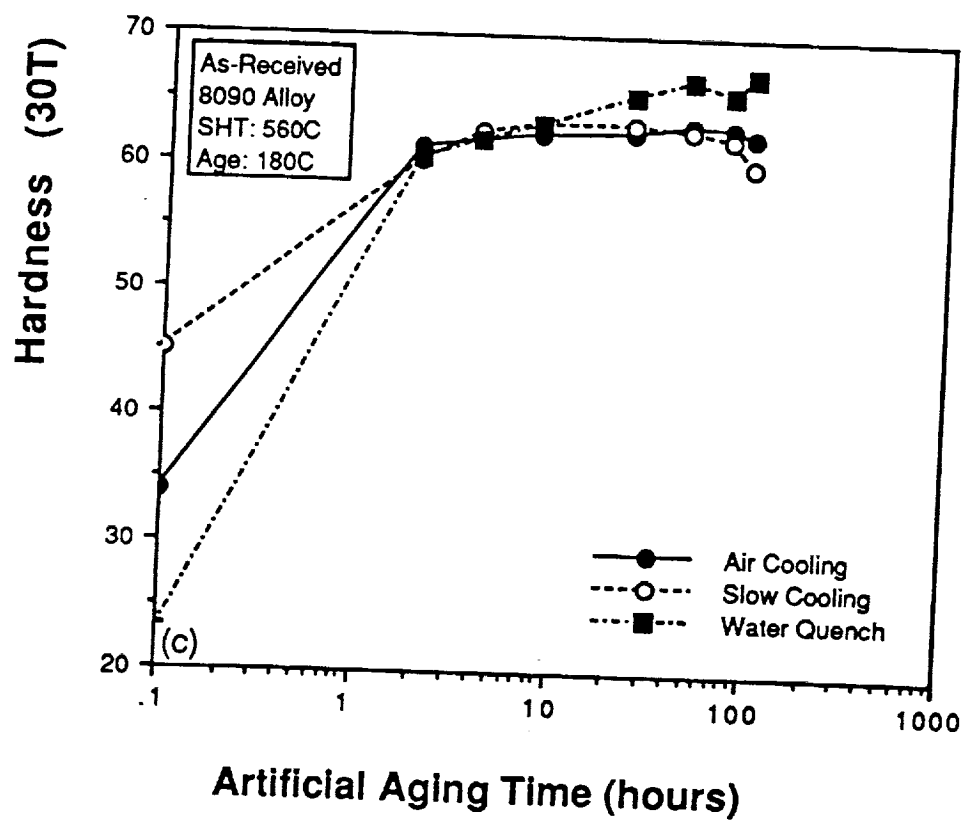


Figure 125 (continued). Effect of cooling rate on the hardness developing with artificial aging time for as-received 8090 alloy, aged at: 180°C (356°F) after solution heat treatment at a. 510°C (950°F), b. 545°C (1013°F), and c. 560°C (1040°F).

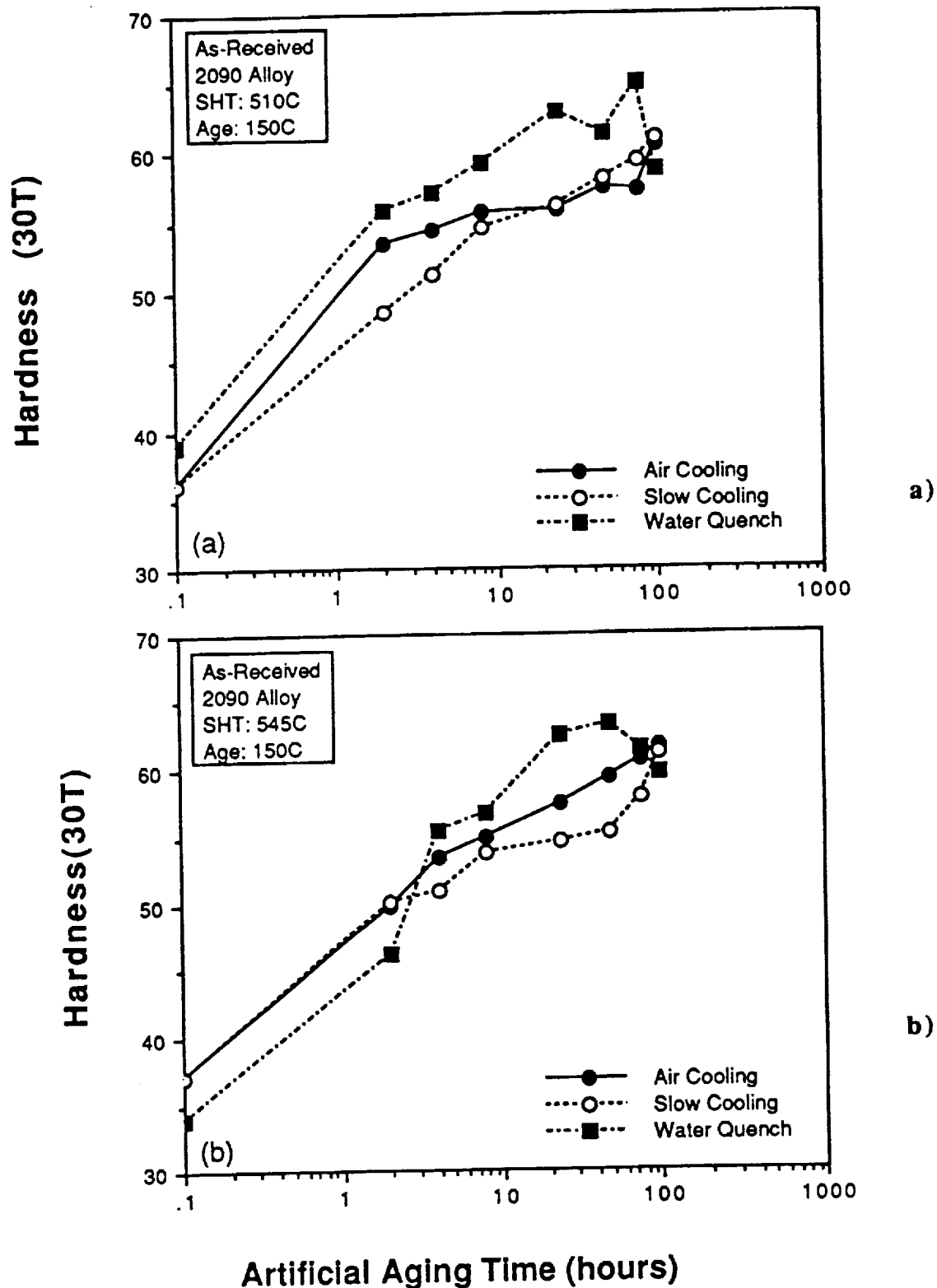


Figure 126. Effect of cooling rate on the hardness developing with artificial aging time for as-received 2090 alloy, aged at: 150°C (302°F) after solution heat treatment at a. 510°C (950°F), b. 545°C (1013°F), and c. 560°C (1040°F).

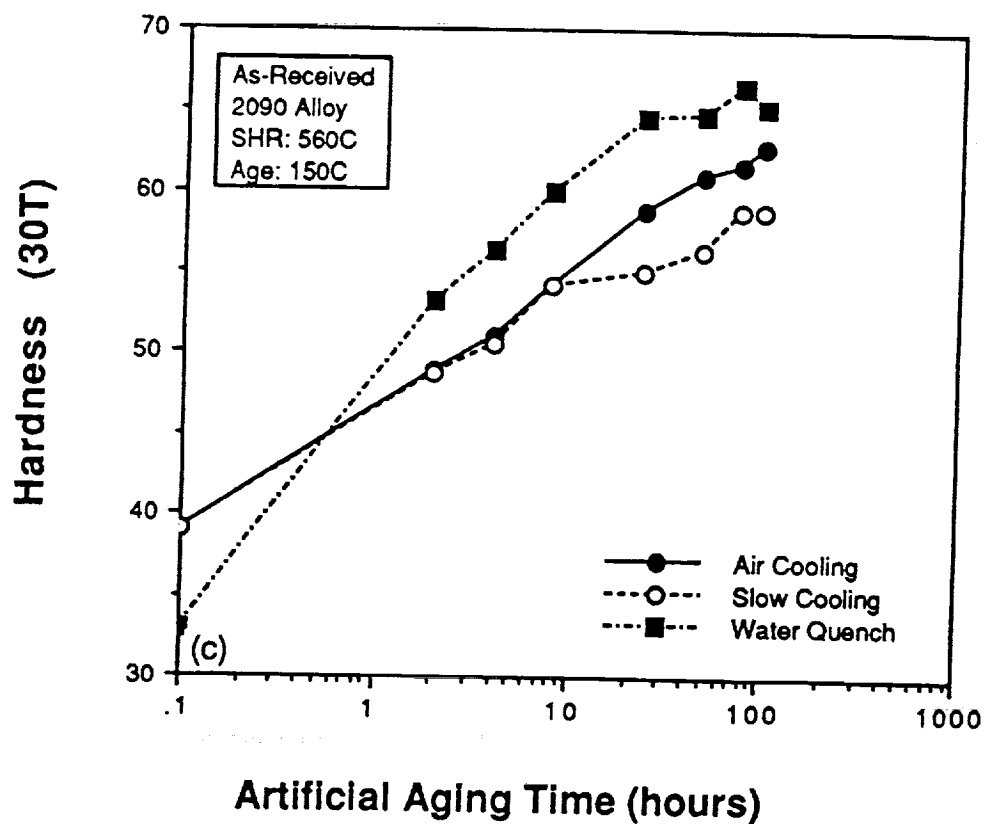


Figure 126 (continued). Effect of cooling rate on the hardness developing with artificial aging time for as-received 2090 alloy, aged at: 150°C (302°F) after solution heat treatment at a. 510°C (950°F), b. 545°C (1013°F), and c. 560°C (1040°F).

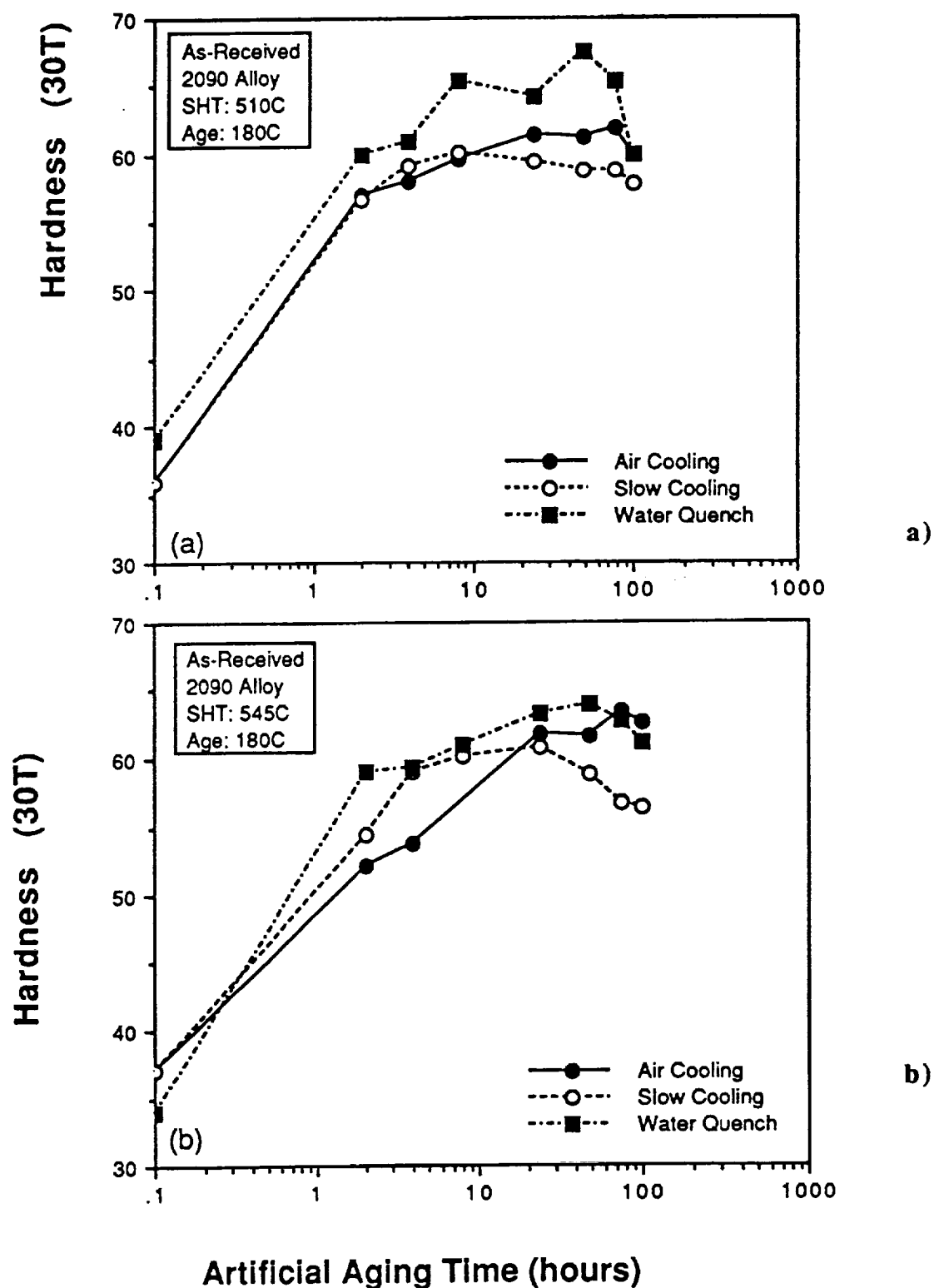


Figure 127. Effect of cooling rate on the hardness developing with artificial aging time for as-received 2090 alloy, aged at: 180°C (356°F) after solution heat treatment at a. 510°C (950°F), b. 545°C (1013°F), and c. 560°C (1040°F).

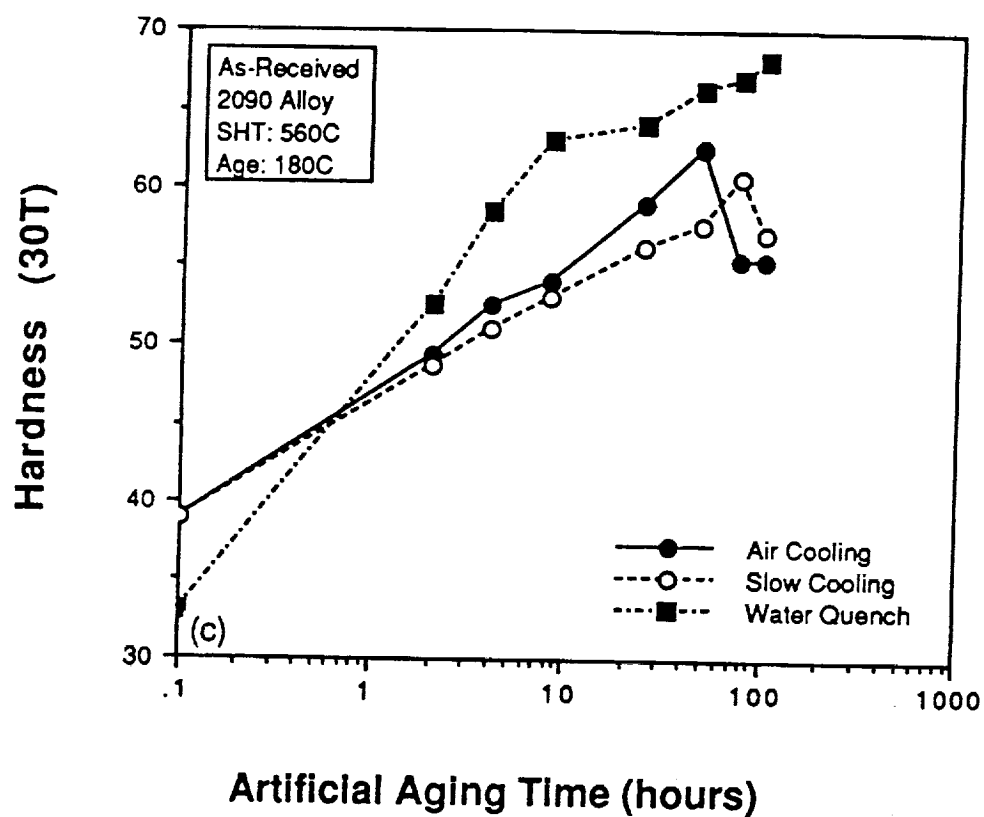


Figure 127 (continued). Effect of cooling rate on the hardness developing with artificial aging time for as-received 2090 alloy, aged at: 180°C (356°F) after solution heat treatment at a. 510°C (950°F), b. 545°C (1013°F), and c. 560°C (1040°F).

Table 55. Tensile Data for As-Received 2090 After Thermal Processing.

Sol'n Heat Treat. Temp. (°F/°C)	Quench Type	Artificial Age Temp. (°F/°C)	Artificial Age Time (Hours)	Fty		Ftu		Elong. (%)
				(ksi)	(MPa)	(ksi)	(MPa)	
950/510	W.Q.	356/180	48	54.7	377.2	69.4	478.5	6.9
950/510	W.Q.	356/180	48	55.6	383.4	69.4	478.5	7.7
1040/560	W.Q.	383/195	48	50.2	346.1	64.1	442.0	5.4
1040/560	W.Q.	383/195	48	50.2	346.1	64.0	440.0	8.4
1040/560	W.Q.	356/180	48	50.7	349.6	65.0	448.2	3.9
1040/560	W.Q.	356/180	48	55.6	383.4	69.9	482.0	3.1
1040/560	W.Q.	329/165	48	50.2	346.1	65.9	454.4	6.0
1040/560	W.Q.	329/165	48	51.5	355.1	67.2	463.3	5.0
1040/560	W.Q.	302/150	48	47.5	327.5	64.0	441.3	4.7
1040/560	W.Q.	302/150	48	---	---	63.0	434.4	---
1040/560	A.C.	302/150	48	48.0	331.0	64.5	444.7	4.3
1000/538	W.Q.	351/177	24	53.8	371.0	67.2	463.3	3.1
1000/538	W.Q.	351/177	24	53.3	367.5	67.2	463.3	4.8
1000/538	W.Q.	250/121	48	46.1	317.9	64.1	442.0	8.4
1000/538	W.Q.	250/121	48	46.1	317.9	64.1	442.0	8.1
1000/538	A.C.	250/121	48	43.0	296.5	61.4	423.4	7.6

Table 56. Tensile Data for As-Received 8090 After Thermal Processing

Sol'n Heat Treat. Temp. (°F/°C)	Quench Type	Artificial Age Temp. (°F/°C)	Artificial Age Time (Hours)	Fty		Ftu		Elong. (%)
				(ksi)	(MPa)	(ksi)	(MPa)	
950/510	W.Q.	356/180	24	56.0	386.1	70.0	482.7	5.2
950/510	W.Q.	356/180	24	56.0	386.1	70.0	482.7	5.4
950/510	W.Q.	356/180	48	57.6	397.2	68.8	474.4	2.8
950/510	W.Q.	356/180	48	56.8	391.6	70.4	485.4	5.3
950/510	W.Q.	302/150	48	58.4	402.7	68.4	471.6	2.2
950/510	A.C.	356/180	48	55.0	379.2	68.0	468.9	5.1
950/510	A.C.	356/180	48	54.0	372.3	69.2	477.1	7.3
950/510	A.C.	356/180	48	53.6	369.6	68.0	468.9	5.5
950/510	A.C.	302/150	48	54.4	375.1	66.4	457.8	2.2
950/510	A.C.	302/150	48	56.4	388.9	68.4	471.6	3.4
1040/560	W.Q.	383/195	48	48.0	331.0	63.2	435.4	8.0
1040/560	W.Q.	356/180	48	53.0	365.4	62.5	430.9	3.7
1040/560	W.Q.	356/180	48	52.8	364.1	64.8	446.8	4.5
1040/560	W.Q.	329/165	48	52.4	361.3	63.2	435.8	5.9
1040/560	W.Q.	329/165	48	52.4	361.3	63.2	435.8	4.1
1040/560	W.Q.	302/150	48	50.4	347.5	62.4	430.2	3.9
1040/560	A.C.	356/180	48	52.5	362.0	64.9	447.5	3.8
1040/560	A.C.	356/180	48	51.6	355.8	65.6	452.3	4.7
1040/560	A.C.	302/150	48	48.0	331.0	59.6	410.9	2.5
1040/560	A.C.	302/150	48	52.4	361.3	65.2	449.6	3.8

4.2.4.3.1 SHT + Natural Aging

Figure 128 shows the natural aging behavior of the 8090 and 2090 Al-Li alloys following in the as-SPF'd and quenched condition and in the post-formed, solution heat treated, and quenched conditions. It appears that natural aging hardness of 8090 in the as-SPF and quenched condition without solution heat treatment is higher than 2090 in all cases. For the 2090 samples that were solution heat treated and aged, the initial hardness was higher than samples of 8090, however, subsequent natural aging resulted in higher hardness levels for the 8090 samples than 2090. It was also noted that there is approximately a 30 hour incubation period before the natural aging results in a measurable hardness increase for 8090, whereas a hardness increase is measured very soon after solution heat treatment for the 2090 material. It is noted that for the as-SPF (at 510°C, 950°F) without solution heat treatment, higher hardness results when natural aging time was over two weeks.

4.2.4.3.2 SHT + Artificial Aging

The information obtained from as-received materials was used as baseline for the as-SPF materials. The peak aging parameters of 150°C (302°F) and 180°C (356°F) were utilized for the as-SPF materials. One group of specimens of the as-SPF alloys were directly aged at the above temperature without SHT while the other two groups of specimens were SHT'd at higher temperatures (higher than SPF temperature of 510°C (950°F)) for comparison. The screening heat treatment results are shown in Figures 129 and 130. It appears that for both alloys the hardness trends are the same as those of as-received materials. It also appears that the 180°C (356°F) aging gives higher strengths than 150°C (302°F) does. It is worth noting that the as-SPF alloys, when directly aged at peak temperature without solution treating, can result in high age-hardened strength, while the results of those solution treated and aged alloys show somewhat lower strengths.

4.2.4.3.3 Microstructure

The microstructure after SPF processing is fully recrystallized, with little evidence of banding as shown in Figures 131 and 132. The grain size is quite small, of the order of 2 to 5 microns as illustrated in Figures 133 and 134. These characteristics are consistent with the results of prior work in which it has been suggested that continuous dynamic recrystallization is the microstructural evolution mechanism operation during the initial stages of superplastic deformation^{17,18,19,20}.

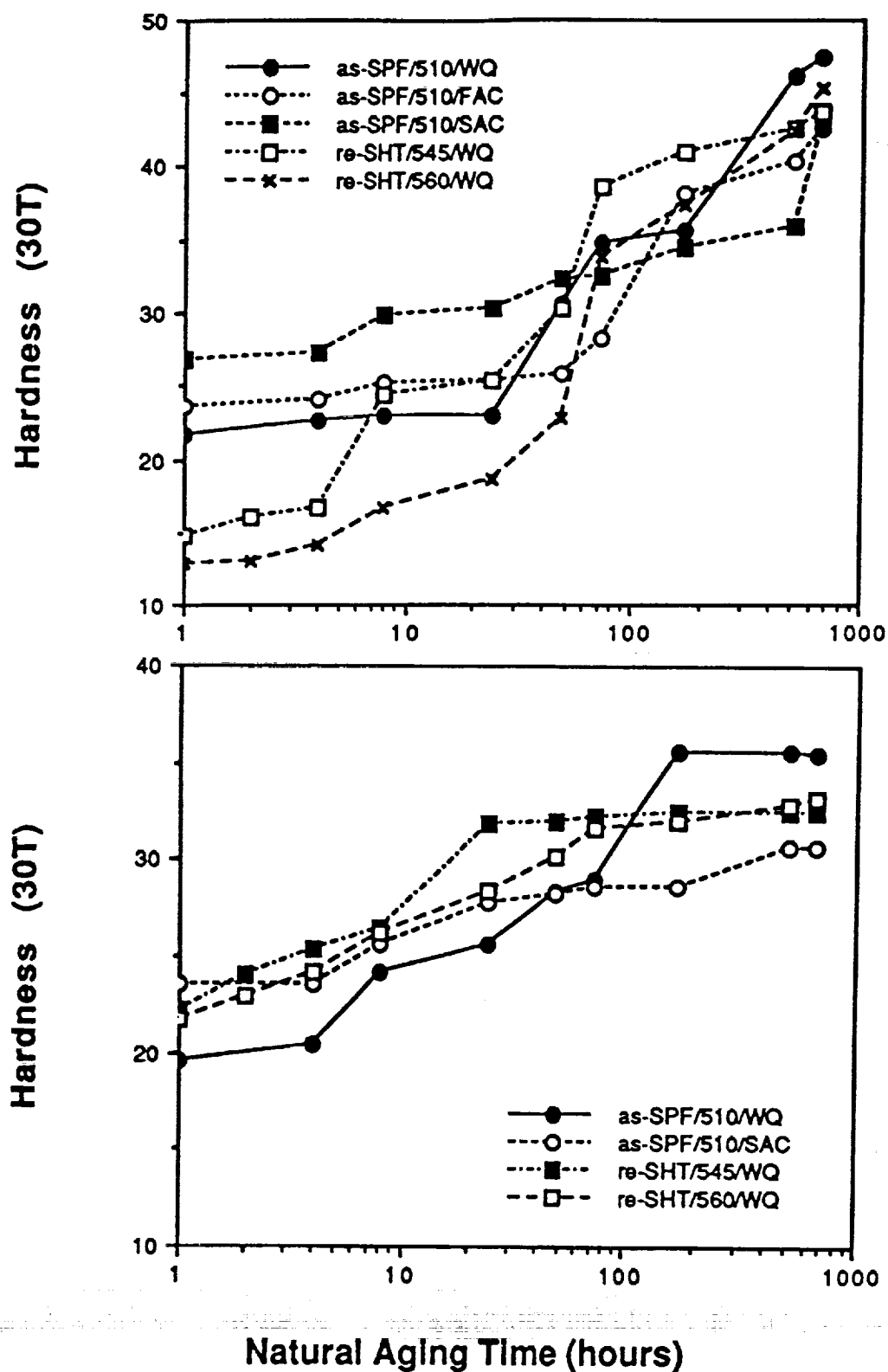


Figure 128 Effect of natural aging on hardness of the SPF-processed a. 8090, and b. 2090 alloys for various solution heat treatment temperatures and cooling rates as indicated on the graphs.

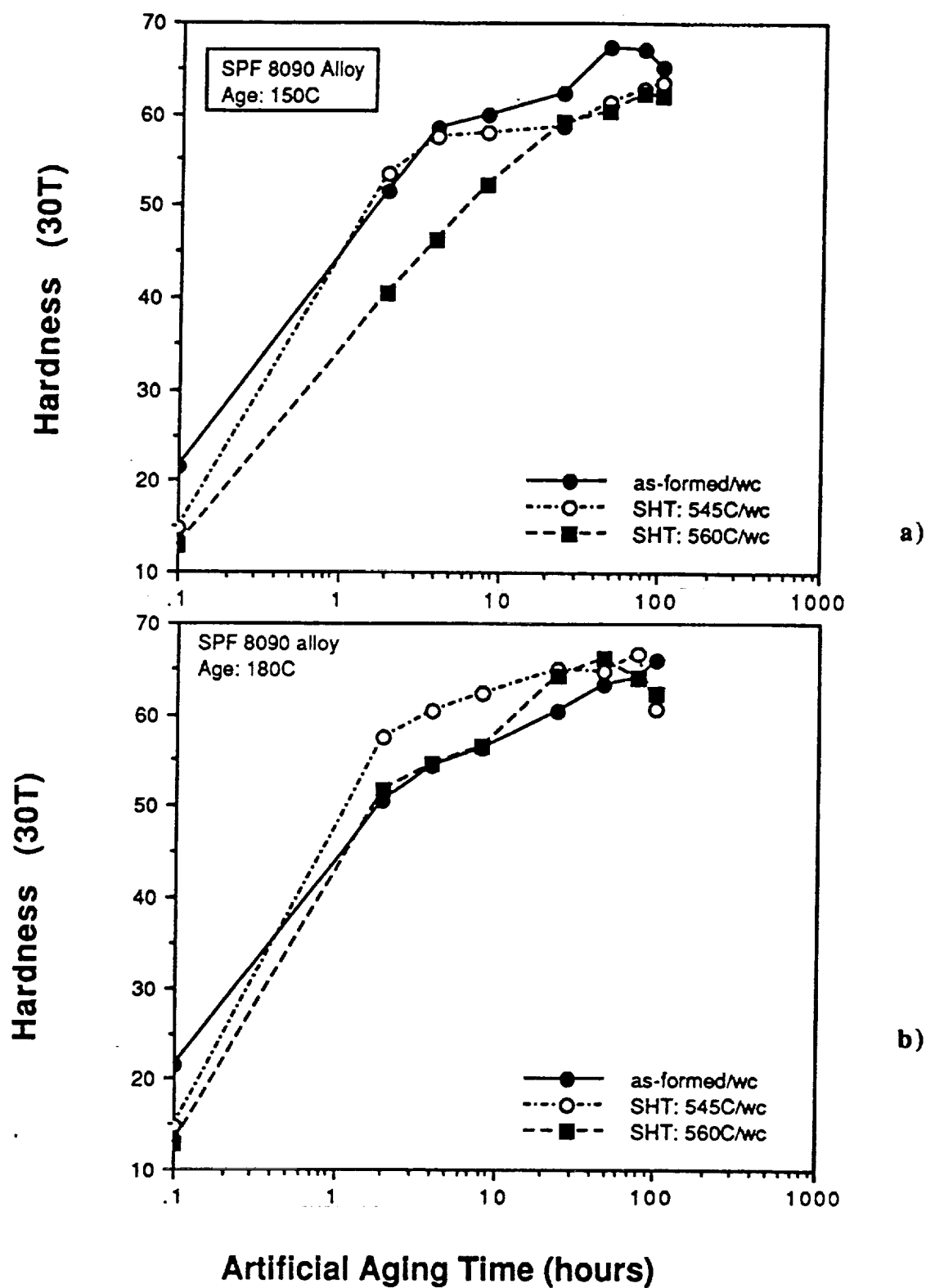


Figure 129. Age hardening characteristics of the SPF-processed 8090 alloy after direct water quenching from the forming temperature, and after re-solution treatment at 545°C (1013°F) and 560°C (1040°F) aged at a. 150°C (302°F), and b. 180°C (356°F).

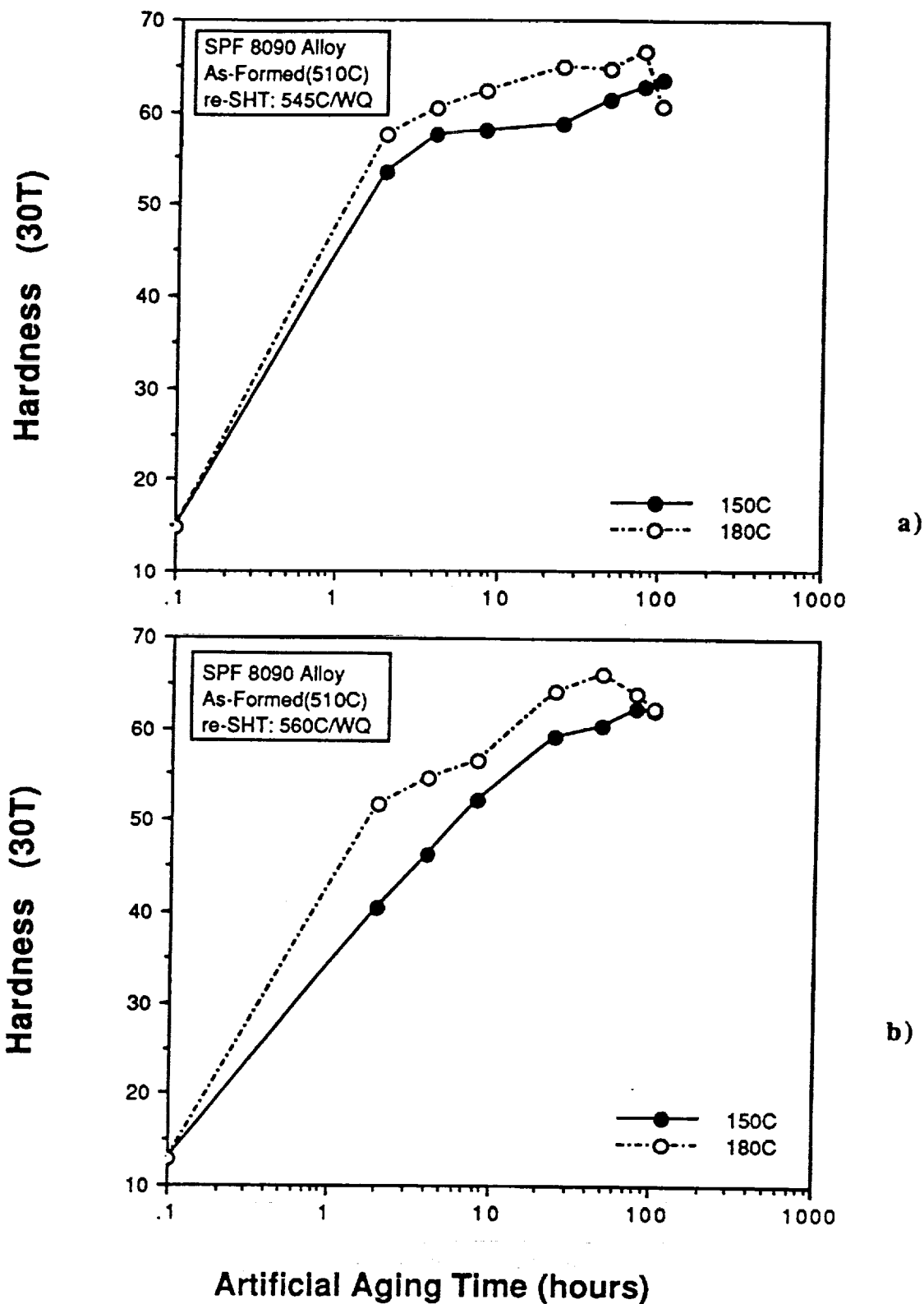
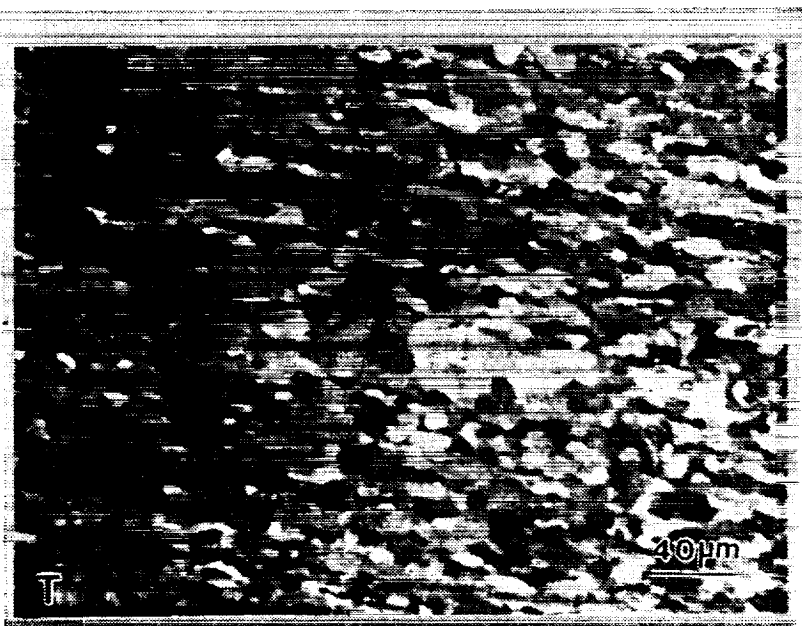


Figure 130. Age hardening characteristics of the SPF-processed 8090 alloy re-solution treated at a. 545°C (1013°F), and b. 560°C (1040°F) and artificially aged at 150°C (302°F) or 180°C (356°F).

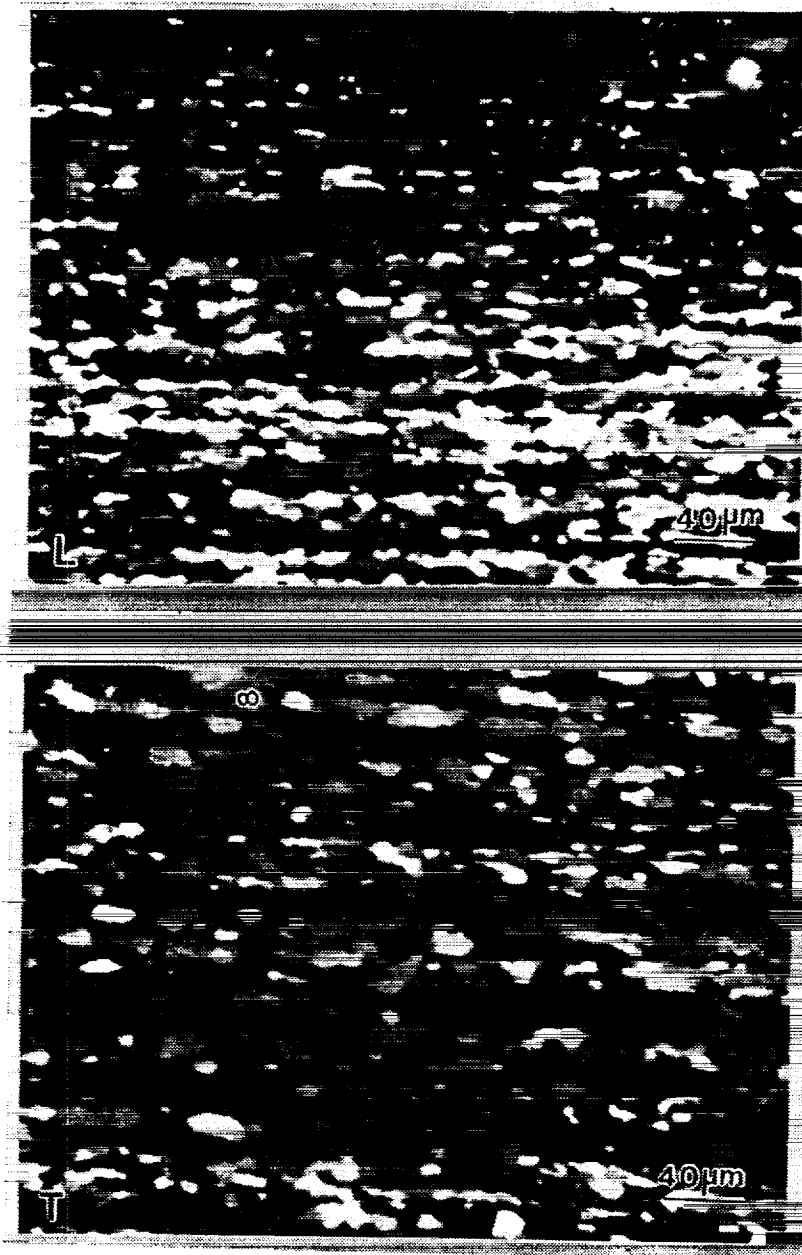


a)



b)

Figure 131. Optical micrographs of the 8090 alloy, as-SPF processed (510°C, 950°F followed by a water quench), a. longitudinal, and b. transverse views.



a)

b)

Figure 132. Optical micrographs of the 2090 alloy, as-SPF processed (510°C, 950°F followed by a water quench), a. longitudinal, and b. transverse views.



Figure 133. TEM photograph of the 8090 alloy after forming and aging: 510°C (950°F) followed by a water quench and artificially aged at 180°C (356°F) for 48 hours.



Figure 134. Electron micrographs of the 2090 alloy in the condition formed at 510°C (950°F) followed by a water quench and artificially aged at 180°C (356°F) for 24 hours. The microstructure appears to have fully recrystallized grains of approximately 1 to 2 microns. A somewhat non-uniform distribution of precipitates was observed.

Careful examination of the metallographic specimens revealed no clear evidence of cavitation. Apparently the superimposed hydrostatic pressure during the forming was effective in controlling the cavitation which would otherwise be clearly evident. The surface depleted layer, as determined by optical metallography and from examination using the back-scattered electron detector on the SEM, appears to be of the order of 0.05 mm thick. This is consistent with results reported by Partridge²¹.

The precipitation visible in Figures 133 to 135 is somewhat heterogeneous. There is evidence of precipitation-free zones (PFZ's), most clearly evident in Figure 135a. Since there is little dislocation structure within the grains, precipitation appears to nucleate on other available sites, such as the grain boundaries. However, within the grains, as can be seen in Figure 136, there appears to be an association of the precipitates with the small dark particles. While not specifically identified here, it is believed that they may be the β' Al_3Zr particles. The ability of the β' particles to act as nucleation sites for δ' , T_1 , and θ' has been suggested previously²².

4.2.4.3.4 Effect of Cooling Rate

Figure 137 and 138 (also 139-143) show the effect that cooling rate after SPF followed by artificial aging has on mechanical properties. It appears that the 8090 alloy exhibits some cooling rate sensitivity when aged at 150°C (302°F), but is cooling rate insensitive when aged at 180°C (356°F). While for the 2090 alloy the trend is reversed; i.e. at 150°C (302°F) age, it is rate insensitive, and at 180°C (356°F), it is rate sensitive. Since the peak age temperature for both as-SPF materials was determined to be 180°C (356°F), in this case, it appears that the 8090 alloy is quite rate insensitive while the 2090 alloy is somewhat more rate sensitive. These results are consistent with those of unrecrystallized materials.

For the 8090 alloy aged at 180°C (356°F), it appears that air cooled specimens may be aging more rapidly than the water quenched, and exhibit some indication of beginning to over-age at times of approximately 100 hours (Figure 136). However, for the practical aging time of 48 hours, fast air cooling appears to develop hardness levels which are quite comparable to that of the water quenched material.

For the 2090 alloy, (Figure 141-143), aged at 180°C (356°F), water quenching appears to be develop superior hardness values to those of slow air cooled materials.



Figure 135. Electron micrographs of the 2090 alloy in the condition formed at 510°C (950°F) followed by a water quench and artificial aging at 180°C (356°F) for 24 hours.

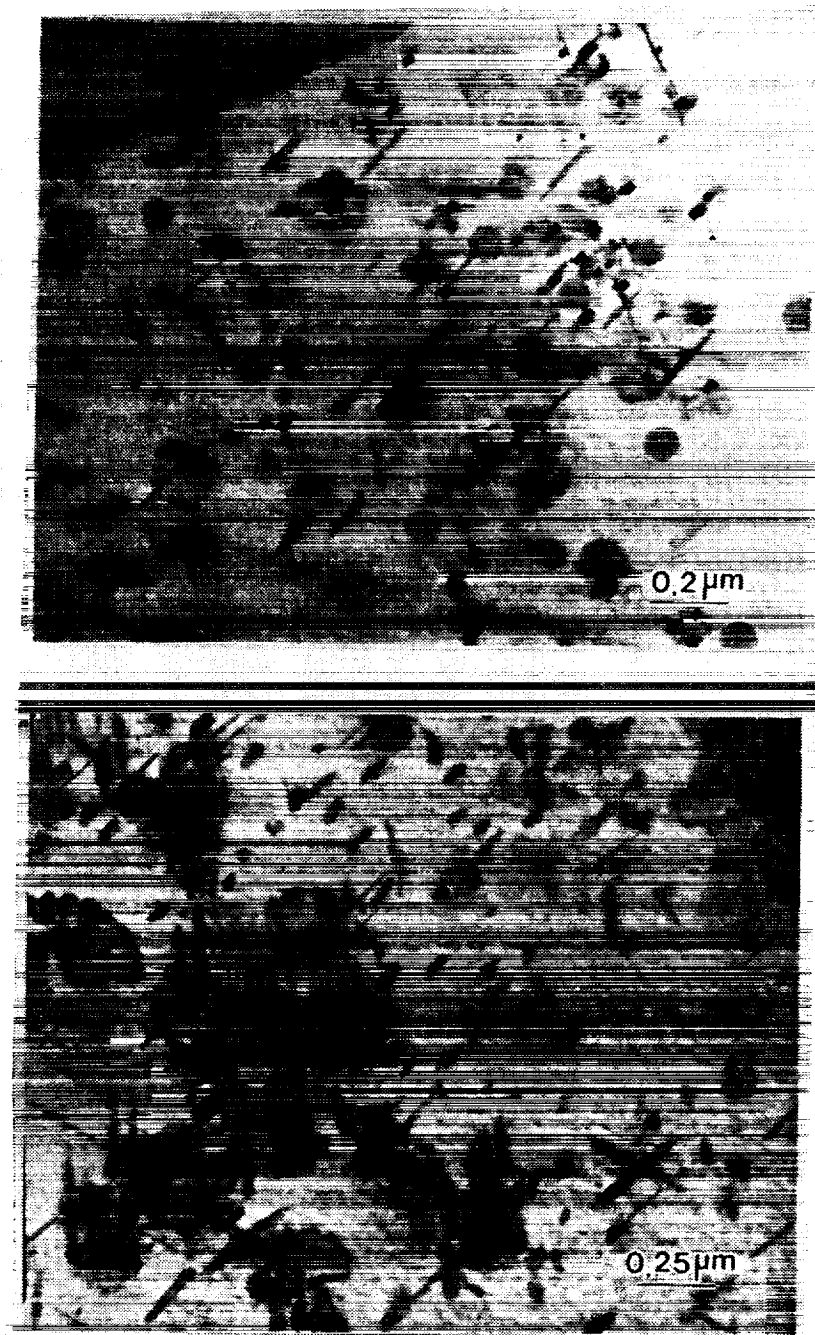
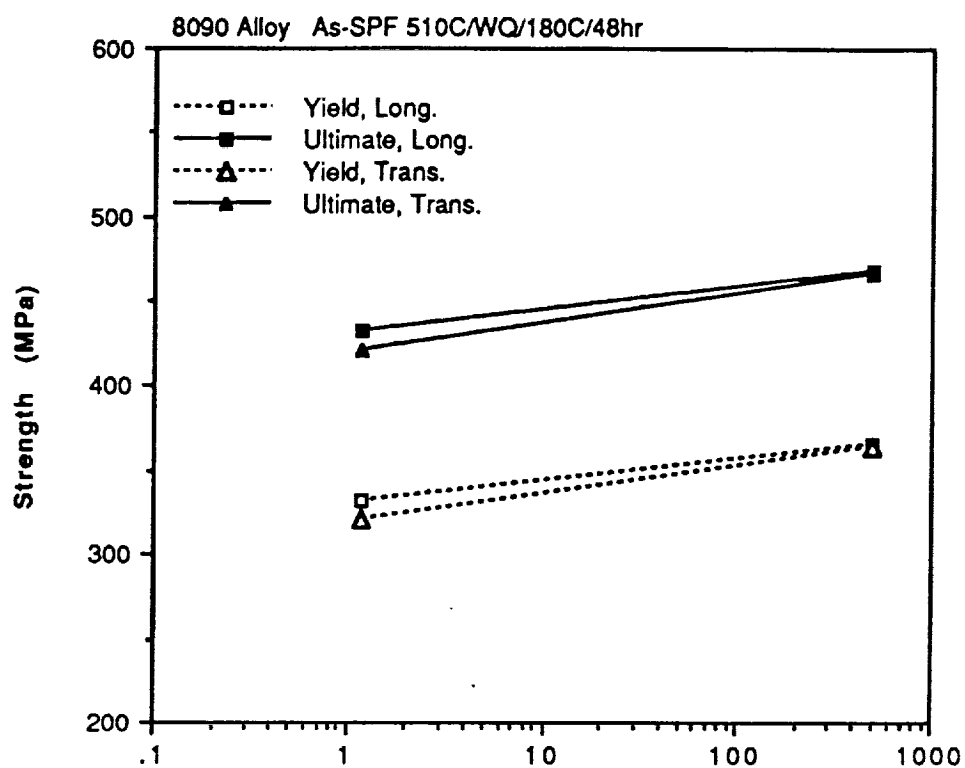
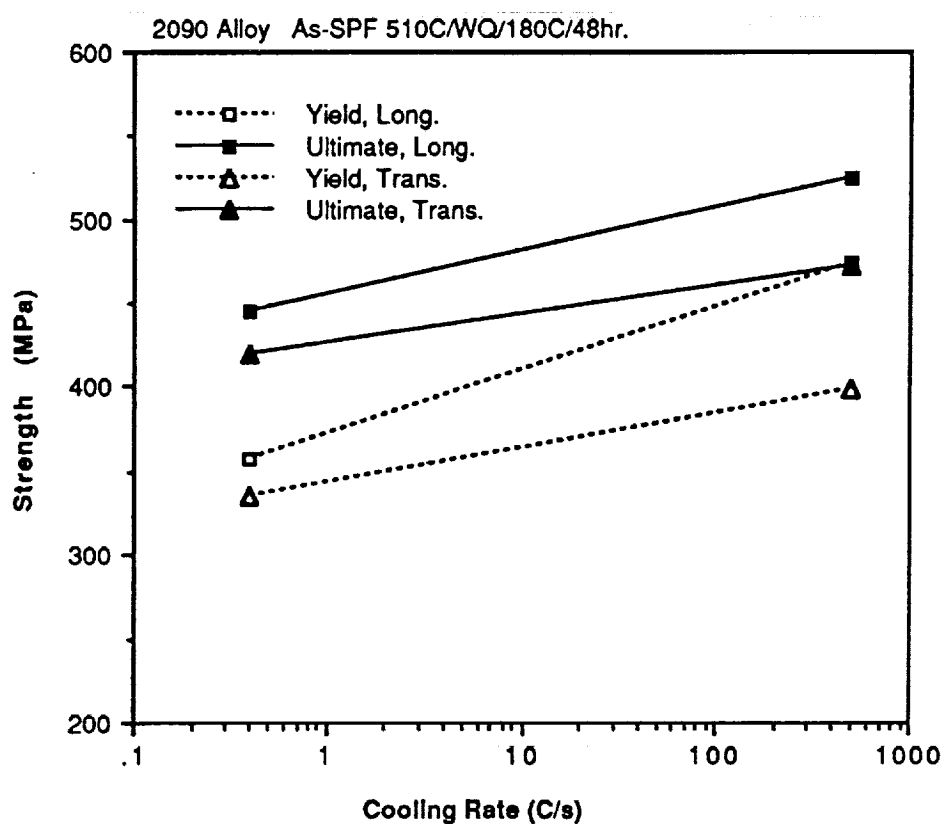


Figure 136. Electron micrographs of the 2090 alloy in the condition formed at 510°C (950°F) followed by a water quench and artificial aging at 180°C (356°F) for 24 hours. The microstructure consists of the δ' as the background "mottled" structure, with the larger T_1 platelets and larger spherical δ' .



a)



b)

Figure 137. Effect of cooling rate on the strength of as-formed, water quenched, and artificially age hardened a. 8090 and b. 2090 alloys.

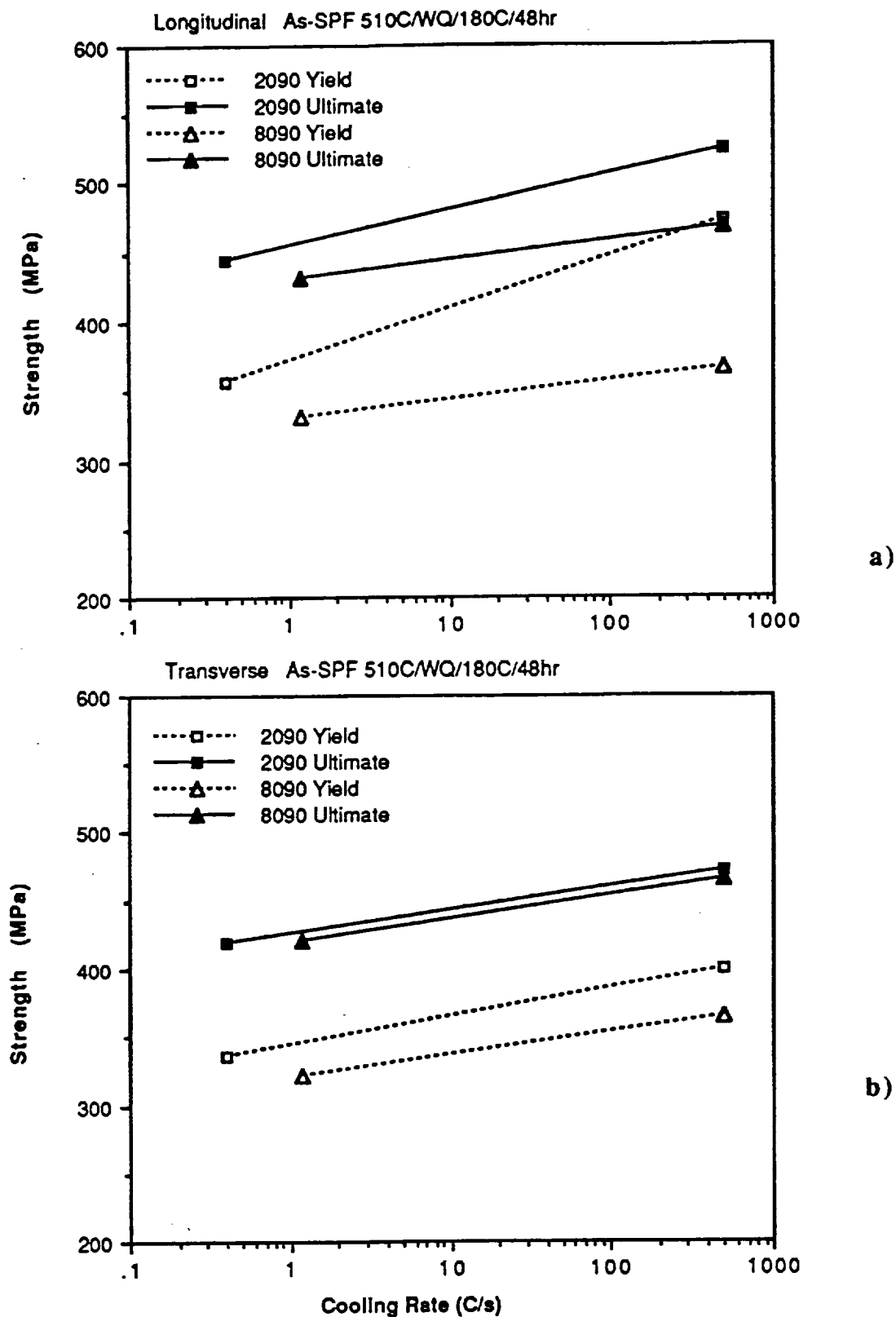


Figure 138. Comparison of the quench-rate effect on the 8090 and 2090 alloys in the as-formed condition, water quenched and age hardened: a. longitudinal orientation, and b. transverse orientation of the tensile test axis.

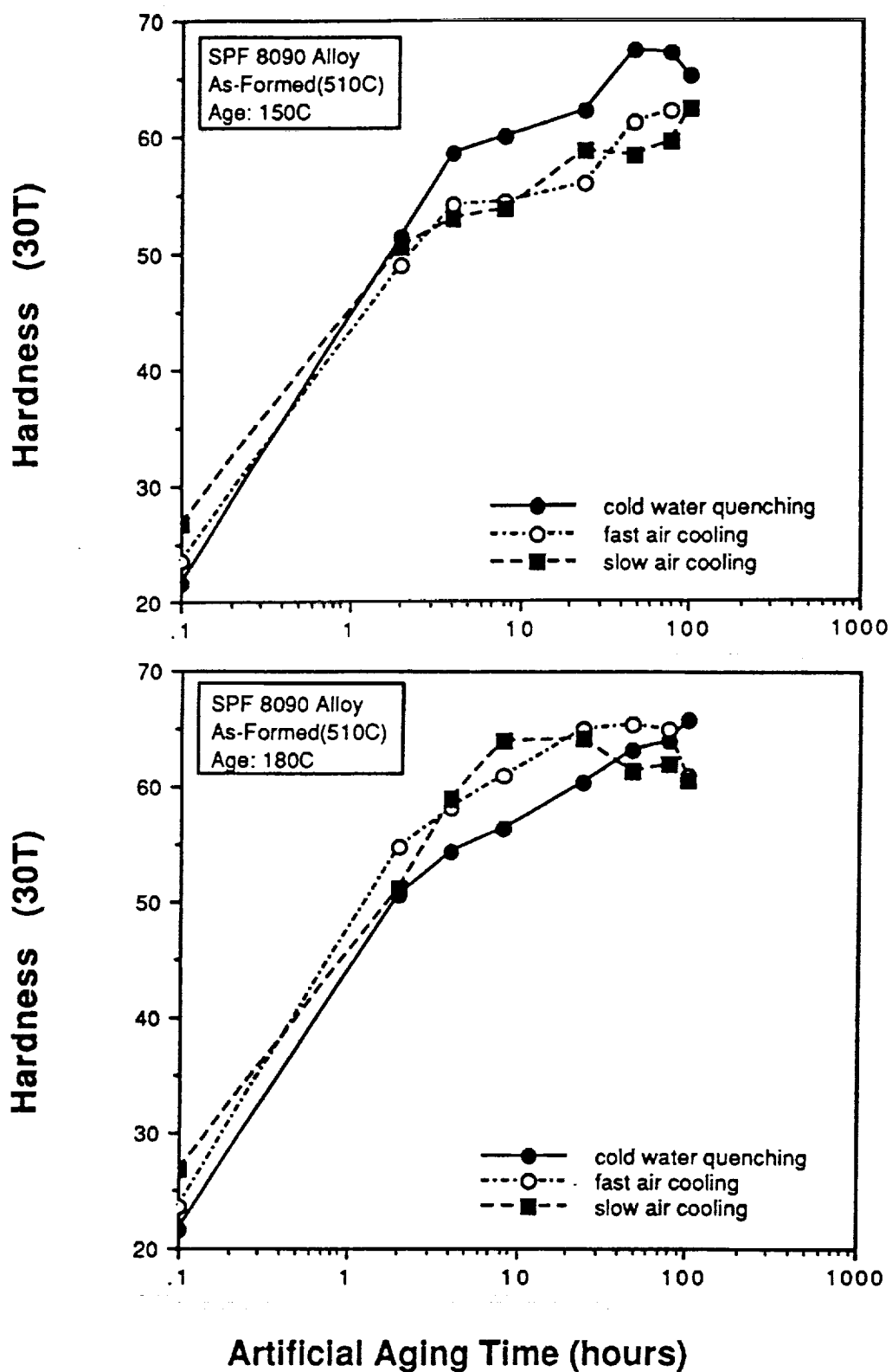
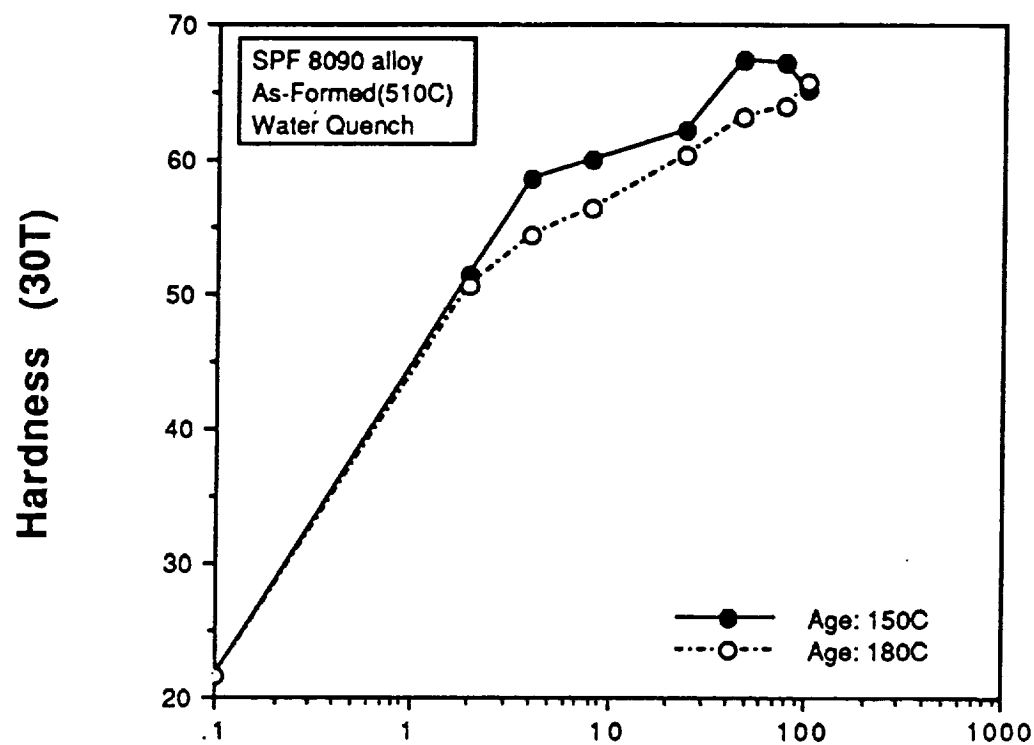
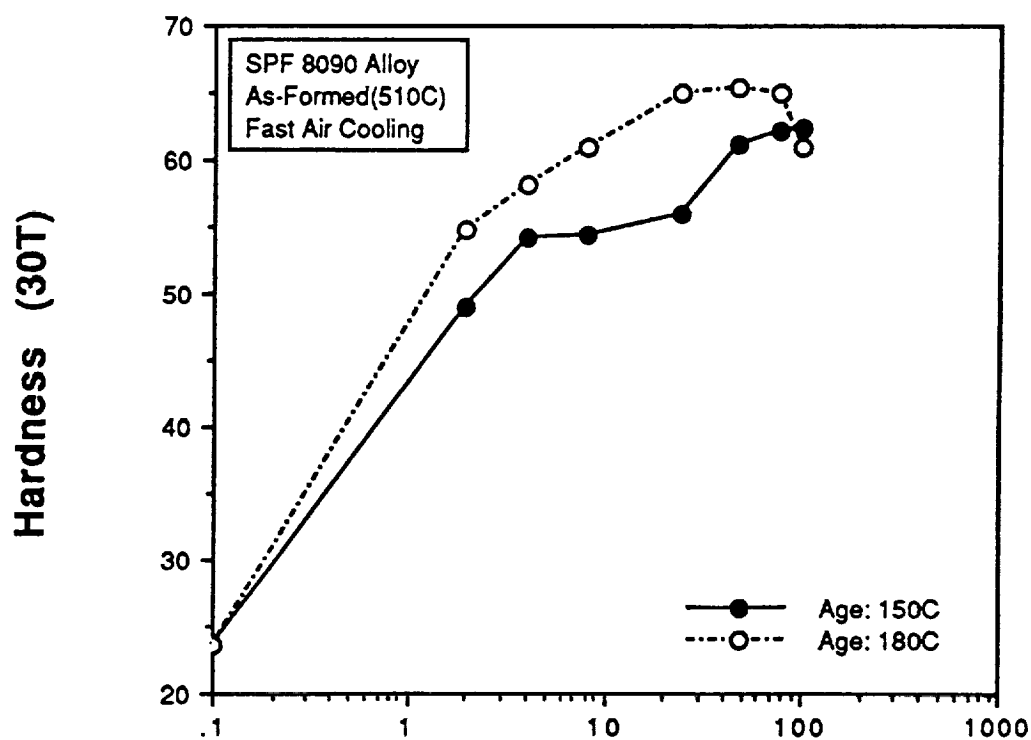


Figure 139. Effect of cooling rate on the age hardening characteristics of the as-SPF processed 8090 alloy for aging at a. 150°C (302°F), and b. 180°C (356°F).



a)



b)

Artificial Aging Time (hours)

Figure 140. Effect of cooling rate on the age hardening characteristics of the as-SPF processed 8090 alloy in the as-formed condition: a. water quenched b. fast air cooled, and c. slow air cooled.

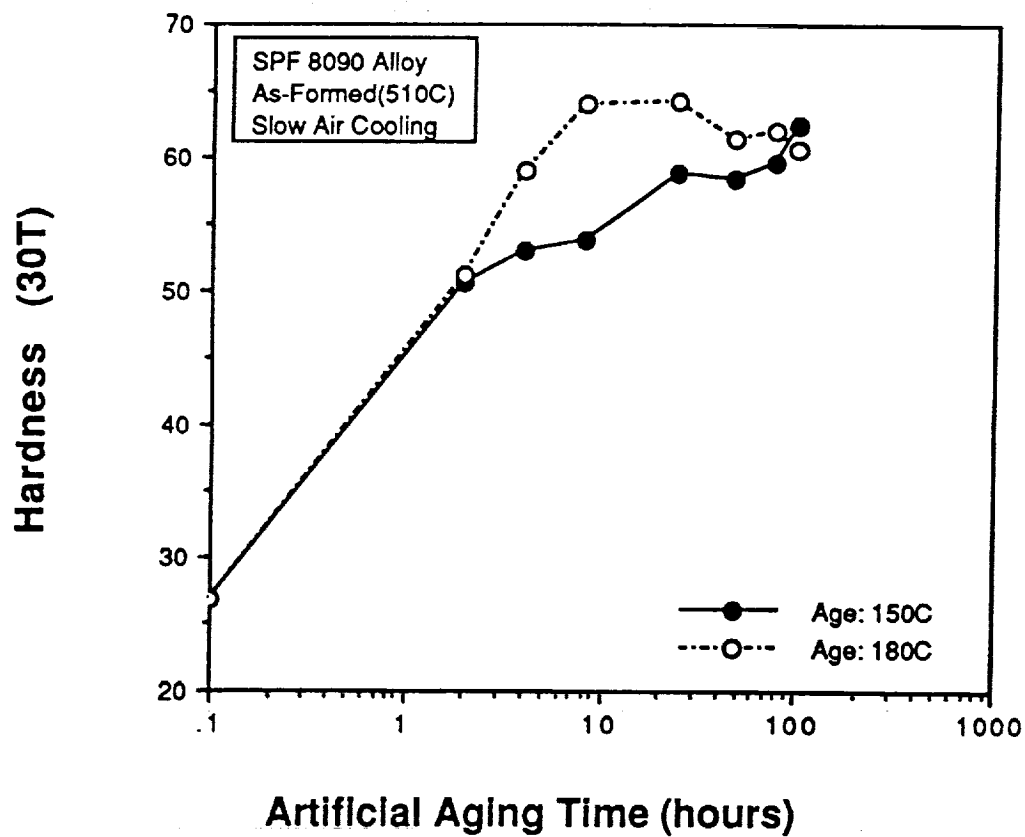
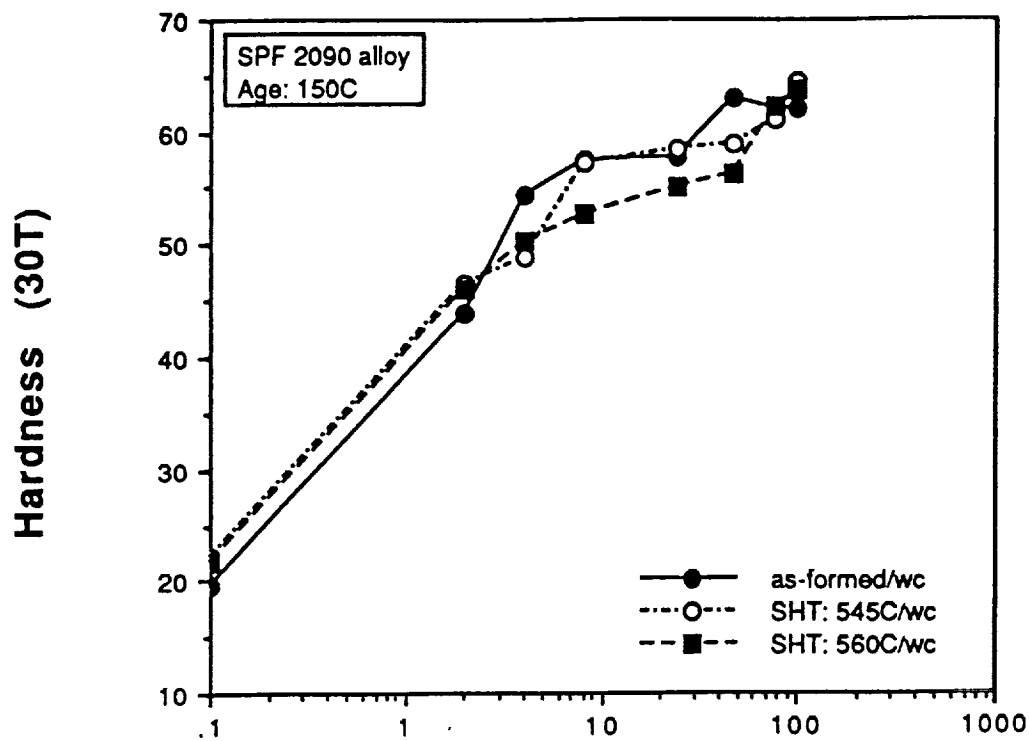
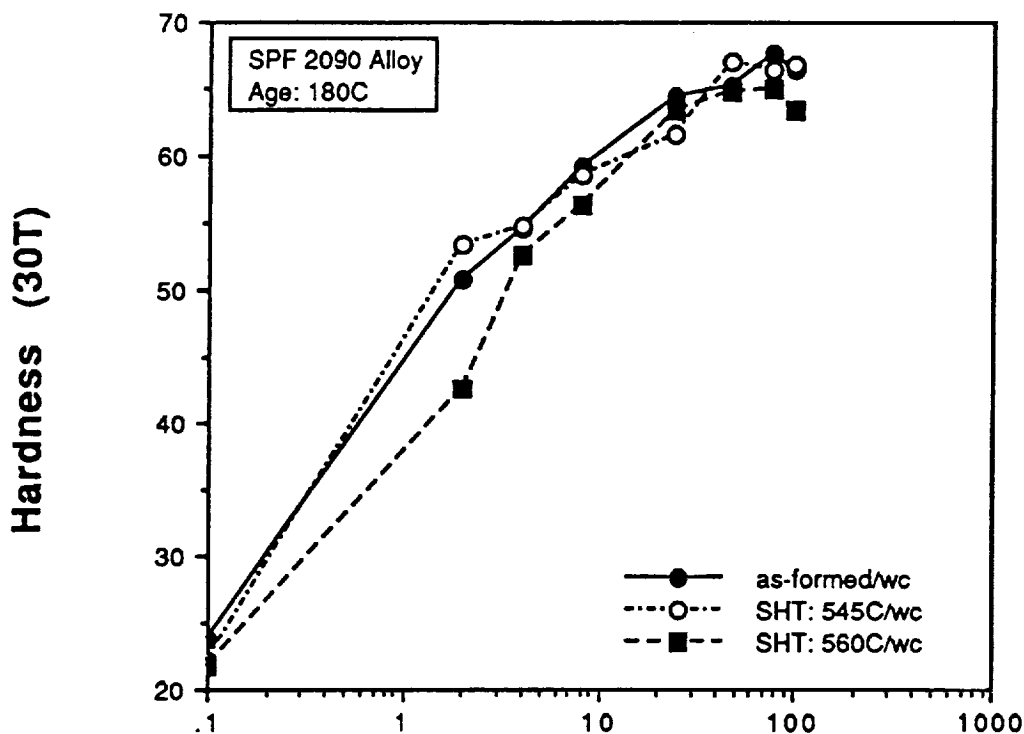


Figure 140 (continued). Effect of cooling rate on the age hardening characteristics of the formed 8090 alloy: a. water quenched b. fast air cooled, and c. slow air cooled.



a)



b)

Artificial Aging Time (hours)

Figure 141. Age hardening characteristics of the SPF-processed 2090 alloy after direct water quenching from the forming temperature, and after solution treatment at 545°C (1013°F) and 560°C (1040°F) aged at a. 150°C (302°F), and b. 180°C (356°F).

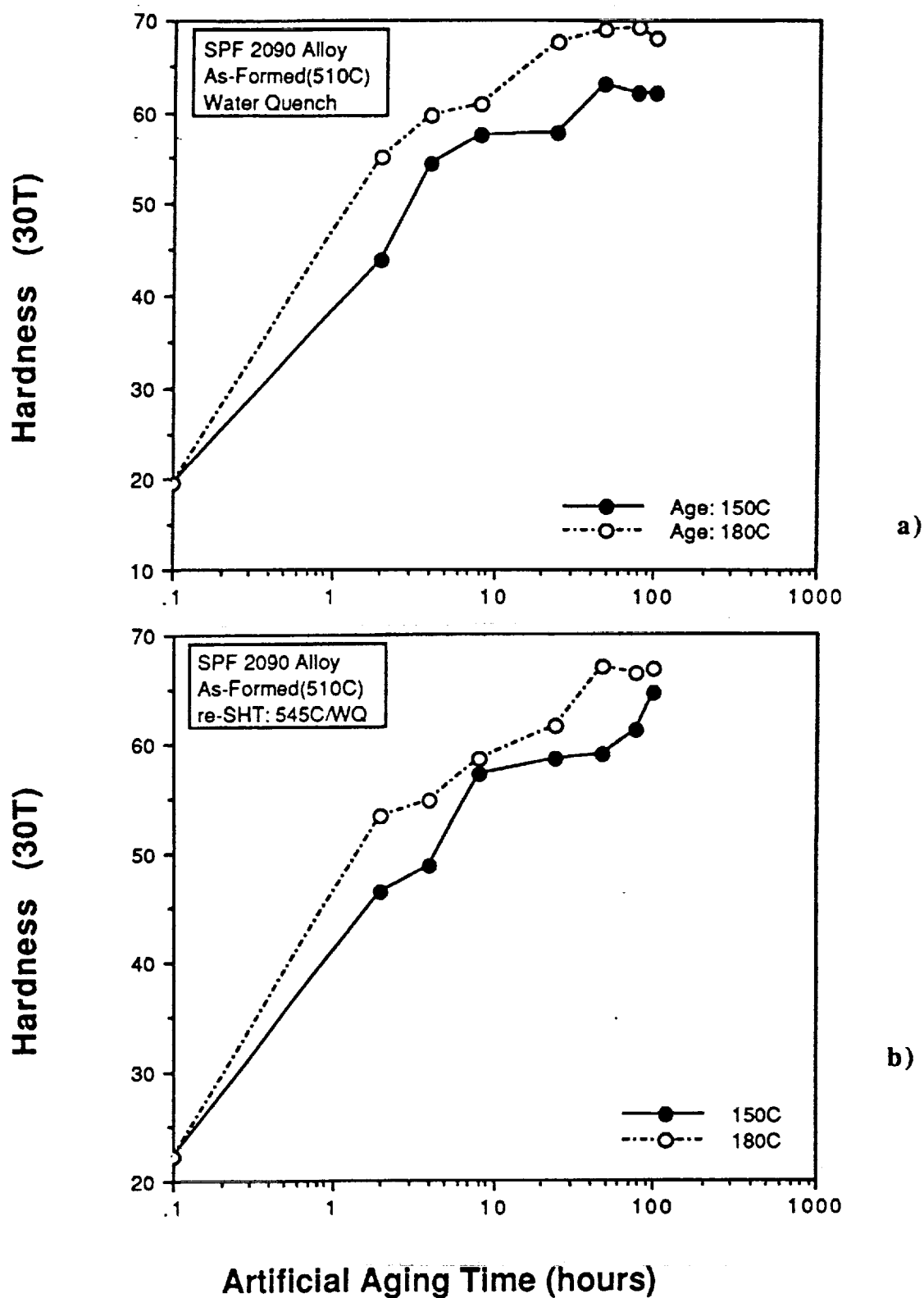
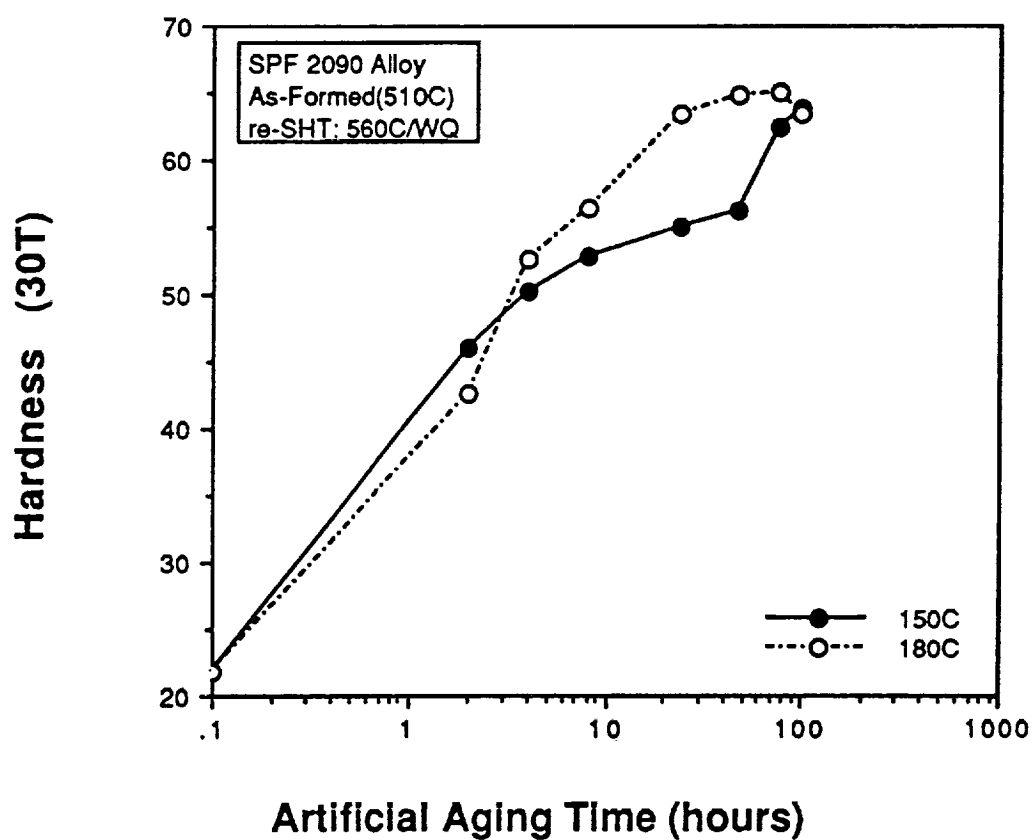
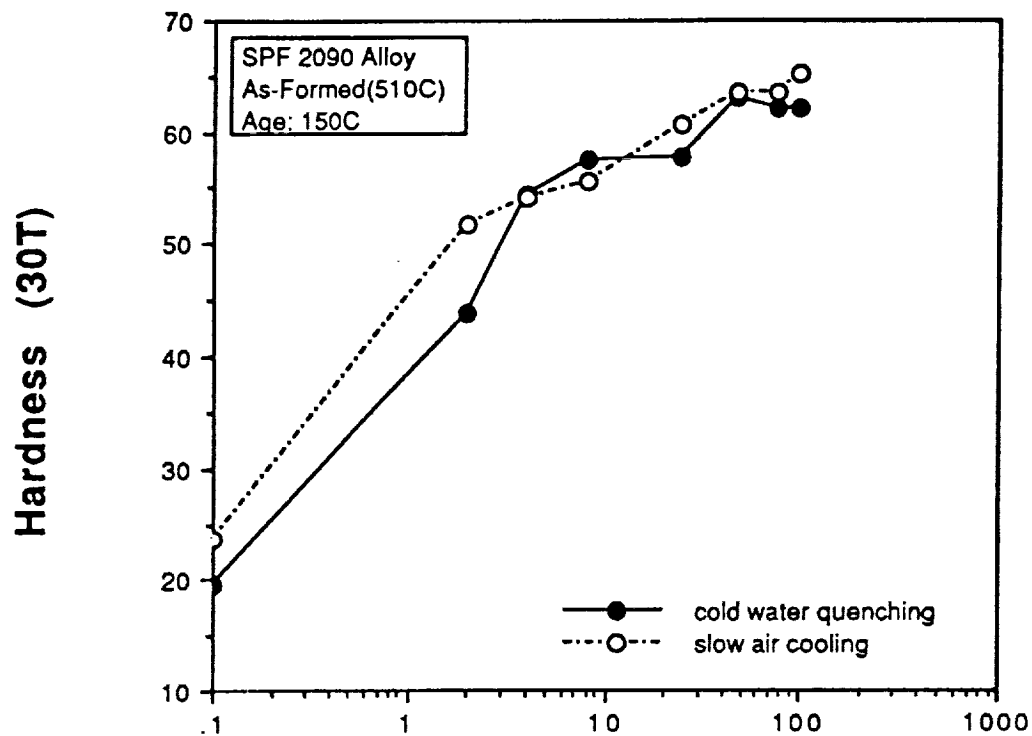


Figure 142. Age hardening characteristics of the SPF-processed 2090 alloy **a.** as-formed and **b.** after solution treatment at 545°C (1013°F), and **c.** after solution treatment at 560°C (1040°F).

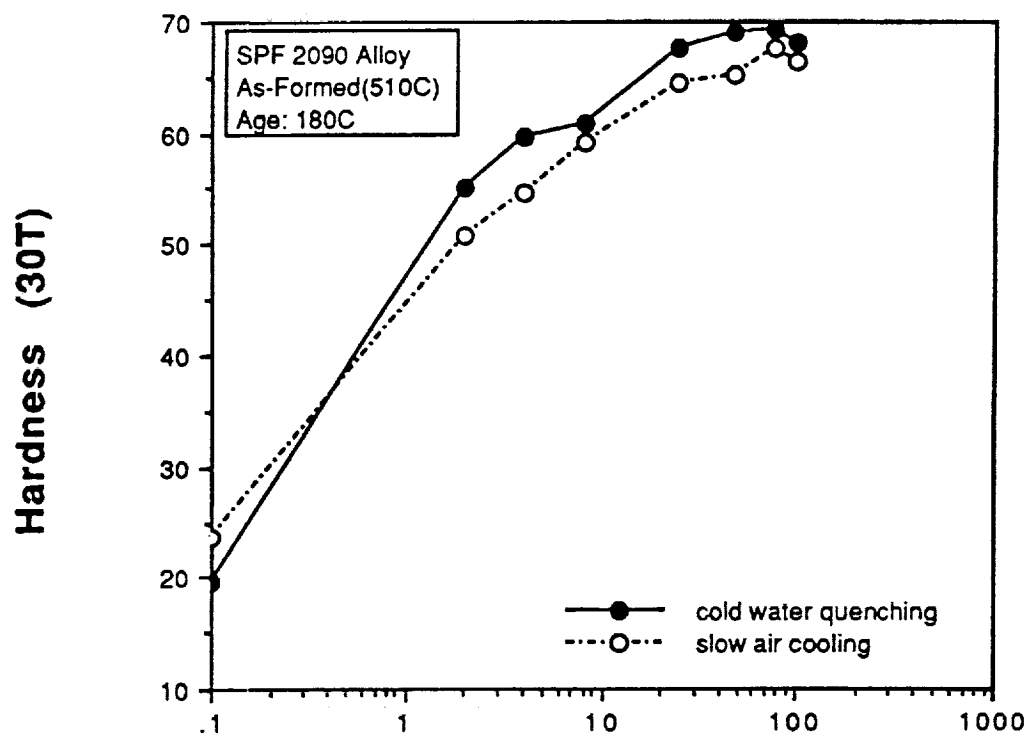


c)

Figure 142 (continued). Age hardening characteristics of the SPF-processed 2090 alloy a. as-formed and b. after solution treatment at 545°C (1013°F), and c. after solution treatment at 560°C (1040°F).



a)



b)

Artificial Aging Time (hours)

Figure 143. Effect of cooling rate on the age hardening characteristics of the as-SPF processed 2090 alloy in the as-formed condition: a. water quenched, and b. slow air cooled.

Subsequent tensile test results support the trends of the hardness testing, and appear to be consistent with results of other work. A comparison of the results of this study and those of Shakesheff et al.²³ for 8090 are shown in Figure 144. The 2090 results are generally consistent with observations reported by Staley and Doherty²⁴.

The effect of the cooling rate on the tendency to form grain boundary precipitation during cooling is illustrated in the electron micrographs of Figure 145 for the 8090 alloy. A general increase in the precipitation with decreasing cooling rates is apparent, and is consistent with observations of past research examinations^{23,24}.

4.2.4.3.5 Tensile Results

The results of the selected tensile tests for both alloys in the as-SPF condition are presented in Table 57 (for 8090 alloy) and 58 (for 2090 alloy). The tensile data appear to be consistent with the hardness results reported previously. It is noteworthy that for both as-SPF alloys, the tensile properties of those aged after SPF processing without a solution heat treatment are as good as, or better than, those with a solution treatment at higher temperatures. These results are consistent with those of as-received (non-SPF) materials which have been solution treated at 510°C (950°F the SPF forming temperature) reported previously. The high strength observed for the water quench plus 180°C (356°F) for 48 hours age is very promising, although the source of this strength increase due to SPF is not understood. Additional tests were conducted to substantiate these strengths, and the data are included in the tables. These strengths are particularly promising since there was no surface removal after SPF, and any surface depleted layer developed during SPF processing is still present.

It should be noted that many of the tensile samples failed outside the marked gage length, as indicated in the tables. It is believed that this is due to the variable thicknesses in the materials as a result of the SPF processing. In order to provide for a supplementary and perhaps more consistent measure of ductility, the fracture strain was determined for each sample by measuring the fracture thickness and width. The fracture strain, ϵ_f , was then computed from the final area, A_f , and the original area, A_0 by using the equation:

$$\epsilon_f = \ln (A_0/A_f)$$

The fracture strain values are tabulated in each table of the tensile test results.

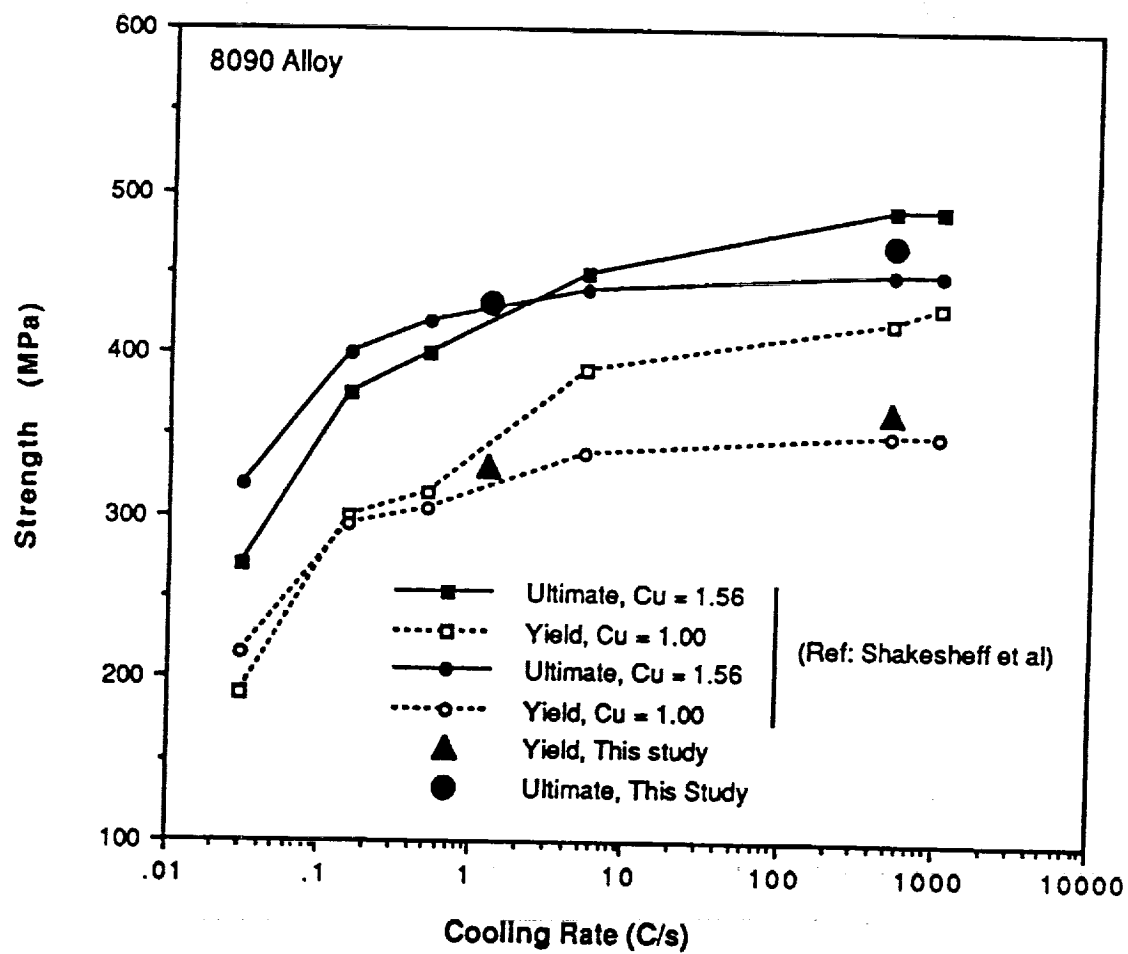


Figure 144. Data showing the effect of the cooling rate on the longitudinal strength of 8090 alloy taken from Shakesheff et. al. and results of this work for comparison.

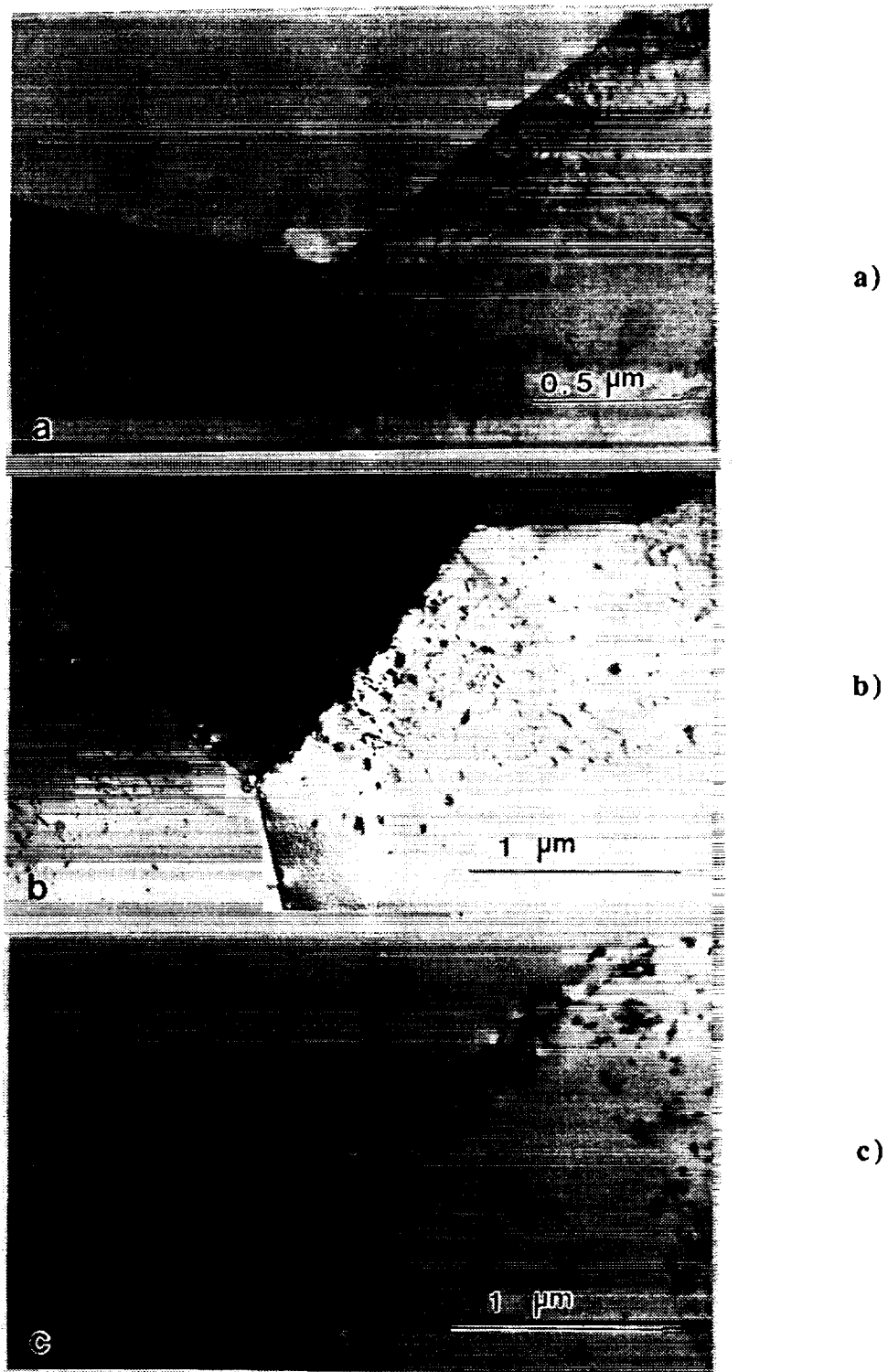


Figure 145. Electron micrographs of the 8090 alloy in the as-formed condition followed by a quench and artificial aging at 180°C (356°F) for 24 hours. Cooling rates were a: water quenched, b. fast air cooling, and c. slow air cooling. An increase in grain boundary precipitation with decreasing cooling rate can be seen.

Table 57. Tensile Properties for SPF 8090 Alloy for Various Heat Treatment Parameters.

Orient.	Sol'n Heat Treat. Temp. (°F/°C)	Quench Type	Artificial Aging Temp. (°F/°C)	Aging Time (Hrs)	F_{ty}		F_{tu}		Elong. (%)	Fracture Strain (%)
L	*950/510	WQ	356/180	48	(ksi) 53.1	(MPa) 366.1	(ksi) 67.9	(MPa) 468.3	5.3	6.3
T	*950/510	WQ	356/180	48	52.9	364.4	67.5	465.1	5.0	6.5
L	*950/510	WQ	356/180	48	53.6	369.6	68.5	472.0	3.3	4.7
T	*950/510	WQ	356/180	24	47.7	329.1	61.0	420.8	7.2	8.6
L	*950/510	SAC	356/180	24	53.7	370.3	66.5	458.2	2.1	4.5
T	*950/510	SAC	356/180	24	48.1	331.3	61.9	426.5	6.5	7.7
L	*950/510	FAC	356/180	48	48.1	331.6	62.7	432.0	5.7	9.1
T	*950/510	FAC	356/180	48	46.6	321.3	60.9	419.9	4.9	7.8
L	*950/510	FAC	356/180	24	47.5	327.5	59.4	409.2	3.8	7.9
L	1010/545	WQ	356/180	48	53.0	365.1	64.7	445.8	1.6	6.4
T	1010/545	WQ	356/180	48	51.2	352.7	65.2	449.6	3.3	5.2
L	1010/545	WQ	356/180	24	44.6	307.2	56.1	386.8	3.6	8.6
T	1010/545	WQ	356/180	24	47.4	326.8	60.3	415.4	2.3	7.7
L	1040/560	WQ	356/180	48	53.4	367.8	63.4	437.1	2.3	9.1
T	1040/560	WQ	356/180	48	43.2	297.9	57.9	399.2	7.3	8.4

*As-formed

Table 58. Tensile Properties for SPF 2090 Alloy for Various Heat Treatment Parameters.

Orient.	Sol'n Heat Treat. Temp. (°F/°C)	Quench Type	Artificial Aging Temp. (°F/°C)	Aging Time (Hrs)	F _{ty}		F _{tu}		Elong. (%)	Fracture Strain (%)
					(ksi)	(MPa)	(ksi)	(MPa)		
L	*950/510	WQ	356/180	48	68.7	473.9	76.2	525.1	1.5	4.8
T	*950/510	WQ	356/180	48	58.0	399.9	68.5	472.3	4.3	9.2
L	*950/510	WQ	356/180	24	64.0	440.9	75.2	518.5	3.2	4.0
T	*950/510	WQ	356/180	24	52.6	362.4	63.7	439.0	5.8	8.4
L	*950/510	SAC	356/180	48	52.0	358.5	64.5	444.9	1.8	6.0
T	*950/510	SAC	356/180	48	48.7	335.8	60.9	419.9	1.8	7.6
L	1000/538	WQ	356/180	20	48.9	336.8	63.4	437.1	1.9	5.4
T	1000/538	WQ	356/180	20	49.1	338.2	63.4	436.8	2.8	5.1
L	1010/545	WQ	356/180	48	48.0	331.0	62.1	427.8	3.9	5.0
T	1010/545	WQ	356/180	48	49.0	337.5	63.4	437.1	4.0	7.6
L	1040/560	WQ	356/180	48	44.2	304.4	57.6	397.2	2.0	6.9
T	1040/560	WQ	356/180	48	46.3	319.2	58.8	405.4	6.4	8.1

* As-formed

While there does appear to be some anisotropy in strength for both alloys, there is very little anisotropy seen for the 8090 alloy in the as-SPF (510°C, 950°F)/WQ/180°C (356°F)/48 hours heat treatment. There does not appear to be a clear anisotropy in the fracture strain for the 8090 alloy; but for the 2090 alloy, the transverse test direction appears to exhibit higher fracture strains in general. It appears that for the 2090 alloy, the value of fracture strain for specimens in longitudinal direction is consistently less, albeit by a small degree, than that in transverse direction for most heat treatment parameters. The exception for the 2090 alloy is the 538°C (1000°F)/WQ/180°C (356°F)/20 hours heat treatment. For the 8090 alloy, there is much less evidence of different ductility in two orientations although some difference is seen with the shorter aging times.

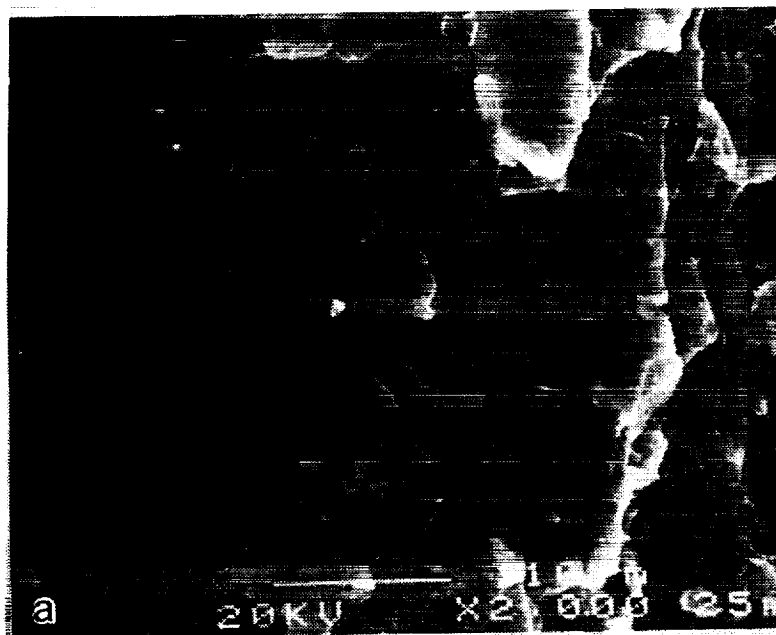
The highest strengths were observed both of the materials when they were superplastically formed and directly quenched in water followed by artificial aging at 180°C (356°F). Both SPF processed alloys show some quench sensitivity, however, high strength values were obtained from all three quench rates used during the study were good. The test results indicated that the faster the cooling rate following SPF process provided the higher the strength values after artificial aging.

The fracture mode of the alloys in the as-received and age hardened condition appears to be mixed mode, consisting of trans-granular and intergranular fracture as shown in Figure 146. After superplastic forming and age hardening, the fracture mode is more consistently intergranular but with ductile dimples evident as shown in Figure 147. This fracture characteristic is consistent with the coarser post-formed grain size and the precipitation free zone (PFZ) along many of the grain boundaries.

4.2.4.4 Discussion of Results

4.2.4.4.1 Microstructure

The microstructure after superplastic deformation is that of a fully recrystallized Al alloy, and is consistent with the observations made for an Al-Li alloy containing Zr^{15,16,17,18,19,20}. The microstructural evolution appears to be that of continuous dynamic recrystallization in which the deformation causes the sub-grain boundaries to overcome the pinning effect of the Al₃Zr particles, and the growth of these sub-grains is accompanied by the development of high angle boundaries resulting in a fully recrystallized material. While the starting material may have a high degree of warm or cold work, the high temperature deformation causes recovery and recrystallization, and there is not a sufficient dislocation density in the grains to aid in the precipitation process. In a previous study on 8091 Al alloy, it was found that the superplastic deformation, if there was no



a)



b)

Figure 146. Scanning electron fractographs taken from the failed tensile test specimens of the a. 2090 and b. 8090 alloys in the unformed but solution heat treated condition (510°C (950°F)) followed by a water quench and artificial age at 180°C (356°F) for 48 hours.



a)

b)

Figure 147. Scanning electron fractographs taken from the failed tensile test specimens of the a. 2090 and b. 8090 alloys in the superplastic formed condition (510°C (950°F)) followed by a water quench and artificial age at 180°C (356°F) for 48 hours. The fracture mode is intergranular, but with ductile dimples on the grain facets.

cavitation or surface alloy depletion, did little to alter the age hardened strength as compared with the solution treated and aged, as-received alloys^{15,16}. While this is generally found here as well, the strength of the formed and aged 2090 seems to be a bit higher than that of the unrecrystallized (unformed) alloy. This effect may be related to the mechanism(s) causing the peak in strength for the 510°C (950°F) solution treatment temperature, the temperature which is also the forming temperature.

4.2.4.4.2 Heat Treatment Results

The results of this study suggest heat treatment parameters suitable for achieving the program goal of acceptable strength levels greater than 50 ksi yield strength for superplastically formed parts produced from the alloys 2090 or 8090. Selected post-SPF heat treatments resulted in yield strengths of the order 50-54 ksi for the 8090 alloy and 57-70 ksi for the 2090 alloy. An unexpected, but interesting result observed was that the higher strengths were generally observed for the alloys when aged directly after forming, where the forming acted as the solution heat treatment. When the same material was solution heat treated and aged, the strength levels were no better, and in many cases lower than, those for the aforementioned condition. This result is highly desirable since it suggests that parts may be superplastically formed and heat treated without need to conduct an additional high temperature process, that of the solution heat treatment.

4.2.4.4.3 Cooling Rates

The cooling rate from the forming operation at 510°C (950°F) is also of considerable interest, since it would be desirable to simply air cool the parts rather than water quench them from the forming operation. Such an air cooling would further simplify the heat treatment of parts, and should minimize the distortion and dimensional losses that could result from rapid quenching. The 8090 alloy has been suggested to be particularly quench-rate insensitive and was of primary interest in this program. The corresponding quench-rate effects on the 2090 was examined as supplementary, and it was intended that this study could show comparative behavior to that of the 8090 alloy. The results of the quench-rate study shows that both alloys exhibit a loss in strength as the quenching rate is decreased from water quenching to air cooling. The strength loss in the 8090 alloy appears to be consistent with that reported previously for high and low Cu content in the 8090 alloy²³. The strength loss in the 2090 alloy appears to be greater than that for the 8090 alloy, but the absolute magnitude of the strength after the reduced cooling rates were generally greater than those for the 8090 alloy since it is a higher strength alloy. Thus, it seems that, on the basis of resulting strength, the 2090 alloy is quite competitive with the 8090 alloy if air cooling is

to be used. However, in both alloys, the resulting yield strength may be 1 or 2 ksi below the program goal of 50 ksi yield strength.

The magnitude of the cooling rate is clearly important, and if a more rapid mild quench than air cooling could be used, for example a water spray, it may then be possible to develop properties which are quite competitive to those of the water quenched materials. From Figure 144, it appears that a quench rate of 10 to 50°C (18 to 90°F) per second may be sufficiently rapid to permit the development of nearly peak strength for the 8090 alloy. As indicated in Figures 137 and 138, the 2090 alloy should achieve higher strengths at these rates than for the 8090 alloy even though the full strengthening capability of this 2090 alloy may not be achieved.

The cause of the strength loss on slower cooling is due to the high temperature precipitation of the hardening phases, especially these phases nucleating and growing on the grain boundaries as shown in Figure 145. It has been suggested by Shakesheff et al.²³ that the phases forming in the grain boundaries such as the T₂ (Al₆CuLi₃) contain significant amounts of the hardening elements Cu and Li, which deplete the surrounding matrix of at least some of the hardening precipitates. Thus, the slower the cooling, the greater the volume fraction of the grain boundary precipitate and the lower the strength of the age hardened alloy. The loss of the strengthening capability should be near the grain boundaries, the width of which would depend on the time spent at the high temperatures near the nose of the TTT curve for the precipitation of the phases.

A peak in hardness was observed for the as-received alloys after SHT at 510°C (950°F) (refer to Figure 120) and generally substantiated with tensile testing for the as-received and superplastic formed alloys (refer to Tables 55 through 58). The source of this additional hardening has not been established in this program. It is expected that the amount of solute going into solution should increase with temperature, and hence it would normally be expected that the higher solution temperatures would produce the greater hardening. It is suggested that the Zr may be playing a role here if there is additional precipitation of Al₃Zr β' phase at the lower temperatures, and if this phase contributes to the precipitation of the δ' and/or the T₁ phases as has been observed previously^{25,26}. In the absence of a pre-strain, which normally introduces an increased dislocation density suitable to encourage nucleation of the hardening precipitates, the β' may participate as a less efficient substitute. In this case, it may be that the additional nucleation sites provided by the β' compensate for the slight loss of solute due to the lower solution temperature. The β' is known to precipitate at temperatures above about 460°C (860°F)²⁷, and solution treating or forming at 510°C (950°F) could be expected to result in a somewhat greater concentration of the β' precipitate than for the higher temperatures. It has also been suggested by Nes²⁸ that superplastic

deformation may cause a re-dissolution of the β' as the low angle boundaries pass, and there may be a subsequent re-precipitation within the grain. This may act to redistribute the grain boundary β' into the matrix where it could then aid the hardening precipitation reaction by providing heterogeneous nucleation sites.

The fracture mode for the SPF-processed alloys is consistently that of intergranular fracture, although there is clear evidence of ductile dimples on the grain boundary facets. The fracture process is a ductile one, but the relatively low over-all ductility is probably related to the localized deformation of the lower strength zones at or near the grain boundaries, perhaps coupled with the tendency of the coarser grain boundary precipitates to crack or separate during exposure to high tensile stress and deformation. Additional fractographs of samples exposed to various thermal treatments utilized during this study are shown as Appendix E.

4.3 JOINING

The built-up cryogenic tank structure approach required attachment of the stiffeners to skin materials in such a way that the tank would remain sealed at both ambient and cryogenic temperatures. Historically, fuel tanks and lines used for cryogenic fuel systems have been fusion welded in order to assure a leak free structure. In the cryogenic fuel tank, the vertical welds (panel to panel) and the welds between the barrel sections and the major ring frames will be fusion welded in order to assure proper sealing of the pressure vessel. However, the attachment of the stiffeners to the outer skins required a permanent, leak free methodology that would be reliable both during storage of the tank and during flight. Since mechanical fastening of the stiffeners to the outer tank skins would not provide for a leak-free surface, alternative attachment methods were examined for the built-up configuration.

The primary method examined during this program was resistance spot welding of the stiffeners to the outer skin panels. The resistance spot welding approach provided a leak-free condition in the cryogenic tank for attachment of the stiffeners to the skins, whether the stiffeners were attached to the inner surface of the tank, or to the outer surface. The second method of attachment examined briefly during the program was adhesive bonding of the stiffeners to the skins on the external surface of the cryogenic tank. Several adhesive systems were examined and tested under laboratory conditions for evaluation of flat-wise tensile and shear behavior at ambient and cryogenic temperatures.

4.3.1 ADHESIVE BONDING

4.3.1.1 Material Selection

An engineering survey of adhesive materials with cryogenic service capabilities was conducted. The list of adhesives that were selected as candidates for the cryogenic tank are shown as Table 59.

Table 59. Candidate Cryogenic Structural Adhesives.

Adhesive	Type	Curing Temperature (°F)
Hysol EA 9330	Epoxy Paste	Room Temp.
Crest 810 A&B	Polyurethane Paste	Room Temp.
Crest 7344 A&B	Epoxy Paste	Room Temp.
Crest 3710 A&B	Polyurethane Paste	Room Temp.
Crest 212 A&B	Polyurethane Paste	Room Temp.
Products Research Corp. PRC 1665	Polyurethane Paste	130
PRC 1649		
BF Goodrich PL-777	Polyurethane Paste	250

Some of the capabilities of the candidate and experimental systems are noted as follows:

- The Hysol EA 9330 epoxy paste adhesive is noted for its high peel strength from -65°F to +150°F
- Products Research Corporation (PRC) polyurethane adhesive PR-1649 is a thixotropic, high-strength, polyurethane-based adhesive formulated to provide excellent physical properties under cryogenic service conditions (recommended for temperatures in the range of -200 °F).
- The laboratory developed adhesive RW2291-83 was formulated for structural use at temperatures of approximately -300 °F.
- Ciba-Geigy Corporation has developed a tough, low-temperature structural adhesive with good toughness and strength. The adhesive (designated LMH263-29) is a modified epoxy adhesive.

Preliminary adhesive testing (lap shear tests were performed per federal specification MMM-A-132, flat-wise tensile tests were performed per Mil-A-25463) were conducted on materials that appeared to be structural adhesives at cryogenic temperature and production-ready materials with aluminum-lithium substrate materials.

The 2090-T83 Al-Li substrates were machined, solvent wiped, etched, rinsed, air dried, and baked at low temperature for fifteen minutes prior to bonding. Cryogenic testing was performed with LN₂ in accordance with industry standards. Lap shear (0.5 in² surface area) and flat-wise tensile (1 in² surface area) results are Al-Li shown in Table 60. Flat-wise tensile results that are reported as NC (not completed) failed the 2090-T83 parent metal in bearing rather than the adhesive. Overall the adhesives performed very well during the evaluation. If adhesives are to be used on the Advanced Launch System for attachment of stiffeners to outer skin panels further testing would provide additional information.

Table 60. Adhesive Preliminary Test Results.

ADHESIVE	TYPE	CURING TEMP. °F	LAP-SHEAR (psi)	FLATWISE TENSILE (psi)	TEST TEMP. °F
CREST'S 810 A&B	PASTE	RT	5970	NC	-320
			6030	NC	-165
			1576	650	RT
7344 A&B	PASTE	RT	2940	NC	-320
			4380	11941	-165
			4565	4542	RT
212 A&B	PASTE	RT	4690	NC	-320
			4680	NC	-165
			839	1927	RT
PRODUCTS Research Corp. PRC 1665	PASTE	130	7190	NC	-320
			5540	NC	-165
			676	1350	RT

4.3.2 RESISTANCE SPOT WELD DEVELOPMENT

Characterization of the resistance spot weld (RSW) parameters for the materials used during this program utilized the Taguchi design of experiments. The Taguchi experiment process minimized the number of coupons that needed to be tested while evaluating the characteristics of the weld process as a function of the processing variables. Both the 7475-T62 to 2219-T81, and the 2090-T62 to 2090-T83 material combinations were examined with the Taguchi methodology. Once the optimum weld parameters had been isolated by this technique, standard test methodologies for development of the behavior of the weld were utilized.

The resistance spot weld equipment used during the program at General Dynamics was a Ferranti-Sciaky PMCO.5STM-400-36 (Refer to Figure 148). The welder was equipped with a microprocessor based controller/monitor, 400 KVA frequency converter transformer, 220,000 maximum secondary short circuit amperage, and has a 20,000 pound maximum electrode force capability.

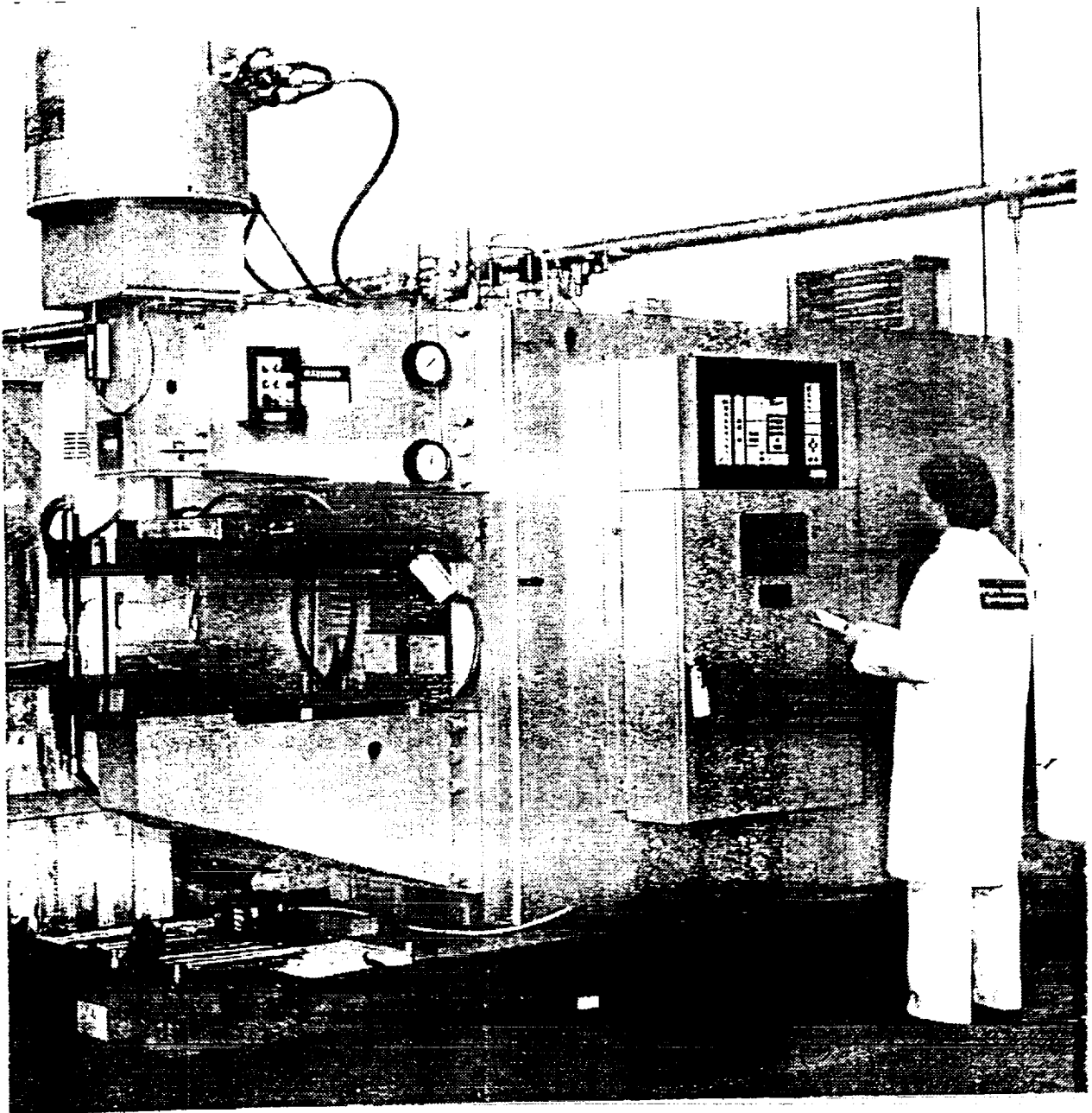


Figure 148. Resistance Spot Welding Equipment at General Dynamics.

ORIGINAL PAGE IS
OF POOR QUALITY

4.3.2.1 Resistance Spot Weld Characterization 7475-T62 to 2219-T81 Aluminum

A Taguchi L9 orthogonal array of tests was performed for the combination of 0.100" 7475-T62 joined to 0.190" 2219-T81 aluminum to identify optimum resistance spot welding parameters for the specified combination. The L9 array consisted of nine (9) tests (as shown in Table 61), each representing a different weld schedule. The four weld parameter variables (or factors) chosen for the L9 array were observed during previous Taguchi tests to have the greatest effect on the success of the weld joint. The variables chosen were weld time as cycles, weld heat as percent, weld force as pounds, and forge force as pounds with each variable having three levels representative of maximum, minimum, and an average value (e.g. Weld Time: Minimum = 5, Average = 6, Maximum = 7).

Table 61. L9 Taguchi Test Matrix for 0.100" 7475-T62 to 0.190" 2219-T81 Al Material Combination.

	A Weld Time Cycles	B Weld Heat Percent	C Weld Force Pounds	D Forge Force Pounds
Test 1	5	28	2400	5600
Test 2	5	33	2950	6400
Test 3	5	38	3400	7200
Test 4	6	28	2950	7200
Test 5	6	33	3400	5600
Test 6	6	38	2400	6400
Test 7	7	28	3400	6400
Test 8	7	33	2400	7200
Test 9	7	38	2950	5600

Each test schedule (1 through 9) was evaluated based upon seven replicate specimens (three lap shear, and four macro cross section examinations). The data was placed into a response table for weld nugget diameter (refer to Table 62) in order to compare the behavior of each test and determine the level of significance between the four factors (weld time, weld heat, weld force, and forge force) on the quality of the weld and with Mil-Handbook requirements. The MIL-W-6858 specification for resistance spot welded aluminum (thickness combination of 0.100" to 0.190") required the following joint constraints be satisfied:

Minimum average shear strength = 1825 pounds

Minimum nugget diameter = 0.250 inch

Nugget penetration = Minimum = 20 percent of thinner sheet

Maximum = 80 percent into each sheet

Table 62. Response Table for Weld Nugget Diameter (inches) of the 0.100" 7475-T62 to 0.190" 2219-T81 Material Combination.

Factor Levels	A Weld Time Cycles	B Weld Heat Percent	C Weld Force Pounds	D Forge Force Pounds
Level 1	0.0	0.0	0.227	0.120
Level 2	0.110	0.117	0.120	0.110
Level 3	0.237	0.230	0.0	0.117
Δ Levels High to Low	0.237	0.230	0.227	0.110

It was determined based upon the weld nugget diameter data that factor A (weld time as cycles) had the greatest effect upon the weld quality (with a response value of 0.237), and that factor B and C (weld heat and weld force) for provided second and third greatest effect on the weld joint. These conclusions were based upon the assumption that a minimum nugget diameter would provide the best structural efficiency (due to the minimized heat affected zone in the outer skin) for the tank structure. The minimum value (excluding zero values) for each factor was selected as the optimum weld schedule (as shown in Table 63). The optimized results were verified with confirmatory tests for reproducibility of results (refer to Table 64).

Table 63. The Optimum Factor Levels were Selected Based Upon Response Table Results for Minimum Nugget Diameter.

Factor A	Level 2 (response value = .110)	Weld Time	= 6 Cycles
Factor B	Level 2 (response value = .117)	Weld Heat	= 33 Percent
Factor C	Level 2 (response value = .120)	Weld Force	= 2950 Pounds
Factor D	Level 2 (response value = .110)	Forge Force	= 6400 Pounds

Table 64. Confirmatory Test of Optimized Weld Schedule for Minimum Nugget Diameter.

Shear Pounds	Nugget Diameter Inches	Nugget Penetration* Percent
2576	0.308	47 / 24
2961	0.303	42 / 25
2943	0.325	60 / 34
	0.315	60 / 34
	0.300	50 / -
Ave.	0.310	52 / 29

* Nugget penetration in 0.100" 7475-T62 sheet / penetration into 0.190" 2219-81 sheet.

The optimum weld schedule for best nugget diameter (developed in accordance with the Taguchi design of experiments) met the MIL-W-6858 specification.

The response table for the lap shear tests is shown as Table 65. The data from the lap shear results were compared and the significance of the weld factors were ranked according to optimum lap shear results. It was concluded, based upon the assumption that a maximum lap shear value was desirable for the joints, that factor B (weld heat) had the greatest effect on the weld joint followed by factors C and A (weld force, and weld time). The maximum lap shear value for each factor was selected as the best level for optimum lap shear performance and are shown as an optimized weld schedule in Table 66. Confirmatory tests were performed to verify the reproducibility of the results as shown in Table 67.

Table 65. Response Table for Shear Test Values (pounds) of the 0.100" 7475-T62 to 0.190" 2219-T81 Material Combination.

Factor Levels	A Weld Time Cycles	B Weld Heat Percent	C Weld Force Pounds	D Forge Force Pounds
Level 1	2395	1896	3119	2982
Level 2	2546	2874	2635	2557
Level 3	3092	3263	2279	2493
Δ Levels High to Low	697	1367	840	488

Table 66. The Optimum Factor Levels were Selected Based Upon Response Table Maximum Lap Shear Test Results.

Factor A	Level 3 (response value = .3092)	Weld Time	= 7 Cycles
Factor B	Level 3 (response value = .3263)	Weld Heat	= 38 Percent
Factor C	Level 1 (response value = .3119)	Weld Force	= 2400 Pounds
Factor D	Level 1 (response value = .2982)	Forge Force	= 7200 Pounds

Table 67. Confirmatory Test of Optimized Weld Schedule for Maximum Lap Shear Result.

Shear Pounds	Nugget Diameter Inches	Nugget Penetration* Percent
3898	0.350	75 / 76
3387	0.355	75 / 79
3782		
Ave. 3689	0.352	75 / 77

* Nugget penetration in 0.100" 7475-T62 sheet / penetration into 0.190" 2219-81 sheet.

The optimum weld schedule for the maximum lap shear values met the MIL-W-6858 specification, however, the welds were rejected due to molten aluminum expulsion during the spot weld formation.

The purpose of utilizing the Taguchi array was to direct the weld engineer toward the range of weld machine settings that would produce the most robust weld schedule for the desired material combination and thickness. Examination of the lap shear and nugget diameter Taguchi tests arrays resulted in the conclusion that development of a weld schedule based upon lap shear results does not provide an optimum weld schedule.

4.3.2.1.1 Weld Cycle Development 7475-T62 Joined to 2219-T81 Aluminum

A second Taguchi orthogonal array of tests (L8) were performed on the 7475-T62 (thickness of 0.100") to 2219-T8 (thickness of 0.190") aluminum to optimize resistance spot welding heat and weld time parameters for the two materials. The L8 array consisted of eight tests (as shown in Table 68), each representing a different weld schedule. Five weld factors were chosen for the L8 array that were observed to be the most significant and sensitive to small changes in setting. The modification provided four levels for weld heat and two levels for the remaining factors.

Table 68. L8 Taguchi Test Matrix for 0.100" 7475-T62 to 0.190" 2219-T81 Al Material Combination.

	A Weld Time Cycles	B Weld Heat Percent	C Weld Force Pounds	D Forge Force Pounds	E Squeeze Cycles
Test 1	6	31	2400	6400	40
Test 2	7	31	2950	7200	55
Test 3	6	33	2400	7200	55
Test 4	7	33	2950	6400	40
Test 5	6	35	2950	6400	55
Test 6	7	35	2400	7200	40
Test 7	6	37	2950	7200	40
Test 8	7	37	2400	6400	55

Each test schedule required ten test specimens (three lap shear specimens, four macro cross section specimens, and three sheet efficiency test specimens). The data from the tests were reduced in order to compare the factor levels and determine the level of significance between the

four factors. The results from analysis of the L8 array data showed that the B factor (weld heat in percent) was the most significant parameter, followed closely by the weld force in pounds. The remaining factors, forge force, weld time and squeeze, in most cases were insignificant. The best overall schedule was chosen based upon the values in the response tables. Three candidates for an optimum weld schedule were obtained and conformation tests were run (refer to Table 69 through 71).

Confirmatory Test Schedule #1

Factor A - Level 2	Weld Time	= 7 Cycles
Factor B - Level 3	Weld Heat	= 35 Percent
Factor C - Level 1	Weld Force	= 2400 Pounds
Factor D - Level 1	Forge Force	= 6400 Pounds
Factor E - Level 2	Squeeze	= 55 Cycles

Confirmatory Test Schedule #2

Factor A - Level 1	Weld Time	= 6 Cycles
Factor B - Level 3	Weld Heat	= 35 Percent
Factor C - Level 1	Weld Force	= 2400 Pounds
Factor D - Level 1	Forge Force	= 6400 Pounds
Factor E - Level 2	Squeeze	= 55 Cycles

Confirmatory Test Schedule #3

Factor A - Level 2	Weld Time	= 7 Cycles
Factor B - Level 2	Weld Heat	= 33 Percent
Factor C - Level 1	Weld Force	= 2400 Pounds
Factor D - Level 1	Forge Force	= 6400 Pounds
Factor E - Level 2	Squeeze	= 55 Cycles

Table 69. Test Results for Confirmatory Run on Schedule #1.

Coupon I.D.	Nugget Diameter inch	Nugget Penetration*		Shear lbs	Weld Quality
		% Upper Sheet	% Lower Sheet		
1C1	0.340	95	21	-	expulsion
1C2	-	-	-	3211	expulsion
1C3	0.335	80	28.9	-	expulsion
1C4	-	-	-	3103	expulsion
1C5	0.340	80	34.2	-	expulsion
1C6	-	-	-	3348	expulsion
1C7	0.335	80	36.8	-	expulsion
Average	0.338	83.8	30.2	3221	

* Nugget penetration in 0.100" 7475-T62 sheet / penetration into 0.190" 2219-81 sheet.

Table 70. Test Results for Confirmatory Run on Schedule #2.

Coupon I.D.	Nugget Diameter inch	Nugget Penetration*		Shear lbs	Weld Quality
		% Upper Sheet	% Lower Sheet		
2C1	-	-	-	3460	good
2C2	0.350	70	26.3	-	good
2C3	-	-	-	3480	good
2C4	0.350	70	34.2	-	good
2C5	-	-	-	3429	good
2C6	0.355	70	34.2	-	good
2C7	0.350	65	36.8	-	good
Average	0.351	68.8	32.9	3456	

* Nugget penetration in 0.100" 7475-T62 sheet / penetration into 0.190" 2219-81 sheet.

Table 71. Test Results for Confirmatory Run on Schedule #3.

Coupon I.D.	Nugget Diameter inch	Nugget Penetration		Shear lbs	Weld Quality
		% Upper Sheet	% Lower Sheet		
3C1	0.325	80	21	-	expulsion
3C2	-	-	-	3502	good
3C3	0.350	65	42.1	-	good
3C4	-	-	-	3225	expulsion
3C5	0.360	75	34.2	-	expulsion
3C6	-	-	-	3663	good
3C7	0.360	80	47.4	-	good
Average	0.338	75.0	36.2	3463	

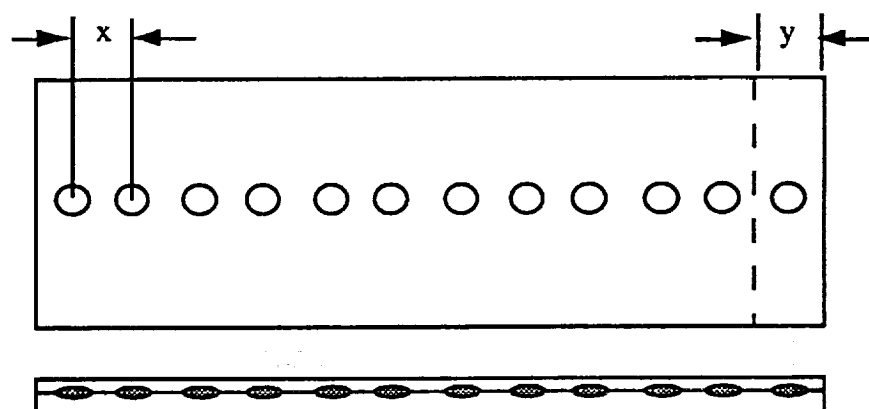
* Nugget penetration in 0.100" 7475-T62 sheet / penetration into 0.190" 2219-81 sheet.

Weld schedule #1 exceeded the maximum depth of penetration into the thin sheet and had considerable weld expulsion. Weld schedule #2 met all of the criteria for the military specification of resistance spot welding, and weld schedule #3, while it met all of the parameters set out in the specification, had weld expulsion three times out of seven, and was found unacceptable. Thus the optimum weld schedule developed under the Taguchi design of experiments was selected as schedule #2.

Resistance spot weld spacing tests were performed in order to determine the effects that inter-spot spacing has on weld strength and quality. Continuous sheet test specimens (refer to Figure 149) were welded from 0.100" 7475-T62 joined to 0.190" 2219-T81 using a certified weld schedule with inter-spot spacings of 0.75", 1.00", 1.25" and 1.5" and the secondary current, nugget expansion, dynamic resistance, weld force, forge force, lap shear values, weld penetration,

and nugget diameters were recorded for all of the tests. Single spot specimens were welded as a control for comparison with the spot spacing specimens. For each of the different spot spacing configurations and single spot specimens, seven test coupons were examined for micro cross sections and three lap shear specimens. The results from the tests are shown in Table 72.

Figure 149. Schematic for inter-spot spacing test.



x = Inter-spot spacing
y = Width of Lap shear coupon

Table 72. Resistance Spot Spacing Test Results for 0.100 inch 7475-T62 to 0.190 inch 2219-T81 Aluminum.

Schedule: Weld Heat (36 percent), Weld Time (6 cycles), Weld Force (15 psi), Forge Force (24 psi), Squeeze (55).

Spot Weld Spacing (inch)	Coupon I.D.	Nugget Diameter (inch)	Nugget Penetration		Shear Strength (Lbs)
			Upper Sheet (inch)	Lower Sheet (inch)	
0.75	1SS1-1	Diffusion	Diffusion	Diffusion	2292
	1SS1-2	Diffusion	Diffusion	Diffusion	
	1SS1-3	Diffusion	Diffusion	Diffusion	
	1SS1-4	Diffusion	Diffusion	Diffusion	
	1SS1-5	Diffusion	Diffusion	Diffusion	
	1SS1-6	Diffusion	Diffusion	Diffusion	
	1SS1-7	Diffusion	Diffusion	Diffusion	
	Average	Diffusion	Diffusion	Diffusion	2379
1.00	1SS2-1	Diffusion	Diffusion	Diffusion	2047
	1SS2-2	Diffusion	Diffusion	Diffusion	
	1SS2-3	0.300	.050	.020 - .040	
	1SS2-4	0.260	.045	.015 - .040	
	1SS2-5	0.260	.045	.015 - .040	
	1SS2-6	0.290	.040	.010 - .030	
	1SS2-7	0.290	.040	.010 - .030	
	Average	0.283	.045	.015 - .037	2254

Table 72 (Continued). Resistance Spot Spacing Test Results for 0.100 inch 7475-T62 to 0.190 inch 2219-T81 Aluminum.

Spot Weld Spacing (inch)	Coupon I.D.	Nugget Diameter (inch)	Nugget Penetration		Shear Strength (Lbs)
			Upper Sheet (inch)	Lower Sheet (inch)	
1.25	1SS3-1	0.300	.045	.015 - .040	2569
	1SS3-2				
	1SS3-3	0.300	.045	.015 - .045	2908
	1SS3-4				
	1SS3-5	Diffusion	Diffusion	Diffusion	2685
	1SS3-6				
	1SS3-7	0.300	.050	.020 - .050	2721
	Average	0.300	.047	.017 - .045	
1.50	1SS4-1	0.300	.060	.020 - .045	2421
	1SS4-2				
	1SS4-3	0.300	.050	.020 - .040	2347
	1SS4-4				
	1SS4-5	0.290	.040	.010 - .025	2394
	1SS4-6				
	1SS4-7	0.325	.050	.025 - .050	2387
	Average	0.304	.050	.019 - .040	
Single Spot	1SS5-1	0.325	.050	.010 - .040	2267
	1SS5-2				
	1SS5-3	0.315	.045	.015 - .030	2769
	1SS5-4				
	1SS5-5	0.300	.045	.020 - .025	2432
	1SS5-6				
	1SS5-7	0.310	.050	.025 - .050	2489
	Average	0.313	.048	.018 - 0.036	

The spot spacing tests revealed that there was not a significant decrease in lap shear values as spot spacings decreased from 1.5" to 0.75", however, a decline in nugget diameters was noted. Furthermore, spot weld penetration into the 0.100" sheet showed a slight decrease with the decrease in spacing. The penetration into the 0.190" sheet resulted in a decrease in minimum penetration as spacing decreased but maximum penetration remained unchanged. The most important observation was that as the spot weld spacing decreased, the greater the shunting effect to the adjoining spot weld, which resulted in a greater probability for diffusion spot welds.

4.3.2.1.2 Ambient Test Data 7475-T62 Joined to 2219-T81 Aluminum

Sheet efficiency tests were performed on the 2219-T81 material in order to determine the "knockdown" against the ultimate tensile strength for a given skin section exposed to the heat generated during the formation of a spot weld. Tensile coupons were prepared by machining 2" x 12" x 0.190" thick pieces into a "dogbone" shape with the gage section reduced in width to 1.00 inch. The sheet efficiency test results are shown in Table 73 for 2219-T81 skin.

Table 73. 0.190" 2219-T81 Aluminum Skin Efficiency (or Reduction in Ultimate Tensile Strength) After Spot Welding of 0.100" 7475-T62 Stiffeners.

Material Type	Test Temperature (°F)	F _{tu} (ksi)	Sheet Efficiency (%)
2219-T81	20	62.1	62.1/65.6* = 94.75

* Note: Ratio taken from actual test data rather than allowable data.

Weld schedules were developed for the crippling test panels (due to thinning in the superplastic formed flange, new cycles were developed, based upon the initial results) and were verified through certification testing. The results from the tests are shown in Table 74. The average lap shear test value for the schedule was 2909 pounds, the minimum being 2565 pounds, and 100% of the individual test values fell within $\pm 12.5\%$ range (the range required for passing certification) of the average value. The average nugget diameter was 0.303" with a minimum nugget diameter requirement of 0.220" per MIL-W-6858D. Nugget penetration into the 7475-T62 (the thinnest sheet) was recorded as a minimum of 61% and a maximum of 80% of the sheet thickness and penetration into the 2219-T81 (the thicker) sheet was recorded as a minimum of 18% and a maximum of 30%. Military specifications on resistance spot welding requires a minimum nugget penetration of twenty percent of the thinnest sheet thickness into both of the sheets being welded, and that maximum penetration shall not exceed eighty percent of the thickness of each sheet. Although the lap shear certification test exceeded the MIL-W-6858D requirement for average lap shear for the thinnest sheet thickness of 0.077" (1202 pounds), the nugget penetration into the lower sheet was insufficient to qualify the schedule for certification. However, due to the quality of the welds and the lap shear values, it was believed that the schedule would exceed the design requirements for the crippling test panels, thus the schedule was utilized during panel fabrication.

4.3.2.1.3 Cryogenic Test Data 7475-T62 Joined to 2219-T81 Aluminum

Sheet efficiency tests were performed under cryogenic temperature on the 2219-T81 material in order to determine the "knockdown" against the ultimate tensile strength for a given skin section exposed to the heat generated during the formation of a spot weld. Tensile coupons were prepared by machining 2" x 12" x 0.190" thick pieces into a "dogbone" shape with the gage section reduced in width to 1.00 inch. The cryogenic sheet efficiency test results are shown in Table 75 for 2219-T81 skin.

Cryogenic Lap Shear Tests on the 0.100" 7475-T62 joined to 0.190" 2219-T81 material combination were performed in order to evaluate the response of the spot welds produced by the certified weld schedule operating under cryogenic temperatures. Fifty spot weld coupons were welded in sequence using the previously certified weld schedule. Forty of the fifty spot welded specimens were tested in Lap Shear at cryogenic temperatures; twenty at LN₂ temperatures of -320°F and twenty at LH₂ temperature of -423°F. The remaining ten coupons were processed for micro cross-section data. The Lap Shear and weld nugget measurements are shown in Table 76 and Table 77 and summary representations of the ambient and cryogenic lap shear, nugget diameter, nugget penetration, and sheet efficiency are shown in Figures 150 through 152.

Table 74. Weld Schedule Certification 0.077" 7475-T62 Joined to 0.190" 2219-T81 Aluminum.

Schedule: Weld Heat (35 percent), Weld Time (6 cycles), Weld Force (16 psi), Forge Force (24 psi), Squeeze (55).

Coupon ID	Nugget Diameter (inch)	Nugget Penetration		Shear (Lbs.)	7475-T62 Thickness (inch)
		% Upper Sheet 7475-T62	% Lower Sheet 2219-T81		
CT4-1	0.315	78.2 - 79.5	24.4	2833	0.071
CT4-2				3076	0.074
CT4-3				2926	0.076
CT4-4				3022	0.077
CT4-5					0.078
CT4-6				3064	0.079
CT4-7				2960	0.080
CT4-8				3025	0.079
CT4-9	0.312	74.0 - 80.5	24.7	2862	0.078
CT4-10					0.077
CT4-11				2693	0.076
CT4-12				2565	0.075
CT4-13				2574	0.072
CT4-14				3046	0.074
CT4-15	0.286	64.5 - 80.0	18.4		0.076
CT4-16				3016	0.078
CT4-17				2968	0.079
CT4-18				2893	0.079
CT4-19				2890	0.080
CT4-20					0.079
CT4-21	0.290	60.8 - 79.7	21.5	2765	0.079
CT4-22				3034	0.077
CT4-23				2956	0.075
CT4-24				3006	0.074
CT4-25					0.072
Average	0.303	70.5	21.4	2909	0.077

Mil-W-6858D Specification Limits for Acceptable Lap Shear Values: 18 out of 20 Test Values Must Fall Within Specification Limits $\pm 12.5\%$ to Pass Evaluation.

Percent Deviation from Shear Value	-25.0%	-12.5%	Mean	+12.5%	+25.0%
Calculated Deviation (Lbs)	2182	2545	2909	3272	3636

MIL-W-6858D Minimum Values for Thinnest Sheet.

Minimum Ave. Shear Strength: = 1202 Lbs

Minimum Nugget Diameter = 0.220 inch

Nugget Penetration: Minimum = 20% of thinner sheet

Maximum = 80% of thinner sheet

Table 75. 0.190" 2219-T81 Aluminum Skin Efficiency (or Reduction in Ultimate Tensile Strength) After Spot Welding of 0.100" 7475-T62 Stiffeners.

Material Type	Test Temperature (°F)	F _{tu} (ksi)	Sheet Efficiency (%)
2219-T81	-320	74.8	74.7/81.9* = 91.3
	-423	86.0	86.0/95.5* = 90.05

* Note: Ratio taken from actual test data rather than allowable data.

From the LN₂ data in Table 76, the average lap shear test value was 4346 lbs., and the minimum value was 3952 lbs. One hundred percent of the individual values were within the $\pm 12.5\%$ range of the average test value. The measured nugget penetrations and diameters for all macros were within MIL-W-6858D requirements.

From the LH₂ data in Table 77, the average lap shear test value was 4134 lbs., and the minimum value was 3550 lbs. Eighty-five percent of the individual test values were within the $\pm 12.5\%$ range of the average test value. The remaining 15% were within the $\pm 25\%$ range of the average test value. The measured nugget penetrations and diameters for all macros were within MIL-W-6858D requirements.

4.3.2.1.4 Exposure After Cleaning

Pre-weld "out-time" cleaning tests were performed in order to determine acceptable cleaning methods for aluminum alloys and determine the amount of time after cleaning that acceptable spot welds could be produced. Standard cleaning methods were used for the materials which consisted of three to five minutes of alkaline clean, followed by a 45 to 60 second chemical etch (hydrofluoric/nitric acid solution) with a final five minute deoxidizer (acid/chromate/sulfate solution) with a final five minute water rinse and a 10 minute oven dry. The "out-time" test was planned for a period of ten days with three tests performed each day.

Prior to welding each day, the coupons were wire brushed and solvent wiped. The results from the test are shown in Table 78 through 80. The test was discontinued after day three due to

weld expulsion however, the entire exposure test was repeated in order to verify the exposure requirements for the aluminum combination.

Table 76. LN₂ (-320°F) Cryogenic Resistance Spot Weld Test Results. 0.100 inch 7475-T62 to 0.190 inch 2219-T81 Aluminum.

Schedule: Weld Heat (36 percent), Weld Time (6 cycles), Weld Force (16 psi), Forge Force (24 psi), Squeeze (55).

Coupon ID	Nugget Diameter (inch)	Nugget Penetration		Shear (lbs)
		% Upper Sheet 7475-T62	% Lower Sheet 2219-T81	
2CRY-1	0.365	80.0	20.0	
2CRY-2				4662
2CRY-3				4129
2CRY-4				4350
2CRY-5				4400
2CRY-6	0.350	60.0	27.0	
2CRY-7				4392
2CRY-8				4411
2CRY-9				4406
2CRY-10				4143
2CRY-11	0.350	60.0	25.0	4468
2CRY-12				4230
2CRY-13				4140
2CRY-14				4375
2CRY-15				
2CRY-16	0.3545	55.0	25.0	4165
2CRY-17				3952
2CRY-18				4326
2CRY-19				4531
2CRY-20				
2CRY-21	0.360	55.0	25.0	4605
2CRY-22				4440
2CRY-23				4306
2CRY-24				4490
2CRY-25				
Average	0.354	62.0	24.4	4346

Mil-W-6858D Specification Limits for Acceptable Lap Shear Values: 18 out of 20 Test Values Must Fall Within Specification Limits $\pm 12.5\%$ to Pass Evaluation.

Percent Deviation from Shear Value	-25.0%	-12.5%	Mean	+12.5%	+25.0%
Calculated Deviation (Lbs)	3260	3803	4346	4889	5433

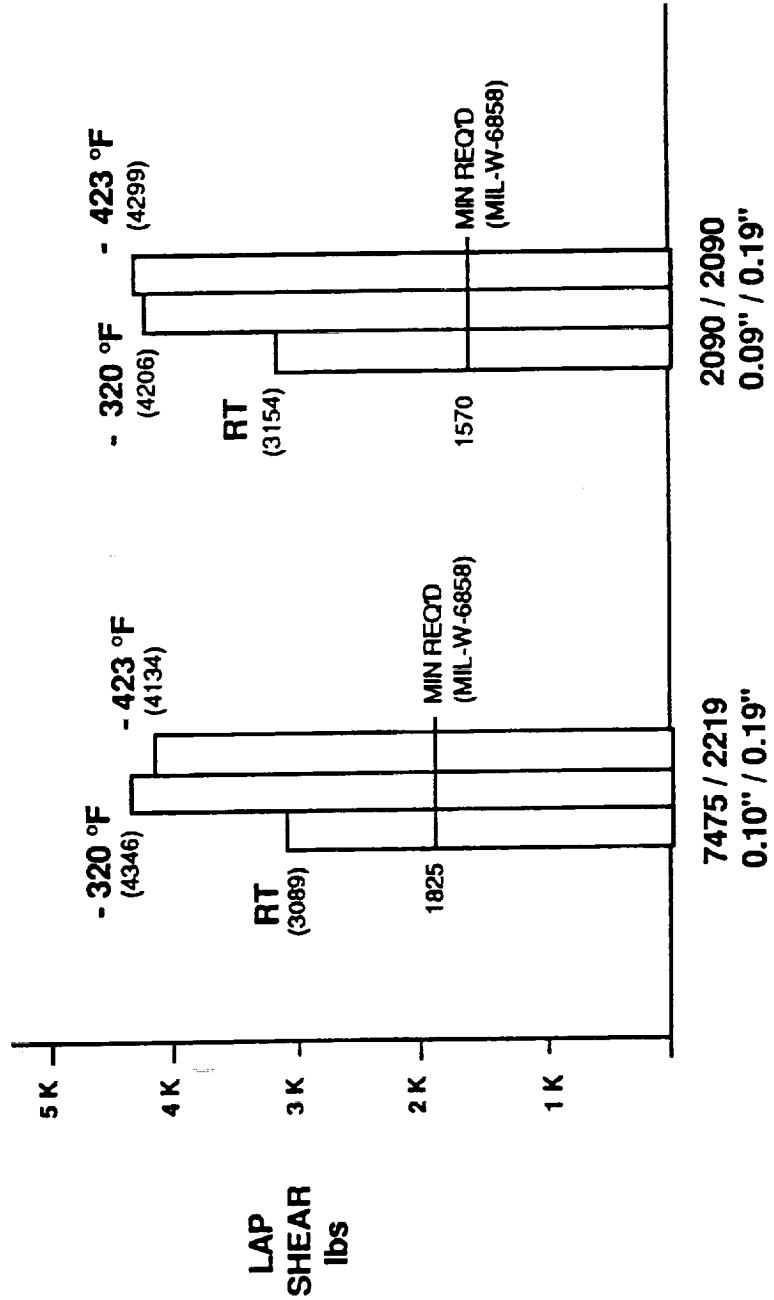
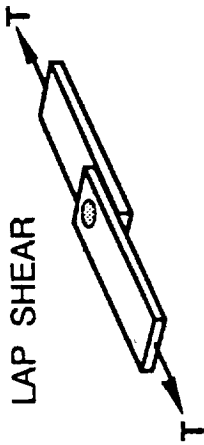


Figure 150. Summary of Mechanical Lap Shear Test Results for 0.100" 7475-T62 joined to 0.190" 2219-T81 Al, and 0.090" 2090-T62 joined to 0.190" 2090-T83 Al-Li.

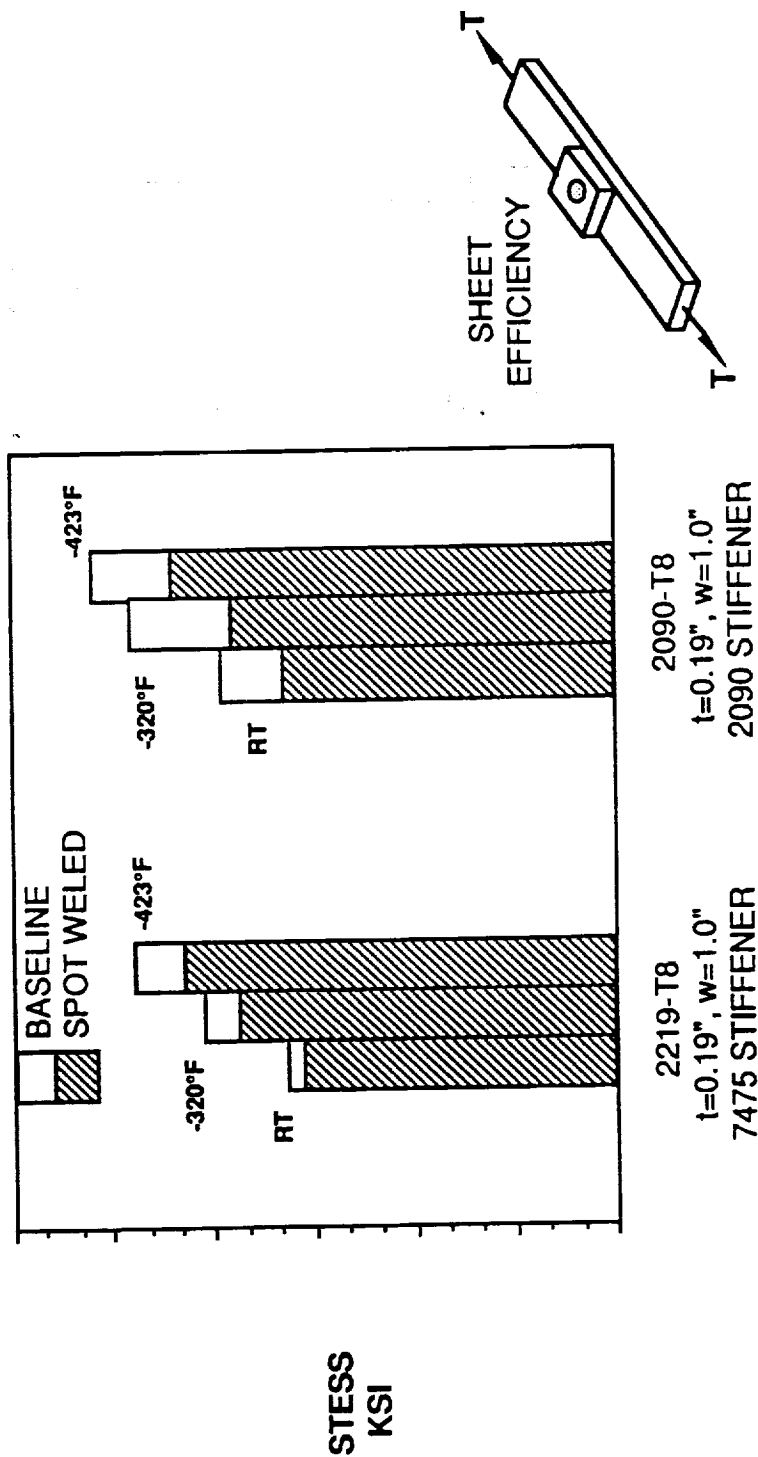
AVERAGE MACRO CROSS-SECTION MEASUREMENTS

NUGGET DIAMETER :	0.349" 0.354" 0.349"	0.406" 0.412" 0.423"	(RT) (LN ₂ , -320°F) (LH ₂ , -423°F)
------------------------------	----------------------------	----------------------------	--

	UPPER SHEET / LOWER SHEET	UPPER SHEET / LOWER SHEET	
NUGGET PENETRATION	62.0 % / 24.8 - 36.8 % : 62.0 % / 24.2 - 29.0 % 62.0 % / 23.6 - 29.0 %	67.0 % / 33.3 - 34.2 % 52.2 % / 33.3 - 37.0 % 52.5 % / 33.3 - 34.0 %	(RT) (LN ₂ , -320°F) (LH ₂ , -423°F)

- MACRO CROSS-SECTION VALUES EXCEED MIL-W-6858 REQUIREMENTS.

Figure 151. Summary of Spot Weld Nugget Quality for 0.100" 7475-T62 joined to 0.190" 2219-T81 Al, and 0.090" 2090-T62 joined to 0.190" 2090-T83 Al-Li.



SHEET EFFICIENCY	RT = 94.5 %	RT = 84.3 %
	-320 = 91.3 %	-320 = 79.6 %
	-423 = 90.2 %	-423 = 84.4 %

Figure 157. Summary of Sheet Efficiency for 0.100" 7475-T62 joined to 0.190" 2219-T81 Al, and 0.090" 2090-T62 joined to 0.190" 2090-T83 Al-Li.

Table 77. LH₂ (-423°F) Cryogenic Resistance Spot Weld Test Results. 0.100 inch 7475-T62 to 0.190 inch 2219-T81 Aluminum.

Schedule: Weld Heat (36 percent), Weld Time (6 cycles), Weld Force (16 psi), Forge Force (24 psi), Squeeze (55).

Coupon ID	Nugget Diameter (inch)	Nugget Penetration		Shear (lbs)
		% Upper Sheet 7475-T62	% Lower Sheet 2219-T81	
1CRY-1	0.355	75.0	30.0	
1CRY-2				3740
1CRY-3				3980
1CRY-4				4050
1CRY-5				3995
1CRY-6	0.355	60.0	20.0	
1CRY-7				4130
1CRY-8				3710
1CRY-9				3605
1CRY-10				3990
1CRY-11				3880
1CRY-12				4200
1CRY-13				4330
1CRY-14				4110
1CRY-15	0.360	65.0	25.0	
1CRY-16				3550
1CRY-17				4470
1CRY-18				4250
1CRY-19				4590
1CRY-20	0.330	50.0	23.0	
1CRY-21				4490
1CRY-22				4840
1CRY-23				4320
1CRY-24				4520
1CRY-25	0.345	60.0	20.0	
Average	0.349	62.0	23.6	4134

Mil-W-6858D Specification Limits for Acceptable Lap Shear Values: 18 out of 20 Test Values Must Fall Within Specification Limits $\pm 12.5\%$ to Pass Evaluation.

Percent Deviation from Shear Value	-25.0%	-12.5%	Mean	+12.5%	+25.0%
Calculated Deviation (Lbs)	3100	3617	4134	4650	5167

Note: 17 out of 20 pass with the 12.5% deviation.

**Table 78. Results from Day One of Set One Pre-Weld Cleaning Test 0.100"
7475-T62 Joined to 0.190" 2219-T81 Aluminum.**

I.D. Set/#	Weld Heat (Cyc. - %)	Nugget Diam. (in.)	Upper Penetration (in.)	Min. Lower Penetration (in.)	Max. Lower Penetration (in.)	Surface Resistance ($\mu\Omega$)	Shear (lbs)
1P1/1	36	0.350	0.075	0.015	0.045	17	3677
1P1/2	36					65	
1P1/3	36	0.325	0.050	0.025	0.055	22	
1P1/4	36					40	
1P1/5	36	0.300	0.050	0.020	0.050	30	
1P1/6	36					52	
1P1/7	36	0.265	0.045	0.010	0.015	27	
Ave 1		0.310	0.055	0.018	0.041	36	3584
1P2/1	36	0.360	0.075	0.015	0.055	25	3250
1P2/2	36					33	
1P2/3	36	0.325	0.050	0.020	0.045	67	
1P2/4	36					35	
1P2/5	36	0.300	0.050	0.020	0.040	27	
1P2/6	36					31	
1P2/7	36	0.300	0.050	0.020	0.055	20	
Ave 2		0.328	0.051	0.019	0.049	34	3563

The second set (set two) of exposure coupons are shown in Table 81 through 85. The conditions and weld schedules used for the re-test sets are provided as follows:

- 1) Bagged or protected material without adjustments to the weld schedule: the weld heat = 38.5%, and weld time = 6 cycles.
- 2) Non-bagged or exposed specimens, without adjustments to the weld schedule: the weld heat = 38.5%, and weld time = 6 cycles.
- 3) Non-bagged or exposed specimens, with an adjustment to the weld schedule: the weld schedule adjustments were made to produce an acceptable weld nugget.

Batch number one of set two, was the control group for the experiment and was welded to represent material that had been cleaned just prior to welding. The control specimens were used to verify that the resistance spot weld machine and the surrounding environment would not cause the formation of unacceptable welds. The control coupons were removed from the vacuum bag and wire brushed and solvent wiped just prior to welding.

Batch two and three of set two were exposed to the environment and welded in order to assess the change in the weld quality with and without adjustments to the weld schedule. On the first day of the experiment, the materials from both of these groups were removed from the

vacuum bags, wire brushed, and exposed to the atmosphere covered only with shop packing paper in order to simulate shop environment. Welds were made each day from each of the sets and evaluated for quality. The test was halted after five days due to the inability to produce acceptable welds in the exposed material.

Table 79. Results from Day Two of Set One Pre-Weld Cleaning Test 0.100" 7475-T62 Joined to 0.190" 2219-T81 Aluminum.

I.D. Set/#	Weld Heat (Cyc. - %)	Nugget Diam. (in.)	Upper Penetration (in.)	Min. Lower Penetration (in.)	Max. Lower Penetration (in.)	Surface Resistance ($\mu\Omega$)	Shear (lbs)
1P3/1	36	0.325	0.050	0.015	0.050	35	3476
1P3/2	36					77	
1P3/3	36	0.365	0.065	0.025	0.040	86	
1P3/4	36					20	
1P3/5	36	0.325	0.050	0.020	0.050	68	
1P3/6	36					35	
1P3/7	36	0.325	0.055	0.025	0.045	95	
Ave 3		0.335	0.055	0.021	0.046	59	3280
1P4/1	36	0.360	0.060	0.010	0.050	25	3609
1P4/2	37					25	
1P4/3	37	0.375	0.075	0.015	0.060	30	
1P4/4	37					26	
1P4/5	37	0.370	0.065	0.025	0.045	20	
1P4/6	37					19	
1P4/7	37	0.350	0.065	0.015	0.060	20	
Ave 4		0.364	0.066	0.016	0.054	24	3498
1P5/1	36	0.350	0.050	0.010	0.045	15	3463
1P5/2	37					17	
1P5/3	37	0.375	0.070	0.025	0.075	30	
1P5/4	37					18	
1P5/5	37	0.350	0.060	0.025	0.065	25	
1P5/6	37					23	
1P5/7	37	0.350	0.060	0.015	0.040	30	
Ave 5		0.356	0.060	0.019	0.056	23	3469

**Table 80. Results from Day Three of Set One Pre-Weld Cleaning Test 0.100"
7475-T62 Joined to 0.190" 2219-T81 Aluminum.**

I.D. Set/#	Weld Heat (Cyc. - %)	Nugget Diam. (in.)	Upper Penetration (in.)	Min. Lower Penetration (in.)	Max. Lower Penetration (in.)	Surface Resistance ($\mu\Omega$)	Shear (lbs)
1P6/1	35	0.370	0.055	0.015	0.050	*	2896
1P6/2	36					150	
1P6/3	36	0.375	0.060	0.025	0.065	*	2933
1P6/4	36					45	
1P6/5	36	0.350	0.050	0.020	0.050	45	3341
1P6/6	36					25	
1P6/7	36	0.350	0.060	0.020	0.050	40	
Ave 6		0.361	0.056	0.020	0.054	61	3057
1P7/1	36	0.350	0.060	0.015	0.050	60	3104
1P7/2	37					54	
1P7/3	37	0.375	0.065	0.030	0.080	42	3167
1P7/4	37					60	
1P7/5	37	0.375	0.050	0.025	0.065	42	3226
1P7/6	37					57	
1P7/7	37	0.325	0.050	0.015	0.040	61	
Ave 7		0.356	0.056	0.021	0.059	54	3166

Welding difficulties were encountered on the first day of the program. However, the testing was continued for five days. The nugget penetration and surface resistance data were recorded throughout the duration of the test and are included as Tables 81 through 85.

Surface resistivity for the material was within the mil-spec requirement of 50 $\mu\Omega$ maximum for every day of testing. However, due to problems encountered with the weld equipment during the entire test program, the minimum and maximum penetration into the lower sheet was far below normal values for the material combination. The nugget penetration for each set of coupons was similar for all of the day one specimens, but appeared to get worse as the week progressed. The steady decline in the penetration values into the lower sheet for the material that had been exposed to the "shop" environment versus the "bagged, or protected" material, did not warrant continuation of the test past day five. It is still unclear as to the maximum duration for spot weld cleanliness for the 7475-T62 to 2219-T81 material combination, however, since two test programs have been completed on this material combination with results indicating problems after five days of welding, it is safe to assume that the material must be vacuum bagged if welding is not to occur during the same week as cleaning.

**Table 81. Results from Day One of Set Two Pre-Weld Cleaning Test 0.100"
7475-T62 Joined to 0.190" 2219-T81 Aluminum.**

I.D. Set/#	Weld Heat (Cyc. - %)	Nugget Diam. (in.)	Min. Upper Penetration (in.)	Max. Upper Penetration (in.)	Min. Lower Penetration (in.)	Max. Lower Penetration (in.)	Surface Resistance ($\mu\Omega$)
1/1	6 - 38.5	0.319	0.047	0.050	0.014	0.043	25
1/2	6 - 38.5	0.327	0.050	0.056	0.013	0.056	20
1/3	6 - 38.5	0.319	0.046	0.050	0.012	0.042	21
1/4	6 - 38.5	0.296	0.044	0.046	0.011	0.025	18
1/5	6 - 38.5	0.334	0.050	0.053	0.016	0.051	15
1/6	6 - 38.5	0.309	0.045	0.046	0.013	0.031	20
Ave 1		0.317	0.047	0.050	0.013	0.041	20
2/1	6 - 38.5	0.330	0.048	0.051	0.019	0.063	30
2/2	6 - 38.5	0.304	0.043	0.046	0.013	0.044	27
2/3	6 - 38.5	0.319	0.049	0.050	0.011	0.036	33
2/4	6 - 38.5	0.306	0.046	0.046	0.011	0.050	30
2/5	6 - 38.5	0.334	0.052	0.057	0.018	0.060	40
2/6	6 - 38.5	0.318	0.047	0.050	0.014	0.052	39
Ave 2		0.319	0.048	0.050	0.014	0.051	33
3/1	6 - 38.5	0.344	0.046	0.050	0.017	0.056	21
3/2	6 - 38.5	0.313	0.046	0.048	0.012	0.037	22
3/3	6 - 38.5	0.332	0.047	0.053	0.015	0.050	15
3/4	6 - 38.5	0.320	0.049	0.051	0.017	0.065	20
3/5	6 - 38.5	0.342	0.054	0.057	0.014	0.054	17
3/6	6 - 38.5	0.309	0.048	0.050	0.014	0.054	20
Ave 3		0.327	0.048	0.052	0.015	0.053	19

**Table 82. Results from Day Two of Set Two Pre-Weld Cleaning Test 0.100"
7475-T62 Joined to 0.190" 2219-T81 Aluminum.**

I.D. Set/#	Weld Heat (Cyc. - %)	Nugget Diam. (in.)	Min. Upper Penetration (in.)	Max. Upper Penetration (in.)	Min. Lower Penetration (in.)	Max. Lower Penetration (in.)	Surface Resistance ($\mu\Omega$)
1/7	6 - 38.5	0.355	0.045	0.051	0.017	0.056	20
1/8	6 - 38.5	0.320	0.043	0.046	0.011	0.037	21
1/9	6 - 38.5	0.329	0.049	0.050	0.013	0.036	21
1/10	6 - 38.5	0.308	0.040	0.040	0.011	0.028	20
1/11	6 - 38.5	0.325	0.046	0.048	0.015	0.050	26
1/12	6 - 38.5	0.281	0.052	0.053	0.015	0.046	25
Ave 1		0.320	0.046	0.048	0.014	0.042	22
2/7	6 - 38.5	0.352	0.055	0.058	0.019	0.060	21
2/8	6 - 38.5	0.325	0.045	0.045	0.013	0.054	20
2/9	6 - 38.5	0.332	0.054	0.056	0.019	0.068	21
2/10	6 - 38.5	0.314	0.047	0.048	0.012	0.044	21
2/11	6 - 38.5	0.333	0.046	0.050	0.012	0.047	20
2/12	6 - 38.5	0.321	0.049	0.050	0.014	0.057	22
Ave 2		0.330	0.040	0.051	0.015	0.055	21

**Table 83. Results from Day Three of Set Two Pre-Weld Cleaning Test 0.100"
7475-T62 Joined to 0.190" 2219-T81 Aluminum.**

I.D. Set/#	Weld Heat (Cyc. - %)	Nugget Diam. (in.)	Min. Upper Penetration (in.)	Max. Upper Penetration (in.)	Min. Lower Penetration (in.)	Max. Lower Penetration (in.)	Surface Resistance ($\mu\Omega$)
1/13	6 - 38.5	0.323	0.045	0.046	0.015	0.046	8
1/14	6 - 38.5	0.349	0.054	0.056	0.017	0.054	8
1/15	6 - 38.5	0.342	0.045	0.049	0.017	0.056	11
1/16	6 - 38.5	0.333	0.051	0.053	0.015	0.054	6
1/17	6 - 38.5	0.346	0.049	0.051	0.015	0.060	8
1/18	6 - 38.5	0.228	0.058	0.060	0.019	0.061	13
Ave 1		0.337	0.050	0.053	0.016	0.055	9
2/13	6 - 38.5	0.319	0.043	0.046	0.007	0.036	23
2/14	6 - 38.5	0.321	0.047	0.049	0.013	0.029	15
2/15	6 - 38.5	0.336	0.051	0.053	0.016	0.058	13
2/16	6 - 38.5	0.296	0.056	0.063	0.015	0.045	15
2/17	6 - 38.5	0.332	0.048	0.052	0.014	0.050	13
2/18	6 - 38.5	0.280	0.042	0.045	0.016	0.032	17
Ave 2		0.314	0.048	0.051	0.014	0.042	16

**Table 84. Results from Day Four of Set Two Pre-Weld Cleaning Test 0.100"
7475-T62 Joined to 0.190" 2219-T81 Aluminum.**

I.D. Set/#	Weld Heat (Cyc. - %)	Nugget Diam. (in.)	Min. Upper Penetration (in.)	Max. Upper Penetration (in.)	Min. Lower Penetration (in.)	Max. Lower Penetration (in.)	Surface Resistance ($\mu\Omega$)
1/19	6 - 38.5	0.255	0.043	0.046	0.006	0.013	5
1/20	6 - 38.5	0.322	0.050	0.052	0.015	0.046	10
1/21	6 - 38.5	0.344	0.056	0.058	0.018	0.067	12
1/22	6 - 38.5	0.300	0.045	0.047	0.016	0.053	15
1/23	6 - 38.5	0.322	0.057	0.059	0.018	0.064	22
1/24	6 - 38.5	0.221	0.050	0.054	0.015	0.037	30
Ave 1		0.311	0.050	0.053	0.015	0.047	16
2/19	6 - 38.5	0.331	0.061	0.063	0.018	0.051	16
2/20	6 - 38.5	0.303	0.043	0.044	0.019	0.052	20
2/21	6 - 38.5	0.317	0.056	0.058	0.008	0.029	15
2/22	6 - 38.5	0.310	0.040	0.041	0.013	0.015	17
2/23	6 - 38.5	0.329	0.061	0.064	0.014	0.054	18
2/24	6 - 38.5	0.321	0.052	0.053	0.008	0.019	23
Ave 2		0.319	0.052	0.054	0.013	0.037	18

Table 85. Results from Day Five of the Pre-Weld Cleaning Test 0.100" 7475-T62 Joined to 0.190" 2219-T81 Aluminum.

I.D. Set/#	Weld Heat (Cyc. - %)	Nugget Diam. (in.)	Min. Upper Penetration (in.)	Max. Upper Penetration (in.)	Min. Lower Penetration (in.)	Max. Lower Penetration (in.)	Surface Resistance ($\mu\Omega$)
1/25	6 - 38.5	0.361	0.046	0.053	0.014	0.047	11
1/26	6 - 38.5	0.315	0.053	0.056	0.013	0.058	10
1/27	6 - 38.5	0.311	0.054	0.055	0.013	0.031	5
1/28	6 - 38.5	0.330	0.053	0.0459	0.012	0.060	6
1/29	6 - 38.5	0.326	0.054	0.058	0.012	0.053	11
1/30	6 - 38.5	0.317	0.053	0.054	0.015	0.036	20
Ave 1		0.327	0.052	0.056	0.013	0.048	11
2/25	6 - 38.5	0.339	0.049	0.051	0.017	0.030	15
2/26	6 - 38.5	0.293	0.043	0.046	0.011	0.025	11
2/27	6 - 38.5	0.281	0.023	0.041	0.002	0.003	25
2/28	6 - 38.5	0.296	0.042	0.043	0.009	0.014	20
2/29	6 - 38.5	0.308	0.050	0.051	0.007	0.019	20
2/30	6 - 38.5	0.313	0.051	0.052	0.012	0.030	21
Ave 2		0.305	0.043	0.047	0.010	0.020	19
3/25	6 - 38.5	0.340	0.058	0.061	0.015	0.050	19
3/26	6 - 38.5	0.323	0.038	0.040	0.009	0.020	15
3/27	6 - 38.5	0.338	0.046	0.048	0.012	0.028	22
3/28	6 - 38.5	0.322	0.040	0.042	0.010	0.024	14
3/29	6 - 38.5	0.358	0.049	0.054	0.012	0.038	11
3/30	6 - 38.5	0.356	0.047	0.049	0.007	0.032	13
Ave 3		0.340	0.046	0.049	0.013	0.032	16

4.3.2.1.5 Weld Cycle Tolerance

A weld heat sensitivity test was conducted in order to determine how high or low the weld heat could be set (tolerance off of optimum setting) and still obtain acceptable spot welds. The results from the tests for the tests are shown as Figures 153 and 155. The heat sensitivity versus nugget diameter show that below 32 percent heat, the nugget diameter for the 7475/2219 Al combination falls below the minimum required by the MIL-W-6858 standard. The nugget diameter continues to climb until approximately 37 percent heat is reached after which it begins to decline again, and expulsion is observed.

The heat sensitivity versus nugget penetration graph (Figure 154) shows that below 33 percent heat, the penetration into the lower sheet (the 2219-T81 skin) is below the requirement called out by the MIL-W-6858 specification. However, as the heat is increased, the percentage of penetration into the lower sheet is increased which if excessive would manifest itself into a reduction in skin efficiency. The lap-shear values versus heat sensitivity are shown as Figure 155.

The increase in lap shear with weld heat percent is clearly shown on the chart. Based upon the behavior noted during the tests, a weld heat of 35% (the heat is adjusted upward slightly for multiple spot panels in order to account for the shunting effects) was selected for weld certification.

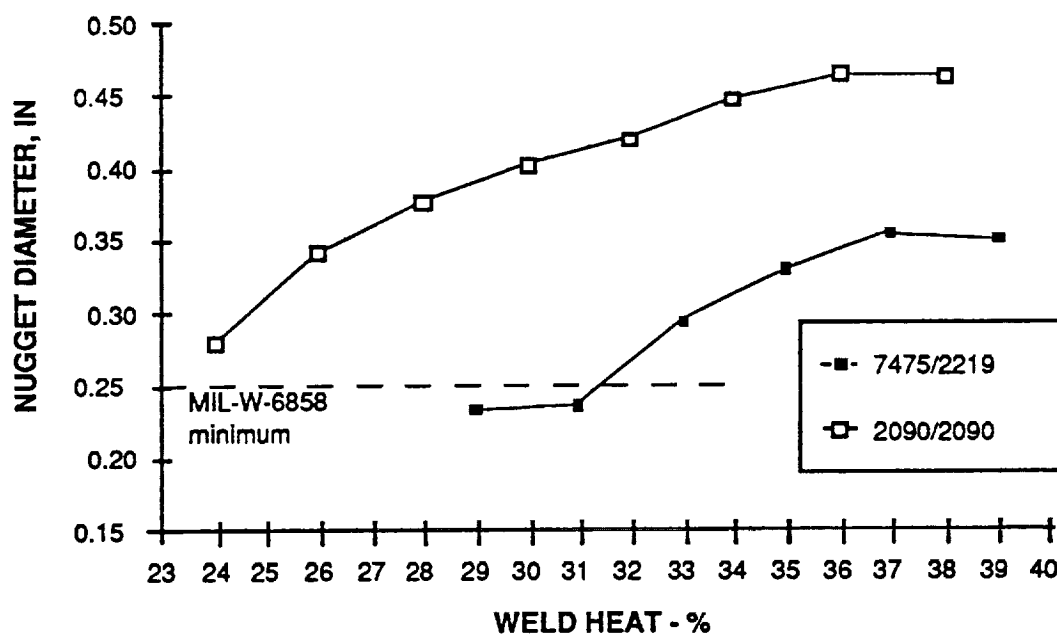


Figure 153. Weld Heat Sensitivity Versus Nugget Diameter for 0.100" 7475-T62 Al Joined to 0.190" and 0.090" 2090-T62 Joined to 0.190" 2090-T83 Al-Li.

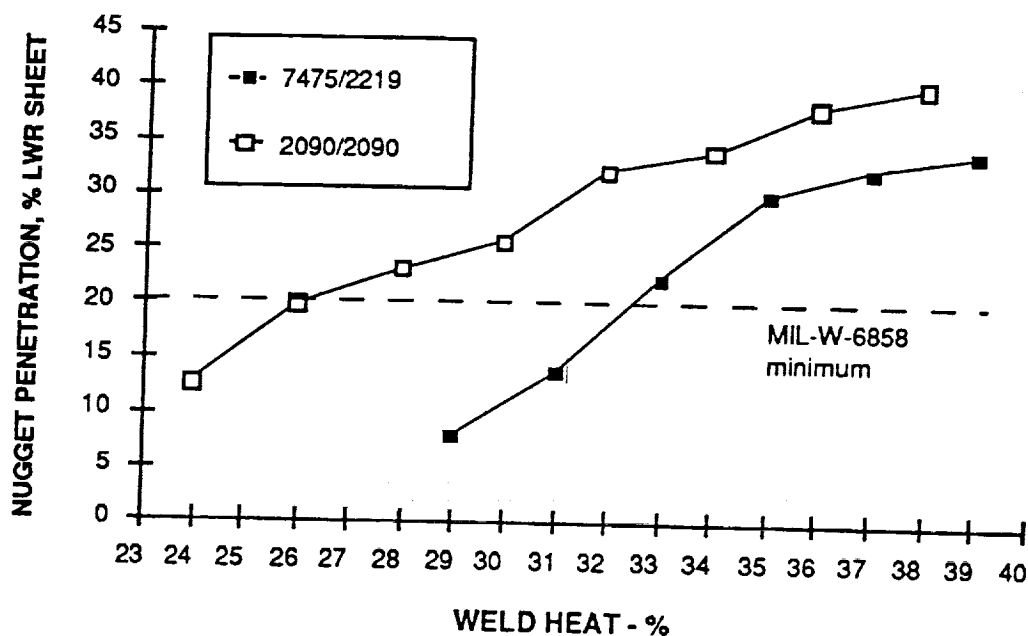


Figure 154. Weld Heat Sensitivity Versus Nugget Penetration into Lower Sheet for 0.100" 7475-T62 Al Joined to 0.190" and 0.090" 2090-T62 Joined to 0.190" 2090-T83 Al-Li.

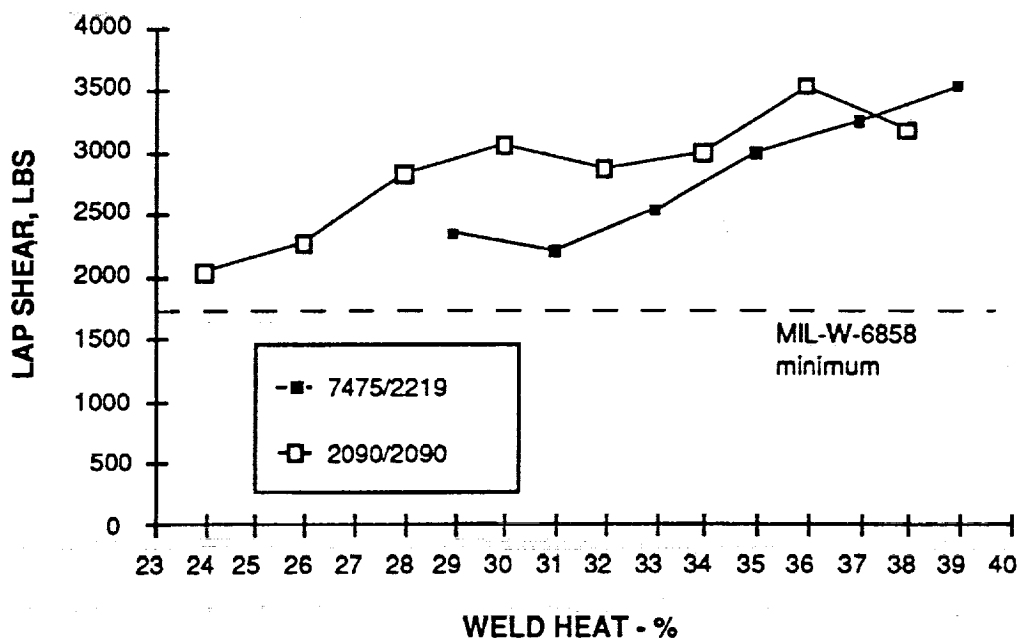


Figure 155. Weld Heat Sensitivity Versus Lap Shear for 0.100" 7475-T62 Al Joined to 0.190" and 0.090" 2090-T62 Joined to 0.190" 2090-T83 Al-Li.

All three values (nugget diameter, nugget penetration, and lap shear) are very sensitive to changes in the overall heat input into the system. All three parameters increased as the heat increased from 29 to 38 percent and definite lowest acceptable heat input (33 %) to the system was recorded for the material combination. Upper boundaries are dependent upon acceptable loss in skin efficiency prior to expulsion of the weld to the design .

4.3.2.2 Resistance Spot Weld Characterization 2090-T62 to 2090-T83 Aluminum-Lithium

The resistance spot weld schedule development was initiated for 0.090" 2090-T62 to 0.190" 2090-T83 aluminum-lithium material using a Taguchi L9 array (refer to Table 86).

Table 86. L9 Taguchi Test Matrix for 0.090" 2090-T62 Al-Li joined to 0.190" 2090-T83 Al-Li.

	A Weld Time Cycles	B Weld Heat Percent	C Weld Force Pounds	D Forge Force Pounds
Test 1	5	26	2400	6000
Test 2	5	32	2700	6500
Test 3	5	38	3000	7000
Test 4	6	26	2700	7000
Test 5	6	32	3000	6000
Test 6	6	38	2400	6500
Test 7	7	26	3000	6500
Test 8	7	32	2400	7000
Test 9	7	38	2700	6000

Each test schedule (one through 9) was performed with ten replicate specimens that were evaluated metallographically, through lap shear, and by tensile for sheet efficiency (three lap shears, four macros, and three sheet efficiency test specimens). Average test values were obtained for each test (one through 9) and the values are presented in Table 87. The data was adjusted to incorporate reduction in the average values due to weld expulsion. The adjusted average values were input into the L9 response tables in order to determine the most significant factors and the optimum weld schedule for the current material combination. The data showed the same trend as previous Taguchi tests, in that the most significant factor for the weld is the heat, followed by the weld force and time. The optimum weld schedule derived from the response tables is as follows: Weld Time = 5 Cycles, Weld Force = 3000 pounds, Weld Heat = 32 percent, Forge Force = 7000 pounds. Confirmatory tests were conducted using the aforementioned schedule. The resistance

spot weld macro examinations (percent penetration, and nugget diameter) and shear testing, and sheet efficiency results from optimum resistance spot weld schedule generated with the Taguchi array are shown on Table 88.

Table 87. Average Test Results for 0.090" 2090-T62 to 0.190" 2090-T83 Al-Li L9 Taguchi Array.

Test I.D.	Nugget Diameter (inch)	Nugget Penetration		Shear (pounds)	Sheet Efficiency (ratio, %)*
		% Upper Sheet	% Lower Sheet		
1	0.360	54.2	17.78	2661	91.3
2	0.406	61.15	30.28	3295	89.6
3	0.228	33.35	12.5	3480	88.2
4	0.376	44.43	23.03	2656	90.0
5	0.485	70.85	41.45	3447	87.3
6	0	0	0	0	0
7	0.404	51.4	34.20	2940	88.0
8	0.373	58.33	38.83	2700	0
9	0	0	0	0	0

*Note: Sheet efficiency is a ratio of the welded to non-welded F_{tu} of the skin material.

Table 88. Conformity Test Results for 0.090" 2090-T62 to 0.190" 2090-T83 Al-Li Optimized Resistance Spot Weld Schedule.

Schedule: Weld Time = 5 Cycles, Weld Force = 3000 pounds, Weld Heat = 32 percent, Forge Force = 7000 pounds

Nugget Diameter inch	Nugget Penetration		Shear Lbs.	Weld Quality
	% Upper Sheet	% Lower Sheet		
0.410	66.7	34.2	-	good
-	-	-	2895	good
0.415	72.2	31.6	-	good
-	-	-	2845	good
0.415	72.2	31.6	-	good
-	-	-	2538	good
0.410	66.7	34.2	-	good
0.4125	69.5	32.9	2759	: Averages

The MIL-W-6858 specification for resistance spot welded aluminum for a 0.090" to 0.190" thickness combination requires the following:

Minimum Average Shear Strength = 1570 pounds

Minimum Nugget Diameter = 0.240"

Nugget Penetration: Minimum = 20% of thinner sheet
Maximum = 80% of thinner sheet

The results from the confirmatory run exceed the standards requirements in all classifications, and the schedule was utilized during the remainder of the testing with this thickness ratio.

4.3.2.2.1 Weld Cycle Development

Resistance spot weld certification tests were performed according to MIL-W-6858D class A requirements. The test was used to certify weld schedules developed by Taguchi design of experiments techniques for optimization of a process. The test results are reported in Table 89.

Table 89. Weld Certification Test Results for 0.090" 2090-T62 to 0.190" 2090-T83 Al-Li Optimized Resistance Spot Weld Schedule.

Schedule: Weld Time = 5 Cycles, Weld Force = 19 psi, Weld Heat = 32 percent, Forge Force = 27 psi, Squeeze = 55

Coupon I.D.	Nugget Diameter inch	Nugget Penetration		Shear Lbs.
		% Upper Sheet	% Lower Sheet	
CT2-1	0.395	55.5	33.0	2940
CT2-2				2834
CT2-3				3430
CT2-4				3105
CT2-5				
CT2-6				3012
CT2-7				2995
CT2-8				3243
CT2-9				3203
CT2-10	0.415	61.1	33.0	
CT2-11				2967
CT2-12				3276
CT2-13				3555
CT2-14	0.410	66.6	33.0	3344
CT2-15				
CT2-16				3196
CT2-17				3119
CT2-18				3352
CT2-19	0.400	61.1	33.0	3272
CT2-20				
CT2-21				3034
CT2-22				3303
CT2-23				3011
CT2-24				2907
CT2-25	0.410	61.1	33.0	
Average	0.406	62.2	33.0	3155

The MIL-W-6858 specification for resistance spot welded aluminum -lithium for a 0.090" to 0.190" thickness combination requires the following:

Percent Deviation	-25.0%	-12.5%	Mean	+12.5%	+25.0%
Calculated Deviation	2366	2761	3155	3549	3944

18 out of 20 test values
fall within this range?

YES

Minimum Average Shear Strength = 1825 pounds	OK
Minimum Nugget Diameter = 0.250"	OK
Nugget Penetration: Minimum = 20% of thinner sheet	OK
Maximum = 80% of thinner sheet	OK

The weld schedule for the 0.090" 2090-T62 joined to 0.190" 2090-T83 aluminum-lithium passed the certification test.

Resistance Spot Weld Spacing Tests were performed to determine the effects of the resistance spot weld spacing on weld strength and quality. Test specimens were welded using the certified weld schedule with spot spacings of .075", 1.00", 1.25", and 1.50". The secondary current, nugget expansion, dynamic resistance, weld force, forge force, lap shear values, weld penetration, and nugget diameters were recorded during the weld process.

Thirty-five 0.090" 2090-T62 to 0.190" 2090-T83 spot weld spacing test specimens and seven single spot test specimens were welded. The single spot specimens were welded for use as control specimens to compare with spot spacing specimens. For each of the four different spot spacing configurations and single spot specimen, seven test coupons were welded. The seven specimens provided four micro cross sections and three lap shears test specimens. Table 90 shows the results of the spot spacing test.

From Table 90 and Figure 156, the average single-spot nugget diameter was 0.418", and the 1.50", 1.25", 1.00" and 0.75" spot spacing average nugget diameters were 0.399", 0.401", 0.372" and 0.363", respectively. There was a decrease of 0.019" from the single-spot value to the 1.50" spot spacing value. The nugget diameter values for spot spacing from 1.50" to 0.75" showed a trend towards decreasing nugget diameter.

From Table 90 and Figure 157, the average single-spot lap shear was 3,417 lbs., and the 1.50", 1.25", 1.00", and 0.75" spot spacing average nugget diameters were 3154, 2876, 3206, and 3024 lbs., respectively. There was a decrease of 263 lbs. from the single-spot value to the 1.50" spot spacing value. The lap shear values for spot spacing from 1.50' to 0.75" did not reveal any conclusive trends.

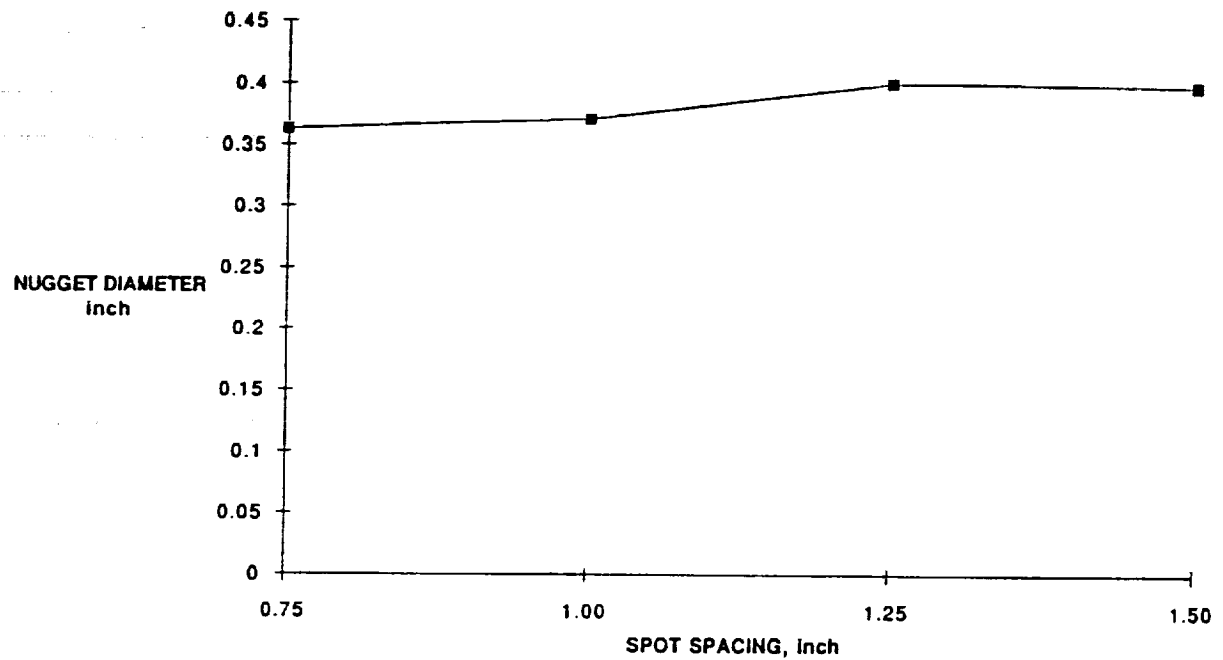


Figure 156. Resistance Spot Weld Spacing Test. Nugget Diameter Versus Spot Spacing 0.090 inch 2090-T62 to 0.190 inch 2090-T8

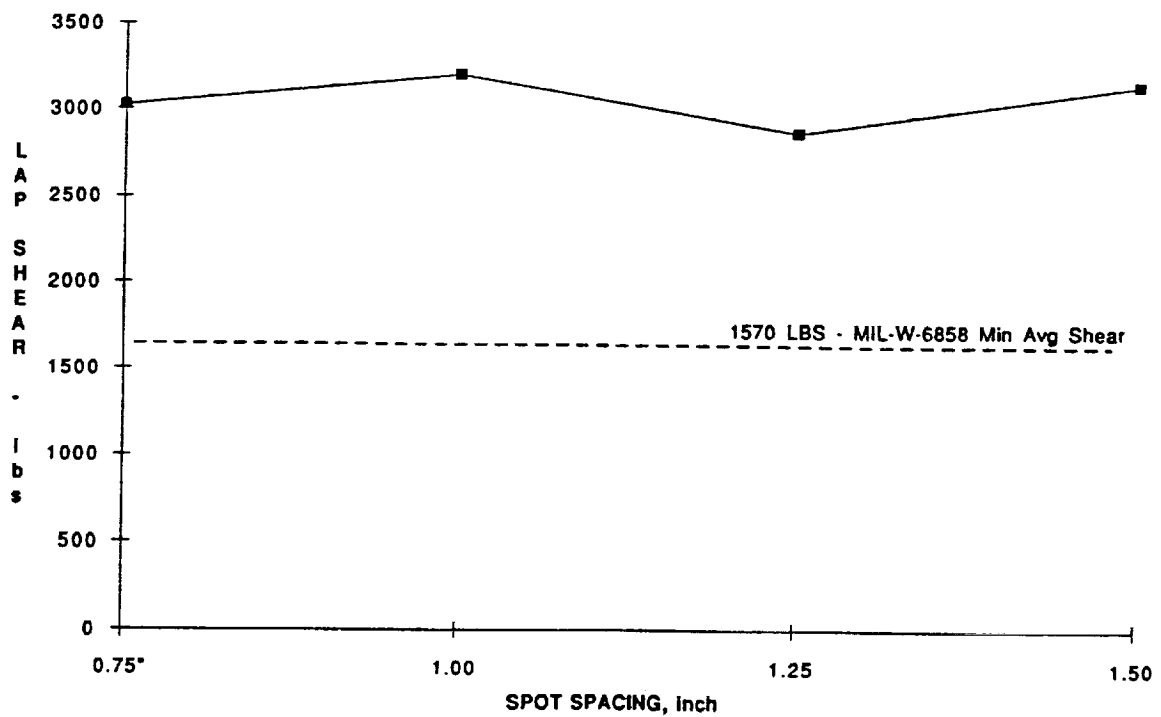


Figure 157. Resistance Spot Weld Spacing Test. Lap Shear Versus Spot Spacing 0.090 inch 2090-T62 to 0.190 inch 2090-T8

From Table 90 and Figures 158 and 159, the spot weld nugget penetration into the 0.090" sheet showed a slight increase in minimum penetration and a slight decrease in maximum penetration with the closer spot weld spacing. The penetration into the 0.190" sheet showed fairly uniform minimum penetration, but the values for maximum penetration showed erratic behavior over the range tested. The overall change in nugget penetration in relationship to the spot spacing was insignificant.

Table 90. Resistance Spot Spacing Test Results for 0.090 inch 2090-T62 to .190 inch 2090-T83 Aluminum-Lithium.

Schedule: Weld Heat (32 percent), Weld Time (5 cycles), Weld Force (19 psi), Forge Force (27 psi), Squeeze (55).

Spot Weld Spacing (inch)	Coupon I.D.	Nugget Diameter (inch)	Nugget Penetration		Shear Strength (Lbs)
			Upper Sheet (inch)	Lower Sheet (inch)	
0.75	2-1-1	0.365	.048 - .048	.021 - .032	2759
	2-1-2				
	2-1-3	0.366	.037 - .037	.023 - .037	
	2-1-4				
	2-1-5	0.355	.048 - .046	.019 - .043	
	2-1-6				
	2-1-7	0.364	.039 - .044	.021 - .036	
	Average	0.363	.043	.029	3024
1.00	2-2-1	0.366	.043 - .046	.020 - .037	2925
	2-2-2				
	2-2-3	0.365	.045 - .049	.020 - .040	
	2-2-4				
	2-2-5	0.366	.045 - .048	.020 - .040	
	2-2-6				
	2-2-7	0.392	.042 - .046	.026 - .037	
	Average	0.372	.045	.030	3206
1.25	2-3-1	0.396	.039 - .046	.022 - .052	2779
	2-3-2				
	2-3-3	0.382	.040 - .053	.023 - .046	
	2-3-4				
	2-3-5	0.417	.045 - .050	.023 - .055	
	2-3-6				
	2-3-7	0.407	.037 - .042	.026 - .047	
	Average	0.401	.044	.037	2876
1.50	2-4-1	0.402	.039 - .047	.020 - .034	2538
	2-4-2				
	2-4-3	0.417	.038 - .043	.025 - .031	
	2-4-4				
	2-4-5	0.377	.039 - .054	.022 - .035	
	2-4-6				
	2-4-7	0.398	.036 - .040	.019 - .038	
	Average	0.399	.042	.048	3154

Table 90 (continued). Resistance Spot Spacing Test Results for 0.090 inch 2090-T62 to .190 inch 2090-T83 Aluminum-Lithium.

Schedule: Weld Heat (32 percent), Weld Time (5 cycles), Weld Force (19 psi), Forge Force (27 psi), Squeeze (55).

Spot Weld Spacing (inch)	Coupon I.D.	Nugget Diameter (inch)	Nugget Penetration		Shear Strength (Lbs)
			Upper Sheet (inch)	Lower Sheet (inch)	
Single Spot	2-5-1	0.416	.040 - .047	.028 - .040	3510
	2-5-2				
	2-5-3	0.415	.033 - .043	.023 - .044	3257
	2-5-4				
	2-5-5	0.425	.036 - .050	.022 - .049	3485
	2-5-6				
	2-5-7	0.415	.035 - .050	.021 - .042	3417
	Average	0.418	.042	.033	

In conclusion, the shunting effect of close spot spacing did not degrade the integrity of the spot weld for this material combination and spot weld schedule. This certified weld schedule could be used to spot weld 0.090" 2090-T62 to 0.190" 2090-T83 at spot spacings of 0.75" or greater.

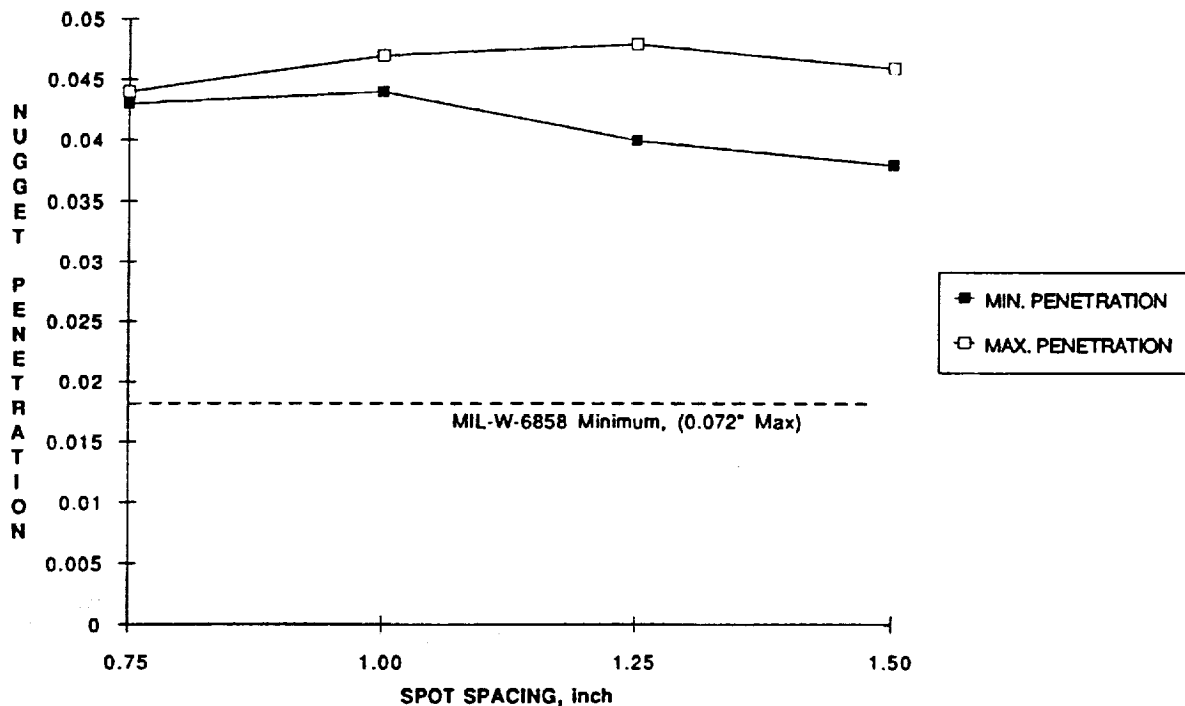


Figure 158. Resistance Spot Weld Spacing Test. 0.090" Sheet Penetration Versus Spot Spacing for 0.090 inch 2090-T62 to 0.190 inch 2090-T8

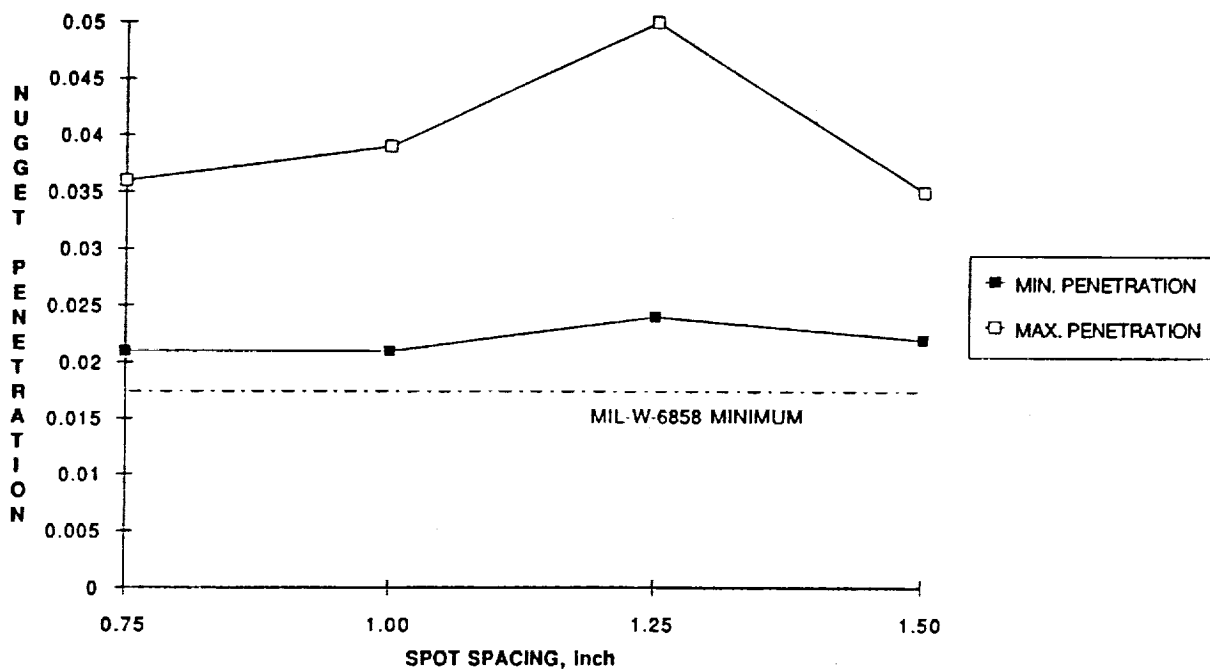


Figure 159. Resistance Spot Weld Spacing Test. 0.190 inch Sheet Penetration Versus Spot Spacing for 0.090 inch 2090-T62 to 0.190 inch 2090-T8

4.3.2.2.2 Ambient Test Data

Sheet efficiency tests were performed on the 2090-T83 material in order to determine the "knockdown" against the ultimate tensile strength for a given skin section exposed to the heat generated during the formation of a spot weld. Tensile coupons were prepared by machining 2" x 12" x 0.190" thick pieces into a "dogbone" shape with the gage section reduced in width to 1.00 inch. The sheet efficiency test results are shown in Table 91 for 2090-T83 skin.

Table 91. 0.190" 2090-T83 Aluminum-Lithium Skin Efficiency (or Reduction in Ultimate Tensile Strength) After Spot Welding of 0.090" 2090-T62 Stiffeners.

Material Type	Test Temperature (°F)	F _{tu} (ksi)	Sheet Efficiency (%)
2090-T83	20	65.9	65.9/78.3* = 84.15

* Note: Ratio taken from actual test data rather than allowable data.

The weld schedules developed for the crippling test panels (modified weld schedule developed for thinner section based upon Taguchi response) were verified through certification testing. The results from the tests are shown in Tables 92.

Table 92. Weld Schedule Certification Test for 2090 Crippling Test Panels.

Schedule: Weld Heat (35 percent), Weld Time (6 cycles), Weld Force (16 psi), Forge Force (24 psi), Squeeze (55).

Coupon ID	Nugget Diameter (inch)	Nugget Penetration		Shear (lbs.)	2090-T62 Thickness (inch)
		% upper Sheet	% Lower Sheet		
CT5-1	0.335	30.0 - 39.7	24.7	2234	0.068
CT5-2				1886	0.069
CT5-3				2080	0.071
CT5-4				2155	0.072
CT5-5					0.073
CT5-6				2087	0.074
CT5-7				2045	0.074
CT5-8				2012	0.074
CT5-9	0.343	38.9 - 50	34.7	2097	0.073
CT5-10					0.072
CT5-11				2024	0.071
CT5-12				1996	0.070
CT5-13				2210	0.068
CT5-14				2708	0.069
CT5-15					0.071
CT5-16				2238	0.072
CT5-17	0.344	36.6 - 49	33.8	2180	0.074
CT5-18				2423	0.074
CT5-19				2274	0.085
CT5-20					0.076
CT5-21				2064	0.075
CT5-22				2229	0.074
CT5-23				2154	0.074
CT5-24	0.338	35.5 - 46	32.9	2413	0.073
CT5-25					0.072
Average	0.340	36 - 47	33.0	2175	0.072

Mil-W-6858D Specification Limits for Acceptable Lap Shear Values: 18 out of 20 Test Values Must Fall Within This Range to Pass Evaluation.

Percent Deviation	-25.0%	-12.5%	Mean	+12.5%	+25.0%
Calculated Deviation (Lbs)	2182	2545	2909	3272	3636

Mil-W-6858D Minimum Values for Thinnest Sheet.

Minimum Average Shear Strength: = 1202 Lbs

Minimum Nugget Diameter = 0.220 inch

Nugget Penetration: Minimum = 20% of thinner sheet
Maximum = 80% of thinner sheet

The material supplied for the certification test consisted of formed material that had been solution heat treated and artificially aged to peak strength (-T62 condition) and sectioned into 1" x 4" test coupons. The certification test panel consisted of resistance spot welding a multi-spot (25 spot weld) test panel configuration, radiographically inspecting the panels and sectioning the panel into lap shear and metallographic specimens.

The weld schedule certification report for the 0.072" $\pm 10\%$ 2090-T62 joined to 0.190" 2090-T83 material combination (refer to Table 92) had an average nugget diameter of 0.340" with a maximum value of 0.344" and a minimum of 0.335". The minimum nugget diameter required per the military specification was 0.212" for a class A weld. The nugget penetration into the thinner sheet was a minimum of 30% with a maximum of 53%. The nugget penetration into the thicker sheet had a minimum of 25% and a maximum of 42%. The requirements for nugget penetration are that it meet or exceed twenty percent of the thickness of the thinner sheet into both sheets, and that the maximum nugget penetration shall not exceed eighty percent of the thickness of each sheet. The average lap shear test value was 2175 pounds, with a minimum of 1886 pounds. Ninety percent of the individual test values fell within the required $\pm 12.5\%$ range of the average value, and the remaining values were within the $\pm 25\%$ range. The specification requirement for average lap shear with a 0.072" thinner sheet is 1063 pounds with a minimum of 847 pounds. The spot weld schedule met the military requirements for class A welds.

4.3.2.2.3 Cryogenic Test Data

Sheet efficiency tests were performed under cryogenic temperature on the 2090-T83 material in order to determine the "knockdown" against the ultimate tensile strength for a given skin section exposed to the heat generated during the formation of a spot weld. Tensile coupons were prepared by machining 2" x 12" x 0.190" thick pieces into a "dogbone" shape with the gage section reduced in width to 1.00 inch. The cryogenic sheet efficiency test results are shown in Table 93 for 2090-T83 skin.

Cryogenic lap shear tests on the 0.090" 2090-T62 joined to 0.190" 2090-T83 material combination were performed in order to evaluate the response of the spot welds produced by the certified weld schedule operating under cryogenic temperatures. Fifty spot weld coupons were welded in sequence using the previously certified weld schedule. Forty of the fifty spot welded specimens were tested in lap shear at cryogenic temperatures; twenty at LN₂ temperatures of -320°F and twenty at LH₂ temperature of -423°F. The remaining ten coupons were processed for

micro cross-section data. The lap shear and weld nugget measurements are shown in Table 94 and Table 95.

Table 93. 0.190" 2090-T83 Aluminum-Lithium Skin Efficiency (or Reduction in Ultimate Tensile Strength) After Spot Welding of 0.090" 2090-T62 Stiffeners.

Material Type	Test Temperature (°F)	F _{tu} (ksi)	Sheet Efficiency (%)
2090-T83	-320	76.1	76.1/95.7 = 79.53
	-423	87.7	87.7/103.9 = 84.4

From the LN₂ data in Table 94, the average lap shear test value was 4206 lbs., and the minimum value was 3730 lbs. One hundred percent of the individual values were within the ± 12.5% range of the average test value. The measured nugget penetrations and diameters for all macros were within MIL-W-6858D requirements.

From the LH₂ data in Table 95, the average lap shear test value was 4299 lbs., and the minimum value was 3720 lbs. Eighty-five percent of the individual test values were within the ± 12.5% range of the average test value. The remaining 15% were within the ± 25% range of the average test value. The measured nugget penetrations and diameters for all macros were within MIL-W-6858D requirements.

4.3.2.2.4 Exposure After Cleaning

Pre-Weld Cleaning Tests were performed to determine acceptable cleaning methods for the aluminum-lithium alloy and determine the out-time after cleaning duration in which acceptable spot welds could be produced with the 0.090" 2090-T62 to 0.190" 2090-T83 material. The spot weld time duration test was planned for ten days with three tests per day totalling to thirty separate test periods; however, since no welding was performed on weekends, the total duration time was fifteen days. Secondary current, nugget expansion, dynamic resistance, weld force, forge force, lap shear values, weld penetration, nugget diameters, and surface resistance were recorded. Surface resistance readings were recorded prior to welding on both brushed and unbrushed areas with a resistance analyzer specifically for resistance spot welding.

All spot weld coupons tested were chemically cleaned, and then wire brushed with a stainless steel brush. As shown in Table 96 and Figure 160, the surface resistance varied up and

down through the duration of the test, but generally tended to increase gradually. In Table 96, values of zero were recorded used to signify a 'no reading' due to localized irregularities in the flatness of the 1" x 4" 2090-T62 spot weld coupons.

Table 94. LN₂ (-320°F) Cryogenic Resistance Spot Weld Test Results. 0.090 inch 2090-T62 to 0.190 inch 2090-T83 Aluminum-Lithium

Schedule: Weld Heat (32 percent), Weld Time (5 cycles), Weld Force (19 psi), Forge Force (27 psi), Squeeze (55).

Coupon ID	Nugget Diameter (inch)	Nugget Penetration		Shear (lbs)
		% Upper Sheet	% Lower Sheet	
3-1	0.400	44.4 - 66.6	38.9 - 66.6	4315
3-2				3930
3-3				4055
3-4				4350
3-5				
3-6				4200
3-7				4265
3-8				4055
3-9				3730
3-10	0.410	38.9 - 61.1	33.3 - 72.2	
3-11				4530
3-12				4425
3-13				4600
3-14	0.400	38.9 - 61.1	33.3 - 77.8	4175
3-15				
3-16				4360
3-17				4215
3-18				4025
3-19				4530
3-20	0.425	38.9 - 66.6	33.3 - 61.1	
3-21				4000
3-22				3910
3-23				4115
3-24				4440
3-25				
Average	0.412	52.2	50.0	4206
Min / Max		38.9 / 66.6	33.3 / 77.8	

Mil-W-6858D Specification Limits for Acceptable Lap Shear Values: 18 out of 20 Test Values Must Fall Within This Range to Pass Evaluation.

Percent Deviation	-25.0%	-12.5%	Mean	+12.5%	+25.0%
Calculated Deviation (Lbs)	3155	3680	4206	4732	5258

Mil-W-6858D Minimum Values for Thinnest Sheet

Minimum Average Shear Strength: = 1570 Lbs

Minimum Nugget Diameter = 0.240 inch

Nugget Penetration: Minimum = 20% of thinner sheet
Maximum = 80% of thinner sheet

Table 95. LH₂ (-423°F) Cryogenic Resistance Spot Weld Test Results. 0.090 inch 2090-T62 to 0.190 inch 2090-T83 Aluminum-Lithium

Schedule: Weld Heat (32 percent), Weld Time (5 cycles), Weld Force (19 psi), Forge Force (27 psi), Squeeze (55).

Coupon ID	Nugget Diameter (inch)	Nugget Penetration		Shear (lbs)
		% Upper Sheet	% Lower Sheet	
4-1	0.410	44.44 - 66.6	27.8 - 55.5	4420
4-2				4840
4-3				4180
4-4				4230
4-5				3900
4-6	0.425	44.4 - 61.1	27.8 - 72.2	4900
4-7				4600
4-8				3720
4-10				4250
4-11				4110
4-12	0.440	38.9 - 61.1	27.8 - 72.2	3860
4-13				4050
4-14				4060
4-15				4780
4-16				3970
4-17	0.415	38.9 - 66.5	27.8 - 72.2	4540
4-18				4070
4-19				4560
4-20				4560
4-21				4400
4-22	0.425	33.3 - 61.1	33.3 - 66.6	
4-23				
4-24				
4-25				
Average	0.423	52.2	47.2	4299
Min / Max		33.3 / 66.6	33.3 / 72.2	

Mil-W-6858D Specification Limits for Acceptable Lap Shear Values: 18 out of 20 Test Values Must Fall Within This Range to Pass Evaluation.

Percent Deviation	-25.0%	-12.5%	Mean	+12.5%	+25.0%
Calculated Deviation (Lbs)	3224	3762	4299	4836	5374

Note: 17 out of 20 pass with the 12.5% deviation.

Mil-W-6858D Minimum Values for Thinnest Sheet.

Minimum Average Shear Strength: = 1570 Lbs

Minimum Nugget Diameter = 0.240 inch

Nugget Penetration: Minimum = 20% of thinner sheet
Maximum = 80% of thinner sheet

Table 96. Resistance Spot Welding Pre-Weld Cleaning Test Results for 0.090 inch 2090-T62 to 0.190 inch 2090-T83 Aluminum-Lithium.

Coupon I.D.	Nugget Diameter (inch)	Nugget Penetration		Shear Strength (Lbs)	S/R Unbrushed ($\mu\Omega$)	S/R Brushed ($\mu\Omega$)
		Upper Sheet (inch)	Lower Sheet (inch)			
Day 1, 12:00PM						
2-1-1	0.440	.035 - .055	.035 - .070		48	20
2-1-2				3406	50	20
2-1-3	0.425	.035 - .060	.027 - .065		48	25
2-1-4				3533	50	16
2-1-5	0.425	.033 - .055	.030 - .060		55	15
2-1-6				3147	65	18
2-1-7	0.435	.035 - .055	.025 - .065		55	24
Average	0.431	.035 - .056	.029 - .065	3362	53	20
Day 2, 12:00PM						
2-2-1	0.435	.036 - .060	.030 - .050		54	
2-2-2				3765	57	31
2-2-3	0.440	.035 - .065	.027 - .070		54	85
2-2-4				2870	65	
2-2-5	0.420	.035 - .065	.025 - .060		55	24
2-2-6				2749		
2-2-7	0.405	.033 - .055	.030 - .060		55	30
Average	0.425	.035 - .061	.028 - .060	3128	57	43
Day 3, 12:00PM						
2-3-1	0.459	.042 - .060	.023 - .041		60	
2-3-2				3604		58
2-3-3	0.413	.043 - .052	.024 - .052		60	
2-3-4				3479	82	
2-3-5	0.393	.042 - .057	.019 - .037		55	50
2-3-6				3386	67	45
2-3-7	0.441	.048 - .048	.018 - .045		55	50
Average	0.427	.044 - .047	.021 - .044	3490	63	51
Day 4, 12:00PM						
2-4-1	0.409	.041 - .051	.025 - .038		50	36
2-4-2				3539	40	24
2-4-3	0.430	.034 - .046	.026 - .055		50	21
2-4-4				3262	60	47
2-4-5	0.423	.040 - .048	.026 - .048		69	50
2-4-6				3394	64	51
2-4-7	0.421	.033 - .0542	.029 - .055		69	48
Average	0.421	.037 - .047	.027 - .049	3398	57	40
Day 5, 12:00PM						
2-5-1	0.423	.041 - .060	.025 - .033		63	36
2-5-2				3470	63	43
2-5-3	0.424	.032 - .043	.034 - .059		63	25
2-5-4				3195	60	60
2-5-5	0.435	.037 - .051	.027 - .051		73	45
2-5-6				3534	63	53
2-5-7	0.392	.033 - .038	.026 - .048		73	51
Average	0.419	.036 - .048	.028 - .048	3400	65	45

Table 96 (continued). Resistance Spot Welding Pre-Weld Cleaning Test Results for 0.090 inch 2090-T62 to 0.190 inch 2090-T83 Aluminum-Lithium.

Coupon I.D.	Nugget Diameter (inch)	Nugget Penetration Upper Sheet (inch) Lower Sheet (inch)		Shear Strength (Lbs)	S/R Unbrushed ($\mu\Omega$)	S/R Brushed ($\mu\Omega$)
Day 8, 12:00PM						
2-6-1	0.427	.039 - .048	.024 - .051		82	45
2-6-2				3250	56	36
2-6-3	0.406	.027 - .039	.034 - .063		82	56
2-6-4				3575	56	31
2-6-5	0.429	.046 - .055	.023 - .042		75	37
2-6-6				3445	50	35
2-6-7	0.422	.030 - .046	.028 - .038		75	27
Average	0.421	.0336 - .047	.027 - .049	3423	68	33
Day 9, 12:00PM						
2-7-1	0.405	.030 - .046	.028 - .038		90	65
2-7-2				3080	95	53
2-7-3	0.434	.039 - .044	.025 - .054		90	67
2-7-4				3525	81	35
2-7-5	0.437	.040 - .055	.027 - .040		73	51
2-7-6				3105	76	56
2-7-7	0.428	.035 - .044	.027 - .052		73	75
Average	0.426	.036 - .047	.027 - .046	3237	83	57
Day 10, 12:00P						
2-8-1	0.456	.031 - .054	.022 - .041		121	55
2-8-2				3072	115	50
2-8-3	0.434	.037 - .047	.025 - .053		121	93
2-8-4				3299	110	44
2-8-5	0.419	.038 - .049	.031 - .041		130	69
2-8-6				3475	109	61
2-8-7	0.397	.039 - .056	.019 - .039		130	75
Average	0.427	.036 - .052	.024 - .044	3282	119	64
Day 11, 12:00PM						
2-9-1	0.449	.025 - .047	.019 - .049		90	65
2-9-2				3224	75	55
2-9-3	0.439	.031 - .046	.028 - .052		90	50
2-9-4				3548	66	30
2-9-5	0.411	.035 - .047	.025 - .039		84	65
2-9-6				3524	61	20
2-9-7	0.416	.041 - .053	.025 - .037		84	60
Average	0.429	.033 - .048	.024 - .044	3432	79	49
Day 14, 12:00PM						
2-10-1	0.423	.032 - .045	.024 - .035		90	45
2-10-2				3162	105	33
2-10-3	0.406	.037 - .049	.030 - .036		90	64
2-10-4				3128	77	43
2-10-5	0.389	.035 - .047	.021 - .033		80	20
2-10-6				3162	64	27
2-10-7	0.411	.027 - .043	.020 - .033		80	27
Average	0.407	.033 - .046	.024 - .034	3151	84	37

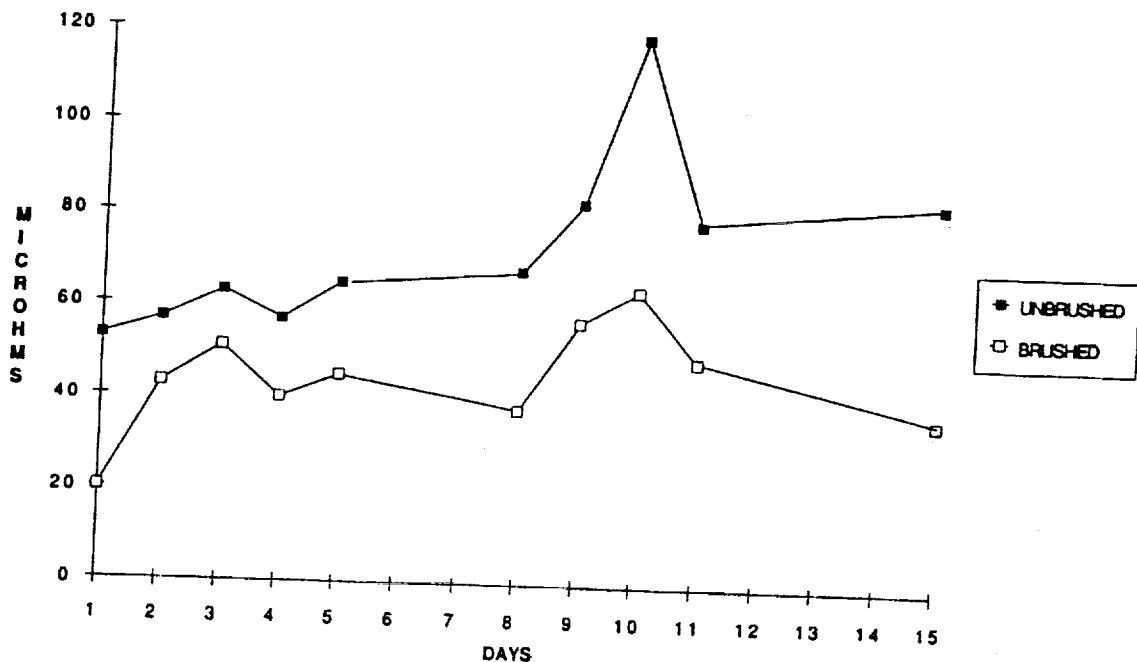


Figure 160. Pre-weld Cleaning Test, Surface Resistance Versus Time. 0.090 inch 2090-T62 to 0.190 inch 2090-T83.

Lap shear values, as shown in Table 96 and Figure 161, did not vary significantly from Day 1 to 15. The average shear value was 3,330 lbs., compared to the spot weld certification value of 3,154 lbs. The high and low values were 3,490 lbs. and 3,128 lbs., respectively, giving a range of 362 lbs. These high and low values varied from -6% to +5% of the 3,330 lbs. average value.

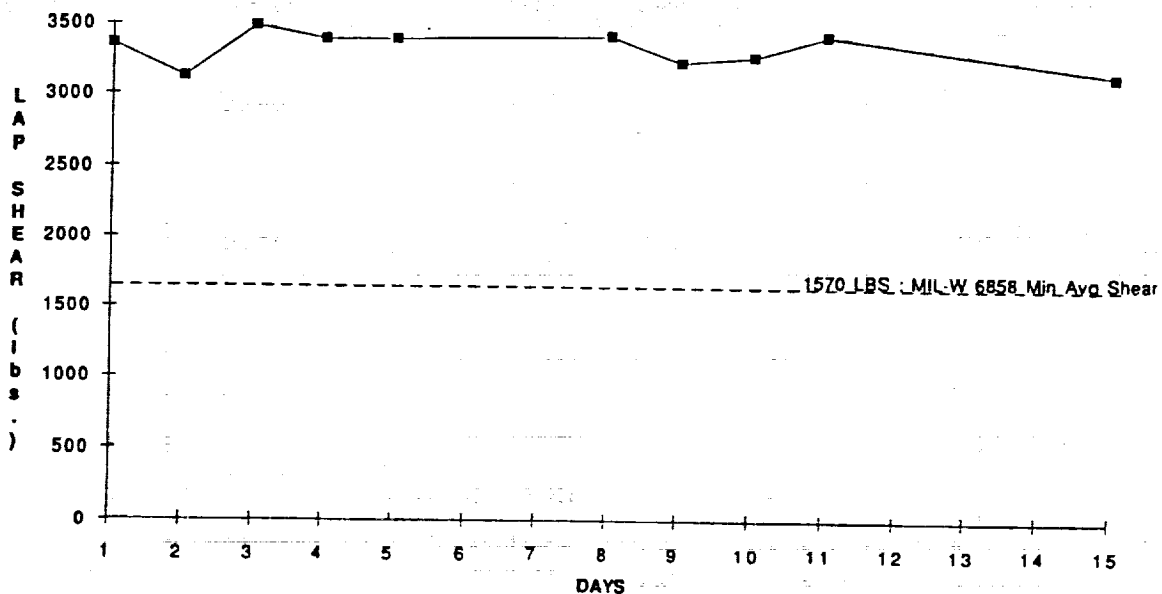


Figure 161. Pre-weld Cleaning Test, Lap Shear Versus Time. 0.090 inch 2090-T62 to 0.190 inch 2090-T83.

Nugget diameters, recorded in Table 96 and Figure 162, did not vary significantly from Day 1 to 15. The average nugget diameter was 0.423", compared to the spot weld certification value of 0.406". The high and low values were 0.431 and 0.407", respectively, giving a range of 0.024". These high and low values varied from -4% to +2% of the 0.406" average value.

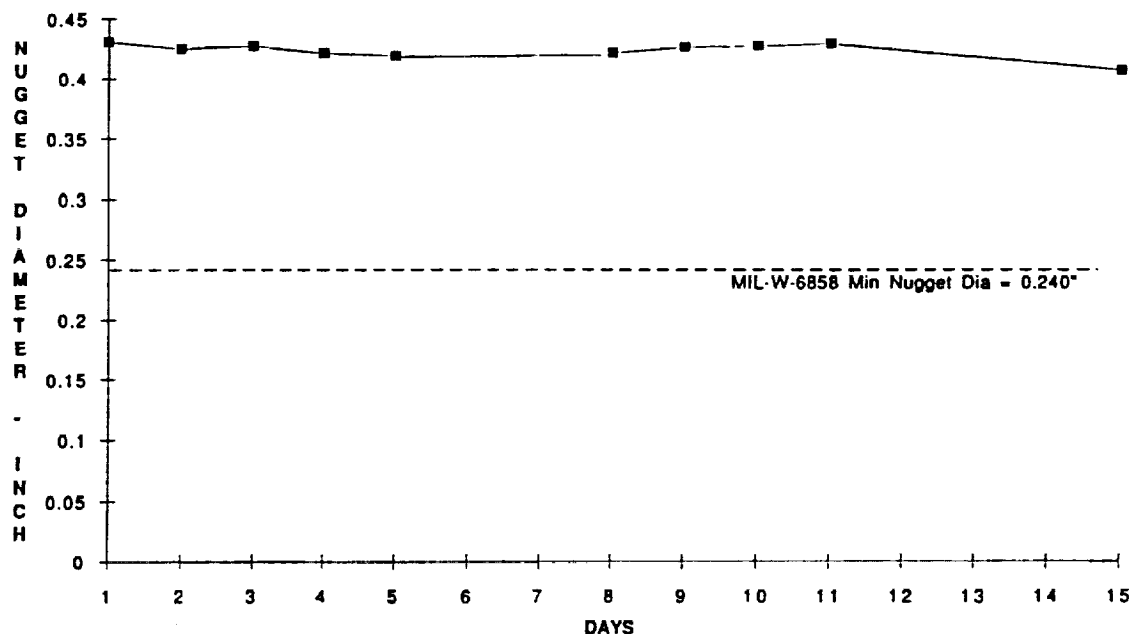


Figure 162. Pre-weld Cleaning Test, Nugget Diameter Versus Time. 0.090 inch 2090-T62 to 0.190 inch 2090-T83.

The minimum nugget penetration (as shown in Table 96 and Figure 163) into the 0.090" sheet had an average value of 0.036". The high and low values were 0.044" and 0.033", respectively, giving a range of 0.011". These high and low values varied from -8% to +22% of the 0.036" average value. The maximum penetration into the 0.090" sheet had an average value of 0.051". The high and low values were 0.061" and 0.046", respectively, giving a range of 0.015". These high and low values varied from -10% to +20% of the 0.051" average value.

The minimum nugget penetration into the 0.190" sheet (refer to Table 96 and Figure 164) had an average value of 0.026". The high and low values were 0.029" and 0.021", respectively, giving a range of 0.008". These high and low values varied from -19% to +20% of the 0.026" average value. The maximum penetration into the 0.090" sheet had an average value of 0.048". The high and low values were 0.065" and 0.034", respectively, giving a range of 0.031". These high and low values varied from -29% to +35% of the 0.048" average value.

In conclusion, the 0.090" 2090-T62 to 0.190" 2090-T83 weld material combination can be successfully resistance spot welded per MIL-W-6858D requirements up to fifteen days after chemical cleaning with only paper (blue-line) packaging.

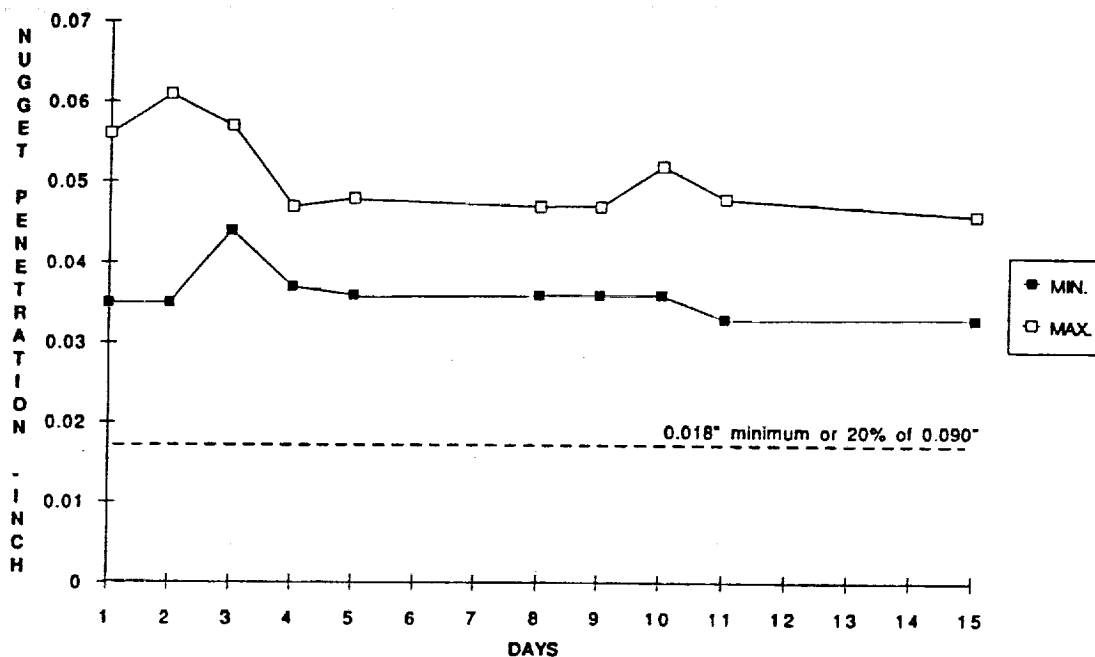


Figure 163. Pre-weld Cleaning Test, 0.090 inch Sheet Penetration Versus Time.

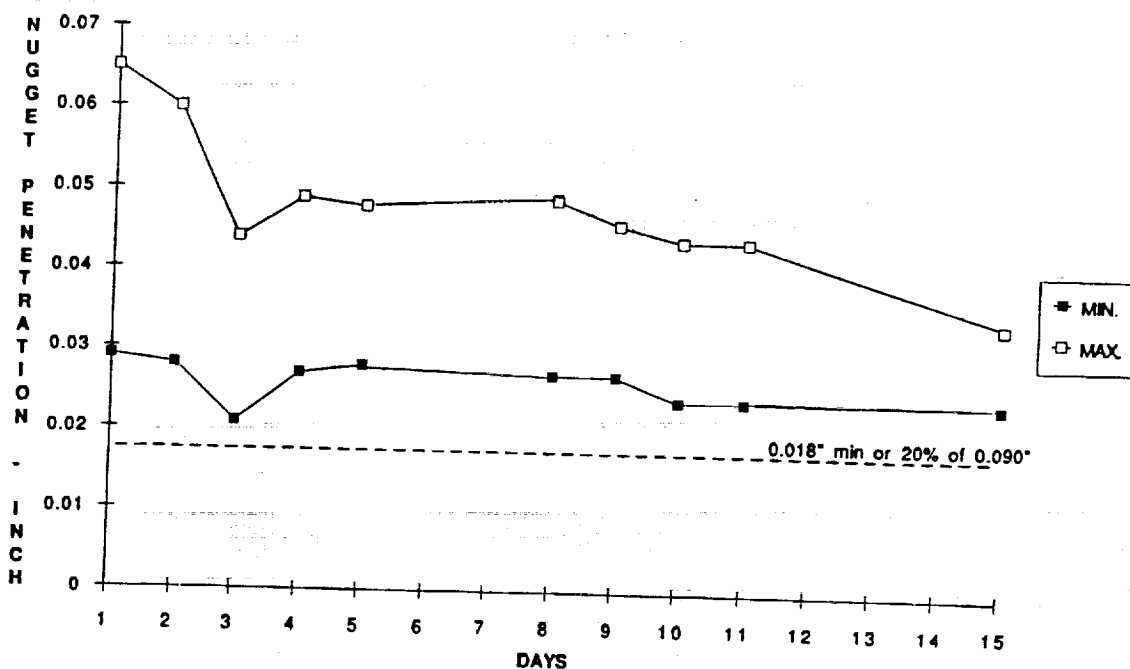


Figure 164. Pre-weld Cleaning Test, 0.190 inch Sheet Penetration Versus Time.

4.3.2.2.5 Weld Cycle Tolerance

Heat sensitivity of 0.090" 2090-T62 joined to 0.190" 2090-T81 material combination was run to determine the effects that variation of the heat would have on the weld quality. The purpose of the test was to determine the range of heat settings that would produce an acceptable weld. The range of weld heat was determined by increasing the weld heat percent until weld expulsion started to occur and decreased until insufficient nugget penetration started to occur. The other parameters (weld time, weld force, and forge force) were held fixed during the test. The results from the tests are shown graphically as nugget diameter and nugget penetration versus weld heat percent, and lap shear strength versus weld heat percent in Figures 153 through 155. The selected weld heat percent selected from the heat sensitivity test was 32%. The 32% heat value was used during the weld certification tests.

4.3.2.2.6 Weld Repair

The objective of this task was to determine the feasibility of repairing defective resistance spot welds in the 0.090" 2090-T62 to 0.190" 2090-T83 aluminum-lithium alloy combination. Defective spot welds were intentionally produced with the aluminum-lithium material combination from variations to the original certified spot weld schedule (refer to Table 97). Three groups of defective welds were made: diffusion welds (a reduction in 11 percentage points of heat from the original certified schedule), undersized nuggets (a reduction in 8 percentage points of heat from the original certified schedule), and nuggets with cracks or voids (a reduction in 2 percentage points of heat and the elimination of the forge force from the original certified schedule).

Fifteen specimens were spot welded per defect group, and sent to radiographic inspection for verification of the defect. Each grouping of fifteen was divided into two areas for post-weld examination: lap shear testing (six of the samples) and metallographic examination (nine of the coupons). Three of the six coupons slated for examination by lap shear were re-welded, using resistance spot weld repair schedules (refer to Table 98), and re-examined by radiographic inspection to verify correction of the defect. The same procedure for repair welding was used for five of the metallographic specimens from each defect group.

The examination of the "diffusion weld" specimens resulted in the removal of the defect by the repair process (refer to Figures 165 and 166). The average shear strength of the diffusion weld was 2203 pounds and the average shear strength of the repair weld was 3344 pounds.

The examination of the "undersized spot weld" specimens resulted in the removal of the defect by the repair process (refer to Figures 167 and 168). The average shear strength of the undersized weld was 2721 pounds and the average shear strength of the repair weld was 3441 pounds.

The examination of specimens with "cracks and voids in the weld" resulted in the removal of the defect by the repair process (refer to Figures 169 and 170). The average shear strength of the cracks and voids in the weld was 3108 pounds and the average shear strength of the repair weld was 3639 pounds.

It was determined that the repair weld process can be successfully used for all of the defect types examined during this program with the aluminum-lithium materials. However, the repairs were accomplished with additional heat placed into the system, which is anticipated to further decrease the skin efficiency. Any quantifiable reduction in skin efficiency is unknown and would depend upon the total heat input.

Table 97. Defect Weld Schedules for 0.090" 2090-T62 Joined to 0.190" 2090-T83 Aluminum-Lithium.

Defect I.D.	Heat Cycles	Heat Percent	Weld Force (lbs)	Forge Force (lbs)
Diffusion Weld	5	24	2900	7000
Undersized Weld	5	27	2900	7000
Cracks or Voids in the Weld	5	33	2900	0

Table 98. Repair Weld Schedules for 0.090" 2090-T62 Joined to 0.190" 2090-T83 Aluminum-Lithium.

Defect I.D.	Heat Cycles	Heat Percent	Weld Force (lbs)	Forge Force (lbs)
Diffusion Weld	12	25	2100	5300
Undersized Weld	12	25	2100	5300
Cracks or Voids in the Weld	12	28	2100	5300



Figure 165. Diffusion Spot Weld in 0.090" 2090-T62 joined to 0.190" 2090-T83 Al-Li.

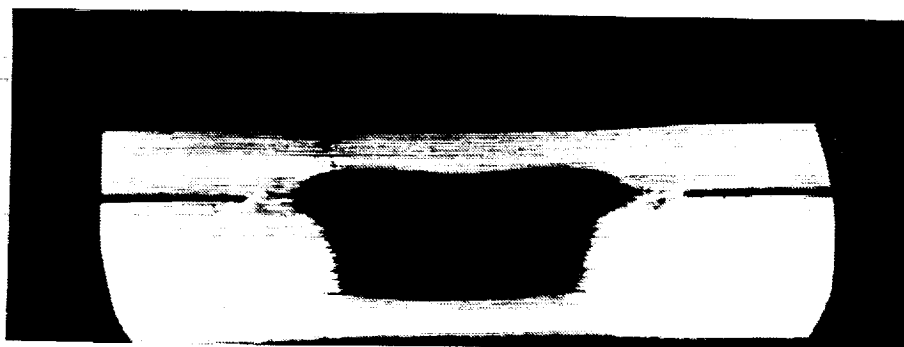


Figure 166. Repaired Diffusion Spot Weld in 0.090" 2090-T62 joined to 0.190" 2090-T83 Al-Li.

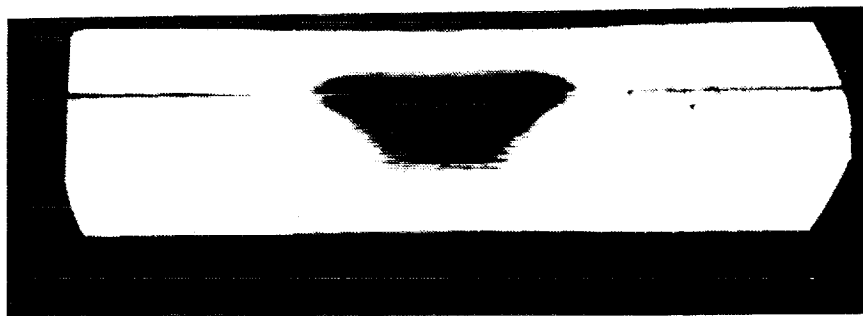


Figure 167. Undersized Spot Weld in 0.090" 2090-T62 joined to 0.190" 2090-T83 Al-Li.

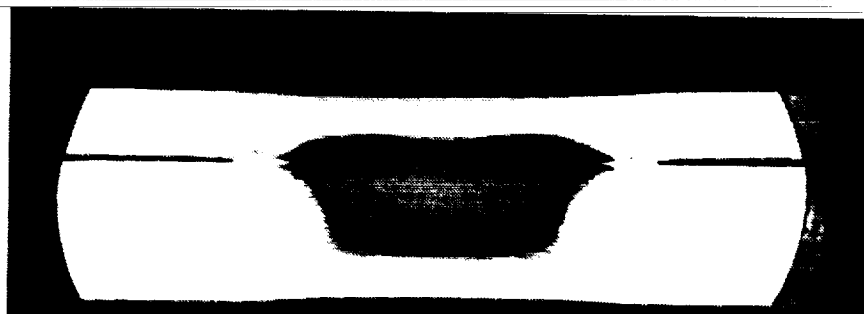


Figure 168. Repaired Undersized Spot Weld in 0.090" 2090-T62 joined to 0.190" 2090-T83 Al-Li.

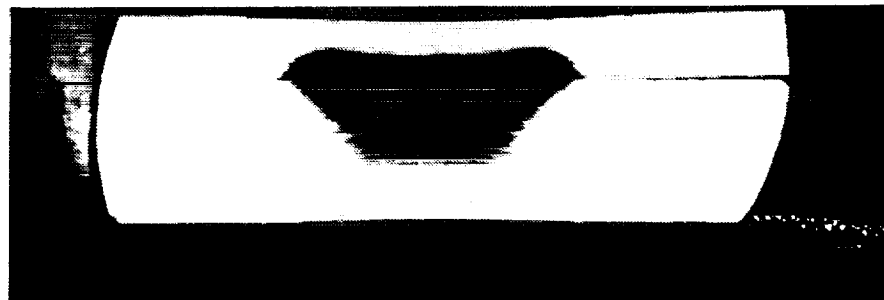


Figure 169. Spot Weld with Cracks and Voids in 0.090" 2090-T62 joined to 0.190" 2090-T83 Al-Li.

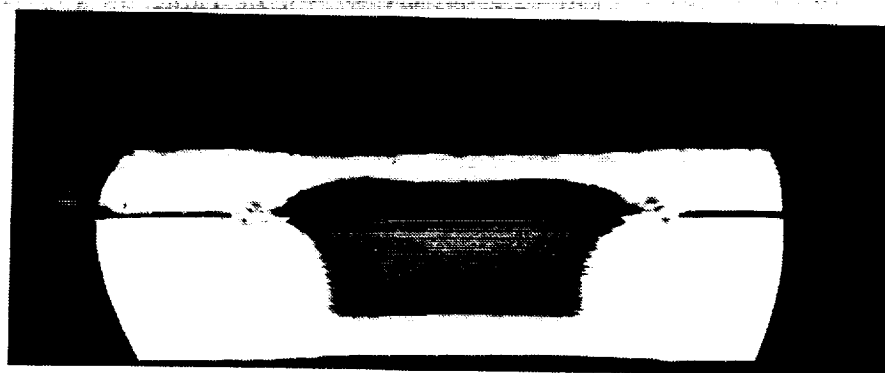


Figure 170. Spot Weld with Cracks and Voids Repaired in 0.090" 2090-T62 joined to 0.190" 2090-T83 Al-Li.

4.3.3 FUSION WELD DEVELOPMENT

Fusion welding is utilized for both the vertical panel to panel joints, and the barrel to major frame joints. In order to minimize the fabrication cost of the cryogenic tank structure (both in minimizing material scrap, and manufacturing time) the vertical welds (panel to panel) were designed so that the requirement for a weld land would be eliminated. The outer skin material would be procured in the required thickness, stiffener panels would be joined to the skin material, and each stiffened segment would be fusion welded together to provide a leak free tank. Since a weld land would not be available to reinforce the joint, a doubler would be placed over the shaved root side of the weld, and attached by resistance spot welding. The doubler reinforced concept has been successfully used on the Atlas and Centaur pressure stabilized configurations for years (although with stainless steel rather than aluminum).

In order to fabricate the doubler reinforced weld joint, fusion weld parameters had to be developed for both the 0.155" 2219-T81 aluminum and 0.155" 2090-T83 aluminum-lithium materials, and the theory of the joint explored through mechanical testing of coupons. Variable Polarity Plasma Arc (VPPA) fusion weld studies were initiated with the aforementioned material systems using a 300 Amp Hobart VPPA welder. A helium purge box was adapted to the VPPA welder so that all of the welding would be controlled under a shielded environment.

4.3.3.1 2219-T81 Aluminum Fusion Weld Development

The variable polarity plasma arc (VPPA) fusion weld development process was initiated and weld certification panels were welded, radiographic inspected and sectioned into tensile test and macro cross-section specimens. The preliminary results of tensile testing on 0.190" and 0.155" thick 2219-T81 aluminum sheet are shown in Table 99 and 100. Additional weld development was performed with 0.155" 2219-T81 Al, results are shown in Figure 171.

As part of the VPPA fusion weld reinforcement study for support of the doubler reinforced fusion weld panel fabrication, General Dynamics welded 2219-T81 aluminum plates (8.0 by 20.0 by 0.155 inches thick) together to create uniaxial test specimens. The plates edges were machined along the 8 inch length prior to VPPA fusion welding in order to assure a parallel weld surface that was free from contaminants. Four sets of 8 by 20 inch panels were successfully fusion welded and radiographically inspected. After inspection, the root side of the weld was shaved to provide a smooth surface for subsequent resistance spot welding of the reinforcement doubler. Two different specimen spot weld patterns were created to vary the spot weld spacing (refer to Figure

172) and are referred to as the pattern 1 (even row) and pattern 2 (staggered row) pattern in further discussions.

Table 99. Tensile Strength of VPPA Fusion Welded 0.190" 2219-T81

Coupon I.D.	Width (in)	Thickness (in)	Area (sq. in)	Load (lbs)	Ftu (psi)
1	0.962	0.192	0.185	7565	40,957
2	0.960	0.191	0.183	7680	41,907
3	0.966	0.190	0.184	7522	40,983
4	0.936	0.191	0.179	7010	39,232
5	0.921	0.191	0.176	6909	39,276
6	0.949	0.189	0.179	7093	39,567
7	0.930	0.188	0.174	6867	39,402
8	0.946	0.187	0.164	6818	38,644
9	0.986	0.187	0.184	7082	38,429
Average					39,822

Table 100. Tensile Strength of VPPA Fusion Welded 0.155" 2219-T81

Coupon I.D.	Width (in)	Thickness (in)	Area (sq. in)	Load (lbs)	Ftu (psi)
A1	0.962	0.145	0.139	5850	41,938
B1	1.027	0.146	0.150	6113	40,769
C1	0.992	0.147	0.146	5953	40,823
Average					<u>41,177</u>
A2	0.997	0.132	0.129	5031	39,011
B2	0.989	0.130	0.129	4794	37,287
C2	1.020	0.135	0.138	5163	37,494
Average					<u>37,930</u>
A3	0.996	0.142	0.141	5310	37,544
B3	1.010	0.141	0.142	5521	38,768
C3	0.9665	0.142	0.137	5244	38,210
Average					<u>38,174</u>

The fusion weld specimens were machined into a tensile coupon (dogbone) configuration and chemically cleaned (doubler and outer skin material) prior to resistance spot welding of the 7475-T62 Al doubler onto the 2219-T81 Al fusion weld specimen. The completed uniaxial specimens were strain gauged (refer to Figure 173) and tested at ambient temperature on a 50 Kips MTS test machine; cross-head speed was 0.05 inches per minute. The strain gauge readings were taken every 3 seconds. Table 101 lists the specimen type, the maximum load reached at failure, the tensile stress at failure, and the percent of parent material strength (weld efficiency) indicated from the coupons during the testing.

VPPAW PARAMETER DEVELOPMENT

350 A HOBART VPPAW POWER SUPPLY
HAWCS CONTROLLER
400 A HOBART TORCH

MATERIAL: 0.155 2219-T81

JOINT DESIGN: SQUARE GROOVE BUTT JOINT



(VERTICAL-UP PROGRESSION)

TENSILE STRENGTH
41.2 ksi AVG

WELD PARAMETERS	KEYHOLE PASS
ARC CURRENT	118 A
CURRENT MODE	VP
STRAIGHT TIME	19 ms
REVERSE TIME	4 ms
REVERSE CURRENT	60 A
ARC VOLTAGE	22.5 V
TRAVEL SPEED	13.5 ipm
WIRE TYPE	2319
WIRE SIZE	1/16
WIRE FEED RATE	38.0 ipm
ELECTRODE DIA.	1/8
ORIFICE SIZE	1/8
CUP SIZE	#13(13/16)
PLASMA GAS TYPE	ARGON
PLASMA GAS FLOW	4.8 cfh
SHIELD GAS TYPE	ARGON
SHIELD GAS FLOW	80 cfh
TRAILER GAS TYPE	N/A
TRAILER GAS FLOW	N/A
BACKSIDE PURGE GAS	N/A

Figure 171. Variable Polarity Plasma Arc Fusion Weld Development for 0.155" 2219-T81.

Table 101. Tensile Response of Fusion Doubler Reinforce Testing for 2219-T81 Al with 7475-T62 Al Doubler.

Specimen ID	Spot Weld Pattern	Width (inch)	Thickness (inch)	Area (sq. in.)	Ultimate Load (pounds)	F _{tu} (Ksi)	Weld Efficiency (percent)
1-F4D1	In-Line	4.84	0.155	0.750	36712	48.9	77.7
1-F3D2	In-Line	4.84	0.155	0.750	41151	54.9	87.0
2-F1D3	Staggered	4.02	0.155	0.620	34720	55.7	88.5
2-F2D4	Staggered	4.02	0.155	0.623	34727	55.7	88.5

All of the test specimens failed in the 2219-T81 skin along the first row of spot welds near the edge of the doubler. There were not any indications of spot weld failure during testing, or permanent deformation in the fusion weld. The first uniaxial specimen failed prematurely in the skin. The premature failure was attributed to the high amount of heat used during resistance spot welding of the initial panel (specimen 1-F4D1). The remaining test panels used lower heat settings during attachment of the doubler. Weld efficiencies for the test specimens were lower than predicted due to the close doubler inter-spot spacing (0.075 inch) used during welding. A summary of the trends in the test data are presented as follows:

- 1) At loads less than 15,000 lbs (20 ksi), all of the strain gage readings were essentially linear.
- 2) At 15,000 lbs., the doubler carried 24.9 percent of the load and the skin carried 75.1 percent. This ratio indicated that the spot stiffness (determined analytically) was 180,000 pounds/inch/spot.
- 3) Data obtained from strain gages 9 and 10 at loads above the 15,000 pounds were non-linear, indicating the area near the fusion weld was yielding, or the sheet was bending near the fusion weld. This effect caused the load ratio to change to 35 percent in the doubler and 65 percent in the basic skin.
- 4) The analytical model indicated that for a spot stiffness of 180,000 pounds/inch/spot the fusion weld would fail before the outer skin material; however, the yielding near the fusion weld caused increased load transfer into the doubler protecting the fusion weld.
- 5) A 35 percent to 65 percent load split results in the effective spot stiffness of 986,000 pounds/inch/spot. The outer skin efficiency is now the weakest component of the system due to the load split considering the minimum fusion weld strength is 36,000 psi.
- 6) The ultimate stress in the outer skin (2219-T81 sheet, F_{tu} = 63 ksi) was 48,936 psi at the first row of spot welds that resulted in a weld efficiency of 77.7 percent.

The results of the doubler reinforced fusion weld testing showed that the in-line configuration provided the best reinforcement of the fusion weld. However, neither reinforcement joint configuration (in-line or staggered) were optimized. As a result of the tests and evaluations of the joint at General Dynamics and Rockwell the inter-spot weld spacing was increased and the center-line offset of the reinforce joint was readjusted.

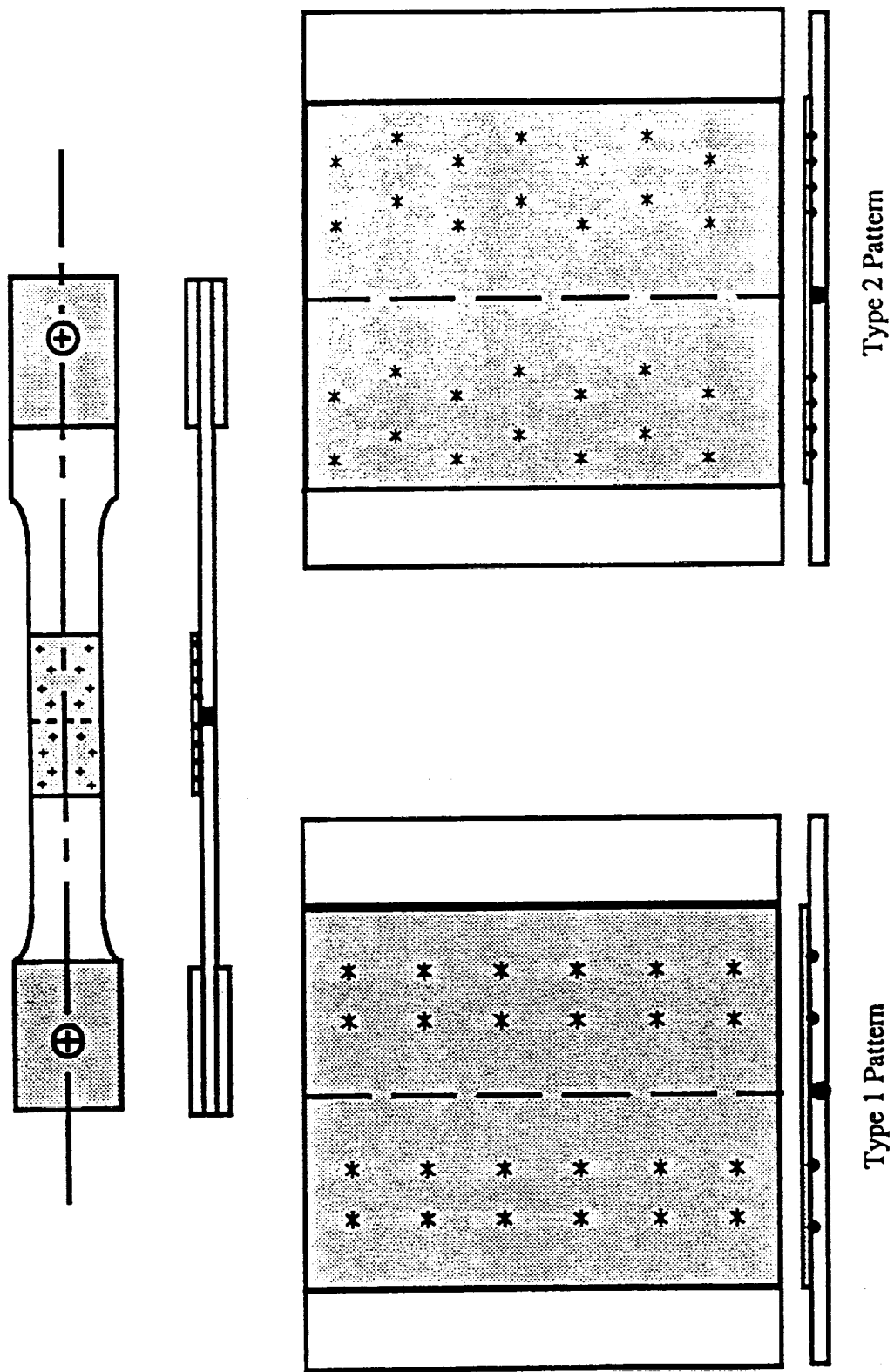
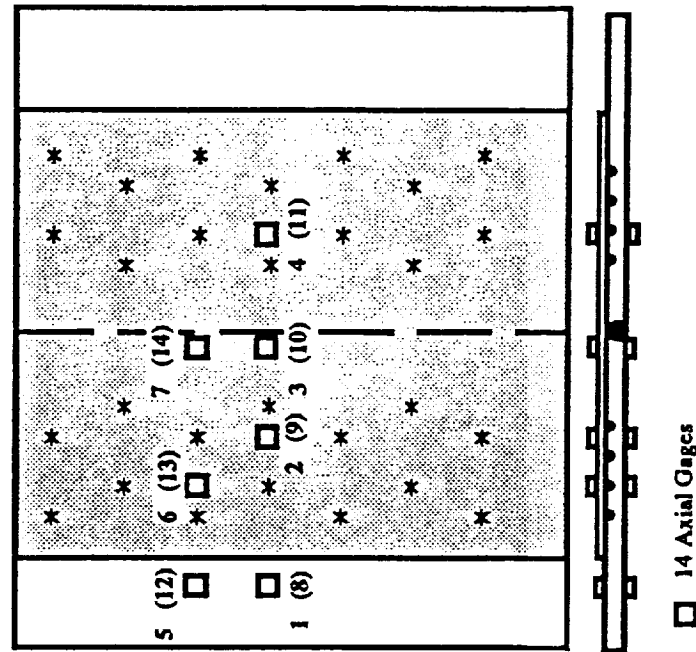
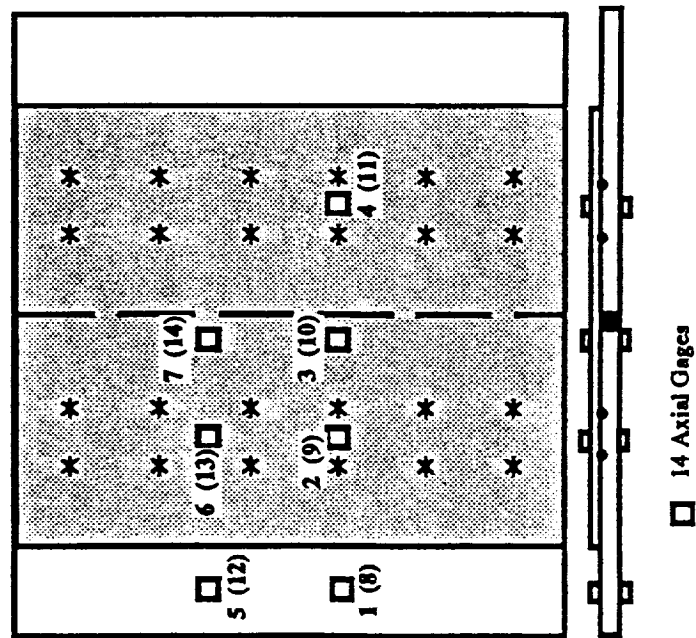


Figure 172. Standard Tension Specimen for Fusion Weld Reinforcement.



Type 2 Pattern



Type 1 Pattern

Figure 173. Strain Gauge Locations for Fusion Weld Efficiency Testing.

4.3.3.2 2090-T83 Aluminum-Lithium Fusion Weld Development

Parameter development on VPPA welding of the 0.155" 2090-T83 material was performed. Radiographic inspection of the single pass welds revealed high quality fusion joints with full penetration, however, the visual appearance of the welds showed small amounts of undercut along the weld length. The initial goal of developing a single pass VPPA weld with full penetration (Keyhole) without a 'cosmetic' cover pass to fill undercut was desirable since panel distortion appeared to be most noticeable after the cover pass. However, the single pass weld schedule could not be enhanced in order to remove the under-cut, and the program goal was modified to include the cover-pass.

The preliminary test panel, 0.155" 2090-T83 Al-Li, was welded and radiographically inspected. The panel passed the acceptance criteria for fusion welding of aluminum and was processed for tensile and metallographic analysis. Data provided for the development work is shown in Table 102. Tensile data was not consistent due to varying amount of undercut on the specimens.

Table 102. Fusion Weld Development of 0.155: 2090-T83 Al-Li

1/8" Tungsten Electrode, 1/8" Orifice, Argon Gas
Current: 110 amps Shielding Gas Flow Rate: 80 CFH
Voltage: 15.5 volts Plasma Gas Flow Rate: 32 CFH
Straight Polarity Time: 44 msec Travel Speed: 9.5 in/min
Reverse Polarity Time: 7 msec Wire Feed Rate: 40 in/min.
Additional Reverse Current: 80 amps

Coupon I.D.	Test Area (sq. in.)	Load (pounds)	F _{tu} (psi)	Elongation (percent)
1	0.141	5871	41,562	5
2	0.144	5269	36,626	5
3	0.141	5766	41,010	4
4	0.146	5313	36,463	5
5	0.145	5276	36,426	5
Average	0.143	5499	38,417	5

The two pass welding process (consisting of a keyhole pass, and a cover pass) resulted in good weld strengths. However, distortion of the panels during welding required changes be made to the fixturing during welding (the addition of chill bars and an increase in the number of fixturing clamps). The 2090-T83 material exhibited greater distortion than the 2219-T81 material.

The VPPA two-pass weld was examined metallographically and by tensile evaluation. The results from the evaluation are shown in Table 103. The tensile specimens 1 through 3 were taken from a section of the panel where mismatch was not present (average $F_{tu} = 41.6$ ksi), specimen 4 was located in a segment of the weld where mismatch was present ($F_{tu} = 39.8$ ksi). The metallographic cross sections of the weld shown as Figure 174 (removed from the area without mismatch) and 175 (removed from the area with mismatch). The photomicrographs revealed small amounts of porosity, however, the quantity and size of the porosity was acceptable per General Dynamics Space Systems fusion weld specification 5-77008-1. Weld parameter development was continued in order to eliminate weld zone porosity.

Table 103. Tensile Results of 0.155" 2090-T83 Two Pass VPPAW

Coupon I.D.#	Width inch	Thickness inch	Test Area sq. inch	F_{tu} psi	Elongation %
1	0.954	0.156	0.149	41169	5
2	1.009	0.157	0.158	41752	5
3	1.005	0.156	0.157	41759	4
4	1.015	0.156	0.158	39832	5
Average			0.156	41128	5

4.3.3.3 Doubler-Reinforced Fusion Weld Development

The initial stress analysis of the LH2 tank longitudinal joint was developed such that both the axial and the hoop loads were represented. The analysis of the loads in the joint was accomplished with a stiffness model which represented the basic skin, the doubler, and the stiffness of the spot weld attachment of the skin to the doubler. The nomenclature of the longitudinal joint for an even row spot weld pattern and a staggered row spot weld pattern is shown in Figure 176 and Figure 1877. The analytical stiffness model of the joint is shown in Figure 178. This model was analyzed by the matrix displacement method to find the internal forces and displacements in the joint in terms of an applied displacement at node 6 with zero displacements at nodes 1 and 2 (boundary conditions).

The initial analysis was performed on a reinforced fusion weld joint configuration (this configuration was used for the tensile dogbone tests using 2219-T81 skin with 7475-T62 doubler) for a range of values of spot weld stiffness. The analysis was done using a constant 9000 lb/in load on the joint. The variables used in the analysis and the resulting computed internal loads are listed in Table 104. This data was generated with the idea that the spot weld stiffness would be found by comparing the failure load of the spot welds or the fusion weld with the curves. However, the tensile dogbone test failures occurred in the basic skin at the first spot weld row;

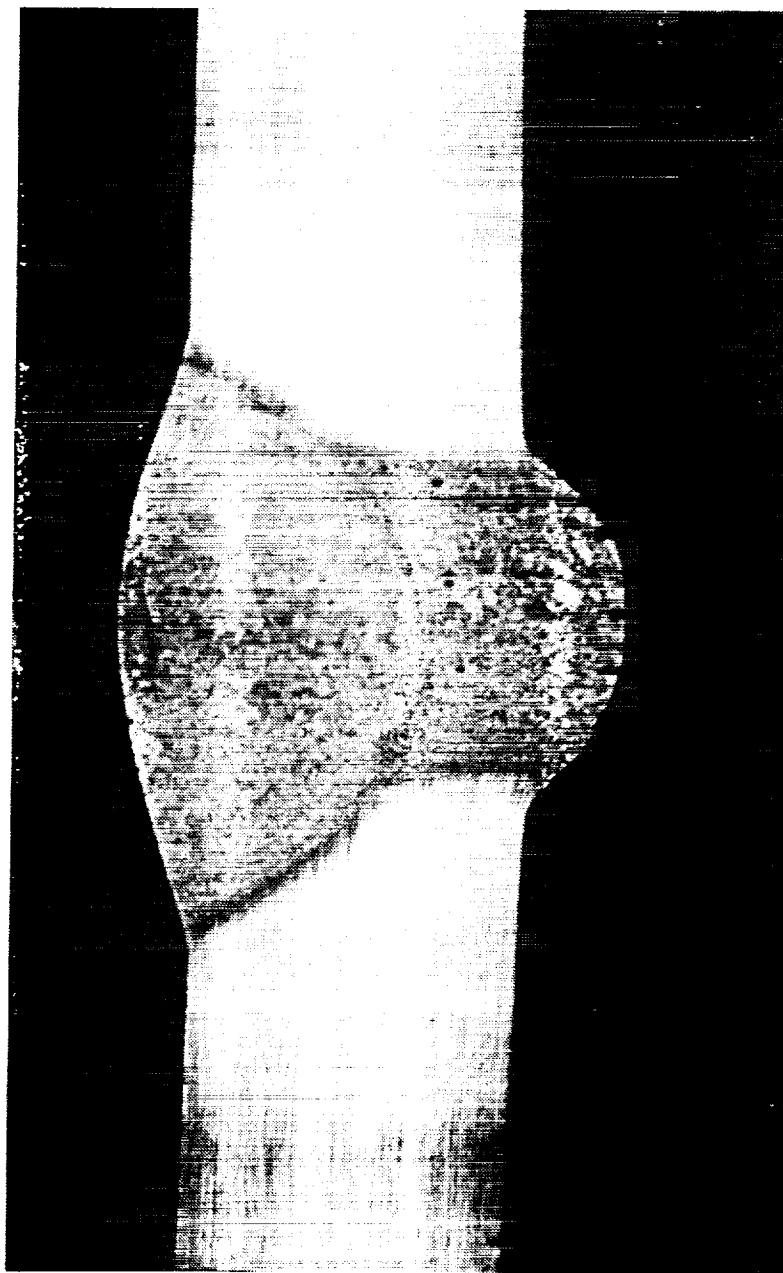


Figure 174. Macro Cross-section of a Double Pass VPPA Weld of 2090-T83, (0.155 inch thickness sheet), some porosity was apparent.



Figure 175. Macro Cross-section of a Double Pass VPPA Weld of 2090-T83, (0.155 inch thickness sheet).

therefore, the spot weld stiffness was found by comparing the load distribution in the joint. The load distribution, or how the load is shared between the doubler and the basic skin, is a function of the spot weld stiffness. Table 105 shows the analytical data for a spot weld stiffness of 180,000 lb/in which best matched the tensile dogbone test data.

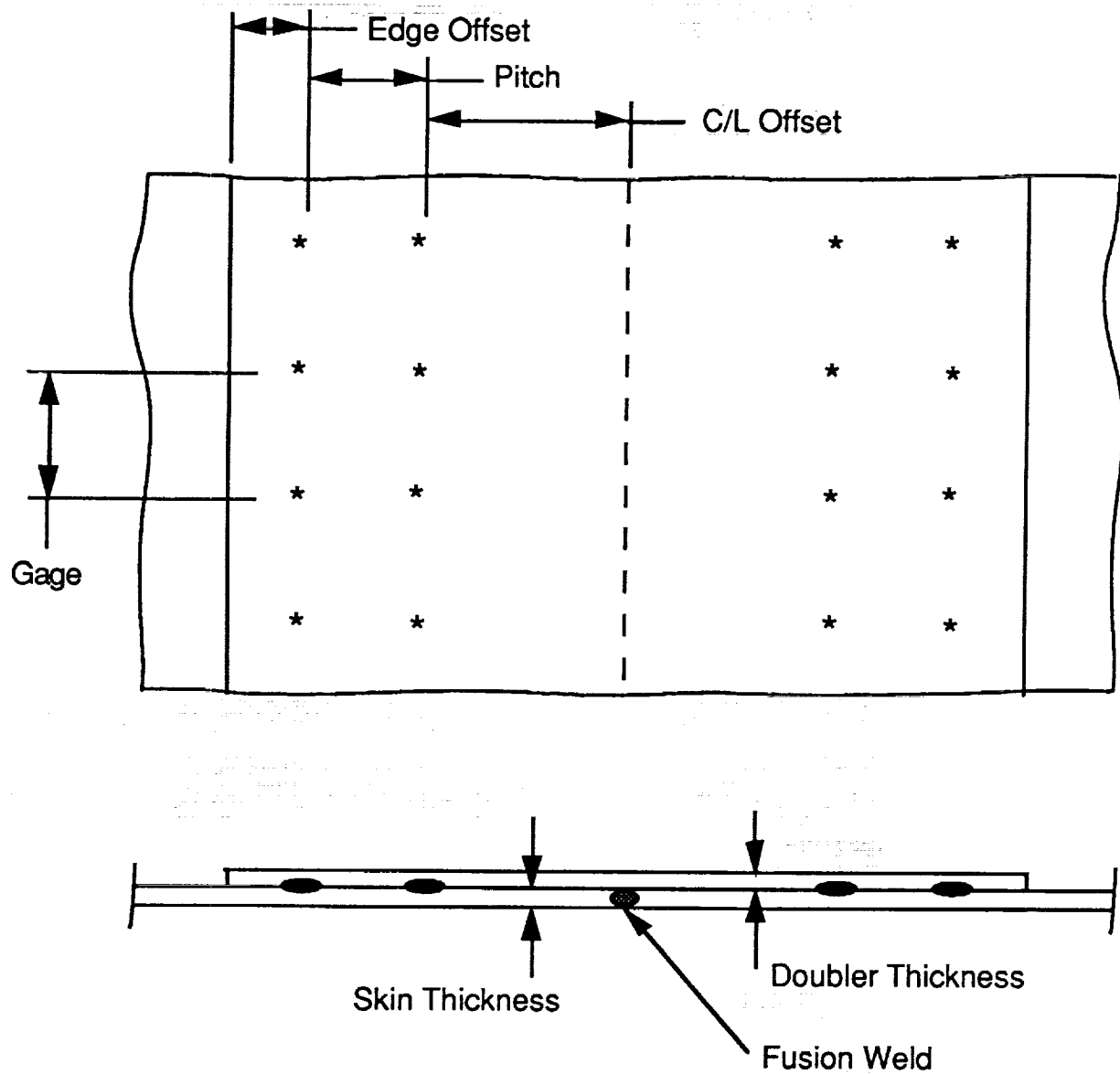


Figure 176. Longitudinal Joint Configuration and Nomenclature for the Even Row Spot Weld Pattern.

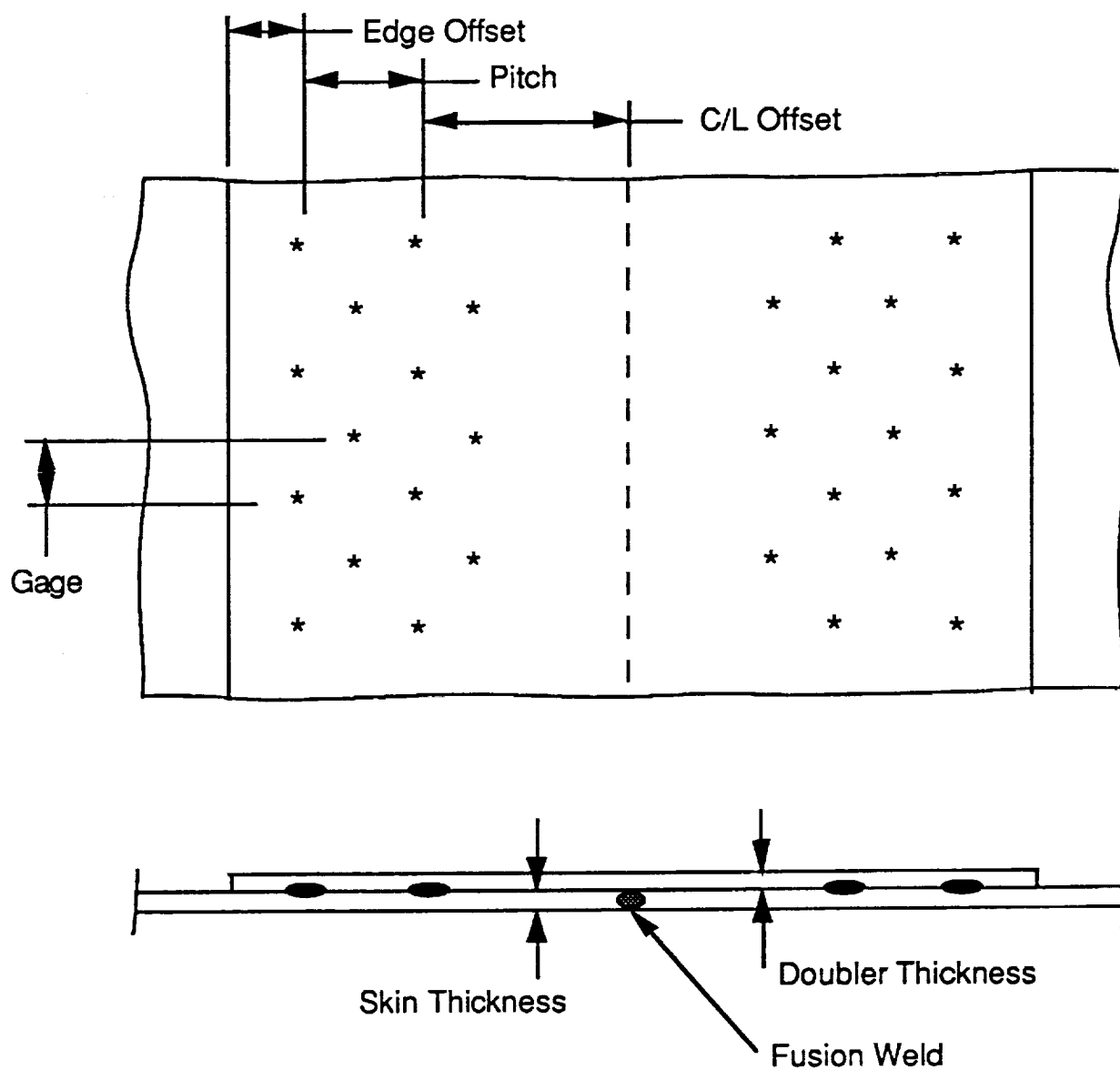
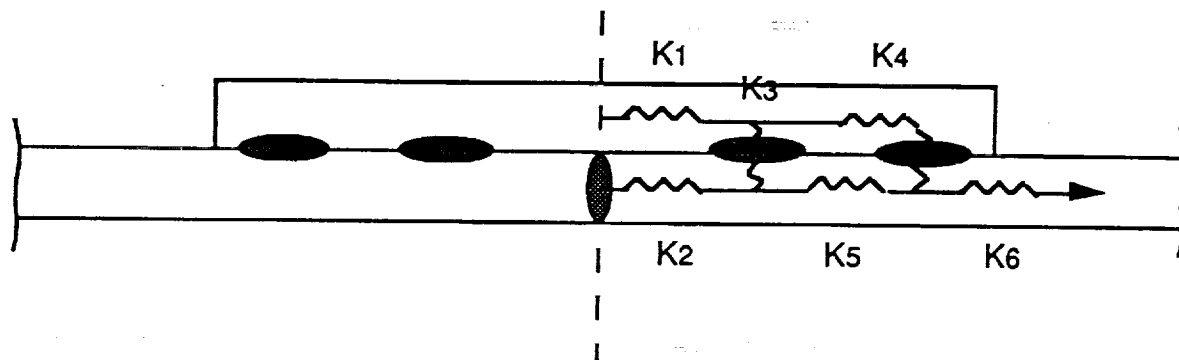


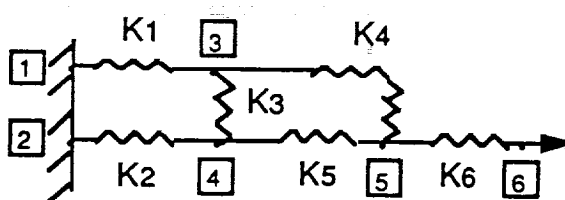
Figure 177. Longitudinal Joint Configuration and Nomenclature for the Staggered Row Spot Weld Pattern.



- K1 is stiffness of doubler from C/L to inside spot row.
- K2 is stiffness of skin from C/L to inside spot row.
- K3 is stiffness of spot weld between skin and doubler.
- K4 is stiffness of spot weld in series with doubler between spot rows.
- K5 is stiffness of skin between spot rows.
- K6 is stiffness of some chosen length of skin from outer spot row.

All stiffnesses based on one gage width.

C/L Symm



- X Node Number
- K_i Element Stiffness Number

Figure 178. Model Representation of a Fusion Weld / Resistance Spotweld Doubler Reinforced Joint

Table 104. Analysis Results for Longitudinal Joint for Various Spot Weld Stiffness Values.

(Staggered Row Pattern Above Shaded Row)
(Even Row Pattern Below Shaded Row)

Gage (in)	Pitch (in)	CL Offset (in)	Edge Offset (in)	Skin Thick (in)	Doubler Thick 1 or 2 (in)	Doubler Skin Modulus (psi)	Doub Modulus (psi)	Spot K (lb/in)	
0.5	1	1.5	0.01	0.155	0.1	1	1.050E+07	1.000E+07	1.233E+05
0.5	1	1	0.5	0.155	0.1	1	1.050E+07	1.000E+07	1.233E+05
0.5	1	1.5	0.01	0.155	0.1	1	1.050E+07	1.000E+07	2.466E+05
0.5	1	1	0.5	0.155	0.1	1	1.050E+07	1.000E+07	2.466E+05
0.5	1	1.5	0.01	0.155	0.1	1	1.050E+07	1.000E+07	4.933E+05
0.5	1	1	0.5	0.155	0.1	1	1.050E+07	1.000E+07	4.933E+05
0.5	1	1.5	0.01	0.155	0.1	1	1.050E+07	1.000E+07	9.865E+05
0.5	1	1	0.5	0.155	0.1	1	1.050E+07	1.000E+07	9.865E+05
0.5	1	1.5	0.01	0.155	0.1	1	1.050E+07	1.000E+07	1.973E+06
0.5	1	1	0.5	0.155	0.1	1	1.050E+07	1.000E+07	1.973E+06
0.5	1	1.5	0.01	0.155	0.1	1	1.050E+07	1.000E+07	3.946E+06
0.5	1	1	0.5	0.155	0.1	1	1.050E+07	1.000E+07	3.946E+06
0.5	1	1.5	0.01	0.155	0.1	1	1.050E+07	1.000E+07	7.892E+06
0.5	1	1	0.5	0.155	0.1	1	1.050E+07	1.000E+07	7.892E+06
0.75	0.75	1.75	0.01	0.155	0.1	1	1.050E+07	1.000E+07	1.233E+05
0.75	0.75	1.75	0.01	0.155	0.1	1	1.050E+07	1.000E+07	2.466E+05
0.75	0.75	1.75	0.01	0.155	0.1	1	1.050E+07	1.000E+07	4.933E+05
0.75	0.75	1.75	0.01	0.155	0.1	1	1.050E+07	1.000E+07	9.865E+05
0.75	0.75	1.75	0.01	0.155	0.1	1	1.050E+07	1.000E+07	1.973E+06
0.75	0.75	1.75	0.01	0.155	0.1	1	1.050E+07	1.000E+07	3.946E+06
0.75	0.75	1.75	0.01	0.155	0.1	1	1.050E+07	1.000E+07	7.892E+06

F1 (lb)	F2 (lb)	F3 (lb)	F4 (lb)	F5 (lb)	F6 (lb)	F. Weld Stress (psi)	Load Dist 1 (F4/F6)	Load Dist 2 (F1/F6)
1013.	3103.	331.	683.	3434.	4116.	40039.	0.1658	0.2461
1087.	3880.	320.	767.	4200.	4967.	50063.	0.1544	0.2188
1256.	2841.	363.	893.	3204.	4097.	36662.	0.2180	0.3065
1419.	3542.	374.	1045.	3915.	4960.	45700.	0.2107	0.2880
1410.	2659.	331.	1079.	2990.	4070.	34314.	0.2652	0.3465
1663.	3304.	362.	1301.	3666.	4967.	42635.	0.2619	0.3348
1486.	2558.	254.	1232.	2812.	4045.	33013.	0.3047	0.3674
1803.	3175.	291.	1511.	3466.	4978.	40964.	0.3036	0.3622
1515.	2512.	168.	1348.	2680.	4027.	32413.	0.3346	0.3762
1866.	3120.	199.	1667.	3319.	4986.	40252.	0.3344	0.3743
1524.	2493.	99.	1425.	2592.	4017.	32172.	0.3547	0.3793
1890.	3101.	120.	1770.	3221.	4992.	40016.	0.3546	0.3787
1544.	2516.	55.	1489.	2571.	4060.	32465.	0.3667	0.3802
1921.	3134.	67.	1854.	3201.	5055.	40435.	0.3667	0.3801
1415.	5351.	539.	877.	5889.	6766.	46026.	0.1296	0.2092
1865.	4901.	660.	1205.	5561.	6766.	42160.	0.1781	0.2758
2207.	4560.	684.	1523.	5244.	6767.	39224.	0.2250	0.3262
2415.	4354.	600.	1814.	4955.	6769.	37458.	0.2680	0.3567
2513.	4249.	448.	2066.	4696.	6762.	36546.	0.3055	0.3717
2552.	4205.	290.	2262.	4495.	6757.	36172.	0.3348	0.3777
2565.	4190.	169.	2396.	4359.	6755.	36039.	0.3547	0.3797

Note: The data above the shaded line for the staggered spot row pattern is given in pairs. One gage width (.5 in) is for two spots which are closer to the edge; a companion gage width (.5 in) is for two spots which are farther from the edge. These two lines of data must be averaged to get the information for a 1 inch gage width.

Table 105. The Analysis Best Matched the Test Data When a Spot Weld Stiffness of 180,000 lb/in was Used.

Gage (in)	Pitch (in)	CL Offset (in)	Edge Offset (in)	Skin Thick (in)	Doubler Thick 1 or 2 (in)	Doubler Skin Modulus (psi)	Doub Modulus (psi)	Spot K (lb/in)	
0.5	0.75	1.5	0.01	0.155	0.1	1	1.050E+07	1.000E+07	1.800E+05
0.5	0.75	1	0.5	0.155	0.1	1	1.050E+07	1.000E+07	1.800E+05
0.75	0.50	1.75	0.01	0.155	0.1	1	1.050E+07	1.000E+07	1.800E+05

F1 (lb)	F2 (lb)	F3 (lb)	F4 (lb)	F5 (lb)	F6 (lb)	F. Weld Stress (psi)	Load Dist 1 (F4/F6)	Load Dist 2 (F1/F6)
1111.	2949.	378.	733.	3328.	4060.	38053.	0.1805	0.2737
1241.	3781.	390.	852.	4171.	5023.	48793.	0.1696	0.2471
1615.	5151.	651.	963.	5803.	6766.	44314.	0.1424	0.2386

Uniaxial tensile dogbone tests (refer to Figure 179) were performed on two doubler reinforced fusion welds configurations using the 7475 Al joined to 2219 Al material combination. A total of 4 specimens were tested; two specimens with even spot row patterns, Figure 180, and two specimens with staggered spot row patterns, Figure 181. Figures 182 through 185 show the strain gage locations for each of the four test specimens. The strain gage traces of microstrain vs. specimen load for each of the four specimens are shown in Figures 186 through 190.

The joint load distribution found from test was matched with analysis runs to find which value of spot weld stiffness yielded the same load distribution. A summary of the dogbone test results with loads and load distributions in the joint are provided along with a comparison of the analytical load distribution for a spot weld stiffness of 180,000 lb/in per spot in Table 106. The first column showing "% Total Load" is the percent of the total load which has been passed into the doubler by the first spot weld row. This would correspond to the percent of load in K4 in the analytical model. The second column showing "% Total Load" is the percent of the total load which has been passed into the doubler by both spot weld rows. This would correspond with the load in K1 in the analytical model.

The strain gage traces from the test specimens were analyzed to determine the loads in the various parts of the joint at a given total load on the specimen. The load point selected for examination of the strain gage data for each specimen was approximately the maximum load at which the strain data was still essentially linear. Once the strain data was determined to be nonlinear, the load corresponding to that strain gage is unknown and the load distribution in the joint is unknown. This load point referred to as the reference load was different for each different specimen configuration. The reference load for F4D1 and F2D4 was approximately 15,000

pounds; the reference load for F1D3 was approximately 20,000 pounds and for F3D2 was approximately 35,000 pounds. Figures 185 through 191 show the calculations of the loads in the various parts of the joints determined from the strain gage readings at the reference loads. A summary of these findings is given in Table 106.

Table 106. Summary of longitudinal joint dogbone tests comparing load distribution in joint with analysis.

Specimen No.	Type	Reference Load (lb)	Basic Sheet Strain Gages (lb)	Doubler Strain Gages 1 (lb)	% Total Load	Doubler Strain Gages 2 (lb)	% Total Load
F4D1	Even	15000.	15951.	2275.	14.3	3969.	24.9
F3D2	Even	35000.	34895.	7840.	22.0	12971.	37.0
ANALYSIS	Even				14.2		23.9
F2D4	Staggered	15000.	15702.	2372.	15.1	4141.	26.4
F1D3	Staggered	20000.	19464.	5065.	26.0	7236.	37.0
ANALYSIS	Staggered				17.5		26.0

Specimen No.	Type	Ultimate Load (lb)	Basic Sheet Stress Result (lb/in)	Basic Sheet Hoop Stress (psi)	Fusion Weld Stress (psi)	Max Spot Shear Load (lb)
F4D1	Even	36712.	7585.	48936.	Linear	Linear
F3D2	Even	41151.	8502.	54853.	36751.	813.
F2D4	Staggered	34727.	8638.	55732.	34557.	1402.
F1D3	Staggered	34720.	8637.	55721.	41019.	652.
					35104.	1123.

The 180,000 lb/in spot weld stiffness yielded analytical load distributions in the joint (shown in Table 106) were very close for two of the test specimens, namely, F4D1 and F2D4. An analytical match with specimens F3D2 and F1D3 could only be achieved if the spot weld stiffness was infinite. In this case the load in the doubler at the center would be about 37% of the total load. With this being the case the data for F4D1 and F2D4 it was concluded that the 180,000 lb/in for the spot weld stiffness was the correct value. It was also found that if the gage used in the analysis were reduced by 0.25 inches the analytical results would more closely match test results. This was attributed to the fact that the spot weld areas occupy some of the gage length and thereby reduces the gage effective length below the centerline-to-centerline distance between spot welds.

An assumption from the test data, which was not observed during the testing in any way, was that the fusion welds may have been close to failure when the specimens failed. If the linear distribution of the loads were applied to the joint at specimen failure; i.e., 24.9% of the ultimate load for the even row specimen and 26.4% of the ultimate load for the staggered row specimen,



Figure 179. Standard Tension Specimen for the Longitudinal Spot Welded Splice Joint Tests.

View A

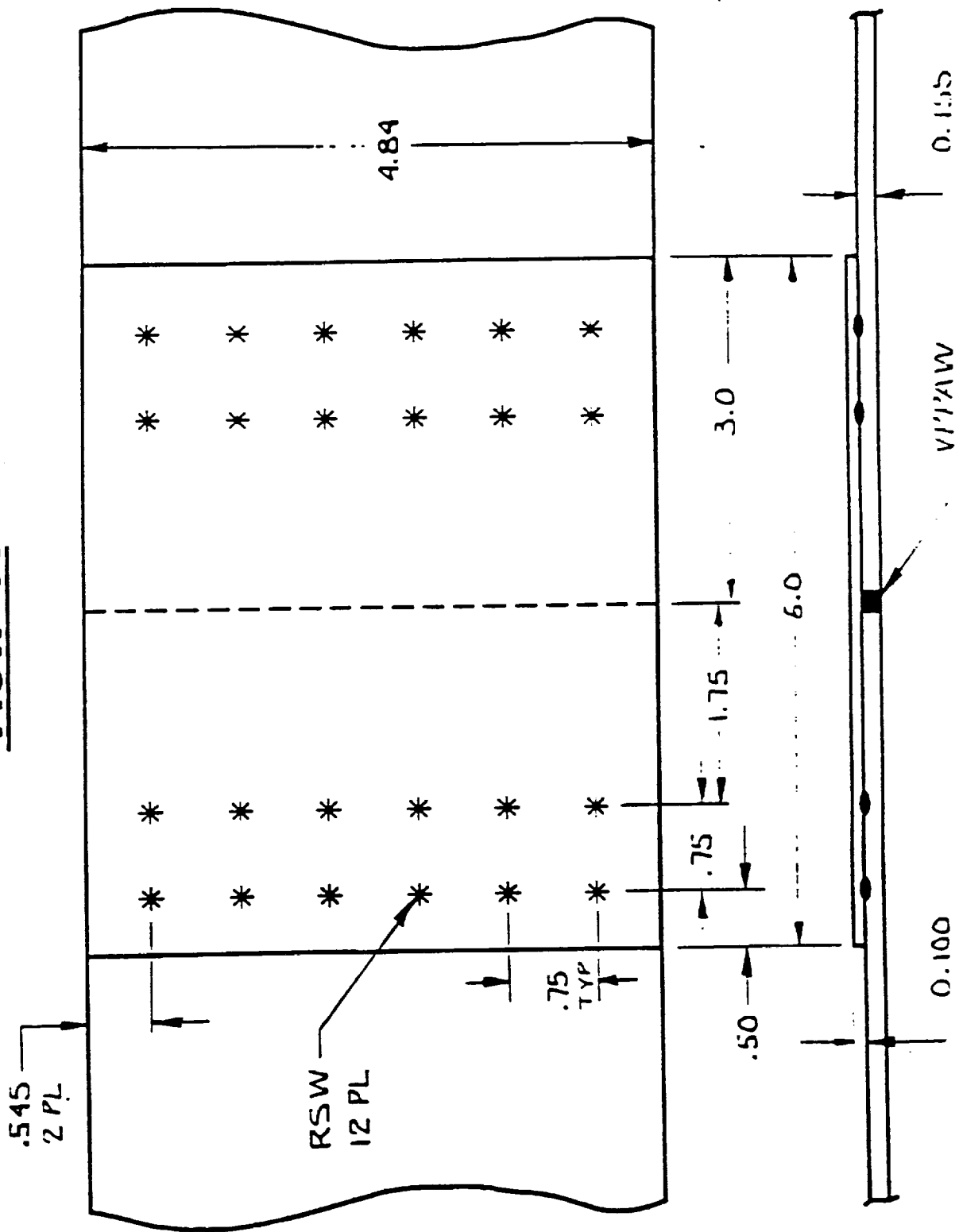


Figure 180. Longitudinal Splice Joint Test Configuration for the Even Row Spot Weld Pattern.

View B

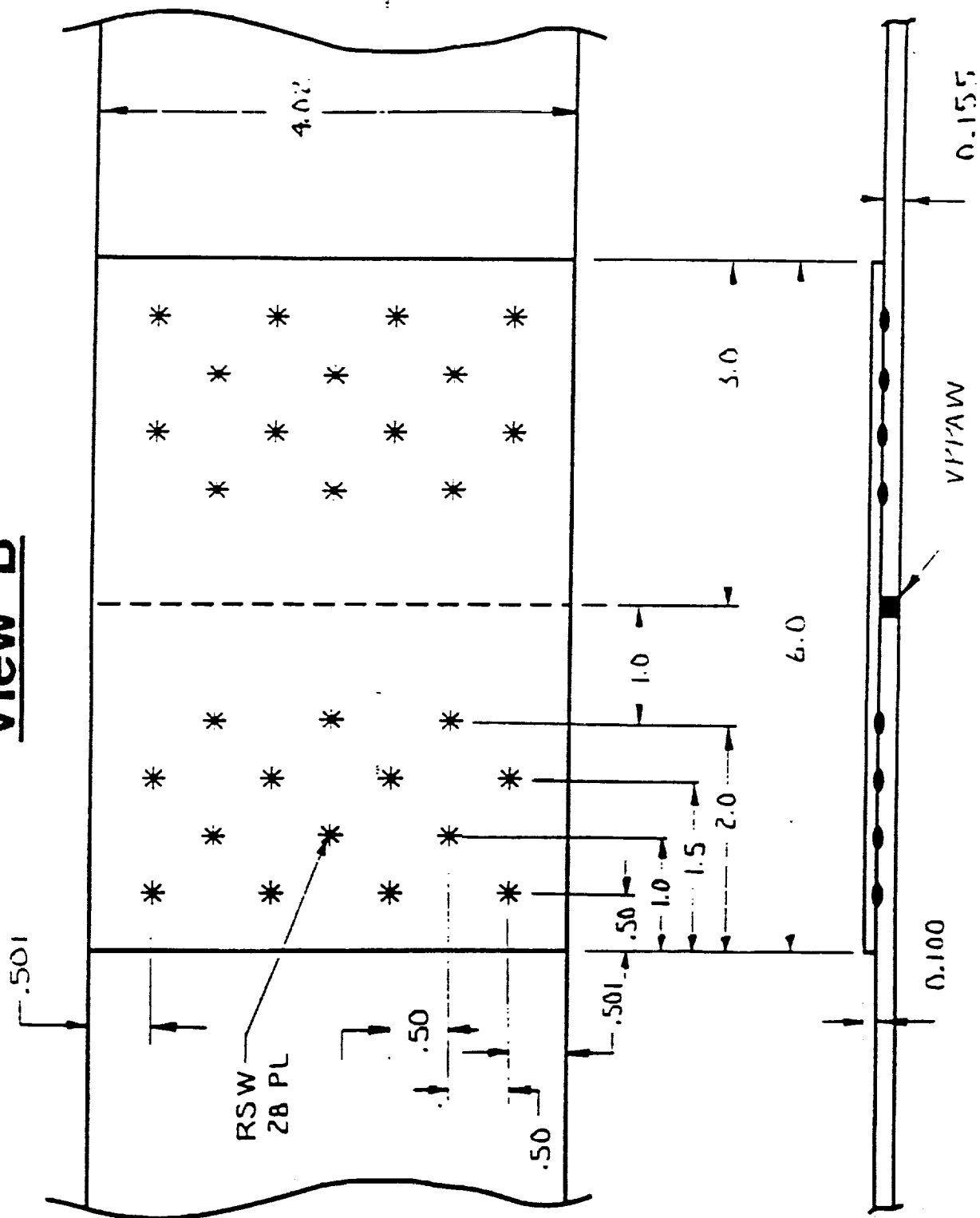
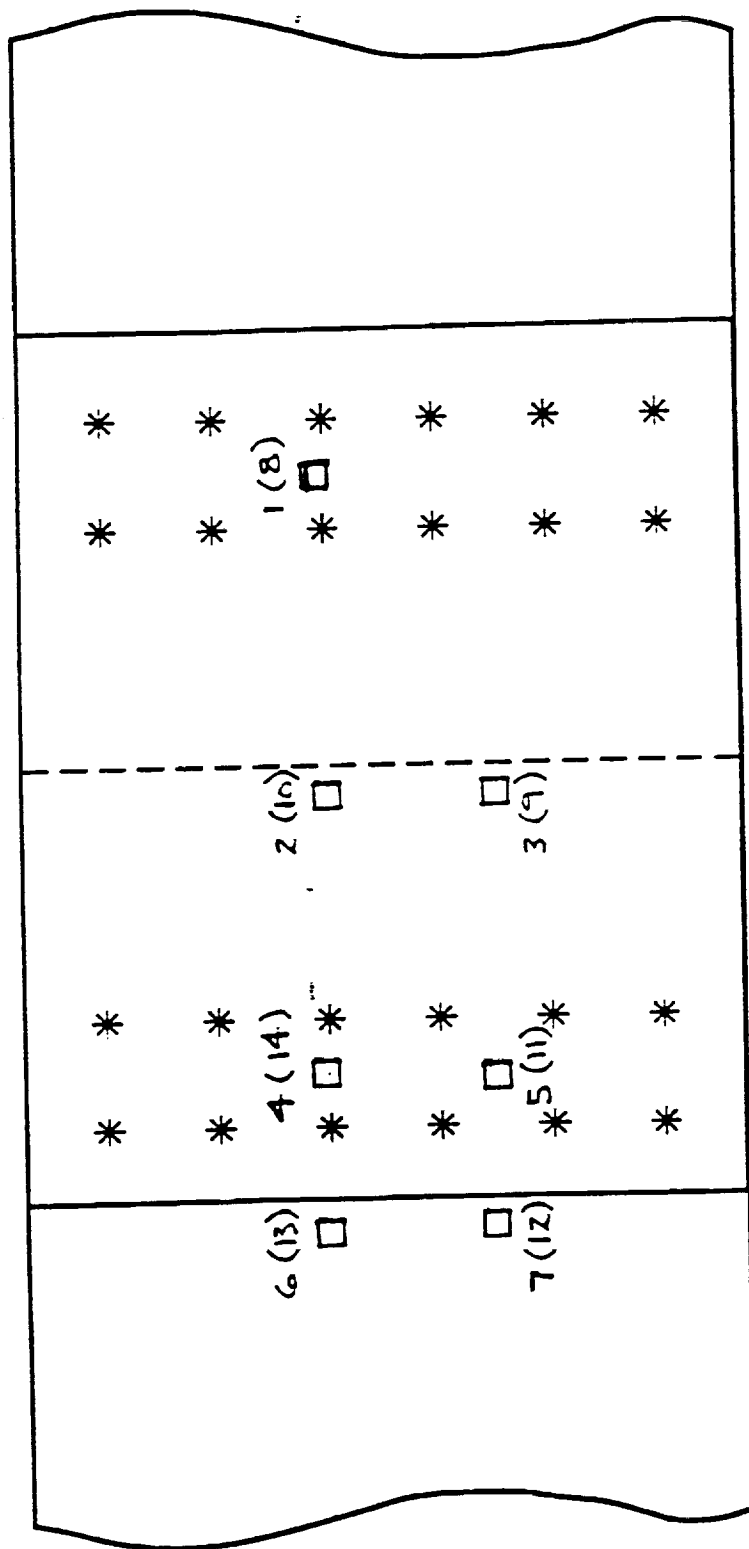


Figure 181. Longitudinal Splice Joint Test Configuration for the Staggered Row Spot Weld Pattern.

View A

F4D1



14 Axial Gages

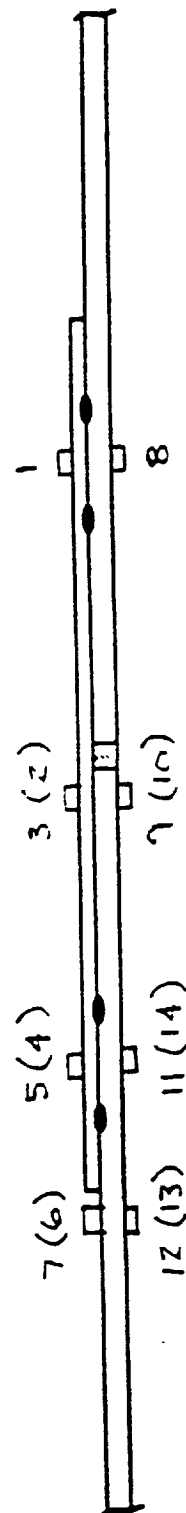
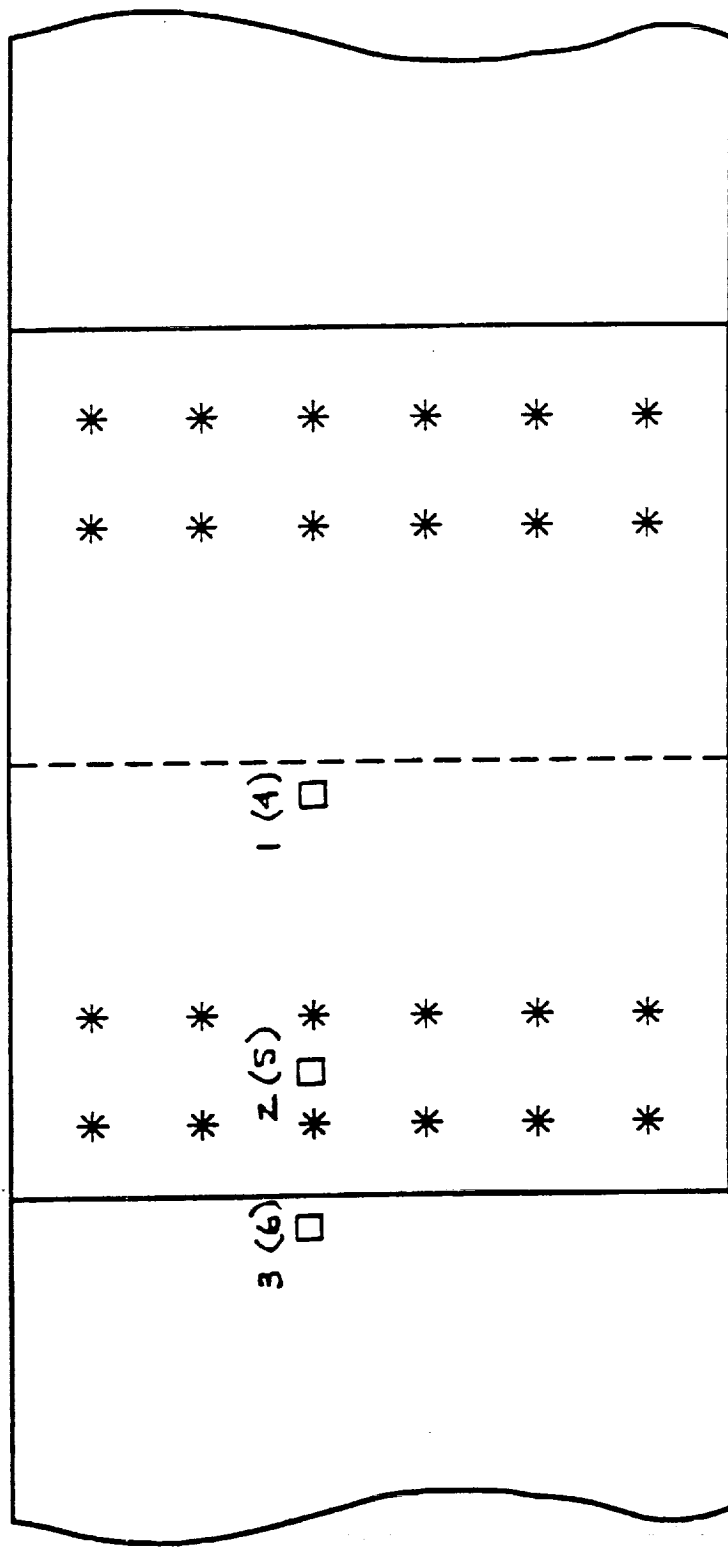


Figure 182. Strain Gage Location for Test Specimen F4D1.

View A

F3D2



6 Axial Gages

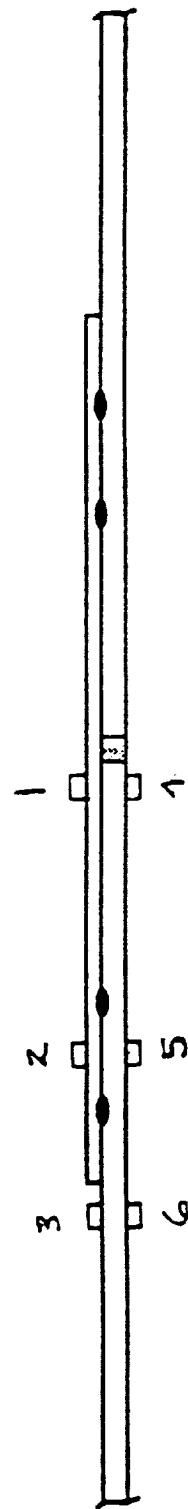
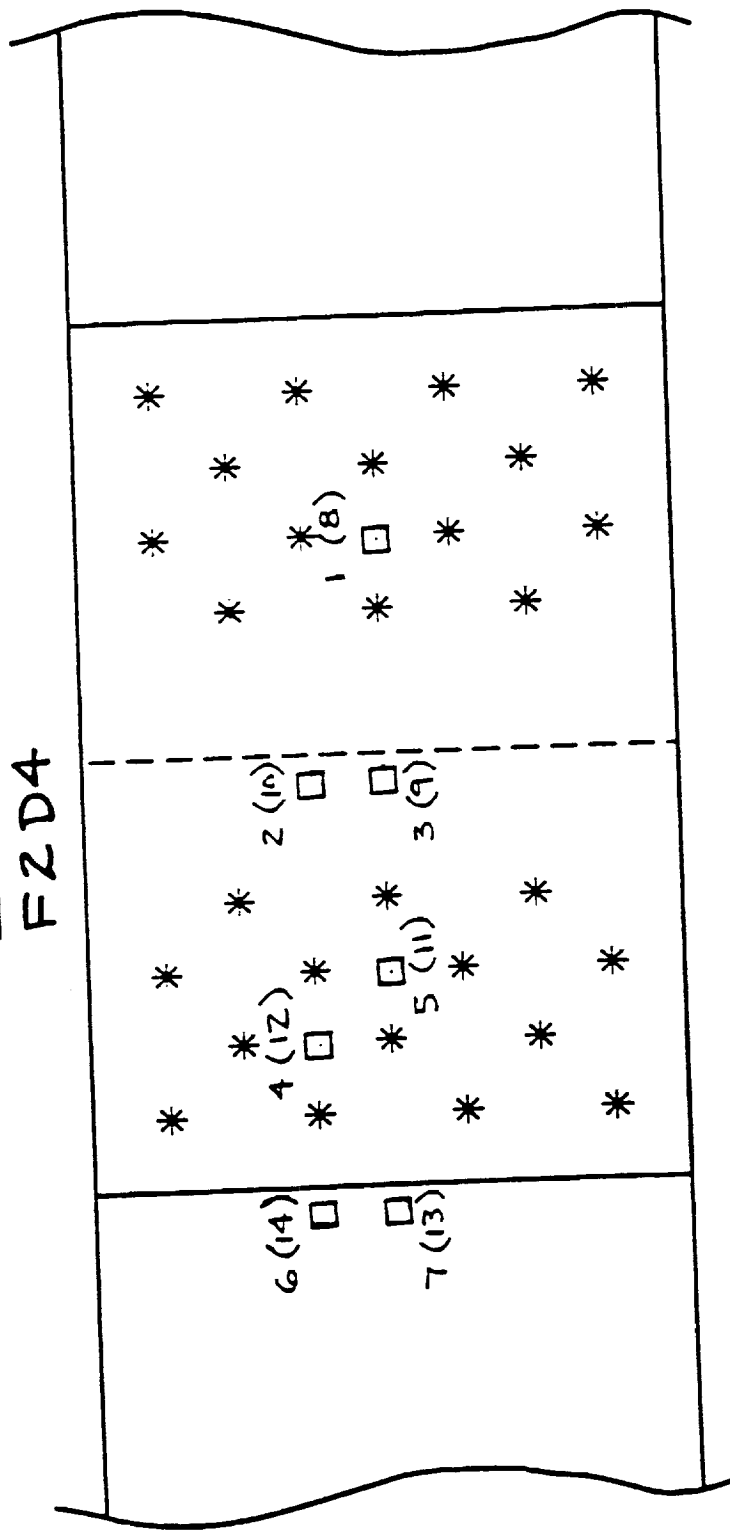


Figure 183. Strain Gage Location for Test Specimen F3D2.

View B

F2D4



14 Axial Gages

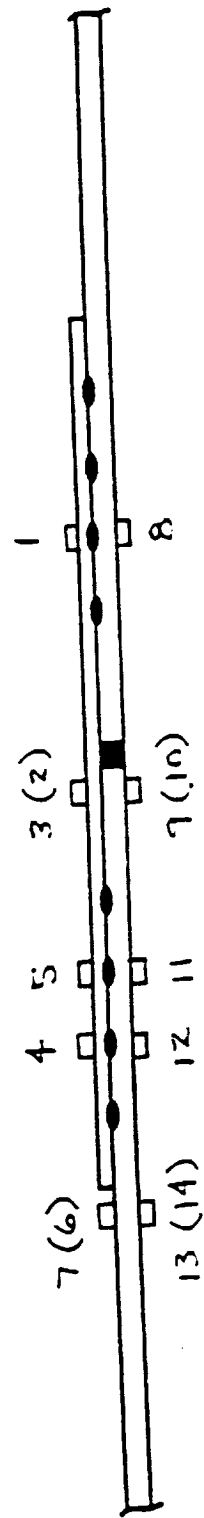
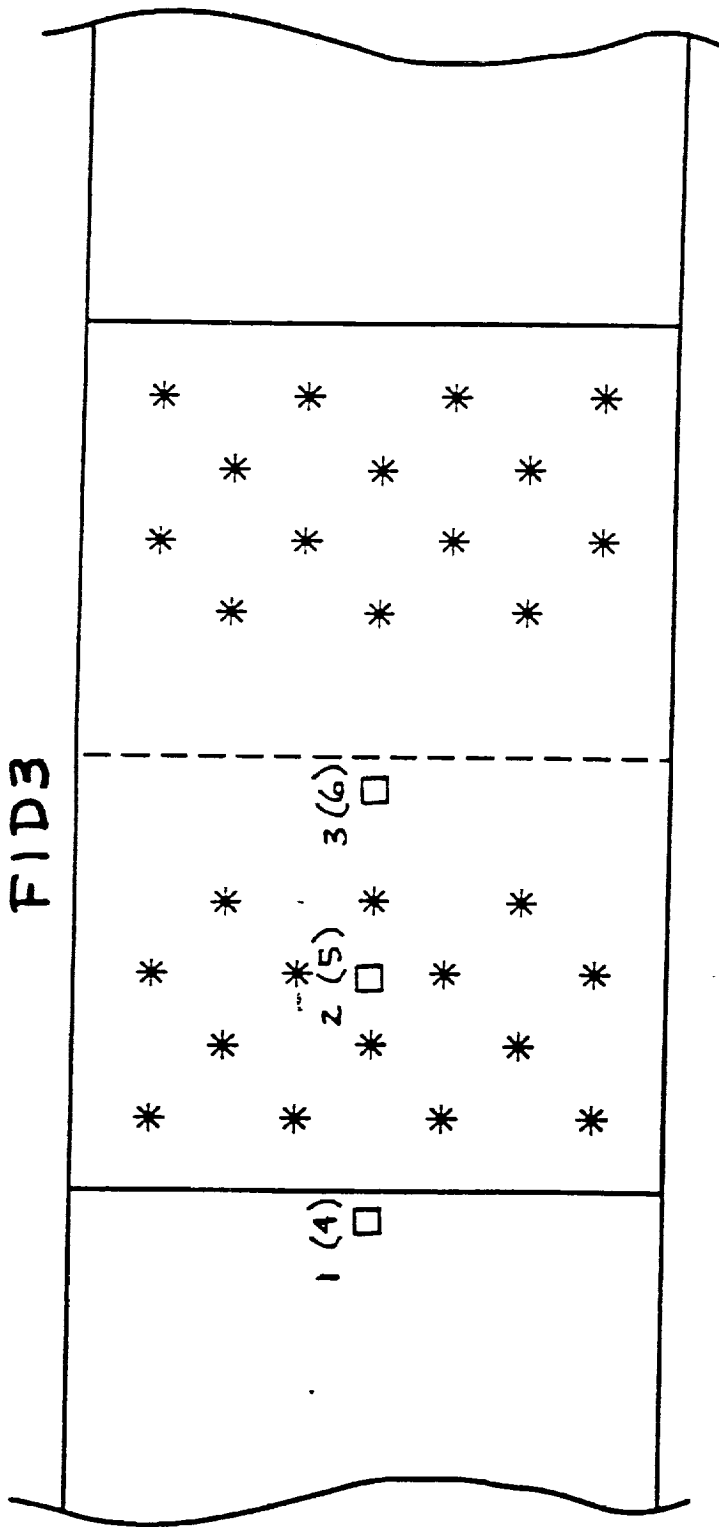


Figure 184. Strain Gage Location for Test Specimen F2D4.

View B

F1D3



6 Axial Gages

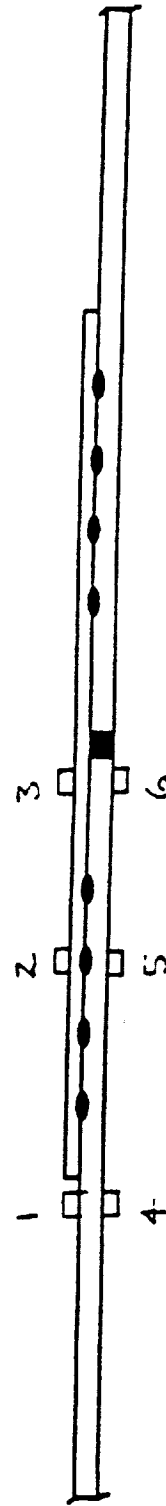


Figure 185. Strain Gage Location for Test Specimen F1D3.

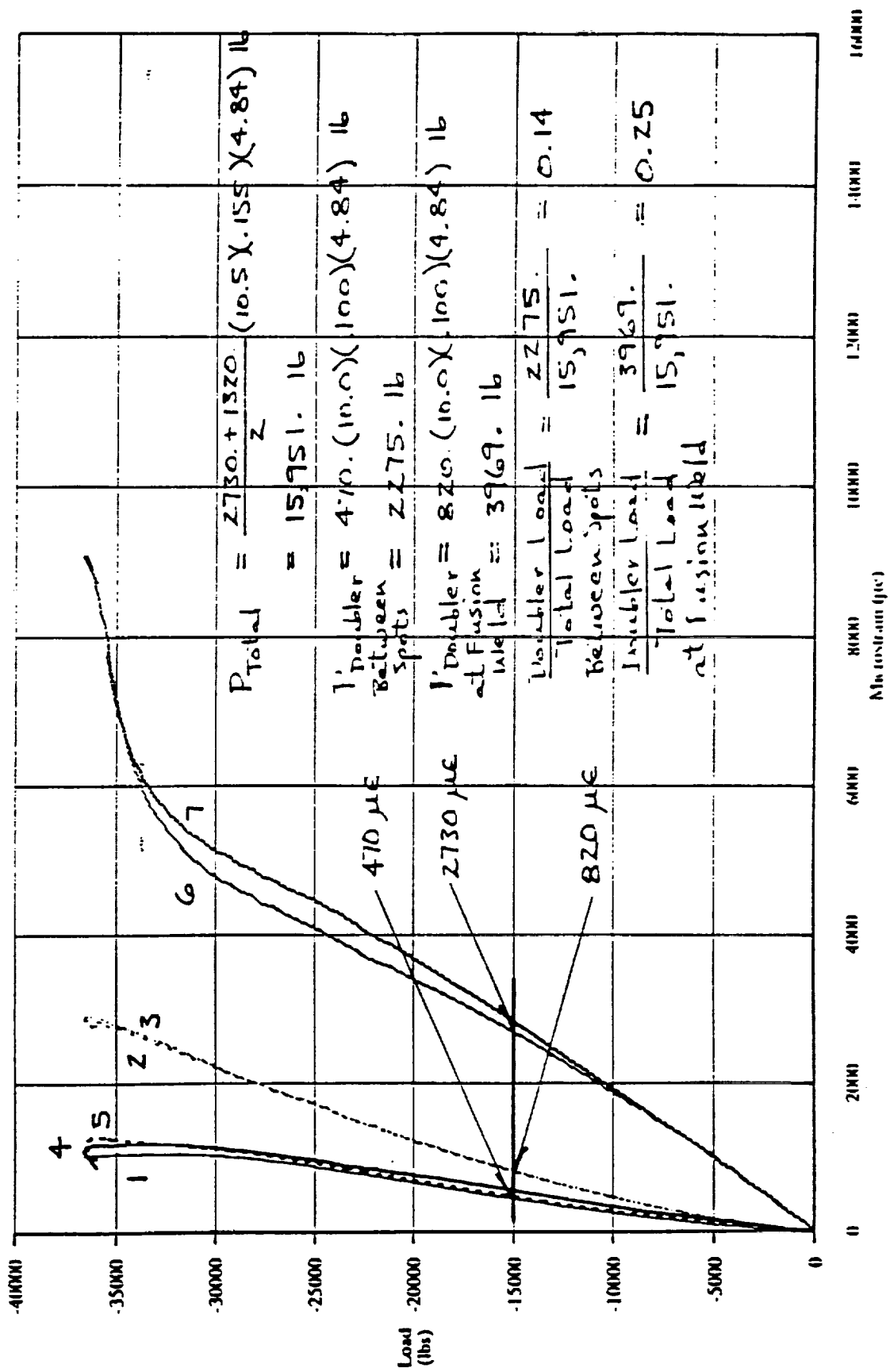


Figure 186. Load Versus Microstrain for Front Strain Gages on Specimen F4D1.

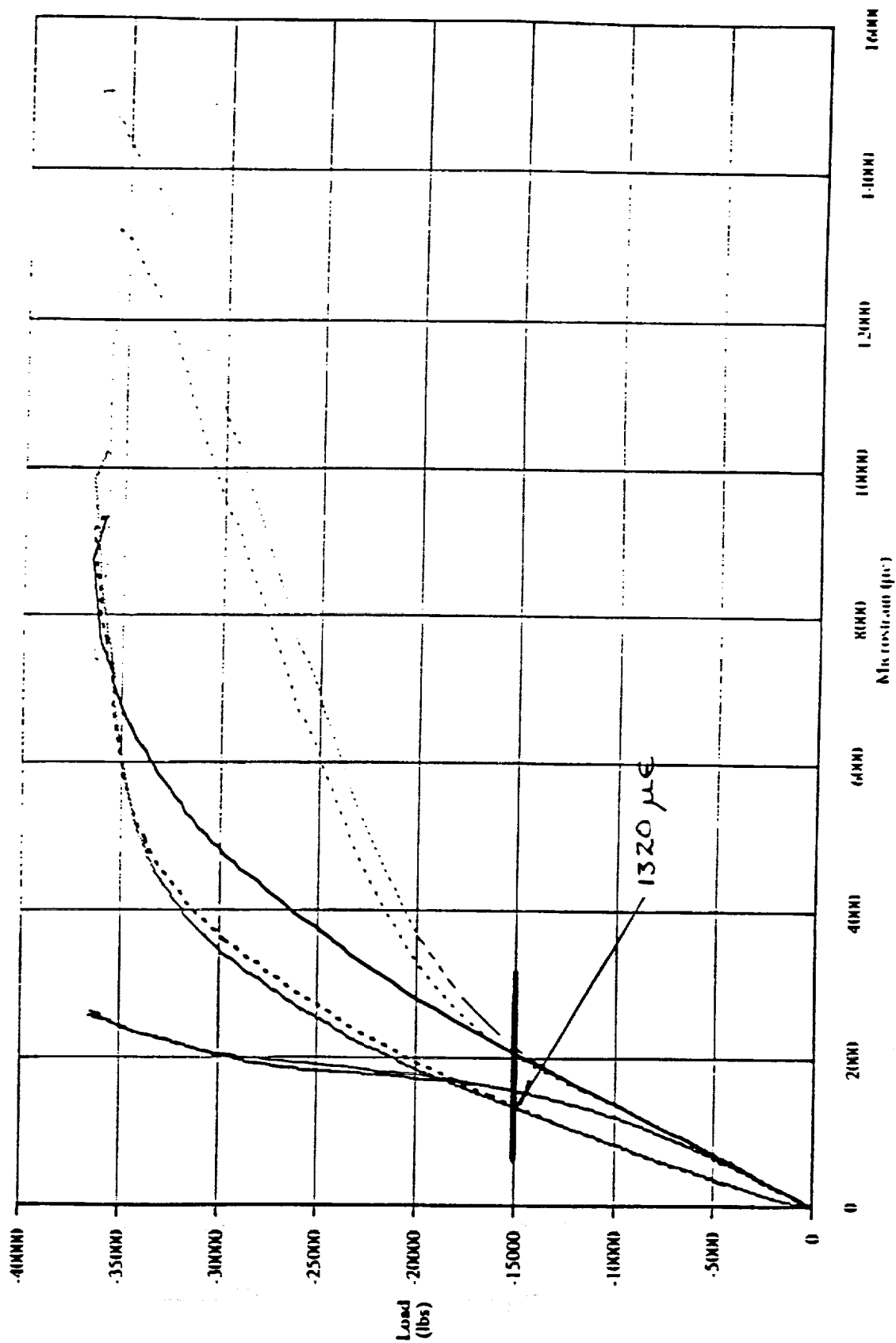


Figure 187. Load Versus Microstrain for Back Strain Gages on Specimen F4D1.

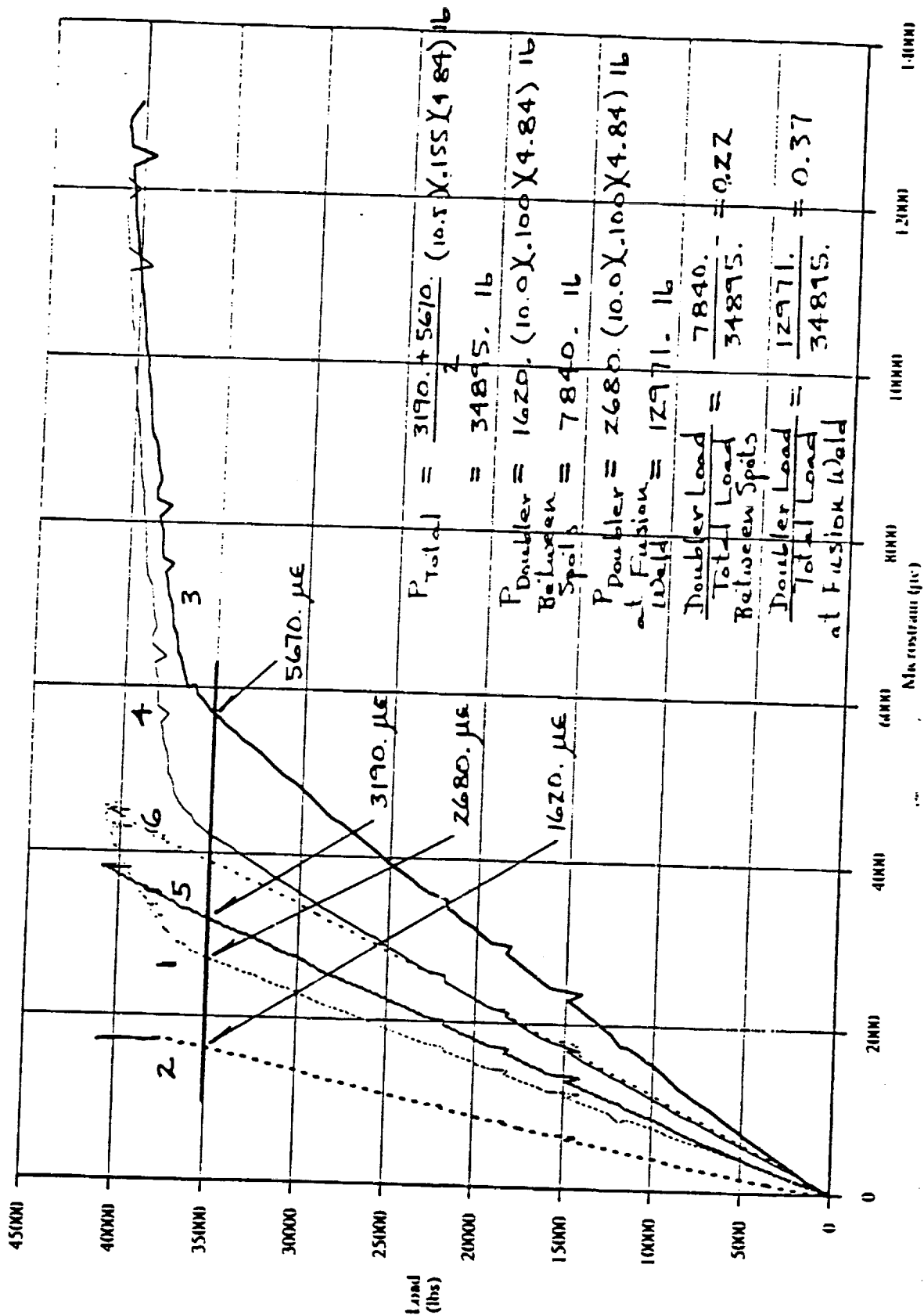


Figure 188. Load Versus Microstrain for Specimen F3D2.

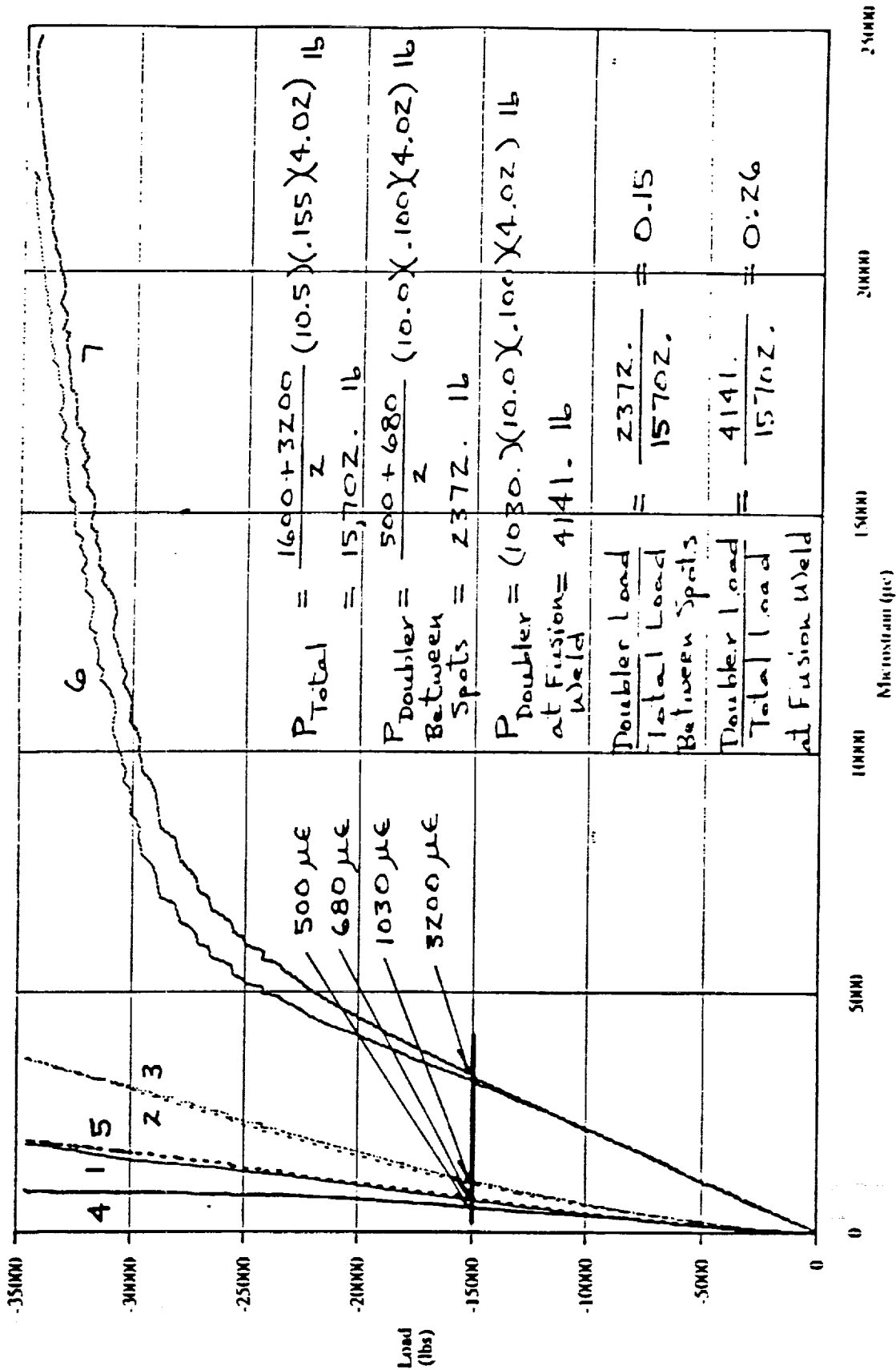


Figure 189. Load Versus Microstrain for Front Strain Gages on Specimen F2D4.

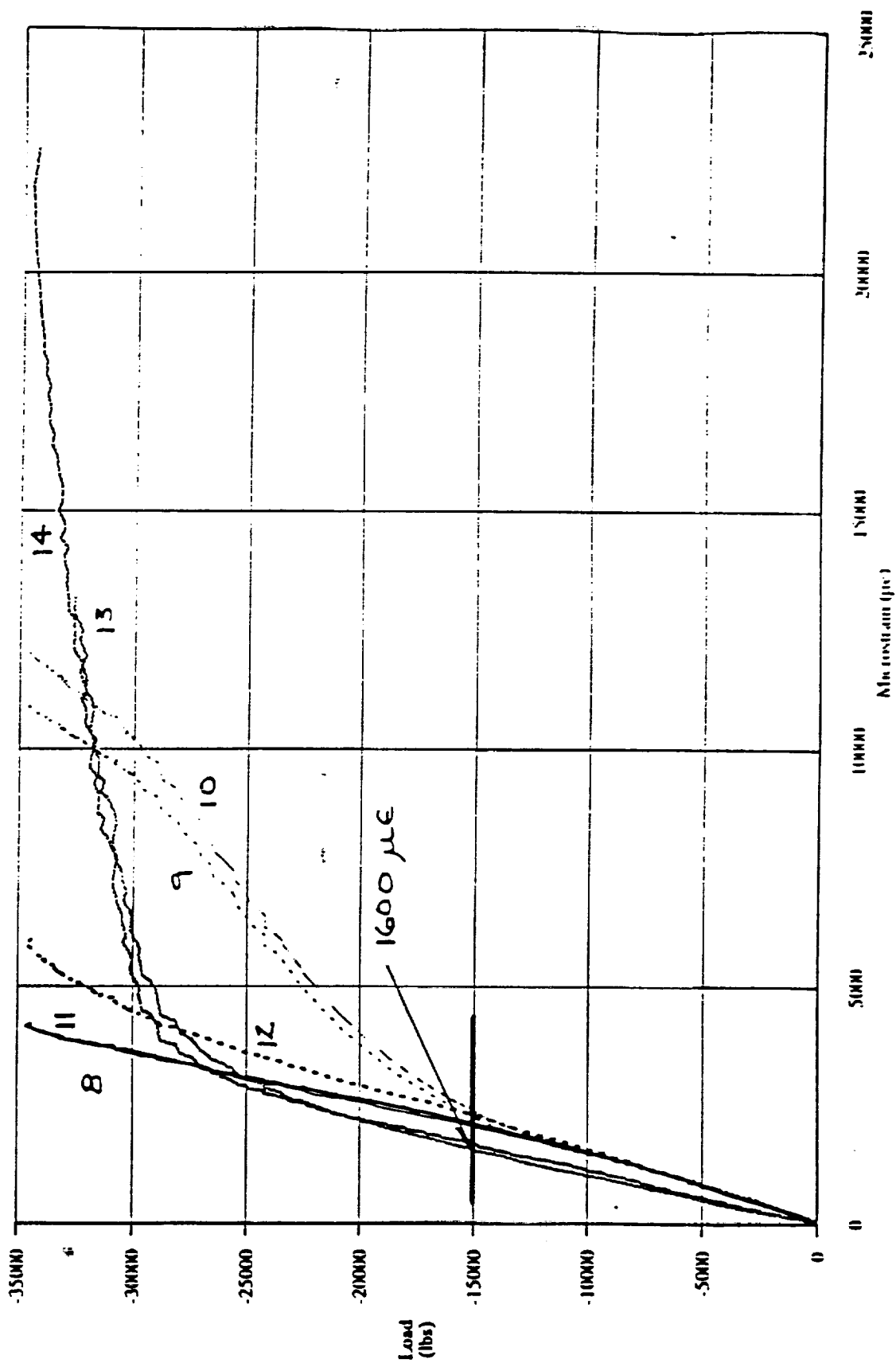


Figure 190. Load Versus Microstrain for Back Strain Gages on Specimen F2D4.

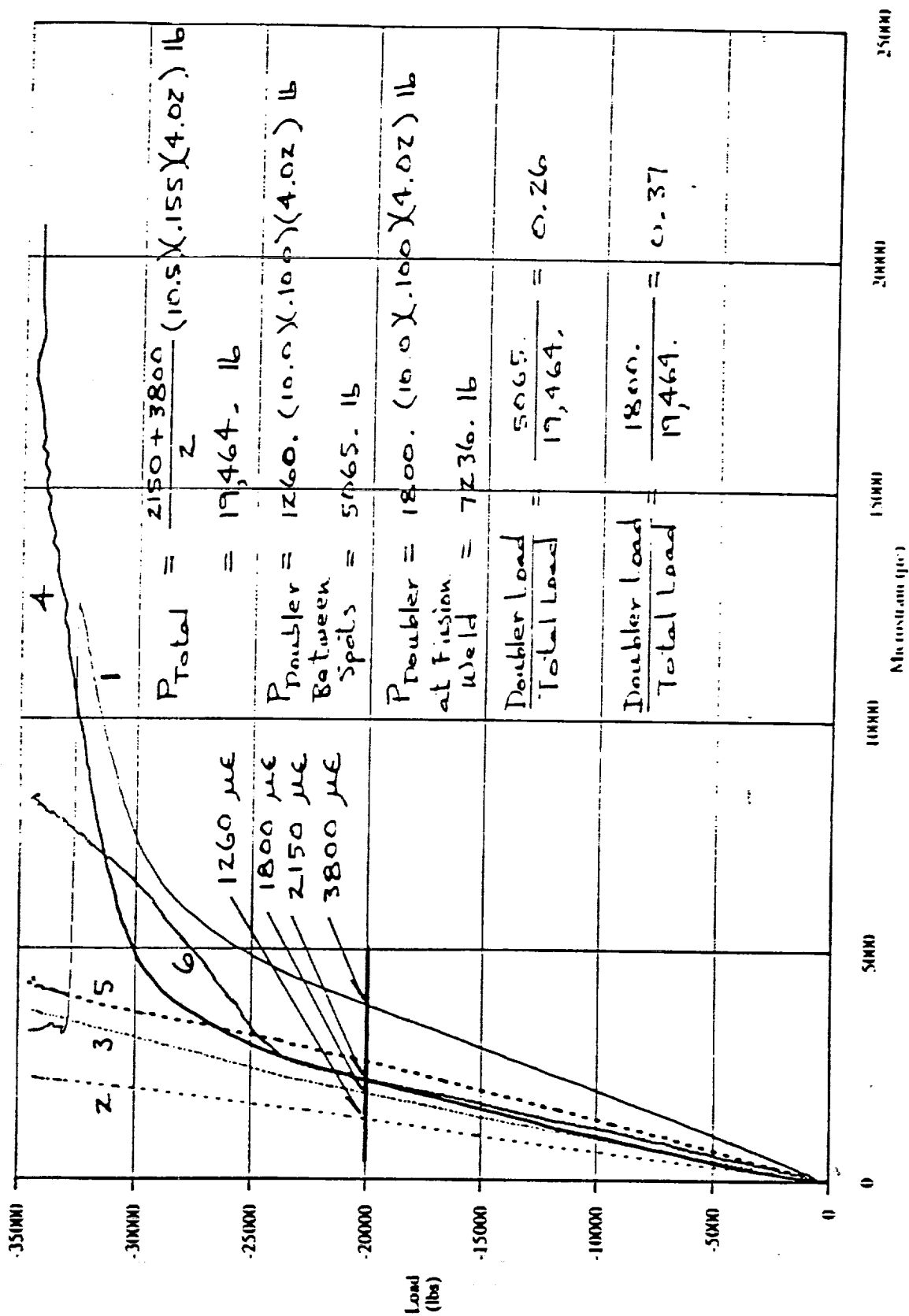


Figure 191. Load Versus Microstrain for Specimen F1D3.

then the fusion weld would be close to the average fusion weld ultimate stress as found by experiment at General Dynamics shown in Table 107. However, it is believed that local yielding in the vicinity of the fusion weld acted to limit the fusion weld stress and therefore offer some degree of protection for the joint. Additionally, it is seen that the spot weld loads are quite modest as compared to the allowable loads listed in Table 107.

Since all specimens failed in the basic skin at the first spot weld row and since the spot weld loads are quite modest then it would suggest that the joint strength could be improved by a process of optimizing the parameters of the joint configuration. For instance, possibly the spot weld spacing could be increased to improve the basic sheet efficiency but yet not overload the spot welds. However, this decrease in the number of spot welds would increase the load at the fusion weld. For this reason the sensitivity curves of Figure 192 through 194 were generated to show the fusion weld stress and the spot weld shear load as a function of the doubler thickness, spot weld gage (spacing), and of the doubler width. These curves were only generated for the even spot row configuration since it was seen that the staggered row configuration had the disadvantage of showing higher fusion weld stresses with no real advantage except lower spot weld shear loads. The curves in Figures 192 through 194 were generated for a constant joint load of 7585 lb/in.

4.4 PANEL FABRICATION AND TEST

4.4.1 FABRICATION AND TESTING OF CRIPPLING PANELS

4.4.1.1 Crippling Panel Fabrication

The crippling panel designs were based upon the analysis of the three selected stiffener configurations. The designs were analyzed and optimized for fabrication and structural testing. The crippling specimens were superplastic formed, heat treated, trimmed, inspected, spot welded to outer skin material and assembled into the test fixtures. Testing was preformed on the three configurations and compared with predicted behavior of the stiffened structures.

4.4.1.1.2 Crippling Panel Tool Design and Fabrication

The SPF tooling was fabricated as a die box with three inserts that were indexed into the bottom of the tool. This type of configuration (die box with inserts) provides for a least cost tooling approach, and maximizes the types of configurations that can be fabricated with the universal tool. The die box and inserts were fabricated from mild steel (1020 steel) shown in Figure 195 and 196. The crippling panel SPF tooling was installed into the automated 300 ton press and evaluated for thermal stability (refer to Figure 197 and 198) and insulation requirements that would be utilized during the forming process. Pressure versus time profiles were run for the

three stiffener configurations for all of the materials used during the program (7475 Al, 2090 Al-Li, 8090 Al-Li, and x2095 Al-Li) refer to Figures 199 through 202

Table 107. Spot Weld and VPPA Fusion Weld Strength Values for Various

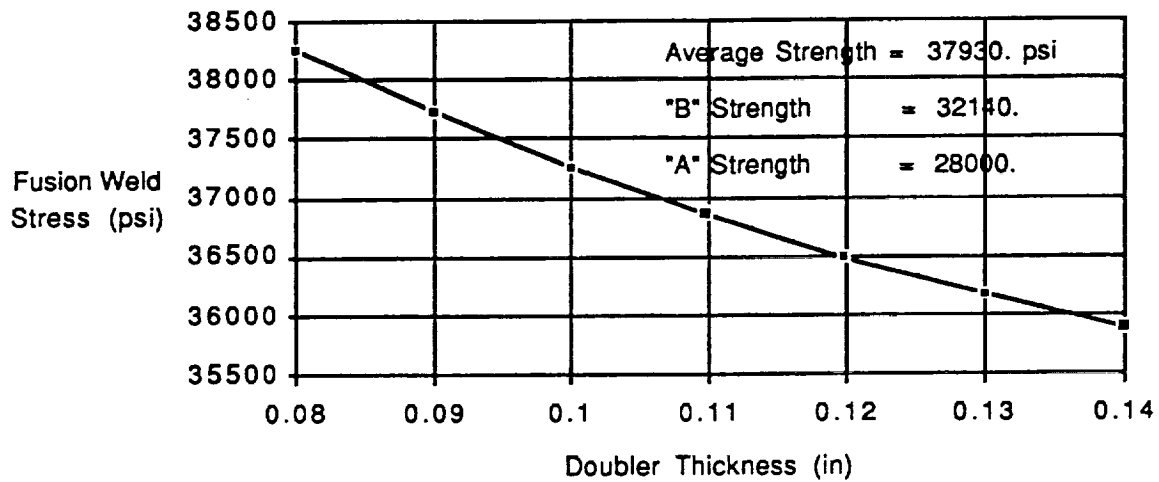
Material Combination (Doubler/Base Sheet)	Reference Temp	Spot Lap Shear Values (lb.)			Sheet Efficiency (ksi)		
		Average	"A" Allowable	"B" Allowable	Average	"A" Allowable	"B" Allowable
0.100" 7475-T62/.155" 2219-T81	R.T.	2616 (6)	1480 (6)	1941 (6)	62.03 (7)	56.36 (7)	58.68 (7)
0.090" 2090-T62/0.155" 2090-T8	R.T.				68.4 (8)		
0.100" 7475-T6/0.190" 2219-T8	R.T.				62.13 (3)	58.73 (3)	60.11 (3)
	LN2				74.74 (3)	69.80 (3)	71.82 (3)
	LH2				82.82 (3)	67.49 (3)	73.72 (3)
0.090" 2090-T62/0.190" 2090-T83	R.T.				65.89 (4)	59.2 (4)	61.92 (4)
	LN2				76.13 (4)	60.43 (4)	66.81 (4)
	LH2				87.68 (4)	72.83 (4)	78.87 (4)
0.072" 2090T-62/0.190" 2090-T83	R.T.	2175 (2)	1570 (2)	1822 (2)			
0.077" 7475-T6/0.190" 2219-T8	R.T.	2909 (1)	2402 (1)	2613 (1)			

- (1) Fourteenth Monthly Report, Table 1
- (2) Fourteenth Monthly Report, Table 2
- (3) Sixteenth Monthly Report, Table 1
- (4) Sixteenth Monthly Report, Table 2
- (5) Eighteenth Monthly Report, page 7
- (6) Eighteenth Monthly Report, page 8
- (7) Eighteenth Monthly Report, Table 5
- (8) Eighteenth Monthly Report, Table 6

Material Combination (Doubler/Base Sheet)	Reference Temp	VPPAW Fusion Weld Strength (ksi)		
		Average	"A" Allowable	"B" Allowable
0.100" 7475-T62/.155" 2219-T81	R.T.	37.93 (5)	28.00 (5)	32.14 (5)
0.090" 2090-T62/0.155" 2090-T8	R.T.			
0.100" 7475-T6/0.190" 2219-T8	R.T.			
	LN2			
	LH2			
0.090" 2090-T62/0.190" 2090-T83	R.T.			
	LN2			
	LH2			
0.072" 2090T-62/0.190" 2090-T83	R.T.			
0.077" 7475-T6/0.190" 2219-T8	R.T.			

Joints.

2219 Long Joint Fusion Weld Stress vs. Doubler Thickness



2219 Long Joint Spot Shear Load vs. Doubler Thickness

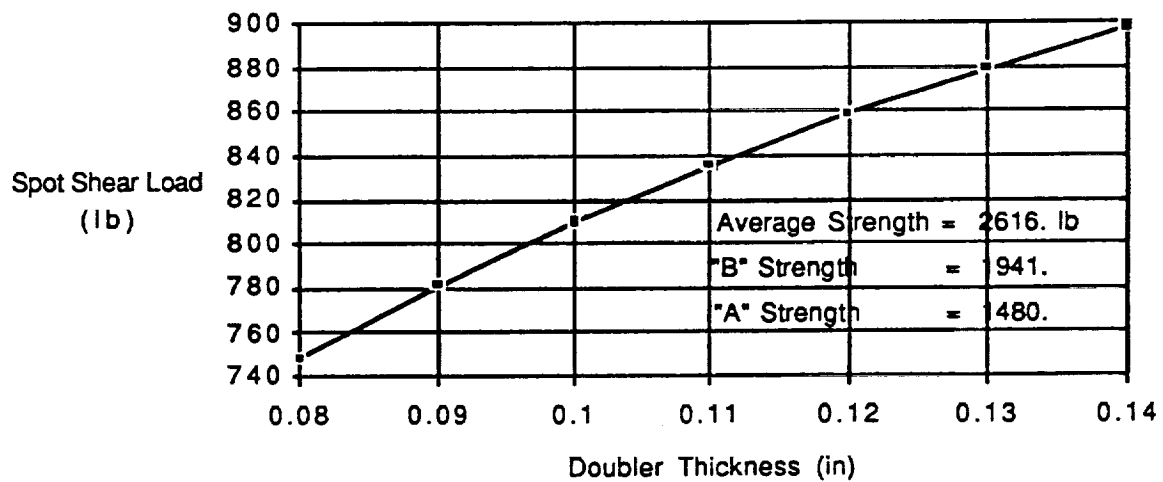
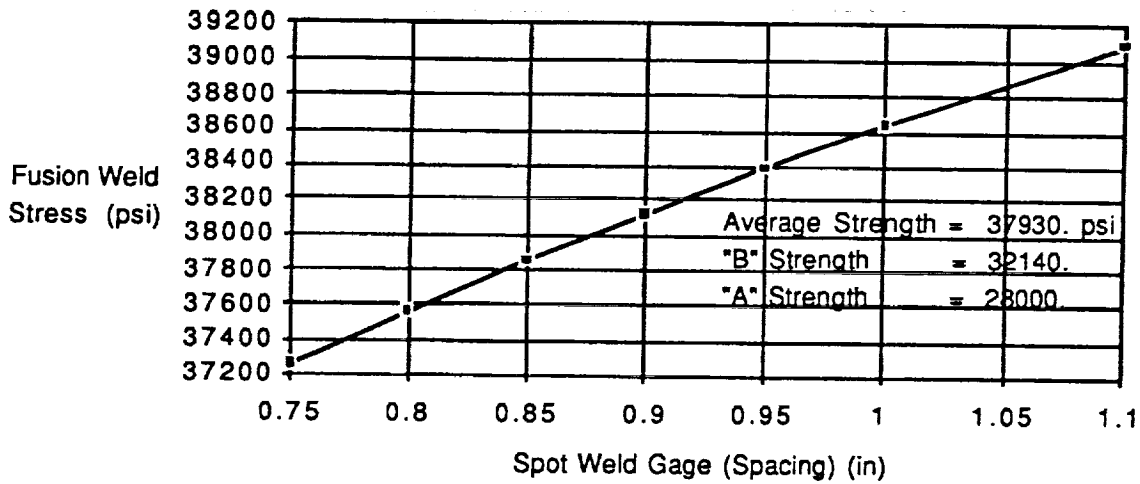


Figure 192. Sensitivities of The Fusion Weld Stress and Spot Shear Load to a Variation in Doubler Thickness.

2219 Long Joint Fusion Weld Stress vs. Spot Weld Gage



2219 Long Joint Spot Shear Load vs. Spot Weld Gage

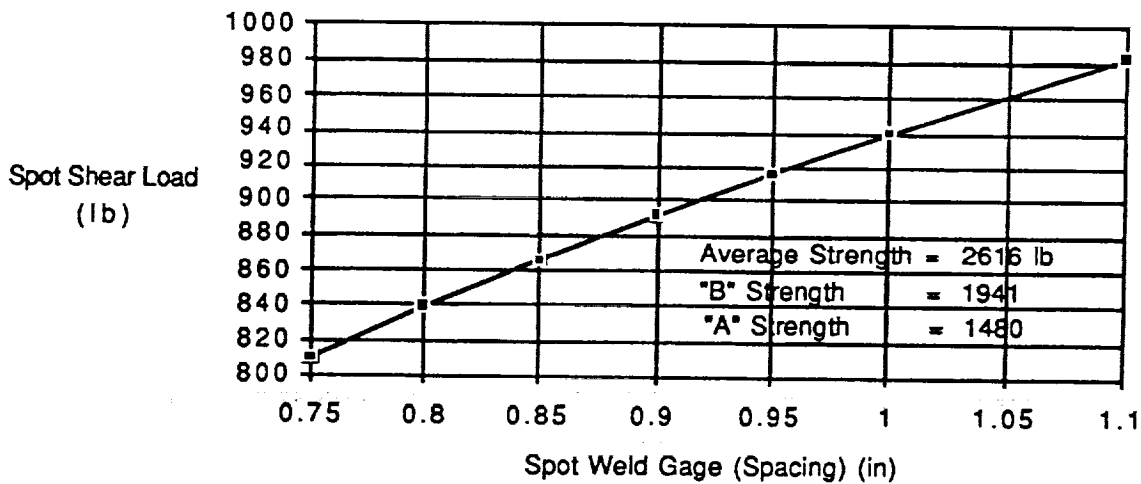
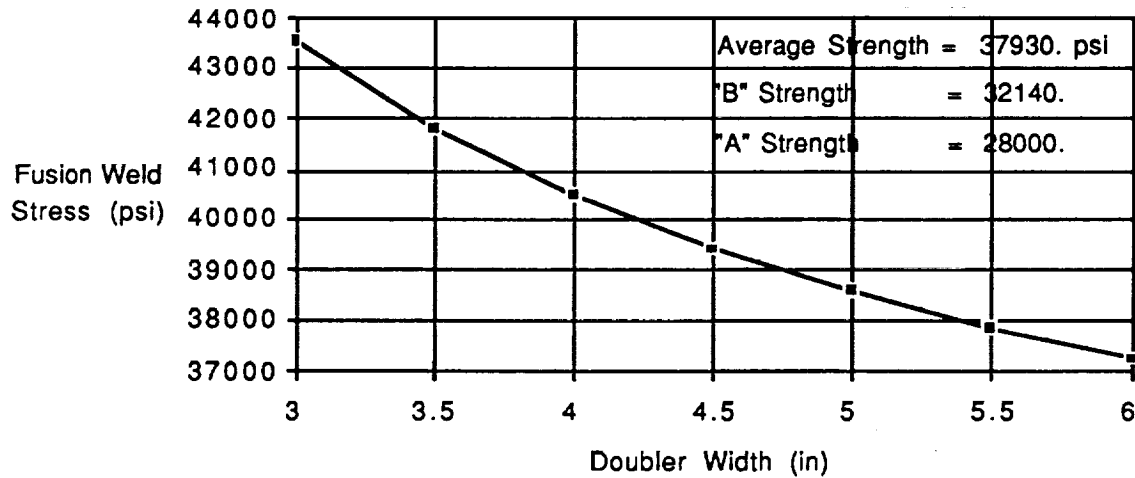


Figure 193. Sensitivities of The Fusion Weld Stress and Spot Shear Load to a Variation in Spot Weld Gage.

2219 Long Joint Fusion Weld Stress vs. Doubler Width



2219 Long Joint Spot Shear Load vs. Doubler Width

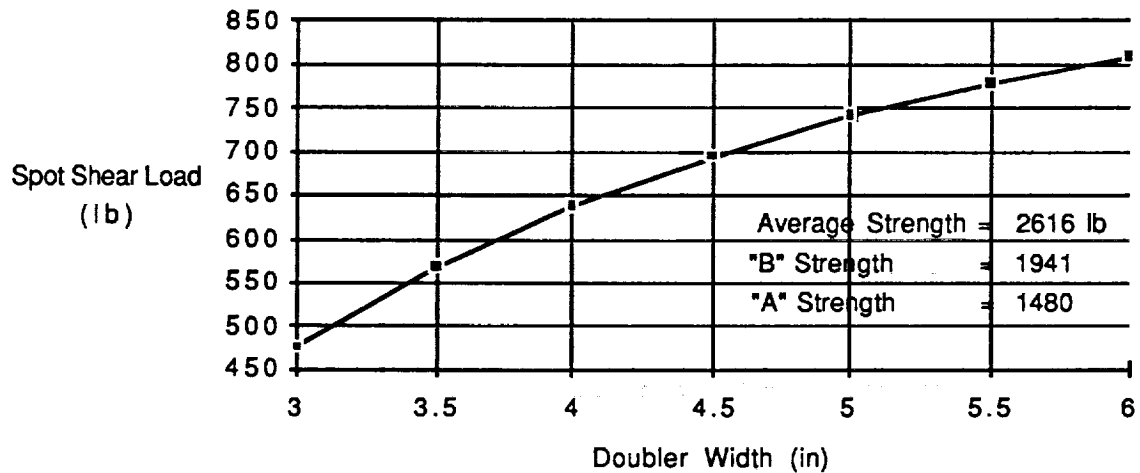


Figure 194. Sensitivities of The Fusion Weld Stress and Spot Shear Load to a Variation in Doubler Width.

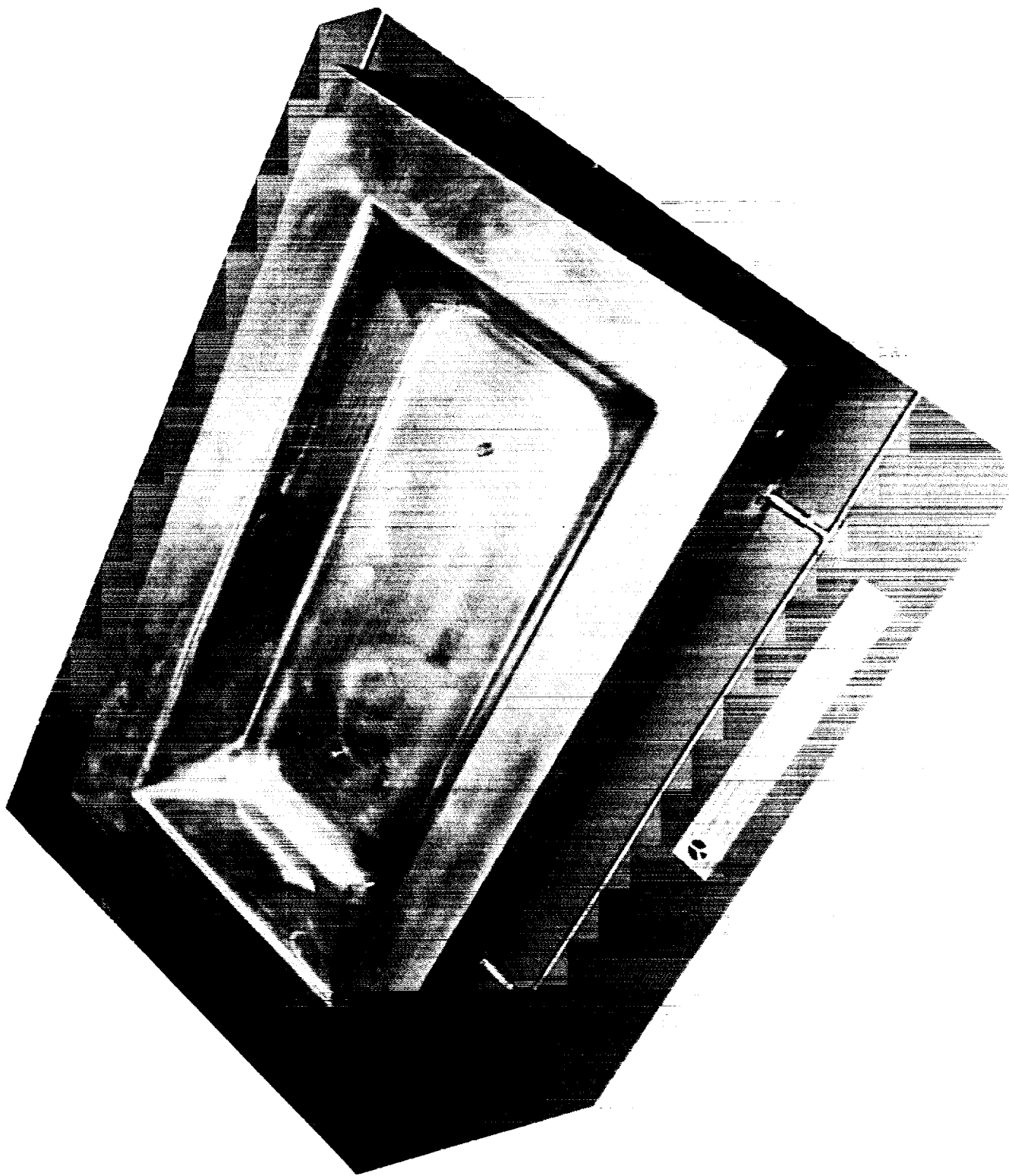


Figure 195. Crippling Specimen Universal Die Box.

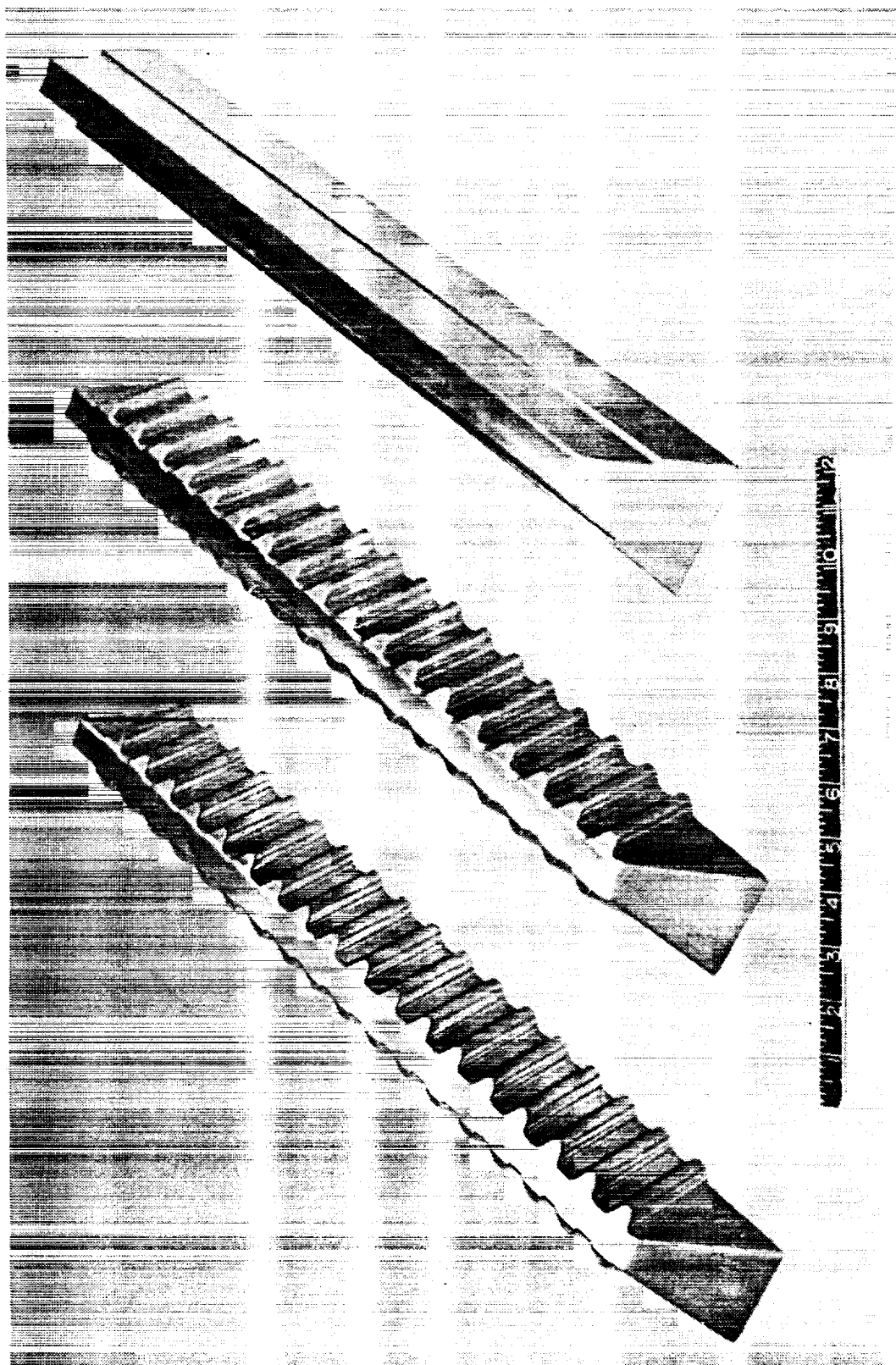


Figure 196. Crippling Stiffener Tool Inserts for Stepped Web Curved Cap Hat, Beaded Web Curved Cap Hat, and Beaded Web Flat Cap Hat.

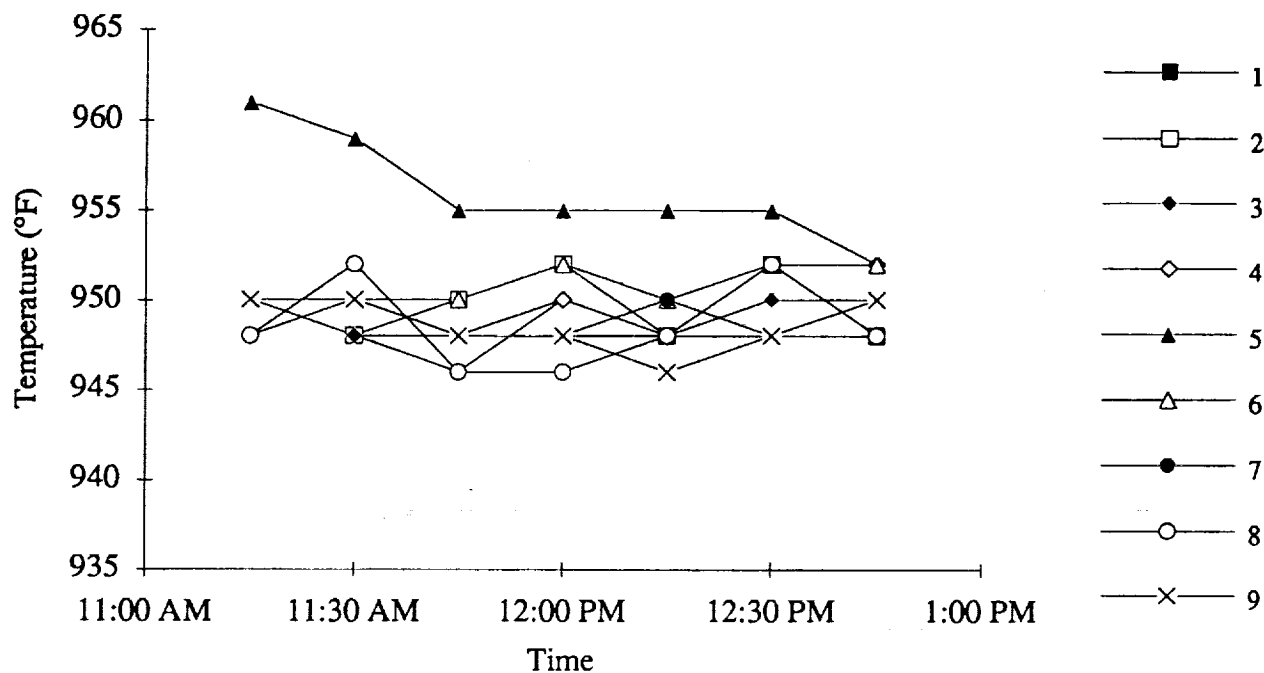


Figure 197. Graphical Representation of the Crippling Tool Thermal Survey.

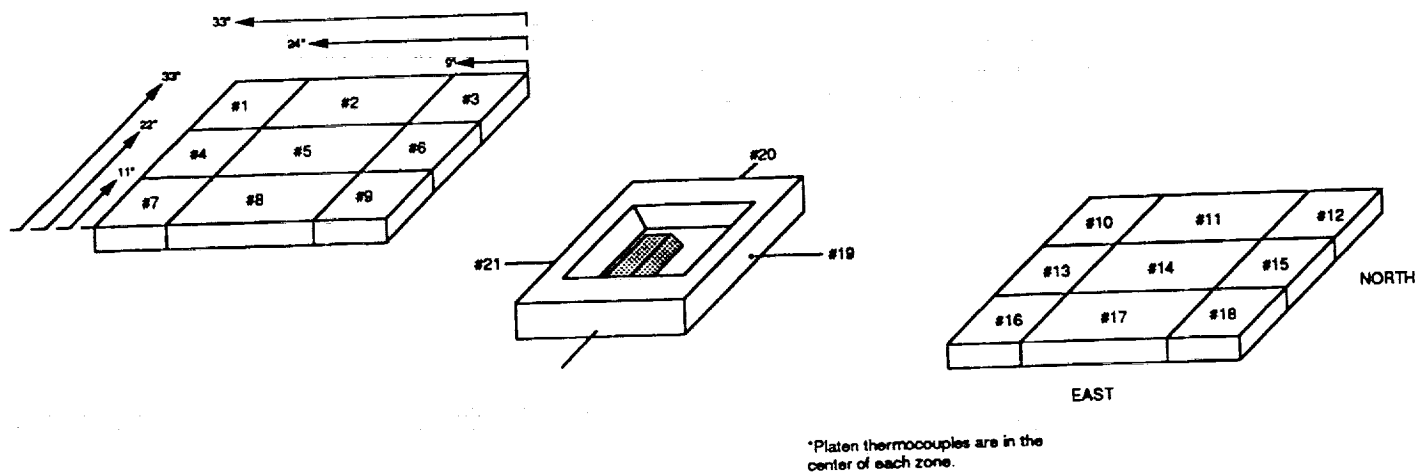


Figure 198. Schematic of Crippling Tool and Platen Thermocouple Layout and Temperature Print Out from Heat Survey.

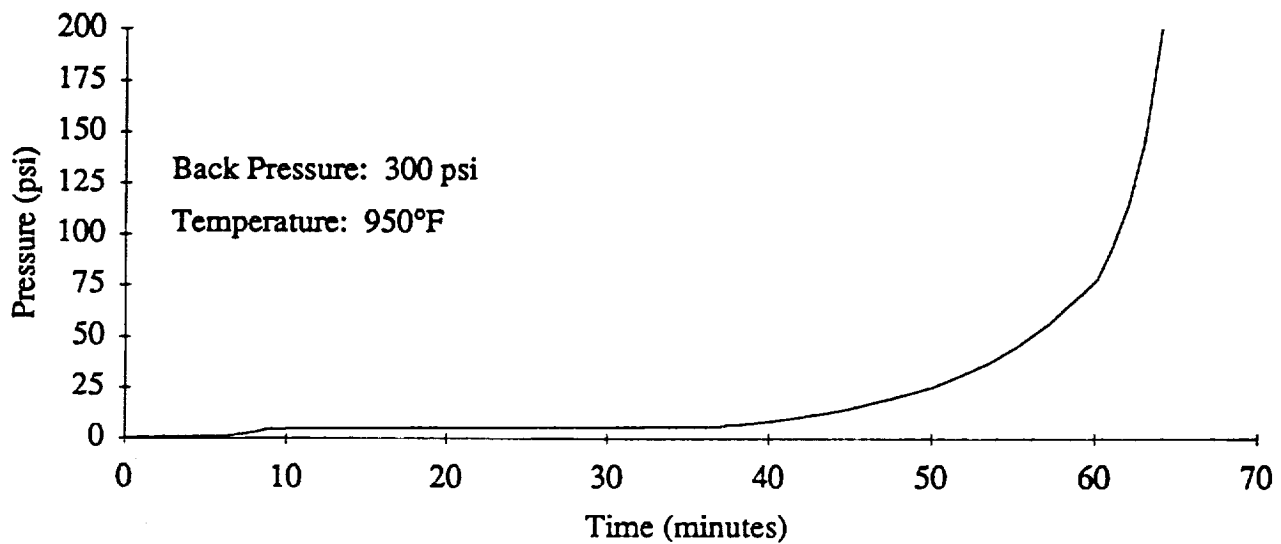


Figure 199. Crippling Panel Pressure Versus Time Profile for 7475 Al.

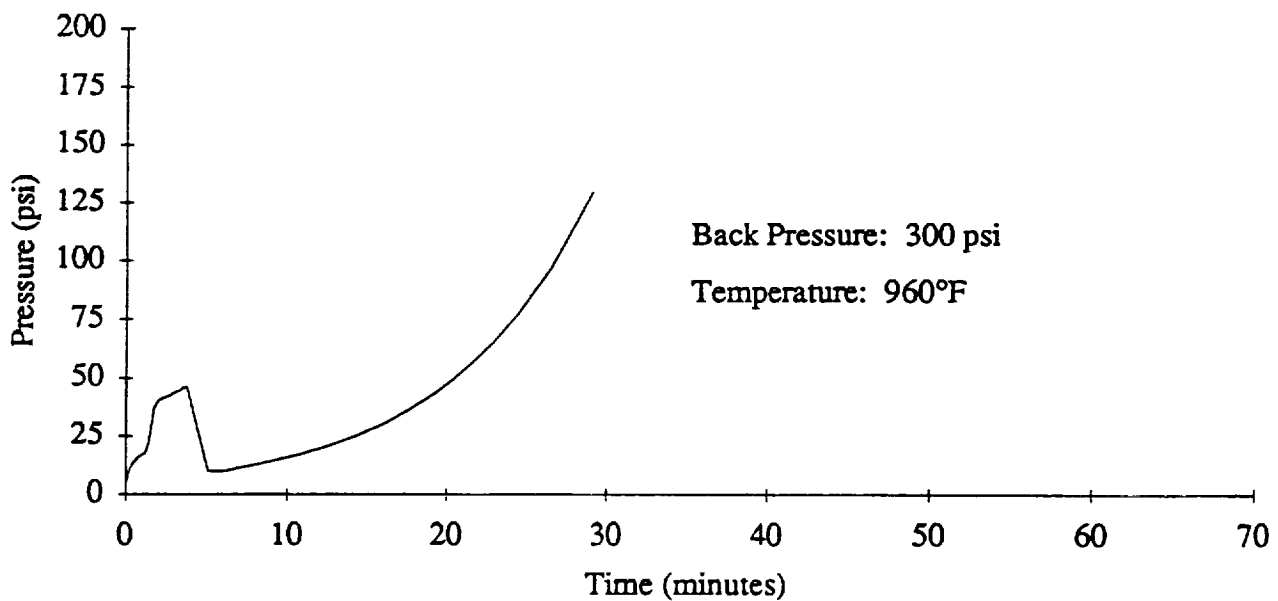


Figure 200. Crippling Panel Pressure Versus Time Profile for 2090 Al-Li.

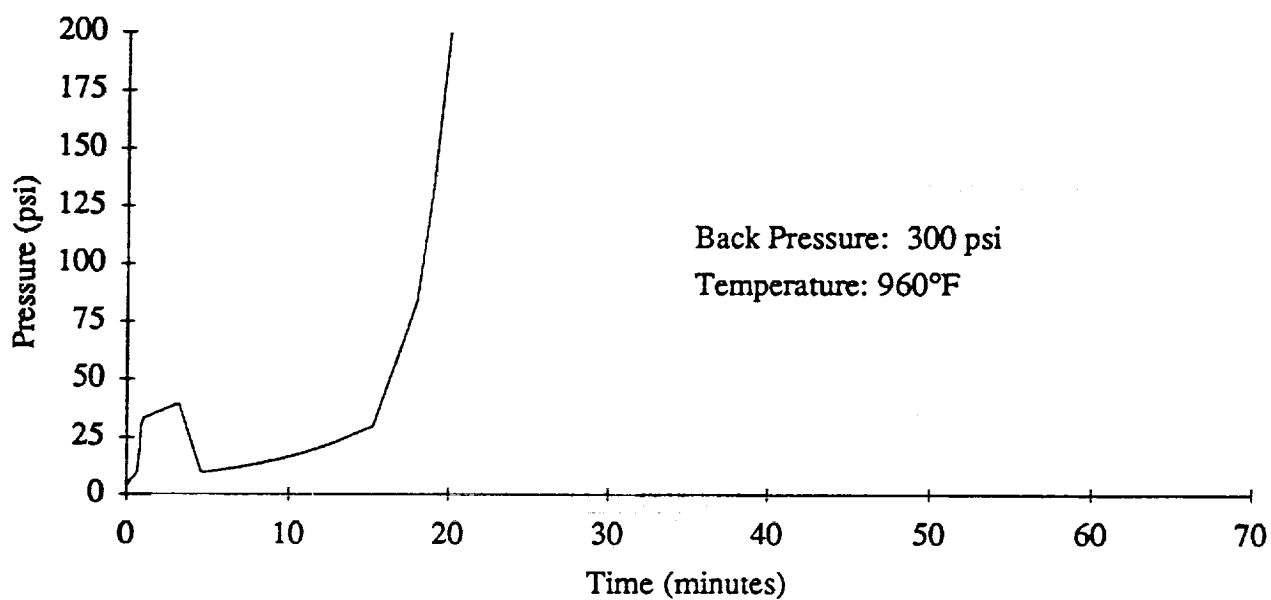


Figure 201. Crippling Panel Pressure Versus Time Profile for 8090 Al-Li.

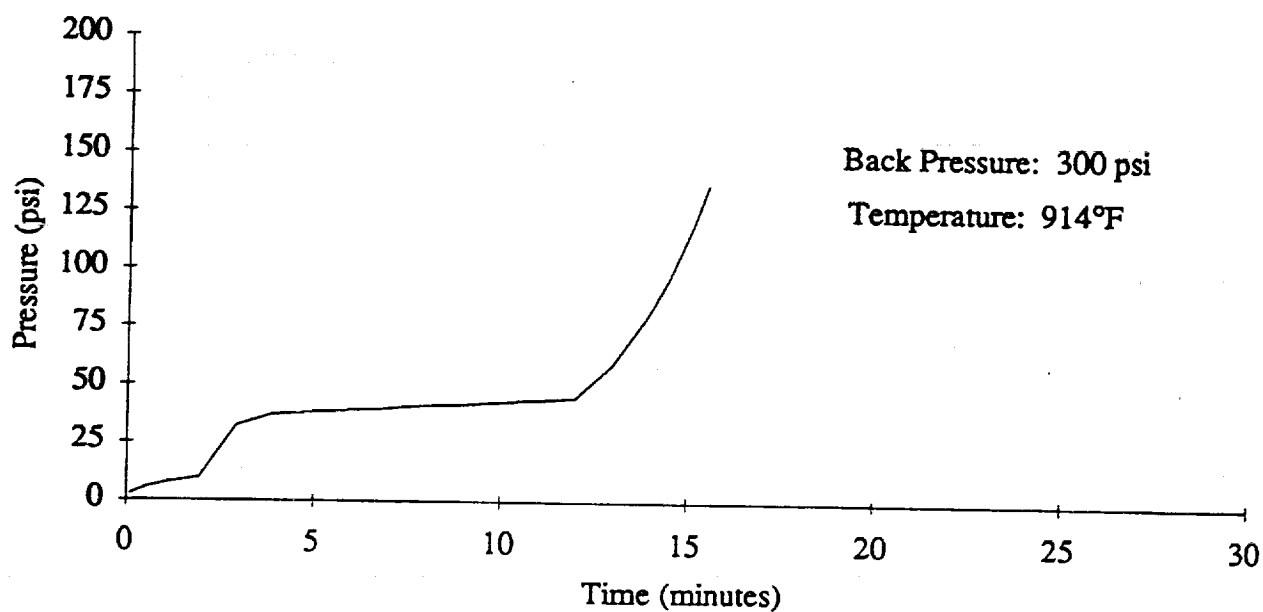


Figure 202. Crippling Panel Pressure Versus Time Profile for 2095 Al-Li.

The part blanks of each material were coated with releasing agent (either sprayed or painted on as shown in Figure 203), hot loaded into the SPF press (refer to Figure 204), formed, hot unloaded (refer to Figure 205) and allowed to slow air cool (refer to Figure 206). The panels were formed, heat treated, trimmed to a net shape configuration (refer to Figures 207 and 208) and inspected (both for surface flaws and for presence of cavitation (initial proof of run part only)) prior to shipment to General Dynamics Space Systems Division for joining and final assembly. Thickness measurements were evaluated for all three panel configurations to assess the predicted versus actual thinning and to map the thinning in the flange area prior to welding. Additional specimens were shipped as dummy specimens for display and verification of the welding procedure.

4.4.1.2 Crippling Panel Test Plan

4.4.1.2.1 Introduction

Three hat stiffener concepts with various material combinations have been designed by Rockwell in conjunction with NASA Langley and General Dynamics to utilize the SPF process in combination with resistance spot welding or an alternate joining concept. The purpose of these concepts is to reduce the manufacturing cost of large cryogenic LH₂ tank designs associated with ALS or future hypersonic vehicles

The objective of this test plan is to delineate the type of loading fixture, instrumentation, failure load predictions, and test procedure that are required to evaluate these stiffener concepts under uniaxial compression for local buckling, crippling and joint effectiveness (referring to the spot weld application or adhesive system).

4.4.1.2.2 Specimen Description

Each specimen consists of a 16.75" x 6" x 0.190" plate skin which is spot-welded at intervals to the inner flanges of a particular 2" high stiffener configuration as shown in Figure 209. The hat stiffener designs were selected to increase structural efficiency and utilize the SPF process are as follows:

- A) Stepped hat with curved outer cap
- B) Beaded web hat with curved outer cap
- C) Beaded web hat with flat outer cap

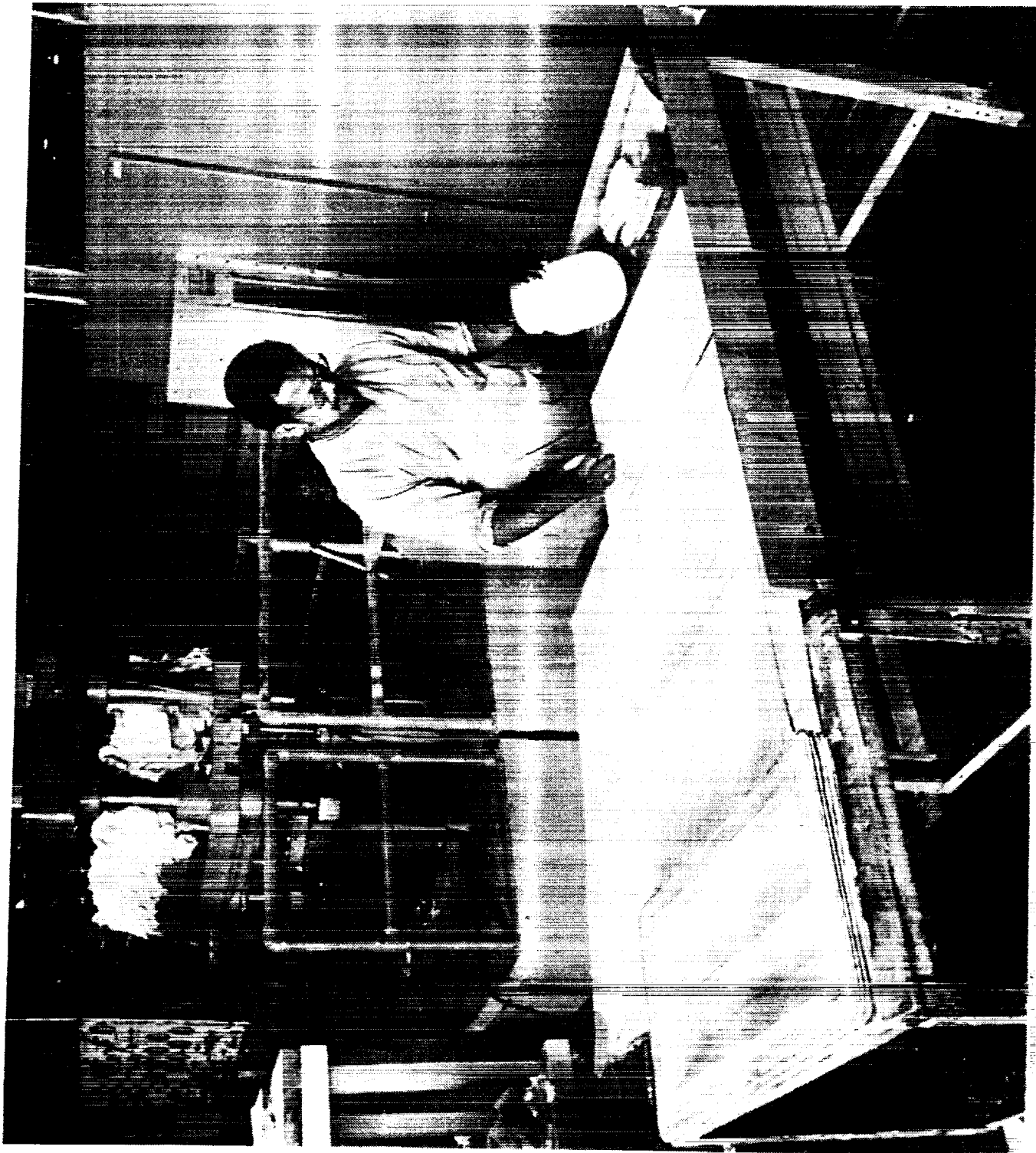


Figure 203. Application of Releasing Agent on Part Blank.

ORIGINAL PAGE
BLACK AND WHITE PHOTOGRAPH

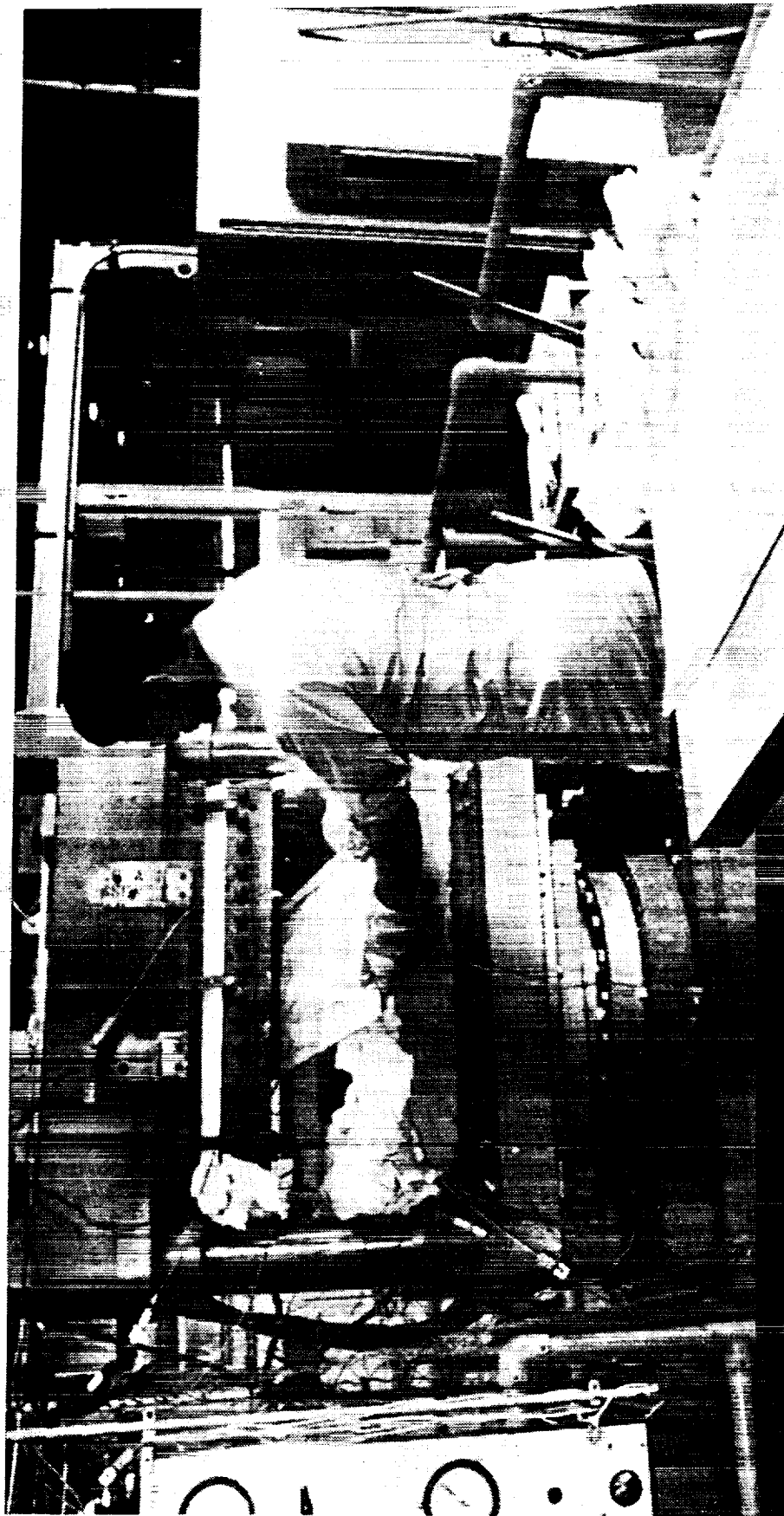


Figure 204. Hot Loading of Part Blank into Automated 300 Ton Press.

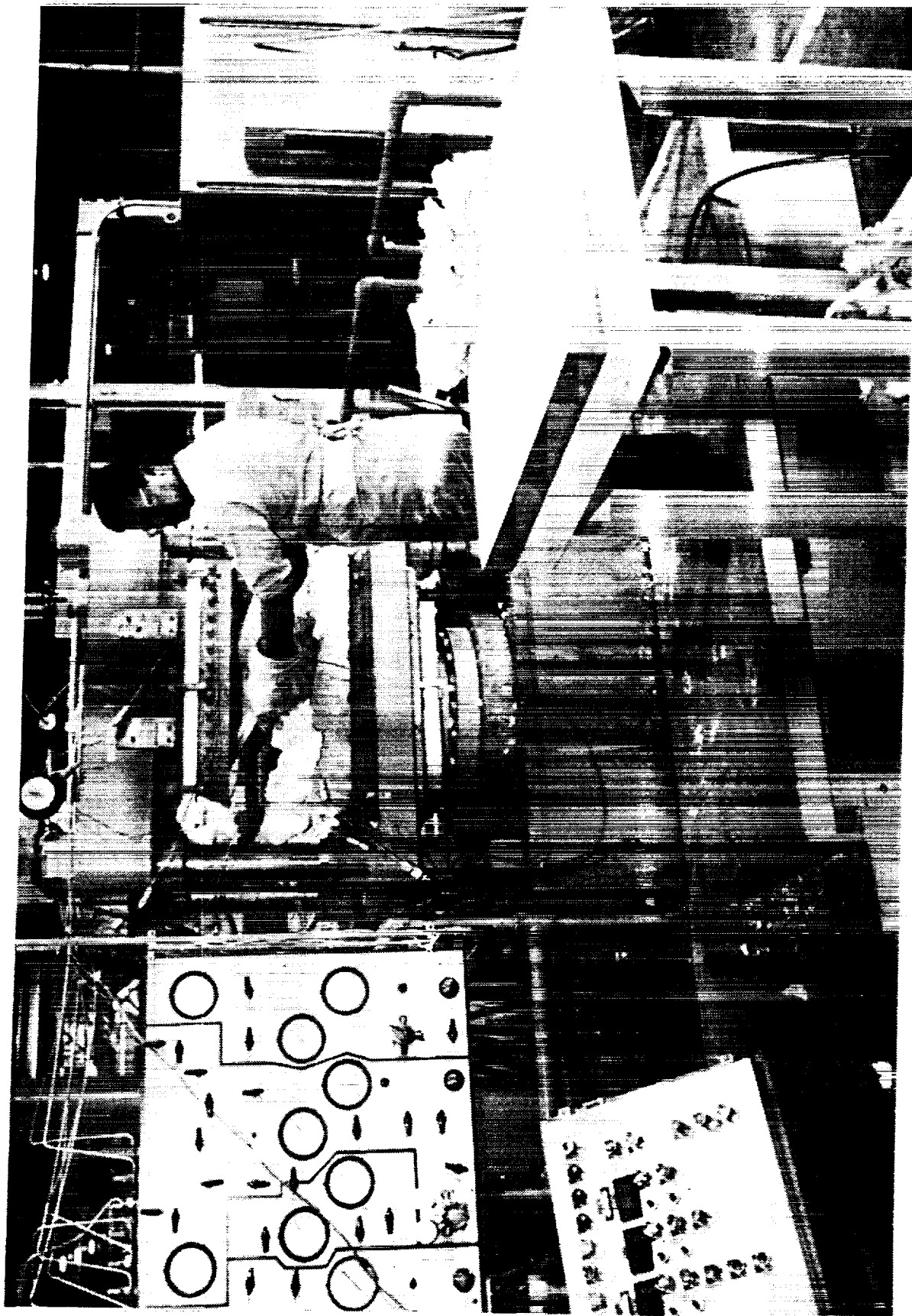


Figure 205. Hot Unload Formed Part.

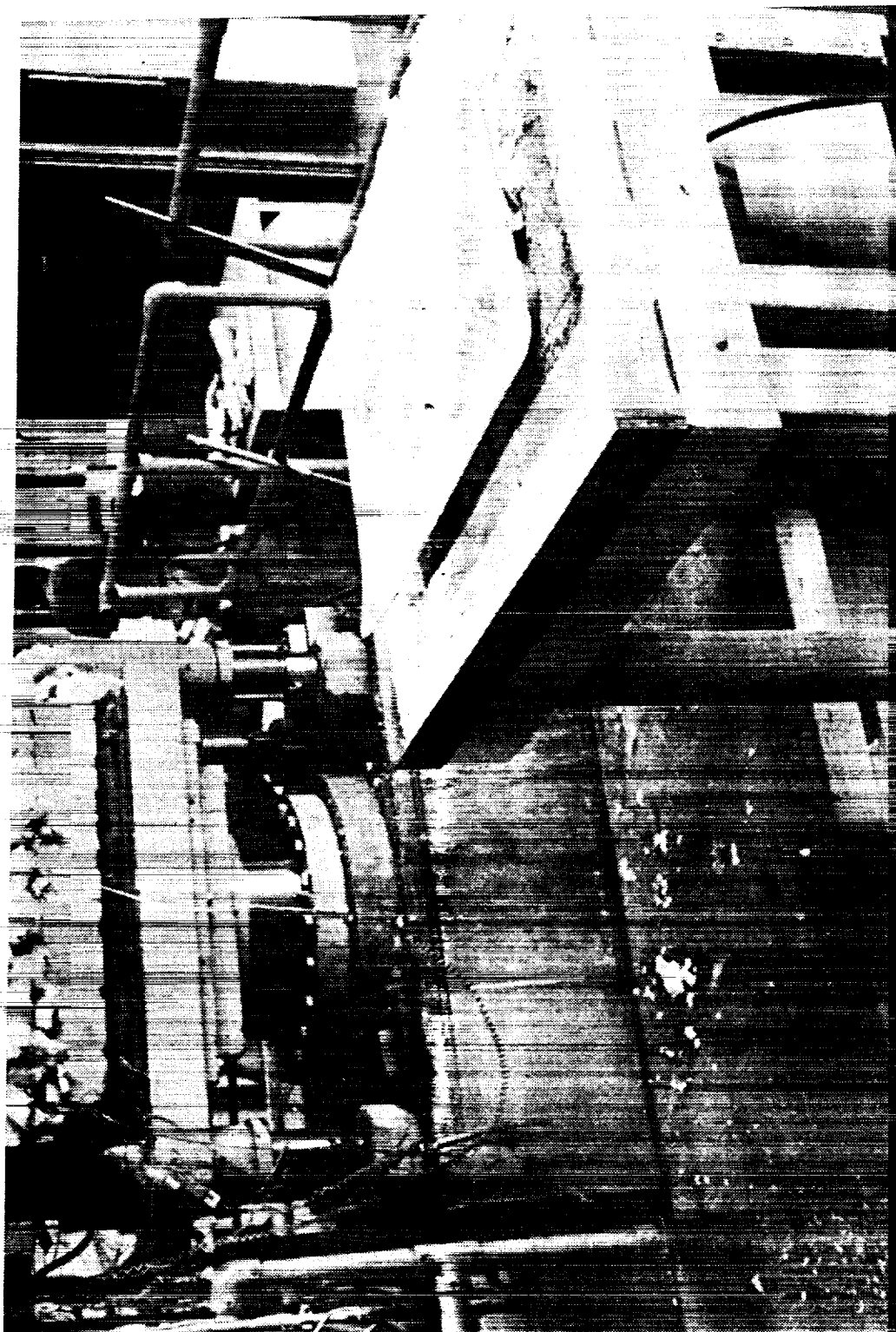


Figure 206. Beaded Crippling Panel.

ORIGINAL PAGE
BLACK AND WHITE PHOTOGRAPH

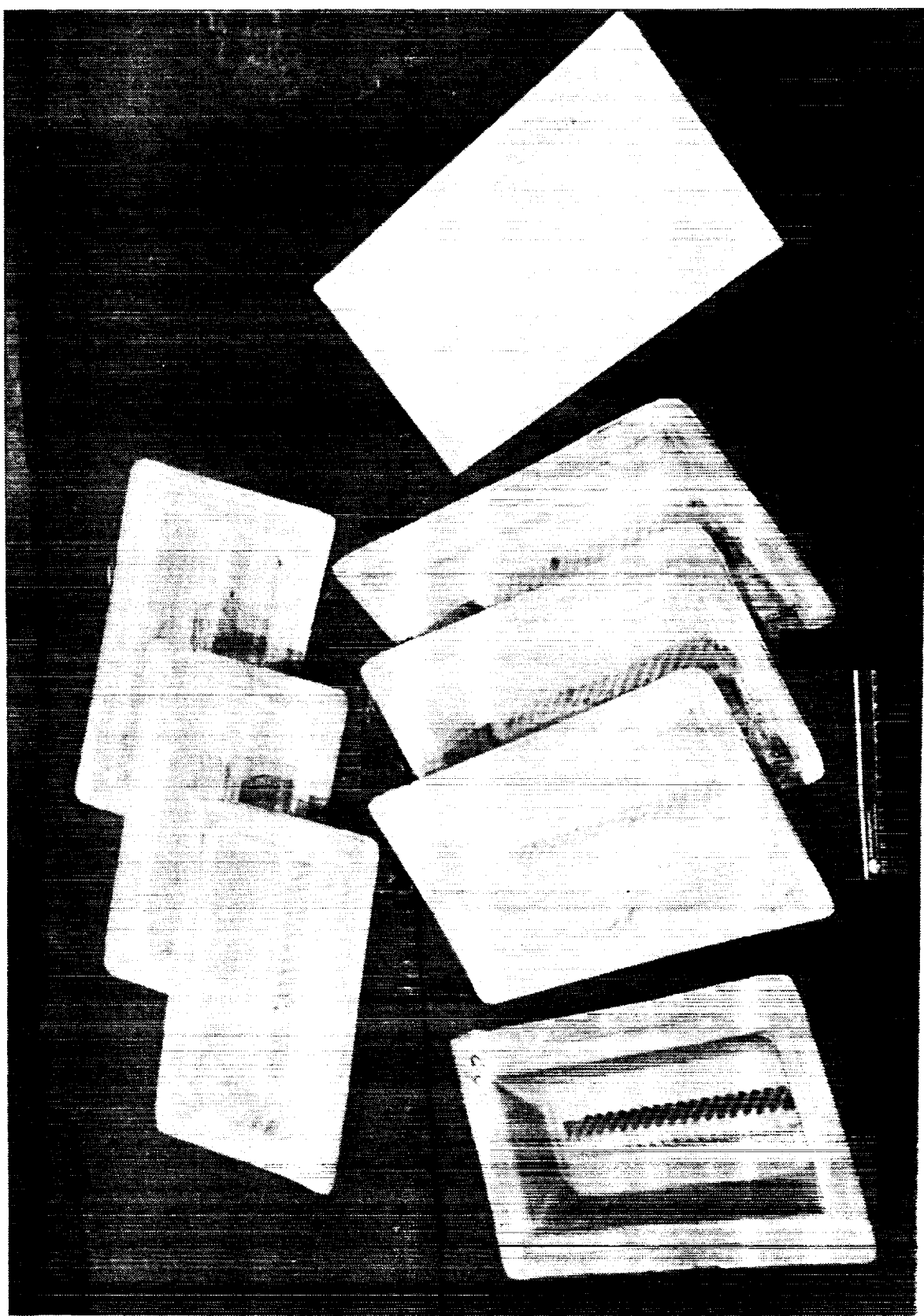


Figure 207. Part Blank and Identical Beaded Hat Sections.

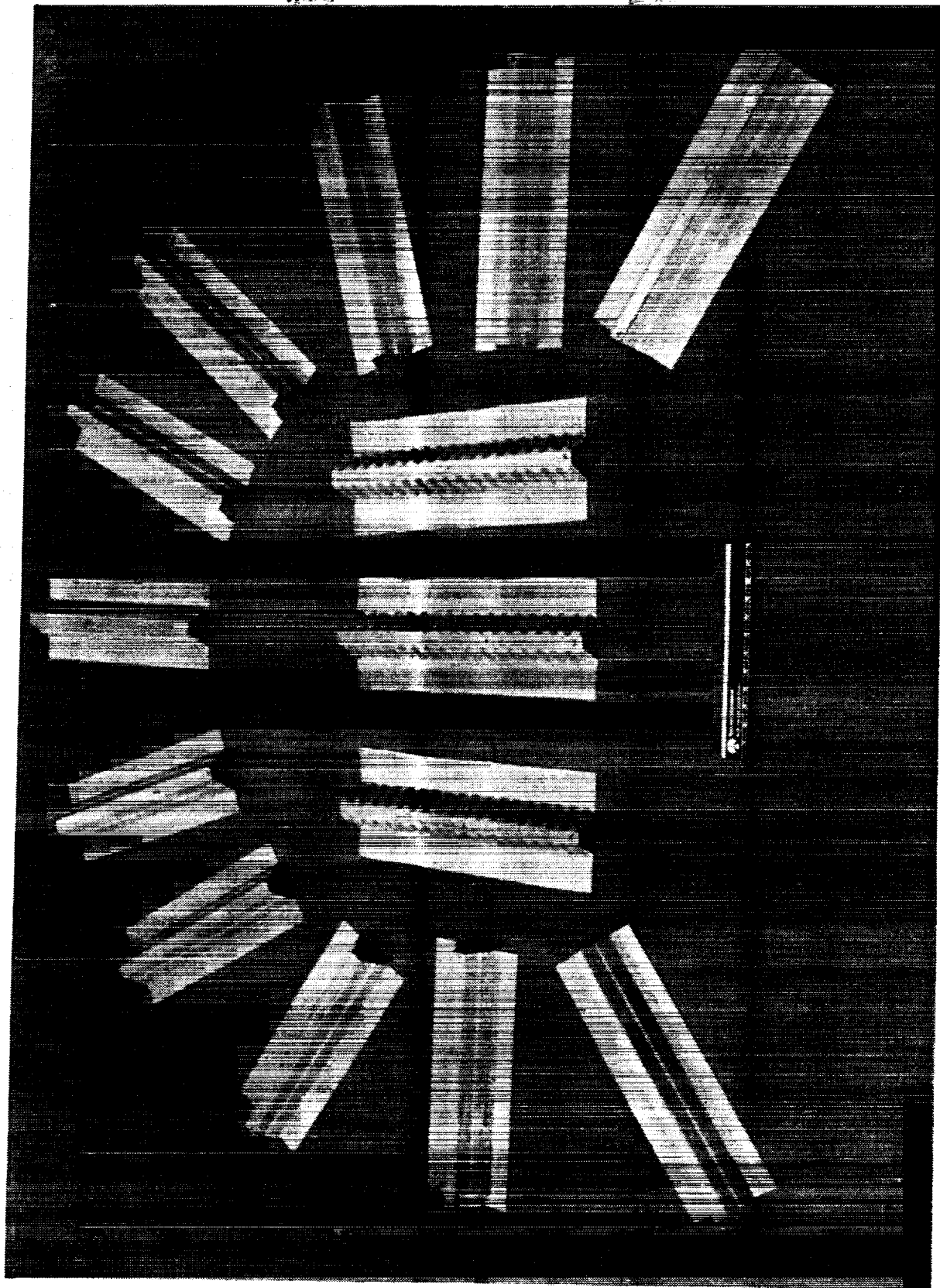
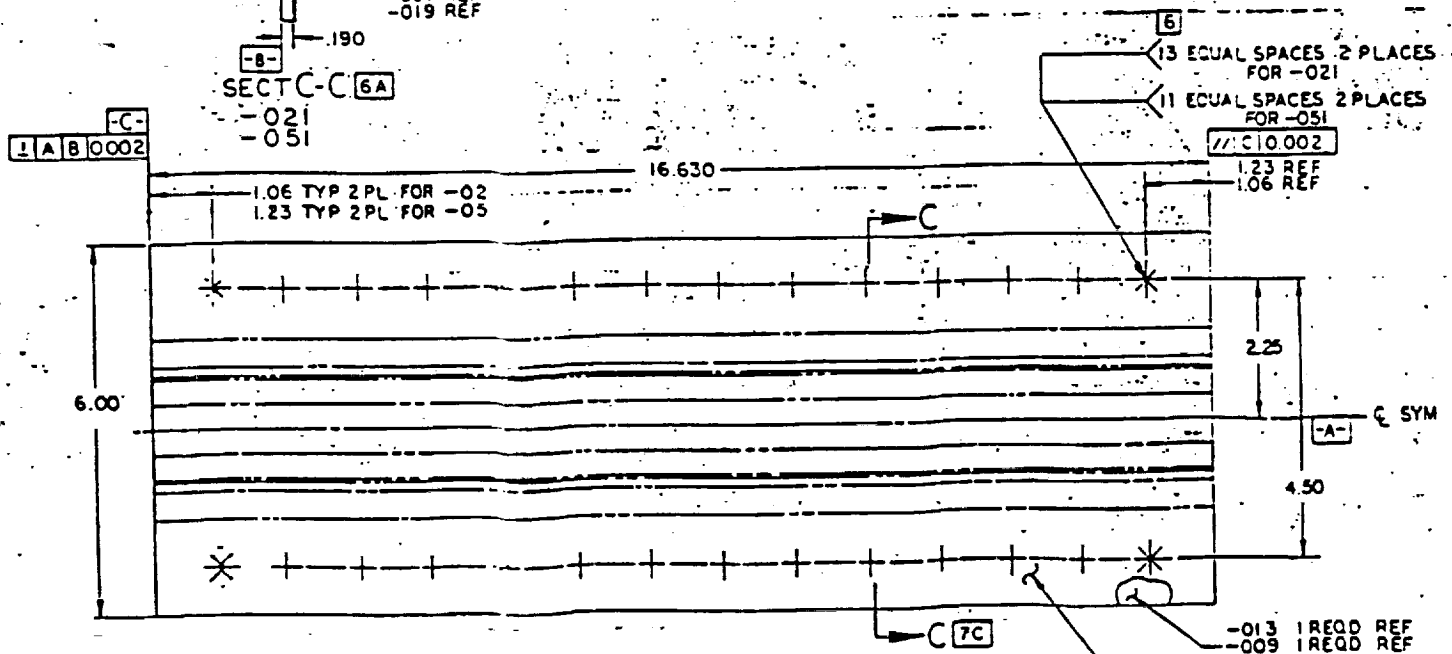


Figure 208. Rough Trimmed Crippling Panels.

THIS PAGE INTENTIONALLY LEFT BLANK.



007 : RECD FOR -021
019 : RECD FOR -051

Each configuration has four (4) stiffener replicates utilizing the following material combinations for a total of twenty four (24) specimens.

Stiffener	Skin
7475 Al	2219 Al
2090 Al-Li	2090 Al-Li

The ends of each stiffener are potted with epoxy to provide local support to the compression edges. The structural test laboratories at NASA Langley will test six test specimens (one of each configuration and material type), while General Dynamics will test eighteen of the test specimens (three of each configuration and material type) at its structural test laboratory (Reference Specimen Drawing L9111392 shown as Figure 209).

4.4.1.2.3 Test Temperature

Ambient test conditions will be utilized for all specimens. Test temperature should be recorded prior to initiation of the structural test for inclusion of data in the test report.

4.4.1.2.4 Test Machine

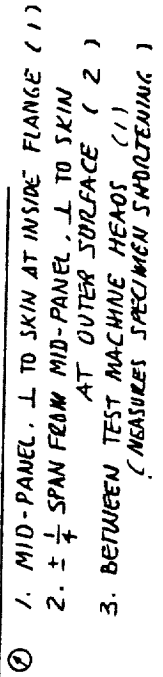
A compression test machine of 120,000 lb or greater capacity capable of a loading rate of 0.05 in/minute should be utilized for the crippling panel tests.

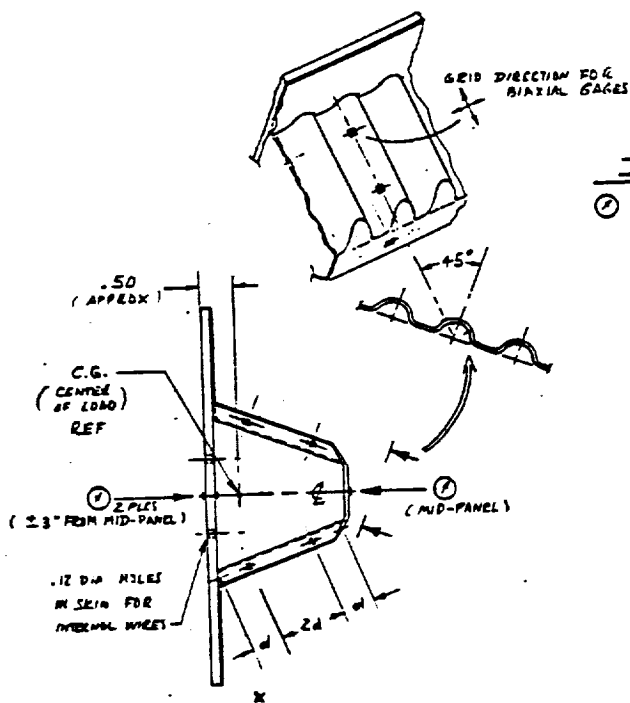
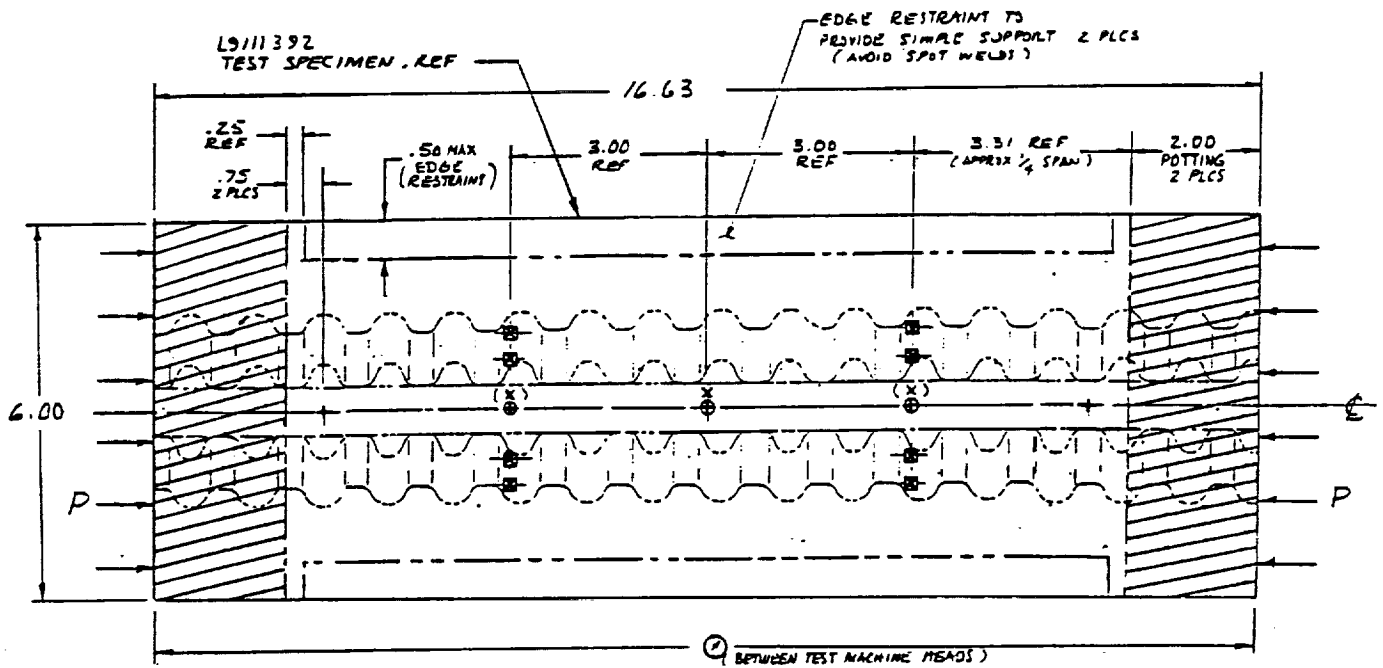
4.4.1.2.5 Instrumentation

Both strain gages and deflectometers will be utilized for instrumentation. The approximate locations of these gages are shown for the stepped hat in Figure 210 and for the beaded web configuration in Figure 211 (Reference drawing L9111398 shown as Figure 212).

4.4.1.2.6 Test Fixtures

The test fixture supports the loaded edges of each specimen to prevent local crippling and to provide simple support boundary conditions to the stiffener side edges. The support of the loaded edges consists of surrounding each edge with a 2" depth potting compound as shown in Figure 213. The side edge support design are shown also in Figure 213. These are simple "clamp-ons" with teflon tape between the specimen and attachment which is based upon past test experience at Rockwell which effectively provides simple support conditions (Reference drawing L9111397 shown as Figure 214).





DEFLECTOMETERS , x

- ① 1. MID-PANEL, ⊥ TO SKIN AT INSIDE FLANGE (1)
2. ± 3" FROM MID-PANEL, ⊥ TO SKIN AT OUTER SURFACE (2)
3. BETWEEN TEST MACHINE HEADS (1)
(MEASURES SPECIMEN SHORTENING)

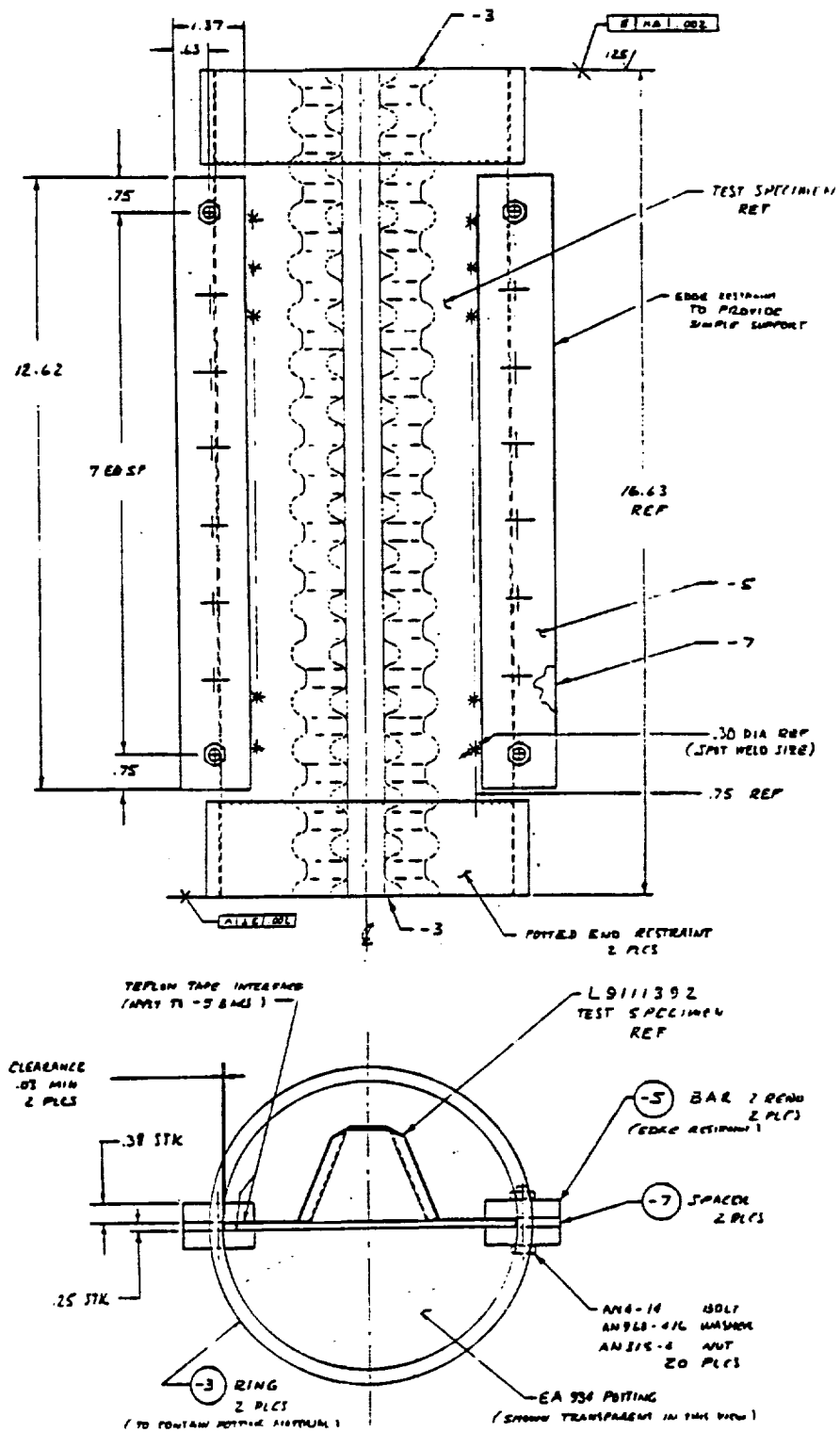
STRAIN GAGE INSTALLATIONS

11 AXIAL & 8 BI-AXIAL
PER LEGEND BELOW:

- - BI-AXIAL ON BEADED WEB (8)
- + - AXIAL ON INSIDE FLANGE (5)
- - BACK-TO-BACK AXIAL ON SKIN, 3 PLCS (6)

Figure 211. Strain Gauge Locations View 2.

THIS PAGE INTENTIONALLY LEFT BLANK.



L9111397 Test Fixture: Type 1 Test Panel
 (End and Edge Restraints for Short Column Compression)

Figure 213. Test Support Fixture.

THIS PAGE INTENTIONALLY LEFT BLANK.

PHOTOGRAPH

4.4.1.2.7 Test Procedure

Each specimen will be mounted and aligned in the test machine for compression loading as shown in Figure 213. The loading of the test specimens was along the center of gravity for each stiffener which was calculated as a 0.47 inch offset for the stepped hat stiffeners, and a 0.18 inch for the beaded web hat stiffeners with respect to the outer mold-line of the stiffener skin. As in standard practice all gages will be zeroed out, and the reading of all gages recorded prior to the start of the loading cycle. Each stiffener will be loaded continuously, with strain gage readings taken at 10 second intervals until failure. The predicted ultimate loads for each stiffener type, and the identification of critical stiffener areas (refer to Figure 215) are summarized in Table 108.

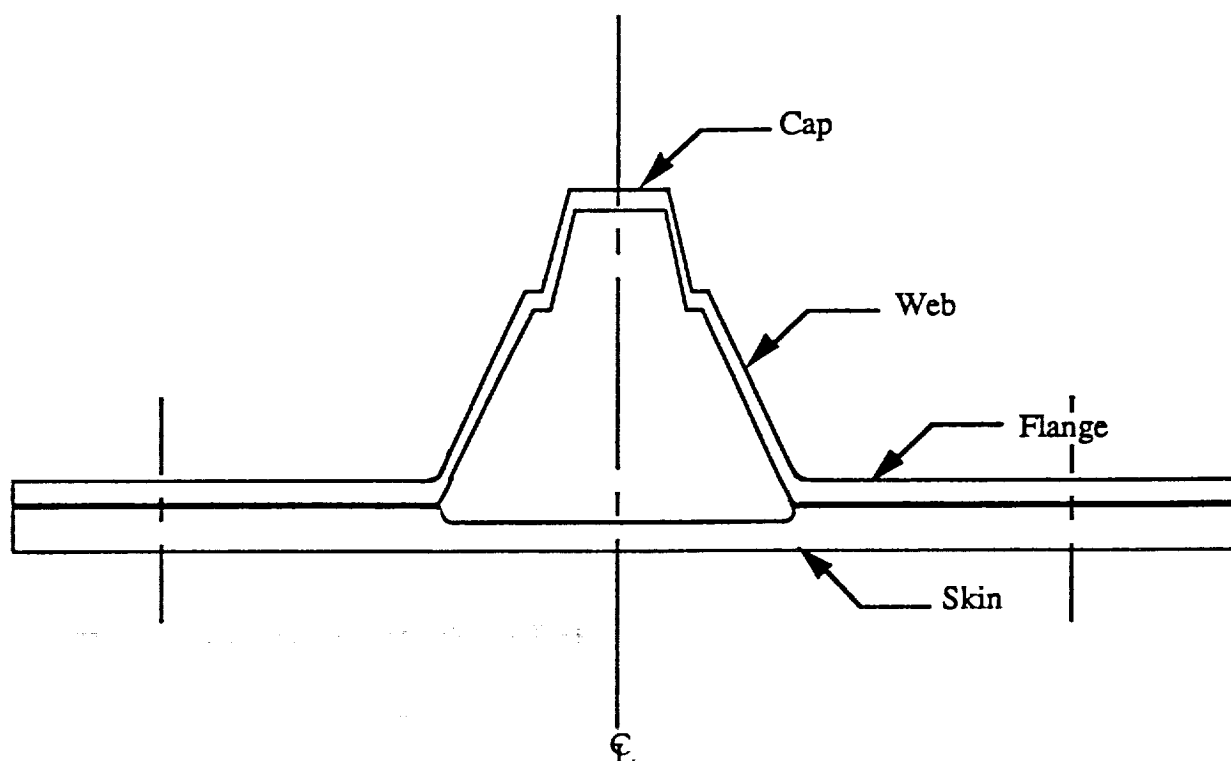


Figure 215. Critical Failure Areas for Stiffener Concepts as Determined by PASCO Modeling.

TABLE 108. Predicted Ultimate Uniaxial Loads.

Stiffener Type	Material Combinations		\bar{t}	Predicted Ultimate Uniaxial Load	Critical Areas
	Skin	Stiffener			
Stepped Hat With Curved Cap	2219 Al	7475 SPF Al	.256	76,800 Lb. 69,000 Lb.	Crippling Yield Skin
Stepped Hat With Curved Cap	2090 Al-Li	2090 SPF Al-Li	.252	68,000 Lb.	Comp Yield Hat
Beaded Web Flat or Curved Cap*	2219 Al	7475 SPF Al	.264	60,000 Lb. 79,200 Lb.	Comp. Yield Skin Skin Wrinkle
Beaded Web Flat or Curved Cap*	2090 Al-Li	2090 SPF Al-Li	.252	60,000 Lb. 68,000 Lb.	Comp. Yield Hat

* Based upon PASCO analysis, the difference in the Ultimate loads for the flat or curved cap configurations was insignificant, thus both configurations are shown together in the table.

- Note: (1) Thinning profiles used during the analysis were developed by C. Anton.
 (2) Critical Design areas are shown in Figure 4.
 (3) Critical Design Loading utilized for the analysis included:
 $N_x = -7607 \text{ lb./in}$
 $N_y = +7002 \text{ lb./in}$
 $N_{xy} = -119 \text{ lb./in}$

4.4.1.2.8 Data Required

All strain gage, load increment, and deflectometer readings for each stiffener test will be recorded. In addition, any observations about the test specimens as they are loaded will be noted and recorded.

One 8-1/2 x 11" glossy and one 85 line screen print with negative will be taken of each stiffener mounted in the test machine. One 8-1/2 x 11" glossy and one 85 line screen print with negative will be taken of each stiffener after failure. A schematic drawing showing the actual measured locations and orientations of all strain gages and deflectometers shall be furnished to the program manager.

4.4.1.2.8 Test Report

A test report summarizing all specimen tests from each testing group will be jointly developed by Rockwell and General Dynamics and submitted within 30 days after test completion of crippling panels for evaluation.:

The test fixture was evaluated with a beaded hat stiffened panel taken up to the point of buckling of the stiffener and skin (67,700 Lbs). The test set-up performed as expected.

4.4.1.3 Assembly of the Crippling Test Panels

Upon receipt at General Dynamics, the stiffener and skin combination was cleaned, re-identified as structural test specimens, and internal strain gauges were applied prior to welding (refer to Figure 216). The stiffener and skin panel combination was placed into a spot weld spacing jig (as shown in Figure 217) and welded (refer to Figure 218 through 220) per the weld schedule developed during task 3.

The 7475-T62 to 2219-T81 Al panels were successfully welded, examined for weld integrity by radiographic analysis and prepared for structural testing (refer to Figures 221 and 222). Weld nugget diameter and lap shear strengths were measured (initially after every panel, but later on the weld certification coupons were tested after each hour of welding) and the results are shown on Table 109 and Figures 223 through 226.

The welded panels were trimmed, assembled into the test fixture, and tested. The initial fully strain gauged crippling panel test was performed on the stepped hat configuration (refer to Figures 227 through 229). Buckling initiated at 77,000 lbs for the stepped hat stiffener but continued to carry load up to 84,000 Lb. The spot welds did not fail during the testing for either the test set-up panel or the initial stepped hat panel.

The results of the 7475-T62/2219-T81 aluminum panels structurally tested at General Dynamics are summarized in Table 110. All testing was performed per the crippling test plan at ambient temperature and the panels were continuously loaded until failure. Side attachments provided support to simulate simple support edge condition. Twenty nine strain gauges and three deflectometers were installed for each panel.

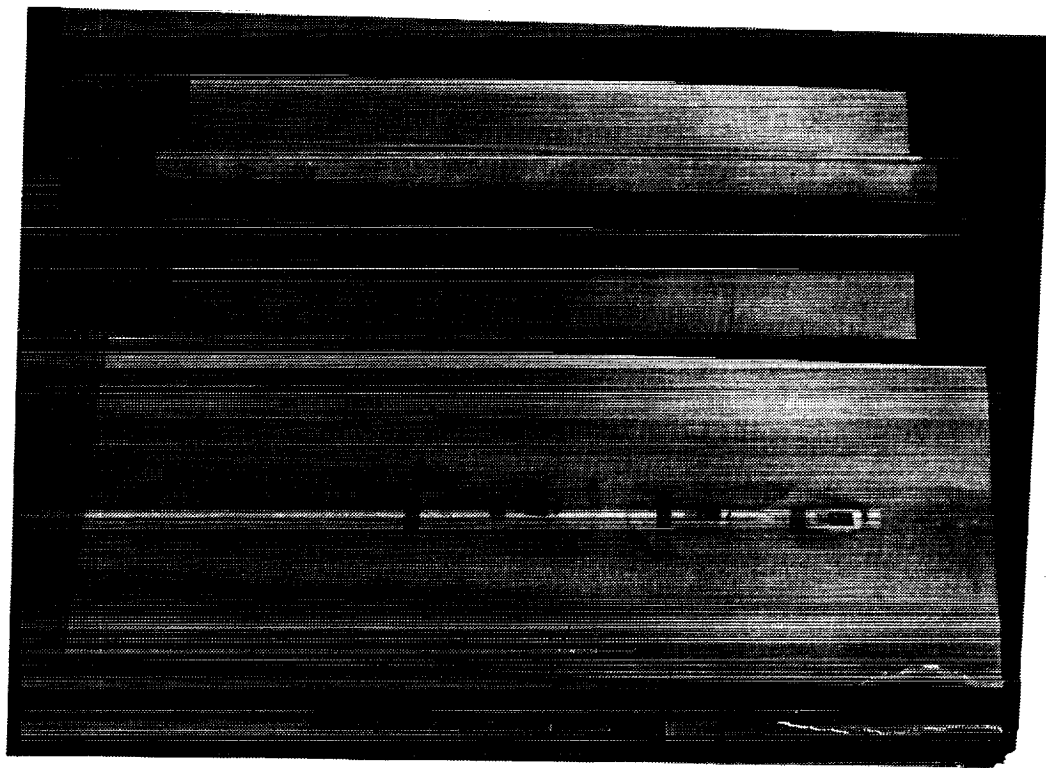


Figure 216. 7475-T62 SPF Stepped Hat Stiffener and 2219-T81 Skin with Strain Gages.

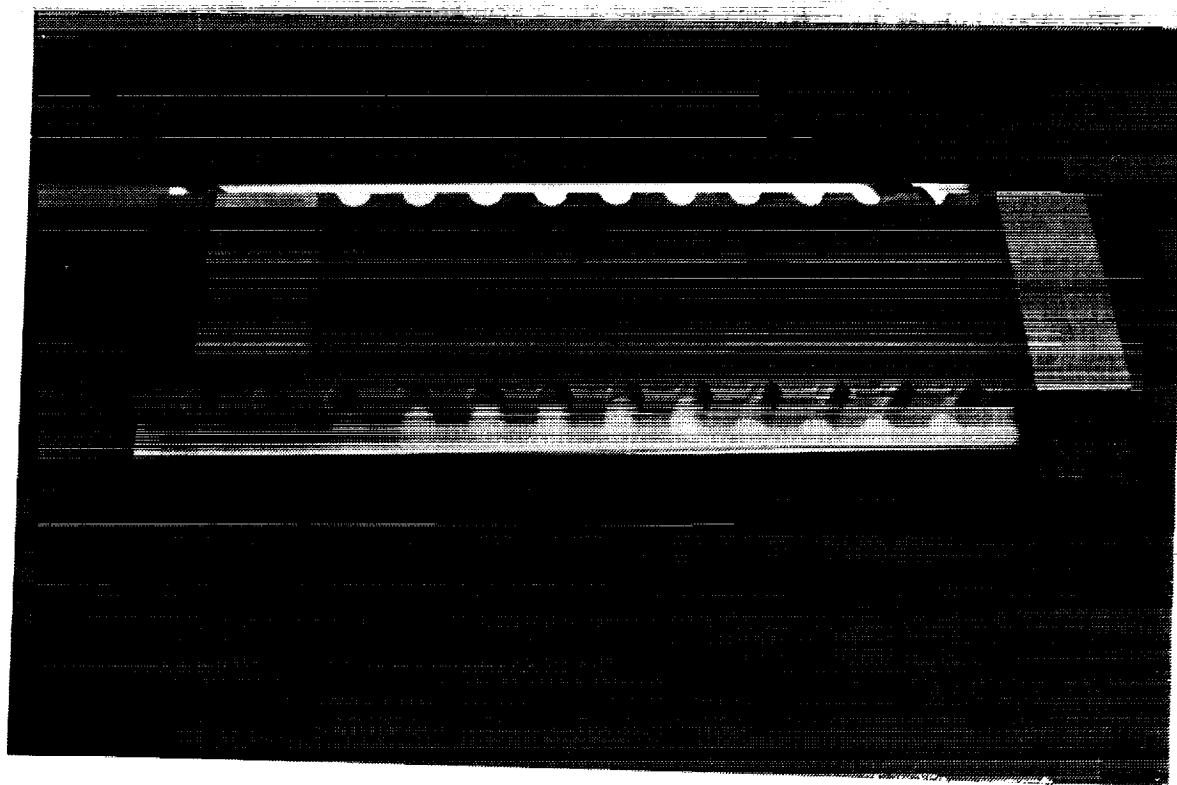


Figure 217. SPF Stepped Hat Stiffener and Skin Clamped With Resistance Spot Spacing Tooling.

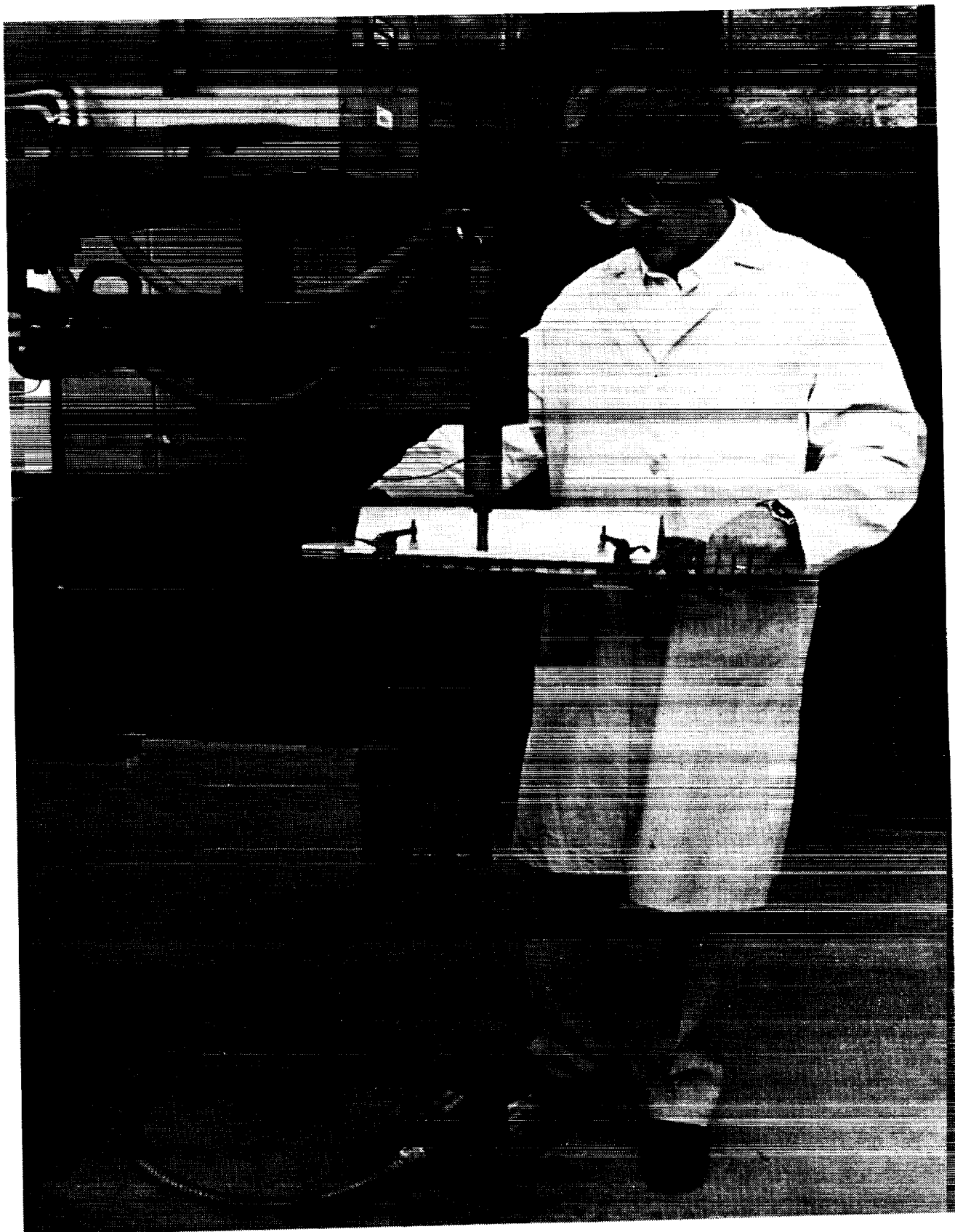


Figure 218. Resistance Spot Welding Crippling Test Panel Stiffener to Skin .



Figure 219. SPF Stepped Hat and Stiffener Being Resistance Spot Welded.

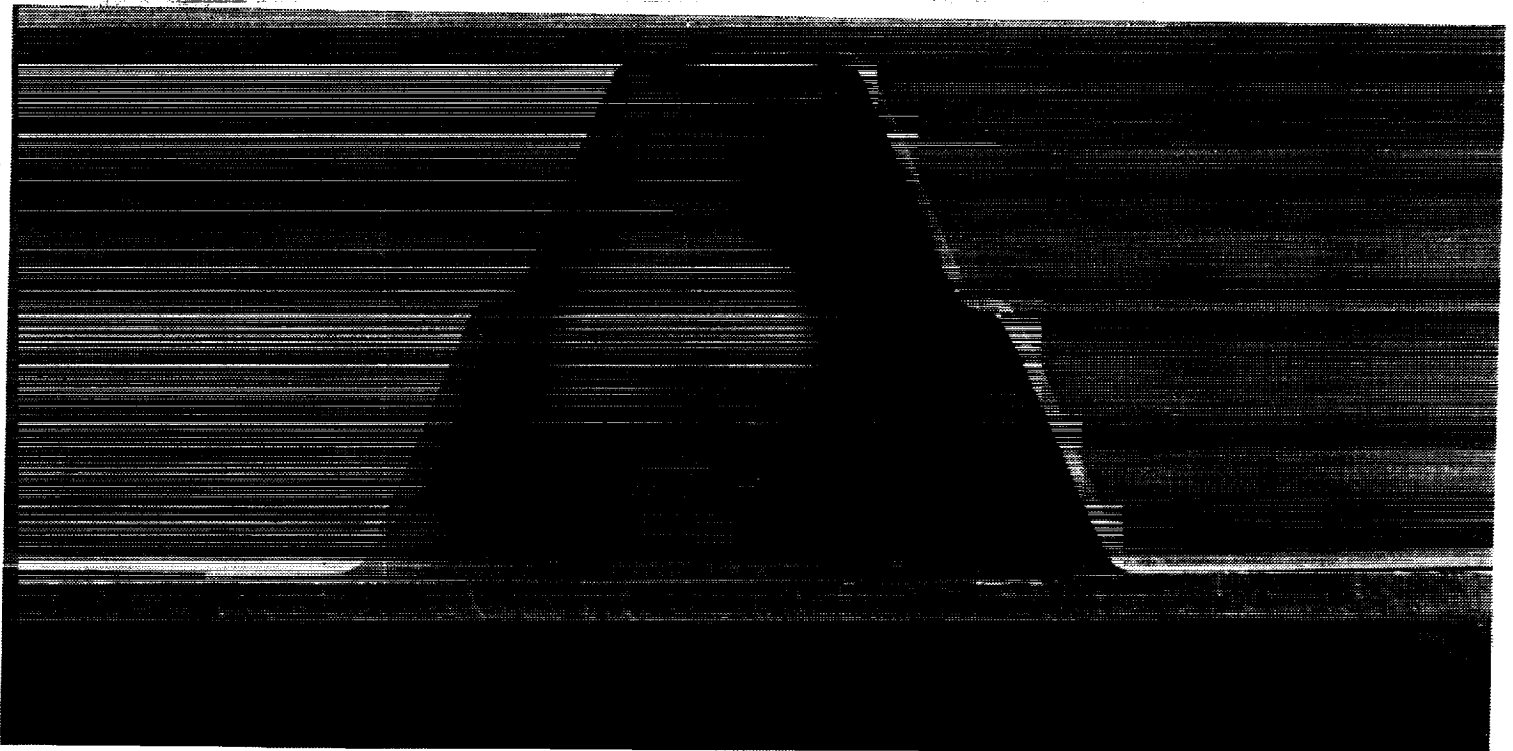


Figure 220. End View of Welded Stepped Hat and Skin Combination.

Table 109. Crippling Panel Weld Certification Testing.

Coupon I.D. (% Heat)	Nugget (inch)	Nugget Penetration		Shear Strength (Lbs)	Material Thickness (inch)
		Upper Sheet (inch)	Lower Sheet (inch)		
Panel 1, 65-3-7-2					
Pre-Test (33.5)	0.314	0.034 - 0.042	0.018 - 0.041		0.073
Pre-Test (35)	0.339	0.042 - 0.043	0.020 - 0.079		0.073
Pre-Test (35)	0.336	0.036 - 0.040	0.018 - 0.084		0.073
Pre-Test (35)				1950	0.075
Pre-Test (35)				2546	0.072
Pre-Test (35)				2551	0.071
Panel 1, 65-3-7-2					
Post-Test (33.5)	0.352	0.034 - 0.038	0.016 - 0.060		0.076
Post-Test (35)	0.334	0.027 - 0.038	0.020 - 0.070		0.077
Post-Test (35)	0.343	0.035 - 0.044	0.018 - 0.063		0.078
Post-Test (35)				2345	0.077
Post-Test (35)				2107	0.073
Post-Test (35)				2322	0.072
Average	0.330	0.035	0.018	2304	0.074
Panel 2, 47-3-7-23					
Post-Test (33.5)	0.341	0.034 - 0.036	0.020 - 0.060		0.071
Post-Test (35)	0.345	0.032	0.017 - 0.064		0.071
Post-Test (35)	0.335	0.033 - 0.036	0.017 - 0.070		0.071
Post-Test (35)				2936	0.078
Post-Test (35)				2140	0.073
Post-Test (35)				2898	0.073
Average	0.340	0.033	0.018	2658	0.073
Panel 3, 50-3-7-26					
Post-Test (33.5)	0.339	0.041	0.022 - 0.065		0.074
Post-Test (35)	0.342	0.041	0.016 - 0.062		0.074
Post-Test (35)	0.360	0.042	0.020 - 0.068		0.075
Post-Test (35)				2522	0.077
Post-Test (35)				3026	0.073
Post-Test (35)				2389	0.075
Average	0.347	0.035	0.020	2646	0.075
Panel 4, 43-3-7-3					
Post-Test (33.5)	0.372	0.041 - 0.043	0.021 - 0.070		0.076
Post-Test (35)	0.350	0.037	0.021 - 0.069		0.076
Post-Test (35)	0.346	0.035	0.022 - 0.080		0.076
Post-Test (35)				2049	0.074
Post-Test (35)				2874	0.071
Post-Test (35)				2577	0.081
Average	0.356	0.035	0.020	2500	0.076

Table 109 (Cont.). Crippling Panel Weld Certification Testing.

Coupon I.D. (% Heat)	Nugget (inch)	Nugget Penetration		Shear Strength (Lbs)	Material Thickness (inch)
		Upper Sheet (inch)	Lower Sheet (inch)		
Panel 5, 1-1-7-7					
Post-Test (35)	0.343	0.038 - 0.040	0.016 - 0.059		0.077
Post-Test (36)	0.335	0.040	0.016 - 0.060		0.077
Post-Test (36)	0.340	0.044	0.024 - 0.070		0.078
Post-Test (36)				2304	0.082
Post-Test (36)				2644	0.079
Post-Test (36)				2908	0.079
Average	0.339	0.041	0.018	2814	0.079
Panel 8, 7-1-7-20					
Post-Test (35)	0.335	0.030 - 0.038	0.020 - 0.055		0.074
Post-Test (36)	0.332	0.030 - 0.036	0.018 - 0.048		0.073
Post-Test (36)	0.348	0.031 - 0.043	0.018 - 0.066		0.072
Post-Test (36)				2304	0.081
Post-Test (36)				2550	0.081
Post-Test (36)				2120	0.080
Average	0.338	0.030	0.019	2325	0.077
Panel 11, 27-2-7-63					
Post-Test (35)	0.344	0.034	0.016 - 0.049		0.078
Post-Test (36)	0.318	0.040	0.018 - 0.054		0.078
Post-Test (36)	0.334	0.044	0.016 - 0.062		0.078
Post-Test (36)				2304	0.078
Post-Test (36)				2550	0.078
Post-Test (36)				2120	0.080
Average	0.332	0.039	0.017	2325	0.078
Panel 12, 30-2-7-36					
Post-Test (35)	0.347	0.031	0.014 - 0.050		0.074
Post-Test (36)	0.319	0.039	0.018 - 0.049		0.077
Post-Test (36)	0.326	0.037	0.019 - 0.055		0.079
Post-Test (36)				2339	0.079
Post-Test (36)				2245	0.073
Post-Test (36)				2126	0.083
Average	0.331	0.036	0.017	2237	0.077
Average of All Panels Welded	0.339	0.036	0.018	2476	0.076

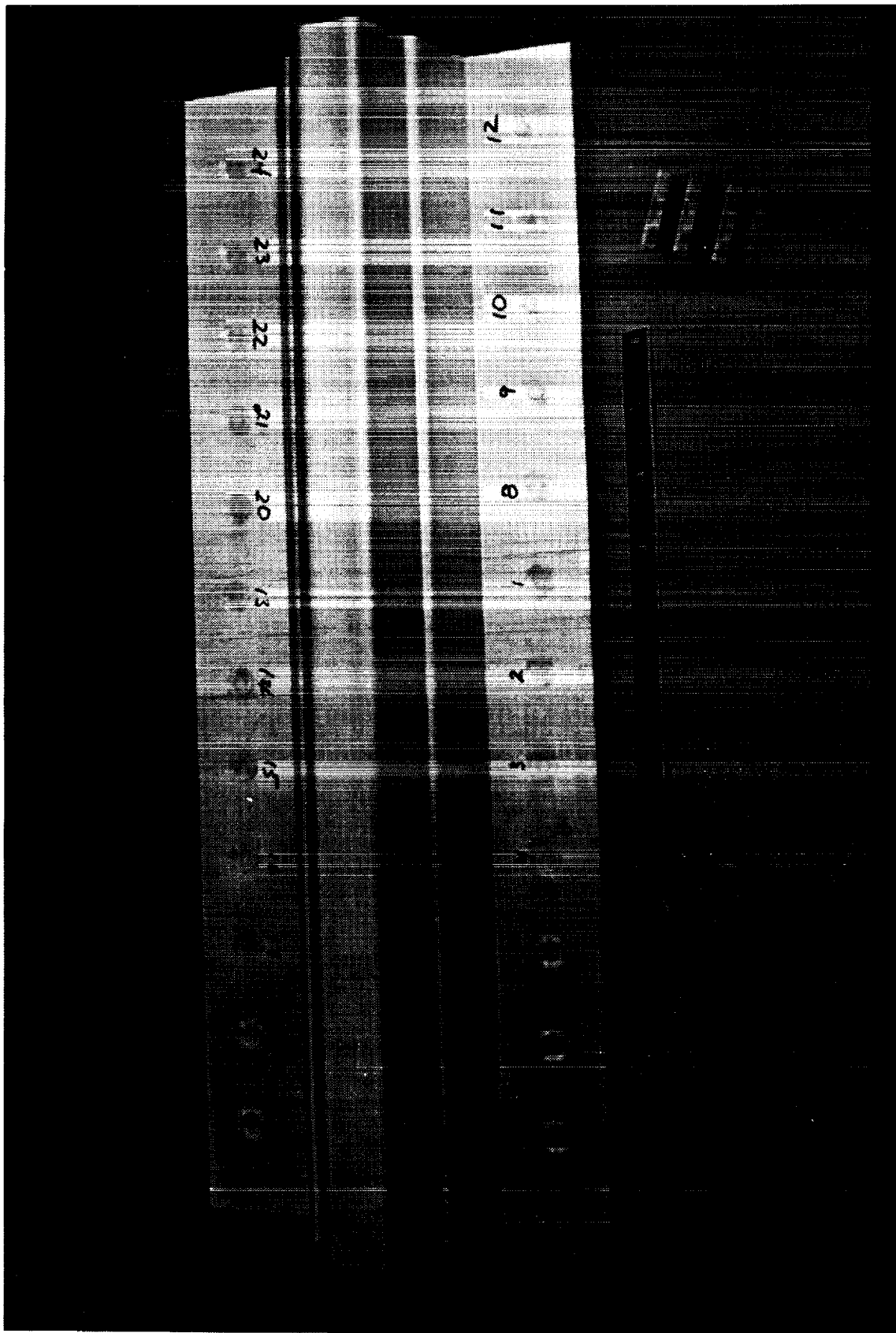


Figure 221. Resistance Spot Welded SPF Crippling Test Panel.

WELD

7

6

5

4

3

2

1

8

9

10

11

12

WELD

19

18

17

16

15

14

13

20

21

22

23

24

Figure 222. Radiographic Image of Resistance Spot Welds for Test Panel 1.

Coupon #3

Coupon #2

Coupon #1

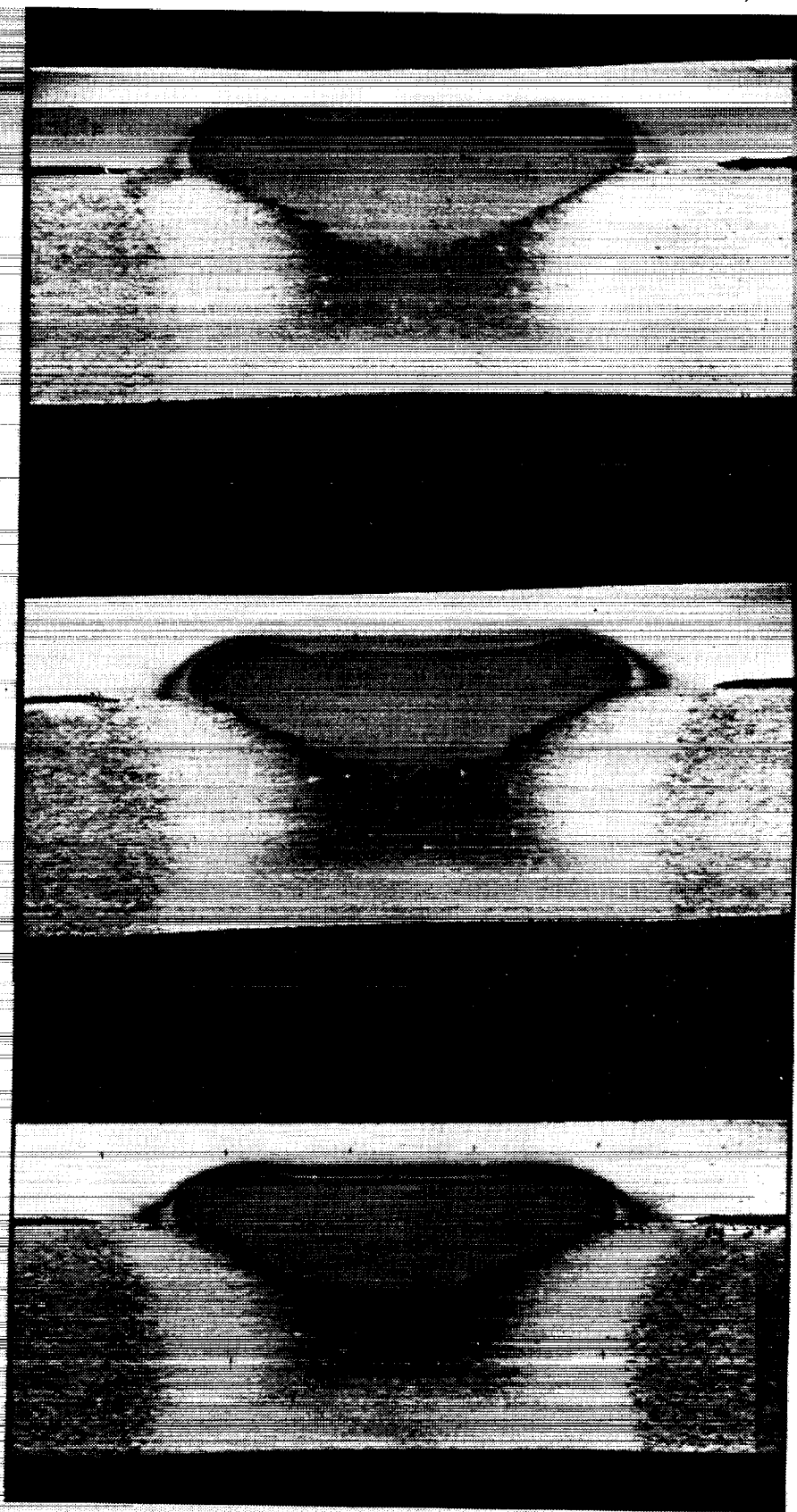


Figure 223. Panel 5 Pre-test Spot Weld Nuggets 0.070" 7475-T62 joined to 0.190" 2219-T81 Al.

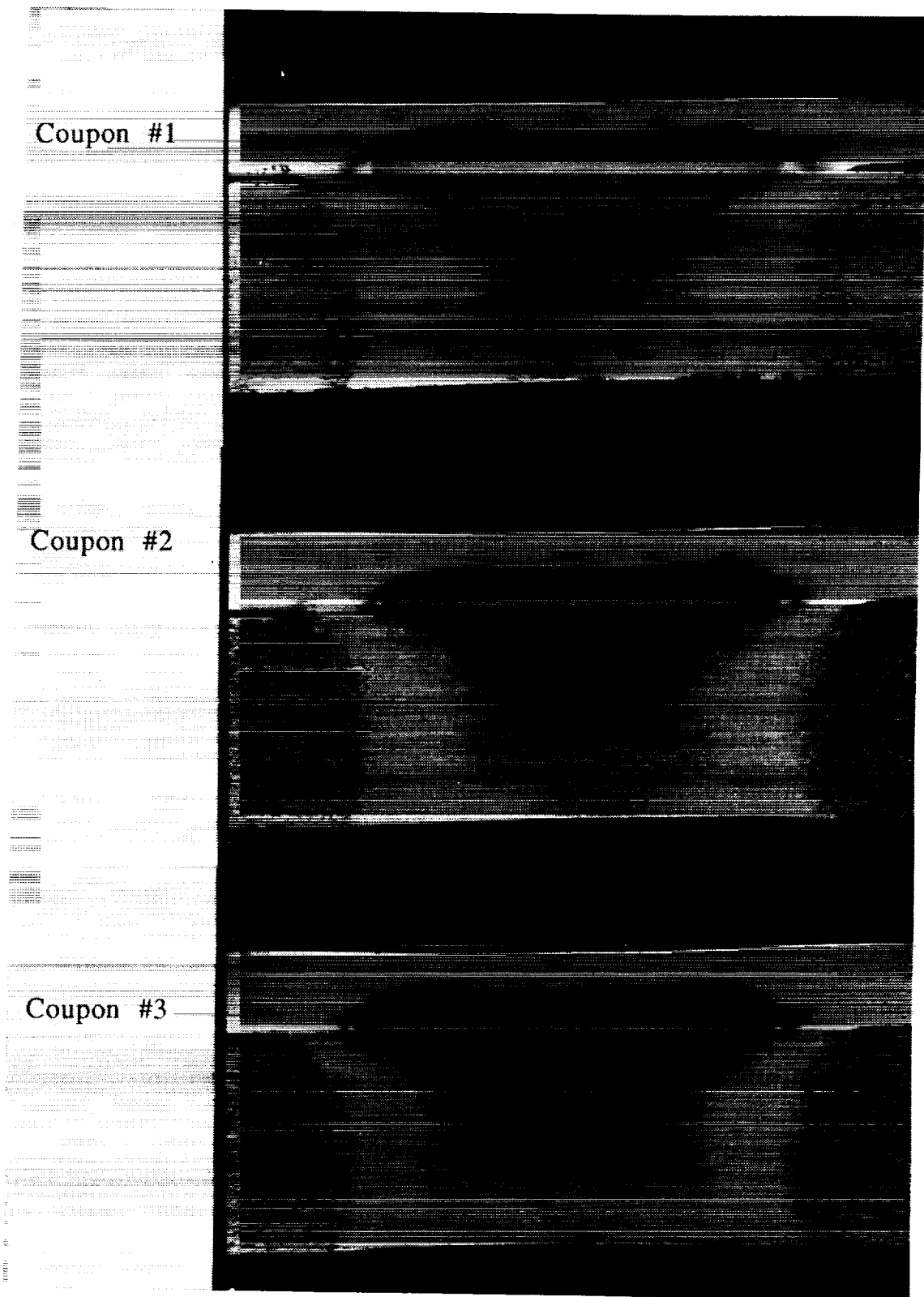
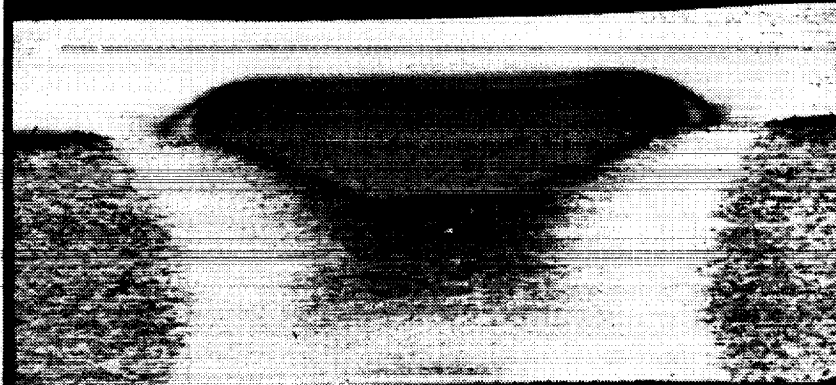
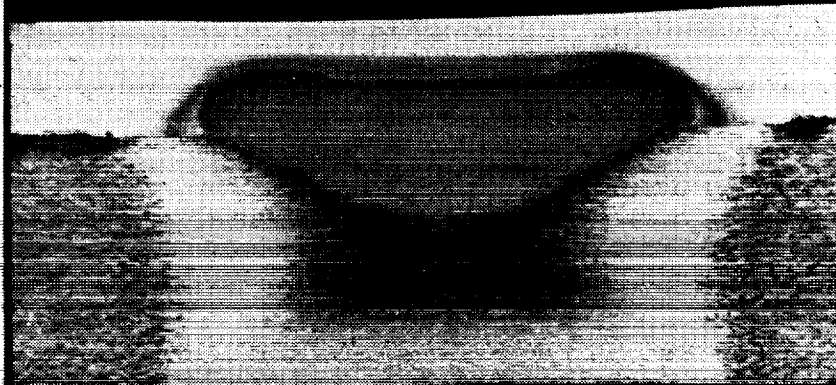


Figure 224. Panel 8 Pre-test Spot Weld Nuggets 0.070" 7475-T62 joined to 0.190" 2219-T81 Al.

Coupon #1



Coupon #2



Coupon #3



Figure 225. Panel 11 Pre-test Spot Weld Nuggets 0.070" 7475-T62 joined to 0.190" 2219-T81 Al.

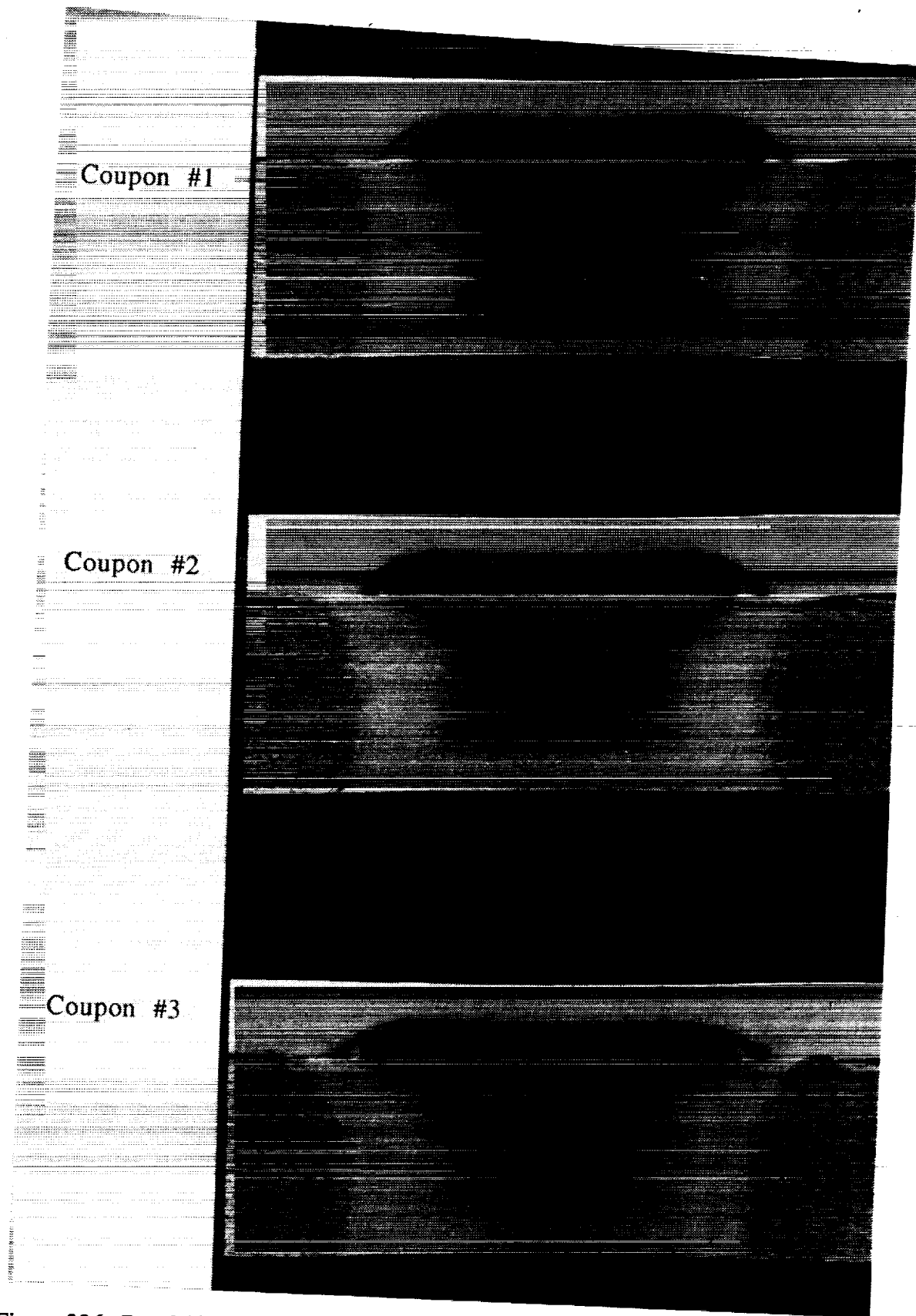


Figure 226. Panel 12 Pre-test Spot Weld Nuggets 0.070" 7475-T62 joined to 0.190" 2219-T81 Al.

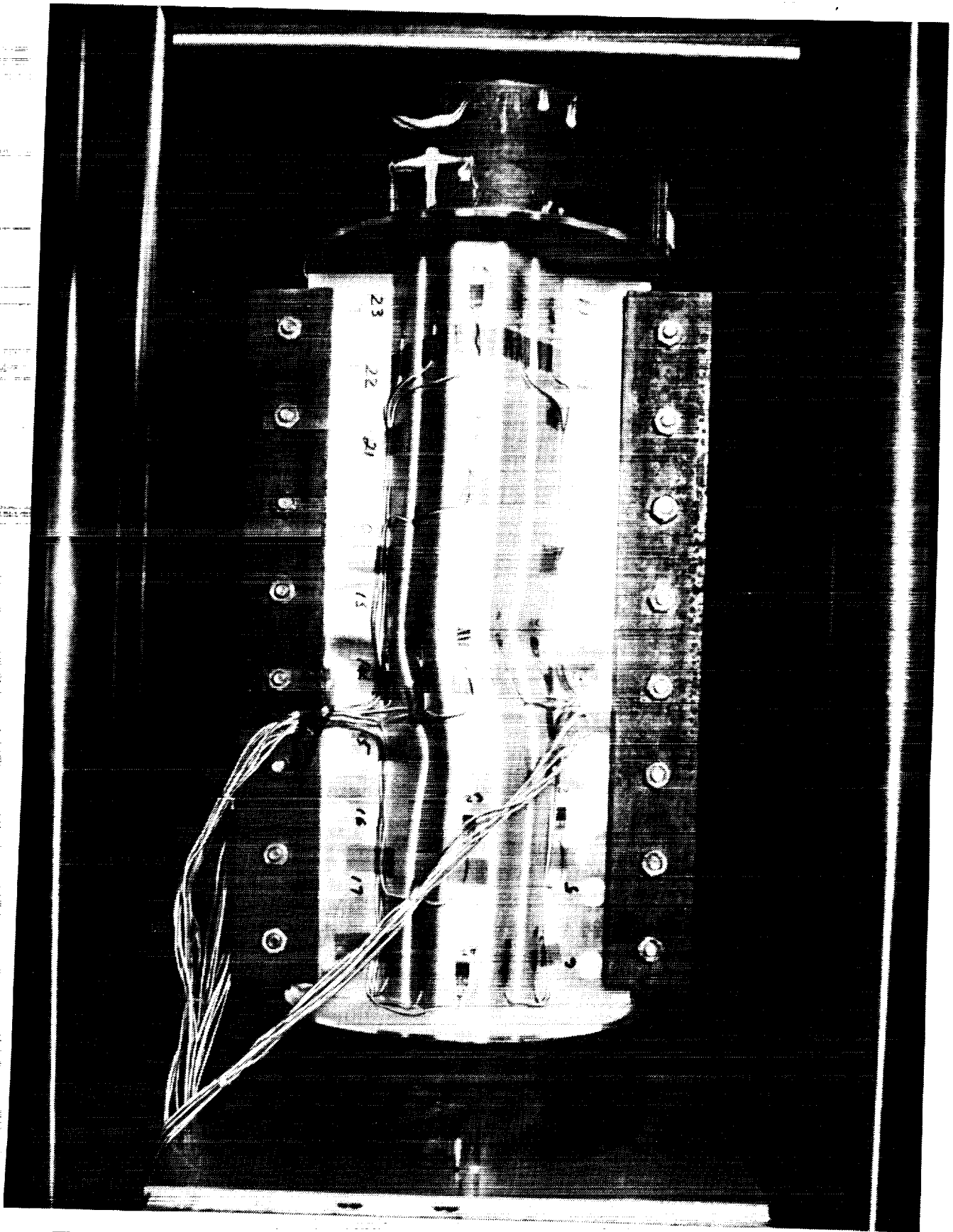


Figure 227. Front View of Initial Test Panel at Completion of Testing at General Dynamics.

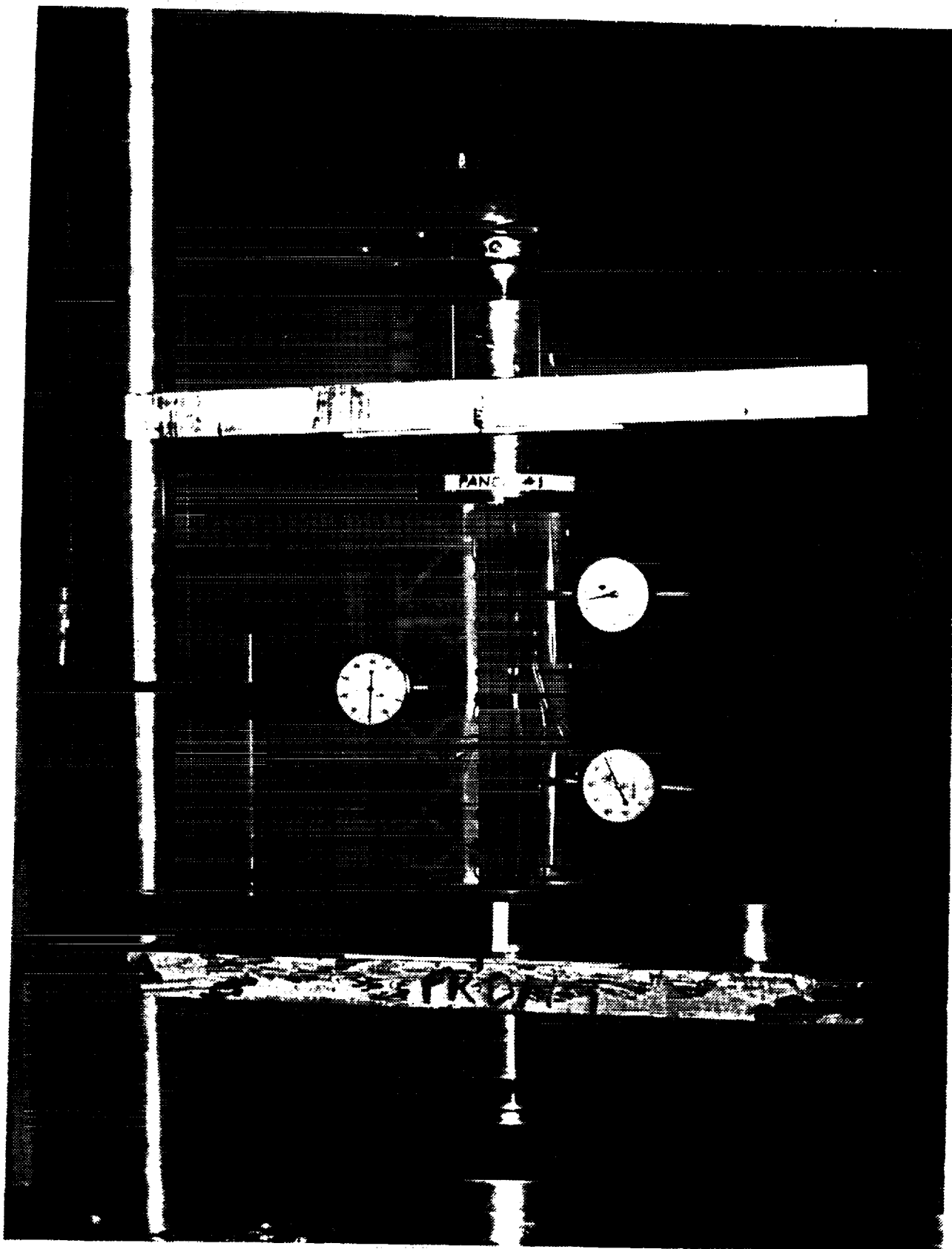


Figure 228. Side View of Initial Test Panel at Completion of Testing at General Dynamics with Deflectometers.

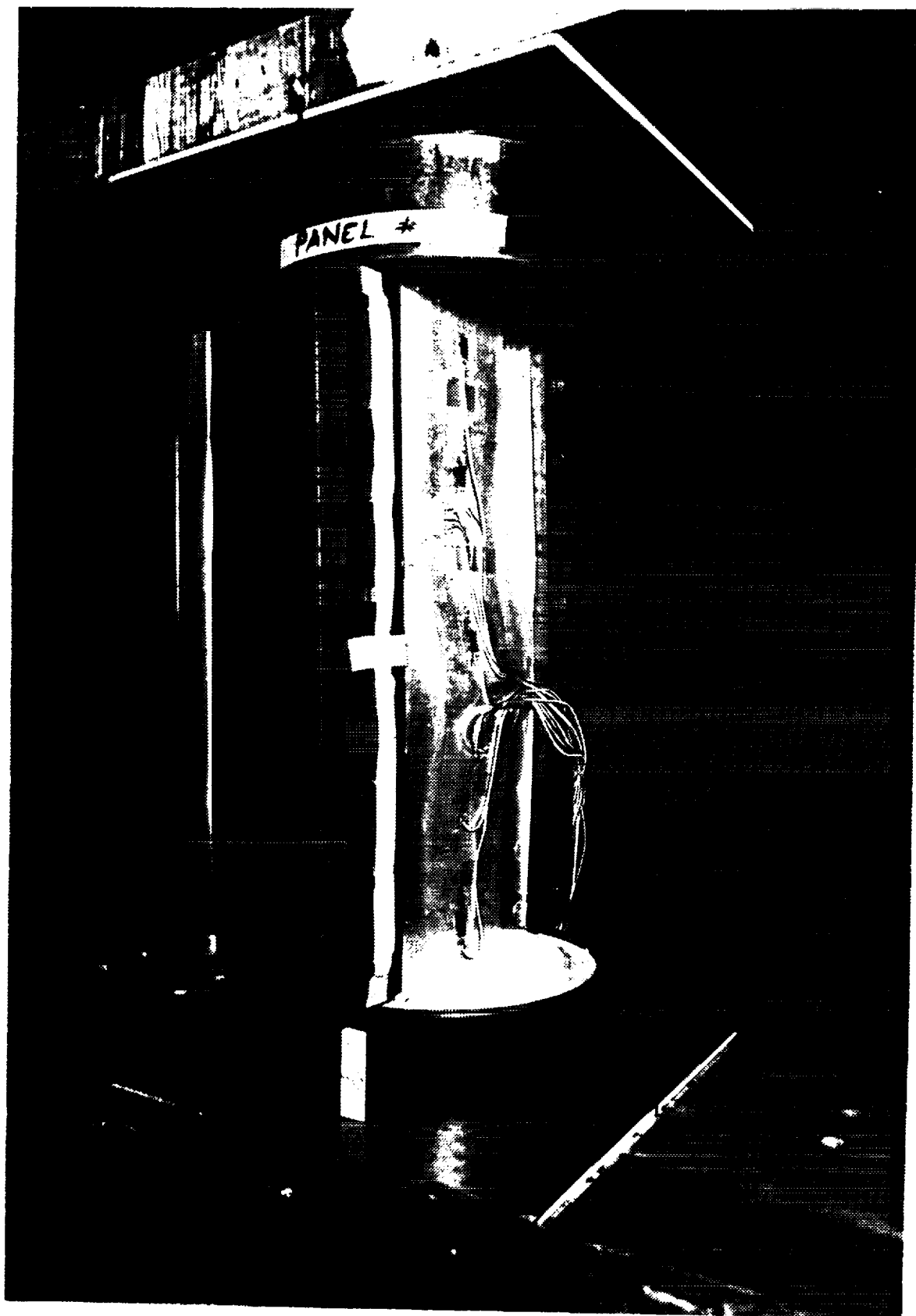


Figure 229. Back View of Initial Test Panel at Completion of Testing at General Dynamics.

Table 110. Crippling Panel Test Results for 7475-T62 Stiffener Joined to 2219-T81 Skin.

Panel and I.D.	Panel Type	Ultimate Load (Lbs)	Comments
Test Panel 1 (47-3-7-23)	Stepped Hat	-84,000	Cracked Spot Welds 1, 2, 14 Cracked Spot Weld 2
Test Panel 2 (50-3-7-26)	Stepped Hat	-79,400	
Test Panel 3 (43-3-7-3)	Stepped Hat	-83,400	
Test Panel 4 (1-1-7-7)	Beaded Web (CC)	-66,500	Cracked Spot Weld 19 Popped Spot Welds 8, 9, 10, 14, 15, 16
Test Panel 5 (3-1-7-16)	Beaded Web (CC)	-67,900	
Test Panel 6 (7-1-7-20)	Beaded Web (CC)	-66,300	
Test Panel 7 (26-2-7-62)	Beaded Web (FC)	-63,000	
Test Panel 8 (27-2-7-63)	Beaded Web (FC)	-67,500	Popped Spot Welds 19, 20, 21
Test Panel 9 (30-2-7-36)	Beaded Web (FC)	-67,000	Cracked Spot Welds 2, 3, 13
			Cracked Spot Welds 1, 2

The test load values were for the 7475-T62 to 2219-T81 aluminum stiffener and skin combination were slightly higher than the predicted load values. The higher results have been attributed to conservative estimates for spot weld strength which translated into reductions in outer skin and stiffener allowables. The predicted ultimate uniaxial test loads for crippling in the hats are re-iterated (reference Table 108) for comparison purposes in the following table:

Predicted Ultimate Uniaxial Test Panel Loads
Aluminum

Stepped Hat	7475-T62 to 2219-T81 Al	76,800 Lb.
Beaded Flat or Curved Cap	7475-T62 to 2219-T81 Al	60,000 Lb.

Aluminum-Lithium

Stepped Hat	2090-T62 to 2090-T83 Al-Li	68,000 Lb.
Beaded Flat or Curved Cap	2090-T62 to 2090-T83 Al-Li	68,000 Lb.

The panel predicted ultimate loads were to fail the stiffener prior to failure of the skin, or simultaneous buckling of the stiffener and the skin material.

The 2090-T62 to 2090-T83 Al-Li panels were successfully welded, examined for weld integrity by radiographic analysis and prepared for structural testing. Weld nugget diameter and lap shear strengths were measured (initially after every panel, but later on the weld certification coupons were tested after each hour of welding) and the results are shown on Tables 111 and 112.

Stiffener configurations were formed, heat treated, trimmed and inspected prior to shipment to General Dynamics for joining of the stiffener to outer pressure vessel skin. Upon receipt at General Dynamics, the stiffener and skin combination was cleaned, re-identified and internal strain

gauges were applied prior to welding. The stiffener and skin panel combination was placed into the spot weld spacing jig and welded per the developed weld schedule for the material combination. The welded panels were trimmed, loaded into the test fixture and structurally tested.

The structural crippling test results are summarized in Table 113. All testing was performed per the crippling test plan at ambient temperature and the panels were continuously loaded until failure. Side attachments provided support to simulate simple support edge condition. Twenty nine strain gauges and three deflectometers were installed for each panel.

The ultimate test load values for the 2090-T62 to 2090-T83 aluminum-lithium stiffener and skin combination were slightly higher than the predicted load values. The higher test results have been attributed to conservative predictions for spot weld strength which resulted in higher knock-downs to outer skin and stiffener allowables. The predicted panel failure modes were crippling of the stiffener prior to the skin, or simultaneous buckling of the stiffener and the skin material.

Table 111. 2090 Al-Li Crippling Panel Weld Certification Testing.

Coupon I.D.	Nugget Diam. (inch)	Nugget Penetration		Shear Strength (Lbs)	Material Thickness (inch)
		Upper Sheet (inch)	Lower Sheet (inch)		
Panel 14, 17-3-2-15	0.361	0.032	0.022 - 0.060	2717	0.069
Panel 15, 126-3-2-91	0.382	0.018	0.017 - 0.085	2341	0.063
Panel 16, 60-3-2-42	0.360	0.018	0.017 - 0.085	2299	0.062
Panel 18, 35-2-2-51	0.328	0.023	0.019 - 0.073	2638	0.068
Panel 19, 39-2-2-55	0.346	0.018	0.021 - 0.083	3123	0.062
Panel 20, 70-2-2-58	0.361	0.037	0.022 - 0.082	2067	0.063
Panel 21, 12-1-2-10	0.363	0.030	0.020 - 0.082	2320	0.065
Panel 23, 87-1-2-77	0.369	0.026	0.019 - 0.082	2758	0.065
Panel 24, 91-1-2-82	0.369	0.026	0.019 - 0.082	2758	0.065
Average of All Panels Welded	0.361	0.027	0.019 - 0.078	543	0.065

Table 112. 2090 Al-Li Crippling Panel Weld Certification Testing.

Coupon I.D.	Nugget Diam. (inch)	Nugget Penetration		Shear Strength (Lbs)	Material Thickness (inch)
		Upper Sheet (inch)	Lower Sheet (inch)		
Panel 13, 56-3-2-35	0.403	0.032	0.020 - 0.056	2938 2779 2974	0.064
	0.408	0.029	0.019 - 0.062		0.064
	0.380	0.038	0.021 - 0.049		0.064
					0.061
	0.361	0.020	0.016 - 0.075		0.059
	0.340	0.021	0.016 - 0.048		0.059
	0.331	0.021	0.016 - 0.048	2674 2164 2550	0.059
					0.0666
					0.064
					0.061
Average	0.371	0.027	0.018 - 0.056	2680	0.062
Panel 14, 17-3-2-15	0.373	0.031	0.022 - 0.061	2682 3208 3127	0.066 0.067 0.069
	0.365	0.041	0.024 - 0.051		
	0.355	0.038	0.033 - 0.057		
	0.366	0.028	0.020 - 0.061		
	0.353	0.029 - 0.033	0.015 - 0.062		
	0.354	0.024 - 0.029	0.015 - 0.069	2541 2240 2504	0.075 0.066 0.071
Average	0.361	0.032	0.022 - 0.060	2717	0.069
Panel 15, 126-3-2-91	0.367	0.022	0.016 - 0.075	2346 2225 2451	0.060
	0.384	0.016	0.020 - 0.100		0.060
	0.395	0.017	0.016 - 0.081		0.060
					0.066
					0.058
					0.063
Average	0.382	0.018	0.017 - 0.085	2341	0.063

Table 112 (Continued). 2090 Al-Li Crippling Panel Weld Certification Testing.

Coupon I.D. (% Heat)	Nugget (inch)	Nugget Penetration		Shear Strength (Lbs)	Material Thickness (inch)
		Upper Sheet (inch)	Lower Sheet (inch)		
Panel 16, 60-3-2-42	0.367	0.022	0.016 - 0.075	2346 2225 2451	0.060
	0.384	0.016	0.020 - 0.100		0.060
	0.395	0.017	0.016 - 0.081		0.060
					0.066
					0.068
					0.063
	0.361	0.019	0.018 - 0.070	2018 2159 2592	0.060
	0.350	0.017	0.019 - 0.074		0.060
	0.305	0.018	0.026 - 0.079		0.060
					0.060
					0.061
					0.062
Average	0.360	0.018	0.017 - 0.085	2299	0.062
Panel 17, 34-2-2-50	0.360	0.033	0.017 - 0.070	2242 2600 2653	0.062
	0.360	0.036	0.024 - 0.071		0.072
	0.366	0.028 0 0.031	0.017 - 0.079		0.070
					0.068
Average	0.362	0.033	0.019 - 0.073	2498	0.068
Panel 18, 35-2-2-51	0.339	0.021	0.015 - 0.055	2648 2631 2635	0.065
	0.309	0.030	0.017 - 0.037		0.069
	0.337	0.018	0.017 - 0.051		0.069
					0.068
Average	0.328	0.023	0.019 - 0.073	2638	0.068
Panel 19, 39-2-2-55	0.360	0.015 - 0.022	0.023 - 0.087	3115 3094 3161	0.057
	0.321	0.017	0.013 - 0.077		0.055
	0.358	0.013 - 0.020	0.028 - 0.086		0.053
					0.069
					0.064
					0.071
Average	0.346	0.018	0.021 - 0.083	3123	0.062

Table 112 (Continued). 2090 Al-Li Crippling Panel Weld Certification Testing.

Coupon I.D. (% Heat)	Nugget (inch)	Nugget Penetration		Shear Strength (Lbs)	Material Thickness (inch)
		Upper Sheet (inch)	Lower Sheet (inch)		
Panel 20, 70-2-2-58	0.352	0.035	0.021 - 0.081		0.060
	0.368	0.042	0.023- 0.088		0.060
	0.363	0.035	0.021 - 0.076		0.060
				1882 2126 2194	0.070 0.065 0.064
Average	0.361	0.037	0.022 - 0.082	2067	0.063
Panel 21, 12-1-2-10	0.380	0.023	0.013 - 0.084		0.062
	0.360	0.025	0.025- 0.074		0.062
	0.354	0.022	0.019 - 0.088		0.062
				2699 2516 2501	0.069 0.069 0.071
Average	0.363	0.030	0.020 - 0.082	2320	0.065
Panel 23, 87-1-2-77	0.380	0.026	0.017 - 0.088		0.062
	0.366	0.032	0.022- 0.088		0.061
	0.375	0.027	0.017 - 0.088		0.062
				3011 2796 3024	0.066 0.068 0.069
Average	0.369	0.026	0.019 - 0.082	2758	0.065
Average of All Panels Welded	0.361	0.027	0.019 - 0.078	543	0.065

Table 113. Crippling Panel Test Results for 2090-T62 Stiffener Joined to 2090-T83 Skin.

Test Panel	I.D.	Panel Type	Ultimate Compressive Load (Lbs)
14	(17-3-2-15)	Stepped Hat	70,300
15	(126-3-2-91)	Stepped Hat	74,600
16	(60-3-2-42)	Stepped Hat	73,800
18	(35-2-2-51)	Beaded Web (FC)	65,000
19	(39-2-2-55)	Beaded Web (FC)	65,000
20	(70-2-2-58)	Beaded Web (FC)	65,200
21	(12-1-2-10)	Beaded Web (CC)	65,800
23	(87-1-2-78)	Beaded Web (CC)	67,200
24	(91-1-2-82)	Beaded Web (CC)	63,770

4.4.1.4 Crippling Panel Test Evaluation

The test plan for the crippling stiffener panels consisted of applying a compression loading continuously to the potted ends of each panel through the center of gravity of each skin/stiffener combination with the side edges simply supported until failure. Strain gage readings were continuously recorded to failure of the panel. In addition, the test machine head travel and transverse deflection at several locations on each stiffener were recorded. The detailed test plan was described in Rockwell TFD-90-1182¹⁰ (refer to section 4.4.1.3).

General Dynamics tested eighteen of the crippling panels and the test results are given in Table 110. The NASA-Langley test results were not available for inclusion in this report. The General Dynamics test results are the basis of the Rockwell test evaluations.

A summary of the test initial buckling and ultimate loads (as derived from General Dynamics test report) versus the predicted loads from the PASCO program are shown in Table 114. The basic failure mode for each stiffener was face wrinkling of the skin, as would be expected with a heavy skin-light stiffener combination. It was noted that very soon after the skin wrinkling for the stepped hat, the web buckled because of the change in skin support condition. This can also be seen in the PASCO analysis for the critical failure eigenvalue. After ultimate load, some inter-spotweld crippling failure was observed. The failure of a typical stepped hat is shown in Figures 230 and 231. Plots of the strain gage readings for the back-to-back skin gages and hat gages for a typical stepped hat are shown in Figures 232 through 234. Strain gage locations are shown in Figure 235. Some of the gages showed divergence typical of a stability-type failure; however, a few of the back-to-back gages (Figure 232) indicated that both sides of the skin were in tension. It was assumed this means that the buckling wave in the skin is going outward away from the stiffener (creating an I-beam effect) that overpowered the compression strain in the skin.

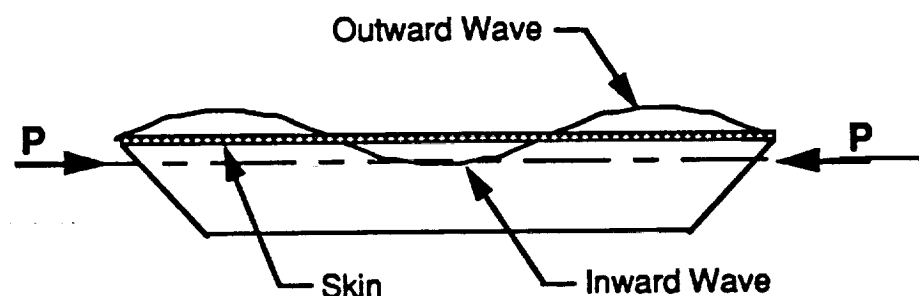


Table 114. Summary of Predicted Loads and Failure Modes for the Crippling Test Panel.

Stiffener Type	Material Skin	Combinations Stiffener	t_{bar}	Predicted Uniaxial Initial Buckling and <i>Ultimate Loads</i> (lbs)	Mode of Failure
Stepped Hat With Curved Cap	2219 Al	7475 SPF Al	0.256	69,600 76,800	Skin Wrinkling Comp. Yield
Stepped Hat With Curved Cap	2090 Al-Li	2090 SPF Al-Li	0.252	68,000 68,000	Skin Wrinkling Comp. Yield
Beaded Web Hat With Flat or Curved Cap	2219 Al	7475 SPF Al	0.264	60,000 79,200	Skin Wrinkling Comp. Yield
Beaded Web Hat With Flat or Curved Cap	2090 Al-Li	2090 SPF Al-Li	0.252	60,000 65,000	Skin Wrinkling Comp. Yield

Note: There is essentially no difference in the predicted loads indicated by the PASCO program between the flat or curved cap configurations of the beaded web stiffener.

Divergence of the gages would indicate an inward wave in the skin (i.e., local bending). Spotweld tension strength appeared very good in these tests since the inter-spotweld crippling after ultimate load produced only a few weld pull-offs or failures.

The beaded web panels exhibited the same type of face wrinkling mode as the stepped hat, but the wavelength of the buckle appeared shorter. The outer caps of some of the beaded-web panels buckled locally near the potted loading end just before ultimate load. This was attributed to the increased thinning of the cap in these areas because of the SPF forming process. It was noted that the stepped-hat configuration did not buckle in these areas; this was attributed to the curvature imposed in the cap.

The beaded-web panels exhibited excellent post-buckling strength after failure (refer to test machine travel versus load plots shown in Figure 236). The stepped hat also had some post-buckling strength, as shown in Figure 236. Typical strain gage plots for the beaded-web panels are shown in Figures 237 through 239. Strain gage locations are shown in Figure 240. Figures 241 and 242 show the failure of typical beaded-web panels in face wrinkling. The inter-weld crippling appears to occur after ultimate load. A summary of test versus predicted loads and failure modes is given in Table 114.

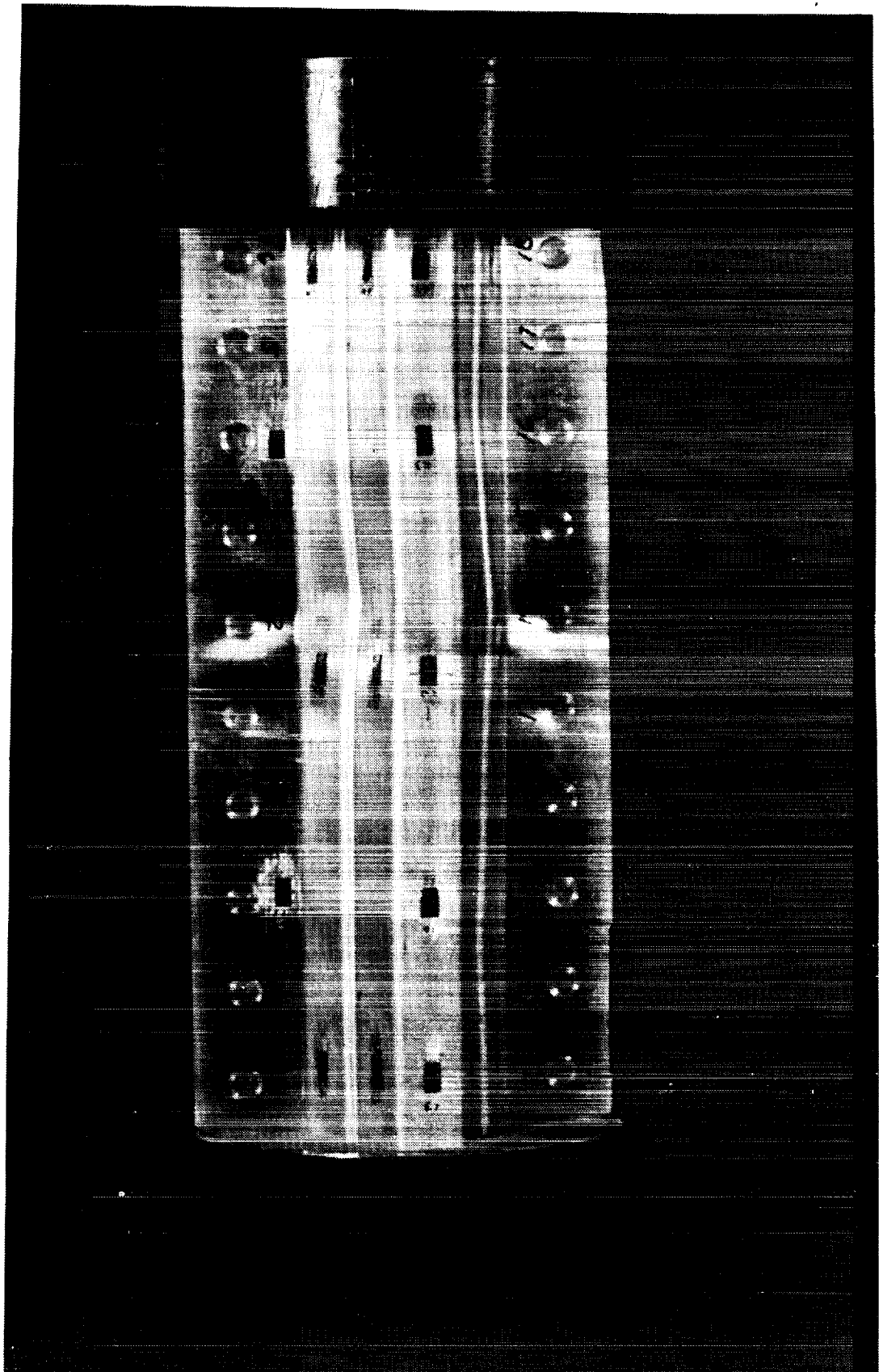


Figure 230. Failure of Panel #4 - 7475 Al Stepped Hat (Front View).

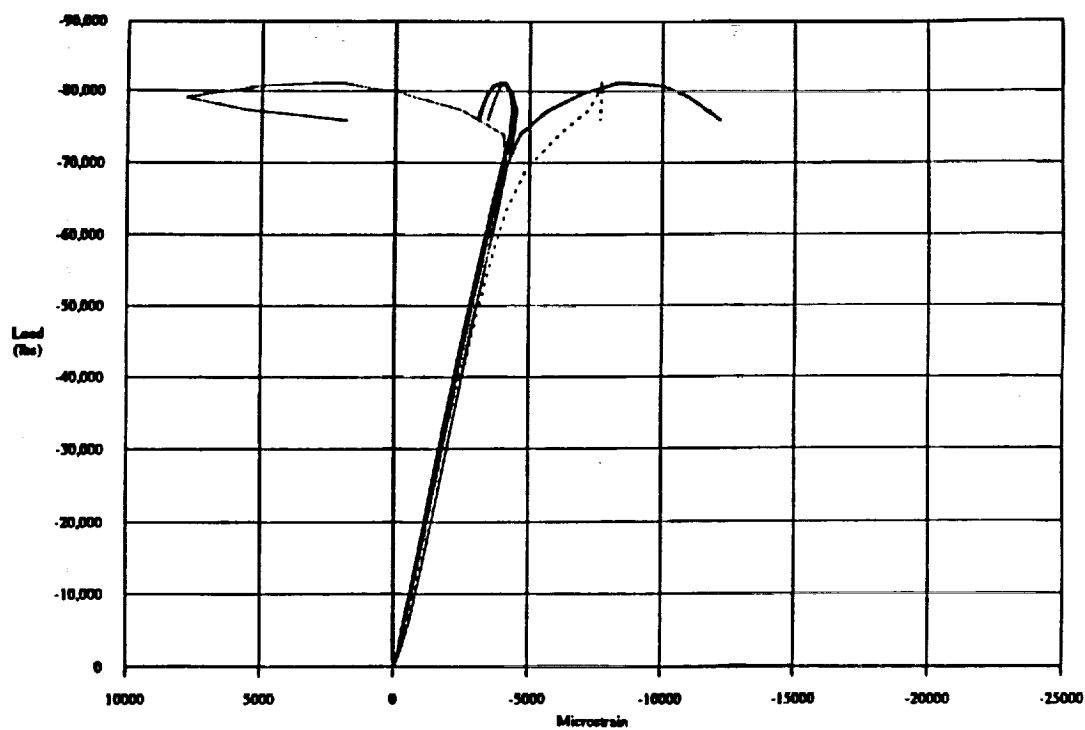
4-333

ORIGINAL PAGE
BLACK AND WHITE PHOTOGRAPH



Figure 231. Failure of Panel #4 - 7475 Al Stepped Hat (Rear View).

SPF Stiffener Tests
Panel #4: 43-3-7-3



SPF Stiffener Tests
Panel #4: 43-3-7-3

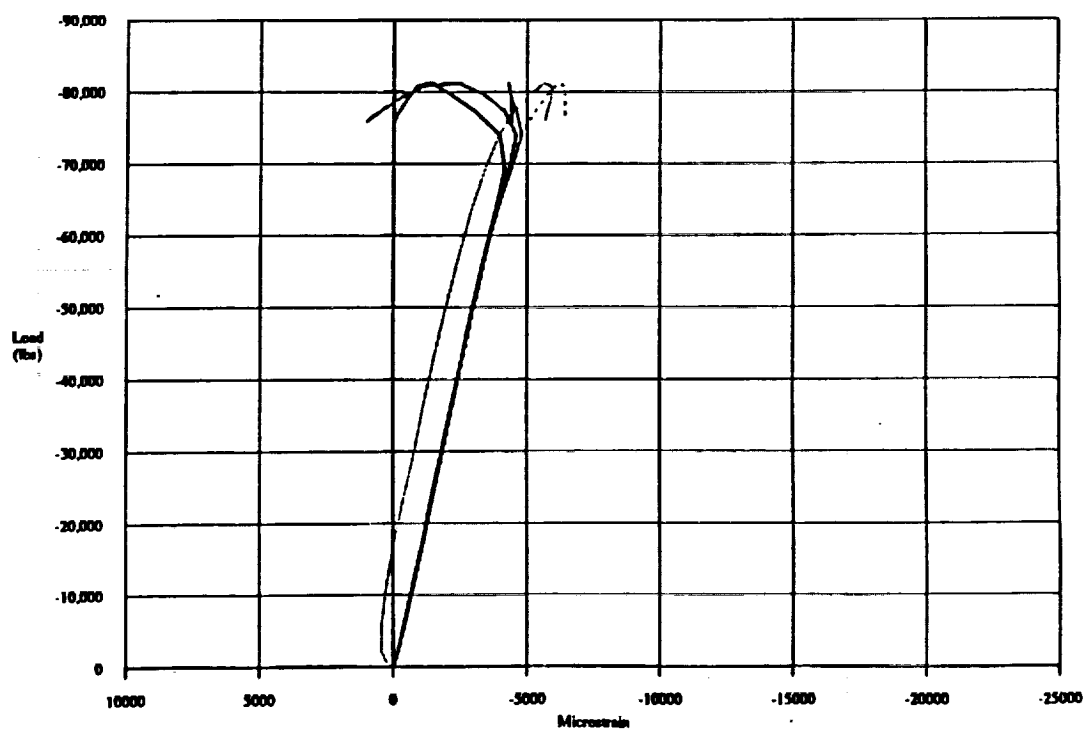
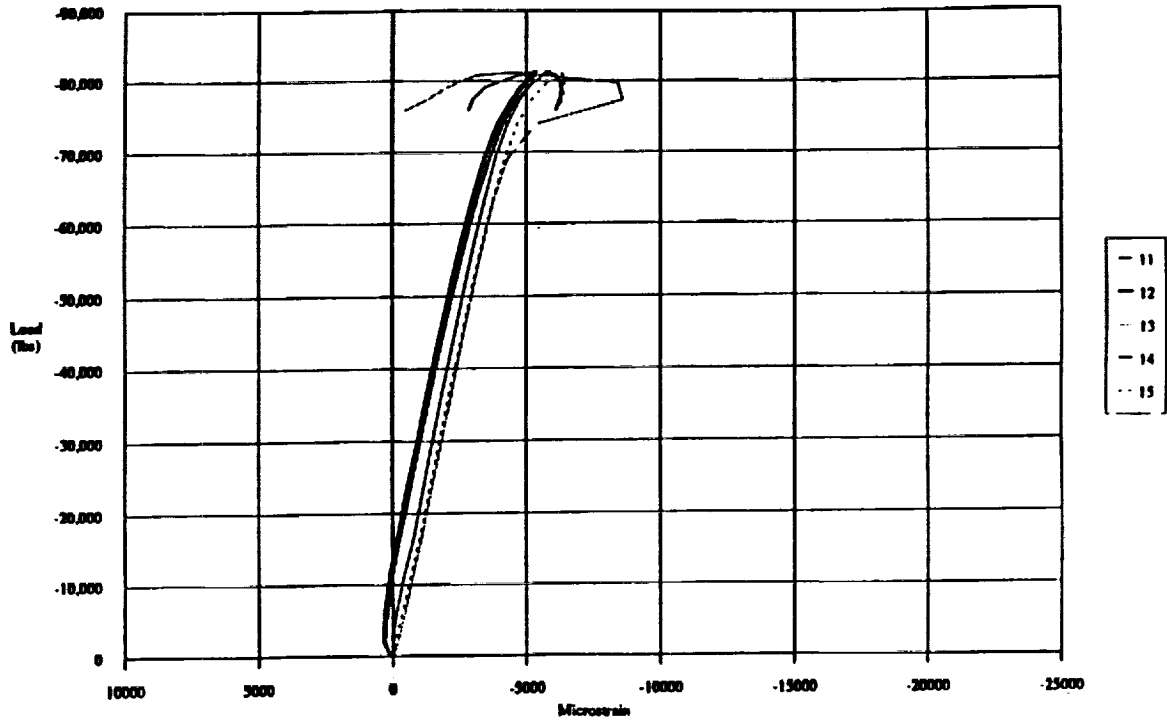


Figure 232. Typical Plots of Compression Strain Versus Load for the 7475-T62 Stepped Hat Stiffener - Panel 4 (Back-to-Back Strain Gages 1 and 6, 2 and 7, 3 and 8, 5 and 9, 5 and 10 are on the Skin).

SPF Stiffener Tests
Panel #4: 43-3-7-3



SPF Stiffener Tests
Panel #4: 43-3-7-3

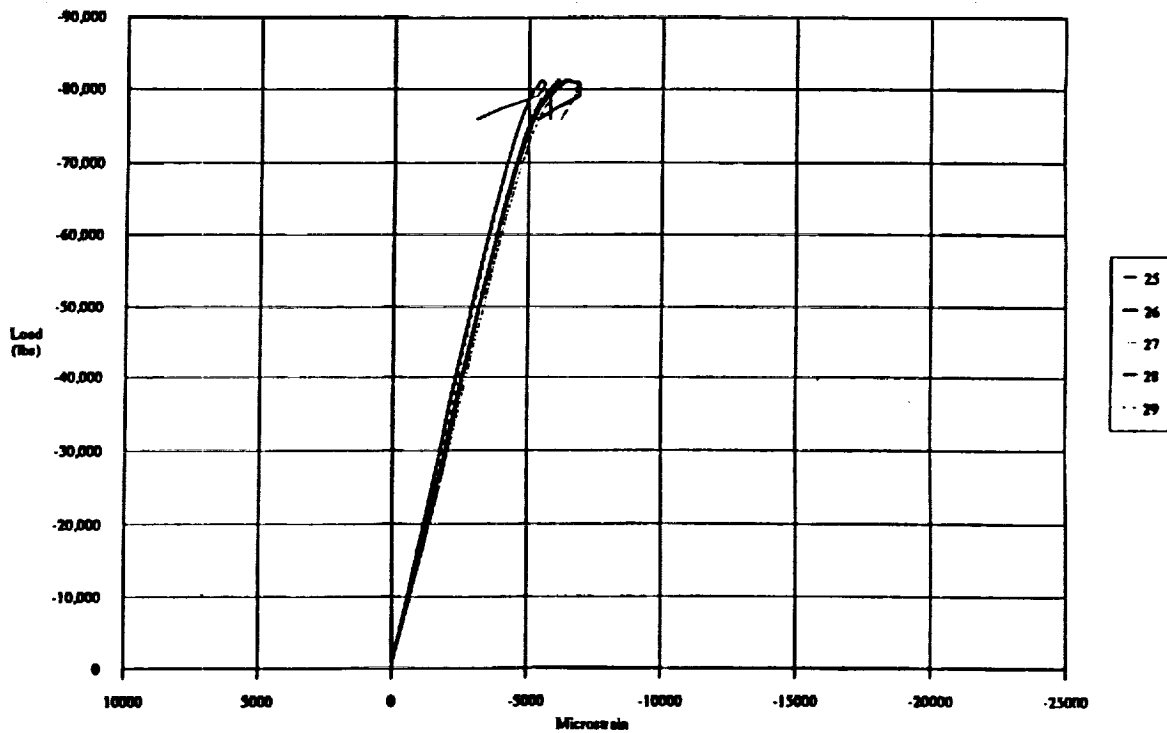


Figure 233. Typical Plots of Compression Strain Versus Load for the 7475-T62 Stepped Hat Stiffener - Panel 4 (Strain Gages at Extreme Ends of Stepped Hat Stiffener).

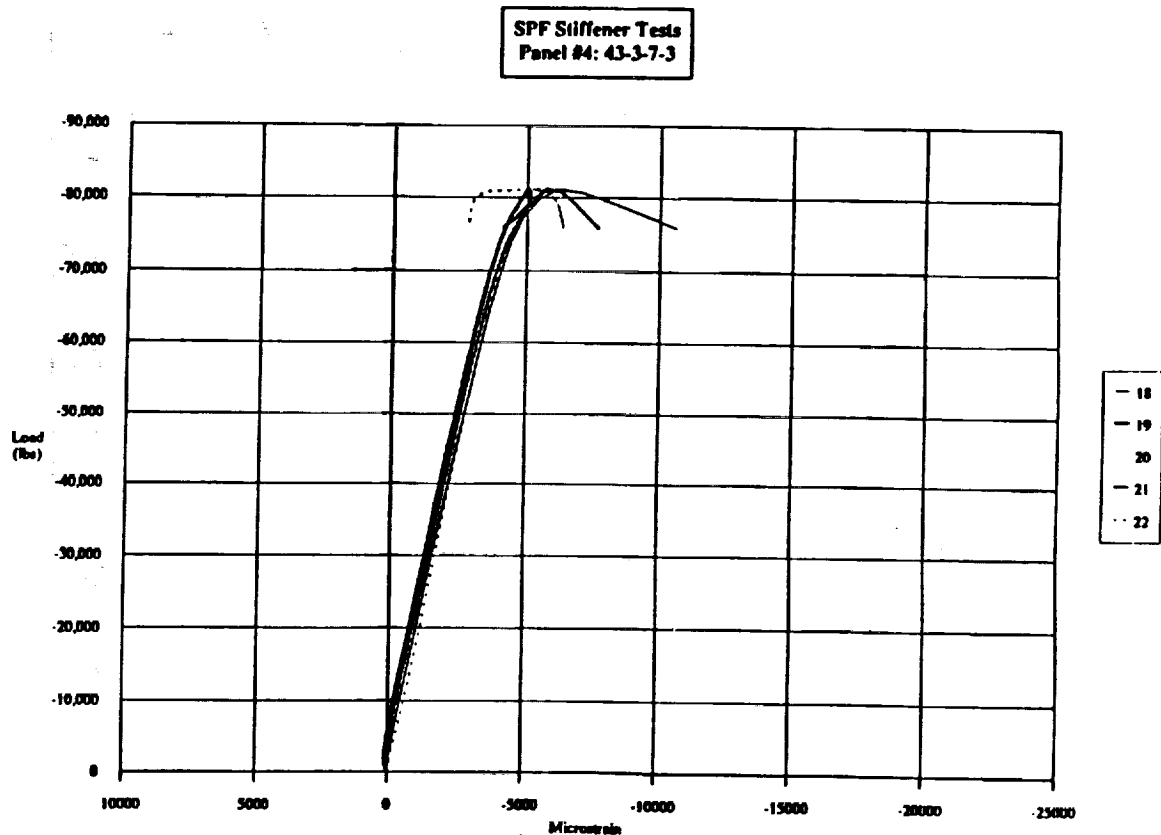
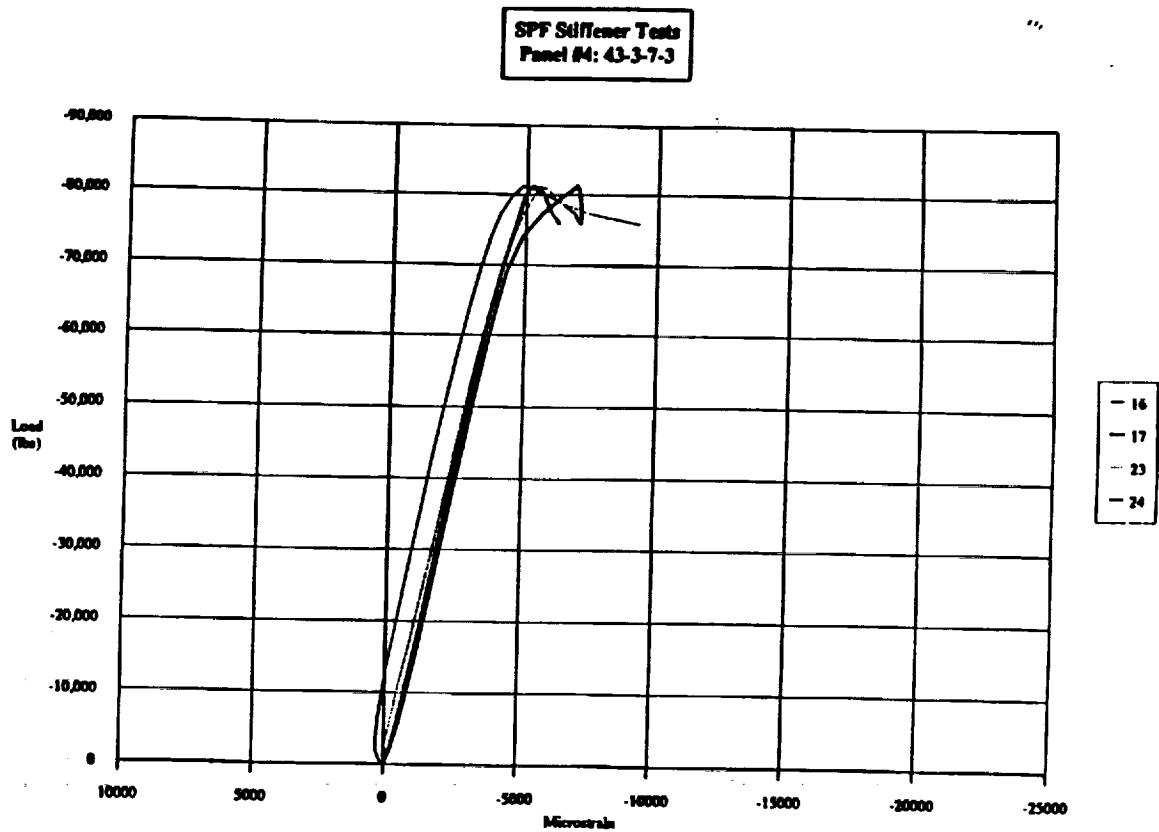
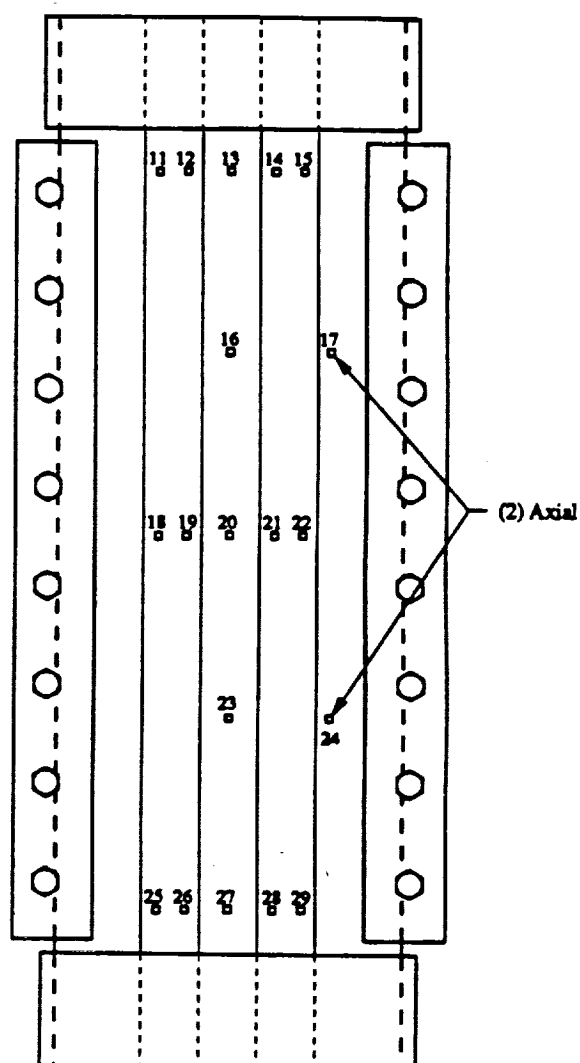
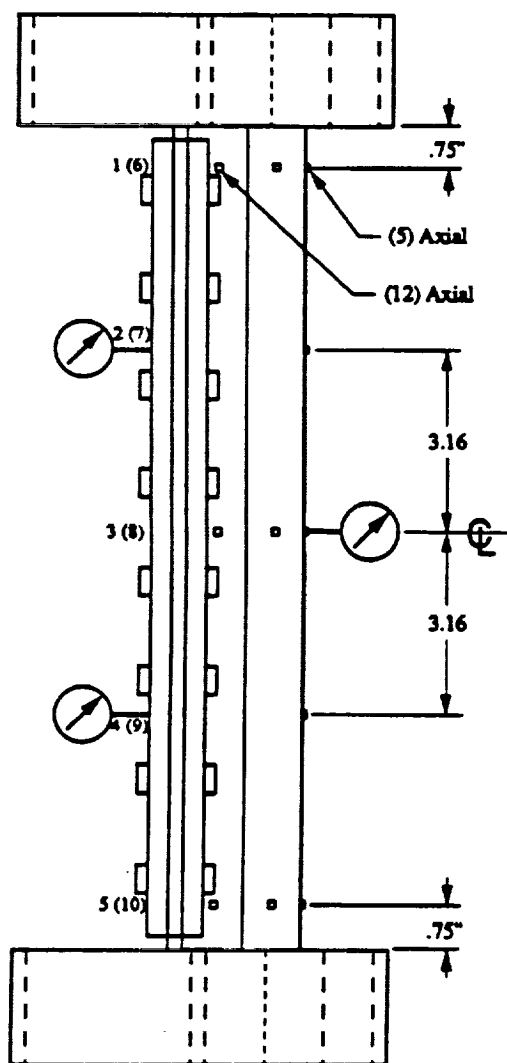
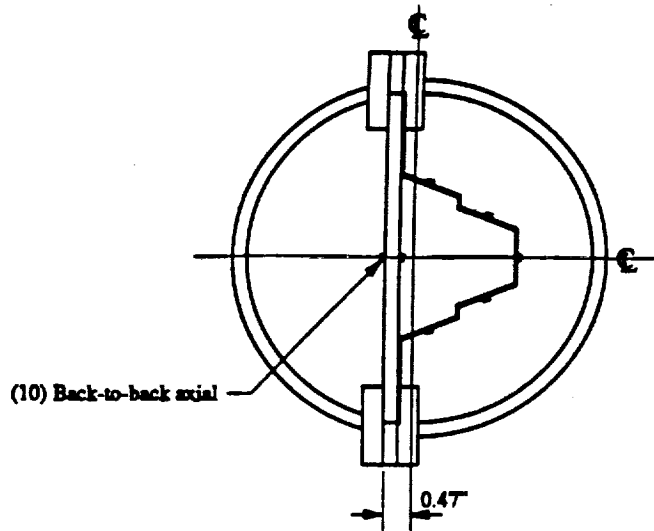


Figure 234. Typical Plots of Compression Strain Versus Load for the 7475-T62 Stepped Hat Stiffener - Panel 4 (Strain Gages are on the Central portions of the Cap and Flange Area of the Hat).



SPF Stiffener Concepts Stepped Hat Specimen

29 Axial Gages
() indicates internal gage

Figure 235. Typical Strain Gage Locations for the Stepped Hat Panels.

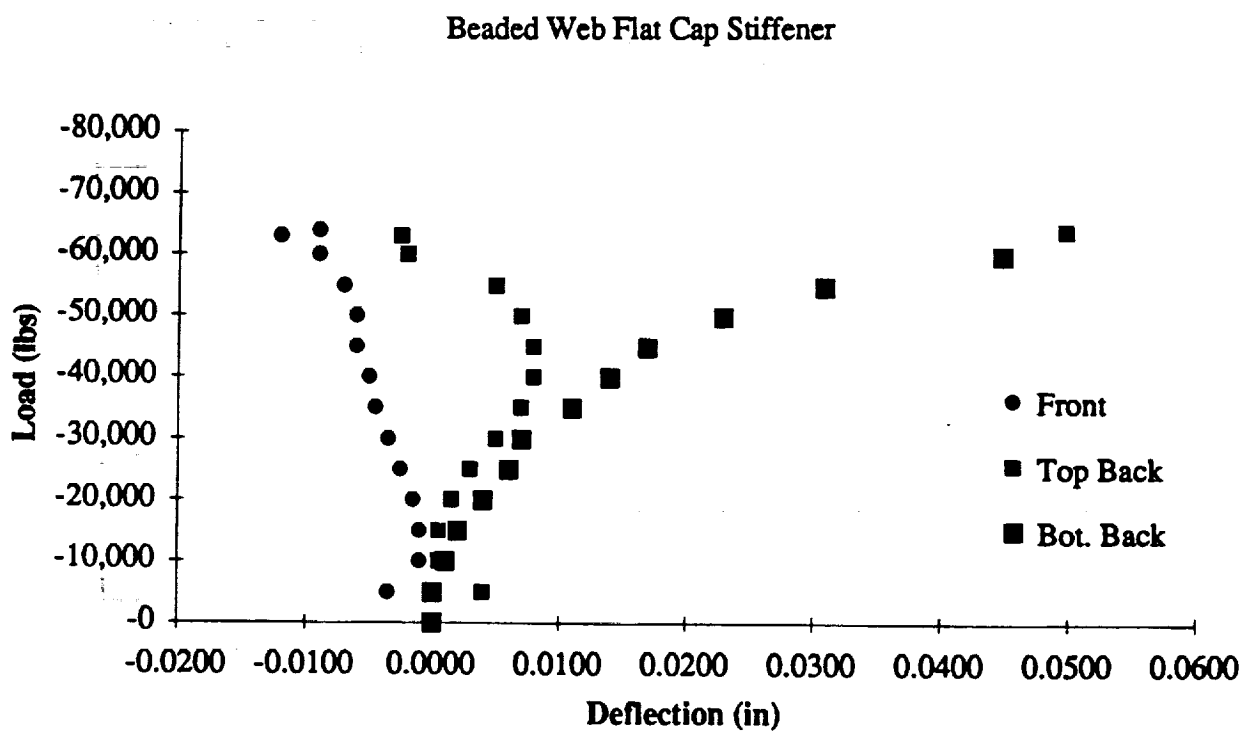
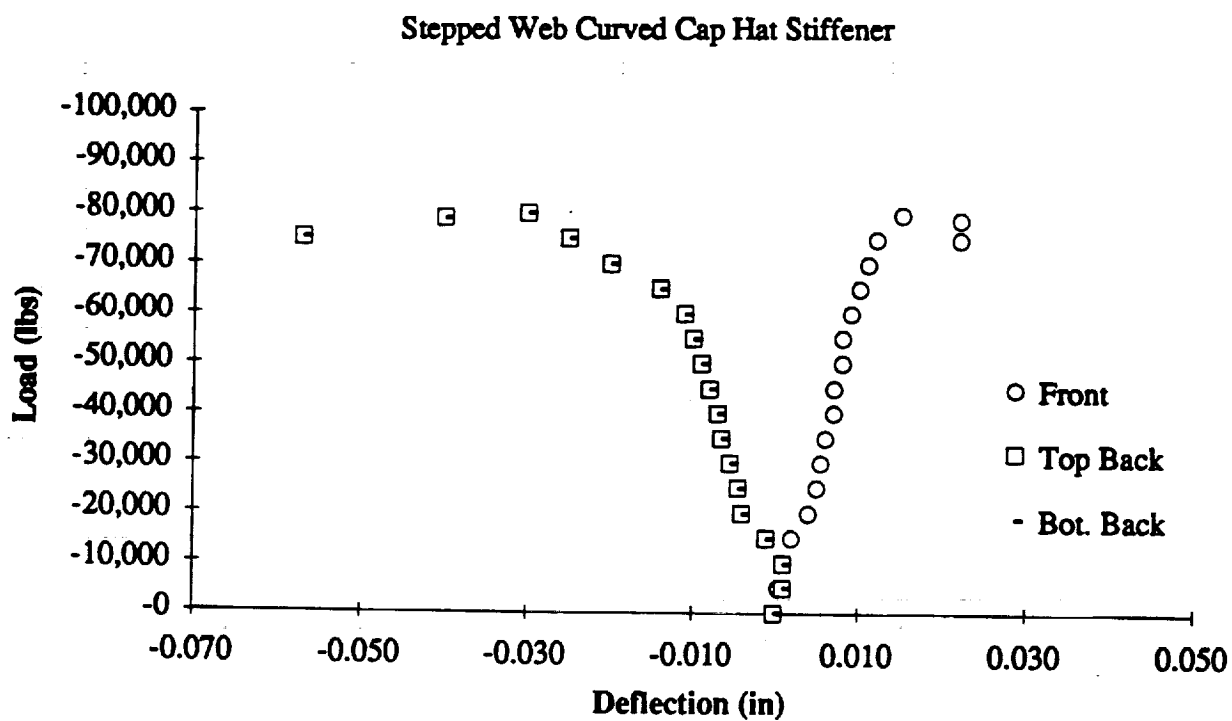
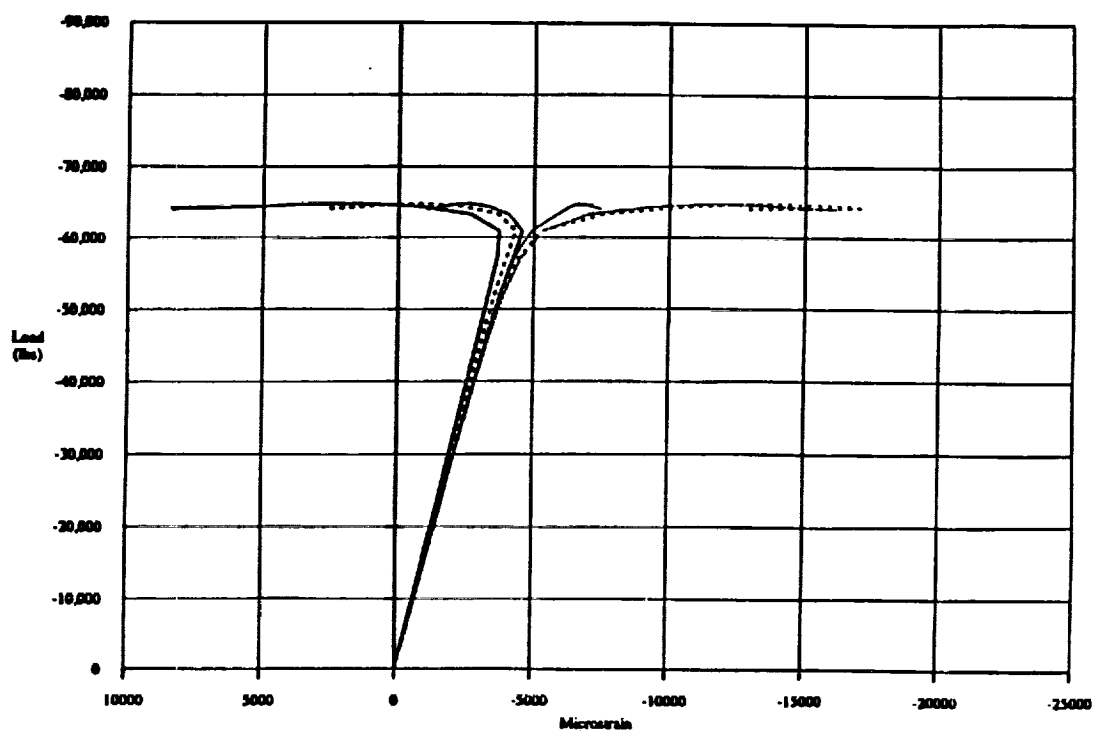
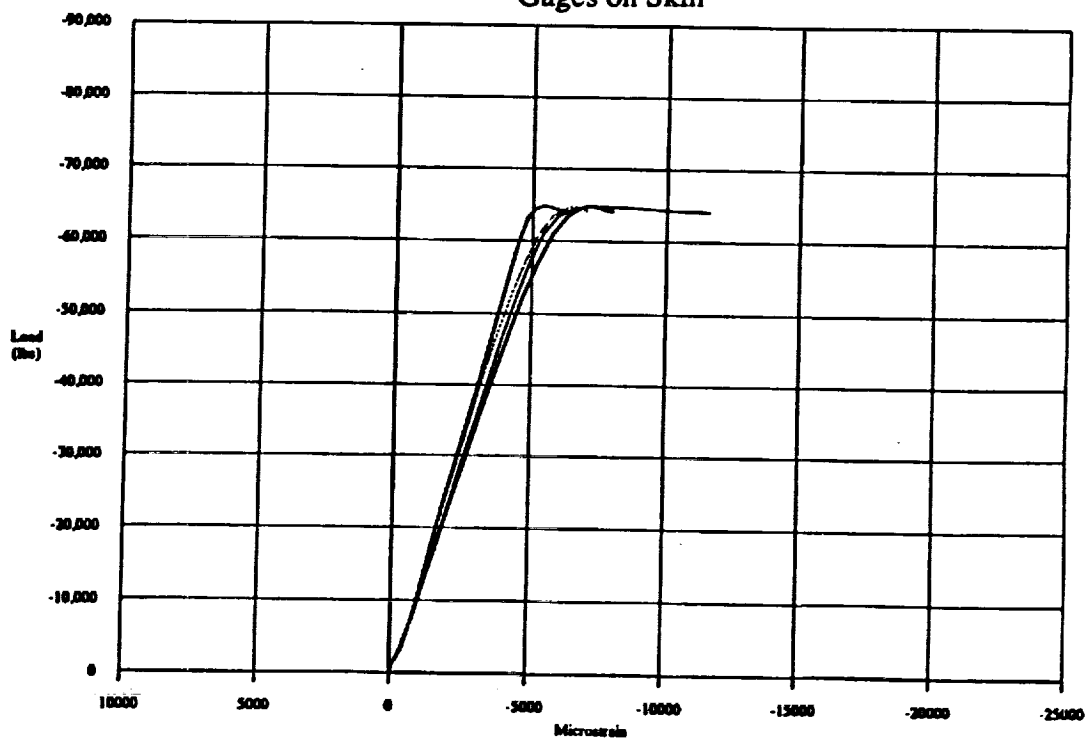


Figure 236. Panel Deflection Versus Load for the 7475-T62 Stepped (Panel 4) and Beaded Hat (Panel 18) Configurations.

SPF Stiffener Tests
Panel 08: 7-1-7-20



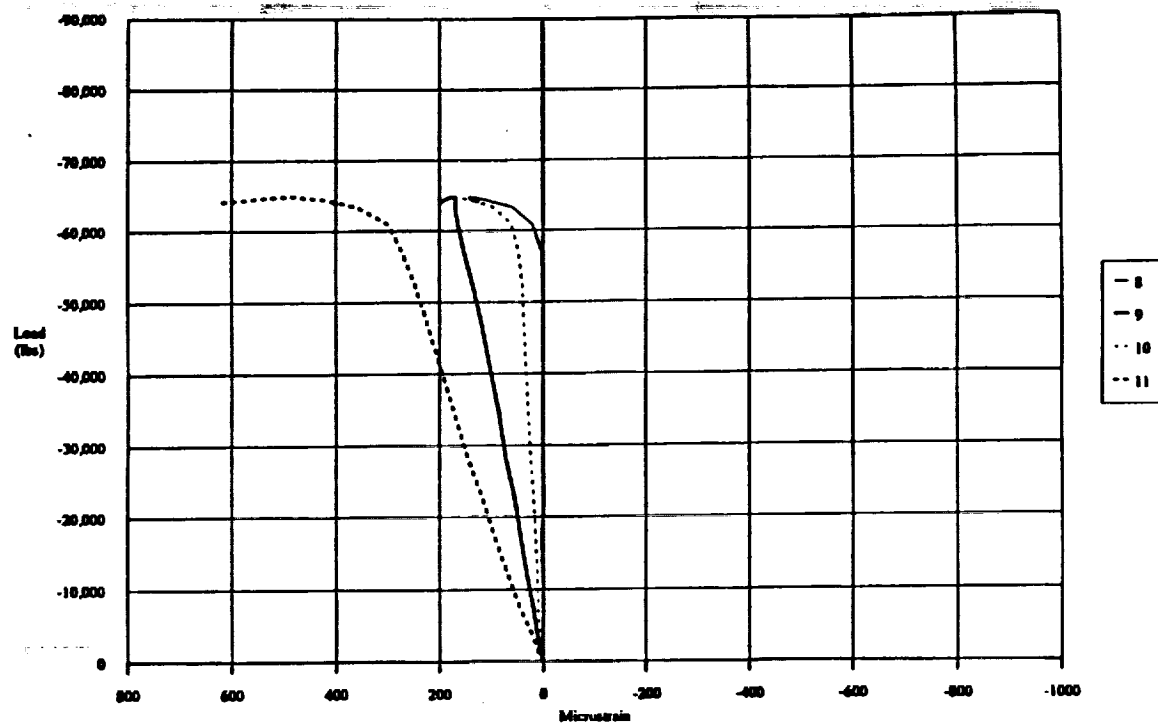
Gages on Skin



Gages on Stiffener Cap

Figure 237. Compression Strain Versus Load for the 7475-T62 Beaded Web Curved Cap Hat Stiffener - Panel 8.

SPF Stiffener Tests
Panel #8: 7-1-7-20



SPF Stiffener Tests
Panel #8: 7-1-7-20

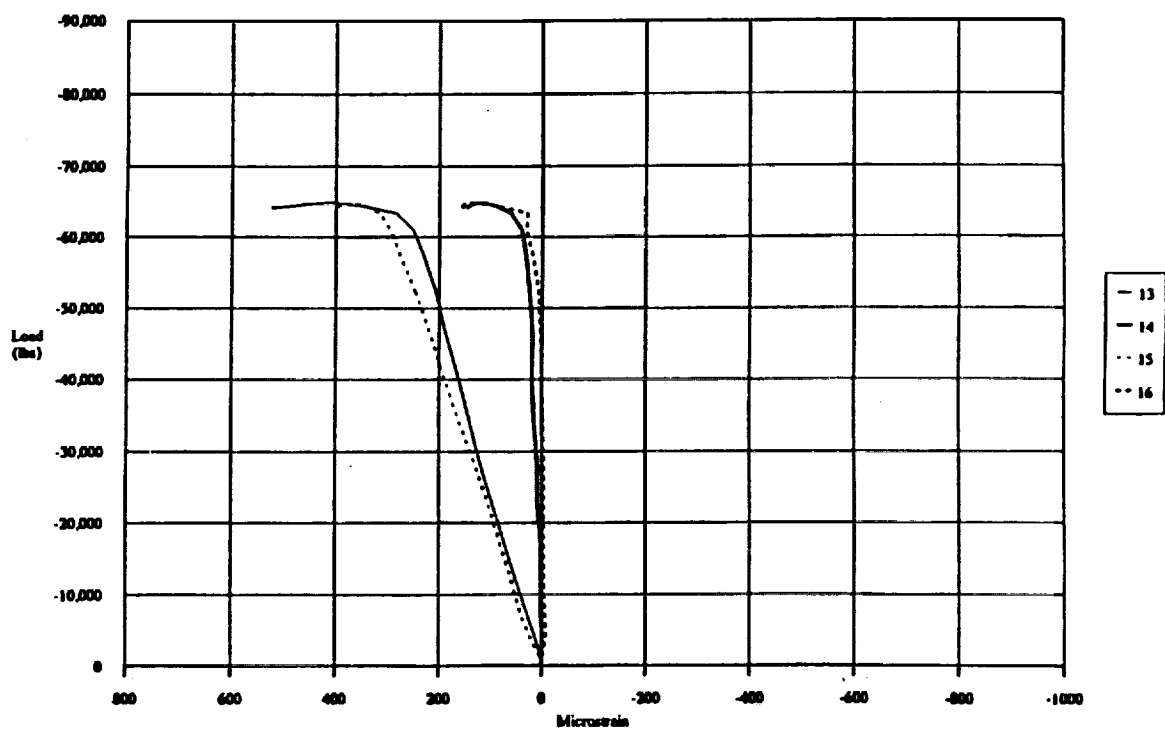
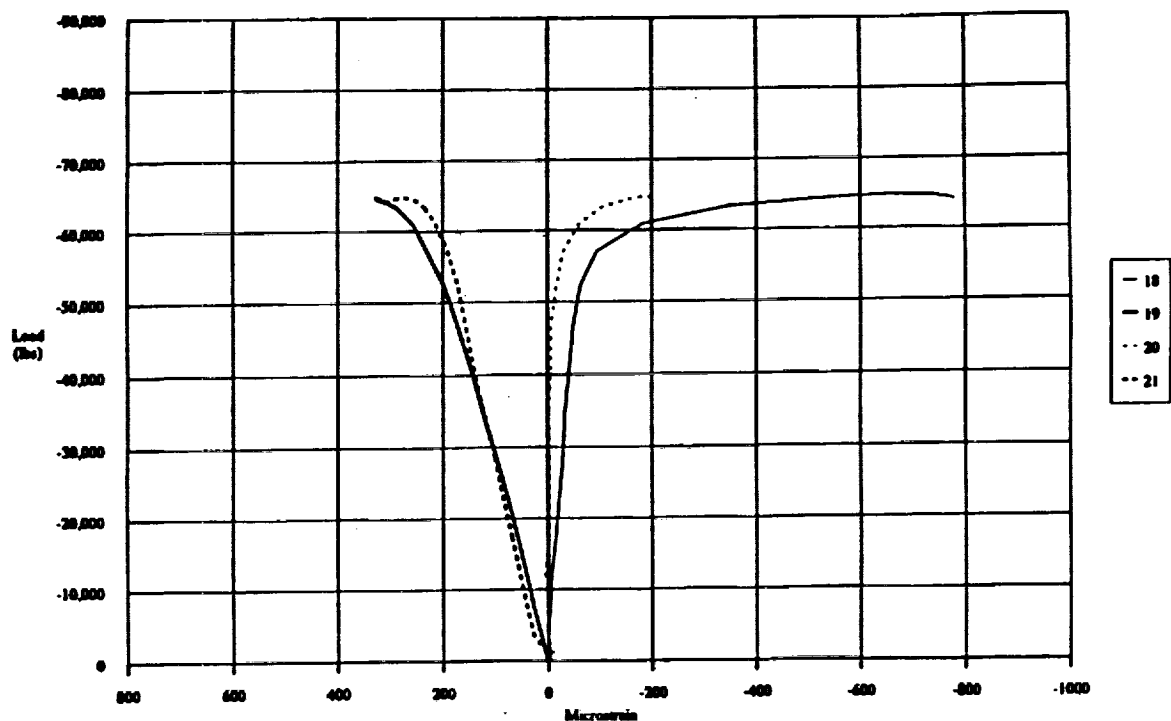


Figure 238. Compression Strain Versus Load for the 7475-T62 Beaded Web Curved Cap Hat Stiffener - Panel 8 (Strain Gages on Upper portion of Web and Flange Areas).

SPF Stiffener Tests
Panel 08: 7-1-7-20



SPF Stiffener Tests
Panel 08: 7-1-7-20

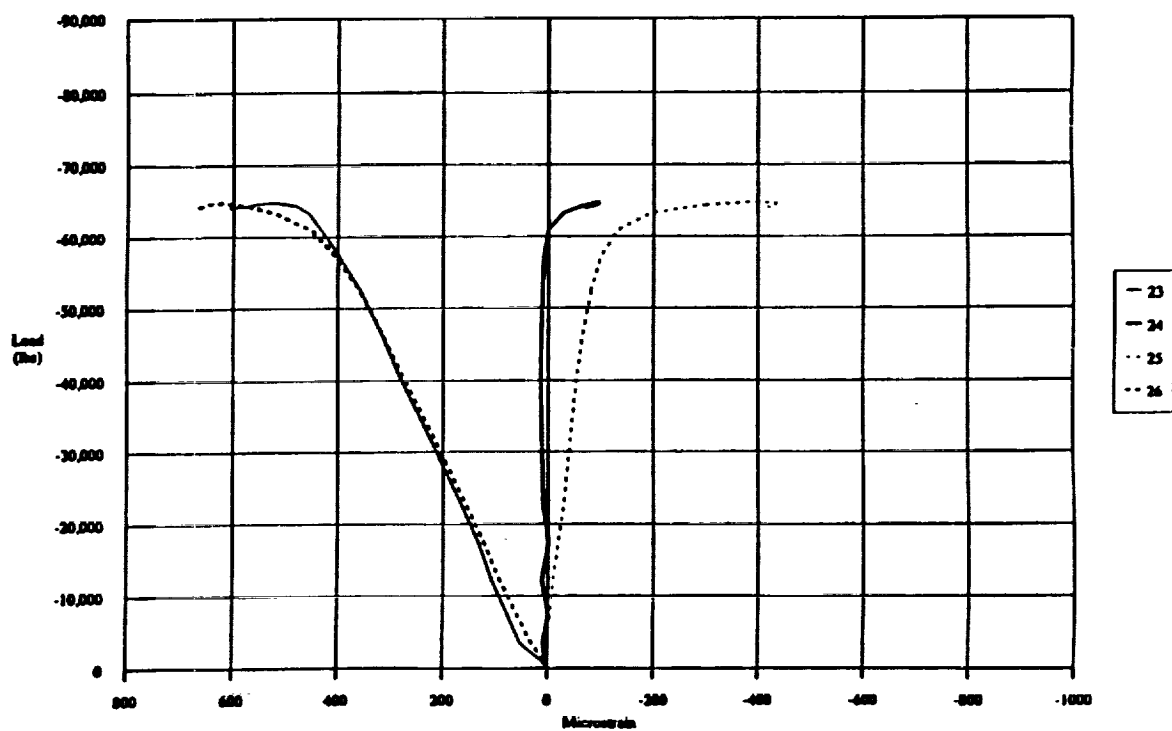
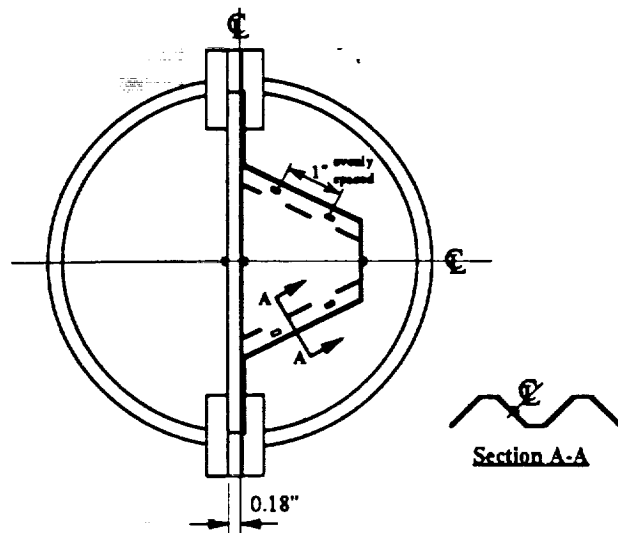


Figure 239. Compression Strain Versus Load for the 7475-T62 Beaded Web Curved Cap Hat Stiffener - Panel 8 (Strain Gages on Lower portion of Web and Flange Areas).



11 Axial
8 Biaxial
() indicates internal gage
A/T indicates axial/transverse

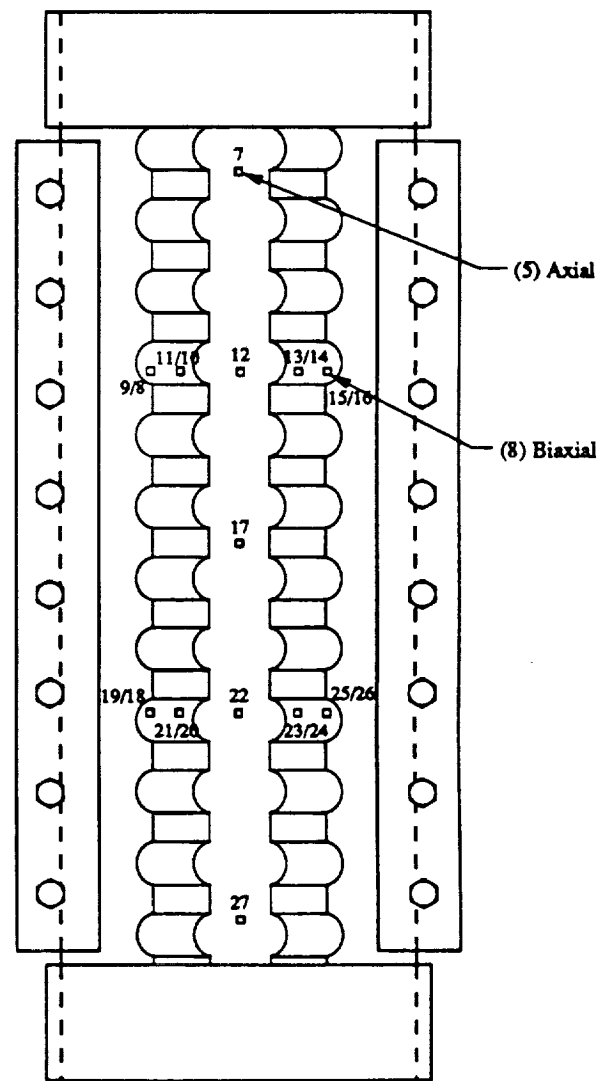
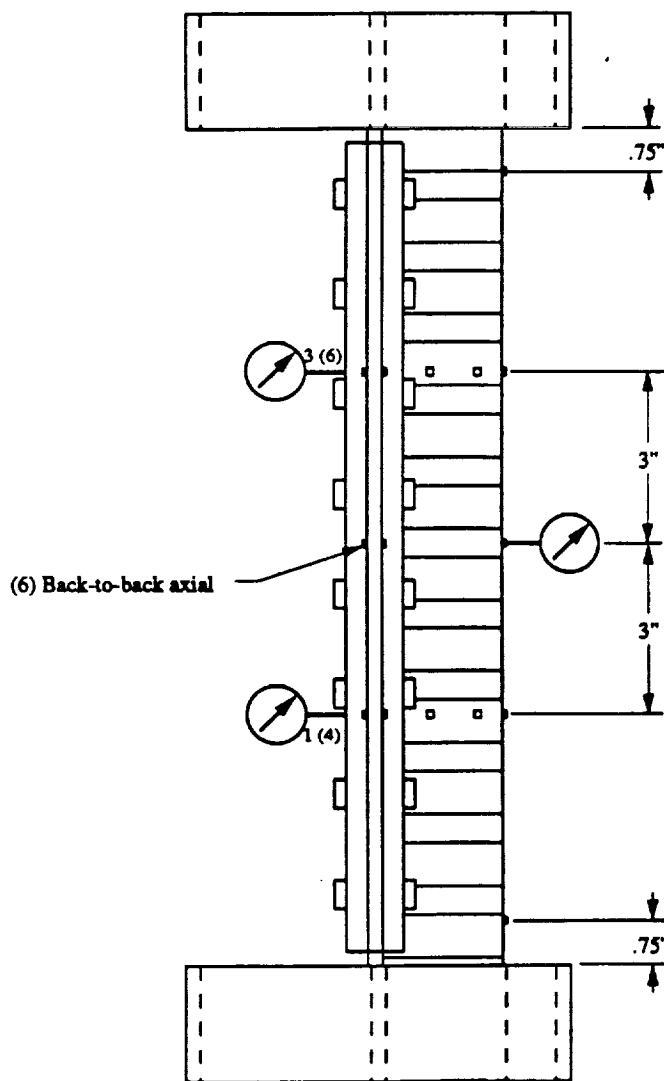


Figure 240. Typical Strain Gage Locations for the Beaded Hat Panels.

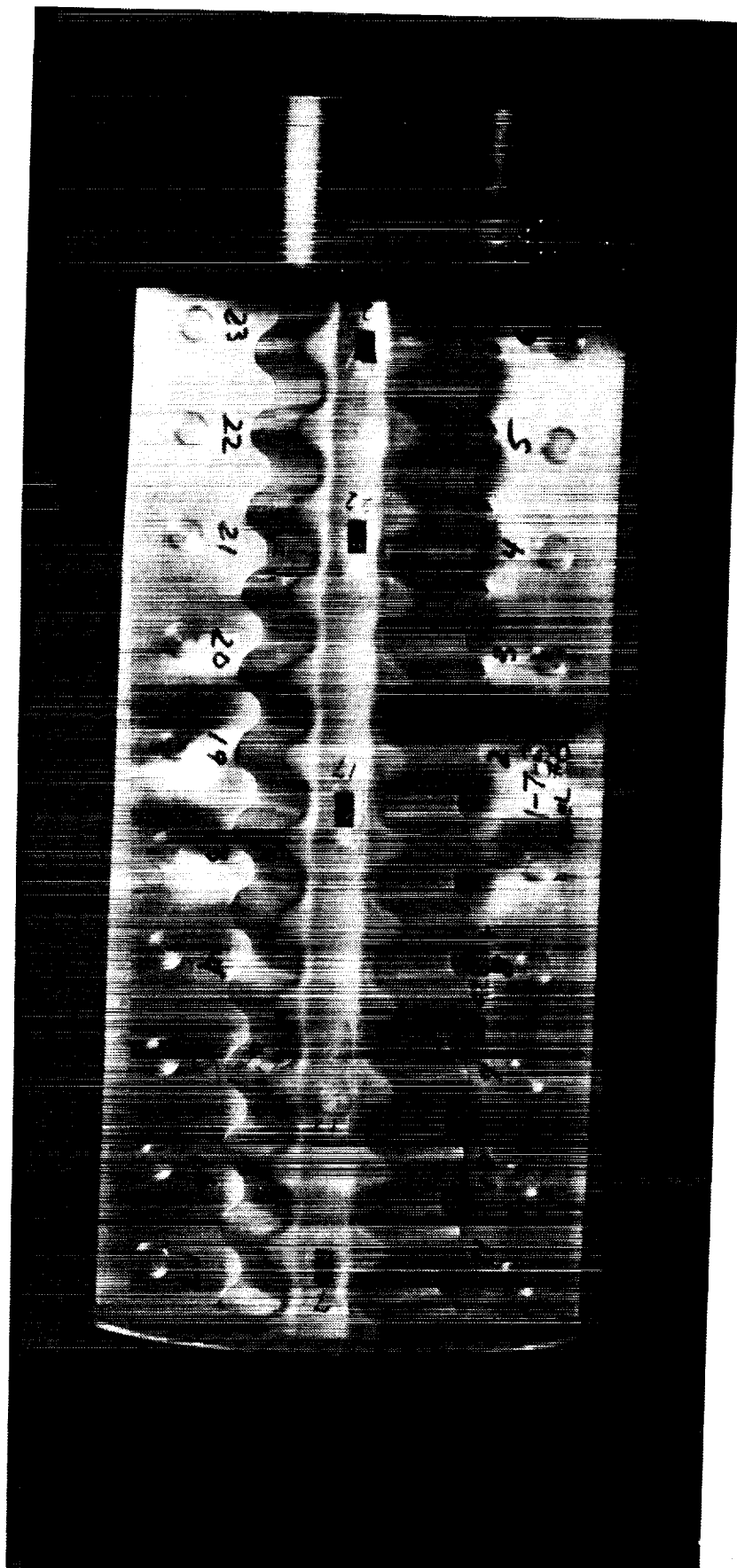


Figure 241. Failure of Panel #8 - 7475 Beaded Web, Curved Cap (Front View).



Figure 242. Failure of Panel #8 - 7475 Beaded Web, Curved Cap (Rear View).

4.4.1.4.1 Initial Buckling

It is of interest to indicate the method of determining the initial buckling load. Normally, the load at which divergence in the back-to-back gage readings occurs as the load is increased is considered buckling (i.e., a Southwell plot). As shown by the plots, the divergence and yield strength were very close, indicating an optimum structure. Thus, to determine the point of face wrinkling, the strains for each back-to-back gage pair were examined. The load at which the first onset of tension in a gage appeared (i.e., reduction in compression strain) was considered initial buckling. Examples of these selections are shown from the tabulated strain data which was taken from the General Dynamics test data for the stepped hat panel number 14 and the beaded hat panel number 18 and are shown in Tables 115 and 116, respectively. The calculated buckling loads for each panel, determined in this manner, are summarized in Table 117.

4.4.1.5 Crippling Panel Test Load Shortening Analysis

The objective of the load shortening analysis was to compare the axial stiffness (EA) of the crippling specimens as determined by test with that of the PASCO model representation of each stiffener/skin material combination.

During testing, machine head deflections versus load were recorded. The head deflections were not valid measurements for stiffener shortening or true computation of the specimen axial stiffness, however, an alternate approach was utilized for determination of the crippling panels load shortening. The alternate method consisted of utilization of average axial strain values at incremental loading of a particular stiffener/skin material combination. A load versus average strain curve was plotted and the slope of the curve in the linear range was utilized as the representative test EA. This translates into a mathematical representation of:

$$\epsilon_{\text{Average}} = \delta / L$$

δ = Shortening Deflection

L = Length of the specimen

$$\text{Thus } \epsilon_{\text{Average}} = \sum \epsilon_i / N \text{ at the load increment}$$

ϵ_i = Axial Strain at i^{th} gage

N = Number of Axial gages utilized

$$\text{Then } P/\epsilon = EA \text{ Where } P/\epsilon \text{ is taken in the curve linear range}$$

It was noted that the stepped hat included axial gages on the webs, whereas the beaded web gages were not included since it was assumed that the beaded configuration was in a pre-buckled state and would have a minimal axial stiffness effect. The plots of P versus ϵ_i are shown for representative stiffener/material combinations in Figures 243 through 248.

**Table 115. Strain Gage and Deflectometer Readings for Panel #14 (7475 Al)
Obtained During Testing at General Dynamics Space Systems Division.**

Time (Sec)	0	49	69	89	109	129	149	169	189	209
Load (Lbs):	0	4004	14,503	28,950	42,834	56,670	68,144	69,423	68,921	67,901
Gage I.D.										
Gage 1 ($\mu\epsilon$)	-28	-305	-1024	-1912	-2757	-3657	-4712	-4003	-3443	-3166
Gage 2 ($\mu\epsilon$)	-19	-249	-830	-1656	-2457	-3294	-4262	-3716	-2840	-2052
Gage 3 ($\mu\epsilon$)	-12	-218	-848	-1679	-2500	-3399	-4726	-10888	-4398	-4310
Gage 4 ($\mu\epsilon$)	-1	-187	-761	-1532	-2233	-2841	-2778	-30	1374	2257
Gage 5 ($\mu\epsilon$)	-4	-290	-947	-1799	-2631	-3489	-4357	-3802	-3205	-2933
Gage 6 ($\mu\epsilon$)	2	-231	-910	-1728	-2495	-3257	-3937	-4893	-4910	-4632
Gage 7 ($\mu\epsilon$)	-3	-242	-862	-1720	-2539	-3363	-3894	-3490	-3158	-2940
Gage 8 ($\mu\epsilon$)	-2	-243	-858	-1714	-2577	-3543	-5050	-6849	-6824	-6589
Gage 9 ($\mu\epsilon$)	-1	-251	-855	-1674	-2459	-3203	-3464	158	2649	3889
Gage 10 ($\mu\epsilon$)	-2	-251	-854	-1662	-2451	-3264	-4107	-4874	-5008	-4892
Gage 11 ($\mu\epsilon$)	7	-354	-1055	-1900	-2729	-3800	-7228	-6543	-6259	-6083
Gage 12 ($\mu\epsilon$)	-10	-359	-1155	-2079	-2995	-3982	-5353	-3598	-2812	-2181
Gage 13 ($\mu\epsilon$)	-11	-323	-1108	-1992	-2861	-3748	-4082	-2925	-2311	-1754
Gage 14 ($\mu\epsilon$)	-8	-314	-1072	-1938	-2755	-3597	-3815	-3800	-3798	-3750
Gage 15 ($\mu\epsilon$)	-17	-309	-963	-1786	-2597	-3364	-3974	-4408	-4697	-4935
Gage 16 ($\mu\epsilon$)	-25	-297	-1048	-1991	-2831	-3715	-4262	-3737	-3324	-2940
Gage 17 ($\mu\epsilon$)	-35	-186	-742	-1447	-2121	-2761	-3200	-3220	-3060	-2744
Gage 18 ($\mu\epsilon$)	-33	-273	-889	-1734	-2553	-3338	-3366	-1515	-1634	-1715
Gage 19 ($\mu\epsilon$)	-18	-271	-921	-1750	-2568	-3349	-3380	-838	880	2280
Gage 21 ($\mu\epsilon$)	-17	-307	-998	-1854	-2731	-3623	-5413	-4016	-2730	-1852
Gage 22 ($\mu\epsilon$)	-12	-306	-950	-1783	-2626	-3471	-3241	-1697	-1264	-1007
Gage 23 ($\mu\epsilon$)	-10	-281	-925	-1784	-2624	-3451	-4309	-3409	-2842	-2379
Gage 24 ($\mu\epsilon$)	1	-259	-900	-1659	-2414	-3127	-3871	-3983	-4016	-3930
Gage 25 ($\mu\epsilon$)	-36	-226	-863	-1631	-2381	-3007	-3074	-3326	-3430	-3480
Gage 26 ($\mu\epsilon$)	-14	-215	-864	-1697	-2515	-3268	-3273	-3142	-3178	-3117
Gage 27 ($\mu\epsilon$)	-2	-248	-913	-1814	-2720	-3600	-3809	-2689	-2188	-1648
Gage 28 ($\mu\epsilon$)	-34	-323	-963	-1806	-2659	-3463	-3579	-2373	-1706	-1107
Gage 29 ($\mu\epsilon$)	-16	-360	-1045	-1857	-2694	-3527	-4235	-3956	-3812	-3627

Load (lbs)	0	-10,000	-20,000	-30,000	-40,000	-50,000	-60,000	-69,000	-68,000
Deflectometers I.D. *									
DF Front (in)	0	-0.0010	0.0000	0.0000	0.0000	0.0010	0.0015	0.0080	0.0040
DF Top Back (in)	0	0.0000	0.0010	0.0020	0.0025	0.0040	0.0040	-0.0080	-0.0210
DF Bottom Back (in)	0	0.0015	0.0025	0.0040	0.0055	0.0090	0.0160	0.0060	0.1500

* Note: Negative deflectometer reading indicates inward movement of the test panel.

**Table 116. Strain Gage and Deflectometer Readings for Panel #18 (2090 Al-Li)
Obtained During Testing at General Dynamics Space Systems Division.**

Time (Sec)	0	55	95	115	135	155	175	195	215	235
Load (Lbs):	0	-5,894	27,113	38,675	49,525	59,618	63,304	63,678	63,507	62,451
Gage I.D.										
Gage 1 ($\mu\epsilon$)	-23	-499	-2039	-2896	-3831	-5325	-6721	-7018	-7051	-7035
Gage 2 ($\mu\epsilon$)	-2	-419	-1781	-2508	-3122	-3093	536	3831	6600	1746
Gage 3 ($\mu\epsilon$)	-1	-431	-1880	-2659	-3332	-3557	-2372	-1273	-614	-146
Gage 4 ($\mu\epsilon$)	-3	-436	-1863	-2652	-3390	-4142	-3416	-2480	-1815	-1280
Gage 5 ($\mu\epsilon$)	-3	-421	-1931	-2800	-3711	-5077	-8056	-10426	-7797	-3883
Gage 6 ($\mu\epsilon$)	-1	-430	-1931	-2786	-3621	-4337	-4258	-3925	-3556	-3296
Gage 7 ($\mu\epsilon$)	-2	368	-1596	-3053	-4216	-5087	-6101	-7527	-8291	-7588
Gage 8 ($\mu\epsilon$)	-5	21	-92	-174	-251	-328	-376	-454	-532	-594
Gage 9 ($\mu\epsilon$)	-4	-13	-21	-16	-24	-67	-211	-288	-308	-292
Gage 10 ($\mu\epsilon$)	-2	11	-243	-405	-578	-804	-856	-881	-901	-862
Gage 11 ($\mu\epsilon$)	-3	-9	1	14	22	9	-60	-71	-68	-57
Gage 12 ($\mu\epsilon$)	0	139	-1421	-2450	-3300	-3862	-3982	-4093	-4138	-3570
Gage 13 ($\mu\epsilon$)	-4	-41	-79	-81	-91	-111	-49	-38	-42	-50
Gage 14 ($\mu\epsilon$)	-3	-20	-31	-24	-25	-63	-41	-8	8	14
Gage 15 ($\mu\epsilon$)	-3	21	-14	-48	-67	-66	-119	-194	-273	-332
Gage 16 ($\mu\epsilon$)	-4	-34	-59	-57	-66	-110	-166	-155	-155	-155
Gage 17 ($\mu\epsilon$)	-1	-108	-1701	-2619	-3388	-4528	-5615	-5659	-2845	3959
Gage 18 ($\mu\epsilon$)	-2	18	89	137	-188	269	435	531	626	698
Gage 19 ($\mu\epsilon$)	-3	12	13	-8	-21	-43	-115	-201	-321	-448
Gage 20 ($\mu\epsilon$)	-6	34	80	80	82	57	-10	-40	-57	-77
Gage 21 ($\mu\epsilon$)	-6	14	29	25	30	19	-48	-78	-94	-111
Gage 22 ($\mu\epsilon$)	-12	-361	-2264	-3207	-4095	-4959	-5843	-6230	-6226	-5420
Gage 23 ($\mu\epsilon$)	-6	75	224	272	316	338	352	379	391	370
Gage 24 ($\mu\epsilon$)	-6	30	59	63	68	67	42	23	-9	-46
Gage 25 ($\mu\epsilon$)	-7	28	142	207	274	349	504	643	-765	864
Gage 26 ($\mu\epsilon$)	-4	44	52	40	37	-54	70	-1	-143	-310
Gage 27 ($\mu\epsilon$)	-0	-578	-2936	-4034	-5747	-7171	-7478	-8931	-9657	-8682

Load (lbs)	0	-10,000	-20,000	-30,000	-40,000	-50,000	-60,000	-64,000
Deflectometers I.D. *								
DF Front (in)	0	-0.0010	-0.0015	-0.0035	-0.0050	-0.0060	-0.0090	-0.0090
DF Top Back (in)	0	0.0005	0.0015	0.0050	0.0080	0.0070	-0.0020	0.0500
DF Bottom Back (in)	0	0.0010	0.0040	0.0070	0.0140	0.0230	0.0450	0.0950

* Note: Negative deflectometer reading indicates inward movement of the test panel.

Table 117. Summary of the Crippling Crippling Panel Test Versus Predicted Loads.

I.D.	Panel Type	Material	Tested By	Ultimate Load (lbs.)	Initial Buckling Load (lbs.)	Average Initial Buckling (lbs)	Predicted							
							Initial Load (lbs)	Init. Vs. Test	Ultimate Load (lbs)	Ult. Vs Test				
1	S.H.	7475 Al	GDSS	84000	71600	67880	69600	1.04	76800	1.09				
2	S.H.	Hat	GDSS	79400	62890			0.91		1.03				
3	S.H.	Joined	NASA	83400	69150			1.00		1.09				
4	S.H.	to	GDSS											
5	B.C.C.	2219 Al	GDSS	66500	62550			1.04		0.84				
6	B.C.C.		NASA	67900	61770	61780	60000	1.03	79200	0.86				
7	B.C.C.		GDSS											
8	B.C.C.		GDSS	66300	61010			1.02		0.84				
9	B.F.C.		GDSS	63000	57230	58500	60000	0.95	79200	0.80				
10	B.F.C.		NASA	67500	62750			1.05		0.85				
11	B.F.C.		GDSS											
12	B.F.C.	V	GDSS	67000	58530			0.98		0.85				
13	S.H	2090 Al-Li	NASA	70300	63415	63695	68000	0.93	68000	1.03				
14	S.H	Hat	GDSS					0.96		1.10				
15	S.H	Joined	GDSS					0.93		1.09				
16	S.H	to	GDSS					60000		68000				
17	B.C.C.	2090 Al-Li	NASA	65000	54820	56820		0.91		0.96				
18	B.C.C.	Skin	GDSS					0.98		0.96				
19	B.C.C.		GDSS					0.95		0.96				
20	B.C.C.		GDSS					60000		68000				
21	B.F.C.		GDSS	65800	56970	57650		0.95		0.97				
22	B.F.C.		NASA	67200	58520			0.98		0.99				
23	B.F.C.		GDSS											
24	B.F.C.	V	GDSS	63770	57470			0.96		0.94				

Panel Type: S.H. = Stepped Hat, B.C.C. = Beaded Web Curved Cap,
B.F.C. = Beaded Web Flat Cap

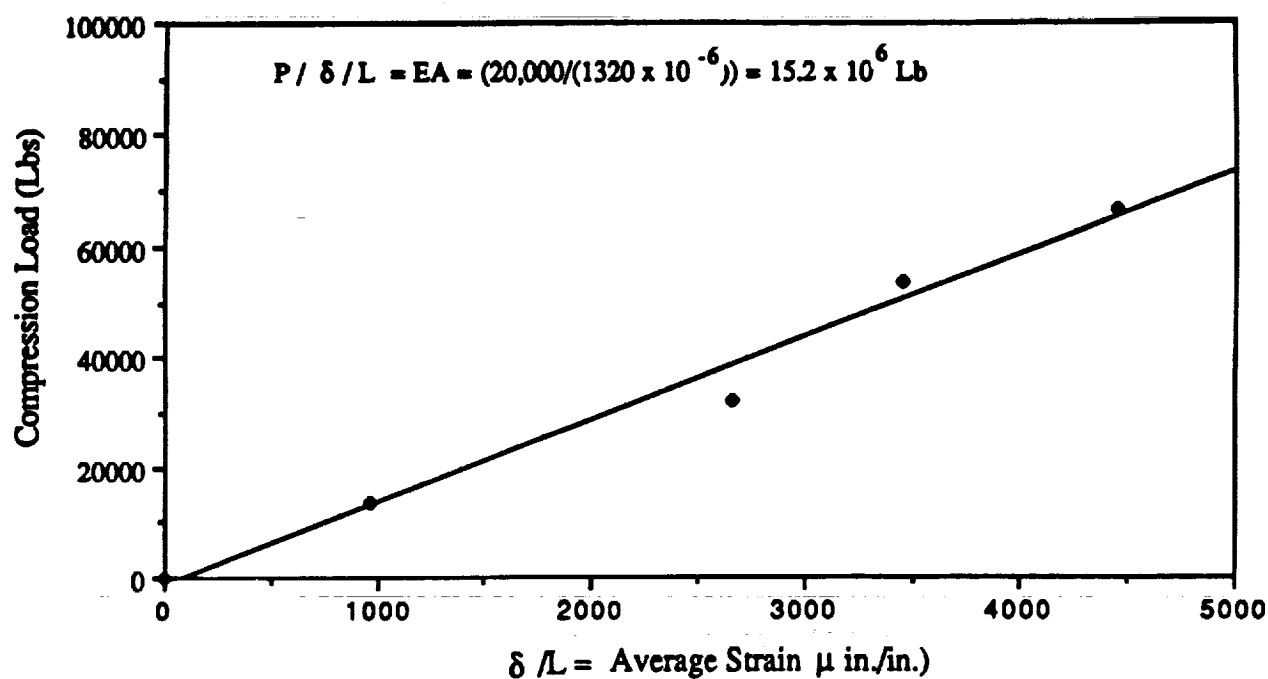


Figure 243. Load Shortening Analysis Panel #1 (65-3-7-28) Stepped Hat with Curved Cap (7475-T62 Al to 2219-T81 Al). Ultimate Load = 84,000 Lb.

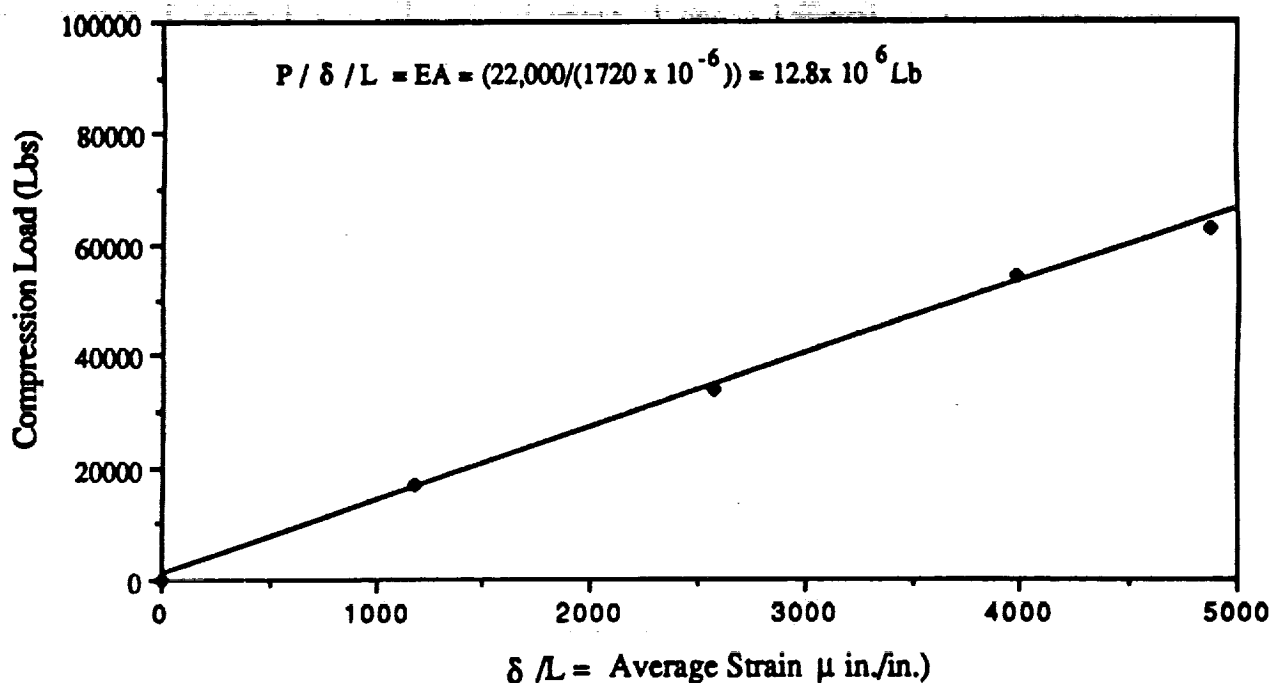


Figure 244. Load Shortening Analysis Panel #8 (7-1-7-20) Beaded Web with Curved Cap (7475-T62 Al to 2219-T81 Al). Ultimate Load = 66,300 Lb.

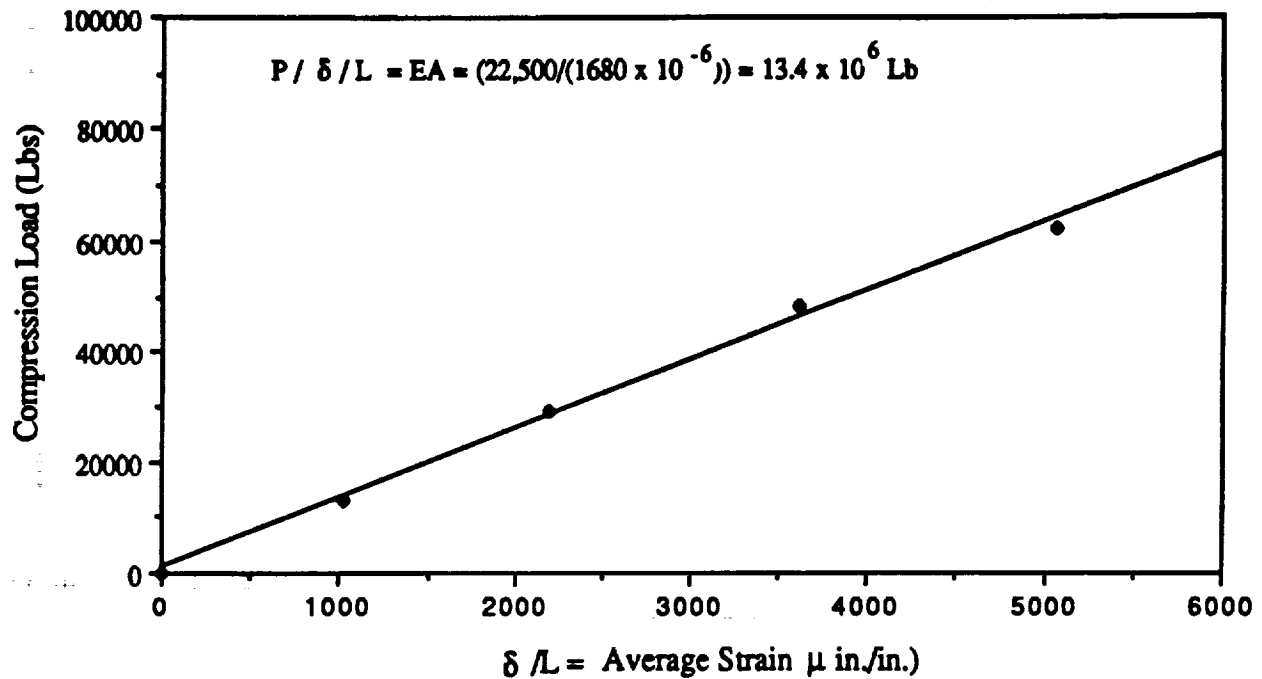


Figure 245. Load Shortening Analysis Panel #12 (30-2-7-36) Beaded Web with Flat Cap (7475-T62 Al to 2219-T81 Al). Ultimate Load = 67,000 Lb.

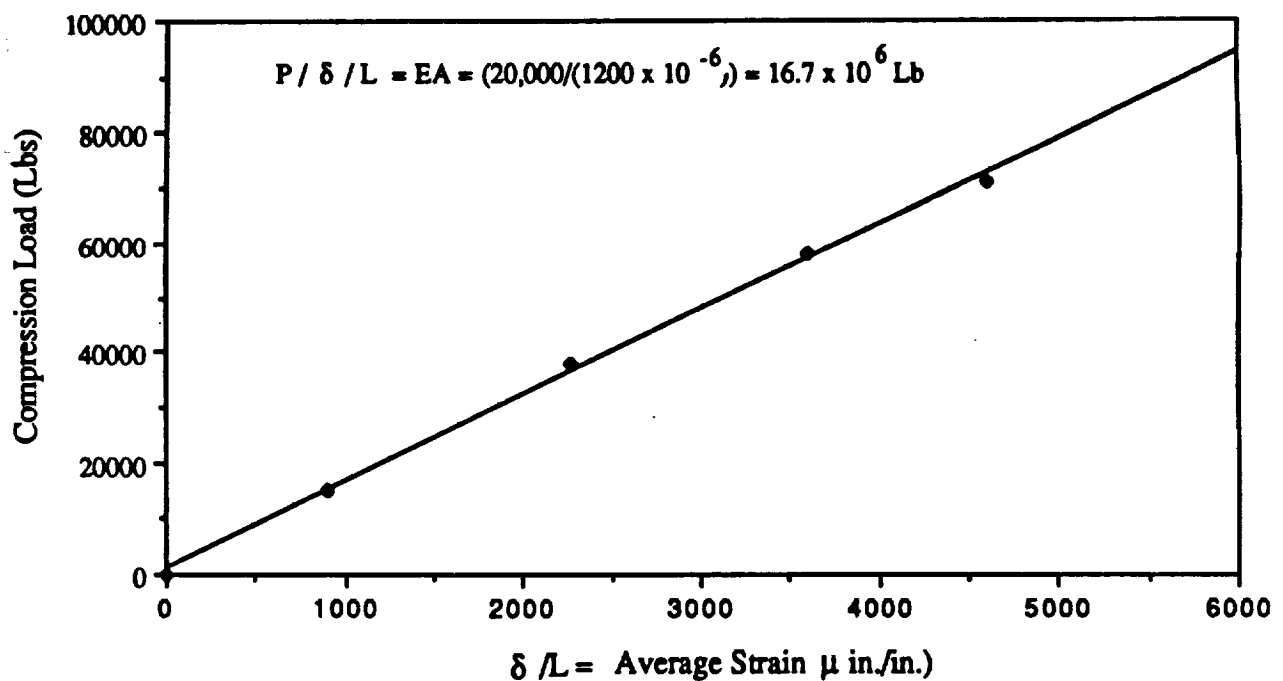


Figure 246. Load Shortening Analysis Panel #15 (126-3-2-91) Stepped Hat with Curved Cap (2090-T62 Al-Li to 2090-T83 Al-Li). Ultimate Load = 74,600 Lb.

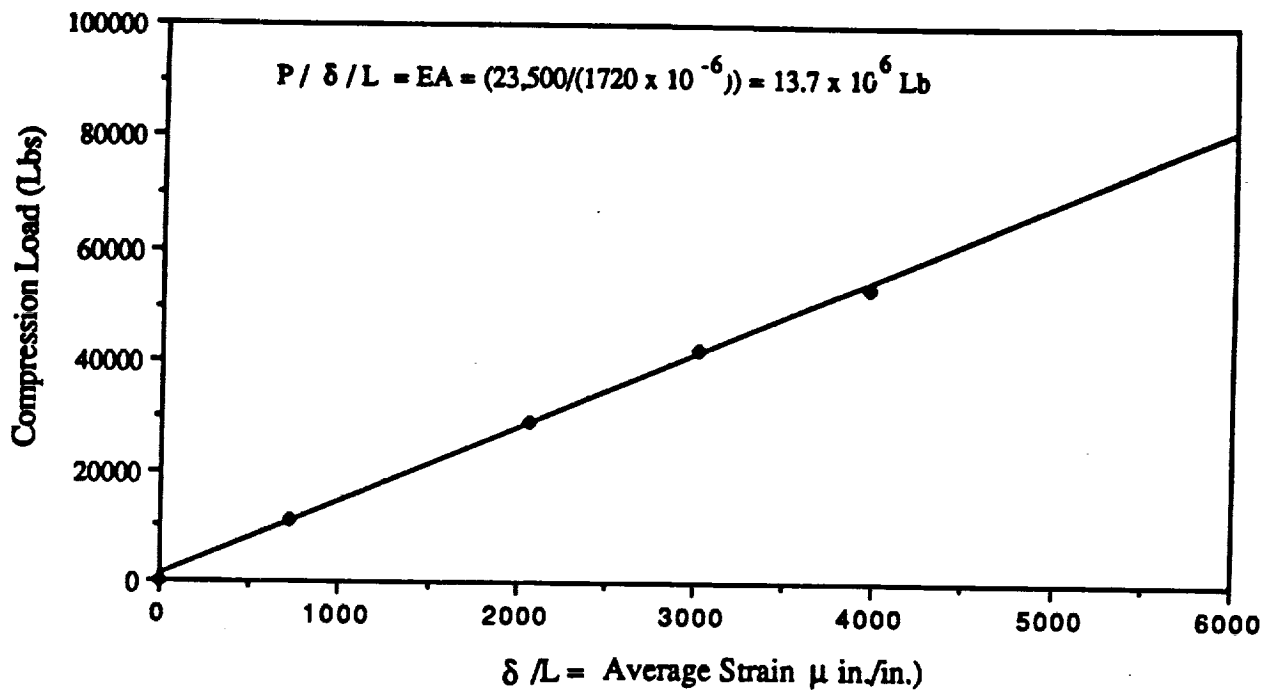


Figure 247. Load Shortening Analysis Panel #19 (39-2-2-55) Beaded Web with Curved Cap (2090-T62 Al-Li to 2090-T83 Al-Li). Ultimate Load = 65,000 Lb.

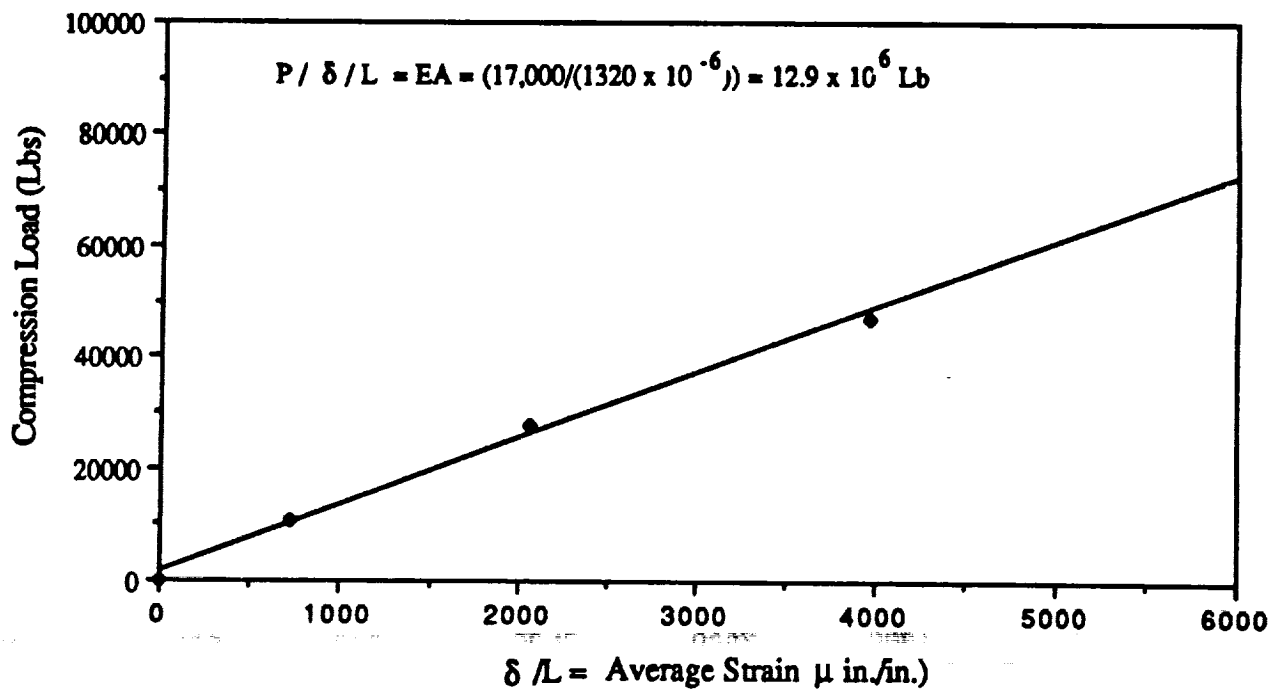


Figure 248. Load Shortening Analysis Panel #23 (87-1-2-78) Beaded Web with Flat Cap (2090-T62 Al-Li to 2090-T83 Al-Li). Ultimate Load = 67,200 Lb.

4.4.1.5 1 Results and Conclusion

The comparisons of the PASCO model axial stiffness and that obtained through the crippling test specimen values are summarized in Table 118. The column of the $E(t_{\text{bar}})x$ specimen width was included as an additional check of the values obtained. The PASCO models presented a satisfactory axial stiffness simulation of the crippling test specimens.

Table 118. Comparison Summary of the Test Panel Versus Predicted Axial Stiffness (EA) of the Crippling Specimens.

Panel No.	Stiffener Type	Material (Stiff/Skin)	A ₁₁ Model (x10 ⁶)	PASCO EA (x10 ⁶)	Test EA (x10 ⁶)	Stiffness t_{bar} (in)	Approximate $E t_{\text{bar}} \times \text{width}$ ($L_b \times 10^6 = EA$)	Ratio Test to Model
#1	SH	7475/2219	2.618	15.7	15.2	0.256	15.4*	0.97
#8	BCC	7475/2219	2.269	13.62	12.8	N/A	N/A	0.94
#12	BFC	7475/2219	2.269	13.62	13.4	N/A	N/A	0.98
#15	SH	2090/2090	2.90	17.4	16.7	0.252	17.1**	0.96
#23	BCC	2090/2090	2.28	13.68	12.9	N/A	N/A	0.94
#19	BFC	2090/2090	2.28	13.68	13.7	N/A	N/A	1.0

* Effective Modulus, Assumed = 10 Msi, ** Effective Modulus, Assumed = 11.3 Msi

t_{bar} = Effective Stiffener to skin thickness

SH = Stepped Hat, BCC = Beaded Curved Cap, BFC = Beaded Flat Cap

Test EA = $P/\delta/L = P/\epsilon$ ave. strain

δ = shortening of specimen (in.)

L = Length of Specimen (in.)

PASCO EA = ($A_{11} \times \text{Width}$)

A_{11} = Stiffness per inch of width

W = Specimen Width (6 in.)

N/A = Not applicable for beaded web panel the PASCO t_{bar} for the beaded web includes the webs, however, the beaded web contribution to the axial load capability of the stiffener is minimal.

4.4.1.6 Crippling Panel Test Conclusions

The following summary conclusions are based on the General Dynamics crippling panel test results:

1. The correlation between test and predicted loads was satisfactory.
2. The mode of initial buckling failure, face wrinkling (similar to column buckling of a beam on an elastic foundation), was expected, since this is typical of a heavy skin-light stiffener combination.

3. General Dynamics produced very satisfactory spotwelds for this application; e.g., no unzipping was observed after the face wrinkling failures of the specimens.
4. Since the t_{bar} for the beaded hat and stepped hat are quite close, the stepped hat offers about 10-14% more efficiency on the basis of initial buckling for the same material.
5. Comparing the ratio of the initial buckling to material density (F_{bu}/ρ) for 2090 and 7475 stepped hats indicates that the 2090 material is slightly more efficient for this application, as would be expected.
6. Since the initial buckling and yield strength were quite close, all the designs appeared to produce a very good optimum structure.
7. All designs met the required design criterion of 51,000 lbs (8474 lbs/in.) uniaxial compression loading for local buckling.
8. The SPF beaded hat could be made a more structurally efficient configuration if the webs were chem-milled to a lower thickness; however, this would increase the cost of fabrication.
9. An improved theoretical thinning profile would be useful in considering any other possible variations of the SPF hat-stiffener configuration.

4.4.1.7 Crippling Panel Test Recommendations

The stepped-hat configuration will be utilized as the column buckling test panel design to maximize stiffener load carrying ability. Integrally stiffened structure (vertical stiffeners and hoop-wise supports integrally formed into the panel) would utilize the beaded web stiffener concept to minimize load transfer through the side walls of the stiffener which could lead to large moments at the point of intersection in the panel. The integrally stiffened panel was not addressed during the panel test and evaluation portion of this program, however, the concept appears to be viable (due to the performance of the structural test specimens and through evaluation of the stress analysis efforts under this program) for vertical and hoop-wise strengthening of built-up cryogenic tank structure.

4.4.2 INTEGRALLY STIFFENED PANEL DEMONSTRATION ARTICLE

The integrally stiffened panel (shown in Figure 249 and 250) was fabricated as a demonstration article. The panel was fabricated as a representation of the type of configuration that could be fabricated for an integral SPF stiffener configuration without optimization of the stiffener or node configuration. An existing die box was sent to Rockwell from NASA Langley and modified so that back pressure could be applied to the part. The part blanks were coated with boron nitride (BN) releasing agent (rather than yttria which is generally used for Al-Li alloys, but

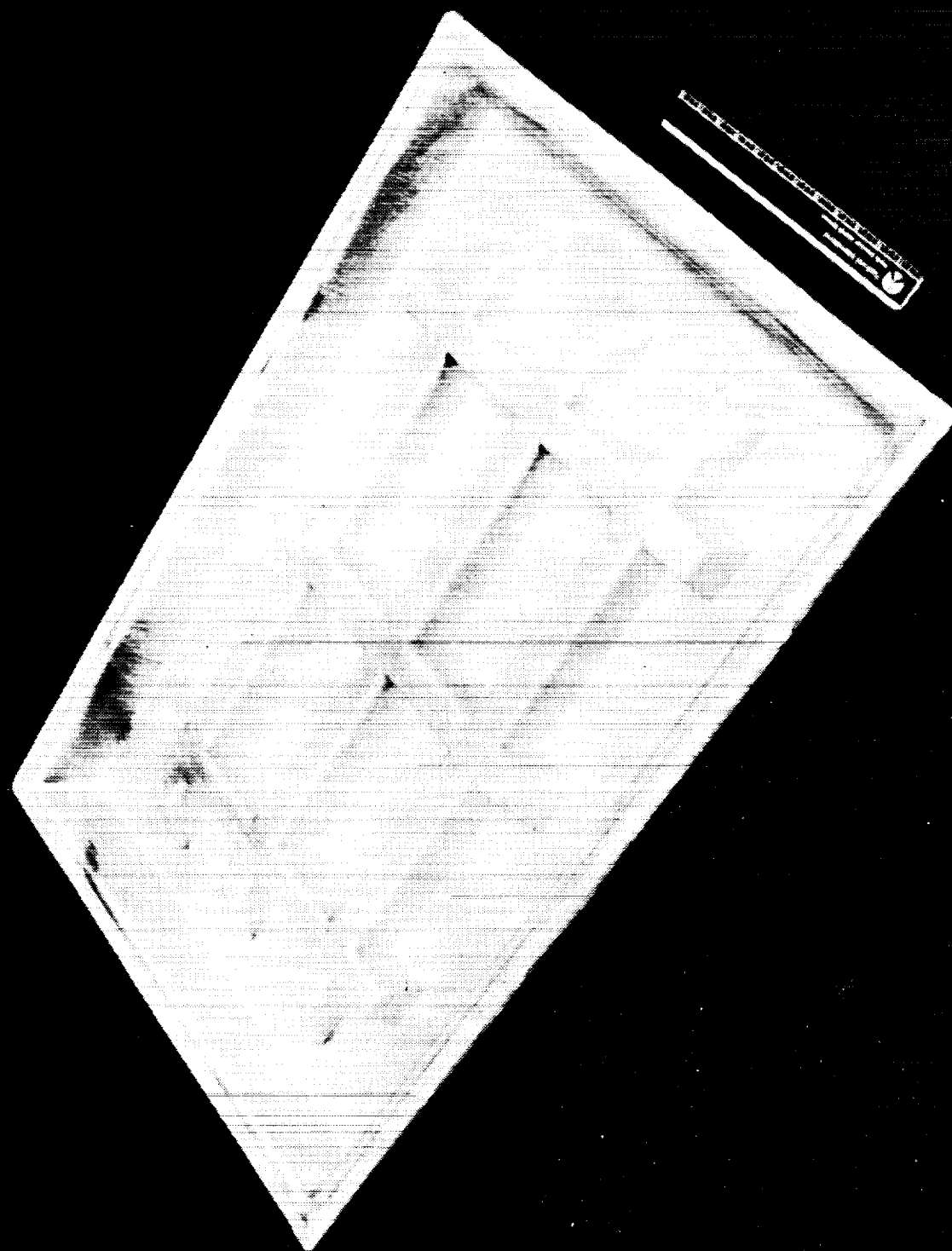


Figure 249. As-Formed and Cleaned Integrally Stiffened Panel.

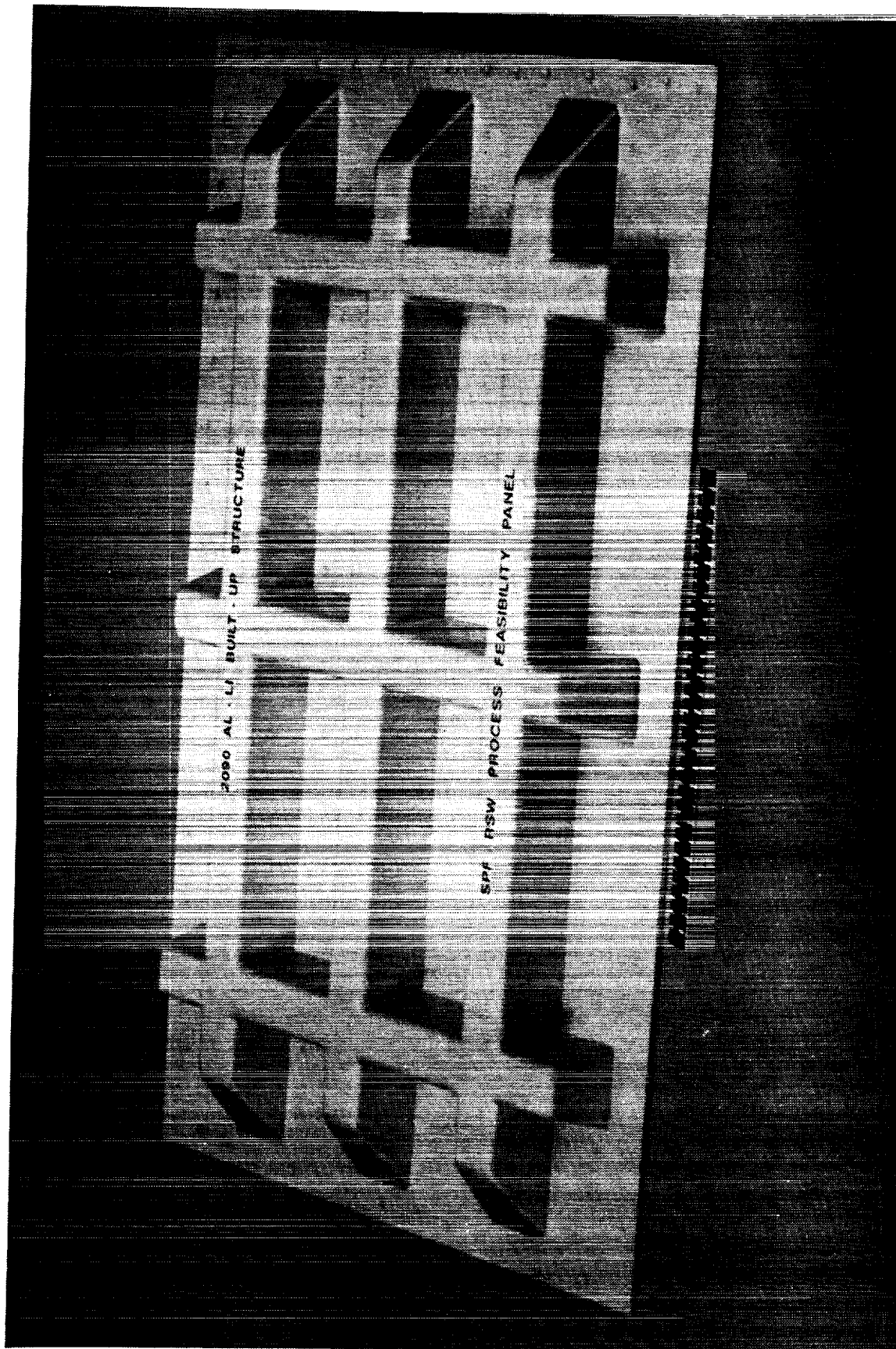


Figure 250. Welded and Trimmed Integrally Stiffened Panel.

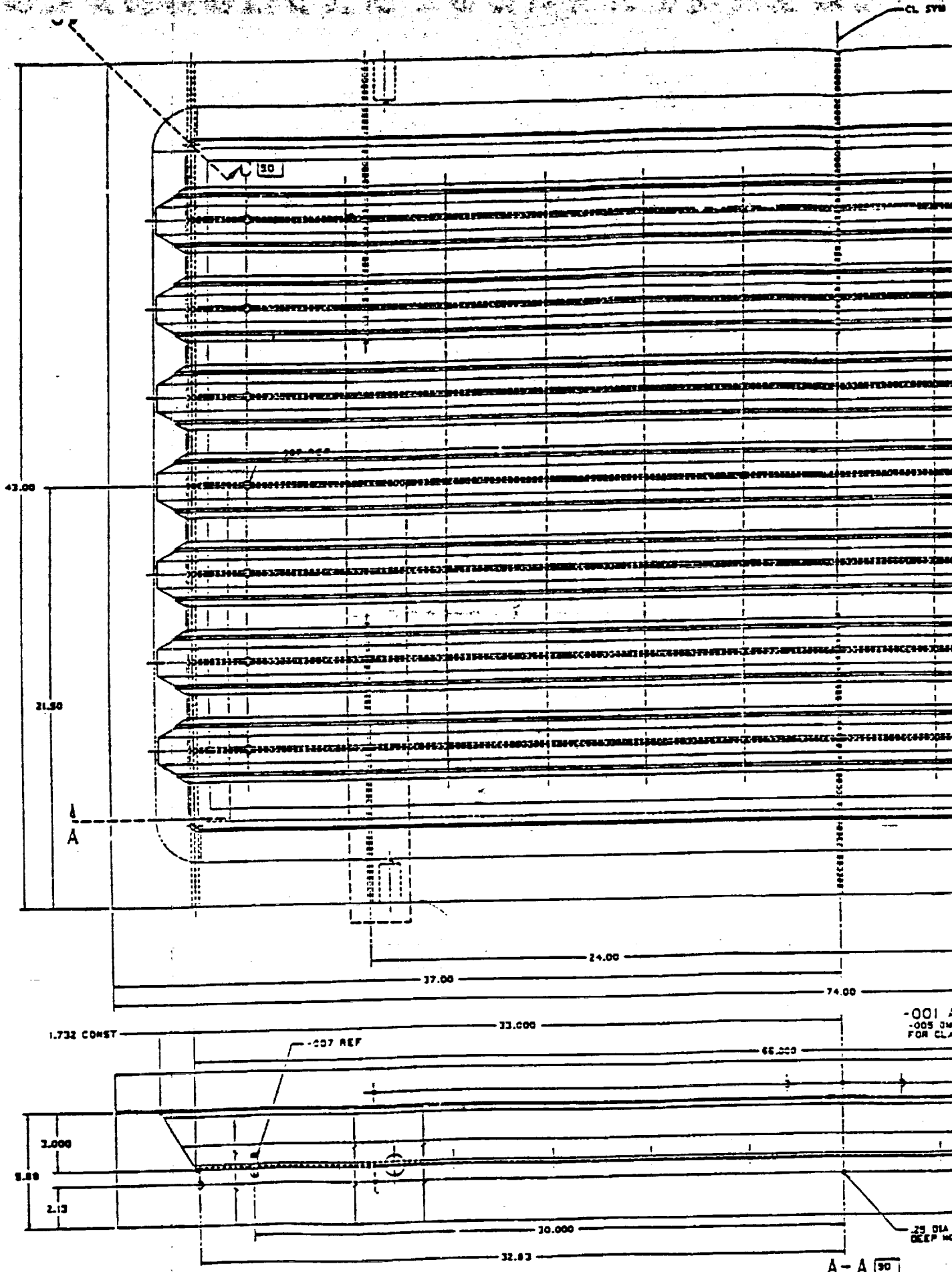
temporarily unavailable during this phase of the program) with mixed results. The initial panels fabricated left severe BN deposits on the tool surface which in turn left indentations on the part surface during the forming cycle, creating an undesirable surface for many of the panels. The mating surface of the part with the outer skin were not effected, thus resistance spot welding was successfully accomplished for the panel on schedule.

4.4.3 COLUMN BUCKLING PANEL FABRICATION

At the completion of the crippling panel tests, the stepped hat stiffener configuration was chosen for continued development based on its load carrying capability. The stepped hat stiffener was modeled (refer to section 4.1 6) under NASTRAN and optimization of the stiffened structure was conducted. PASCO analysis of the stepped hat stiffener was conducted with a larger cap width to enhance the overall stability of the structure. The panel configuration was chosen based upon the desired length of the panel (column of at least 60 inches) and limited by the width of available material (48" minus sealing area). The resulting panel design (refer to Figure 26) maintained the inter-stiffener and inter-spot spacing optimized for the crippling stiffener panels.

The tooling concept for the universal die chamber and insert combination used a base-plate for assured release of the gas pressure during forming with separate stiffener configurations indexed onto the gas plate with locator pins (as shown in Figure 252). The die chamber and upper surface tool were machined out of a solid plates of mild steel (6" x 43" x 74" and 2" x 43" x 74"). The stiffeners were machined separately out of bar stock in order to minimize material scrap and keep handling of the tooling configuration simple. The gas pressure plate was also machined out of plate material and was chamfered along the bottom periphery and grooved to allow for gas flow away from the final part to the gas outlets. The tooling was completed, inspected, and gas lines were welded onto the outer surface of the tool for introduction of gas pressure and installed into the 4500 ton press in El Segundo (refer to Figure 252). Surveys of the thermal stability of the tool were performed in order to assess the insulation requirements for the die chamber. Proof of process parts were formed (refer to Figures 253 and 254) for both the 7475 Al and 2090 Al-Li materials (using pressure versus profiles generated by the Rockwell model and uniaxial SPF tensile data generated under Task 2). The proof of process parts were inspected for thickness variations along the flange and for the presence of cavitation in the formed configuration. Cavitation evaluation showed that the parts were free from cavitation, thus structural performance of the panels (barring external damage) would not be affected by voids in the material.

THIS PAGE INTENTIONALLY LEFT BLANK.



FOLDOUT FRAME

ORIGINAL PAGE IS
OF POOR QUALITY

PRECEDING PAGE BLANK NOT FILMED

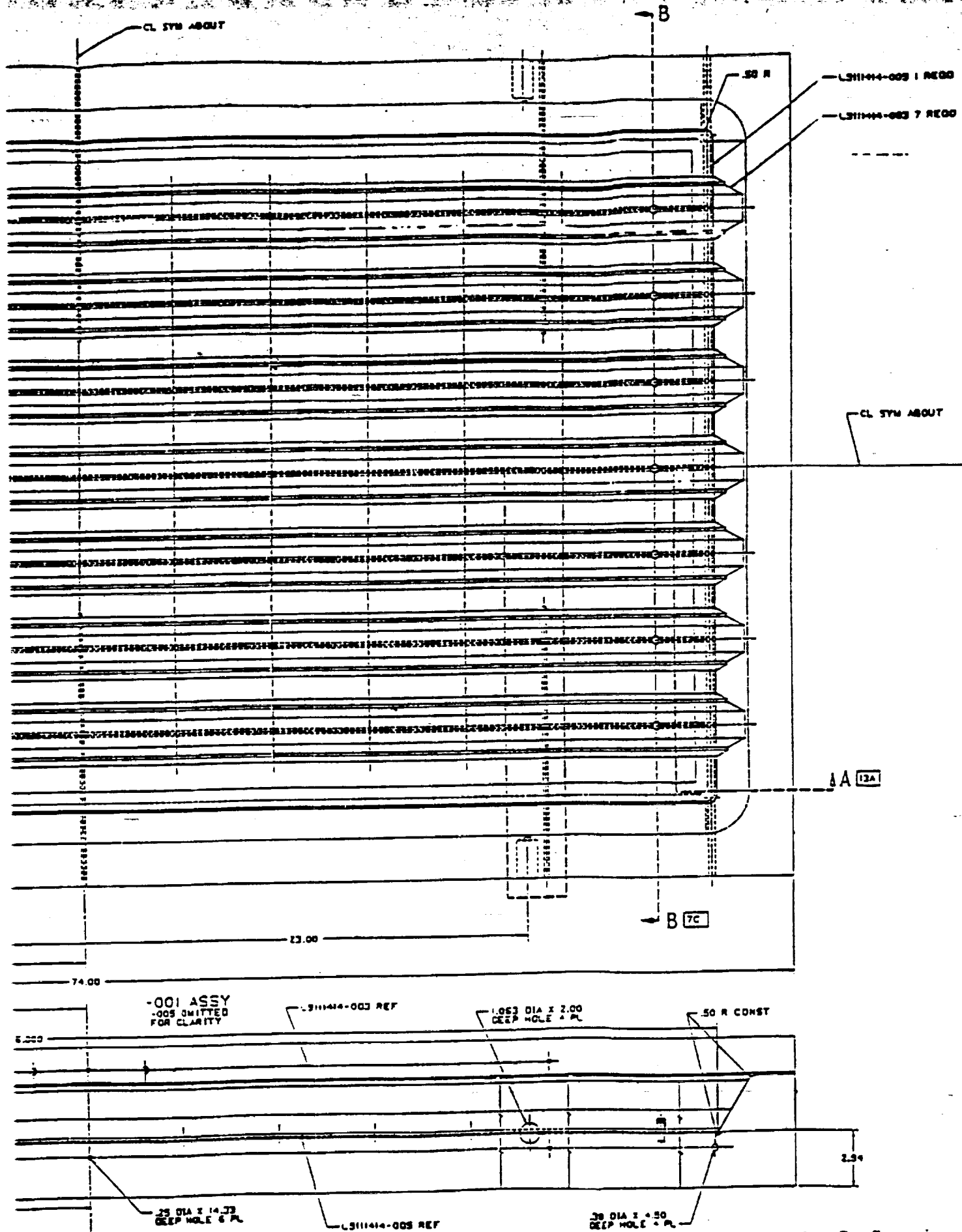


Figure 251. Column Buckling Panel Tooling Configuration.

FOLDOUT FRAME 2. ORIGINAL PAGE IS
OF POOR QUALITY



Figure 252. Column Buckling Panel Die Chamber.



Figure 253. Loading of Column Buckling Panel Part Blank into Heated Die Chamber.



Figure 254. Hot Removal of Column Buckling Panel from 4500 Ton Press.

During forming of the initial proof parts, it was noted that the gas pressure release from the tool at the completion of forming was very slow. Future tool designs of this size and nature will require incorporation of larger gas holes in order to allow for a maximum flow rate (to minimize the time necessary to remove the gas from the tool at the completion of the forming cycle). Modification to the tooling was not performed since the fabrication schedule would not permit any loss of time during this phase of the program.

During fabrication of the column buckling panels, several panels appeared to have an increasing variance in distance between stiffeners. Fabrication was stopped in order to assess the situation. It was determined that the outer two stiffeners of the last column buckling panel were misaligned due to shearing of the three locating pins (the pins used were hollow rather than solid) on the two outer inserts, which caused them to shift and reduce the spacing between the two outer stiffeners on each side from 1.25 inches to 0.80 inches. The die chamber was removed from the press, cleaned and the two outer stiffener inserts were re-aligned and tack welded into place to assure proper location during the fabrication of the final four panels.

The column buckling test panels were solution heat treated, water quenched, straightened, and artificially aged. The panels were trimmed, chemically cleaned (refer to Figure 255), and strain gauged prior to shipment of the panels to General Dynamics. The assembly plan for the column buckling panels is included application of all internal strain gages to the panels at Rockwell (refer to Figures 256 through 258) and welding of the stiffeners and skins along with final assembly at General Dynamics (refer to Figure 259 through 263). Weld certification coupons were cleaned at the same time as the column buckling panels and outer skins to assure identical oxide conditions to the panels at the time of welding. After completion of the welding process, the panels were inspected and final machined to net dimensions (refer to Figure 264 to 268). The panels were shipped directly to NASA LaRC for final assembly and testing.

The test plan and predicted behavior of the panels are discussed in section 4.1.6 and in Appendix C.

4.4.4 DOUBLER-REINFORCED FUSION WELD PANEL

The final panel configuration that was examined during this program was the vertical fusion weld or panel-to-panel joint. The joints are fusion butt-welded together and reinforced with a spot-welded doubler over the weld. This doubler-reinforced concept eliminates the need for machined

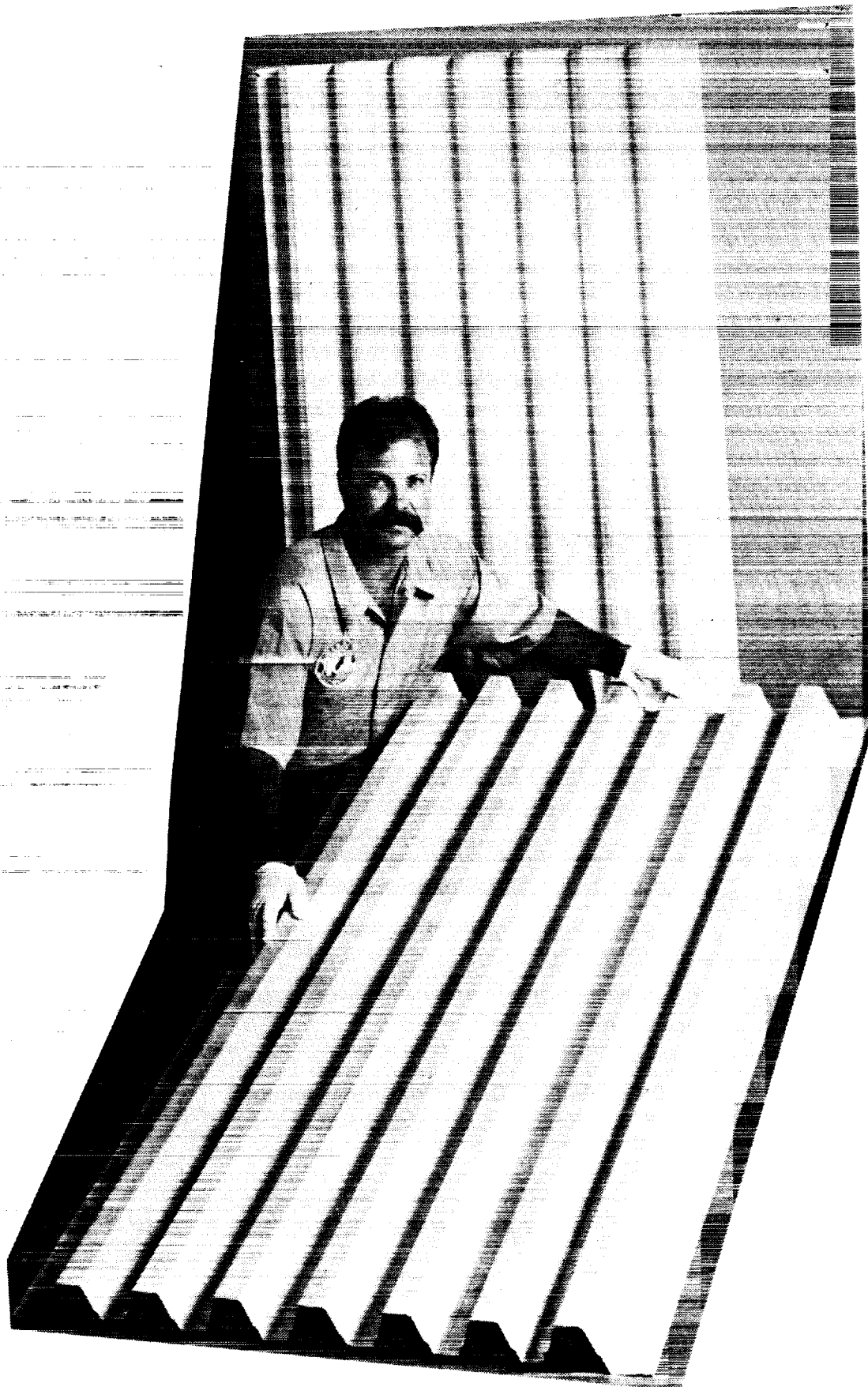


Figure 255. Trimmed and Cleaned Column Buckling Panels.



Figure 256. Strain Gage Location for Inner Surface of Column Buckling Stiffener Panel #1, 7475-T62.

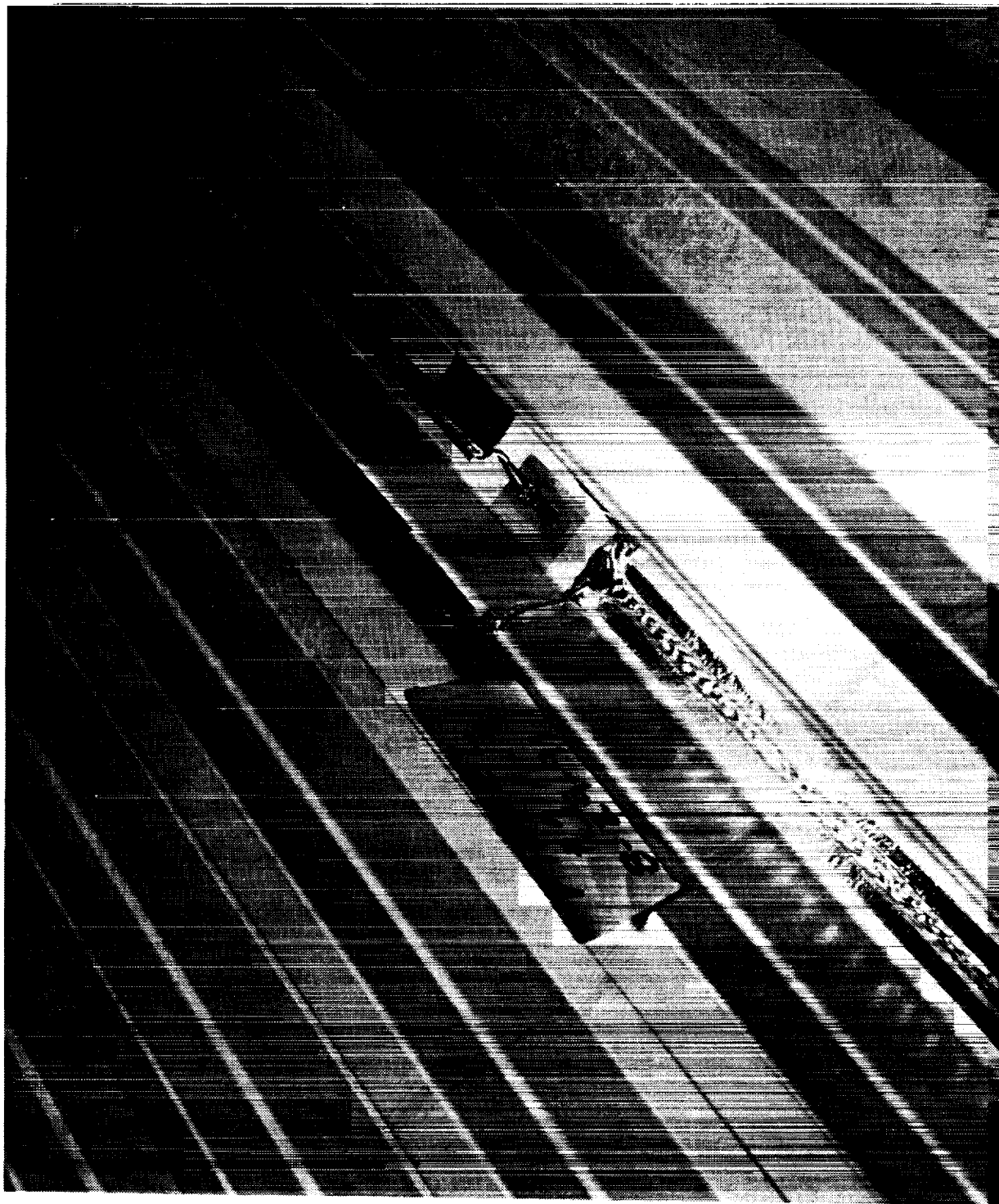


Figure 257. Close-up of Strain Gage Location for Inner Surface of Column Buckling Stiffener Panel #1, 7475-T62.

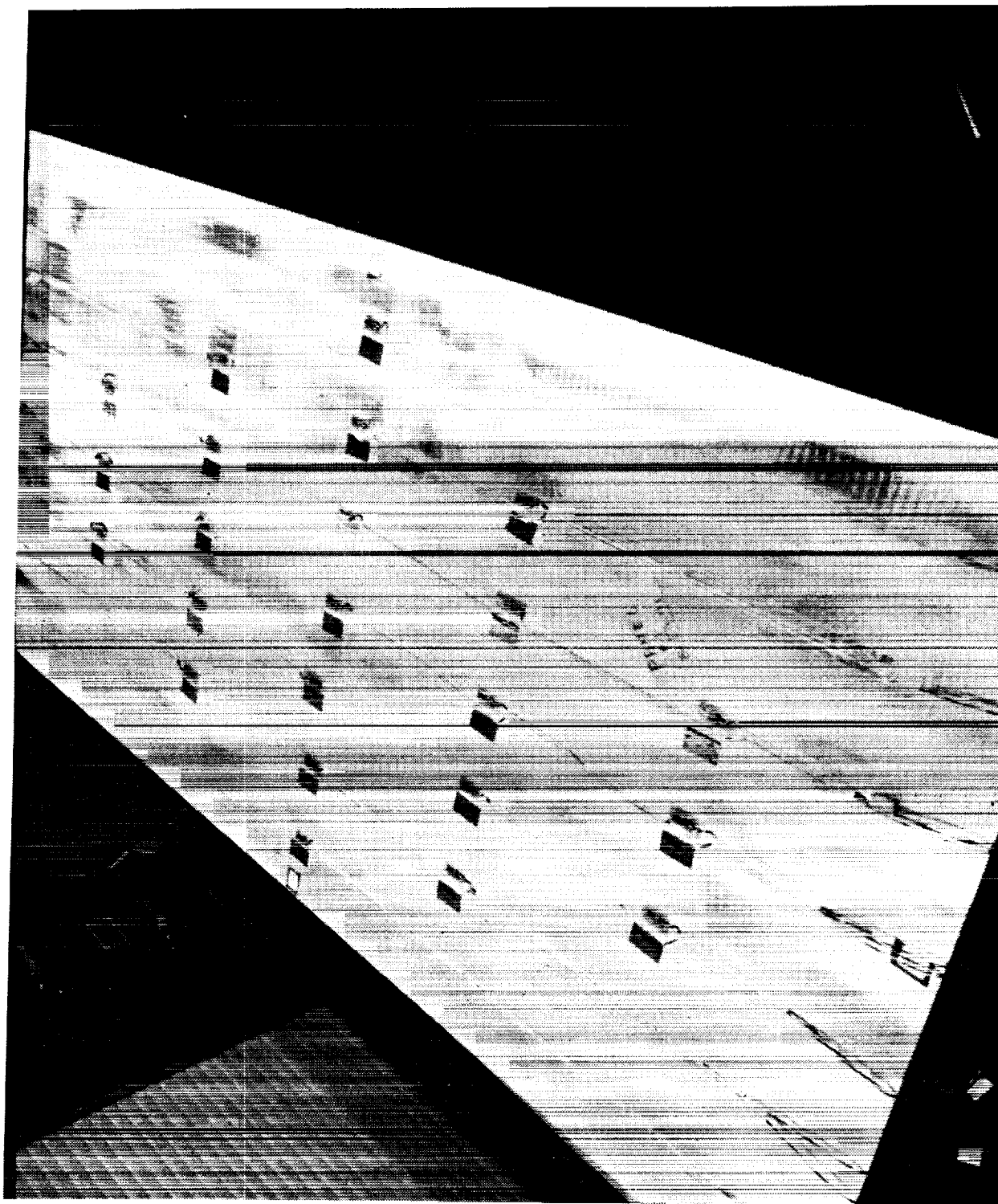


Figure 258. Strain Gage Location for Inner Surface of Column Buckling Skin Panel #1, 2219-T81.

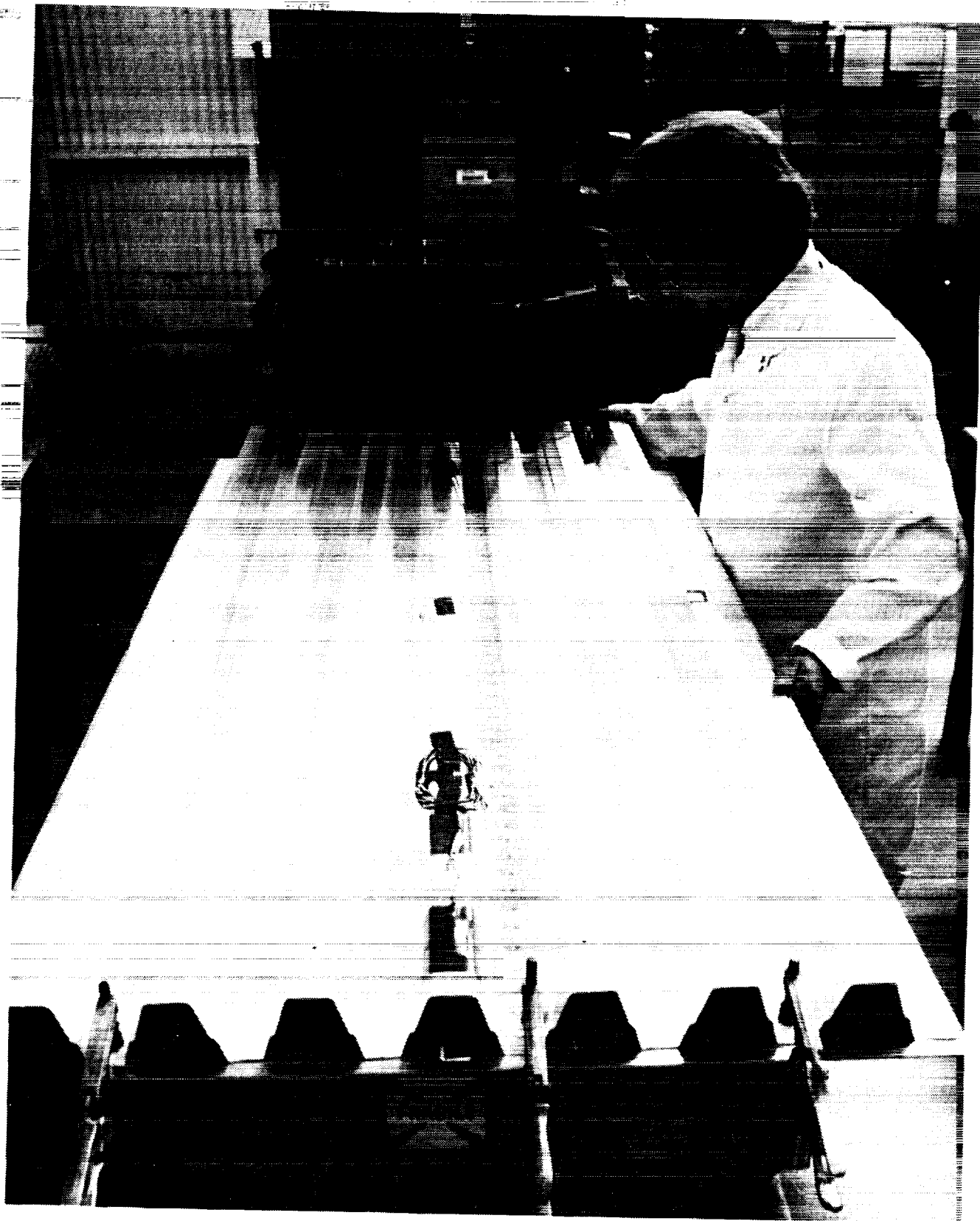


Figure 259. Spot welding of Column Buckling Panel.

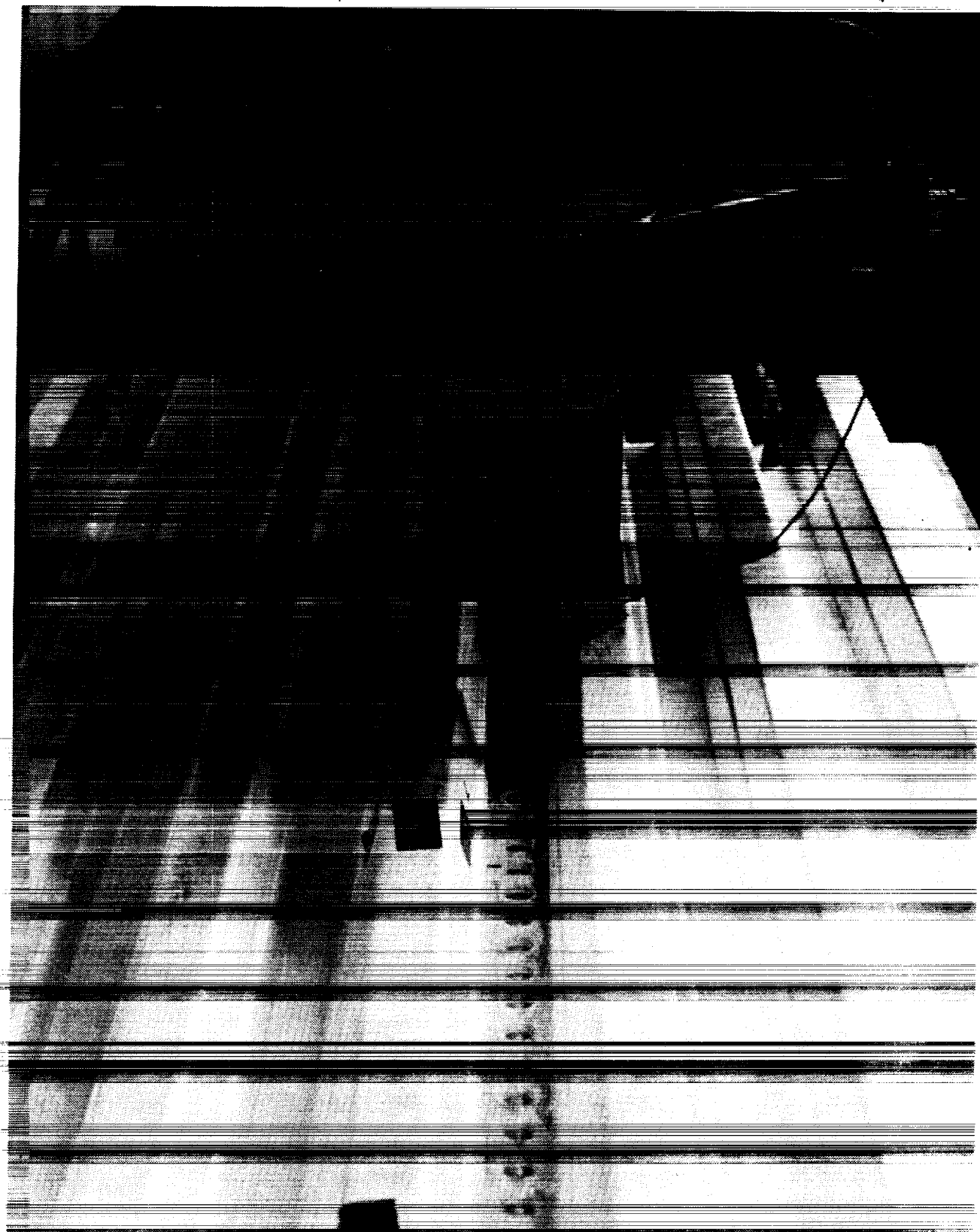


Figure 260. Spot welding of Column Buckling Panel with Tooling for Spot Weld Location.

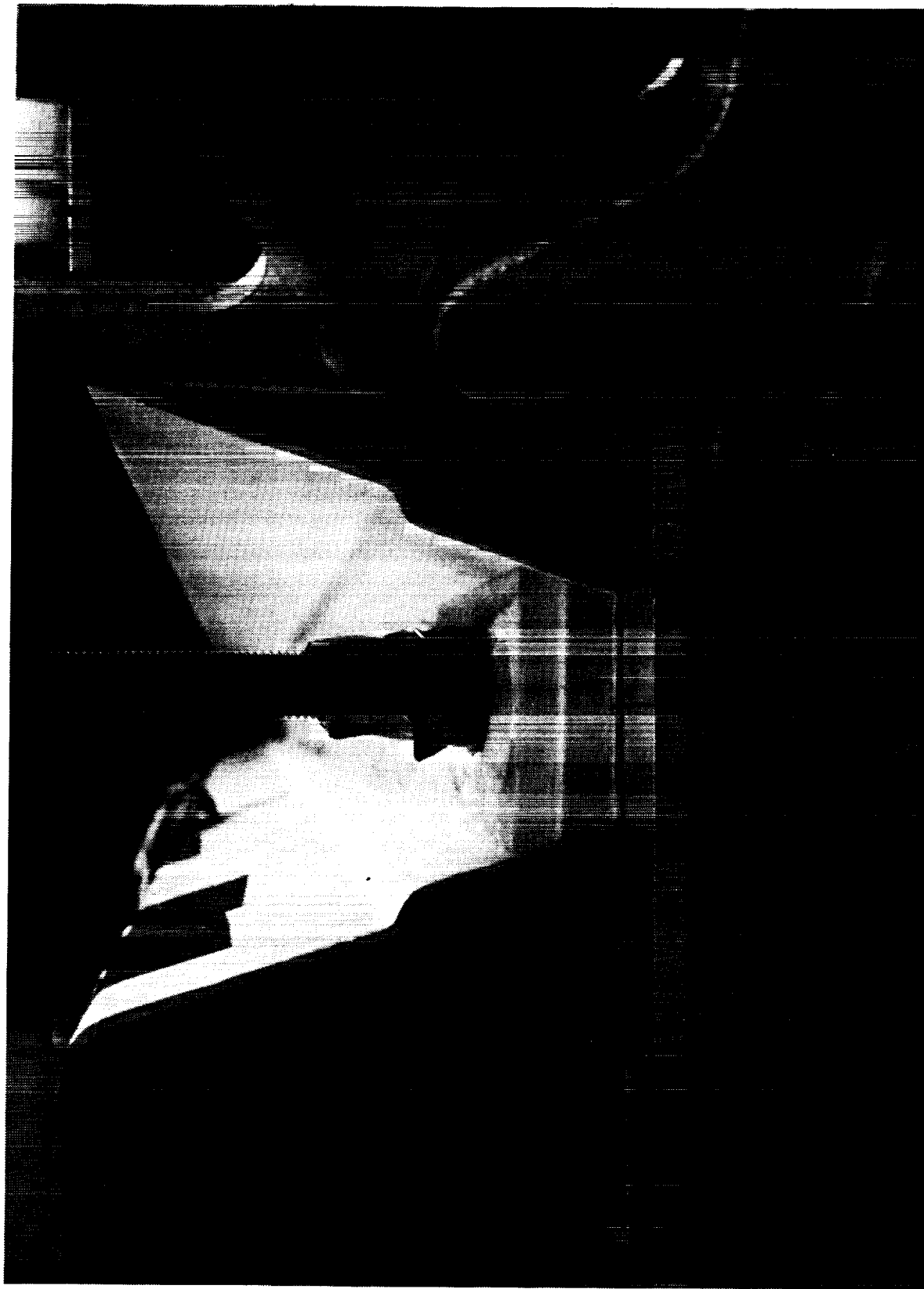


Figure 261. Close-up of Resistance Spot welding of Column Buckling Panel.

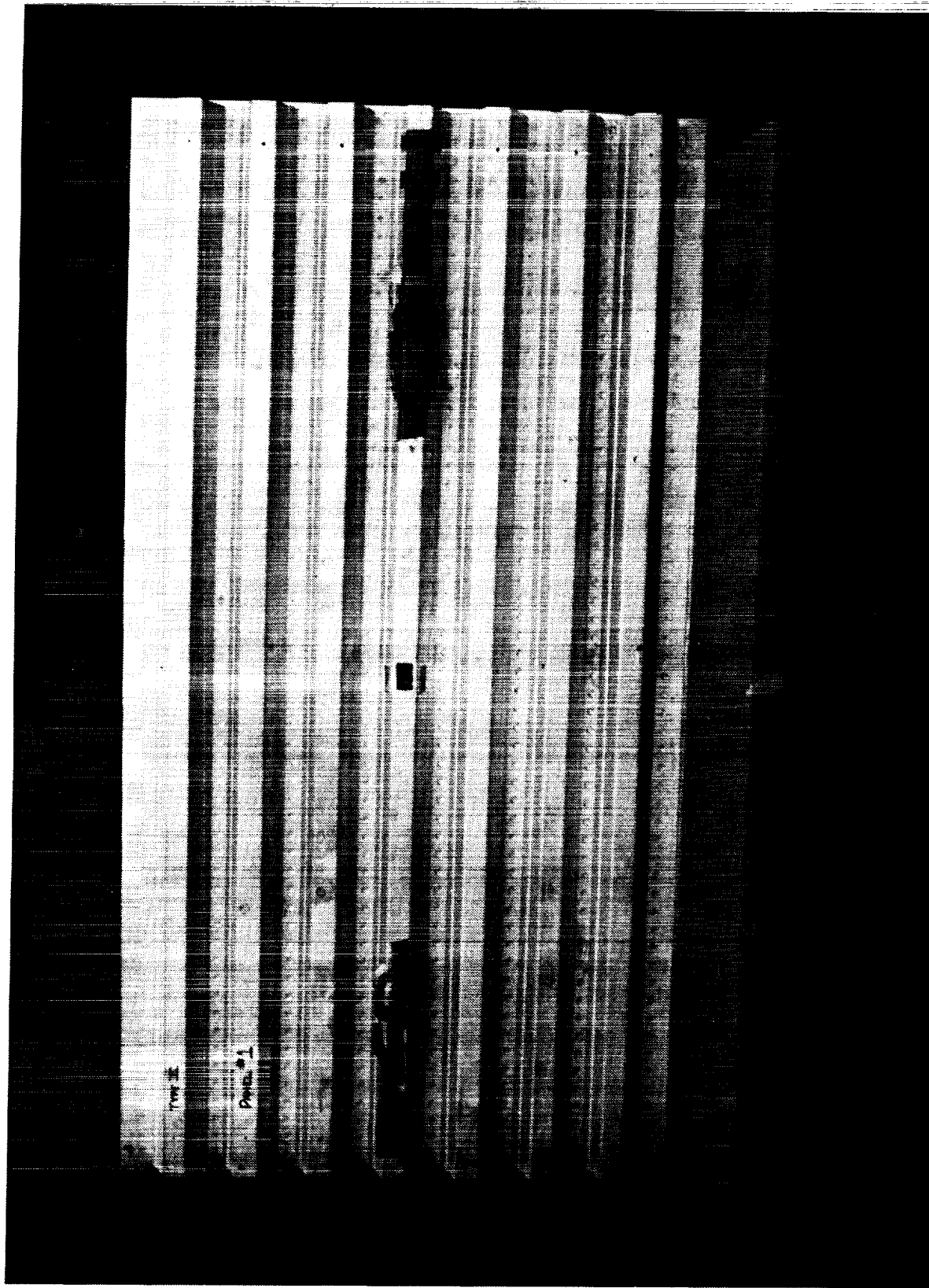


Figure 262. Welded Column Buckling Panel (Front View).

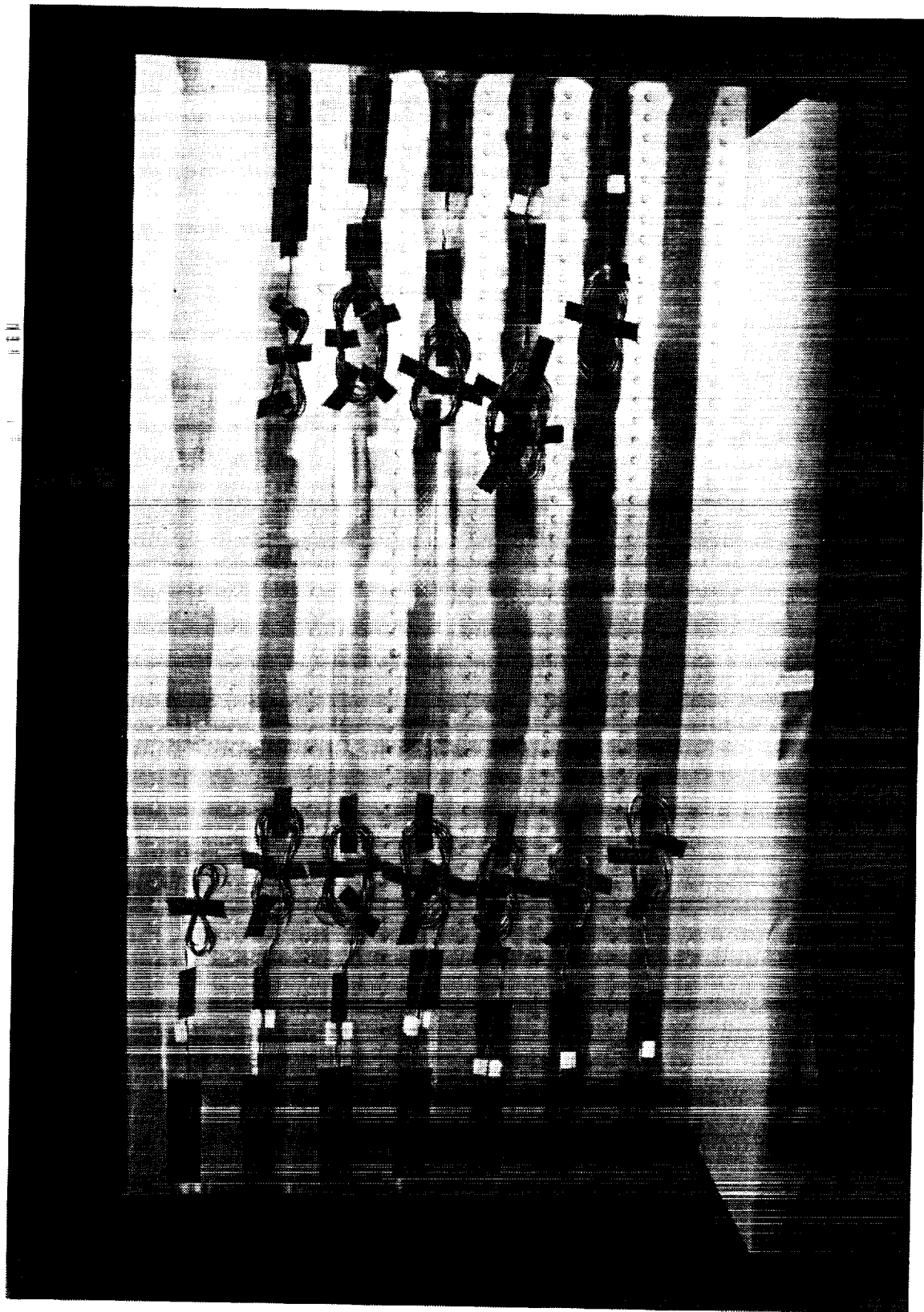


Figure 263. Welded Column Buckling Panel (Back View).

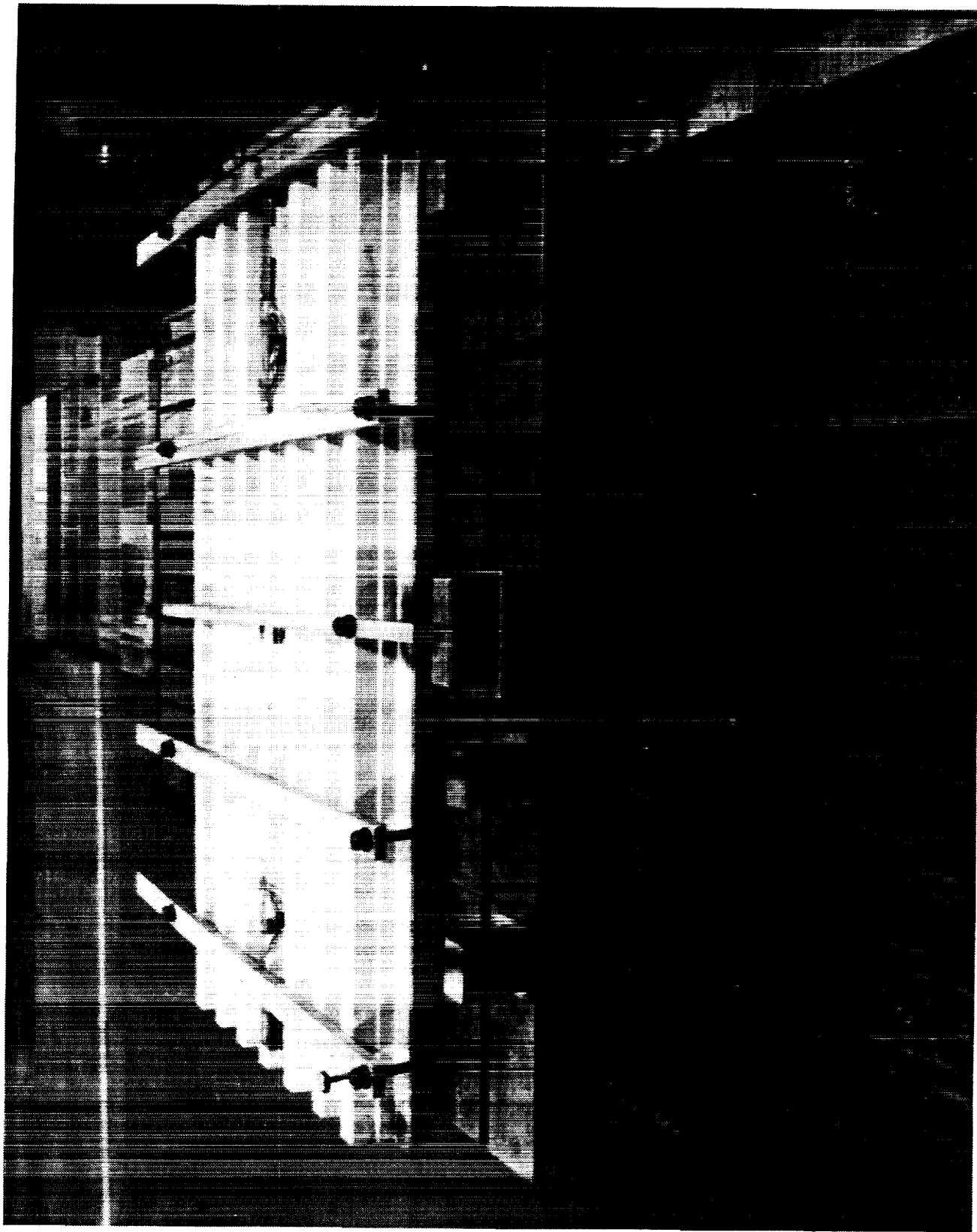


Figure 264. Welded Column Buckling Panel Fixtured for Edge Clean-up.

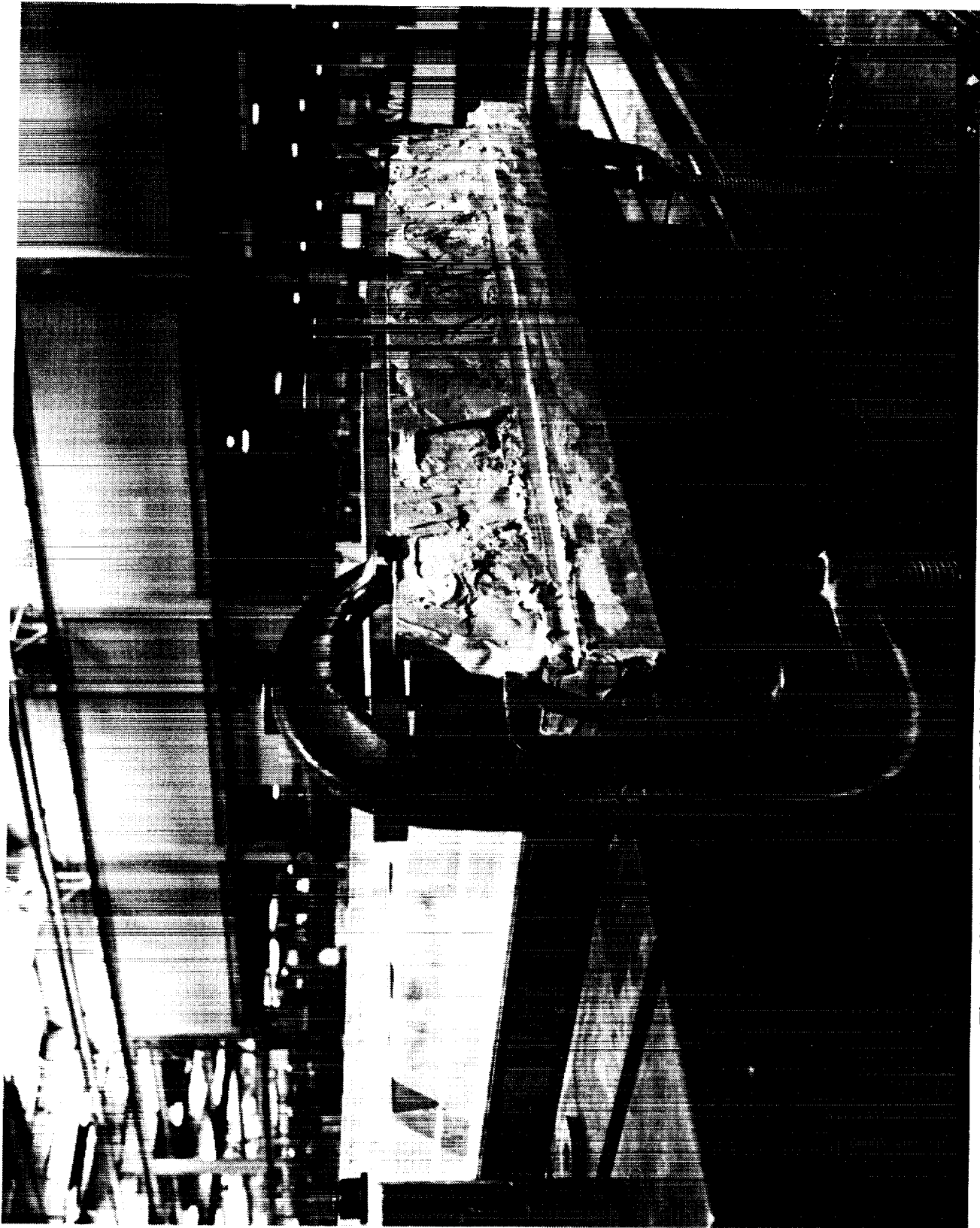


Figure 265. End View of Welded Column Buckling Panel Fixtured for Edge Machining.



Figure 266. Welded Column Buckling Panel Being Machined Flat and Parallel.



Figure 267. Welded Column Buckling Panel After Machining.



Figure 268. Close-up of Welded Column Buckling Panel After Machining.

4-376

ORIGINAL PAGE
BLACK AND WHITE PHOTOGRAPH

weld lands (commonly used for launch vehicle pressure vessels at an increased fabrication cost, and weight penalty to the structure) to reinforce the joint by utilizing the doubler as a major load carrying member for the fusion weld. The development of the joint was based upon the fusion weld and resistance spot weld data generated during task 3 (section 4.3) of this program. Specific doubler testing was conducted under task 3 that provided a greater understanding of the behavior of the doubler over the Variable Polarity Plasma Arc (VPPA) fusion weld for load transfer. The test data was then utilized with finite element modeling techniques to predict the behavior of the fusion weld joint during bi-axial (axial and hoop) loading conditions.

4.4.4.1 Bi-Axial Panel Fabrication

The fusion weld test panels were fabricated from two skins (machined from 0.190" to 0.155" thickness) fusion welded together with a doubler attached to the outer skin over the fusion weld and two crippling stiffeners attached to the skin material. Prior to assembly of the panels, weld verification testing was performed on the fusion weld. Welding of the 2219-T81 and 2090-T83 fusion weld panels were completed and inspected (visually and radiographically). Mechanical property tests were performed on coupons welded during the panel fabrication in order to assess the fusion weld strength. The coupon tests were broken into three groups:

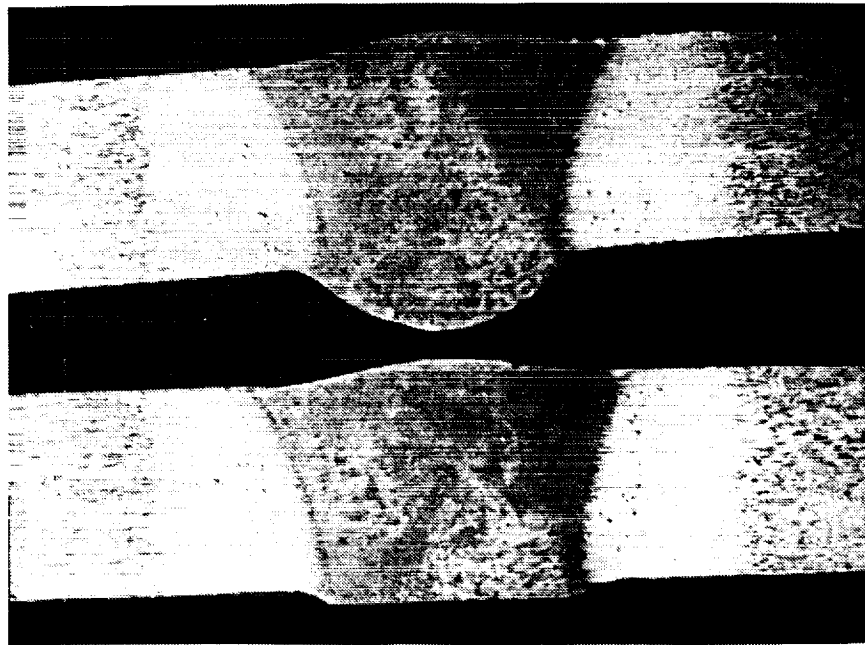
- 1) the fusion weld bead was left intact,
- 2) the root side of the weld bead was removed to within 0.010" of the original skin contour, and
- 3) the weld bead was ground flush to the skin contour on both sides of the fusion weld.

Extensometers were attached to all the test specimens during the tensile testing. Axial strain gages were applied to the fusion weld zone for coupons with the weld bead ground flush on both sides of the coupon. The results from the ambient temperature testing of the specimens are shown in Tables 119 through 125. Optical microscopy of the fusion weld sections (as welded, and with the bead shaved) is shown as Figure 269 for 0.155" 2219-T81 Al and an as-welded specimen of 0.155" 2090-T83 Al-Li (refer to Figure 270). Analysis of cross-sections from the 2219-T81 and 2090-T83 fusion welds verified the radiographic inspection results showing that the weld was defect-free.

4.4.4.1.1 Test Procedure

Twenty 9.0 by 1.5 inch dog-bone specimens were removed from each fusion weld test panels (2219-T81 and 2090-T83). Five of the specimens were tested in the as-welded condition (weld bead left on the specimen), five were tested with the weld bead shaved down to the parent

UPPER MACRO : AS WELDED



Lower Macro: Weld Bead Shaved on Root Side

Figure 269. Variable Polarity Plasma Arc Weld Macro of 0.155" 2219-T81 Al.

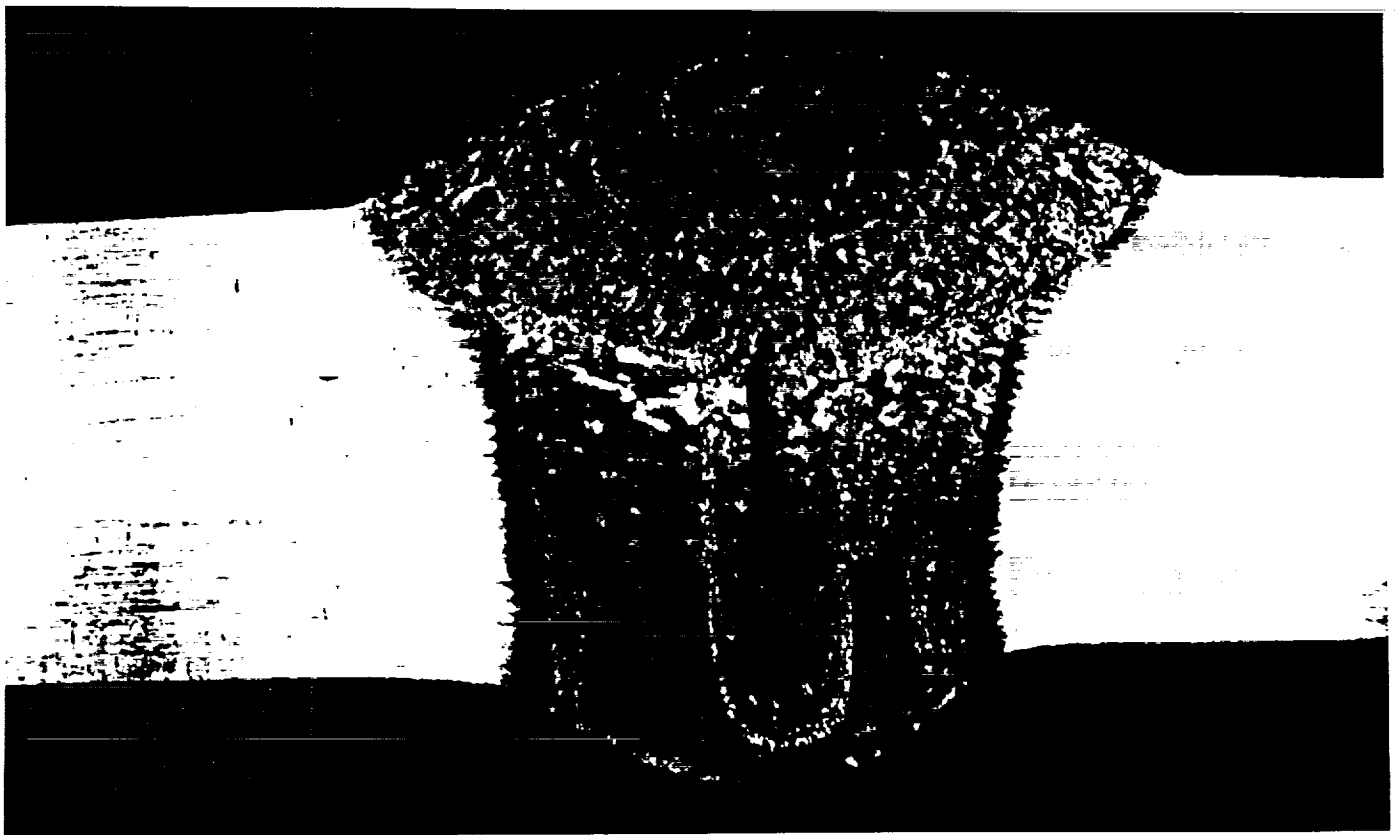


Figure 270. Variable Polarity Plasma Arc Weld Macro of 0.155" 2090-T83 Al-Li.

metal on one side, and five were tested with the weld bead shaved down to the parent metal on both sides of the specimen. Specimen thickness measurements A and C were taken from the parent metal, and B was taken at the weld bead for each specimen.

All specimens were tested on a 20 Kip capacity Instron 1125 electro-mechanical test machine under ambient conditions. A 0.5 inch extensometer was positioned over the weld in order to measure specimen deformation. Elongation was determined over 0.5, 1.0, and 2.0 inches through the use of gage marks on the specimen (ink, rather than scribe). Width and thickness measurements were taken at the weld and on either side of the specimen. Specimens that retained part of the weld bead were tested at a cross-head rate of 0.05 inch per minute to failure. The specimens that had the weld bead shaved on both sides of the specimen were instrumented with FAE-13-06A-35S13 axial strain gages bonded back-to-back with M-Bond 200 adhesive. These specimens were loaded at a cross-head rate of 0.02 inch per minute until failure. Load versus strain data was recorded at one second intervals using an Orion/Macintosh Data Acquisition System.

Table 119. Test Results of the As-Welded 2219-T81 VPPA Fusion Weld Tensile Specimens.

Specimen I.D.	Width (in)	Thickness (in)	F _{tu} (ksi)	F _{ty} (ksi)	E (msi)	% Elongation Over the Gage Length		
						1/2"	1.0"	2.0"
3-1 A B C	0.5027	0.1548						
	0.5020	0.2378						
	0.5026	0.1563	42.45	16.55	7.65	12.0	9.0	4.0
3-2 A B C	0.5034	0.1559						
	0.5022	0.2405						
	0.5026	0.1571	43.19	17.26	7.00	12.0	7.0	3.5
3-3 A B C	0.5020	0.1550						
	0.5007	0.2347						
	0.5018	0.1569	41.66	18.33	5.75	10.0	5.5	2.5
3-4 A B C	0.5015	0.1550						
	0.5009	0.2313						
	0.5016	0.1571	42.77	18.43	6.95	12.0	5.0	2.5
3-5 A B C	0.5028	0.1552						
	0.5019	0.2350						
	0.5026	0.1564	43.13	18.45	7.35	12.0	5.0	3.0
Average Value			42.64	17.80	6.94	11.6	6.3	3.1
Standard Deviation			0.62	0.86	0.72	0.9	1.7	0.7
Coefficient of Variance (%)			1.46	4.82	10.42	7.71	27.26	21.03

Note: Modulus data was very low. Phenomena attributed to the non-uniform area of the as-welded bead. The majority of the elongation was occurring in the weld due to its lower yield strength as compared to the parent material.

Table 120. Test Results of the 2219-T81 VPPA Fusion Weld with the Bead Ground Down on One Side of Each Tensile Specimen.

Specimen I.D.	Width (in)	Thickness (in)	F _{tu} (ksi)	F _{ty} (ksi)	E (msi)	% Elongation Over the Gage Length		
						1/2"	1.0"	2.0"
2-2 A	0.5032	0.1562						
	0.5019	0.1796						
	0.5024	0.1532	40.34	17.50	9.75	12.0	7.0	4.0
2-4 A	0.5029	0.1559						
	0.5016	0.1709						
	0.5020	0.1519	40.26	17.70	8.65	14.0	7.0	3.5
2-6 A	0.5026	0.1546						
	0.5016	0.1714						
	0.5018	0.1510	40.19	18.28	8.95	14.0	6.5	3.5
2-8 A	0.5002	0.1536						
	0.5014	0.1635						
	0.5018	0.1520	39.33	17.90	10.85	16.0	8.0	4.0
2-10 A	0.5028	0.1533						
	0.5012	0.1675						
	0.5022	0.1513	40.14	17.37	12.25	14.0	7.0	3.5
Average Value			40.05	17.75	10.09	14.0	7.1	3.7
Standard Deviation			0.41	0.36	1.48	1.4	0.5	0.3
Coefficient of Variance (%)			1.02	2.01	14.64	10.10	7.71	7.40

Table 121. Test Results of the 2219-T81 VPPA Fusion Weld with the Bead Ground Down on Both Sides of Each Tensile Specimen.

Specimen I.D.	Width (in)	Thickness (in)	F _{tu} (ksi)	F _{ty} (ksi)	E (msi)	% Elongation Over the Gage Length		
						1/2"	1.0"	2.0"
2-1 A	0.5030	0.1497						
	0.5019	0.1476						
	0.5023	0.1517	36.94	16.18	10.90	16.0	8.0	4.0
2-3 A	0.5036	0.1526						
	0.5025	0.1518						
	0.5026	0.1463	38.83	17.64	11.40	14.0	8.0	4.0
2-5 A	0.5033	0.151						
	0.5022	0.1497						
	0.5029	0.1475	38.76	18.36	12.50	14.0	8.0	4.0
2-7 A	0.5027	0.1520						
	0.5014	0.1486						
	0.5025	0.1494	38.25	18.59	11.40	16.0	7.0	3.5
2-9 A	0.5026	0.1523						
	0.5014	0.1495						
	0.5023	0.1511	37.81	17.52	9.70	16.0	8.0	4.0
Average Value			38.12	17.66	11.18	15.2	7.8	3.9
Standard Deviation			0.78	0.94	1.01	1.1	0.4	0.2
Coefficient of Variance (%)			2.03	5.34	9.06	7.72	5.73	5.73

Table 122. Results of 2090-T83 VPPA Fusion Weld Tensile Tests.

Specimen I.D.	Width (in)	Thickness (in)	F _{tu} (ksi)	F _{ty} (ksi)	E (msi)	% Elongation Over the Gage Length		
						1/2"	1.0"	2.0"
2	A	0.5004						
	B	0.4997						
	C	0.5008	35.31	19.93	13.80	8.0	4.0	2.5
4	A	0.4989						
	B	0.4984						
	C	0.5000	36.78	18.84	15.10	9.0	5.0	2.5
6	A	0.4991						
	B	0.4986						
	C	0.4994	34.60	18.33	12.70	8.0	5.0	2.0
8	A	0.5004						
	B	0.4997						
	C	0.5008	34.83	18.12	12.50	8.0	4.0	2.50
10	A	0.4999	30.68	18.45	12.40	7.0	4.0	2.5
	B	0.4995						
	C	0.5005						
12	A	0.4993						
	B	0.4983						
	C	0.4997	36.96	19.00	12.30	10.0	5.5	3.0
Average Value			34.86	18.78	13.13	8.3	4.6	2.4
Standard Deviation			2.27	0.65	1.11	1.0	0.7	0.4
Coefficient of Variance (%)			6.52	3.47	8.43	12.39	14.50	15.57

Table 123. Results of 2090-T83 VPPA Fusion Weld Tensile Tests, Weld Bead Ground Flush on One Side.

Specimen I.D.	Width (in)	Thickness (in)	F _{tu} (ksi)	F _{ty} (ksi)	E (msi)	% Elongation Over the Gage Length		
						1/2"	1.0"	2.0"
1	A	0.5009						
	B	0.5000						
	C	0.5016	38.08	18.20	13.4	10.0	5.5	3.0
3	A	0.4999						
	B	0.4990						
	C	0.5003	39.19	18.35	13.4	10.0	6.0	3.5
5	A	0.5000	39.18	18.56	15.6	12.0	7.0	3.5
	B	0.4990						
	C	0.5007						
7	A	0.4999						
	B	0.4992						
	C	0.5002	35.31	17.94	17.40	8.0	5.0	2.5
9	A	0.4997	27.94	16.44	14.70	9.0	4.5	2.0
	B	0.4985						
	C	0.5010						
11	A	0.4995	36.62	19.64	14.40	10.0	5.5	2.5
	B	0.4986						
	C	0.5003						
Average Value			35.72	18.19	14.82	9.8	5.6	2.8
Standard Deviation			4.28	1.04	1.52	1.3	0.9	0.6
Coefficient of Variance (%)			11.98	5.71	10.23	13.52	15.42	21.37

Table 124. Results of 2090-T83 VPPA Fusion Weld Tensile Test.

Specimen I.D.		Width	Thickness	F _{tu}	F _{ty}	E	% Elongation Over the Gage Length		
		(in)	(in)	(ksi)	(ksi)	(msi)	1/2"	1.0"	2.0"
2-01	A	0.4993	0.1565	35.2	19.6	16.0	8.0	5.0	2.5
	B		0.1566						
2-02	A	0.4993	0.1570	37.0	18.4	14.2	9.0	5.0	3.0
	B		0.1569						
2-03	A	0.4990	0.1568	35.2	19.0	14.2	8.0	5.0	2.5
	B		0.1567						
2-04	A	0.4994	0.1548	36.5	21.4	12.5	9.0	5.0	3.0
	B		0.1547						
Average Value				35.94	19.63	14.23	8.5	5.0	2.8
Standard Deviation				0.91	1.28	1.43	0.6	0.0	0.3
Coefficient of Variance (%)				2.54	6.52	10.05	6.79	0.0	10.5

Table 125. Results of 2090-T83 VPPA Fusion Weld Tensile Tests, Weld Bead Ground Flush on One Side.

Specimen I.D.	Width (in)	Thickness (in)	F _{tu} (ksi)	F _{ty} (ksi)	E (msi)	% Elongation Over the Gage Length		
						1/2"	1.0"	2.0"
1-01 A B	0.4990	0.1556	35.0	18.2	13.5	8.0	5.0	2.5
		0.1559						
1-02 A B	0.4993	0.1558	35.8	19.4	12.8	8.0	6.0	3.5
		0.1557						
1-03 A B	0.4989	0.1556	33.6	19.5	15.2	10.0	4.0	2.5
		0.1557						
1-04 A B	0.4996	0.1556	34.7	20.1	16.1	9.0	5.0	2.5
		0.1557						
1-05 A B	0.4997	0.1556	32.9	19.9	14.3	10.0	5.0	2.5
		0.1557						
1-06 A B	0.4990	0.1549	36.9	18.7	12.9	10.0	5.0	2.5
		0.1545						
Average Value			34.8	19.3	14.13	9.2	5.0	2.7
Standard Deviation			1.44	0.72	1.32	1.0	0.6	0.4
Coefficient of Variance (%)			4.15	3.73	9.35	10.73	12.65	15.31

The fusion welded panels were accepted after the weld verification testing, and machined to a net shape condition. The reinforcement doubler was resistance spot welded onto panel over the shaved weld bead (refer to Figure 271). The SPF stepped hat stiffeners were subsequently located and welded onto the test panel and the entire panels was inspected (refer to Figure 272). The finished test panels were machined to final contour (flat and parallel) and inspected for dimensional integrity. Final assembly of the fusion weld panels into the test fixture (refer to Figures 273 through 275) was initiated at General Dynamics. The doubler reinforced fusion weld panels were shipped to NASA Langley for completion of assembly and final testing. The predicted behavior of the panels is covered under section 4.1.8 and the test plan is included as Appendix F.

4.5 NDE & QUALITY ASSURANCE

The NDE and quality assurance of SPF structure and resistance spot weld joints was evaluated and enhanced wherever possible during the program. The superplastic forming process has been widely studied for titanium, steel, inconel and aluminum materials. Material and fabrication procedures have been developed for each material system that allow for real-time process control during fabrication (generally through the control of variables such as temperature, gas pressure, manufacturing tolerances, gas cleanliness, tooling materials, releasing agent, inspection methods, etc.). Another area that has been widely developed for quality control of the SPF process is predictive forming methodologies. Forming methodologies enable the design to be critically evaluated for manufacturability prior to design freeze and fabrication. The in-process control of superplastic forming, when combined with the predictive methodologies of the forming process, ensure the highest quality of the desired structure.

Existing process specifications for aluminum at Rockwell were modified to include 2090 and 8090 Al-Li. The modifications to the specification were based upon uniaxial test data and producibility analysis (based upon the predictive modeling of the material prior to forming) carried out under this program. The main areas that were critical for understanding the materials were the strain rate and forming temperature that result in the lowest flow stress (with the highest uniform elongation) and the cavitation behavior of each material (refer to section 4.2). The evaluation of the superplastic material variables resulted in selection of a duplex strain rate for both the 2090 and 8090 materials (2E-3 for strains up to 0.5 after which the strain rate is decreased to 2E-4 for the remainder of the forming process), thermal control of $950 \pm 10^\circ\text{F}$ with a maximum back pressure of 600 psi (minimum of 200 psi). Post-formed thermal processing included a non-optimized heat treatment with the minimum resulting properties as shown in Table 126.

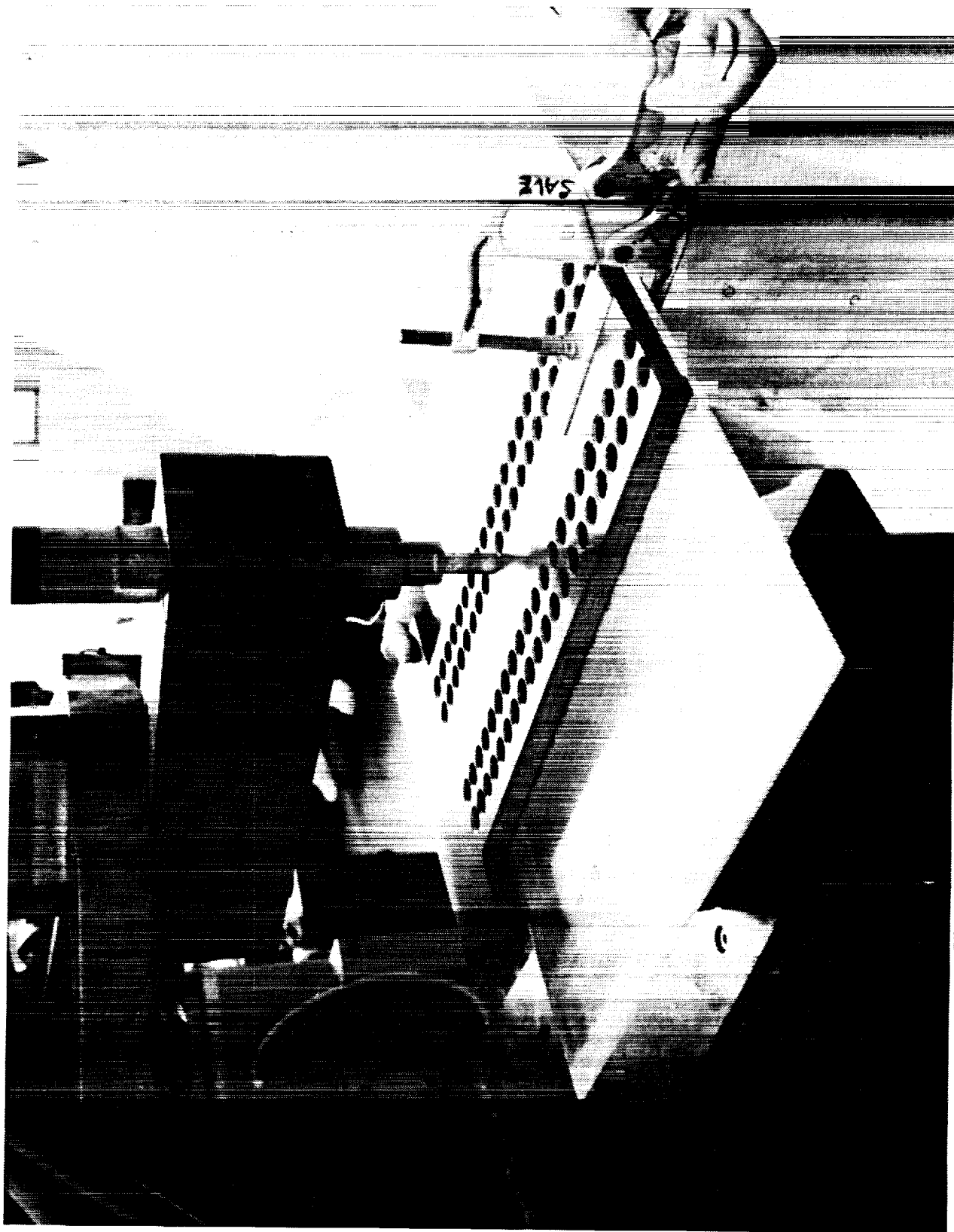


Figure. 27/1. Resistance Spot Welding of Doubler over the Fusion Weld.



Figure 272. Resistance Spot Welding of Doubler Reinforced Fusion Weld with Stepped Hat Stiffeners.

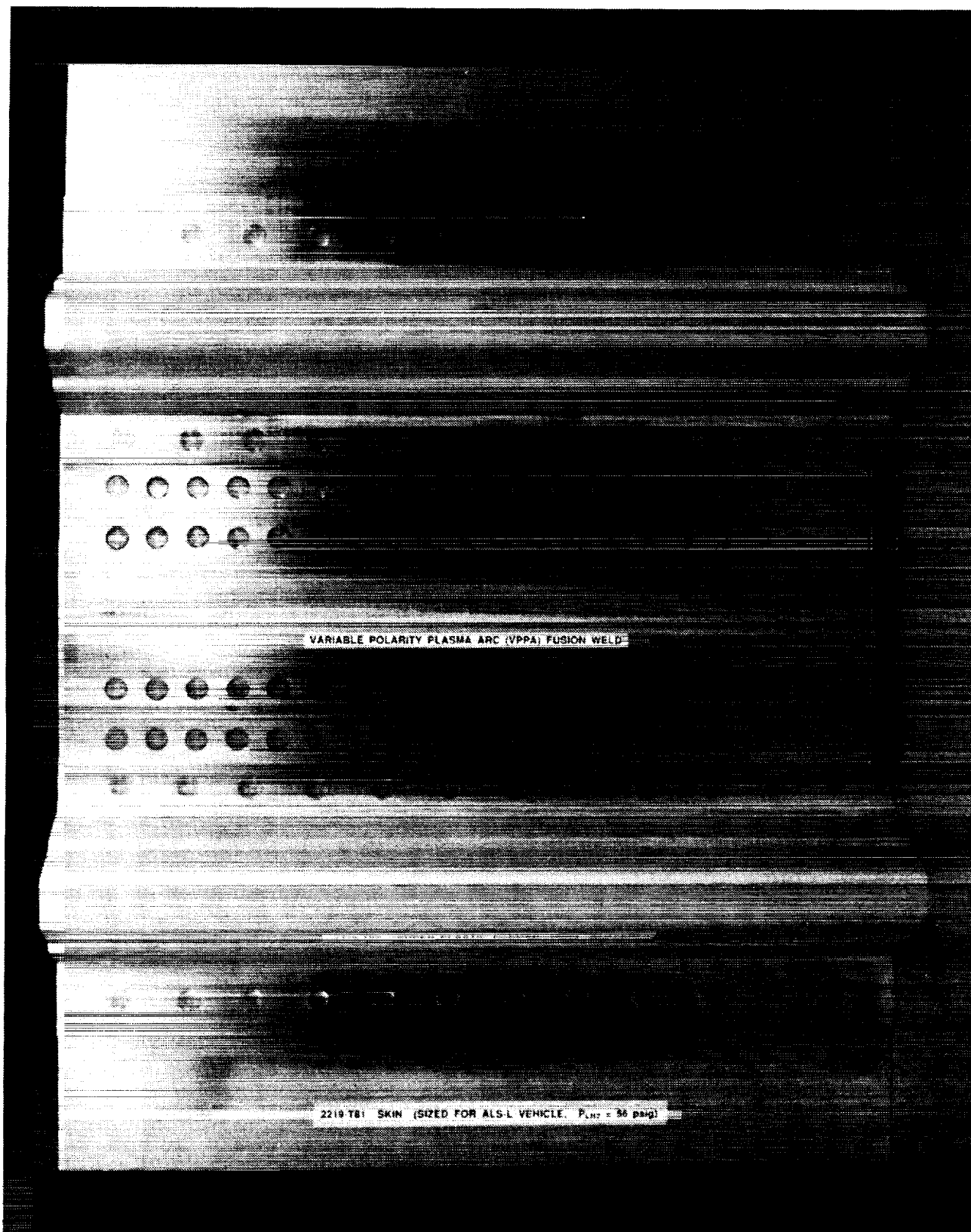


Figure 273. Front View of Double Reinforced Fusion weld.

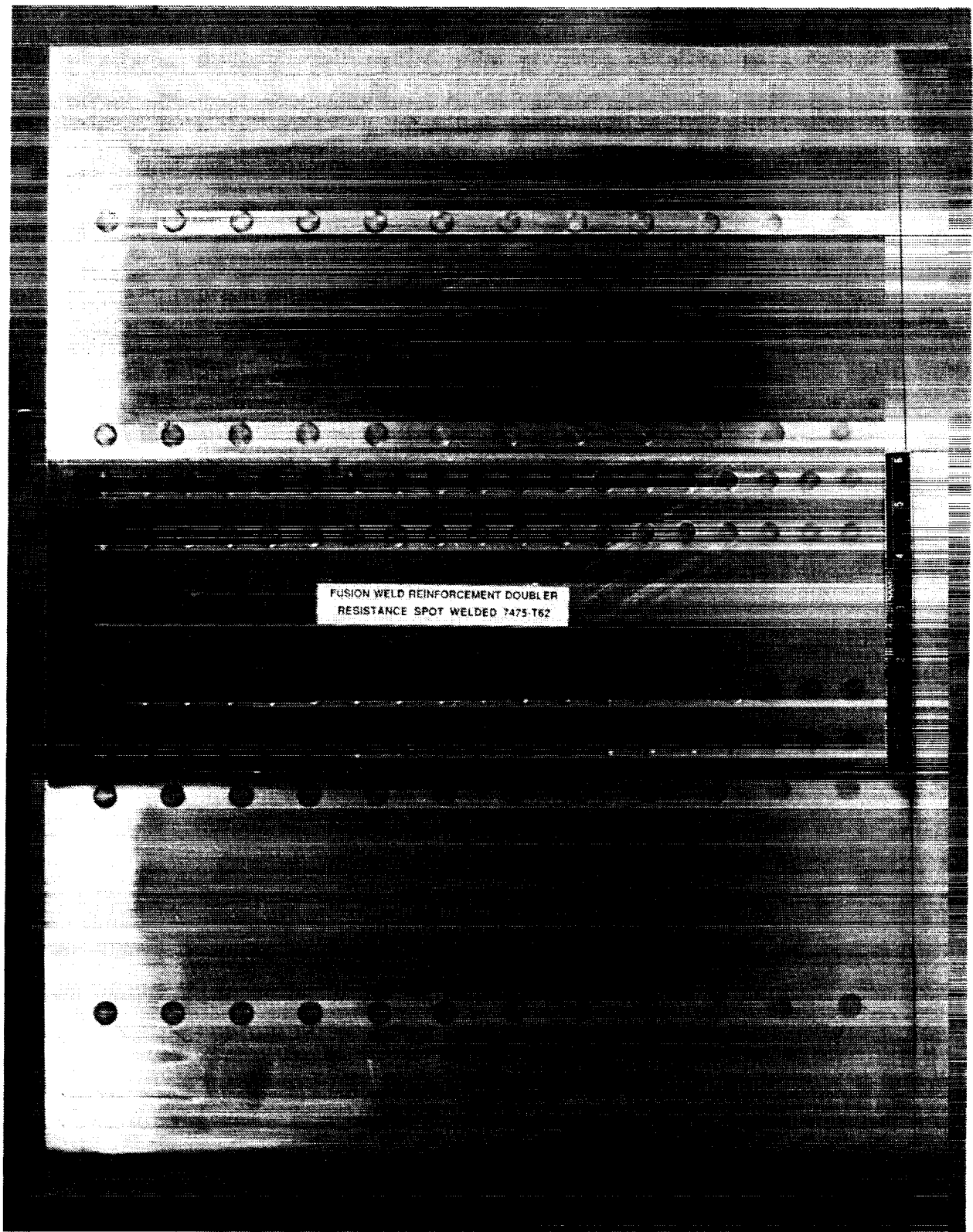


Figure 274. Back View of Doubler Reinforced Fusion weld.

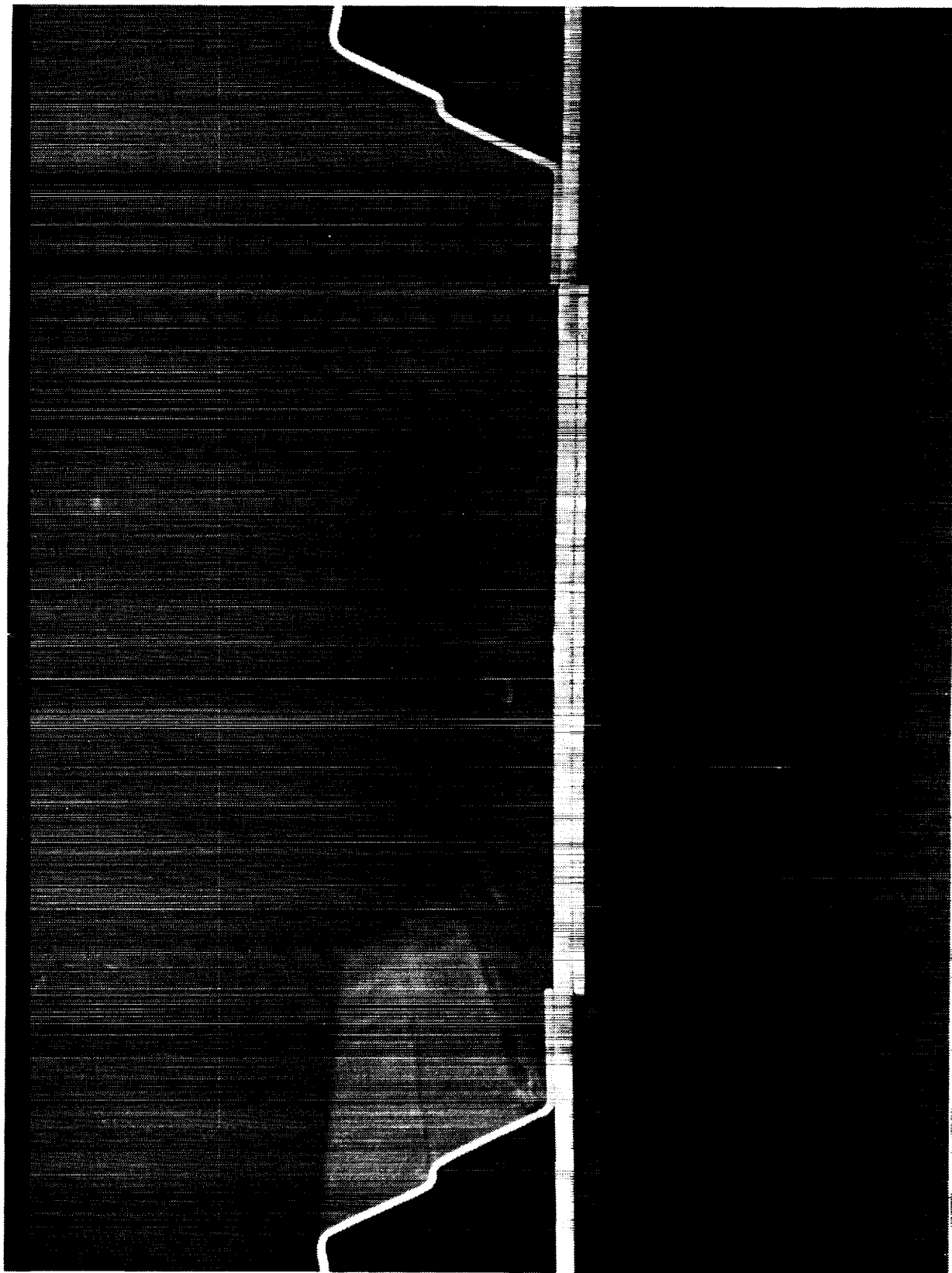


Figure 275. End View of Doubler Reinforced Fusion Weld Panel With Stepped Hat Stiffeners.

The welding NDE and quality control issues were addressed during resistance spot welding development (refer to section 4.3) The evaluation of weld quality was based upon monitoring of the process parameters for resistance spot welding (forge force, heat, current, etc.) that were recorded during each welding operation and evaluating the parameters for an acceptable versus unacceptable weld. The out-of-tolerance control areas for the welding process were determined through evaluations of information generated during the Taguchi design of experiment tests and the heat sensitivity testing. The acceptable limits for each variable in the welding process were identified and used as boundaries (upper and lower limits) for the fabrication of acceptable resistance spot welds (however, radiographic inspection, lap shear testing, and metallographic examination of welds was performed during this program in order to fully characterize the process). The next step for complete NDE of the resistance spot weld process would be to include automatic feed-back control (or in-process control) for the welding equipment that would control the settings of the weld equipment so that out-of-tolerance welds could not be made. However, investigation of automatic feedback control for resistance spot welding was out of the scope of this program.

Table 126. T62 Heat Treatment of Al-Li and Minimum Resultant Tensile Properties.

Alloy	Thermal Treatment	Temperature (°F)	Time at Temperature	F _{tu} (ksi)	F _{ty} (ksi)	Elongation (%)
2090 8090	Solution	1000 ± 10	30 minutes	58	48	2
	Artificial Age	350 ± 5	20 hours			
	Solution	1013 ± 10	30 minutes	57	45	2
	Artificial Age	300 ± 5	36 to 48 hours			

4.6 LIFE CYCLE COST ANALYSIS

The "Low Cost, SPF Aluminum Cryogenic Tank Structures for ALS and Future Hypersonic Vehicles" examined the application of superplastic formed (SPF) structure as a cost effective means to fabricate a cryogenic tank. The goal of the life cycle cost (LCC) study was to evaluate the cost savings or penalty associated with utilizing a built-up structures approach versus integrally machined structure for the Hydrogen tank. The built-up concept uses stiffeners, specifically, superplastically formed stiffener panels, brake formed hat sections, or "I" extrusions,

joined to a skin panel. The flow of the LCC study included evaluation of three built-up concepts represented by two different material systems, and a baseline concept, integral machining. A representation of the LCC analysis flow is shown as Figure 276 for review.

The General Dynamics ALS "L" vehicle configuration (described under section 4.1 of this report) was utilized as the baseline for the study (refer to Figure 277). The ALS cryogenic tank is a load-bearing member of the vehicle and is not pressure stabilized. Thus the tank must be able to support both its weight, and the loading conditions for the vehicle: ground (payload, and weather loads such as wind which would induce bending) and thrust during launch. The axial loads are transferred through the combination of the vertical stiffeners and skin, and the hoop or pressure loads are transferred through the skin and the hoop direction stiffeners. The stiffener concepts (both built-up and integrally machined) examined during the LCC analysis for the Hydrogen tank are shown in Figures 278 through 282. Each fabrication method utilized a fabrication flow for processing and assembly of the panels shown as Figures 283 through 289.

4.6.1 Ground Rules and Assumptions

The General Dynamics Space Systems Division ALS vehicle cost model was utilized for this study to examine the effects that structural weight and fabrication costs have on the life cycle cost (LCC) of the vehicle. The information was gathered for each fabrication process examined for the LH₂ tank. The fabrication and assembly data used during the analysis was compiled by both General Dynamics and Rockwell International. The generation of the cost data was divided such that one company provided information on fabrication of the structural components, and the other provided data on handling and assembly of the LH₂ tank structure. The division was made to assure continuity in estimating the fabrication hours for each process.

The data gathered for the life cycle cost analysis included the costs of the raw materials (extrusions and sheet materials: "T" extrusions, -T3 sheet for outer skins, superplastic sheet, and -T3 sheet for brake forming), fabrication hours for the superplastic formed (SPF) stiffener panels and braked formed hat structure, special tooling (recurring and non-recurring costs and hours), and hours for bar code identification, heat treatment, trimming, inspection, cleaning, storage (temporary), joining, and final assembly. Both groups of data (fabrication and assembly) were reviewed and accepted by each company and consolidated into a fabrication package, prior to inclusion into the analysis. The LCC cost estimating methodology, ground-rules and break-down of the hours, costs and weights for each process are shown in Tables 127 through 136.

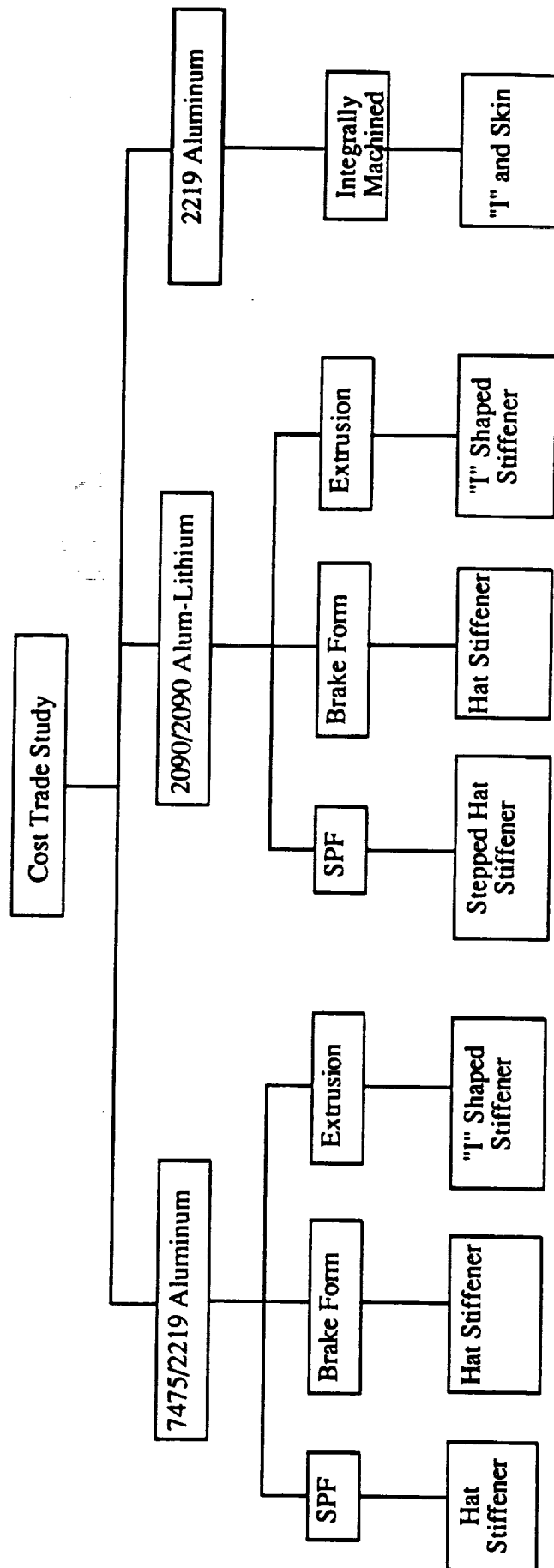


Figure 276. Life Cycle Cost Trade Flow.

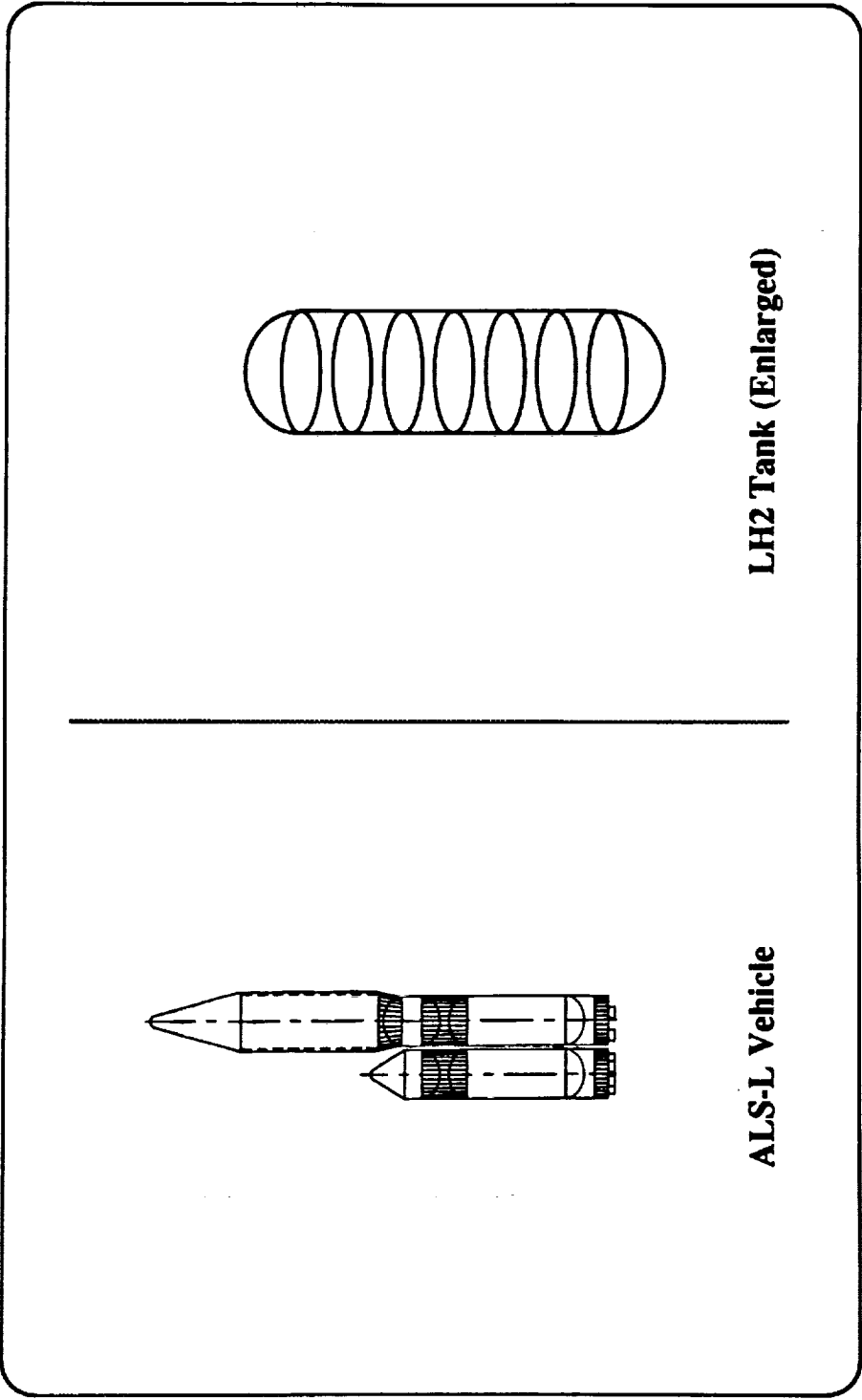
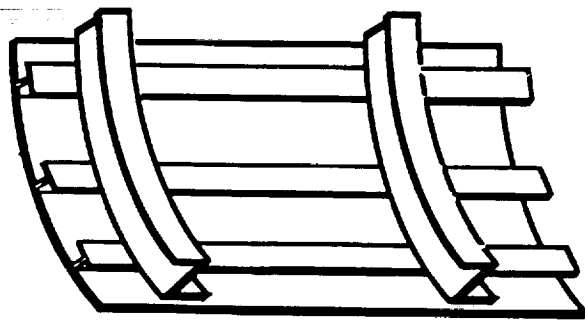
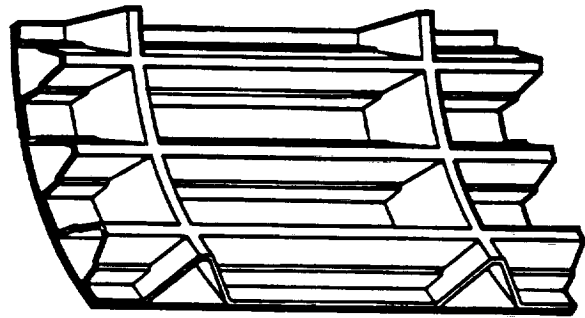


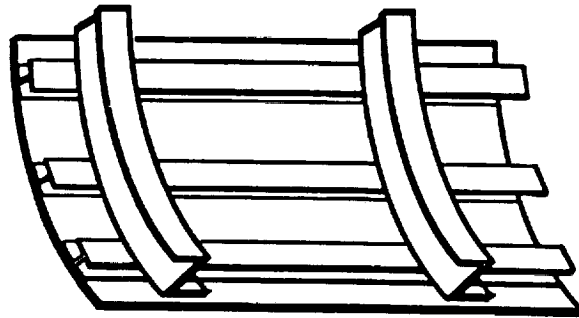
Figure 277. Cryogenic Tank Vehicle Concepts Utilized for Life Cycle Cost Analysis.



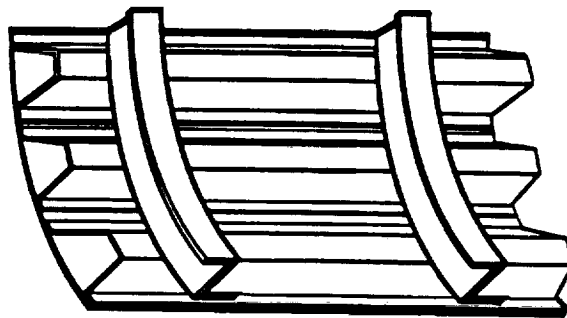
**INTEGRALLY
MACHINED**



**SUPERPLASTIC FORMED
BUILT-UP
STIFFENER PANEL
(STIFFENER AND SKIN)**



**EXTRUSION
BUILT-UP
STIFFENER PANEL
(MULTIPLE STIFFENERS
JOINED TO SKIN)**



**BRAKE FORMED
BUILT-UP
STIFFENER PANEL
(MULTIPLE STIFFENERS
JOINED TO SKIN)**



Figure 278. Cryogenic Tank Structural Options Investigated During the Life Cycle Cost Analysis.

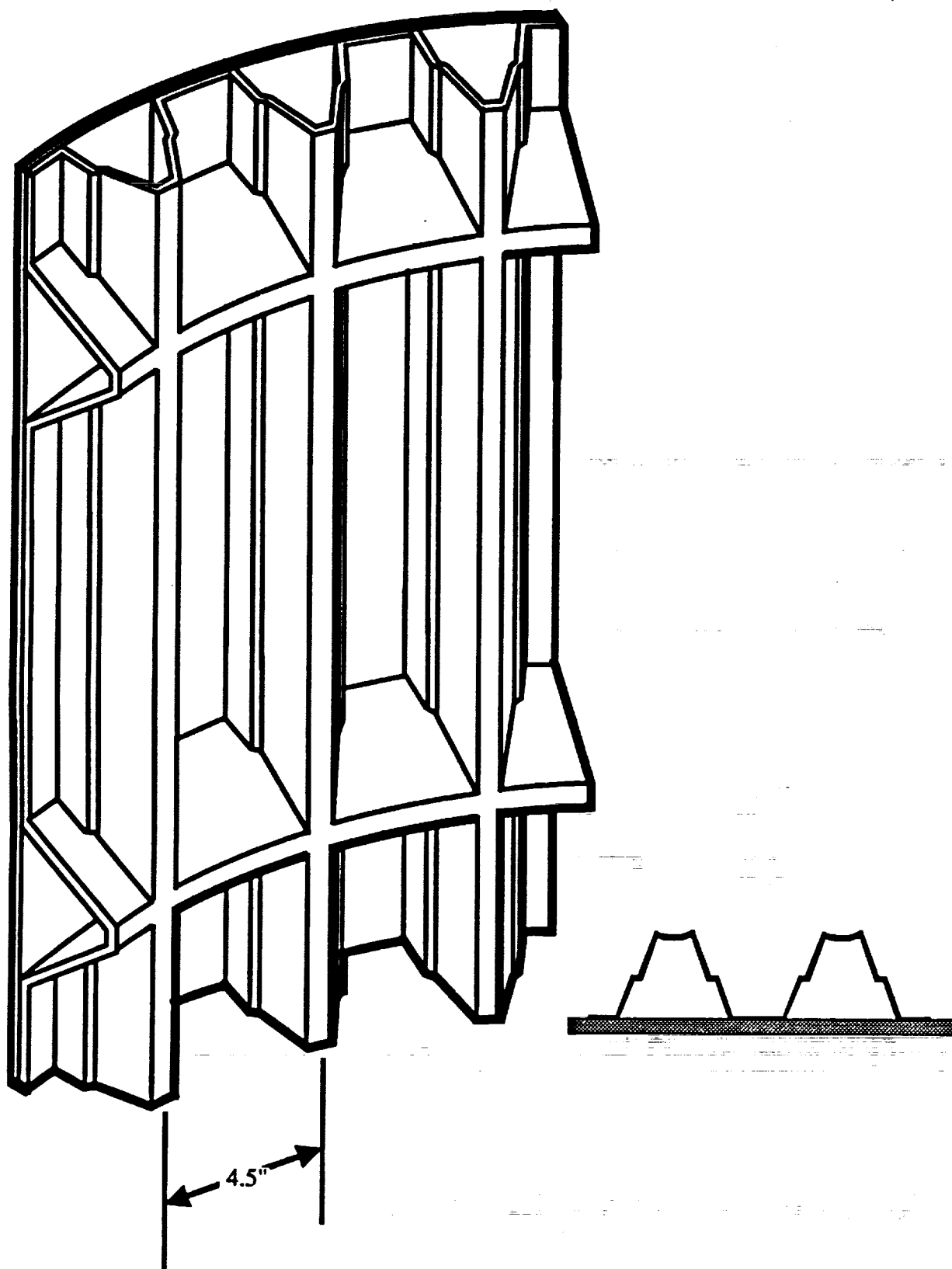


Figure 279. Built-Up SPF Stiffener Panel Configuration.

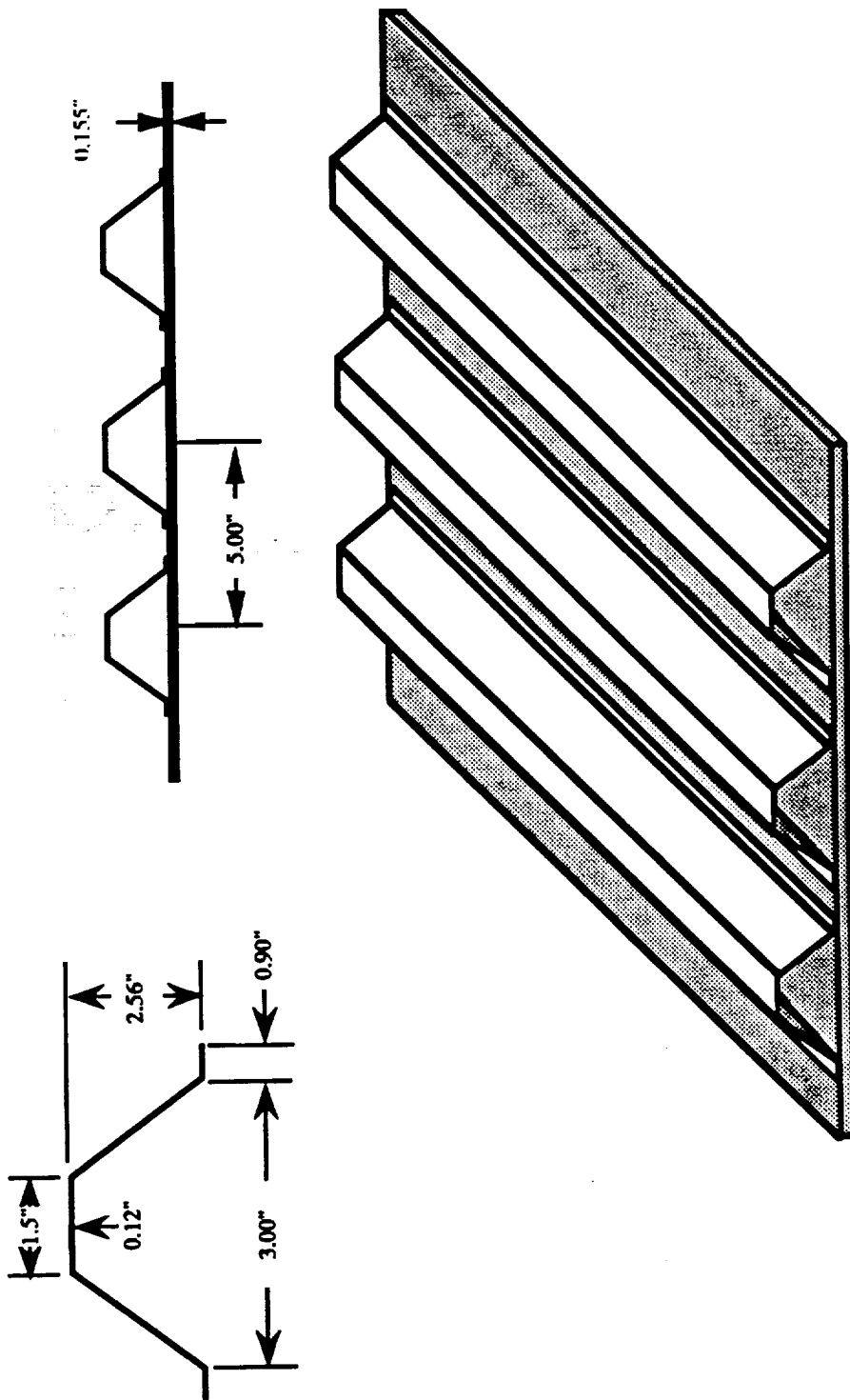


Figure 280. Built-Up Brake Formed Stiffener Panel Configuration.

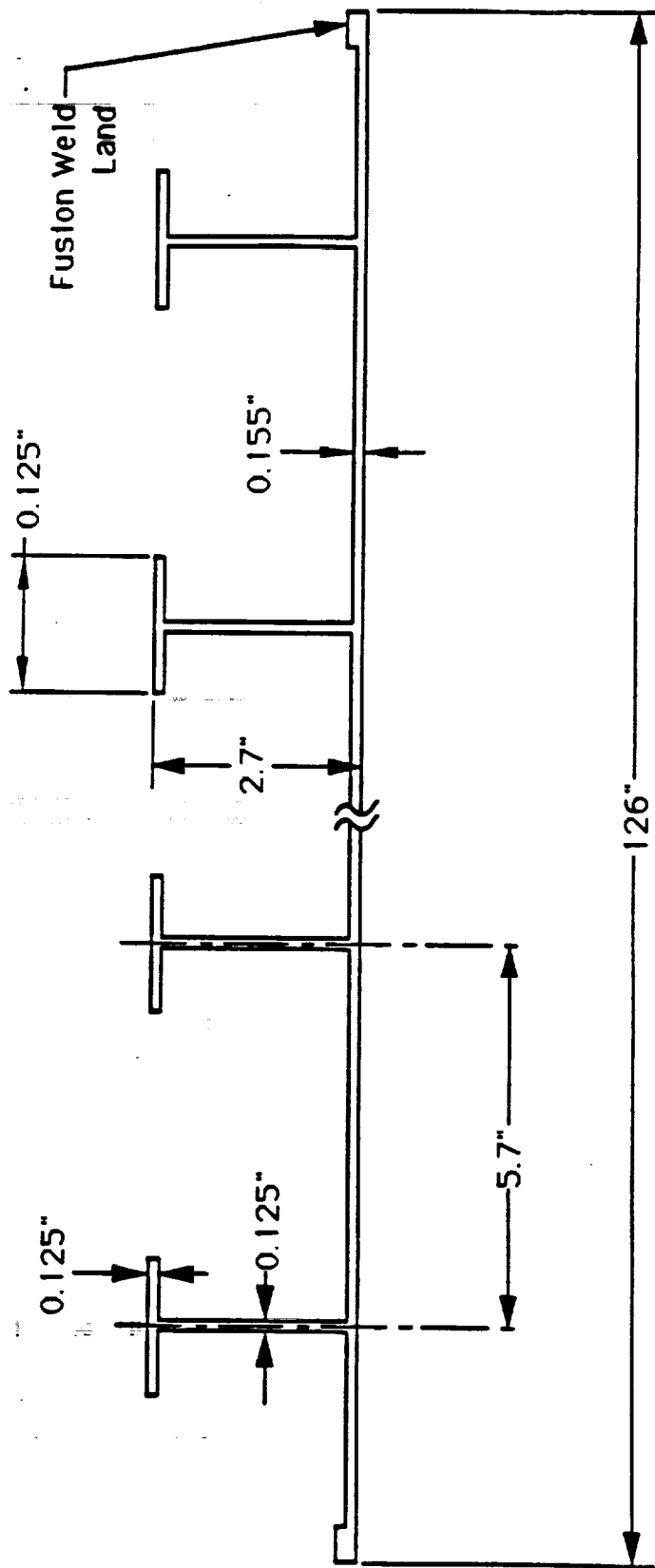


Figure 282. Machined Panel Configuration, Integrally Stiffened.

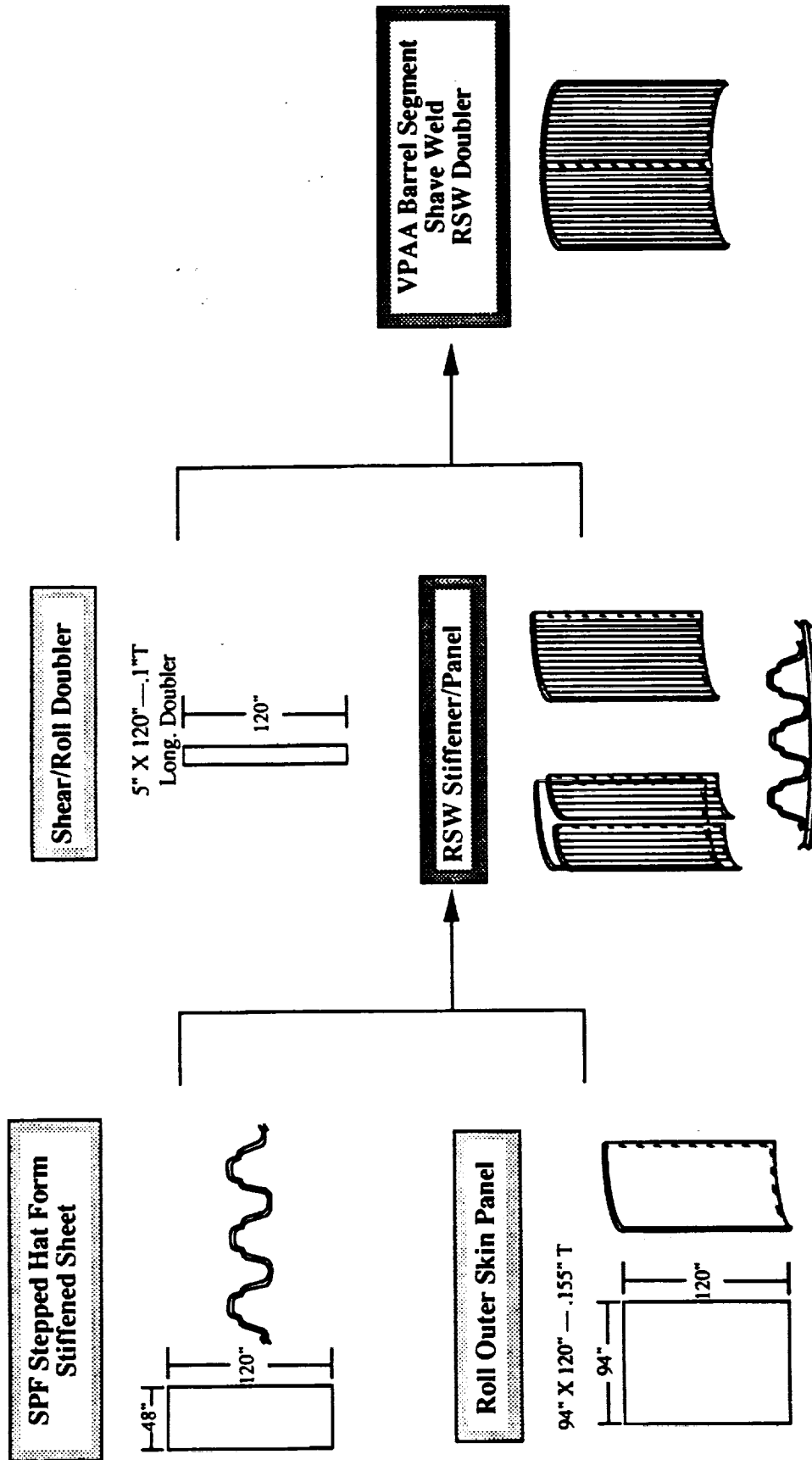


Figure 283. Manufacturing Process Flow for 2090 Al-Li SPF Stiffener Panel Fabrication and Assembly Into Barrel Sections.

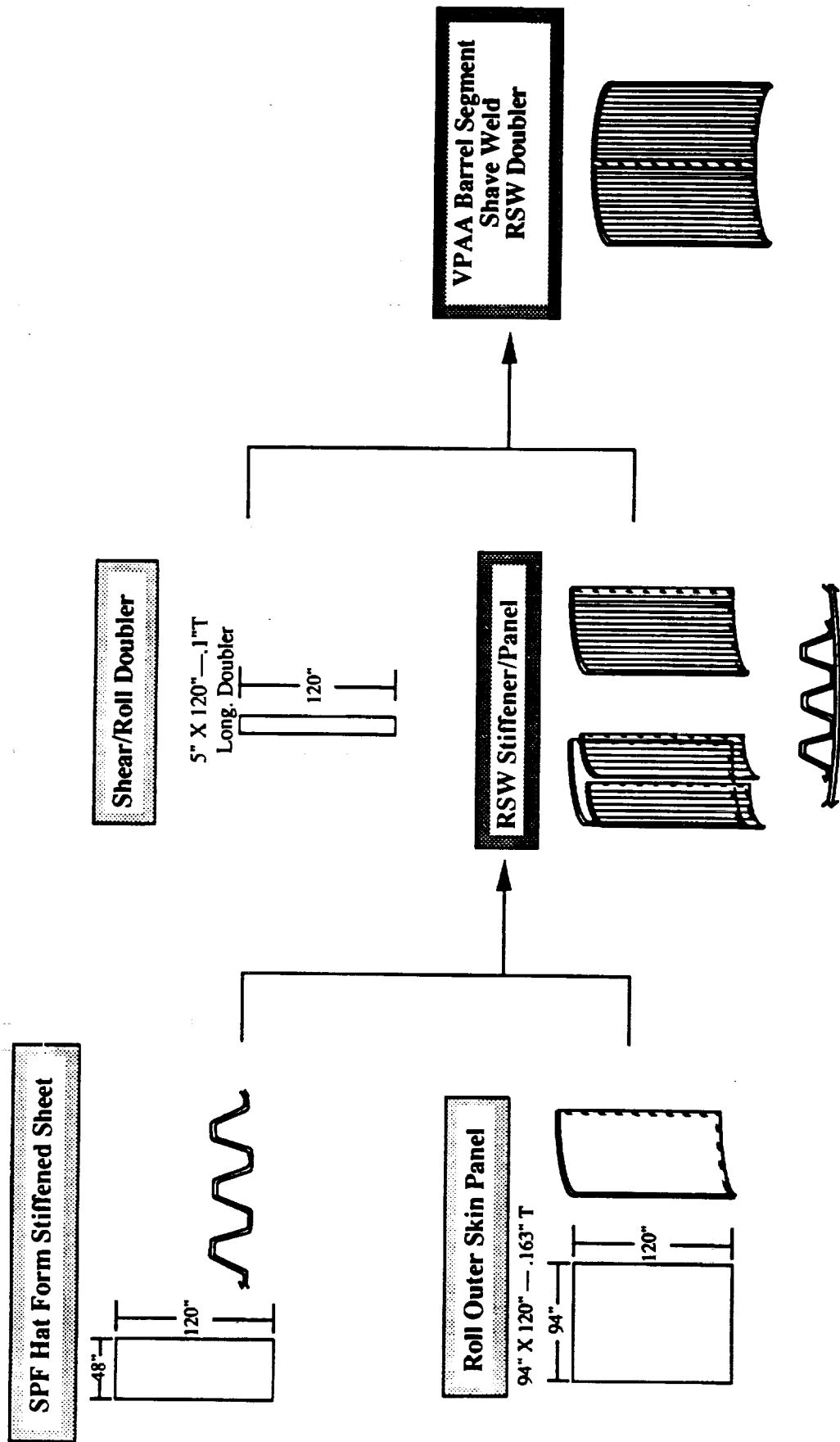


Figure 284. Manufacturing Process Flow for 7475 Al SPF Stiffener Panel Fabrication and Assembly Into Barrel Sections.

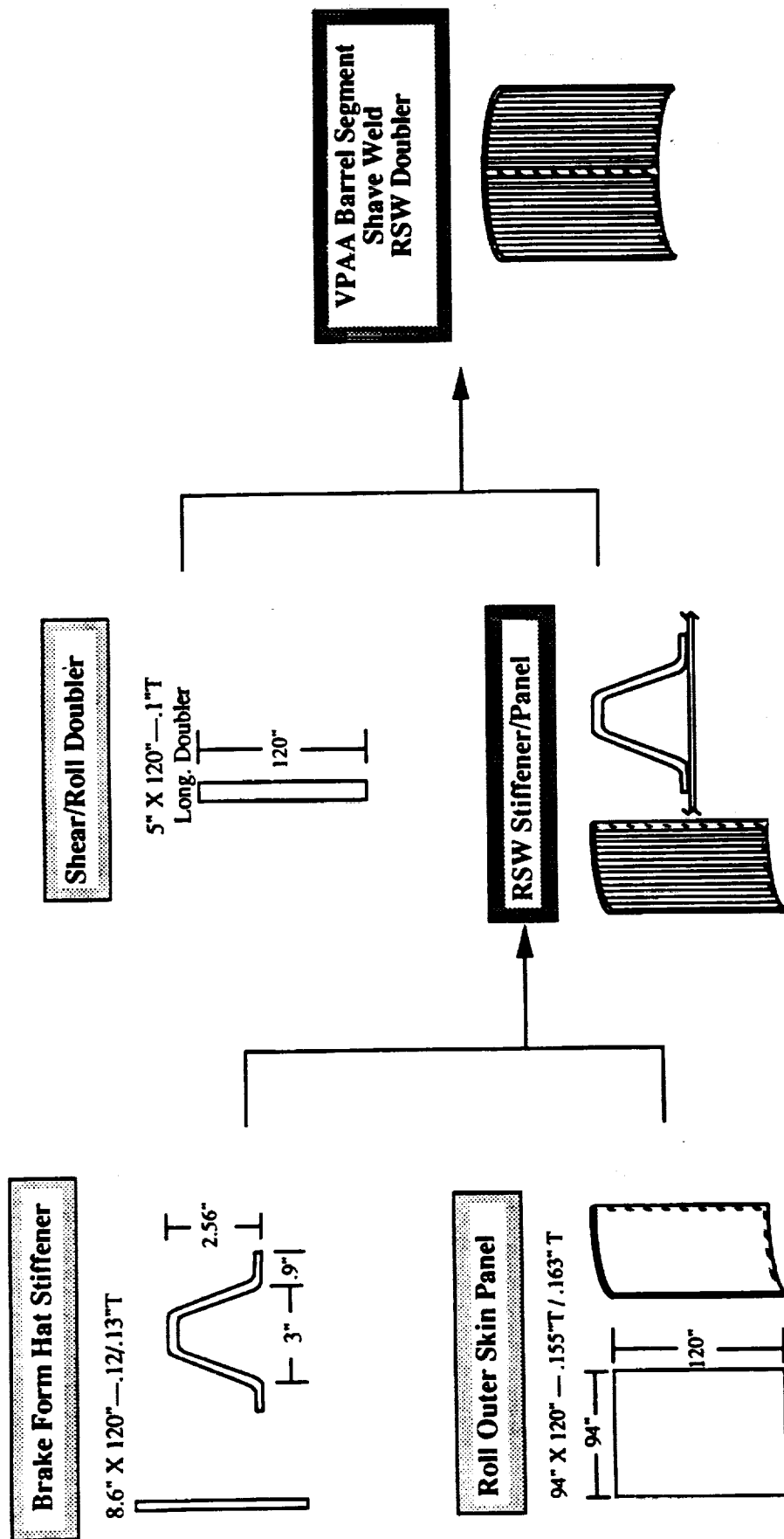


Figure 285. Manufacturing Process Flow for 2090 Al-Li or 2219 Al Brake Formed Stiffener Components and Assembly Into Barrel Sections.

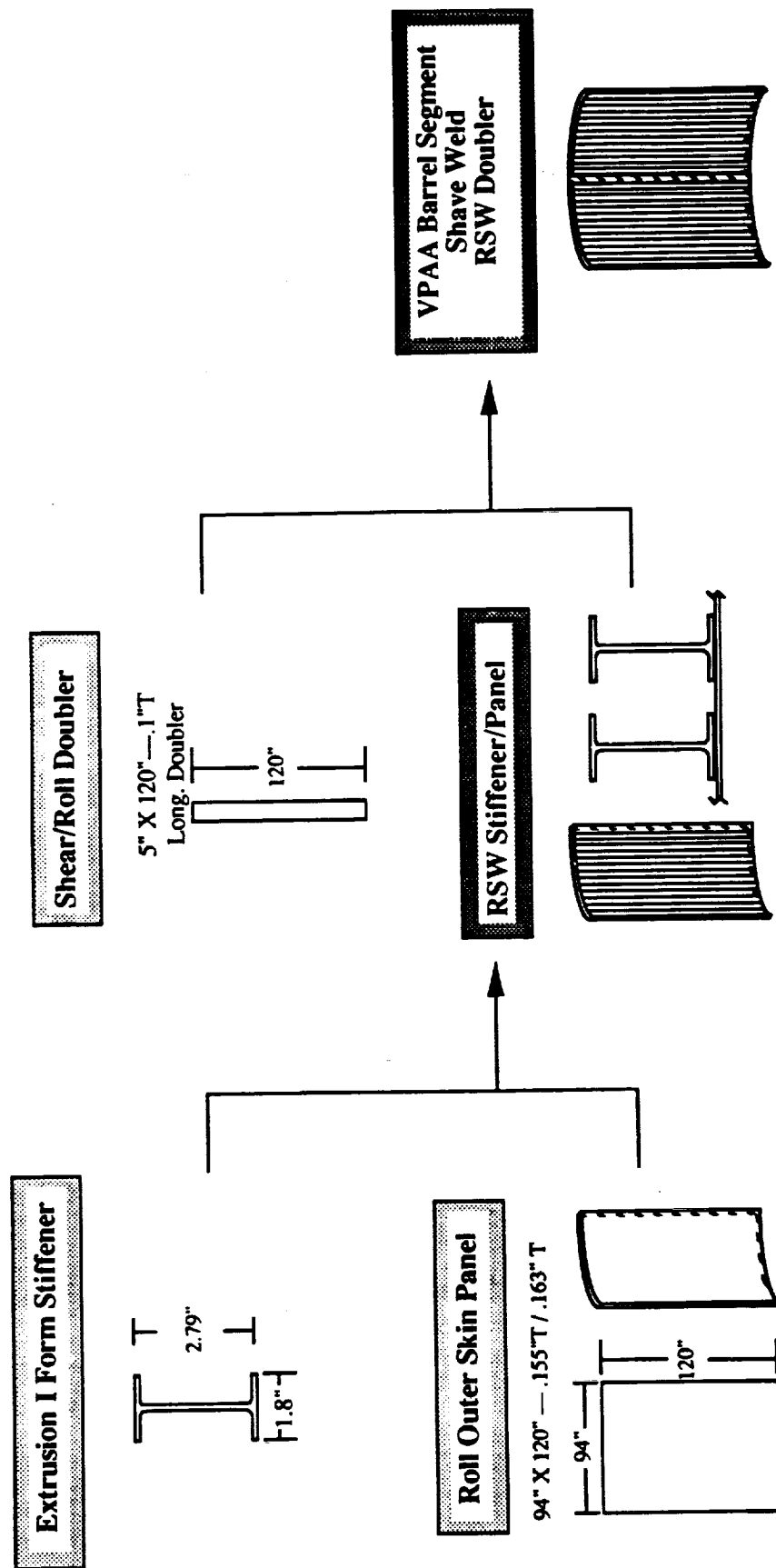


Figure 286. Manufacturing Process Flow for 2090 Al-Li or 2219 Al "I" Extrusion Stiffener Components and Assembly Into Barrel Sections.

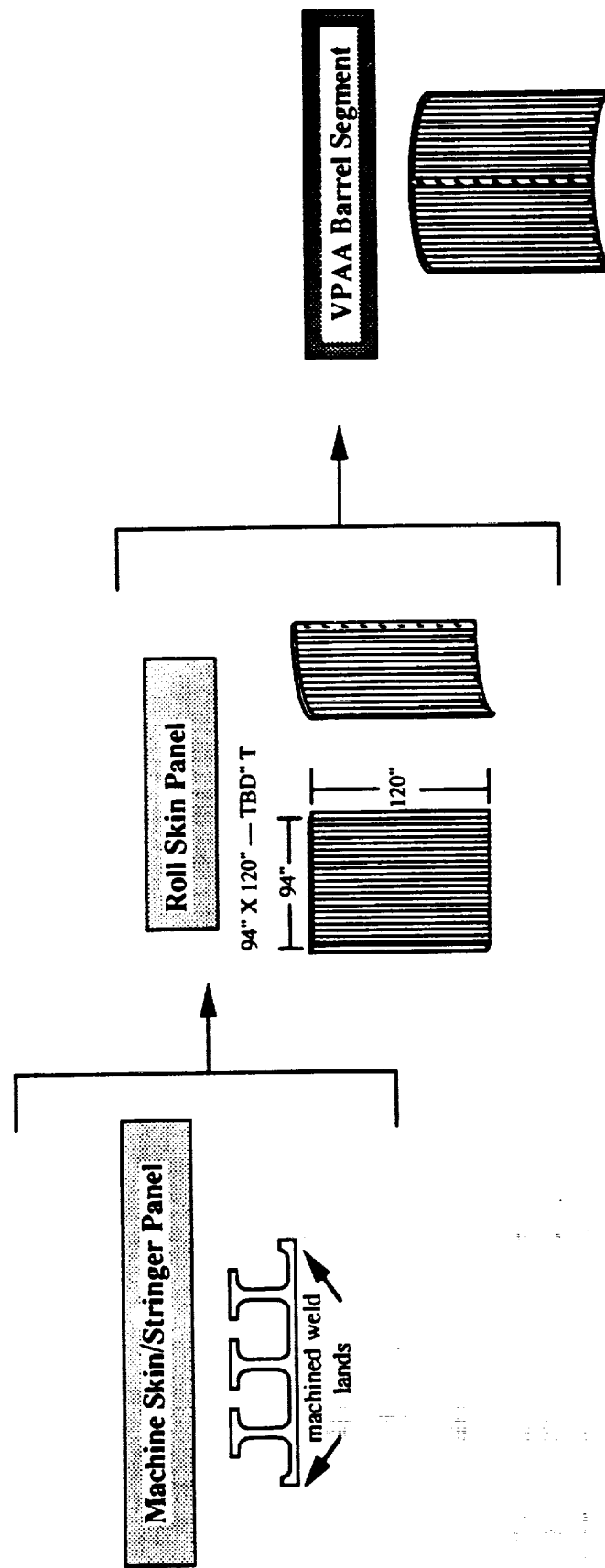


Figure 287. Manufacturing Process Flow for Integrally Machined 2219 Al Panels and Assembly Into Barrel Sections.

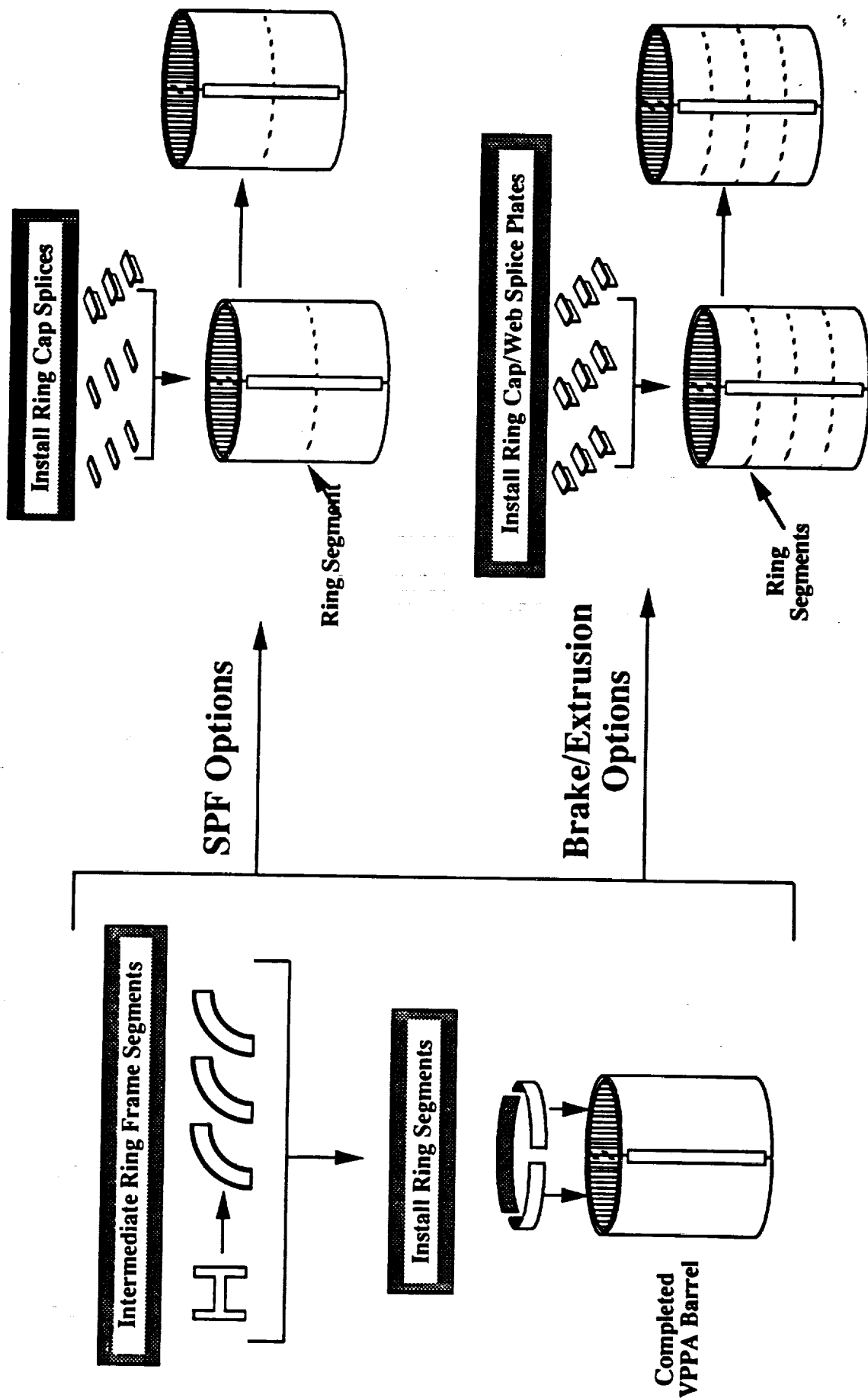


Figure 288. Manufacturing Process Flow for Barrel Section Forming.

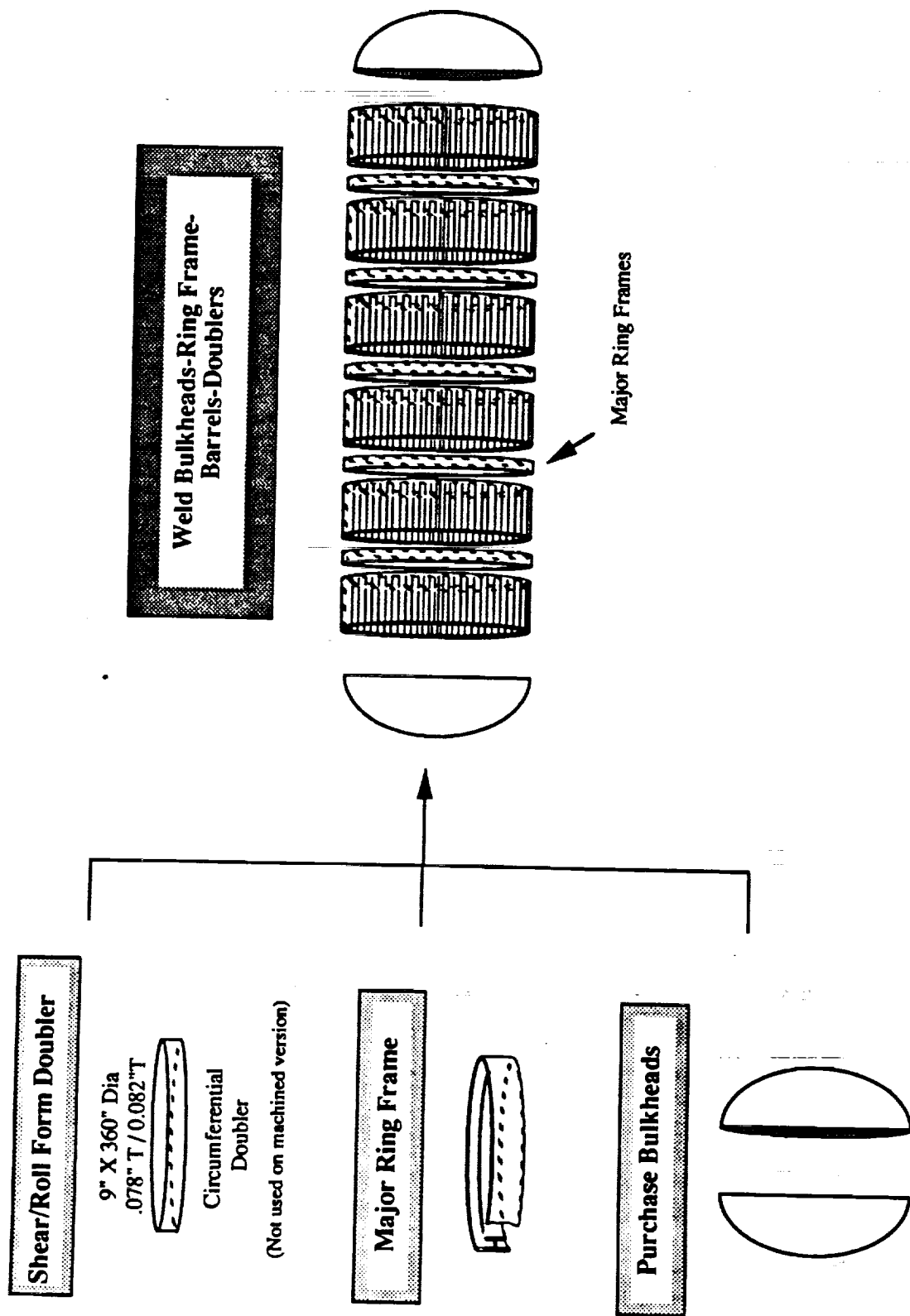
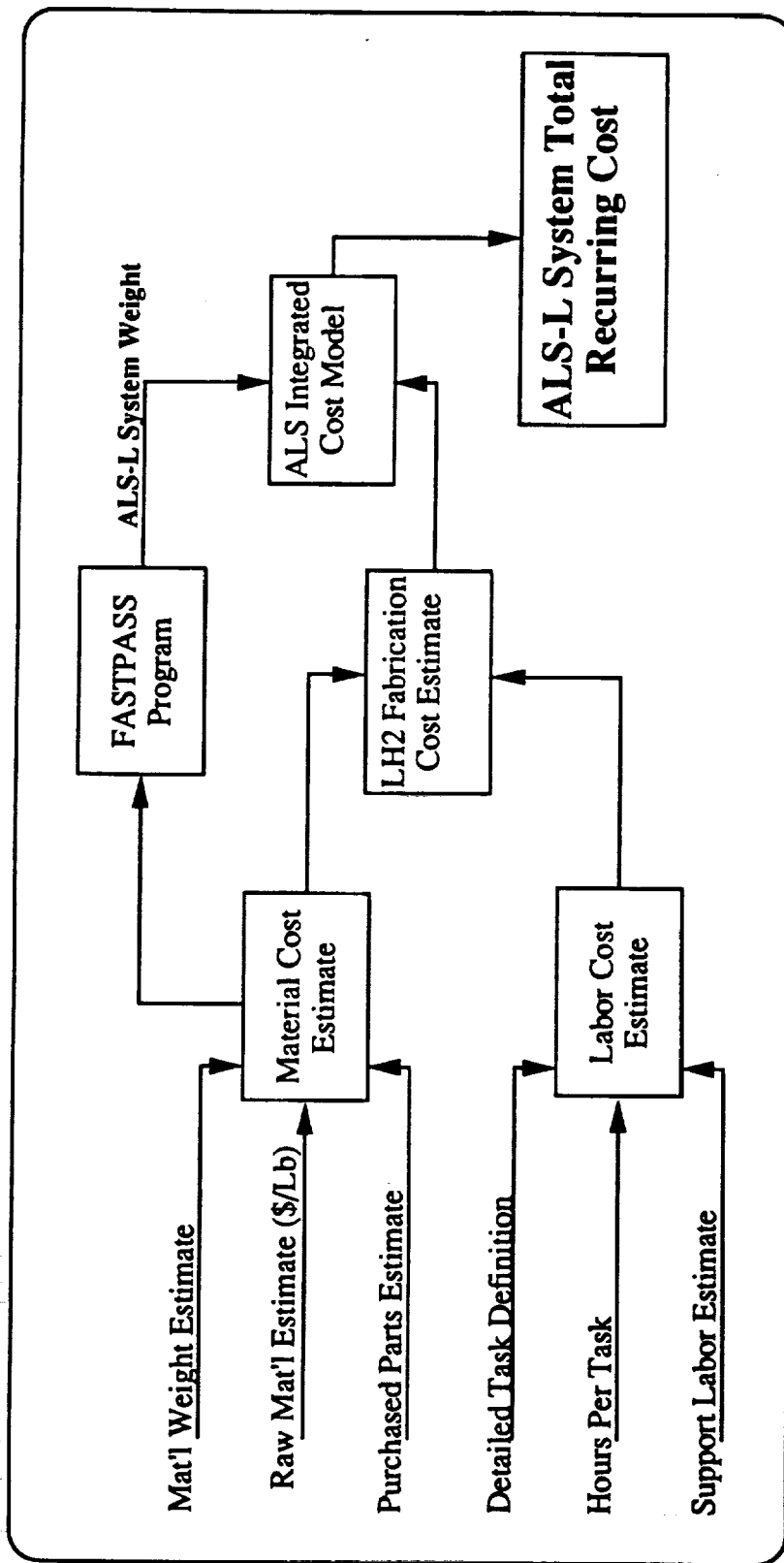


Figure 289. Manufacturing Process Flow for Major Cylinder Assembly.

Table 127. Cost Estimating Methodology for the LCC Analysis.



**DO THIS PROCESS FOR EACH OPTION --> THEN
COMPARE ALS-L SYSTEM RECURRING COSTS**

Table 128. Ground Rules for LCC Analysis.

Preliminary Information:

- # of Vehicles per Year = 20
- 47 panels/vehicle
- All Stiffener to Outer Skin Joints are Resistance Spot Welding
- All Panel to Panel Joints are variable polarity plasma arc fusion welded with resistance spot welded sheet doublers over the joints
- All Dollars are in Yr. 2000
- Panel Size = 60" x 282.7"
- Outer skin = 2090 Aluminum-Lithium in the -T3 condition
- SPF Aluminum = Heat Treated to -T62
- Brake Formed Aluminum = -T3 Aged to -T8
- Extrusions Aluminum = -T8
- Material will be available in 60" widths
- Tooling for SPF will be fabricated out of high grade corrosion resistant Steel)

4.6.2 Summary of Life Cycle Cost Analysis

The results of the analysis represented in Tables 130 through 136 showed the cost to fabricate one vehicles cryogenic tanks (T1 dollars, two tanks per vehicle), 307 vehicles (T307 dollars, two tanks per vehicle), and a projected build of 1000 vehicles (T1000, two tanks per vehicle). A summary of the costs for the tanks are shown as Table 137. The integrally machined configuration (integrally machined 2219 Al) is the most costly system at T1, and at T307 (or the 307th vehicle built) however at T1000, the disparity in purchase price between built-up configurations and the integrally machined concept begins to become less apparent.

In the coarse of the program, it was difficult to ascertain the value of weight to the vehicle versus amount of payload that would have to be sacrificed for each pound of structural weight. However, if the value were similar to a Shuttle type vehicle in that each pound saved for the vehicle allowed for increase to the payload manifest, each pound could be worth up to \$300. In that case the modified purchase price, due to weight savings or penalty, (refer to Table 138) is shown in Table 139 for each configuration (based off of the integrally machined concept). Using the \$300/lb ratio, the SPF Al-Li concepts provide for approximately 40 to 48% cost savings over the integrally machined concept, while the SPF Al concept provided a 17 to 26% cost savings. The cost savings or penalties are shown as Table 140. Since this is an expendable vehicle, the goal of minimization of fabrication and material cost is of the utmost importance. However, weight savings should be kept in the picture as it relates to potential payload into space.

Table 129. LCC Weight Breakdowns for Each Configuration.

LH2 TANK COMPONENTS	2090-T83 AL-LI SKIN			2219-T851 AL SKIN			2219-T851 MACHINED
	2090-T6(3PF) SPF Stopped Hat	2090-T8 Hat Section	2090-T86 I - Section	2219-T6(3PF) SPF Stopped Hat	2219-T851 Hat Section	2219-T851 I - Section	
Tank Geometry							
Cylinder Length, inches	706.8	727.6	724.8	721.2	736.8	732	732
Cylinder Diameter, inches	360	360	360	360	360	360	360
Tank Skin Thickness, in.	0.155	0.155	0.155	0.163	0.163	0.163	0.163
Circumferential Splice Plate Geometry							
Fusion Weld Reinforcement Doubler Thickness	0.078	0.078	0.078	0.082	0.082	0.082	0.163
Width	9.00	9.00	9.00	9.00	9.00	9.00	9.00
Number of Splices	6	6	6	6	6	6	3
Longitudinal Splice Plate Geometry							
Fusion Weld Reinforcement Doubler Thickness	0.100	0.100	0.100	0.100	0.100	0.100	0.326
Width	5.00	5.00	5.00	5.00	5.00	5.00	2.00
Number of Splices	12	12	12	12	12	12	6
Axial Reinforcement Stiffeners							
Stiffener Spacing	7.05	9	5.76	9	9	6	5.7
Stiffener Area	0.549	1.030	0.700	1.088	1.061	0.746	0.309
Calculated No. Of Stiffeners	169	126	196	126	126	188	198
Equivalent 'hat' (includes skin + stiffener)	0.377			0.285			
Major Ring Frame - Fusion Welded							
Ring Frame Spacing, inches	117.8	121.3	120.8	120.2	122.8	122.0	244.0
Cross-Section Area, sq in	2.64	2.64	2.64	2.64	2.64	2.64	2.64
Number of Frames	5	5	5	5	5	5	2
60-Inch Intermediate Ring Frame							
Ring Frame Spacing, inches	58.90	60.63	60.40	58.75	58.75	58.75	58.75
Cross-Section Area, sq in	2.64	2.64	2.64	2.64	2.64	2.64	2.64
Number of Frames	6	6	6	6	6	6	6
Attachment Fasteners (4 per stiffener)	3840	3000	4704	3000	3000	4512	4752
30-Inch Intermediate Ring Frame							
Ring Frame Spacing, inches	29.45	30.32	30.20	29.38	29.38	29.38	29.38
Cross-Section Area, sq in	0.19	1.2	1.2	0.19	1.2	1.2	1.2
Number of Frames	12	12	12	12	12	12	12
Attachment Fasteners (2 per stiffener)	0 (RSW'd)	3000	4704	0 (RSW'd)	3000	4512	4752
External Reaction Rings (Booster-Core)							
Area (Total for two rings), in2	39.68	39.68	39.68	39.68	39.68	39.68	39.68
Weight Breakdowns							
Skin Weight	11523	11842	11816	13694	13990	13899	13899
Axial Stiffener Weight	7496	8220	8562	8027	9237	9700	7247
Major Ring Weight	1538	1538	1538	1538	1538	1538	615
60" Intermediate Ring Weight	1628	1632	1629	1808	1808	1807	1807
30" Intermediate Ring Weight	236	1487	1485	262	1657	1657	1657
Intermediate Ring Attach Fasteners	19	30	56	15	30	54	57
Intermediate Ring Splices (2% of Total Wt)	37	62	62	41	69	69	69
Circumferential Splice Weight	440	440	440	513	513	513	513
Longitudinal Splice Weight	364	376	374	413	423	420	284
Bulkhead Weight (Total for 2 Bulkheads)	3707	3707	3707	4106	4106	4106	4106
Total Weight of Cylinder	23282	25647	25963	26311	29265	29657	26149
Manufacturing Tolerances & Buildup	1115	1148	1144	1260	1287	1279	1279
Miscellaneous Contingency - 3%	732	804	813	827	917	928	823
Total Structure Weight of LH2 Tank	28836	31386	31627	32545	38576	38976	32366
Scrap Weights							
Skin Weight - 5%, 78%	668	891	889	789	810	805	73833
Axial Stiffener Weight, 3%-10%-3%	225	822	428	241	924	485	
Ring Extrusion Weight - 5%	170	233	233	180	230	230	204
Fusion Weld/Ring Splice Plates - 5%	42	44	44	48	30	30	43
Total Wt. of LH2 Tank Mod.	29942	33096	33028	33763	37689	37561	106456

Table 130. LCC Hours and Cost Information for Superplastic Formed Stiffened Panels for 2090 Aluminum LH₂ Tank Structure at T1, T307 and T1000.

SPF SUMMARY - 2090						
RECURRING ESTIMATE	# PARTS	T1 Hours		AVG. HRS FOR 1 Tank		
		Per Part	T1 Hours	T307 Hours	T1000 Hours	
FAB SEALING FRAME	6	30.4	182.4	60.5	48.2	
PREPARE BLANK FOR FORMING	6	22.0	132.0	43.8	34.9	
FORM PART	6	59.6	357.6	222.2	203.4	
HAT POST FORM PROCESS	6	176.5	1059.0	386.7	317.0	
OUTER SKIN	6	101.8	610.8	356.2	322.8	
DOUBLERS	6	43.2	259.2	113.5	97.4	
RING FRAME CAPS	6	29.5	177.0	58.7	46.8	
FORM BARREL SECTION	6	820.6	4923.4	1810.8	1487.6	
MAJOR CYL ASSY	1	1842.6	1842.6	830.6	717.5	
SUBTOTAL			9544.0	3883.1	3275.5	
SUPPORT LABOR			5089.3	4344.7	1763.1	
TOTAL LABOR HRS			14633.3	8227.8	5038.6	
				T1\$ FY'87 \$K	T307\$ FY'87 \$K	T1000\$ FY'87 \$K
LABOR DOLLARS FOR 2 TANKS				\$1,463K	\$823K	\$504K
RADIOGRAPHIC MATL (\$10/HR WELDING)					\$14.93K	
PURCHASE BULKHEAD-\$188K ea			3707 lbs	2 /Veh	\$752.0K	
PURCHASE SKIN MATL @ \$ 10.8 /lb			14038 lbs	2 /Veh	\$303.2K	
PURCHASE STIFF MATL (SPF) @ \$ 27.0 /lb			7721 lbs	2 /Veh	\$416.9K	
PURCHASE SPLICE MATL @ \$ 10.8 /lb			884 lbs	2 /Veh	\$19.1K	
PURCHASE FABRICATED RINGS (AVG. 307 VEH.)						
MAJOR RING FRAME @ \$ 95.8 /lb			1615 lbs	2 /Veh	\$309.4K	
60-INCH RING FRAME, 3 SECT @ \$ 79.4 /lb			1710 lbs	2 /Veh	\$271.5K	
30-INCH RING FRAME, 3 SECT @ \$ 10.8 /lb			248 lbs	2 /Veh	\$5.4K	
FASTENERS (HUCK BLIND RIVOT @ \$ 180.2 /lb			19 lbs	2 /Veh	\$6.8K	
Average Cost of 2 Tanks (1 Vehicle)				\$3,563K	\$2,922.1K	\$2,603.2K
Average Cost of 1 Tank				\$1,781.4K	\$1,461.1K	\$1,301.6K
Total Weight of One Tank			28,836 lbs			
Average Recurring Dollars per Pound for 1 Vehicle				@ \$ 61.8 /lb	@ \$ 50.7 /lb	@ \$ 45.1 /lb
MATERIAL COSTS HAVE BEEN ADJUSTED FROM FY90 TO FY87 \$ (ESCALATION FACTOR = 1.111 TO GET FROM FY87 TO FY 90) AL-LI SHEET = \$12/LB IN FY90, \$10.80/LB IN FY87 AL-LI SHEET (SPF GRADE) = \$30/LB IN FY90, \$27/LB IN FY87 AL-LI EXTRUSION = \$20/LB IN FY90, \$18/LB IN FY87						
NON-RECURRING ESTIMATE						
TOOLING						
SPF TOOL				\$63.2K		
* 2 TANKS PER VEHICLE						

Table 131. LCC Hours and Cost Information for Superplastic Formed Stiffened Panels for 7475 Aluminum LH₂ Tank Structure at T1, T307 and T1000.

SPF SUMMARY - 7475						
RECURRING ESTIMATE	# PARTS	T1 Hours		AVG. HRS FOR 1 Tank		
		Per Part	T1 Hours	T307 Hours	T1000 Hours	
FAB SEALING FRAME	6	30.4	182.4	60.5	48.2	
PREPARE BLANK FOR FORMING	6	22.0	132.0	43.8	34.9	
FORM PART	6	59.6	357.6	222.2	203.4	
HAT POST FORM PROCESS	6	176.5	1059.0	386.7	317.0	
OUTER SKIN	6	101.8	610.8	356.2	322.8	
DOUBLERS	6	43.2	259.2	113.5	97.4	
RING FRAME CAPS	6	29.5	177.0	58.7	46.8	
FORM BARREL SECTION	6	714.8	4288.8	3006.4	2437.4	
MAJOR CYL ASSY	1	1842.6	1842.6	830.6	717.5	
SUBTOTAL			8909.4	5078.7	4225.4	
SUPPORT LABOR			4752.6	4301.4	2267.1	
TOTAL LABOR HRS			13662.0	9380.1	6492.4	
				T1\$ FY'87 \$K	T307\$ FY'87 \$K	T1000\$ FY'87 \$K
LABOR DOLLARS FOR 2 TANKS				\$1,366K	\$938K	\$649K
RADIOGRAPHIC MATL (\$10/HR WELDING)					\$14.78K	
PURCHASE BULKHEAD-\$188K ea			4106 lbs 2 /Veh		\$752.0K	
PURCHASE SKIN MATL @ \$ 3.1 /lb			16570 lbs 2 /Veh		\$102.7K	
PURCHASE STIFF MATL (AL-LI Sh @ \$ 10.8 /lb			8267 lbs 2 /Veh		\$178.6K	
PURCHASE SPLICE MATL @ \$ 3.1 /lb			1016 lbs 2 /Veh		\$6.3K	
PURCHASE FABRICATED RINGS (AVG. 307 VEH.)						
MAJOR RING FRAME @ \$ 95.8 /lb			1615 lbs 2 /Veh		\$309.4K	
60-INCH RING FRAME, 3 SECT @ \$ 79.4 /lb			1898 lbs 2 /Veh		\$301.4K	
30-INCH RING FRAME, 3 SECT @ \$ 3.1 /lb			276 lbs 2 /Veh		\$1.7K	
FASTENERS (HUCK BLIND RIVOT @ \$ 180.2 /lb			15 lbs 2 /Veh		\$5.4K	
Average Cost of 2 Tanks (1 Vehicle)				\$3,039K	\$2,610.3K	\$2,321.6K
Average Cost of 1 Tank				\$1,519.3K	\$1,305.2K	\$1,160.8K
Total Weight of One Tank			32,505 lbs			
Average Recurring Dollars per Pound for 1 Vehicle				@ \$ 46.7 /lb	@ \$ 40.2 /lb	@ \$ 35.7 /lb
MATERIAL COSTS HAVE BEEN ADJUSTED FROM FY90 TO FY87 \$ (ESCALATION FACTOR = 1.111 TO GET FROM FY87 TO FY 90) 2219 SHEET = \$3.43/LB IN FY90, \$3.09/LB IN FY87 7475 SHEET (SPF GRADE) = \$12/LB IN FY90, \$10.80/LB IN FY87 STD EXTRUSION = \$4.50/LB IN FY90, \$4.05/LB IN FY87 30-INCH RING MATERIAL PRICE = SKIN MATERIAL PRICE						
NON-RECURRING ESTIMATE						
TOOLING						
SPF TOOL						
				\$63.2K		
* 2 TANKS PER VEHICLE						

Table 132. LCC Hours and Cost Information for Brake Formed Stiffened Panels for 2090 Aluminum LH₂ Tank Structure at T1, T307 and T1000.

BRAKE FORMING SUMMARY - 2090					
RECURRING ESTIMATE	# PARTS	T1 Hours Per Part	AVG. HRS FOR 1 Tank		
			T1 Hours	T307 Hours	T1000 Hours
BRAKE FORM HAT	6	120.0	720.0	353.5	310.7
HAT POST FORM PROCESS	6	112.5	675.0	246.9	202.5
OUTER SKIN	6	101.5	609.0	355.6	322.3
DOUBLERS	6	43.2	259.2	113.5	97.4
FORM BARREL SECTION	6	1152.7	6916.2	2544.5	2090.4
MAJOR CYL ASSY	1	1842.6	1842.6	830.6	717.5
SUBTOTAL			11022.0	4444.7	3740.8
SUPPORT LABOR			5873.5	4334.8	2010.0
TOTAL LABOR HRS			16895.5	8779.5	5750.7

	T1\$ FY'87 \$K	T307\$ FY'87 \$K	T1000\$ FY'87 \$K
LABOR DOLLARS FOR 2 TANKS	\$1,690K	\$878K	\$575K
RADIOGRAPHIC MATL (\$10/HR WELDING)		\$20.39K	
PURCHASE BULKHEAD-\$188K ea		\$752.0K	
PURCHASE SKIN MATL @ \$ 10.8 /lb		\$313.3K	
PURCHASE STIFF MATL (AL-LI Sh @ \$ 10.8 /lb		\$195.3K	
PURCHASE SPLICE MATL @ \$ 10.8 /lb		\$19.9K	
PURCHASE FABRICATED RINGS (AVG. 307 VEH.)			
MAJOR RING FRAME @ \$ 95.8 /lb		\$309.4K	
60-INCH RING FRAME, 3 SECT @ \$ 79.4 /lb		\$272.0K	
30-INCH RING FRAME, 3 SECT @ \$ 79.4 /lb		\$248.0K	
FASTENERS (HUCK BLIND RIVOT @ \$ 180.2 /lb		\$10.8K	
Average Cost of 2 Tanks (1 Vehicle)	\$3,831K	\$3,019.2K	\$2,716.3K
Average Cost of 1 Tank	\$1,915.4K	\$1,509.6K	\$1,358.2K
Total Weight of One Tank	31,306 lbs		
Average Recurring Dollars per Pound for 1 Vehicle	@ \$ 61.2 /lb	@ \$ 48.2 /lb	@ \$ 43.4 /lb

MATERIAL COSTS HAVE BEEN ADJUSTED FROM FY90 TO FY87 \$
 (ESCALATION FACTOR = 1.111 TO GET FROM FY87 TO FY 90)
 AL-LI SHEET = \$12/LB IN FY90, \$10.80/LB IN FY87
 AL-LI SHEET (SPF GRADE) = \$30/LB IN FY90, \$27/LB IN FY87
 AL-LI EXTRUSION = \$20/LB IN FY90, \$18/LB IN FY87

NON-RECURRING ESTIMATE	
TOOLING	
PRESS BRAKE	\$74.5K
DIE	\$2.5K
TOTAL	\$77.0K

* 2 TANKS PER VEHICLE

Table 133. LCC Hours and Cost Information for Brake Formed Stiffened Panels for 2219 Aluminum LH₂ Tank Structure at T1, T307 and T1000.

BRAKE FORMING SUMMARY - 2219					
RECURRING ESTIMATE	# PARTS	Per Part	T1 Hours	AVG. HRS FOR 1 Tank	
			T1 Hours	T307 Hours	T1000 Hours
BRAKE FORM HAT	6	120.0	720.0	353.5	310.7
HAT POST FORM PROCESS	6	112.5	675.0	246.9	202.5
OUTER SKIN	6	101.5	609.0	355.6	322.3
DOUBLERS	6	43.2	259.2	113.5	97.4
FORM BARREL SECTION	6	1152.7	6916.2	2544.5	2090.4
MAJOR CYL ASSY	1	1842.6	1842.6	830.6	717.5
SUBTOTAL			11022.0	4444.7	3740.8
SUPPORT LABOR			5873.5	3804.5	2010.0
TOTAL LABOR HRS			16895.5	8249.2	5750.7

	T1\$ FY'87 \$K	T307\$ FY'87 \$K	T1000\$ FY'87 \$K
LABOR DOLLARS FOR 2 TANKS	\$1,690K	\$825K	\$575K
RADIOGRAPHIC MATL (\$10/HR WELDING)		\$20.39K	
PURCHASE BULKHEAD-\$188K ea		\$752.0K	
PURCHASE SKIN MATL @ \$ 3.1 /lb		\$105.4K	
PURCHASE STIFF MATL (AL Sheet) @ \$ 3.1 /lb		\$63.0K	
PURCHASE SPLICE MATL @ \$ 3.1 /lb		\$6.5K	
PURCHASE FABRICATED RINGS (AVG. 307 VEH.)			
MAJOR RING FRAME @ \$ 95.8 /lb		\$309.4K	
60-INCH RING FRAME, 3 SECT @ \$ 79.4 /lb		\$301.4K	
30-INCH RING FRAME, 3 SECT @ \$ 79.4 /lb		\$276.3K	
FASTENERS (HUCK BLIND RIVOT @ \$ 180.2 /lb		\$10.8K	
Raw Material Weight and Average Cost of 307 Vehicles	\$3,535K	\$2,670.2K	\$2,420.4K
AVERAGE COST OF 614 TANKS*	\$1,767.4K	\$1,335.1K	\$1,210.2K

Total Weight of One Tank	35,576 lbs		
Average Recurring Dollars per Pound for 307 Vehicles	@ \$ 49.7 /lb	@ \$ 37.5 /lb	@ \$ 34.0 /lb

MATERIAL COSTS HAVE BEEN ADJUSTED FROM FY90 TO FY87 \$
(ESCALATION FACTOR = 1.111 TO GET FROM FY87 TO FY 90)
 2219 SHEET = \$3.43/LB IN FY90, \$3.09/LB IN FY87
 7475 SHEET (SPF GRADE) = \$12/LB IN FY90, \$10.80/LB IN FY87
 STD EXTRUSION = \$4.50/LB IN FY90, \$4.05/LB IN FY87

NON-RECURRING ESTIMATE			
TOOLING			
PRESS BRAKE			\$74.5K
DIE			\$2.5K
TOTAL			\$77.0K

* 2 TANKS PER VEHICLE

Table 134. LCC Hours and Cost Information for "T" Extrusion Stiffened Panels for 2090 Aluminum LH₂ Tank Structure at T1, T307 and T1000.

Extrusion SUMMARY - 2090					
RECURRING ESTIMATE	# PARTS	AVG. HRS FOR 1 Tank			
		T1 Hours Per Barrel	T1 Hours	T307 Hours	T1000 Hours
CUT EXTRUSION TO SIZE	6	19.2	115.2	38.2	30.5
HAT POST FORM PROCESS	6	78.7	472.2	156.7	124.8
OUTER SKIN	6	101.8	610.8	356.2	322.8
DOUBLERS	6	43.2	259.2	113.5	97.4
FORM BARREL SECTION	6	1501.1	9006.6	3318.6	2727.4
MAJOR CYL ASSY	1	1842.6	1842.6	830.6	717.5
SUBTOTAL			12306.6	4813.9	4020.4
SUPPORT LABOR			6555.2	4730.1	2158.3
TOTAL LABOR HRS			18861.8	9544.0	6178.8

	T1\$ FY'87 \$K	T307\$ FY'87 \$K	T1000\$ FY'87 \$K
LABOR DOLLARS FOR 2 TANKS	\$1,886K	\$954K	\$618K
RADIOGRAPHIC MATL (\$10/HR WELDING)		\$25.91K	
PURCHASE BULKHEAD-\$188K ea 3707 lbs 2 /Veh		\$752.0K	
PURCHASE SKIN MATL @ \$ 10.8 /lb 14462 lbs 2 /Veh		\$312.4K	
PURCHASE STIFF MATL (EXTRUS @ \$ 18.0 /lb 8990 lbs 2 /Veh		\$323.6K	
PURCHASE DOUBLER MATL @ \$ 10.8 /lb 921 lbs 2 /Veh		\$19.9K	
PURCHASE FABRICATED RINGS(AVG. 307 VEH.)			
MAJOR RING FRAME @ \$ 95.8 /lb 1615 lbs 2 /Veh		\$309.3K	
60-INCH RING FRAME, 3 SECT @ \$ 79.4 /lb 1710 lbs 2 /Veh		\$271.5K	
30-INCH RING FRAME, 3 SECT @ \$ 79.4 /lb 1559 lbs 2 /Veh		\$247.6K	
FASTENERS (HUCKBOLT) @ \$ 131.3 /lb 56 lbs 2 /Veh		\$14.8K	
Average Cost of 2 Tanks (1 Vehicle) 33020 lbs	\$4,163K	\$3,231.5K	\$2,895.0K
Average Cost of 1 Tank	\$2,081.6K	\$1,615.8K	\$1,447.5K
Total Weight of One Tank 31,627 lbs			
Average Recurring Dollars per Pound for 1 Vehicle	@ \$ 65.8 /lb	@ \$ 51.1 /lb	@ \$ 45.8 /lb

MATERIAL COSTS HAVE BEEN ADJUSTED FROM FY90 TO FY87 \$
(ESCALATION FACTOR = 1.111 TO GET FROM FY87 TO FY 90)
AL-LI SHEET = \$12/LB IN FY90, \$10.80/LB IN FY87
AL-LI SHEET (SPF GRADE) = \$30/LB IN FY90, \$27/LB IN FY87
AL-LI EXTRUSION = \$20/LB IN FY90, \$18/LB IN FY87
AL-LI SHEET (SPF GRADE) = \$30/LB IN FY90, \$27/LB IN FY87
AL-LI EXTRUSION = \$20/LB IN FY90, \$18/LB IN FY87

TOOLING	\$2.0K
Extrusion Die	

Table 135. LCC Hours and Cost Information for "T" Extrusion Stiffened Panels for 2219 Aluminum LH₂ Tank Structure at T1, T307 and T1000.

Extrusion SUMMARY - 2219						
RECURRING ESTIMATE	# PARTS	T1 Hours		AVG. HRS FOR 1 Tank		
		Per Barrel	T1 Hours	T307 Hours	T1000 Hours	
CUT EXTRUSION TO SIZE	6	19.8	118.8	39.4	31.4	
HAT POST FORM PROCESS	6	81.0	486.0	131.3	128.4	
OUTER SKIN	6	101.8	610.8	356.2	322.8	
DOUBLERS	6	43.2	259.2	113.5	97.4	
FORM BARREL SECTION	6	1521.4	9128.4	3367.5	2768.6	
MAJOR CYL ASSY	1	1842.6	1842.6	830.6	717.5	
SUBTOTAL			12445.8	4838.5	4066.1	
SUPPORT LABOR			6629.1	4051.6	2182.6	
TOTAL LABOR HRS			19074.9	8890.2	6248.7	
				T1\$ FY'87 \$K	T307\$ FY'87 \$K	T1000\$ FY'87 \$K
LABOR DOLLARS FOR 2 TANKS				\$1,907K	\$889K	\$625K
RADIOGRAPHIC MATL (\$10/HR WELDING)					\$25.91K	
PURCHASE BULKHEAD-\$188K ea	4106 lbs	2 /Veh			\$752.0K	
PURCHASE SKIN MATL @ \$ 3.1 /lb	16912 lbs	2 /Veh			\$104.9K	
PURCHASE STIFF MATL (EXTRUS @ \$ 4.1 /lb	10185 lbs	2 /Veh			\$83.5K	
PURCHASE DOUBLER MATL @ \$ 3.1 /lb	1052 lbs	2 /Veh			\$6.5K	
PURCHASE FABRICATED RINGS(AVG. 307 VEH.)						
MAJOR RING FRAME @ \$ 95.8 /lb	1615 lbs	2 /Veh			\$309.3K	
60-INCH RING FRAME, 3 SECT @ \$ 79.4 /lb	1898 lbs	2 /Veh			\$301.4K	
30-INCH RING FRAME, 3 SECT @ \$ 79.4 /lb	1740 lbs	2 /Veh			\$276.3K	
FASTENERS (HUCKBOLT) @ \$ 131.3 /lb	54 lbs	2 /Veh			\$14.2K	
Average Cost of 2 Tanks (1 Vehicle)	37562 lbs			\$3,782K	\$2,763.1K	\$2,498.9K
Average Cost of 1 Tank				\$1,890.8K	\$1,381.5K	\$1,249.5K
Total Weight of One Tank	35,970 lbs					
Average Recurring Dollars per Pound for 1 Vehicle				@ \$ 52.6 /lb	@ \$ 38.4 /lb	@ \$ 34.7 /lb
MATERIAL COSTS HAVE BEEN ADJUSTED FROM FY90 TO FY87 \$ (ESCALATION FACTOR = 1.111 TO GET FROM FY87 TO FY 90) AL-LI SHEET = \$12/LB IN FY90, \$10.80/LB IN FY87 AL-LI SHEET (SPF GRADE) = \$30/LB IN FY90, \$27/LB IN FY87 AL-LI EXTRUSION = \$20/LB IN FY90, \$18/LB IN FY87 AL-LI SHEET (SPF GRADE) = \$30/LB IN FY90, \$27/LB IN FY87 AL-LI EXTRUSION = \$20/LB IN FY90, \$18/LB IN FY87						
TOOLING					\$2.0K	
Extrusion Die						

Table 136. LCC Hours and Cost Information for Integrally Stiffened Machined Panels for 2219 Aluminum LH₂ Tank Structure at T1, T307 and T1000.

Machined Summary - 2219						
RECURRING ESTIMATE	# PARTS	T1 Hours Per Part	AVG. HRS FOR 1 Tank			
			T1 Hours	T307 Hours	T1000 Hours	
OUTER SKIN		3	7,580	6,155	6,009	
FORM BARREL SECTION		3	7,580	1,348	111	
MAJOR CYL ASSY		1	2,527	1,417	1,273	
SUBTOTAL			17687.6	8919.6	7393.2	
SUPPORT LABOR			9410.5	7278.5	3948.0	
TOTAL LABOR HRS			27098.1	16198.1	11341.3	
				T1\$ FY'87 \$K	T307\$ FY'87 \$K	T1000\$ FY'87 \$K
LABOR DOLLARS FOR 2 TANKS				\$2,710K	\$1,619.8K	\$1,134K
RADIOGRAPHIC MATL (\$10/HR WELDING)					\$7.3K	
PURCHASE BULKHEAD-\$120K ea		4106 lbs	2 /Veh		\$480.0K	
PURCHASE SKIN MATL @ \$ 3.1 /lb		95908 lbs	2 /Veh		\$594.6K	
PURCHASE FABRICATED RINGS (AVG. 307 VEH.)						
MAJOR RING FRAME @ \$ 95.8 /lb		646 lbs	2 /Veh		\$123.8K	
60-INCH RING FRAME, 3 SECT @ \$ 79.4 /lb		2989 lbs	2 /Veh		\$474.7K	
30-INCH RING FRAME, 3 SECT @ \$ 79.4 /lb		1827 lbs	2 /Veh		\$290.1K	
FASTENERS (HUCK RIVOT) @ \$ 131.3 /lb		75 lbs	2 /Veh		\$19.7K	
Average Cost of 2 Tanks (1 Vehicle)				\$4,225K	\$3,610.0K	\$2,649.6K
Average Cost of 1 Tank				\$2,112.6K	\$1,805.0K	\$1,324.8K
Total Weight of One Tank			32,356 lbs			
Average Recurring Dollars per Pound for 1 Vehicle				@ \$ 65.3 /lb	@ \$ 55.8 /lb	@ \$ 40.9 /lb
MATERIAL COSTS HAVE BEEN ADJUSTED FROM FY90 TO FY87 \$ (ESCALATION FACTOR = 1.111 TO GET FROM FY87 TO FY 90) 2219 SHEET= \$3.43/LB IN FY90, \$3.09/LB IN FY87						
NON-RECURRING ESTIMATE						
TOOLING					\$3.0K	
CREATE NC MACHINE TAPE (60 HRS)					\$7.0K	
FABRICATE VACUUM CHUCK (140 HRS)					\$10.0K	
TOTAL						
* 2 TANKS PER VEHICLE						
** AVERAGE TANK FAB HOURS FOR 614 TANKS(307 BOOSTERS, 307 CORES)						

Table 137. Summary of Cost Trade Analysis.

Fabrication Method - Material	T1 Dollars	T307 Dollars	T1000 Dollars
Built-Up Structures			
Superplastic Forming Al-Li	3,563,000	2,922,100	2,603,200
Superplastic Forming Al	3,039,000	2,610,300	2,321,600
Brake Forming Al-Li	3,831,000	3,019,200	2,716,300
Brake Forming Al	3,535,000	2,670,200	2,420,400
Extrusion Al-Li	4,163,000	3,231,500	2,895,000
Extrusion Al	3,782,000	2,763,100	2,498,900
Integrally Machined Al	4,225,000	3,610,000	2,649,600

In summary, the built-up approach can provide significant cost savings over conventionally machined cryogenic tank structure. This analysis was performed with standard manufacturing methods and realistic data inputs. It is believed that the aluminum-lithium family of materials can provide additional benefits to an NLS type vehicle by reducing overall structural weight. Additional cost savings can be realized with utilization of alternative fabrication methods for cryogenic tank structure.

Table 138. Summary of Weight Analysis.

Fabrication Method - Material	Structural Weight (Lbs)
Built-Up Structures	
Superplastic Forming Al-Li	28,836
Superplastic Forming Al	32,505
Brake Forming Al-Li	31,306
Brake Forming Al	35,576
Extrusion Al-Li	31,627
Extrusion Al	35,970
Integrally Machined Al	32,356

Table 139. Predicted LCC Behavior.

Fabrication Method - Material	T1 Dollars	T307 Dollars	T1000 Dollars
Built-Up Structures			
Superplastic Forming Al-Li	2,507,000	1,866,100	1,547,200
Superplastic Forming Al	3,486,000	2,655,000	2,366,300
Brake Forming Al-Li	3,516,000	2,704,200	2,401,300
Brake Forming Al	4,501,000	3,636,200	3,386,400
Extrusion Al-Li	3,944,300	3,012,800	2,676,300
Extrusion Al	4,866,200	3,847,300	3,583,100
Integrally Machined Al	4,225,000	3,610,000	2,649,600

Table 140. Cost Savings or Penalties for Cryogenic Tank Structures Versus the Integrally Machined Concept.

Fabrication Method - Material	T1 Savings	T307 Savings	T1000 Savings
Built-Up Structures			
Superplastic Forming Al-Li	40.7 %	48.3 %	41.6 %
Superplastic Forming Al	17.5 %	26.5 %	10.7 %
Brake Forming Al-Li	16.8 %	25.1 %	9.4 %
Brake Forming Al	(6.5 %)	(0.7 %)	(27.8 %)
Extrusion Al-Li	6.6 %	16.5 %	1 %
Extrusion Al	(15.2 %)	(6.6 %)	(35.7 %)
Integrally Machined Al	0	0	0

4.7 AUTOMATION AND SCALE-UP

Investigations into automation of the fabrication process for NLS cryogenic tanks were limited to planning the type of facilities that could be most cost-effective for the nation. An automated fabrication cell for superplastic forming (refer to Figures 290 through 293) could be included in the plan that would eliminate the requirement for digging a large pit (which would eliminate the concern of toxic waste entering into the ground through hydraulic fluid leaks, and lower maintenance and installation costs). This above ground forming concept has been studied at Rockwell for several years and is the recommendation for re-facilitization efforts. The automated fabrication well would provide for automatic loading of a part blank, forming, part removal and

quenching (air quench if aluminum-lithium materials are to be utilized). The parts would be loaded immediately after forming into a cleaning and heat treatment carousel after which time it would be trimmed and welded onto the outer skins (refer to Figure 294). The welded panels would then be joined into barrel sections (refer to Figure 295) and finally into cryogenic tank structure. The preliminary plan would utilize existing facilities where available (or modify existing facilities if possible) in order to minimize any re-facilitization costs.

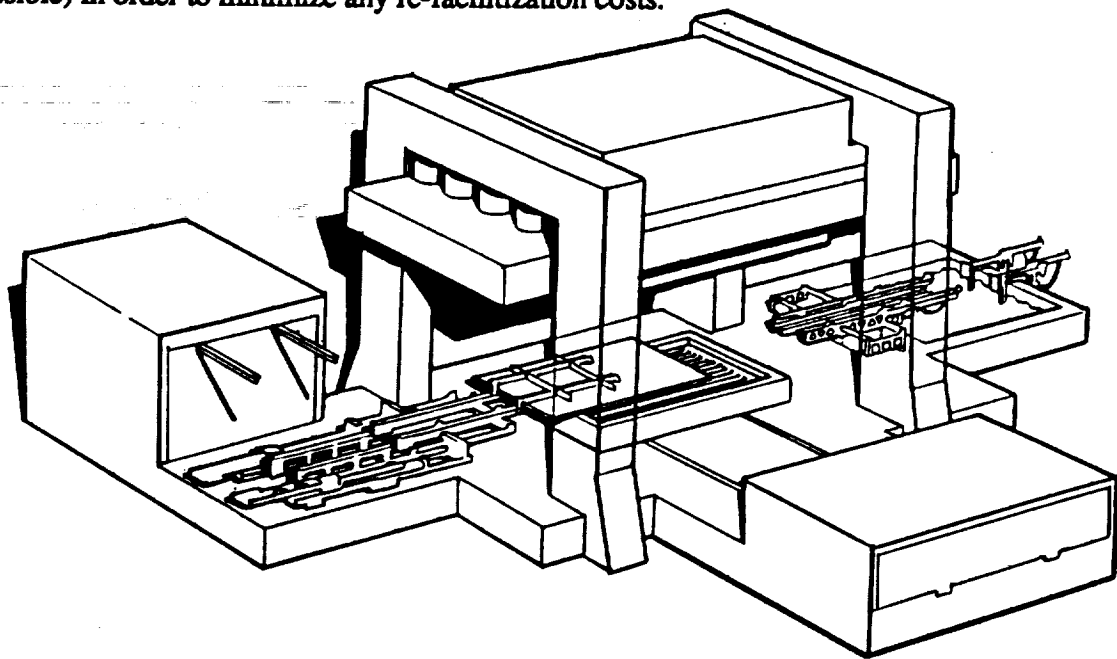


Figure 290. Hot Loading Part Blank into Automated SPF Press.

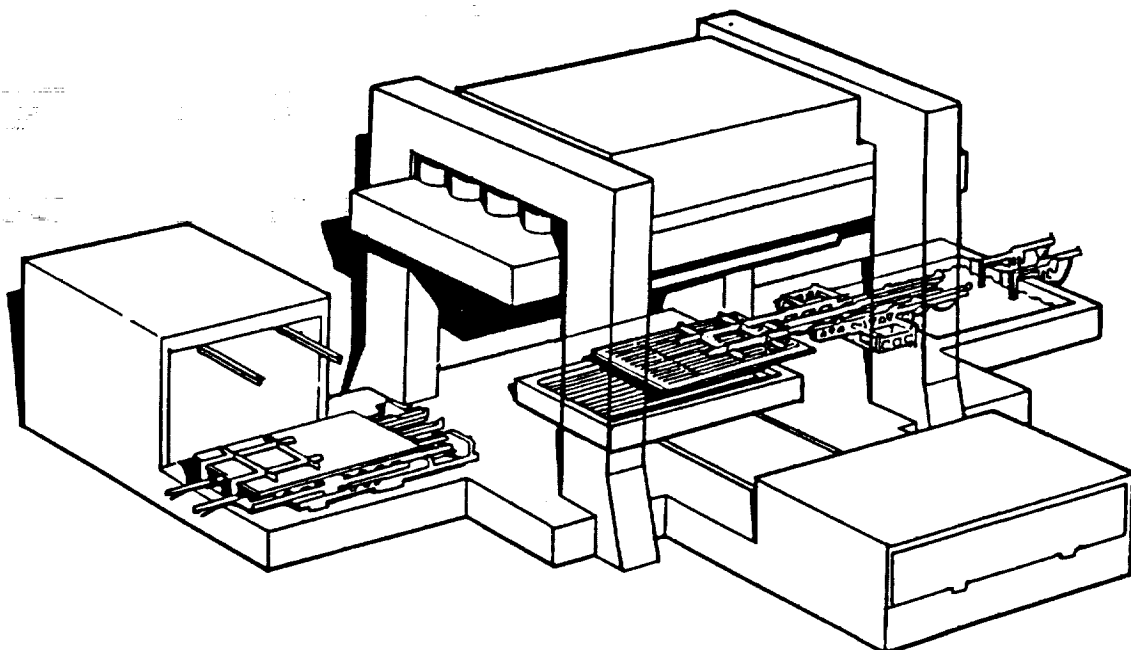


Figure 291. Hot Unloading Part.

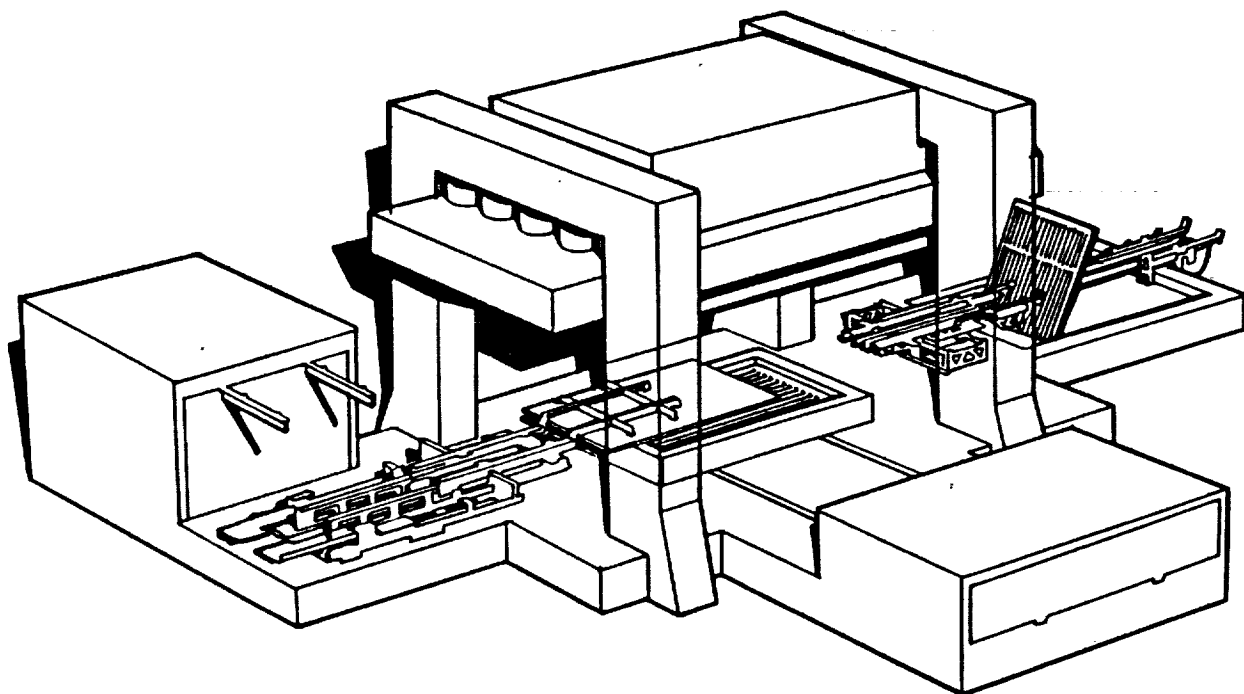


Figure 292. Hot Loading of Blank and Quench of Formed Part.

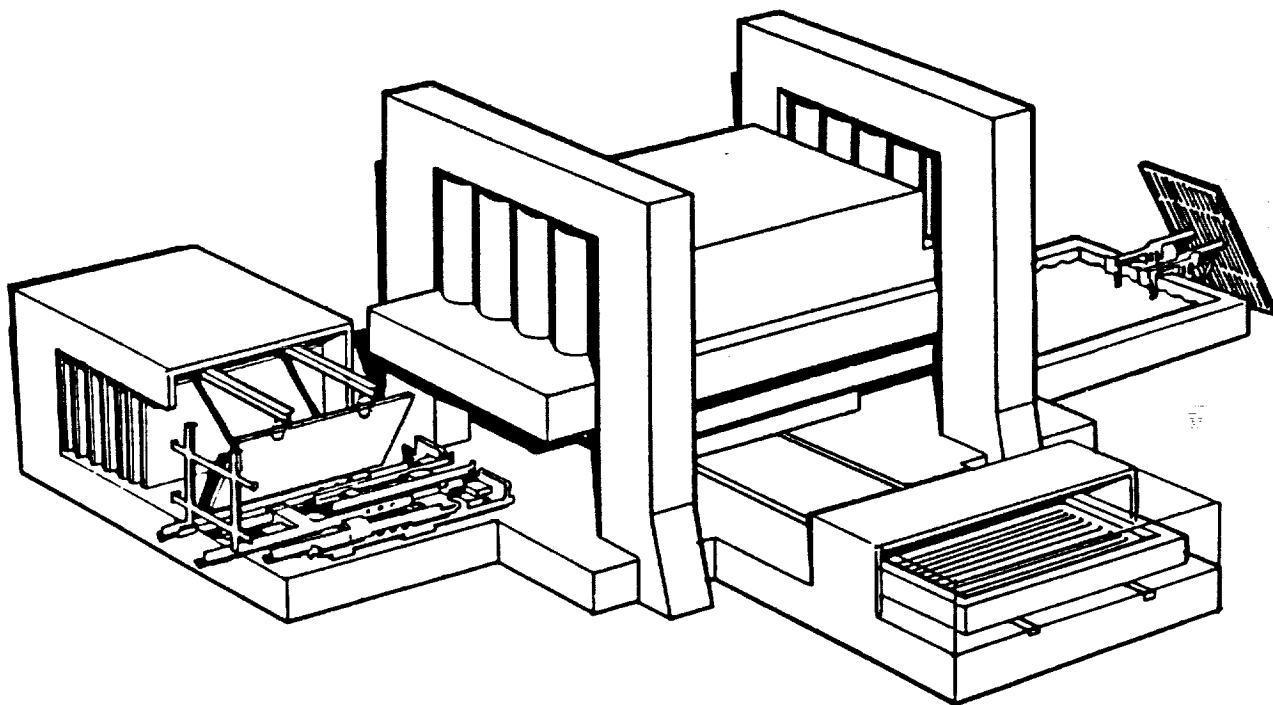


Figure 293. Forming Blank and Loading Part for Thermal Processing.

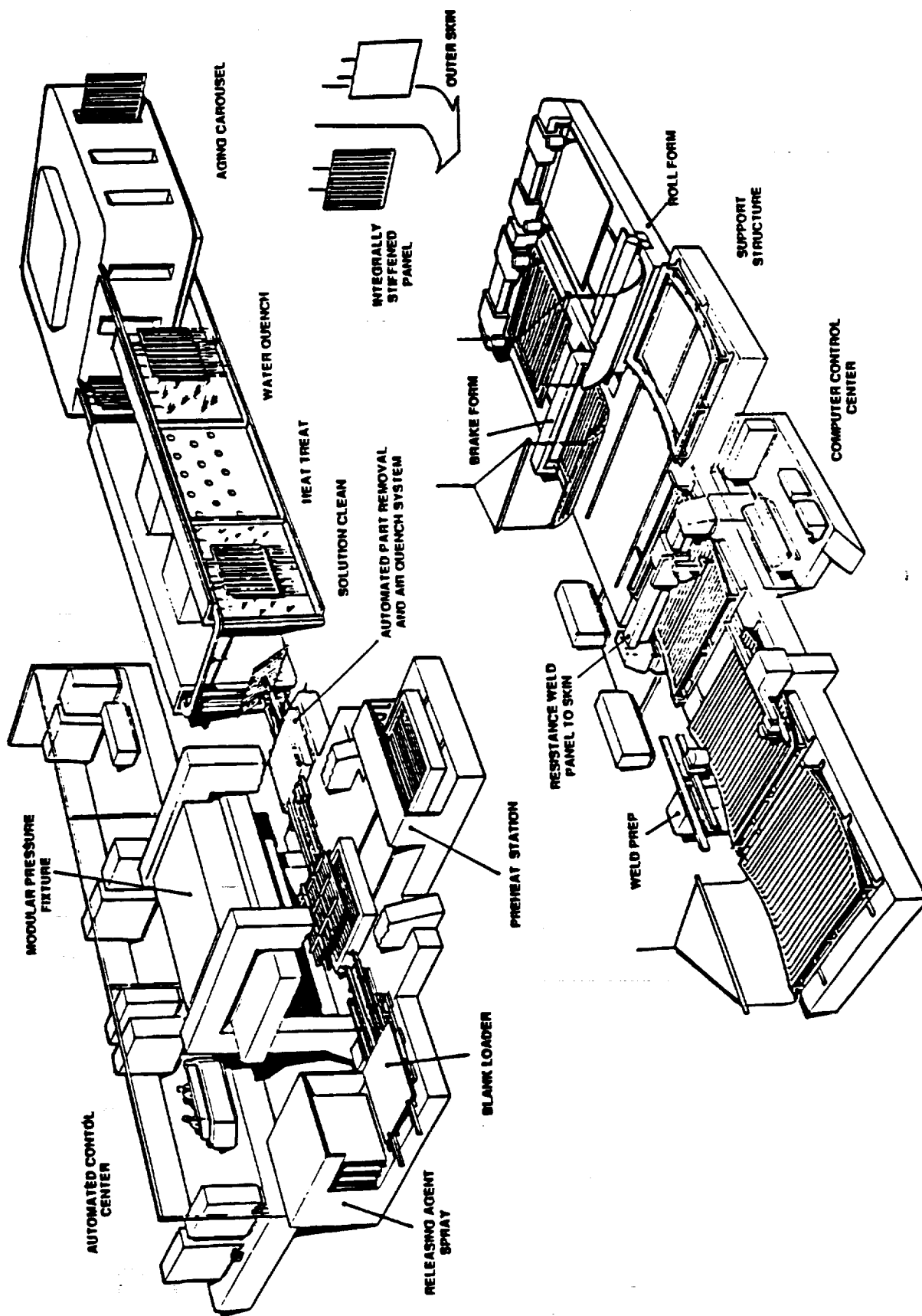


Figure 294. Heat Treatment, Trimming and Welding of Stiffened Panel to Outer Skin.

NLS TANK MANUFACTURING CONCEPT

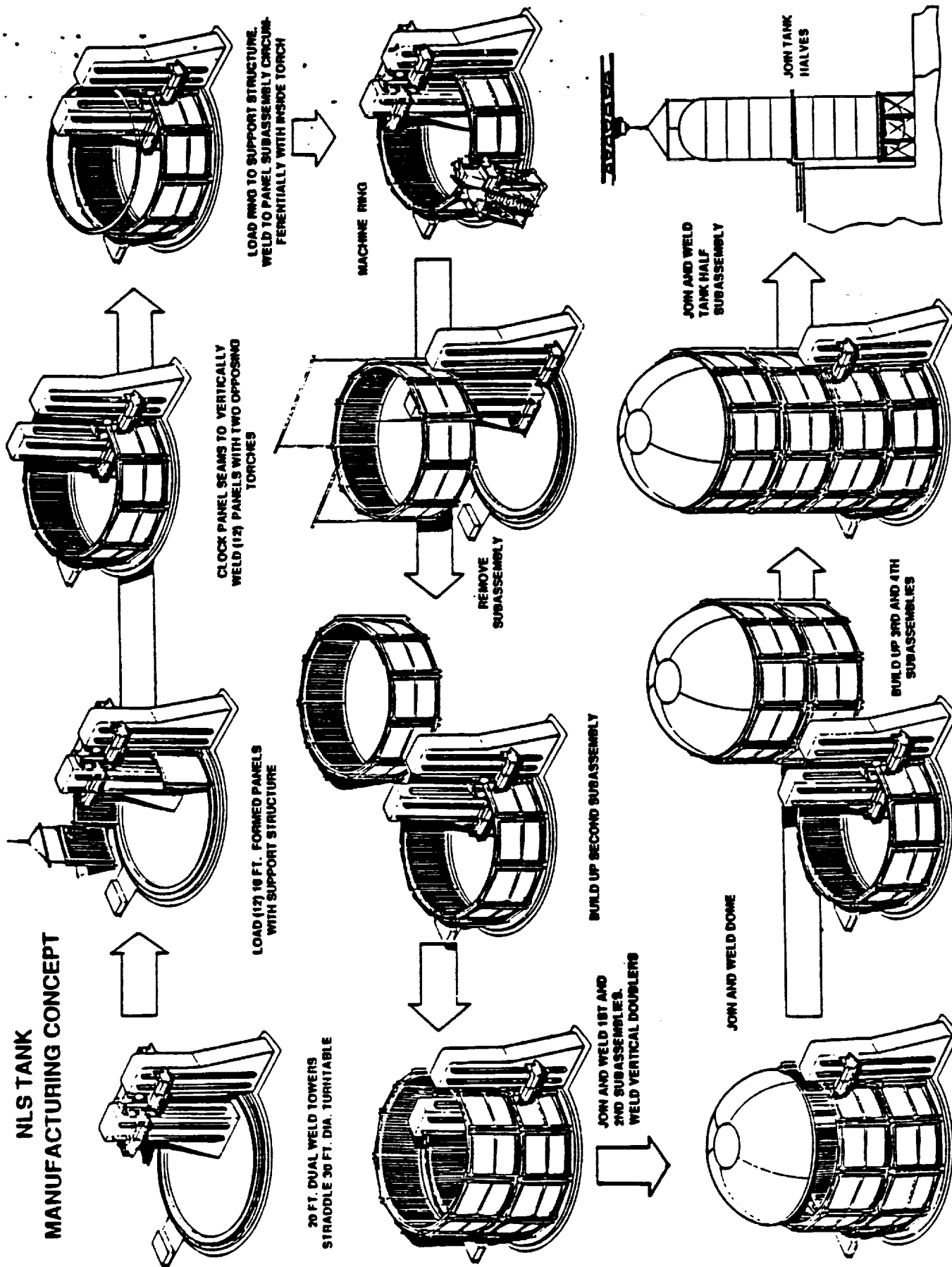


Figure 295. Assembly of Cryogenic Tank.

5.0 REFERENCES

- 1 General Dynamics, "Baseline ALS Loads", August 1989.
- 2 Anton, C.E., Monthly Status Report NAS1-18590-Task 5, NA-89-1270-4, September 1989.
- 3 Anton, C.E., Monthly Status Report NAS1-18590-Task 5, NA-89-1270-4, September 1989.
- 4 MIL-HDBK-5E, "Metallic Materials and Elements for Aerospace Vehicle Structures", Naval Publications and Forms Center, 1986, 8-133.
- 5 Qualitative Trade Study Developed under Air Force Flight Dynamics Laboratory Contract F333615-87-C-3223, Final Report.
- 6 Bushness, David, and Panda, Z., "Program for Minimum Weight Design of Stiffened Panels", Lockheed Research Laboratory, 1986.
- 7 Anderson, Melvin, and Stroud, W. Jefferson, "PASCO: Structural Panel Analysis and Sizing Code", NASA Technical Memorandum 80181, January 1980.
- 8 Davis, Randall, Royster, D., and Bales, Thomas, "Analysis and Test of Supercritical Formed Titanium Hat-Stiffened Panels Under Compression", NASA Technical Memorandum 88989, January 1987.29
- 9 Davis, Randall, Mills, Charles, Prabhakaran, R., and Jackson, L. Robert, "Structural Efficiency Studies of Corrugated Compression Panels With Curved Caps and Beaded Webs", NASA TP 2272, February 1984.
- 10 Davis, Randall, "Beaded (0.25 R) Sine Wave A&D Matrix Using PASCO", May 1990.
- 11 Davis, Randall, "3-Layer Program to Determine Moduli and Layer Thickness for PASCO Input", May 1990.
- 12 ASTM G85-85, "Standard Practice for Modified Salt Spray (Fog) Testing", 1990 Annual Book of ASTM Standards, Pages 357-361.
- 13 ASTM G44-88, "Standard Practice for Evaluating Stress Corrosion Cracking Resistance of Metals and Alloys by Alternate Immersion in 3.5% Sodium Chloride Solution", 1988 Annual Book of ASTM Standards, Pages 166-169.
- 14 Sprowls, D.O., Bucci, R.J., Ponchel, B.M., Brazill, R.L., and Bretz, P.E., "A Study of Environmental Characterization of Conventional and Advanced Aluminum Alloys for Selection and Design", NAS1-16424, NASA Langley Research Center, Hampton, VA, August, 1984.
- 15 C. E. Anton and G. R. Martin, "Superplastic Formed Aluminum-Lithium Aircraft Structures," WRDC-TR-90-3015, Flight Dynamics Laboratory, Wright Research and Development Center, Wright-Patterson Air Force Base, Ohio, June 1990.
- 16 R. D. Tucker, Master's Thesis, Washington State University, (1989).
- 17 B. Ren, C. H. Hamilton and B. A. Ash, "An Approach to Rapid SPF of an Al-Li-Cu-Zr Alloy," Fifth International Aluminum-Lithium Conference, (1989), 131-139.
- 18 B. Ash and C. H. Hamilton, "Factors Affecting Superplastic Stability in an Al-Li-Cu-Zr Alloy," Superplasticity and Superplastic Forming, (1988), 239-244.
- 19 B. A. Ash and C. H. Hamilton, "Strain and Strain Rate Hardening Characteristics of a Superplastic Al-Zr-Cu-Zr Alloy," Scripta Metallurgica, 22, (1988), 277-282.
- 20 C. H. Hamilton, B. A. Ash, D. Sherwood and H. C. Heikkinen, "Effect of Microstructural Dynamics on Superplasticity in Al Alloys," Superplasticity in Aerospace, (1988), 29-50.
- 21 P. G. Partridge, "Oxidation of Aluminum-Lithium Alloys in the Solid and Liquid States," International Materials Reviews, 35(1), (1990), 37-58.

REFERENCES (CONTINUED)

- 22 R.J. Bucci, R.C. Malcolm, E.L. Colvin, S.J. Murtha, and R.S. Hames, "Cooperative Test Program for the Evaluation of Engineering Properties of Al-Li Alloy 2090-T8X Sheet, Plate, and Extrusion Products", NSWC TR 89-106, Naval Surface Warfare Center, Dahlgren, VA, September, 1989, 13-14.
- 23 A. J. Shakesheff, D. S. McDermid and P. J. Gregson, "Effects of Cooling Rate and Copper Content on the Properties of Al-Li-Mg-Zr Alloy 8090," Materials Letters, 7(9,10), (1989), 17-22.
- 24 J. T. Staley and R. D. Doherty, "Quench Sensitivity of an Al-Cu-Li Alloy Plate," Fifth International Aluminum-Lithium Conference, (1989), 345-354.
- 25 J. M. Galbraith, M. H. Tosten and P. R. Howell, "On the Precipitation of Theta Prime and T1 on Al₃Zr Precipitates in Al-Li-Cu-Zr Alloys," Journal of Materials Science, 22, (1987), 27-36.
- 26 F. W. Gayle and J. B. Vander Sande, "'Composite' Precipitates in an Al-Li-Zr Alloy," Scripta Metallurgica, 18, (1984), 473-478.
- 27 E. Nes, "Precipitation of the Metastable Cubic Al₃Zr-Phase in Subperitectic Al-Zr Alloys," Acta Metallurgica, 20, (1972), 499-506.
- 28 E. Nes, "Continuous Recrystallization and Grain Growth During Superplastic Flow," Superplasticity, (1985), 7.1-7.14.

APPENDIX A
PASCO INPUT

Typical PASCO Input for 2090 Al-Li Beaded Hat Stiffener Concept.

Regular Hat with Beaded Web - HA15 - 2090 Hat, 2090 Skin - Measured

\$CONDATS

\$PANEL

B = 0.3, 3.9, 0.65, 3*.718022, 1.0, 1.0, 0.3713907,

T = -0.0775, 0.030, 0.090, 0.045, 0.040,

THET = 5*0.0,

MAT(1,1) = 1,

MAT(2,1) = 1,

MAT(3,1) = 2,

MAT(4,1) = 3,

MAT(5,1) = 1,

KWALL(1,1) = 1, 2,

KWALL(1,2) = 1,

KWALL(1,3) = 2,

KWALL(1,4) = 3, 4,

KWALL(1,5) = 3, 4,

KWALL(1,6) = 3, 4,

KWALL(1,7) = 5,

IWALL = 1, 2, 3, 4, 5, 6, 7, 1, 1,

HCARD = 4, -11, 4, -9, 8,

4, -12, 5, -9, 8,

4, -13, 6, -9, 8,

4, -14, 6, 9, 8,

4, -15, 5, 9, 8,

4, -16, 4, 9, 8,

10, 20, 3, 11, 12, 13, 7, 14, 15, 16, 3,

5, 30, 1, 2, -20, 1,

ICARD = 5, 1, 2, 1, -990, 9000,

5, 2, 11, 2, 3, 3,

3, 3, 4, 11,

3, 4, 5, 12,

3, 5, 6, 13,

3, 6, 7, 7,

3, 7, 8, 14,

3, 8, 9, 15,

3, 9, 10, 16,

3, 10, 11, 3,

3, 11, 12, 1,

3, 12, -990, 9000,

EL = 15.0, IP = -2, JPRINT = 1, MAXJJJ = 0

MINLAM = 15, NOBAY = 1, FSTIFF = 1.0, NLAM(1) = 5, 7, 9, 11, 13, 15,

NX(1) = 10000,

NY(1) = 0,

NXY(1) = 0,

\$

\$MATER

E1(1) = 11.5 E6, E2(1) = 11.5 E6, E12(1) = 4.4 E6, ANU1(1) = 0.33, RHO(1) = 0.094,

E1(2) = 2.41 E4, E2(2) = 3.23 E6, E12(2) = 3.25 E5, ANU1(2) = 0.0, RHO(2) = 0.017,

E1(3) = 2.11 E4, E2(3) = 1.07 E6, E12(3) = 8.11 E5, ANU1(3) = 0.0, RHO(3) = 0.017,

ALLOW(1,1) = 1, 60.0 E3, -63.0 E3, 60.0 E3, -63.0 E3, 35.0 E3,

ALLOW(1,2) = 1, 50.0 E3, -60.0 E3, 50.0 E3, -60.0 E3, 29.0 E3,

ALLOW(1,3) = 1, 50.0 E3, -60.0 E3, 50.0 E3, -60.0 E3, 29.0 E3,

\$

APPENDIX B
PASCO OUTPUT

PASCO Output for Crippling Stiffener Panel

PPPP
PPPP
PPPP

1

0 THE LENGTH OF COMMON /BL57 = 10209 DECIMAL OR 023741 DCTAL

TIME IN SECONDS = 59.279

LOADFU= 33472
IXMBC= 13711

IN THE FOLLOWING--

ASTERISKS PRINTED FOR DL, TL, AND THEYL INDICATE THE ASSOCIATED DIMENSION IS NOT A DESIGN VARIABLE

THE INTEGER SUBSCRIPTS HAVE THE FOLLOWING MEANINGS:

- I REFERS TO PLATE
- IV REFERS TO WALL NUMBER
- J REFERS TO GENERAL LAYER J
- K REFERS TO THE KTH LAYER IN A GIVEN WALL
- L REFERS TO A LOAD CASE L
- N REFERS TO AXIAL HALF-WAVE NUMBER
- MA REFERS TO MATERIAL MA
- N REFERS TO EQUATION NUMBER N LINKING VARIABLES

PLATE ELEMENT WIDTHS

VARIABLE NO.	BC(I)	LOWER BOUND BL(I)	UPPER BOUND BU(I)	WALL NO.	VIPASA PLATE NO.	FRYCTI	FRYCTI
1	.300000	*****	-.100000E+11	1	1	0.000000	0.000000
2	3.900000	*****	-.100000E+11	2	2	0.000000	0.000000
3	.500000	*****	-.100000E+11	3	3	0.000000	0.000000
4	1.096586	*****	-.100000E+11	4	4	0.000000	0.000000
5	.150000	*****	-.100000E+11	5	5	0.000000	0.000000
6	1.096586	*****	-.100000E+11	6	6	0.000000	0.000000
7	.800000	*****	-.100000E+11	7	7	0.000000	0.000000
8	1.000000	*****	-.100000E+11	8	8	0.000000	0.000000
9	.410365	*****	-.100000E+11	9	9	0.000000	0.000000

LAYER CHARACTERISTICS

7 6

ICARD

5 1 2 1 -990 9000

5 2 11 2 3 3

3 3 4 11

3 4 5 5

3 5 6 12

3 6 7 7

3 7 8 14

3 8 9 5

3 9 10 13

3 10 11 3

3 11 12 1

3 12 -990 9000

MATERIAL PROPERTIES(ORTHOTROPIC ONLY)

E1(MA)	E2(MA)	E12(MA)	ANUI(MA)	RHO(MA)	ALFA1(MA)	ALFA2(MA)
.105000E+08	.105000E+08	.400000E+07	.330000E+00	.192000E+00	0.	0.
.100000E+08	.100000E+08	.380000E+07	.330000E+00	.181000E+00	0.	0.

ALLOW(1,MA)	ALLOW(2,MA)	ALLOW(3,MA)	ALLOW(4,MA)	ALLOW(5,MA)	ALLOW(6,MA)	ALLOW(7,MA)
1.0000	50000.0000	-63000.0000	50000.0000	-50000.0000	30000.0000	0.0000
1.0000	64000.0000	-74000.0000	64000.0000	-64000.0000	45000.0000	0.0000

BUCKLING LOAD CALCULATED FOR AT LEAST THE FOLLOWING N NUMBERS

NLAN(M)= 1 5 7 9 11 13 15

WAVE NO. SAFETY FACTOR NUMBER OF EIGENVALUES

CLAN(M) MEIG(M)

1	1.000	1
2	1.000	1
3	1.000	1
4	1.000	1
5	1.000	1
6	1.000	1
7	1.000	1
8	1.000	1
9	1.000	1
10	1.000	1
11	1.000	1

12	1.000	1
13	1.000	1
14	1.000	1
15	1.000	1

ANALYSIS ONLY

BOUNDARY CONDITIONS DETERMINED FROM ICARD INPUT

COMMON CONTROL PARAMETERS

AB08J1	ALPHAX	CTL	CTLMIN	DABFUM	DELFUN	IPRINT	ITMAX	ITAM	LIAOBJ	MICAL	THETA
.10000E+00	.10000E+00	-.10000E-01	.10000E-05	.10000E-05	.10000E-04	1	15	0	0	0	.10000E+01

TIME IN SECONDS AT THE BEGINNING OF THE FINAL VIPASA ANALYSIS IS 39.354

IVIPASA RESULTS

INPUT DEVICE NUMBER IS 7 OUTPUT DEVICE NUMBER IS 6
 OCCURRENT FIELD LENGTH IS 103100

NRK	NSK	NSC	IPAST	NSM	NSK	NOLAN
32	12	10	100	91	0	15

IPLOY	NSPAC	PAGE	AMP
-2	0	0.00	0.00

ADDITION TO BLANK COMMON IS 4111

OCCURRENT FIELD LENGTH IS 113200

NUMBER OF PROBLEMS IS 1

1 DATA FOR PROBLEM NUMBER 1

STEPPED MAT 9.5° WIDE WITH 0.0° CAP - WA15 - 7475 MAT, 2219 SKIN

1	1	500.0	1.00000	0.00000	0.0000	0.0000	0.00000000
15.0000	-1.0000	15.0000	1.0000	0.0	0.000	0.00000000	

THE ABOVE TWO DATA CARDS HAVE THE FOLLOWING MEANING

THE PROBLEM IS TO FIND ALL EIGENVALUES FROM NUMBER 1 DOWN TO NUMBER 1

INCLUSIVE, TO AN ACCURACY OF AT LEAST ONE IN 500.0

THE LENGTH L OF THE STRUCTURE IS 15.00000 AND LAMBDA TAKES

SUCCESSIVE VALUES IN THE SERIES L/1, L/2, L/3... STARTING AT L/ 1

AND STOPPING AT L/ 15
 MODES ARE FOUND AT ALL EIGENVALUES
 THE NUMBERS OF PLATES DEFINED IN SIMPLIFIED WAY, OF PLATES DEFINED IN
 GENERAL WAY, INDICATOR OF GENUINE SPRING SUPPORTS, NUMBERS OF
 SUB-STRUCTURES AND OF CARDS DEFINING FINAL STRUCTURE ARE, RESPECTIVELY,
 0 0 0 6 12

IG= 3 IFAST= 2 IEP= 1
 THE FIXED LONGITUDINAL STRAIN IS 0.000000
 THE VARIABLE LONGITUDINAL STRAIN IS 1.000000
 EIGENVALUE DETERMINED ONLY IF LESS THAN THAT FOR PREVIOUS LAMBDA
 CONVERGENCE MAY NOT BE OBTAINED IF THERE ARE NEGATIVE ROOTS AT FACTOR=0

MATERIAL INPUT

MATERIAL	E1	E2	E12	NU1	KMO	ALFA1	ALFA2
1	.105E+00	.105E+00	.400E+07	.330E+00	.102E+00	0.	0.
2	.100E+00	.100E+00	.300E+07	.330E+00	.101E+00	0.	0.

1 B-6

WALL NUMBER 1

MAT	Y	THET	TEM
1	.0775000	0.00000	0.00000
2	.0310000	0.00000	0.00000
2	.0310000	0.00000	0.00000
1	.0775000	0.00000	0.00000

ZREF FOR WALL NO. 1= .1005E+00

MASS PER UNIT AREA OF WALL NO. 1= .2207E-01

A-MATRIX FOR WALL NO. 1 D-MATRIX FOR WALL NO. 1 CIT

.2522E+07	.0323E+06	0.	.1002E+05	.3307E+04	0.
.0323E+06	.2522E+07	0.	.3307E+04	.1002E+05	0.
0.	0.	.0556E+06	0.	0.	.3402E+00

LAMINATE PROPERTIES

	E1	E2	E12	NU1	NU2	ALFA1	ALFA2
1	-103571E+00	-103571E+00	-394206E+07	-3300000	-3300000	0.	0.

WALL NUMBER 2

MAT	T	THEY	TER
-----	---	------	-----

1	-0775000	0.00000	0.00000
1	-0775000	0.00000	0.00000

ZREF FOR WALL NO. 2= -7750E-01

MASS PER UNIT AREA OF WALL NO. 2= -1501E-01

A-MATRIX FOR WALL NO. 2 D-MATRIX FOR WALL NO. 2 CIT

-1026E+07	-6027E+06	0.	-3657E+04	-1207E+04	0.
-6027E+06	-1026E+07	0.	-1207E+04	-3657E+04	0.
0.	0.	-6200E+06	0.	0.	-1207E+04

LAMINATE PROPERTIES

	E1	E2	E12	NU1	NU2	ALFA1	ALFA2
1	-103000E+00	-103000E+00	-400000E+07	-3300000	-3300000	0.	0.

WALL NUMBER 3

MAT	T	THEY	TER
-----	---	------	-----

2	-0310000	0.00000	0.00000
2	-0310000	0.00000	0.00000

ZREF FOR WALL NO. 3= -3100E-01

MASS PER UNIT AREA OF WALL NO. 3= -6262E-02



A-MATRIX FOR WALL NO. 3 D-MATRIX FOR WALL NO. 3 CIT

.6958E+06 .2296E+06 0. .2229E+03 .7355E+02 0. 0.
 .2296E+06 .6958E+06 0. .7355E+02 .2229E+03 0. 0.
 0. 0. .2356E+06 0. 0. .7547E+02 0. 0.

E1 E2 E12 LAMINATE PROPERTIES MUI MUI2 ALFA1 ALFA2
 1 .10000E+08 .10000E+08 .38000E+07 .338000 .330000 0. 0.

WALL NUMBER 4

MAT	T	THET	TEN
2	.931000	0.0000	0.0000
2	.931000	0.0000	0.0000

ZREF FOR WALL NO. 4= .3188E-01

MASS PER UNIT AREA OF WALL NO. 4= .6262E-02

A-MATRIX FOR WALL NO. 4 D-MATRIX FOR WALL NO. 4 CIT

.6958E+06 .2296E+06 0. .2229E+03 .7355E+02 0. 0.
 .2296E+06 .6958E+06 0. .7355E+02 .2229E+03 0. 0.
 0. 0. .2356E+06 0. 0. .7547E+02 0. 0.

E1 E2 E12 LAMINATE PROPERTIES MUI MUI2 ALFA1 ALFA2
 1 .10000E+08 .10000E+08 .38000E+07 .338000 .330000 0. 0.

WALL NUMBER 5

MAT	T	THET	TEN
2	.931000	0.0000	0.0000
2	.931000	0.0000	0.0000

ZREF FOR WALL NO. 5= .3100E-01

MASS PER UNIT AREA OF WALL NO. 5= .6262E-02

A-MATRIX FOR WALL NO. 5 U-MATRIX FOR WALL NO. 5 CITY

.6950E+06	.2296E+06 0.	.2229E+03	.7355E+02 0.	0.
.2296E+06	.6950E+06 0.	.7355E+02	.2229E+03 0.	0.
0.	0.	.2356E+06 0.	0.	.7547E+02 0.

E1	E2	E12	MU1	MU2	ALFA1	ALFA2
.100000E+08	.100000E+08	.300000E+07	.330000	.330000 0.	0.	0.

WALL NUMBER 6

WALL NUMBER 6

2	.231000	0.0000	0.0000
2	.031000	0.0000	0.0000

ZREF FOR WALL NO. 6= .3100E-01

MASS PER UNIT AREA OF WALL NO. 6= .6262E-02

A-MATRIX FOR WALL NO. 6 U-MATRIX FOR WALL NO. 6 CITY

.6950E+06	.2296E+06 0.	.2229E+03	.7355E+02 0.	0.
.2296E+06	.6950E+06 0.	.7355E+02	.2229E+03 0.	0.
0.	0.	.2356E+06 0.	0.	.7547E+02 0.

E1	E2	E12	MU1	MU2	ALFA1	ALFA2
.100000E+08	.100000E+08	.300000E+07	.330000	.330000 0.	0.	0.

WALL NUMBER 7

WALL NUMBER 7

MAT		I		THEY		TEN	
2		.0350000		0.00000		0.00000	
2		.0350000		0.00000		0.00000	
ZREF FOR WALL NO. 7= .3500E-01							
MASS PER UNIT AREA OF WALL NO. 7= .7070E-02							
A-MATRIX FOR WALL NO. 7				D-MATRIX FOR WALL NO. 7			
.7855E+06		.2592E+06 0.		.3200E+03		.1859E+03 0.	
.2592E+06		.7855E+06 0.		.1859E+03		.3200E+03 0.	
0.		.2650E+06 0.		0.		.1000E+03 0.	
LAMINATE PROPERTIES							
E1		E2		E12		NU1	
.100000E+08		.100000E+08		.300000E+07		.3300000	
1				NU2		ALFA1	
				.3300000 0.		0.	
ALFA2							
0.							
NEGATIVE WALL NUMBERS INDICATE ANISOTROPIC STIFFNESS TERMS NEGLECTED							
PLATE FORCES ARE FOR UNIFORM AXIAL STRAIN							
PLATE WALL							
NO.		NO.		BREATH		MTV	
1		-1		.30000		0.00	
2		-2		3.90800		0.00	
3		-3		.50000		0.00	
4		-4		1.09659		0.00	
5		-5		.15000		0.00	
6		-6		1.09659		0.00	
7		-7		.80000		0.00	
8		-1		1.00000		0.00	
9		-1		.41836		0.00	
SUB-STRUCTURES ARE DEFINED AS FOLLOWS							
4		-11		4		-9	
4		-12		6		-9	
4		-13		4		9	
4		-14		6		9	
10		20		3		11	
5		30		1		2	
						13	

THE FINAL STRUCTURE IS DEFINED AS FOLLOWS

5 1 2 1-9909000
 5 2 11 2 3 3
 3 3 4 11
 3 4 5 5
 3 5 6 12
 3 6 7 7
 3 7 8 14
 3 8 9 5
 3 9 10 13
 3 10 11 3
 3 11 12 1
 3 12-9909000

OBJ = MASS/(AREA*LENGTH) = .17299E-02
 TOTAL PANEL MASS = .174249E+01
 PANEL WIDTH = .950000E+01

B-11

SHEARED PANEL STIFFNESSES ASSIGNED TO PLATE 33
 A11 A22 A33 D11 D22 D33 ZBAR AM
 -261806E+07 -180332E+07 -835701E+06 -150777E+07 -768769E+04 -977913E+06 -457107E+00 -258147E-01

EIGENVALUES CALCULATED TO AN ACCURACY OF COMVI ARE DETERMINED AS FOLLOWS TO IDENTIFY CRITICAL WAVELENGTHS

ITER	WEIG	LAMBDA	FACTOR	LIMITS ON FACTOR	MX	MY	MAY
11	1	.150000000E+02	-279118177E+01	-279058905E+01	-279286564E+01	-279118E+05	0.
11	1	.750000000E+01	-183316175E+01	-183284028E+01	-183335185E+01	-183316E+05	0.
9	1	.580000000E+01	-139749507E+01	-139689727E+01	-139798186E+01	-139750E+05	0.
8	1	.375000000E+01	-116382115E+01	-116289196E+01	-116456447E+01	-116382E+05	0.
11	1	.300000000E+01	-119932541E+01	-119877677E+01	-120011939E+01	-119933E+05	0.
11	1	.214285714E+01	-165505089E+01	-165412176E+01	-165714633E+01	-165505E+05	0.
17	1	.156666667E+01	-219991835E+01	-219968793E+01	-220350187E+01	-219992E+05	0.
16	1	.136363636E+01	-254039619E+01	-253952290E+01	-254393396E+01	-254040E+05	0.
15	1	.115384615E+01	-281668855E+01	-281378038E+01	-281828964E+01	-281669E+05	0.
15	1	.180000000E+01	-303961356E+01	-303728741E+01	-304161403E+01	-303961E+05	0.

SUMMARY OF CRITICAL WAVELENGTHS AND EIGENVALUES

N	LAMDA	FACTOR
1	15.0000	2.7912
2	3.7500	1.1638
3	3.0000	1.1993
4	2.1429	1.6551
5	1.6667	2.1999
6	1.3636	2.5404
7	1.1538	2.8167
8	1.0000	3.0396

EIGENVALUES FOR CRITICAL WAVELENGTHS ARE NOW CALCULATED TO AN ACCURACY CONV2

ITER	WEIG	LAMBDA	FACTOR	LIMITS ON FACTOR	MX	MY	MNY
18	1	.15000000E+02	.27911810E+01	.27911808E+01	.27911845E+01	U.	U.
17	1	.37500000E+01	.11638218E+01	.11638206E+01	.11638226E+01	U.	U.
19	1	.30000000E+01	.119932691E+01	.119932597E+01	.119932730E+01	U.	U.
17	1	.21285714E+01	.165505674E+01	.165505632E+01	.165505782E+01	U.	U.

PLATE FORCES INCLUDING LATERAL PRESSURE AND IMPERFECTION. BENDING MOMENT= 0.00000000 EVALUATED AT FACTOR= 1.000000

PLATE WALL NO.	BREADTH	MTV	MLV	MSV	0*MLV
1	-1	.30000	8584.59	0.00	2575.38
2	-2	3.90800	6216.43	0.00	24244.07
3	-3	.50900	2368.16	0.00	1104.00
4	-4	1.09659	2368.16	0.00	2596.89
5	-5	.15000	2368.16	0.00	355.22
6	-6	1.09659	2368.16	0.00	2596.89
7	-7	.80000	2673.73	0.00	2138.99
8	-1	1.00800	8584.59	0.00	8584.59
9	-1	.41836	8584.59	0.00	3522.81

PLATE STRAINS AND STRESSES

PLATE LAYER NO	EP1	EP2	EP12	SIG1	SIG2	SIG12
1	.381962E-02	-.125047E-02	U.	.401060E+05	U.	U.
1	.381962E-02	-.126047E-02	U.	.381962E+05	U.	U.

2	1	.381962E-02	-.126047E-02	0.	.401060E+05	.017623E-10	0.
3	2	.381962E-02	-.126047E-02	0.	.381962E+05	.770689E-10	0.
4	3	.381962E-02	-.126047E-02	0.	.381962E+05	.770689E-10	0.
5	4	.381962E-02	-.126047E-02	0.	.381962E+05	.770689E-10	0.
6	5	.381962E-02	-.126047E-02	0.	.381962E+05	.770689E-10	0.
7	6	.381962E-02	-.126047E-02	0.	.381962E+05	.770689E-10	0.
8	1	.381962E-02	-.126047E-02	0.	.401060E+05	0.	0.
8	2	.381962E-02	-.126047E-02	0.	.381962E+05	0.	0.
9	1	.381962E-02	-.126047E-02	0.	.401060E+05	0.	0.
9	2	.381962E-02	-.126047E-02	0.	.381962E+05	0.	0.

LLMM-JJ BUCKLING-LOAD CASE L, AXIAL MODE M, EIGENVALUE J

JJCLII-KKMM STRENGTH-CRITERIA JJ, LOAD CASE L, PLATE NO. I, LAYER NO. K, ALLOW(M)

LLMM STIFFNESS-LOAD CASE L, M=1-2 AXIAL, M=3-4 SHEAR, M=5-6 BENDING, M ODD IS LOWER BOUND, M EVEN IS UPPER BOUND

104.0108	-.16
105.0100	-.20
107.0100	-.66
10101.0102	-.20
10101.0202	-.40
10102.0102	-.20
10103.0202	-.40
10104.0302	-.40
10105.0402	-.40
10106.0502	-.40
10107.0602	-.40
10108.0702	-.20
10108.0202	-.40
10109.0102	-.20
10109.0202	-.40

TIME IN SECONDS AT THE BEGINNING OF PLOTTING IS 64.898

PLATE AND SUBSTRUCTURE COORDINATES

ENTRY Y-CORR. Z-CORR. M



1	0.	0.	-1
2	.30000000E+00	0.	0
3	0.	0.	-2
4	.39000000E+01	0.	0
5	0.	0.	-3
6	.50000000E+00	0.	0
7	0.	0.	-4
8	.10965900E+01	0.	0
9	0.	0.	-5
10	.15000000E+00	0.	0
11	0.	0.	-6
12	.10965900E+01	0.	0
13	0.	0.	-7
14	.00000000E+00	0.	0
15	0.	0.	-8
16	.10000000E+01	0.	0
17	0.	0.	-9
18	.41036000E+00	0.	0
19	0.	0.	-11
20	.45000103E+00	.10000000E+01	0
21	0.	0.	-12
22	.45000103E+00	.10000000E+01	0
23	0.	0.	-13
24	.45000103E+00	.10000000E+01	0
25	0.	0.	-14
26	.45000103E+00	.10000000E+01	0
27	0.	0.	-20
28	.50000000E+00	0.	0
29	.95000103E+00	.10000000E+01	0
30	.10000000E+01	.10000000E+01	0
31	.15500037E+01	.20000000E+01	0
32	.23500037E+01	.20000000E+01	0
33	.28000055E+01	.10000000E+01	0
34	.29500055E+01	.10000000E+01	0
35	.34000073E+01	0.	0
36	.39000073E+01	0.	0
37	0.	0.	-30
38	.30000000E+00	0.	0
39	.42000000E+01	0.	0
40	.30000000E+00	0.	1
41	.00000000E+00	0.	0
42	.12500000E+01	.10000000E+01	0
43	.140000010E+01	.10000000E+01	0

44	.18500037E+01	.20000000E+01	0
45	.26500037E+01	.20000000E+01	0
46	.31000055E+01	.10000040E+01	0
47	.32500055E+01	.10000040E+01	0
48	.37000073E+01	0.	0
49	.42000073E+01	0.	0
50	.42000000E+01	0.	1
51	.45000000E+01	0.	0
52	0.	0.	-990

FINAL STRUCTURE COORDINATES

ENTRY	Y-CORR.	Z-CORR.	M1
1	0.	0.	-1
2	.30000000E+00	0.	0
3	.30000000E+00	0.	-2
4	.30000000E+00	0.	-2
5	.42000000E+01	0.	0
6	.42000000E+01	0.	-11
7	.30000000E+00	0.	-2
8	.80000000E+00	0.	0
9	.80000000E+00	0.	-3
10	.80000000E+00	0.	-3
11	.12500010E+01	.10000040E+01	0
12	.12500010E+01	.10000040E+01	-4
13	.12500010E+01	.10000040E+01	-4
14	.14000010E+01	.10000040E+01	0
15	.14000010E+01	.10000040E+01	-5
16	.14000010E+01	.10000040E+01	-5
17	.18500037E+01	.20000000E+01	0
18	.18500037E+01	.20000000E+01	-6
19	.18500037E+01	.20000000E+01	-6
20	.26500037E+01	.20000000E+01	0
21	.26500037E+01	.20000000E+01	-7
22	.26500037E+01	.20000000E+01	-7
23	.31000055E+01	.10000040E+01	0
24	.31000055E+01	.10000040E+01	-8
25	.31000055E+01	.10000040E+01	-8
26	.32500055E+01	.10000040E+01	0
27	.32500055E+01	.10000040E+01	-9
28	.32500055E+01	.10000040E+01	-9

29	.37000073E+01	0.	0
30	.37000073E+01	0.	-10
31	.37000073E+01	0.	-10
32	.42000073E+01	0.	0
33	.42000073E+01	0.	-11
34	.42000073E+01	0.	-11
35	.45000073E+01	0.	0
36	.45000073E+01	0.	-12
37	.45000073E+01	0.	-12
38	0.	0.	-901

COORDINATES OF MODES

MODE Y Z

1	0.	0.	
2	.30000000E+00	0.	
3	.80000000E+00	0.	
4	.12500010E+01	.10000000E+01	
5	.14000010E+01	.10000000E+01	
6	.18500037E+01	.20000000E+01	
7	.26300037E+01	.20000000E+01	
8	.31000035E+01	.10000000E+01	
9	.32500035E+01	.10000000E+01	
10	.37000073E+01	0.	
11	.42000073E+01	0.	
12	.45000073E+01	0.	

B-16

LAMBDA= 15.000 EIGENVALUE NO. = 1 EIGENVALUE= 2.791

MODE	THEYA	V	U
1	.481268E-35	.224469E+00	-.132123E-33
2	.252260E-02	.224840E+00	.297004E-04
3	-.100000E+00	.179904E+00	.124128E-03
4	.881655E-02	.173872E+00	.116614E-01
5	.529419E-02	.174732E+00	.114600E-01
6	.585769E-02	.176493E+00	.132611E-02
7	-.585790E-02	.176493E+00	.132593E-02
8	-.529430E-02	.174731E+00	.114599E-01
9	-.881664E-02	.173872E+00	.115614E-01
10	.100000E+00	.179904E+00	-.124121E-03
11	-.252261E-02	.224840E+00	-.297047E-04
12	-.481272E-35	.224469E+00	.132125E-33

LAMBDA= 3.750 EIGENVALUE NO. = 1 EIGENVALUE= 1.164

MODE	THETA	W	V	U
1	.141598E-35	-.404810E-01	.191724E-34	-.483239E-03
2	-.248098E-02	-.408465E-01	-.229878E-04	.527733E-06
3	.100800E+00	.175983E-03	.163882E-03	.116610E-03
4	.363342E-03	.142227E-01	-.301343E-01	.155879E-02
5	-.477577E-02	.141233E-01	-.300908E-01	-.191371E-02
6	-.224436E-01	.106989E-02	-.585174E-04	-.260601E-03
7	.221307E-01	.106535E-02	.549088E-04	-.261708E-03
8	.477266E-02	.141137E-01	.300841E-01	-.191267E-02
9	-.363786E-03	.142130E-01	.301196E-01	.155798E-02
10	-.399847E-01	.173370E-03	-.162968E-03	.118579E-03
11	.248118E-02	-.408453E-01	-.224737E-04	.389903E-05
12	-.148504E-35	-.404798E-01	0.	0.

LAMBDA= 3.000 EIGENVALUE NO. = 1 EIGENVALUE= 1.199

MODE	THETA	W	V	U
1	-.398937E-35	.404430E-01	-.171987E-34	.363762E-04
2	.328985E-02	.409302E-01	-.242029E-04	.340876E-04
3	-.999964E-01	-.528390E-03	-.174783E-03	.480962E-04
4	.401304E-03	-.133277E-01	.272425E-01	-.177991E-02
5	.335108E-02	-.132802E-01	.272043E-01	.210660E-02
6	.213410E-01	-.152318E-02	.313182E-04	-.524493E-04
7	-.218433E-01	-.152393E-02	-.318583E-04	-.526514E-04
8	-.335262E-02	-.132901E-01	-.272074E-01	.210691E-02
9	-.401739E-03	-.133298E-01	-.272456E-01	-.178019E-02
10	.100800E+00	-.528883E-03	.173185E-03	.486376E-04
11	-.328981E-02	.409306E-01	.244352E-04	.352755E-04
12	.398960E-35	.404441E-01	.172944E-34	.382624E-04

LAMBDA= 2.143 EIGENVALUE NO. = 1 EIGENVALUE= 1.655

MODE	THETA	W	V	U
1	-.864014E-35	.363689E-01	-.607379E-36	.375233E-04
2	.527538E-02	.373501E-01	-.703035E-05	.456795E-04

3	--.999992E-01	--.149082E-02	--.932658E-04	.347234E-03
4	.287049E-02	--.156687E-01	.303855E-01	--.286915E-02
5	.257651E-02	--.154044E-01	.303497E-01	.305184E-02
6	.278659E-01	--.226302E-02	.263399E-04	--.019746E-03
7	--.278663E-01	--.226313E-02	--.264125E-04	--.019781E-03
8	--.257684E-02	--.154047E-01	--.303503E-01	.305190E-02
9	--.287061E-02	--.156691E-01	--.303861E-01	--.286922E-02
10	.108000E+00	--.149080E-02	.935847E-04	.347359E-03
11	--.527538E-02	.373543E-01	.718026E-05	.361890E-04
12	.864022E-35	.365690E-01	.676205E-36	.385172E-04
THE TOTAL JOB TIME IS. 65.239 SECONDS				

THIS PAGE INTENTIONALLY LEFT BLANK.

APPENDIX C
COLUMN BUCKLING PANEL TEST PLAN

SERIAL NO.

TEST PLAN
FOR
TYPE III COLUMN BUCKLING PANEL
SPF STIFFENER CONCEPT

CONTRACT: Technology for Hypersonic Vehicles, NAS 1-18590 TASK Order 5, "Low Cost
SPF Aluminum Cryogenic Tank Concepts for ALS and Future Hypersonic Vehicles"

Prepared By:

C. E. Thompson
R. A. Latham
A. R. Del Mundo
G. H. Arvin

Approved By:



C. E. Anton
Program Manager
Low Cost, SPF Aluminum Cryogenic Tank
Concepts for ALS and Future Hypersonic Vehicles

DATE January 17, 1991
NO. OF PAGES Title + ii + 6 + Appendix A + Appendix B



Rockwell International

North American Aircraft Operations
Rockwell International Corporation
P.O. Box 92098
Los Angeles, California 90009

FOREWORD

The work reported herein covers the proposed effort for the Type III hat-stiffened panels for the NASA contract NAS 1-18590 Task Order 5, "Low Cost SPF Aluminum Cryogenic Tank Concepts for ALS and Future Hypersonic Vehicles", C. E. Anton, Program Manager.

TABLE OF CONTENTS

	Page
FOREWORD	C-2
TABLE OF CONTENTS.....	C-3
1.0 INTRODUCTION.....	C-4
2.0 SPECIMEN DESCRIPTION	C-4
3.0 TEST TEMPERATURE.....	C-6
4.0 TEST MACHINE	C-6
5.0 INSTRUMENTATION.....	C-6
6.0 TEST FIXTURES.....	C-6
7.0 TEST PROCEDURE.....	C-6
8.0 DATA REQUIRED.....	C-8
9.0 TEST REPORT.....	C-8

1.0 INTRODUCTION

On the basis of the Type I panel tests, the stepped hat configuration was selected for the Type III panel tests. The column length selected for these tests was 60 inches in accordance with an agreement with General Dynamics for baseline comparisons of configurations having no intermediate frames.

The objective of this report is to delineate the type of loading fixture, instrumentation, failure load predictions, and test procedure required to evaluate the Type III stepped-hat panels under uniaxial loading.

1.1 TECHNICAL CONTACTS

C. E. Thompson	Stress	213-647-3541
R. A. Latham	Stress	213-647-6776
A. R. Del Mundo	Project Engineer (Deasign)	213-922-0929

2.0 SPECIMEN DESCRIPTION

Each specimen consists of seven 2.6-inch-high stepped hat stiffeners spotwelded to a 36- x 60- x 0.155-inch plate skin with a 1-inch longitudinal spotweld pitch (Figure 1). The spotweld rows in the two hat flanges are 4.5 inches apart (hoopwise direction). The increased height of the stiffeners was necessary to account for the increased column length required for baseline comparison. The test specimen drawing, L9111403, is furnished as Appendix A.

Because of limited material availability, the SPF stiffeners were restricted to the following "starting gages":

7475 Al	$t_{\text{start}} = 0.100$ inch
2090 Al	$t_{\text{start}} = 0.125$ inch

The predicted failure loads were constrained to these limitations.

Each of the two specimen types shown in the following table has two replicates, comprising a total of four specimens.

	Stiffener	Skin
#1	7475 Al	2219 Al
#2	2090 Al-Li	2090 Al-Li

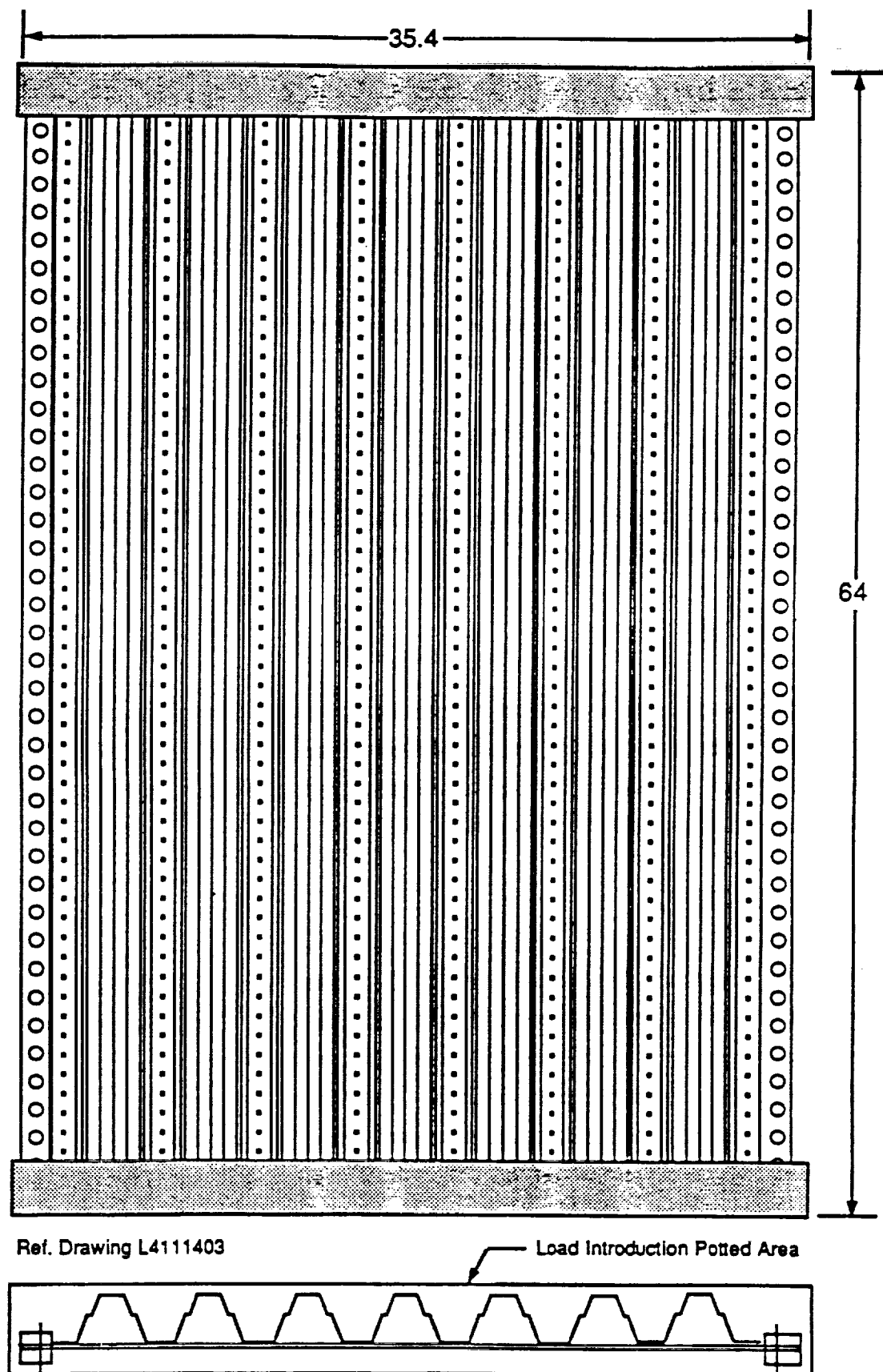


Figure 1. Type III SPF Panel Configuration

The ends of each panel are potted with Velstone to provide local support for the introduction of the compression loads.

The structural test laboratories at NASA-Langley will test all four panels.

3.0 TEST TEMPERATURE

All specimens will be tested at ambient temperature conditions. Test temperature should be recorded prior to each test for inclusion in the test report.

4.0 TEST MACHINE

A compression test machine with a load capacity of 500,000 pounds or greater and a loading rate of 0.05 inch/minute should be used for the Type III panel tests.

5.0 INSTRUMENTATION

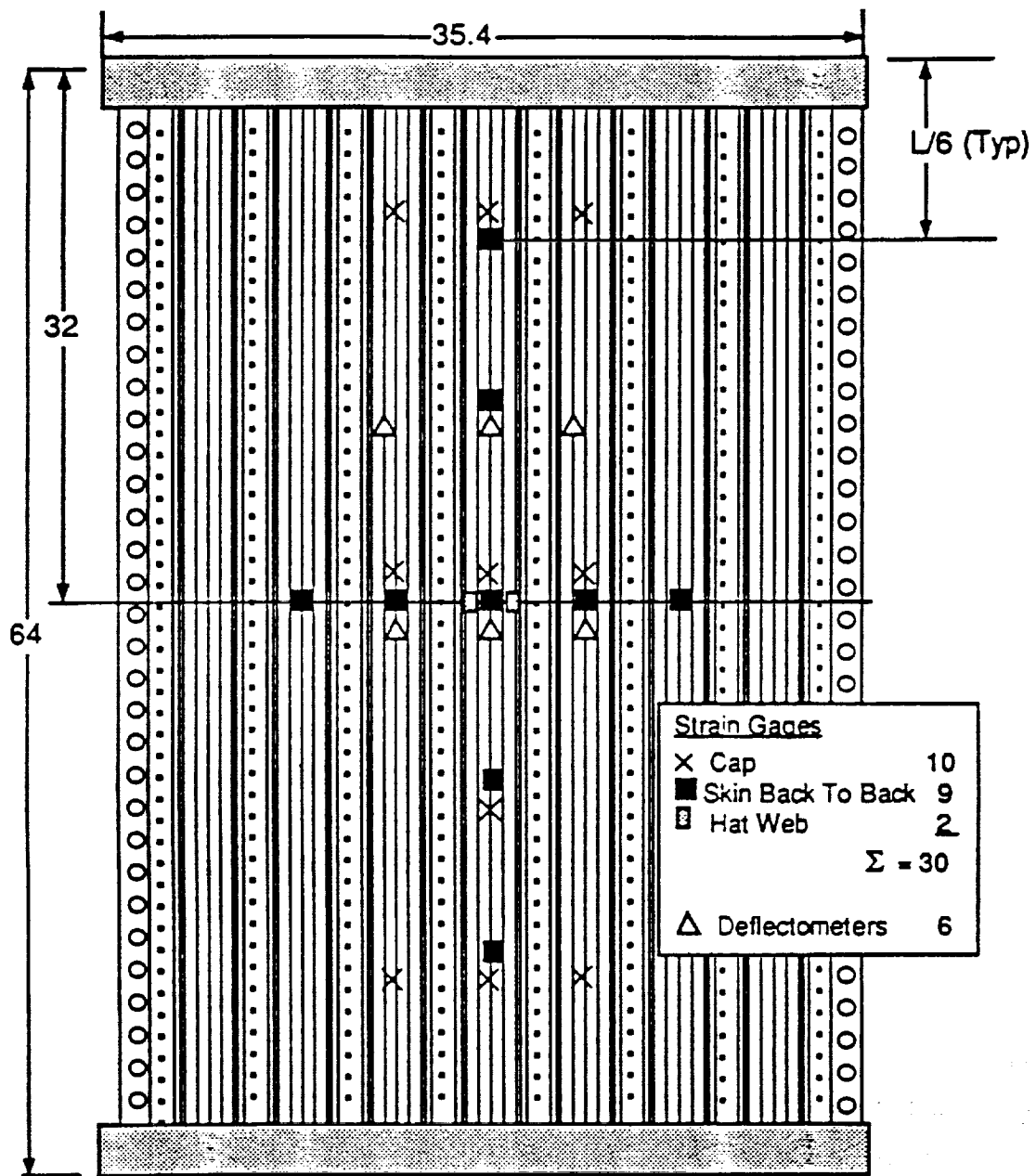
Instrumentation will be designed to provide both strain gage data and deflection data for test results evaluation. A total of 30 strain gages and 6 deflectometers are specified for Panel III tests, as shown in Figure 2. General Dynamics will install all strain gages prior to panel shipment to NASA. The instrumentation reference drawing is L91111412.

6.0 TEST FIXTURES

The test fixture supports the loaded edges of each specimen to prevent local crippling and to provide simple-support boundary conditions to the stiffener side edges. The support of the loaded edges consists of encapsulating each loading edge with 2-inch-deep Velstone potting compound. The side edge support design is shown in Appendix B. These are simple "clamp-on" fixtures with Teflon tape between the specimen and fixtures. Previous Rockwell experience has shown that the tape is effective in providing simple-support conditions. The reference drawing for the test fixture is L9111411.

7.0 TEST PROCEDURE

Each panel will be mounted in the compression test machine in a similar manner to that used in Type I panel testing. The load will be applied through the combined centroid of the skin/stiffener system. The



Ref. Drawing L4111412

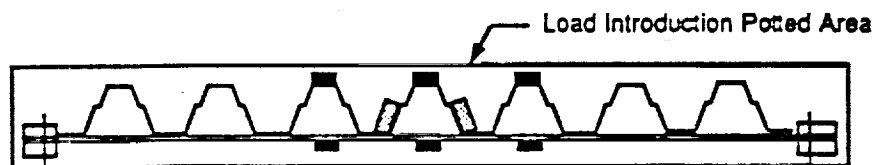


Figure 2. Type III SPF Panel Instrumentation

c.g. was calculated by using the PASCO program and is referenced to the outer mold line of the skin, as shown in the following table:

Stiffener/Skin Material	t_{start}	c.g. (Ref OML)
7475-T62 Al/ 2219-T8	0.100	0.75
2090-T62 Al-Li/ 2090-T8	0.125	0.85

For each panel test, all gages will be zeroed out as standard practice prior to the start of the loading cycle. Each panel will be loaded continuously, with strain gage readings recorded every 10 seconds until failure. The predicted ultimate loads for each stiffener type, together with the predicted failure mode, are shown in Table I.

8.0 DATA REQUIRED

All strain gage and deflectometer readings at each load increment will be recorded for each panel test. In addition, all relevant observations concerning specimen appearance, procedure incidents, and anomalous indications will be noted and recorded relative to the corresponding load level.

One 8.5- x 11-inch glossy photographic print and one 85-line screen print with negative will be furnished by the test facility for each test panel both after mounting in the test machine and after failure.

A schematic drawing showing the actual measured locations and orientations of all strain gages and deflectometers will be furnished to the program manager.

9.0 TEST REPORT

A preliminary test report tabulating all strain gage and deflection data will be prepared by the NASA Structures Laboratory and submitted within 30 days after testing of the Type III panels to:

Rockwell International, Space Division
C. E. Anton, NAS1-18590 Task 5 Program Manager
D/284, 841-NA40
12214 Lakewood Blvd
Downey, CA 90241

for preparation of the final test report.

Table I
**PREDICTED ULTIMATE UNIAXIAL COMPRESSION LOADS
 FOR TYPE III PANELS**

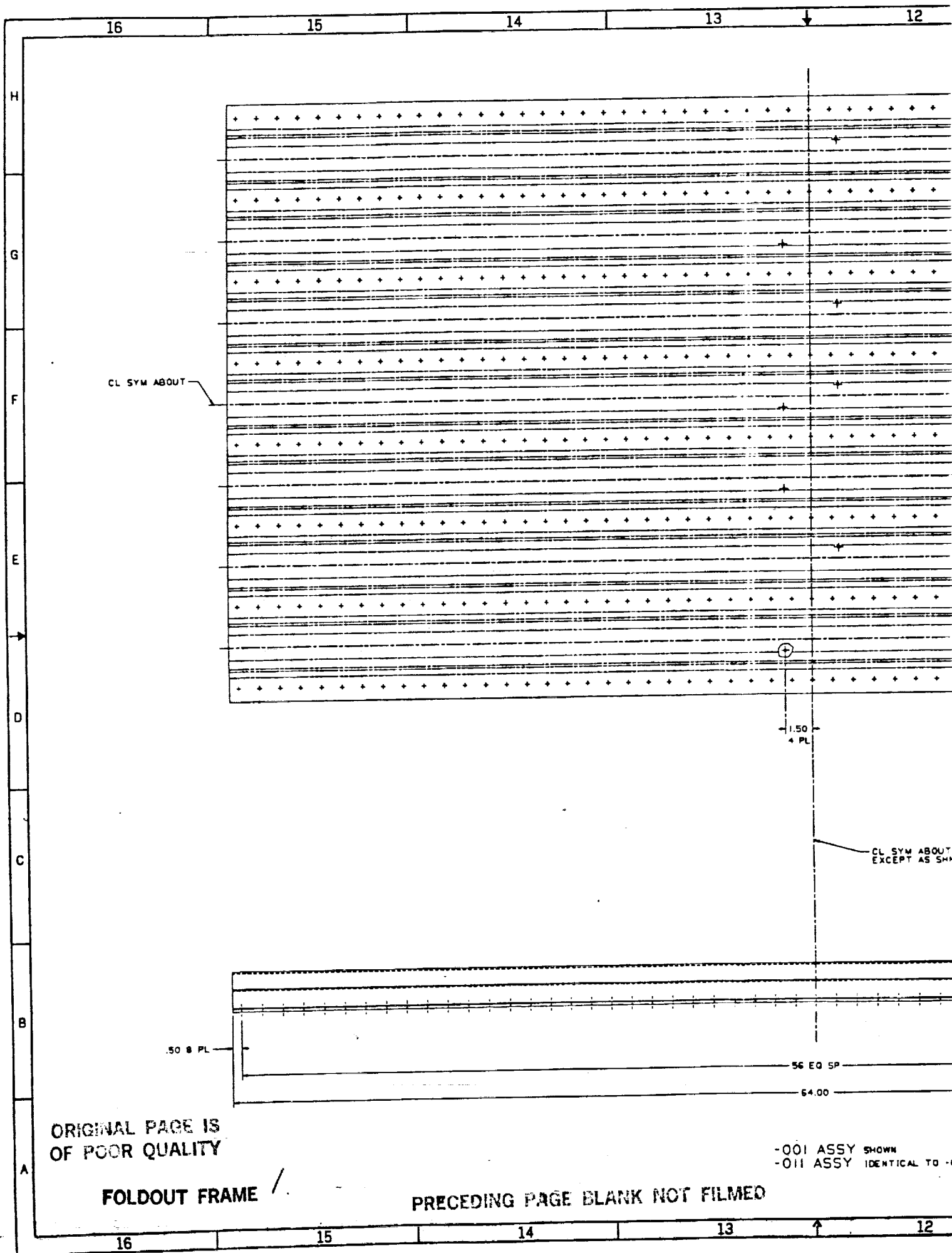
Stiffener Type	Skin Material	Stiffener Material	Predicted Ultimate Panel Load	Critical Area
Stepped Hat Curved Cap (0.10 t_{start})	2219 Al	7475 Al	233,000 lbs (6573 lb/in.)	Column Buckling
Stepped Hat Curved Cap (0.125 t_{start})	2090 Al-Li	2090 Al-Li SPF	312,000 lbs* (8825 lb/in.)	Column Buckling

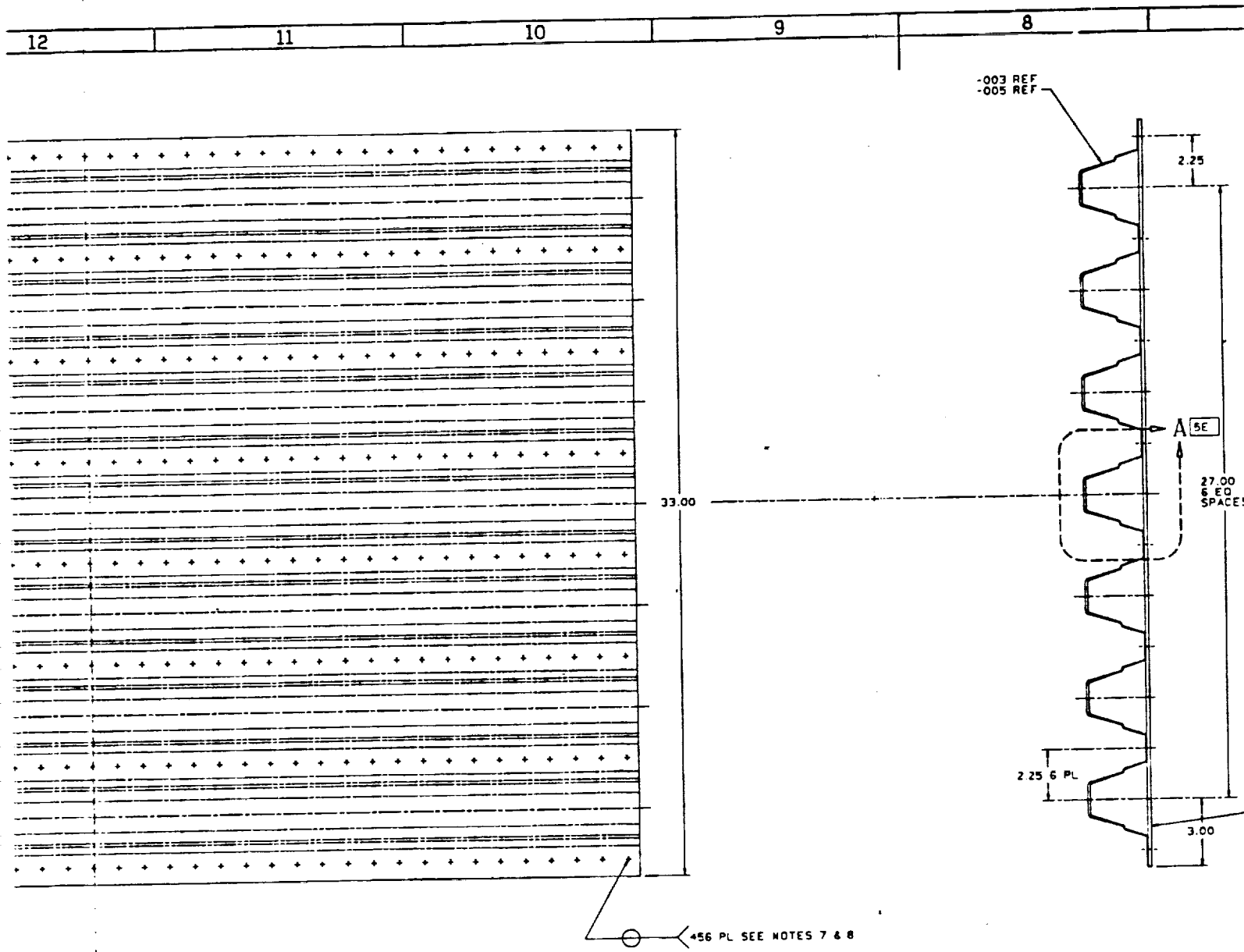
NOTES:

1. Load prediction calculations made for available starting gages, $t_{start} = 0.100$ and 0.125 inch; panel length = 60 inches; skin gage = 0.155 inch.
 2. Thinning profiles were estimated from Type I panel data.
- * Meets design criteria loading.

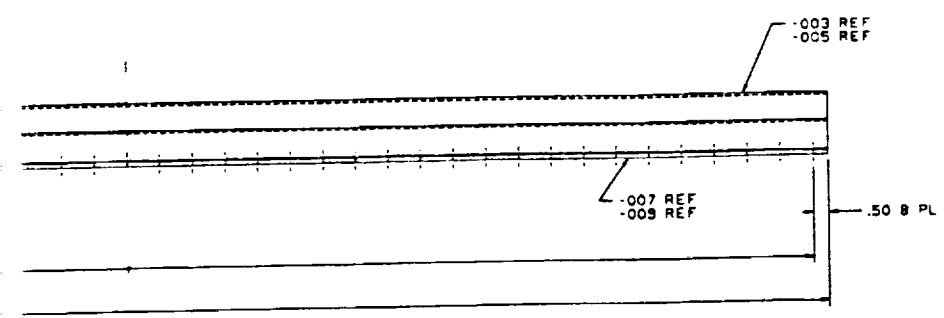
TYPE III PANEL
REFERENCE DRAWING L9111403

THIS PAGE INTENTIONALLY LEFT BLANK.





SYM ABOUT
EPT AS SHN



ORIGINAL PAGE IS
OF POOR QUALITY

FOLDOUT FRAME 2

ICAL TO -001 EXCEPT AS NOTED

FOLDOUT FRAME	
L9111403	REV 1

THIS PAGE INTENTIONALLY LEFT BLANK.

TYPE III PANEL
REFERENCE DRAWINGS FOR
FIXTURES AND INSTRUMENTATION

7 sheets

24

23

22

21

H

G

F

E

D

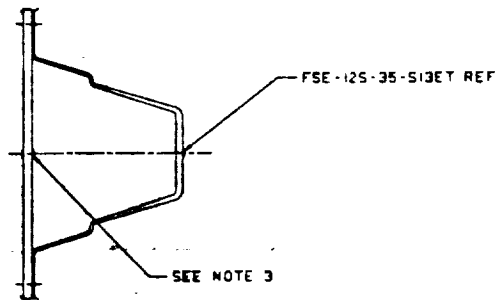
C

B

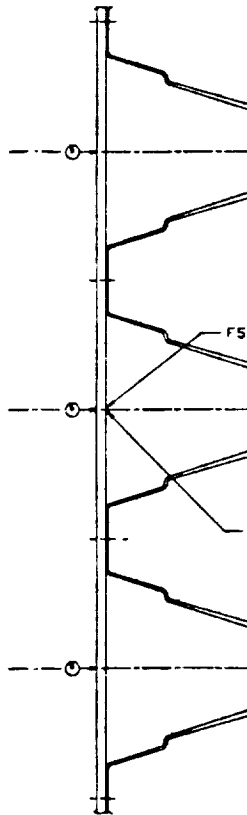
A

ORIGINAL PAGE IS
OF POOR QUALITY

FOLDOUT FRAME



D-D 138
SCALE 1



C-C 139
SCALE 1

24

23

22

21

ORIGINAL PAGE IS
OF POOR QUALITY

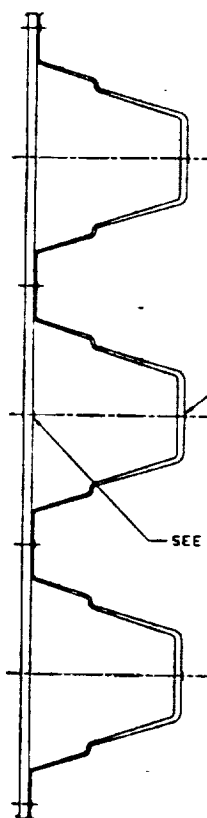
S13ET REF

FSE-125-35-S13ET REF

SEE NOTE 3

2.
FOLDOUT FRAME

C-C 118
SCALE 1

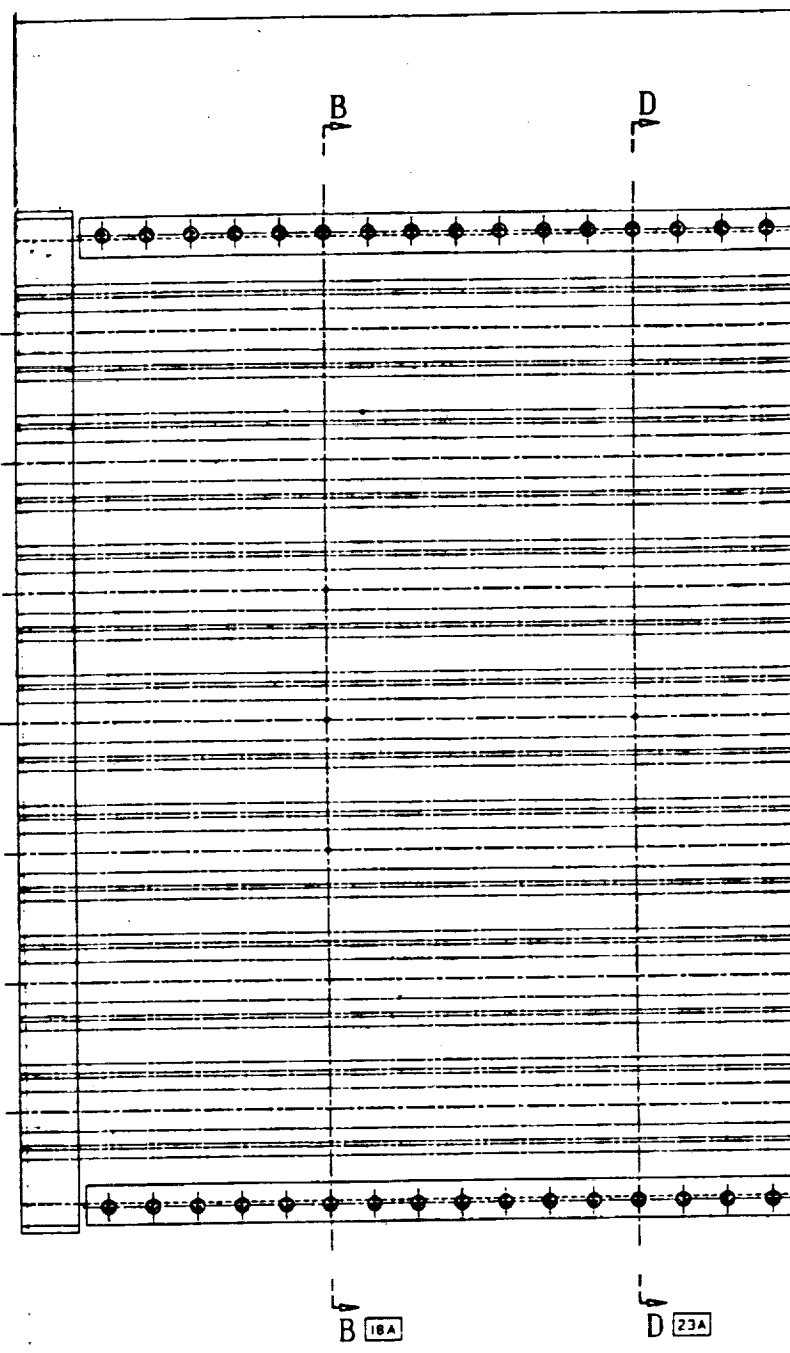


FSE-125-35-S13ET REF

SEE NOTE 3

B-B 148 118
SCALE 1

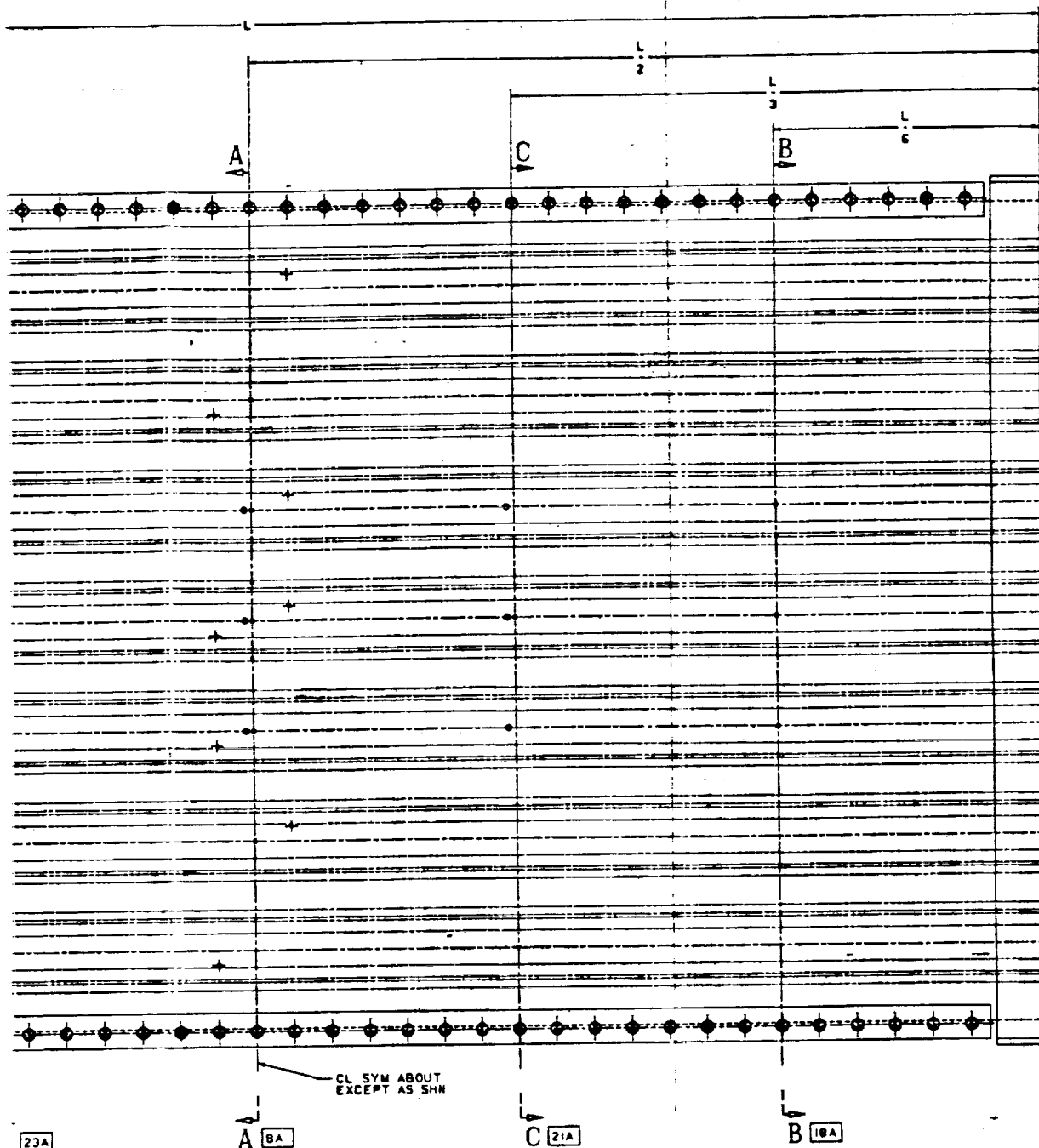
FORM 10 FRA
L911



CL SYM ABOUT

E-125-35-S13ET REF

FOLDOUT FRAME 3.



DEFLECTOMETER,
TOP AND BOTTOM
FSE-125-36-S

-001 ASSY SHOWN
-011 ASSY IDENTICAL TO -001 EXCEPT AS NOTED

FOLDOUT, FRAME 4/

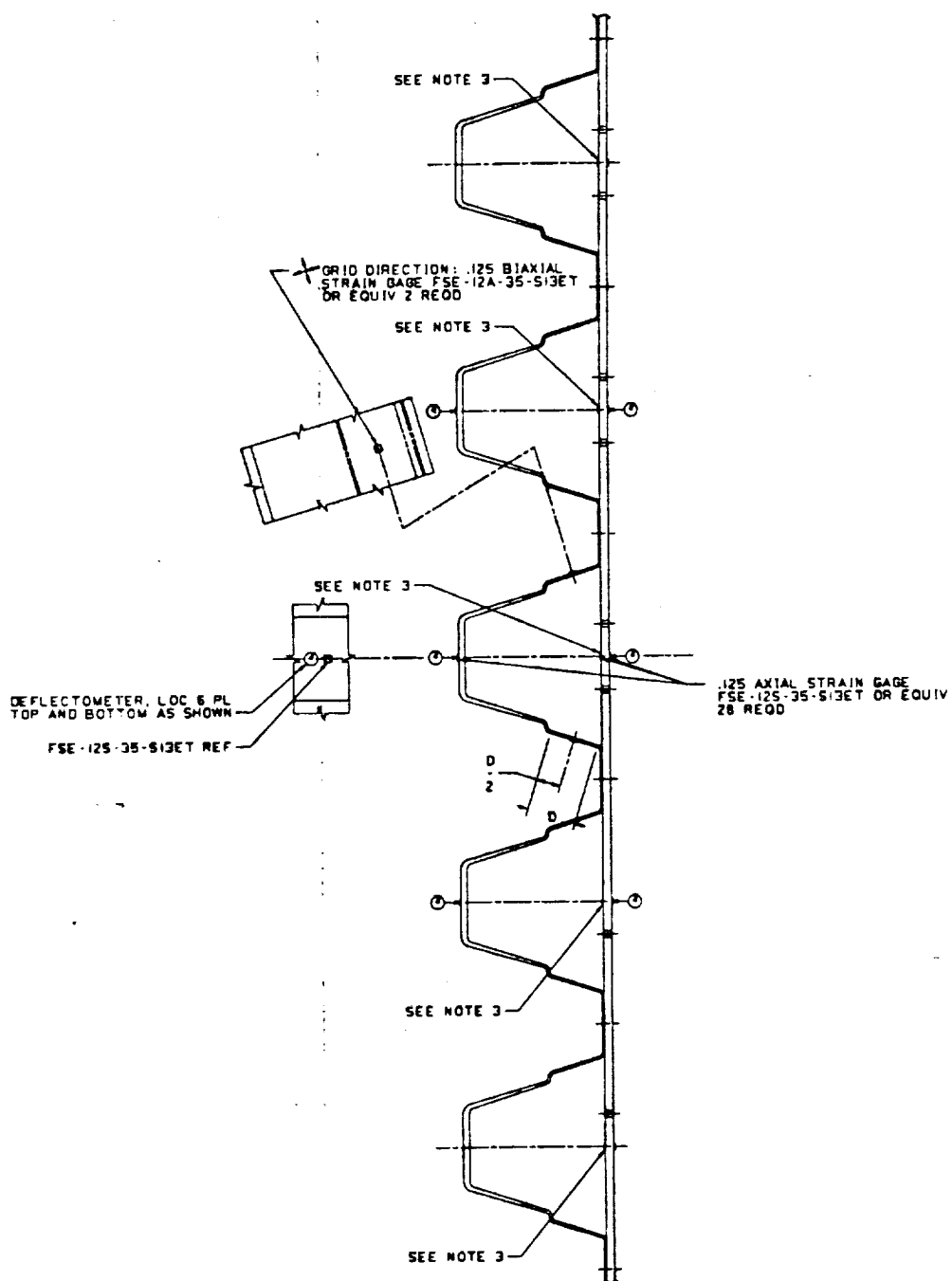
9

8

7

6

5



FOLDOUT FRAME

5

A-A 138
SCALE 1ORIGINAL PAGE IS
OF POOR QUALITY

REV	DATE	BY	CHK
1	-	1	

L9111412

3. THIS STRAIN GAGE MUST BE INSTALLED
 2. IDENTIFY PER LAD104-C26, EXC. METAL IMPRESSION STAMP
 1. SHEET METAL EXTRUSION, STANDARD DETAIL PER LAD102-C
- NOTES: UNLESS OTHERWISE SPECIFIED

9

8

7

6

5

ORIGINAL PAGE IS
OF POOR QUALITY

JAN 25 1991
#5-1

L9111412

NEXT ASSEMBLY		END	ITEM	QTY	REQD	DASH NO	IDENT	PART OR IDENTIFYING NUMBER	NOMENCLATURE OR DESCRIPTION	NOTE	ZONE	ITEM NO
								L910411-011	PANEL ASSY			90
								L910411-001	PANEL ASSY			90
				2	2			FSET-12A-35-13ET	BIAXIAL STRAIN GAGE (.125 STACKED)			21E
				20	20			FSE-125-25-813ET	AXIAL STRAIN GAGE (.125)			20C
								1-011	ASSY			13B
								1-001	ASSY			13B

FOLDOUT FRAME

STRAIN GAGE MUST BE INSTALLED PRIOR TO SPOT WELDING PANEL, TYP 9 PL
TIFY PER LAD104-026, EXCEPT DO NOT
AL IMPRESSION STAMP
T METAL EXTRUSION,
BOARD DETAIL PER LAD102-012
S: UNLESS OTHERWISE SPECIFIED

ORIGINAL PAGE IS
OF POOR QUALITY

PARTS LIST		F31302-13417-11400		General International Corporation North American Aircraft Operations P.O. Box 6000, L.B. Smith, Ok.	
UNLESS OTHERWISE SPECIFIED ALL DIMENSIONS ARE IN INCHES. TOLERANCES ARE: FRACTIONS DECIMALS ANGLES .1250 .001 .01 .01 .001 .001 .01 .01 .001 .001 .01 .01		REVISED BY: J. L. GORDON DATE: 1-15-91 BY: J. L. GORDON DATE: 1-15-91		INSTRUMENTATION INSTL-TYPE III PNL (STEPPED HAT)	
TYPICAL AND STANDARD DIMENSIONS ARE: TYPICAL AND STANDARD DIMENSIONS ARE: TYPICAL AND STANDARD DIMENSIONS ARE:		J 43999		L9111412	
CAD DATABASE AVAIL-CADDS 4					

THIS PAGE INTENTIONALLY LEFT BLANK.

THIS PAGE INTENTIONALLY LEFT BLANK.

APPENDIX D
R-CURVES

PRECEDING PAGE BLANK NOT FILMED

Aluminum Company of America
Alcoa Technical Center
Product Design and Mechanics Division

R-curve Fracture Toughness Test Report
Report Date and Time: 03-04-1991 16:36:13
ASTM Test Methods: B646-87 & E561-86
Data reduction program: RCURV3_1.BAS Ver 1.02

Mechanical Test No.: 900822-004
Specimen ID: 590316-1-L-T-4
Job Order No.:
Author: RLB

Material/Test Data

Alloy - Temper: 2090-T62
Product: Sheet
Lot/Sample No.: 590316-1
Specimen No.: 4
Test Comment: T62 PRE-SFF
Material Modulus = 11.4 Msi
Tensile Yield Strength, σ_{ys} = 50.0 ksi

Specimen Orientation: L-T
Specimen Type: M(T)
Product Thickness: 0.090 in
Test Date: 910222
Test Temperature: 72 deg. F
Test Operator: PDE
Test Plane: T/2

Specimen Data:

Thickness, b = 0.0909 in
Initial Crack Length, $2a_0$ = 1.475 in

Width, w = 4.000 in
Gage Span, $2y_0$ = 0.832 in

Fatigue Precracking Data:

Maximum Fatigue Load, P_{fmax} = 2300.0 lb
Fatigue Cycles = 31,020
Load Ratio, R = 0.1
 $\sigma_{fnetmax}/\sigma_{ys}$ = 0.20

$\sigma_{fnetmax}$ = 10.02 ksi
Pretcrack Date: 910222
 K_{fmax} = 10.5 ksi \sqrt{in}
Pass if < 0.5 : Yes

Fracture Curve Data Analysis Results:

Fracture Data File Name: TEST52A.PRN
Number of data points: 612

K rate = 2.39 ksi \sqrt{in}/sec
E/Eeff = 1.01

	Obs #	Time (sec)	Load (lb)	COD (in)
Critical points:				
Maximum load:	557	22.24	8466.9	0.0098
Final data point:	612	24.44	0.0	0.0382
Best fit linear data:				
Lower limit:	107	4.24	575.6	0.0004
Upper limit:	199	7.92	2498.1	0.0020

Slope (lb/in)	Y-int (lb)	X-int (in)	r^2	# pts in fit	Step size	Eeff (Msi)
1216016	50.8	-0.0000	0.999952	93	2	11.327

R-curve data stored in file: RC52.DAT
 Specimen ID: 590316-1-L-T-4
 Material: 2090-T62
 Test comment: T62 PRE-SPF
 MTH: 900822-004

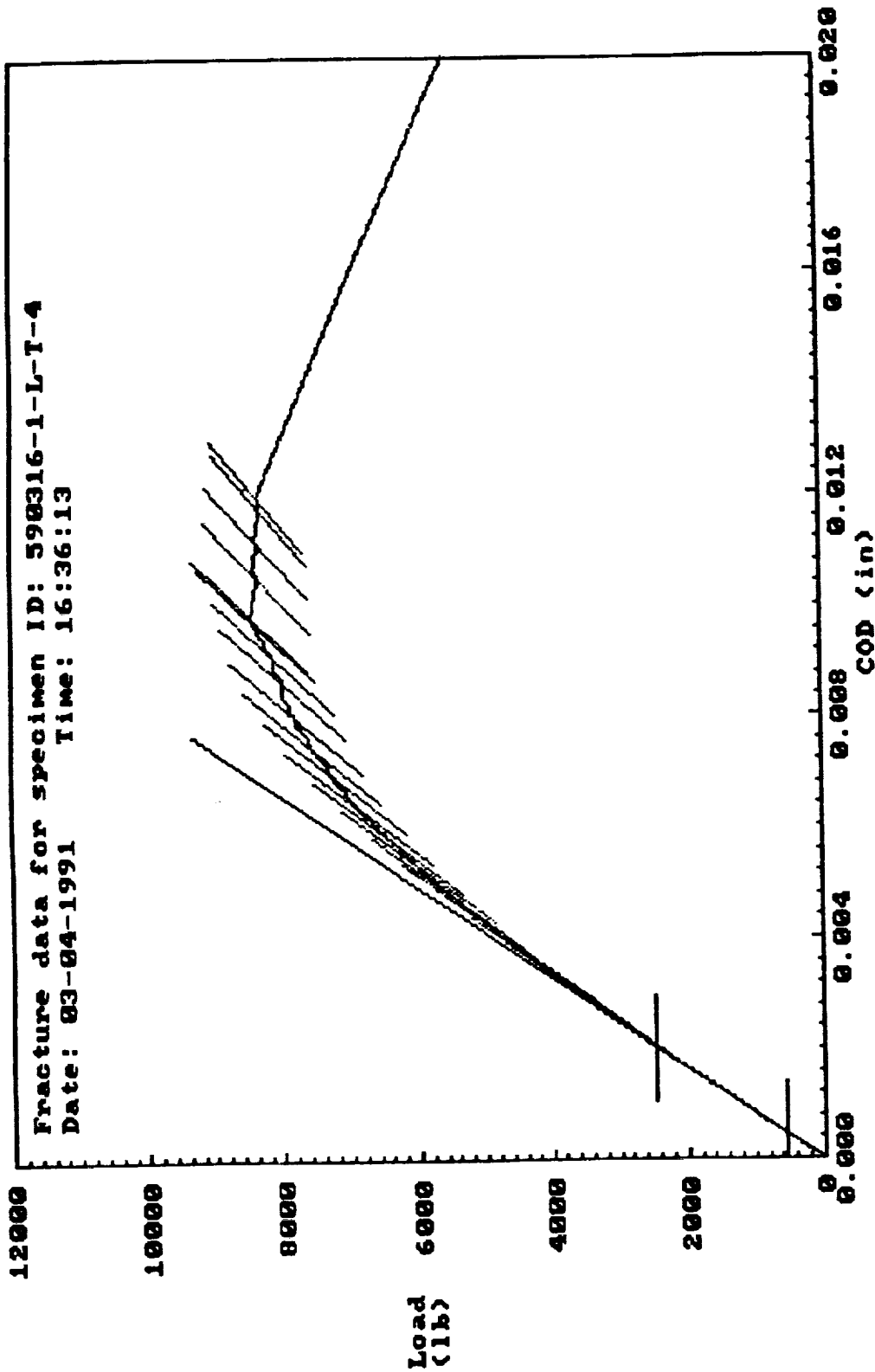
Obs #	Secant Slope (lb/in)	Load (lb)	COD (in)	Delta aeff (in)	Kr (ksi Jin)	K rate (ksi Jin/sec)	σnet (ksi)	Kapp (ksi Jin)	Valchk = σnet/σys	Valchk < 0.8?
199	1215119	2498.1	0.0020	0.000	11.44	2.4	10.89	11.43	0.22	Y
226	1202966	3010.6	0.0025	0.007	13.87	2.3	13.19	13.78	0.26	Y
253	1191944	3521.3	0.0029	0.013	16.31	2.3	15.50	16.11	0.31	Y
280	1182740	4031.9	0.0034	0.018	18.77	2.3	17.82	18.45	0.36	Y
309	1171135	4566.9	0.0039	0.025	21.38	2.3	20.29	20.90	0.41	Y
338	1159094	5085.0	0.0043	0.032	23.96	2.2	22.72	23.27	0.45	Y
366	1144859	5555.6	0.0048	0.040	26.38	2.2	24.99	25.42	0.50	Y
391	1123696	6002.5	0.0053	0.052	28.83	2.5	27.28	27.47	0.55	Y
417	1101577	6436.9	0.0058	0.066	31.30	2.4	29.59	29.46	0.59	Y
441	1077341	6862.5	0.0063	0.081	33.83	2.6	31.95	31.40	0.64	Y
464	1046996	7223.8	0.0069	0.101	36.26	2.6	34.21	33.06	0.68	Y
485	1011480	7555.6	0.0074	0.125	38.76	3.0	36.54	34.58	0.73	Y
502	972824	7801.9	0.0080	0.153	41.03	3.3	38.68	35.70	0.77	Y
517	925411	7976.9	0.0086	0.189	43.32	3.8	40.88	36.50	0.82	N
530	894226	8123.1	0.0090	0.214	45.12	3.4	42.63	37.17	0.85	N
550	866421	8386.3	0.0096	0.238	47.56	3.1	45.02	38.38	0.90	N
557	860034	8466.9	0.0098	0.243	48.25	2.5	45.70	38.75	0.91	N
558	793101	8364.4	0.0105	0.305	50.35	52.4	48.03	38.28	0.96	N
565	750057	8376.9	0.0111	0.347	52.41	7.4	50.34	38.33	1.01	N
571	707026	8319.4	0.0117	0.393	54.27	7.8	52.61	38.07	1.05	N
577	696046	8363.1	0.0120	0.405	55.17	3.8	53.64	38.27	1.07	N

Kc calculations at maximum load:

557	860034	8466.9	0.0098	0.243	48.25	2.5	45.70	38.75	0.91	N
-----	--------	--------	--------	-------	-------	-----	-------	-------	------	---

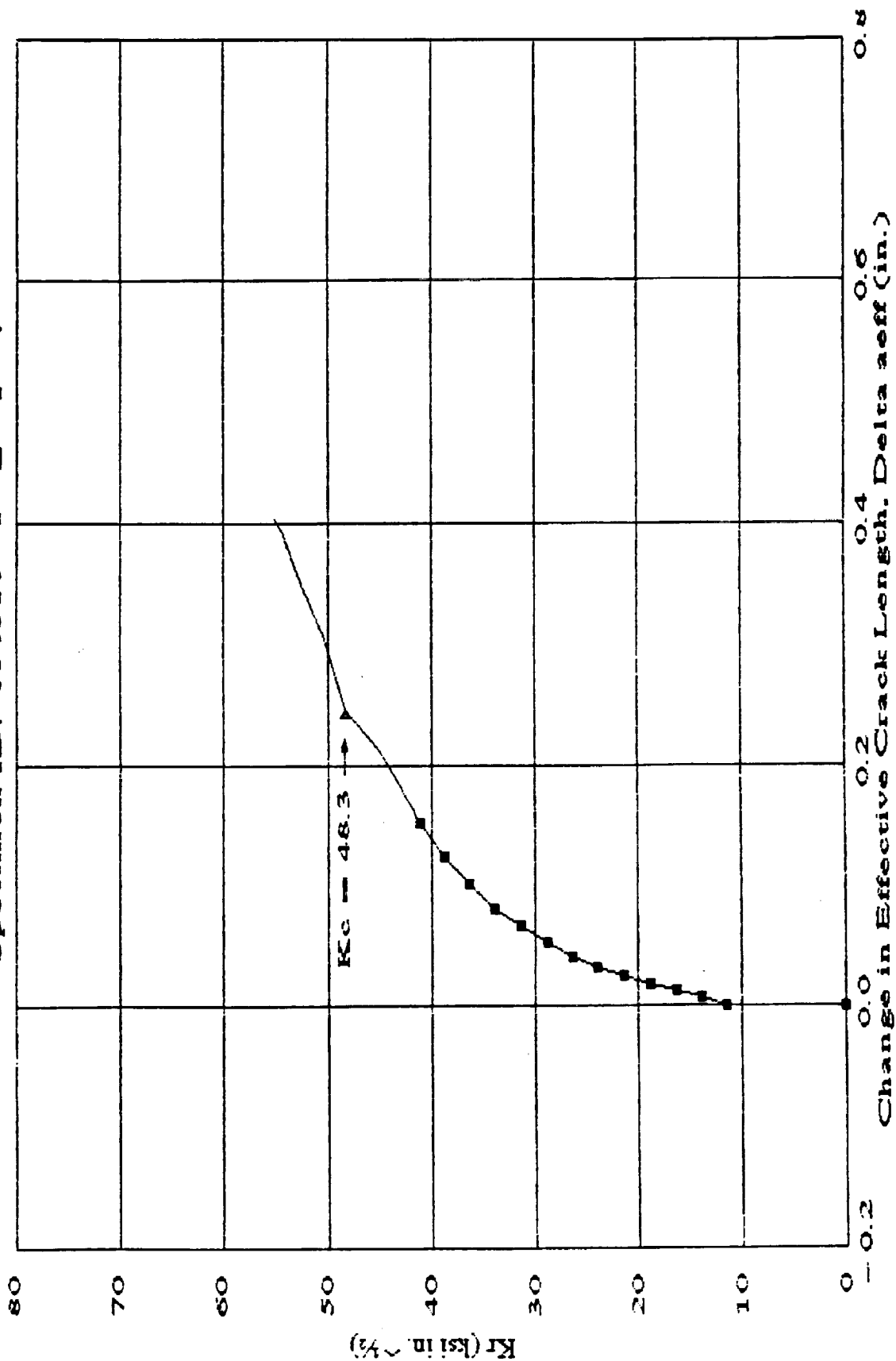
Kc = 48.3 ksi Jin Crack length = 0.981 in Valchk = 0.91
 Kc point is INVALID.

Analysis stopped because load went negative.



E = 11.40 Eff = 11.33
 Enter file name to store rcurve data: RC52.DAT
 File already exists? Y
 Are you sure {Y or N}? Y
 Screen copy? Y

R-curve
Specimen ID: 590316-1-L-T-4

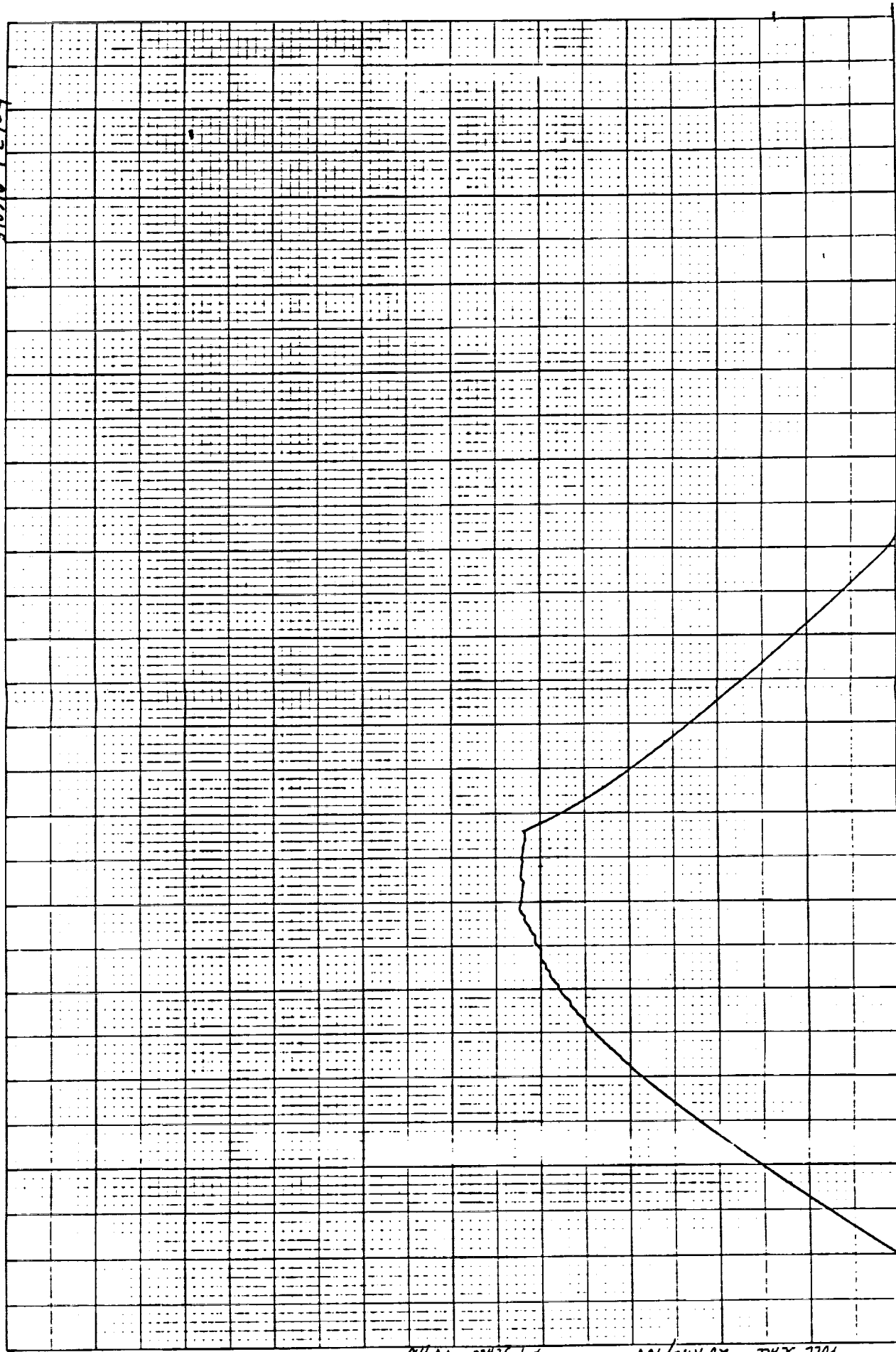


— R-curve (valid) — R-curve (invalid) — Kc value

Material: 2090-T62

NIT#: 900822-004 Test comment: T62 PRE-SFF

590316-1-1-1-4



0.00

X-Y SCALE = 1.50/IN

FULL SCALE = 0.050"/IN

X-Y SCALE = 1.00/IN

FULL SCALE = 20 KI/PS/100

5-D-5

UNITED STATES OF AMERICA
NAVY CONTROLS CORPORATION
BOSTON, MASS. 02106

NO. XY 1101-SP5

Aluminum Company of America
Alcoa Technical Center
Product Design and Mechanics Division

R-curve Fracture Toughness Test Report
Report Date and Time: 03-01-1991 15:38:51
ASTM Test Methods: B646-87 & E561-86
Data reduction program: RCURV3_1.BAS Ver.1.02

Mechanical Test No.: 900822-004
Specimen ID: 590316-3-L-T-2
Job Order No.:
Author: RLB

Material/Test Data

Alloy - Temper: 2090-T62
Product: Sheet
Lot/Sample No.: 590316-3
Specimen No.: 2
Test Comment: T62 PRE-SPF
Material Modulus = 11.8 Msi
Tensile Yield Strength, σ_{ys} = 50.0 ksi

Specimen Orientation: L-T
Specimen Type: M(T)
Product Thickness: 0.090 in
Test Date: 910222
Test Temperature: 72 deg. F
Test Operator: PDE
Test Plane: T/2

Specimen Data:

Thickness, b = 0.0905 in
Initial Crack Length, $2a_0$ = 1.465 in

Width, w = 4.000 in
Gage Span, $2y_0$ = 0.832 in

Fatigue Precracking Data:

Maximum Fatigue Load, P_{fmax} = 2300.0 lb
Fatigue Cycles = 23,955
Load Ratio, R = 0.1
 $\sigma_{fnetmax}/\sigma_{ys}$ = 0.20

$\sigma_{fnetmax}$ = 10.03 ksi
Pretcrack Date: 910222
 K_{fmax} = 10.5 ksi $\sqrt{\text{in}}$
Pass if < 0.5 : Yes

Fracture Curve Data Analysis Results:

Fracture Data File Name: TEST51A.PRN
Number of data points: 662

K rate = 2.18 ksi $\sqrt{\text{in/sec}}$
 E/E_{eff} = 1.14

Warning: E/E_{eff} is outside recommended limits of $[0.9 \leq E/E_{eff} \leq 1.1]$.
Recommend checking calibration and input data. Data will still
be corrected with E_{eff} , but use with caution.

	Obs #	Time (sec)	Load (lb)	COD (in)
Critical points:				
Maximum load:	611	24.40	8852.5	0.0115
Final data point:	662	26.48	-5.6	0.0380
Best fit linear data:				
Lower limit:	231	9.20	2806.3	0.0022
Upper limit	287	11.44	3873.1	0.0032

Slope (lb/in)	Y-int (lb)	X-int (in)	r^2	# pts in fit	Step size	E_{eff} (Msi)
1110228	349.7	-.0003	0.999908	57	2	10.307

R-curve data stored in file: RC51.DAT
 Specimen ID: 590316-3-L-T-2
 Material: 2090-T62
 Test comment: T62 PRE-SPF
 MTH: 900822-004

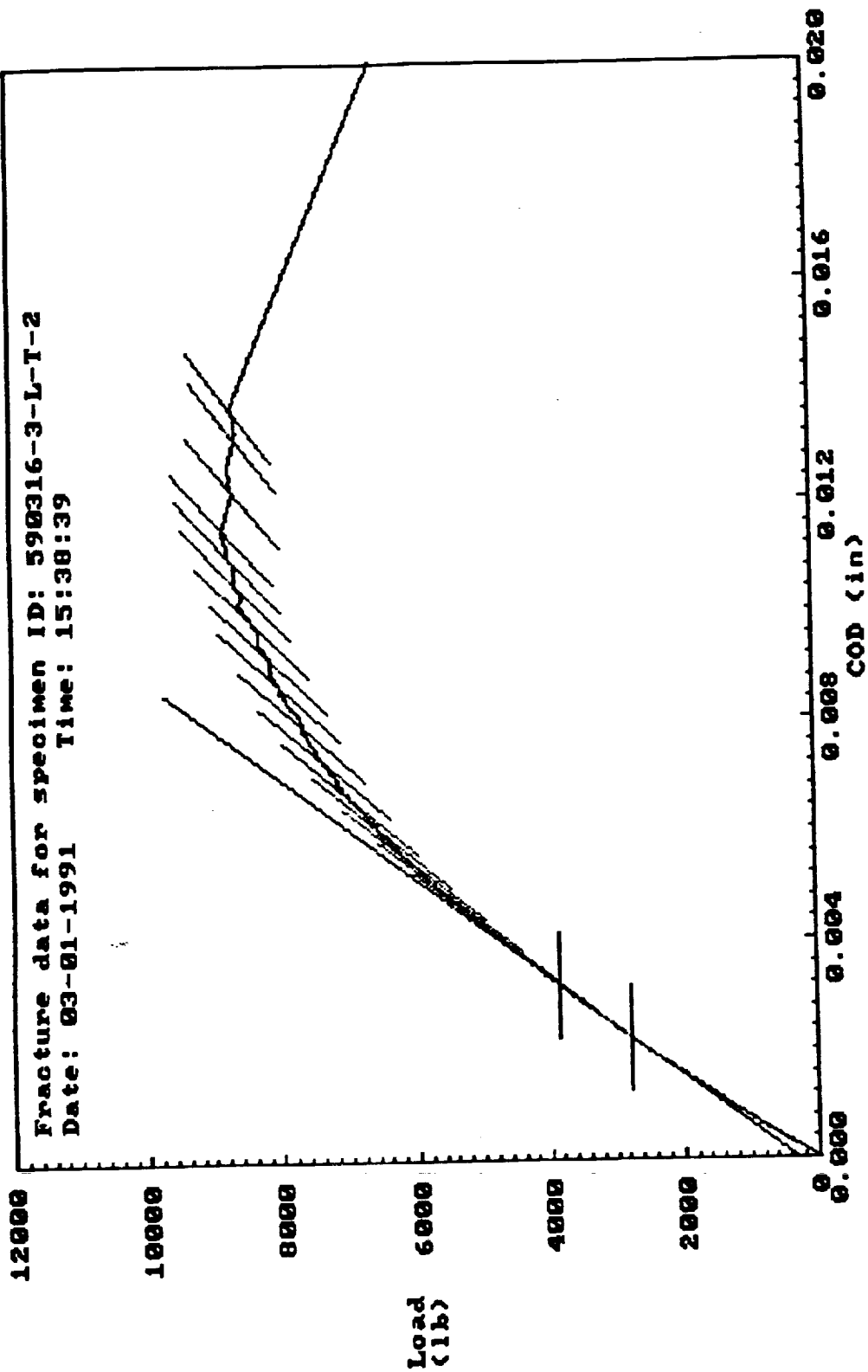
Obs #	Secant Slope (lb/in)	Load (lb)	COD (in)	Delta aeff (in)	Kr (ksi Jin)	K rate (ksi Jin/sec)	σ_{net} (ksi)	K_{app} (ksi Jin)	Valchk = σ_{net}/σ_{ys}	Valchk < 0.8?
287	1110772	3873.1	0.0032	-0.000	17.71	2.2	16.88	17.72	0.34	Y
318	1102102	4436.9	0.0037	0.005	20.39	2.2	19.41	20.30	0.39	Y
349	1093144	4991.9	0.0043	0.010	23.05	2.1	21.93	22.84	0.44	Y
379	1080230	5516.9	0.0048	0.018	25.66	2.2	24.39	25.24	0.49	Y
409	1060289	6031.3	0.0054	0.030	28.38	2.3	26.93	27.59	0.54	Y
438	1039646	6515.0	0.0060	0.043	31.03	2.3	29.40	29.81	0.59	Y
466	1014736	6978.8	0.0066	0.060	33.73	2.4	31.92	31.93	0.64	Y
490	979377	7353.8	0.0072	0.084	36.34	2.7	34.32	33.64	0.69	Y
512	936074	7678.1	0.0079	0.115	39.03	3.1	36.81	35.13	0.74	Y
538	896717	8030.6	0.0086	0.146	41.95	2.8	39.55	36.74	0.79	Y
549	863223	8156.9	0.0091	0.173	43.66	3.9	41.17	37.32	0.82	N
570	830670	8410.0	0.0098	0.201	46.15	3.0	43.57	38.47	0.87	N
591	801149	8661.9	0.0105	0.228	48.68	3.0	46.02	39.63	0.92	N
602	774047	8763.1	0.0110	0.253	50.38	3.9	47.74	40.09	0.95	N
611	750552	8852.5	0.0115	0.276	51.96	4.4	49.35	40.50	0.99	N
612	695261	8679.4	0.0122	0.335	53.68	43.0	51.41	39.71	1.03	N
623	641142	8655.0	0.0132	0.397	56.67	6.8	54.93	39.60	1.10	N
633	620725	8697.5	0.0137	0.422	58.29	4.1	56.84	39.79	1.14	N

Kc calculations at maximum load:

611	750552	8852.5	0.0115	0.276	51.96	4.4	49.35	40.50	0.99	N
-----	--------	--------	--------	-------	-------	-----	-------	-------	------	---

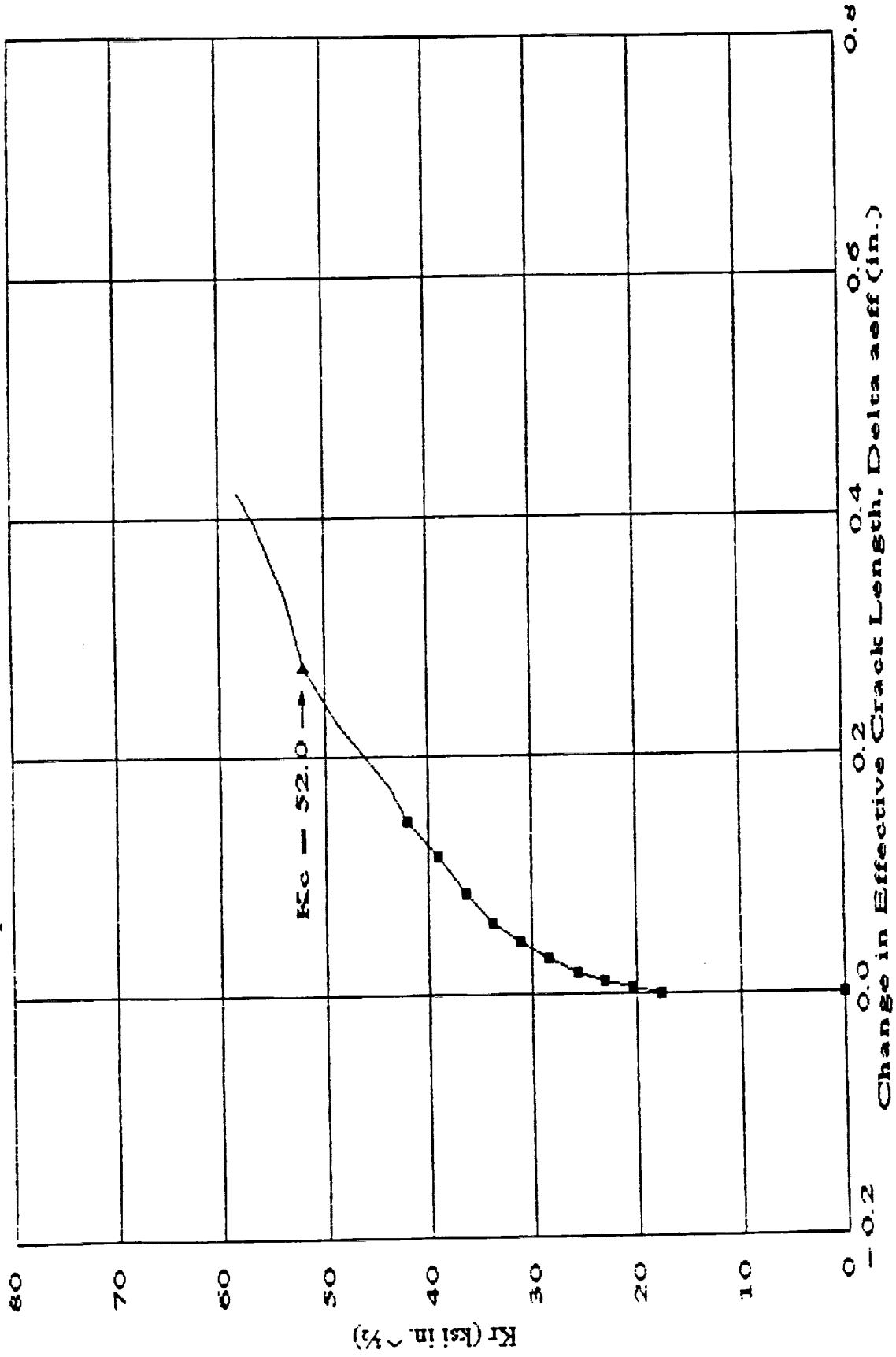
Kc = 52.0 ksi Jin Crack length = 1.009 in Valchk = 0.99
 Kc point is INVALID.

Analysis stopped because $2a/w$ is outside of valid compliance region ($2a/w > 0.8$).



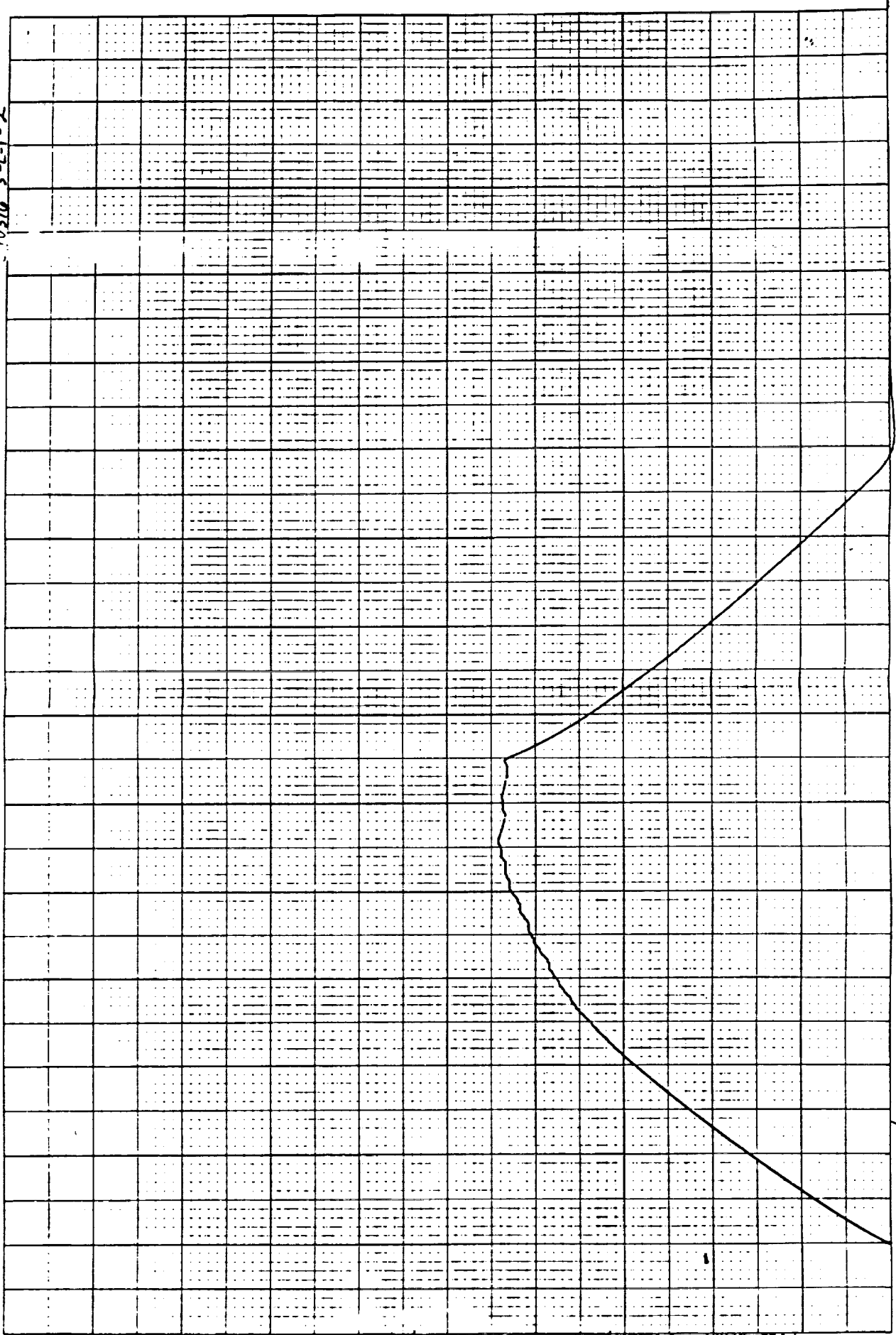
E = 11.80 Eff = 10.31
 Enter file name to store curve data: RC51.DAT
 Screen copy? Y

Specimen ID: 590316-3-L-T-2



--- R-curve (valid) — R-curve (invalid) ▲ Kc value
 Material: 2090-T62 Test comment: T62 PRE-SPF
 MT#: 900822-004

570316-3-L-T-2



COD

X-Y SCALE = .5V/IN

FULL SCALE = 0.05 IN/10V

X-Y SCALE = 1V/IN

FULL SCALE = 20 KIPS/10V

LOAD

NO. XY 1101-SP5

D-10

GRAPHIC CONTROLS CORPORATION
PRINTED IN U.S.A.

Aluminum Company of America
Alcoa Technical Center
Product Design and Mechanics Division

R-curve Fracture Toughness Test Report
Report Date and Time: 03-01-1991 15:56:32
ASTM Test Methods: B646-87 & E561-86
Data reduction program: RCURV3.1.BAS Ver 1.02

Mechanical Test No.: 900822-004
Specimen ID: 590324-L-T-5
Job Order No.:
Author: RLB

Material/Test Data

Alloy - Temper: 2090-T62
Product: Sheet
Lot/Sample No.: 590324
Specimen No.: 5
Test Comment: T62 POST-SPF
Material Modulus = 11.4 Msi
Tensile Yield Strength, σ_{ys} = 50.0 ksi

Specimen Orientation: L-T
Specimen Type: M(T)
Product Thickness: 0.090 in
Test Date: 910225
Test Temperature: 72 deg. F
Test Operator: PDE
Test Plane: T/2

Specimen Data:

Thickness, b = 0.0701 in
Initial Crack Length, $2a_0$ = 1.480 in

Width, w = 4.000 in
Gage Span, $2y_0$ = 0.832 in

Fatigue Precracking Data:

Maximum Fatigue Load, P_{fmax} = 2300.0 lb
Fatigue Cycles = 7,008
Load Ratio, R = 0.1
 $\sigma_{fnetmax}/\sigma_{ys}$ = 0.26

$\sigma_{fnetmax}$ = 13.02 ksi
Pretack Date: 910225
 K_{fmax} = 13.7 ksi \sqrt{in}
Pass if < 0.5 : Yes

Fracture Curve Data Analysis Results:

Fracture Data File Name: TEST54A.PRN
Number of data points: 816

K rate = 2.54 ksi \sqrt{in}/sec
 E/E_{eff} = 1.02

* K rate greater than maximum of 150 ksi \sqrt{in}/min recommended by ASTM-E399.

	Obs #	Time (sec)	Load (lb)	COD (in)
Critical points:				
Maximum load:	709	28.32	5411.3	0.0081
Final data point:	816	32.60	1746.3	0.0281
Best fit linear data:				
Lower limit:	400	15.96	932.5	0.0010
Upper limit:	488	19.48	2438.1	0.0027

Slope (lb/in)	Y-int (lb)	X-int (in)	r^2	# pts in fit	Step size	E_{eff} (Msi)
918939	-12.2	0.0000	0.999961	89	3	11.142

R-curve data stored in file: RC54.DAT
 Specimen ID: 590324-L-T-5
 Material: 2090-T62
 Test comment: T62 POST-SPF
 MTH: 900822-004

Obs #	Secant Slope (lb/in)	Load (lb)	COD (in)	Delta aeff (in)	Kr (ksi Jin)	K rate (ksi Jin/sec)	σ_{net} (ksi)	K_{app} (ksi Jin)	σ_{net}/σ_{ys}	Valchk < 0.8?
488	917050	2438.1	0.0027	0.001	14.52	2.5	13.82	14.50	0.28	Y
509	909483	2777.5	0.0031	0.007	16.62	2.5	15.81	16.52	0.32	Y
529	902573	3107.5	0.0035	0.012	18.69	2.6	17.76	18.48	0.36	Y
550	892459	3414.4	0.0038	0.019	20.67	2.4	19.63	20.31	0.39	Y
577	879070	3738.1	0.0043	0.029	22.84	2.0	21.66	22.23	0.43	Y
596	851715	3994.4	0.0047	0.050	24.89	2.7	23.55	23.76	0.47	Y
614	830310	4246.9	0.0051	0.068	26.88	2.8	25.41	25.26	0.51	Y
633	818524	4528.1	0.0055	0.078	28.92	2.7	27.31	26.93	0.55	Y
651	801677	4776.9	0.0060	0.092	30.91	2.8	29.17	28.41	0.58	Y
670	753020	4998.8	0.0067	0.136	33.65	3.6	31.72	29.73	0.63	Y
688	737196	5238.1	0.0071	0.151	35.74	2.9	33.70	31.16	0.67	Y
697	698822	5313.8	0.0076	0.190	37.53	5.0	35.42	31.61	0.71	Y
707	669881	5393.1	0.0081	0.221	39.16	4.1	37.03	32.08	0.74	Y
709	666069	5411.3	0.0081	0.225	39.44	3.5	37.31	32.19	0.75	Y
710	587359	5277.5	0.0090	0.320	41.88	60.9	40.06	31.39	0.80	N
711	562983	5240.6	0.0093	0.353	42.83	23.8	41.21	31.17	0.82	N
714	559435	5246.9	0.0094	0.358	43.08	2.0	41.48	31.21	0.83	N

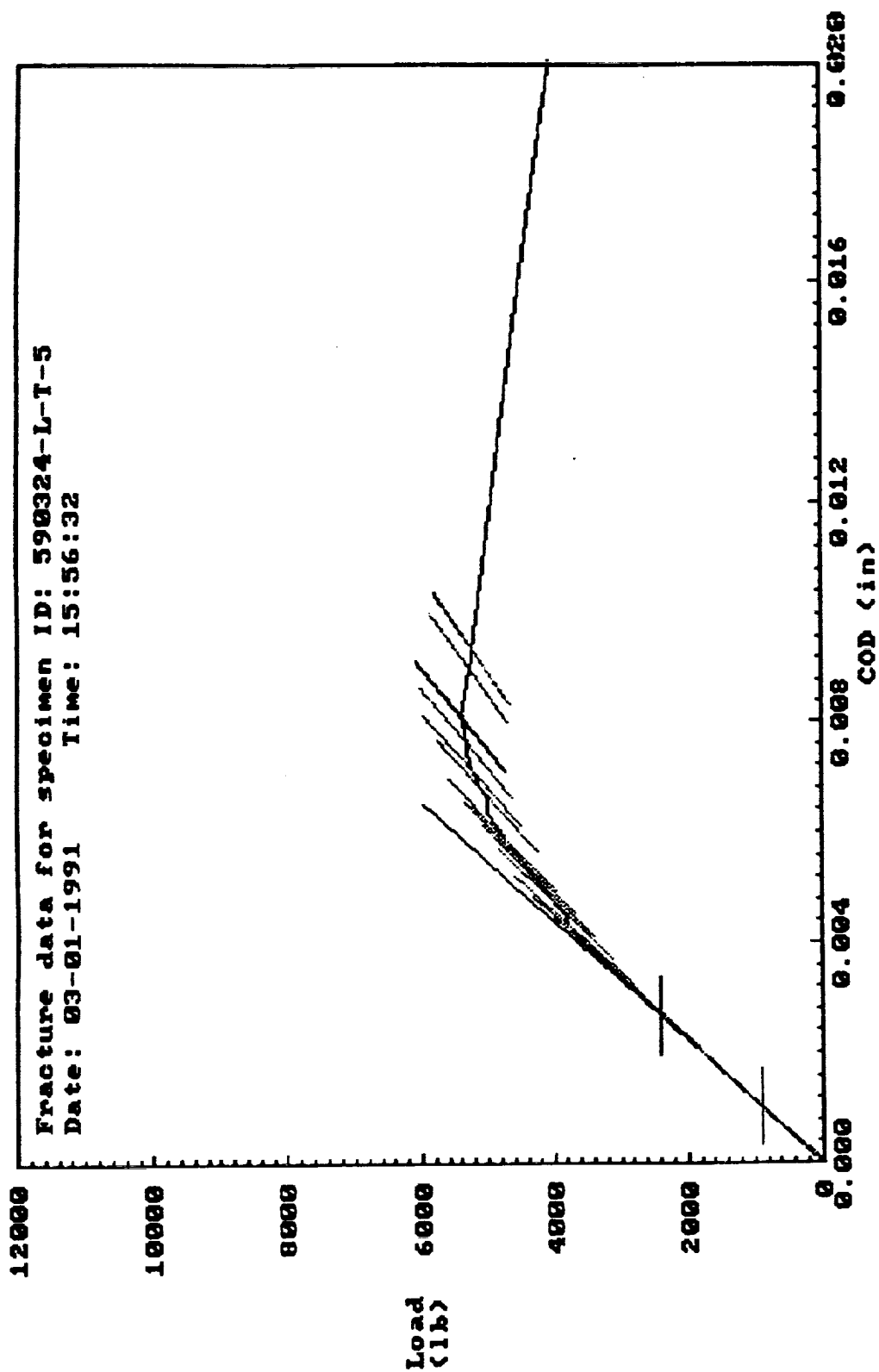
Kc calculations at maximum load:

709	666069	5411.3	0.0081	0.225	39.44	3.5	37.31	32.19	0.75	Y
-----	--------	--------	--------	-------	-------	-----	-------	-------	------	---

Kc = 39.4 ksi Jin Crack length = 0.965 in Valchk = 0.75

Kc point is valid.

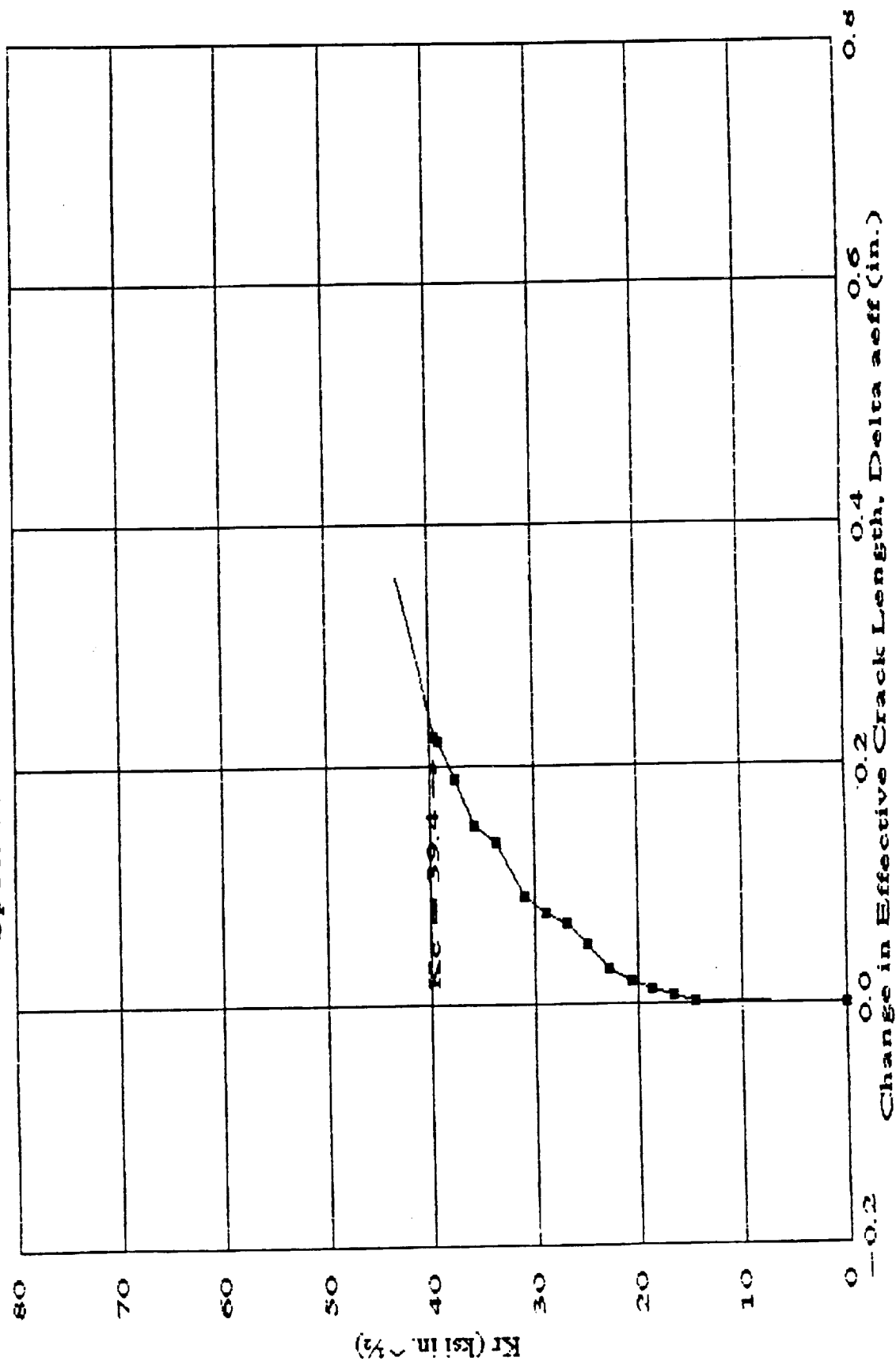
Analysis stopped because $2a/w$ is outside of valid compliance region ($2a/w > 0.8$).



E = 11.40 Eff = 11.14
Enter file name to store curve data: RC34.DAT
Screen copy? y

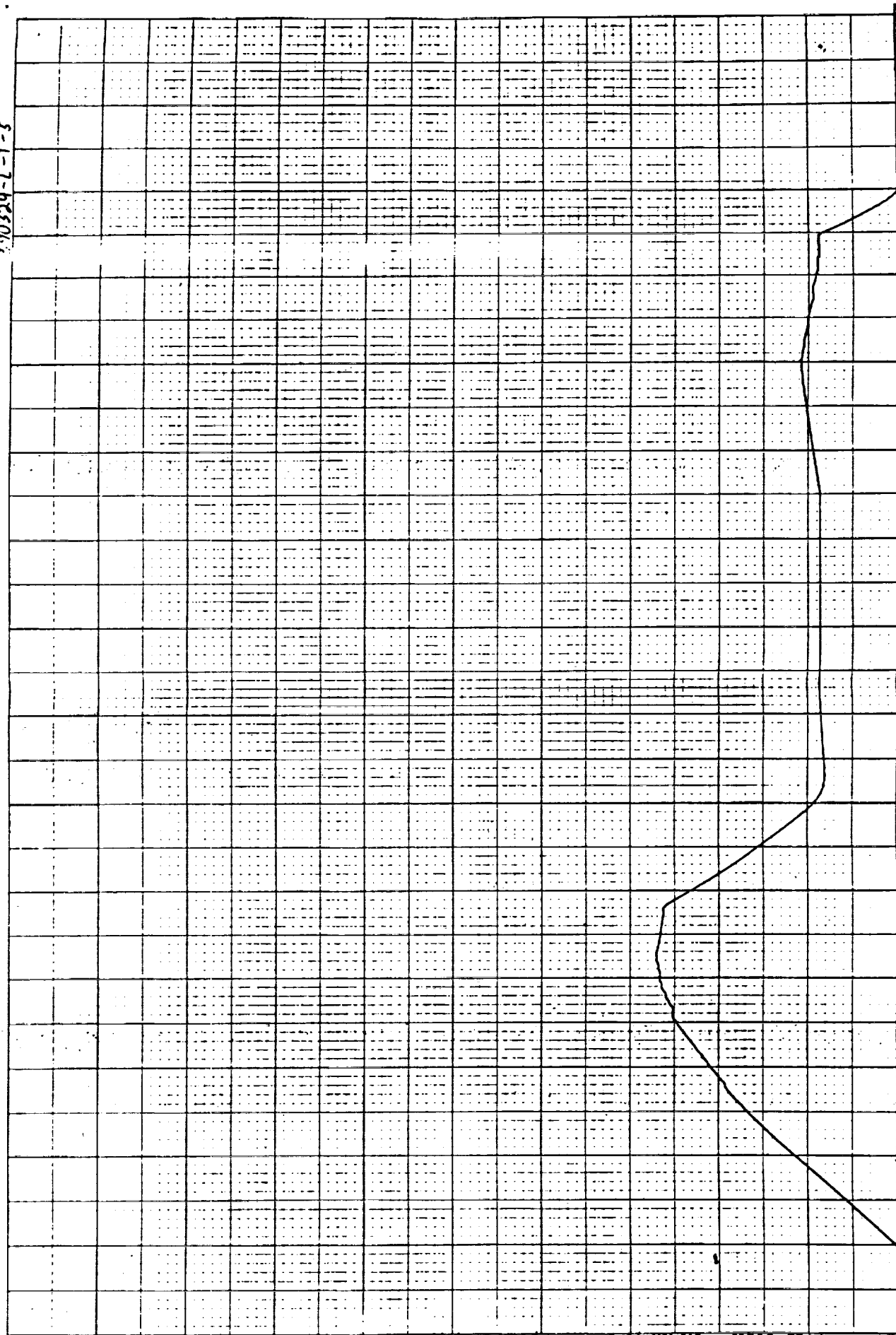
Specimen ID: 590324-L-T-5

R-curve



Material: 2090-T62
 NIT#: 900822-004
 Test comment: T62 POST-SPF

50324-L-T-5



COD

X-SCALE = 0.5V/M

FULL SCALE = 0.050"/10V

FULL SCALE = 20 KIP/10V
Y-SCALE = 1V/M

LOAD
D-15

NO. XY 1101-SP5

GRAPHIC CON. & INFORMATION
DRAWN BY: J. L. H. 1000
CHECKED BY: J. L. H. 1000
DATE: 10/1/70

Aluminum Company of America
Alcoa Technical Center
Product Design and Mechanics Division

R-curve Fracture Toughness Test Report
Report Date and Time: 03-01-1991 15:48:52
ASTM Test Methods: E646-87 & E561-86
Data reduction program: RCURV3 1.BAS Ver 1.02

Mechanical Test No.: 900822-004
Specimen ID: 590325-L-T-4
Job Order No.:
Author: RLB

Material/Test Data

Alloy - Temper: 2090-T62
Product: Sheet
Lot/Sample No.: 590325
Specimen No.: 4
Test Comment: T62 POST-SPF
Material Modulus = 11.8 Msi
Tensile Yield Strength, σ_{ys} = 50.0 ksi

Specimen Orientation: L-T
Specimen Type: M(T)
Product Thickness: 0.090 in
Test Date: 910222
Test Temperature: 72 deg. F
Test Operator: PDE
Test Plane: T/2

Specimen Data:

Thickness, b = 0.0732 in
Initial Crack Length, $2a_0$ = 1.500 in

Width, w = 4.000 in
Gage Span, $2y_0$ = 0.832 in

Fatigue Precracking Data:

Maximum Fatigue Load, P_{fmax} = 2300.0 lb
Fatigue Cycles = 10,076
Load Ratio, R = 0.1
 $\sigma_{fnetmax}/\sigma_{ys}$ = 0.25

$\sigma_{fnetmax}$ = 12.57 ksi
Pretack Date: 910222
 K_{fmax} = 13.2 ksi \sqrt{in}
Pass if < 0.5 : Yes

Fracture Curve Data Analysis Results:

Fracture Data File Name: TEST53A.PRN
Number of data points: 612

K rate = 2.39 ksi $\sqrt{in/sec}$
 E/E_{eff} = 1.12

Warning: E/E_{eff} is outside recommended limits of $[0.9 \leq E/E_{eff} \leq 1.1]$.
Recommend checking calibration and input data. Data will still
be corrected with E_{eff} , but use with caution.

	Obs #	Time (sec)	Load (lb)	COD (in)
Critical points:				
Maximum load:	507	20.24	5835.6	0.0126
Final data point:	612	24.44	-2.5	0.0351
Best fit linear data:				
Lower limit:	153	6.08	1291.3	0.0013
Upper limit:	217	8.64	2353.8	0.0025

Slope (lb/in)	Y-int (lb)	X-int (in)	r^2	# pts in fit	Step size	E_{eff} (Msi)
896582	157.2	-0.0002	0.999943	65	2	10.571

R-curve data stored in file: RC53.DAT

Specimen ID: 590325-L-T-4

Material: 2090-T62

Test comment: T62 POST-SPF

MTN: 900822-004

Obs #	Secant Slope (lb/in)	Load (lb)	COD (in)	Delta aeff (in)	Kr (ksi Jin)	K rate (ksi Jin/ sec)	σ_{net} (ksi)	Kapp (ksi Jin)	Valchk = $\sigma_{net}/$ σ_{ys}	Valchk < 0.8?
217	894035	2353.8	0.0025	0.000	13.54	2.4	12.87	13.53	0.26	Y
244	886116	2820.6	0.0030	0.008	16.33	2.6	15.51	16.22	0.31	Y
272	874824	3263.1	0.0036	0.016	19.04	2.4	18.07	18.76	0.36	Y
304	858653	3684.4	0.0041	0.029	21.75	2.1	20.61	21.18	0.41	Y
331	841768	4089.4	0.0047	0.042	24.44	2.5	23.12	23.51	0.46	Y
358	816398	4467.5	0.0053	0.063	27.21	2.6	25.71	25.68	0.51	Y
383	792375	4835.0	0.0059	0.084	30.00	2.8	28.31	27.80	0.57	Y
404	763585	5141.3	0.0066	0.110	32.66	3.2	30.79	29.56	0.62	Y
428	737336	5436.9	0.0072	0.134	35.31	2.8	33.29	31.26	0.67	Y
434	602242	5322.5	0.0087	0.284	39.51	17.5	37.64	30.60	0.75	Y
454	571730	5501.3	0.0094	0.324	42.32	3.5	40.57	31.63	0.81	N
467	546607	5610.6	0.0101	0.358	44.54	4.3	42.98	32.26	0.86	N
477	518740	5692.5	0.0108	0.399	46.92	5.9	45.68	32.73	0.91	N
491	478952	5709.4	0.0117	0.461	49.89	5.3	49.41	32.82	0.99	N
506	460022	5814.4	0.0125	0.492	52.38	4.1	52.39	33.43	1.05	N
507	457852	5835.6	0.0126	0.496	52.76	9.5	52.84	33.55	1.06	N
511	423490	5733.8	0.0134	0.556	55.07	14.5	56.41	32.97	1.13	N
514	421793	5743.1	0.0134	0.559	55.34	2.2	56.76	33.02	1.14	N

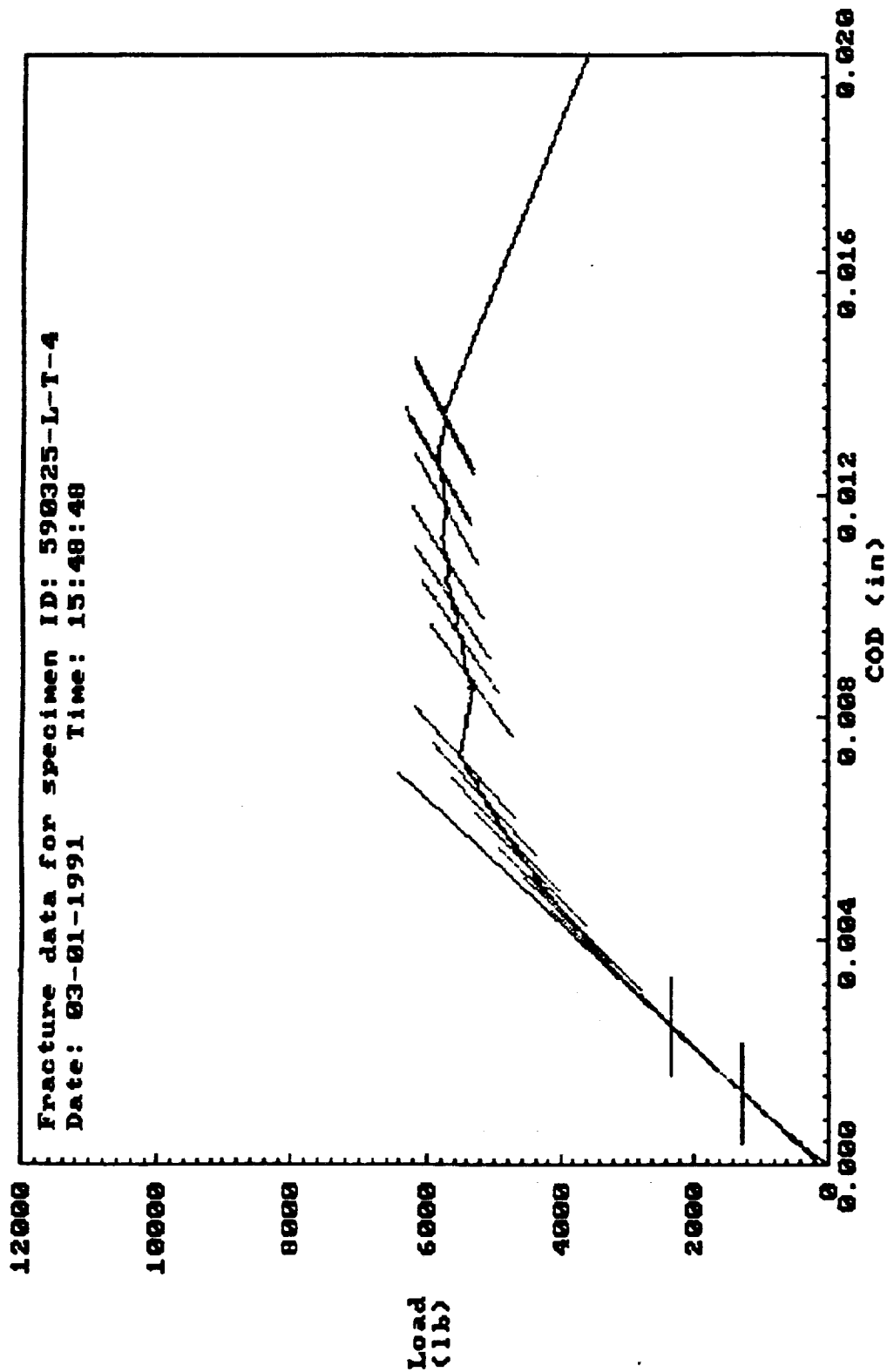
Kc calculations at maximum load:

507	457852	5835.6	0.0126	0.496	52.76	9.5	52.84	33.55	1.06	N
-----	--------	--------	--------	-------	-------	-----	-------	-------	------	---

Kc = 52.8 ksi Jin Crack length = 1.246 in Valchk = 1.06

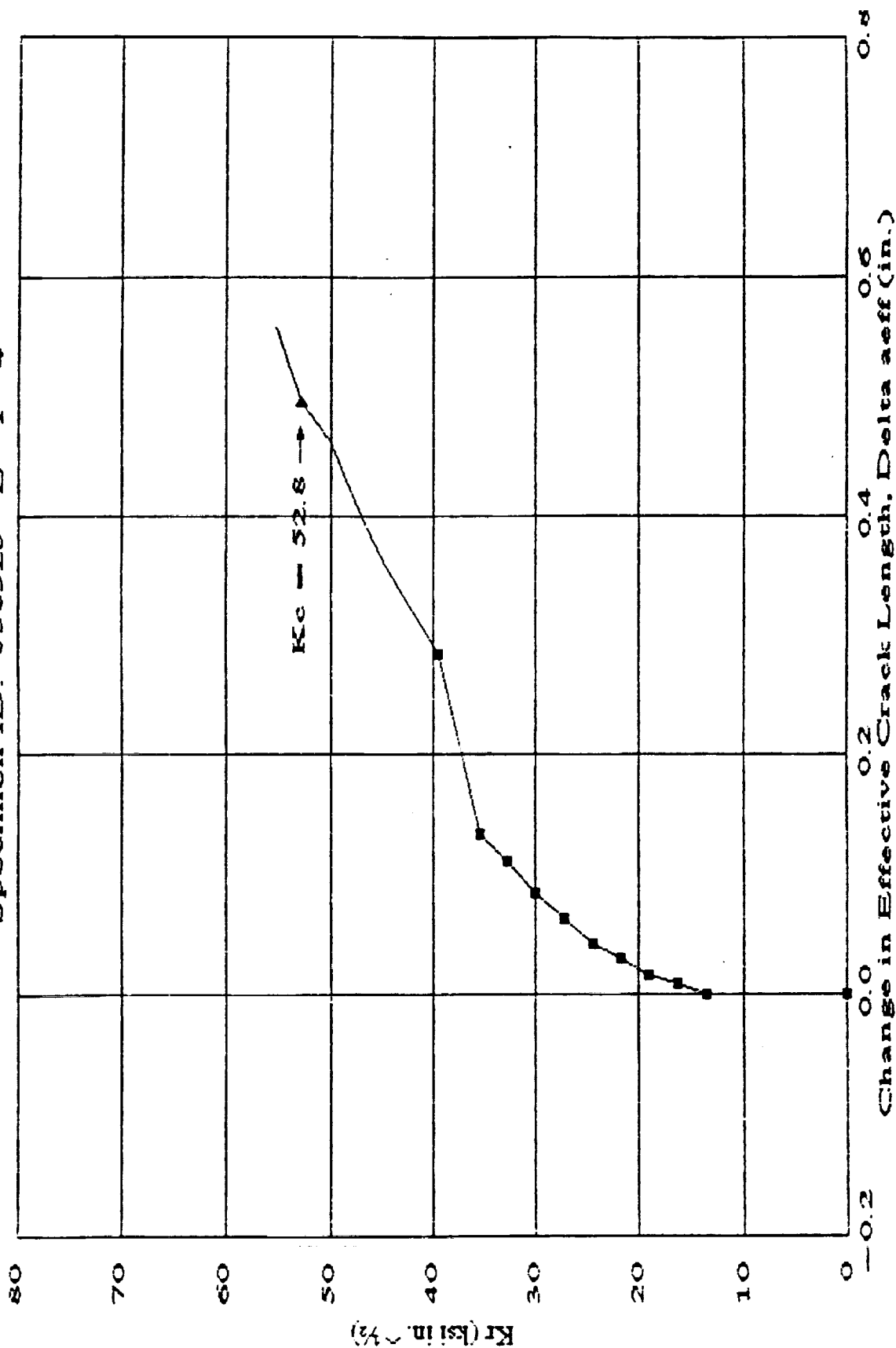
Kc point is INVALID.

Analysis stopped because $2a/w$ is outside of valid compliance region ($2a/w > 0.8$).



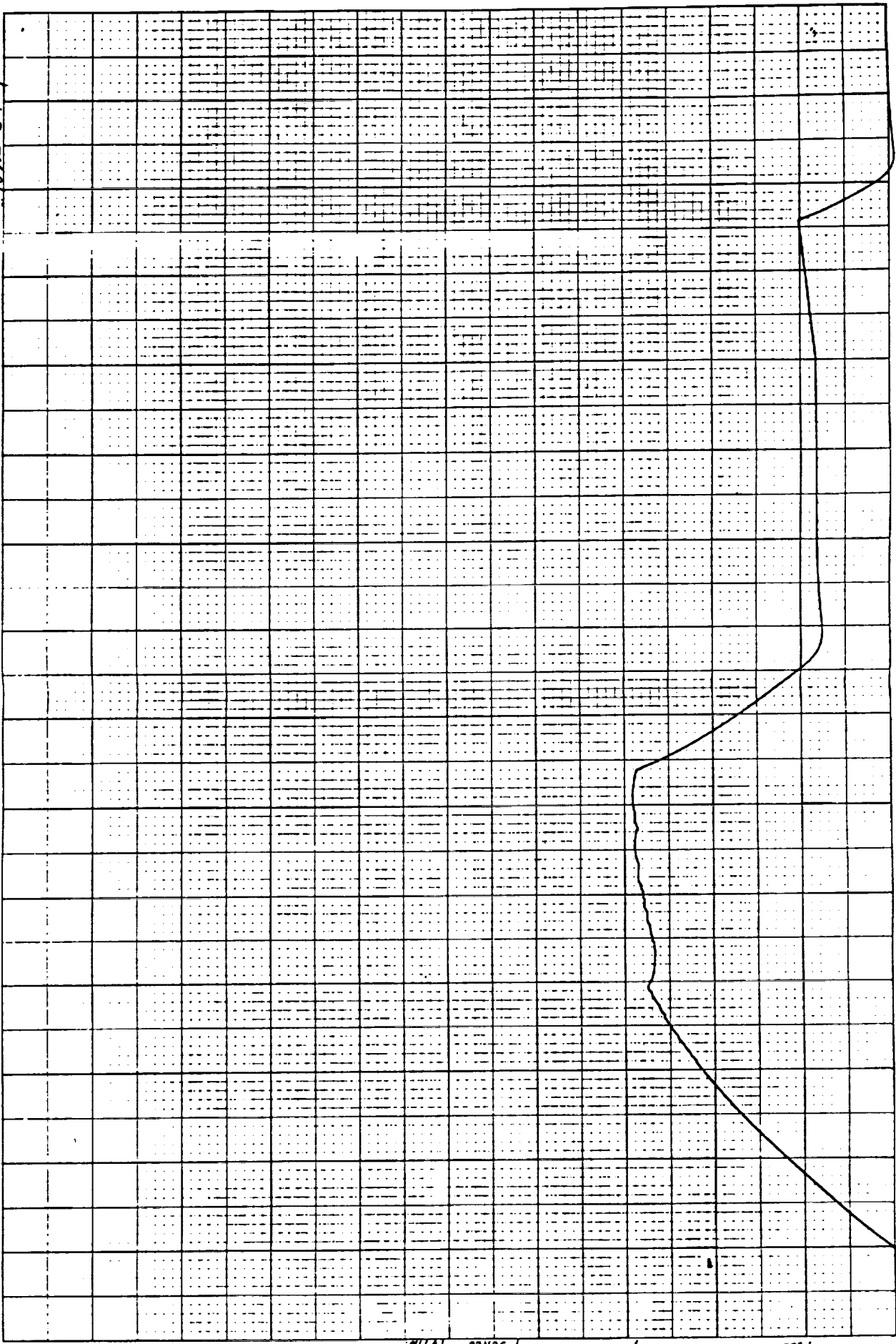
E = 11.80 E_{eff} = 10.57
Enter file name to store rcurve data: RC53.DAI
Screen copy? Y

R-curve Specimen ID: 590325-L-T-4



-- R-curve (valid) R-curve (invalid) Kc value
Material: 2090-T62
MT#: 900822-004 Test comment: T62 POST-SPF

590325-1-1-4



(0.1)

X SCALE = .5 V / IN.

Y SCALE = 0.05 V / IN.

FULL SCALE = 20 KIPS / 10V

LOAD

D-20

NO. XY 1101-SP5

GRAPHIC CONTROLS CORPORATION
PRINTED IN U.S.A.
SHEET NO. 1000

Aluminum Company of America
Alcoa Technical Center
Product Design and Mechanics Division

3-curve Fracture Toughness Test Report
Report Date and Time: 03-01-1991 15:25:32
ASTM Test Methods: B646-87 & E561-86
Data reduction program: RCURV3_1.BAS Ver 1.02

Mechanical Test No.: 900822-004
Specimen ID: 590315-1-L-T-4
Job Order No.:
Author: RLB

Material/Test Data

Alloy - Temper: 8090-T62
Product: Sheet
Lot/Sample No.: 590315-1
Specimen No.: 4
Test Comment: T62 PRE-SPF
Material Modulus = 10.8 Msi
Tensile Yield Strength, σ_{ys} = 55.0 ksi

Specimen Orientation: L-T
Specimen Type: M(T)
Product Thickness: 0.088 in
Test Date: 910221
Test Temperature: 72 deg. F
Test Operator: PDE
Test Plane: T/2

Specimen Data:

Thickness, b = 0.0885 in
Initial Crack Length, $2a_0$ = 1.570 in

Width, w = 3.980 in
Gage Span, $2y_0$ = 0.832 in

Fatigue Precracking Data:

Maximum Fatigue Load, P_{fmax} = 2000.0 lb
Fatigue Cycles = 45,635
Load Ratio, R = 0.1
 $\sigma_{fnetmax}/\sigma_{ys}$ = 0.17

$\sigma_{fnetmax}$ = 9.38 ksi
Pretcrack Date: 910221
 K_{fmax} = 9.9 ksi \sqrt{in}
Pass if < 0.5 : Yes

Fracture Curve Data Analysis Results:

Fracture Data File Name: TEST48A.PRN
Number of data points: 765

K rate = 1.47 ksi $\sqrt{in/sec}$
E/Eeff = 0.95

	Obs #	Time (sec)	Load (lb)	COD (in)
Critical points:				
Maximum load:	695	27.76	8172.5	0.0112
Final data point:	765	30.56	-3.8	0.0421
Best fit linear data:				
Lower limit:	52	2.04	26.9	-0.0001
Upper limit:	269	10.72	2613.8	0.0023

Slope (lb/in)	Y-int (lb)	X-int (in)	r^2	# pts in fit	Step size	Eeff (Msi)
1097543	93.0	-0.0001	0.999946	218	3	11.350

R-curve data stored in file: RC48.DAT
 Specimen ID: 590315-1-L-T-4
 Material: 8090-T62
 Test comment: T62 PRE-SPF
 MTH: 900822-004

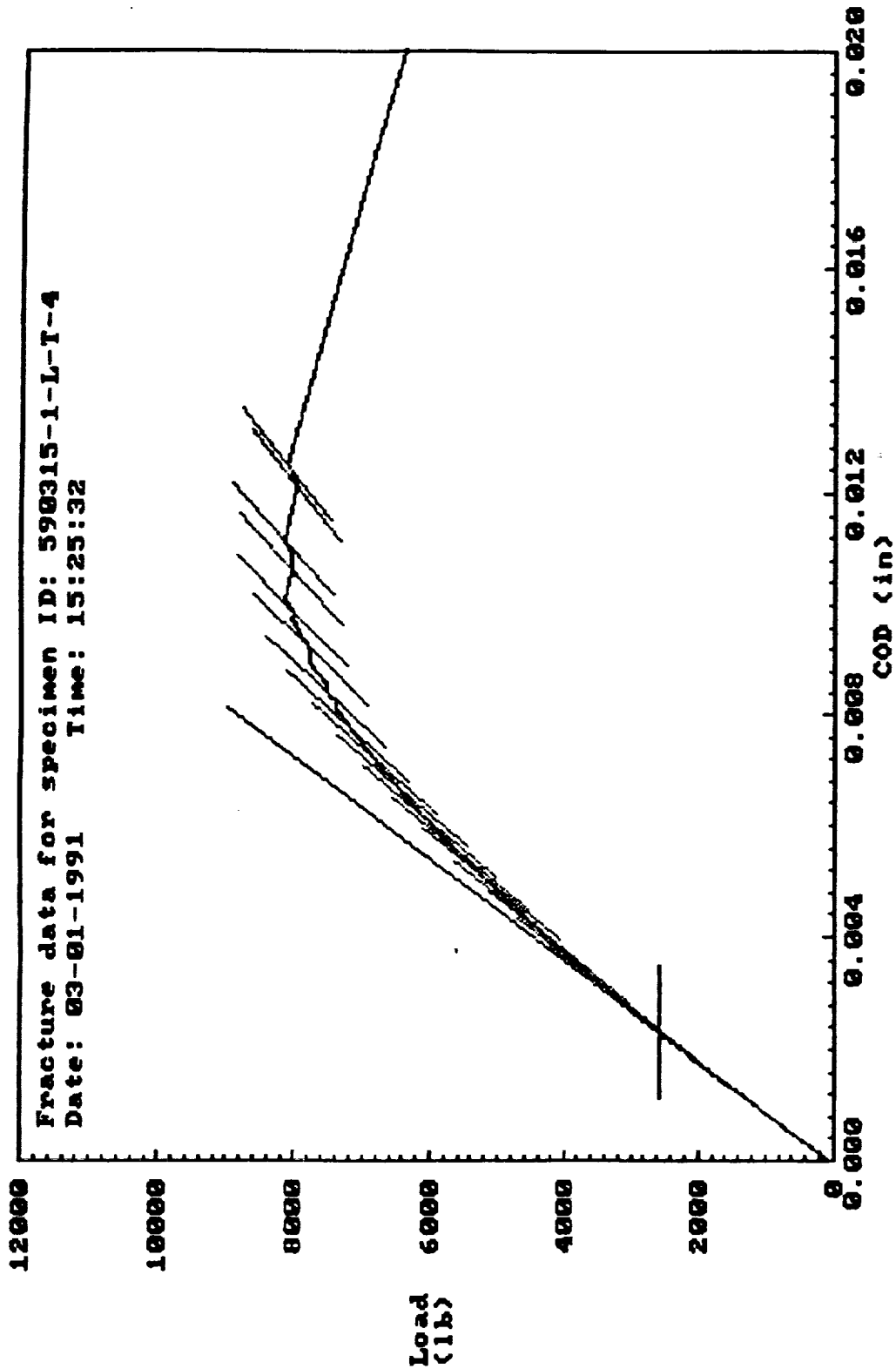
Obs #	Secant Slope (lb/in)	Load (lb)	COD (in)	Delta aeff (in)	Kr (ksi Jin)	K rate (ksi Jin/sec)	σ_{net} (ksi)	Kapp (ksi Jin)	Valchk = σ_{net}/σ_{ys}	Valchk < 0.8?
269	1091762	2613.8	0.0023	0.004	12.96	1.5	12.29	12.92	0.22	Y
299	1077264	3124.4	0.0028	0.013	15.62	2.2	14.80	15.44	0.27	Y
337	1062817	3625.6	0.0033	0.022	18.28	1.7	17.31	17.92	0.31	Y
365	1045068	4108.8	0.0038	0.033	20.93	2.4	19.81	20.30	0.36	Y
401	1031113	4619.4	0.0044	0.043	23.73	1.9	22.45	22.83	0.41	Y
436	1014466	5104.4	0.0049	0.054	26.49	2.0	25.05	25.22	0.46	Y
466	996969	5563.1	0.0055	0.066	29.19	2.2	27.60	27.49	0.50	Y
504	978492	6015.0	0.0061	0.079	31.94	1.8	30.19	29.72	0.55	Y
532	957125	6425.0	0.0066	0.095	34.60	2.4	32.70	31.75	0.59	Y
561	934222	6823.1	0.0072	0.112	37.32	2.3	35.28	33.72	0.64	Y
593	914407	7211.3	0.0078	0.128	39.99	2.1	37.82	35.63	0.69	Y
623	886411	7543.1	0.0084	0.150	42.69	2.2	40.41	37.27	0.73	Y
646	838542	7773.8	0.0092	0.191	45.63	3.2	43.33	38.41	0.79	Y
672	806248	8035.0	0.0099	0.221	48.42	2.7	46.12	39.70	0.84	N
684	752466	8068.1	0.0106	0.273	50.97	5.3	48.90	39.87	0.89	N
695	727025	8172.5	0.0112	0.299	52.88	4.3	50.97	40.38	0.93	N
696	655849	7997.5	0.0121	0.378	55.71	70.6	54.66	39.52	0.99	N
707	645119	8115.6	0.0125	0.391	57.22	3.4	56.33	40.10	1.02	N

Kc calculations at maximum load:

695	727025	8172.5	0.0112	0.299	52.88	4.3	50.97	40.38	0.93	N
-----	--------	--------	--------	-------	-------	-----	-------	-------	------	---

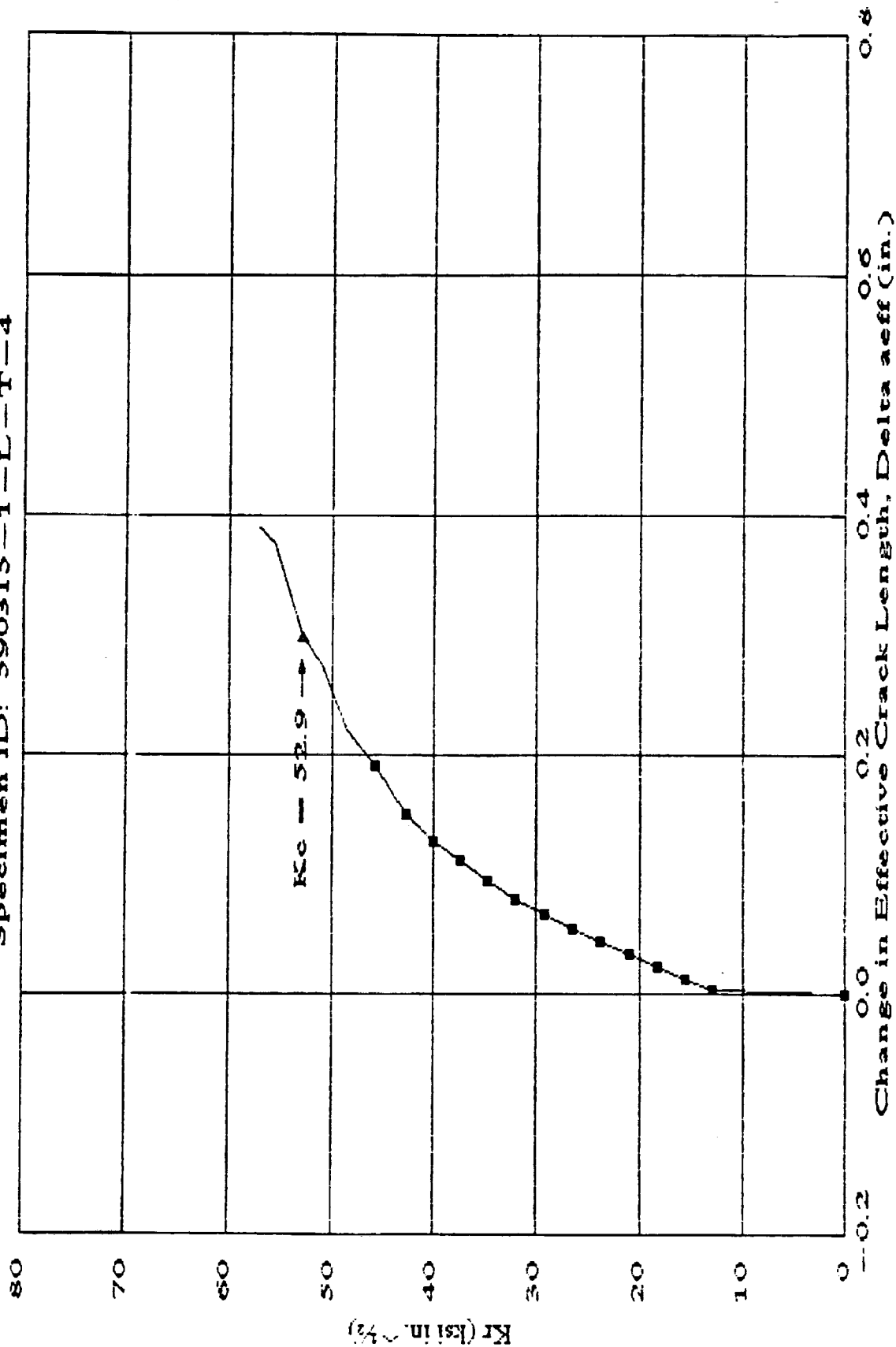
Kc = 52.9 ksi Jin Crack length = 1.084 in Valchk = 0.93
 Kc point is INVALID.

Analysis stopped because $2a/w$ is outside of valid compliance region ($2a/w > 0.8$).



E = 10.80 Eff = 11.35
Enter file name to store rcurve data: RC48.DAT
File already exists? Y
Are you sure you want to write over it (Y or N)? Y
Screen copy? Y

R-curve
Specimen ID: 590315-1-L-T-4



— R-curve (valid) — R-curve (invalid) ▲ Kc value

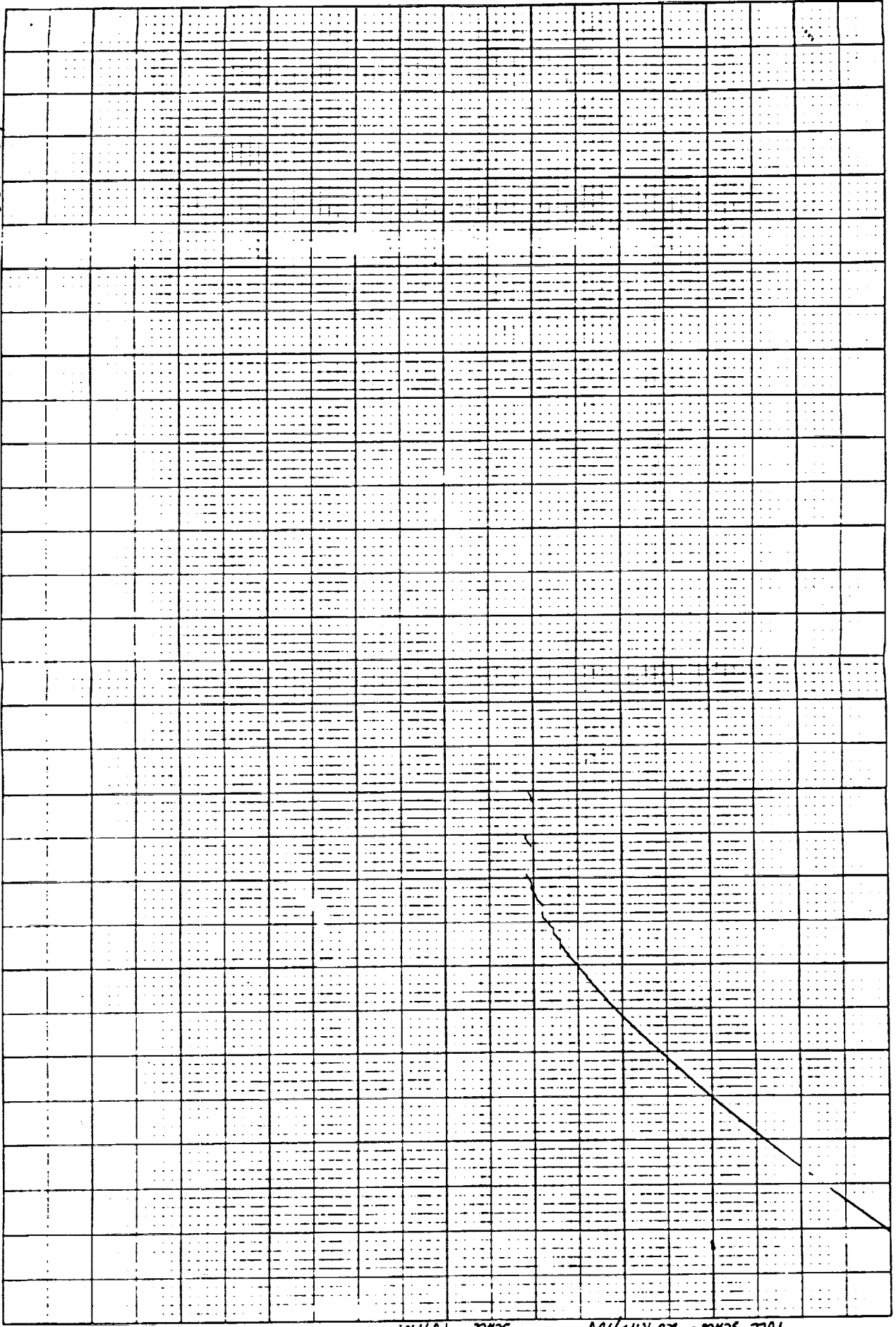
Material: 8090-T62

NTT#: 900822-004

Test comment: T62 PRE-SPF

59035-1-1-7-4

PLS



FULL SCALE = .050 in / 10V
SCALE = 0.5V / in.
COD

Full scale = 20 KIPS / 10V
Scale = 1V / in.
LOND

NO. XY 1101-SP5

D-25

GRAPHIC CORPORATION
PAPER & SUPPLIES
NEW YORK, N.Y.

Aluminum Company of America
Alcoa Technical Center
Product Design and Mechanics Division

R-curve Fracture Toughness Test Report
Report Date and Time: 03-01-1991 15:32:08
ASTM Test Methods: B646-87 & E561-86
Data reduction program: RCURV3_1.BAS Ver 1.02

Mechanical Test No.: 900822-004
Specimen ID: 590315-2-L-T-3
Job Order No.:
Author: RLB

Material/Test Data

Alloy - Temper: 8090-T62
Product: Sheet
Lot/Sample No.: 590315-2
Specimen No.: 3
Test Comment: T62 PRE-SPF
Material Modulus = 11.9 Msi
Tensile Yield Strength, σ_{ys} = 55.0 ksi

Specimen Orientation: L-T
Specimen Type: M(T)
Product Thickness: 0.088 in
Test Date: 910220
Test Temperature: 72 deg. F
Test Operator: PDE
Test Plane: T/2

Specimen Data:

Thickness, b = 0.0880 in
Initial Crack Length, $2a_0$ = 1.500 in

Width, w = 4.000 in
Gage Span, $2y_0$ = 0.832 in

Fatigue Precracking Data:

Maximum Fatigue Load, P_{fmax} = 2500.0 lb
Fatigue Cycles = 12,269
Load Ratio, R = 0.1
 $\sigma_{fnetmax}/\sigma_{ys}$ = 0.21

$\sigma_{fnetmax}$ = 11.36 ksi
Pretack Date: 910220
 K_{fmax} = 12.0 ksi $\sqrt{\text{in}}$
Pass if < 0.5 : Yes

Fracture Curve Data Analysis Results:

Fracture Data File Name: TEST47A.FRN
Number of data points: 867

K rate = 7.70 ksi $\sqrt{\text{in/sec}}$
 E/E_{eff} = 1.01

* K rate greater than maximum of 150 ksi $\sqrt{\text{in/min}}$ recommended by ASTM-E399.

	Obs #	Time (sec)	Load (lb)	COD (in)
Critical points:				
Maximum load:	828	33.08	9036.3	0.0143
Final data point:	867	34.64	-3.8	0.0455
Best fit linear data:				
Lower limit:	265	10.56	1226.9	0.0010
Upper limit	284	11.32	2450.6	0.0020

Slope (lb/in)	Y-int (lb)	X-int (in)	r^2	# pts in fit	Step size	E_{eff} (Msi)
1206579	32.1	-.0000	0.999975	20	3	11.833

R-curve data stored in file: RC47.DAT

Specimen ID: 590315-2-L-T-3

Material: 8090-T62

Test comment: T62 PRE-SPF

MT#: 900822-004

Obs #	Secant Slope (lb/in)	Load (lb)	COD (in)	Delta aeff (in)	Kr (ksi Jin)	K rate (ksi Jin/ sec)	σ_{net} (ksi)	Kapp (ksi Jin)	Valchh = $\sigma_{net}/$ σ_{ys}	Valchh < 0.8?
284	1206417	2450.6	0.0020	0.000	11.72	7.7	11.14	11.72	0.20	Y
305	1182431	3115.0	0.0026	0.013	15.08	4.0	14.31	14.90	0.26	Y
351	1159042	3770.6	0.0032	0.027	18.48	1.8	17.51	18.03	0.32	Y
397	1137058	4404.4	0.0038	0.040	21.84	1.8	20.67	21.06	0.38	Y
439	1115339	5031.3	0.0045	0.053	25.25	2.0	23.87	24.06	0.43	Y
485	1090359	5625.6	0.0051	0.068	28.64	1.8	27.05	26.90	0.49	Y
530	1065909	6195.6	0.0058	0.084	31.99	1.9	30.19	29.63	0.55	Y
577	1039986	6738.8	0.0065	0.101	35.34	1.8	33.33	32.23	0.61	Y
619	1008482	7240.6	0.0072	0.123	38.72	2.0	36.50	34.63	0.66	Y
651	964520	7636.3	0.0079	0.155	42.01	2.6	39.62	36.52	0.72	Y
682	916143	7981.9	0.0087	0.192	45.41	2.7	42.88	38.17	0.78	Y
726	843130	8270.6	0.0098	0.254	49.72	2.4	47.19	39.55	0.86	N
753	775983	8482.5	0.0109	0.317	53.96	3.9	51.68	40.57	0.94	N
763	732488	8564.4	0.0117	0.362	56.73	6.9	54.78	40.96	1.00	N
781	691662	8694.4	0.0125	0.406	60.01	4.6	58.53	41.58	1.06	N
811	668126	8958.1	0.0134	0.433	63.41	2.8	62.29	42.84	1.13	N
816	636931	8925.0	0.0140	0.470	65.46	10.3	65.01	42.68	1.18	N
828	630529	9036.3	0.0143	0.478	66.78	2.8	66.49	43.21	1.21	N
829	630715	9035.0	0.0143	0.478	66.76	-0.6	66.46	43.21	1.21	N

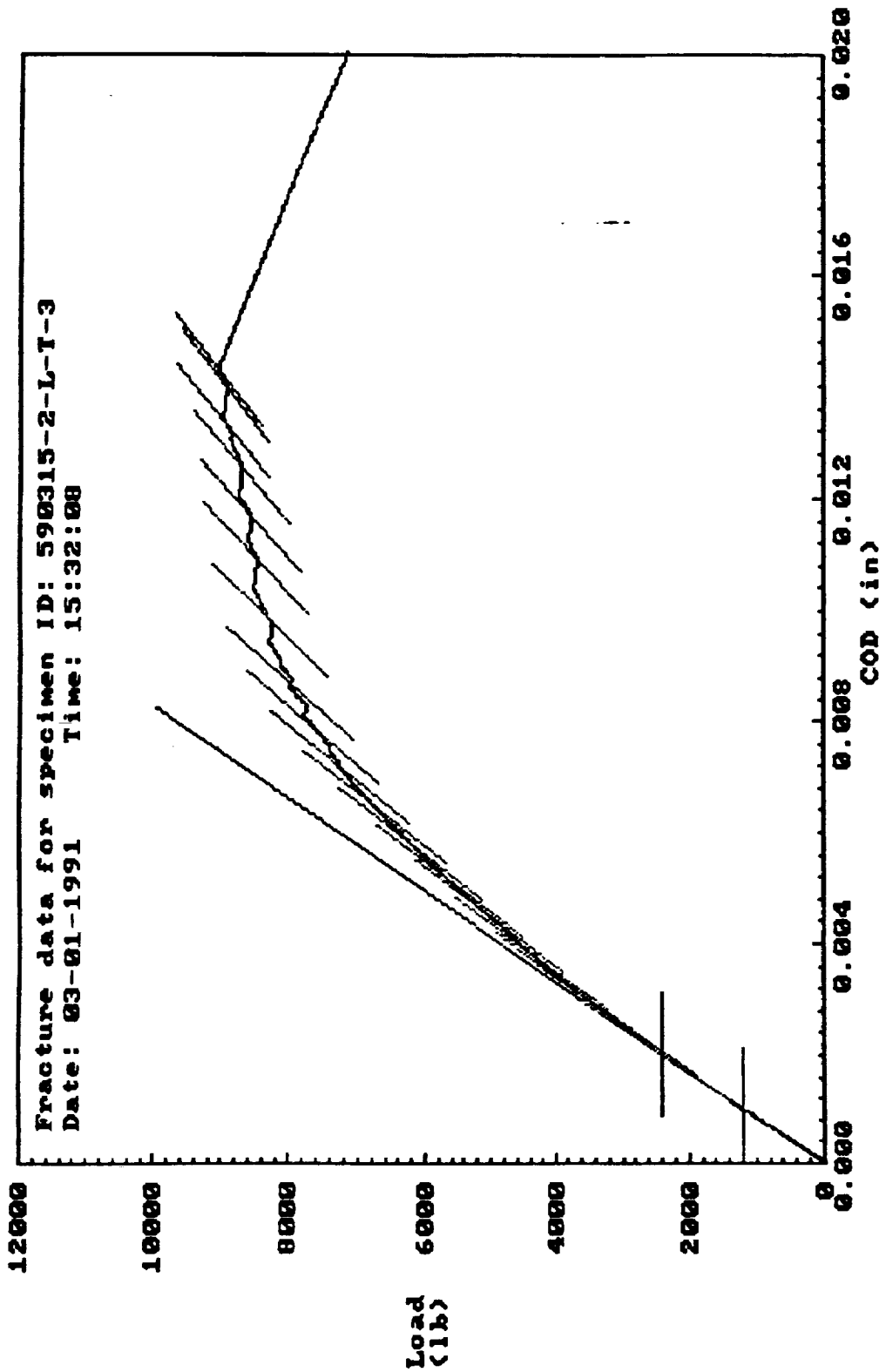
Kc calculations at maximum load:

828	630529	9036.3	0.0143	0.478	66.78	2.8	66.49	43.21	1.21	N
-----	--------	--------	--------	-------	-------	-----	-------	-------	------	---

Kc = 66.8 ksi Jin Crack length = 1.228 in Valchh = 1.21

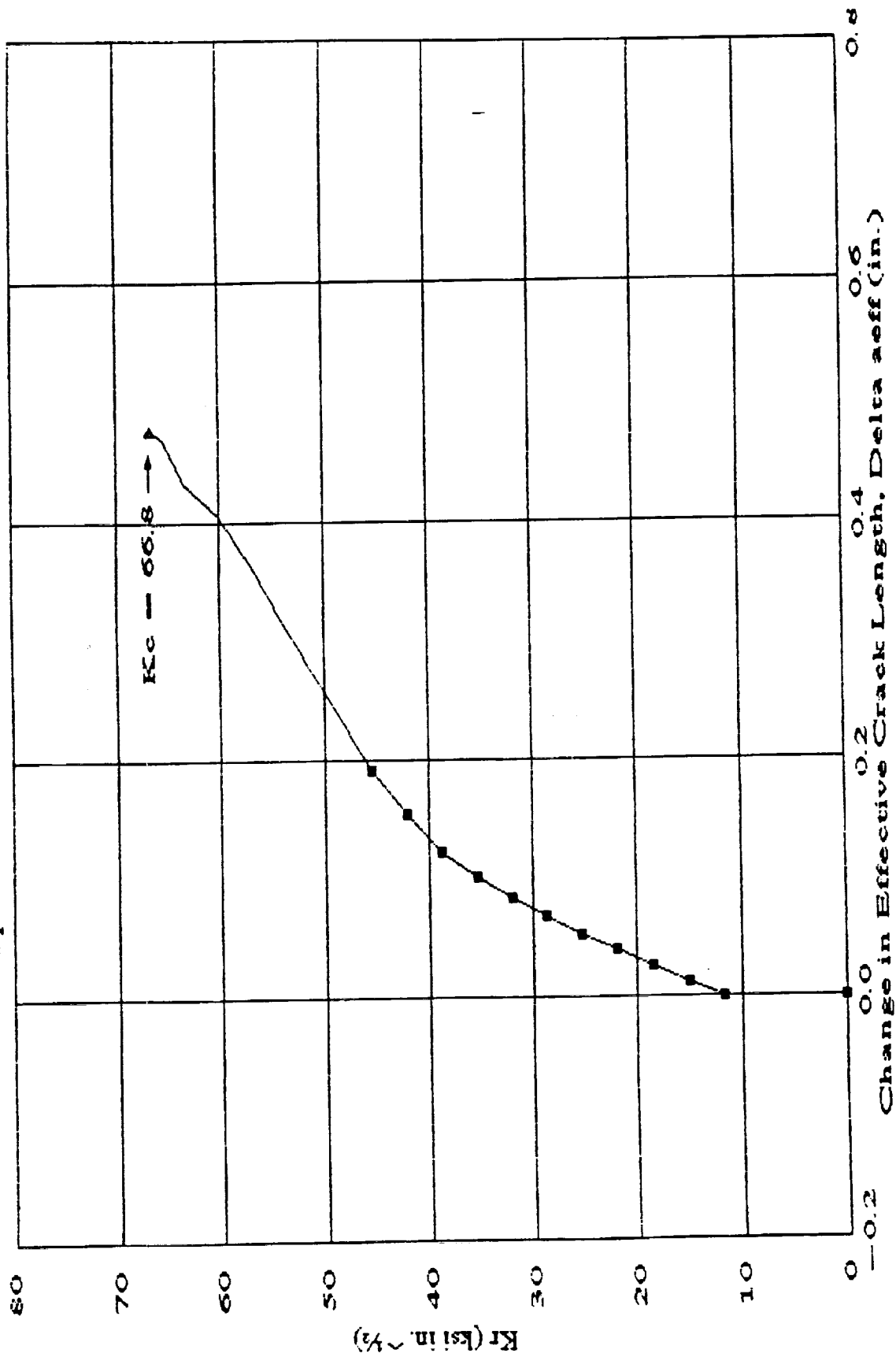
Kc point is INVALID.

Analysis stopped because $2a/w$ is outside of valid compliance region ($2a/w > 0.8$).



E = 11.90 Eff = 11.83
Enter file name to store rcurve data: RC47.DAT
Screen copy? y

H-curve
Specimen ID: 590315-2-L-T-3



-- R-curve (valid) — R-curve (invalid) Kc value
Material: 8090-T62
MT#: 900822-004 Test comment: T62 PRE-SPF

20 kV

10. XY 1101-SP5

Load

D-30

GRAPHIC CONTROLS CORPORATION
BUFFALO, NEW YORK
PRINTED IN U.S.A.

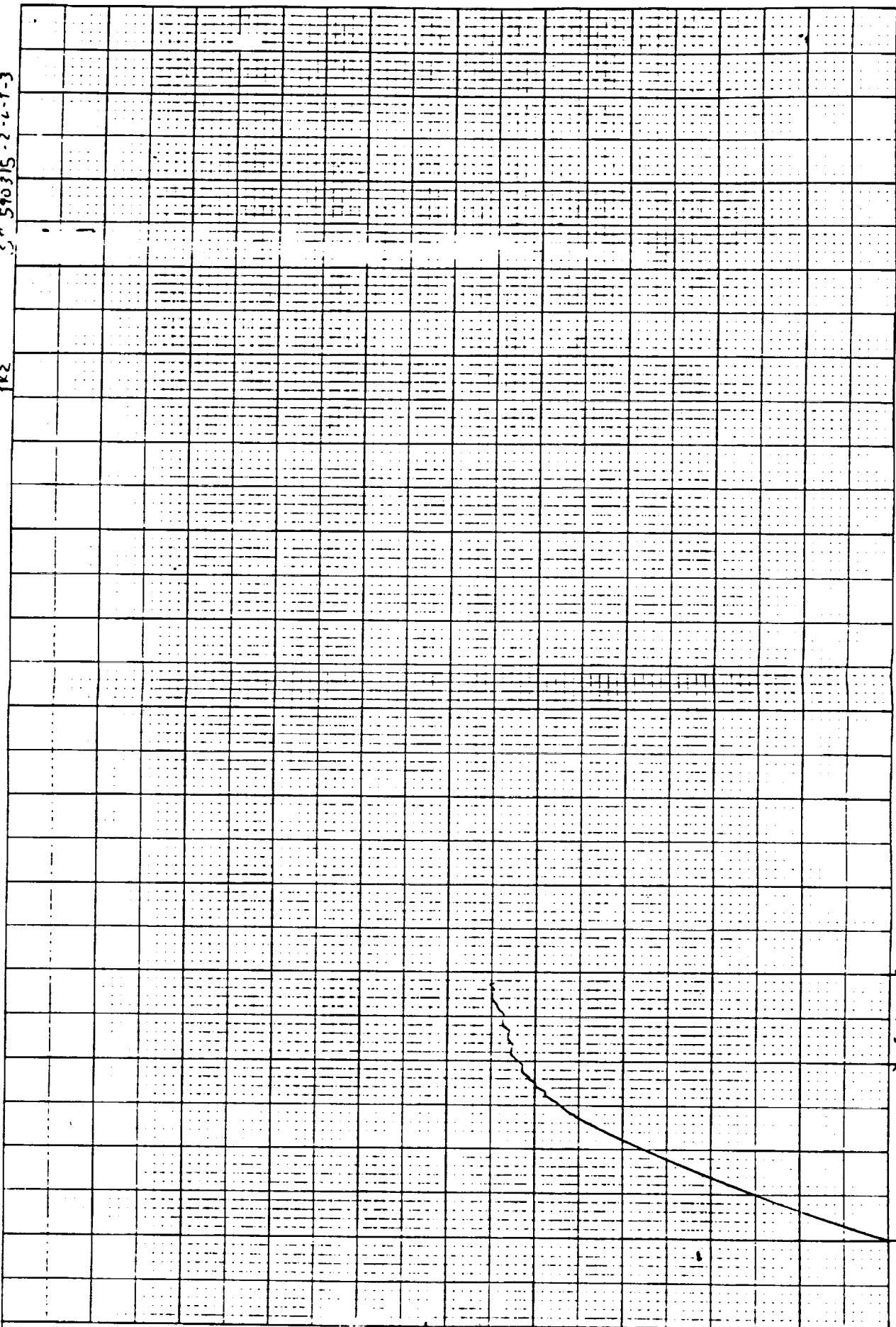
FULL SCALE = 20 KIIPS
(10V)

SCALE = 1V/IN

FULL SCALE = .050 IN/10V
SCALE = 1V/IN
20V

S# 590315-2-6-T-3

PRZ



Aluminum Company of America
Alcoa Technical Center
Product Design and Mechanics Division

R-curve Fracture Toughness Test Report
Report Date and Time: 03-04-1991 16:29:40
ASTM Test Methods: B646-87 & E561-86
Data reduction program: RCURV3 1.BAS Ver 1.02

Mechanical Test No.: 980822-004
Specimen ID: 590319-L-T-4
Job Order No.:
Author: RLB

Material/Test Data

Alloy - Temper: 8090-T62
Product: Sheet
Lot/Sample No.: 590319
Specimen No.: 4
Test Comment: T62 POST-SPF
Material Modulus = 12.9 Msi
Tensile Yield Strength, σ_{ys} = 55.0 ksi

Specimen Orientation: L-T
Specimen Type: M(T)
Product Thickness: 0.088 in
Test Date: 910221
Test Temperature: 72 deg. F
Test Operator: PDE
Test Plane: T/2

Specimen Data:

Thickness, b = 0.0771 in
Initial Crack Length, $2a_0$ = 1.455 in

Width, w = 4.000 in
Gage Span, $2y_0$ = 0.832 in

Fatigue Precracking Data:

Maximum Fatigue Load, P_{fmax} = 2300.0 lb
Fatigue Cycles = 18,037
Load Ratio, R = 0.1
 $\sigma_{fnetmax}/\sigma_{ys}$ = 0.21

$\sigma_{fnetmax}$ = 11.72 ksi
Pretack Date: 910221
 K_{fmax} = 12.3 ksi \sqrt{in}
Pass if < 0.5 : Yes

Fracture Curve Data Analysis Results:

Fracture Data File Name: TEST49A.PRN
Number of data points: 816

K rate = 11.37 ksi $\sqrt{in/sec}$
 E/E_{eff} = 1.09

* K rate greater than maximum of 150 ksi $\sqrt{in/min}$ recommended by ASTM-E399.

	Obs #	Time (sec)	Load (lb)	COD (in)
Critical points:				
Maximum load:	749	29.92	8000.0	0.0121
Final data point:	816	32.60	-3.8	0.0443
Best fit linear data:				
Lower limit:	274	10.92	1260.0	0.0009
Upper limit:	287	11.44	2366.3	0.0019

Slope (lb/in)	Y-int (lb)	X-int (in)	r^2	# pts in fit	Step size	E_{eff} (Msi)
1098993	243.3	-.0002	0.999911	14	3	11.884

R-curve data stored in file: RC49.DAT
 Specimen ID: 590319-L-T-4
 Material: 8090-T62
 Test comment: T62 POST-SPF
 MTN: 900R22-004

Obs #	Secant Slope (lb/in)	Load (lb)	COD (in)	Delta aeff (in)	Kr (ksi Jin)	K rate (ksi Jin/sec)	σ_{net} (ksi)	Kap ₀ (ksi Jin)	Valchk = σ_{net}/σ_{ys}	Valchk < 0.8?
287	1096870	2366.3	0.0019	0.001	12.66	11.4	12.07	12.65	0.22	Y
306	1083047	2928.8	0.0025	0.009	15.79	4.1	15.04	15.65	0.27	Y
345	1066130	3459.4	0.0030	0.020	18.83	1.9	17.91	18.49	0.33	Y
387	1049538	3976.3	0.0036	0.030	21.86	1.8	20.75	21.25	0.38	Y
426	1032079	4487.5	0.0041	0.041	24.92	2.0	23.63	23.99	0.43	Y
467	1013821	4986.3	0.0047	0.053	28.00	1.9	26.52	26.65	0.48	Y
505	995098	5485.0	0.0053	0.066	31.15	2.1	29.47	29.32	0.54	Y
541	970924	5931.3	0.0059	0.082	34.21	2.1	32.32	31.70	0.59	Y
576	937298	6317.5	0.0065	0.107	37.24	2.2	35.15	33.77	0.64	Y
614	915147	6743.1	0.0071	0.124	40.36	2.0	38.06	36.04	0.69	Y
638	879938	7041.9	0.0078	0.151	43.21	3.0	40.73	37.64	0.74	Y
655	842337	7231.9	0.0084	0.183	45.63	3.6	43.04	38.65	0.78	Y
685	802908	7505.6	0.0091	0.218	48.86	2.7	46.15	40.12	0.84	N
699	757041	7648.1	0.0099	0.262	51.76	5.2	49.06	40.88	0.89	N
715	695348	7721.3	0.0109	0.326	55.36	5.6	52.90	41.27	0.96	N
735	657272	7853.1	0.0117	0.369	58.55	4.0	56.37	41.97	1.02	N
749	646976	8000.0	0.0121	0.381	60.32	3.1	58.21	42.76	1.06	N
750	586609	7843.8	0.0132	0.457	63.47	78.8	62.38	41.92	1.13	N
760	585137	7959.4	0.0134	0.459	64.53	2.6	63.45	42.54	1.15	N

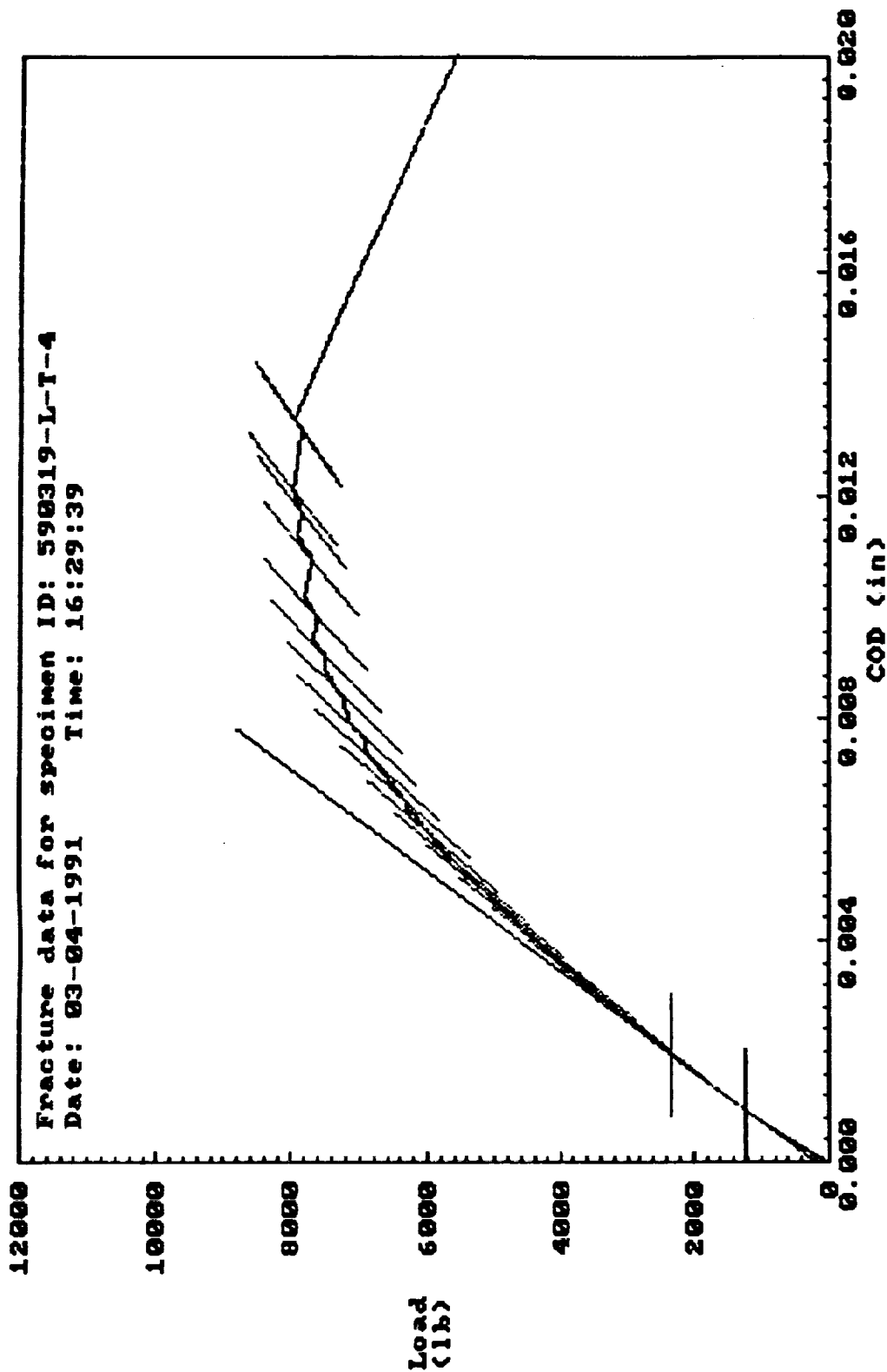
Kc calculations at maximum load:

749	646976	8000.0	0.0121	0.381	60.32	3.1	58.21	42.76	1.06	N
-----	--------	--------	--------	-------	-------	-----	-------	-------	------	---

Kc = 60.3 ksi Jin Crack length = 1.109 in Valchk = 1.06

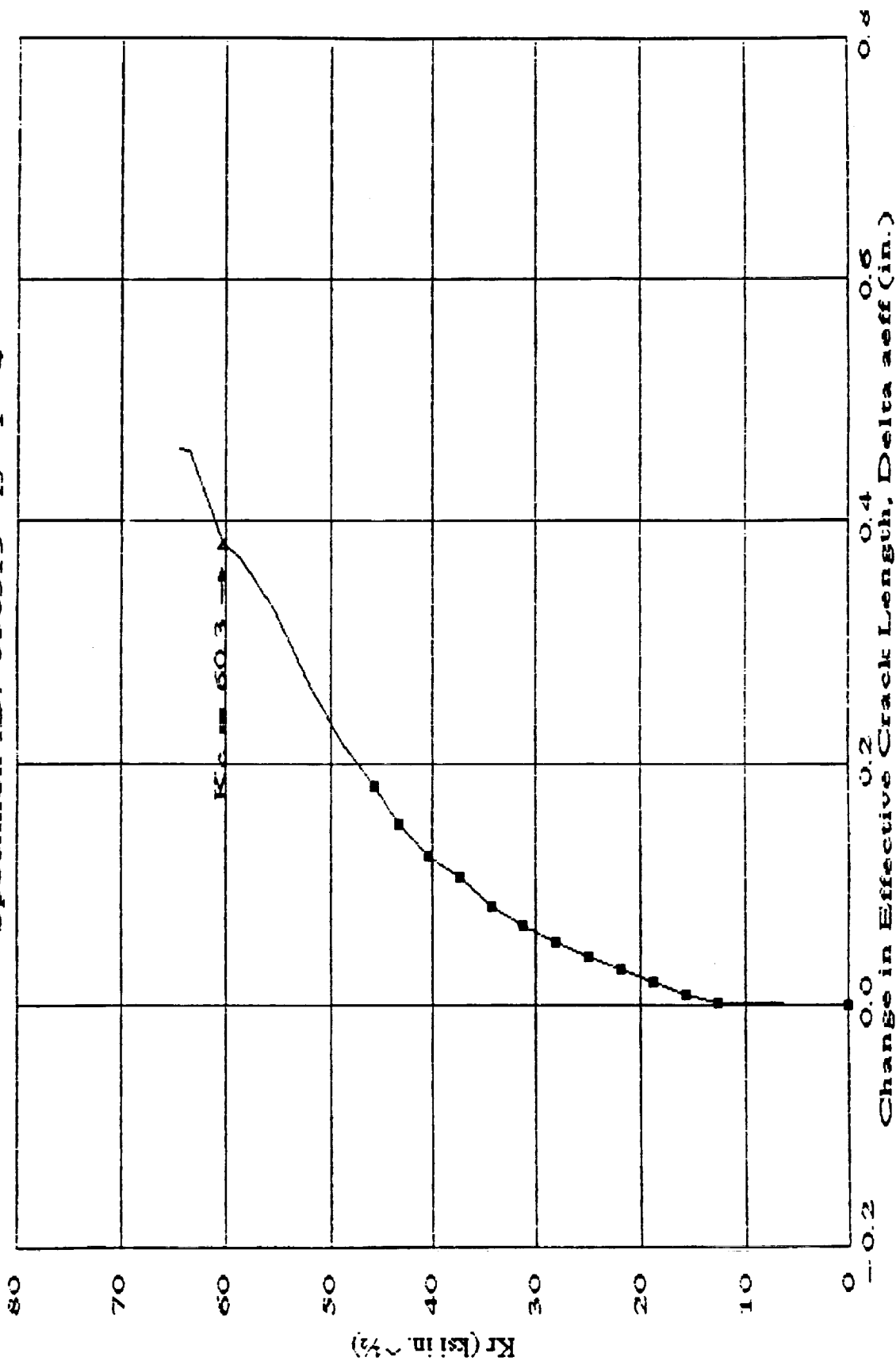
Kc point is INVALID.

Analysis stopped because load went negative.



E = 12.90 Eff = 11.88
 Enter file name to store rcurve data: RC49.DAT
 File already exists. Do you want to write over it (Y or N)? Y
 Are you sure? Y
 Screen copy? Y

R-curve
Specimen ID: 590319-L-T-4



-- R-curve (valid) --- R-curve (invalid) * Kc value
Material: 8090-T62
MT#: 900822-004 Test comment: T62 POST-SPF

Post

NO. XY 1101-SP5

D-35 28

RECEIVED
JAN 10 1964
U.S. DEPARTMENT OF AGRICULTURE
WASHINGTON, D.C.

SCALE: 1/16"

FULL SCALE = 20 KIPS/10V

← 5145.12 →

FUL. S.N. 6 = 0.05 IN/10V SENSE 0.5V/M. COLD

'

Aluminum Company of America
Alcoa Technical Center
Product Design and Mechanics Division

R-curve Fracture Toughness Test Report
Report Date and Time: 03-01-1991 15:08:45
ASTM Test Methods: B646-87 & E561-86
Data reduction program: RCURV3_1.BAS Ver 1.02

Mechanical Test No.: 900822-004
Specimen ID: 590320-L-T-1
Job Order No.:
Author: RLB

Material/Test Data

Alloy - Temper: 8090-T62
Product: Sheet
Lot/Sample No.: 590320
Specimen No.: 1
Test Comment: T62 POST-SPF
Material Modulus = 12.4 Msi
Tensile Yield Strength, σ_{ys} = 55.0 ksi

Specimen Orientation: L-T
Specimen Type: M(T)
Product Thickness: 0.088 in
Test Date: 910222
Test Temperature: 72 deg. F
Test Operator: PDE
Test Plane: T/2

Specimen Data:

Thickness, b = 0.0731 in
Initial Crack Length, $2a_0$ = 1.450 in

Width, w = 4.000 in
Gage Span, $2y_0$ = 0.832 in

Fatigue Precracking Data:

Maximum Fatigue Load, P_{fmax} = 2300.0 lb
Fatigue Cycles = 11,516
Load Ratio, R = 0.1
 $\sigma_{fnetmax}/\sigma_{ys}$ = 0.22

$\sigma_{fnetmax}$ = 12.34 ksi
Pretcrack Date: 910222
 K_{fmax} = 12.9 ksi \sqrt{in}
Pass if < 0.5 : Yes

Fracture Curve Data Analysis Results:

Fracture Data File Name: TEST50A.PRN
Number of data points: 612

K rate = 2.35 ksi \sqrt{in}/sec
 E/E_{eff} = 1.24

Warning: E/E_{eff} is outside recommended limits of $[0.9 \leq E/E_{eff} \leq 1.1]$.
Recommend checking calibration and input data. Data will still
be corrected with E_{eff} , but use with caution.

	Obs #	Time (sec)	Load (lb)	COD (in)
Critical points:				
Maximum load:	551	22.00	6990.6	0.0113
Final data point:	612	24.44	2135.6	0.0311
Best fit linear data:				
Lower limit:	153	6.08	1330.6	0.0016
Upper limit:	223	8.88	2499.4	0.0029

Slope (lb/in)	Y-int (lb)	X-int (in)	r^2	# pts in fit	Step size	E_{eff} (Msi)
878443	-56.7	0.0001	0.999927	71	2	9.980

R-curve data stored in file: rc50.dat

Specimen ID: 590320-L-T-1

Material: 8090-T62

Test comment: T62 POST-SPF

MTN: 900822-004

Obs #	Secant Slope (lb/in)	Load (lb)	COD (in)	Delta aeff (in)	Kr (ksi f/in)	K rate (ksi f/in/ sec)	σ_{net} (ksi)	K_{app} (ksi f/in)	σ_{net}/σ_{ys}	Valchk < 0.8?
223	877118	2499.4	0.0029	0.001	14.07	2.3	13.42	14.06	0.24	Y
248	868420	2916.9	0.0034	0.007	16.52	2.4	15.74	16.40	0.29	Y
276	859162	3327.5	0.0039	0.014	18.97	2.2	18.05	18.71	0.33	Y
309	849999	3736.9	0.0045	0.021	21.44	1.9	20.39	21.02	0.37	Y
336	839841	4145.0	0.0050	0.029	23.96	2.3	22.76	23.31	0.41	Y
362	830204	4545.0	0.0055	0.037	26.46	2.4	25.11	25.56	0.46	Y
389	817317	4943.1	0.0061	0.047	29.05	2.4	27.54	27.80	0.50	Y
413	802140	5303.8	0.0067	0.060	31.53	2.6	29.85	29.83	0.54	Y
437	781819	5627.5	0.0073	0.077	33.99	2.6	32.14	31.65	0.58	Y
460	756893	5918.8	0.0079	0.100	36.48	2.7	34.44	33.29	0.63	Y
483	743312	6248.1	0.0085	0.112	38.95	2.7	36.75	35.14	0.67	Y
498	698569	6402.5	0.0092	0.156	41.51	4.3	39.13	36.01	0.71	Y
516	668294	6623.1	0.0100	0.188	44.18	3.7	41.67	37.25	0.76	Y
526	646350	6728.8	0.0105	0.212	45.87	4.2	43.31	37.84	0.79	Y
546	625686	6941.9	0.0112	0.236	48.34	3.1	45.71	39.04	0.83	N
551	622884	6990.6	0.0113	0.240	48.83	2.4	46.18	39.32	0.84	N
552	551939	6805.0	0.0124	0.331	51.57	68.6	49.29	38.27	0.90	N
564	490026	6774.4	0.0139	0.422	55.83	8.9	54.34	38.10	0.99	N
573	482809	6833.8	0.0142	0.434	56.93	3.0	55.57	38.43	1.01	N

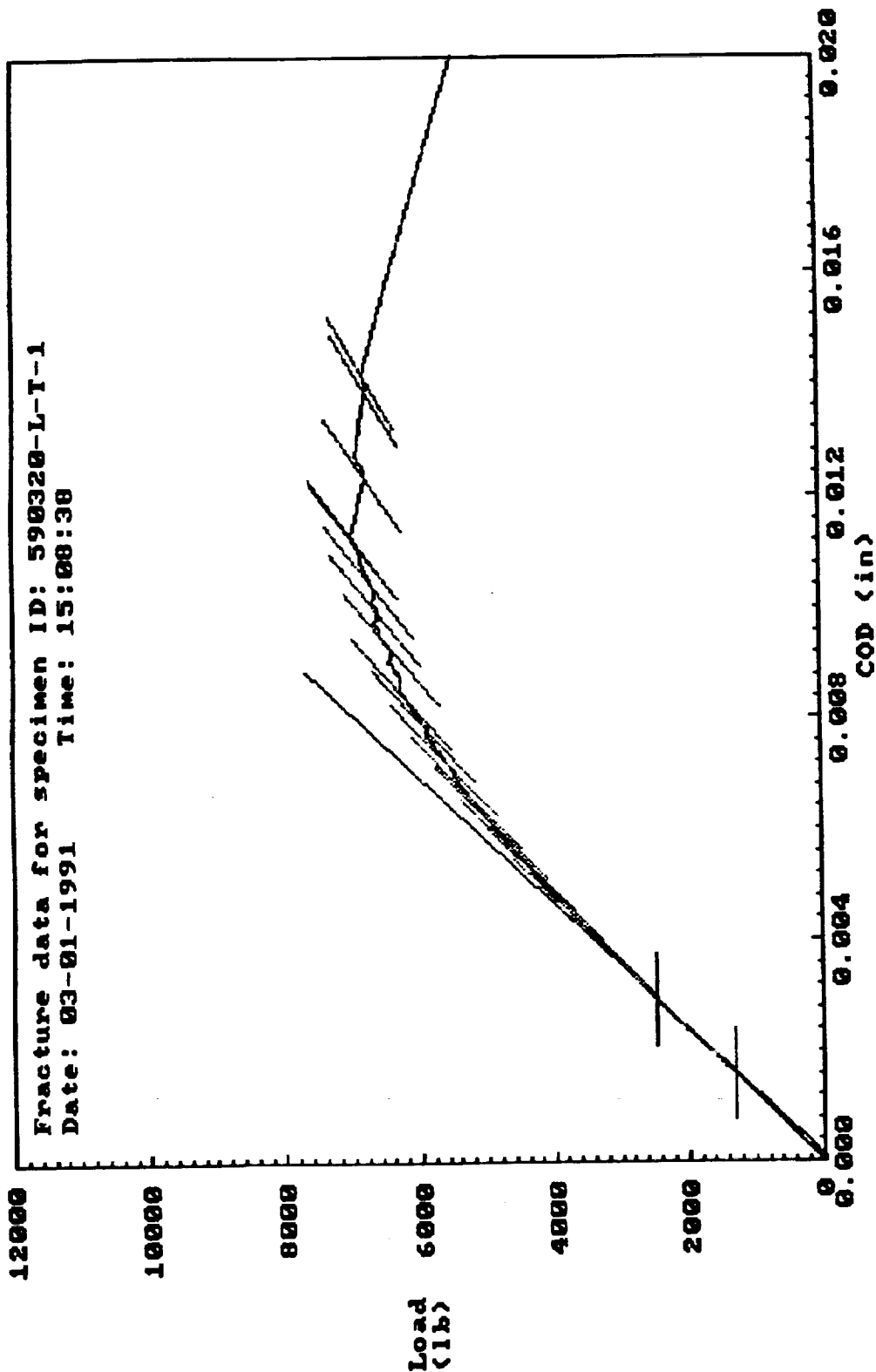
Kc calculations at maximum load:

551	622884	6990.6	0.0113	0.240	48.83	2.4	46.18	39.32	0.84	N
-----	--------	--------	--------	-------	-------	-----	-------	-------	------	---

Kc = 48.8 ksi f/in Crack length = 0.965 in Valchk = 0.84

Kc point is INVALID.

Analysis stopped because $2a/w$ is outside of valid compliance region ($2a/w > 0.8$).

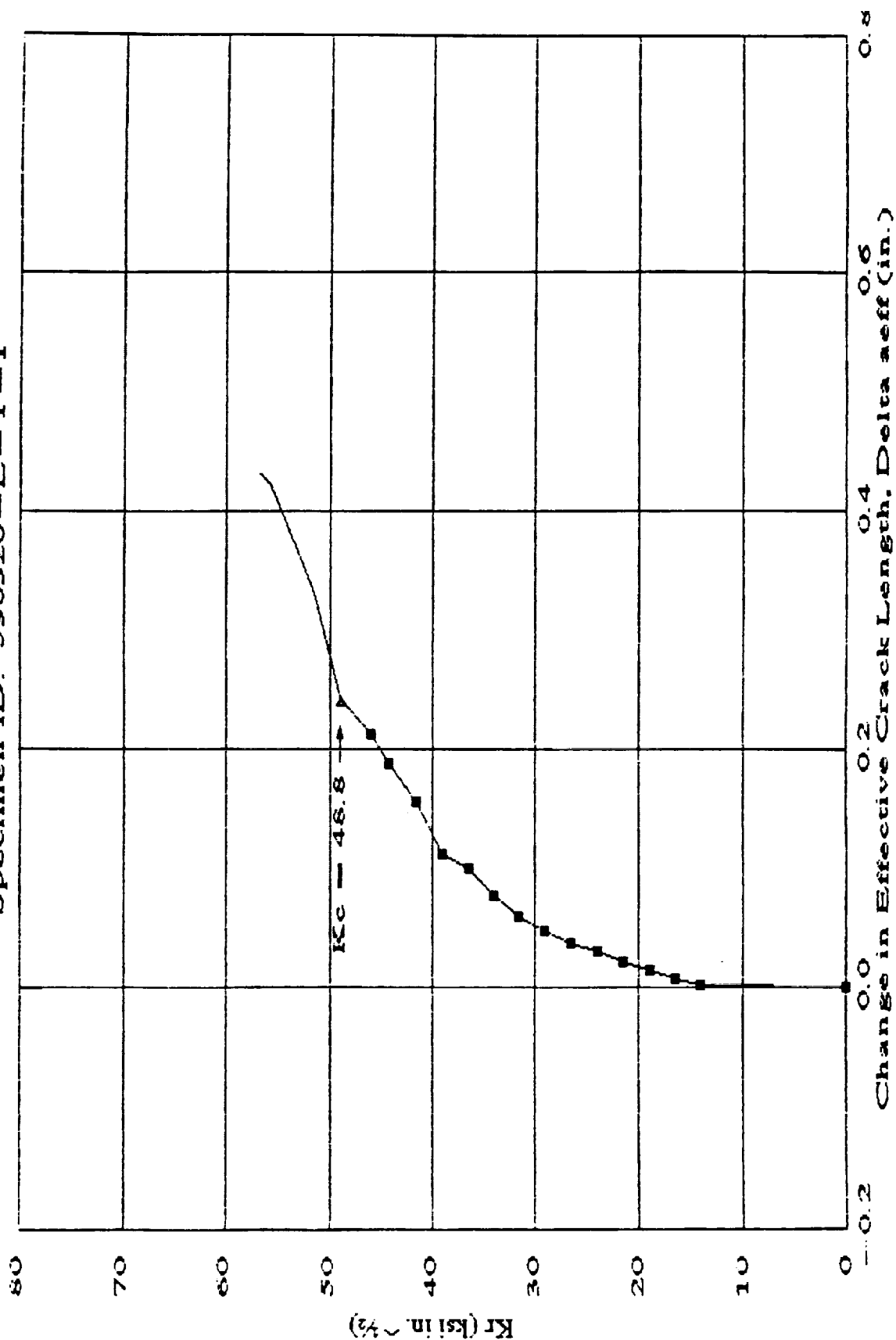


ORIGINAL PAGE IS
OF POOR QUALITY

D-38

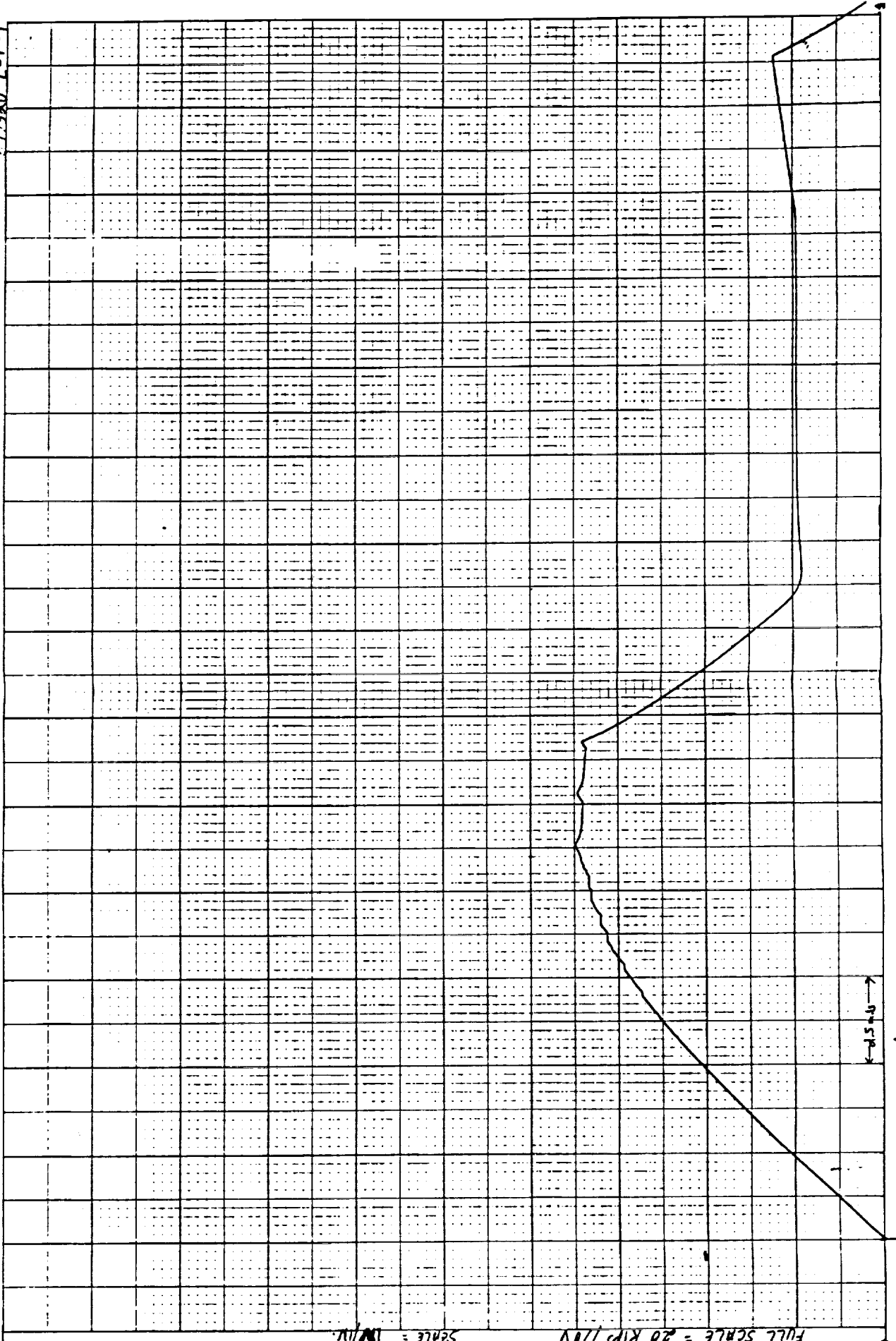
F = 12.40 Eff = 9.98
Enter file name to store rcurve data: rc50.dat
File already exists? Do you want to write over it (Y or N)? y
Are you sure (Y or N)? y
Screen copy? y

R-curve Specimen ID: 590320-L-T-1



— R-curve (valid) — R-curve (invalid) Kc value
 Material: 8090-T62
 NIT#: 900822-004 Test comment: T62 POST-SPF

691320-1-T-1



SCALE 0.5V/IN

FULL SCALE 0.05 IN/10V

FULL SCALE = 20 KIIPS/10V

SCALE = 1V/IN

20

NO. XY 1101-SPS

D-40

RESEARCH-CALIBRATION
SIGNAL CONDITIONING CORPORATION
BURLINGAME, CALIF. 94010
PRINTED IN U.S.A.

THIS PAGE INTENTIONALLY LEFT BLANK.

APPENDIX E

TRANSMISSION ELECTRON MICROSCOPY AND DIFFRACTION PATTERNS OF 2090 AND 8090 HEAT TREATMENT ANALYSIS

PRECEDING PAGE BLANK NOT FILMED



E-1

2090 WQ + age







ORIGINAL PAGE IS
OF POOR QUALITY

E-4

2090 fan cool + age





E-6

2090 - slow cool + age



E-7

2090 slow cool +age



2090 slow cool + age.



2090- slow cool +age



ORIGINAL PAGE IS
OF POOR QUALITY

E-10

2090 slow cool + age



2090 slow cool + age



21.0KN559

8090 WA + age.



8090 WQ + age.

31.0KN.5.6.4



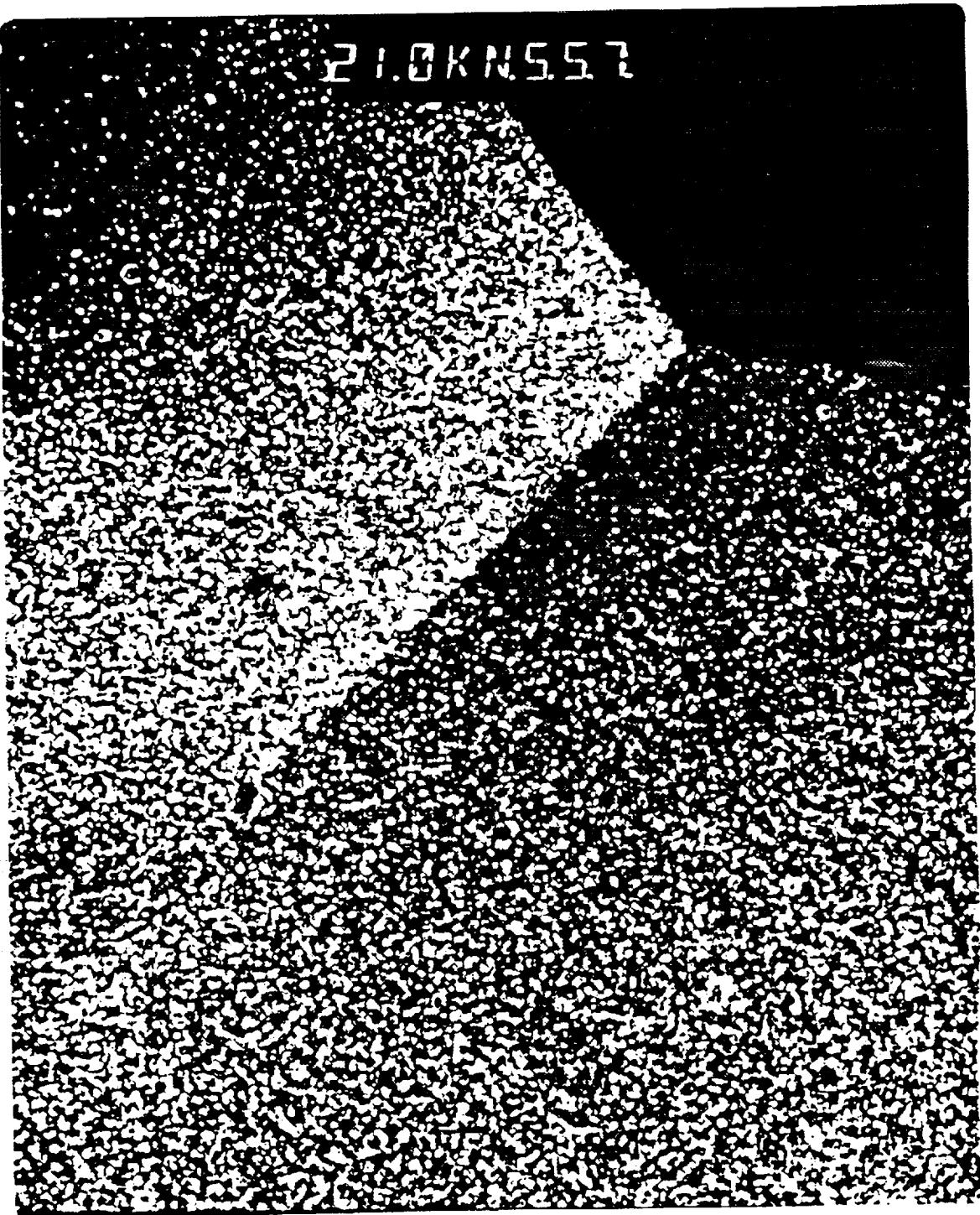
8090 WA + age.
8090 poor cool age



E-15

8090 W2 + age.

21.0KN557



3090 W2.

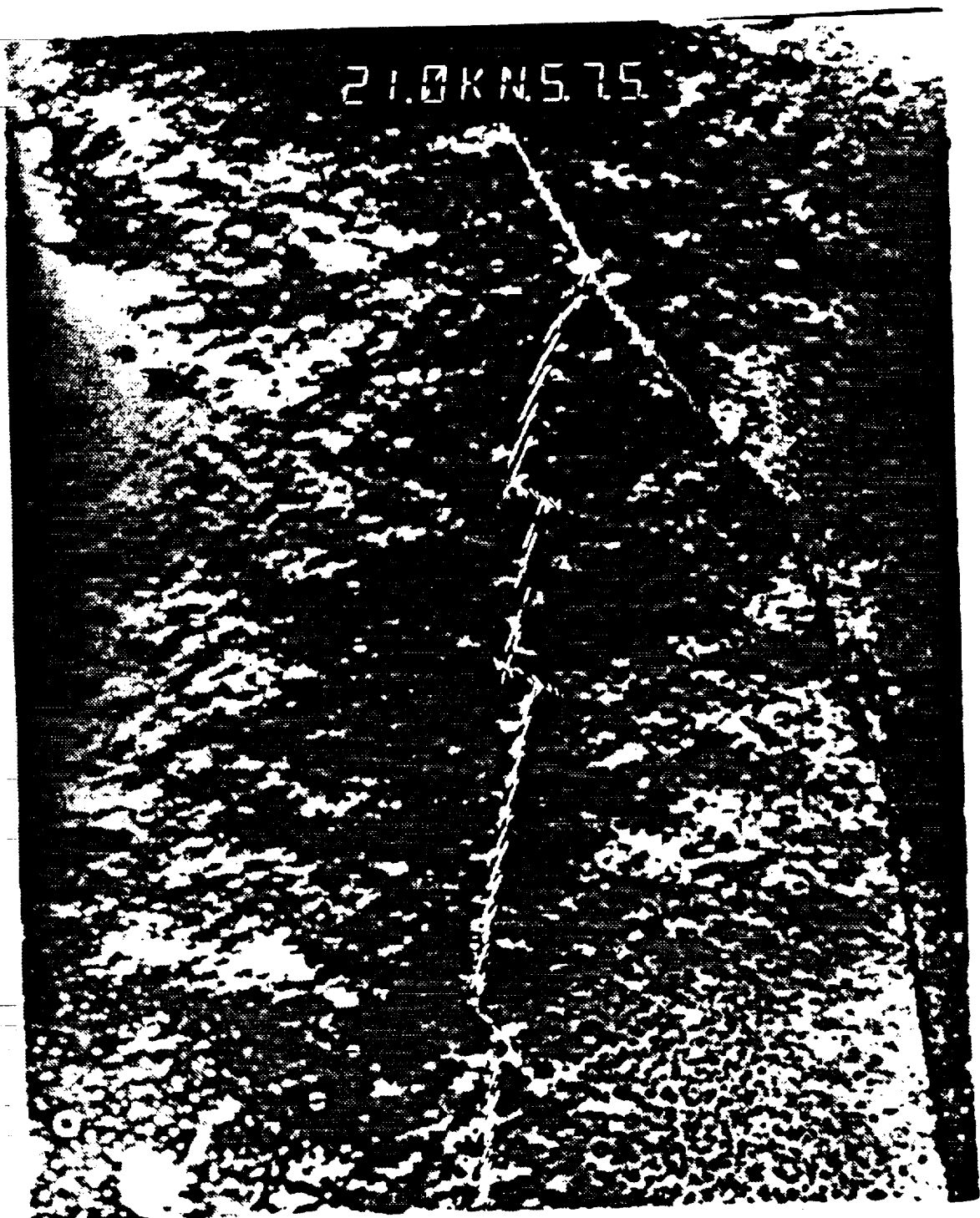
ORIGINAL PAGE IS
OF POOR QUALITY

E-16

e-7



8090 fan cool + age

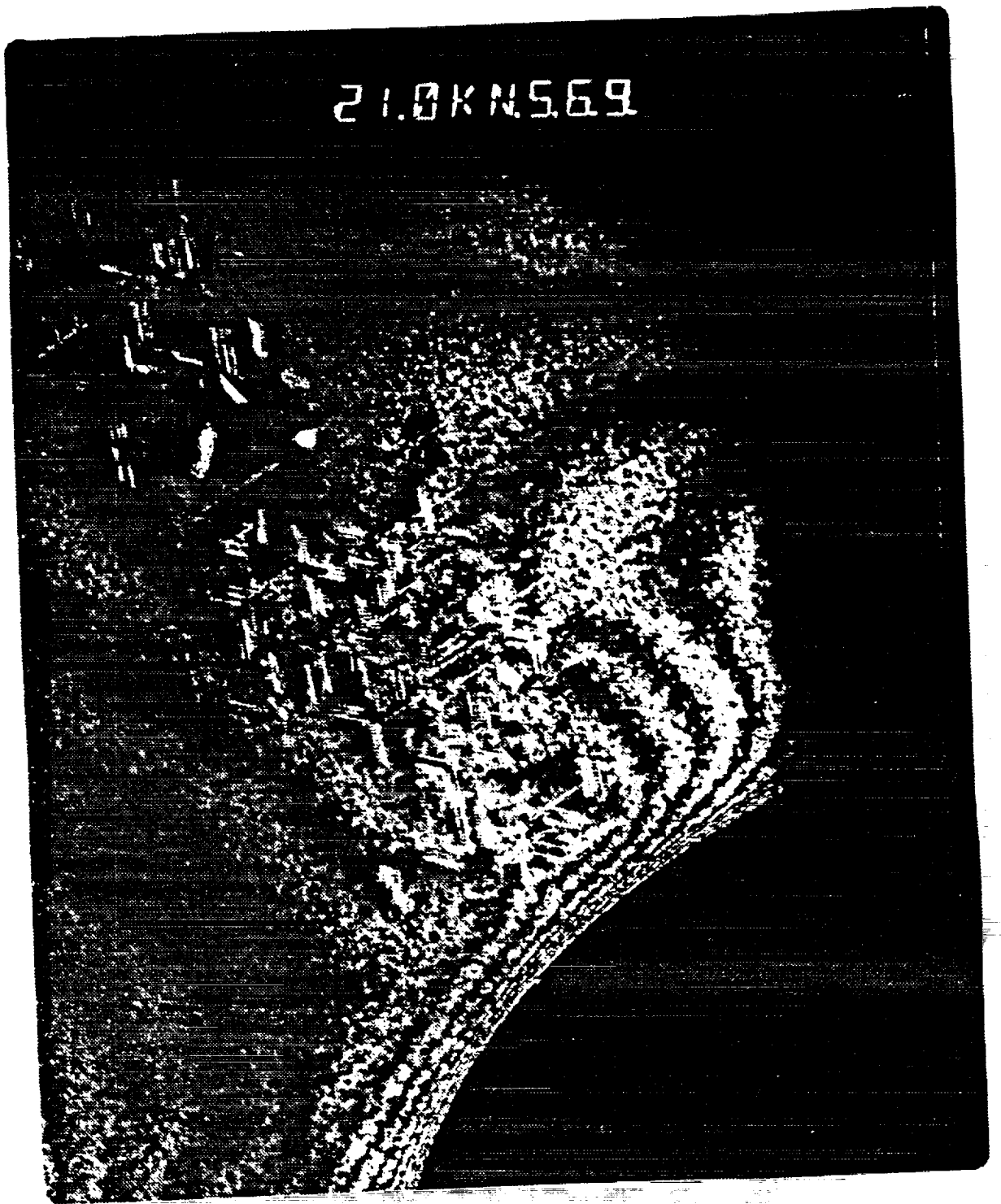


8090 fan cool rag

ORIGINAL PAGE IS
OF POOR QUALITY

E-18

21.0KN5.69



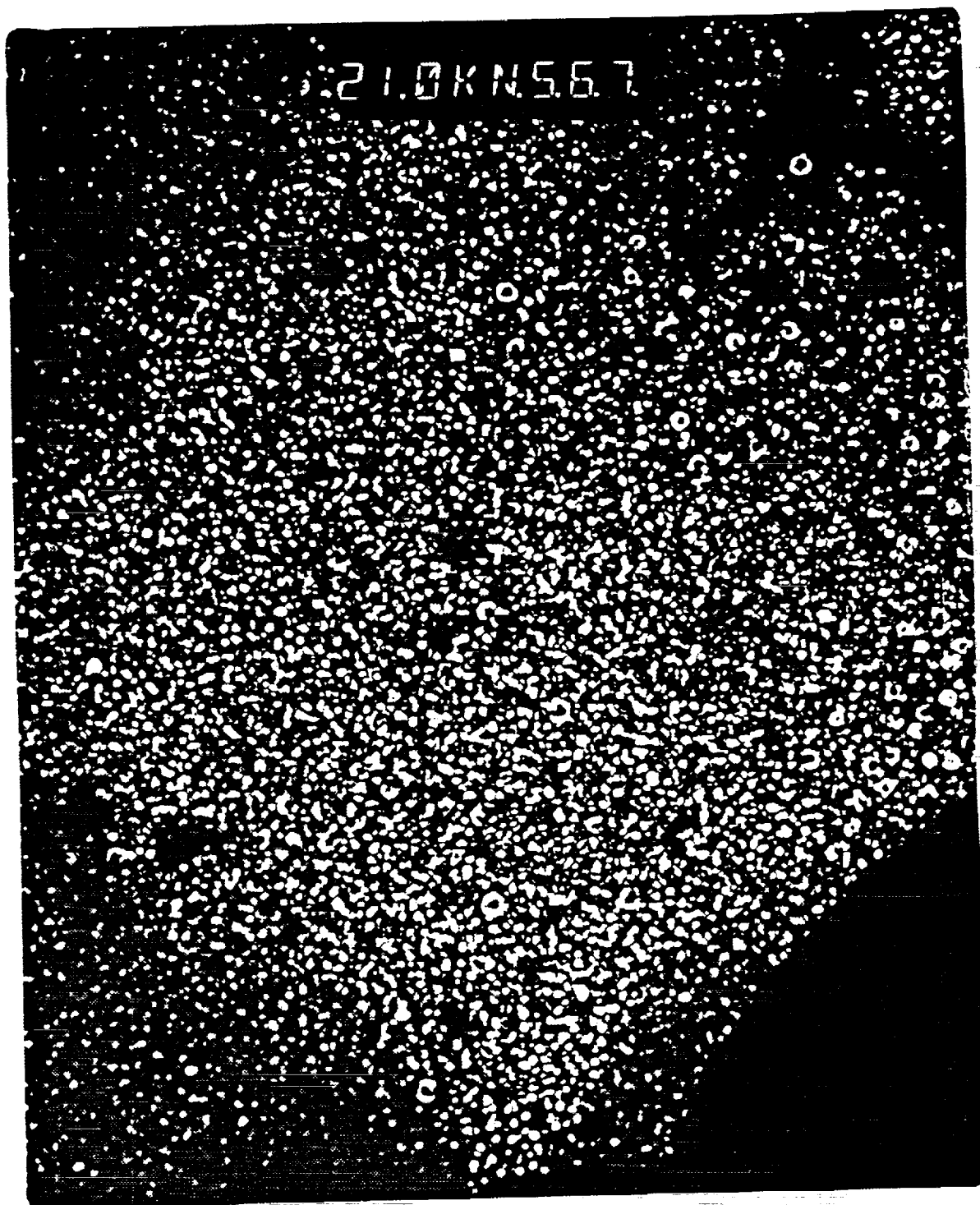
8090 fan cool + age



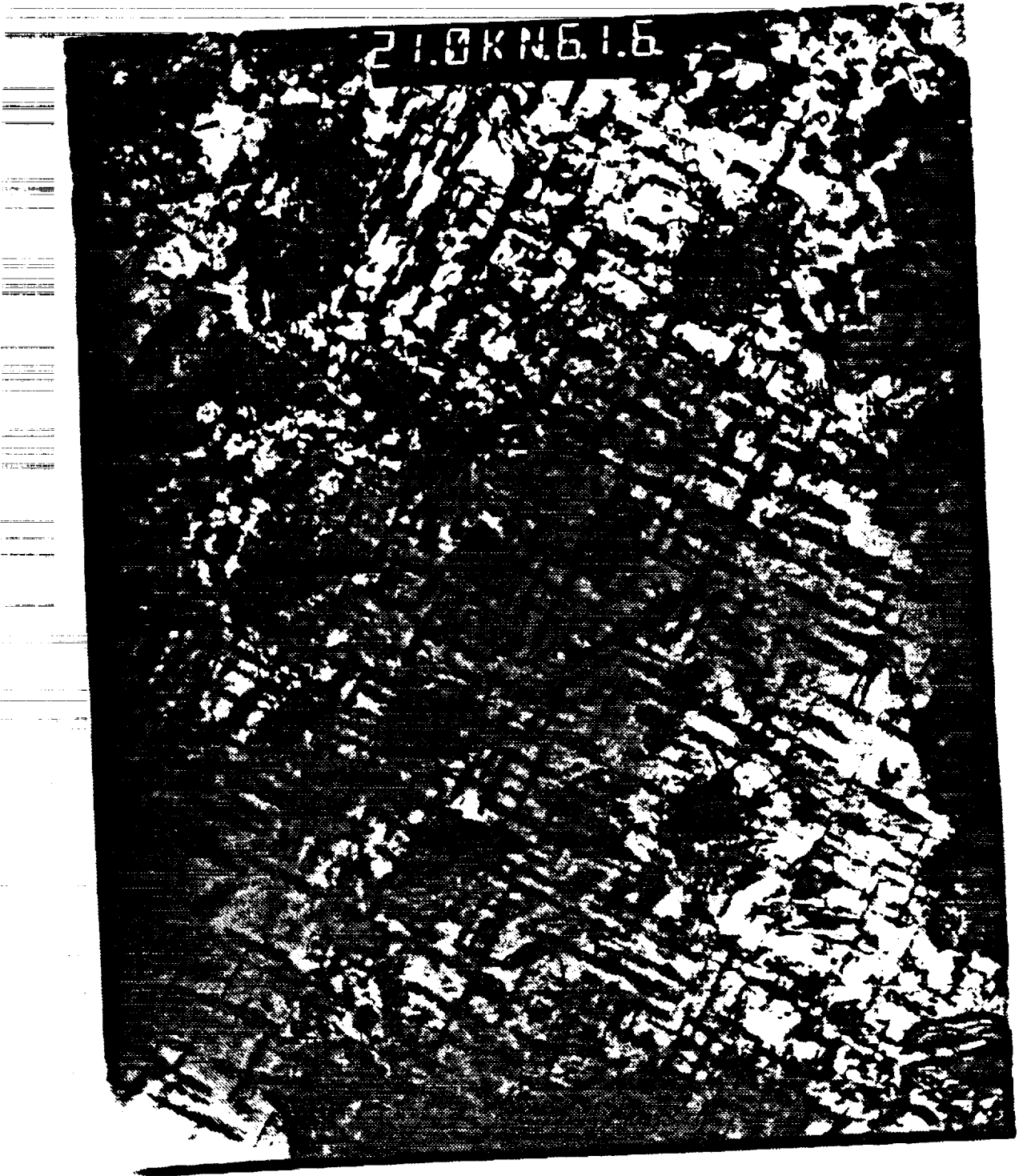
8090 fan cool + age

ORIGINAL PAGE IS
OF POOR QUALITY

E-20



8090 fan cool + age



8090 slow cool + age



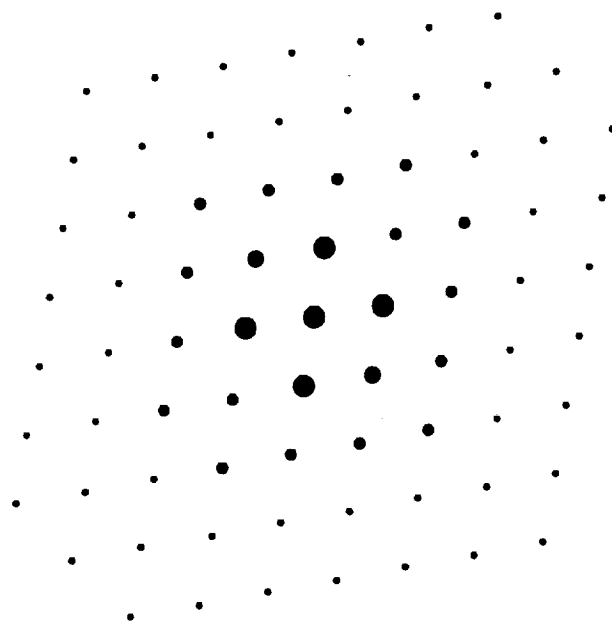
8090 slow cool + ad



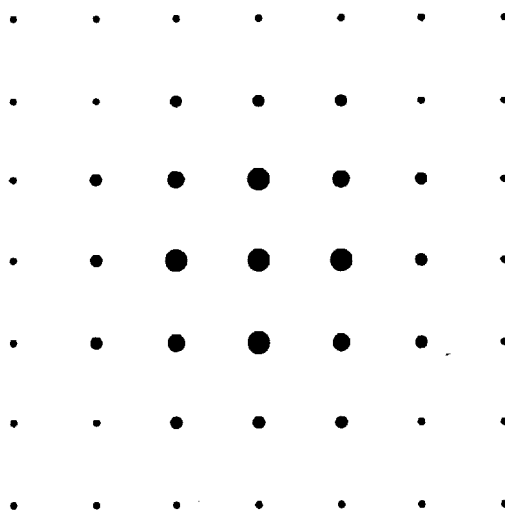
8090 slow cool + age



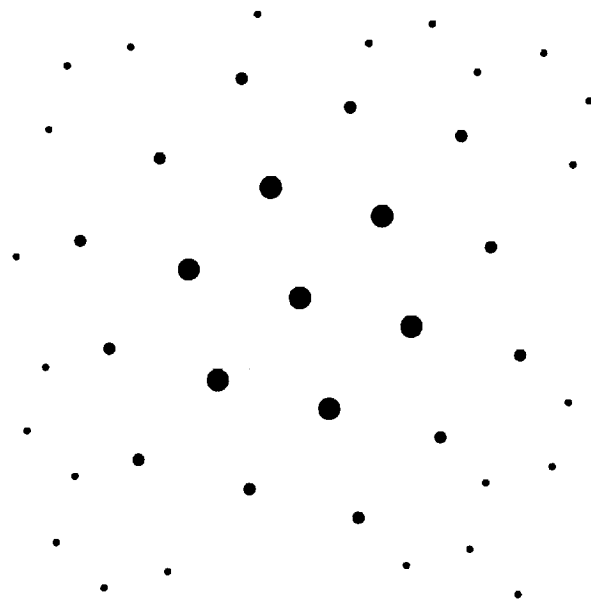
Selected Area Diffraction Pattern
Aluminum (110)



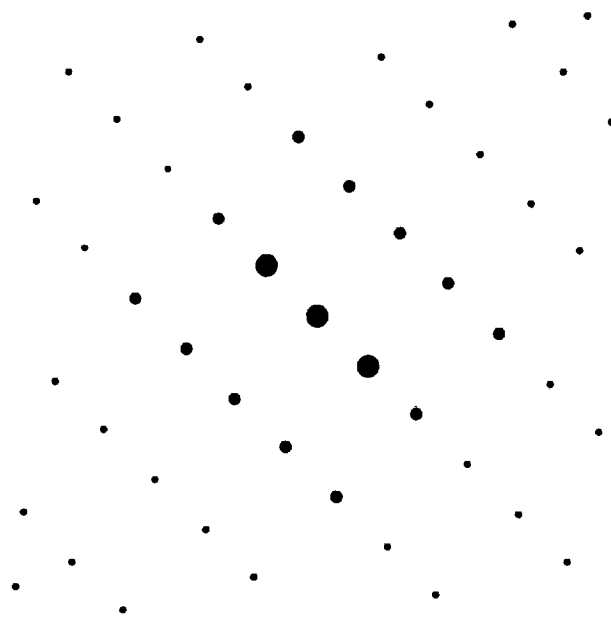
Selected Area Diffraction Pattern
Aluminum (001)



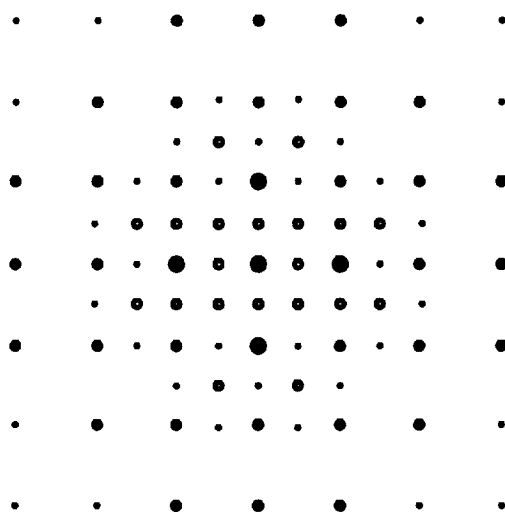
Selected Area Diffraction Pattern
Aluminum (111)



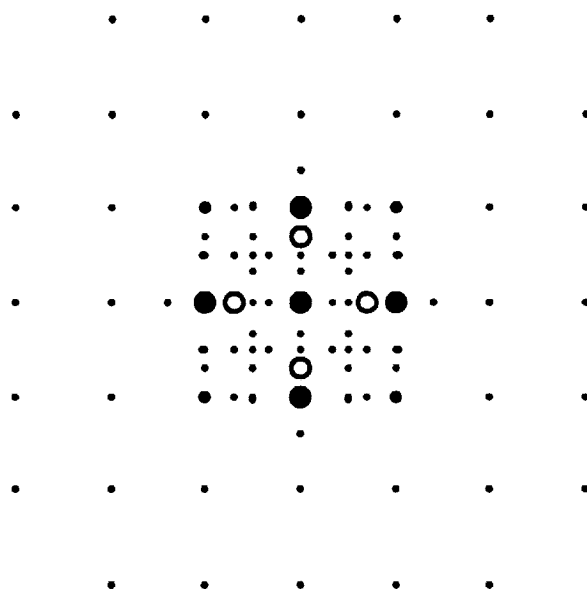
Selected Area Diffraction Pattern
Aluminum (112)



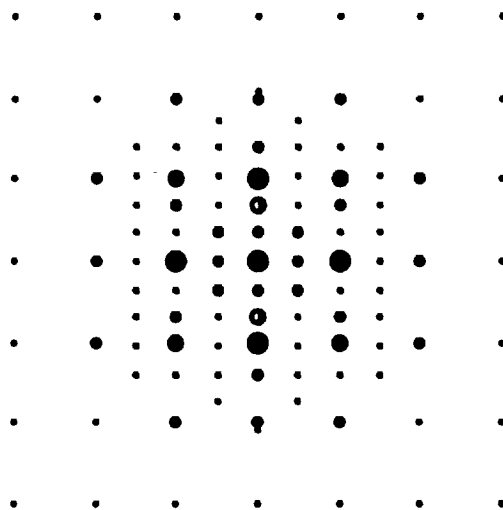
Selected Area Diffraction Pattern
Al (100) + Al₃Li 50nm particles, cube-cube orientation



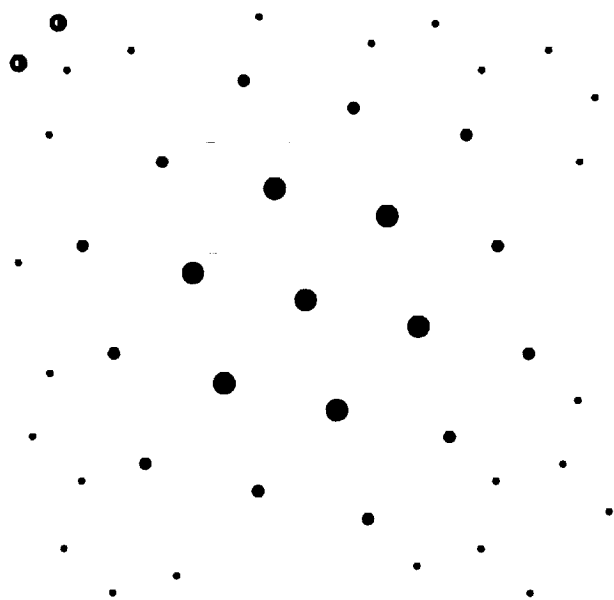
Al₂Cu in Al 100 zone axis



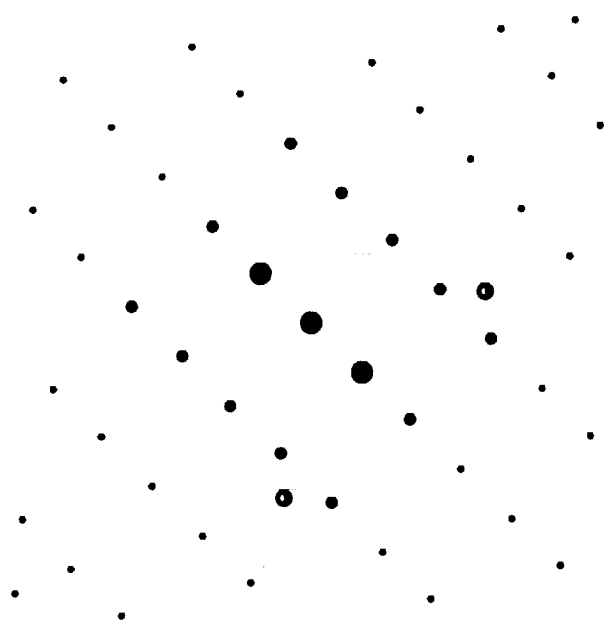
Selected Area Diffraction Pattern
(100) Al + Al₂Cu



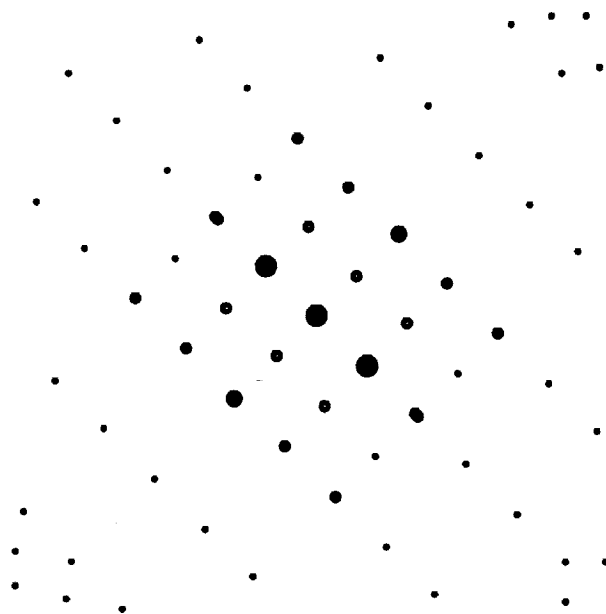
Selected Area Diffraction Pattern
(111) Al + Al₂Cu



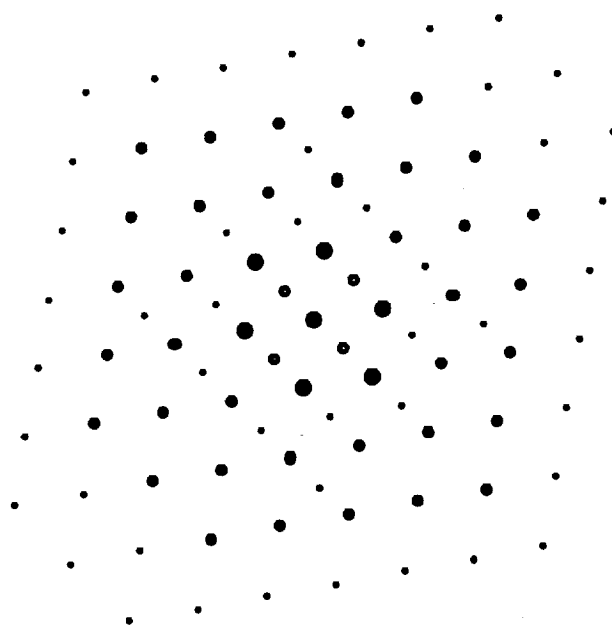
Selected Area Diffraction Pattern
(112) Al + Al₂Cu



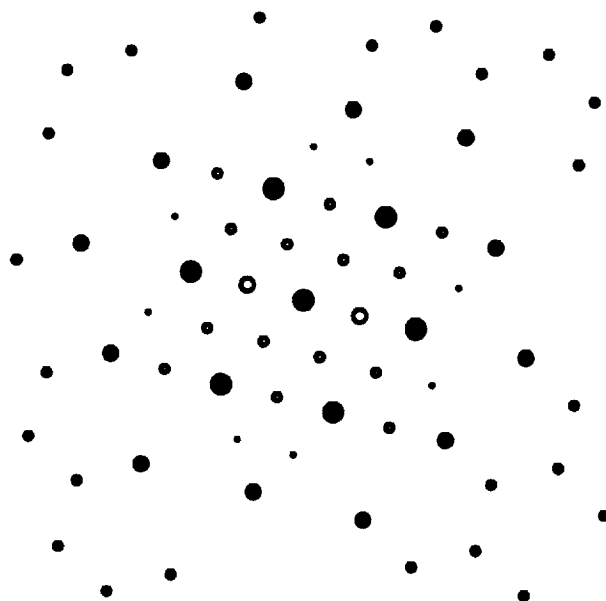
Selected Area Diffraction Pattern
(112) Al + Al₃Li



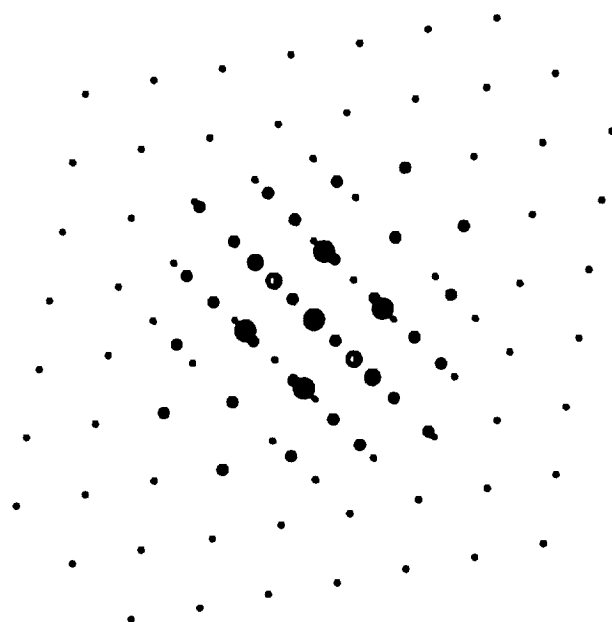
Selected Area Diffraction Pattern
(110) Al + Al₃Li

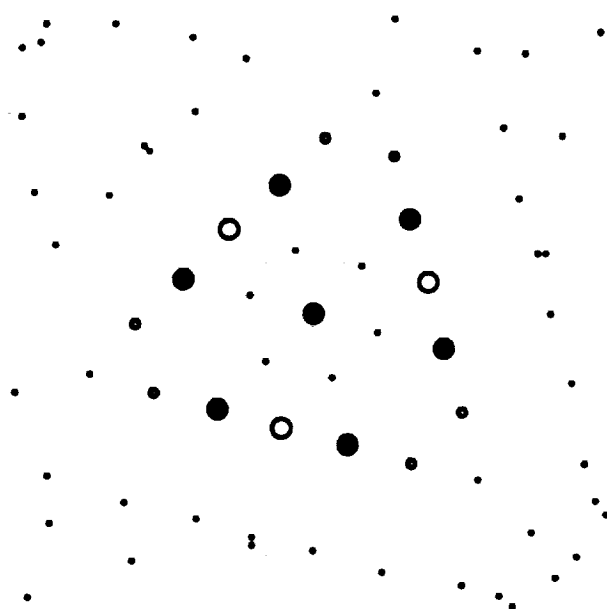


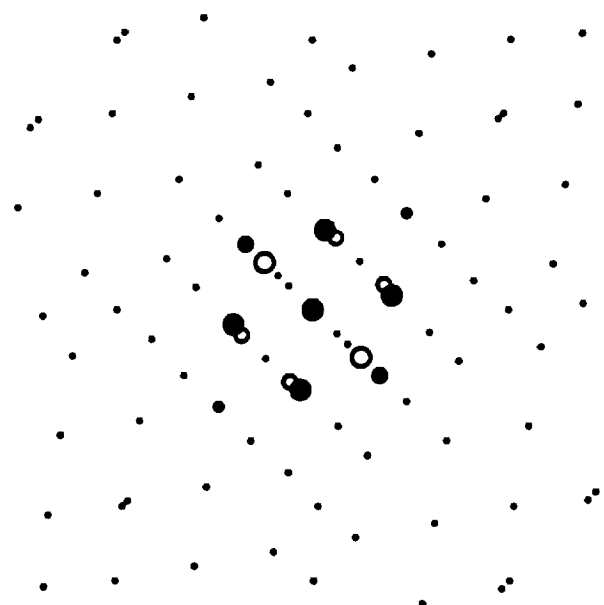
Selected Area Diffraction Pattern
(111) Al + Al₃Li



Selected Area Diffraction Pattern
(110) Al + Al₂Cu







THIS PAGE INTENTIONALLY LEFT BLANK.

APPENDIX F
DOUBLER REINFORCED FUSION WELD PANEL TEST PLAN

PRECEDING PAGE BLANK NOT FILMED

TEST PLAN
FOR
TYPE IV FUSION WELD PANEL
SPF STIFFENER CONCEPT

CONTRACT: Technology for Hypersonic Vehicles, NAS 1-18590 TASK Order 5, "Low Cost
SPF Aluminum Cryogenic Tank Concepts for ALS and Future Hypersonic Vehicles"

Prepared By:

C. E. Thompson
R. A. Latham
A. R. Del Mundo
G. H. Arvin

Approved By:



C. E. Anton
Program Manager
Low Cost, SPF Aluminum Cryogenic Tank
Concepts for ALS and Future Hypersonic Vehicles

DATE January 17, 1991
NO. OF PAGES Title + ii + 7



Rockwell International

North American Aircraft Operations
Rockwell International Corporation
P.O. Box 92098
Los Angeles, California 90009

FOREWORD

, The work reported herein covers the proposed effort for the Type IV hat-stiffened panels for the NASA contract NAS 1-18590 Task Order 5, "Low Cost SPF Aluminum Cryogenic Tank Concepts for ALS and Future Hypersonic Vehicles", C. E. Anton, Program Manager.

TABLE OF CONTENTS

	<u>Page</u>
FOREWORD	F-2
TABLE OF CONTENTS.....	F-3
1.0 INTRODUCTION.....	F-4
2.0 SPECIMEN DESCRIPTION	F-4
3.0 TEST TEMPERATURE.....	F-4
4.0 TEST MACHINE	F-6
5.0 INSTRUMENTATION.....	F-6
6.0 TEST FIXTURES.....	F-6
7.0 TEST PROCEDURE.....	F-6
8.0 DATA REQUIRED.....	F-9
9.0 TEST REPORT.....	F-9

1.0 INTRODUCTION

The assembly of the overall tank structure for large cryogenic LH₂ designs requires longitudinal splice joints between the SPF stiffened-panel sections. The objective of this report is to define the type of loading fixture, test instrumentation, failure load prediction, and test procedure that are required to evaluate the combined fusion weld and resistance spotweld doubler splice joint under the biaxial loads of bending and pressure.

1.1 TECHNICAL CONTACTS

C. Thompson	Stress	213-647-3541
R. Latham	Stress	213-647-6776
A. Del Mundo	Project Engineer(Design)	213-922-0929

2.0 SPECIMEN DESCRIPTION

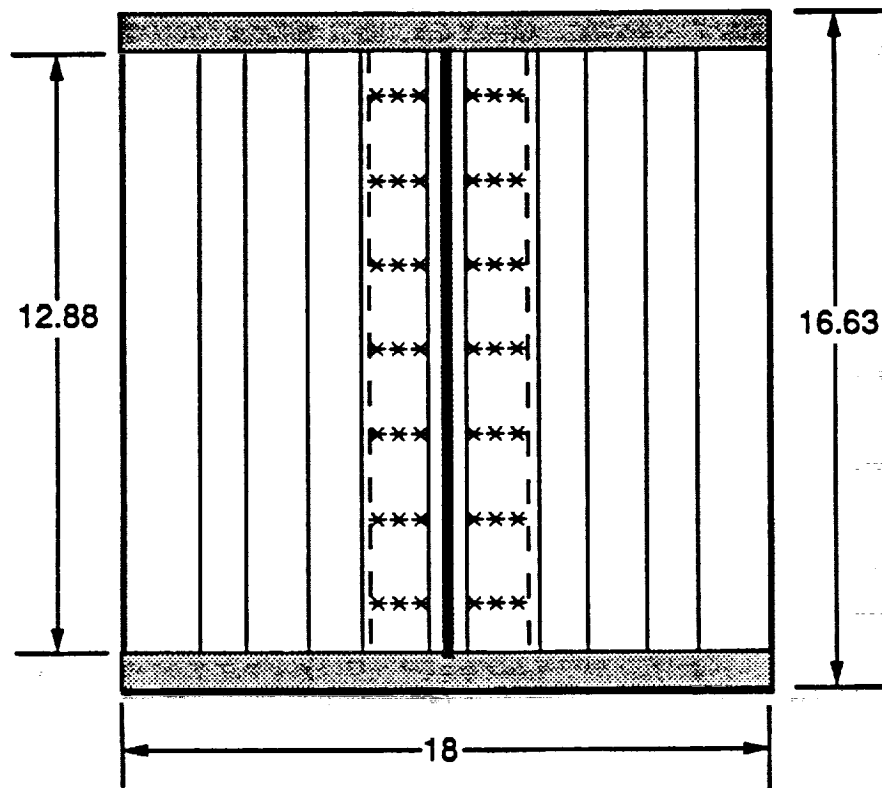
Each specimen consists of two 9- x 6.75- x 0.155-inch plates fusion edge-welded together, reinforced by an overlapping spotwelded doubler, combined with two Type I stepped-hat stiffeners. The pressure load across the joint (hoop tension) is carried by spotwelding the stiffener flanges, skin, and doubler together with three-spotweld clusters, as shown in Figure 1. Two replicates for each of the following material combinations will be tested:

	Stiffener	Skin	Doubler
#1	7475 Al	2219 Al	2219 Al
#2	2090 Al-Li	2090 Al-Li	2090 Al-Li

The reference drawing is L9111413

3.0 TEST TEMPERATURE

Ambient test conditions will be specified for all specimens. Test temperature should be recorded prior to the structural test for inclusion in the test report.



Ref. Drawing L9111413

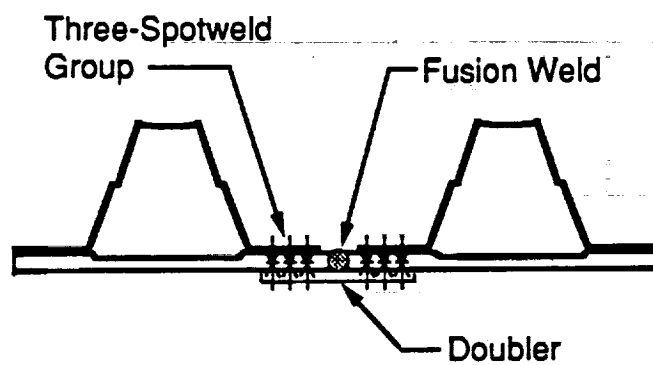


Figure 1. Type IV SPF Panel Configuration

4.0 TEST MACHINE

A compression test machine with a load capacity of 200,000 pounds or greater and a loading rate of 0.05 inch/minute should be used for applying the axial load to each Type IV panel. Actuators with total load capacity of 150,000 pounds will be used to apply the transverse load to each panel.

5.0 INSTRUMENTATION

Both strain gage and deflectometer data will be measured, with eleven strain gages and five deflectometers required for each panel. The locations of these gages and deflectometers are shown in Figure 2.

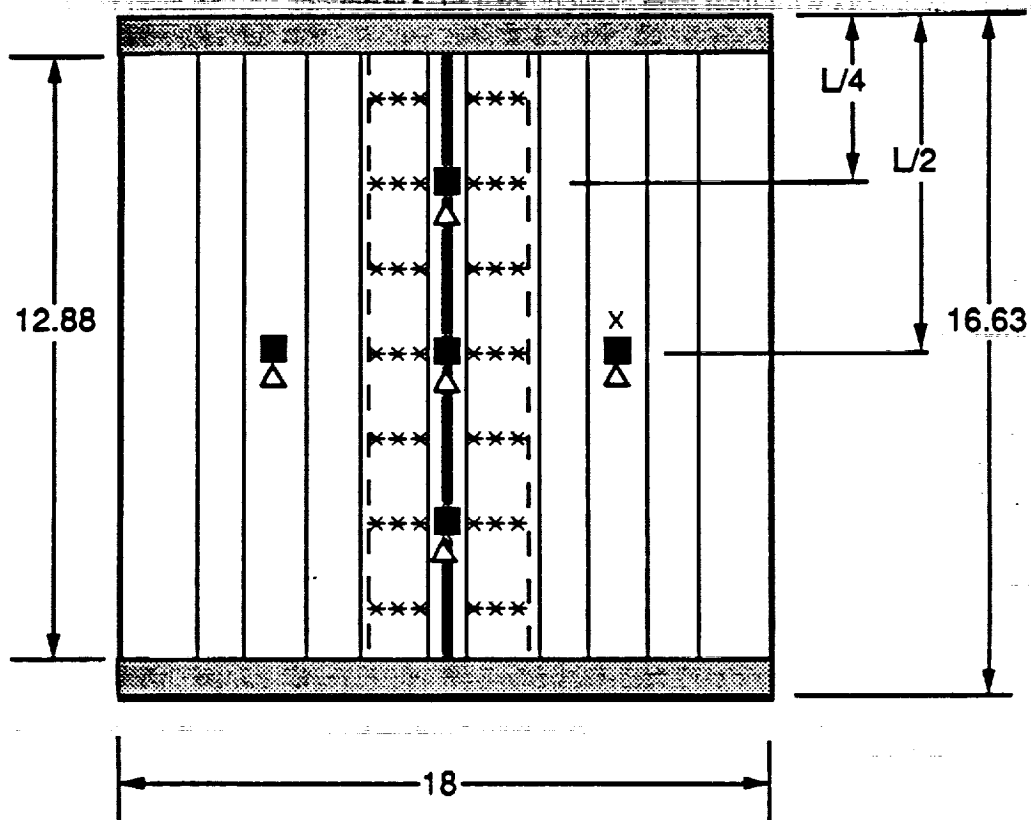
6.0 TEST FIXTURES

The support of the loaded axial (N_x) edges consists of potting the ends with Velstone to a depth of two inches surrounding the stiffener and skin. The panel side edges will be held in guided supports that have been radiused to provide simple support and still allow introduction of the transverse load (pressure) to the specimen. The transverse load will be introduced to the panel with small segmented pads to prevent the edges from accepting axial load introduction by the longitudinal test machine. A whiffletree arrangement will be used so that only two actuators will be needed to apply the transverse loading, as shown in Figure 3.

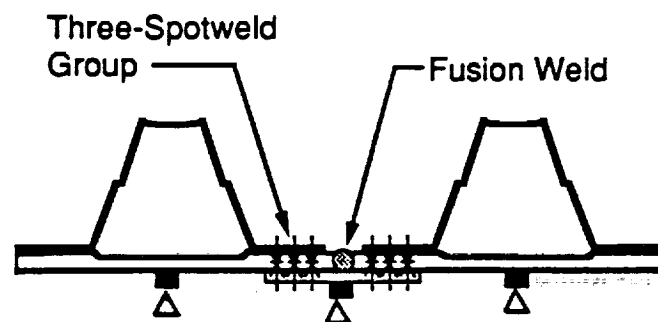
The reference drawing for the test fixture is L9111441

7.0 TEST PROCEDURE

Each specimen will be mounted in the test machine and aligned with the side edges surrounded by the guides to provide simple support (Figure 3). The transverse loads will be introduced by the actuators through the whiffletree system. The loading will be applied in the ratio of $N_x/N_y = -1.086$ (ultimate biaxial loading criteria) continuously until failure is achieved. The application of the P_1 axial load will be through the centroid of the two stiffeners plus joint splice configuration. This centroid has been calculated to be 0.32 inch with reference to the outer skin mold line.



Ref. Drawing # L9111411

Strain Gages

x Axial Cap	1
■ Bi-Axial (Skin)	10
Total	11
△ Deflectometers	5

Figure 2. Type IV SPF Panel Instrumentation

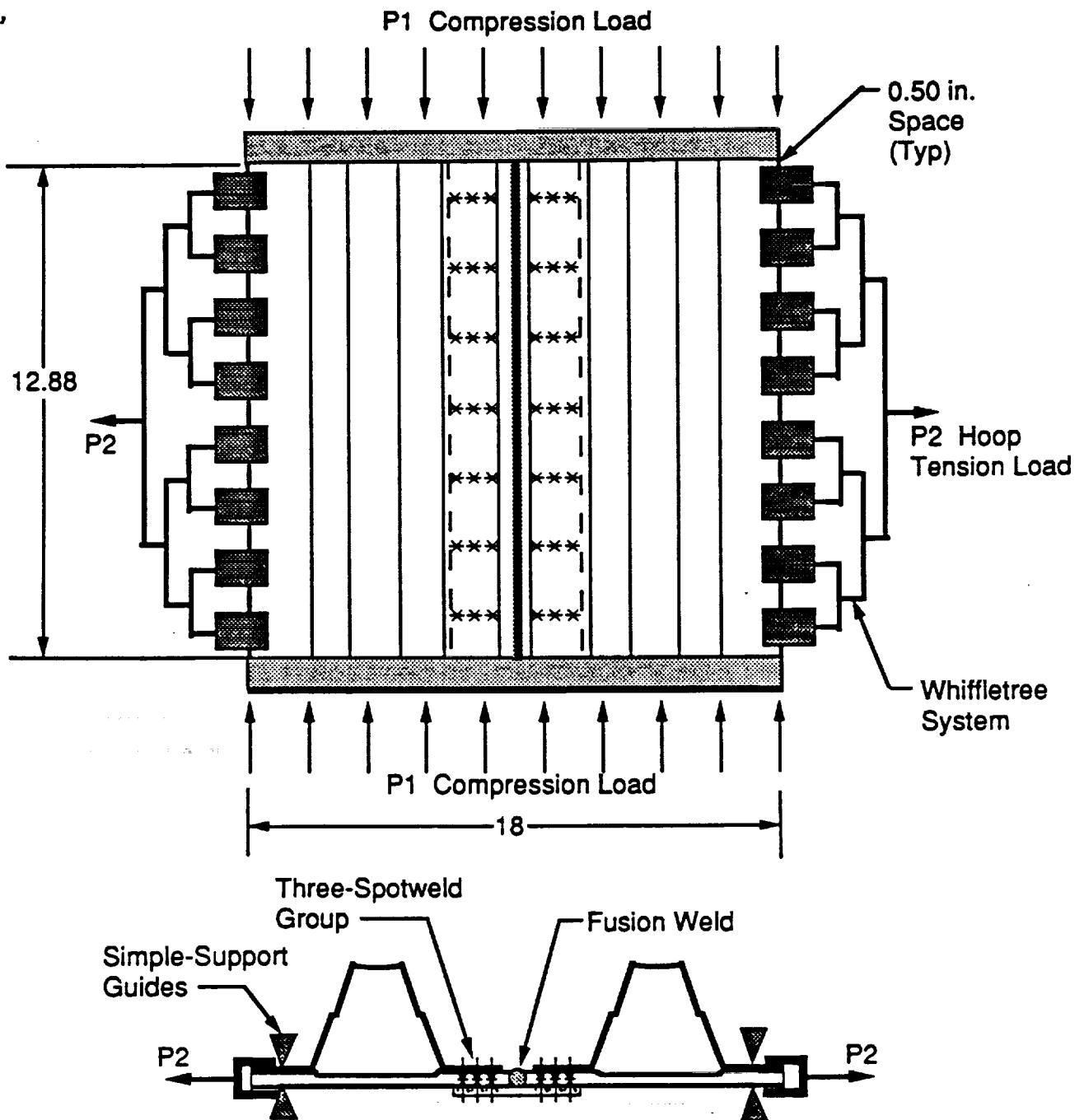


Figure 3. Type IV SPF Panel Loading Setup

The strain gages and deflectometers will be read at 10-second intervals until failure. As is standard practice, all gages will be zeroed out prior to the start the of loading for each panel. The predicted ultimate loads for each Type IV panel are summarized in Table I.

8.0 DATA REQUIRED

All strain gage and deflectometer readings at each load increment will be recorded for each panel test. In addition, all relevant observations concerning specimen appearance, procedure incidents, and anomalous indications will be noted and recorded relative to the corresponding load level.

One 8.5- x 11-inch glossy photographic print and one 85-line screen print with negative will be furnished by the test facility for each test panel both after mounting in the test machine and after failure

A schematic drawing showing the actual measured locations and orientations of all strain gages and deflectometers will be furnished to the program manager.

9.0 TEST REPORT

A preliminary test report tabulating all strain gage and deflection data will be prepared by the NASA-Langley Structures Laboratory and submitted within 30 days after testing of the Type IV panels to:

Rockwell International, Space Division
C. E. Anton, NAS1-18590 Task 5 Program Manager
D/284, 841-NA40
12214 Lakewood Blvd
Downey, CA 90241

for preparation of the final test report.

Table I

PREDICTED BIAXIAL FAILURE LOADS FOR TYPE IV PANELS

Panel Type	Predicted Load Intensity* Lb/in.	P ₁ Total Load Lbs	P ₂ Total Load Lbs	Predicted Failure Mode
7475/2219	N _x = -9125 N _y = +8402	164,250	108,218	SHEAR-1st Spotweld
2090/2090	N _x = -5975 N _y = +5500	107,550	70,840	SHEAR-1st Spotweld

* Based on preliminary GD weld allowables. The ratio $N_x/N_y = -1.086$ will be maintained throughout the loading to failure.

NOTES:

1. Splice doubler thickness = 0.09 inch
2. The predicted failure loads P₁ and P₂ are the load intensity values times the respective panel dimensions.

THIS PAGE INTENTIONALLY LEFT BLANK.

24 23 22 21

H

G

F

E

D

C

B

A

PRECEDING PAGE BLANK NOT FILMED

FOLDOUT FRAME

ORIGINAL PAGE IS
OF POOR QUALITY

59.50

38.00

DET -031 ASS

SHIM AS REQD BETWEEN
-007 & -009, SEE NOTE 7

.187 FOR -009

9C

009

24 23 22 21

A-A 9C

— 59.50 —

38 EO 5

DET -031 ASS

SHIM AS REQD BETWEEN
-007 & -009, SEE NOTE 7

.187 FOR -009

-009

PRECEDING PAGE BLANK NOT FILMED

FOLDOUT FRAME

ORIGINAL PAGE IS
OF POOR QUALITY

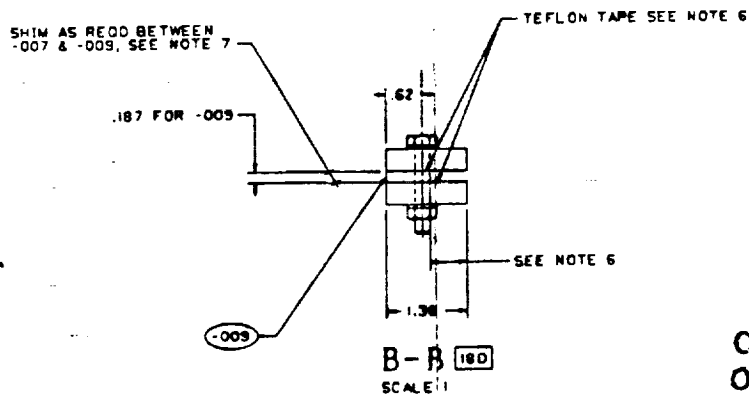
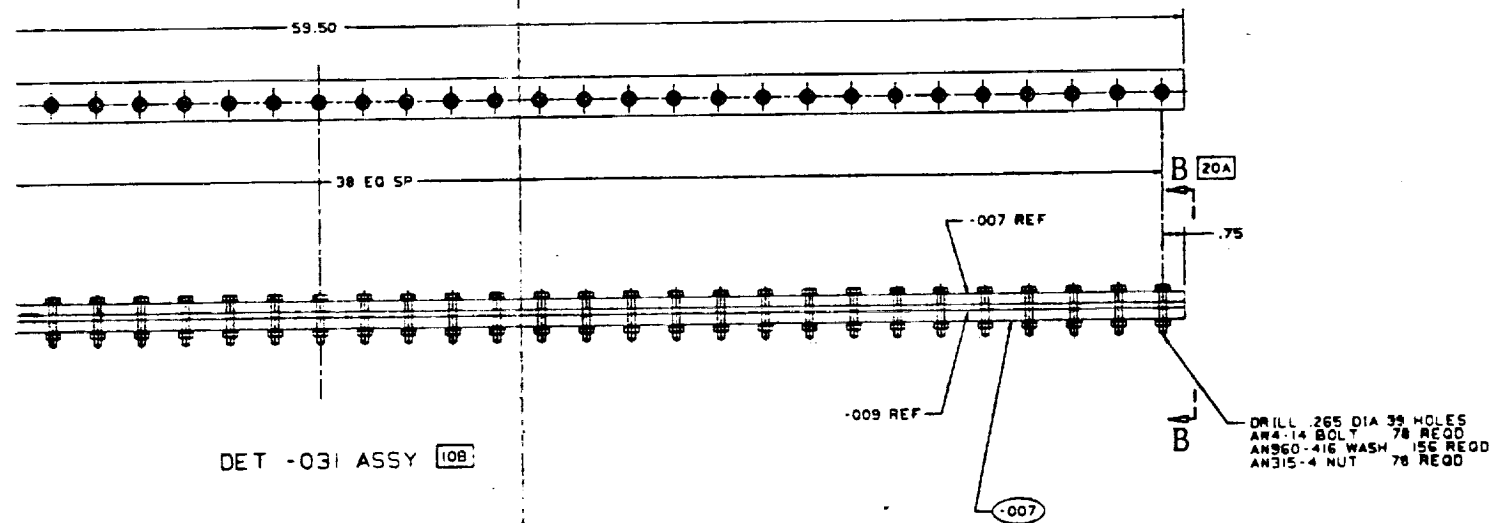
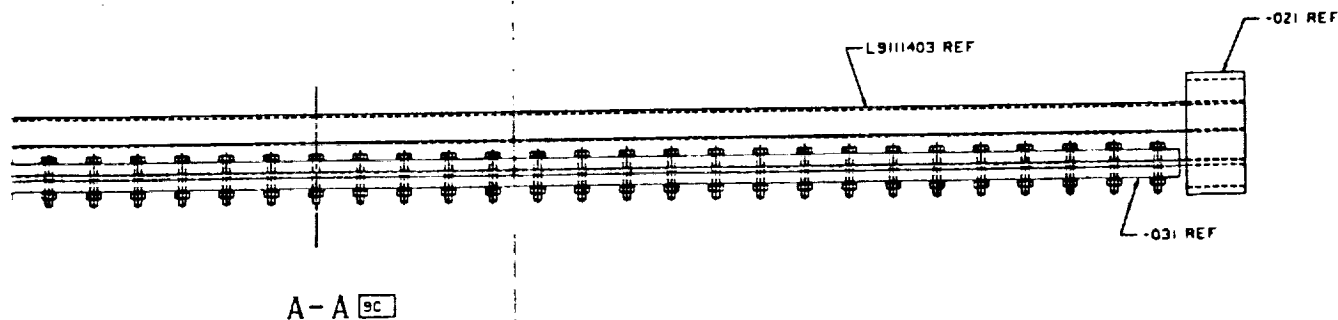
1. The first part of the document is a list of the names of the persons who have been appointed to the various offices of the Board of Directors of the Corporation. The names are as follows:

2. The second part of the document is a list of the names of the persons who have been appointed to the various offices of the Board of Directors of the Corporation. The names are as follows:

3. The third part of the document is a list of the names of the persons who have been appointed to the various offices of the Board of Directors of the Corporation. The names are as follows:

4. The fourth part of the document is a list of the names of the persons who have been appointed to the various offices of the Board of Directors of the Corporation. The names are as follows:

5. The fifth part of the document is a list of the names of the persons who have been appointed to the various offices of the Board of Directors of the Corporation. The names are as follows:

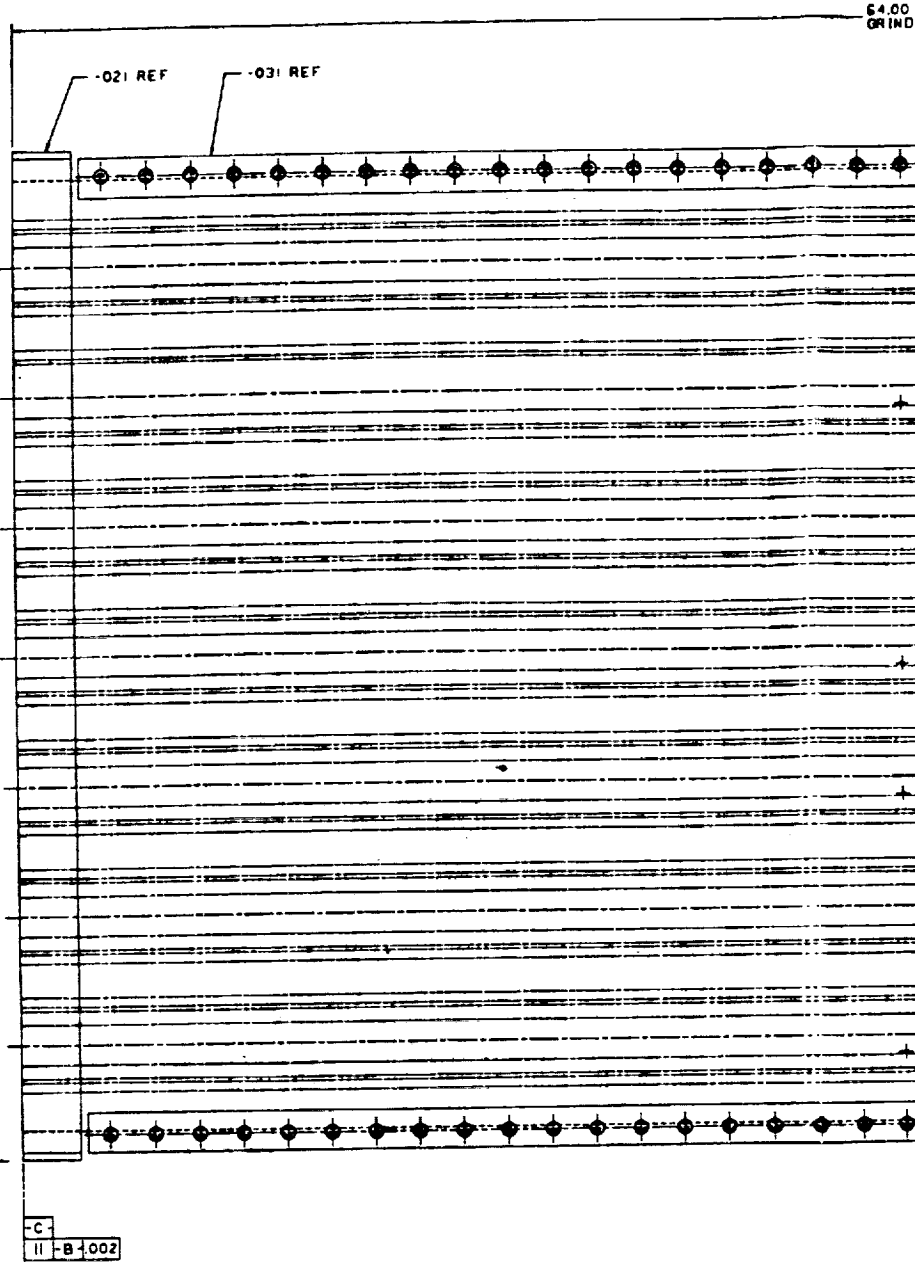


ORIGINAL PAGE IS
OF POOR QUALITY

FOLDOUT FRAME

FIG.	FRAME	REV	BY
L9111411	-	1	

021 REF

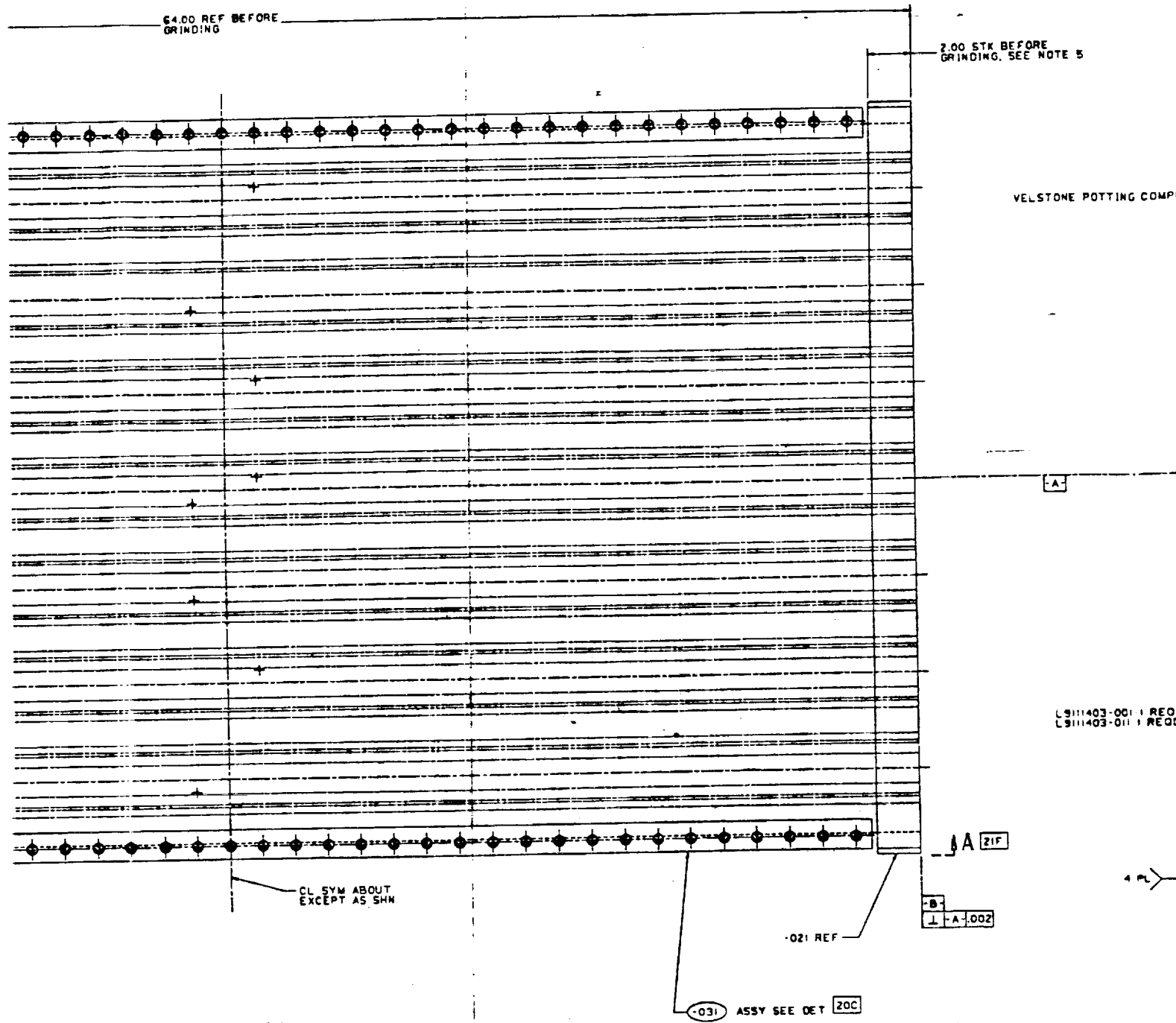


L .265 DIA 39 HOLES
 14 BOLT 78 REQD
 60-416 WASH 156 REQD
 15-4 NUT 78 REQD

3.
 FOLDOUT FRAME

ORIGINAL PAGE IS
 OF POOR QUALITY

FOLDOUT FRAME	
L9111411	REV 1



-001 ASSY SHOWN
 -011 ASSY IDENTICAL TO -001 EXCEPT AS NOTED

FOLDOUT FRAME

ORIGINAL PAGE IS
 OF POOR QUALITY

FRAME	REV. NO.
L9111411	1

2.00 STX BEFORE GRINDING, SEE NOTE 5

VELSTONE POTTING COMPOUND

LS111403-001 I RECD ON -001
LS111403-011 I RECD ON -011

-031 REF

-003
-021 WELD ASSY

A 21F

B
A-002

FOLDOUT FRAME

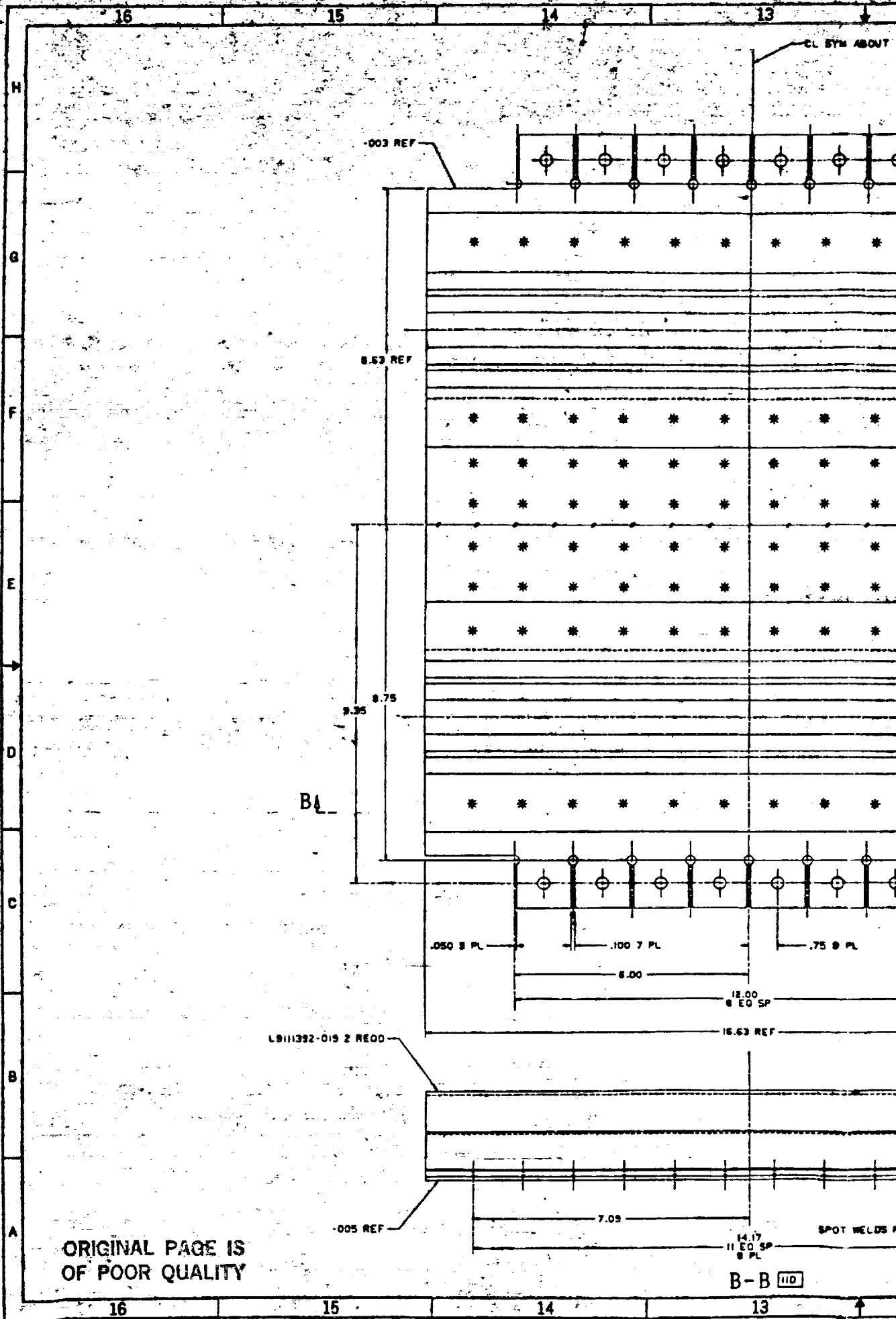
ORIGINAL FACE IS OF POOR QUALITY

REV	DATE	BY	CHK	APP
1				

- THE -031 ASSYS SHOULD BE FIT & SHOULD NOT BE TIGHT
- APPLY TEFLON TAPE TO THE BARS TO INTERFACE WITH THE
- GRIND SPECIMEN ENDS AND PARALLEL 1.06 MAX EACH E
- USE 1/2 DIA STRAIN GAGE WHEN APPLYING VELSTONE
- VELSTONE POTTING COMPOUND INTERNAL AS WELL AS EXTERNAL FROM THE END
- IDENTIFY PER LAD104-026, IMPRESSION STAMP
- SHEET METAL OR EXTRUSION LAD102-012

NOTES: UNLESS OTHERWISE

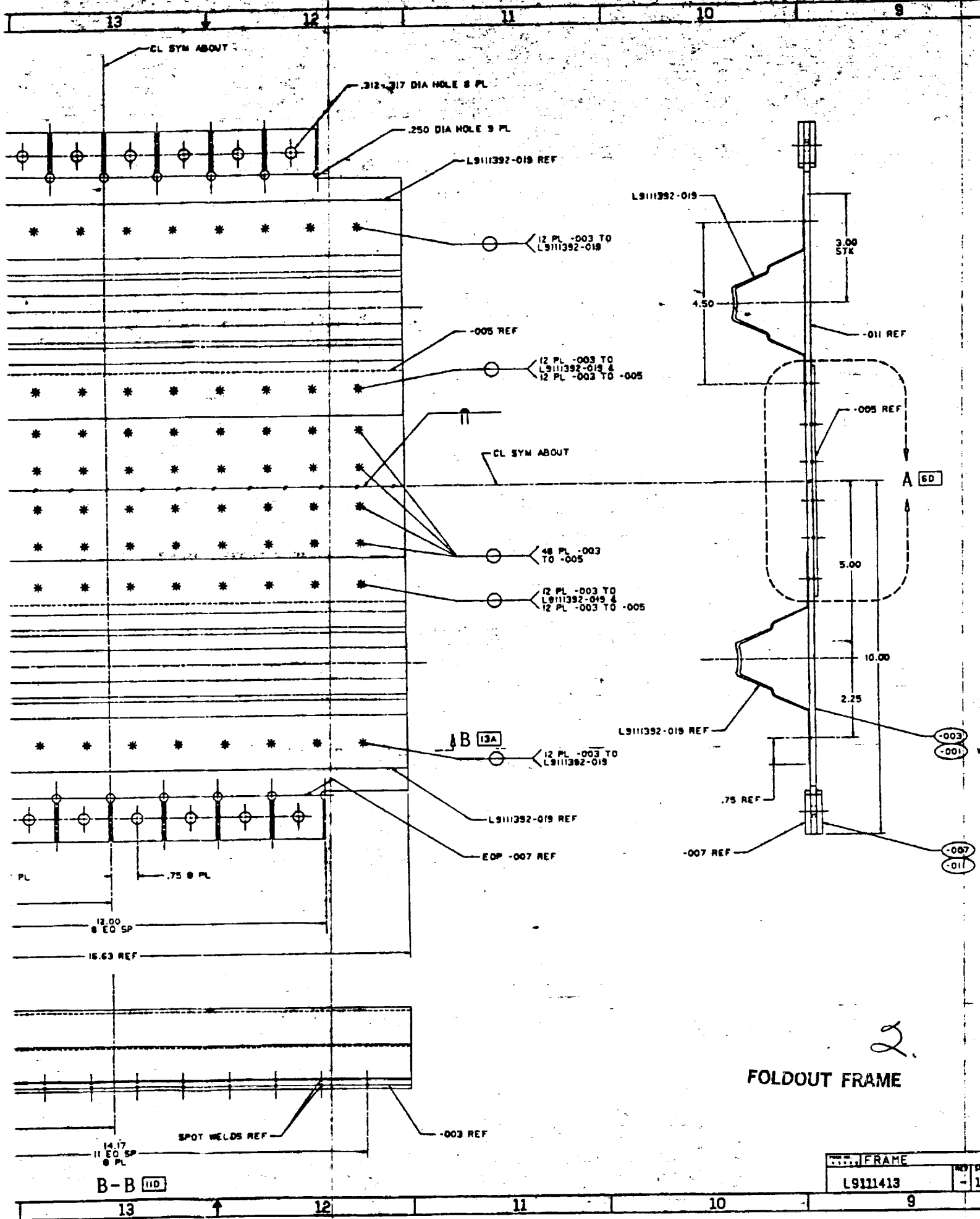
1000000

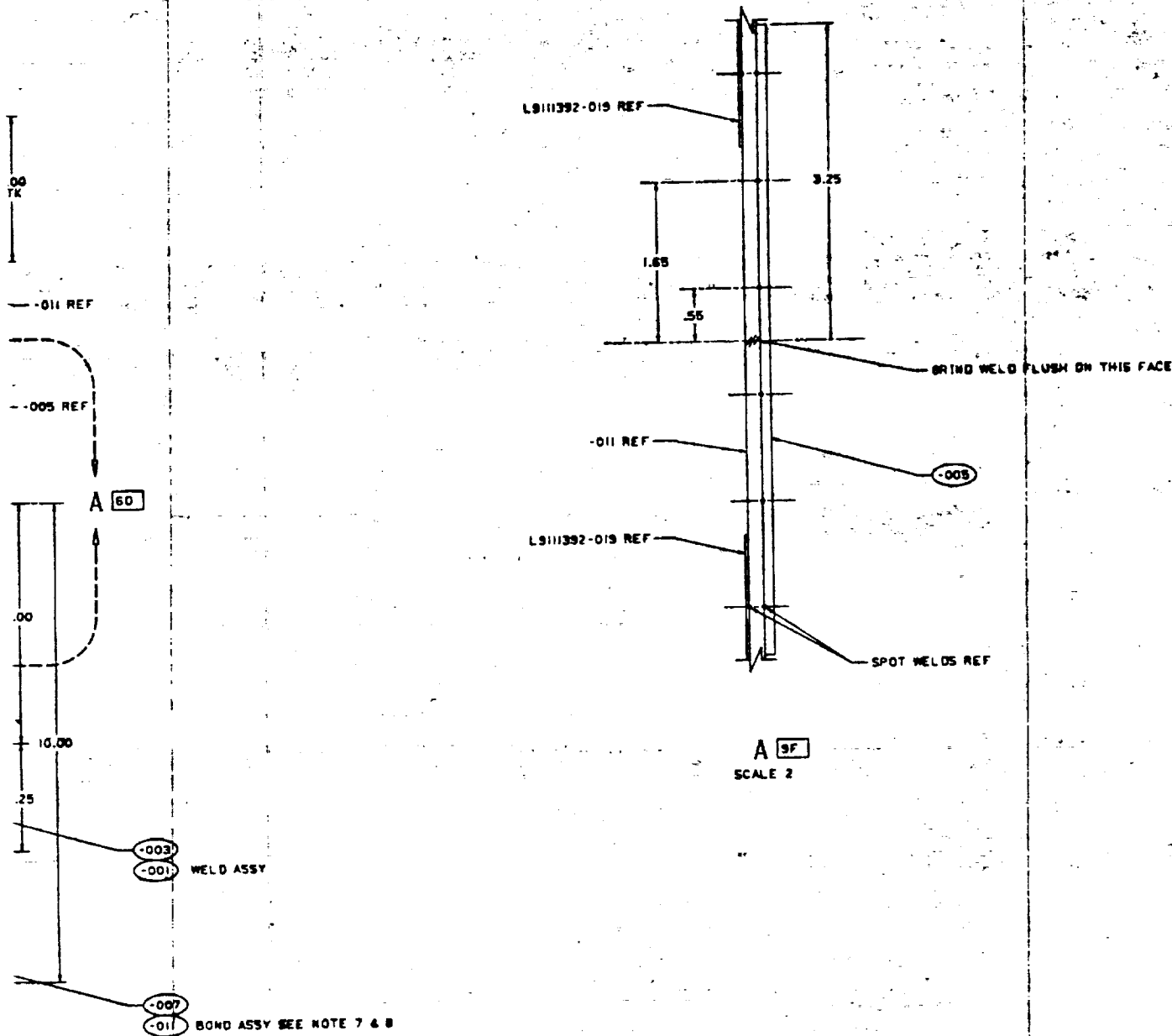


FOLDOUT FRAME

ORIGINAL PAGE IS
OF POOR QUALITY

B-B 110





FRAME
9111413

ORIGINAL PAGE IS
OF POOR QUALITY

6. ROOM TEMPERATURE BOND -007 TO -003 USE 7344 A & B ADHESIVE
 7. BOND -007 TO -003 BEFORE MACHINING .250 DIA HOLES; -007 MAY BE MADE FROM WD X 12.00 LG SHTS OF MATERIAL FOR
 8. WELD SYMBOLS PER SY05000020P
 9. RADIOGRAPHIC AND VISUAL INSPECT PER
 10. RESISTANCE WELD PER MIL-W-68580
 11. IDENTIFY PER LA0104-0026, EXCEPT
 12. MACHINE PER LA0103-004
 13. STANDARD DETAIL PER LA0102-012
- NOTES: UNLESS OTHERWISE SPECIFIED

ORIGINAL PAGE IS
OF POOR QUALITY

10M TEMPERATURE BOND -002 TO -003 PER MIL-A-25483;
E 7344 A & B ADHESIVE

NEXT ASSEMBLY

RD -007 TO -003 BEFORE MACHINING FINGERS & DRILLING
30 DIA HOLES; -007 MAY BE MADE FROM 2 INCH THK X 1.25
X 12.00 LB SHTS OF MATERIAL FOR EACH -003 ASSY

LD SYMBOLS PER STD0000070P

DIAGRAPHIC AND VISUAL INSPECT PER MIL-W-68600

FINANCE WELD PER MIL-W-68580

ENTIFY PER LAG104-0026, EXCEPT DO NOT METAL IMPRESSION STAMP

CHINE PER LAG103-004

ANDARD DETAIL PER LAG102-048


ES: UNLESS OTHERWISE SPECIFIED

JAN 23 1931
#5-1

L9111413

				2		L9111292-051	L9111292-051		15B
				2		-011	BOND ASSY		9C
				NS		-007	DOUBLER, STD170LB0048, 2219-T62 CLAD AL ALY, .156 THK X 1.25 WD X 1.40 LG	7.9	9C
				1		-005	DOUBLER, STD170LB0048, 2219-T62 CLAD AL ALY, .100 THK X 6.50 WD X 16.63 LG		6F
				1		-003	SKIN, STD170LB0048, 2219-T62 CLAD AL ALY, .156 THK X 10.00 WD X 16.63 LG		8D
				1		-001	WELD ASSY		8D
NEXT ASSEMBLY	END ITEM			-011-001	ONE IDENT	PART OR IDENTIFYING NUMBER	1	1	STEM NO
BOMENCLATURE OR DESCRIPTION							NOTE	ZONE	NO

PARTS LIST

		PANEL - TYPE IV BI-AXIAL TEST ASSY
J 43999	L9111413	OF

CAD DATABASE AVAIL-CADD5 4

